RECENT ADVANCES IN PRECISION VACCINE DISCOVERY & DEVELOPMENT

EDITED BY: Ofer Levy, Simon Daniel Van Haren, Scott James Tebbutt, Francesco Borriello and Jay Evans

PUBLISHED IN: Frontiers in Immunology and Frontiers in Pediatrics

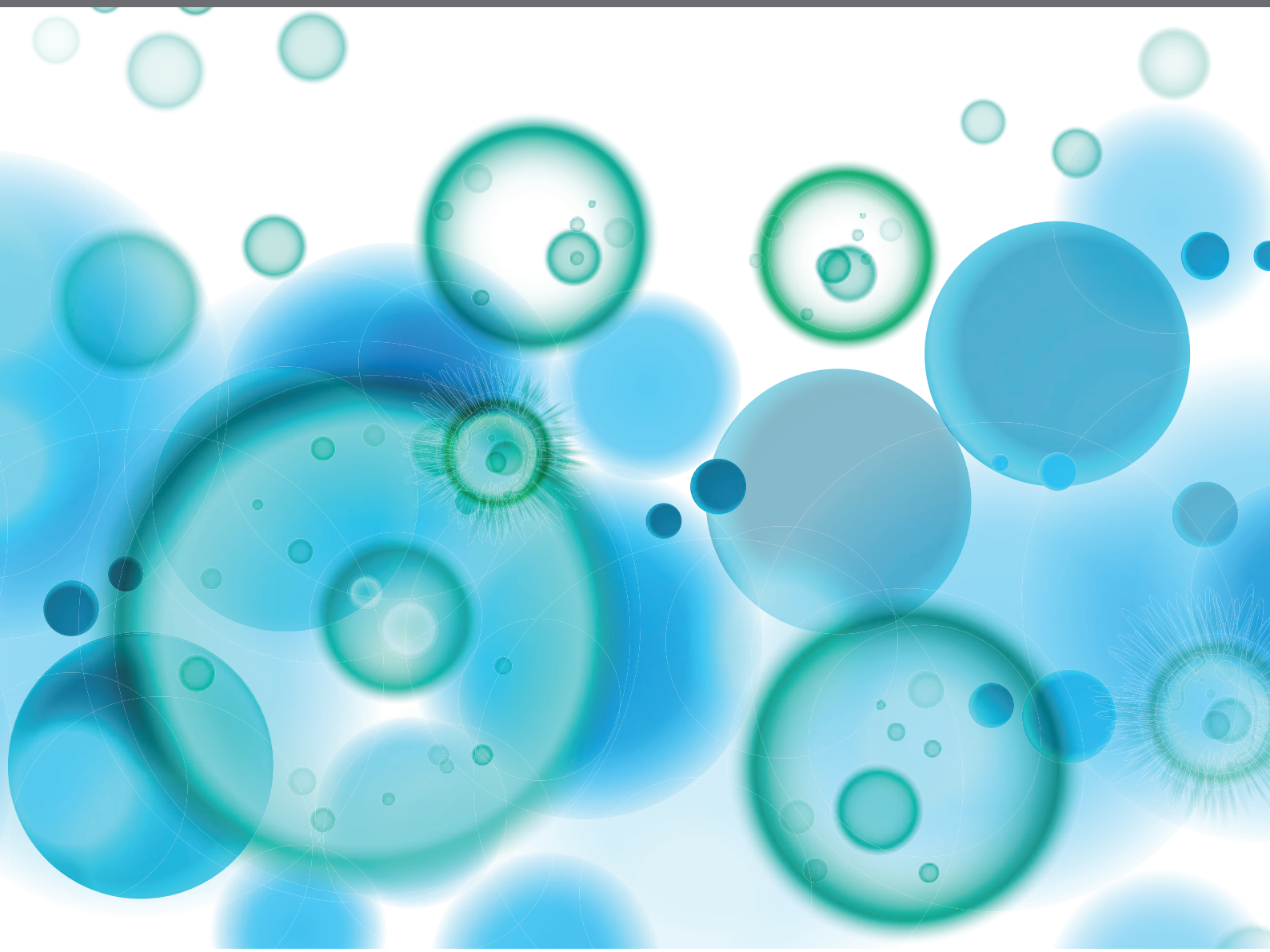

frontiers Research Topics

frontiers

ISSN 1664-8714
ISBN 978-2-88971-658-6
DOI 10.3389/978-2-88971-658-6

About Frontiers

Frontiers is more than just an open-access publisher of scholarly articles: it is a pioneering approach to the world of academia, radically improving the way scholarly research is managed. The grand vision of Frontiers is a world where all people have an equal opportunity to seek, share and generate knowledge. Frontiers provides immediate and permanent online open access to all its publications, but this alone is not enough to realize our grand goals.

Frontiers Journal Series

The Frontiers Journal Series is a multi-tier and interdisciplinary set of open-access, online journals, promising a paradigm shift from the current review, selection and dissemination processes in academic publishing. All Frontiers journals are driven by researchers for researchers; therefore, they constitute a service to the scholarly community. At the same time, the Frontiers Journal Series operates on a revolutionary invention, the tiered publishing system, initially addressing specific communities of scholars, and gradually climbing up to broader public understanding, thus serving the interests of the lay society, too.

Dedication to Quality

Each Frontiers article is a landmark of the highest quality, thanks to genuinely collaborative interactions between authors and review editors, who include some of the world's best academicians. Research must be certified by peers before entering a stream of knowledge that may eventually reach the public - and shape society; therefore, Frontiers only applies the most rigorous and unbiased reviews.
Frontiers revolutionizes research publishing by freely delivering the most outstanding research, evaluated with no bias from both the academic and social point of view. By applying the most advanced information technologies, Frontiers is catapulting scholarly publishing into a new generation.

What are Frontiers Research Topics?

Frontiers Research Topics are very popular trademarks of the Frontiers Journals Series: they are collections of at least ten articles, all centered on a particular subject. With their unique mix of varied contributions from Original Research to Review Articles, Frontiers Research Topics unify the most influential researchers, the latest key findings and historical advances in a hot research area! Find out more on how to host your own Frontiers Research Topic or contribute to one as an author by contacting the Frontiers Editorial Office: frontiersin.org/about/contact

RECENT ADVANCES IN PRECISION VACCINE DISCOVERY & DEVELOPMENT

Topic Editors:
Ofer Levy, Boston Children's Hospital, United States
Simon Daniel Van Haren, Harvard Medical School, United States
Scott James Tebbutt, University of British Columbia, Canada
Francesco Borriello, Harvard Medical School, United States
Jay Evans, University of Montana, United States

Topic Editor Jay Evans is the co-founder, President and CEO of Inimmune Corporation. The other Topic Editors declare no competing interests with regard to the Research Topic subject.

Citation: Levy, O., Van Haren, S. D., Tebbutt, S. J., Borriello, F., Evans, J., eds. (2021). Recent Advances in Precision Vaccine Discovery & Development. Lausanne: Frontiers Media SA. doi: 10.3389/978-2-88971-658-6

Table of Contents

frontiers in Immunology

ORIGINAL RESEARCH
published: 10 March 2020
doi: 10.3389/fimmu.2020.00406

Novel Lipidated Imidazoquinoline TLR7/8 Adjuvants Elicit Influenza-Specific Th1 Immune Responses and Protect Against Heterologous H3N2 Influenza Challenge in Mice

Shannon M. Miller[1,2], *Van Cybulski*[1,2], *Margaret Whitacre*[1,2], *Laura S. Bess*[1,3], *Mark T. Livesay*[1,3], *Lois Walsh*[1,3], *David Burkhart*[1,3], *Hélène G. Bazin*[1,3] *and Jay T. Evans*[1,2*]

[1] *Center for Translational Medicine, University of Montana, Missoula, MT, United States,* [2] *Division of Biological Sciences, University of Montana, Missoula, MT, United States,* [3] *Department of Biomedical and Pharmaceutical Sciences, University of Montana, Missoula, MT, United States*

OPEN ACCESS

Edited by:
Anke Huckriede, University Medical Center Groningen, Netherlands

Reviewed by:
Michael Schotsaert, Icahn School of Medicine at Mount Sinai, United States
Gunnveig Grødeland, University of Oslo, Norway

***Correspondence:**
Jay T. Evans
jay.evans@umontana.edu

Specialty section:
This article was submitted to Vaccines and Molecular Therapeutics, a section of the journal Frontiers in Immunology

Received: *13 November 2019*
Accepted: *20 February 2020*
Published: *10 March 2020*

Citation:
Miller SM, Cybulski V, Whitacre M, Bess LS, Livesay MT, Walsh L, Burkhart D, Bazin HG and Evans JT (2020) Novel Lipidated Imidazoquinoline TLR7/8 Adjuvants Elicit Influenza-Specific Th1 Immune Responses and Protect Against Heterologous H3N2 Influenza Challenge in Mice. Front. Immunol. 11:406. doi: 10.3389/fimmu.2020.00406

Most licensed seasonal influenza vaccines are non-adjuvanted and rely primarily on vaccine-induced antibody titers for protection. As such, seasonal antigenic drift and suboptimal vaccine strain selection often results in reduced vaccine efficacy. Further, seasonal H3N2 influenza vaccines demonstrate poor efficacy compared to H1N1 and influenza type B vaccines. New vaccines, adjuvants, or delivery technologies that can induce broader or cross-seasonal protection against drifted influenza virus strains, likely through induction of protective T cell responses, are urgently needed. Here, we report novel lipidated TLR7/8 ligands that act as strong adjuvants to promote influenza-virus specific Th1-and Th17-polarized T cell responses and humoral responses in mice with no observable toxicity. Further, the adjuvanted influenza vaccine provided protection against a heterologous H3N2 influenza challenge in mice. These responses were further enhanced when combined with a synthetic TLR4 ligand adjuvant. Despite differences between human and mouse TLR7/8, these novel lipidated imidazoquinolines induced the production of cytokines required to polarize a Th1 and Th17 immune response in human PBMCs providing additional support for further development of these compounds as novel adjuvants for the induction of broad supra-seasonal protection from influenza virus.

Keywords: adjuvant, Vaccine, influenza, TLR4 (Toll-like receptor 4), Influenza challenge model, precision vaccines, TLR7/8 agonists

INTRODUCTION

The connection between the innate andadaptive immune system is instrumental for eliciting protective, durable, vaccine-elicited protection against infectious diseases. Current seasonal influenza virus vaccines can be effective if well-matched to the circulating strains; however, mismatch between vaccine strains and circulating strains, particularly in the case of H3N2 (1), leads to a sharp drop in vaccine effectiveness (2, 3). Further, recent analyses have indicated

that intraseasonal waning immunity against seasonal influenza is significant, and reductions in vaccine effectiveness may occur more rapidly for H3N2 than for H1N1 strains (4–8). Along with neutralizing antibodies [reviewed in (9)], previous studies have demonstrated that protection against influenza correlates with pre-existing levels of influenza-specific Th1-type CD4 T cells (10) and that passively transferred Th1 or Th17 memory T cells can protect naïve mice against influenza (11). However, current licensed seasonal and pandemic influenza vaccines fail to elicit efficient T cell responses (12).

One solution to this challenge is to develop novel adjuvants that target distinct innate immune receptors and trigger the required innate immune response to subsequently shape the desired adaptive immune response. Thus far, defining the required innate immune stimulators, or adjuvants, to subsequently elicit a protective, durable T cell response has been difficult. Promisingly, new vaccine adjuvants based on Toll-like receptor (TLR) ligands have been approved for human use including monophosphoryl lipid A, a TLR4 agonist and a component of the clinically approved adjuvant systems AS01 and AS04 (13–17), and CpG, a TLR9 agonist (18, 19). In the case of pandemic influenza virus vaccines, emulsion based adjuvant systems such as AS03 [reviewed in (15)] and MF59 [reviewed in (20)] have proven safe and effective at inducing strong humoral immunity to the matched vaccine and challenge strains. However, we still lack an influenza vaccine capable of eliciting consistent protection against drifted influenza strains. Two particularly promising adjuvant targets are TLR4 and TLR7/8. TLRs recognize various bacterial and viral components [reviewed in (21)]. TLR7 and TLR8 are expressed in the endosome and specifically recognize single stranded RNA (ssRNA) (22, 23). As the influenza virus is a single-stranded RNA virus and is recognized by TLR7/8 amongst other pattern recognition receptors (PRRs) (24), TLR7 and TLR8 are attractive targets for influenza virus vaccine adjuvants. Ligation of TLR7/8 elicits production of pro-inflammatory cytokines, such as TNFα, as well as the anti-viral cytokine IFNα, and induces upregulation of co-stimulatory molecules on antigen-presenting cells (APCs) that are critical for enhancing antigen-specific T cell responses (25–27). The anti-viral effects of TLR7/8 agonists are primarily generated through TLR7 ligation in plasmacytoid dendritic cells (pDCs) and their secretion of IFNα (25, 26) while pro-inflammatory responses generated through TLR8 ligation in myeloid dendritic cells [mDCs; (28, 29)] help shape the resulting innate and adaptive immunity. TLR4 has several known ligands, the most well-known of which is lipopolysaccharide (LPS). TLR4 is unique in that it can signal via the MyD88 pathway when TLR4 is engaged on the cell surface, resulting in production of proinflammatory cytokines [reviewed in (30)], whereas endosomal TLR4 signals via the TRIF pathway and induces the production of type I interferons (31, 32), which are critical for anti-viral immune responses, and pro-IL-1β (33–35).

TLR7/8-based adjuvants have a long history of efficacy in a pre-clinical and clinical setting. Early investigations into first generation TLR7/8 agonists as vaccine adjuvants, such as R848, demonstrated high reactogenicity when administered orally or intravenously limiting their widespread use (36). Novel TLR7/8 agonists which do not result in systemic immune responses but nevertheless activate the innate and, subsequently, the adaptive immune system, are of great interest. Recently, several groups have developed lipidated or alum adsorbed TLR7/8 ligands to overcome the rapid systemic distribution and toxicity noted with the previous compounds (37–44). Additionally, previous work has demonstrated that the combination of a TLR4 agonist with a TLR7/8 agonist leads to synergistic upregulation of IFNγ, IL-12p70, and IFNα (45–49), cytokines which induce and enhance Th1 type immune responses that are particularly effective at controlling viral infections [reviewed in (50)].

We have previously reported on the discovery and activity of core (non-lipidated) TLR7/8 agonists, one of which enhanced humoral and cell-mediated immunity to the CRM197 mutant diphtheria toxin protein in pigs (51). Here, we build upon these studies by reporting on novel lipidated imidazoquinoline TLR7/8 ligands, alone or in combination with a synthetic TLR4 ligand, and their ability to elicit strong antigen-specific humoral and Th1- or Th17-mediated T cell responses to a co-administered seasonal split H3N2 influenza vaccine in mice. We found that lipidated imidazoquinolines TLR7/8 agonists can elicit a Th1-biased influenza specific immune response in mice and when combined with a TLR4 agonist, elicit a Th17 response as well. Further, the adjuvanted vaccine-induced adaptive immune responses provided durable protection from a heterosubtypic H3N2 influenza virus challenge, particularly in the case of a combination TLR4 and TLR7/8 adjuvant. When tested in human PBMCs, these adjuvants were able to elicit a cytokine profile suggestive of Th1- and Th17-polarization.

REAGENTS

TLR7/8 Agonist Compounds and Formulation

CRX-601 (TLR4 agonist) (52), UM-3001 (non-lipidated TLR7/8 agonist) (53), and UM-3003, -3004, and -3005 (54) were synthesized following established procedures and formulated in 2% glycerol in water as previously reported (51). Physical characteristics are presented in **Table S1**.

HEK293 TLR7 and TLR8 Reporter Assays

Human TLR7 or TLR8 and mouse TLR7 or TLR8 expressing HEK cells were obtained from Invivogen (San Diego, CA) or Novus (human TLR7 only). Cells were cultured according to the manufacturer's instructions in DMEM with 10% FBS and selection antibiotics. HEK cells were plated at a density of 3×10^5 cells/well in a flat bottom 96 well-plate and incubated for 18–24 h at 37°C with indicated concentrations of various TLR7/8 agonists. Cell supernatants were harvested and analyzed for NFκB via the manufacturer's instructions using the QuantiBlue kit (Invivogen). SEAP activity was assessed by reading the optical density (OD) at 620–655 nm with a microplate reader. Data are expressed as the fold change in OD over vehicle treated cells.

Human Peripheral Blood Mononuclear Cell (PBMC) Isolation and Stimulation

Human blood was obtained from healthy adult donors through a University of Montana Institutional Review Board (IRB)-approved protocol. PBMCs were separated from whole blood via density gradient separation using Histopaque 1,077 (Sigma). For PBMC-based assays, cells were resuspended at the desired cell concentration in complete media (RPMI1640+10% FBS+antibiotics). Cells were treated with the indicated compound concentrations and stimulated for 6–24 h depending on the assay as indicated in the figure legends and assays outlined below.

PBMC Cytokine Analysis

For Luminex assays, supernatants were harvested from treated human PBMCs following 18–24 h of incubation. Supernatants were analyzed using Luminex multiplex panel for analytes IL-1β, IL-12p70, IL-23, IL-6, TNFα, IFNα, and IL-4 (R&D Systems) per the manufacturer's instructions. Multiplex analysis was performed using a Luminex 200 instrument (Luminex Corporation) and analyzed with StarStation2.3 software.

For flow cytometry analysis of innate cytokines, PBMCs were stimulated with indicated concentration of compound for 1 h followed by 5 h incubation with GolgiPlug (BD, 1 μL/mL) at 37°C. Post-stimulation, cells were harvested and surface stained with viability dye, and monoclonal antibodies targeting CD3 AF700 (Tonbo Bioscience, UCHT1), CD19 AF700 (Tonbo Bioscience, HIB19), CD56 AF700 (Biolegend, 5.1H11), HLA-DR BV785 (Biolegend, L243), CD14 APC-Cy7 (Biolegend, 63D3), CD16 PE-Dazzle594 (Biolegend, 3G8), CD11c BV421 (Biolegend, 3.9), and CD123 APC (Biolegend, 6H6). Following fixation and permeabilization with BD Cytofix/Cytoperm buffers, cells were stained with monoclonal antibodies targeting the intracellular cytokines IL-12p40 PE (a shared IL-12 and IL-23 subunit, Biolegend, C11.5), IL-6 FITC (Biolegend MQ2-13A5), IL-4 BV605 (Biolegend, MP4-25D2), and LAP (TGF-β) PE Cy7 [latency-associated peptide (55), Biolegend TW4-2F8]. Data were collected using an LSRII flow cytometer (BD) and analyzed using FlowJo 10.0 software (TreeStar).

In vivo Experiments

Animal studies were carried out in accordance with University of Montana's IACUC guidelines for the care and use of laboratory animals. Groups of 6 female BALB/c mice were vaccinated intramuscularly with 0.3 μg HA equivalent monovalent detergent-split A/Victoria/210/2009 (H3N2; monovalent detergent split influenza vaccine was provided by GSK Vaccines) influenza vaccine with or without the indicated concentrations of TLR agonists in 50 μL total volume per injection (compounds and antigen were diluted as needed in 2% glycerol in water). After 14 days, blood samples were collected via submandibular bleeds for antibody analysis and a secondary vaccination was administered. At day 19 (5 days post-secondary vaccination), mice were euthanized and spleens were harvested for the assessment of cell-mediated immunity. For influenza challenge experiments, 16 female Balb/c mice per group were vaccinated intramuscularly with 0.3 μg detergent-split A/Victoria influenza vaccine with or without the indicated concentrations of TLR agonists in 50 μL total volume per injection. After 14 days, blood samples were collected for antibody analysis and a secondary vaccination was administered. At day 19 (5 days post-secondary vaccination), 6 mice per group were euthanized and spleens were harvested to assess T cell responses. Fourteen days after secondary vaccination, blood was collected from remaining 10 mice via submandibular bleeds for serum antibody analysis. Three weeks following the secondary vaccination, the remaining 10 mice in each group were anesthetized with approximately 10 mg/kg ketamine/xylazine i.p. and challenged with 10 μL per nare with mouse-adapted A/Hong Kong/1/68 (H3N2) at a dose of $3LD_{50}$. Clinical body scores, temperatures, body weights and mortality were recorded daily for each mouse. The humane endpoint for euthanasia included any of the following: (1) 30% weight loss, (2) body temperature <25°C two consecutive days, or (3) clinical score of 4.

ELISA for Anti-influenza Antibody Quantification

Blood was collected from mice 14 days post-primary, serum was isolated and diluted according to the expected antibody response (between 1:10 and 1:5000). Plates were coated with 100 μL of detergent-split A/Victoria influenza vaccine at 1 μg/mL. Following washing (PBS plus tween 20) and blocking (SuperBlock, Scytek Laboratories), plates were incubated with diluted serum for 1 hr followed by anti-mouse IgG, IgG1 or IgG2a-HRP secondary antibody (Bethyl Laboratories) and TMB substrate (BD). Plates were read at 450 nm. Antibody titers were determined by calculating titer of each sample at OD 0.3.

Splenocyte Restimulation and Cell-Mediated Immunity Analysis

Spleens were harvested from vaccinated mice 5 days after secondary injections and processed cells by disruption of the spleens through a 100 μm filter. Red blood cells were lysed by incubation with red blood cell lysis buffer (Sigma) for 5 min followed by washing in 1x PBS. Cells were plated in a 96 well-plate at 5×10^6 cells/well in 200 μL complete RPMI1640 media. Cells were incubated with 1 μg/mL whole influenza antigen (detergent split A/Victoria or whole HK68 as indicated) plus 1 μg/mL αCD28 and 1 μg/mL αCD49d for 6 h at 37°C. After 6 h, 1 μL/mL GolgiPlug (Brefeldin A, BD Biosciences) was added to each well and cells were incubated at 37°C for a further 12 h. Following incubation, cells were stained with the cell surface antibodies against CD3e PerCP-Cy5.5 (Tonbo Biosciences, 145-2C11), CD4a APC-Cy7 (Tonbo Biosciences, RM4-5) and CD8a PE-Cy7 (Tonbo Biosciences, 53-6.7) and viability stain (Ghost 510, Tonbo Biosciences). Cells were treated with Cytofix/Cytoperm (BD) and stained with anti-IFNγ PE-CF594 (BD, XMG1.2), anti-IL2 FITC (Biolegend, JES6-5H4), anti-IL-5 BV421 (BD, TRFK5), anti-IL17A PE (Biolegend, TC11-18H10.1), and anti-TNFα APC (Invitrogen, MP6-XT22). Data was collected using an LSRII flow cytometer (BD) and analyzed using FlowJo 10.0 software (TreeStar).

Secreted cytokines following spleen harvest and antigen restimulation (1 μg/mL whole influenza antigen, detergent split A/Victoria or whole HK68 as indicated) were measured after 72 h of stimulation by MesoScale Discovery (MSD) U-PLEX Assay Platform (MesoScale Diagnostics) to detect mouse IFNγ, IL-17, TNFα, IL-2, and IL-5.

RESULTS

Structure and Activity of Novel Lipidated TLR7/8 Agonists

Compounds shown in **Figure 1A** were formulated in 2% glycerol and tested in human and mouse TLR7 and TLR8 HEK293-SEAP reporter cells to determine their relative TLR7 and TLR8 receptor specificity and potency. Briefly, the HEK reporter system consists of HEK293 cells that express either human or mouse TLR7 or TLR8. When signaling occurs through the expressed TLR resulting in activation of NFkB, a SEAP reporter is expressed and measured via a colorimetric assay using cell culture supernatants (**Figures 1B,C**). UM-3001 (non-lipidated) demonstrated strong NFkB activation through both human TLR8 (EC50 = 0.53 μM, **Figure 1C** and TLR7 (EC50 = 1.12 μM, **Figure 1B**) while UM-3005 (lipidated at the 7-position) elicited strong NFkB activation through human TLR8 (EC50 = 0.27 μM, **Figure 1C**) but was much less potent with respect to NFkB activation via human TLR7 (EC50 = 499.2 μM, **Figure 1B**). Moving the phospholipid from the 7-position to the 2-position of the core imidazoquinoline compound altered the TLR7/8 signaling as demonstrated for compounds UM-3004 and UM-3003, both lipidated at the 2-position. UM-3004 induced signaling through NFkB via both TLR7 (EC50 = 60.5 μM; **Figure 1B**) and TLR8 (EC50 = 24.6 μM; **Figure 1C**). UM-3003 behaved similarly to UM-3004, signaling through NFkB via TLR7 (EC50 = 34.7 μM; **Figure 1B**) and minimally via TLR8 (EC50 = 52.5 μM; **Figure 1C**). As has been previously reported (56), mouse TLR8 is not readily activated by imidazoquinolines and other TLR8 ligands [**Figure 1E**; R848 plus polyDT was included as a positive control for mouse TLR8 activity as reported in (56) shown in **Figure S1**], despite their ability to signal through human TLR8 (**Figure 1C**). However, all compounds activated mouse TLR7 as demonstrated in **Figure 1D**. UM-3001, UM-3004, and UM-3005 were more potent activators of mouse TLR7 than UM-3003, as demonstrated by lower EC50s (UM-3001 = 0.48 μM, UM-3004 = 0.86 μM, UM-3005 = 1.14 μM, UM-3003 = 12.64 μM) in the HEK293 assay system (**Figure 1D**). None of the compounds shown in **Figure 1A** elicited signaling via NFkB when tested in the HEK Null line containing the NFkB-SEAP reporter without human or murine TLR7/8 (**Figure S1**). CRX-601 has been previously published and validated as a TLR4 agonist (57).

TLR7/8 Adjuvanted Influenza Vaccination Elicits a Th1/Th17-Biased Immune Response in Mice

Previous success using lipidated TLR7/8 agonists by other groups, namely 3M-052 (43) and 1V270 (58), led us to hypothesize that these novel imidazoquinolines may serve as potent adjuvants for influenza vaccination in mice. Additionally, we hypothesized that the addition of a synthetic TLR4 agonist may further enhance the adaptive immune responses as previous reports have noted synergy between TLR4 agonists and TLR7/8 agonists, especially with respect to the generation of a Th1 type immune response (45–49, 58). To investigate these hypotheses, a monovalent detergent-split A/Victoria/210/2009 (H3N2; A/Vic) influenza vaccine (0.3 μg/mouse) was adjuvanted with either low dose TLR7/8 agonist (1 μg/mouse) with or without 0.1 μg CRX-601 (1:10 ratio of CRX-601:TLR7/8 agonist), or high dose TLR7/8 agonist (10 μg/mouse) with or without 0.1 μg CRX-601 [1:100 ratio of CRX-601:TLR7/8 agonist; (56)]. Two injections were administered intramuscularly (i.m.) 14 days apart. Mice were bled 14 days post-primary injection (14pd1) to measure influenza-specific antibody responses and spleens were harvested 5 days post-secondary injection (5dp2) to assess influenza-specific T cell responses. Total influenza-specific IgG serum titers were increased by high-dose lipidated adjuvants (UM-3003, UM-3005, and UM-3004) alone or in combination with 601 (**Figure 2A**). Low dose UM-3004 alone and low dose UM-3004 and UM-3005 plus 601 also significantly increased total influenza-specific IgG serum titers. Influenza-specific IgG1 was significantly increased only by 601 alone, high dose UM-3001 (non-lipidated TLR7/8 adjuvant), and high dose UM-3001 with 601 (**Figure 2B**). Conversely, influenza-specific IgG2a was significantly increased in the majority of groups that contained a lipidated TLR7/8 agonist (**Figure 2C**): all groups adjuvanted with UM-3005, all groups adjuvanted with high dose lipidated TLR7/8 agonist plus 601, as well as high dose UM-3003 alone, and low dose UM-3004 alone. The ability of lipidated TLR7/8 agonists to drive an IgG2a response compared to the ability of non-lipidated TLR7/8 agonists to drive an IgG1 response is illustrated in **Figure 2D**, where the average fold change of adjuvanted influenza-specific IgG1 or IgG2a titers over A/Vic alone (no adjuvant) was calculated (**Figure 2D**; solid or open bars indicate IgG2a fold change, patterned bars indicate IgG1 fold change). This calculation allows for a direct comparison between the change in IgG2a vs. IgG1 antibody titers in mice vaccinated with adjuvant plus antigen compared to mice vaccinated with antigen alone, demonstrating whether an adjuvant drives IgG2a or IgG1 antibody production. Lipidated TLR7/8 adjuvants drove a predominantly IgG2a influenza-specific response compared to non-adjuvanted A/Vic (**Figure 2D**) as evidenced by the fact that IgG2a titers were increased more than IgG1 titers by adjuvanting with UM-3003, -3004, and -3005 compared to A/Vic alone. The non-lipidated TLR7/8 adjuvant, UM-3001, produced an approximately equal increase in both IgG2a and IgG1 titers compared to A/Vic alone (**Figure 2D**).

Influenza-specific T cell responses were measured in splenocytes harvested at 5 days post-secondary vaccination and re-stimulated *ex vivo* with A/Vic (H3N2) split flu antigen, followed by flow cytometry to detect intracellular cytokines and MesoScale Discovery (MSD) multiplex cytokine array to detect secreted cytokines. Here, we used the A/Vic only vaccinated mice as a control as opposed to the more commonly seen method of using unstimulated splenocytes as a control, allowing the changes

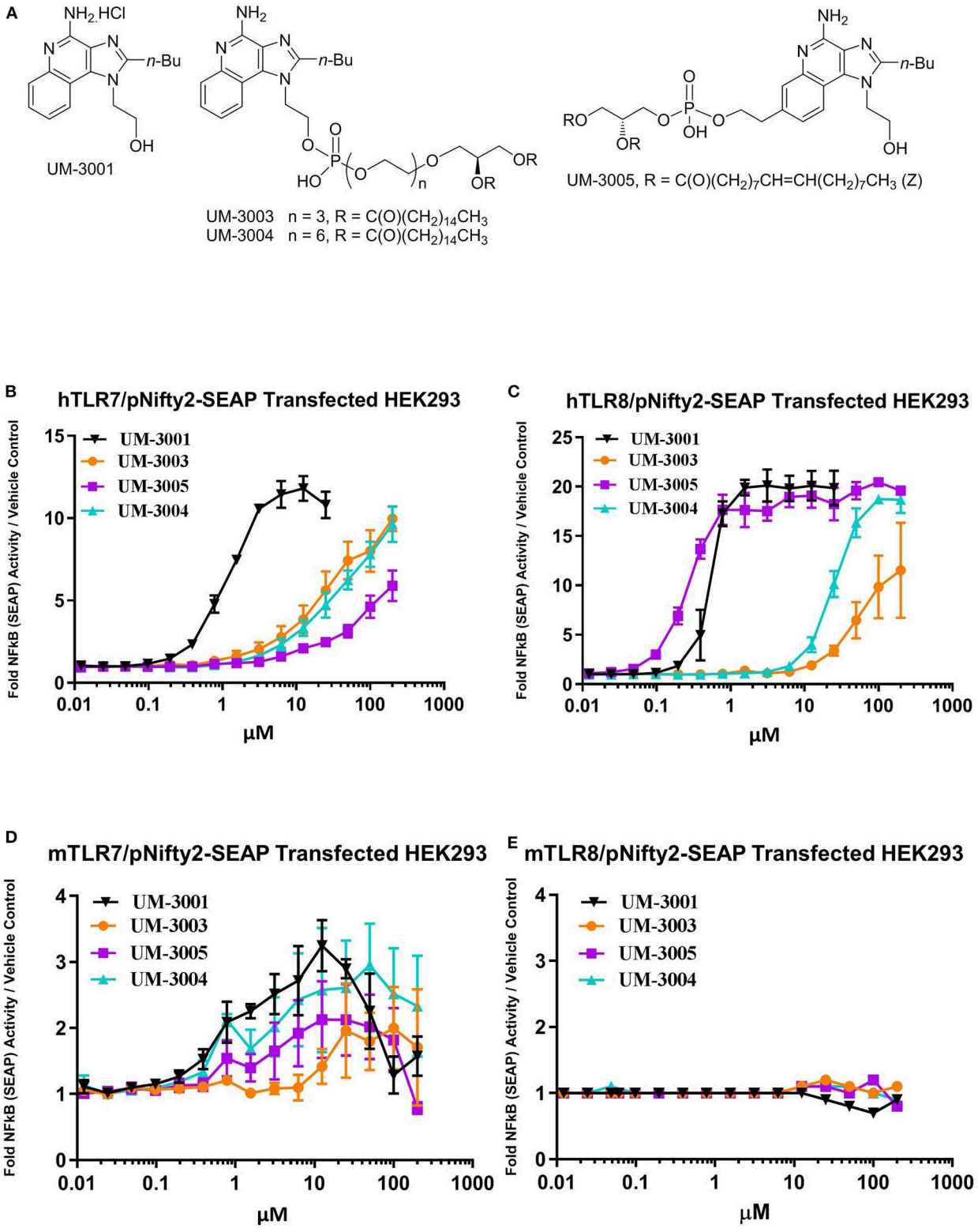

FIGURE 1 | Novel imidazoquinolines as TLR7/8 agonists. **(A)** Chemical structures of synthesized imidazoquinoline small molecules. **(B,C)** Activity of imidazoquinolines in human embryonic kidney (HEK) reporter cells expressing human TLR7 (**B**; $n = 2$) or human TLR8 (**C**; $n = 2$). **(D,E)** Activity of imidazoquinolines in human embryonic kidney (HEK) reporter cells expressing mouse TLR7 (**D**; $n = 3$) or mouse TLR8 (**E**, $n = 3$). In b-e, cells were stimulated with imidazoquinolines formulated in 2% glycerol at the indicated concentrations for 24 h. HEK reporter activity is expressed as fold change over media only control.

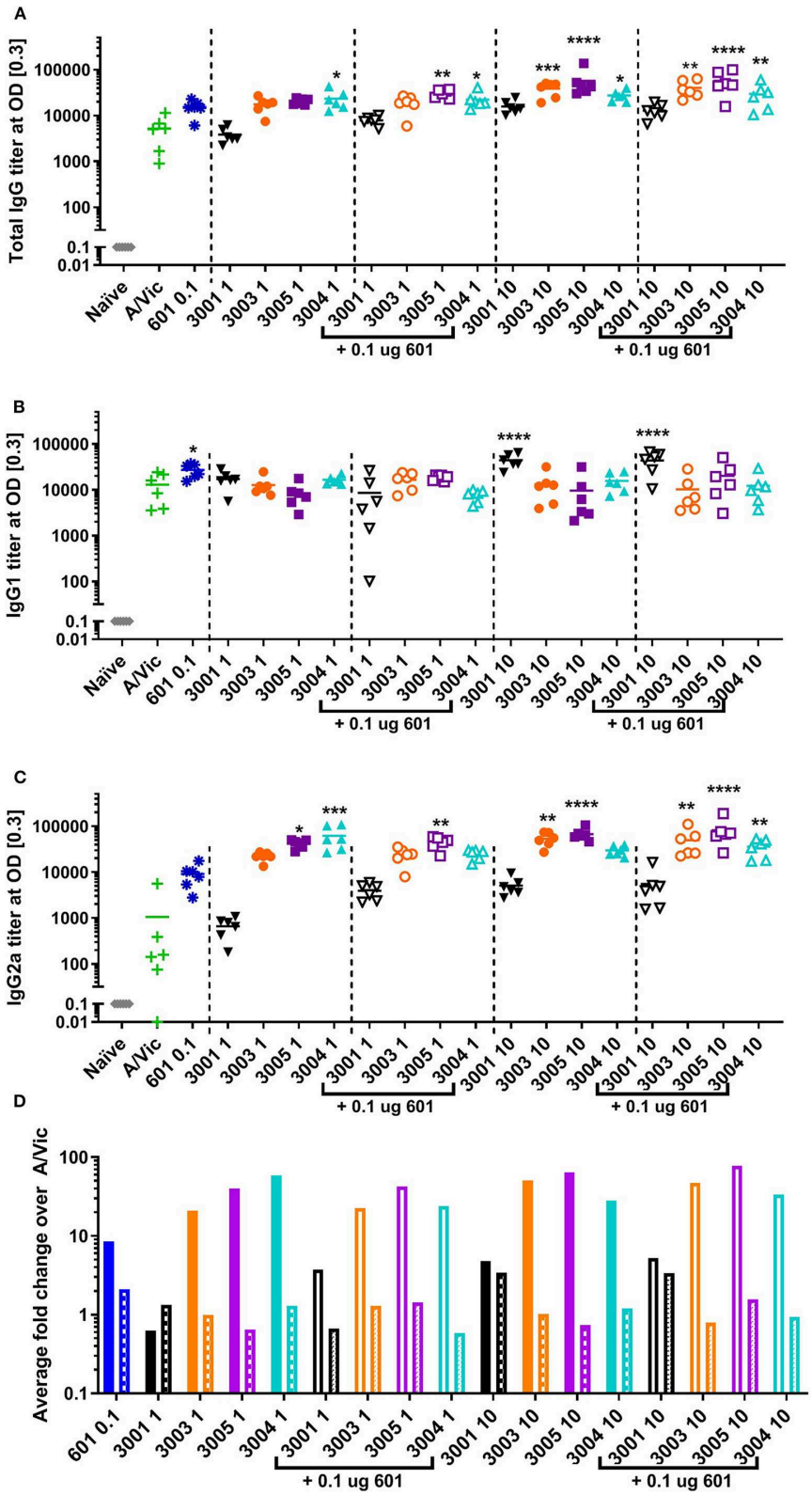

FIGURE 2 | Lipidated imidazoquinolines elicit an IgG2a-biased influenza-specific antibody response after a single intramuscular vaccination. Balb/c mice (6 per group) were injected once i.m. with 0.3 μg/mouse A/Vic monovalent detergent-split influenza vaccine adjuvanted with indicated TLR4 (0.1 μg), TLR7/8 (1 or 10 μg as

(Continued)

FIGURE 2 | indicated), or combination TLR4 + TLR7/8 agonists as indicated. Fourteen days post-injection, mice were bled, serum was collected, and A/Vic-specific total IgG **(A)**, IgG1 **(B)** and IgG2a **(C)** antibody titers were measured. **(D)** Fold change of IgG2a (solid bars) or IgG1 (patterned bars) titers with indicated adjuvant normalized to non-adjuvanted (A/Vic alone) control. Statistical signficance determined by one-way ANOVA (GraphPad Prism 7) followed by Fishers LSD for multiple comparisons; asterisks indicate significance compared to the A/Vic alone group (green "+") where $^{*}p \leq 0.05$, $^{**}p \leq 0.01$, $^{***}p \leq 0.001$, $^{****}p \leq 0.0001$.

in the immune response that are directly due to the adjuvant to be determined. Mice vaccinated with A/Vic plus non-lipidated TLR7/8 (UM-3001) did not exhibit any significantly increased cytokine production compared to mice vaccinated with A/Vic alone (**Figure 3**: high dose adjuvant T cell responses; **Figure S3**: low dose adjuvant T cell responses). In contrast, mice vaccinated with lipidated TLR7/8 agonists UM-3003, UM-3005 or UM-3004 exhibited primarily a Th1 influenza-specific response in mice (**Figures 3A,B**; flow gating and example cytokine staining shown in **Figure S2**; low dose adjuvant T cell responses shown in **Figure S3**) which correlates with the IgG2a biased antibody responses also elicited by these adjuvants (see **Figure 2**). High dose lipidated TLR7/8 agonists, with or without the addition of a TLR4 agonist, also elicited significantly increased frequencies of influenza-specific multifunctional CD4 T cells (IFNγ+ IL2+ TNFα+, **Figure 3B**; individual secreted cytokines shown in **Figures 3B,F,H**), which have previously been shown to be beneficial for protection against heterologous influenza challenge (59). Frequencies CD8 IFNγ+ cells, of particular interest when trying to elicit an anti-viral response, were significantly increased through adjuvanting A/Vic antigen with high dose UM-3005 with or without a TLR4 agonist (**Figure 3G**). Interestingly, the addition of a TLR4 agonist did not boost influenza-specific Th1 responses but did significantly increase influenza-specific Th17 responses when combined with high dose lipidated TLR7/8 agonists (**Figures 3C,D**). Splenocytes from vaccinated mice adjuvanted with only CRX-601 also demonstrate IL-17 secretion after *ex vivo* antigen restimulation (**Figure 3D**). None of the adjuvants produced significant increases in CD4 IL-5+ frequencies or in concentration of secreted IL-5; in fact, cytokine secretion as measured by MSD indicates that all adjuvants, except high dose UM-3004 alone, reduced IL-5 secretion compared to non-adjuvanted A/Vic antigen (**Figure 3J**, **Figure S3J**). These T cell data are in agreement with antibody data, demonstrating that lipidated TLR7/8 agonists biased a Th1 response without boosting the Th2 type response whereas the non-lipidated TLR7/8 agonist did not elicit any measurable antigen-specific T cell responses. T cell data also demonstrates that very low dose TLR4 agonist elicited a low level Th17 response and, when added to lipidated TLR7/8 agonists, increased their ability to elicit a Th17 response as well.

TLR7/8 Adjuvanted Influenza Vaccine Protects Against Heterologous H3N2 Influenza Challenge in Mice

Based on promising vaccine-induced influenza-specific antibody and T cell responses, we next evaluated whether or not vaccinated mice are protected against a heterologous H3N2 influenza virus challenge. For this purpose, we used a mouse-adapted A/Hong Kong/1/68 (HK68) challenge virus. Groups of 16 mice were vaccinated as above with A/Vic antigen alone or A/Vic antigen adjuvanted with TLR4 agonist (CRX-601, 0.1 μg/mouse), TLR7/8 agonist (UM-3003 10 μg/mouse or UM-3005 10 μg/mouse), or combination TLR4 agonist plus TLR7/8 agonist (0.1 μg/mouse TLR4 + 10 μg/mouse TLR7/8; 1:100 ratio). Lead compounds, combinations, ratios and doses were selected based on previous results (see above, **Figures 2**, **3**). UM-3005 is structurally unique compared to UM-3003 and -3004 and elicited the strongest Th1-biased T cell and antibody responses at 10 μg, either alone or in combination with CRX-601. We also elected to continue experiments with 10 μg UM-3003 alone and in combination with CRX-601. Due to UM-3004's structural similarity to UM-3003 and similar but slightly less promising immune profile, this compound was not carried forward into challenge studies. Influenza-specific antibody titers (14dp1) and T cell responses (5dp2) were assessed to confirm that immune responses as described above (**Figures 2**, **3**) were replicated. Influenza-specific IgG2a (**Figure 4A**, left), IgG1 (**Figure 4B**, left) and T cell responses (**Figures S4A–H**) were very similar to those observed in the adjuvant response study (**Figures 2**, **3**, **Figures S2**, **S3**) with one exception: UM-3003 plus A/Vic antigen no longer elicited a significantly higher IL-17 response compared to A/Vic antigen alone (**Figures S4E,F**). However, all other responses were replicated both in terms of humoral response IgG2a bias (**Figure 4C**, left) and Th1 (**Figures S4A–C**) and Th17 (**Figures S4E,F**) CD4 T cell responses. In addition, serum antibody titers were measured 14 days following the secondary vaccination (14dp2; **Figure 4**, right column). Both IgG2a (**Figure 4A**, right) and IgG1 (**Figure 4B**, right) influenza-specific antibody titers continued to increase compared to 14dp1; particularly the group vaccinated with A/Vic with CRX-601 plus UM-3005 (**Figures 4A,B**). As demonstrated at 14dp1, at 14dp2 all adjuvanted groups compared to non-adjuvanted A/Vic alone increased average IgG2a titers to a greater degree than average IgG1 titers (**Figure 4C**, right), demonstrating that after a second injection, the Th1 humoral bias remains. All remaining mice (10 per group) were challenged with $3LD_{50}$ mouse-adapted A/Hong Kong/1/68 (H3N2; HK68) 21 days after the secondary vaccination via the intranasal/intrapulmonary route (10 μL/nare). As expected, all of the naïve (non-vaccinated) mice succumbed to the 3LD50 influenza virus challenge with 100% mortality by day 10 following challenge (**Figure 5A**). Mice vaccinated with A/Vic antigen (no adjuvant) demonstrated limited protection with 10% survival (1 mouse out of 10). All groups that received adjuvanted A/Vic antigen were protected when challenged with the heterologous mouse adapted A/HK/68 influenza virus (**Figure 5A**; protection is considered as 80% survival or greater). However, some groups experienced significantly greater weight loss indicating differences in the

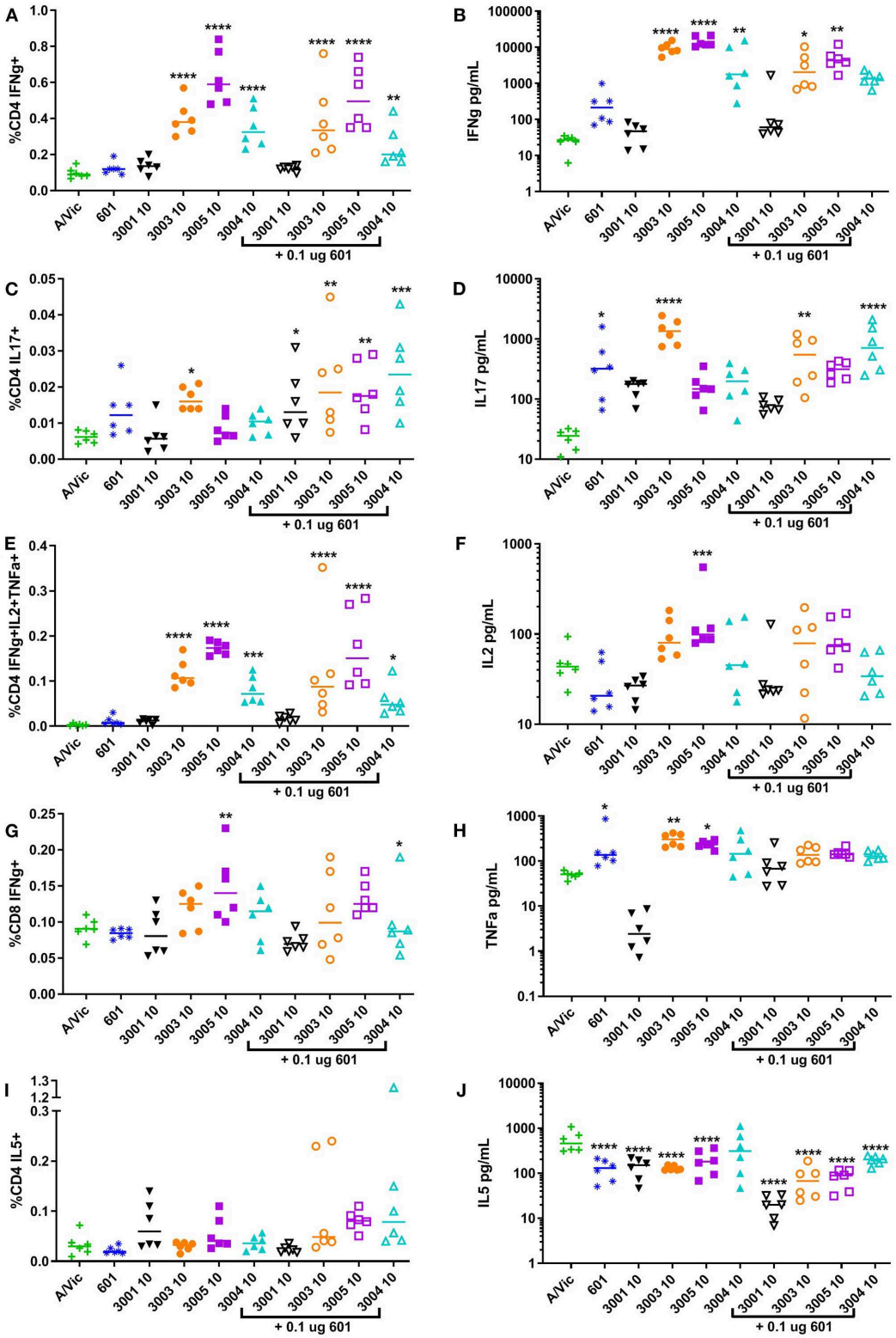

FIGURE 3 | High-dose lipidated imidazoquinolines elicit an influenza-specific Th1 response and, in combination with a TLR4 agonist, an influenza-specific Th17 response. Balb/c mice (6 per group) were injected twice i.m. fourteen days apart with 0.3 μg/mouse A/Vic monovalent detergent-split influenza vaccine adjuvanted with indicated TLR4 (0.1 μg/mouse), TLR7/8 (10 μg/mouse), or combination TLR4 + TLR7/8 agonists. Five days post-secondary injection (5dp2), mice were

(Continued)

FIGURE 3 | euthanized and spleens were harvested, disaggregated and restimulated with 1 μg/mL A/Vic + 1 μg/mL αCD28 + 1 μg/mL αCD49d for flow cytometry or 1 μg/mL A/Vic alone for MSD. The indicated cytokines were measured by flow cytometry cytokines after 6 h of stimulation plus a further 12 h with GolgiPlug (BD Biosciences) followed by intracellular cytokine staining (left column; **A**, **C**, **E**, **G**, **I**). Secreted cytokines were measured via MesoScale Discovery (MSD) assay after 72 h of stimulation (right column; **B**, **D**, **F**, **H**, **J**). Lines indicate means. Statistical signficance determined by one-way ANOVA followed by Fishers LSD for multiple comparisons (GraphPad Prism 7); asterisks indicate significance compared to the A/Vic alone group (green "+") where $*p \leq 0.05$, $**p \leq 0.01$, $***p \leq 0.001$, $****p \leq 0.0001$.

level of protection observed. Mice vaccinated with A/Vic antigen plus CRX-601 (a TLR4 ligand) experienced significantly greater weight loss compared to mice that received A/Vic antigen and CRX-601 in combination with UM-3005 or UM-3003 (**Figures 5B,C**; dark purple and dark orange lines, respectively). Weight loss in mice receiving antigen plus UM-3005 was somewhat greater than that experienced by mice adjuvanted with UM-3005 in combination with CRX-601 although this difference was not statistically significant (**Figure 5B**). Interestingly, weight loss experienced by mice vaccinated with antigen and CRX-601 plus UM-3005 vs. CRX-601 plus UM-3003 was not statistically different (**Figures 5B,C**), despite the fact that mice vaccinated with UM-3003 plus antigen experienced significantly greater weight loss than those receiving UM-3003 plus CRX-601 (**Figure 5C**). These data indicate that a combination adjuvant including a synthetic TLR4 agonist and a lipidated TLR7/8 agonist induces better protection against influenza-induced weight loss than a TLR4 adjuvant or a TLR7/8 agonist alone (**Figure 5C**).

TLR7/8 Stimulation of PBMCs Elicits a Th1/Th17 Polarizing Innate Cytokine Response

To determine if the lipidated TLR7/8 ligands may be capable of eliciting a similar T cell response in humans, we investigated production of T cell polarizing cytokines in human PBMCs both by flow cytometry and via R&D Systems multiplex cytokine array (Luminex). In addition to evaluating the TLR7/8 ligands alone, we also evaluated potential synergies between CRX-601 and the TLR7/8 ligands. IL-12p70, the canonical Th1-polarizing cytokine (60–62), is produced to various degrees by all four TLR7/8 agonists, both lipidated and non-lipidated (**Figure 6A**), although UM-3003 only produces low levels of IL-12p70 at the highest tested concentration (**Figure 6A**, right). As previously reported for other TLR7/8 agonists *in vitro* (44–46], the addition of a TLR4 ligand CRX-601 at a 1:10 ratio boosted IL-12p70 production when combined with the non-lipidated TLR7/8 ligand UM-3001 (**Figure 6A**, left) while CRX-601 stimulation alone did not elicit a detectable IL-12p70 response (**Figure 6A**, left). IL-23 and IL-1β are important for Th17 polarization (63). This combination of cytokines was also produced to various degrees by all four TLR7/8 agonists investigated here (**Figures 6B–D**), again with UM-3003 eliciting low concentrations of IL-23 and IL-1β at the highest tested dose (**Figures 6B,C**, right). Interestingly, the addition of CRX-601 strongly enhanced IL-1β production despite eliciting low levels of IL-1β by itself (**Figure 6C**, left), suggesting there may be a synergistic IL-1β response to TLR4 plus TLR7/8 stimulation. IL-6, also shown to contribute to Th17 polarization (citation as above, 61) was also elicited by all adjuvants, including CRX-601 alone (**Figure S5A**). IL-4 production, which polarizes Th2 cells, was found to be secreted only at very low concentrations by these TLR7/8 agonists (**Figure 6G**). Additionally, IFNα, an important cytokine for protection against viral infections and Th1 polarization [reviewed in (64)], is secreted in response to lipidated imidazoquinolines UM-3003, UM-3005, and UM-3004 but not by the non-lipidated TLR7/8 ligand UM-3001 (**Figure S5B**) despite its potent TLR7 activity in the HEK293 reporter assay (see **Figure 1B**).

IL-12p40, the shared subunit of IL-12 and IL-23, is produced mainly by myeloid dendritic cells (mDCs) and monocytes in response to both UM-3005 and UM-3001 (**Figure 7A**, left (mDCs) and right (monocytes)). Lower frequencies of mDC and classical monocytes produce IL-12p40 in response to the weaker TLR7/8 agonists (UM-3004) and the weak TLR7 agonist (UM-3003) (**Figure 7A**). Interestingly, the addition of a TLR4 agonist reduced frequencies of IL-12p40+ mDC and monocytes (**Figure 7A**). Additionally, approximately 20% of mDC and classical monocytes produce IL-12p40 (the shared IL-12 and IL-23 subunit) in response to UM-3005 and, in the case of mDC, UM-3001 (**Figure 4B**). Interestingly, TLR4 stimulation induces a high frequency of mDC (median 60%) and classical monocytes (median 80%) to produce IL-6 (**Figure 7B**). In combination with weak TLR7/8 stimulation (UM-3004 and UM-3003), frequency of IL-6 production is somewhat lowered compared to TLR4 stimulation alone but when in combination with a strong TLR7/8 agonist (UM-3001), the frequency of IL-6 producing mDC or classical monocytes is lower than of either alone (**Figure 7B**), suggesting either activation-induced cell death or that excessive activation is inducing negative regulators that serve to terminate signaling. TGFβ [as measured by latency-associated peptide, LAP (55), an intracellular immature form of TGFβ] is expressed by low frequencies of mDC and classical monocytes in response to CRX-601 plus UM-3001 and UM-3001 alone (**Figure 7C**). Interestingly, TGFβ/LAP production appears to have higher donor-to-donor variability compared to other cytokines measured here. Only very low frequencies of mDC, or classical monocytes (<6%) were found to express IL-4 in response to any of the TLR agonists investigated here (**Figure 7D**). In contrast to mDC and monocytes, pro-inflammatory/T cell polarizing pDC responses with respect to TLR7/8 stimulation were of lower frequency, as expected based on the expression of TLR7 but not TLR8 in pDCs (65) (**Figure 7**, right column). Data presented here confirm that the cytokine secretion as measured in **Figure 6** comes from professional antigen-presenting cells that are best suited to present antigen to T cells and induce their polarization and differentiation. Further, secreted cytokine data shown in

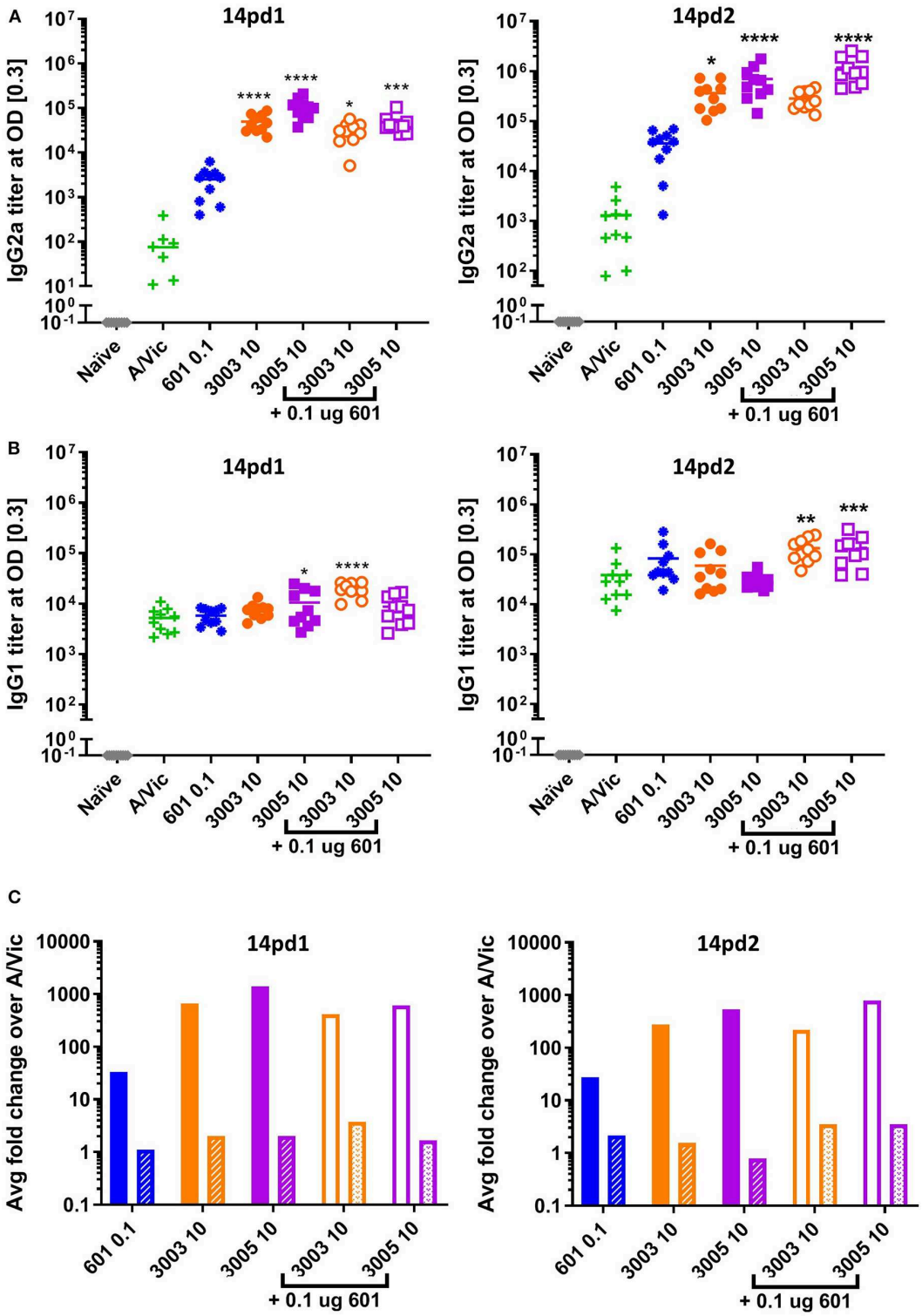

FIGURE 4 | Th1 humoral bias is maintained after two vaccinations. Balb/c mice (10 per group) were vaccinated i.m. with A/Vic detergent-split monovalent influenza vaccine (0.3 μg/mouse) with indicated adjuvants (CRX-601 = 0.1 μg/mouse, UM-3003 or UM-3005 = 10 μg/mouse). At 14dp1 and 14dp2 mice were bled and influenza-specific IgG2a **(A)** and IgG1 **(B)** titers were measured. **(C)** Fold change of adjuvanted IgG2a (solid bars) or IgG1 (patterned bars) compared to non-adjuvanted control (A/Vic only) at 14dp1 (left) and 14dp2 (right). Lines indicate mean. Statistical signficance determined by one-way ANOVA followed by Fishers LSD for multiple comparisons (GraphPad Prism 7); asterisks indicate significance compared to the A/Vic alone group (green "+") where $*p \leq 0.05$, $**p \leq 0.01$, $***p \leq 0.001$, $****p \leq 0.0001$.

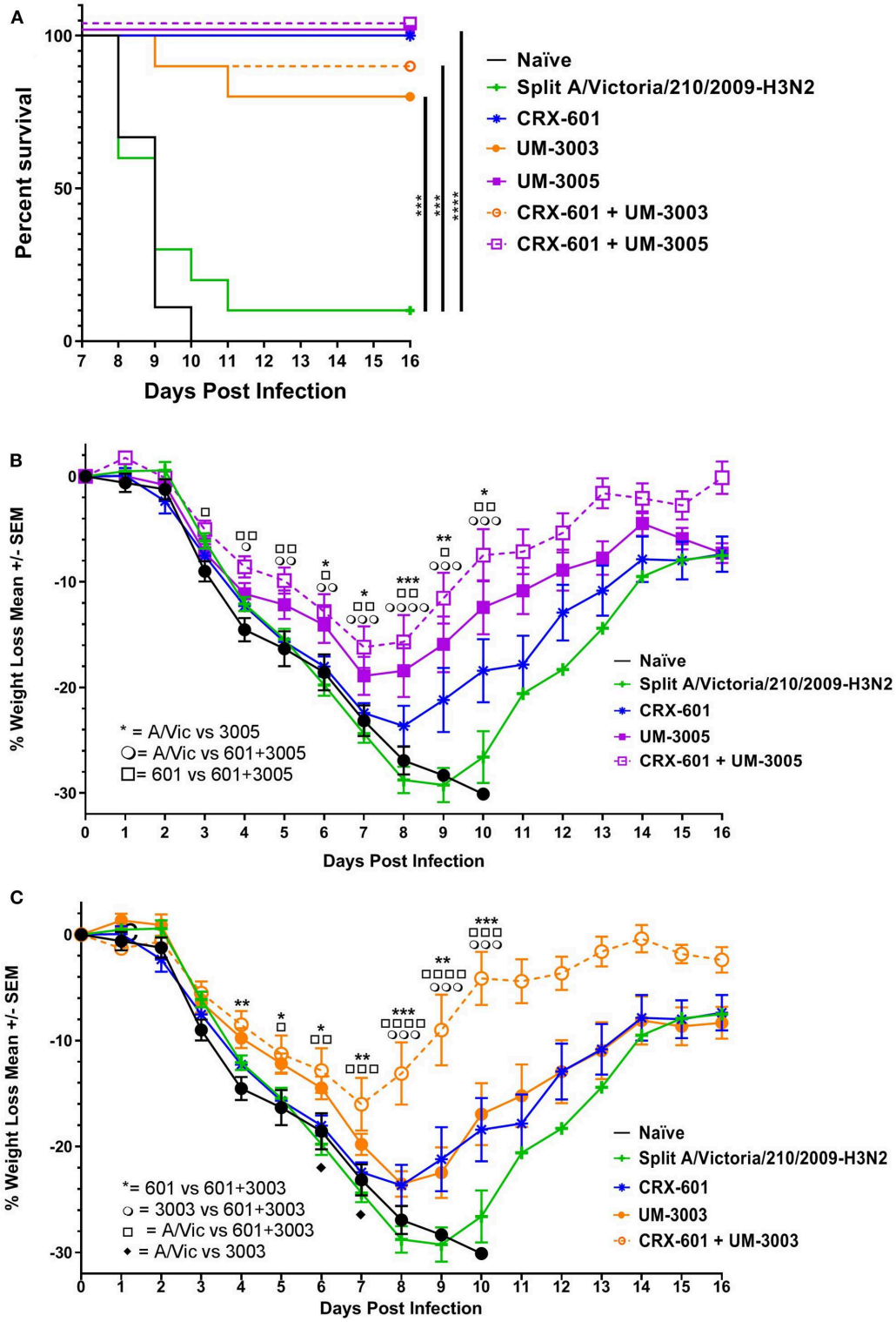

FIGURE 5 | Lipidated imidazoquinolines with or without a TLR4 agonist protect against lethal, heterologous H3N2 challenge. Balb/c mice were immunized i.m. twice, 14 days apart, with A/Vic monovalent detergent-split influenza vaccine (0.3 μg/mouse) adjuvanted with indicated TLR4 (0.1 μg/mouse), TLR7/8 (10 μg/mouse), or TLR4 + TLR7/8 agonists. Three weeks after the second immunization, 10 mice per group were challenged i.n. with 3LD50 HK68 (H3N2) mouse-adapted influenza virus. Mice were monitored daily for weight loss, temperature, and body condition. **(A)** Percent of surviving mice in each group. **(B,C)** Average percent

(Continued)

FIGURE 5 | weight loss per group, +/- SEM. Survival statistics determined by log-rank (Mantel-Cox) test, weight loss significance determined by one-way ANOVA at a given timepoint followed by Fishers LSD for multiple comparisons (GraphPad Prism 7); $^{*}p \leq 0.05$, $^{**}p \leq 0.01$, $^{***}p \leq 0.001$, $^{****}p \leq 0.0001$. For ease of comparison, data for UM-3005 and CRX-601 + UM-3005 adjuvanted mice are displayed in **(B)** along with control groups (CRX-601 adjuvanted mice, A/Vic vaccinated mice, and naïve mice). Similarly, data for UM-3003 and CRX-601 + UM-3003 are displayed in **(C)** along with control groups (CRX-601 adjuvanted mice, A/Vic vaccinated mice, and naïve mice).

Figure 6 and the intracellular cytokine staining data (**Figure 7**) support the human HEK activity data shown in **Figure 1B**–UM-3005, the most strongly TLR8-biased compound, elicits the highest concentrations and frequencies of pro-inflammatory and Th1/Th17 biasing cytokines while UM-3003, the least TLR8-biased compound, elicits low concentrations and low frequencies of pro-inflammatory and Th1/Th17 polarizing cytokines but is the most potent inducer of IFNα, indicative of TLR7 activity. Taken together, the combination of cytokines expressed by mDC and classical monocytes, as well as secreted cytokine data, suggests a Th1 and Th17 polarizing innate cytokine environment upon stimulation with these TLR7/8 agonists in human PBMCs, particularly by UM-3005. Interestingly, UM-3005 was also the most potent single adjuvant with respect to polarizing an influenza-specific Th1 immune response in mice as well as protection against influenza virus challenge in vaccinated mice.

DISCUSSION

Here, we explored the ability of novel lipidated imidazoquinolines (TLR7/8 agonists) to act as adjuvants to confer protection against drifted H3N2 influenza both with and without a TLR4 agonist in mice. We found that these compounds elicited a Th1/Th17 type T cell response as well as a strongly Th1-biased humoral response. When used as adjuvants in combination with low dose A/Vic, these compounds were protective against the pandemic H3N2 strain HK68. When combined with a low dose of TLR4 agonist at a 1:100 ratio, mice were still protected from challenge with HK68 and weight loss was reduced when 601+UM-3003 was used as an adjuvant compared to UM-3003 alone. No vaccine-induced reactogenicity (as determined by visual inspection of the mice, e.g., ruffled fur, hunched posture, reluctance to move, or visible weight loss) was observed in any mouse at any time. Given the dissimilarity of TLR7 and TLR8 in mice compared to humans, we also evaluated the cytokine profile elicited by these compounds in human PBMCs. Promisingly, we found that cytokines required to generate a Th1 and Th17 response were produced by PBMCs in response to TLR7/8 agonists while they did not elicit cytokines required to bias a Th2 response. Although some donor-to-donor variability was observed in the frequency of cells producing a specific cytokine or the amount of cytokine that each donor's PBMCs secreted in response to adjuvant stimulation, all six donors responded to imidazoquinoline TLR7/8 stimulation with the same combination of cytokines. Taken together, these data indicate that imidazoquinolines lipidated at the 2-position or 7-position function as potent Th1/Th17 adjuvants in mice, protect against lethal influenza challenge, and elicit the cytokines required to generate the same Th1/Th17 response in humans.

Previous work has demonstrated the efficacy of using a TLR4 agonist in combination with a lipidated TLR7/8 agonist or a lipidated TLR7/8 agonist alone in protecting against influenza challenge (43, 58) either in a DMSO, liposome, or emulsion formulation. The work shown here extends these previous studies by demonstrating that lipidated imidazoquinolines in an aqueous formulation, with or without the addition of a TLR4 agonist, also serve as potent influenza adjuvants. The aqueous formulation used here, 2% glycerol, includes no excipients that may confound the adjuvant effect of the TLR7/8 or TLR4 compounds by inducing an immune response by itself, unlike emulsions or liposomes in which some of the immune response and protective effect was shown to be due to the emulsion or liposome formulation alone (43), demonstrating the adjuvant effects of the small molecule compounds themselves. Further, we found the potency of the adjuvants explored in this work may allow antigen dose sparing as we found protection was induced at an antigen dose of 0.3 μg HA per mouse after two injections whereas previous groups have used an antigen dose of 5 μg HA per mouse (58). In a pandemic setting, adjuvants that allow antigen dose sparing will be critical for allowing production of enough vaccine doses for mass vaccination.

H3N2 strains, regardless of reported antigenic mismatch, are more difficult to protect against than drifted H1N1 or influenza type B–a recent meta-analysis calculated that between 2004 and 2015, vaccine effectiveness against H3N2 strains was only 33% compared to 54% for influenza type B and 61–73% for H1N1 (1). Reasons for the low efficacy of H3N2 vaccination, especially against drifted strains, are still mostly unknown. A recent report demonstrated that egg-grown H3N2 vaccines lack a glycosylation site that is found in circulating H3N2 strains and that non-egg grown vaccines were able to induce higher neutralizing antibody titers against H3N2 viruses containing the glycosylation site compared to egg grown vaccines (66) which may partially explain poor vaccine-induced responses to circulating H3N2 viruses. In addition to moving toward cell-based methods of vaccine production, data presented in this manuscript demonstrate that adjuvanting with a lipidated imidazoquinoline in combination with a TLR4 agonist would likely provide broader protection against drifted H3N2 viruses.

Data suggest that while antibody responses, B cells, CD4 and CD8 T cells are all required to optimally clear an influenza infection protect against further infection (11, 67–75), transfer of influenza-specific CD4 T cells protects influenza-naïve mice from challenge in the absence of B cells or CD8 T cells (11). Further, T cell responses are critical for broad protection against different influenza viruses (73, 76–80). Here, we demonstrate that the small molecule adjuvants investigated induce significant influenza-specific IFNγ+ T cells and/or IL17 production compared to A/Vic alone. In the case

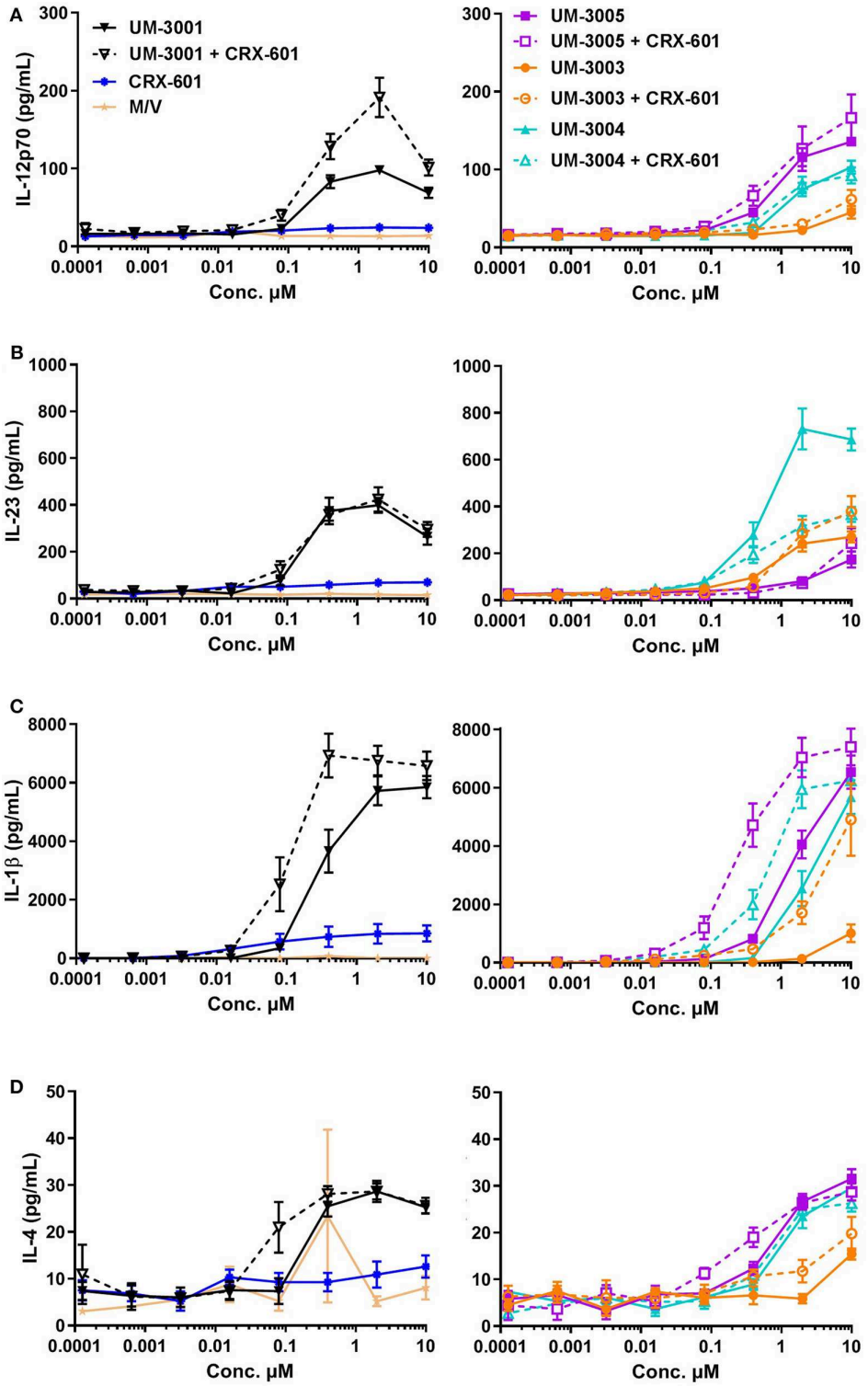

FIGURE 6 | Lipidated imidazoquinolines elicit a Th1/Th17-inducing innate cytokine profile from human PBMCs. PBMCs from 6 healthy, adult blood donors were stimulated with indicated concentrations of TLR7/8 agonists with and without a TLR4 agonist. Secreted cytokines were measured after 24 h via Luminex assay. Supernanant concentrations of **(A)** IL-12p70, **(B)** IL-23, **(C)** IL-1β, and **(D)** IL-4 were determined. For clarity, cytokine secretion data from PBMCs stimulated with media only (M/V), CRX-601, non-lipidated TLR7/8 agonist UM-3001, and UM-3001+CRX-601 are displayed in left plots while cytokine secretion data from PBMCs stimulated with lipidated TLR7/8 agonists alone and in combination with CRX-601 are diplayed on right plots. Note that for each cytokine measured, the y-axis scale used for the left and right plots is identical for ease of comparison.

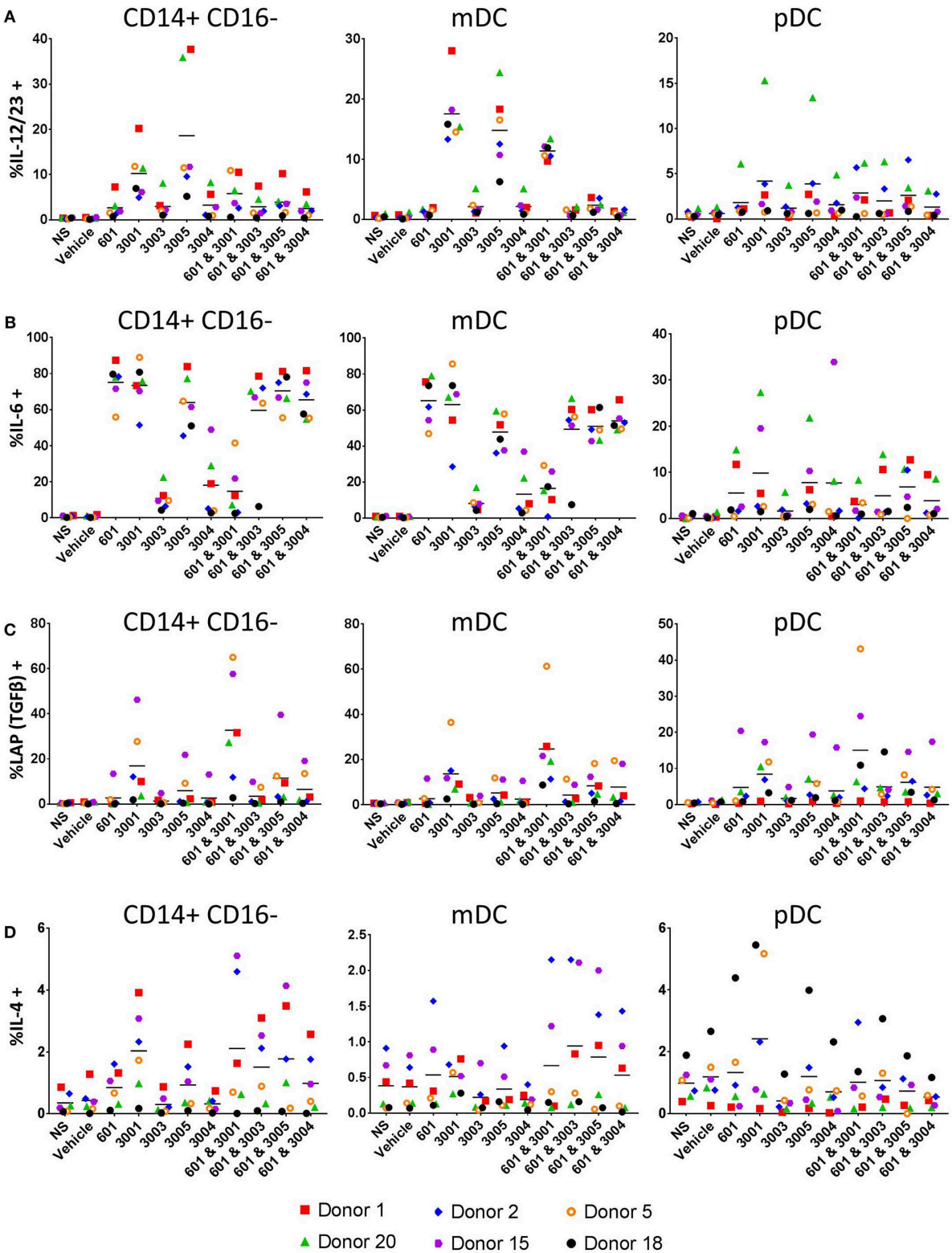

FIGURE 7 | Lipidated imidazoquinolines elicit T cell polarizing cytokines primarily from APCs. PBMCs from 6 healthy, adult blood donors were stimulated with 2 μM indicated TLR7/8, TLR4, or combination TLR4 + TLR7/8 agonists. After 1 h, brefeldin A (GolgiPlug) was added and cells were incubated for a further 5 h. Cells were then harvested and stained with surface antibodies for phenotyping, fixed and permeablized and stained with antibodies to detect intracellular cytokines. **(A)** Frequency of IL-12/IL-23+ cells, **(B)** frequency of IL-6+ cells, **(C)** frequency of TGFβ (LAP)+ cells, and **(D)** frequency of IL-4+ cells.

of lipidated imidazoquinolines, with or without the addition of CRX-601, an influenza-specific Th1 humoral bias was also produced. Compared to A/Vic vaccination alone, all mice that received adjuvanted A/Vic had either significantly increased A/Vic-specific IFNγ responses or IL-17 responses and were protected from mortality upon challenge. Mice who received A/Vic adjuvanted with a combination of UM-3003 or UM-3005 plus CRX-601 demonstrated an IgG2a-biased humoral response and significantly increased A/Vic-specific IFNγ and IL-17 T cell responses, and were the best protected from weight loss in a heterologous challenge model. This suggests that in this model both a Th1-biased humoral response as well as Th1 and Th17 T cell responses are required for optimal protection against heterologous H3N2 infection.

Despite the differences between mouse and human TLR7/8, the cytokine profile elicited by the lipidated imidazoquinoline TLR7/8 agonists investigated in this manuscript is that which is required to elicit a Th1/Th17 biased T cell response. Further, we demonstrated that these T cell polarizing cytokines were produced by mDC and classical monocytes, cell types that are critical as APCs in an infection setting. Although most cytokines measured were not boosted through the addition of CRX-601, addition of 601 did boost IL-1β production compared to TLR7/8 agonists alone. This is particularly striking as IL-1β induces Th17 differentiation (81, 82) and IL-17+ T cell frequencies were boosted in mice *in vivo* with the addition of CRX-601 to the TLR7/8 agonists, further strengthening connection between *in vivo* mouse data and *ex vivo* human data. While our group has previously demonstrated that too much IL-17 production can be detrimental in influenza infection (57), it is likely that some Th17 cells are important for viral clearance as mice adjuvanted with CRX-601 + TLR7/8 agonist experienced reduced weight loss and quicker recovery than those adjuvanted with CRX-601 or TLR7/8 agonist alone. Also, previous reports have shown that transferred influenza-specific Th17 memory cells can protect naïve mice against influenza challenge (11). Further, TLR7/8 adjuvants, particularly those with a TLR8 bias, demonstrated robust activity in activating human infant APCs (28) and increased neonatal macaque pneumococcus immunogenicity *in vivo* (41). A TLR8 biased adjuvant therefore, such as UM-3005, may be particularly efficacious at increasing infant responses to influenza. Taken together, these data suggest that UM-3003 and UM-3005 when used in combination with CRX-601 vaccine adjuvants in a detergent split influenza vaccine may provide much needed cross-protection against heterologous strains of H3N2 in humans.

DATA AVAILABILITY STATEMENT

The datasets generated for this study are available on request to the corresponding author.

ETHICS STATEMENT

The studies involving human participants were reviewed and approved by the University of Montana Institutional Review Board. The patients/participants provided their written informed consent to participate in this study. The animal study was reviewed and approved by the University of Montana Institutional Animal Care and Use Committee.

AUTHOR CONTRIBUTIONS

SM and JE designed experiments and analyzed data and wrote the manuscript draft. SM, VC, and MW performed experiments, data collection, and analysis. LB, ML, and HB synthesized compounds. LW and DB formulated compounds and provided physical characteristics. All authors discussed data, and reviewed and edited the final manuscript.

FUNDING

This work was supported by the NIAID Adjuvant Discovery Contract HHSN2722009900036C.

ACKNOWLEDGMENTS

H3N2 vaccine (A/Vic) and virus (HK68) were generously provided by GlaxoSmithKline (GSK). Compounds were first prepared at GSK. UM-3003, UM-3004, and UM-3005 are proprietary GSK compounds.

SUPPLEMENTARY MATERIAL

The Supplementary Material for this article can be found online at: https://www.frontiersin.org/articles/10.3389/fimmu.2020.00406/full#supplementary-material

REFERENCES

1. Belongia EA, Simpson MD, King JP, Sundaram ME, Kelley NS, Osterholm MT, et al. Variable influenza vaccine effectiveness by subtype: a systematic review and meta-analysis of test-negative design studies. *Lancet Infect Dis.* (2016) 16:942–51. doi: 10.1016/S1473-3099(16)00129-8
2. De Jong JC, Beyer WE, Palache AM, Rimmelzwaan GF, Osterhaus AD. Mismatch between the 1997/1998 influenza vaccine and the major epidemic A(H3N2) virus strain as the cause of an inadequate vaccine-induced antibody response to this strain in the elderly. *J Med Virol.* (2000) 61:94–9. doi: 10.1002/(SICI)1096-9071(200005)61:1<94::AID-JMV15>3.0.CO;2-C
3. Xie H, Wan XF, Ye Z, Plant EP, Zhao Y, Xu Y, et al. H3N2 mismatch of 2014–15 northern hemisphere influenza vaccines and head-to-head comparison between human and ferret antisera derived antigenic maps. *Sci Rep.* (2015) 5:15279. doi: 10.1038/srep15279
4. Kissling E, Nunes B, Robertson C, Valenciano M, Reuss A, Larrauri A, et al. I-MOVE multicentre case–control study 2010/11 to 2014/15: is there within-season waning of influenza type/subtype vaccine effectiveness with increasing time since vaccination? *Euro Surveill.* (2016) 21. doi: 10.2807/1560-7917.ES.2016.21.16.30201

5. Radin JM, Hawksworth AW, Myers CA, Ricketts MN, Hansen EA, Brice GT. Influenza vaccine effectiveness: maintained protection throughout the duration of influenza seasons 2010–2011 through 2013–2014. *Vaccine.* (2016) 34:3907–12. doi: 10.1016/j.vaccine.2016.05.034
6. Ferdinands JM, Fry AM, Reynolds S, Petrie JG, Flannery B, Jackson ML, et al. Intraseason waning of influenza vaccine protection: evidence from the US influenza vaccine effectiveness network, 2011–2012 through 2014–2015. *Clin Infect Dis.* (2017) 64:544–50. doi: 10.1093/cid/ciw816
7. Young B, Sadarangani S, Jiang L, Wilder-Smith A, Chen MI-C. Duration of influenza vaccine effectiveness: a systematic review, meta-analysis, and meta-regression of test-negative design case-control studies. *J Infect Dis.* (2017) 217:731–41. doi: 10.1093/infdis/jix632
8. Rambhia KJ, Rambhia MT. Early bird gets the flu: what should be done about waning intraseasonal immunity against seasonal influenza? *Clin Infect Dis.* (2018) 68:1235–40. doi: 10.1093/cid/ciy748
9. Corti D, Cameroni E, Guarino B, Kallewaard NL, Zhu Q, Lanzavecchia A. Tackling influenza with broadly neutralizing antibodies. *Curr Opin Virol.* (2017) 24:60–9. doi: 10.1016/j.coviro.2017.03.002
10. Wilkinson TM, Li CK, Chui CS, Huang AK, Perkins M, Liebner JC, et al. Preexisting influenza-specific CD4(+) T cells correlate with disease protection against influenza challenge in humans. *Nat Med.* (2012) 18:274–80. doi: 10.1038/nm.2612
11. Mckinstry KK, Strutt TM, Kuang Y, Brown DM, Sell S, Dutton RW, et al. Memory CD4+ T cells protect against influenza through multiple synergizing mechanisms. *J Clin Invest.* (2012) 122:2847–56. doi: 10.1172/JCI63689
12. Clemens E, Van De Sandt C, Wong S, Wakim L, Valkenburg S. Harnessing the power of T cells: the promising hope for a universal influenza vaccine. *Vaccines.* (2018) 6:18. doi: 10.3390/vaccines6020018
13. Control CFD, and Prevention. *FDA Licensure of Bivalent Human Papillomavirus Vaccine (HPV2, Cervarix) for Use in Females and Updated HPV Vaccination Recommendations From the Advisory Committee on Immunization Practices (ACIP).* MMWR. Morbidity and mortality weekly report (2010) (Atlanta, GA: Center for Disease Control and Prevention). p. 9:626.
14. Szarewski A. HPV vaccine: cervarix. *Expert Opin Biol Ther.* (2010) 10:477–87. doi: 10.1517/14712591003601944
15. Garçon N, Di Pasquale A. From discovery to licensure, the adjuvant system story. *Hum Vaccin Immunother.* (2017) 13:19–33. doi: 10.1080/21645515.2016.1225635
16. James SF, Chahine EB, Sucher AJ, Hanna C. Shingrix: the new adjuvanted recombinant herpes zoster vaccine. *Ann Pharmacother.* (2018) 52:673–80. doi: 10.1177/1060028018758431
17. Syed YY. Recombinant zoster vaccine (Shingrix®): a review in herpes zoster. *Drugs Aging.* (2018) 35:1031–40. doi: 10.1007/s40266-018-0603-x
18. Jackson S, Lentino J, Kopp J, Murray L, Ellison W, Rhee M, et al. Immunogenicity of a two-dose investigational hepatitis B vaccine, HBsAg-1018, using a toll-like receptor 9 agonist adjuvant compared with a licensed hepatitis B vaccine in adults. *Vaccine.* (2018) 36:668–74. doi: 10.1016/j.vaccine.2017.12.038
19. Schillie S, Harris A, Link-Gelles R, Romero J, Ward J, Nelson N. *Recommendations of the Advisory Committee On Immunization Practices for Use of a Hepatitis B Vaccine With a Novel Adjuvant*. Morbidity and Mortality Weekly Report (2018). p. 67:455. doi: 10.15585/mmwr.mm6715a5
20. Black S. Safety and effectiveness of MF-59 adjuvanted influenza vaccines in children and adults. *Vaccine.* (2015) 33:B3–B5. doi: 10.1016/j.vaccine.2014.11.062
21. Tartey S, Takeuchi O. Pathogen recognition and toll-like receptor targeted therapeutics in innate immune cells. *Int Rev Immunol.* (2017) 36:57–73. doi: 10.1080/08830185.2016.1261318
22. Diebold SS, Kaisho T, Hemmi H, Akira S, Reis E Sousa C. Innate antiviral responses by means of TLR7-mediated recognition of single-stranded RNA. *Science.* (2004) 303:1529–31. doi: 10.1126/science.1093616
23. Heil F, Hemmi H, Hochrein H, Ampenberger F, Kirschning C, Akira S, et al. Species-specific recognition of single-stranded RNA via toll-like receptor 7 and 8. *Science.* (2004) 303:1526–9. doi: 10.1126/science.1093620
24. Jensen S, Thomsen AR. Sensing of RNA viruses: a review of innate immune receptors involved in recognizing RNA virus invasion. *J Virol.* (2012) 86:2900–10. doi: 10.1128/JVI.05738-11
25. Loré K, Betts MR, Brenchley JM, Kuruppu J, Khojasteh S, Perfetto S, et al. Toll-like receptor ligands modulate dendritic cells to augment cytomegalovirus- and HIV-1-specific T cell responses. *J Immunol.* (2003) 171:4320–8. doi: 10.4049/jimmunol.171.8.4320
26. Russo C, Cornella-Taracido I, Galli-Stampino L, Jain R, Harrington E, Isome Y, et al. Small molecule Toll-like receptor 7 agonists localize to the MHC class II loading compartment of human plasmacytoid dendritic cells. *Blood.* (2011) 117:5683–91. doi: 10.1182/blood-2010-12-328138
27. Desmet CJ, Ishii KJ. Nucleic acid sensing at the interface between innate and adaptive immunity in vaccination. *Nat Rev Immunol.* (2012) 12:479–91. doi: 10.1038/nri3247
28. Levy O, Suter EE, Miller RL, Wessels MR. Unique efficacy of Toll-like receptor 8 agonists in activating human neonatal antigen-presenting cells. *Blood.* (2006) 108:1284–90. doi: 10.1182/blood-2005-12-4821
29. Poulin LF, Salio M, Griessinger E, Anjos-Afonso F, Craciun L, Chen J-L, et al. Characterization of human DNGR-1+ BDCA3+ leukocytes as putative equivalents of mouse CD8α+ dendritic cells. *J Exp Med.* (2010) 207:1261–71. doi: 10.1084/jem.20092618
30. Bryant CE, Symmons M, Gay NJ. Toll-like receptor signalling through macromolecular protein complexes. *Mol Immunol.* (2015) 63:162–5. doi: 10.1016/j.molimm.2014.06.033
31. Fitzgerald KA, Rowe DC, Barnes BJ, Caffrey DR, Visintin A, Latz E, et al. LPS-TLR4 signaling to IRF-3/7 and NF-κB involves the toll adapters TRAM and TRIF. *J Exp Med.* (2003) 198:1043–55. doi: 10.1084/jem.20031023
32. Yamamoto M, Sato S, Hemmi H, Hoshino K, Kaisho T, Sanjo H, et al. Role of adaptor TRIF in the MyD88-independent toll-like receptor signaling pathway. *Science.* (2003) 301:640–3. doi: 10.1126/science.1087262
33. Maelfait J, Vercammen E, Janssens S, Schotte P, Haegman M, Magez S, et al. Stimulation of Toll-like receptor 3 and 4 induces interleukin-1β maturation by caspase-8. *J Exp Med.* (2008) 205:1967–73. doi: 10.1084/jem.20071632
34. He S, Liang Y, Shao F, Wang X. Toll-like receptors activate programmed necrosis in macrophages through a receptor-interacting kinase-3–mediated pathway. *Proc Natl Acad Sci USA.* (2011) 108:20054–9. doi: 10.1073/pnas.1116302108
35. Moriwaki K, Bertin J, Gough PJ, Chan FK-M. A RIPK3–caspase 8 complex mediates atypical pro–IL-1β processing. *J Immunol.* (2015) 194:1938–44. doi: 10.4049/jimmunol.1402167
36. Pockros PJ, Guyader D, Patton H, Tong MJ, Wright T, Mchutchison JG, et al. Oral resiquimod in chronic HCV infection: safety and efficacy in 2 placebo-controlled, double-blind phase IIa studies. *J Hepatol.* (2007) 47:174–82. doi: 10.1016/j.jhep.2007.02.025
37. Smirnov D, Schmidt JJ, Capecchi JT, Wightman PD. Vaccine adjuvant activity of 3M-052: an imidazoquinoline designed for local activity without systemic cytokine induction. *Vaccine.* (2011) 29:5434–42. doi: 10.1016/j.vaccine.2011.05.061
38. Buonsanti C, Balocchi C, Harfouche C, Corrente F, Stampino LG, Mancini F, et al. Novel adjuvant Alum-TLR7 significantly potentiates immune response to glycoconjugate vaccines. *Sci Rep.* (2016) 6:29063. doi: 10.1038/srep29063
39. Cortez A, Li Y, Miller AT, Zhang X, Yue K, Maginnis J, et al. Incorporation of phosphonate into benzonaphthyridine toll-like receptor 7 agonists for adsorption to aluminum hydroxide. *J Med Chem.* (2016) 59:5868–78. doi: 10.1021/acs.jmedchem.6b00489
40. Fox CB, Orr MT, Van Hoeven N, Parker SC, Mikasa TJ, Phan T, et al. Adsorption of a synthetic TLR7/8 ligand to aluminum oxyhydroxide for enhanced vaccine adjuvant activity: a formulation approach. *J Control Release.* (2016) 244:98–107. doi: 10.1016/j.jconrel.2016.11.011
41. Dowling DJ, Van Haren SD, Scheid A, Bergelson I, Kim D, Mancuso CJ, et al. TLR7/8 adjuvant overcomes newborn hyporesponsiveness to pneumococcal conjugate vaccine at birth. *JCI Insight.* (2017) 2:e91020. doi: 10.1172/jci.insight.91020

42. Misiak A, Leuzzi R, Allen AC, Galletti B, Baudner BC, D'oro U, et al. Addition of a TLR7 agonist to an acellular pertussis vaccine enhances Th1 and Th17 responses and protective immunity in a mouse model. *Vaccine*. (2017) 35:5256–63. doi: 10.1016/j.vaccine.2017.08.009
43. Van Hoeven N, Fox CB, Granger B, Evers T, Joshi SW, Nana GI, et al. A formulated TLR7/8 agonist is a flexible, highly potent and effective adjuvant for pandemic influenza vaccines. *Sci Rep*. (2017) 7:46426. doi: 10.1038/srep46426
44. Dowling DJ. Recent advances in the discovery and delivery of TLR7/8 agonists as vaccine adjuvants. *ImmunoHorizons*. (2018) 2:185–97. doi: 10.4049/immunohorizons.1700063
45. Napolitani G, Rinaldi A, Bertoni F, Sallusto F, Lanzavecchia A. Selected Toll-like receptor agonist combinations synergistically trigger a T helper type 1-polarizing program in dendritic cells. *Nat Immunol.* (2005) 6:769–76. doi: 10.1038/ni1223
46. Ghosh TK, Mickelson DJ, Solberg JC, Lipson KE, Inglefield JR, Alkan SS. TLR-TLR cross talk in human PBMC resulting in synergistic and antagonistic regulation of type-1 and 2 interferons, IL-12 and TNF-alpha. *Int Immunopharmacol.* (2007) 7:1111–21. doi: 10.1016/j.intimp.2007.04.006
47. Ouyang X, Negishi H, Takeda R, Fujita Y, Taniguchi T, Honda K. Cooperation between MyD88 and TRIF pathways in TLR synergy via IRF5 activation. *Biochem Biophys Res Commun.* (2007) 354:1045–51. doi: 10.1016/j.bbrc.2007.01.090
48. Pufnock JS, Cigal M, Rolczynski LS, Andersen-Nissen E, Wolfl M, Mcelrath MJ, et al. Priming CD8+ T cells with dendritic cells matured using TLR4 and TLR7/8 ligands together enhances generation of CD8+ T cells retaining CD28. *Blood.* (2011) 117:6542–51. doi: 10.1182/blood-2010-11-317966
49. Orr MT, Duthie MS, Windish HP, Lucas EA, Guderian JA, Hudson TE, et al. MyD88 and TRIF synergistic interaction is required for TH1-cell polarization with a synthetic TLR4 agonist adjuvant. *Eur J Immunol.* (2013) 43:2398–408. doi: 10.1002/eji.201243124
50. Sallusto F. Heterogeneity of human CD4+ T cells against microbes. *Annu Rev Immunol.* (2016) 34:317–34. doi: 10.1146/annurev-immunol-032414-112056
51. Smith AJ, Li Y, Bazin HG, St-Jean JR, Larocque D, Evans JT, et al. Evaluation of novel synthetic TLR7/8 agonists as vaccine adjuvants. *Vaccine.* (2016) 34:4304–12. doi: 10.1016/j.vaccine.2016.06.080
52. Bazin HG, Murray TJ, Bowen WS, Mozaffarian A, Fling SP, Bess LS, et al. The 'Ethereal' nature of TLR4 agonism and antagonism in the AGP class of lipid A mimetics. *Bioorg Med Chem Lett.* (2008) 18:5350–4. doi: 10.1016/j.bmcl.2008.09.060
53. Gerster JF, Lindstrom KJ, Miller RL, Tomai MA, Birmachu W, Bomersine SN, et al. Synthesis and structure–activity-relationships of 1H-Imidazo(4,5-c)quinolines that induce interferon production. *J Med Chem.* (2005) 48:3481–91. doi: 10.1021/jm049211v
54. Bazin HG, Bess LS, Livesay MT, Mwakwari SC, Johnson DA. Phospholipidation of TLR7/8-active imidazoquinolines using a tandem phosphoramidite method. *Tetrahedron Lett.* (2016) 57:2063–6. doi: 10.1016/j.tetlet.2016.03.091
55. Robertson IB, Rifkin DB. Regulation of the bioavailability of TGF-β and TGF-β-related proteins. *Cold Spring Harb Perspect Biol.* (2016) 8:a021907. doi: 10.1101/cshperspect.a021907
56. Gorden KK, Qiu XX, Binsfeld CC, Vasilakos JP, Alkan SS. Cutting edge: activation of murine TLR8 by a combination of imidazoquinoline immune response modifiers and polyT oligodeoxynucleotides. *J Immunol.* (2006) 177:6584–7. doi: 10.4049/jimmunol.177.10.6584
57. Maroof A, Yorgensen YM, Li Y, Evans JT. Intranasal vaccination promotes detrimental Th17-mediated immunity against influenza infection. *PLoS Pathog.* (2014) 10:e1003875. doi: 10.1371/journal.ppat.1003875
58. Goff PH, Hayashi T, Martínez-Gil L, Corr M, Crain B, Yao S, et al. Synthetic toll-like receptor 4 (TLR4) and TLR7 ligands as influenza virus vaccine adjuvants induce rapid, sustained, and broadly protective responses. *J Virol.* (2015) 89:3221–35. doi: 10.1128/JVI.03337-14
59. Moris P, Van Der Most R, Leroux-Roels I, Clement F, Dramé M, Hanon E, et al. H5N1 influenza vaccine formulated with AS03 A induces strong cross-reactive and polyfunctional CD4 T-cell responses. *J Clin Immunol.* (2011) 31:443–54. doi: 10.1007/s10875-010-9490-6
60. Trinchieri G, Wysocka M, D'andrea A, Rengaraju M, Aste-Amezaga M, Kubin M, et al. Natural killer cell stimulatory factor (NKSF) or interleukin-12 is a key regulator of immune response and inflammation. *Prog Growth Factor Res.* (1992) 4:355–68. doi: 10.1016/0955-2235(92)90016-B
61. Hsieh CS, Macatonia SE, Tripp CS, Wolf SF, O'garra A, Murphy KM. Development of TH1 CD4+ T cells through IL-12 produced by Listeria-induced macrophages. *Science.* (1993) 260:547–9. doi: 10.1126/science.8097338
62. Bustamante J, Boisson-Dupuis S, Abel L, Casanova JL. Mendelian susceptibility to mycobacterial disease: genetic, immunological, and clinical features of inborn errors of IFN-γ immunity. In: *Seminars in Immunology*. (2014) (Amsterdam: Elsevier). p. 454–470. doi: 10.1016/j.smim.2014.09.008
63. Ghoreschi K, Laurence A, Yang XP, Tato CM, Mcgeachy MJ, Konkel JE, et al. Generation of pathogenic T(H)17 cells in the absence of TGF-beta signalling. *Nature.* (2010) 467:967–71. doi: 10.1038/nature09447
64. Crouse J, Kalinke U, Oxenius A. Regulation of antiviral T cell responses by type I interferons. *Nat Rev Immunol.* (2015) 15:231. doi: 10.1038/nri3806
65. Gorden KB, Gorski KS, Gibson SJ, Kedl RM, Kieper WC, Qiu X, et al. Synthetic TLR agonists reveal functional differences between human TLR7 and TLR8. *J Immunol.* (2005) 174:1259–68. doi: 10.4049/jimmunol.174.3.1259
66. Zost SJ, Parkhouse K, Gumina ME, Kim K, Perez SD, Wilson PC, et al. Contemporary H3N2 influenza viruses have a glycosylation site that alters binding of antibodies elicited by egg-adapted vaccine strains. *Proc Natl Acad Sci USA.* (2017) 114:12578–83. doi: 10.1073/pnas.1712377114
67. Allan W, Tabi ZCleary A, Doherty P. Cellular events in the lymph node and lung of mice with influenza. Consequences of depleting CD4+ T cells. *J Immunol.* (1990) 144:3980–6.
68. Eichelberger M, Allan W, Zijlstra M, Jaenisch R, Doherty P. Clearance of influenza virus respiratory infection in mice lacking class I major histocompatibility complex-restricted CD8+ T cells. *J Exp Med.* (1991) 174:875–80. doi: 10.1084/jem.174.4.875
69. Bender BS, Croghan T, Zhang L, Small P. Transgenic mice lacking class I major histocompatibility complex-restricted T cells have delayed viral clearance and increased mortality after influenza virus challenge. *J Exp Med.* (1992) 175:1143–5. doi: 10.1084/jem.175.4.1143
70. Scherle P, Palladino G, Gerhard W. Mice can recover from pulmonary influenza virus infection in the absence of class I-restricted cytotoxic T cells. *J Immunol.* (1992) 148:212–7.
71. Epstein S, Misplon J, Lawson C, Subbarao E, Connors M, Murphy B. Beta 2-microglobulin-deficient mice can be protected against influenza A infection by vaccination with vaccinia-influenza recombinants expressing hemagglutinin and neuraminidase. *J Immunol.* (1993) 150:5484–93.
72. Graham MB, Braciale TJ. Resistance to and recovery from lethal influenza virus infection in B lymphocyte–deficient mice. *J Exp Med.* (1997) 186:2063–8. doi: 10.1084/jem.186.12.2063
73. Epstein SL, Lo C-Y, Misplon JA, Bennink JR. Mechanism of protective immunity against influenza virus infection in mice without antibodies. *J Immunol.* (1998) 160:322–7.
74. Topham DJ, Doherty PC. Clearance of an influenza A virus by CD4+ T cells is inefficient in the absence of B cells. *J Virol.* (1998) 72:882–5. doi: 10.1128/JVI.72.1.882-885.1998
75. Riberdy JM, Christensen JP, Branum K, Doherty PC. Diminished primary and secondary influenza virus-specific CD8+ T-cell responses in CD4-depleted Ig–/– mice. *J Virol.* (2000) 74:9762–5. doi: 10.1128/JVI.74.20.9762-9765.2000
76. Benton KA, Misplon JA, Lo C-Y, Brutkiewicz RR, Prasad SA, Epstein SL. Heterosubtypic immunity to influenza A virus in mice lacking IgA, all Ig, NKT cells, or γδ T cells. *J Immunol.* (2001) 166:7437–45. doi: 10.4049/jimmunol.166.12.7437
77. Richards KA, Chaves FA, Sant AJ. Infection of HLA-DR1 transgenic mice with a human isolate of influenza a virus (H1N1) primes a diverse CD4 T-cell repertoire that includes CD4 T cells with heterosubtypic cross-reactivity to avian (H5N1) influenza virus. *J Virol.* (2009) 83:6566–77. doi: 10.1128/JVI.00302-09
78. Guo H, Santiago F, Lambert K, Takimoto T, Topham DJ. T cell-mediated protection against lethal 2009 pandemic H1N1 influenza virus infection in a mouse model. *J Virol.* (2011) 85:448–55. doi: 10.1128/JVI.01812-10
79. Hillaire ML, Van Trierum SE, Kreijtz JH, Bodewes R, Geelhoed-Mieras MM, Nieuwkoop NJ, et al. Cross-protective immunity against influenza

pH1N1 2009 viruses induced by seasonal influenza A (H3N2) virus is mediated by virus-specific T-cells. *J General Virol.* (2011) 92:2339–49. doi: 10.1099/vir.0.033076-0

80. Weinfurter JT, Brunner K, Capuano Iii SV, Li C, Broman KW, Kawaoka Y, et al. Cross-reactive T cells are involved in rapid clearance of 2009 pandemic H1N1 influenza virus in nonhuman primates. *PLoS Pathog.* (2011) 7:e1002381. doi: 10.1371/journal.ppat.1002381
81. Zielinski CE, Mele F, Aschenbrenner D, Jarrossay D, Ronchi F, Gattorno M, et al. Pathogen-induced human T H 17 cells produce IFN-γ or IL-10 and are regulated by IL-1β. *Nature.* (2012) 484:514. doi: 10.1038/nature10957
82. Mailer RK, Joly A-L, Liu S, Elias S, Tegner J, Andersson J. IL-1β promotes Th17 differentiation by inducing alternative splicing of FOXP3. *Sci Rep.* (2015) 5:14674. doi: 10.1038/srep14674

Conflict of Interest: VC, MW, LB, ML, LW, DB, HB, and JE were employees of GlaxoSmithKline Vaccines when TLR7/8 compounds described here were first synthesized.

The remaining author declares that the research was conducted in the absence of any commercial or financial relationships that could be construed as a potential conflict of interest.

frontiers in Immunology

ORIGINAL RESEARCH
published: 09 April 2020
doi: 10.3389/fimmu.2020.00642

Determining Whether Agonist Density or Agonist Number Is More Important for Immune Activation via Micoparticle Based Assay

*Peter Deak, Flora Kimani, Brittney Cassaidy and Aaron Esser-Kahn**

Pritzker School of Molecular Engineering, The University of Chicago, Chicago, IL, United States

It is unknown if surface bound toll-like-receptor (TLR) agonists activate cells via density or total molecular number. To answer this question, we developed a TLR agonist surface conjugated polystyrene microparticle (MP) system. Using a library of MPs with varying TLR agonist density and number, we simultaneously observed innate immune cell MP uptake and TNFα expression using ImageStream flow cytometry on a cell by cell basis. The data shows that total TLR number and not density drives cellular activation with a threshold of approximately 10^5–10^6 TLR agonists. We believe that this information will be crucial for the design of particulate vaccine formulations.

Keywords: toll-like-receptor, innate immunity, microparticle, activation threshold, *In vitro* quantification

OPEN ACCESS

Edited by:
Jay Evans,
University of Montana, United States

Reviewed by:
Tom Mitchell,
University of Louisville, United States
Howard B. Cottam,
University of California, San Diego, United States

****Correspondence:***
Aaron Esser-Kahn
aesserkahn@uchicago.edu;
apekay@gmail.com

Specialty section:
This article was submitted to Vaccines and Molecular Therapeutics, a section of the journal Frontiers in Immunology

Received: *03 February 2020*
Accepted: *20 March 2020*
Published: *09 April 2020*

Citation:
Deak P, Kimani F, Cassaidy B and Esser-Kahn A (2020) Determining Whether Agonist Density or Agonist Number Is More Important for Immune Activation via Micoparticle Based Assay. Front. Immunol. 11:642. doi: 10.3389/fimmu.2020.00642

INTRODUCTION

Toll-like-receptors (TLRs) initiate responses in the innate immune system by recognizing molecules present on the surfaces of bacteria and fungi. Given their importance for initiating an immune response, TLR agonists are widely studied for understanding innate immune responses and for their usefulness as vaccine adjuvants (1). Recently, researchers showed that TLR agonist activation can be enhanced by presenting the agonists in a particulate (2–4). TLR agonists have been packaged inside microparticles (MPs), conjugated to polymers and conjugated on MP surfaces to form "pathogen mimetic" MPs (5–10). Improvements in vaccine activity occur when agonists are attached to a particle, likely due to increases in valency and antigen proximity, but the different systems lack a basis for comparison as the particle structure, size and agonist density have not been consistent. One great example of probing agonist density and identity comes from the Roy lab, in part, but this study focused on the exciting differences *in vivo* responses (11). Therefore, to date, there has not been a direct characterization of how surface bound TLR agonists effect innate immune cell activation. Answering this question would help guide the design of future vaccines and immune-therapies that rely on particulate presentation to enhance immune responses.

This study seeks to quantitatively determine an activation threshold for micro-particle surface bound TLR agonists using mouse derived dendritic cells (BMDCs). A threshold for particle-surface TLR agonists could be the result of either a fixed surface density or an absolute concentration of agonists. We developed a system to answer two questions: (1) Is innate immune cell activation by surface bound TLR agonists a function of TLR agonist density on the particle or dictated by the total

Abbreviations: BCA, bicinchoninic acid assay; BMDC, mouse derived dendritic cells; CpG, oligonucleotide; MP, microparticle; MPLA, monophosphoryl lipid A; Pam_2, Pam_2CSK_4; PS, polystyrene; TLR, toll-like-receptor.

number of TLR-TLR agonist interactions? and (2) if one mechanism is dominant, can we quantify the threshold at which a cell becomes activated? To answer these questions, we synthesized particles of different sizes and densities and directly measured if density or absolute concentration trigger similar of different TNFα responses (**Figure 1**). By quantifying the number of agonists and/or the density of agonists on each MP, we correlate agonist number or density to immune activation.

MATERIALS AND METHODS

A full description of the Materials and Methods used in this study are provided in the **Supplementary Material**.

RESULTS

TLR Agonist Conjugated Microparticle Synthesis

To achieve fine control of agonist density and absolute concentration, we developed a synthesis strategy for conjugating a TLR agonist oligonucleotide (CpG) to siloxane coated polystyrene (PS) microparticles (MPs) (12). Using a similar strategy, we conjugated $PamCSK_4$ (Pam), a TLR2/6 agonist, and monophosphoryl lipid A (MPLA), a TLR4 agonist, to siloxane coated PS MPs (**Supplementary Figure S1**). In this study, we quantified the number of TLR agonists conjugated to MPs of varying sizes, incubated them with BMDCs and other immune cell lines and observed immune activation via TNFα secretion – a common indicator of immune action (**Figure 1**) (13).

TLR Agonist Surface Conjugation Estimation

An estimate of a surface bound TLR agonist threshold has been difficult to obtain. Inconsistent conjugation and the heterogeneous nature of TLR make direct quantification of each difficult. In addition, TLR agonists activate their receptors with as low as picomolar concentrations. Some of the most potent agonists, such as lipopolysaccharide (LPS), are a heterogeneous mixture of large macromolecules of various sizes (14, 15). Additionally, given that most TLR agonists are large hydrophobic molecules, they can be challenging to chemically modify and to determine if they covalently attach to a MP or simply non-specifically associate to their surfaces (16). Finally, many polymeric MPs activate innate immune

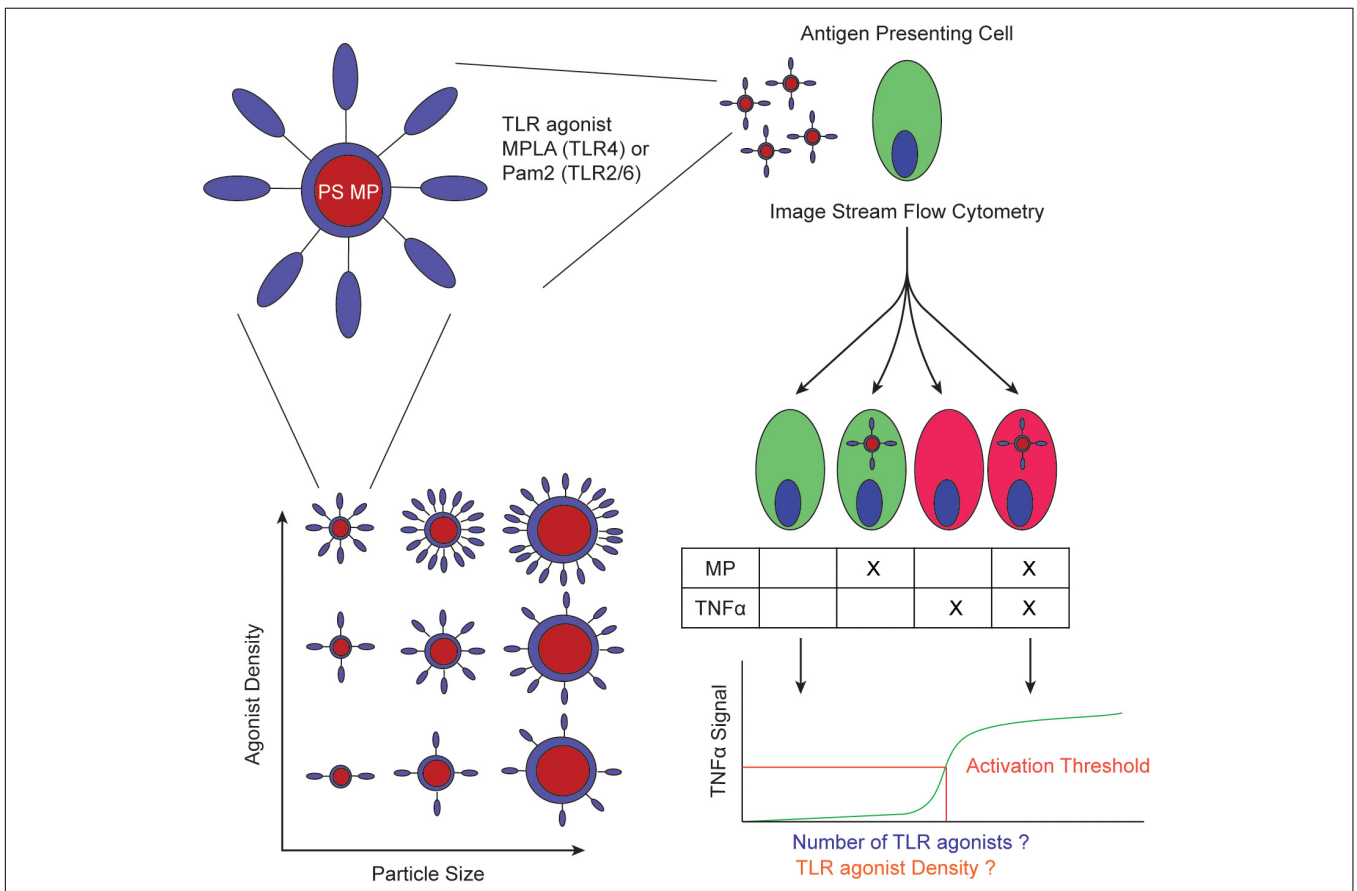

FIGURE 1 | Schematic of experimental workflow. PS MPs are conjugated with TLR agonists with varying number of molecules and/or density and quantified **(left)**. These MPs are incubated with APCs to determine if the activation threshold is determined by total number of TLR agonists or TLR agonist density **(right)**.

cells non-specifically and this background noise complicates analysis (12).

To address the issues of quantification, consistency in conjugation and characterization, we employed multiple strategies. For background activation, we used polystyrene (PS) MPs with a siloxane coating – reducing the immune activation to background levels (12). We modified this PS MP system to generate MPs of various sizes, 0.25, 2, and 5 μm diameter which when coated with similar agonist concentrations yield different densities and confirmed that they do no aggregate in aqueous conditions (**Supplementary Figure S2A**). We carefully selected our TLR agonist system to ensure consistency and ease of characterization. MPLA and Pam2 are small (MW > 2000 Da) compared to other agonists and have well defined structures. Both MPLA and Pam2 are readily synthesized or modified for conjugation to PS MPs using maleimide-thiol chemistry (**Figure 2A** and **Supplementary Figure S1**). This chemistry is very efficient and highly consistent, specifically for surface conjugations to larger particles (16). Additionally, both molecules can be quantified via their amide bonds using a bicinchoninic acid assay (BCA).

These functionalities make the PS MP system ideal for quantitatively measuring TLR agonists conjugated on MP surfaces. This chemistry is important as accurately determining the number of agonist molecules on a MP surface is crucial to answer our overall question if TLR agonist density or number is more critical. To obtain greater accuracy, we used three independent quantification methods to count the number of agonist conjugations on the particle surface. First, we used a BCA assay to directly quantify the number of agonist molecules on the surface (17). The BCA does not interfere with particles as it relies on soluble material to quantify amide bonds. However, because the BCA measures any amide bond, the assay can result in high background measurements when testing MPs, due to non-specific absorption of molecules on the particle surface. In our case, this background was exacerbated by the presence of an amide bond in the maleimide linker. For all experiments, we subtracted a maleimide-linker conjugated MP as our control (**Figures 2B,C**).

To ensure accuracy, we used two other methods that measure the total number of reactive maleimides on the particle surface and determined the number of molecules on the surface via subtractive measurement. Both methods are indirect, but when combined provide further accuracy in our measurement. The first method measures the total number of free thiols on an unmodified MP and the number of maleimide molecules after reaction with the maleimide linker by observing a decrease in a known amount of L-cysteine in solution (**Supplementary Figure S3**). The data indicated that the maleimide conjugation is nearly 100%. To quantify the number of unreacted maleimides, we used a modified Ellman's assay to determine a drop in a known L-cysteine concentration (16). As a third confirmation, we used a commercially available fluorescent maleimide quantification kit for both Pam2 and MPLA conjugated MPs (**Figures 2B,C**). We conjugated the MPs with varying concentrations of MPLA or Pam2 (50–0.1 μg/mL), which provided a large range of total agonists (3×10^6–1×10^5 molecules/MP).

TLR Agonist Modified MPs Activate Immune Cells

After quantifying the number of MPLA and Pam2 molecules on the MP surface, we tested these MPs using a RAW blue activation assay to confirm that they stimulate immune cells (**Figures 2D,E**) (12). The RAW blue data not only shows that the MP are immunostimulatory, but also indicates a cell-MP ratio necessary to stimulate bulk immune activation. When sufficient quantities of innate immune cells are activated simultaneously, paracrine signaling often results in high levels of bulk activation, even in cells that do not encounter the activating agent (in this case the TLR agonist) (18). In our experiments, we sought to observe on a cell by cell basis if a phagocytosis event of a MP triggers activation of a cell and remove the secondary activation mechanisms of paracrine signaling. Another possibility we wished to avoid is that MPs bind their TLRs transiently and then dissociate before being phagocytosed. This transient activation is possible given that TLR2/6 and TLR4 are both surface expressed. Based on the RAW blue data, we expect that cells dosed with a 1 to 5 ratio of MPs to cells would have little to no paracrine activation and transient TLR binding, due to the shortage of MPs. Additionally, cells were dosed with a paracrine signaling blocking agent, brefeldin A (BFA), prior to MP stimulation to further reduce the non-TLR mediated cellular activation and to sequester TNFα (19).

ImageStream Analysis of Endocytosed MPs

To observe the number of endocytosed microparticles, we developed an ImageStream workflow to count particles within individual cells. The method also allows us to correlate TNFα production within each individual cell with the number of particles with that same cell. After a 16 h incubation, innate immune cells (BMDCs, RAW 264.7 or THP-1) were washed, fixed, permeabilized and stained for TNFα. The single cell suspension was then analyzed with Image Stream flow cytometry (**Supplementary Figure S4**) (20). Image Stream provides images of individual cells. With these images, we then count the number of fluorescently labeled MPs in each cell and the TNFα intensity (21). Due to the cell to MP ratio of 5:1, there was a bimodal distribution of cells, a small population of cells (<10%) that contained a MP, which was the focus of this study. To prevent skewing data toward the non-MP cells, we first confirmed that this population had a normal distribution of TNFα intensity and used only the averages for each independent experiment in all plots and significance tests (**Supplementary Figure S5**). In order to obtain a sufficiently large population of BMDCs with MPs, we analyzed at least 100,000 cells in biological triplicates for all variation of TLR coated MPs (**Figures 3A,B** and **Supplementary Figure S6**). BMDCs that uptake MPs with more agonist molecules per MP require fewer MPs to increase TNFα signal for both Pam2 and MPLA. This result occurred in all our test innate immune cell lines, THP-1 and RAW 264.7 (**Supplementary Figures S7, S8**). To readout immune activation further upstream of TNFα in cells, we used the nuclear co-localization of NFκB taken at 15 min post stimulation rather than overnight with TNFα. However, NFκB was more readily

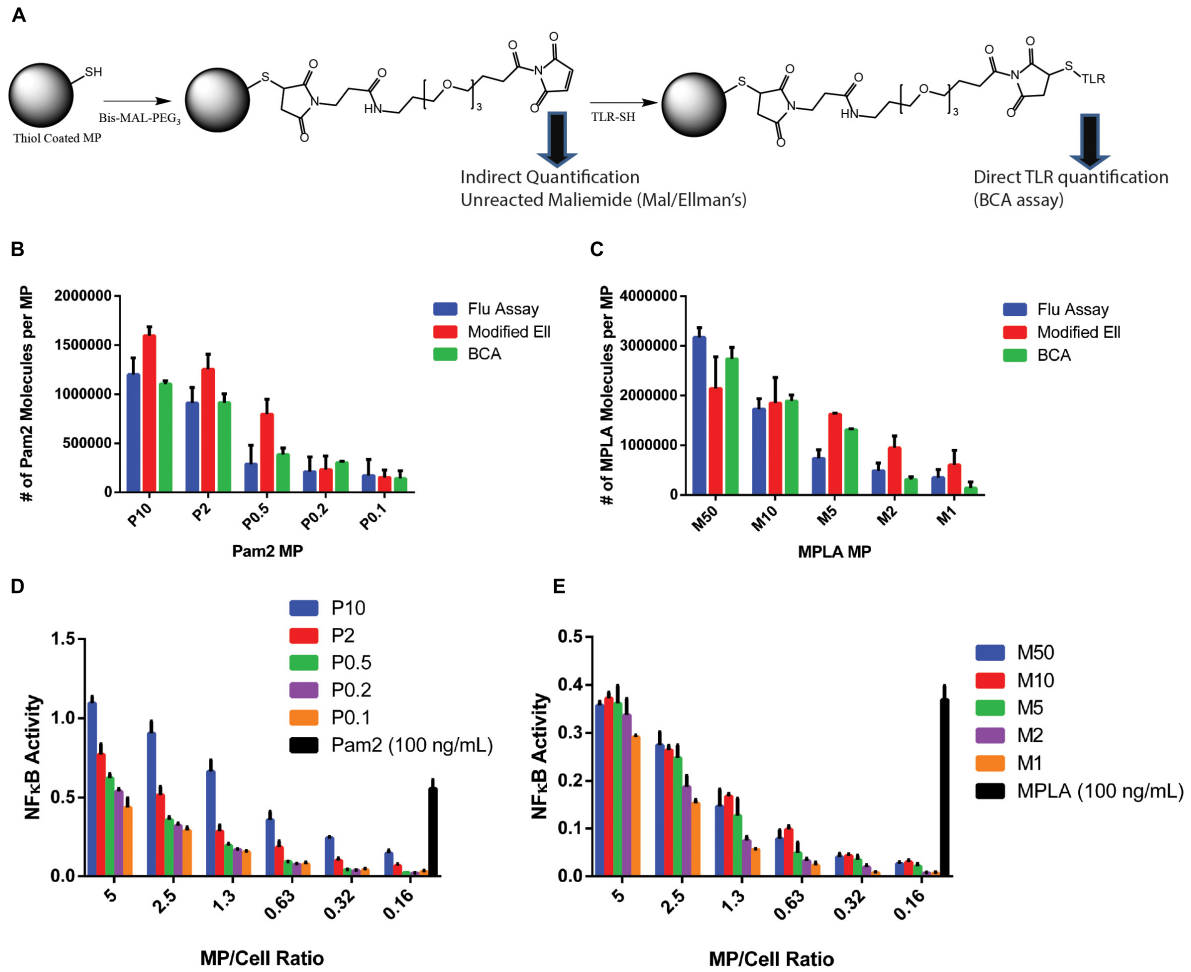

FIGURE 2 | TLR agonists surface conjugation and quantification. **(A)** Chemistry schematic for MP modification with TLR ligands. **(B)** After conjugating Pam2 to 2 μm diameter MPs and washing to remove unreacted TLR agonists, the total TLR agonist conjugated to MPs were tested with the three analytical quantification methods, Fluorescence, Ellmans or BCA. **(C)** The analysis from part B was repeated with MPLA conjugated MPs. **(D)** one million RAW Blue cells were incubated with varying numbers of Pam2 conjugated MPs formulations or free Pam2 (100 ng/mL) for 16 h, then tested using a Quanti-blue SEAP reporter assay for NFkB activity. Experiments were performed as technical triplicates. The red line indicates baseline activation. **(E)** Repeated analysis of part **(D)** with MPLA conjugated MPs and 100 ng/mL free MPLA. Error bars represent standard deviation of triplicate experiments. MP labeling scheme: P for Pam2 and M for MPLA, number represents concentration of agonist during reaction in μg/mL (e.g., P10- MPs conjugated with 10 μg/ml Pam2).

activated at even the lowest number of agonists on a single MP for both Pam2 and MPLA. This activation level suggests that NFκB nuclear colocalization requires less stimulus than TNFα secretion. For example, for the MP with the fewest Pam2 or MPLA agonists (P0.1 or M1) cells required the uptake of at least 3 MPs to trigger TNFα production, while cells only required one MP to stimulate NFκB (**Supplementary Figure S9**).

Total Agonist Number on MPs More Critical for Immune Activation Than Agonist Density

To probe ligand concentration versus ligand density, we generated MPLA and Pam2 conjugated MPs of different sizes (5 μm and 0.25 μm diameter) and quantified them in a similar fashion. We estimated the ligand density for each particle by calculating the surface area of the particle (assuming a sphere, πd^2) and dividing the total number of agonists by the surface area. We achieved a wide range of both total agonist ligands per particle and agonist density. For agonists per particle, we synthesized a range of 5×10^4 to 1×10^7 (**Figure 3B**, **Supplementary Figure S10**, and **Supplementary Table S1**). For ligand density, this data can be represented as a range of 1×10^4 to 1.6×10^6 molecules per μm^2. For MP endocytosis, a similar trend was observed where more ligands per particle required fewer endocytosed MPs to trigger TNFα, but also the larger 5 μm particles with more ligands (10^6–10^7 molecules/MP or 10^4–10^5 molecules/μm^2) required only either 1 or 2 MPs for each condition and smaller 0.25 μm particles (5×10^4–3×10^5 molecules/MP or 2.5×10^5–1.5×10^6 molecules/μm^2) required over 1 MP for all but one condition, P10 (3×10^5

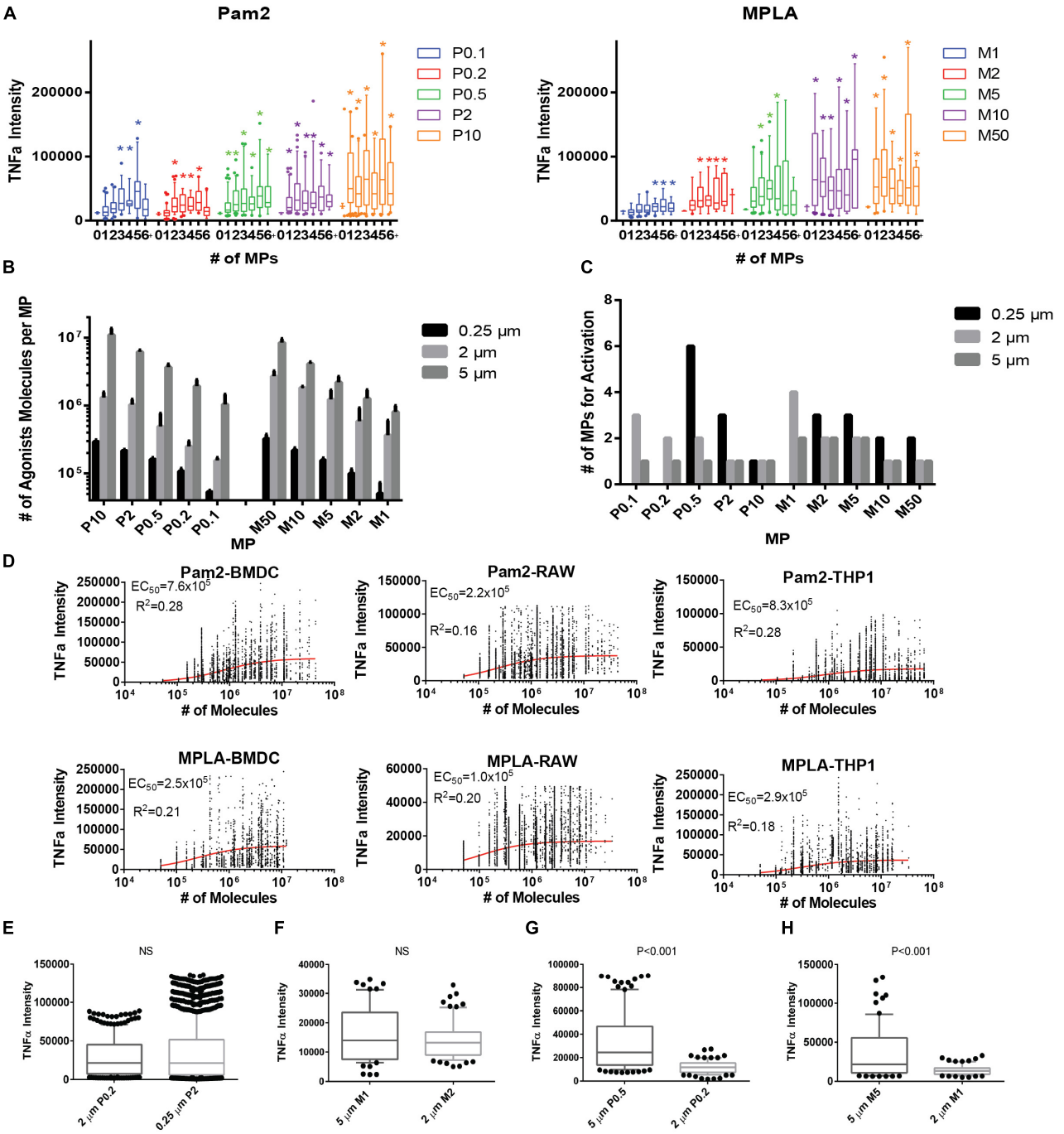

MP	Agonist ($x10^5$)	Agonist /nm²
2 um P0.2	2.5	0.020
0.25 um P2	2.1	1.092

MP	Agonist ($x10^5$)	Agonist /nm²
5 um M1	8.0	0.010
2 um M2	7.8	0.097

MP	Agonist ($x10^5$)	Agonist /nm²
5 um P0.5	36.4	0.046
2 um P0.5	4.9	0.039

MP	Agonist ($x10^5$)	Agonist /nm²
5 um M5	21.9	0.028
2 um M1	3.6	0.029

FIGURE 3 | Continued

FIGURE 3 | TLR coated MPs induce innate immune cell TNFα expression, which correlates with total number of TLR agonists exposed to cells. **(A)** 10 million BMDCs were incubated with two million varying Pam2 or MPLA conjugated 2 μm MPs overnight in 1 μg/mL brefeldin **(A)** BMDCs were then washed, fixed, permabilized, stained and analyzed with imagestream (>100,000 cells per run, done in triplicate then combined). TNFα expression was then compared to the number of particles which cells uptake (1, 2, 3, 4, 5, or >5 which we call 6+) and compared to baseline TNFα (the average TNFα expression of unstimulated BMDCs). Conditions with a significant ($p < 0.05$) increase in TNFα when compared to unstimulated cells are marked with a colored star. Data for Pam2 is on right and MPLA is on the left. For each condition, box and whisker plots represent one standard deviation (box) and error bars for **(A)** and **(B)** represent 90/10% range with dots >90 or <10% range, with $N > 10$ and significance as $p < 0.05$. **(B)** After conjugating Pam2 or MPLA to 0.25 and 5 μm diameter MPs and washing to remove unreacted TLR agonists, the total TLR agonist conjugated to MPs were tested with the three analytical quantification methods, Fluorescence, Ellmans or BCA, then averaged. Error bars represent standard deviation from all three testing methods. **(C)** Bar graph representing number of MPs that BMDCs uptake for each MP formulation that had a significant average TNFα signal above the average unstimulated BMDC. **(D)** TNFα expression is well correlated with total number of TLR agonists on MP surfaces. By further analyzing the imagestream data, the TNFα expression for BMDCs that uptake any number of MPs was compared with the total number of TLR agonists that interact on a BMDC surface (calculated by multiplying the number of molecules per MP by the number of MPs that cells uptake). Included are curvefits for Pam2 (top) or MPLA (bottom) MPs with BMDCs (left), RAWs (middle) or THP-1 (right). EC_{50} and R^2 values were determined using a Hill curve fit model in Graphpad 7 software. **(E)** We selected two MP formulated that either had similar total number of Pam2 agonists per MP (see table below) and compared the levels of TNFα secretion when BMDCs with a single MP. Statistical difference between the two group is shown above graph, if $p > 0.05$ then it is not significant (NS). **(F)** similar to part **(E)** but for MPLA MPs **(G)** Similar analysis as in part **(E)**, but comparing two MP formulations with similar Pam2 agonist density. **(H)** Similar to **(G)** but with MPLA MPs.

TABLE 1 | List of TNFα activation threshold.

Cell Line	BMDC			RAW			THP-1		
Agonist	**EC_{50} (×10^5) molecule**	**CI (×10^5) molecule**	**R^2**	**EC_{50} (×10^5) molecule**	**CI (×10^5) molecule**	**R^2**	**EC_{50} (×10^5) molecule**	**CI (×10^5) molecule**	**R^2**
Pam_2	7.6 ± 0.5	6.6–8.6	0.28	2.2 ± 0.1	2.0–2.5	0.16	8.3 ± 0.5	7.3–9.3	0.28
MPLA	2.5 ± 0.2	2.1–2.9	0.21	1.0 ± 0.06	0.9–1.1	0.20	2.9 ± 0.17	2.5–3.2	0.18

molecules/MP or 1.5 × 10^6 molecules/μm^2, **Figure 3C** and **Supplementary Figures S11–S13**).

With the insight that density and ligand number were both variables, we analyzed a complete data set to observe larger trends. We compared the correlation between agonist density on MPs or total number of agonist-TLR interaction and TNFα intensity. To estimate the total number of TLR agonists encountered by a BMDC, we estimated each particle could fully expose its agonists to the endocytic environment. We calculated the agonists per MP by multiplying the total number of MPs phagocytosed by a BMDC for all MP sizes and agonist conjugation ratios. We then plotted this data with the corresponding TNFα intensity and performed a curve fit analysis using Graphpad Prism 6 (**Figure 3D**). Both MPLA and Pam2 have a highly significant positive trend between number of agonists and TNFα intensity ($p < 10^{-3}$) and reasonable R^2 values for the curve fit given the degree of biological variability inherent in an immune response (**Table 1**). Moreover, we observed no significant trend when the TNFα intensity was compared to agonist density on MPs (**Supplementary Figure S14**), indicating that BMDC activation is largely a function of total agonist molecules and not agonist density on MP surfaces. This trend is also seen in other cell lines, such as THP-1 and RAW 264.7 cells (**Figure 3D** and **Table 1**).

We next sought to determine if density was impacting cell activation in any quantifiable way. While the correlation between the numbers of MP bound TLR agonists and immune activation is clear in the large analysis, the high biological variability of innate activation partially masked a more interesting phenomenon when comparing individual sets. In essence, the variability in cell activation across sets meant that statistical analysis had much greater power when comparing individual sets. To determine if density had an effect, we directly compared systems with different agonist densities but similar total number of agonists. As shown in **Figure 3E**, the 2 μm P0.2 MP (2.4 × 10^6 molecules/MP, 2.0 × 10^4 molecules/μm^2) has a similar total number of agonists per MP as the 0.25 μm P2 MP (2.1 × 10^6 molecules/MP, 1.1 × 10^6 molecules/μm^2). BMDCs that endocytose a single MP in each case have a similar levels of TNFα activation. This effect is also seen in MPLA MPs (**Figure 3F**). In contrast, MPs with similar levels of agonist density have dissimilar TNFα intensity (**Figures 3G,H**). For example, the 5 μm M5 MP (2.1 × 10^6 molecules/MP, 7.0 × 10^3 molecules/μm^2) and the 2 μm M2 MP (3.6 × 10^5 molecules/MP, 7.2 × 10^3 molecules/μm^2) had similar agonists densities and dissimilar total agonist numbers but had a statistically significant difference in TNFα expression (**Figure 3H**, $p < 0.001$). We observed these relationships in all MP density comparisons (**Supplementary Figure S15**) – comparing across particle size and total agonist numbers. Based on this data, we concluded that the immune activating potential for TLR agonists when bound to a MP is correlated more with the total number of agonists on the particle and not with the density of agonist conjugation.

In an effort to provide further insight, we estimated the order of magnitude for the activation threshold (the number of agonists required to engage TLRs) to trigger innate immune activation. We calculated an EC_{50} value to estimate the activation threshold for BMDCs by plotting the number of molecules per particle compared to the TNFα intensity (**Figure 3D**). This estimate varies slightly between the TLR agonist used (7.6 × 10^5 for Pam2 vs. 2.5 × 10^5 for MPLA). This estimate likewise varies slightly for THP-1 or RAW 264.7 cells (**Table 1**). Despite these small

variations, we generate a range between 10^5–10^6 MPLA or Pam2 molecules required on MP surfaces to activate an innate immune cell. This information provides a minimum guideline for the design of any surface bound TLR agonist vaccine formulation and suggests a range of activation for APCs more generally.

DISCUSSION

This result strongly suggests that the total number of ligand-receptor interactions is the primary driver of antigen presenting cell activation and not the density of ligands. While this evidence strongly supports agonist number, it does not rule out that particle density can influence immune responses in other ways. TLR agonist density alters downstream responses including Th1/Th2 bias, CD8 T-cell responses, and Fc receptor density (10, 22–24). Taking into account these finding, we propose a potential two-step process in which a cell is activated and then uses density and concentration to inform the type of response that develops.

It should be noted that this type of analysis has some limitations. Namely, our estimate is not a description of the total number of agonist-TLR interactions required to initiate downstream immune activation, rather it is an empirical observation of the number of agonists required on the MP surface to stimulate innate immune cells. Determining a quantitative estimate of the number of agonist-TLR interactions is challenging because the total number of TLR on APCs has not been definitely determined and obtaining estimates of total number of binding events in such highly multivalent systems as MPs is notoriously difficult (25). Instead, our analysis sidesteps these issues and focuses exclusively on quantifying the number of TLR agonists necessary to generate APC activation. While this analysis lacks mechanistic insights on TLR mediated APC activation, it provides more of a practical guideline for particulate vaccine formulations.

For this study, we provide the following overall insights into particulate immune activation, namely (1) initial TLR mediated APC activation has a threshold dictated by the absolute number of TLR agonists and not density and (2) to activate an APC, a particle must have on the order of 10^5–10^6 TLR agonists on its surface. To test this, we employed a PS MP based system, which allowed for discrete and quantifiable conjugation of molecules per MP and a mechanism for tracking which cells bind TLR agonists (via fluorescence). In combination with ImageStream flow cytometry, this MP system reliably tracked innate immune cell activation and determined a TLR agonist activation threshold. The analysis from this approach is limited to observing just APC activation, but future work will track downstream adaptive immune responses. Using the MP system, we envision stimulating APCs with MPs for T-cell expansion and *in vivo* experiments. TLR agonist MP formulations are a promising new direction for vaccine development and have many potential applications to enhance current vaccine formulations (11). These types of quantitative measurements will aid the design of these MPs, allowing optimal immune activation while reducing extraneous TLR agonists and excess inflammation which contribute to reduced tolerability in vaccines and potential side effects in immune-therapies.

DATA AVAILABILITY STATEMENT

All datasets generated for this study are included in the article/**Supplementary Material**.

ETHICS STATEMENT

The animal study was reviewed and approved by the University of Chicago IACUC.

AUTHOR CONTRIBUTIONS

PD and AE-K designed the study and developed the initial ideal. BC performed the SEM microparticle analysis. FK synthesized, purified, and performed the analysis on thiol modified Pam_2 molecules. PD performed all other experiments, synthesized the other compounds, performed the analysis, created the figures, and wrote the text of the manuscript. PD and AE-K edited and provided the feedback on the manuscript.

FUNDING

This work was supported by NIH NIAID grants 7U01AI124286-03 and NIH 1 F32 AI147517.

SUPPLEMENTARY MATERIAL

The Supplementary Material for this article can be found online at: https://www.frontiersin.org/articles/10.3389/fimmu.2020.00642/full#supplementary-material

REFERENCES

1. Duthie MS, Windish HP, Fox CB, Reed SG. Use of defined TLR Ligands as adjuvants within human vaccines. *Immunol Rev*. (2011) 239:178–96. doi: 10.1111/j.1600-065X.2010.00978.x
2. Akira S, Takeda K. Toll-like receptor signalling. *Nat Rev Immunol*. (2004) 4:499–511. doi: 10.1038/nri1391
3. Akira S, Takeda K, Kaisho T. Toll-like receptors: critical proteins linking innate and acquired immunity. *Nat Immunol*. (2001) 2:675–80. doi: 10.1038/90609
4. Agnihotri G, Crall BM, Lewis TC, Day TP, Balakrishna R, Warshakoon HJ, et al. Structure–activity relationships in Toll-like receptor 2-agonists leading to simplified monoacyl lipopeptides. *J. Med. Chem*. (2011) 54:8148–60. doi: 10.1021/jm201071e
5. Hafner AM, Corthésy B, Merkle HP. Particulate formulations for the delivery of Poly(I:C) as vaccine adjuvant. *Adv Drug Deliv Rev*. (2013) 65:1386–99. doi: 10.1016/j.addr.2013.05.013
6. Ebrahimian M, Hashemi M, Maleki M, Hashemitabar G, Abnous K, Ramezani M, et al. Co-delivery of dual Toll-like receptor agonists and antigen in poly(Lactic-Co-Glycolic) acid/polyethylenimine cationic hybrid nanoparticles

promote efficient in vivo immune responses. *Front Immunol*. (2017) 8:1077. doi: 10.3389/fimmu.2017.01077
7. Siefert AL, Caplan MJ, Fahmy TM. Artificial bacterial biomimetic nanoparticles synergize pathogen-associated molecular patterns for vaccine efficacy. *Biomaterials*. (2016) 97:85–96. doi: 10.1016/j.biomaterials.2016.03.039
8. Demento SL, Siefert AL, Bandyopadhyay A, Sharp FA, Fahmy TM. Pathogen-associated molecular patterns on biomaterials: a paradigm for engineering new vaccines. *Trends Biotechnol*. (2011) 29:294–306. doi: 10.1016/j.tibtech.2011.02.004
9. Petersen LK, Ramer-Tait AE, Broderick SR, Kong C-S, Ulery BD, Rajan K, et al. Activation of innate immune responses in a pathogen-mimicking manner by amphiphilic polyanhydride nanoparticle adjuvants. *Biomaterials*. (2011) 32:6815–22. doi: 10.1016/j.biomaterials.2011.05.063
10. Lynn GM, Laga R, Darrah PA, Ishizuka AS, Balaci AJ, Dulcey AE, et al. In Vivo characterization of the physicochemical properties of polymer-linked TLR agonists that enhance vaccine immunogenicity. *Nat Biotech*. (2015) 33:1201–10. doi: 10.1038/nbt.3371
11. Madan-Lala R, Pradhan P, Roy K. Combinatorial delivery of dual and triple TLR agonists via polymeric pathogen-like particles synergistically enhances innate and adaptive immune responses. *Sci Rep*. (2017) 7:2530. doi: 10.1038/s41598-017-02804-y
12. Moser BA, Steinhardt RC, Esser-Kahn AP. Surface coating of nanoparticles reduces background inflammatory activity while increasing particle uptake and delivery. *ACS Biomater Sci Eng*. (2017) 3:206–13. doi: 10.1021/acsbiomaterials.6b00473
13. Trevejo JM, Marino MW, Philpott N, Josien R, Richards EC, Elkon KB, et al. TNF-α-dependent maturation of local dendritic cells is critical for activating the adaptive immune response to virus infection. *Proc Natl Acad Sci*. (2001) 98:12162–7. doi: 10.1073/pnas.211423598
14. Wang Y, Su L, Morin M, Jones B, Whitby L, Surakattula M, et al. Identification of novel and potent synthetic TLR agonists. *J Immunol*. (2017) 198 (1 Suppl.):129.3. doi: 10.1038/mi.2014.93
15. Lu Y-C, Yeh W-C, Ohashi PS. LPS. /TLR4 signal transduction pathway. *Cytokine*. (2008) 42:145–51. doi: 10.1016/j.cyto.2008.01.006
16. Moser M, Behnke T, Hamers-Allin C, Klein-Hartwig K, Falkenhagen J, Resch-Genger U. Quantification of PEG-maleimide ligands and coupling efficiencies on nanoparticles with ellman's reagent. *Anal Chem*. (2015) 87:9376–83. doi: 10.1021/acs.analchem.5b02173
17. Yap WT, Song WK, Chauhan N, Scalise PN, Agarwal R, Shea LD. Quantification of particle-conjugated or -encapsulated peptides on interfering reagent backgrounds. *Biotechniques*. (2014) 57:39–44. doi: 10.2144/000114190
18. Shalek AK, Satija R, Shuga J, Trombetta JJ, Gennert D, Lu D, et al. Single cell RNA seq reveals dynamic paracrine control of cellular variation. *Nature*. (2014) 510:363–9. doi: 10.1038/nature13437
19. Xue Q, Lu Y, Eisele MR, Sulistijo ES, Khan N, Fan R, et al. Analysis of single-cell cytokine secretion reveals a role for paracrine signaling in coordinating macrophage responses to TLR4 stimulation. *Sci Signal*. (2015) 8:ra59–59. doi: 10.1126/scisignal.aaa2155
20. Maguire O, Collins C, O'Loughlin K, Miecznikowski J, Minderman H. Quantifying nuclear P65 as a parameter for NF-KB activation: correlation between imagestream cytometry, Microscopy, and Western Blot. *Cytometry A*. (2011) 79:461–9. doi: 10.1002/cyto.a.21068
21. Headland SE, Jones HR, D'Sa ASV, Perretti M, Norling LV. Cutting-edge analysis of extracellular microparticles using imagestream^x imaging flow cytometry. *Sci Rep*. (2014) 4:5237. doi: 10.1038/srep05237
22. Pacheco P, White D, Sulchek T. Effects of microparticle size and fc density on macrophage phagocytosis. *PLoS One*. (2013) 8:e60989. doi: 10.1371/journal.pone.0060989
23. Leleux JA, Pradhan P, Roy K. Biophysical attributes of CpG presentation control TLR9 signaling to differentially polarize systemic immune responses. *Cell Rep*. (2017) 18:700–10. doi: 10.1016/j.celrep.2016.12.073
24. Lynn GM, Chytil P, Francica JR, Lagová A, Kueberuwa G, Ishizuka AS, et al. Impact of polymer-TLR-7/8 agonist (Adjuvant) morphology on the potency and mechanism of CD8 T cell induction. *Biomacromolecules*. (2019) 20:854–70. doi: 10.1021/acs.biomac.8b01473
25. Jang S, Park J-S, Won Y-H, Yun S-J, Kim S-J. The expression of Toll-like receptors (TLRs) in cultured human skin fibroblast is modulated by histamine. *Chonnam Med J*. (2012) 48:7–14. doi: 10.4068/cmj.2012.48.1.7

Conflict of Interest: The authors declare that the research was conducted in the absence of any commercial or financial relationships that could be construed as a potential conflict of interest.

frontiers in Pediatrics

STUDY PROTOCOL
published: 30 April 2020
doi: 10.3389/fped.2020.00197

Clinical Protocol for a Longitudinal Cohort Study Employing Systems Biology to Identify Markers of Vaccine Immunogenicity in Newborn Infants in The Gambia and Papua New Guinea

Olubukola T. Idoko[1,2,3,4], Kinga K. Smolen[2,5], Oghenebrume Wariri[1], Abdulazeez Imam[1], Casey P. Shannon[6], Tida Dibassey[1], Joann Diray-Arce[2,5], Alansana Darboe[1], Julia Strandmark[1], Rym Ben-Othman[7], Oludare A. Odumade[2,4,8], Kerry McEnaney[2,9], Nelly Amenyogbe[10], William S. Pomat[11], Simon van Haren[2,5], Guzmán Sanchez-Schmitz[2,5], Ryan R. Brinkman[12,13], Hanno Steen[2,5,14], Robert E. W. Hancock[15], Scott J. Tebbutt[6,16,17], Peter C. Richmond[10,18], Anita H. J. van den Biggelaar[10], Tobias R. Kollmann[10†], Ofer Levy[2,5,19*†], Al Ozonoff[2,5†], Beate Kampmann[1,4*†] and on behalf of The EPIC Consortium*

[1] Vaccines and Immunity Theme, Medical Research Council Unit the Gambia at London School of Hygiene and Tropical Medicine, Fajara, Gambia, [2] Precision Vaccines Program, Division of Infectious Diseases, Boston Children's Hospital, Boston, MA, United States, [3] CIH LMU Center for International Health, Medical Center of the University of Munich (LMU), Munich, Germany, [4] The Vaccine Centre, London School of Hygiene and Tropical Medicine, London, United Kingdom, [5] Harvard Medical School, Boston, MA, United States, [6] PROOF Centre of Excellence, Vancouver, BC, Canada, [7] Department of Pediatrics, BC Children's Hospital, University of British Columbia, Vancouver, BC, Canada, [8] Division of Medicine Critical Care, Harvard Medical School, Boston Children's Hospital, Boston, MA, United States, [9] Department of Cardiology, Boston Children's Hospital, Boston, MA, United States, [10] Wesfarmers Centre of Vaccines and Infectious Diseases, Telethon Kids Institute, University of Western Australia, Nedlands, WA, Australia, [11] Papua New Guinea Institute of Medical Research, Goroka, Papua New Guinea, [12] BC Cancer Agency, Vancouver, BC, Canada, [13] Department of Medical Genetics, University of British Columbia, Vancouver, BC, Canada, [14] Department of Pathology, Boston Children's Hospital, Boston, MA, United States, [15] Department of Microbiology & Immunology, University of British Columbia, Vancouver, BC, Canada, [16] Centre for Heart Lung Innovation, University of British Columbia, Vancouver, BC, Canada, [17] Division of Respiratory Medicine, Department of Medicine, UBC, Vancouver, BC, Canada, [18] Division of Pediatrics, School of Medicine, Perth Children's Hospital, University of Western Australia, Nedlands, WA, Australia, [19] Broad Institute of MIT & Harvard, Cambridge, MA, United States

Background: Infection contributes to significant morbidity and mortality particularly in the very young and in low- and middle-income countries. While vaccines are a highly cost-effective tool against infectious disease little is known regarding the cellular and molecular pathways by which vaccines induce protection at an early age. Immunity is distinct in early life and greater precision is required in our understanding of mechanisms of early life protection to inform development of new pediatric vaccines.

Methods and Analysis: We will apply transcriptomic, proteomic, metabolomic, multiplex cytokine/chemokine, adenosine deaminase, and flow cytometry immune cell phenotyping to delineate early cellular and molecular signatures that correspond to vaccine immunogenicity. This approach will be applied to a neonatal cohort in The Gambia ($N \sim 720$) receiving at birth: (1) Hepatitis B (HepB) vaccine alone, (2) Bacille Calmette Guerin (BCG) vaccine alone, or (3) HepB and BCG vaccines, (4) HepB and

OPEN ACCESS

Edited by:
Eric Giannoni, CHU de Lausanne (CHUV), Switzerland

Reviewed by:
Riccardo Castagnoli, University of Pavia, Italy
Claus Klingenberg, Arctic University of Norway, Norway

***Correspondence:**
Olubukola T. Idoko
bukkyidoko@gmail.com;
Olubukola.Idoko@lshtm.ac.uk
Ofer Levy
ofer.levy@childrens.harvard.edu
Beate Kampmann
bkampmann@mrc.gm

† These authors have contributed equally to this work and shares senior authorship

Specialty section:
This article was submitted to Pediatric Immunology, a section of the journal Frontiers in Pediatrics

Received: *30 December 2019*
Accepted: *01 April 2020*
Published: *30 April 2020*

Citation:
Idoko OT, Smolen KK, Wariri O, Imam A, Shannon CP, Dibassey T, Diray-Arce J, Darboe A, Strandmark J, Ben-Othman R, Odumade OA, McEnaney K, Amenyogbe N, Pomat WS, Haren S, Sanchez-Schmitz G, Brinkman RR, Steen H, Hancock REW, Tebbutt SJ, Richmond PC, van den Biggelaar AHJ, Kollmann TR, Levy O, Ozonoff A and Kampmann B (2020) Clinical Protocol for a Longitudinal Cohort Study Employing Systems Biology to Identify Markers of Vaccine Immunogenicity in Newborn Infants in The Gambia and Papua New Guinea. Front. Pediatr. 8:197. doi: 10.3389/fped.2020.00197

BCG vaccines delayed till day 10 at the latest. Each study participant will have a baseline peripheral blood sample drawn at DOL0 and a second blood sample at DOL1,−3, or−7 as well as late timepoints to assess HepB vaccine immunogenicity. Blood will be fractionated via a "small sample big data" standard operating procedure that enables multiple downstream systems biology assays. We will apply both univariate and multivariate frameworks and multi-OMIC data integration to identify features associated with anti-Hepatitis B (anti-HB) titer, an established correlate of protection. Cord blood sample collection from a subset of participants will enable human *in vitro* modeling to test mechanistic hypotheses identified *in silico* regarding vaccine action. Maternal anti-HB titer and the infant microbiome will also be correlated with our findings which will be validated in a smaller cohort in Papua New Guinea ($N \sim 80$).

Ethics and Dissemination: The study has been approved by The Gambia Government/MRCG Joint Ethics Committee and The Boston Children's Hospital Institutional Review Board. Ethics review is ongoing with the Papua New Guinea Medical Research Advisory Committee. All de-identified data will be uploaded to public repositories following submission of study output for publication. Feedback meetings will be organized to disseminate output to the study communities.

Clinical Trial Registration: Clinicaltrials.gov Registration Number: NCT03246230

Keywords: markers, newborn, vaccine, immunogenicity, systems biology, OMICS

BACKGROUND AND RATIONALE FOR THE STUDY

Infection remains a major cause of morbidity and mortality accounting for over 30% of global deaths occurring each year in children under the age of 5 years (1). The burden of infectious disease is highest among the very young and in low- and middle-income countries (1, 2). In 2017, 5.4 million deaths occurred in children under the age of five accounting for 38.9 deaths per thousand live births (2). Roughly 2.5 million (47%) of these under five deaths occurred in the first 28 days of life (1). The leading causes of under-five mortality in 2016 were complications of prematurity (18%), pneumonia (16%) intrapartum related events (12%), congenital anomalies (9%), diarrhea (8%), neonatal sepsis (7%), and malaria (5%) (1). Thus, infectious disease remains a leading cause of mortality and indeed morbidity during the most vulnerable period of life.

Immunization is a powerful and highly cost-effective approach to prevent infection (3–5). It is estimated that for every public dollar spent on immunization, there is a $44 return on investment (6), and that vaccines have contributed to saving over 20 million lives and $350 billion between 2001 and 2017 in 73 low and middle income countries alone (6). Vaccines are thought to save 2–3 million lives each year worldwide (7) and have contributed to disease eradication (8–10) with prospects for eradicating another disease in sight (11–13). However, there are few vaccines specifically licensed for use at the extremes of age partly because little is known regarding the molecular pathways by which vaccines induce protection, particularly in the "developing" immune system of the very young (14).

Systems biology, is a powerful approach to gain deep insight into biology and has increasingly been applied to vaccinology to obtain insights into vaccine protection (15). However, these powerful techniques have not been applied to the most vulnerable: newborns in resource poor settings (16). To meet this need, an international group of academic biomedical centers have partnered to form the Expanded Program on Immunization Consortium (EPIC) (**Figure 1**) partnering to utilize systems biology to unravel the complex relationships between vaccine immunogenicity via early, vaccine-induced transcriptomic, metabolomic, proteomic, multiplex cytokine/chemokine, adenosine deaminase and immune cell phenotype ("OMIC") signatures. With funding from the United States National Institute of Health (NIH), through National Institute of Allergy and Infectious Diseases (NIAID) U19 Initiative for the Human Immune Project Consortium (HIPC), the study described below will be conducted to explore these complex relationships.

Previous EPIC pilot studies (EPIC-001) conducted at the Medical Research Council Unit The Gambia at London School of Hygiene and Tropical Medicine (MRCUG at LSHTM) and the Papua New Guinea Institute of Medical Research (PNGIMR) between 2015 and 2017 demonstrated the feasibility of measuring robust and cogent "OMIC" readouts from small volume blood

Abbreviations: Ab, Antibody; BCG, Bacille Calmette-Guérin; CMI, Cell Mediated Immunity; EPI, Expanded Programme on Immunization; EPIC-HIPC, Expanded Programme on Immunization Consortium- Human Immune Project Consortium; HBV, Hepatitis B virus; HepB, Hepatitis B; HB-sAg, Hepatitis B Surface antigen; Anti-HBs, anti-Hepatitis B surface antigen; LSHTM, London School of Hygiene and Tropical Medicine; MRCG, Medical Research Council Unit The Gambia; PNG, Papua New Guinea; PNGIMR, Papua New Guinea Institute of Medical Research; WBA, Whole Blood Assay.

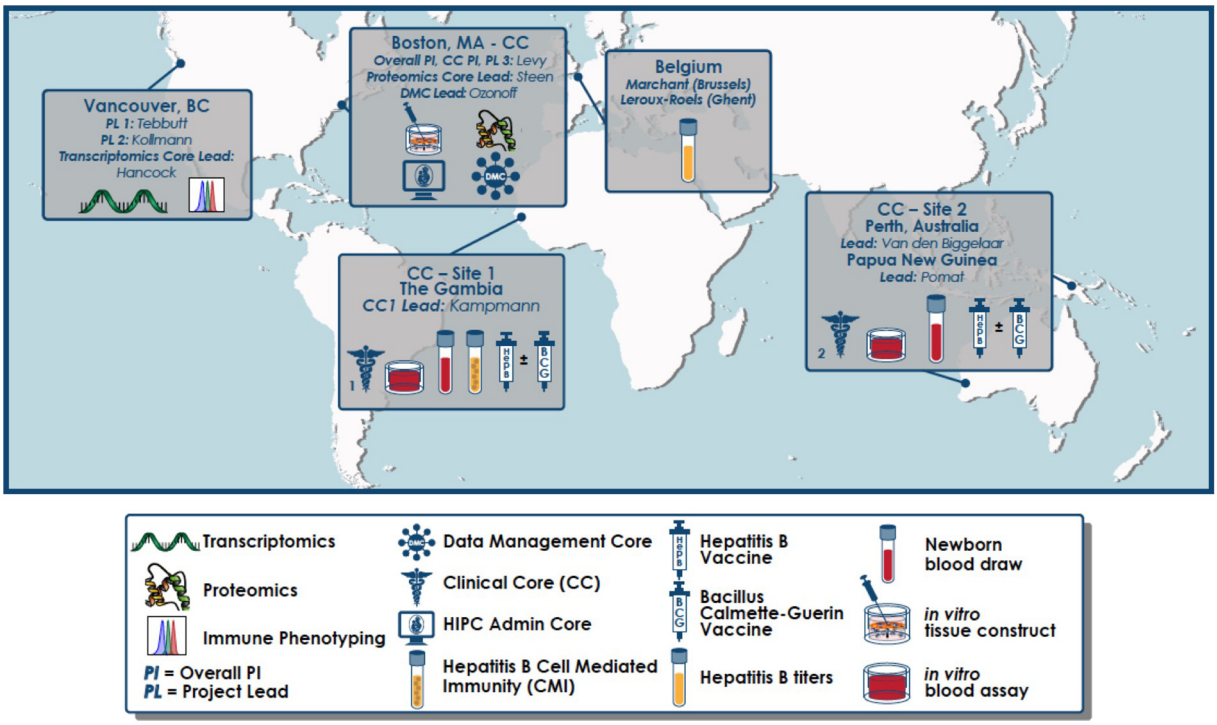

FIGURE 1 | Geographical distribution of partnering sites for the EPIC-002 study. An overarching administrative core, clinical core (CC), data management core (DMC), as well as an *in vitro* vaccine modeling project are based at Boston Children's Hospital (Boston, MA). Clinical Core Sites are located in The Gambia (West Africa) and Papua New Guinea (Australasia). End-point assays are conducted in The Gambia (whole blood assay and cell mediated immunity), PNG (whole blood assay), University of British Columbia (flow cytometry and RNASeq), BCH (multiplex cytokines/chemokines, plasma proteomics, *in vitro* modeling including WBA and tissue constructs) as well as the Center for Vaccinology (CEVAC; Ghent, Belgium; anti-hepatitis B surface antigen titres).

samples to obtain "OMIC" signatures (17). Based on the pilot data, the current EPIC research project will focus on the immunogenicity of Hepatitis B (HepB) vaccine for which a clear correlate of protection exists (i.e., anti-hepatitis B surface antigen antibody (Ab) titres) (18, 19). Cell mediated immunity (CMI) though not validated as a correlate of protection but which appears to play a role in long-term immunity (post-primary series titres of 10 mIU/ml or greater have been shown to correlate with the induction of memory T helper-and B-cell responses) (20), will also be assessed. In addition, we will examine if concomitant vaccination with Bacille Calmette Guérin (BCG) can modulate the response to HepB vaccine. Both vaccines are recommended for routine use at birth in these countries and in similar settings.

The HepB vaccine is safe, immunogenic and highly effective and is on the list of Expanded Programme on Immunization (EPI) recommended childhood vaccines. The first dose is recommended on the day of birth to prevent vertical and horizontal transmission of Hepatitis B virus (HBV) (18). The HepB vaccine has one of the best-characterized serologic correlates of protection (CoP), and is the only clear CoP for any neonatal vaccine (18). First described in The Gambia, this CoP is the lower limit of the peak Ab response measured >1 month after the primary series (3 or 4 doses), defined as an anti-Hepatitis B surface antigen (anti-HBs) Ab level of >10 mIU/mL (18, 19). Importantly, while an anti-HBs threshold of >10 mIU/ml represents the minimal level for protection from infection, a relationship exists in direct quantitative correlation between Ab level and duration of protection (i.e., the higher the anti-HBs titer the better and longer protection) (19). In addition, there is evidence to suggest that the higher the titer after the first dose of HepB vaccine, the higher the titer after the last dose, and persistence (18, 19). This implies that variability in response to the first dose (21) of HepB vaccine may predict long-term immunogenicity (18). Substantial quantitative inter-participant variation in absolute anti-HBs levels are the norm after each dose of HepB vaccine as with many other vaccines. Such inter-participant variability represents a key ingredient for meaningful analyses using a systems vaccinology approach (21).

The neonatal HepB vaccine immune response has been reported to be altered by co-administration of BCG, which is co-administered as part of the standard EPI, and likely to perturb the immune response to HepB vaccine *in vivo* (22, 23). Maternal antibodies to HepB have also been documented to impair the post vaccination immune response to HepB vaccine in newborns (18, 24, 25). The mechanisms that underlie HepB vaccine-induced immunogenicity in newborns, including Ab and CMI, are incompletely characterized particularly as it relates to variations in response.

Given the many advantages, HepB vaccine represents an ideal model in which to decipher what governs immunogenicity in

early life. Similar reasoning regarding HepB vaccine as a model for systems biology have led to deciphering of mechanisms relevant for the immune response in older adults (26). This project will study the systems biology responses of newborns receiving HepB vaccination with and without concomitant BCG vaccine compared to a group of infants receiving both vaccines later in the first week of life to allow us to observe any changes occurring over the first week of life as a result of immune ontogeny rather than induced by vaccination. *In vitro* tissue constructs will also be set up to model the *in vivo* responses and maternal antibodies will be assayed to enable correlation with the infant responses.

The ability to show a correlation between age-specific molecular patterns ("signatures") and vaccine-mediated protection (our main outcome measure) should accelerate the development and optimization of vaccines against childhood infections of major global health importance.

STUDY QUESTIONS, OBJECTIVES

The overall goal of the project is the characterization of vaccine-specific "OMIC" signatures that correlate with vaccine-type specific immunogenicity in human newborns.

The EPIC-002 study will characterize vaccine-induced "OMIC" signatures and their relationship to HepB vaccine CoP and characterization of the impact of BCG and maternal antibodies (MatAbs), thereby informing development of vaccines optimized for early life immunization.

Specific Objectives:

1. Measure adaptive immune responses to HepB vaccine, enabling correlation of *in vivo* "OMIC" signatures and *in vitro* vaccine Modeling assays with established correlates of protection.
2. Characterize the pre-vaccine "OMIC" and immune *in vivo* signatures that may predict immunogenicity of HepB vaccine in human newborns.
3. Characterize the impact of HepB vaccine with or without BCG on neonatal "OMIC" and immune *in vivo* signatures that predict immunogenicity of HepB vaccine.
4. Measure maternal antibodies (MatAbs) to HBV in relation to vaccine-induced neonatal and infant "OMIC" vaccine signatures and adaptive responses.
5. Interrogate functional correlations identified *in silico* using novel human *in vitro* platforms.
6. Validate identified "OMIC" signatures in a distinct and independent newborn cohort recruited from Papua New Guinea (PNG).

STUDY DESIGN

The program consists of two neonatal cohort studies. A longitudinal neonatal cohort study will be conducted in The Gambia with a total follow-up time of roughly 5 months that serves as the program's core study. Following completion and analysis of The Gambian study, a validation cohort study will be conducted in Papua New Guinea to validate the key findings of the Gambian study. The two studies will harmonize procedures and protocols.

Participants will be recruited within the first 24 h of life into one of four broad groups as detailed below to receive either HepB vaccine alone, BCG vaccine alone or both HepB and BCG vaccines at this time point. The fourth group will have the birth doses of vaccines deferred till a time point within the first week of life. All infants will receive the recommended birth dose of polio vaccine a maximum of 10 days post-vaccination depending on the group assignment.

Two mL of venous blood will be drawn from each participant at the point of recruitment to assess "OMIC" responses. Each participant will have a maximum of two blood draws within the first week of life. In the core cohort in The Gambia, infants will be randomized into three subgroups that will have the second blood sample collected at 1, 3, or 7 days following the initial sampling. The cohort in The Gambia therefore consists of 12 different groups (**Table 1**). For the PNG cohort, all infants will have the second blood draw on the same day of life: analysis of The Gambia cohort will inform whether this will be at day 1, 3, or 7 of life. Subsequent visits and blood draws are as detailed in the Clinical Cohort Table below (**Table 1**)

In vitro effects of the HepB vaccine and BCG vaccines will be studied in two *in vitro* assays using blood derived from the same study participants immunized *in vivo*: (a) whole blood assay (WBA) run at the recruitment sites on the day of sample collection and (b) in three-dimensional microphysiologic tissue constructs employing cryopreserved cord blood-derived mononuclear cells and plasma (27), enabling *in vitro* mechanistic interrogation of cellular and molecular signatures that correlate with anti-HepBsAg (anti-Hepatitis B surface antigen) titres *in vivo*.

Blood samples and rectal swabs for epigenetic and microbiome analysis will be collected and stored from participants in The Gambia. Maternal blood samples to enable correlation of maternal anti-HB Abs to infant responses will also be collected.

STUDY ANALYSIS PLAN

This study aim is to identify "OMIC" signatures that correlate with HepB vaccine responses, as assessed by anti-HB titer (a well-established CoP), by leveraging both pre- and post-vaccine transcriptomic, proteomic, metabolomic, and cellular profiles. Our intention is to apply both univariate and multivariate frameworks to identify either a ranked list of molecular features associated with anti-HB titer or subsets of the molecular features best able to predict anti-HB titer, respectively. We plan to derive signatures in three distinct groups of newborns (corresponding to the distinct vaccination schedules) and compare across groups to gain a better understanding of the molecular basis of adjuvantation of HepB vaccine with BCG (given before, after or simultaneously). We further plan to derive robust multi-"OMIC" signatures correlating with effective HepB immunization by integrating across all available "OMIC" datasets. These signatures will then be validated in a distinct and independent newborn

TABLE 1 | Clinical cohort table for infants recruited in The Gambia (discovery cohort) and Papua New Guinea (validation cohort).

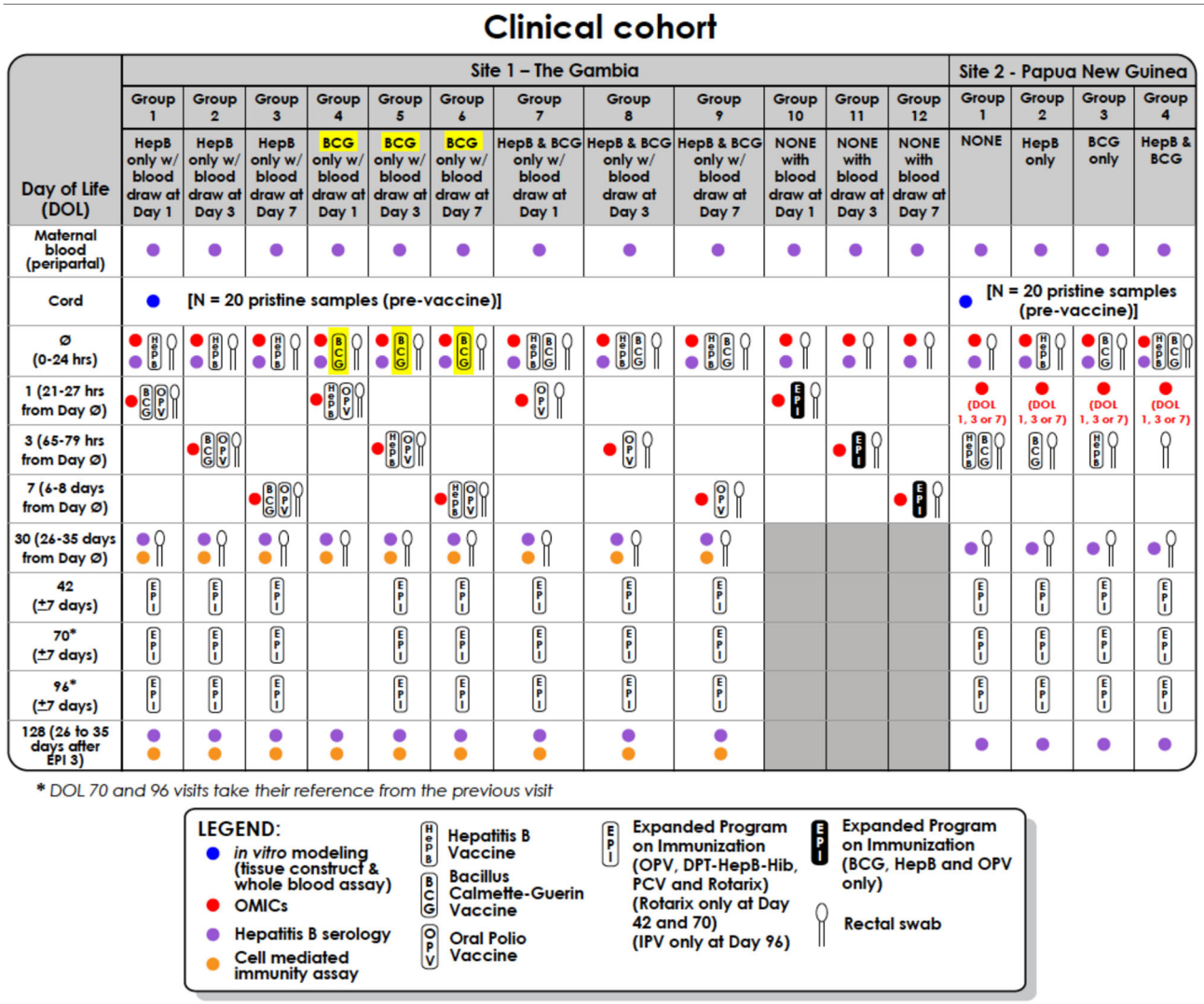

Table courtesy Kristin Johnson, Boston Children's Hospital.

cohort recruited from PNG. Finally, the correlations identified by these various *in silico* analyses will be tested using the novel human *in vitro* platforms.

We will apply these methods to define baseline cellular and molecular pathways/hubs/nodes that predict vaccine immunogenicity and assess specific signatures *in vitro* that provide insight into vaccine mechanisms of action (MOA).

SAMPLE SIZE/BIOSTATISTICAL CONSIDERATIONS

The cohort design included careful consideration of statistical power and sample size. Power calculations in the setting of traditional OMIC designs are well-documented (28) and we performed power calculations for OMIC platforms or flow cytometry based on preliminary data (unpublished data). Although we intended our tests of hypothesis to borrow strength across data types, little has been published on statistical power for integrative analyses or cross-platform comparisons, so this characteristic of our design was not taken into account when determining sample size. Power calculations were carried out using group sizes ranging between $n = 30$ or $n = 60$ per group, two-sided significance criterion (alpha) of 0.05, and a target 80% power to detect.

Since preliminary data for flow cytometry were not available, we performed a worst-case power analysis using a real-world published data on the most variable cell subpopulation where a significant difference was still identified comparing healthy, immunosuppressed, and transplant-tolerant individuals (29). This provided a lower bound of the minimum sample size required to detect a significant difference in cell sub-populations that could act as potential biomarkers. We found $n = 30$ would result in 80% power to detect a 2.3-fold difference in the relative abundance of a cell population, while $n = 60$ would result in 80% power to detect 1.8-fold difference, assuming a balanced design.

OMIC Analyses

We considered power to detect correlations between biomarker signals of any type and the CoP. We assumed approximate normality, after data transformation (e.g., log-transformation) and calculated detectable Pearson coefficients for samples using group size $n = 30$ or $n = 60$. We concluded that our design offered 80% power to detect correlations between continuous measures as small as $r = 0.25–0.48$. Additional parameters were included when carrying out power calculations for the transcriptomic analysis to account for variable coverage [e.g., read depth across biosamples using RNASeqPower v1.10 (28)]. Here we considered power to detect differentially abundant transcripts between two groups and estimated within-group standard deviation from preliminary data, as before. We found $n = 30$ would result in 80% power to detect a 2.4-fold difference in the relative abundance of a transcript, while $n = 60$ would result in 80% power to detect 1.4-fold difference, assuming a balanced design.

TRIAL REGISTRATION AND FUNDING

The study is registered on clinicaltrials.gov with registration number NCT03246230.

The study is funded primarily by a grant received from the U.S. National Institute of Health; Grant number U19AI118608. These funders are not involved in study design, collection, management or analysis and interpretation of data, or publication of output. Additional funding is provided by the *Precision Vaccines Program*, supported in part by the Department of Pediatrics and Chief Scientific Office of Boston Children's Hospital.

The study will be conducted according to Declaration of Helsinki International Conference Harmonization Good Clinical Practice (ICH-GCP) and local ethical guidelines. Internal governance SOP's will be followed, and study-specific procedures developed by the study team.

ETHICAL CONSIDERATIONS

Ethical approvals have been obtained for the core study in The Gambia from The Gambia Government/MRCG Joint Ethics Committee (Scientific Coordinating Committee number: 1513); for the validation study in PNG from the PNGIMR Institute Review Board (IRB number: 18.12) and the protocol has been approved by the PNG Medical Research Advisory Committee (IRB number 18.14). Ethical approval has also been obtained from the Boston Children's Hospital Institutional Review Board (IRB-P00024239).

PARTICIPANT SELECTION

Study Sites

In the Gambia, 720 mother-infant pairs (60 per group) will be recruited through delivery rooms at one secondary level care institution; The Kanifing General Hospital and one primary health facility; The Banjullinding Health Center in The Gambia. In PNG, 80 mother-infant pairs will be recruited at Goroka Hospital, the only tertiary hospital in the Eastern Highland Province of PNG. Maternal infant pairs will be recruited within the first 24 h of the infants' life.

Rationale for Selection of Participants

As infection is most prevalent in the newborn, the study will target this most vulnerable group to help improve our understanding of vaccine-induced cellular and molecular signatures associated with vaccine-induced correlate of protection i.e., anti-HBs Abs.

INFORMED CONSENT

Community Consent

Community consent will be sought prior to the commencement by providing information to individuals in the communities served by the participating health centers. Village heads and key opinion leaders in the communities will be engaged in large community meetings during which information regarding the study will be provided and opportunities given to ask questions, in line with previous practice at the MRCG and PNGIMR.

Individual Consent

Women presenting for antenatal care in the 2nd or 3rd trimester of pregnancy will be approached at the antenatal care clinic and given information regarding the study using a detailed informed consent document. Individuals expressing interest in participating will then be provided with a copy of the informed consent document (**Appendix**) to take home to discuss with their partners or other significant decision maker in the family. Opportunities will be given to ask questions including the provision of contact details to allow potential participants to reach members of the study team after the clinic visit. Follow-up contact will then be made with each potential participant to verify spousal assent, as male members of the family are typically key decision makers in this setting. In addition, families will be asked to confirm if other members of the household need to assent including grandparents of the child in question.

When the mother of the potential participant presents in labor or shortly following delivery, the consent signature will be obtained, and eligibility assessed. Written consent will be obtained from biological mothers of participants in each mother-infant pair only. The consent process will continue throughout the study with confirmation of willingness to continue participation at each contact.

FUTURE USE OF STORED SAMPLES

Written informed consent will also be sought for the future use of left-over biological samples for studies which would require approval by the relevant ethics committees.

INCLUSION/EXCLUSION CRITERIA

Maternal

Healthy women delivering at term will be recruited into the study. Inclusion and exclusion criteria are as detailed below.

Inclusion

Reported gestation of at least 37 weeks
Spontaneous vaginal delivery
Written informed consent.

Exclusion

Antibiotic use in the week prior to delivery
HIV or HepB positive—Rapid test done in labor or shortly after delivery
TB Diagnosis in mother or family member in the past 6 weeks
Severe intrapartum condition such as severe pre-eclampsia
Physicians assessment of high risk or previous contraindicative obstetric history such as multiple early neonatal deaths.

Infant

Healthy term newborns will be recruited into the study. Details of inclusion and exclusion criteria are as follows:

Inclusion

Healthy, term infant as determined by medical history, physical examination, and judgment of the study physician.
Weight of 2.5 kg or greater at the time of enrolment.

Exclusion

Previous vaccination with any EPI vaccine
Major known congenital malformation
Apgar score < 8 at 5th min.

Physician assessment of potential high-risk infant including significant risk factors for sepsis/morbidity (such as maternal symptoms suggestive of urinary tract infection in the peri-partal period), or macrosomia (birth weight above 4 kilograms).

RANDOMIZATION AND BLINDING

Following assessment of eligibility by the study physician, newborns will be randomly assigned to 1 of 12 groups in The Gambia (60 per group), and 1 of 4 groups in PNG (20 per group), using a computer-generated block randomization sequence. In The Gambia, the code will allow block randomization of 720 study participants into 12 groups, using random block sizes of 24 and 48. In PNG, block sizes of 8 will be used. Each study participant will be assigned sequential identification numbers (IDs) starting from 001 to 720 for The Gambia, and 1,001–1,080 in PNG. A check digit character will be augmented to each of these numbers to make up the participant IDs which will be generated using the Damm algorithm (https://en.wikipedia.org/wiki/Damm_algorithm; date accessed 08 November 2016). Here the check digit numbers 0–9 will be converted to letters A-H and J-K. The IDs for the Gambian cohort will be prefixed with the letter "G" which stands for Gambia. The randomization code will use the web application developed by the Statistics and Bioinformatics department at MRCG to generate the IDs including the check digit and prefix as detailed above (the app is available on https://stats.mrc.gm/chkdgt-id/). Randomization code for the PNG cohort will be generated at BCH using similar methods. Randomization groups will be printed on cards labeled with the participant identification number and allocated in the sequence in which the infants will be recruited. Cards will be sequentially allocated by clinical staff as participants are screened.

Due to the nature of randomized groups and difficulty of blinding to randomized vaccine groups, staff in direct contact with participants will be unblinded, while all laboratory staff at the sites will be blinded to participants assigned group throughout the study.

STUDY PROCEDURES

Cohort Overview

The cohort overview is detailed in **Table 1**.

Screening

Following the informed consent signature and pre-test counseling, a detailed medical and pregnancy history will be obtained from each eligible woman. Women will be screened for Human Immunodeficiency Virus (HIV)-I and -II and HB-sAg using rapid diagnostic tests. Individuals positive for any of these antigens will be excluded from the study, offered post-test counseling and referred for care as appropriate. It will be essential to exclude HB-sAg positive mothers to ensure that infants born to these mothers receive HepB vaccine at birth to minimize transmission risk as recommended by the World Health Organization (WHO). The study team will ensure receipt of this vaccine within 24 h of life for all infants whose mothers tested positive for HepB, but these infants will remain excluded from further study procedures. Similarly, infants born to HIV-positive mothers will be excluded and referred for further management. Inclusion of HIV-exposed or positive infants could impact on the biological signatures. Each newborn infant will then undergo a full newborn exam to rule out obvious congenital anomalies and other signs of ill health.

Enrolment

Eligible mother-infant pairs will be randomized to one of 12 or 4 groups in The Gambia and PNG cohorts, respectively, and study procedures carried out as detailed below.

Follow-Up

The mother's participation will end following this initial visit while the infant will be followed up longitudinally over a 5-months period as dictated by the study design detailed in **Table 1**.

Termination

Participation in the study will be completed 1 month after the primary infant series vaccination, corresponding to 1-month post the 4th dose of HepB vaccine, or following the week one follow-up visit for infants in the delayed vaccine group (Groups 10 to 12) in The Gambia. Participation in PNG will be complete after the second visit for PNG; **Table 1**).

Early Termination

Infants will exit the study prior to the above if consent is withdrawn; the study team can no longer reach the participant's caregiver and/or caregiver does not present for a visit at the clinic (lost to follow-up); the participant moves out of the study area; or the infant dies.

Discontinuation Criteria

Study participation could also be discontinued for individual participants if in the judgement of the investigator participation poses an additional risk to the participant other than the already anticipated minimal risk. The study could also be discontinued following assessment by the Ethics Committee that the study posed significant unacceptable risk to the participants based on safety signals.

Strategies to Enhance Retention

To enhance participant retention and adherence to follow-up schedule, a field calendar will be set up which automatically generates the follow-up schedule in REDCap [a browser-based, metadata-driven electronic data capture (EDC) software and workflow methodology for designing clinical and translational research databases (https://www.project-redcap.org)], following enrolment. Each participant will be assigned to a field worker on the day of enrolment. This individual will keep a record of the follow-up schedule in their logbook. In addition, daily follow-up calendars will be printed from REDCap by field supervisors to ensure a double check for follow-ups. As an additional check, the clinician will maintain a field diary on which visits can checked off as they occur. The responsible field worker will call the participant to remind him/her of the scheduled visit at least 24 h prior to the visit (first week of life visit) or the weekend prior to the scheduled visit and again 24 h prior to the visit (subsequent visits). Participants will be picked up by a study vehicle for the first week of life visits to ease logistics during a time when mother and infant will be recovering from the birth process. Participants will be encouraged to share travel plans with the responsible field worker as soon as possible to allow for rescheduling of visits.

Clinical/Laboratory Procedures

Blood Samples

The following samples will be collected as detailed in **Table 1**:

Two milliliters (ml) of blood will be collected at two time points within the first week of life, as described above. Immediately following blood draw into sodium heparinized tube (BD Vacutainer^{R}, Cat. No. 368884), 200 μl of blood will be pipetted into a tube containing 552 μl/ ucl of Paxgene ^{R} fluid (BD Biosciences, Cat. No. 762165) for RNA stabilization in preparation for later sequencing. The remaining sample will be transported to the laboratory within 4 hours of collection along with RNA sample. Whole blood will be centrifuged to separate plasma. Plasma will be separated into 4×100 μl aliquots for onward shipment to analytical laboratories. Homogeneity of plasma aliquots will be ensured by first separating the total volume, mixing using micro pipetting, and subsequently separated into respective aliquots. Next, 900 μl of 1:1 whole blood and RPMI Medium 1640-GlutaMAX^{TM}-I (Gibco^{R}, Cat. No. 72400-047) will be aliquoted for immunophenotyping using the SMARTube system. Lastly, the remaining blood will be pelleted to obtain white blood cell. All fractionated samples will be stored at −70°C while awaiting and during shipment to endpoint laboratories.

Two additional samples of 3 ml each will be collected 30 days following enrolment and at Day 128 post enrolment which corresponds to 28 days post the 4th dose of HBV to measure anti-HBs Ag; a cell mediated immunity (CMI) assay will also be conducted using these samples. All samples will be collected by drip method into commercial tubes heparinized with sodium heparin (BD vacutainers).

Cord blood samples will be collected from a random subset of participants determined by logistics; where the mother has signed consent prior to delivery of the placenta and the infant is subsequently found eligible for enrolment. A total of 20 pristine cord blood samples will be targeted for collection at each site.

Rectal Swabs

Rectal swabs will be collected at the first study visit (within 24 h of life) if the child has passed meconium, and subsequently during the second visit (24 h, 72 h, or 7 days post first study visit) and at Day 30 post-enrolment to enable exploration of the infant microbiome. The swabs (FLOQSwabs (Copan, Cat. No. 608CS01R) will be collected using standard swabs and placed directly in 1 ml of guanidine thiocyanate transport media. They will be stored at −70°C before and during transport to analytical laboratories.

Vaccinations

Infants will be randomized into 1 of 4 groups (each split into 3 further subgroups to reflect day of second blood sample collection in The Gambia), to receive vaccinations as detailed in **Table 1**. Although not routinely recommended in PNG, the infants at this site will also receive bivalent oral polio vaccine within the first week of life as part of our efforts to harmonize schedules.

All subsequent childhood vaccines will be given in line with the World Health Organization (WHO) recommended EPI schedule, including 13-valent pneumococcal conjugate vaccine, rotavirus vaccine, Pentavalent vaccine containing diphtheria, whole cell pertussis, tetanus toxoid, HepB and *Haemophilus influenzae* type b antigens, oral polio vaccine and inactivated polio vaccine, as detailed in **Table 1**. Of note, the routine schedule in The Gambia involves vaccinations at 2, 3, and 4 months of age beyond the birth doses (**Supplementary Table 1A**), while that of PNG is 1, 2, and 3 months (**Supplementary Table 1B**). In an effort to harmonize between the two study sites, the WHO schedule of 6, 10, and 14 weeks will be utilized at both sites, and the rotavirus vaccine (Rotarix), not routinely given in PNG, will be administered. While there is heterogeneity between vaccines formulations routinely used in the two countries, vaccines from the same manufacturers will be utilized for both sites. The routine EPI schedules for both countries are detailed in **Supplementary Tables 1A,B**.

The specific vaccines which will be utilized for the study are detailed in **Tables 2**, **3**.

Laboratory Assays

The following assays are planned on samples collected (**Supplementary Figure 1**):

TABLE 2 | Vaccines to be studied in EPIC-002.

Vaccine	Acronym	Source	Type	Route	Adjuvant
Hepatitis B vaccine	HepB vaccine	SIIL	Sub-unit	IM	Alum
DwPT-HepB-Hib (HepB component)	Pentavalent vaccine	SIIL	Killed/toxoid	IM	Aluminum phosphate
Bacille Calmette–Guérin	BCG	SIIL	Live	ID	Self-adjuvanted live attenuated vaccine

Ab, antibody; ID, intradermal; IM, intramuscular; EPI, WHO Expanded Programme on Immunization; DwPT-HepB-Hib, Diphtheria, whole cell pertussis, tetanus, Hepatitis B and Haemophilus influenza type b vaccine; SIIL, Serum institute of India Limited.

TABLE 3 | Other vaccines to be received during the EPIC-002 study.

Vaccine	Acronym	Source	Type	Route
Oral polio vaccine	OPV	SIIL	Killed	Oral
Inactivated polio vaccine	IPV	SIIL	Live	IM
13 -valent Pneumococcal Conjugate Vaccine	PCV13	Pfizer	Killed	IM
Rotavirus vaccine	Rotarix	GSK	Live	Oral

ID, intradermal; IM, intramuscular; EPI, WHO Expanded Programme on Immunization; SIIL, Serum Institute of India Ltd.; GSK, GlaxoSmithKline; IPV, Inactivated polio vaccine; OPV, Oral polio vaccine; PCV13, 13-vallent pneumococcal conjugate vaccine.

Transcriptomics

RNA Sequencing (RNASeq) at the University of British Columbia (UBC) Vancouver to assess the changes in gene expression in the blood samples collected within the first week of life.

Proteomics

Plasma samples will be subjected to nanospray liquid chromatography tandem mass spectrometry (LC-MS/MS) at Boston Children's Hospital (BCH) for protein identification and quantification by liquid chromatography mass spectrometry.

Flow cytometry

Flow cytometry will be run by UBC/TKI to analyze the changes in cell composition in the samples collected within the first week of life.

Basal plasma cytokines

Plasma samples will be analyzed utilizing multiplex cytokine assays to quantify cytokine and chemokine plasma concentrations across the first week of life using a custom multiplex kit (Milliplex MAP Kit: Human Cytokine/Chemokine Magnetic Bead Panel HCYTMAG60K-PX41) at BCH.

Cell mediated immunity (CMI)

Assays will be carried out at MRCG to assess the antigen-specific CD4 T-cell response following HepB and BCG vaccines for the Gambian cohort only.

In vitro modeling of vaccine responses using cord whole blood assays (WBAs; at MRCG and BCH) and microphysiologic tissue constructs (TCs) will be conducted at BCH.

Microbiome

Fecal (stool) microbiome composition and functional potential will be determined over the first month of life via 16S amplicon sequencing as well as metagenomics on selected samples to capture changes in association with vaccine responses.

Metabolomics

Plasma metabolomics will be analyzed using Metabolon's HD4 platform LC-MS/MS for identification of global plasma metabolites.

Epigenetics

To compare differential gene methylation patterns (epigenetics) following vaccination genome-wide changes in the epigenome will be assessed via the Infinitum Methylation EPIC bead array. The analytical laboratory for this assay is yet to be determined.

Sample Management

Sample management and tracking will use ItemTracker; a sample tracking and management system (http://www.itemtracker.com) to track samples from the point of collection to the analytic laboratories by scanning a sample-specific barcode which carries a unique sample identifier (visit ID).

SAFETY CONSIDERATIONS AND OVERSIGHT

Risks and Benefits

We recently reported major cellular and molecular changes which occur over the first week of life demonstrating a dynamic baseline (17). For this reason, we will have a delayed vaccination group in order to distinguish basic immune ontogeny signatures from vaccine-induced changes.

To minimize risks, we will carefully screen mothers and infants to avoid any risk for the infants included in the delayed vaccination group by the following measures: (a) only newborns to HB-sAg negative mothers will be included; (b) any women with history of tuberculosis (TB) or TB contact will be excluded; (c) BCG vaccination is recommended for any time before 3 months of age and infants within the delayed vaccination group will be vaccinated within 10 days of birth. There is indeed evidence to suggest that delayed BCG vaccination may actually be beneficial (30). The continued recommendation for birth doses of the vaccine is to ensure coverage and avoid missed opportunities for vaccination during contact with a health facility. Polio vaccine is recommended at birth in The Gambia and will be delayed by a maximum of 10 days for all infants in our cohort. This infection has not been diagnosed in The Gambia for over 20 years. The risk posed from this slight delay is therefore considered minimal.

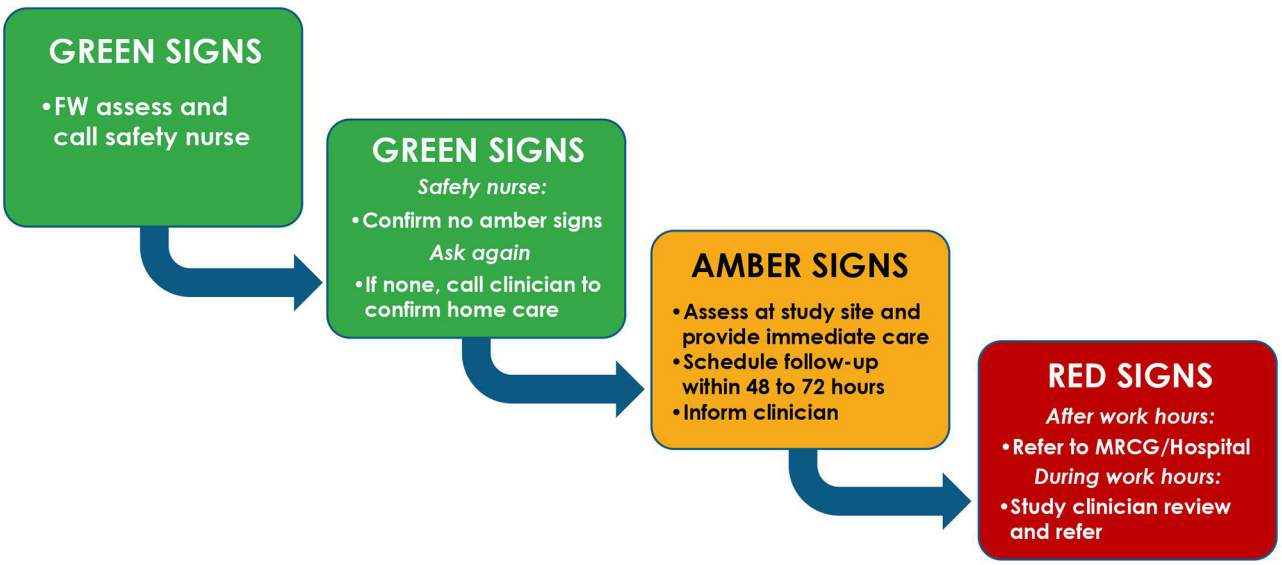

FIGURE 2 | Field algorithm for management of intercurrent illness during the EPIC-002 study. Green, amber and red signs are as defined in **Supplementary Table 2**. FW, Field worker.

Overall, the Ethics Committees have determined that the study to pose minimal risk to participants, consisting of transient pain when drawing blood and possibly mild discomfort during the rectal swab. Rare complications could include bleeding from or inflammation/infection of puncture sites.

There are no direct benefits for the individual participants other than access to care at the research facility allowing for closer surveillance and higher likelihood of detecting illness early. Participants excluded due to maternal HepB positivity will have the added benefit of accessing the HepB vaccine within 24 h after birth from the study team. Despite being recommended by WHO, this practice is not yet uniformly carried out in many low-income countries including The Gambia and PNG, and largely depends on whether the child is born during working hours vs. the weekend and/or late night. In addition, in The Gambia vaccinations given after the tradition of infant naming at the age of 7 days of age is a common local practice also contributing to delayed vaccinations in the real-life setting.

All costs related to medical care of participants will be covered by the study for the duration of the study. Institutional insurance for participants exists for all research projects conducted at the MRCG Unit. Sponsors cover insurance for study participants at the site in PNG.

Safety Oversight

Since the study infants are enrolled at an age at which they are particularly prone to illness, including infections, rigorous clinical oversight will be ensured. Oversight for participant safety will be provided by the lead study pediatrician with support from a local safety monitor—a pediatrician with experience caring for children at this age who could provide input as an independent party, in The Gambia, and a pediatrician affiliated with Goroka Hospital in PNG.

Field staff will conduct a home visit during the first week of life to evaluate for sick infants, such that all participants will have a total of 2 visits (home or clinic) prior to day 7 of life. Participants will also receive phone numbers at the point of enrolment to enable them reach study staff in the event of emergencies/concerns. Field staff trained to identify danger signs will utilize an escalation system where clinical signs are categorized into green (low risk), amber (intermediate risk), or red (high risk) as detailed in **Supplementary Table 2** and **Figure 2** to ensure prompt care for intercurrent illnesses.

DATA HANDLING, RECORDS, AND ANALYSIS PLATFORMS

In The Gambia, all data will be collected using electronic case report forms (CRFs) with built-in quality checks designed on REDCap except for consent forms and certified copies of medical records. Data capture using this platform could be done online or offline to allow entry in settings where internet access is suboptimal. In PNG, data will first be collected using paper CRFs before entry into an electronic REDCap database. Data will be prioritized into three Tiers: Tier-1 data considered essential to accomplish primary study objectives; Tier-2 data considered potentially useful for identifying confounders which might influence analysis of the primary study questions and to address secondary study questions; and Tier-3 data considered additional exploratory data. Data will be checked for congruency and completeness at the site and quality control (QC) checks

will be completed by data assistants and a data manager at MRCG and PNGIMR. Queries will be generated and resolved by responsible staff, following which data forms will be locked by delegated personnel to prevent inadvertent changes. This will be followed by data extraction prioritized from Tier-1 to−3, and data will be sent securely to the centralized Data Management Core (DMC) at BCH. Further quality assurance (QA) processes will be performed by the DMC and queries raised to allow resolution of discrepancies/clarify unclear details prior to data sharing across the project. Following this process for all tiers of data, the database will be locked, and data downloads will be restricted to read-only access.

The DMC will use an innovative operational structure for data curation and integrative analysis. The digital backbone of the DMC will leverage an institutional partnership with Amazon Web Services (AWS) to provide secure dedicated cloud-based access and computational tools to research programs based at BCH. This will allow for controlled and timely updates of key infrastructure components, resources, and policies.

CONFIDENTIALITY

All electronic data capture will be performed using secure password-protected encrypted devices. Papers records including consent forms, and medical records will be stored in locked cabinets in secure locations with restricted access at the study sites.

QUALITY CONTROL AND QUALITY ASSURANCE

Written Standard Operating Procedures (SOPs) and Study Specific Procedures (SSPs) will be developed and implemented for each activity. Staff engaged in the activity will be trained to carry out the specific procedure in accordance with the written SOPs and SSPs. Copies of these procedures will then be provided to each staff member for reference and additional copies will be located at each study site for ease of reference.

A number of general QC and QA measures will be observed for the study including: (a) having study staff work in pairs and cross check one another's procedures and entries, including checking all procedures and entries before marking as complete; (b) having senior team members validate procedures and entries carried out by junior members and conduct spot checks for ongoing work of junior team members; (c) disallowing any blank fields on completed forms to ensure that where data is not available this is clearly documented and not just an omission in entry; and (d) requiring transmittal logs for materials/samples transported from one location to another to ensure that these can be tracked to their current location at all times.

Laboratory Quality Control Measures

Controls and standards will be run for each assay. In addition, to minimize batch effects related to laboratory assays, additional Universal Reference Standard (URS) samples will be included with each batch of samples to allow comparison or data normalization to minimize potential run-to-run or plate-to-plate variation. As a further measure to reduce batch effects and mitigate potential confounding of these effects across platforms, sample batches for all "OMIC" platforms will be aligned with the study block randomization as follows:

- Each sample batch will include two study visits per study participant to minimize variation across time points;
- Sample batches will be generated and assigned using 48 or 96 samples (i.e., 24–48 participants over two visits) per block, with equal representation of each of the 12 vaccine sub-groups within each sample batch;
- Each assay team will predefine criteria for quality control of each experimental sample and assay to ensure data quality.

The overall approach will be to have each endpoint laboratory define its own quality control (QC) procedures with additional quality assurance (QA) performed by the centralized Data Management Core at BCH.

DISSEMINATION POLICY

All data will be uploaded to public repositories such as NIAID ImmPort, https://immport.org and Gene Expression Omnibus (GEO) and will be publicly available following submission of study output for publication.

Study output will be published by the study team adhering to IJMCE authorship criteria in peer reviewed journals. Results will be disseminated at conferences and stakeholder meetings.

Community feedback will be undertaken to disseminate study results to participating communities.

AUTHOR'S NOTE

This protocol has been prepared in keeping with SPIRIT guidance.

AUTHOR CONTRIBUTIONS

OL, TK, and BK conceived the study. OL, TK, BK, RH, HS, RB, PR, ST, and AO developed study design. OI and AB developed protocol draft and contributed to study design. OI, OL, TK, BK, CS, KS, AB, and AO development of protocol content. OI and BK provide clinical oversight and developed site clinical protocols and procedures. All authors critical review of protocol content and review of final draft.

FUNDING

This study was funded primarily by a grant received from the U.S. National Institute of Health; Grant number: NIAID U19AI118608. These funders are not involved in study design, collection, management or analysis and interpretation of data, or publication of output. Additional funding is provided by the Precision Vaccines Program, supported in part by the

Department of Pediatrics and Chief Scientific Office of Boston Children's Hospital.

ACKNOWLEDGMENTS

The authors acknowledge the study communities and staff of the study sites involved in preparing the sites. Authors also acknowledge all members of the EPIC Consortium and Kristin Johnson of Boston Children's Hospital for graphical support with **Table 1**, and **Figures 1** and **2**.

SUPPLEMENTARY MATERIAL

The Supplementary Material for this article can be found online at: https://www.frontiersin.org/articles/10.3389/fped.2020.00197/full#supplementary-material

REFERENCES

1. United Nations InterAgency Group on Child Mortality Estimation. *Levels and Trends in Child Mortality* (2017).
2. Global Burden of Disease. Global, regional, and national age-sex specific mortality for 264 causes of death, 1980-2016: a systematic analysis for the Global Burden of Disease Study 2016. *Lancet.* (2017). 390:1151–210. doi: 10.1016/S0140-6736(17)32152-9
3. Duclos P, Okwo-Bele JM, Gacic-Dobo M, Cherian T. Global immunization: status, progress, challenges and future. *BMC Int Health Hum Rights.* (2009) 9 (Suppl. 1):S2. doi: 10.1186/1472-698X-9-S1-S2
4. Ozawa S, Stack ML. Public trust and vaccine acceptance–international perspectives. *Hum Vaccin Immunother.* (2013) 9:1774–8. doi: 10.4161/hv.24961
5. Idoko OT, Kochhar S, Agbenyega TE, Ogutu B, Ota MO. Impact, challenges, and future projections of vaccine trials in Africa. *Am J Trop Med Hyg.* (2013) 88:414–9. doi: 10.4269/ajtmh.12-0576
6. Ozawa S, Clark S, Portnoy A, Grewal S, Stack ML, Sinha A, et al. Estimated economic impact of vaccinations in 73 low- and middle-income countries, 2001-2020. *Bull World Health Organ.* (2017) 95:629–38. doi: 10.2471/BLT.16.178475
7. Delany I, Rappuoli R, De Gregorio E. Vaccines for the 21st century. *EMBO Mol Med.* (2014) 6:708–20. doi: 10.1002/emmm.201403876
8. Birn AE. Small(pox) success? *Cien Saude Colet.* (2011) 16:591–7. doi: 10.1590/S1413-81232011000200022
9. Okwo-Bele JM, Cherian T. The expanded programme on immunization: a lasting legacy of smallpox eradication. *Vaccine.* (2011) 29 (Suppl. 4):D74–9. doi: 10.1016/j.vaccine.2012.01.080
10. Henderson DA. The eradication of smallpox–an overview of the past, present, and future. *Vaccine.* (2011). 29 (Suppl. 4):D7–9. doi: 10.1016/j.vaccine.2011.06.080
11. Bagcchi S. Polio endgame: overcoming the final barriers. *Lancet Infect Dis.* (2016). 16:644. doi: 10.1016/S1473-3099(16)30093-7
12. Garon J, Seib K, Orenstein WA, Ramirez Gonzalez A, Chang Blanc D, Zaffran M, et al. Polio endgame: the global switch from tOPV to bOPV. *Expert Rev Vaccines.* (2016) 15:693–708. doi: 10.1586/14760584.2016.1140041
13. Patel M, Menning L, Bhatnagar P. Polio eradication and endgame plan - victory within grasp. *Indian Pediatr.* (2016) 53 (Suppl. 1):S28–32.
14. Kollmann TR, Kampmann B, Mazmanian SK, Marchant A, Levy O. Protecting the newborn and young infant from infectious diseases: lessons from immune ontogeny. *Immunity.* (2017) 46:350–63. doi: 10.1016/j.immuni.2017.03.009
15. Hagan T, Pulendran B. Will systems biology deliver its promise and contribute to the development of new or improved vaccines? From data to understanding through systems biology. *Cold Spring Harb Perspect Biol.* (2018) 10:a028894. doi: 10.1101/cshperspect.a028894
16. Amenyogbe N, Levy O, Kollmann TR. Systems vaccinology: a promise for the young and the poor. *Philos Trans R Soc Lond B Biol Sci.* (2015) 370. doi: 10.1098/rstb.2014.0340
17. Lee AH, Shannon CP, Amenyogbe N, Bennike TB, Diray-Arce J, Idoko OT, et al. Dynamic molecular changes during the first week of human life follow a robust developmental trajectory. *Nat Commun.* (2019) 10:1092. doi: 10.1038/s41467-019-08794-x
18. Schillie SF, Murphy TV. Seroprotection after recombinant hepatitis B vaccination among newborn infants: a review. *Vaccine.* (2013) 31:2506–16. doi: 10.1016/j.vaccine.2012.12.012
19. Jack AD, Hall AJ, Maine N, Mendy M, Whittle HC. What level of hepatitis B antibody is protective? *J Infect Dis.* (1999) 179:489–92. doi: 10.1086/314578
20. Stubbe M, Vanderheyde N, Goldman M, Marchant A. Antigen-specific central memory CD4+ T lymphocytes produce multiple cytokines and proliferate *in vivo* in humans. *J Immunol.* (2006) 177:8185–90. doi: 10.4049/jimmunol.177.11.8185
21. Tsang JS. Utilizing population variation, vaccination, and systems biology to study human immunology. *Trends Immunol.* (2015). 36:479–93. doi: 10.1016/j.it.2015.06.005
22. Ota MO, Vekemans J, Schlegel-Haueter SE, Fielding K, Sanneh M, Kidd M, et al. Influence of *Mycobacterium bovis* bacillus calmette-guerin on antibody and cytokine responses to human neonatal vaccination. *J Immunol.* (2002) 168:919–25. doi: 10.4049/jimmunol.168.2.919
23. Ritz N, Mui M, Balloch A, Curtis N. Non-specific effect of Bacille Calmette-Guerin vaccine on the immune response to routine immunisations. *Vaccine.* (2013) 31:3098–103. doi: 10.1016/j.vaccine.2013.03.059
24. Hu Y, Wu Q, Xu B, Zhou Z, Wang Z, Zhou YH. Influence of maternal antibody against hepatitis B surface antigen on active immune response to hepatitis B vaccine in infants. *Vaccine.* (2008) 26:6064–7. doi: 10.1016/j.vaccine.2008.09.014
25. Van Herck K, Van Damme P. Benefits of early hepatitis B immunization programs for newborns and infants. *Pediatr Infect Dis J.* (2008) 27:861–9. doi: 10.1097/INF.0b013e318173966f
26. Fourati S, Cristescu R, Loboda A, Talla A, Filali A, Railkar R, et al. Pre-vaccination inflammation and B-cell signalling predict age-related hyporesponse to hepatitis B vaccination. *Nat Commun.* (2016) 7:10369. doi: 10.1038/ncomms10369
27. Sanchez-Schmitz G, Stevens CR, Bettencourt IA, Flynn PJ, Schmitz-Abe K, Metser G, et al. Microphysiologic human tissue constructs reproduce autologous age-specific BCG and HBV primary immunization *in vitro*. *Front Immunol.* (2018) 9:2634. doi: 10.3389/fimmu.2018.02634
28. Hart SN, Therneau TM, Zhang Y, Poland GA, Kocher JP. Calculating sample size estimates for RNA sequencing data. *J Comput Biol.* (2013) 20:970–8. doi: 10.1089/cmb.2012.0283
29. Newell KA, Asare A, Kirk AD, Gisler TD, Bourcier K, Suthanthiran M, et al. Identification of a B cell signature associated with renal transplant tolerance in humans. *J Clin Invest.* (2010) 120:1836–47. doi: 10.1172/JCI39933
30. Kagina BM, Abel B, Bowmaker M, Scriba TJ, Gelderbloem S, Smit E, et al. Delaying BCG vaccination from birth to 10 weeks of age may result in an enhanced memory CD4 T cell response. *Vaccine.* (2009) 27:5488–95. doi: 10.1016/j.vaccine.2009.06.103

Conflict of Interest: The authors declare that the research was conducted in the absence of any commercial or financial relationships that could be construed as a potential conflict of interest.

APPENDICES

1. Informed consent document version 3.1 of 16 Feb 2018 (MRCG) and version 1.0 of 19 September 2018 (PNG)
2. Algorithm for identifying danger signs among study participants adapted from National Institute for Health and Care Excellence (NICE) guideline.
3. Routine EPI schedule for The Gambia and PNG
4. Sample processing flow chart

In addition to the named authors on the title page, The EPIC Consortium includes:
Alec Plotkin, Amrit Singh, Amy Lee, Arnaud Marchant, Asimenia Angelidou, Benoit Fatou, Bhav Dillon, Bianca Dy, Bing Cai, Daniel He, Danny Harbeson, David Ferrari, Diana Vo, Ebrima Trawally, Adam Jeng-Barry, Modou L. Fofana, AruKumba Baldeh, Joseph Kanu, Elena Morrochi, Fatoumatta Cole, Fatoumatta Ceesay, Frederic Clement, Geert Leroux-Roels, Geraldine Masiria, Gerard Saleu, Giulia Conti, Jensen Pak, John-Paul Matlam, Ken Kraft, Kim-Anh Le Cao, Maren Smith, Matthew Pettengill, Mehrnoush Malek, Mitch Cooney, Njilan Johnson, Rebecca Ford, Reza Falsafi, Sam Hinshaw, Sarah Javati, Sebastiano Montante, Shun Rao, Sofia Vignolo, Susan Farmer, Travis Blikie, Tue B. Bennike, Wendy Kirarock, Erin E. Gill, Shun Rao, Miriam Wathuo, Zaineb Wurie.

frontiers in Pediatrics

CORRECTION
published: 17 November 2020
doi: 10.3389/fped.2020.610461

Corrigendum: Clinical Protocol for a Longitudinal Cohort Study Employing Systems Biology to Identify Markers of Vaccine Immunogenicity in Newborn Infants in The Gambia and Papua New Guinea

Olubukola T. Idoko[1,2,3,4], Kinga K. Smolen[2,5], Oghenebrume Wariri[1], Abdulazeez Imam[1], Casey P. Shannon[6], Tida Dibassey[1], Joann Diray-Arce[2,5], Alansana Darboe[1], Julia Strandmark[1], Rym Ben-Othman[7], Oludare A. Odumade[2,4,8], Kerry McEnaney[2,9], Nelly Amenyogbe[10], William S. Pomat[11], Simon van Haren[2,5], Guzmán Sanchez-Schmitz[2,5], Ryan R. Brinkman[12,13], Hanno Steen[2,5,14], Robert E. W. Hancock[15], Scott J. Tebbutt[6,16,17], Peter C. Richmond[10,18], Anita H. J. van den Biggelaar[10], Tobias R. Kollmann[10†], Ofer Levy[2,5,19*†], Al Ozonoff[2,5†], Beate Kampmann[1,4*†] and on behalf of The EPIC Consortium*

[1] Vaccines and Immunity Theme, Medical Research Council Unit the Gambia at London School of Hygiene and Tropical Medicine, Fajara, Gambia, [2] Precision Vaccines Program, Division of Infectious Diseases, Boston Children's Hospital, Boston, MA, United States, [3] CIH LMU Center for International Health, Medical Center of the University of Munich (LMU), Munich, Germany, [4] The Vaccine Centre, London School of Hygiene and Tropical Medicine, London, United Kingdom, [5] Harvard Medical School, Boston, MA, United States, [6] PROOF Centre of Excellence, Vancouver, BC, Canada, [7] Department of Pediatrics, BC Children's Hospital, University of British Columbia, Vancouver, BC, Canada, [8] Division of Medicine Critical Care, Harvard Medical School, Boston Children's Hospital, Boston, MA, United States, [9] Department of Cardiology, Boston Children's Hospital, Boston, MA, United States, [10] Wesfarmers Centre of Vaccines and Infectious Diseases, Telethon Kids Institute, University of Western Australia, Nedlands, WA, Australia, [11] Papua New Guinea Institute of Medical Research, Goroka, Papua New Guinea, [12] BC Cancer Agency, Vancouver, BC, Canada, [13] Department of Medical Genetics, University of British Columbia, Vancouver, BC, Canada, [14] Department of Pathology, Boston Children's Hospital, Boston, MA, United States, [15] Department of Microbiology & Immunology, University of British Columbia, Vancouver, BC, Canada, [16] Centre for Heart Lung Innovation, University of British Columbia, Vancouver, BC, Canada, [17] Division of Respiratory Medicine, Department of Medicine, UBC, Vancouver, BC, Canada, [18] Division of Pediatrics, School of Medicine, Perth Children's Hospital, University of Western Australia, Nedlands, WA, Australia, [19] Broad Institute of MIT & Harvard, Cambridge, MA, United States

Keywords: markers, newborn, vaccine, immunogenicity, systems biology, OMICS

OPEN ACCESS

Approved by:
Frontiers Editorial Office, Frontiers Media SA, Switzerland

****Correspondence:***
Olubukola T. Idoko
bukkyidoko@gmail.com;
Olubukola.Idoko@lshtm.ac.uk
Ofer Levy
ofer.levy@childrens.harvard.edu
Beate Kampmann
bkampmann@mrc.gm

† These authors have contributed equally to this work and shares senior authorship

Specialty section:
This article was submitted to Pediatric Immunology, a section of the journal Frontiers in Pediatrics

Received: *25 September 2020*
Accepted: *28 September 2020*
Published: *17 November 2020*

Citation:
Idoko OT, Smolen KK, Wariri O, Imam A, Shannon CP, Dibassey T, Diray-Arce J, Darboe A, Strandmark J, Ben-Othman R, Odumade OA, McEnaney K, Amenyogbe N, Pomat WS, van Haren S, Sanchez-Schmitz G, Brinkman RR, Steen H, Hancock REW, Tebbutt SJ, Richmond PC, van den Biggelaar AHJ, Kollmann TR, Levy O, Ozonoff A and Kampmann B (2020) Corrigendum: Clinical Protocol for a Longitudinal Cohort Study Employing Systems Biology to Identify Markers of Vaccine Immunogenicity in Newborn Infants in The Gambia and Papua New Guinea. Front. Pediatr. 8:610461. doi: 10.3389/fped.2020.610461

A Corrigendum on

Clinical Protocol for a Longitudinal Cohort Study Employing Systems Biology to Identify Markers of Vaccine Immunogenicity in Newborn Infants in The Gambia and Papua New Guinea

by Idoko, O. T., Smolen, K. K., Wariri, O., Imam, A., Shannon, C. P., Dibassey, T., et al. (2020). Front. Pediatr. 8:197. doi: 10.3389/fped.2020.00197

In the original article, there was an omission in the legend for **Figure 2** as published. **"FW" in the figure stands for Field worker.** The correct legend appears below.

Figure 2 | Field algorithm for management of intercurrent illness during the EPIC-002 study. Green, amber and red signs are as defined in Supplementary Table 2. FW, Field worker.

TABLE 1 | Clinical cohort table for infants recruited in The Gambia (discovery cohort) and Papua New Guinea (validation cohort).

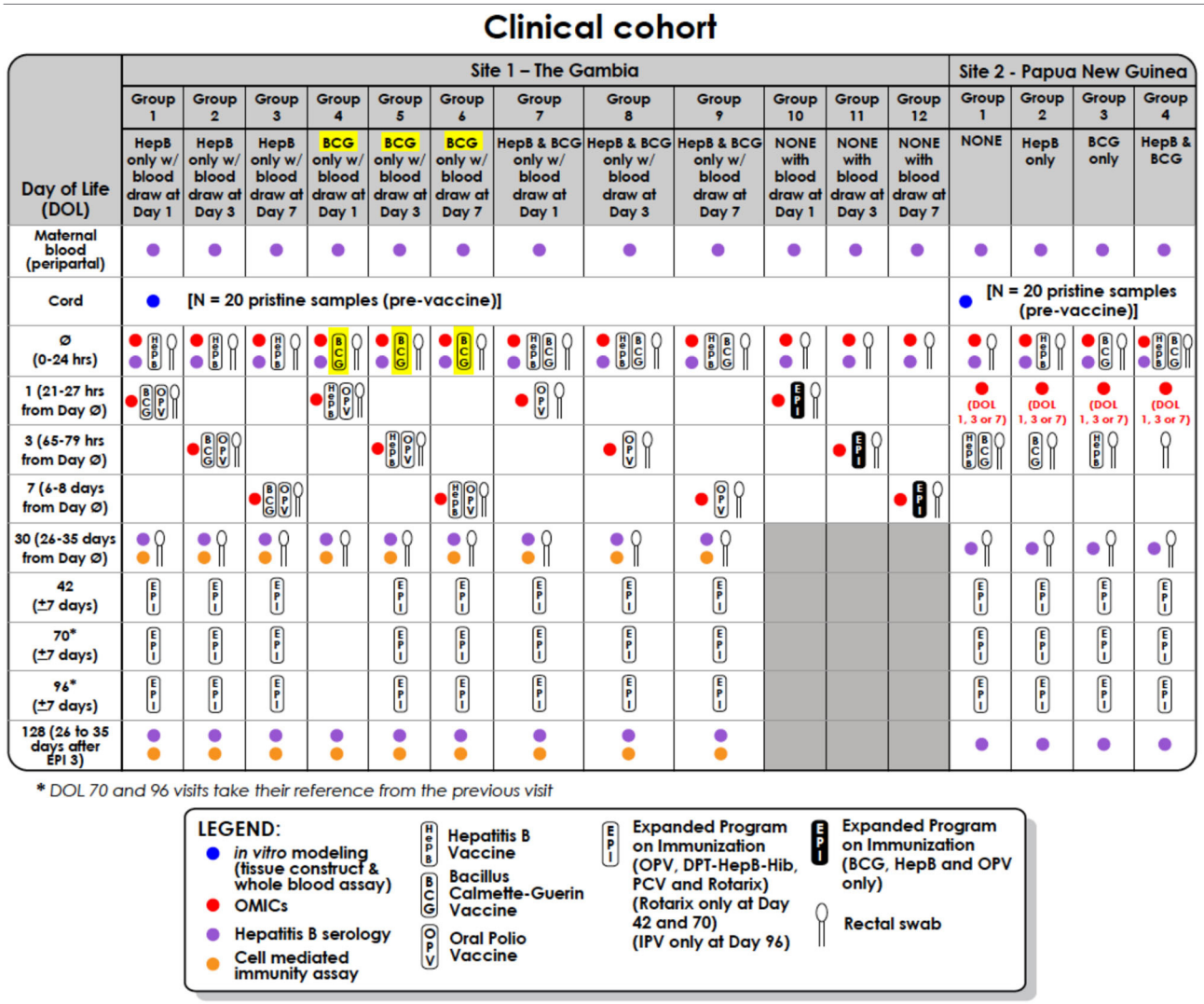

In the original article, there was a mistake in **Table 1** as published. Column headings below groups 4, 5, and 6 should read BCG and not HepB. The corrected **Table 1** appears above.

The authors apologize for this error and state that this does not change the scientific conclusions of the article in any way. The original article has been updated.

frontiers in Immunology

ORIGINAL RESEARCH
published: 07 May 2020
doi: 10.3389/fimmu.2020.00803

Intrapulmonary (i.pulmon.) Pull Immunization With the Tuberculosis Subunit Vaccine Candidate H56/CAF01 After Intramuscular (i.m.) Priming Elicits a Distinct Innate Myeloid Response and Activation of Antigen-Presenting Cells Than i.m. or i.pulmon. Prime Immunization Alone

Aneesh Thakur[1], Fernanda Endringer Pinto[2], Harald Severin Hansen[3], Peter Andersen[4], Dennis Christensen[4], Christian Janfelt[1] and Camilla Foged[1]*

[1] Department of Pharmacy, Faculty of Health and Medical Sciences, University of Copenhagen, Copenhagen, Denmark, [2] Department of Chemistry, Federal University of Espírito Santo, Vitoria, Brazil, [3] Department of Drug Design and Pharmacology, Faculty of Health and Medical Sciences, University of Copenhagen, Copenhagen, Denmark, [4] Department of Infectious Disease Immunology, Statens Serum Institut, Copenhagen, Denmark

OPEN ACCESS

Edited by:
Jay Evans,
University of Montana, United States

Reviewed by:
Elizabeth B. Norton,
Tulane University, United States
David J. Dowling,
Boston Children's Hospital,
United States

***Correspondence:**
Aneesh Thakur
aneesh.thakur@sund.ku.dk

Specialty section:
This article was submitted to Vaccines and Molecular Therapeutics, a section of the journal Frontiers in Immunology

Received: 11 November 2019
Accepted: 08 April 2020
Published: 07 May 2020

Citation:
Thakur A, Pinto FE, Hansen HS, Andersen P, Christensen D, Janfelt C and Foged C (2020) Intrapulmonary (i.pulmon.) Pull Immunization With the Tuberculosis Subunit Vaccine Candidate H56/CAF01 After Intramuscular (i.m.) Priming Elicits a Distinct Innate Myeloid Response and Activation of Antigen-Presenting Cells Than i.m. or i.pulmon. Prime Immunization Alone. Front. Immunol. 11:803. doi: 10.3389/fimmu.2020.00803

Understanding the *in vivo* fate of vaccine antigens and adjuvants and their safety is crucial for the rational design of mucosal subunit vaccines. Prime and pull vaccination using the T helper 17-inducing adjuvant CAF01 administered parenterally and mucosally, respectively, has previously been suggested as a promising strategy to redirect immunity to mucosal tissues. Recently, we reported a promising tuberculosis (TB) vaccination strategy comprising of parenteral priming followed by intrapulmonary (i.pulmon.) mucosal pull immunization with the TB subunit vaccine candidate H56/CAF01, which resulted in the induction of lung-localized, H56-specific T cells and systemic as well as lung mucosal IgA responses. Here, we investigate the uptake of H56/CAF01 by mucosal and systemic innate myeloid cells, antigen-presenting cells (APCs), lung epithelial cells and endothelial cells in mice after parenteral prime combined with i.pulmon. pull immunization, and after parenteral or i.pulmon. prime immunization alone. We find that i.pulmon. pull immunization of mice with H56/CAF01, which are parenterally primed with H56/CAF01, substantially enhances vaccine uptake and presentation by pulmonary and splenic APCs, pulmonary endothelial cells and type I epithelial cells and induces stronger activation of dendritic cells in the lung-draining lymph nodes, compared with parenteral immunization alone, which suggests activation of both innate and memory responses. Using mass spectrometry imaging of lipid biomarkers, we further show that (i) airway mucosal immunization with H56/CAF01 neither induces apparent local tissue damage nor inflammation in the lungs, and (ii) the presence of CAF01 is accompanied by evidence of an altered phagocytic activity in alveolar macrophages, evident from

co-localization of CAF01 with the biomarker bis(monoacylglycero)phosphate, which is expressed in the late endosomes and lysosomes of phagocytosing macrophages. Hence, our data demonstrate that innate myeloid responses differ after one and two immunizations, respectively, and the priming route and boosting route individually affect this outcome. These findings may have important implications for the design of mucosal vaccines intended for safe administration in the airways.

Keywords: H56/CAF01, tuberculosis, subunit vaccine, pulmonary administration, myeloid cells, antigen-presenting cells, mass spectrometry imaging, drug delivery

INTRODUCTION

Tuberculosis (TB) is one of the top 10 causes of death worldwide, and the disease killed an estimated 1.3 million people in 2017 (1). Approximately one fourth of the world's population is latently infected with *Mycobacterium tuberculosis* (*Mtb*), and these individuals remain susceptible to active TB for the rest of their life (1). With the emergence of multi-drug resistant *Mtb* strains, a novel vaccine, which is more effective than the currently available Bacillus Calmette-Guérin (BCG) vaccine, is required to achieve the World Health Organization's important goal of ending the global TB epidemic by 2035 (2). In this respect, mucosal delivery via intrapulmonary (i.pulmon.) administration of subunit vaccines having excellent safety profiles (3, 4) is a promising strategy to induce protective lung-localized *Mtb*-specific T-cell responses (5). However, little is known about the *in vivo* fate of inhaled vaccine antigens and adjuvants, and their safety.

Innate myeloid cells include mononuclear phagocytes, monocytes, dendritic cells (DCs), and granulocytes. These cells play essential roles in pathogen clearance, initiation, regulation and resolution of inflammation, and antigen presentation (6, 7). Following repeated immunizations, i.e., prime – pull immunization strategies, there is a continuous cross-talk between innate and adaptive immune cells and vaccine components. Hence, knowledge about these events is crucial to improve the immunogenicity, protective efficacy and safety of vaccines. Recent advances in the understanding of the diversity of myeloid and non-myeloid antigen-presenting cells (APCs) clearly suggest that for vaccines to induce specific immune profiles, they should be targeted to immune cell subsets capable of inducing that specific type of immune response (8, 9). For different subunit vaccines administered i.pulmon., inconsistencies exist in the immune responses they induce, and these differences may be due to factors like (i) the diversified localization of different APC subsets in the respiratory tract and the lung-draining lymph nodes (LNs), (ii) their functional differences, (iii) the size of the antigen, and (iv) the physicochemical properties of the adjuvant (10–13). Therefore, an understanding of the initial interactions taking place between the vaccine [antigen(s) and adjuvant] and the immune system is crucial for the rational design of safe vaccines, which have the capability to induce long-lasting protective immunity in the lungs (14).

The subunit vaccine antigen H56 is a fusion protein composed of the *Mtb* antigens Ag85B, ESAT-6, and Rv2660c, and in combination with the cationic adjuvant formulation 01 (CAF01) administered parenterally, this antigen elicits a polyfunctional Th1/Th17 $CD4^+$ T cell response and causes a significant reduction in *Mtb* burden (15–17). CAF01 is composed of cationic liposomes based on the surfactant dimethyldioctadecylammonium (DDA) bromide and the glycolipid trehalose-6,6'-dibehenate (TDB) (18). CAF01 delivers antigen and activates DCs (19), induces both humoral and cell-mediated memory immune responses, and it has been tested in phase I clinical trials, demonstrating an excellent safety and immunogenicity profile (20–22). Our recent data suggests that a parenteral prime – mucosal pull immunization strategy using CAF01 can be applied to redirect immunity to mucosal tissues (23). Recently, we reported an immunization strategy comprising intramuscular (i.m.) priming followed by i.pulmon. mucosal pull immunization with the H56/CAF01 vaccine, which resulted in the induction of lung-localized, H56-specific T cells and systemic as well as lung mucosal IgA responses (24). However, the role of (i) H56/CAF01 deposition within lung tissue, (ii) CAF01 internalization by phagocytic cells, and (iii) antigen presentation in the lungs and the lung-draining LNs on the induction of immune responses after pulmonary administration are unknown. In addition, an outstanding research question is the safety of CAF01 upon pulmonary administration.

Here, we applied multicolor flow cytometry to investigate H56/CAF01 uptake by innate myeloid cells and APCs in the lungs, the spleen, and the lung-draining LNs in mice after i.m. or i.pulmon. prime or i.m. prime – i.pulmon. pull immunization. We compared homologous prime – pull immunization with prime immunization alone to examine if pre-existing systemic H56-specific immunity induced by H56/CAF01 leads to different safety issues as compared to pulmonary prime immunization alone. We did not include mucosal prime – boost immunization as previous studies have showed no overt immunological advantage applying this immunization strategy (25). Mass spectrometry imaging (MSI) was used to follow the time-dependent biodistribution of CAF01 and selected lipid biomarkers in lung tissue.

MATERIALS AND METHODS

Materials

Dimethyldioctadecylammonium was obtained from Avanti Polar Lipids (Alabaster, AL, United States). TDB was purchased from Niels Clauson-Kaas A/S (Farum, Denmark). Xenolight

1,1′-dioctadecyl-3,3,3′,3′-tetramethylindotricarbocyanine iodide (DiR) near infra-red fluorescent dye was purchased from Perkin Elmer (Waltham, MA, United States). H56 protein was produced recombinantly in *E. coli* as previously described (15), reconstituted in 20 mM glycine buffer (pH 8.8), checked for purity, and validated for residual DNA, endotoxins and bioburden following internal good manufacturing practice standards at Statens Serum Institut as described previously (16). Alexa Fluor® 647-labeling of H56 was performed commercially (Thermo Fischer Scientific, Eugene, OR, United States). 2,5-dihydroxybenzoic (DHB), 1,5-diaminonaphthalene (DAN), trifluoroacetic acid (TFA), and Meyer's hematoxylin solution and eosin (H&E) solution were purchased from Sigma-Aldrich (St. Louis, MO, United States). Methanol was obtained from Th. Geyer (Renningen, Germany). Water was prepared by using a Millipore Direct-Q3 UV system (Billerica, MA, United States). All other chemicals and reagents were of analytical grade and were acquired from commercial suppliers.

Preparation of CAF01

Liposomes were prepared by using the thin film method and characterized for average intensity-weighted hydrodynamic diameter (*z*-average), polydispersity index (PDI) and zeta-potential as previously described (24). Briefly, weighed amounts of DDA and TDB (5:1, w/w) were dissolved in chloroform/methanol (9:1, v/v) in a round bottom flask. The lipid mixture was dried overnight by rotary evaporation under vacuum after cleaning with 99% (v/v) ethanol. The lipid film was rehydrated in 10 mM Tris buffer (pH 7.4), sonicated for 5 min using an ultrasound cleaner (Branson Ultrasonic Cleaner, Danburry, CT, United States), and heated to 60°C for 1 h in a water bath with vortexing every 10 min. The liposomes were tip-sonicated for 20 s, 20 min after the rehydration by using a MISONIX S-4000 probe sonicator (LLC, Newtown, CT, United States) (amplitude 70; power 16 W) to reduce their size. The final concentration of CAF01 was 20/4 mg/mL of DDA/TDB, corresponding to a molar ratio of 89:11. Solutions of unlabeled or Alexa Fluor® 647-labeled H56 were mixed with equal volumes of CAF01 dispersions at concentrations of 5 and 10 μg/mL, respectively, and the antigen was allowed to adsorb to the liposomes for 30 min at room temperature before administration. Fluorescently labeled CAF01 was prepared by addition of Xenolight DiR dissolved in ethanol during the preparation of the lipid film, resulting in a DiR concentration of 0.025 mg/mL in the final formulation.

Immunizations

Six-to-eight-week old female BALB/c mice (Scanbur, Karlslunde, Denmark) were allowed to acclimatize for 1 week upon arrival. All experimental work was approved by the Danish National Experiment Inspectorate under permit 2016-15-0201-01026 and was performed in accordance with the European Community directive 86/609 for the care and use of laboratory animals. Mice (6–12/group) were immunized once by i.m. or i.pulmon administration, or by i.m. priming followed by i.pulmon. pull immunization after an interval of 2 weeks. For the i.m. immunizations, 5 μg Alexa Fluor® 647-labeled unadjuvanted H56 or 5 μg Alexa Fluor® 647-labeled H56 adjuvanted with DiR-labeled CAF01 (250/50 μg DDA/TDB) was injected in the right thigh muscles. For the i.pulmon. immunizations, 10 μg Alexa Fluor® 647-labeled unadjuvanted H56 or 10 μg Alexa Fluor® 647-labeled H56 adjuvanted with DiR-CAF01 (125/25 μg DDA/TDB) was used, and they were performed as described previously (24). All vaccines were formulated and administered in a dose-volume of 50 μL in isotonic Tris buffer. Mice dosed i.m. or i.pulmon. with 50 μL isotonic Tris buffer served as negative controls.

Organ Collection and Cell Preparation

Mice were euthanized 3, 24, or 72 h after the immunizations, and the lungs, spleens, and draining LNs (inguinal and popliteal LNs to which vaccines administered i.m. are draining, and the tracheobronchial and mediastinal LNs to which vaccines administered i.pulmon. are draining) were isolated. For the MSI study, mice were euthanized after 6, 24, 48, and 72 h, and 7, 10, and 14 days. To collect lung tissue, a previously described protocol was used that involves flushing the pulmonary circulation and inflating the lung with dispase during tissue harvest, followed by homogenization and digestion in a DNase and collagenase solution (26). Briefly, following euthanasia of mice, the trachea was intubated transorally. The pulmonary circulation was flushed with 2 mL phosphate-buffered saline (PBS) followed by instillation of 1 mL dispase (Corning Life Sciences, Tewksbury, MA, United States). Subsequently, a volume of 0.7 mL dispase was administered *via* the endotracheal catheter, followed by administration of 0.5 mL 1% (w/v) low-melting-point agarose (Sigma-Aldrich, Brøndby, Denmark) heated to 50°C, which served as a semi-solid plug when cooled to keep the enzyme solution in close proximity to the lung tissue. The lungs were excised, placed in RPMI 1640 (Sigma-Aldrich) at 4°C, and dissociated in gentleMACS C tubes (Miltenyi Biotec Norden, Lund, Sweden) containing 2 mL RPMI 1640, 5% (v/v) fetal calf serum (FCS, Gibco Thermo Fisher, Hvidovre, Denmark), 1.5 mg/mL collagenase type IV (Sigma-Aldrich), and 20 units/mL DNase (Sigma-Aldrich) by using the gentleMACS dissociator (Miltenyi Biotec Norden AB). After 1 h incubation at 37°C, the lung pieces were dissociated again by using the gentleMACS dissociator and centrifuged at 700 × *g* for 5 min. Lung cell pellets were forced through a 70 μm cell-strainer (Falcon, Durham, NC, United States) and washed twice with RPMI 1640. Single cell suspensions of splenocytes were obtained by homogenizing the spleens through a nylon-mesh cell-strainer (Falcon) followed by two washings with RPMI 1640. The LNs were treated with 2 mL RPMI supplemented with 1 mg/mL Collagenase type IV and 20 units/mL DNase. After 30 min of incubation at 37°C, the LNs were passed through the nylon-mesh cell-strainer, followed by two washings with RPMI 1640. For each lung, spleen or LN, 1×10^6 cells (or everything, if the sample contained less cells) were resuspended in RPMI 1640 supplemented with 5×10^{-5} M 2-mercaptoethanol (Gibco Thermo Fisher), 1% (v/v) sodium pyruvate (Sigma-Aldrich), 1% (v/v) penicillin-streptomycin (Gibco Thermo Fisher), 1% (v/v) HEPES (Gibco Thermo Fisher), and 10% (v/v) FCS (Gibco Thermo Fisher) and transferred to 96-well, V-bottomed plates.

Flow Cytometry

Single cell suspensions of lungs, spleen, and LNs from immunized mice were washed with PBS and resuspended in FACS-buffer [PBS supplemented with 1% (v/v) fetal calf serum and 0.1% (w/v) sodium azide]. Following treatment with Fc-block (BD Biosciences, Lyngby, Denmark), the cells were stained for 30 min at 4°C for surface markers using mAbs (**Supplementary Table S1**). Dead cells were excluded by using the fixable viability dyes FVS510 or FVS700 (BD). The cells were washed twice, resuspended in FACS buffer and analyzed using an LSRFortessa flow cytometer (BD). Gates for the surface markers are based on fluorescence-minus-one controls. The gating strategy used for identifying distinct cell populations in the lungs, the spleen, and the draining lymph nodes is based on previous reports (26–28) and is further described in the **Supplementary Figures S1–S3**. All flow cytometry analyses were performed using the FlowJo software v10 (Tree Star, Ashland, OR, United States).

Tissue Preparation for Matrix-Assisted Laser Desorption/Ionization Mass Spectrometry Imaging (MALDI-MSI)

Following euthanasia, the lungs were removed, snap-frozen on crushed dry ice and stored at −80°C until analysis. Analysis time points selected for imaging were 6, 24, 48, 72, and 96 h and 7, 10, and 14 days with one mouse analyzed at each time point and one control animal. The frozen lungs were mounted onto a cryo-microtome sample specimen disk (Leica Biosystems Inc., Buffalo Grove, IL, United States) with 5% (w/v) carboxymethyl cellulose aqueous gel (Sigma-Aldrich) at −24°C. The lungs were cut into coronal sections of 18 μm thickness using a Leica CM3050S cryo-microtome (Leica Microsystems, Wetzlar, Germany), thaw-mounted onto microscope glass slides (VWR, Søborg, Denmark) and stored in a −80°C freezer until MSI analysis.

Prior to matrix application, the tissue sections were transferred directly from the freezer to a vacuum desiccator for 10 min. For the positive ion mode analysis, a solution of freshly prepared 30 mg/mL DHB in methanol/water (50:50, v/v) supplemented with 1% (w/v) TFA was used. For the negative ion mode analysis, a freshly prepared solution of 3 mg/mL DAN in methanol/water (90:10, v/v) was used. A volume of 300 μL matrix solution was sprayed onto the surface of the tissue sections using an in-house built pneumatic sprayer with the sample rotating at 150 rpm (for the application of the DHB matrix) or 250 rpm (for the application of the DAN matrix), and the matrix solution was pneumatically sprayed at a flow rate of 30 μL/min using a nebulizer gas pressure of 2 bar (29). The quality of matrix deposition (homogeneity and crystal size) was checked by inspection with reflected light optical microscopy.

MALDI-MSI and Image Analysis

The samples were analyzed using a Thermo Q Exactive Orbitrap mass spectrometer (Thermo Scientific, Bremen, Germany) equipped with an AP-SMALDI10 ion source (TransMIT, Giessen, Germany). The AP-SMALDI10 ion source was equipped with a nitrogen laser with a wavelength of 337 nm, and a frequency of 60 Hz, operated using 30 laser pulses per pixel. Analysis was performed in the positive and negative ion modes, respectively, using a scan range of 300–1200 Da, a mass resolving power of 140,000 at *m/z* 200, a lock mass of *m/z* 431.037 corresponding to a signal from the DHB matrix in the positive ion mode, and a lock mass of *m/z* 311.130 corresponding to a signal from DAN matrix in the negative ion mode. Images were acquired at a pixel size of 100 μm with the ablation craters well separated. After imaging, the sections were stained with H&E as described in detail elsewhere (30), and images were acquired using an optical microscope. The raw files were converted to imzML files (31), and the MSiReader program was used for image generation (32). Images were generated with a bin width of ±0.002 Da (±5 ppm). Semi-quantitative data analysis (i.e., intensity ratio) was performed for measuring changes in the abundance of CAF01 lipids [DDA (m/z 550.629) and TDB (m/z 1025.726)] relative to endogenous tissue lipids, i.e., phosphatidylcholine {[PC (34:1)], m/z 798.541} and phosphatidylserine {[PS (38:4)], m/z 810.529}. For calculating the intensity ratio, a region of interest (ROI) was manually selected along the lung section, and the mean intensity of the lipid (i.e., DDA or TDB) in the ROI was divided by the mean intensity of endogenous tissue lipid (PC or PS) in that specific ROI. We also analyzed the distribution of phospholipids, i.e., lysophosphatidylcholines (LysoPC) and bis(monoacylglycero)phosphate (BMP), sphingolipids (ceramides), and cholesteryl esters in the lungs following i.pulmon. administration of CAF01.

Statistical Analysis

Two-way ANOVA followed by Tukey's multiple comparisons test was used to analyze the difference between the immunization groups using the GraphPad Prism software (GraphPad Software Inc., La Jolla, CA, United States). A value of $p < 0.05$ was considered significant.

RESULTS

Mucosal (i.pulmon.) Pull Immunization of Mice Parenterally (i.m.) Primed With H56/CAF01 Induces Higher Vaccine Uptake by Pulmonary APCs as Compared to i.m. or i.pulmon. Priming Alone

Similar to our previous study using an i.m. prime – i.pulmon. pull immunization strategy for the H56/CAF01 vaccine, which induced strong lung mucosal $CD4^+$ T-cell immunity (24), mice were primed once by i.m. immunization followed by i.pulmon. pull immunization. The cellular uptake of Alexa Fluor®-labeled H56/DiR-labeled CAF01 in the lungs was evaluated by multicolor flow cytometry 3, 24, and 72 h post-immunization and compared with the cellular uptake after i.pulmon. and i.m. priming immunizations alone (**Supplementary Figure S1**).

The fluorescent labeling of CAF01 and its cellular uptake using flow cytometry was performed as previously reported (33). H56 was commercially labeled with Alexa Fluor® 647 as previously reported for ovalbumin (33) and the fluorescent labeling did not influence the physicochemical properties of H56 (data not shown). Moreover, we have previously shown that radiolabeling of H56 did not influence its physicochemical properties (24). In general, we observed that at 72 h, i.pulmon. pull immunization induced a significantly higher vaccine uptake by immune cells in the lungs as compared to i.pulmon. priming immunization alone (**Figure 1** and **Supplementary Table S2**). As expected, we did not observe any vaccine$^+$ cells in the lungs after i.m. priming alone. In addition, there was a rapid influx of neutrophils into the lungs within the first 24 h after i.pulmon. pull immunization, and the number of neutrophils was significantly higher than the number of neutrophils detected at 24 and 72 h post-immunization in the lungs of mice only primed by i.pulmon. immunization (**Figure 1A**). A comparable trend was observed for alveolar macrophages (**Figure 1B**) and inflammatory monocytes (**Figure 1C**). At 72 h, a significantly higher number of vaccine$^+$ B cells was detected following i.pulmon. priming as compared to i.pulmon. pull immunization (**Figure 1D**). Among the studied DC subsets, vaccine$^+$ monocyte-derived DCs (moDCs) (**Figure 1E**), CD11b$^+$ DCs (**Figure 1F**), and plasmacytoid DCs (pDCs) (**Figure 1G**) were detected at significantly higher numbers 72 h after i.pulmon. pull immunization than after i.pulmon. priming immunization alone, whereas there was no statistical significant difference in the number of CD103$^+$ DCs at this time point (**Figure 1H**). Similarly, at 72 h, the numbers of vaccine$^+$ interstitial macrophages (**Figure 1I**) and eosinophils (**Figure 1J**) were highest following i.pulmon. pull immunization. We also assessed the total fraction of each cell subset in the lungs 3, 24, and 72 h post-immunization (**Figure 1K**), though none of the subpopulation changes were different between groups. We did observe a non-significant trend that the neutrophils and the B cell population were the most abundant cell subsets in the lungs at the designated time points following the different immunization regimens. The CD11b$^+$ DCs constituted a major fraction of the vaccine$^+$ cell subsets, whereas the CD103$^+$ DCs only made up a minor fraction, in particular at 3 and 72 h following i.m. or i.pulmon. immunization. The vaccine was also associated with pDCs, but vaccine association with this cell subset was only detectable at 72 h after i.pulmon. pull immunization. Evaluation of the H56$^+$ uptake by the immune cells in the lungs (**Figure 2**) showed almost similar trends as the vaccine (H56/CAF01) uptake, except that the numbers of cells taking up the vaccine were 1.5–7.5 times higher than the numbers of cells displaying detectable H56 uptake. Another major difference was that the majority of the cellular subsets had taken up H56 as early as 24 h post-immunization as compared to 72 h in case of H56/CAF01. In general, the number of vaccine$^+$ and H56$^+$ cells were higher for the group vaccinated using the i.m. prime – i.pulmon. strategy as compared to the groups only vaccinated by prime immunization, which suggests activation of both innate and memory responses.

H56/CAF01 Parenteral Prime-Airway Mucosal Pull Immunization Enhances Vaccine Uptake by Lung Endothelial Cells and Type I Epithelial Cells as Compared to Parenteral or Airway Mucosal Prime Immunization Alone

We also evaluated the uptake of the fluorescently labeled H56/CAF01 vaccine by pulmonary epithelial cells, endothelial cells, hematopoietic lineage cells, and lineage-negative cells (**Supplementary Figure S2**). No significant differences in the vaccine uptake by hematopoietic lineage cells could be measured between the i.pulmon. prime versus i.pulmon. pull immunization (**Figure 3A**). At 3 and 24 h post-immunization, no significant differences were observed in the vaccine uptake by the majority of the lung cell populations following i.pulmon. priming or i.pulmon. pull immunization (**Figures 3B–E**). However, the number of vaccine$^+$ type II epithelial cells was significantly higher following i.pulmon. pull immunization than i.pulmon. priming immunization alone (**Figure 3D**). At 72 h, a significantly higher number of vaccine$^+$ endothelial cells (**Figure 3B**), type I epithelial cells (**Figure 3C**), and lineage-negative cells (**Figure 3E**) were measured following i.pulmon. pull as compared to the number of cells after i.pulmon. prime immunization alone. Evaluation of the total fraction of these pulmonary cell populations in the lungs (**Figure 3F**) did not show any significant differences among the groups. The data showed a non-significant trend that the hematopoietic cells were largely the dominant cell subsets in the lungs at the examined time points when applying different immunization regimens. Endothelial cells and type I epithelial cells constituted the other fraction of vaccine$^+$ cell subsets. The vaccine$^+$ lineage-negative cells comprised the dominant fraction of cells 3 h after i.m. immunization, and this was observed at all time points following the i.m prime – i.pulmon. pull immunization. We also evaluated the H56 uptake by the endothelial cells and epithelial cells in the lungs (**Figure 4**) and found an almost similar cellular distribution as for the H56/CAF01 uptake. However, the numbers of cells taking up the vaccine (H56 + CAF01) were in general 2–3.75 times higher than the number of cells that displayed detectable levels of H56 uptake.

Differential Splenic Cellular Pharmacokinetics of H56/CAF01 Upon Prime and Prime-Pull Immunization

We also assessed the cellular uptake of the H56/CAF01 vaccine by innate myeloid cells and APCs in the spleen (**Supplementary Figure S3**). Overall, we found differences in the vaccine uptake by splenocyte populations when applying the three different immunization strategies (**Figure 5** and **Supplementary Table S2**). At 3 h post-i.m. immunization, a significantly higher number of vaccine$^+$ neutrophils was observed as compared to mucosal immunizations (**Figure 5A**). At 24 h, significantly higher numbers of pDCs (**Figure 5B**) and inflammatory monocytes (**Figure 5C**) were observed after i.pulmon. and i.m. – i.pulmon. immunization as compared to i.m. immunization alone. No other differences were observed at 3 and 24 h among the

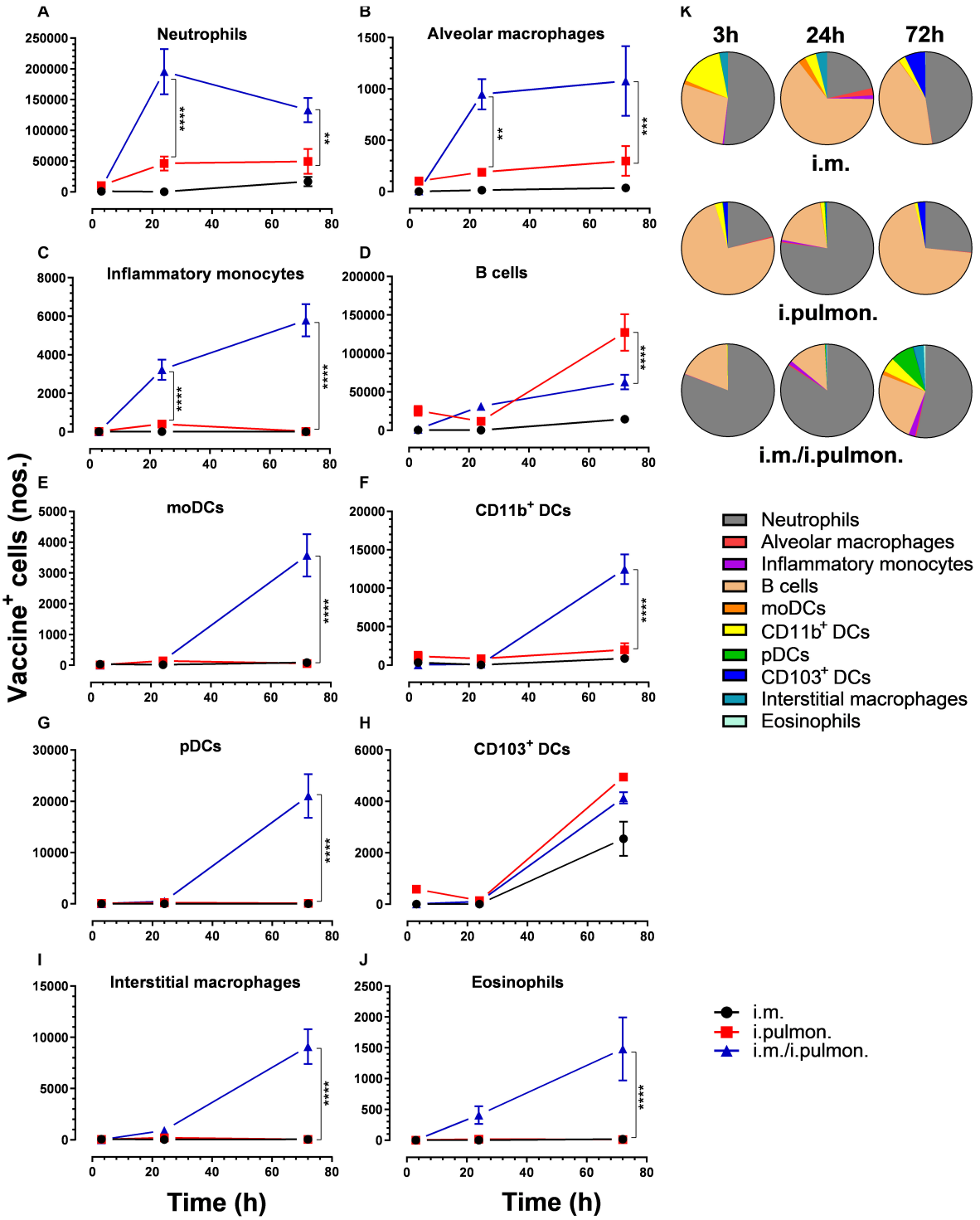

FIGURE 1 | Airway mucosal pull immunization after parenteral immunization with H56/CAF01 increases vaccine uptake by innate myeloid cells in the lungs as compared to parenteral or airway mucosal priming alone. BALB/c mice were immunized with Alexa Fluor® 647-labeled H56/DiR-labeled CAF01 *via* the i.m. or i.pulmon. or i.m. – i.pulmon. routes, and the vaccine uptake by lung cells was assessed by flow cytometry 3, 24, and 72 h post-immunization. Numbers of vaccine$^+$ (H56$^+$/CAF01$^+$) **(A)** neutrophils (Ly6G$^+$), **(B)** alveolar macrophages (F4/80$^+$CD11b$^-$), **(C)** inflammatory monocytes (Ly6C$^+$CD11b$^+$), **(D)** B cells (CD19$^+$), **(E)** moDCs (CD11c$^+$F4/80$^+$CD11b$^+$CD64$^+$), **(F)** CD11b$^+$ DCs (CD11c$^+$CD11b$^+$), **(G)** pDCs (CD11c$^+$Ly6C$^+$F4/80$^-$CD11b$^-$), **(H)** CD103$^+$ DCs (CD11c$^+$CD11b$^-$CD103$^+$), **(I)** interstitial macrophages (F4/80$^+$CD11b$^+$), and **(J)** eosinophils (SiglecF$^+$) in the lungs. **(K)** Fraction of vaccine$^+$ (H56$^+$/CAF01$^+$) cells in the lungs at 3, 24, and 72 h post-immunization. Data points represent $n = 4$, and they display mean values ± SEM. $^{**}p < 0.01$, $^{***}p < 0.001$, $^{****}p < 0.0001$ vs. i.pulmon. immunization *via* two-way ANOVA with Tukey's post-test.

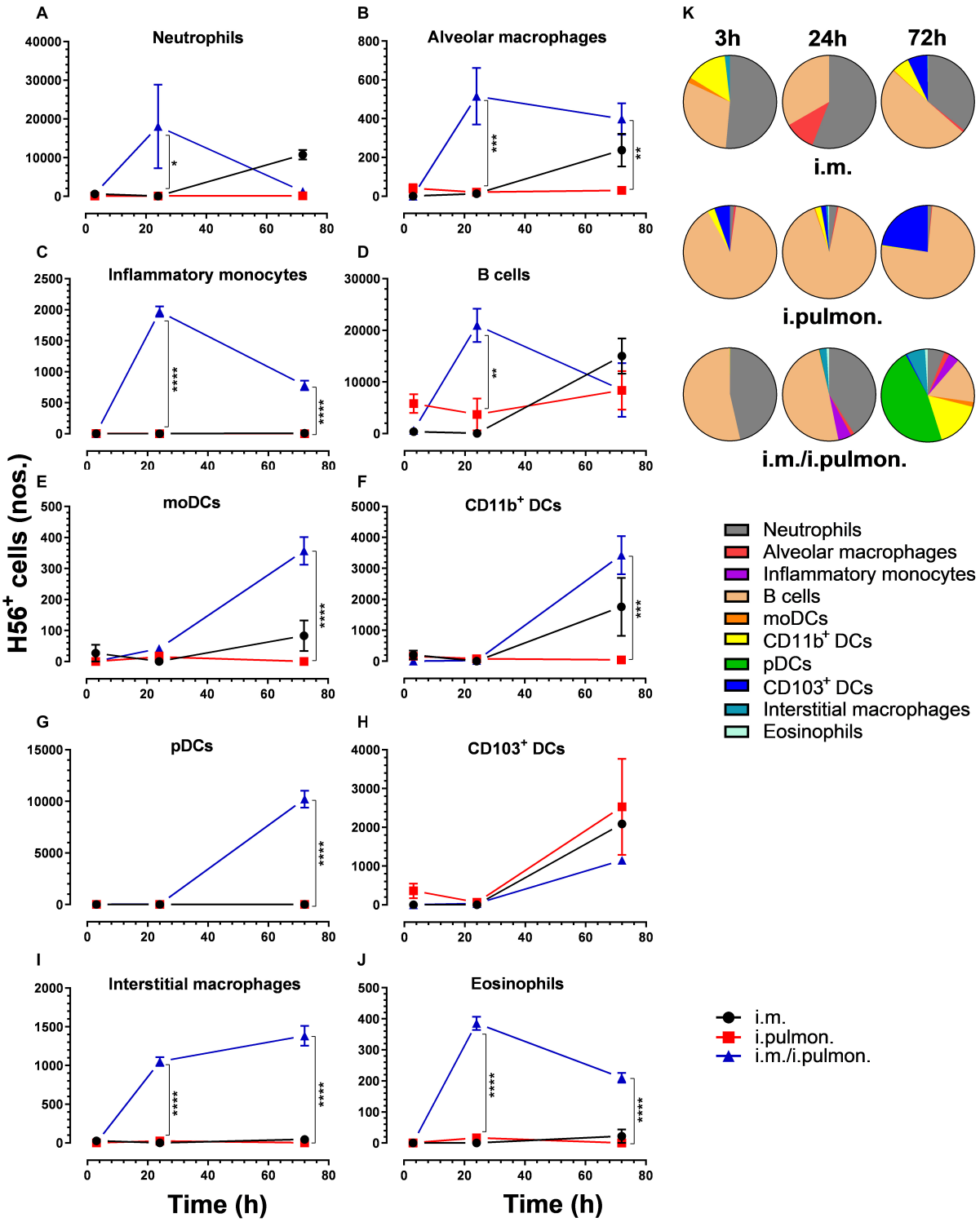

FIGURE 2 | H56 uptake by different immune cells in the lungs following prime or prime – pull immunization with H56/CAF01. BALB/c mice were immunized with Alexa Fluor® 647-labeled H56/DiR-labeled CAF01 *via* i.m. or i.pulmon. or i.m. – i.pulmon. routes, and the $H56^+$ uptake by lung cells was assessed by flow cytometry 3, 24, and 72 h post-immunization. Numbers of $H56^+$ **(A)** neutrophils ($Ly6G^+$), **(B)** alveolar macrophages ($F4/80^+CD11b^-$), **(C)** inflammatory monocytes ($Ly6C^+CD11b^+$), **(D)** B cells ($CD19^+$), **(E)** moDCs ($CD11c^+F4/80^+CD11b^+CD64^+$), **(F)** $CD11b^+$ DCs ($CD11c^+CD11b^+$), **(G)** pDCs ($CD11c^+Ly6C^+F4/80^-CD11b^-$), **(H)** $CD103^+$ DCs ($CD11c^+CD11b^-CD103^+$), **(I)** interstitial macrophages ($F4/80^+CD11b^+$), and **(J)** eosinophils ($SiglecF^+$) in the lungs. **(K)** Fraction of $H56^+$ cells in the lungs at 3, 24 and 72 h post-immunization. Data points represent $n = 2$, and they display mean values ± SEM. $^*p < 0.05$, $^{**}p < 0.01$, $^{***}p < 0.001$, $^{****}p < 0.0001$ vs. i.pulmon. immunization *via* two-way ANOVA with Tukey's post-test.

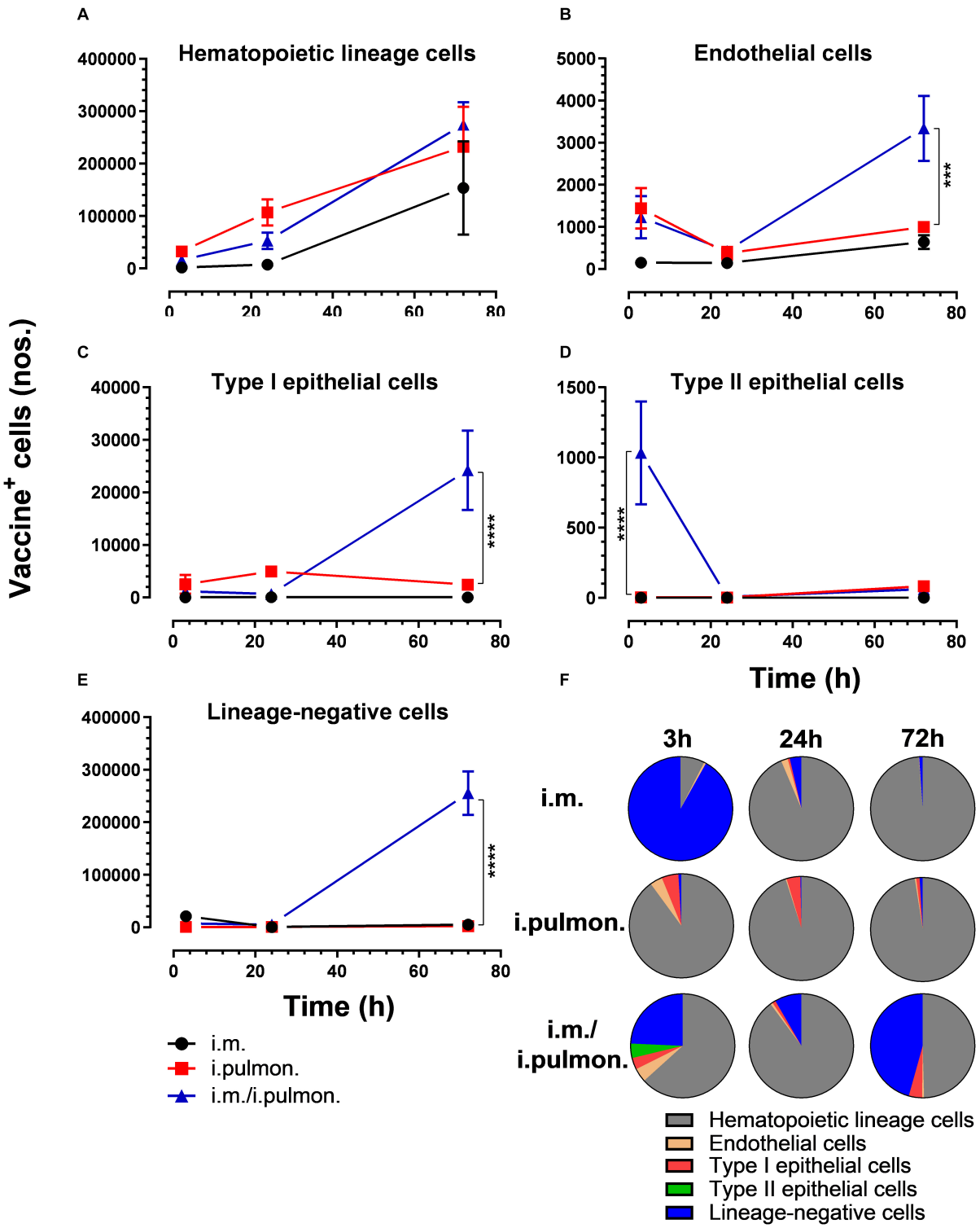

FIGURE 3 | Intramuscular (i.m.) prime-intrapulmonary (i.pulmon.) pull immunization with H56/CAF01 increases vaccine uptake by lung endothelial cells and type I epithelial cells as compared to either i.m. or i.pulmon. immunization alone. BALB/c mice were immunized with Alexa Fluor-labeled H56/DiR-labeled CAF01 *via* the i.m. or i.pulmon. or i.m. – i.pulmon. routes, and vaccine uptake by lung cells was assessed by flow cytometry 3, 24, and 72 h post-immunization. Numbers of vaccine$^+$ (H56$^+$/CAF01$^+$) **(A)** hematopoietic lineage cells (CD45$^+$CD31$^-$CD326$^-$), **(B)** endothelial cells (CD45$^-$CD31$^+$CD326$^-$), **(C)** type I epithelial cells (CD45$^-$CD31$^-$CD326$^+$CD74$^-$Podoplanin$^+$), **(D)** type II epithelial cells (CD45$^-$CD31$^-$CD326$^+$CD74$^+$Podoplanin$^-$), and **(E)** lineage-negative cells (CD45$^-$CD31$^-$CD326$^-$) in the lungs. **(F)** Fraction of vaccine$^+$ (H56$^+$/CAF01$^+$) cells in the lungs at 3, 24, and 72 h post-immunization. Data points represent mean values ± SEM (n = 4). ***$p < 0.001$, ****$p < 0.0001$ vs. i.pulmon. immunization *via* two-way ANOVA with Tukey's post-test.

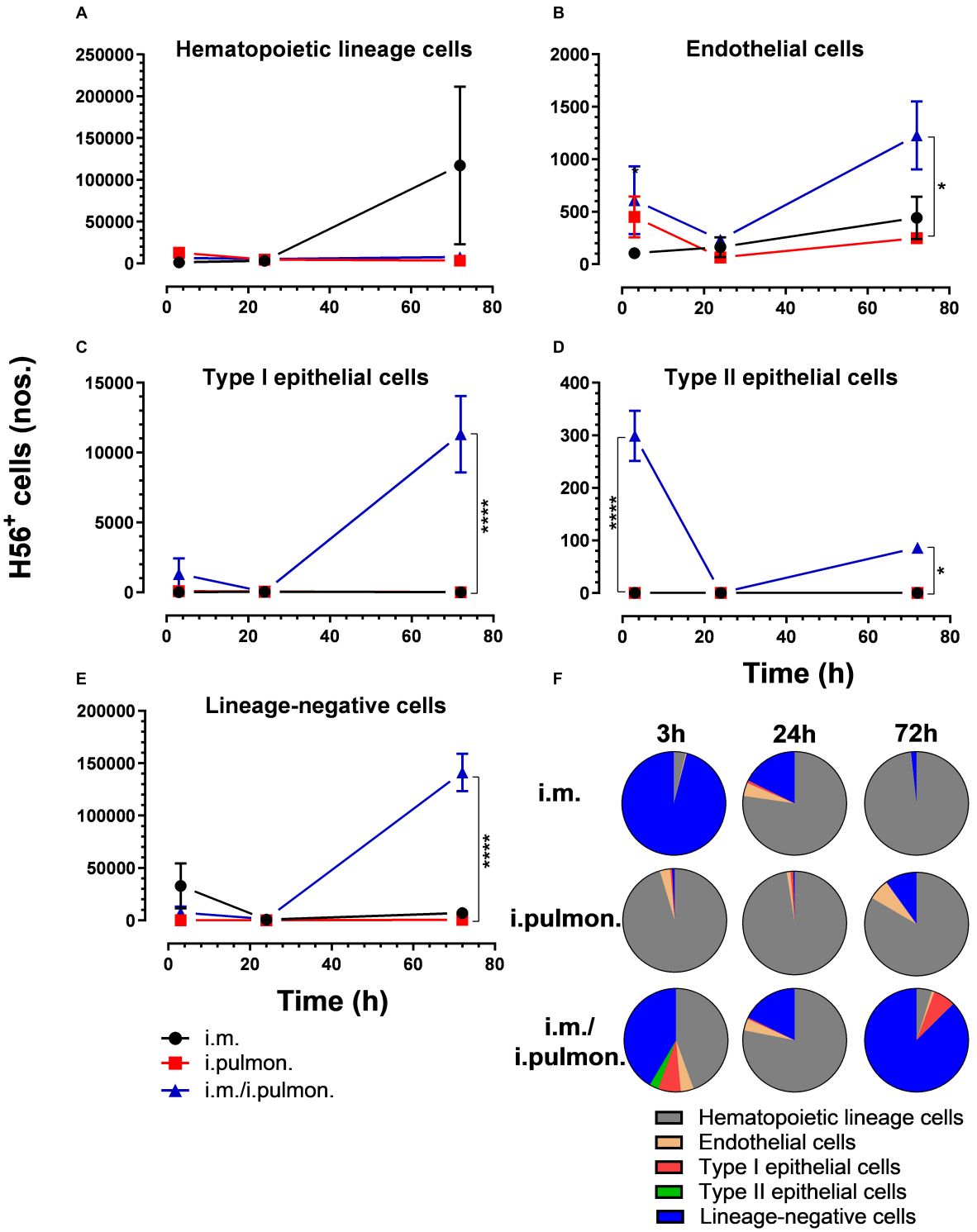

FIGURE 4 | H56 uptake by epithelial cells, endothelial cells, hematopoietic lineage cells, and lineage-negative cells in the lungs following prime or prime – pull immunization with H56/CAF01. BALB/c mice were immunized with Alexa Fluor® 647-labeled H56/DiR-labeled CAF01 *via* the i.m. or i.pulmon. or i.m. – i.pulmon. routes, and the $H56^+$ uptake by lung cells was assessed by flow cytometry 3, 24 and 72 h post-immunization. Numbers of vaccine$^+$ ($H56^+/CAF01^+$) **(A)** hematopoietic lineage cells ($CD45^+CD31^-CD326^-$), **(B)** endothelial cells ($CD45^-CD31^+CD326^-$), **(C)** type I epithelial cells ($CD45^-CD31^-CD326^+CD74^-Podoplanin^+$), **(D)** type II epithelial cells ($CD45^-CD31^-CD326^+CD74^+Podoplanin^-$), and **(E)** lineage-negative cells ($CD45^-CD31^-CD326^-$) in the lungs. **(F)** Fraction of $H56^+$ cells in the lungs at 3, 24, and 72 h post-immunization. Data points represent $n = 2$ and display mean values ± SEM. $^*p < 0.05$, $^{****}p < 0.0001$ vs. i.pulmon. immunization *via* two-way ANOVA with Tukey's post-test.

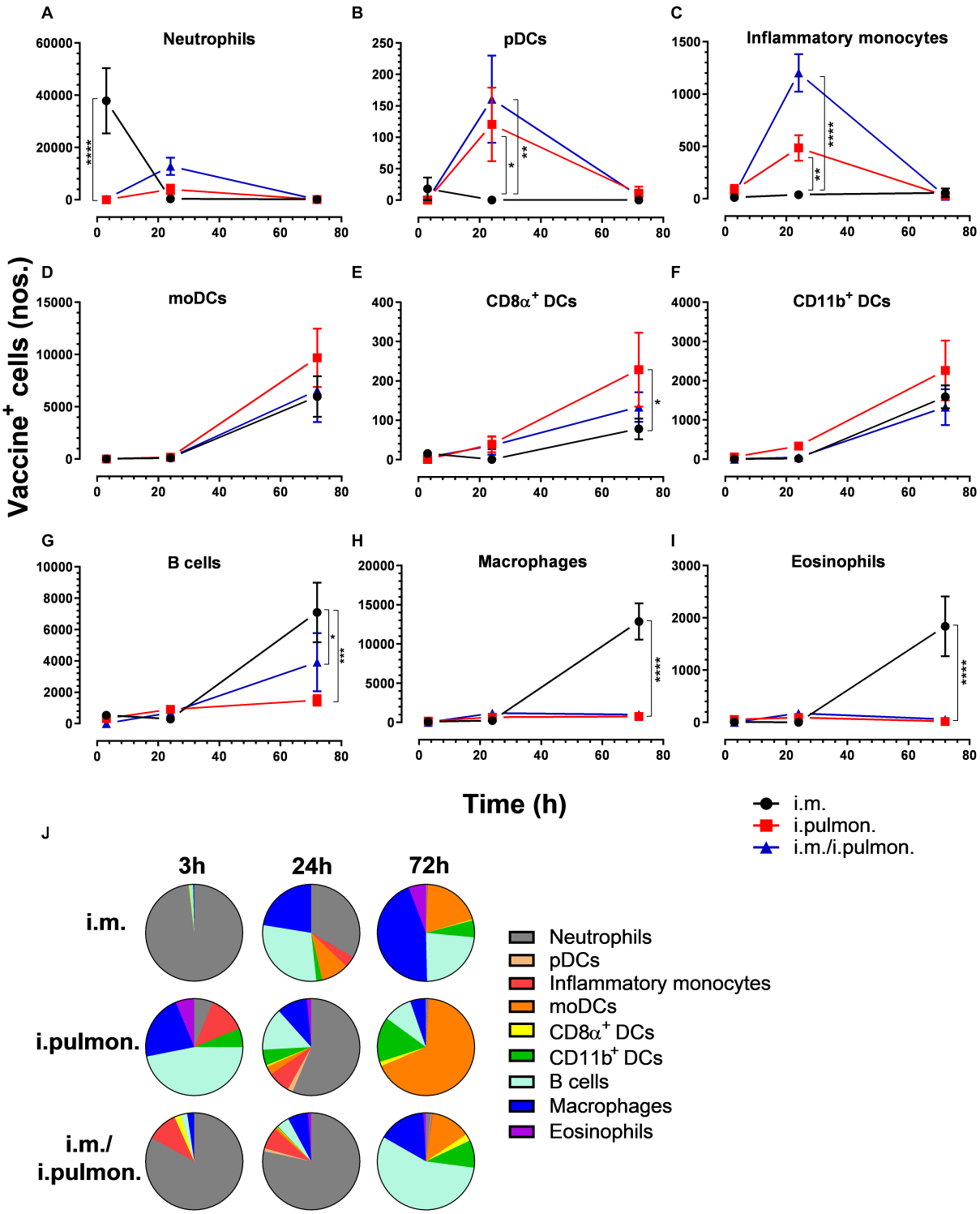

FIGURE 5 | Differential vaccine uptake by innate myeloid and antigen-presenting cells following parenteral or mucosal prime and parenteral prime-mucosal pull immunization with H56/CAF01. BALB/c mice were immunized with Alexa Fluor®-labeled H56/DiR-labeled CAF01 *via* the i.m. or i.pulmon. or i.m. – i.pulmon. routes, and the vaccine uptake by spleen cells was assessed by flow cytometry 3, 24, and 72 h post-immunization. Numbers of vaccine$^+$ ($H56^+/CAF01^+$) **(A)** neutrophils ($Ly6G^+$), **(B)** pDCs ($CD11c^+Ly6C^+F4/80^-CD11b^-$), **(C)** inflammatory monocytes ($Ly6C^+CD11b^+$), **(D)** moDCs ($CD11c^+F4/80^+CD11b^+CD64^+$), **(E)** $CD8\alpha^+$ DCs ($CD11c^+CD11b^-CD8\alpha^+$), **(F)** $CD11b^+$ DCs ($CD11c^+CD11b^+$), **(G)** B cells ($CD19^+$), **(H)** macrophages ($F4/80^+CD11b^+$), and **(I)** eosinophils ($SiglecF^+$) in the spleen. **(J)** Fraction of vaccine$^+$ ($H56^+/CAF01^+$) cells in the spleen at 3, 24, and 72 h post-immunization. Data points represent $n = 4$, and they display mean values ± SEM. $^*p < 0.05$, $^{**}p < 0.01$, $^{***}p < 0.001$, $^{****}p < 0.0001$ vs. i.m. immunization *via* two-way ANOVA with Tukey's post-test.

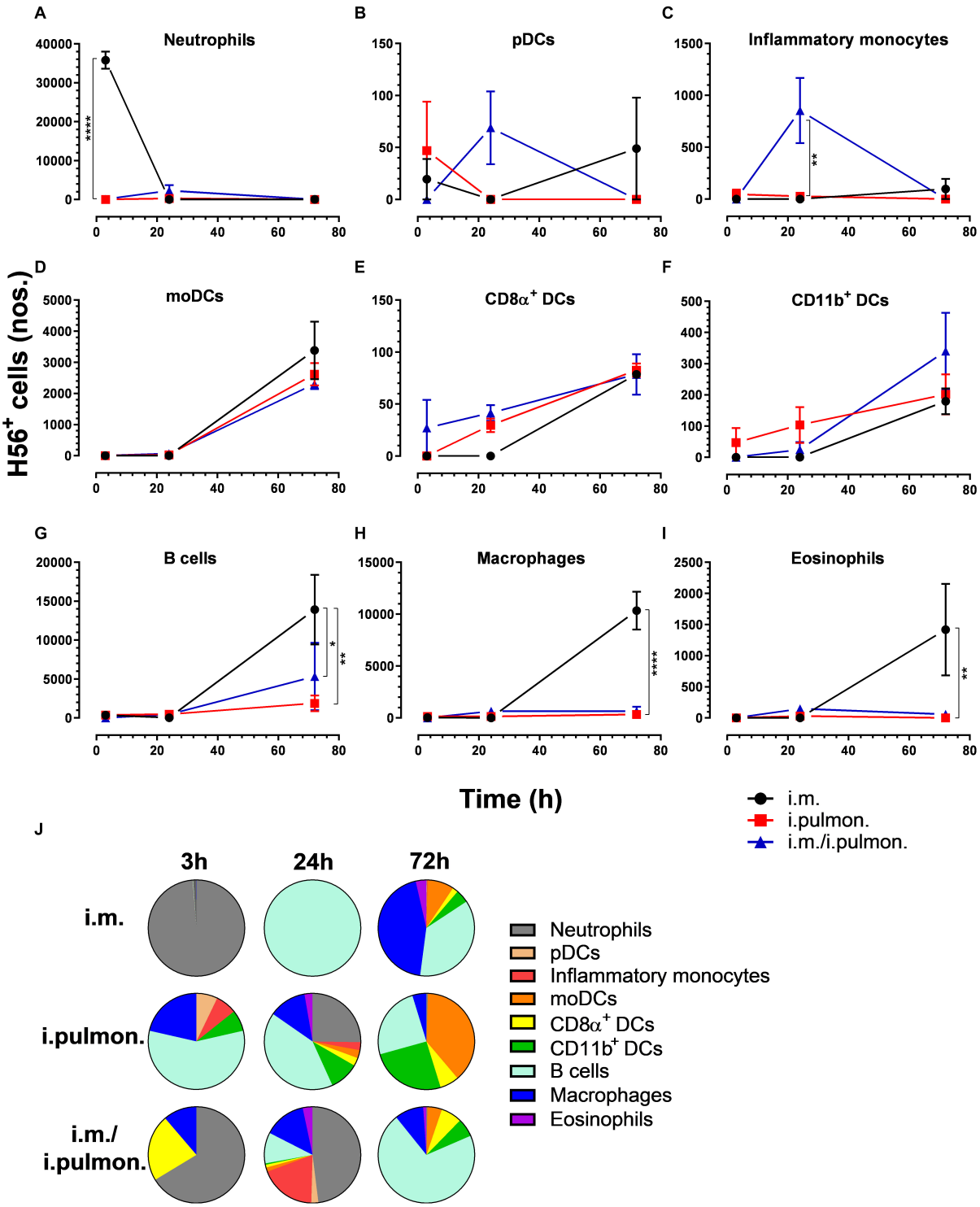

FIGURE 6 | H56 uptake by splenic cells following parenteral or airway mucosal prime or parenteral prime – airway mucosal pull immunization with H56/CAF01. BALB/c mice were immunized with Alexa Fluor® 647-labeled H56/DiR-labeled CAF01 *via* i.m. or i.pulmon. or i.m. – i.pulmon. routes, and the $H56^+$ uptake by spleen cells was assessed by flow cytometry 3, 24, and 72 h post-immunization. Numbers of **(A)** neutrophils ($Ly6G^+$), **(B)** pDCs ($CD11c^+Ly6C^+F4/80^-CD11b^-$), **(C)** inflammatory monocytes ($Ly6C^+CD11b^+$), **(D)** moDCs ($CD11c^+F4/80^+CD11b^+CD64^+$), **(E)** $CD8\alpha^+$ DCs ($CD11c^+CD11b^-CD8\alpha^+$), **(F)** $CD11b^+$ DCs ($CD11c^+CD11b^+$), **(G)** B cells ($CD19^+$), **(H)** macrophages ($F4/80^+CD11b^+$), and **(I)** eosinophils ($SiglecF^+$) in the spleen. **(J)** Fraction of $H56^+$ cells in the spleen at 3, 24, and 72 h post-immunization. Data points represent $n = 2$, and they display mean values ± SEM. $^*p < 0.05$, $^{**}p < 0.01$, $^{****}p < 0.0001$ vs. i.m. immunization *via* two-way ANOVA with Tukey's post-test.

different immunization strategies. At 72 h, the vaccine$^+$ moDCs (**Figure 5D**), CD8α$^+$ DCs (**Figure 5E**), and CD11b$^+$ DCs (**Figure 5F**) were higher for all immunization groups than at 3 and 24 h, but were not different among the immunization strategies used. A significantly higher number of vaccine$^+$ CD8α$^+$ DCs were observed following i.pulmon. immunization as compared to the i.m. immunization. The numbers of vaccine$^+$ neutrophils (**Figure 5A**), pDCs (**Figure 5B**), and inflammatory monocytes (**Figure 5C**) at 72 h decreased, as compared to the number of vaccine$^+$ cells measured 24 h post-immunization, and the numbers of cells were not different among the groups. For mice vaccinated by i.m. immunization, significantly higher numbers of vaccine$^+$ B cells (**Figure 5G**), macrophages (**Figure 5H**), and eosinophils (**Figure 5I**) were detected, as compared to the numbers of cells measured after i.pulmon. prime or pull immunization at 72 h. Among the total fraction of vaccine$^+$ splenic cell types at 3, 24, and 72 h post-immunization (**Figure 5J**), we did not observe any significant differences between the groups. However, the percentage subpopulations of all the H56$^+$ splenic cells (**Figure 6J**) were statistically higher ($p < 0.05$) following 24 h of i.m./i.pulmon. immunization as compared to i.m. immunization. We did observe a non-significant trend that the neutrophils, macrophages and B cells were the predominant cell populations taking up the vaccine, independently of the immunization strategy. The CD11b$^+$ DCs and moDCs constituted the dominant DC subsets, in particular at 72 h post-immunization. In general, there was a diversified participation of innate myeloid cells and APCs in the vaccine uptake in the spleen following i.pulmon. immunization. For the H56$^+$ uptake (**Figure 6**), almost similar trends were apparent, as compared to the vaccine uptake, but the numbers of cells taking up the vaccine were 1.2-8 times higher than the numbers of cells displaying detectable H56 uptake.

Mucosal Pull Immunization of Mice Parenterally Primed With H56/CAF01 Promotes Upregulation of CD86 Expression by Dendritic Cells in the Lung-Draining Lymph Nodes as Compared to Parenteral or Mucosal Prime Immunization Alone

Clear differences were observed in the vaccine uptake by immune cells in the lungs of mice vaccinated using different immunization strategies. Therefore, we investigated if differences in the draining lymph node innate environment after mucosal pull immunization may contribute to the differences measured in the vaccine uptake when using the three immunization strategies (**Supplementary Figure S3**) and to the higher cell-mediated and humoral immune responses following i.m. prime – i.pulmon. pull immunization, as reported previously (24). We found that the activation states, assessed as the CD86 surface expression by B cells (at 24 h, **Figure 7A**), moDCs (at 72 h, **Figure 7B**), CD8α$^+$ DCs (at 24 h, **Figure 7C**), and CD11b$^+$ DCs (at 72 h, **Figure 7D**) in the tracheobronchial lymph nodes (TLNs) and mediastinal lymph nodes (MLN) draining the lungs in i.m. prime and i.pulmon. pull immunized mice, were significantly higher than the activation states after i.m. or i.pulmon. immunization alone. There were no differences between the immunization strategies in the CD86 surface expression by pDCs (**Figure 7E**) and macrophages (**Figure 7F**) in the TLNs and MLNs. Interestingly, B cells (**Figure 7G**) and pDCs (**Figure 7K**) were activated distal to the site of immunization in the inguinal lymph nodes (ILNs) and the popliteal lymph nodes (PLNs) at 24 h post-prime-pull immunization, and only DCs showed increased activation after i.m. immunization. However, there was no difference in the surface expression of CD86 between the immunization strategies in moDCs (**Figure 7H**), CD8α$^+$ DCs (**Figure 7I**), CD11β$^+$ DCs (**Figure 7J**), and macrophages (**Figure 7L**). Overall, there was an increased activation state of vaccine$^+$ DCs in the lymph nodes draining the lungs after i.m. prime – i.pulmon. pull immunization with H56/CAF01.

A Uniform DDA Distribution and Signal Intensity in the Lungs Can Be Detected for at Least 2 Weeks After Intrapulmonary Administration of CAF01

To investigate the spatiotemporal distribution of the CAF01 constituent lipids (DDA and TDB) in the lungs, MALDI-MSI was performed on cryo-sections of lung tissue isolated 6, 24, 48, and 72 h, and 7, 10, and 14 days after i.pulmon. administration of CAF01 to mice, and we compared the results with the signals obtained from cryo-sections of lungs from naïve mice. At these specific time points, we then compared the signal intensity ratios between DDA and TDB, respectively, and the endogenous lipid PC (34:1) in the positive ion mode in a semi-quantitative way. We found that DDA (m/z 550.62) could be detected at all examined time points after i.pulmon. administration of CAF01 (**Figure 8**). In addition, DDA displayed a homogeneous tissue distribution in the lungs at all examined time points at comparable signal intensities. Lung cryo-sections from negative control mice did not display any detectable MS signals of DDA and TDB. Ionized PC (34:1) (m/z 798.541) was also uniformly expressed in the lung cryo-sections at all investigated time points (**Supplementary Figure S4**). Co-localization analysis showed that DDA and PC (34:1) were present together in the lung sections (**Figure 8A**), and the signal intensity ratio of DDA and PC (34:1) appeared rather constant throughout the study (**Figure 8B**). As compared to DDA, the signal intensity for TDB (m/z 1025.726) was relatively lower, and the signal was apparently not distributed homogeneously in the lung sections (**Supplementary Figure S5A**). The signal intensity ratio of TDB relative to PC (34:1) increased from 6 h and reached a maximum at 48 h post-administration, after which the intensity ratio remained low until day 14, where the TDB signal was no longer detectable (**Supplementary Figure S5B**).

Increased BMP Lipids in Alveloar Macrophages Following Intrapulmonary Administration of CAF01 Is Suggestive of Altered Phagocytic Activity

From the same imaging experiments, images were generated of selected biomarker phospholipids, i.e., BMP and lysoPC,

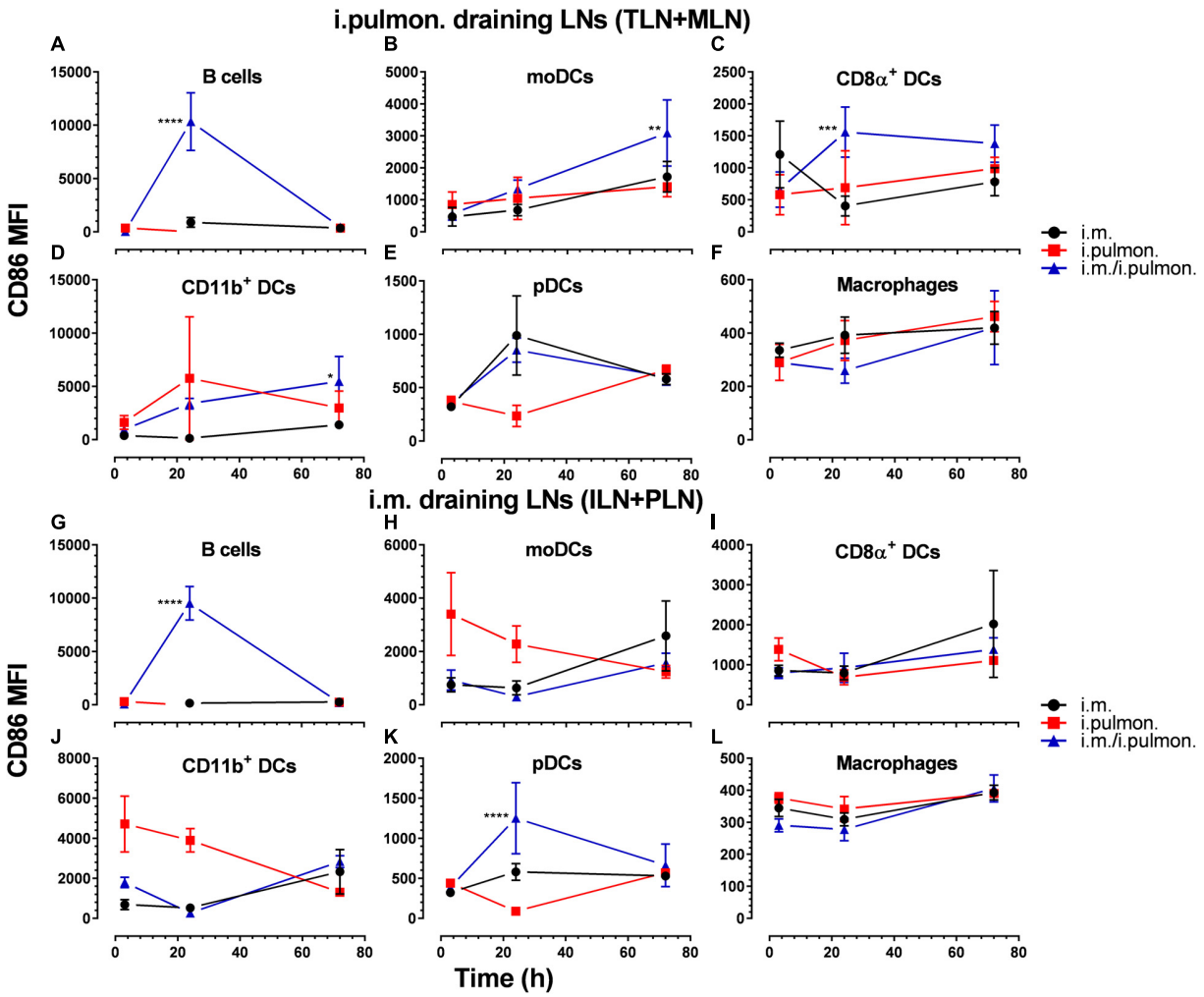

FIGURE 7 | The expression of CD86 by dendritic cells in the lung-draining lymph nodes is upregulated after parenteral prime and mucosal pull immunization of mice with H56/CAF01, as compared to the CD86 levels in mice vaccinated by parenteral or mucosal prime immunization alone. BALB/c mice were immunized with Alexa Fluor®-labeled H56/DiR-labeled CAF01 *via* the i.m. or i.pulmon. or i.m. – i.pulmon. routes, and the vaccine uptake in the lymph nodes draining the i.m. administration site [inguinal (ILN) and popliteal (PLN)] or the i.pulmon. administration site [tracheobronchial (TLN) and mediastinal (MLN)] was assessed by flow cytometry 3, 24, and 72 h post-immunization. The relative surface expression of CD86 by antigen-presenting cells was assessed and expressed as mean fluorescence intensity (MFI). CD86 surface expression by vaccine$^+$ (H56$^+$/CAF01$^+$) **(A)** B cells (CD19$^+$), **(B)** moDCs (CD11c$^+$F4/80$^+$CD11b$^+$CD64$^+$), **(C)** CD8α$^+$ DCs (CD11c$^+$CD11b$^-$CD8α$^+$), **(D)** CD11b$^+$ DCs (CD11c$^+$CD11b$^+$), **(E)** pDCs (CD11c$^+$Ly6C$^+$F4/80$^-$CD11b$^-$), and **(F)** macrophages (F4/80$^+$CD11b$^+$) in the TLN and MLN, and **(G)** B cells (CD19$^+$), **(H)** moDCs (CD11c$^+$F4/80$^+$CD11b$^+$CD64$^+$), **(I)** CD8α$^+$ DCs (CD11c$^+$CD11b$^-$CD8α$^+$), **(J)** CD11b$^+$ DCs (CD11c$^+$CD11b$^+$), **(K)** pDCs (CD11c$^+$Ly6C$^+$F4/80$^-$CD11b$^-$), and **(L)** macrophages (F4/80$^+$CD11b$^+$) in the ILN and PLN at 3, 24, and 72 h post-immunization. Data points represent $n = 4$, and they display mean values ± SEM. *$p < 0.05$, **$p < 0.01$, ***$p < 0.001$, ****$p < 0.0001$ vs. i.m. immunization *via* two-way ANOVA with Tukey's post-test.

and sphingolipids, i.e., ceramides, in the lungs after i.pulmon. administration of CAF01. BMP is a recognized biomarker of phagocytozing macrophages (34), and it is abundantly expressed in the late endosomes and lysosomes of alveolar macrophages (35), while lysoPC (36) and ceramides (37) are known biomarkers of inflammation. We observed that 6 h after i.pulmon. administration of CAF01, the BMP (22:6/22:6, m/z 865.503) expression level in the lungs was comparable to the BMP level measured for control animals (**Figure 9A**). However, from 24 h and onward, the BMP signal increased consistently reaching a maximum at day 10 of the study, after which it was decreased at day 14. The ionized PS (38:4) (m/z 810.529), which is the most abundant phosphatidylserine species in the lungs (38), was expressed in the lung sections at all studied time points (**Supplementary Figure S6**). Analysis of the signal intensity ratio of BMP (22:6/22:6) as compared to PS (38:4) (m/z 810.529) showed that the intensity ratio of BMP/PS was increased from 24 h post-administration, reached a threshold at day 10 of the study, after which it was decreased at day 14 (**Figure 9B**). The increased level of BMP after i.pulmon. administration of CAF01 therefore suggests an altered phagocytic activity in alveolar macrophages. We did not observe any expression of ceramides and cholesteryl esters at the investigated time points after administration of

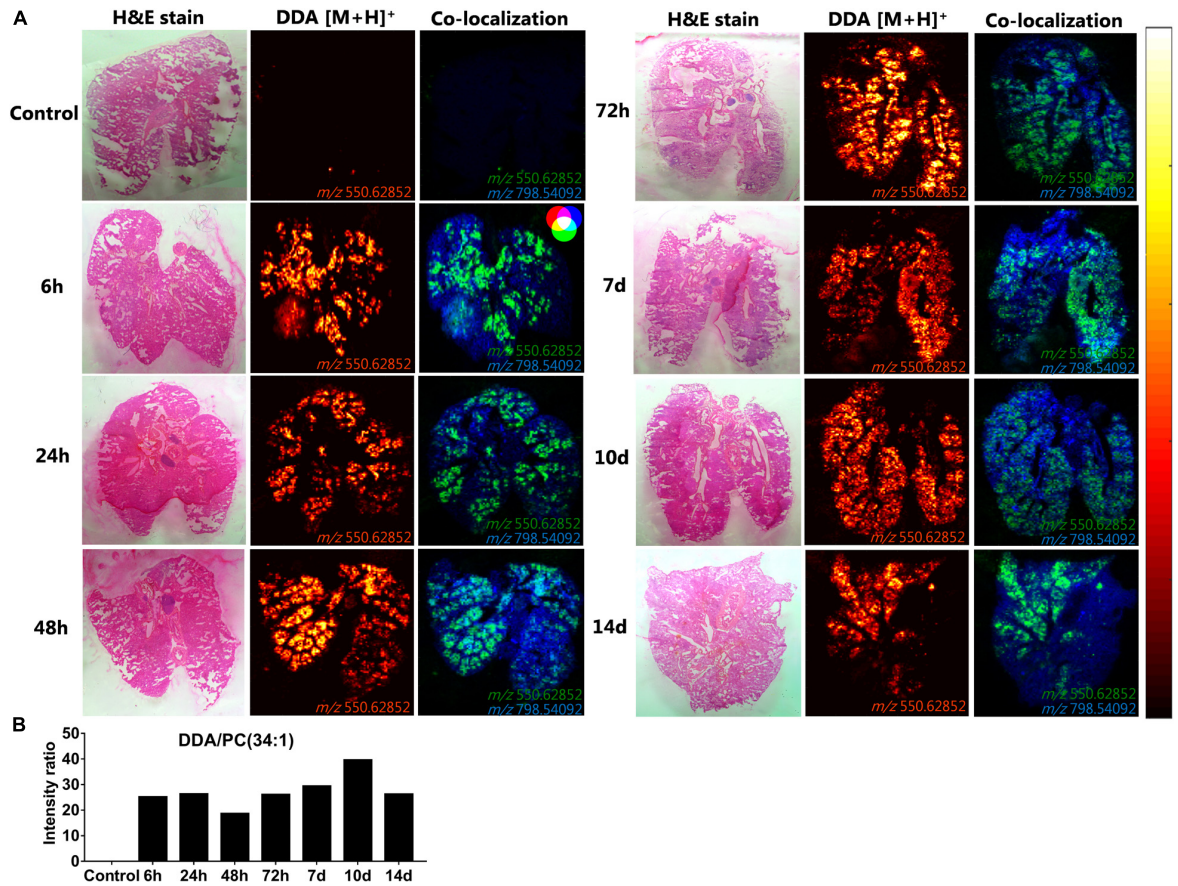

FIGURE 8 | Uniform distribution and signal intensity of dimethyldioctadecylammonium (DDA) bromide in cryo-sections of lungs of mice, which have been dosed intrapulmonary (i.pulmon.) with CAF01. BALB/c mice were immunized once with CAF01 *via* the i.pulmon. route, and matrix-assisted laser desorption/ionization mass spectrometry imaging (MALDI-MSI) was performed on lung cryo-sections at 6, 24, 48, and 72 h, and 7, 10, and 14 days after the immunization. Untreated mice served as negative control. **(A)** Hematoxylin and eosin (H&E) staining (left panels), MALDI-MSI-based distribution of DDA $[M + H]^+$ (m/z 550.629 ± 0.002, middle panels), and mass spectrometry (MS) co-localization images (right panels) of DDA $[M + H]^+$ (green) and PC (34:1) $[M + K]^+$ (m/z 798.541 ± 0.002) (blue) in the lungs at different time points after i.pulmon. administration of CAF01. **(B)** Signal intensity ratios between DDA and PC (34:1) at different time points of the study, which were calculated after drawing a region of interest (ROI) across the lung sections and comparing the MS signal intensities in the respective ROIs. All images were measured in the positive ion mode by MALDI-MSI at a pixel size of 100 μm.

CAF01 (data not shown). The phospholipid LysoPC (16:0) (m/z 518.323) was primarily distributed homogeneously in the lungs following CAF01 administration (**Supplementary Figure S7A**). Analysis of the signal intensity ratio of LysoPC (16:0)/PC (34:1) confirmed this observation. The intensity ratio of LysoPC/PC after administration of CAF01 remained low until day 10, or at the same level at day 14, compared to negative control lungs (**Supplementary Figure S7B**). This data therefore suggests that i.pulmon. administration of CAF01 does not induce any apparent inflammation or tissue damage in the lungs because the LysoPC and ceramides levels are not influenced by CAF01 administration.

DISCUSSION

Here, we investigated further our previous finding that parenteral prime and airway mucosal pull immunization with the H56/CAF01 vaccine induces higher humoral and cell-mediated immune responses than parenteral immunization alone (24) by providing a cellular basis that may explain the enhanced immunogenicity. We show that the i.m. prime – i.pulmon. pull immunization regimen with H56/CAF01 induces a higher vaccine uptake by pulmonary APCs, endothelial cells, and type I epithelial cells as well as splenic inflammatory macrophages as compared to the vaccine uptake measured after i.m. and i.pulmon. immunization, respectively. In addition, there is an increased activation state of vaccine$^+$ DCs and B cells in the lung- and intramuscular-draining lymph nodes following i.m. prime – i.pulmon. pull immunization with H56/CAF01, as compared to the activation state measured after immunization using the i.m. and i.pulmon. routes of administration, respectively. A major difference between the evaluated immunization strategies is the activation of innate immunity after i.m. and i.pulmon. prime immunization alone, as compared to the activation of both innate and memory immune responses after i.m. prime – i.pulmon pull

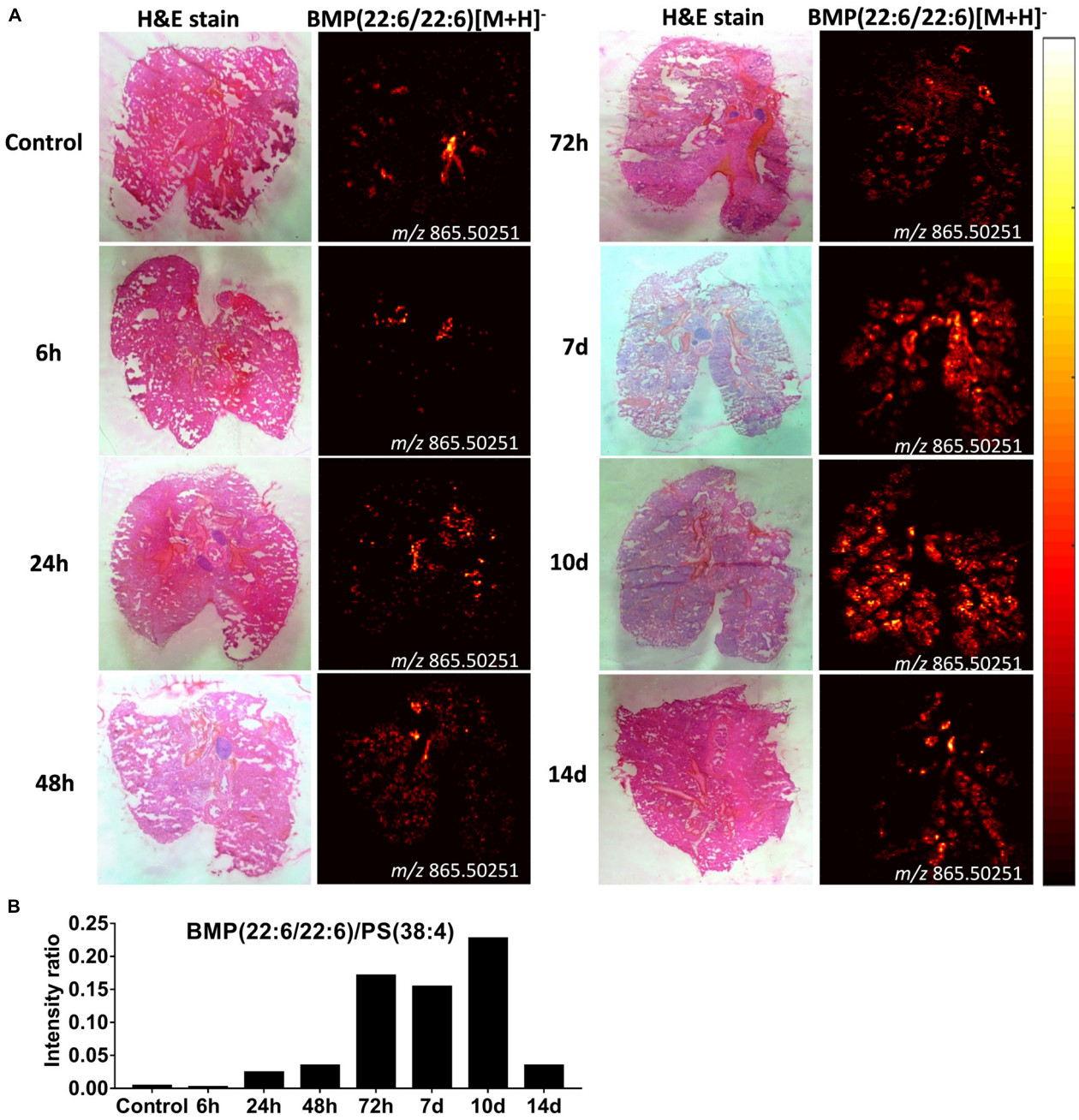

FIGURE 9 | Increased bis(monoacylglycero)phosphate (BMP) expression in the lungs of mice dosed intrapulmonary (i.pulmon.) with CAF01. BALB/c mice were immunized once with CAF01 *via* the i.pulmon. route, and matrix-assisted laser desorption/ionization mass spectrometry imaging (MALDI-MSI) was performed on lung cryo-sections collected 6, 24, 48, 72 h, and 7, 10, and 14 days after immunization. Untreated mice served as negative control. **(A)** Hematoxylin and eosin (H&E) staining (left panels) and MALDI-MSI-based distribution of BMP (22:6/22:6) $[M + H]^-$ (m/z 865.503, right panels) in cryo-sections of lungs isolated at different time points after i.pulmon. dosing with CAF01. **(B)** Signal intensity ratios between BMP and PS (38:4) $[M + H]^-$ (m/z 810.529 ± 0.002) at different time points of the study, which were calculated by drawing a region of interest (ROI) across the lung sections and comparing the MS signal intensities in the respective ROIs. All images were measured in the negative ion mode by using MALDI-MSI at a pixel size of 100 μm.

immunization, in particular at the 24 h time point of the study. Importantly, we show for the first time that MSI is a useful tool to investigate the biodistribution of a lipid-based vaccine adjuvant. We report that following pulmonary immunization, CAF01 is homogeneously distributed in the lung parenchyma and is present in the lungs for at least 2 weeks without inducing any measurable local tissue damage or inflammation. We further report an increased BMP signal in the lungs following immunization, which in ischemic brain tissue has been shown to correlate with an increased phagocytic activity of cerebral

macrophages (34). Hence, the increased BMP activity measured in the lungs after administration of CAF01 may be correlated with an altered phagocytic activity in alveolar macrophages.

The lungs are highly vascularized with a large surface area and an extensive network of immune cells surveilling the mucosa against microbial attacks, which make lung tissue an attractive target for the administration of subunit vaccine antigens and immunopotentiating adjuvants (39). Subunit vaccines may elicit immunopotentiating effects by interacting with the highly specialized network of immune cells, e.g., DCs and macrophages that capture the vaccines via pattern-recognition receptors and transport them (antigen + adjuvant) to the regional lymph nodes, where antigen-specific T cell activation takes place (14). T cell-mediated protection against *Mtb* is recognized to be dependent on the ability of the antigen-specific T-cells to home back to the lung parenchyma and directly interact with infected cells (40, 41). Accordingly, a number of airway mucosal immunization strategies, based on either mucosal BCG vaccination or heterologous mucosal vaccination with viral vectors encoding *Mtb* antigens following BCG priming, have been tested and found to enhance the number of protective lung-resident T cells against TB (42–44). Hence, pulmonary delivery of subunit vaccines represents an attractive strategy for inducing antigen-specific T cell immunity in the lungs (39, 45). We envisage to use this strategy for immunization of adolescents and adults with H56/CAF01 vaccine. BCG is administered to newborns immediately after birth and has over 70% protective efficacy against tuberculous meningitis and miliary TB (46), while in adults, BCG vaccination fails to completely protect against pulmonary TB and has a very variable protective efficacy (0–80%) (47). BCG vaccination also reduces mortality in newborn and children because of non-specific cross-protection induced by this vaccine against other unrelated pathogens (48). Therefore, keeping in view the beneficial effects of BCG vaccination in children, our long term strategy is to boost the BCG-primed immune responses (in infants and neonates) with parenteral prime and mucosal pull immunization of H56/CAF01 vaccine (in adolescents and adults).

Recently, we demonstrated that parenteral prime and i.pulmon. pull immunization with the H56/CAF01 vaccine induces significantly higher airway mucosal as well as systemic IgA and polyfunctional $CD4^+$ T cells as compared to parenteral prime and pull immunization (24). However, the cellular basis of this increased immune response after parenteral prime and mucosal pull immunization was unknown. The results of our current work provide strong evidence that this enhanced immunity may be by virtue of an increased vaccine uptake by pulmonary APCs, including DCs and macrophages, and/or an enhanced activation of DCs in the lung-draining lymph nodes. In the lungs, several DC subsets and macrophages reside possessing specialized functions with respect to antigen uptake, presentation and initiation of immune responses (49). In the steady state, the lungs are populated by two major subsets of conventional DCs (cDCs), i.e., $CD103^+$ and $CD11b^+$ cDCs, and pDCs, while moDCs migrate into the lung parenchyma in response to inflammation (28). In our study, the H56/CAF01 vaccine is taken up by respiratory tract APCs, but the extent of uptake is highly dependent on the specific immunization strategy. Pulmonary DCs and macrophages were strongly positive for H56/CAF01 administered by applying the parenteral prime – mucosal pull immunization strategy as compared to the H56/CAF01 levels measured after parenteral immunization alone.

Using virosomes and liposomes as delivery systems without or with conjugated ovalbumin, it has previously been shown that DCs and macrophages take up equally well nanoparticles administered intranasally (50). However, another study reported enhanced uptake of latex particles by alveolar macrophages, as compared to pulmonary DCs, after intranasal administration (51). Recently, airway mucosal pull immunization by H56/CAF01 immunization was demonstrated to induce significantly increased numbers and activation state of alveolar macrophages in the lungs (23). At the earliest time point investigated in the present study, i.e., 3 h after administration, our measurements did not show any detectable vaccine uptake in the airways or trafficking to the lung-draining LNs, as reported previously (12). Only 24 h after immunization, there were visible differences in the vaccine uptake between the different APCs, depending on the specific immunization strategy. We also observed a significantly higher number of $vaccine^+$ neutrophils following mucosal pull immunization as compared to the number of $vaccine^+$ neutrophils after single immunizations. Among the visceral organs, the lungs contain the highest proportion of neutrophils, which might facilitate the activation and differentiation of antigen-specific $CD4^+$ T cells *via* cross-talk with DCs (52, 53). Therefore, our results show that there are distinct differences in the vaccine uptake by innate myeloid APCs and B cells, depending on the specific immunization strategy (prime versus prime – pull). Similarly, a high phenotypic diversity of neutrophils, monocytes, and DCs was observed between prime and pull immunization of cynomolgus macaques with the modified vaccinia virus Ankara (54).

In addition to professional APCs, a variety of other cell types may present antigens to T-helper cells, including epithelial cells (55, 56). Lung epithelial cells can present antigens, and they play an important role for the induction of local immune responses in the lungs (55, 57). We found that mucosal pull immunization induces a higher number of $vaccine^+$ type II epithelial cells within 3 h and a higher number of type I epithelial cells at 72 h post-immunization as compared to parenteral immunization alone. Both type I (57) and II (58) epithelial cells possess the ability to present antigens, but they differ in their expression levels of major histocompatibility complex II molecules with higher expression levels in type II cells than in type I cells (57). We also observed lower major histocompatibility complex II expression in $vaccine^+$ type I epithelial cells in this study (data not shown). The potential role of lung epithelial cells in antigen capture and presentation in immune responses is restricted to stimulate T cells previously presented to antigens by other APCs (59, 60). We found that the hematopoietic lineage and lineage-negative cells took up the vaccine, in particular at 72 h after immunization. Lineage-negative cells primarily include fibroblasts, smooth muscle cells and mesenchymal stem cells (26). The mesenchymal stem cells have the capability to capture and release antigens, which are subsequently captured by APCs (61).

The distinct differences in vaccine uptake by pulmonary immune cells after vaccine administration applying the three different immunization strategies correlated well with the subsequent activation state of DCs measured in the draining LNs. Previously, it has been shown that the activation state of CAF04- and CAF09-induced $CD4^+$ and $CD8^+$ T cells coincided with the activation of resident and migratory DCs in the spleen and the draining LNs after parenteral immunization (33). In the lung-draining LNs, resident $CD8\alpha^+$ and migratory $CD11b^+$ DCs were significantly activated at 24 and 72 h after mucosal pull immunization, respectively, than after parenteral immunization. This increased activation state of $vaccine^+$ DCs in the lung-draining lymph nodes (TLN + MLN) by i.m. prime – i.pulmon. pull immunization with H56/CAF01 supports our previous results where we observed that this immunization strategy induces high lung mucosal and systemic antibody and $CD4^+$ responses (24). On the other hand, in the LNs draining the i.m. site of immunization (ILN + PLN), no significant differences between the activation state of $CD8\alpha^+$ and $CD11b^+$ DCs were observed among the different immunization strategies used. Interestingly, B cells and pDCs are significantly activated in ILN + PLN at 24 h post-prime-pull immunization, and the fact that only DCs showed increased activation after i.m. immunization is supported by previous studies (62). Similarly, we found that all immunization strategies used for administering the H56/CAF01 vaccine promote differential cellular uptake by innate myeloid APCs present in the spleen. Our previous results show that i.m. prime – i.pulmon. pull immunization with H56/CAF01 induces highly comparable antibody and $CD4^+$ responses in the spleen as the i.m. immunization (24). Overall, there were marked differences in the vaccine uptake by innate myeloid APCs, epithelial cells, and B cells and in the activation state of APCs between prime and prime – pull immunization with the H56/CAF01 vaccine. Recently, it was shown that the innate myeloid cells following the prime – pull with the modified vaccinia virus Ankara displayed higher activation states and enhanced expression of molecules involved in phagocytosis, antigen presentation, co-stimulation, chemotaxis, and inflammation (54). Recently, we showed that mucosal (intranasal) pull immunization of H56/CAF01 immunization significantly increased the early lung-localized vaccine T-cell response and increased early protection to a pulmonary *Mtb* challenge in mice (23). Therefore, our results demonstrating an improved antigen uptake and s stronger immune response following i.pulmon. pull immunization of H56/CAF01 immunization (24) are certainly promising for our efforts to develop a thermostable, dry powder-based H56/CAF01 vaccine intended for i.pulmon. immunization of BCG-primed individuals (63).

Mass spectrometry imaging can be used to identify the distribution and expression levels of molecules, e.g., biomarkers, peptides and proteins, and metabolites or drugs in tissue sections with high sensitivity and specificity, without the need to label the analyte (34, 64). This imaging technique can also be used to identify the spatiotemporal distribution of different phospholipids in various tissues, including the lungs (34, 65). Using SPECT-CT imaging, we have previously measured the pharmacokinetics of CAF01 for up to day 6 after pulmonary administration (24). However, there is still insufficient data on the long-term fate and safety of CAF01 administered in the respiratory tract. Here, we show using MSI that DDA distributes uniformly in the lungs and is detectable for at least 2 weeks post-i.pulmon. administration of CAF01. Both DDA and TDB co-localize with the endogenous phospholipids PC (34:1) in the positive ion mode and PS (38:4) in the negative ion mode. The phospholipid lysoPC (16:0) (36) and the sphingolipid ceramide (37) are well-known biomarkers of inflammation and local tissue damage, respectively. The absence of enhanced ceramide expression in the lungs of mice immunized with CAF01, and the lack of difference in the expression levels of LysoPC between the immunized mice and the negative control animal, suggest that i.pulmon. administration of CAF01 may be safe and does not induce any apparent inflammation in the lungs during the investigated time period. Using intranasal (66, 67) and i.pulmon. immunization (24, 68), our previous results have consistently shown the safety of immunization with the CAF01 adjuvant in preclinical animal models and most recently in phase I clinical trials in humans following intranasal immunization with a *Chlamydia* antigen (69). Therefore, in this study we did not expect any difference in the number of inflammatory cells among the immunization strategies and did not compare histopathological changes in lung tissue sections. BMP (22:6/22:6) is a negatively charged glycerophospholipid, which is primarily localized in the late endosomes/lysosomes (70). The BMP content is enriched in alveolar macrophages, as compared to other cell types, and it is primarily localized in phagosomes (35). BMP (22:6/22:6) has been shown to co-localize with the macrophage biomarker CD11b in ischemic brain tissue, and it is a reported biomarker for phagocytozing macrophages (34). The increased level of BMP after i.pulmon. administration of CAF01 liposomes measured in our study suggests an increased phagocytic activity in alveolar macrophages. In addition, the flow cytometry data demonstrates an increased number of alveolar macrophages 24 and 72 h after i.pulmon. administration of the H56/CAF01 vaccine. Hence, these results collectively suggest that after i.pulmon. administration of CAF01, there is (i) an increased alveolar macrophage activity, as well as (ii) an increased number of alveolar macrophages that takes up the vaccine. In a previous study, cholesteryl esters were shown to co-localize with BMP during resolution of cerebral inflammation due to phagocytosis of cholesterol-containing dead cells or cell debris (34). However, in our study, the BMP expression was not accompanied by increased levels of cholesteryl esters. The lack of cholesteryl ester expression in our study suggests that (i) there is no increased phagocytosis of dead cells following CAF01 administration in the lungs, and (ii) applying this administration route does not cause any measurable local inflammation.

In this study, we chose to investigate multiple time points by MSI post-i.pulmon. administration of CAF01, rather than including more animals in each group and fewer time points. We believe that this imaging method is a very robust method for evaluating even low doses/expression levels of proteins, lipids and their metabolites. However, to improve the statistical strength of our data, more biological replicates should be

included in future studies. In addition, commonly investigated biomarkers for systemic inflammation, e.g., plasma C-reactive protein and interferon-γ inducible protein-10 concentrations, should be evaluated to investigate further the safety of pulmonary vaccination.

CONCLUSION

In conclusion, we show that there are pronounced differences in the vaccine uptake by innate myeloid APCs in the lungs and the spleen and epithelial cells in the lungs, and in the activation state of APCs in the lung-draining lymph nodes after i.m. prime and i.pulmon. mucosal pull immunization with the H56/CAF01 vaccine, as compared to i.m. or i.pulmon. priming alone, which suggests activation of both innate and memory response by prime – pull immunization. Using phospholipid analysis by MALDI-MSI, we further conclude that airway mucosal immunization with H56/CAF01 is a safe immunization approach, which is critical to consider in the rational design of vaccines for pulmonary delivery. Overall, the differences in vaccine uptake by innate myeloid cells and activation of APCs among the different immunization strategies described here can be valuable to tailor vaccine-induced immunity.

DATA AVAILABILITY STATEMENT

The datasets generated for this study are available on request to the corresponding author.

ETHICS STATEMENT

The animal study was reviewed and approved by the Danish National Experiment Inspectorate under permit 2016-15-0201-01026.

AUTHOR CONTRIBUTIONS

AT, DC, and CF designed the study. AT and FP performed the laboratory work and analyzed the data. AT, HH, DC, CJ, and CF interpreted the data. AT, FP, and CF drafted the manuscript. AT, HH, PA, DC, CJ, and CF provided scientific input throughout the study period and draft of the manuscript.

FUNDING

This work was supported by The Danish Council for Independent Research, Technology and Production Sciences (Grant Number DFF-4184-00422). Support from the Carlsberg Foundation and The Danish Council for Independent Research, Medical Sciences (Grant Number DFF-4002-00391) for MALDI-MSI instrumentation is gratefully acknowledged. This study was financed in part (support to FP) by the Coordenação de Aperfeiçoamento de Pessoal de Nível Superior – Brazil (CAPES) (Finance Code 001).

ACKNOWLEDGMENTS

We are grateful to the staff of the animal facility at Department of Drug Design and Pharmacology, University of Copenhagen, for their animal husbandry services. We thank the Core Facility for Flow Cytometry, Faculty of Health and Medical Sciences, University of Copenhagen, for the flow cytometry. We also thank Fabrice Rose for technical assistance and Karolina Sanicka for help with the cell studies.

SUPPLEMENTARY MATERIAL

The Supplementary Material for this article can be found online at: https://www.frontiersin.org/articles/10.3389/fimmu.2020.00803/full#supplementary-material

REFERENCES

1. WHO *Global Tuberculosis Report 2018*. Geneva: World Health Organization. (2018).
2. Uplekar M, Weil D, Lonnroth K, Jaramillo E, Lienhardt C, Dias HM, et al. WHO's new end TB strategy. *Lancet*. (2015) 385:1799–801. doi: 10.1016/S0140-6736(15)60570-0
3. Foged C. Subunit vaccines of the future: the need for safe, customized and optimized particulate delivery systems. *Ther Deliv*. (2011) 2:1057–77. doi: 10.4155/tde.11.68
4. Delany I, Rappuoli R, De Gregorio E. Vaccines for the 21st century. *EMBO Mol Med*. (2014) 6:708–20. doi: 10.1002/emmm.201403876
5. Beverley PC, Sridhar S, Lalvani A, Tchilian EZ. Harnessing local and systemic immunity for vaccines against tuberculosis. *Mucosal Immunol*. (2014) 7:20–6. doi: 10.1038/mi.2013.99
6. Iqbal AJ, Fisher EA, Greaves DR. Inflammation-a critical appreciation of the role of myeloid cells. *Microbiol Spectr*. (2016) 4:MCHD-0027-2016.. doi: 10.1128/microbiolspec.MCHD-0027-2016
7. Jaillon S, Galdiero MR, Del Prete D, Cassatella MA, Garlanda C, Mantovani A. Neutrophils in innate and adaptive immunity. *Semin Immunopathol*. (2013) 35:377–94. doi: 10.1007/s00281-013-0374-8
8. Hashimoto D, Miller J, Merad M. Dendritic cell and macrophage heterogeneity in vivo. *Immunity*. (2011) 35:323–35. doi: 10.1016/j.immuni.2011.09.007
9. Gerner MY, Casey KA, Kastenmuller W, Germain RN. Dendritic cell and antigen dispersal landscapes regulate T cell immunity. *J Exp Med*. (2017) 214:3105–22. doi: 10.1084/jem.20170335
10. Desch AN, Henson PM, Jakubzick CV. Pulmonary dendritic cell development and antigen acquisition. *Immunol Res*. (2013) 55:178–86. doi: 10.1007/s12026-012-8359-6
11. Condon TV, Sawyer RT, Fenton MJ, Riches DW. Lung dendritic cells at the innate-adaptive immune interface. *J Leukoc Biol*. (2011) 90:883–95. doi: 10.1189/jlb.0311134
12. Blank F, Stumbles PA, Seydoux E, Holt PG, Fink A, Rothen-Rutishauser B, et al. Size-dependent uptake of particles by pulmonary antigen-presenting cell populations and trafficking to regional lymph nodes. *Am J Respir Cell Mol Biol*. (2013) 49:67–77. doi: 10.1165/rcmb.2012-0387OC
13. Fromen CA, Robbins GR, Shen TW, Kai MP, Ting JP, DeSimone JM. Controlled analysis of nanoparticle charge on mucosal and systemic antibody responses following pulmonary immunization. *Proc Natl Acad Sci USA*. (2015) 112:488–93. doi: 10.1073/pnas.1422923112
14. Blank F, Fytianos K, Seydoux E, Rodriguez-Lorenzo L, Petri-Fink A, von Garnier C, et al. Interaction of biomedical nanoparticles with the pulmonary

immune system. *J Nanobiotechnology*. (2017) 15:6. doi: 10.1186/s12951-016-0242-5

15. Aagaard C, Hoang T, Dietrich J, Cardona PJ, Izzo A, Dolganov G, et al. A multistage tuberculosis vaccine that confers efficient protection before and after exposure. *Nat Med*. (2011) 17:189–94. doi: 10.1038/nm.2285
16. Knudsen NP, Olsen A, Buonsanti C, Follmann F, Zhang Y, Coler RN, et al. Different human vaccine adjuvants promote distinct antigen-independent immunological signatures tailored to different pathogens. *Sci Rep*. (2016) 6:19570. doi: 10.1038/srep19570
17. Lin PL, Dietrich J, Tan E, Abalos RM, Burgos J, Bigbee C, et al. The multistage vaccine H56 boosts the effects of BCG to protect cynomolgus macaques against active tuberculosis and reactivation of latent *Mycobacterium tuberculosis* infection. *J Clin Invest*. (2012) 122:303–14. doi: 10.1172/JCI46252
18. Davidsen J, Rosenkrands I, Christensen D, Vangala A, Kirby D, Perrie Y, et al. Characterization of cationic liposomes based on dimethyldioctadecylammonium and synthetic cord factor from *M. tuberculosis* (trehalose 6,6'-dibehenate)-a novel adjuvant inducing both strong CMI and antibody responses. *Biochim Biophys Acta*. (2005) 1718:22–31. doi: 10.1016/j.bbamem.2005.10.011
19. Kamath AT, Rochat AF, Christensen D, Agger EM, Andersen P, Lambert PH, et al. A liposome-based mycobacterial vaccine induces potent adult and neonatal multifunctional T cells through the exquisite targeting of dendritic cells. *PLoS One*. (2009) 4:e5771. doi: 10.1371/journal.pone.0005771
20. van Dissel JT, Joosten SA, Hoff ST, Soonawala D, Prins C, Hokey DA, et al. A novel liposomal adjuvant system, CAF01, promotes long-lived *Mycobacterium tuberculosis*-specific T-cell responses in human. *Vaccine*. (2014) 32:7098–107. doi: 10.1016/j.vaccine.2014.10.036
21. Roman VR, Jensen KJ, Jensen SS, Leo-Hansen C, Jespersen S, da Silva Te D, et al. Therapeutic vaccination using cationic liposome-adjuvanted HIV type 1 peptides representing HLA-supertype-restricted subdominant T cell epitopes: safety, immunogenicity, and feasibility in Guinea-Bissau. *AIDS Res Hum Retroviruses*. (2013) 29:1504–12. doi: 10.1089/AID.2013.0076
22. Karlsson I, Brandt L, Vinner L, Kromann I, Andreasen LV, Andersen P, et al. Adjuvanted HLA-supertype restricted subdominant peptides induce new T-cell immunity during untreated HIV-1-infection. *Clin Immunol*. (2013) 146:120–30. doi: 10.1016/j.clim.2012.12.005
23. Woodworth JS, Christensen D, Cassidy JP, Agger EM, Mortensen R, Andersen P. Mucosal boosting of H56:CAF01 immunization promotes lung-localized T cells and an accelerated pulmonary response to *Mycobacterium tuberculosis* infection without enhancing vaccine protection. *Mucosal Immunol*. (2019) 12:816–26. doi: 10.1038/s41385-019-0145-5
24. Thakur A, Rodriguez-Rodriguez C, Saatchi K, Rose F, Esposito T, Nosrati Z, et al. Dual-Isotope SPECT/CT imaging of the tuberculosis subunit vaccine H56/CAF01: induction of strong systemic and mucosal IgA and T-cell responses in mice upon subcutaneous prime and intrapulmonary boost immunization. *Front Immunol*. (2018) 9:2825. doi: 10.3389/fimmu.2018.02825
25. Woodland DL. Jump-starting the immune system: prime-boosting comes of age. *Trends Immunol*. (2004) 25:98–104. doi: 10.1016/j.it.2003.11.009
26. Singer BD, Mock JR, D'Alessio FR, Aggarwal NR, Mandke P, Johnston L, et al. Flow-cytometric method for simultaneous analysis of mouse lung epithelial, endothelial, and hematopoietic lineage cells. *Am J Physiol Lung Cell Mol Physiol*. (2016) 310:L796–801. doi: 10.1152/ajplung.00334.2015
27. Misharin AV, Morales-Nebreda L, Mutlu GM, Budinger GR, Perlman H. Flow cytometric analysis of macrophages and dendritic cell subsets in the mouse lung. *Am J Respir Cell Mol Biol*. (2013) 49:503–10. doi: 10.1165/rcmb.2013-0086MA
28. Pulendran B. The varieties of immunological experience: of pathogens, stress, and dendritic cells. *Annu Rev Immunol*. (2015) 33:563–606. doi: 10.1146/annurev-immunol-020711-075049
29. Bouschen W, Schulz O, Eikel D, Spengler B. Matrix vapor deposition/recrystallization and dedicated spray preparation for high-resolution scanning microprobe matrix-assisted laser desorption/ionization imaging mass spectrometry (SMALDI-MS) of tissue and single cells. *Rapid Commun Mass Spectrom*. (2010) 24:355–64. doi: 10.1002/rcm.4401
30. Janfelt C, Wellner N, Leger PL, Kokesch-Himmelreich J, Hansen SH, Charriaut-Marlangue C, et al. Visualization by mass spectrometry of 2-dimensional changes in rat brain lipids, including N-acylphosphatidylethanolamines, during neonatal brain ischemia. *FASEB J*. (2012) 26:2667–73. doi: 10.1096/fj.11-201152
31. Schramm T, Hester A, Klinkert I, Both JP, Heeren RM, Brunelle A, et al. imzML–a common data format for the flexible exchange and processing of mass spectrometry imaging data. *J Proteomics*. (2012) 75:5106–10. doi: 10.1016/j.jprot.2012.07.026
32. Robichaud G, Garrard KP, Barry JA, Muddiman DC. MSiReader: an open-source interface to view and analyze high resolving power MS imaging files on Matlab platform. *J Am Soc Mass Spectrom*. (2013) 24:718–21. doi: 10.1007/s13361-013-0607-z
33. Schmidt ST, Khadke S, Korsholm KS, Perrie Y, Rades T, Andersen P, et al. The administration route is decisive for the ability of the vaccine adjuvant CAF09 to induce antigen-specific CD8(+) T-cell responses: the immunological consequences of the biodistribution profile. *J Control Release*. (2016) 239:107–17. doi: 10.1016/j.jconrel.2016.08.034
34. Nielsen MM, Lambertsen KL, Clausen BH, Meyer M, Bhandari DR, Larsen ST, et al. Mass spectrometry imaging of biomarker lipids for phagocytosis and signalling during focal cerebral ischaemia. *Sci Rep*. (2016) 6:39571. doi: 10.1038/srep39571
35. Akgoc Z, Iosim S, Seyfried TN. Bis(monoacylglycero)phosphate as a Macrophage enriched phospholipid. *Lipids*. (2015) 50:907–12. doi: 10.1007/s11745-015-4045-5
36. Qin X, Qiu C, Zhao L. Lysophosphatidylcholine perpetuates macrophage polarization toward classically activated phenotype in inflammation. *Cell Immunol*. (2014) 289:185–90. doi: 10.1016/j.cellimm.2014.04.010
37. Kurz J, Parnham MJ, Geisslinger G, Schiffmann S. Ceramides as novel disease biomarkers. *Trends Mol Med*. (2019) 25:20–32. doi: 10.1016/j.molmed.2018.10.009
38. von Halling Laier C, Gibson B, Moreno JAS, Rades T, Hook S, Nielsen LH, et al. Microcontainers for protection of oral vaccines, in vitro and in vivo evaluation. *J Control Release*. (2018) 294:91–101. doi: 10.1016/j.jconrel.2018.11.030
39. Blank F, Stumbles P, von Garnier C. Opportunities and challenges of the pulmonary route for vaccination. *Expert Opin Drug Deliv*. (2011) 8:547–63. doi: 10.1517/17425247.2011.565326
40. Khader SA, Bell GK, Pearl JE, Fountain JJ, Rangel-Moreno J, Cilley GE, et al. IL-23 and IL-17 in the establishment of protective pulmonary CD4+ T cell responses after vaccination and during *Mycobacterium tuberculosis* challenge. *Nat Immunol*. (2007) 8:369–77. doi: 10.1038/ni1449
41. Srivastava S, Ernst JD. Cutting edge: direct recognition of infected cells by CD4 T cells is required for control of intracellular *Mycobacterium tuberculosis* in vivo. *J Immunol*. (2013) 191:1016–20. doi: 10.4049/jimmunol.1301236
42. Jeyanathan M, Shao Z, Yu X, Harkness R, Jiang R, Li J, et al. AdHu5Ag85A respiratory mucosal boost immunization enhances protection against pulmonary tuberculosis in BCG-primed non-human primates. *PLoS One*. (2015) 10:e0135009. doi: 10.1371/journal.pone.0135009
43. Satti I, Meyer J, Harris SA, Manjaly Thomas ZR, Griffiths K, Antrobus RD, et al. Safety and immunogenicity of a candidate tuberculosis vaccine MVA85A delivered by aerosol in BCG-vaccinated healthy adults: a phase 1, double-blind, randomised controlled trial. *Lancet Infect Dis*. (2014) 14:939–46. doi: 10.1016/S1473-3099(14)70845-X
44. Perdomo C, Zedler U, Kuhl AA, Lozza L, Saikali P, Sander LE, et al. Mucosal BCG vaccination induces protective lung-resident memory T cell populations against tuberculosis. *MBio*. (2016) 7:e01686-16. doi: 10.1128/mBio.01686-16
45. Foged C. Thermostable subunit vaccines for pulmonary delivery: how close are we? *Curr Pharm Des*. (2016) 22:2561–76. doi: 10.2174/1381612822666160202141603
46. Thakur A, Andrea A, Mikkelsen H, Woodworth JS, Andersen P, Jungersen G, et al. Targeting the mincle and TLR3 receptor using the dual agonist cationic adjuvant formulation 9 (CAF09) induces humoral and polyfunctional memory T cell responses in calves. *PLoS One*. (2018) 13:e0201253. doi: 10.1371/journal.pone.0201253
47. Mangtani P, Abubakar I, Ariti C, Beynon R, Pimpin L, Fine PE, et al. Protection by BCG vaccine against tuberculosis: a systematic review of randomized controlled trials. *Clin Infect Dis*. (2014) 58:470–80. doi: 10.1093/cid/cit790

48. de Bree LCJ, Koeken V, Joosten LAB, Aaby P, Benn CS, van Crevel R, et al. Non-specific effects of vaccines: current evidence and potential implications. *Semin Immunol*. (2018) 39:35–43. doi: 10.1016/j.smim.2018.06.002
49. Guilliams M, Lambrecht BN, Hammad H. Division of labor between lung dendritic cells and macrophages in the defense against pulmonary infections. *Mucosal Immunol*. (2013) 6:464–73. doi: 10.1038/mi.2013.14
50. Blom RAM, Amacker M, van Dijk RM, Moser C, Stumbles PA, Blank F, et al. Pulmonary delivery of virosome-bound antigen enhances antigen-specific CD4(+) T cell proliferation compared to liposome-bound or soluble antigen. *Front Immunol*. (2017) 8:359. doi: 10.3389/fimmu.2017.00359
51. Jakubzick C, Tacke F, Llodra J, van Rooijen N, Randolph GJ. Modulation of dendritic cell trafficking to and from the airways. *J Immunol*. (2006) 176:3578–84. doi: 10.4049/jimmunol.176.6.3578
52. Hufford MM, Richardson G, Zhou H, Manicassamy B, Garcia-Sastre A, Enelow RI, et al. Influenza-infected neutrophils within the infected lungs act as antigen presenting cells for anti-viral CD8(+) T cells. *PLoS One*. (2012) 7:e46581. doi: 10.1371/journal.pone.0046581
53. Blomgran R, Ernst JD. Lung neutrophils facilitate activation of naive antigen-specific CD4+ T cells during *Mycobacterium tuberculosis* infection. *J Immunol*. (2011) 186:7110–9. doi: 10.4049/jimmunol.1100001
54. Palgen JL, Tchitchek N, Elhmouzi-Younes J, Delandre S, Namet I, Rosenbaum P, et al. Prime and boost vaccination elicit a distinct innate myeloid cell immune response. *Sci Rep*. (2018) 8:3087. doi: 10.1038/s41598-018-21222-2
55. Wosen JE, Mukhopadhyay D, Macaubas C, Mellins ED. Epithelial MHC Class II expression and its role in antigen presentation in the gastrointestinal and respiratory tracts. *Front Immunol*. (2018) 9:2144. doi: 10.3389/fimmu.2018.02144
56. Hershberg RM, Mayer LF. Antigen processing and presentation by intestinal epithelial cells - polarity and complexity. *Immunol Today*. (2000) 21:123–8. doi: 10.1016/s0167-5699(99)01575-3
57. Kumari M, Saxena RK. Relative efficacy of uptake and presentation of *Mycobacterium bovis* BCG antigens by type I mouse lung epithelial cells and peritoneal macrophages. *Infect Immun*. (2011) 79:3159–67. doi: 10.1128/IAI.05406-11
58. Corbiere V, Dirix V, Norrenberg S, Cappello M, Remmelink M, Mascart F. Phenotypic characteristics of human type II alveolar epithelial cells suitable for antigen presentation to T lymphocytes. *Respir Res*. (2011) 12:15. doi: 10.1186/1465-9921-12-15
59. Rothermel AL, Wang Y, Schechner J, Mook-Kanamori B, Aird WC, Pober JS, et al. Endothelial cells present antigens in vivo. *BMC Immunol*. (2004) 5:5. doi: 10.1186/1471-2172-5-5
60. Perez VL, Henault L, Lichtman AH. Endothelial antigen presentation: stimulation of previously activated but not naive TCR-transgenic mouse T cells. *Cell Immunol*. (1998) 189:31–40. doi: 10.1006/cimm.1998.1362
61. Sanchez-Abarca LI, Alvarez-Laderas I, Diez Campelo M, Caballero-Velazquez T, Herrero C, Muntion S, et al. Uptake and delivery of antigens by mesenchymal stromal cells. *Cytotherapy*. (2013) 15:673–8. doi: 10.1016/j.jcyt.2013.01.216
62. Kamath AT, Mastelic B, Christensen D, Rochat AF, Agger EM, Pinschewer DD, et al. Synchronization of dendritic cell activation and antigen exposure is required for the induction of Th1/Th17 responses. *J Immunol*. (2012) 188:4828–37. doi: 10.4049/jimmunol.1103183
63. Thakur A, Ingvarsson PT, Schmidt ST, Rose F, Andersen P, Christensen D, et al. Immunological and physical evaluation of the multistage tuberculosis subunit vaccine candidate H56/CAF01 formulated as a spray-dried powder. *Vaccine*. (2018) 36:3331–9. doi: 10.1016/j.vaccine.2018.04.055
64. Ferguson CN, Fowler JW, Waxer JF, Gatti RA, Loo JA. Mass spectrometry-based tissue imaging of small molecules. *Adv Exp Med Biol*. (2014) 806:283–99. doi: 10.1007/978-3-319-06068-2_12
65. Berry KA, Li B, Reynolds SD, Barkley RM, Gijon MA, Hankin JA, et al. MALDI imaging MS of phospholipids in the mouse lung. *J Lipid Res*. (2011) 52:1551–60. doi: 10.1194/jlr.M015750
66. Ciabattini A, Prota G, Christensen D, Andersen P, Pozzi G, Medaglini D. Characterization of the antigen-specific CD4(+) T cell response induced by prime-boost strategies with CAF01 and CpG adjuvants administered by the intranasal and subcutaneous routes. *Front Immunol*. (2015) 6:430. doi: 10.3389/fimmu.2015.00430
67. Lorenzen E, Follmann F, Boje S, Erneholm K, Olsen AW, Agerholm JS, et al. Intramuscular priming and intranasal boosting induce strong genital immunity through secretory IgA in minipigs infected with chlamydia trachomatis. *Front Immunol*. (2015) 6:628. doi: 10.3389/fimmu.2015.00628
68. Thakur A, Rose F, Ansari SR, Koch P, Martini V, Ovesen SL, et al. Design of gadoteridol-loaded cationic liposomal adjuvant CAF01 for MRI of lung deposition of intrapulmonary administered particles. *Mol Pharm*. (2019) 16:4725–37. doi: 10.1021/acs.molpharmaceut.9b00908
69. Abraham S, Juel HB, Bang P, Cheeseman HM, Dohn RB, Cole T, et al. Safety and immunogenicity of the chlamydia vaccine candidate CTH522 adjuvanted with CAF01 liposomes or aluminium hydroxide: a first-in-human, randomised, double-blind, placebo-controlled, phase 1 trial. *Lancet Infect Dis*. (2019) 19:1091–100. doi: 10.1016/S1473-3099(19)30279-8
70. van der Goot FG, Gruenberg J. Intra-endosomal membrane traffic. *Trends Cell Biol*. (2006) 16:514–21. doi: 10.1016/j.tcb.2006.08.003

Conflict of Interest: PA and DC are employed by Statens Serum Institut, a nonprofit government research facility, of which the CAF adjuvants and H56 are proprietary products.

The remaining authors declare that the research was conducted in the absence of any commercial or financial relationships that could be construed as a potential conflict of interest.

frontiers in Immunology

REVIEW
published: 16 June 2020
doi: 10.3389/fimmu.2020.01055

Challenges in Dengue Vaccines Development: Pre-existing Infections and Cross-Reactivity

Abdullah M. Izmirly[1,2,3], *Sana O. Alturki*[2,3], *Sawsan O. Alturki*[2,3], *Jennifer Connors*[1,2] *and Elias K. Haddad*[1,2]*

[1] Division of Infectious Diseases and HIV Medicine, Department of Medicine, Drexel University College of Medicine, Philadelphia, PA, United States, [2] Department of Microbiology and Immunology, Drexel University College of Medicine, Philadelphia, PA, United States, [3] Department of Medical Technology, Faculty of Applied Medical Sciences, King Abdulaziz University, Jeddah, Saudi Arabia

Dengue is one of the most frequently transmitted mosquito-borne diseases in the world, which creates a significant public health concern globally, especially in tropical and subtropical countries. It is estimated that more than 390 million people are infected with dengue virus each year and around 96 million develop clinical pathologies. Dengue infections are not only a health problem but also a substantial economic burden. To date, there are no effective antiviral therapies and there is only one licensed dengue vaccine that only demonstrated protection in the seropositive (Immune), naturally infected with dengue, but not dengue seronegative (Naïve) vaccines. In this review, we address several immune components and their interplay with the dengue virus. Additionally, we summarize the literature pertaining to current dengue vaccine development and advances. Moreover, we review some of the factors affecting vaccine responses, such as the pre-vaccination environment, and provide an overview of the significant challenges that face the development of an efficient/protective dengue vaccine including the presence of multiple serotypes, antibody-dependent enhancement (ADE), as well as cross-reactivity with other flaviviruses. Finally, we discuss targeting T follicular helper cells (Tfh), a significant cell population that is essential for the production of high-affinity antibodies, which might be one of the elements needed to be specifically targeted to enhance vaccine precision to dengue regardless of dengue serostatus.

Keywords: dengue (DENV), adenosine deaminase (ADA), antibody dependent enhancement (ADE), challenges of vaccine development, T follicular helper cells (Tfh), cross-reactivity

OPEN ACCESS

Edited by:
Simon Daniel Van Haren, Boston Children's Hospital, Harvard Medical School, United States

Reviewed by:
Rong Hai, University of California, Riverside, United States
Navin Khanna, International Centre for Genetic Engineering and Biotechnology, India

***Correspondence:**
Elias K. Haddad
ee336@drexel.edu

Specialty section:
This article was submitted to Vaccines and Molecular Therapeutics, a section of the journal Frontiers in Immunology

Received: *15 March 2020*
Accepted: *01 May 2020*
Published: *16 June 2020*

Citation:
Izmirly AM, Alturki SO, Alturki SO, Connors J and Haddad EK (2020) Challenges in Dengue Vaccines Development: Pre-existing Infections and Cross-Reactivity. Front. Immunol. 11:1055. doi: 10.3389/fimmu.2020.01055

EPIDEMIOLOGY OF DENGUE INFECTION

Dengue is a global health threat in tropical and subtropical countries with a vast number of dengue infections that has been estimated to be more than 390 million cases annually. Among them, ∼96 million people develop clinical pathologies (1). In 2019, there were many cases of dengue infection reported worldwide, of which more than 3 million cases were confirmed by the Pan American Health Organization (PAHO). The majority of the cases were reported in Brazil with an estimated 1.5 millions in 2019 (PAHO). This accounted for more than 10-fold increase compared with the year before. In addition to South American countries, dengue infection occurs in multiple countries in Asia and Southeast Asia, including Bangladesh, Malaysia,

the Maldives, and the Philippines, where dramatic increases in dengue infection cases are on the rise. Countries in the Indian Ocean, Australia, and the Pacific have reported many dengue cases as well. A complete list of countries with dengue infection is found in **Table 1**. Dengue infections are not only a health problem but also a huge economic burden that has been estimated with a total annual burden of ∼$5.71 billion dollars in 2016 (2). This economic burden has risen dramatically from the estimate of 2013, which was $1.51 billion dollars and is likely to continue to rise yearly (2). Thus, there is an urgent need to develop a dengue vaccine and this exemplified by the international collaborative efforts from many world health organizations and federal institutions.

CLINICAL MANIFESTATIONS OF DENGUE INFECTION

There are three phases of dengue infection: the febrile phase, the critical phase, and the recovery phase. The febrile phase is the initial phase and usually begins with a high fever that appears with several flu-like symptoms, including vomiting, headaches, myalgia, and joint pain. This phase lasts for about a week and most people recover without further complications (3). The critical phase, or the life-threatening phase, is where most of the severe symptoms, such as internal bleeding and plasma leakage, occur. During the recovery phase, the vascular permeability returns to normal, and symptoms start to subside rapidly (3) **(Figure 1)**. In general, the most severe form of the disease is

TABLE 1 | List of total dengue cases by year and country.

Country	Cases 2019	Cases 2020	
Indian Ocean			
Mayotte	9	904	French Regional Health Agency (ARS)
Reunion	3,048	353	French Regional Health Agency (ARS)
Pacific Islands Countries and Australia			
Australia	1,038	54	Department of Health, Australia
French Polynesia	3,496	168	Center for Occupational Health and Public Safety, French Polynesia
New Caledonia	319	11	Network of sentinel physicians, New Caledonia
Asia			
Cambodia	56,000	330	Ministry of Health, Cambodia
China	20,000	268	National Health Commission, China
Viet Nam	370,702	NA	General Department of Preventative Medicine, Ministry of Health, Viet Nam
Lao PDR	2,300	285	National Centre for Laboratory and Epidemiology, Ministry of Health, Lao PDR
Malaysia	100,803	18,473	Department of Health, Malaysia
The Philippines	27,245	15,817	
Singapore	2,506	1,729	Communicable Diseases Division, Ministry of Health, Singapore
Thailand	136,000**	2,097	Bureau of Epidemiology, Department of Disease Control, Ministry of Public Health
Indonesia	110,000***	NA	WHO
Sri Lanka	99,120	14,730	Epidemiology Unit of the Ministry of Health, Sri
Americas and the Caribbean			
North America	1,158	35	Pan American Health Organization (PAHO)
Central America Ithsmus and Mexico	672,168	30,460	
Andean Subregion	185,320	56,077	
Southern Cone (incl Brazil)	2,241,974	273,565	
Latin Caribbean	23,472	1,267	
Non-Latin Caribbean	16,557	3,401	
Europe	NA	NA	European Centre for Disease Prevention and Control

**No official updates for Bangladesh, the Maldives, and India.*
***No official update since November 2019.*
****No official update since October 2019.*
All numbers reported for 2020 are as of February 5, 2020.

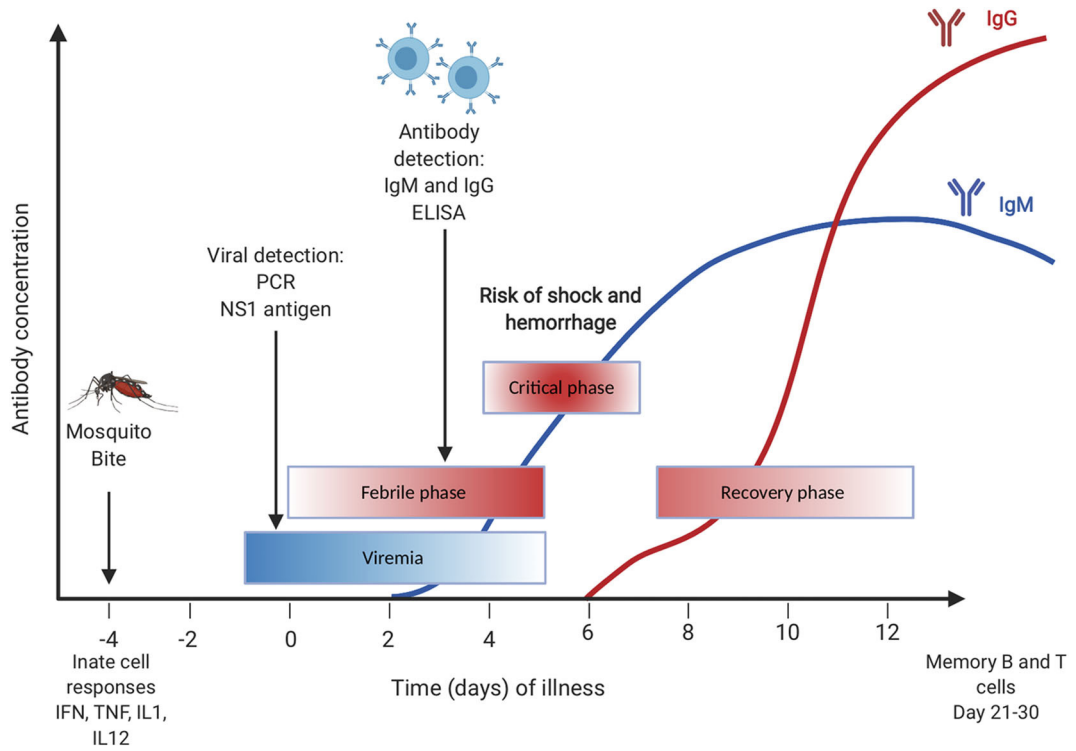

FIGURE 1 | Primary dengue infection with timing of diagnostic testing.

developing dengue hemorrhagic fever (DHF) and dengue shock syndrome (DSS) both of which are associated with antibody-dependent enhancement (ADE) (4, 5). ADE occurs when an antibody that is generated previously to one of the four serotypes binds but does not neutralize another dengue serotype. This binding then facilitates the entry of viruses via FC receptors which results in increased viremia (5).

VIROLOGY OF DENGUE VIRUS

Dengue virus (DENV) is an arthropod-borne pathogen that infects humans by a bite of an infected mosquito (6). Two types of mosquitos can be infected by the dengue virus: *Aedes aegypti* or *Aedes albopictus* (1). Dendritic cells (DCs) and macrophages are primarily targeted by the virus in the first days of dengue virus infections (7). There is no human-to-human transmission, and the virus is only transmitted through mosquitos when taking blood from a viremic individual. Viremia and systemic infection can be accomplished due to lymphotropic characteristics of the virus in which the DENV infects skin-draining lymph nodes (dLNs) and the cells that traffic into them, such as DCs and monocytes (8).

DENV is an enveloped virus that consists of a positive-stranded RNA that belongs to the Flavivirus genus of the Flaviviridae family. When the virus is matured, it encompasses three structural proteins namely the nucleocapsid (C), envelope (E), and membrane (M) and seven non-structural proteins (NS1, NS2A, NS2B, NS3, NS4A, NS4B, and NS5) (9). These play significant roles in virus genome replication, immune system evasion and modulation, virion assembly, and viral genome synthesis (10). DENV has four antigenically distinct serotypes (DENV1-4) that share up to 65% of their viral genome (11, 12). The differences in the serotypes create a great challenge for dengue vaccine development. The dengue virus enters the host cell through various internalization pathways as clathrin-dependent receptor endocytosis when bound to a cognate receptor. During natural infection, DENV primarily infects cells bearing C-type lectin receptors on mononuclear phagocyte lineage cells like monocytes, DCs, and macrophages. Such C-type lectin receptors are, for example, DC-specific intracellular adhesion molecule 3 (ICAM-3) and grabbing non-integrin (DC-SIGN, CD209) (6). In secondary infections, DENV depends on the pre-existing antibodies to be taken up by target Fcγ receptor-bearing cells to enter the host cells. Upon entering the cell by endocytosis, DENV can escape the endosome, due to a pH-dependent conformational change, and release its genome to the cytoplasm (13). Following translation of the structural and non-structural proteins, the capsid and the genome associate together to form a nucleocapsid in the cytoplasm. Nucleocapsids are directed by an unknown mechanism to the ER and bud into the lumen of the ER to acquire the bilipid membrane coated with prM/M proteins and E proteins (6, 13). This will form a spike-like shaped immature virus which will then be directed to the Golgi apparatus for additional structural changes in prM. The slightly

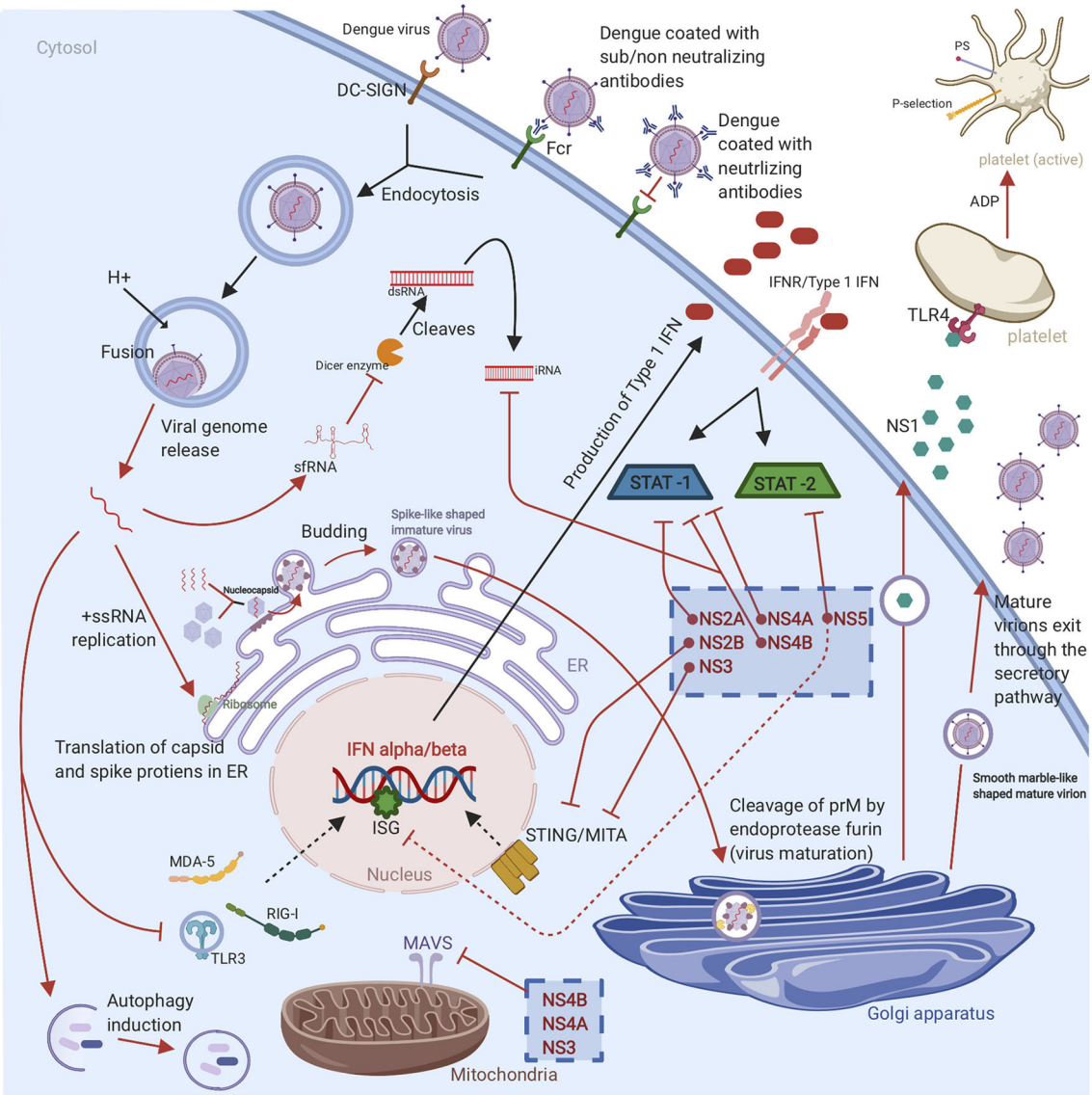

FIGURE 2 | Graphical representation of DENV life cycle and subversion of the innate immune response: The virus enters the host cell through receptor mediated endocytosis or antibody dependent enhancement. Once the virus is endocytosed, the viral RNA escapes the endosome, followed by RNA translation in ER and replication in cytoplasm. Then the newly replicated viral genome is assembled with the C protein to form a nucleocapsid which buds into ER to obtain a lipid membrane coated with prM/M and E proteins. The virion bunds out of ER as immature virion which is characterized by spiky appearance. For further maturation, the virion travel to Golgi apparatus where the prM protein is cleaved by the cellular endoprotease furin to form a mature virion which exists the cell through secretory pathways and infect new cells. The non-structural proteins (NS1, NS2A, NS2B, NS3, NS4A, NS4B, and NS5) of DENV have various evasion mechanisms. These evasion mechanisms include TLR, RIG-I, and MDA5 signaling cascades disruption, suppression of IFN α/β-mediated antiviral responses, MITA/STING cleavage, interference with RNAi response, enhance viral replication by autophagy induction, inhibition the cleavage of double-stranded RNA by Dicer enzyme, suppression the ISGs, inhibition the upstream and downstream of MAVS pathway, STAT1 phosphorylation inhibition, and STAT2 degradation. Finally, the non-structural proteins are able to induce platelet activation, aggregation, and apoptosis that leads to vascular leakage and thrombocytopenia (Red arrows represent various countermeasures that have been developed by dengue to evade and or to hinder antiviral innate immune response. The cellular antiviral response against DENV is indicated with black arrows).

acidic pH of the trans-Golgi network (TGN) and the presence of the host cell endoprotease furin enable the cleavage of prM to generate a smooth marble-like shaped mature virion-associated M and a soluble peptide (14).

It is important to highlight the significant role of DENV in regulating cellular lipid metabolism and autophagy to enhance replication, maturation, and production of the infectious virions. The mature virions and NS1 hexamers exit the infected cell through the host secretory pathway (13) **(Figure 2)**. It is worth noting that the concentration of secreted NS1 have been shown to be positively corelated with disease severity as high counts of NS1 are associated with DHF and DSS (15). The proposed

mechanism is that NS1 binds to platelets via toll-like receptor (TLR) 4, activating the platelets, and induces the expression of the activation marker P-selection and the apoptosis marker phosphatidylserine (PS) on the surface of the platelets. The expression of P-selection on the surface increases the adherence to endothelial cells and the PS exposure triggers phagocytosis by macrophages, which leads to thrombocytopenia in dengue infections **(Figure 2)**. This adhesion to endothelial cells also induces vascular leakage and can cause a cytokine storm (16). NS1 can also enhance platelet aggregation with the presence of adenosine diphosphate (ADP) which is secreted by the activated platelets. Thus, TLR4/NS1 interaction triggers platelet activation, aggregation, and apoptosis (16).

IMMUNE RESPONSE TO DENGUE VIRUS

Innate Immunity

The production of interferons (IFNs) is the first line of defense to DENV that can control early viral replication in target cells (6). Once DENV enters the skin, it is recognized by the pattern recognition receptors (PRRs) such as TLRs and C-type lectin receptors that are expressed on the immune sentinels (8). PRR activation enhances antiviral innate immune responses through activation downstream pathway leading to the production of interferons (IFNs) and tumor-necrosis factor (TNF) (17). TLR-3 and −7 stimulation induces the production of IFN- α and IFN- β. IFN-αβ production play a crucial role in inhibiting DENV infection. The produced IFNs bind to IFN receptors express on cells in an autocrine and paracrine manner. This binding leads to the JAK/STAT pathway activation, hence the production of more than 100 effector proteins (18). All the above-mentioned responses will stimulate DC maturation and B and T cells activation, and consequently, promote the adaptive immune response. However, DENV has developed several strategies to hijack IFN machinery. The NS1 protein is secreted from infected cells as a hexamer into patient's sera. The protease NS2B/3 of DENV has the ability to interfere with IFN α/β induction pathways to downregulate antiviral responses through cleaving the human mediator of interferon regulatory factor 3 (IRF3) activator (MITA or STING) (19). In addition, the non-structural proteins of DENV (NS2A, NS4A and NS4B) can partially block STAT signaling pathway which in turn interfere with IFN signaling between the cells (20) **(Figure 2)**.

Intracellular sensors such as the helicases melanoma differentiation-associated protein 5 (MDA5) and retinoic acid-inducible gene 1 (RIG-I) are also considered to be the first line of defense that are able to recognize the viral RNA and are involved in IFN- β production (13). Both RIG-I and MDA5 are involved in IFN-β production (21). In secondary infections, DENV complexed to non-neutralizing antibodies infects Fc**γ** receptor-bearing cells in a manner known as antibody dependent enhancement (ADE). ADE causes down-regulation of TLR signaling as well as interference with RIG-I- and MDA5-signaling cascades causing the inhibition of the IFN α/β-mediated antiviral response (13). During RIG-I activation, RIG-I will recognize viral RNA and is translocated to the mitochondria where it interacts with an adaptor protein called a mitochondrial antiviral-signaling protein (MAVS). RIG-I/MAVS interaction induces the development of MAVS aggregates, which serve as an immune signalosome that activates the transcription factor IRF3 and nuclear factor kB (NF-κB). Afterward, these transcription factors translocate to the nucleus and induce the production of type I IFN.

DENV has developed evasion strategies to inhibit upstream and downstream from MAVS pathway. DENV protein NS3 is able to prevent the translocation of RIG-I to mitochondria (22). On the other hand, NS4A is able to bind to MAVS CARD domains and effectively prevent RIG-I/MAVS interaction (23). The interference RNA (RNAi) pathway is a vital antiviral response however, DENV has evolved multiple mechanisms to interfere or evade it. The most well-studied of these mechanisms is the generation of a subgenomic flavivirus RNA (sfRNA) from the 3'-untranslated region of the viral RNA (vRNA) (24). The production of sfRNA inhibits the cleavage of double-stranded RNA by the Dicer enzyme to hinder the innate antiviral immunity. Another strategy that has been developed to interfere with RNAi pathway is the expression of the sub-structural protein NS4B which can modulate the host RNAi/miRNA pathway to favor DENV replication (25). The protein NS5 is able to prevent IFN production by suppressing IFN-stimulated genes (ISGs) through inhibiting recruitment of the transcription complex PAF1C (26). As mentioned above, dengue non-structural proteins interplay with innate immunity depicted in **Figure 2**. It has been shown that the activated mast cell in the skin is the responsible cell for initiating the recruitment of cytotoxic cells including natural killer (NK) cells, natural killer T (NKT) cells, and CD8+ T cells. The recruitment of cytotoxic cells to the site of infection promotes the clearance of virus and limits the infection in the draining lymph nodes (27). In addition to the crucial role of DCs in producing IFNs, TNFs, and blocking the spread and replication of the virus, DCs also link the innate immune response to adaptive immune response by presenting the antigen to T cells after migrates to the draining LNs (8).

Adaptive Immunity (T Cells)

T cells have been reported to have both pathological and protective function during dengue infection. Dengue-infected DCs present the antigen to CD8+ and CD4+ T cells in the T-cell zones of the draining LN, where the adaptive immune response begins. The activated CD4+ T cells will then provide help to CD8+ T cells that are then able to directly kill dengue infected cells through recognition a variety of dengue proteins including the non-structural NS3 and NS1.2a proteins (8, 28). High numbers of activated CD4+ T cells have been seen in asymptomatic cases in controlling the dengue infection demonstrating its protective role. CD8+ T cells are mostly directed against non-structural proteins whereas CD4+ T cells are skewed toward envelope, capsid, and NS1 epitopes (29). It has been reported that in immune-recall responses to secondary DENV infection the presence of heterologous memory and cross-reactive CD4+ T specific for a primary DENV serotype will exacerbate immune pathology (30).

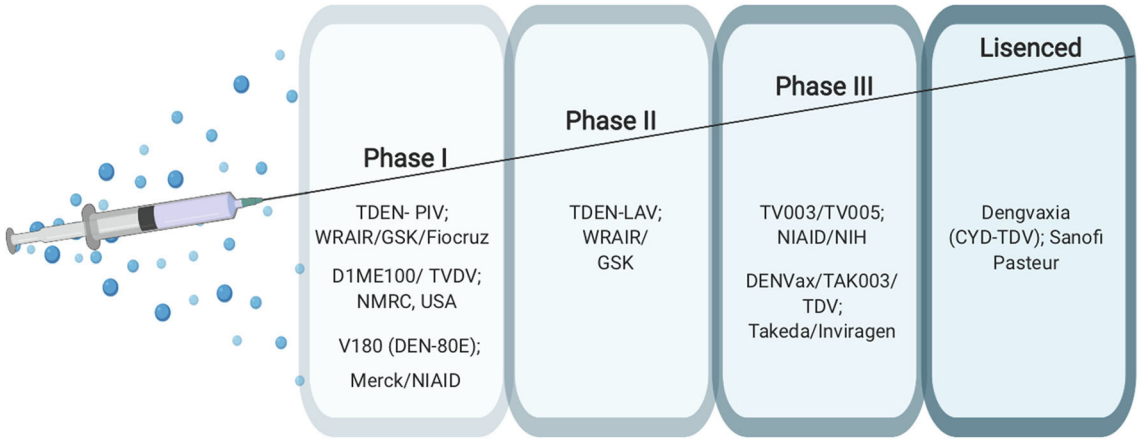

FIGURE 3 | Current dengue vaccines.

CURRENT DENGUE VACCINES

Licensed Vaccine

Developing an effective vaccine against dengue is challenging due to the fact that the DENV has four serotypes with all four types have the ability to cause disease. In addition, ADE, which is induced by pre-existing antibodies against DENV, creates an obstacle for vaccine development since neutralizing antibodies need to be generated to all serotypes of dengue to confer protection (31). Yet there are several promising dengue vaccine candidates under clinical evaluation (32, 33). So far, Dengvaxia (CYD-TDV) developed by Sanofi Pasteur is the only vaccine licensed and in use in many countries worldwide since 2015 (34, 35). This vaccine is a live attenuated, chimeric, tetravalent vaccine with a Yellow fever 17D strain virus backbone (36, 37). The prM and E proteins of the yellow fever are replaced with the prM and E proteins from the four DENV serotypes (37). This vaccine is licensed to be given only to dengue seropositive individuals with the age group of 9–45 years in dengue endemic countries It is administered subcutaneously in a three-dosage series of 6 months apart (0, 6, 12 months) (35). Despite the fact that CYD-TDV has shown great efficacy in protecting against severe disease in dengue positive individuals, it placed seronegative individuals at an increased risk of developing severe dengue disease (38). For this reason, research to find other possible dengue vaccines is still underway. There are several other vaccine candidates in clinical trials at different advanced stages ranging from Phase I to Phase III. These include live attenuated, purified inactivated and DNA vaccine platforms (39–43) **(Figure 3)**.

Phase III Vaccines

TV003/TV005 (NCT01506570) and TDV/DENVax/TAK003 (NCT02302066) are two promising live-attenuated vaccine candidates currently ongoing in phase 3 clinical trials (39, 40). The TV003/TV005 vaccine candidate is a live attenuated vaccine developed by The National Institute of Allergy and Infectious Diseases NIAID/NIH (44). This vaccine contains a mixture of four live attenuated dengue serotypes (4). The TV003 vaccine has been shown to induce neutralizing antibodies to all four serotypes in humans. This vaccine contains 10^3 PFU from each of the four-dengue serotypes 1, 2, 3, and 4 (4). TV005 is identical to TV003 with only a higher dose of 10^4 PFU of the DENV2 component. Both vaccines have showed promising results in clinical trials with TV003 eliciting the highest robust immune response to all DENV serotypes (DENV1-4) after only a single dose (31, 44). TDV, which is also known as DENVax/TAK003, is a chimeric, tetravalent live attenuated vaccine that was developed by Takeda/Inviragen (NCT01511250). This vaccine consists a chimera of prM and E proteins of DENV1, 3 and 4 serotypes based on a whole live-attenuated DENV2 PDK53 backbone (45). It has shown to induce neutralizing antibody titers against all DENV serotypes and the ability to produce humoral and cellular responses as well (46, 47) **(Figure 3)**.

Phase II, I, Preclinical Vaccines

TDEN-LAV (NCT01702857) (36) and TDEN-PIV (NCT01666652) (37) are two other vaccine candidates which were developed by the Walter Reed Army Institute of Research (WRAIR) and GlaxoSmithKline Vaccines (GSK). TDEN-LAV is a live attenuated tetravalent vaccine requiring two doses that contains the four serotypes of DENV and is currently in a phase II clinical trial. It has undergone serial passaging in primary dog kidney (PDK) cells and three more passages in fetal rhesus lung cells (FRhL) to reduce infectivity. TDEN-LAV was made in two different formulations termed F17 and F19 with both being tolerated well by healthy adults regardless of their prior priming status with the dengue virus. The F17 formulation produced stable titers for all four serotypes while F19 formulation had loss of infectivity with DENV-4. During the trial, unprimed vaccine recipients did not develop responses to all 4 serotypes after the first vaccine dose yet both formulations elicited immunogenicity across all subtypes after 2 doses. However, the level of neutralizing antibody was not measured and so is unknown.

Live-attenuated vaccine platforms come with one caveat: often, study subjects will develop antibodies against only one

dominant serotype rather than all that are included. To combat this problem, it was reasonable to pursue an inactivated dengue vaccine platform. TDEN-PIV (DPIV) is a purified, formalin-inactivated tetravalent DENV vaccine currently in phase I clinical trial (37). DPIV was formulated with either alum or $AS01_E$ or $AS03_B$ adjuvant systems with two different antigen concentrations. The vaccine regimen includes three doses, one initial dose with two boosters. The study participants were all sero-negative for all four serotypes at the time of vaccine administration. All formulations were well-tolerated by study participants and moderately immunogenic against all four serotypes however there was a waning and a plateau of neutralizing antibodies (48, 49).

Another Phase I vaccine candidate, D1ME100/TVDV, is being developed by the Naval Medical Research Center (NMRC), USA (NCT00290147) (43). It is a monovalent DNA vaccine with a plasmid vector expressing the prM and E genes of DENV-1 under the control of the cytomegalovirus promoter of the plasmid vector VR1012. The vaccine was tested in dengue-naïve participants, and immunogenicity and safety were determined after three doses. DNA vaccines offer several advantages including potent CTL responses and ability to preserve humoral immunity. This is accomplished by producing non-living, non-replicating, and non-spreading antigens that essentially results in mimicking natural infection (50). D1ME100/TVDV induced anti-dengue T cell IFN gamma responses but only 5 of 12 patients that received a high-dose formulation had detectable neutralizing antibody responses that, while long-lasting, were low level (43, 51) indicating that the TVDV vaccine to be safe and favorably reactogenic but without important humoral responses (43).

There are many recombinant subunit vaccine candidates in the vaccine pipeline. V180 (DEN-80E) MERCK (NCT01477580) is one of the most promising vaccine candidates that has completed phase I clinical trial (52). It is an envelope protein-based vaccine containing 80% of the N-terminal of the envelope protein (DEV-80E) for all four DENV serotypes produced using the S2 Drosophila cell line (53). The preclinical trial study used a mixture of this vaccine candidate with ISCOMATRIX™ adjuvant on mice and monkeys to show efficacy in inducing strong neutralizing antibodies against all DENV serotypes and protection against viremia (53, 54). The MERCK phase I clinical trial used flavivirus-naïve adult volunteers who were injected with V180 formulations, including the adjuvant ISCOMATRIX™. Study participants showed a positive robust immunity but formulations with aluminum adjuvant and without adjuvants were poorly immunogenic. The vaccine, when coupled with ISCOMATRIX™, was shown to be associated with more favorable events when compared with formulations with aluminum and non-adjuvanted formulations and overall, all formulations were well-tolerated (55) **(Figure 3)**.

Several other vaccine candidates with different platforms are being tested in preclinical trials with mice and non-human primates including virus-vectored (56–58), recombinant protein (59–61) and virus-like particles (VLPs) (62–64) vaccines but so far, none have made it into phase I trials.

PRE-VACCINE ENVIRONMENT EFFECT ON VACCINE RESPONSE

The pre-vaccination microenvironment is poorly understood for vaccine development. There are known and generally well-studied factors that affect vaccine response include age, gender, genetic background, differences in physical environment, and pre-existing immunity. For example, one study looked at the comparison of the response to the licensed yellow fever vaccine YF-17D in healthy adults from different origins and gender. The results show that men of mixed European decent have higher antibody levels when compared with females of the same decent, or individuals of African descent or Hispanics (65). Recently, researchers from Oxford published a study outlining just how genetic variation can affect vaccine response and the persistence of immunity after childhood vaccinations. They detail the considerable variability in the magnitude and persistence of vaccine-induced immunity due to genetic factors using genome-wide association study (GWAS) in the childhood vaccines capsular group C meningococcal (MenC), Hemophilus influenzae type b, and tetanus toxoid (TT) vaccines. In doing so, they were able to define associations between the single nucleotide polymorphisms (SNPs) in the human leukocyte antigen (HLA) locus and the persistence of immunity (66). Aging has also been shown to play a large factor in vaccine response. For example, two large-scale clinical trials compared the highly successful yellow fever vaccine YF-17D immunogenicity between adults and elderly individuals. One found no difference between the generation of neutralizing antibodies between the two groups, but the other trial found that the elderly cohort had a delayed antibody response and higher viremia (67).

Pre-existing immunity or "original antigenic sin" is a well-known barrier to a productive vaccine especially for flaviviruses which are all antigenically related. This phenomenon can modulate immune response to sequential infections or vaccinations. In general, the immune memory to cross-reactive antigenic sites and the formation of immune complexes can affect antibody responses in any sequential infections or immunizations with similar antigens. This was shown in a recent paper in 2019 where pre-existing yellow fever immunity from infection impaired the antibody response to the tick-borne encephalitis vaccination (68). It is important to consider this prospect especially in dengue vaccine development.

Nevertheless, the pre-vaccine microenvironment, like the levels of inflammation and immune activation that is already active in an individual, has a great impact on how a patient will respond to a particular vaccine. In a study published in 2014, researchers looked at the pre-vaccination environment and vaccine responses between study participants from either Entebbe, Uganda or Lausanne, Switzerland that were vaccinated against yellow fever with the licensed yellow fever vaccine YF-17D. They found fundamental differences in the subsequent cellular or humoral responses after vaccination including a substantially lower CD8+ T cells and B cells from the Entebbe cohort compared with immunized individuals

from Lausanne meaning an impaired vaccine response. The researchers also observed higher frequencies of differentiated T and B cell subsets, exhausted and activated NK cells, and proinflammatory monocytes suggesting that an activated immune microenvironment in the Entebbe cohort prior to vaccination led to differences in vaccination responses. The activation of the proinflammatory monocytes at baseline resulted in a negative correlation with YF-1D neutralizing antibody titers after vaccination (69). Though we have known that aging plays a role in how a subject will respond to a vaccination, it is only recently that the mechanisms have been researched. Researchers in 2015 reported that the pre-vaccination inflammation and blunted B cell signaling due to aging correlates with the hyporesponse to the hepatitis B (HBV) vaccination (70). Specifically, using transcriptional and cytometric profiling of whole blood collected before vaccination, they show that there is an increase in inflammatory response transcripts and pro-inflammatory monocytes in the older cohort that correlates with poor vaccine response to the HBV vaccine. Conversely, augmented B cells responses and a higher frequency of B cells correlated with a stronger response to the vaccine in the younger individuals. This study was the first to identify baseline responses that could predict responses to the HBV vaccine and possibly others. Therefore, the existence of the pre-vaccine immune microenvironment should be taken into consideration for the development of any vaccine.

CHALLENGES FACE DENGUE VACCINE DEVELOPMENT

Antibody Dependent Enhancement (ADE)

Unlike other highly effective vaccines developed against other flaviviruses, the development of a dengue vaccine is highly challenging due to that fact that the virus has four antigenically different serotypes (DENV1–4). For an ideal dengue vaccine, the vaccine should be effective against all four serotypes at the same time. Primary DENV infections are usually asymptomatic or with mild flu like symptoms **(Figure 4A)**. Post DENV infection it takes antibodies ∼1 week to develop. During primary infection with one DENV serotype, antibodies produced by this serotype usually results in a long-lasting protection against that particular serotype and short lived protection against other serotypes (5). Antibodies play a dual role in controlling DENV infection, in which they can either neutralize or enhance the entry of the virus (4). A study that analyzed antibodies produced in human post-primary DENV infection found low amounts of highly specific and neutralizing antibodies that were mainly against the envelope EDIII domain. On the other hand, they found that most weakly cross-reactive antibodies were against prM (71). Preexisting neutralizing antibodies can prevent DENV attachment to its natural receptor on the cell surface thus inhibiting virus entry **(Figure 4B)**. However, antibodies from heterologous infection can be cross-reactive and facilitate a process known as antibody dependent enhancement or ADE. This mechanism allows the virus to enter and escape the endosome and go through a manner similar to the primary infection pathway causing a higher virus burden and ultimately enhancement of disease (5, 72). ADE has been observed for a variety of viruses including HIV, Ebola, and possibly the virus responsible for the recent pandemic, SARS-CoV2. Fc receptor (FcR)-dependent ADE is accepted as the most common mechanism of ADE among many viruses, including dengue, HIV, and influenza A. Virus-antibody complexes will bind to cells that have a FcR like macrophages, monocytes, B cells, and neutrophils through the interaction between the Fc portion of the antibody and the FcR on the cell surface. This essentially creates an immune synapse that increases the attachment of viruses to the cells (73) **(Figure 4C)**. Another possible mechanism of ADE involves the activation of the complement classical pathway. While FcRs are only expressed on immune cells, complement receptors (CRs) are broadly expressed on most cells (74). For example, HIV ADE can occur via FcR or by virus-C3 fragment complexes and classical CRs that will facilitate normal virus entry by viral surface protein gp120 and its receptors and coreceptors (75). Additionally, Ebola utilizes another complement mediated ADE mechanism in in which antibodies bind in proximity, allowing C1q to bind to the Fc portion of the antibodies. This complex (virus, antibodies, and C1q) binds to C1q receptors (C1qR) which facilitates either endocytosis or binding of the virus to Ebola-specific receptors (74, 76). Recently, Wan et al. published an ADE mechanism in Coronaviruses.. Their results indicate that ADE of coronaviruses may be mediated by neutralizing antibodies that target the receptor binding domains of the coronavirus spikes. Interestingly and unlike dengue that involves ADE with the different serotypes, the same coronavirus strains that produce fully neutralizing antibodies can be mediated to go through ADE by the same neutralizing antibodies (77). It is also unclear as to whether virus-specific receptors are required for ADE entry. It may depend on whether the virus is enveloped or non-enveloped and the mechanism of ADE but if a virus relies on surface receptors only for binding, the virus may be able to infect the cells via FcR without a natural receptor. This models how non-susceptible cells that do not express a virus's natural receptor can be infected when FcR is expressed like in FcR-mediated ADE of foot and mouth disease (78).

The reason behind the high number of infected cells and high viral particles following ADE have been shown in a study in which DENV-immune complexes can suppress the antiviral immune response by down regulating the production of IL-12, TNF-a, IFN-γ, and nitric oxide radicals (NO), and enhancing the expression of IL-6 and IL-10, thus promoting virus particle production (79). ADE occurs in dengue-infected individuals who previously had been infected with different serotype from the first one or other flavivirus. ADE could also occur upon poor response to vaccination. Both anti-E and anti-prM antibodies have been shown to enhance DENV entry into the target cells through Fc**γ**- mediated ADE (4). A study published in 2010 suggested that response toward cross-reactive epitopes such as prM could be a part of the immune evasion mechanism by DENV. Furthermore, they have advised the reduction of anti-prM response in dengue vaccine design to reduce ADE (80). One example of a DENV vaccine candidate that steered away from prM is a preclinical vaccine. This vaccine is VLP

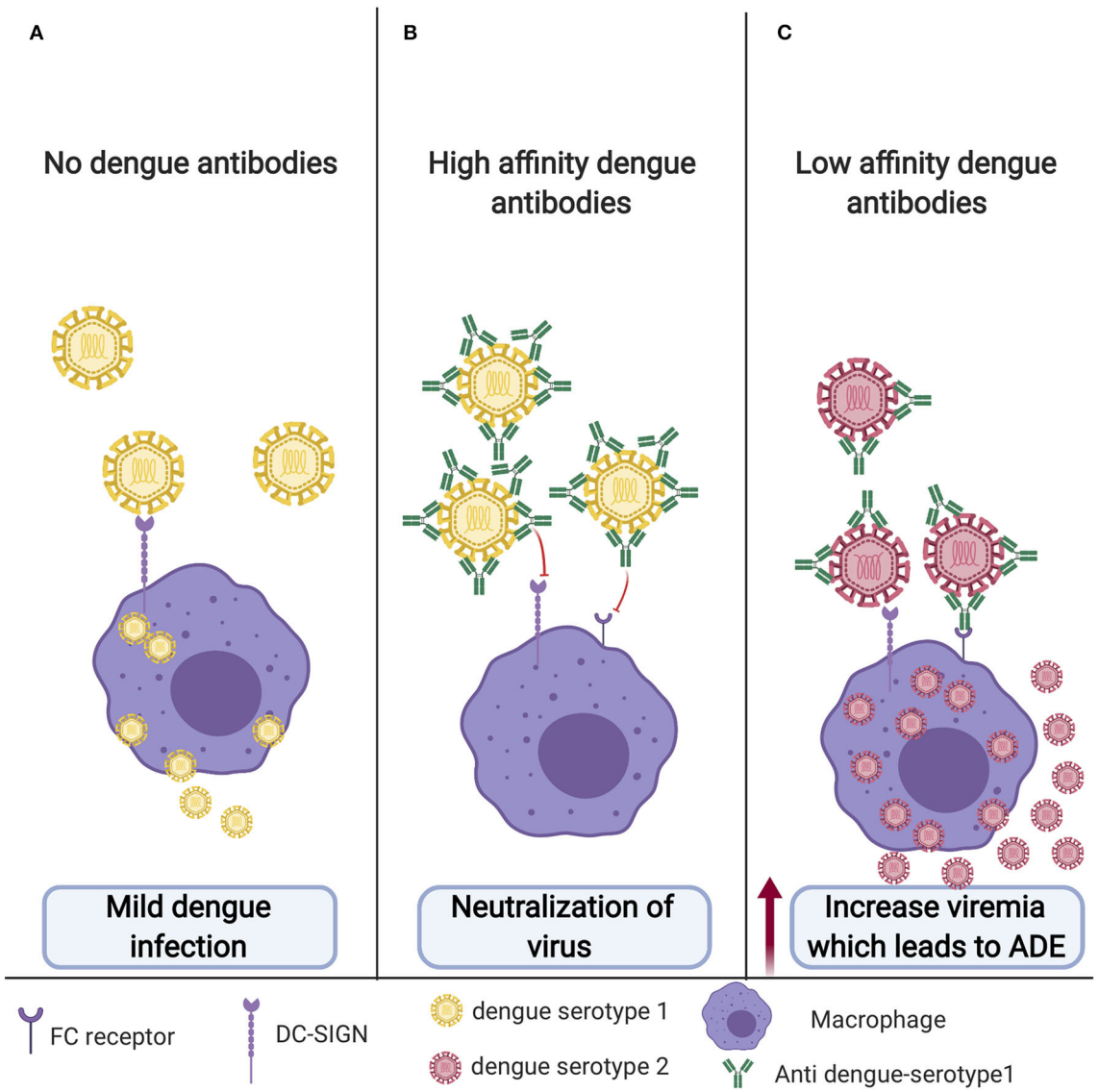

FIGURE 4 | Antibody dependent enhancement (ADE): **(A)** Primary infection with no previous vaccination. DENV will enter macrophage through its cognate receptor; however, most of the time, it will result in mild disease, and sometime this could even be symptomatic or with mild flu-like symptoms. **(B)** DENV in the presence of neutralizing antibodies for the same serotype. DENV will not be able to enter the cells and establish infection. **(C)** Cross-reactive antibodies from previous unsuccessful dengue vaccine or dengue infection with different serotypes will bind but not neutralize the virus. This low-affinity binding will facilitate the entry of the virus to the macrophage through FC receptor resulting in increased viremia leading to ADE.

based designed to produce antibodies against the EDIII domain and has demonstrated decreased ADE in animal models (62). Additionally, a recent study in 2019 using molecular simulations found that higher cross-reactive DENV antibodies were linked to higher ADE and that poorly immunogenic vaccine enhances ADE (81). Ultimately, ADE is the main causative factor in the progression of the self-limited dengue fever to DHF and DSS (4, 82–84) **(Figure 4)**.

Cross Reactivity With Other Flaviviruses

There are several challenges that have hindered the development of the dengue vaccine. One of these challenges is the structural similarities between DENV and other members of the Flaviviridae family viruses such as the Zika virus (ZIKV), Yellow fever virus (YFV), Japanese encephalitis virus (JEV) and West Nile virus (WNV). The envelope protein (E) is both structurally conserved among flaviviruses and the most exposed protein to which the immune system generates antibodies against in order to neutralize the virus. The E protein consists of three functionally and structurally distinct domains EDI, EDII, and EDIII (85). The envelope protein (E) of DENV shares more than 50% homology with the ZIKV E protein, resulting in cross reactivity (86). The cross reactivity contributes to either protection or pathogenic enhancement to a second infection

with one of the members depending on the quantity and the specificity of the generated antibodies. In 2016, ZIKV outbreaks overlapped the regions where the DENV was endemic in the north of Brazil and Mexico (85, 87). Consequently, the individuals that have been infected by ZIKV were likely to be pre-exposed to DENV and vice versa. This created a concern among researchers since preexisting immunity to other flaviviruses affects immune responses induced by DENV which may result in severe dengue manifestation.

Studies show that both humoral and cellular immunity contribute to disease pathogenesis with humoral immunity being the main causative factor of ADE. However, high concentrations of pre-existing cross-reactive antibodies have been found to have the ability to reduce the probability of symptomatic dengue infections (88). Therefore, the threshold of cross-reactive antibody concentration must be reached to effectively neutralize and inhibit virus attachment and entry. On the other hand, if the cross-reactive antibody titers do not reach the threshold, ADE occurs, and the neutralization fails. One recent study done within the Mexican population determined the response of cross-reacting antibodies in the sera of patients with DENV against the recombinant envelope protein of ZIKV (85). They demonstrated that the serum samples of the dengue-infected patients have cross-reactive antibodies against the E protein of ZIKV which can either mediate ADE or neutralize the infection depending on the concentration of the antibodies (85). It has been observed that the protection against severe infections lasts for 2 years following the primary infection after which the neutralizing antibodies decay and the risk of symptomatic and severe dengue infection increases upon secondary heterologous infection (88). There is some evidence that a simultaneous re-exposure is required to maintain the cross-reactive neutralizing antibodies for a longer time (89). Most of the effectual vaccines provide protection against pathogens by generating neutralizing antibodies. Long-lived antibody-secreting plasma cells are produced by the germinal centers (GC) that are formed in the secondary lymphoid tissues with the help of T follicular helper cells (Tfh) (90). Harnessing this mechanism for long-lived antibody secreting plasma cells is vital for a thoroughly effective dengue vaccine.

TARGETING TFH CELLS TO ENHANCE DENGUE VACCINE EFFICACY

Germinal center (GC) responses are supported by a specialized type of CD4+ T cells called Tfh cells. Tfh are mainly located in the GC, however, counterparts of these cells are present in the peripheral blood which can be identified by expression of CXCR5, ICOS, and PD-1 (91, 92). There are growing interest in studying circulating peripheral blood Tfh (cTfh) instead of GC Tfh and using them as biomarkers of GC activity since collecting a healthy human lymphoid tissue can be more difficult than peripheral blood (93, 94). CTfh cells come in different subtypes with each expressing different cytokines and therefore having different abilities to provide help for the B cells (95, 96). CTfh1 are mostly considered as the inefficient helper while cTfh2 and cTfh17 are the efficient helper subtypes. Furthermore, these cells have been highly correlated with broadly neutralizing antibodies (95, 97). These cTfh cells provide a great tool for monitoring vaccine responses. Generally, Tfh activate GC B cells by producing IL-21 and up-regulating various proteins and transcriptional factors such as ICOS, Bcl-6, PD-1, and CD40 (98). Antigen-activated B cells migrate to the B cell follicle in the secondary lymph tissue where they differentiate, proliferate, and undergo through class switching, somatic gene hypermutation (SHM) and, affinity maturation. B cells that have been through SHM exit the division cycle to test their recently mutated B cell receptor by interacting with the antigens expressed by the antigen-presenting cell follicular dendritic cells (FDC). Finally, the B cells must undergo the selection process to exit the GC as long-lived plasma cells and durable memory cells. The selection process occurs by presenting the processed antigen on B cells to Tfh cells to select B cells with higher affinity for the pathogen (98). A recent study showed an increased activation of the Tfh cells in the critical phase of illness compared to mild and moderate phase of illness that was highly correlated with high frequency of plasma blasts. Furthermore, the number of activated peripheral Tfh in secondary DENV infections is increased compared with primary DENV infections (99). This might be due to the activation of Tfh cells specific only for one serotype resulting in ADE and disease pathogenesis. However, we hypothesize that enhancing Tfh cells specific to all serotypes would solve ADE. Eventually, Tfh cells support the GC response and positively regulate the magnitude of the GC response. Using Adenosine deaminase-1 (ADA-1) as an adjuvant has been shown to be one of the potential strategies to modify and enhance Tfh function. ADA-1 is an intracellular enzyme which converts adenosine into inosine through the deamination process. ADA-1 is also involved in the development and maintenance of the immune system by potentiating the differentiation of naive T cells to effector, regulatory, and memory CD4+ T cells (100). It has a central role in the immune system as mutation of ADA-1 leads to severe immunological disorders and loss of functional T, B, and NK cells (101). One study, using PBMCs and tonsil cells from HIV-infected patients, shows that ADA-1 is essential for an efficient GC-Tfh response and promotes antibody affinity maturation within the GC by providing a favorable cytokine microenvironment (102). Many studies have shown a strong correlation between efficient induction of memory B cells and plasma cells that will produce specific neutralizing antibodies against influenza and Ebola and increasing Tfh cells in the context of the immunizations (93, 97, 103). It is important to identify potential adjuvants that will efficiently target and induce a Tfh response for future vaccine design. Most vaccines depend on adjuvants to improve the immune response, increase neutralizing antibody titers, induce long-lasting immunity, and reduce required vaccine doses. In the context of Tfh induction, water-in-oil adjuvants have been shown to selectively promote the Tfh response, such as incomplete Freund's adjuvant (IFA), Montanide ISA 720, and ISA-51 (104). Another study showed the MF59 oil-in-water adjuvant mediates a potent Tfh response that directly promotes GC responses (105). Other adjuvants such as TLR4, TLR6, TLR7, TLR8, and TLR9 agonists had extensive interest in the use of vaccine adjuvants as TLR agonists can all

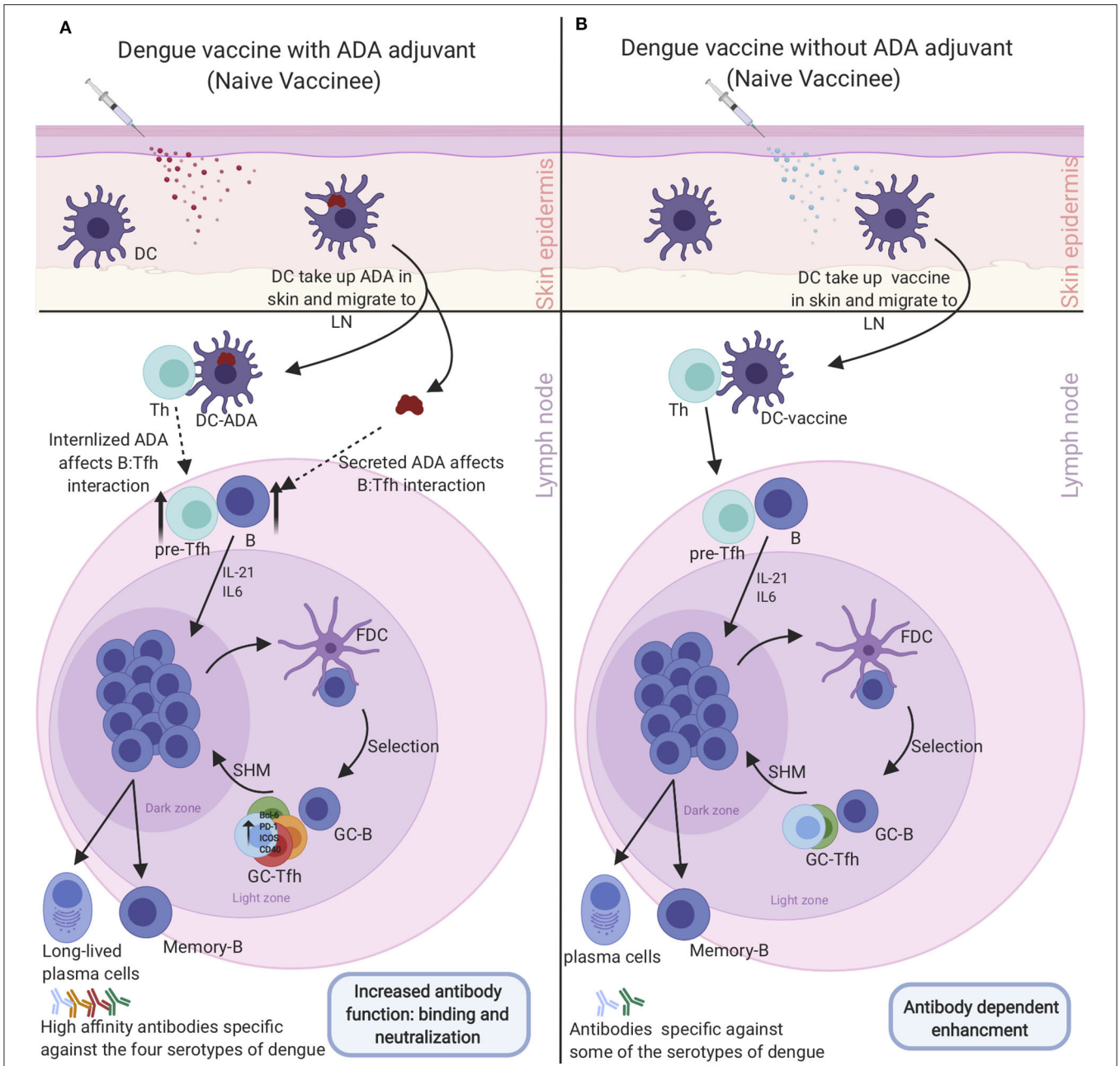

FIGURE 5 | Enhancement of dengue vaccine by targeting Tfh cells to overcome dengue serostatus effect: **(A)** Administering dengue vaccine to naive dengue individual with Tfh Adjuvant (ADA) will be taken up by DC that travels to the LN and prompt enhanced Tfh-B cell interaction. The enhanced interaction induces Tfh-specific cells to the four dengue serotypes leading to differentiation of memory B cells and plasmablasts that produce high-affinity neutralizing antibodies against all the serotypes which neutralize the dengue virus. **(B)** Administrating dengue vaccine to naive individuals without Tfh adjuvant (ADA). Vaccine will be taken up by DC, which will travel to the LN and induce medium Tfh-B cell interaction. The medium interaction will give rise to Tfh, B cells, and plasmablasts that are specific to some serotypes of dengue. Antibodies produced by this response will make them vulnerable to ADE and enhanced dengue diseases upon infection with a different dengue serotype virus that they have sub-neutralizing antibodies against.

enhance Tfh cells (106). The Tfh cells have to be selectively and potently enhanced to overcome the seronegative group setback in dengue vaccination in order to generate specificity to all 4 serotypes concurrently using a potent adjuvant such as ADA **(Figure 5)**. On the other hand, enhancement of Tfh activity has been linked with multiple autoimmune diseases such as Systemic Lupus Erythematosus (SLE), Rheumatoid Arthritis (RA) and, multiple sclerosis (MS) (107–110). In conclusion, Tfh cells are a double-edged sword and transient enhancement of their activity would be beneficial for the development of a precise dengue

vaccine that would generate neutralizing antibody titers to all dengue serotypes regardless of vaccines dengue serostatus.

SUMMARY

DENV is a significant health concern and the development of the best vaccine possible is needed to decrease the burden of this disease on society. Dengue is a very tricky and challenging virus because it has four separate dengue serotypes. That means that in order to design an effective dengue vaccine, it has to induce neutralizing high-affinity antibodies to the 4 serotypes simultaneously to avoid ADE. So far, the only licensed dengue vaccine Dengvaxia (CYD-TDV), developed by Sanofi Pasteur, taught us a vital lesson that dengue serostatus affects vaccine response. With Dengvaxia, dengue naïve individuals did not respond appropriately to the vaccine compared to immune individuals. This difference between the two groups needs to be investigated at the prevaccination microenvironment level to address this issue. However, we speculate that the low activation of Tfh cells, specific to each of the four serotypes, is the fundamental difference between the two groups. This issue could be addressed by adding adjuvants such as ADA that potently activate the Tfh cells and give rise to Tfh specifics to the 4 serotypes of the virus. We believe this could make the naïve individuals respond to the vaccine and give rise to high-affinity neutralizing antibodies to all the 4 serotypes and make them respond as well as dengue immune vaccinated individuals.

AUTHOR CONTRIBUTIONS

SanA, SawA, and JC contributed to writing sections of the paper and figure design. EH and AI contributed to the concept, structure, and writing up the paper. All authors contributed to the article and approved the submitted version.

FUNDING

This work was supported by NIH funding as part of Human Immune Project Consortium (HIPC) to EH # U19 AI128910 and AI125202. Figures were created using biorender.com.

ACKNOWLEDGMENTS

The authors would like to acknowledge King Abdulaziz University and thier fellowship program for their support.

REFERENCES

1. Bhatt S, Gething PW, Brady OJ, Messina JP, Farlow AW, Moyes CL, et al. The global distribution and burden of dengue. *Nature.* (2013) 496:504–7. doi: 10.1038/nature12060
2. Hariharan D, Das MK, Shepard DS, Arora NK. Economic burden of dengue illness in India from 2013 to 2016: A systematic analysis. *Int J Infect Dis.* (2019) 84S:S68–73. doi: 10.1016/j.ijid.2019.01.010
3. Simmons CP, Farrar JJ, Nguyen v V, Wills B. Dengue. *N Engl J Med.* (2012) 366:1423–32. doi: 10.1056/NEJMra1110265
4. Huang KJ, Yang YC, Lin YS, Huang JH, Liu HS, Yeh TM, et al. The dual-specific binding of dengue virus and target cells for the antibody-dependent enhancement of dengue virus infection. *J Immunol.* (2006) 176:2825–32. doi: 10.4049/jimmunol.176.5.2825
5. Halstead SB. Neutralization and antibody-dependent enhancement of dengue viruses. *Adv Virus Res.* (2003) 60:421–67. doi: 10.1016/S0065-3527(03)60011-4
6. Rodenhuis-Zybert IA, Wilschut J, Smit JM. Dengue virus life cycle: viral and host factors modulating infectivity. *Cell Mol Life Sci.* (2010) 67:2773–86. doi: 10.1007/s00018-010-0357-z
7. Kyle JL, Beatty PR, Harris E. Dengue virus infects macrophages and dendritic cells in a mouse model of infection. *J Infect Dis.* (2007) 195:1808–17. doi: 10.1086/518007
8. John ALS, Rathore AP. Adaptive immune responses to primary and secondary dengue virus infections. *Nat Rev Immunol.* (2019) 19:218–30. doi: 10.1038/s41577-019-0123-x
9. Tremblay N, Freppel W, Sow AA, Chatel-Chaix L. The interplay between dengue virus and the human innate immune system: a game of hide and seek. *Vaccines.* (2019) 7:145. doi: 10.3390/vaccines7040145
10. Chong HY, Leow CY, Bakar AMA, Leow CH. Flavivirus Infection-A review of immunopathogenesis, immunological response, and immunodiagnosis. *Virus Res.* (2019) 274:197770. doi: 10.1016/j.virusres.2019.197770
11. Holmes EC. Molecular epidemiology and evolution of emerging infectious diseases. *Br Med Bull.* (1998) 54:533–43. doi: 10.1093/oxfordjournals.bmb.a011708
12. Rodriguez-Barraquer I, Mier-y-Teran-Romero L, Schwartz IB, Burke DS, Cummings DA. Potential opportunities and perils of imperfect dengue vaccines. *Vaccine.* (2014) 32:514–20. doi: 10.1016/j.vaccine.2013.11.020
13. Guzman MG, Harris E. Dengue. *Lancet.* (2015) 385:453–65. doi: 10.1016/S0140-6736(14)60572-9
14. Zybert IA, van der Ende-Metselaar H, Wilschut J, Smit JM. Functional importance of dengue virus maturation: infectious properties of immature virions. *J Gen Virol.* (2008) 89:3047–51. doi: 10.1099/vir.0.2008/002535-0
15. Paranavitane SA, Gomes L, Kamaladasa A, Adikari TN, Wickramasinghe N, Jeewandara C, et al. Dengue NS1 antigen as a marker of severe clinical disease. *BMC Infect Dis.* (2014) 14:570. doi: 10.1186/s12879-014-0570-8
16. Chao CH, Wu WC, Lai YC, Tsai PJ, Perng GC, Lin YS, et al. Dengue virus nonstructural protein 1 activates platelets via Toll-like receptor 4, leading to thrombocytopenia and hemorrhage. *PLoS Pathog.* (2019) 15:e1007625. doi: 10.1371/journal.ppat.1007625
17. Ho LJ, Wang JJ, Shaio MF, Kao CL, Chang DM, Han SW, et al. Infection of human dendritic cells by dengue virus causes cell maturation and cytokine production. *J Immunol.* (2001) 166:1499–506. doi: 10.4049/jimmunol.166.3.1499
18. Ho LJ, Hung LF, Weng CY, Wu WL, Chou P, Lin YL, et al. Dengue virus type 2 antagonizes IFN-α but not IFN-γ antiviral effect via down-regulating Tyk2-STAT signaling in the human dendritic cell. *J Immunol.* (2005) 174:8163–72. doi: 10.4049/jimmunol.174.12.8163
19. Aguirre S, Maestre AM, Pagni S, Patel JR, Savage T, Gutman D, et al. DENV inhibits type I IFN production in infected cells by cleaving human STING. *PLoS Pathog.* (2012) 8:e1002934. doi: 10.1371/journal.ppat.1002934
20. Munoz-Jordán JL, Laurent-Rolle M, Ashour J, Martínez-Sobrido L, Ashok M, Lipkin WI, et al. Inhibition of alpha/beta interferon signaling by the NS4B protein of flaviviruses. *J Virol.* (2005) 79:8004–13. doi: 10.1128/JVI.79.13.8004-8013.2005
21. Nasirudeen A, Wong HH, Thien P, Xu S, Lam KP, Liu DX. RIG-I, MDA5 and TLR3 synergistically play an important role in restriction of dengue virus infection. *PLoS Negl Trop Dis.* (2011) 5:e926. doi: 10.1371/journal.pntd.0000926
22. Liu HM, Loo YM, Horner SM, Zornetzer GA, Katze MG, Gale M Jr. The mitochondrial targeting chaperone 14–3-3ε regulates a RIG-I translocon that

mediates membrane association and innate antiviral immunity. *Cell Host Microbe.* (2012) 11:528–37. doi: 10.1016/j.chom.2012.04.006
23. He Z, Zhu X, Wen W, Yuan J, Hu Y, Chen J, et al. Dengue virus subverts host innate immunity by targeting adaptor protein MAVS. *J Virol.* (2016) 90:7219–30. doi: 10.1128/JVI.00221-16
24. Schnettler E, Sterken MG, Leung JY, Metz SW, Geertsema C, Goldbach RW, et al. Noncoding flavivirus RNA displays RNA interference suppressor activity in insect and Mammalian cells. *J Virol.* (2012) 86:13486–500. doi: 10.1128/JVI.01104-12
25. Kakumani PK, Ponia SS, Sood V, Chinnappan M, Banerjea AC, Medigeshi GR, et al. Role of RNA interference (RNAi) in dengue virus replication and identification of NS4B as an RNAi suppressor. *J Virol.* (2013) 87:8870–83. doi: 10.1128/JVI.02774-12
26. Shah PS, Link N, Jang GM, Sharp PP, Zhu T, Swaney DL, et al. Comparative flavivirus-host protein interaction mapping reveals mechanisms of dengue and Zika virus pathogenesis. *Cell.* (2018) 175:1931–45.e18. doi: 10.1016/j.cell.2018.11.028
27. John ALS, Rathore AP, Yap H, Ng ML, Metcalfe DD, Vasudevan SG, et al. Immune surveillance by mast cells during dengue infection promotes natural killer (NK) and NKT-cell recruitment and viral clearance. *Proc Natl Acad Sci USA.* (2011) 108:9190–5. doi: 10.1073/pnas.1105079108
28. Mathew A, Kurane I, Rothman AL, Zeng LL, Brinton MA, Ennis FA. Dominant recognition by human CD8+ cytotoxic T lymphocytes of dengue virus nonstructural proteins NS3 and NS1. 2a. *J Clin Invest.* (1996) 98:1684–91. doi: 10.1172/JCI118964
29. Simon-Loriere E, Duong V, Tawfik A, Ung S, Ly S, Casademont I, et al. Increased adaptive immune responses and proper feedback regulation protect against clinical dengue. *Sci Transl Med.* (2017) 9:eaal5088. doi: 10.1126/scitranslmed.aal5088
30. Mongkolsapaya J, Dejnirattisai W, Xu XN, Vasanawathana S, Tangthawornchaikul N, Chairunsri A, et al. Original antigenic sin and apoptosis in the pathogenesis of dengue hemorrhagic fever. *Nat Med.* (2003) 9:921–7. doi: 10.1038/nm887
31. Kirkpatrick BD, Whitehead SS, Pierce KK, Tibery CM, Grier PL, Hynes NA, et al. The live attenuated dengue vaccine TV003 elicits complete protection against dengue in a human challenge model. *Sci Transl Med.* (2016) 8:330ra36. doi: 10.1126/scitranslmed.aaf1517
32. Shrivastava A, Tripathi NK, Dash PK, Parida M. Working towards dengue as a vaccine-preventable disease: challenges and opportunities. *Exp Opin Biol Ther.* (2017) 17:1193–9. doi: 10.1080/14712598.2017.1356284
33. Thisyakorn U, Thisyakorn C. Latest developments and future directions in dengue vaccines. *Ther Adv Vaccines.* (2014) 2:3–9. doi: 10.1177/2051013613507862
34. WHO. World Health Organization. *International Travel and Health – Chapter 6. Vaccine-Preventable Diseases and Vaccines.* (2017). Available online at: http://www.who.int/ith/en/ (accessed June 4, 2020).
35. Thomas SJ, Yoon IK. A review of Dengvaxia(R): development to deployment. *Hum Vaccin Immunother.* (2019) 15:2295–314. doi: 10.1080/21645515.2019.1658503
36. Dorigatti I, Aguas R, Donnelly CA, Guy B, Coudeville L, Jackson N, et al. Modelling the immunological response to a tetravalent dengue vaccine from multiple phase-2 trials in Latin America and South East Asia. *Vaccine.* (2015) 33:3746–51. doi: 10.1016/j.vaccine.2015.05.059
37. Guy B, Briand O, Lang J, Saville M, Jackson N. Development of the Sanofi Pasteur tetravalent dengue vaccine: one more step forward. *Vaccine.* (2015) 33:7100–11. doi: 10.1016/j.vaccine.2015.09.108
38. Sridhar S, Luedtke A, Langevin E, Zhu M, Bonaparte M, Machabert T, et al. Effect of dengue serostatus on dengue vaccine safety and efficacy. *N Engl J Med.* (2018) 379:327–40. doi: 10.1056/NEJMoa1800820
39. Whitehead SS, Durbin AP, Pierce KK, Elwood D, McElvany BD, Fraser EA, et al. In a randomized trial, the live attenuated tetravalent dengue vaccine TV003 is well-tolerated and highly immunogenic in subjects with flavivirus exposure prior to vaccination. *PLoS Negl Trop Dis.* (2017) 11:e0005584. doi: 10.1371/journal.pntd.0005584
40. Sáez-Llorens X, Tricou V, Yu D, Rivera L, Tuboi S, Garbes P, et al. Safety and immunogenicity of one versus two doses of Takeda's tetravalent dengue vaccine in children in Asia and Latin America: interim results from a phase 2, randomised, placebo-controlled study. *Lancet Infect Dis.* (2017) 17:615–25. doi: 10.1016/S1473-3099(17)30166-4
41. Bauer K, Esquilin IO, Cornier AS, Thomas SJ, del Rio AIQ, Bertran-Pasarell J, et al. A phase II, randomized, safety and immunogenicity trial of a re-derived, live-attenuated dengue virus vaccine in healthy children and adults living in Puerto Rico. *Am J Trop Med Hyg.* (2015) 93:441–53. doi: 10.4269/ajtmh.14-0625
42. Schmidt AC, Lin L, Martinez LJ, Ruck RC, Eckels KH, Collard A, et al. Phase 1 randomized study of a tetravalent dengue purified inactivated vaccine in healthy adults in the United States. *Am J Trop Med Hyg.* (2017) 96:1325–37. doi: 10.4269/ajtmh.16-0634
43. Beckett CG, Tjaden J, Burgess T, Danko JR, Tamminga C, Simmons M, et al. Evaluation of a prototype dengue-1 DNA vaccine in a Phase 1 clinical trial. *Vaccine.* (2011) 29:960–8. doi: 10.1016/j.vaccine.2010.11.050
44. Kirkpatrick BD, Durbin AP, Pierce KK, Carmolli MP, Tibery CM, Grier PL, et al. Robust and balanced immune responses to all 4 dengue virus serotypes following administration of a single dose of a live attenuated tetravalent dengue vaccine to healthy, flavivirus-naive adults. *J Infect Dis.* (2015) 212:702–10. doi: 10.1093/infdis/jiv082
45. Osorio JE, Partidos CD, Wallace D, Stinchcomb DT. Development of a recombinant, chimeric tetravalent dengue vaccine candidate. *Vaccine.* (2015) 33:7112–20. doi: 10.1016/j.vaccine.2015.11.022
46. Brewoo JN, Kinney RM, Powell TD, Arguello JJ, Silengo SJ, Partidos CD, et al. Immunogenicity and efficacy of chimeric dengue vaccine (DENVax) formulations in interferon-deficient AG129 mice. *Vaccine.* (2012) 30:1513–20. doi: 10.1016/j.vaccine.2011.11.072
47. Osorio JE, Huang CY-H, Kinney RM, Stinchcomb DT. Development of DENVax: a chimeric dengue-2 PDK-53-based tetravalent vaccine for protection against dengue fever. *Vaccine.* (2011) 29:7251–60. doi: 10.1016/j.vaccine.2011.07.020
48. Thomas SJ, Eckels KH, Carletti I, De La Barrera R, Dessy F, Fernandez S, et al. A phase II, randomized, safety and immunogenicity study of a re-derived, live-attenuated dengue virus vaccine in healthy adults. *Am J Trop Med Hyg.* (2013) 88:73–88. doi: 10.4269/ajtmh.2012.12-0361
49. Fernandez S, Thomas SJ, De La Barrera R, Im-Erbsin R, Jarman RG, Baras B, et al. An adjuvanted, tetravalent dengue virus purified inactivated vaccine candidate induces long-lasting and protective antibody responses against dengue challenge in rhesus macaques. *Am J Trop Med Hyg.* (2015) 92:698–708. doi: 10.4269/ajtmh.14-0268
50. Flingai S, Czerwonko M, Goodman J, Kudchodkar S, Muthumani K, Weiner D. Synthetic DNA vaccines: improved vaccine potency by electroporation and co-delivered genetic adjuvants. *Front Immunol.* (2013) 4:354. doi: 10.3389/fimmu.2013.00354
51. Porter KR, Raviprakash K. Nucleic acid (DNA) immunization as a platform for dengue vaccine development. *Vaccine.* (2015) 33:7135–40. doi: 10.1016/j.vaccine.2015.09.102
52. Manoff SB, George SL, Bett AJ, Yelmene ML, Dhanasekaran G, Eggemeyer L, et al. Preclinical and clinical development of a dengue recombinant subunit vaccine. *Vaccine.* (2015) 33:7126–34. doi: 10.1016/j.vaccine.2015.09.101
53. Clements DE, Coller B-AG, Lieberman MM, Ogata S, Wang G, Harada KE, et al. Development of a recombinant tetravalent dengue virus vaccine: immunogenicity and efficacy studies in mice and monkeys. *Vaccine.* (2010) 28:2705–15. doi: 10.1016/j.vaccine.2010.01.022
54. Govindarajan D, Meschino S, Guan L, Clements DE, ter Meulen JH, Casimiro DR, et al. Preclinical development of a dengue tetravalent recombinant subunit vaccine: immunogenicity and protective efficacy in nonhuman primates. *Vaccine.* (2015) 33:4105–16. doi: 10.1016/j.vaccine.2015.06.067
55. Manoff SB, Sausser M, Falk Russell A, Martin J, Radley D, Hyatt D, et al. Immunogenicity and safety of an investigational tetravalent recombinant subunit vaccine for dengue: results of a Phase I randomized clinical trial in flavivirus-Naïve adults. *Hum Vaccin Immunother.* (2019) 15:2195–204. doi: 10.1080/21645515.2018.1546523
56. Brandler S, Ruffie C, Najburg V, Frenkiel MP, Bedouelle H, Desprès P, et al. Pediatric measles vaccine expressing a dengue tetravalent antigen elicits neutralizing antibodies against all four dengue viruses. *Vaccine.* (2010) 28:6730–9. doi: 10.1016/j.vaccine.2010.07.073

57. Harahap-Carrillo SI, Ceballos-Olvera I, Valle RJ. Immunogenic subviral particles displaying domain III of dengue 2 envelope protein vectored by measles virus. *Vaccines.* (2015) 3:503–18. doi: 10.3390/vaccines3030503
58. White LJ, Sariol CA, Mattocks MD, Wahala MPBW, Yingsiwaphat V, Collier ML, et al. An alphavirus vector-based tetravalent dengue vaccine induces a rapid and protective immune response in macaques that differs qualitatively from immunity induced by live virus infection. *J Virol.* (2013) 87:3409. doi: 10.1128/JVI.02298-12
59. Versiani AF, Astigarraga RG, Rocha ESO, Barboza APM, Kroon EG, Rachid MA, et al. Multi-walled carbon nanotubes functionalized with recombinant Dengue virus 3 envelope proteins induce significant and specific immune responses in mice. *J Nanobiotechnol.* (2017) 15:26. doi: 10.1186/s12951-017-0259-4
60. Chiang CY, Pan CH, Chen MY, Hsieh CH, Tsai JP, Liu HH, et al. Immunogenicity of a novel tetravalent vaccine formulation with four recombinant lipidated dengue envelope protein domain IIIs in mice. *Sci Rep.* (2016) 6:30648. doi: 10.1038/srep30648
61. Gil L, Cobas K, Lazo L, Marcos E, Hernández L, Suzarte E, et al. A tetravalent formulation based on recombinant nucleocapsid-like particles from dengue viruses induces a functional immune response in mice and monkeys. *J Immunol.* (2016) 197:3597. doi: 10.4049/jimmunol.1600927
62. Ramasamy V, Arora U, Shukla R, Poddar A, Shanmugam RK, White LJ, et al. A tetravalent virus-like particle vaccine designed to display domain III of dengue envelope proteins induces multi-serotype neutralizing antibodies in mice and macaques which confer protection against antibody dependent enhancement in AG129 mice. *PLOS Negl Trop Dis.* (2018) 12:e0006191. doi: 10.1371/journal.pntd.0006191
63. Shukla R, Rajpoot RK, Arora U, Poddar A, Swaminathan S, Khanna N. Pichia pastoris-expressed bivalent virus-like particulate vaccine induces domain III-focused bivalent neutralizing antibodies without antibody-dependent enhancement *in vivo*. *Front Microbiol.* (2018) 8:2644. doi: 10.3389/fmicb.2017.02644
64. Urakami A, Ngwe Tun MM, Moi ML, Sakurai A, Ishikawa M, Kuno S, et al. An envelope-modified tetravalent dengue virus-like-particle vaccine has implications for flavivirus vaccine design. *J Virol.* (2017) 91:e01181–17. doi: 10.1128/JVI.01181-17
65. Monath TP, Cetron MS, McCarthy K, Nichols R, Archambault WT, Weld L, et al. Yellow fever 17D vaccine safety and immunogenicity in the elderly. *Hum Vaccines.* (2005) 1:207–14. doi: 10.4161/hv.1.5.2221
66. O'Connor D, Png E, Khor CC, Snape MD, Hill AVS, van der Klis F, et al. Common genetic variations associated with the persistence of immunity following childhood immunization. *Cell Rep.* (2019) 27:3241–53.e4. doi: 10.1016/j.celrep.2019.05.053
67. Roukens AH, Soonawala D, Joosten SA, de Visser AW, Jiang X, Dirksen K, et al. Elderly subjects have a delayed antibody response and prolonged viraemia following yellow fever vaccination: a prospective controlled cohort study. *PLoS ONE.* (2011) 6:e27753. doi: 10.1371/journal.pone.0027753
68. Bradt V, Malafa S, von Braun A, Jarmer J, Tsouchnikas G, Medits I, et al. Pre-existing yellow fever immunity impairs and modulates the antibody response to tick-borne encephalitis vaccination. *NPJ Vaccines.* (2019) 4:38. doi: 10.1038/s41541-019-0133-5
69. Muyanja E, Ssemaganda A, Ngauv P, Cubas R, Perrin H, Srinivasan D, et al. Immune activation alters cellular and humoral responses to yellow fever 17D vaccine. *J Clin Invest.* (2014) 124:3147–58. doi: 10.1172/JCI75429
70. Fourati S, Cristescu R, Loboda A, Talla A, Filali A, Railkar R, et al. Pre-vaccination inflammation and B-cell signalling predict age-related hyporesponse to hepatitis B vaccination. *Nat Commun.* (2016) 7:10369. doi: 10.1038/ncomms10369
71. de Alwis R, Beltramello M, Messer WB, Sukupolvi-Petty S, Wahala WM, Kraus A, et al. In-depth analysis of the antibody response of individuals exposed to primary dengue virus infection. *PLoS Negl Trop Dis.* (2011) 5:e1188. doi: 10.1371/annotation/f585335f-ff77-40ae-a8b6-ad6019af31aa
72. Tirado SMC, Yoon KJ. Antibody-dependent enhancement of virus infection and disease. *Viral Immunol.* (2003) 16:69–86. doi: 10.1089/088282403763635465
73. Hawkes RA. Enhancement of the infectivity of arboviruses by specific antisera produced in domestic fowls. *Aust J Exp Biol Med Sci.* (1964) 42:465–82. doi: 10.1038/icb.1964.44
74. Takada A, Ebihara H, Feldmann H, Geisbert TW, Kawaoka Y. Epitopes required for antibody-dependent enhancement of ebola virus infection. *J Infect Dis.* (2007) 196(Suppl. 2):S347–56. doi: 10.1086/520581
75. Lund O, Hansen J, Søorensen AM, Mosekilde E, Nielsen JO, Hansen JE. Increased adhesion as a mechanism of antibody-dependent and antibody-independent complement-mediated enhancement of human immunodeficiency virus infection. *J Virol.* (1995) 69:2393–400. doi: 10.1128/JVI.69.4.2393-2400.1995
76. Ghiran I, Tyagi SR, Klickstein LB, Nicholson-Weller A. Expression and function of C1q receptors and C1q binding proteins at the cell surface. *Immunobiology.* (2002) 205:407–20. doi: 10.1078/0171-2985-00142
77. Wan Y, Shang J, Sun S, Tai W, Chen J, Geng Q, et al. Molecular mechanism for antibody-dependent enhancement of coronavirus entry. *J Virol.* (2020) 94, 1–15. doi: 10.1128/JVI.02015-19
78. Mason PW, Rieder E, Baxt B. RGD sequence of foot-and-mouth disease virus is essential for infecting cells via the natural receptor but can be bypassed by an antibody-dependent enhancement pathway. *Proc Natl Acad Sci USA.* (1994) 91:1932–6. doi: 10.1073/pnas.91.5.1932
79. Chareonsirisuthigul T, Kalayanarooj S, Ubol S. Dengue virus (DENV) antibody-dependent enhancement of infection upregulates the production of anti-inflammatory cytokines, but suppresses anti-DENV free radical and pro-inflammatory cytokine production, in THP-1 cells. *J Gen Virol.* (2007) 88:365–75. doi: 10.1099/vir.0.82537-0
80. Dejnirattisai W, Jumnainsong A, Onsirisakul N, Fitton P, Vasanawathana S, Limpitikul W, et al. Cross-reacting antibodies enhance dengue virus infection in humans. *Science.* (2010) 328:745–8. doi: 10.1126/science.1185181
81. Ripoll DR, Wallqvist A, Chaudhury S. Molecular simulations reveal the role of antibody fine specificity and viral maturation state on antibody-dependent enhancement of infection in dengue virus. *Front Cell Infect Microbiol.* (2019) 9:200. doi: 10.3389/fcimb.2019.00200
82. Kliks SC, Nisalak A, Brandt WE, Wahl L, Burke DS. Antibody-dependent enhancement of dengue virus growth in human monocytes as a risk factor for dengue hemorrhagic fever. *Am J Trop Med Hyg.* (1989) 40:444–51. doi: 10.4269/ajtmh.1989.40.444
83. Burke DS, Nisalak A, Johnson DE, Scott RM. A prospective study of dengue infections in Bangkok. *Am J Trop Med Hyg.* (1988) 38:172–80. doi: 10.4269/ajtmh.1988.38.172
84. Sangkawibha N, Rojanasuphot S, Ahandrik S, Viriyapongse S, Jatanasen S, Salitul V, et al. Risk factors in dengue shock syndrome: a prospective epidemiologic study in Rayong, Thailand: I. The 1980 outbreak. *Am J Epidemiol.* (1984) 120:653–69. doi: 10.1093/oxfordjournals.aje.a113932
85. Montecillo-Aguado MR, Montes-Gómez AE, García-Cordero J, Corzo-Gómez J, Vivanco-Cid H, Mellado-Sánchez G, et al. Cross-reaction, enhancement, and neutralization activity of dengue virus antibodies against zika virus: a study in the mexican population. *J Immunol Res.* (2019) 2019:7239347. doi: 10.1155/2019/7239347
86. Sirohi D, Chen Z, Sun L, Klose T, Pierson TC, Rossmann MG, et al. The 3.8 Å resolution cryo-EM structure of Zika virus. *Science.* (2016) 352:467–70. doi: 10.1126/science.aaf5316
87. Nogueira ML, Júnior NN, Estofolete CF, Terzian AB, Guimarães GdF, Zini N, et al. Adverse birth outcomes associated with Zika virus exposure during pregnancy in São José do Rio Preto, Brazil. *Clin Microbiol Infect.* (2018) 24:646–52. doi: 10.1016/j.cmi.2017.11.004
88. Katzelnick LC, Montoya M, Gresh L, Balmaseda A, Harris E. Neutralizing antibody titers against dengue virus correlate with protection from symptomatic infection in a longitudinal cohort. *Proc Natl Acad Sci USA.* (2016) 113:728–33. doi: 10.1073/pnas.1522136113
89. Ghosh A, Dar L. Dengue vaccines: challenges, development, current status and prospects. *Indian J Med Microbiol.* (2015) 33:3–15. doi: 10.4103/0255-0857.148369
90. Havenar-Daughton C, Newton IG, Zare SY, Reiss SM, Schwan B, Suh MJ, et al. Normal human lymph node T follicular helper cells and germinal center B cells accessed via fine needle aspirations. *J Immunol Methods.* (2020) 479:112746. doi: 10.1016/j.jim.2020.112746
91. Ueno H. Human circulating T follicular helper cell subsets in health and disease. *J Clin Immunol.* (2016) 36:34–9. doi: 10.1007/s10875-016-0268-3

92. Simpson N, Gatenby PA, Wilson A, Malik S, Fulcher DA, Tangye SG, et al. Expansion of circulating T cells resembling follicular helper T cells is a fixed phenotype that identifies a subset of severe systemic lupus erythematosus. *Arthritis Rheum.* (2010) 62:234–44. doi: 10.1002/art.25032
93. Bentebibel S-E, Lopez S, Obermoser G, Schmitt N, Mueller C, Harrod C, et al. Induction of ICOS+ CXCR3+ CXCR5+ TH cells correlates with antibody responses to influenza vaccination. *Sci Transl Med.* (2013) 5:176ra32. doi: 10.1126/scitranslmed.3005191
94. He J, Tsai LM, Leong YA, Hu X, Ma CS, Chevalier N, et al. Circulating precursor CCR7loPD-1hi CXCR5+ CD4+ T cells indicate Tfh cell activity and promote antibody responses upon antigen reexposure. *Immunity.* (2013) 39:770–81. doi: 10.1016/j.immuni.2013.09.007
95. Schmitt N, Bentebibel SE, Ueno H. Phenotype and functions of memory Tfh cells in human blood. *Trends Immunol.* (2014) 35:436–42. doi: 10.1016/j.it.2014.06.002
96. Morita R, Schmitt N, Bentebibel SE, Ranganathan R, Bourdery L, Zurawski G, et al. Human blood CXCR5(+)CD4(+) T cells are counterparts of T follicular cells and contain specific subsets that differentially support antibody secretion. *Immunity.* (2011) 34:108–21. doi: 10.1016/j.immuni.2011.01.009
97. Locci M, Havenar-Daughton C, Landais E, Wu J, Kroenke MA, Arlehamn CL, et al. Human circulating PD-1+CXCR3-CXCR5+ memory Tfh cells are highly functional and correlate with broadly neutralizing HIV antibody responses. *Immunity.* (2013) 39:758–69. doi: 10.1016/j.immuni.2013.08.031
98. Victora GD, Schwickert TA, Fooksman DR, Kamphorst AO, Meyer-Hermann M, Dustin ML, et al. Germinal center dynamics revealed by multiphoton microscopy with a photoactivatable fluorescent reporter. *Cell.* (2010) 143:592–605. doi: 10.1016/j.cell.2010.10.032
99. Haltaufderhyde K, Srikiatkhachorn A, Green S, Macareo L, Park S, Kalayanarooj S, et al. Activation of peripheral T follicular helper cells during acute dengue virus infection. *J Infect Dis.* (2018) 218:1675–85. doi: 10.1093/infdis/jiy360
100. Martinez-Navio JM, Casanova V, Pacheco R, Naval-Macabuhay I, Climent N, Garcia F, et al. Adenosine deaminase potentiates the generation of effector, memory, and regulatory CD4+ T cells. *J Leuk Biol.* (2011) 89:127–36. doi: 10.1189/jlb.1009696
101. Bradford KL, Moretti FA, Carbonaro-Sarracino DA, Gaspar HB, Kohn DB. Adenosine deaminase (ADA)-deficient severe combined immune deficiency (SCID): molecular pathogenesis and clinical manifestations. *J Clin Immunol.* (2017) 37:626–37. doi: 10.1007/s10875-017-0433-3
102. Tardif V, Muir R, Cubas R, Chakhtoura M, Wilkinson P, Metcalf T, et al. Adenosine deaminase-1 delineates human follicular helper T cell function and is altered with HIV. *Nat Commun.* (2019) 10:1–15. doi: 10.1038/s41467-019-08801-1
103. Farooq F, Beck K, Paolino KM, Phillips R, Waters NC, Regules JA, et al. Circulating follicular T helper cells and cytokine profile in humans following vaccination with the rVSV-ZEBOV Ebola vaccine. *Sci Rep.* (2016) 6:27944. doi: 10.1038/srep27944
104. Riteau N, Radtke AJ, Shenderov K, Mittereder L, Oland SD, Hieny S, et al. Water-in-oil–only adjuvants selectively promote T follicular helper cell polarization through a type I IFN and IL-6–dependent pathway. *J Immunol.* (2016) 197:3884–93. doi: 10.4049/jimmunol.1600883
105. Gavillet BM, Eberhardt CS, Auderset F, Castellino F, Seubert A, Tregoning JS, et al. MF59 mediates its B cell adjuvanticity by promoting T follicular helper cells and thus germinal center responses in adult and early life. *J Immunol.* (2015) 194:4836–45. doi: 10.4049/jimmunol.1402071
106. Kasturi SP, Skountzou I, Albrecht RA, Koutsonanos D, Hua T, Nakaya HI, et al. Programming the magnitude and persistence of antibody responses with innate immunity. *Nature.* (2011) 470:543–7. doi: 10.1038/nature09737
107. Yang X, Yang J, Chu Y, Xue Y, Xuan D, Zheng S, et al. T follicular helper cells and regulatory B cells dynamics in systemic lupus erythematosus. *PLoS ONE.* (2014) 9, 1–9. doi: 10.1371/journal.pone.0088441
108. Wang J, Shan Y, Jiang Z, Feng J, Li C, Ma L, et al. High frequencies of activated B cells and T follicular helper cells are correlated with disease activity in patients with new-onset rheumatoid arthritis. *Clin Exp Immunol.* (2013) 174:212–20. doi: 10.1111/cei.12162
109. Christensen JR, Börnsen L, Ratzer R, Piehl F, Khademi M, Olsson T, et al. Systemic inflammation in progressive multiple sclerosis involves follicular T-helper, Th17-and activated B-cells and correlates with progression. *PLoS ONE.* (2013) 8:e57820. doi: 10.1371/journal.pone.0057820
110. Linterman MA, Rigby RJ, Wong RK, Yu D, Brink R, Cannons JL, et al. Follicular helper T cells are required for systemic autoimmunity. *J Exp Med.* (2009) 206:561–76. doi: 10.1084/jem.20081886

Conflict of Interest: The authors declare that the research was conducted in the absence of any commercial or financial relationships that could be construed as a potential conflict of interest.

frontiers in Immunology

ORIGINAL RESEARCH
published: 19 June 2020
doi: 10.3389/fimmu.2020.01207

A Novel Synthetic Dual Agonistic Liposomal TLR4/7 Adjuvant Promotes Broad Immune Responses in an Influenza Vaccine With Minimal Reactogenicity

*Fumi Sato-Kaneko[1], Shiyin Yao[1], Fitzgerald S. Lao[1], Jonathan Shpigelman[1], Karen Messer[2], Minya Pu[2], Nikunj M. Shukla[1], Howard B. Cottam[1], Michael Chan[1], Paul J. Chu[1], David Burkhart[3], Roman Schoener[3], Takaji Matsutani[4], Dennis A. Carson[1], Maripat Corr[5] and Tomoko Hayashi[1]**

[1] Moores Cancer Center, University of California, San Diego, La Jolla, CA, United States, [2] Division of Biostatistics, University of California, San Diego, La Jolla, CA, United States, [3] Inimmune Corp., Missoula, MT, United States, [4] Repertoire Genesis Inc., Saito-Asagai, Osaka, Japan, [5] Department of Medicine, University of California, San Diego, La Jolla, CA, United States

OPEN ACCESS

Edited by:
Simon Daniel Van Haren, Harvard Medical School, Boston Children's Hospital, United States

Reviewed by:
Hongpeng Jia, The Johns Hopkins Hospital, United States
Matej Sova, University of Ljubljana, Slovenia

***Correspondence:**
Tomoko Hayashi
thayashi@health.ucsd.edu

Specialty section:
This article was submitted to Vaccines and Molecular Therapeutics, a section of the journal Frontiers in Immunology

Received: 25 March 2020
Accepted: 14 May 2020
Published: 19 June 2020

Citation:
Sato-Kaneko F, Yao S, Lao FS, Shpigelman J, Messer K, Pu M, Shukla NM, Cottam HB, Chan M, Chu PJ, Burkhart D, Schoener R, Matsutani T, Carson DA, Corr M and Hayashi T (2020) A Novel Synthetic Dual Agonistic Liposomal TLR4/7 Adjuvant Promotes Broad Immune Responses in an Influenza Vaccine With Minimal Reactogenicity. Front. Immunol. 11:1207. doi: 10.3389/fimmu.2020.01207

The limited efficacy of seasonal influenza vaccines is usually attributed to ongoing variation in the major antigenic targets for protective antibody responses including hemagglutinin (HA) and neuraminidase (NA). Hence, vaccine development has largely focused on broadening antigenic epitopes to generate cross-reactive protection. However, the vaccine adjuvant components which can accelerate, enhance and prolong antigenic immune responses, can also increase the breadth of these responses. We previously demonstrated that the combination of synthetic small-molecule Toll-like receptor 4 (TLR4) and TLR7 ligands is a potent adjuvant for recombinant influenza virus HA, inducing rapid, and sustained antibody responses that are protective against influenza viruses in homologous and heterologous murine challenge models. To further enhance adjuvant efficacy, we performed a structure-activity relationship study for the TLR4 ligand, *N*-cyclohexyl-2-((5-methyl-4-oxo-3-phenyl-4,5-dihydro-3H-pyrimido[5,4-*b*]indol-2-yl)thio)acetamide ($C_{25}H_{26}N_4O_2S$; **1Z105**), and identified the 8-(furan-2-yl) substituted pyrimido[5,4-*b*]indole analog ($C_{29}H_{28}N_4O_3S$; **2B182C**) as a derivative with higher potency in activating both human and mouse TLR4-NF-κB reporter cells and primary cells. In a prime-boost immunization model using inactivated influenza A virus [IIAV; A/California/04/2009 (H1N1)pdm09], **2B182C** used as adjuvant induced higher serum anti-HA and anti-NA IgG1 levels compared to **1Z105**, and also increased the anti-NA IgG2a responses. In combination with a TLR7 ligand, **1V270**, **2B182C** induced equivalent levels of anti-NA and anti-HA IgG1 to **1V270+1Z105**. However, the combination of **1V270+2B182C** induced 10-fold higher anti-HA and anti-NA IgG2a levels compared to **1V270+1Z105**. A stable liposomal formulation of **1V270+2B182C** was developed, which synergistically enhanced anti-HA and anti-NA IgG1 and IgG2a responses without demonstrable reactogenicity after intramuscular injection. Notably, vaccination with IIAV plus the liposomal formulation of **1V270+2B182C** protected mice against lethal homologous influenza virus (H1N1)pdm09 challenge and reduced lung viral

titers and cytokine levels. The combination adjuvant induced a greater diversity in B cell clonotypes of immunoglobulin heavy chain (IGH) genes in the draining lymph nodes and antibodies against a broad spectrum of HA epitopes encompassing HA head and stalk domains and with cross-reactivity against different subtypes of HA and NA. This novel combination liposomal adjuvant contributes to a more broadly protective vaccine while demonstrating an attractive safety profile.

Keywords: vaccine, combination adjuvant, synthetic TLR4 agonist, synthetic TLR7 agonists, small molecule, influenza virus infection

INTRODUCTION

Global public health emergencies from zoonotic infections stress the imperative need for vaccines with rapid protective immune responses (1, 2). Lasting protection against infectious diseases induced by vaccines largely depends on adjuvants as well as antigen selection (3–5). For example, past epidemics and pandemics have demonstrated that influenza viruses are continuously evolving, and antigenic drift and shift of surface glycoproteins, including hemagglutinin (HA) and neuraminidase (NA), cause mismatches between vaccine containing strains and circulating strains (1, 2). Typically, existing licensed seasonal vaccines contain 3 or 4 strains of inactivated influenza virus including H1N1, H3N2 and influenza B viruses, and afford only a limited protection (1, 2, 6, 7). However, the gap in protection cannot be exclusively attributed to the antigenic component as most vaccines only contain aluminum salts, such as $Al(OH)_3$ and $AlPO_4$, as the adjuvant and preferentially enhance humoral responses to the major surface protein HA (3, 8). These adjuvants also skew away from balanced T helper (Th) 1 and 2 responses to a Th2 predominant response that is mediated by induction of antigen specific IgG1 (9), Furthermore, the thermostability of aluminum adjuvant may not be robust (10). Newer vaccines with greater potency like FLUAD, which uses a squalene-based adjuvant microfluidized emulsion 59 (MF59) (11, 12), induced long term and broadly reactive antibodies against HAs (11, 13). Adjuvant System 04 (ASO4) and AS01 containing 3-O-desacyl-4′-monophosphoryl lipid A (MPL) are used in the vaccine against human paplillomavirus and varicella zoster virus infections, respectively, and are reported to induce long lasting effective protection (14, 15). Although these adjuvants have been demonstrated to be useful in high risk groups such as the elderly (11), mild to moderate adverse effects were reported, including pain and bruising at the injection site, as well as muscular ache (13). Also, MPL is chemically modified from biologically derived lipid A from *Salmonella minnesota* R595 lipopolysaccharide, which results in high production cost and variability (16). In addition, many other adjuvants have failed to advance into clinical trials for safety concerns from reactogenicity (17). Hence, it is still of major importance to develop vaccine adjuvants that do not cause adverse effects and that are easy to access at low cost.

Our approach to improve the protective efficacy of vaccines is to activate innate immune cells through multiple receptors thereby simultaneously heightening the responses of antigen presenting cells (APCs) like dendritic cells. In prior work we generated a phospholipid conjugated small molecule TLR7 ligand (TLR-L), **1V270**, which induced robust IgG2a responses in mice (18). In a separate study using a high throughput screen (HTS), pyrimido[5,4-*b*]indoles were identified as NF-κB activators and an initial structure-activity relationship (SAR) study identified a first-in-class small molecule TLR4 agonist, **1Z105** (19). In combination, **1Z105** and **1V270** worked additively as a potent adjuvant for recombinant influenza virus HA protein, inducing rapid and sustained immunity that was protective against influenza viruses in homologous, heterologous, and heterosubtypic murine challenge models (20, 21).

In this study, to further enhance adjuvanticity, we performed further SAR analysis on **1Z105** and identified an 8-(furan-2-yl) substituted pyrimido[5,4-*b*]indole analog (**2B182C**) with greater potency in stimulating mouse and human cells compared to **1Z105**. In a prime-boost preclinical model using inactivated influenza A virus [IIAV; A/California/04/2009 (H1N1)pdm09], and **2B182C** as an adjuvant, increased IgG1 levels against both HA and NA were observed compared to **1Z105**. A liposomal formulation of **1V270** and **2B182C** with IIAV protected mice against lethal homologous virus (H1N1)pdm09 challenge and reduced lung viral titers and cytokine levels. In addition, the liposomal combined adjuvant increased populations of T follicular helper (Tfh) cells, germinal center (GC) B cells, plasmablasts and plasma cells, and B cell receptor diversity in the draining lymph nodes. This combination also induced humoral responses against a broader spectrum of epitopes encompassing HA head and stalk regions and with cross-reactivity against different subtypes of HA and NA with minimal *in vivo* reactogenicity.

RESULTS

Structure-Activity Relationship Study of 1Z105 Yields 2B182C

We previously synthesized and characterized **1Z105**, *N*-cyclohexyl-2-((5-methyl-4-oxo-3-phenyl-4,5-dihydro-3H-pyrimido[5,4-*b*]indol-2-yl)thio)acetamide ($C_{25}H_{26}N_4O_2S$), a fully synthetic TLR4 ligand with *in vivo* efficacy as a vaccine adjuvant (19). To further improve the potency of **1Z105**,

additional SAR was performed probing the C8 position on the pyrimidoindole scaffold, which was previously found to be tolerant of variation with retained activity as seen with a C8-phenyl substitution (**2B110**) (22). The chemical space was explored with a series of substitutions including various alkyl, alkynyl, aryl, and heteroaryl substitutions (**Figure 1A**). First, we explored alkyl and alkynyl groups at this position. We introduced a *N*5-methyl initially by methylation of indole analog compound **2** (**Figure 1A**) as this substituent was previously found to reduce cytotoxicity (22). A "Sonogashira" reaction was then performed to introduce the alkyne on the indole ring (**3a**-**d**). These analogs were then reacted with phenylisothiocyanate to obtain thiourea analogs (**4a**-**d**), followed by ring closing condensation using sodium ethoxide to obtain pyrimidoindole ring compounds (**5a**-**d**). The S-alkylation of these compounds provided compounds (**6a**-**d**). In parallel, alkynes **3a**-**c** were reduced using hydrogenation to obtain alkyl substituted compounds (**3e**-**g**). These alkyl bearing analogs were further processed as discussed earlier to obtain C8-alkyl analogs **6e**-**g** (**Figure 1A**). For the next set of compounds, the advanced intermediate **7** (22) was reacted with several different aryl boronic acids via a "Suzuki" coupling reaction to obtain a series of C8-aryl compounds (**8a**-**t**) (**Figure 1B**).

Titration curves of **1Z105** and derivatives were used to assess their potency in stimulating human and mouse TLR4 response using HEK NF-κB reporter cells (HEK-Blue^{TM} hTLR4 and mTLR4, respectively). The areas under the curve for dose response curves relative to vehicle (0.5% DMSO) were normalized to the greatest activity as 100% of **2B110** for both assays (**Figure 1C**). The compounds were also tested for *in vitro* toxicity by MTT assay (**Figure 1C**, **Supplementary Figure 1**). Among the C8-alkynyl compounds, the 6-carbon chain analog **6b** showed the highest level of TLR4 activation, whereas compounds with shorter chain length (2 carbon chain, **6a**) or compounds with greater chain lengths (8-carbon chain, **6c**) showed a reduction in TLR4 activity, and the 12-carbon chain analog **6d** was completely inactive. These compounds had a relatively high toxicity in cell-based assay suggesting C8-alkynyl substitution was not ideal. The C8-alkyl substituted compounds (**6e**-**g**) showed a similar trend in TLR4 activity and the toxicity of this set of compounds improved compared to that of the corresponding C8-alkynyl compounds.

Moving on to the C8-aryl substituted compounds, we began first with small modifications to the structure of **2B110** starting with *ortho*, *meta*, and *para*-methyl substituted compounds **8a**-**c**, respectively. While all these compounds showed potent TLR4 agonistic activities in both mTLR4 and hTLR4 reporter cells, these compounds were relatively toxic. We continued probing the length of alkyl substitution at the *para* position to obtain *p*-ethyl and *p*-*n*-butyl compounds **8d** and **8e**, respectively. However, both these compounds showed relatively high toxicity, while maintaining TLR4 activity. These results on the *para*-substituted compounds prompted us to further explore the *meta* substituted compounds as availability of *ortho*-substituted boronic acids were limited likely due to steric hindrance. The first set of compounds included non-ionic hydrophobic substituents such as *m*-phenyl, *m*-isopropyl, and *m*-trifluoromethyl substituted analogs **8f**, **8g**, and **8i**, respectively. In parallel, we also synthesized *m*-methoxy (**8h**) and *m*-isopropoxy (**8j**) analogs. Most of these compounds retained murine TLR4 activity. However, bulky *m*-phenyl bearing compound **8f** and hydrogen bond accepting *m*-methoxy substituted compound **8h** showed dramatic loss of human TLR4 activity.

Continuing the SAR, we synthesized polar hydrophilic substituent bearing analogs including *m*-amino (**8k**), *m*-carboxylic acid (**8l**), and *m*-hydroxy (**8m**). However, all of these compounds showed significant loss of both human and murine TLR4 activity, suggesting that the binding pocket in TLR4-MD2 does not tolerate hydrophilic substituents at the C8 position. We then introduced hydrogen bond-accepting hydrophobic substituents to obtain the *m*-cyano and *m*-nitro substituted analogs **8n** and **8o**, respectively. While these compounds retained murine TLR4 activity, they were less potent than **2B110** in hTLR4 reporter cells (**Figure 1C**). The final set of C-8 aryl substituted compounds included bioisosteric replacements of C8-phenyl with 4-pyridyl (**8p**), 3-pyridyl (**8q**), 3-furyl (**8r**), 2-furyl (**8s**), and 3-thienyl (**8t**). While the pyridyl substituted compounds **8p**-**q** were either inactive or toxic, the five membered ring analogs showed potent TLR4 activity in both reporter cells with compound **8s** showing potency equivalent to that of compound **2B110** (**Figure 1C**). Thus, these SAR studies pointed us to our lead compound **8s** (herein designated as **2B182C**) along with previous lead **1Z105** and **2B110**, the structures of which are shown in **Figure 1D**. Among the SAR compounds, **2B182C** and **2B110** derivatives had high TLR4 stimulatory potency in both mTLR4 and hTLR4 reporter cells. However, **2B110** had slightly higher toxicity in MTT assays than did **2B182C** (**Supplementary Figure 1**); hence **2B182C** was chosen as a lead compound for further analyses and **2B110** was held in reserve as an alternate.

The relative potency of **2B182C** was compared to that of **1Z105** in a series of *in vitro* tests with TLR4 reporter cells and primary human and mouse cells (**Figure 2**). Notably **2B182C** was 4-fold more potent than **1Z105** (EC_{50} =1.65 μM and EC_{50} =7.49 μM, respectively) in stimulating a mTLR4 reporter line. However, **2B182C** was approximately 800-fold more potent in stimulating the hTLR4 reporter cells than **1Z105** (**Figure 2A**). This activity was confirmed in human and mouse primary cells, peripheral blood mononuclear cells (hPBMCs) and mouse bone marrow derived dendritic cells (mBMDCs). **2B182C** induced higher level of IL-8 secretion by hPBMCs compared to **1Z105** (**Figure 2B**). **2B182C** effectively induced cytokine production in primary mBMDCs at relatively low concentrations: IL-12 (EC_{50} = 0.20 μM) and IL-6 (EC_{50} = 0.16 μM; **Figure 2C**).

As a vaccine adjuvant, stimulating dendritic cells to mature into antigen-presenting cells is critical. Hence, we tested expression levels of co-stimulatory molecules CD40 and CD86 on BMDC using flow cytometry as measures of APC maturation. In mBMDCs, 1 μM **2B182C** induced significantly higher expression levels of costimulatory molecules CD40 and CD86 compared to **1Z105** (**Figure 2D**). These data confirmed that the SAR study successfully yielded a derivative, **2B182C**, with higher TLR4 stimulatory potency, especially for human TLR4.

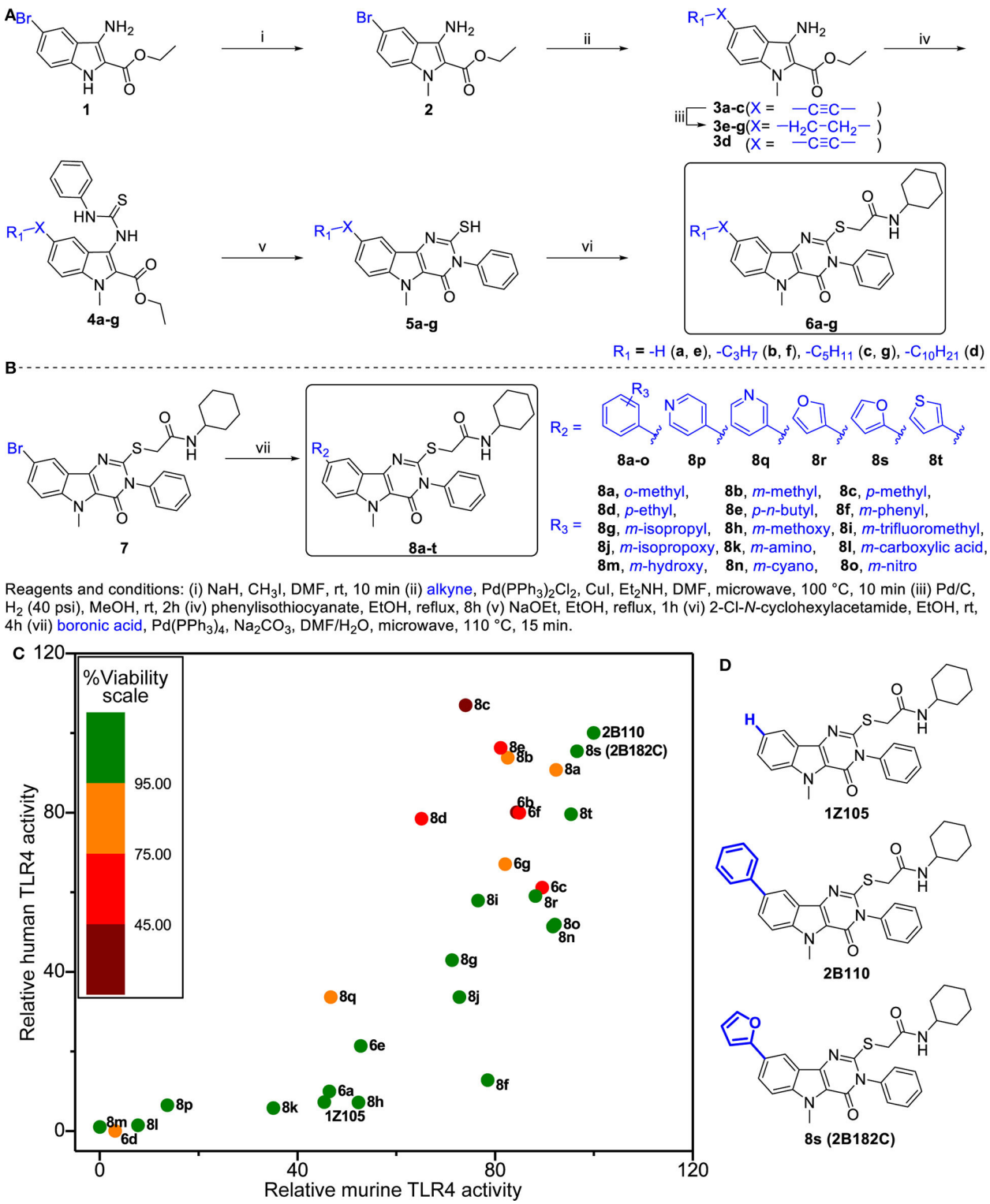

FIGURE 1 | Structure-activity relationship studies in TLR4 agonistic pyrimidoindoles. **(A)** Syntheses of C8-alkynyl and C8-alkyl analogs. **(B)** Syntheses of C8-aryl analogs. **(C)** Scatter plot of hTLR4 and mTLR4 agonistic activity in TLR4-NF-κB HEK reporter cells (HEK-Blue^{TM} hTLR4 and HEK-Blue^{TM} mTLR4, respectively). NF-κB inducible NF-κB SEAP levels in culture supernatants were measured according to manufacturer's protocol. The TLR4 agonistic potency was evaluated as area under the curve (AUC) calculated for dose response curve using 2-fold serial dilutions from 10 μM, and normalized to the AUC for **2B110** as 100% on both axes. AUC of **2B110** for mTLR4 and hTLR4 reporter cells were 28.43 ± 5.49 units and 14.95 ± 1.95, respectively. The color of each point is based on cell viability in TLR4-NF-κB reporter cells for compounds evaluated at 5 μM concentration. Viability data was normalized to vehicle control (Vehicle $OD_{570-650}$ = 0.58 ± 0.01). **(D)** Structures of the lead compounds with differences at C8 substitution highlighted in blue.

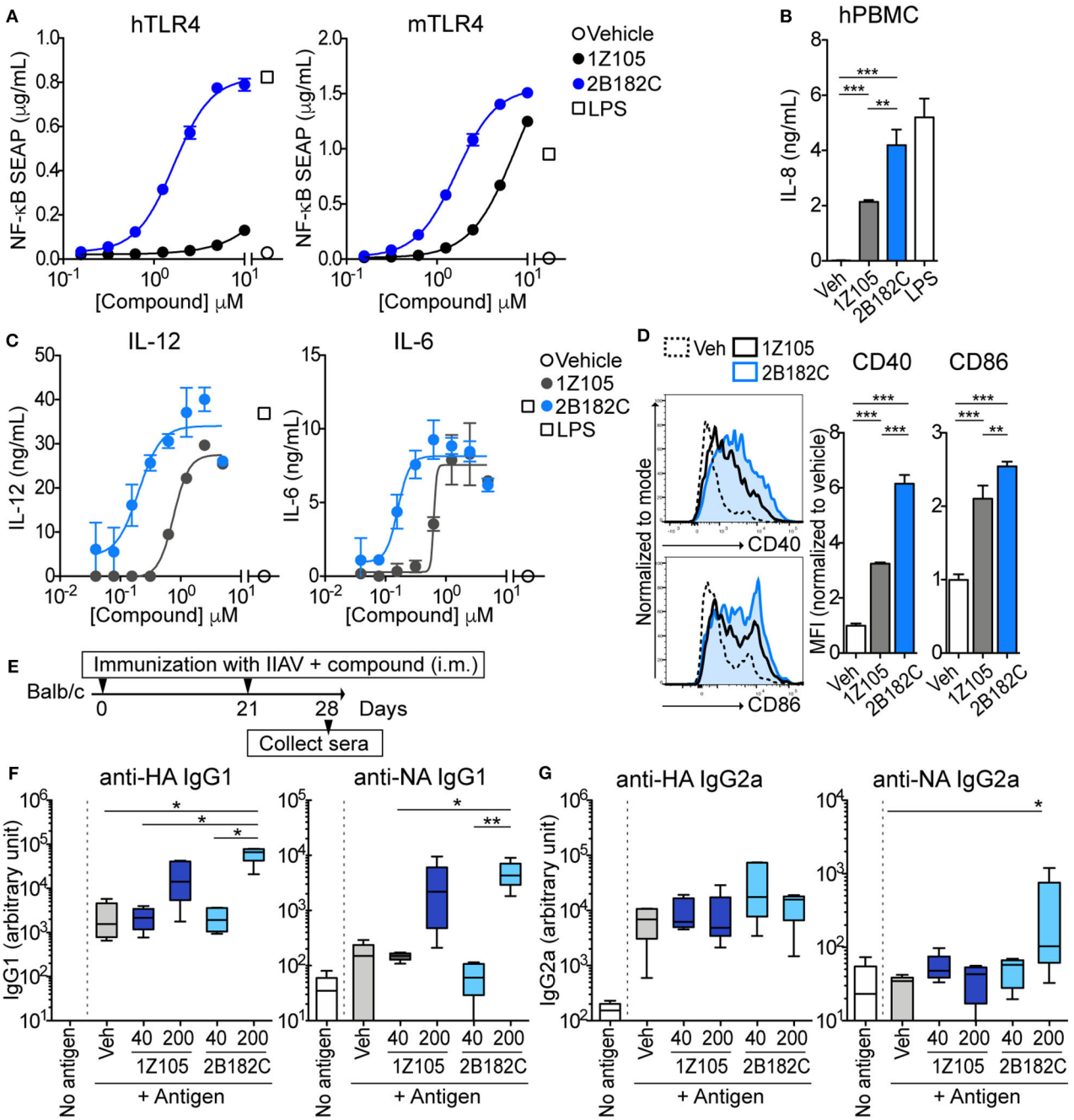

FIGURE 2 | 2B182C is more potent than **1Z105** in both human and mouse cells and induced higher levels of anti-NA IgG2a. **(A)** TLR4-NF-κB HEK reporter cells (HEK-Blue^{TM} hTLR4 and HEK-Blue^{TM} mTLR4) were treated with compounds **1Z105** and **2B182C** (2-fold serial dilutions from 10 μM) for 20 h. NF-κB inducible NF-κB SEAP levels in culture supernatants were measured according to manufacturer's protocol. EC_{50} of **1Z105** and **2B182C** were 1,445 and 1.66 μM, respectively, on hTLR4 reporter cells. EC_{50} of **1Z105** and **2B182C** were 7.49 and 1.65 μM, respectively on mTLR4 reporter cells. Data represent means ± SD and are representative of two independent experiments with similar results. **(B)** IL-8 release from hPBMC. Data shown are means of triplicates ± SD from one donor and are representative of two donors with similar results. **(C)** IL-12 and IL-6 production levels in BMDCs. EC_{50} of **1Z105** and **2B182C** were 0.77 and 0.20 μM for IL-12, and 0.63 and 0.12 μM for IL-6, respectively. **(D)** Expression levels of costimulatory molecules CD40 and CD86 on BMDCs. Mean fluorescence intensity of CD40 and CD86 were analyzed by flow cytometry. **(B,D)** $^{**}P < 0.01$, $^{***}P < 0.0001$, one-way ANOVA with Tukey's *post-hoc* test. **(A–D)** Data shown are means ± SD. **(E)** Experimental protocol for comparison of two TLR agonists **1Z105** and **2B182C**. BALB/c mice ($n = 5$/group) were i.m. immunized with IIAV (10 μg/injection) plus a TLR4 agonist **1Z105** or **2B182C** (40 and 200 nmol/injection) on days 0 and 21, and were bled on day 28. The sera were evaluated for IgG1 **(F)** and IgG2a **(G)** against hemagglutinin (HA) and neuraminidase (NA) by ELISA. Ten percentage DMSO was used as vehicle. In each box plot, the line within the box represents the median, the bounds are the upper and lower quartiles and the bars indicate minimum and maximum values. Data shown are means ± SEM. $^{*}P < 0.05$, $^{**}P < 0.01$, Kruskal-Wallis test with Dunn's *post-hoc* test.

TLR4 Agonist 2B182C Enhances Antigen Specific IgG1 Production

Our previous report demonstrated that TLR4-L **1Z105** and TLR7-L **1V270** separately induced antigen specific Th2-mediated IgG1, and Th1-mediated IgG2a levels when administered as an adjuvant with antigen in mice (20, 21). Since **2B182C** demonstrated higher potency compared to **1Z105** *in vitro*, we first tested whether a vaccine formulated in 10% DMSO and adjuvanted with **2B182C** induced higher levels of antigen specific IgG secretion compared to that induced by a **1Z105** adjuvanted vaccine. BALB/c mice were intramuscularly (i.m.) immunized with IIAV [A/California/04/2009 (H1N1)pdm09] mixed with **1Z105** or **2B182C** at 40 or 200 nmol/injection on days 0 and 21. The mice were bled on day 28, and sera were evaluated by ELISA for antibodies (IgG1 and IgG2a) against two glycoproteins on the surface of the virus, hemagglutinin (HA) and neuraminidase (NA; **Figure 2E**). At a dose of 200 nmol/injection **2B182C** significantly increased IgG1 antibody production against both HA and NA compared to the vehicle control group (**Figure 2F**). Interestingly, 200 nmol/injection of **2B182C**, but not **1Z105**, enhanced anti-NA specific IgG2a compared to the vehicle control (**Figure 2G**).

2B182C Enhances Antigen Specific IgG2a Production Induced by 1V270

In our previous studies, the combination adjuvant with the TLR4-L **1Z105** and the TLR7-L **1V270** worked additively with a recombinant HA to induce rapid, long-lasting, and balanced Th1- and Th2-type immunity (20, 21). Thus, we next compared effects of the two TLR4 ligands as co-adjuvants in combination with **1V270** on antibody production using IIAV as an antigen (**Figure 3**). BALB/c mice were i.m. immunized with IIAV mixed with **1V270** (1 nmol/injection) alone or mixed with **1V270** and **2B182C** (200 nmol/injection) or **1Z105** (200 nmol/injection) on days 0 and day 21. Immunization with **1V270+2B182C** increased IgG1 specific for HA and NA to a similar degree as **1V270+1Z105**, when compared to **1V270** alone (**Figure 3A**). In contrast, **1V270+2B182C** notably enhanced induction of anti-HA and anti-NA IgG2a compared to **1V270** alone and **1V270+1Z105** (**Figure 3B**). Hence, immunization with **1V270+1Z105** produced both Th1 and Th2 associated IgG2a and IgG1 responses, respectively, as previously reported (20). However, **1V270+2B182C** augmented both Th1 and Th2 associated humoral responses resulting in an overall skewing toward a relatively Th1 biased response (**Figure 3C**).

Liposomal Formulation Enhances Immunostimulatory Effects of the Combination 1V270+2B182C Adjuvant With Minimal Reactogenicity

In order to avoid unwanted cytotoxicity and reactogenicity, while maintaining a robust immune response from a vaccine, adjusting the formulation is an important step in the development of vaccine adjuvants (23). The adjuvant formulation has significant effects on the induction of humoral and cell mediated immune

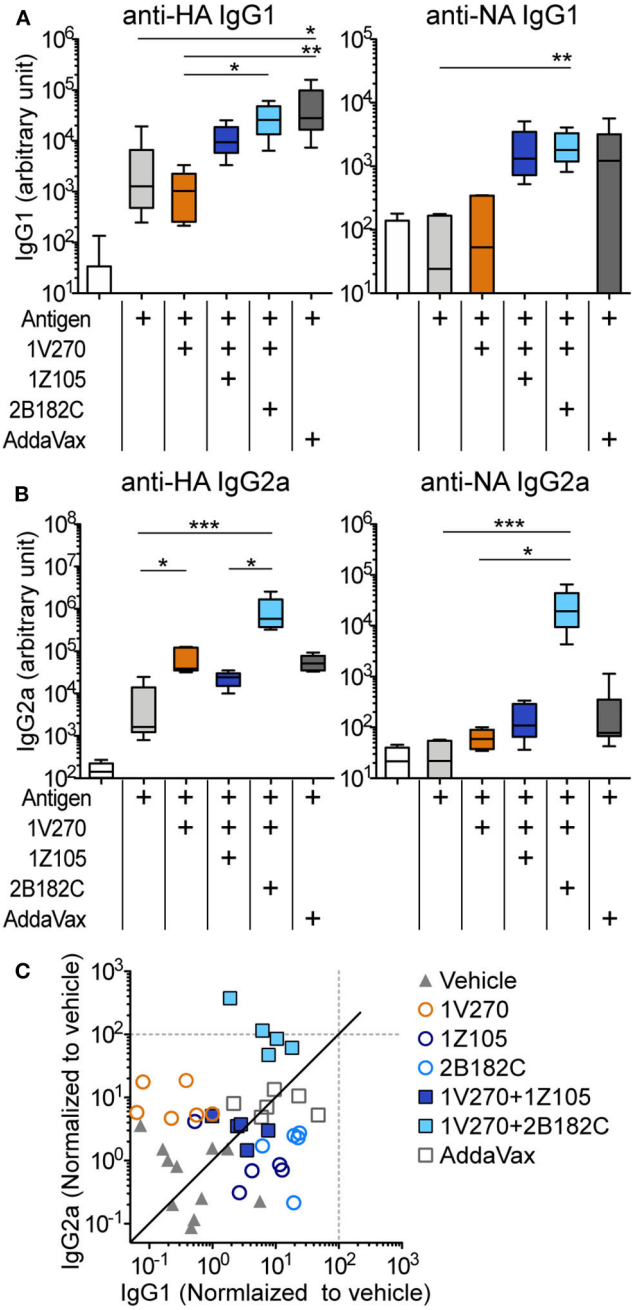

FIGURE 3 | 2B182C (TLR4-L) enhanced antigen specific IgG2a production induced by **1V270** (TLR7-L). **(A–C)** BALB/c mice ($n = 5–6$) were immunized with IIAV (10 μg/injection) and adjuvants (1 nmol/injection **1V270**, 200 nmol/injection **1Z105** or 200 nmol/injection **2B182C**) and bled on day 28 as shown in **Figure 2E**. AddaVax™ was used as a positive control. Sera anti-HA and anti-NA IgG1 **(A)**, and IgG2a **(B)** were determined by ELISA. In each box plot, the line within the box represents the median, the bounds are the upper and lower quartiles and the bars indicate minimum and maximum values. $^*P < 0.05$, $^{**}P < 0.01$, $^{***}P < 0.001$, Kruskal-Wallis test with Dunn's *post-hoc* test. **(C)** Anti-HA IgG1 and IgG2a levels induced by all combination treatments (normalized to vehicle) are shown. Data for **1Z105**, **2B182C** alone (200 nmol/injection) and vehicle from **Figure 2** are also shown in **(C)**. Each dot indicates an individual mouse. Identity line in solid black.

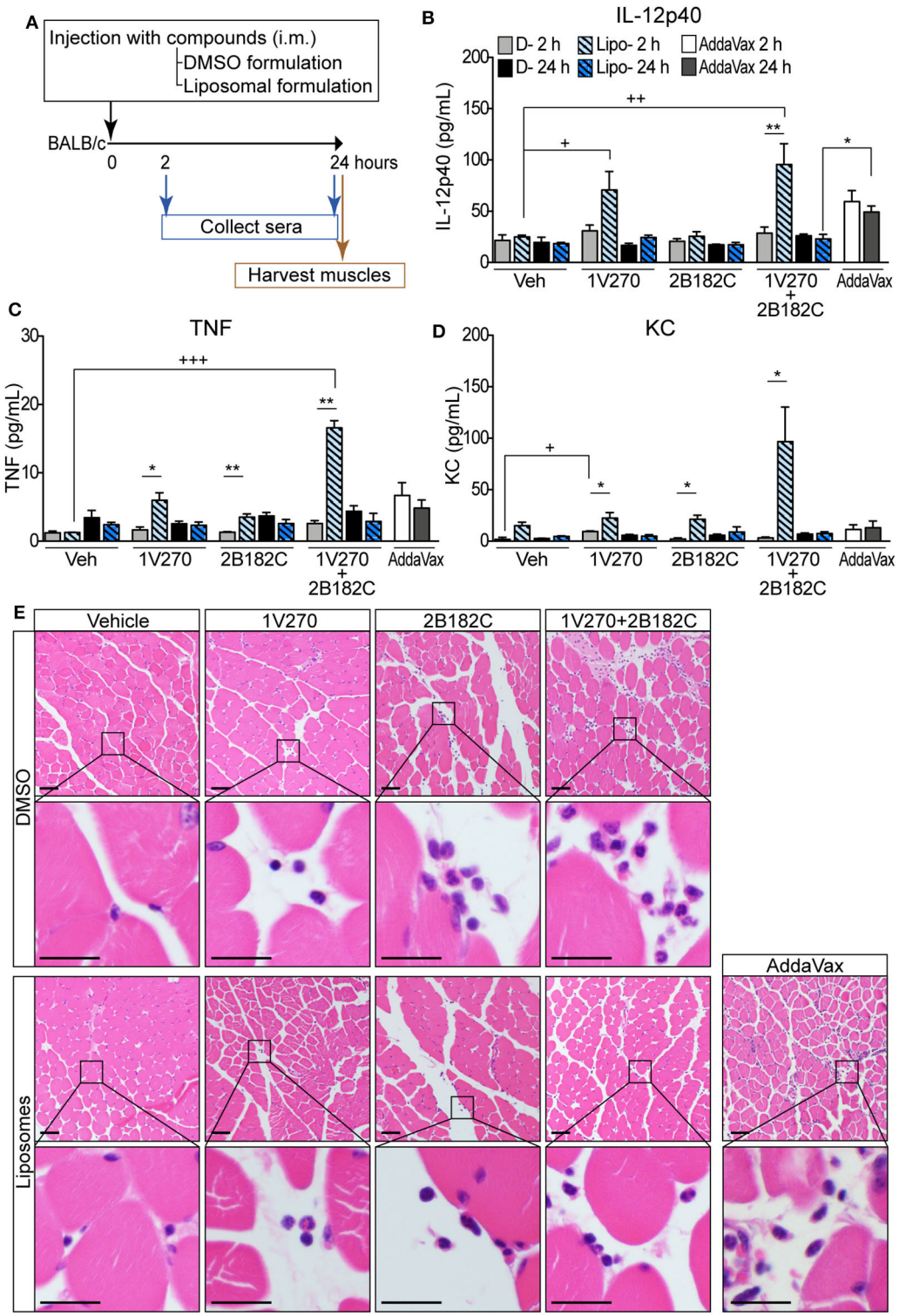

FIGURE 4 | Liposomal formulation enhanced immunostimulatory effects of combination adjuvant with reduced reactogenicity. **(A)** BALB/c mice ($n = 5$/group) were i.m. injected with vehicle, **1V270**, **2B182C**, **1V270+2B182C** with DMSO formulation or liposomal formulation (1 nmol/injection **1V270** and 200 nmol/injection **2B182C** in a volume of 50 μL). AddaVax™ (25 μL/injection) was used as a positive control. Two and 24 h following the injection, sera were collected and examined for **(B)** IL-12p40, **(C)** TNFα, and **(D)** KC levels by Luminex multiplex cytokine assay. Data shown are means ± SEM. $^{*}P < 0.05$, $^{**}P < 0.01$, two-tailed Mann-Whitney *U*-test. $+P < 0.05$, $++P < 0.01$, $+++P < 0.0001$, Kruskal-Wallis with Dunn's *post-hoc* test to compare 4 groups (vehicle, **1V270**, **2B182C**, **1V270+2B182C** in the same formulation). **(E)** Micrographs of H&E stained histological sections of muscles at injected sites (scale bar 50 μm) where squares indicate areas captured at higher magnification in the rows below (scale bar 20 μm).

responses in many vaccines (24–26). Therefore, **1V270** and **2B182C** were co-encapsulated in liposomes by Inimmune Corp (Missoula, MT). These liposomal formulations were prepared by the lipid film rehydration method using DOPC:cholesterol in a molar ratio of 2:1, respectively. In the studies above using DMSO formulations, we determined that the optimal ratio of **1V270**:**2B182C** was 1:200 (1 nmol/injection of **1V270** and 200 nmol/injection of **2B182C** in a volume of 50 μL). To evaluate whether the liposomal formulation affected immunostimulatory potency, we examined the *in vivo* systemic and local effects. BALB/c mice were i.m. injected with **1V270** and **2B182C** in DMSO as a control formulation, or in the liposomal (Lipo-) formulation and bled at 2 and 24 h after administration (**Figure 4A**). Intramuscular injections with Lipo-**1V270**, Lipo-**2B182C**, and Lipo-(**1V270+2B182C**) induced measurable increases of IL-12p40, TNF, and KC levels in serum at 2 h, but these values returned to basal levels by 24 h post injection (**Figures 4B–D**). Histological analyses of muscles at the injected sites indicated that DMSO-**2B182C** and DMSO-(**1V270+2B182C**) augmented immune cell infiltration, whereas Lipo-**2B182C**, and Lipo-(**1V270+2B182C**) induced minimal cell infiltration (**Figure 4E**).

Co-encapsulated Combination Adjuvant Lipo-(1V270+2B182C) Synergistically Enhances Anti-HA and Anti-NA IgG1 and IgG2a Production

We next evaluated the activity of the combination adjuvant of liposomal **1V270+2B182C** *in vivo* using a prime-boost regimen as depicted in **Figure 2E**. Two types of combinations of **1V270** and **2B182C** were assessed; a co-encapsulation with **1V270** and **2B182C** in the same liposomes [Lipo-(**1V270+2B182C**)], and an admixed combination of liposomes with individual compounds [(Lipo-**1V270**)+(Lipo-**2B182C**)]. In the prime-boost model, sera harvested on day 28 were assessed for anti-HA and anti-NA antibodies by ELISA (**Figure 5**). Liposomal **2B182C** (Lipo-**2B182C**) induced higher levels of IgG1, which was consistent with DMSO-**2B182C** (**Figure 5A**). Unlike DMSO-**1V270**, liposomal **1V270** (Lipo-**1V270**) alone did not enhance IgG2a production (**Figure 5B**). When the two compounds were combined in the same liposome [Lipo-(**1V270+2B182C**)], anti-NA IgG1, and anti-HA, and anti-NA IgG2a levels were greater than those for mice immunized with Lipo-**1V270**, Lipo-**2B182C**, or control liposome (Lipo-Veh) (**Figures 5A,B**). Vaccination with the co-encapsulated combination developed antigen specific Th1-biased immune responses (**Figure 5C**), consistent with the trend observed with the DMSO formulation.

Lipo-2B182C and Lipo-(1V270+2B182C) Protect Mice Against Homologous Influenza Viral Challenge

To test whether the augmented antibody responses to HA and NA seen with the co-encapsulated combination adjuvant Lipo-(**1V270+2B182C**) could provide immunologic

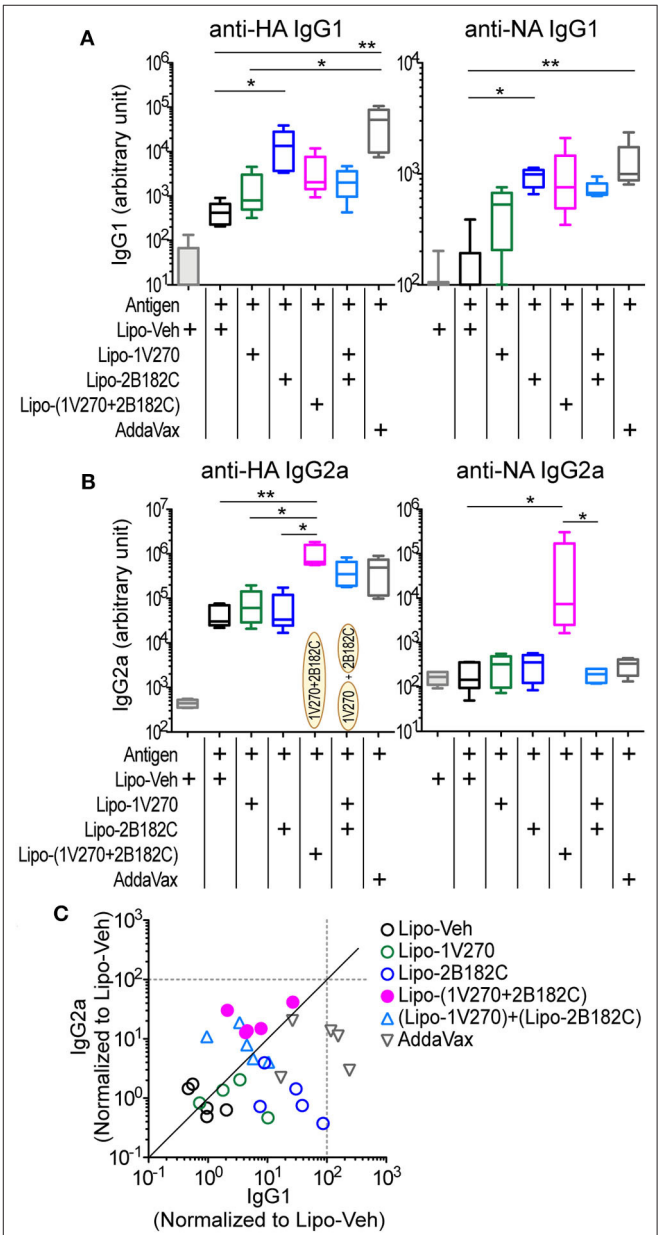

FIGURE 5 | Liposomal **1V270** and **2B182C** synergistically enhanced anti-HA and anti-NA IgG1 and IgG2a production. **(A–C)** BALB/c mice ($n = 5$/group) were i.m. immunized on days 0 and 21 with IIAV (10 μg/injection) with formulated adjuvants as shown in **Figure 2E**. Liposomal **1V270** (Lipo-**1V270**, 1 nmol/injection), liposomal **2B182C** (Lipo-**2B182C**, 200 nmol/injection), and co-encapsulated liposomal with **1V270** and **2B182C** [Lipo-(**1V270+2B182C**)], and admixed combination with **1V270** and **2B182C** [(Lipo-**1V270**)+(Lipo-**2B182C**)] were injected. Blank liposomes (Lipo-Veh) was used as a control. AddaVax™ was used as a positive control. Sera were collected on day 28 and anti-HA or anti-NA IgG1 **(A)** and IgG2a **(B)** were determined by ELISA. Data shown are means ± SEM and representative of two independent experiments with similar results. $^{*}P < 0.05$, $^{**}P < 0.01$, Kruskal-Wallis test with Dunn's *post-hoc* test. **(C)** Anti-HA IgG1 and IgG2a levels induced by all combination treatments (normalized to vehicle) are shown. Each dot indicates an individual mouse. Identity line is shown in solid black.

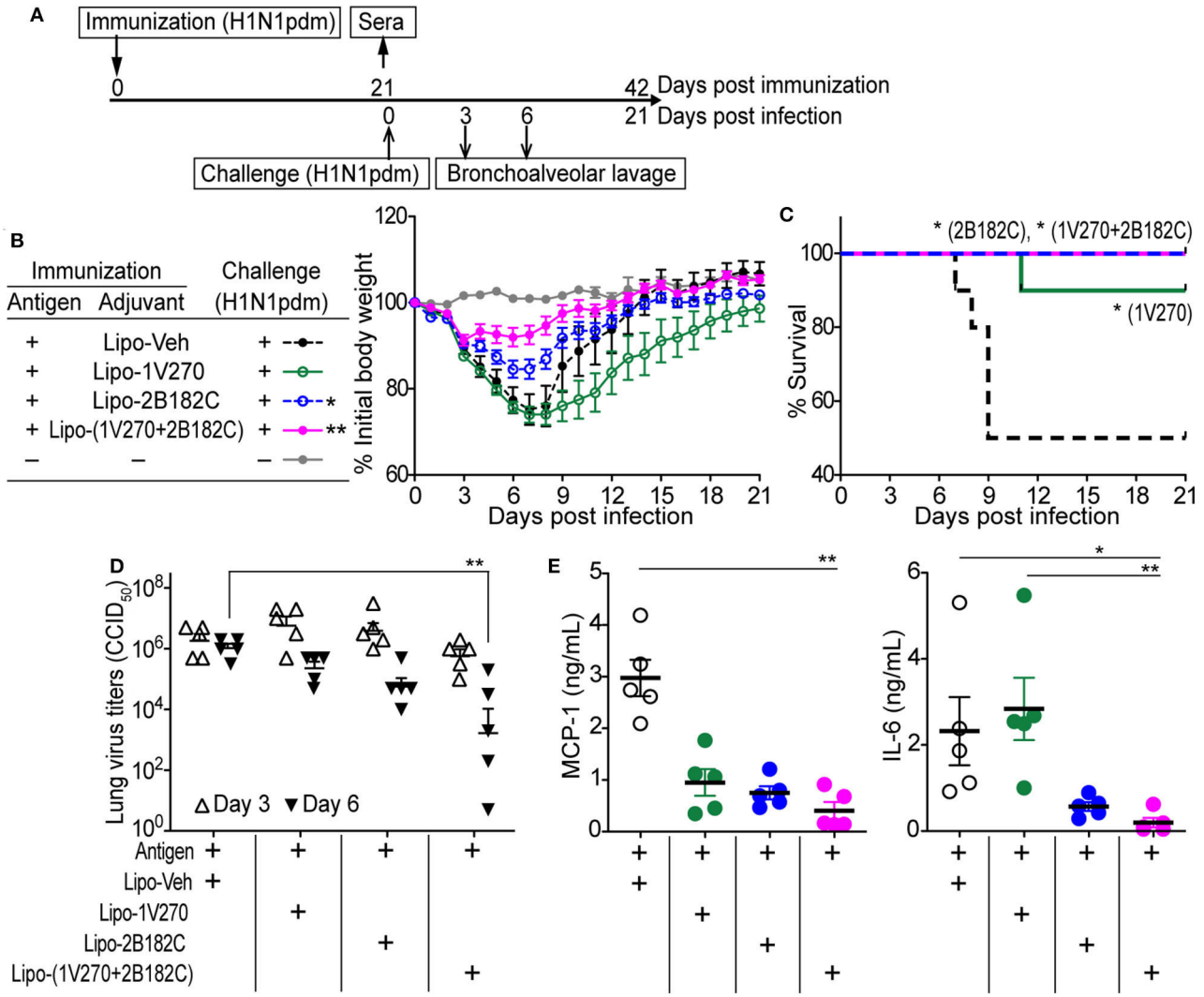

FIGURE 6 | Lipo-**2B182C** and Lipo-**(1V270+2B182C)** protected mice against homologous influenza virus. **(A)** Experimental schedule of homologous influenza virus challenge. BALB/c mice were immunized with IIAV adjuvanted with Lipo-Veh, Lipo-**1V270**, Lipo-**2B182C**, and Lipo-(**1V270+2B182C**) on day 0 and were infected with homologous influenza virus (H1N1)pdm09 on day 21. Body weights and survival were monitored. Three and 6 days after viral challenge, bronchioalveolar lavage samples were collected for lung virus titers and cytokine levels. **(B)** Mean body weight changes after challenge are indicated by % initial body weight (100% = 19.75 ± 0.12 g). *$P < 0.05$, **$P < 0.01$, one-way ANOVA with Dunnett's *post-hoc* test compared to Lipo-Veh. **(C)** Survival rates of mice post challenge with homologous virus (H1N1)pdm09. Kaplan-Meier curves with Log-rank test are shown (*$P < 0.05$). Lung virus titer **(D)** and cytokine levels **(E)** in lung fluids on day 6 were evaluated. *$P < 0.05$, **$P < 0.01$, Kruskal-Wallis with Dunn's *post-hoc* test.

protection against infection, the adjuvant was tested in a mouse adapted influenza lethal challenge model (**Figure 6**). BALB/c mice were i.m. vaccinated on day 0 with IIAV plus Lipo-**1V270**, Lipo-**2B182C**, or Lipo-(**1V270+2B182C**) and were intranasally challenged with homologous influenza virus (H1N1)pdm09 on day 21 post vaccination (**Figure 6A**). Body weights and survival were monitored over the next 21 days (**Figures 6B,C**). Lipo-**2B182C** and Lipo-(**1V270+2B182C**) significantly limited body weight loss after viral challenge (**Figure 6B**). Furthermore, Lipo-**1V270** showed 90% protection, and Lipo-**2B182C** and Lipo-(**1V270+2B182C**) completely protected mice against homologous influenza virus challenge (**Figure 6C**).

To evaluate if survival correlates with viral titers in the lung, bronchoalveolar lavage (BAL) was performed on days 3 and 6. Lipo-(**1V270+2B182C**) effectively reduced virus titers in the lungs on day 6 (**Figure 6D**). Since the levels of cytokine and chemokine in airway epithelial cells (e.g., MCP-1, IL-6, etc) have been correlated with lethal lung injury and pneumonia (27, 28), we evaluated IL-6 and MCP-1 levels in BAL fluids collected on day 6 using the Quansys multiplex ELISA. Use of lipo-(**1V270+2B182C**) as adjuvant significantly reduced MCP-1

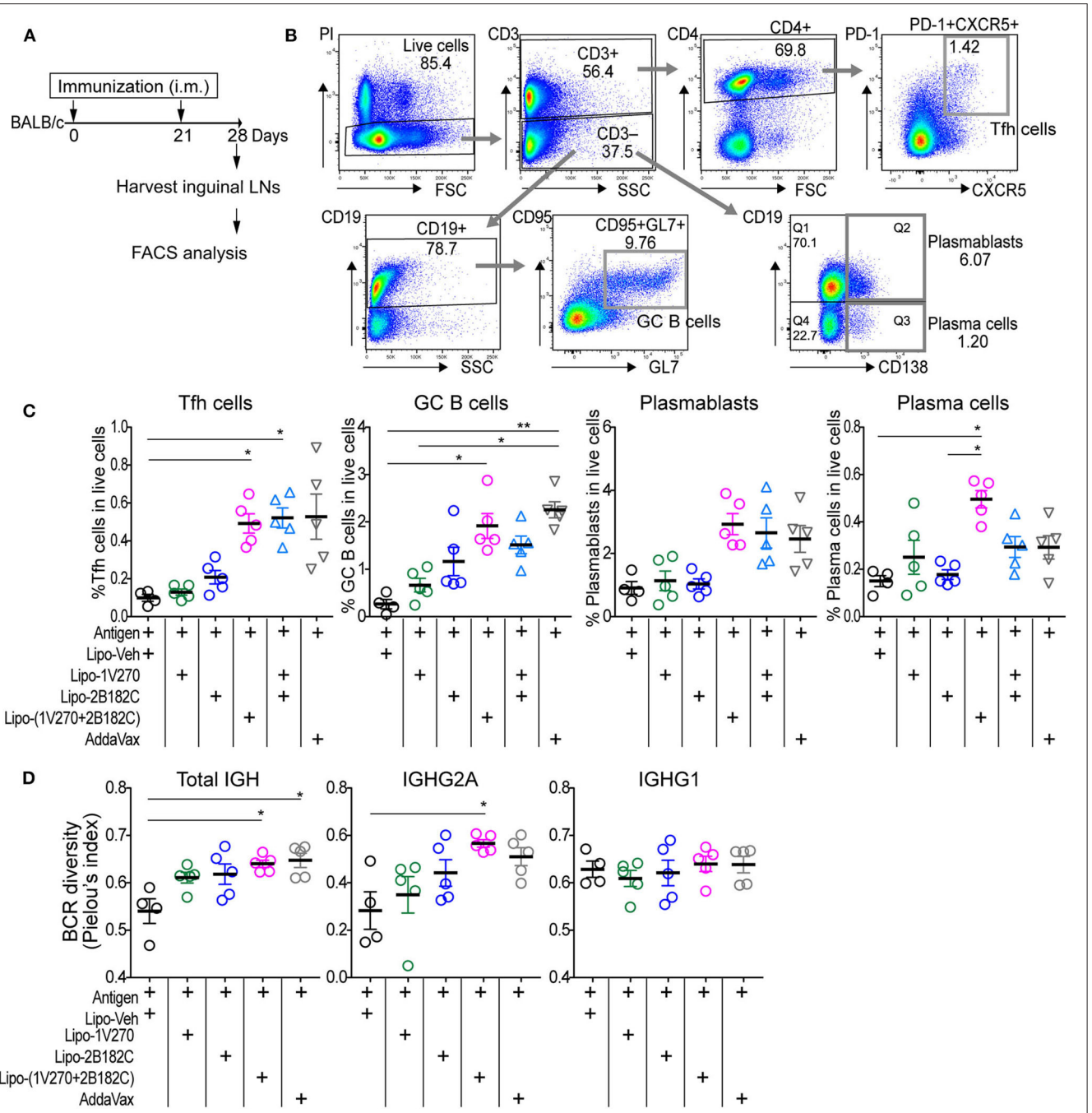

FIGURE 7 | Co-encapsulated combination adjuvant Lipo-**(1V270+2B182C)** increased populations of Tfh cells, antibody secreting cells, and BCR diversity. **(A)** Scheme of immunization strategy. **(B)** BALB/c mice (n = 4–5/group) were vaccinated on days 0 and 21 with IIAV (10 μg/injection) with **1V270** (1 nmol/injection) and/or **2B182C** (200 nmol/injection) in a total volume of 50 μL. Twenty-eight days later, lymphocytes in inguinal lymph nodes were harvested for FACS analysis. Gating strategy for Tfh cells ($CD3^+CD4^+PD\text{-}1^+CXCR5^+$), GC B cells ($CD3^-CD19^+CD95^+GL7^+$), plasmablasts ($CD3^-CD19^+CD138^+$), and plasma cells ($CD3^-CD19^-CD138^+$) are shown. **(C)** %Tfh cells, GC B cells, plasmablasts, and plasma cells of total live cells. Bars indicate means ± SEM. $^*P < 0.05$, $^{**}P < 0.01$, Kruskal-Wallis with Dunn's *post-hoc* test. Data are representative of two independent experiment with similar results. **(D)** BALB/c mice (n = 4–5/groups) were immunized on days 0 and 21 with IIAV (10 μg /injection) with liposomal adjuvants [**1V270** (1 nmol/injection), **2B182C** (200 nmol/injection) and **1V270+2B182C** (1nmo/injection + 200 nmol/injection)] and draining (inguinal) lymph nodes were harvested on day 28 for BCR repertoire analysis. BCR diversity of total IGH, IGHG1, and IGHG2A are shown by Pielou's index. Bars indicate means ± SEM. $^*P < 0.05$, Kruskal-Wallis with Dunn's post-*hoc test*.

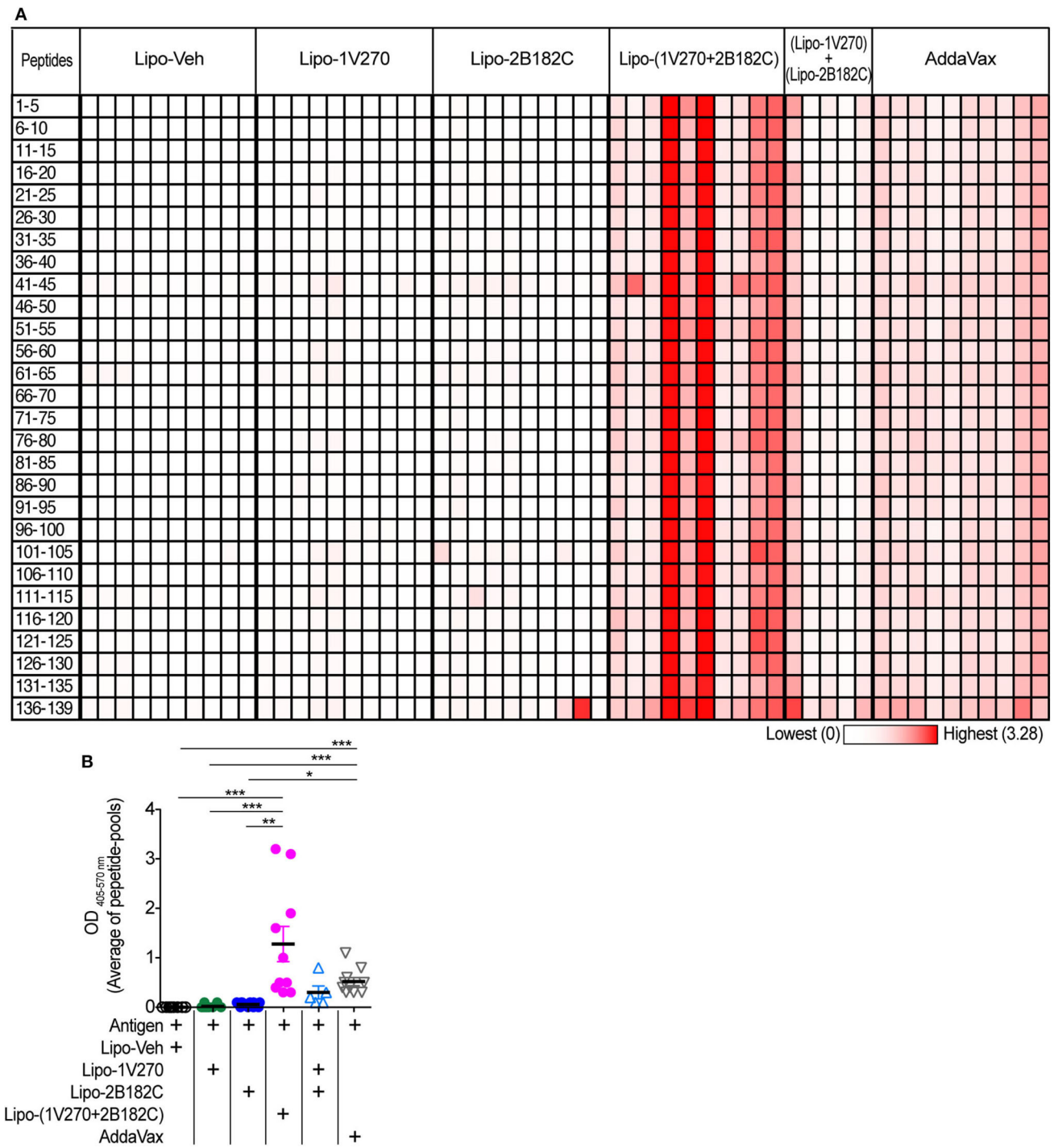

FIGURE 8 | Sera binding profile to A/California/04/2009 (H1N1)pdm09 HA peptide array. **(A,B)** BALB/c mice [$n = 5$ in a group of (Lipo-**1V270**)+(Lipo-**2B182C**), $n = 10$ in other groups)] were immunized with IIAV plus Lipo-Veh, Lipo-**1V270**, Lipo-**2B182C**, Lipo-(**1V270+2B182C**) (co-encapsulated combination), or (Lipo-**1V270**)+(Lipo-**2B182C**) (admixed combination) on days 0 and 21, and were bled on day 28. Peptide arrays of HA of A/California/04/2009 (H1N1)pdm09 were obtained from BEI resources. Pools of 5 peptides per cluster were generated. **(A)** Heatmap of $OD_{405-570nm}$ summarizing antibody binding patterns. Each row and column indicate each peptide pool and mouse, respectively. **(B)** The average absorbance of antibody binding for the 28 peptide pools for individual mice are shown. $^{*}P < 0.05$, $^{**}P < 0.01$, $^{***}P < 0.0001$, Kruskal-Wallis with Dunn's *post-hoc* test.

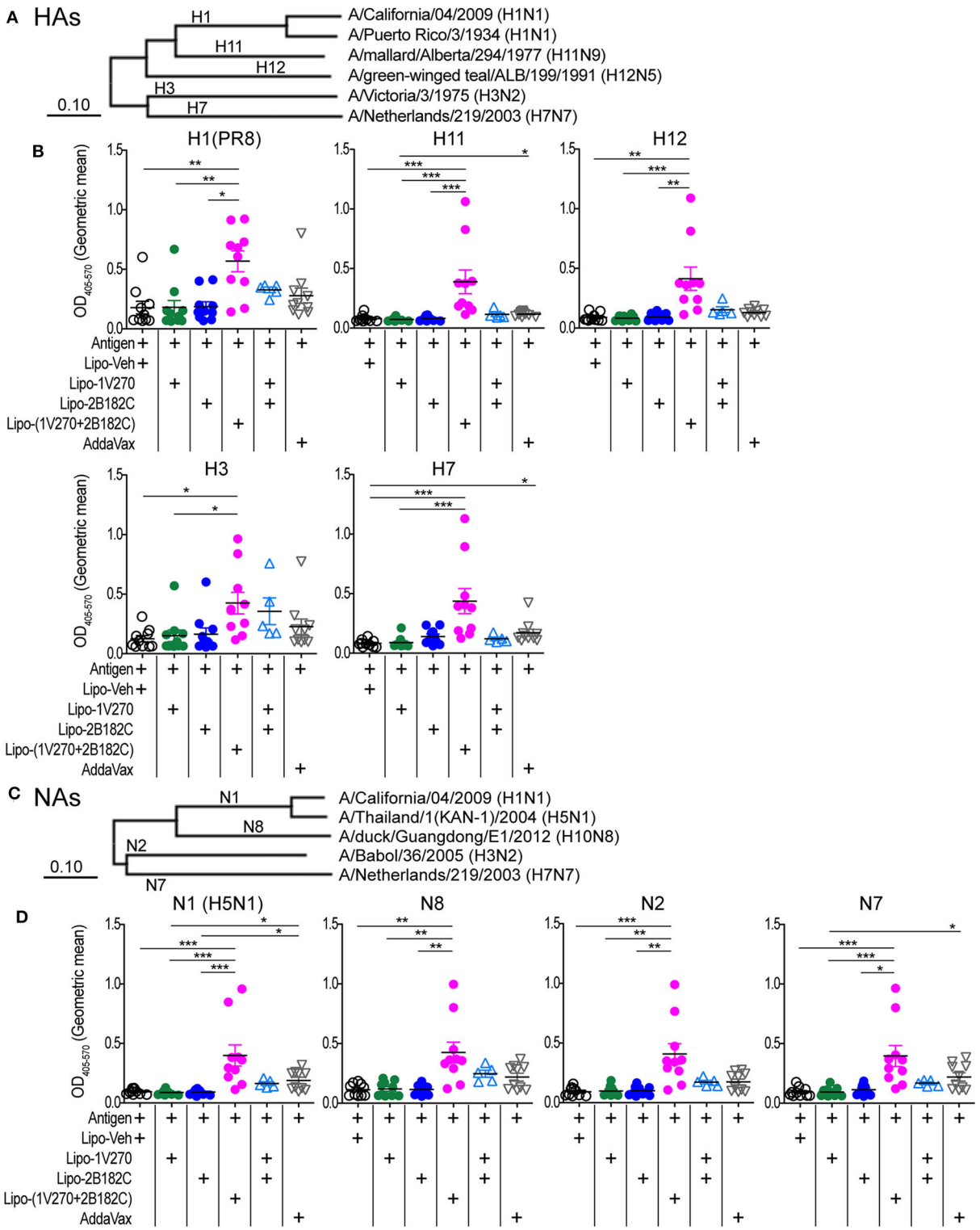

FIGURE 9 | Lipo-(**1V270+2B182C**) induced cross reactive antibodies. **(A–D)** Phylogenetically distinct HAs and NAs of influenza A viruses were tested. **(A,C)** Amino acid sequences of proteins used in ELISA were aligned by the MUSCLE algorithm using the Influenza Research Database. Phylogenetic trees were constructed by the neighbor-joining method using MEGAX software. **(B,D)** BALB/c (n = 5–10/group) mice were immunized with IIAV [A/California/04/2009 (H1N1)pdm09] plus Lipo-Veh, Lipo-**1V270**, Lipo-**2B182C**, Lipo-(**1V270+2B182C**), or (Lipo-**1V270**)+(Lipo-**2B182C**) on days 0 and 21 and were bled on day 28. Sera were serially diluted (1:100 to 1:409600) and assessed for total IgG levels against **(B)** HA of PR8 H1N1, H11N9, H12N5, H3N2, and H7N7 and **(D)** NA of H5N1, H10N8, H3N2, and H7N7 by ELISA. Geometric means of total IgG titer curves of individual mice are shown. Total IgG titer curves of HA and NA proteins are shown in **Supplementary Figure 2**. *$P < 0.05$, **$P < 0.01$, ***$P < 0.001$, Kruskal-Wallis with Dunn's *post-hoc* test.

and IL-6 production in the airways of infected mice (**Figure 6E**), suggesting lipo-(**1V270+2B182C**) adjuvanted vaccine prevented lung inflammation due to the reduced viral titers.

Lipo-(1V270+2B182C) Promotes B Cell Responses in Draining Lymph Nodes

The liposomal combined adjuvant increased the levels of anti-HA and anti-NA antibodies (**Figure 5**) and protected mice from a lethal challenge by influenza (**Figure 6**). We further characterized the mechanisms contributing to these beneficial responses. Formation of germinal centers (GC) is essential for long lasting humoral immune responses (29, 30). Naïve B cells differentiate into memory B cells and antibody-secreting plasma cells in GCs in draining lymph nodes. Within the GCs, T follicular helper (Tfh) cells are specialized helper cells that support B cell functions (31, 32). Thus, we investigated whether the liposomal combined adjuvant had an effect on the populations of Tfh cells, GC B cells, plasmablasts, and plasma cells in draining lymph nodes. In the prime-boost immunization protocol described above, lymphocytes in the draining inguinal lymph nodes were harvested on day 28 (1 week after the boost) for analysis by flow cytometry (**Figures 7A,B**). The percentage of Tfh cells ($CD3^+$ $CD4^+$ $PD\text{-}1^+$ $CXCR5^+$) was significantly increased in mice vaccinated with Lipo-(**1V270+2B182C**) compared to Lipo-Veh or Lipo-**1V270** (**Figure 7C**). Additionally, Lipo-(**1V270+2B182C**) injection significantly increased the populations of GC B cells ($CD3^-$ $CD19^+$ $CD95^+$ $GL7^+$), plasmablasts ($CD3^-$ $CD19^+$ $CD138^+$), and plasma cells ($CD3^-$ $CD19^+$ $CD138^-$) in the draining lymph nodes compared to Lipo-Veh injected mice (**Figure 7C**).

B Cell Receptor Diversities Are Increased After Immunization With 1V270 Plus 2B182C

To examine whether the cellular expansion in the lymph nodes after Lipo-(**1V270+2B182C**) injection was associated with a change in the diversity of the B cell receptors (BCR), we performed next generation sequencing analysis for immunoglobulin heavy chain gene (IGH). Mice were immunized in the prime-boost protocol and lymphocytes in the draining lymph nodes were collected on day 28 (**Figure 7A**). BCR sequencing analyses showed that the Shannon diversity of total IGH and IGHG2A normalized to total number of clonotypes (Pielou's index) was significantly increased by Lipo-(**1V270+2B182C**), compared to Lipo-Veh (**Figure 7D**).

Liposomal Combined Adjuvant, Lipo-(1V270+2B182C), Extends Cross Reactivity of Sera Specific to HA and NA

Currently approved seasonal influenza vaccines often do not provide broad humoral protection, limiting their effectiveness. Adjuvants that expand the epitopes recognized by the neutralizing antibody response, including less variable regions like the HA stalk protein would provide greater protection against antigenic drift (33–36). Hence we tested the sera from mice by ELISA against pools of peptides derived from the sequence of HA from (H1N1)pdm09. Vaccination with IIAV plus Lipo-(**1V270+2B182C**) promoted broad reactions to peptides of HA and in aggregate the serologic response was greater than that of the other vaccine groups (**Figures 8A,B**).

Given the results above, we further evaluated whether Lipo-(**1V270+2B182C**) could provide broader protection against various subtypes of HA and NA. Cross-reactivity to recombinant HA and NA proteins from antigenically distinct phylogenetic groups were evaluated by ELISA (**Figures 9A–D**, **Supplementary Figures 2A–D**). Total IgG levels against the HAs of H1N1, H11N9, H12N5, H3N2, and H7N7 viral subtypes were significantly enhanced by Lipo-(**1V270+2B182C**) compared to liposomes with vehicle (Lipo-Veh) and Lipo-**1V270** (**Figure 9B**, **Supplementary Figure 2B**). In addition, serum IgG binding to recombinant NAs of H5N1, H10N8, H3N2, and H7N7 viral subtypes were also increased in mice immunized with Lipo-(**1V270+2B182C**) and the inactivated H1N1 subtype (**Figure 9D**, **Supplementary Figure 2D**).

DISCUSSION

The overall average effectiveness of seasonal influenza vaccines in the past 10 years is ∼40% and the highest protection rate reported was 60% in 2010–2011. Furthermore, the effectiveness for high risk groups, such as children (6 months to 18 years old) and elderly subjects, remains low (39 and 25%, respectively) (37–39). Therefore, the development of an adjuvanted influenza vaccine that can provide rapid, broad and sustained protective immunity is still needed. Toll-like receptor ligands (TLRL) have been widely investigated as potential vaccine adjuvants (40) and MPLA, a semi-synthetic TLR4 ligand, has been approved for clinical use (41, 42). However, the use of more than one TLR ligand in combination has been demonstrated to improve the potency of an adjuvant response. Here we demonstrated that further optimization of a vaccine adjuvant with fully synthetic TLR agonists and a co-encapsulated liposomal formulation produced a vaccine that effectively protected mice against lethal homologous influenza virus challenge and reduced lung viral titers and cytokine levels.

The small molecule TLR agonists used in our studies were identified after extensive evaluation of structure-activity relationship (SAR) studies generated for both TLR4 and TLR7 agonists (18, 19, 22). We previously developed a TLR4 agonist, **1Z105**, as a vaccine adjuvant that induced rapid and broad immunity in combination with a TLR7 agonist, **1V270** (20, 21). In this study, we identified a highly potent derivative of this TLR4 agonist, **2B182C**, that strongly enhanced NF-κB activation and cytokine production in both mouse and human primary cells. Both **1V270** and **2B182C** are novel synthetic agonists that are easy to prepare and manufacture in 7-step and 9-step processes, respectively. The TLR4 agonist, **2B182C**, in particular, represents the lead compound identified from a 3rd-generation SAR effort to enhance the potency and broaden the species specificity of the TLR4 activity. The novel finding that substitution at the C8 position of the pyrimidoindole scaffold with an aryl or heteroaryl

group provided potent human TLR4 agonistic activity was a critical observation. A major advantage of this TLR4 agonist over other established agonists, such as MPLA, is that it is fully synthetic, easy to prepare and to scale up for clinical use.

In our study the formulation of the combination of synthetic ligands also improved vaccine efficacy. A prime-boost vaccination protocol of IIAV adjuvanted with **2B182C** induced anti-HA and anti-NA IgG1 production and enhanced antigen specific IgG2a production induced by the TLR7 agonist **1V270**. Notably, the co-encapsulation of **1V270** and **2B182C** in a liposome [Lipo-(**1V270+2B182C**)] induced a greater response than that of liposomes with each compound mixed together. In addition, the Lipo-(**1V270+2B182C**) promoted both Th1 and Th2 associated antibody responses against IIAV. The co-encapsulated adjuvant Lipo-(**1V270+2B182C**) also stimulated a germinal center reaction similar to AddaVax, that was associated with increased populations of Tfh cells, GC B cells, plasmablasts, and plasma cells. Therefore, the liposomal combined adjuvant likely enhanced clonal expansion of B cells in the GC.

Antigenic drift of the surface proteins HA and NA allows influenza viruses to escape from the immunosurveillance elicited by annual vaccination. One of the strategies for providing broader protection against viral variation is to create a vaccine that induces humoral responses to relatively conserved stem HA epitopes in the stalk domain (33–36, 43). In this study, immunized IIAV adjuvanted with the co-encapsulated combination Lipo-(**1V270+2B182C**) elevated total IgG levels against multiple clusters of peptides of HA in both head and stalk domains. In contrast, Lipo-**1V270**, Lipo-**2B182C** increased antibody responses to only a few clusters of peptides in each head and stem region. This epitope spreading phenomenon induced by Lipo-(**1V270+B182C**) was consistent with the trend that Lipo-(**1V270+2B182C**) increased the diversity of BCR of B cells in the draining lymph nodes. Since broadly reactive antibodies recognizing HA and NA from multiple viral strains are associated with protection against various influenza virus infection (44–46), this could be one of the critical criteria for a successful vaccine. Therefore, the reactivities of the sera against HA from antigenically distinct phylogenetic groups (H11, H12, H3, and H7) were tested by ELISA. The sera in mice immunized with IIAV (H1N1)pdm09 adjuvanted with the co-encapsulated Lipo-(**1V270+2B182C**) were cross reactive to all the HA subtypes that we tested, suggesting that our novel co-encapsulated adjuvant may effectively support cross-strain protection against lethal infection with this virus.

Since NA is responsible for viral entry and releasing viral particles into cells, inhibition of the NA enzyme has been a primary treatment of influenza [e.g., including oseltamivir (Tamiflu)] (47, 48). Antibodies that bind to NA were suggested to provide durable and broad protection against divergent influenza strains (49–52). It should also be noted that **2B182C** (alone and in combination) enhanced anti-NA IgG2a production, whereas other adjuvants including **1V270** alone and AddaVax did not. Our data demonstrated that the co-encapsulated adjuvant with **1V270** and **2B182C**, Lipo-(**1V270+2B182C**), induced cross reactivity with NAs of other virus strains. A B cell response that targets the major surface glycoprotein NA responses in conjunction with an anti-HA response would broaden host protection (47, 49).

Adjuvants for vaccines often have safety concerns related to solubility and off-target effects of the compounds that may cause reactogenicity and systemic adverse effects (17). Compounds that have strong indications of toxicity or side effects in preclinical studies do not proceed into clinical trials. Thus, a balance of efficacy and reduced reactogenicity of compounds is a key issue in adjuvant development. Liposomes containing DOPC and cholesterol were chosen as both components are biocompatible and have low background immunogenicity. Additionally, this lipid system has been demonstrated to efficiently incorporate various lipidated TLR4 agonists, including MPLA (53), and **1V270**, a lipidated TLR7 agonist (20). Lipo-(**1V270+2B182C**) induced comparable levels of a GC reaction similar to that of AddaVax. There was only a transient increase in IL12, TNF and KC 2 h after injection with Lipo-(**1V270+2B182C**) which resolved back to baseline by 24 h.

In summary, we identified a novel small molecule TLR4 ligand, **2B182C**, which was highly active in both mouse and human APCs. A stable liposomal formulation in combination with a TLR7 ligand (**1V270**) was developed that enhanced anti-HA and anti-NA IgG1 and IgG2a responses after i.m. immunization. The co-encapsulated liposomal formulation of **1V270+2B182C** as an adjuvant for vaccination with IIAV (H1N1)pdm09 protected mice from a homologous viral challenge, reduced lung viral titers and lowered cytokine levels compared to mice that received an unadjuvanted vaccine. Serologic examination showed that the combination adjuvant induced antibodies against a broader spectrum of epitopes encompassing HA head and stalk domains, and with cross-reactivity against different subtypes of HA and NA. These data and the lower reactogenicity suggest that the novel liposomal adjuvant Lipo-(**1V270+2B182C**) might be attractive for development of a universal influenza virus vaccine.

METHODS

Mice

Female 6–8 week-old BALB/c mice were purchased from Jackson laboratory (Bar Harbor, MA). The mouse experiments using IIAV as an antigen were performed at University of California (UC) San Diego Animal Facility. The influenza challenge studies with live virus were performed by Institute for Antiviral Research, Utah State University using female 6 week-old BALB/c mice (Charles River Laboratories, Wilmington, MA). All animal experiments received prior approval by the Institutional Animal Care and Use Committee (IACUC) for UC San Diego or Utah State University.

Cells and Reagents

TLR4/NF-κB reporter cell lines HEK-Blue™ humanTLR4 and HEK-Blue™ murineTLR4 cells were purchased from InvivoGen (#hkb-htlr4, # hkb-mtlr4, San Diego, CA). Human PBMC were isolated using Ficoll-Paque Plus (GE Healthcare) from buffy coats. Mouse primary BMDCs were prepared from bone marrow cells harvested from femurs of C57BL/6 mice as

previously described (54, 55). Human PBMC and mBMDCs were treated with indicated compounds in RPMI supplemented with 10% FBS (Omega, Tarzana, CA) and penicillin/streptomycin (100 unit/mL/100 μg/mL, Thermo Fisher Scientific, Waltham, MA). AddaVax™ were purchased from InvivoGen (vac-adx-10, San Diego, CA). Inactivated Influenza A virus (IIAV) A/California/04/2009 (H1N1)pdm09 was obtained from BEI resources (# NR-49450, Manassas, VA). TLR7 agonist **1V270** (18), TLR4 agonists **1Z105** (19), and its derivatives including **2B182C** were synthesized in our laboratory. Detailed chemistry is shown in **Supplementary Methods**.

Preparation of Liposomal Formulation of 1V270 and 2B182C

1V270 and **2B182C** were submitted to Inimmune Corp. and liposomal formulation of **1V270** (20 μM), **2B182C** (4 mM), and **1V270+2B182C** (20 μM + 4 mM) was prepared by Inimune corp (Missoula, MT). 1,2-dioleoyl-sn-glycero-3-phosphocholine (DOPC) was purchased from Avanti Polar Lipids (Alabaster, AL), cholesterol was purchased from Sigma (St. Louis, MO). For **2B182C** containing liposomes the adjuvant target concentration was 4 mM and for **1V270** the target concentration was 20 μM. Concentration of each adjuvant was determined by RP-HPLC using a gradient method. The DOPC:cholesterol liposomes were produced with a mass ratio of 60:15 mg/mL, respectively. Liposomes were prepared using the thin-film rehydration method (56). Briefly, lipids were individually dissolved in 9:1 chloroform:methanol to make stocks, and lipid stocks were added to a round bottom flask and mixed. Solvent was evaporated using a Rotavap set to 150 rpm in a water bath at 45–50°C, and residual solvent was removed by storing overnight under reduced pressure at room temperature. Thin films were rehydrated with 10 mM sodium phosphate at pH 7.1. Formulations were sonicated in an Elma 9331 bath sonicator at temperatures below 50°C (above the transition temperature of all compounds) until particle size was reduced below 0.22 μm or the samples appeared opalescent and particle size did not change upon further sonication. Since the presence of endotoxin would cause unwanted TLR4 agonism, all liposomes were made in a BioChemGard biosafety cabinet using aseptic technique, endotoxin-free consumables, and depyrogenated glassware.

TLR4/NF-κB Reporter Cell Assay

TLR4/NF-κB activation was assessed using HEK-Blue™ hTLR4 and HEK-Blue™ mTLR4 (InvivoGen). The cells were treated with **1Z105** and **2B182C** (2-fold serial dilutions starting from 10 μM) for 20 h. NF-κB inducible secreted embryonic alkaline phosphatase (SEAP) protein in the culture supernatant was measured according to manufacturer's protocol. To evaluate cell viability, 0.5 mg/mL 3-[4,5-dimethylthiazol-2-yl]-2,5-dipheyl tetrazolium bromide (MTT, Thermo Fisher Scientific) solution was added to each well and incubated at 37°C. Six hours later, formazan crystals were lysed with lysis buffer (15% SDS and 0.12% 12 N HCl) and the absorbance was measured at 570 nm using 650 nm as a reference with a plate reader (Tecan, Switzerland).

Cytokine Assay Using Human and Mouse Primary Cells

Human PBMC (10^6 cells/mL) were treated with 5 μM **1Z105** and **2B182C** overnight and the culture supernatant assessed for human IL-8 by ELISA. Mouse BMDCs (10^6 cells/mL) were incubated with serially diluted compounds (2-fold dilution from 5 μM). 0.5% DMSO was used as vehicle. IL-12 and IL-6 levels in the supernatant were measured by ELISA. ELISA was performed as previously described (57). Reagents and dilution factors of antibodies are described in **Supplementary Table 1**.

Prime-Boost Vaccination Model

BALB/c mice were i.m. immunized with IIAV (H1N1)pdm09 (10 μg/injection) plus indicated adjuvants in gastrocnemius of hind legs (both legs) on days 0 and 21. IIAV and adjuvants were mixed in a total volume of 50 μL for injection. Details for concentrations of adjuvants and the number of mice in each treatment group are described in each figure legend. Sera were collected on day 28 (1 week after the boost) and evaluated for antigen-specific antibodies. For studies with DMSO formulation, 10% DMSO was used as vehicle. In the experiments using the liposomal-formulated adjuvant, blank liposomes, 1,2-dioleoyl-sn-glycero-3-phosphocholine and cholesterol (DOPC/Chol, control liposomes), was used as vehicle. AddaVax™, which is an oil-in-water adjuvant MF59 (11, 12, 58), was used as a positive control (25 μL/injection).

Flow Cytometry Analysis

Detailed information for reagents used in flow cytometry analysis are shown in **Supplementary Table 2**. For co-stimulatory molecules on mBMDCs, mBMDCs (10^6 cells/mL) were incubated with 1 μM **1Z105** and **2B182C** for 20 h. 0.5% DMSO was uses as vehicle. After removing the supernatant, cells were washed with the stain buffer (BD Biosciences, San Diego, CA) and incubated with anti-mouse CD16/32 antibody for blocking FcR. Cells were then stained with an antibody cocktail with anti-CD40 and anti-CD86 antibodies for 20–30 min at 4°C. For analysis of lymphocytes harvested from draining lymph nodes, two antibody cocktails were prepared; (1) anti-CD3, anti-CD4, anti-PD-1, and anti-CXCR5 antibodies for Tfh cell analysis, (2) anti-CD3, anti-CD19, anti-CD95, anti-CD138, and anti-GL7 antibodies for B cell analysis. After blocking with anti-CD16/CD32 antibody, 2×10^6 cells were stained in each antibody cocktail. For Tfh cell analysis, after staining with primary antibodies, cells were washed with PBS, and incubated with streptavidin-PE. Cells were then washed and stained with propidium iodide to determine live/dead cells. Data were acquired using MACSQuant Analyzer 10 (Miltenyi Biotec, Germany) and analyzed using FlowJo (version 10.6.1, Becton Dickinson, Ashland, OR).

ELISA for Serum IgG Levels

Reagents used in the ELISA are listed in Supplementary Table 3. ELISA for anti-HA IgG1, anti-NA IgG1, anti-HA IgG2a, and anti-NA IgG2a antibodies (**Figures 2–5**) were performed as previously described (18) using recombinant HA and NA

proteins of A/California/04/2009 (H1N1)pdm09. In brief, plates were coated with HA and NA proteins, blocked, then incubated with sera serially diluted in blocking buffer. An initial dilution of sera was 1:100, followed by 4-fold serial dilutions. After incubation with sera, plates were washed and incubated with detecting antibody, followed by wash and incubation with p-nitrophenyl phosphate substrate. Plates were read at 405 nm on a plate reader (Tecan, Switzerland). For the peptide binding assay, a peptide array of HA of (H1N1)pdm09 was obtained from BEI resources (NR-15433). Sera diluted in 1–200 in blocking buffer were analyzed by peptide ELISA as previously described (59). For evaluation of cross-reactivity of antibody, half-area 96-well-plates were coated with each protein (HAs of H1N1, H11N9, H12N5, H3N2, and H7N7, and NAs of H5N1, H10N8, H3N2, and H7N7), overnight at 4°C. Sera were diluted 1:100 in blocking buffer followed by 1:4 serial dilutions (dilution factors were from 100 to 40,9600). Plates were processed as described above. Phylogenetic relationships of HAs and NAs used in this assay is shown in **Figure 9**, **Supplementary Figure 2**. Amino acid sequences of the proteins were aligned by MUSCLE (Multiple Sequence Comparison by Log-Expectation) algorithm (60) using Influenza Research Database (https://www.fludb.org/brc/home.spg?decorator=influenza). Phylogenetic tree was constructed by Neighbor-joining method (61) using Molecular Evolutionary Genetics Analysis software MEGAX (https://www.megasoftware.net/) (62).

Next-Generation Sequencing for B Cell Receptor Repertoire

The prime-boost model described above was used. Briefly, BALB/c mice were immunized with IIAV (H1N1)pdm09 plus the liposomal formulation of **1V270** and **2B182C** on days 0 and 21. Mice were sacrificed on day 28 and lymphocytes in the draining lymph nodes in the injected sides (inguinal lymph nodes) were collected. The lymphocytes preserved in RNAprotect® Cell Reagent (#76526, QIAGEN) were submitted to Repertoire Genesis Inc. (Osaka, Japan). For BCR analysis, total RNA was extracted from lymphocytes using RNeasy Mini Kit (Qiagen, Hilden, Germany) and the quality of RNA was confirmed by Agilent 2200 TapeStation System (Agilent, Santa Clara, CA). Next-generation sequencing (NGS) was performed with unbiased BCR repertoire analysis technology (Repertoire Genesis Inc., Osaka, Japan) according to the method with some modifications described in previous reports (63, 64). In brief, total RNA was converted to complementary DNA (cDNA) with Superscript III reverse transcriptase (Invitrogen, Carlsbad, CA). Then, double strand (ds)-cDNA was synthesized and an P20EA/P10EA adaptor was ligated to the 5′ end of the ds-cDNA and then cut with *Sph*I restriction enzyme. PCR was performed with KAPA HiFi DNA Polymerase (Kapa Biosystems, Woburn, MA) using P20EA and IgG constant region-specific primer mCG1 (GACAGGGMTCCAKAG TTCC). The second PCR was performed with P20EA and mCG2 (ACYGRCTCAGGGAARTAVCC) using the same PCR conditions. After Tag PCR amplification with mCG-ST1-R (TCGTCGGCAGCGTCAGATGTGTATAAGAGACAGCC YTTGACMAGGCAYCC) and P22EA-ST1-R, index (barcode) sequences were added by amplification with Nextera XT index kit v2 setA (Illumina, San Diego, CA). Sequencing was done with the Illumina Miseq paired-end platform (2 × 300 bp). Data processing, assignment, and data aggregation were automatically performed using repertoire analysis software originally developed by Repertoire Genesis, Inc. Normalized Shannon index (Pielou's index) (65, 66) was calculated based on the number of read of each unique sequence read (abundance data) with vegan 2.5-6 package of R version 3.5.3.

Evaluation for Protection From Lethal Influenza Virus Challenge

BALB/c mice were i.m. vaccinated with formulated **1V270** and **2B182C** with IIAV (H1N1)pdm09 (3 μg/injection) on day 0 and intranasally challenged with homologous influenza A virus, (H1N1)pdm09 on day 21. Body weight and survival of mice were monitored. The immunization dose of IIAV of 3 μg/injection was determined to be protective for 30–50% of mouse from the challenge with homologous virus was previously determined. For influenza virus challenge, groups of mice were anesthetized by intraperitoneal injection of ketamine/xylazine (50 mg/kg//5 mg/kg) prior to intranasal challenge with 1×10^5 ($3 \times LD_{50}$) cell culture infectious doses ($CCID_{50}$) of [(H1N1)pdm09] virus in a 90-μL suspension.

Virus

Influenza virus (H1N1)pdm09, strain designation 175190 for challenge study, was received from Dr. Elena Govorkova (Department of Infectious Diseases, St. Jude Children's Research Hospital, Memphis TN). The virus was adapted to replication in the lungs of BALB/c mice by 9 sequential passages in mice. Virus was plaque purified in Madin-Darby Canine Kidney (MDCK) cells and a virus stock was prepared by growth in embryonated chicken eggs and then MDCK cells.

Determination of Lung Virus Titers and Lung Inflammation

Six days after virus challenge, the bronchioalveolar lavage (BAL) procedure was performed immediately after blood collection and was completed within 5–10 min postmortem. A volume of 0.75 mL of PBS was slowly delivered into the lung through the tracheal tube. Immediately after delivery, the fluid was slowly withdrawn by gentle suction and the samples were stored at −80°C. The procedure was repeated a total of three times and lavage fluids from each mouse were pooled. To determine lung virus titers, BAL samples were centrifuged at 2,000 g for 5 min. Varying 10-fold dilutions of BAL supernatants were assayed in triplicate for infectious virus in MDCK cells, with virus titers calculated as described previously (67). For determination of lung cytokine levels, a sample (200 μL) from each lung lavage was tested for MCP-1 and IL-6 using a chemiluminescent multiplex ELISA-based assay according to

the manufacturer's instructions (Quansys Biosciences Q-Plex™ Array, Logan, UT).

Statistical Analyses

Data obtained *in vivo* studies are presented as means with standard error of mean (SEM) and *in vitro* data are shown as means with standard deviation (SD). For *in vitro* data, one-way ANOVA with Tukey's *post-hoc* test was used for multiple comparison. For continuous/ordinal outcomes (antigen specific antibodies, immune cell populations, BCR diversities, lung virus titers, and lung cytokine levels), Kruskal-Wallis tests with Dunn's *post-hoc* test were applied. To compare two groups in mouse experiments, a two-tailed Mann-Whitney test was used. For body weight, last-value-carried-forward approach was used to impute missing values after a mouse was sacrificed, and the average weight over time was used as an outcome for comparison. A log rank test was used to test for a significant difference between Kaplan-Meier survival curves. Prism 5 software (GraphPad Software, San Diego, CA) was used. $P < 0.05$ was considered statistically significant.

DATA AVAILABILITY STATEMENT

The datasets presented in this study can be found in online repositories. The names of the repository/repositories and accession number(s) can be found below: https://www.ebi.ac.uk/arrayexpress/, E-MTAB-8870.

ETHICS STATEMENT

The animal study was reviewed and approved by University of California San Diego, Institutional Animal Care and Use Committee.

AUTHOR CONTRIBUTIONS

FS-K, DC, MCo, and TH designed research, interpreted data and drafted the manuscript. FS-K, SY, FL, JS, and TM conducted experiments. DB and RS formulated compounds in liposomes. TM performed BCR analyses. FS-K, KM, and MP performed statistical analyses. NS, HC, MCh, and PC performed SAR studies including design and syntheses of compounds. All authors contributed to discussions and had opportunity to review and revise the manuscript.

FUNDING

This study was supported by the National Institute of Health/National Institute of Allergy and Infectious Diseases under contracts HHSN272201400051C, 75N93019C00042, and HHSN272202800048C (Subcontract No. PG19-61078-01).

SUPPLEMENTARY MATERIAL

The Supplementary Material for this article can be found online at: https://www.frontiersin.org/articles/10.3389/fimmu.2020.01207/full#supplementary-material

REFERENCES

1. Krammer F. The human antibody response to influenza A virus infection and vaccination. *Nat Rev Immunol.* (2019) 19:383–97. doi: 10.1038/s41577-019-0143-6
2. Krammer F, Smith GJD, Fouchier RAM, Peiris M, Kedzierska K, Doherty PC, et al. Influenza. *Nat Rev Dis Primers.* (2018) 4:3. doi: 10.1038/s41572-018-0002-y
3. Tregoning JS, Russell RF, Kinnear E. Adjuvanted influenza vaccines. *Hum Vaccin Immunother.* (2018) 14:550–64. doi: 10.1080/21645515.2017.1415684
4. Nachbagauer R, Palese P. Is a universal influenza virus vaccine possible? *Annu Rev Med.* (2020) 71:315–27. doi: 10.1146/annurev-med-120617-041310
5. Reed SG, Bertholet S, Coler RN, Friede M. New horizons in adjuvants for vaccine development. *Trends Immunol.* (2009) 30:23–32. doi: 10.1016/j.it.2008.09.006
6. World Health Organization. *Recommended Composition of Influenza Virus Vaccines for Use in the 2020 - 2021 Northern Hemisphere Influenza Season.* (2020). Available online at: https://www.who.int/influenza/vaccines/virus/recommendations/2020-21_north/en/ (accessed March 18, 2020)
7. Wei CJ, Crank MC, Shiver J, Graham BS, Mascola JR, Nabel GJ. Next-generation influenza vaccines: opportunities and challenges. *Nat Rev Drug Discov.* (2020) 19:239–52. doi: 10.1038/s41573-019-0056-x
8. He P, Zou Y, Hu Z. Advances in aluminum hydroxide-based adjuvant research and its mechanism. *Hum Vaccin Immunother.* (2015) 11:477–88. doi: 10.1080/21645515.2014.1004026
9. Oleszycka E, Lavelle EC. Immunomodulatory properties of the vaccine adjuvant alum. *Curr Opin Immunol.* (2014) 28:1–5. doi: 10.1016/j.coi.2013.12.007
10. Clapp T, Siebert P, Chen D, Jones Braun L. Vaccines with aluminum-containing adjuvants: optimizing vaccine efficacy and thermal stability. *J Pharm Sci.* (2011) 100:388–401. doi: 10.1002/jps.22284
11. Clark TW, Pareek M, Hoschler K, Dillon H, Nicholson KG, Groth N, et al. Trial of 2009 influenza A (H1N1) monovalent MF59-adjuvanted vaccine. *N Engl J Med.* (2009) 361:2424–35. doi: 10.1056/NEJMoa0907650
12. Domnich A, Arata L, Amicizia D, Puig-Barbera J, Gasparini R, Panatto D. Effectiveness of MF59-adjuvanted seasonal influenza vaccine in the elderly: a systematic review and meta-analysis. *Vaccine.* (2017) 35:513–20. doi: 10.1016/j.vaccine.2016.12.011
13. Tsai TF. MF59 adjuvanted seasonal and pandemic influenza vaccines. *Yakugaku Zasshi.* (2011) 131:1733–41. doi: 10.1248/yakushi.131.1733
14. Naud PS, Roteli-Martins CM, De Carvalho NS, Teixeira JC, de Borba PC, Sanchez N, et al. Sustained efficacy, immunogenicity, and safety of the HPV-16/18 AS04-adjuvanted vaccine: final analysis of a long-term follow-up study up to 9.4 years post-vaccination. *Hum Vaccin Immunother.* (2014) 10:2147–62. doi: 10.4161/hv.29532
15. Didierlaurent AM, Laupeze B, Di Pasquale A, Hergli N, Collignon C, Garcon N. Adjuvant system AS01: helping to overcome the challenges of modern vaccines. *Expert Rev Vaccines.* (2017) 16:55–63. doi: 10.1080/14760584.2016.1213632
16. Gregg KA, Harberts E, Gardner FM, Pelletier MR, Cayatte C, Yu L, et al. Rationally designed TLR4 ligands for vaccine adjuvant discovery. *mBio.* (2017) 8:e00492-17. doi: 10.1128/mBio.00492-17
17. Petrovsky N. Comparative safety of vaccine adjuvants: a summary of current evidence and future needs. *Drug Saf.* (2015) 38:1059–74. doi: 10.1007/s40264-015-0350-4

18. Chan M, Hayashi T, Kuy CS, Gray CS, Wu CC, Corr M, et al. Synthesis and immunological characterization of toll-like receptor 7 agonistic conjugates. *Bioconjug Chem.* (2009) 20:1194–200. doi: 10.1021/bc900054q
19. Chan M, Hayashi T, Mathewson RD, Nour A, Hayashi Y, Yao S, et al. Identification of substituted pyrimido[5,4-b]indoles as selective Toll-like receptor 4 ligands. *J Med Chem.* (2013) 56:4206–23. doi: 10.1021/jm301694x
20. Goff PH, Hayashi T, Martinez-Gil L, Corr M, Crain B, Yao S, et al. Synthetic Toll-like receptor 4 (TLR4) and TLR7 ligands as influenza virus vaccine adjuvants induce rapid, sustained, and broadly protective responses. *J Virol.* (2015) 89:3221–35. doi: 10.1128/JVI.03337-14
21. Goff PH, Hayashi T, He W, Yao S, Cottam HB, Tan GS, et al. Synthetic toll-like receptor 4 (TLR4) and TLR7 ligands work additively via MyD88 to induce protective antiviral immunity in mice. *J Virol.* (2017) 91:e01050-17. doi: 10.1128/JVI.01050-17
22. Chan M, Kakitsubata Y, Hayashi T, Ahmadi A, Yao S, Shukla NM, et al. Structure-activity relationship studies of pyrimido[5,4-b]indoles as selective toll-like receptor 4 ligands. *J Med Chem.* (2017) 60:9142–61. doi: 10.1021/acs.jmedchem.7b00797
23. Erbelding EJ, Post DJ, Stemmy EJ, Roberts PC, Augustine AD, Ferguson S, et al. A universal influenza vaccine: the strategic plan for the national institute of allergy and infectious diseases. *J Infect Dis.* (2018) 218:347–54. doi: 10.1093/infdis/jiy103
24. Hui GS, Hashimoto CN. Adjuvant formulations possess differing efficacy in the potentiation of antibody and cell mediated responses to a human malaria vaccine under selective immune genes knockout environment. *Int Immunopharmacol.* (2008) 8:1012–22. doi: 10.1016/j.intimp.2008.03.005
25. Orr MT, Fox CB, Baldwin SL, Sivananthan SJ, Lucas E, Lin S, et al. Adjuvant formulation structure and composition are critical for the development of an effective vaccine against tuberculosis. *J Control Release.* (2013) 172:190–200. doi: 10.1016/j.jconrel.2013.07.030
26. Abhyankar MM, Orr MT, Lin S, Suraju MO, Simpson A, Blust M, et al. Adjuvant composition and delivery route shape immune response quality and protective efficacy of a recombinant vaccine for entamoeba histolytica. *NPJ Vaccines.* (2018) 3:22. doi: 10.1038/s41541-018-0060-x
27. Gurczynski SJ, Nathani N, Warheit-Niemi HI, Hult EM, Podsiad A, Deng J, et al. CCR2 mediates increased susceptibility to post-H1N1 bacterial pneumonia by limiting dendritic cell induction of IL-17. *Mucosal Immunol.* (2019) 12:518–30. doi: 10.1038/s41385-018-0106-4
28. Zhou J, Wang D, Gao R, Zhao B, Song J, Qi X, et al. Biological features of novel avian influenza A (H7N9) virus. *Nature.* (2013) 499:500–3. doi: 10.1038/nature12379
29. Suan D, Sundling C, Brink R. Plasma cell and memory B cell differentiation from the germinal center. *Curr Opin Immunol.* (2017) 45:97–102. doi: 10.1016/j.coi.2017.03.006
30. Bannard O, Cyster JG. Germinal centers: programmed for affinity maturation and antibody diversification. *Curr Opin Immunol.* (2017) 45:21–30. doi: 10.1016/j.coi.2016.12.004
31. Vinuesa CG, Linterman MA, Yu D, MacLennan IC. Follicular helper T cells. *Annu Rev Immunol.* (2016) 34:335–68. doi: 10.1146/annurev-immunol-041015-055605
32. Crotty S. T follicular helper cell biology: a decade of discovery and diseases. *Immunity.* (2019) 50:1132–48. doi: 10.1016/j.immuni.2019.04.011
33. Mallajosyula VV, Citron M, Ferrara F, Temperton NJ, Liang X, Flynn JA, et al. Hemagglutinin sequence conservation guided stem immunogen design from influenza A H3 subtype. *Front Immunol.* (2015) 6:329. doi: 10.3389/fimmu.2015.00329
34. Yassine HM, Boyington JC, McTamney PM, Wei CJ, Kanekiyo M, Kong WP, et al. Hemagglutinin-stem nanoparticles generate heterosubtypic influenza protection. *Nat Med.* (2015) 21:1065–70. doi: 10.1038/nm.3927
35. Fan X, Hashem AM, Chen Z, Li C, Doyle T, Zhang Y, et al. Targeting the HA2 subunit of influenza A virus hemagglutinin via CD40L provides universal protection against diverse subtypes. *Mucosal Immunol.* (2015) 8:211–20. doi: 10.1038/mi.2014.59
36. Ellebedy AH, Krammer F, Li GM, Miller MS, Chiu C, Wrammert J, et al. Induction of broadly cross-reactive antibody responses to the influenza HA stem region following H5N1 vaccination in humans. *Proc Natl Acad Sci USA.* (2014) 111:13133–8. doi: 10.1073/pnas.1414070111
37. Restivo V, Costantino C, Bono S, Maniglia M, Marchese V, Ventura G, et al. Influenza vaccine effectiveness among high-risk groups: a systematic literature review and meta-analysis of case-control and cohort studies. *Hum Vaccin Immunother.* (2018) 14:724–35. doi: 10.1080/21645515.2017.1321722
38. Shang M, Chung JR, Jackson ML, Jackson LA, Monto AS, Martin ET, et al. Influenza vaccine effectiveness among patients with high-risk medical conditions in the United States, 2012-2016. *Vaccine.* (2018) 36:8047–53. doi: 10.1016/j.vaccine.2018.10.093
39. Center for Disease Control and Prevention. *CDC Seasonal Flu Vaccine Effectiveness Studies.* (2020). Available online at: https://www.cdc.gov/flu/vaccines-work/effectiveness-studies.htm (accessed March 18, 2020)
40. Reed SG, Orr MT, Fox CB. Key roles of adjuvants in modern vaccines. *Nat Med.* (2013) 19:1597–608. doi: 10.1038/nm.3409
41. Mata-Haro V, Cekic C, Martin M, Chilton PM, Casella CR, Mitchell TC. The vaccine adjuvant monophosphoryl lipid A as a TRIF-biased agonist of TLR4. *Science.* (2007) 316:1628–32. doi: 10.1126/science.1138963
42. Reed SG, Hsu FC, Carter D, Orr MT. The science of vaccine adjuvants: advances in TLR4 ligand adjuvants. *Curr Opin Immunol.* (2016) 41:85–90. doi: 10.1016/j.coi.2016.06.007
43. Krammer F, Palese P. Universal influenza virus vaccines that target the conserved hemagglutinin stalk and conserved sites in the head domain. *J Infect Dis.* (2019) 219:S62–7. doi: 10.1093/infdis/jiy711
44. Frasca D, Blomberg BB. B Cell-specific biomarkers for optimal antibody responses to influenza vaccination and molecular pathways that reduce B cell function with aging. *Crit Rev Immunol.* (2016) 36:523–37. doi: 10.1615/CritRevImmunol.2017020113
45. Corti D, Cameroni E, Guarino B, Kallewaard NL, Zhu Q, Lanzavecchia A. Tackling influenza with broadly neutralizing antibodies. *Curr Opin Virol.* (2017) 24:60–9. doi: 10.1016/j.coviro.2017.03.002
46. Laursen NS, Wilson IA. Broadly neutralizing antibodies against influenza viruses. *Antiviral Res.* (2013) 98:476–83. doi: 10.1016/j.antiviral.2013.03.021
47. Wohlbold TJ, Krammer F. In the shadow of hemagglutinin: a growing interest in influenza viral neuraminidase and its role as a vaccine antigen. *Viruses.* (2014) 6:2465–94. doi: 10.3390/v6062465
48. Gubareva L, Mohan T. Antivirals targeting the neuraminidase. *Cold Spring Harb Perspect Med.* (2020) 5:401–9. doi: 10.1101/cshperspect.a038455
49. Chen YQ, Wohlbold TJ, Zheng NY, Huang M, Huang Y, Neu KE, et al. Influenza infection in humans induces broadly cross-reactive and protective neuraminidase-reactive antibodies. *Cell.* (2018) 173:417–29 e410. doi: 10.1016/j.cell.2018.03.030
50. Krammer F, Fouchier RAM, Eichelberger MC, Webby RJ, Shaw-Saliba K, Wan H, et al. NAction! how can neuraminidase-based immunity contribute to better influenza virus vaccines? *mBio.* (2018) 9:e02332-17. doi: 10.1128/mBio.02332-17
51. Smith GE, Sun X, Bai Y, Liu YV, Massare MJ, Pearce MB, et al. Neuraminidase-based recombinant virus-like particles protect against lethal avian influenza A(H5N1) virus infection in ferrets. *Virology.* (2017) 509:90–7. doi: 10.1016/j.virol.2017.06.006
52. Liu WC, Lin CY, Tsou YT, Jan JT, Wu SC. Cross-reactive neuraminidase-inhibiting antibodies elicited by immunization with recombinant neuraminidase proteins of H5N1 and pandemic H1N1 influenza A viruses. *J Virol.* (2015) 89:7224–34. doi: 10.1128/JVI.00585-15
53. Garcon N, Van Mechelen M. Recent clinical experience with vaccines using MPL- and QS-21-containing adjuvant systems. *Expert Rev Vaccines.* (2011) 10:471–86. doi: 10.1586/erv.11.29
54. Lutz MB, Kukutsch N, Ogilvie AL, Rossner S, Koch F, Romani N, et al. An advanced culture method for generating large quantities of highly pure dendritic cells from mouse bone marrow. *J Immunol Methods.* (1999) 223:77–92. doi: 10.1016/S0022-1759(98)00204-X
55. Datta SK, Redecke V, Prilliman KR, Takabayashi K, Corr M, Tallant T, et al. A subset of Toll-like receptor ligands induces cross-presentation by bone marrow-derived dendritic cells. *J Immunol.* (2003) 170:4102–10. doi: 10.4049/jimmunol.170.8.4102
56. Zhang H. Thin-film hydration followed by extrusion method for liposome preparation. *Methods Mol Biol.* (2017) 1522:17–22. doi: 10.1007/978-1-4939-6591-5_2
57. Cho HJ, Takabayashi K, Cheng PM, Nguyen MD, Corr M, Tuck S, et al. Immunostimulatory DNA-based vaccines induce cytotoxic lymphocyte

activity by a T-helper cell-independent mechanism. *Nat Biotechnol.* (2000) 18:509–14. doi: 10.1038/75365
58. Baudner BC, Ronconi V, Casini D, Tortoli M, Kazzaz J, Singh M, et al. MF59 emulsion is an effective delivery system for a synthetic TLR4 agonist (E6020). *Pharm Res.* (2009) 26:1477–85. doi: 10.1007/s11095-009-9859-5
59. Wang Z, Huang B, Thomas M, Sreenivasan CC, Sheng Z, Yu J, et al. Detailed mapping of the linear B Cell epitopes of the hemagglutinin (HA) protein of swine influenza virus. *Virology.* (2018) 522:131–7. doi: 10.1016/j.virol.2018.07.013
60. Edgar RC. MUSCLE: multiple sequence alignment with high accuracy and high throughput. *Nucleic Acids Res.* (2004) 32:1792–7. doi: 10.1093/nar/gkh340
61. Saitou N, Nei M. The neighbor-joining method: a new method for reconstructing phylogenetic trees. *Mol Biol Evol.* (1987) 4:406–25.
62. Kumar S, Nei M, Dudley J, Tamura K. MEGA: a biologist-centric software for evolutionary analysis of DNA and protein sequences. *Brief Bioinform.* (2008) 9:299–306. doi: 10.1093/bib/bbn017
63. Shalapour S, Lin XJ, Bastian IN, Brain J, Burt AD, Aksenov AA, et al. Inflammation-induced IgA+ cells dismantle anti-liver cancer immunity. *Nature.* (2017) 551:340–5. doi: 10.1038/nature24302
64. Kitaura K, Yamashita H, Ayabe H, Shini T, Matsutani T, Suzuki R. Different somatic hypermutation levels among antibody subclasses disclosed by a new next-generation sequencing-based antibody repertoire analysis. *Front Immunol.* (2017) 8:389. doi: 10.3389/fimmu.2017.00389
65. Tumeh PC, Harview CL, Yearley JH, Shintaku IP, Taylor EJ, Robert L, et al. PD-1 blockade induces responses by inhibiting adaptive immune resistance. *Nature.* (2014) 515:568–71. doi: 10.1038/nature13954
66. Carey AJ, Hope JL, Mueller YM, Fike AJ, Kumova OK, van Zessen DBH, et al. Public clonotypes and convergent recombination characterize the naive CD8(+) T-cell receptor repertoire of extremely preterm neonates. *Front Immunol.* (2017) 8:1859. doi: 10.3389/fimmu.2017.01859
67. Liu G, Tarbet B, Song L, Reiserova L, Weaver B, Chen Y, et al. Immunogenicity and efficacy of flagellin-fused vaccine candidates targeting 2009 pandemic H1N1 influenza in mice. *PLoS ONE.* (2011) 6:e20928. doi: 10.1371/journal.pone.0020928

Conflict of Interest: DB and RS were employed by the company Inimmune Corp. TM was employed by the company Repertoire Genesis Inc.

The remaining authors declare that the research was conducted in the absence of any commercial or financial relationships that could be construed as a potential conflict of interest.

frontiers in Immunology

PERSPECTIVE
published: 30 July 2020
doi: 10.3389/fimmu.2020.01683

Systems Biology Approaches to Understanding the Human Immune System

Bhavjinder K. Dhillon[1], *Maren Smith*[1], *Arjun Baghela*[1], *Amy H. Y. Lee*[1,2] *and Robert E. W. Hancock*[1]*

[1] Centre for Microbial Diseases and Immunity Research, University of British Columbia, Vancouver, BC, Canada, [2] Molecular Biology & Biochemistry Department, Simon Fraser University, Burnaby, BC, Canada

Systems biology is an approach to interrogate complex biological systems through large-scale quantification of numerous biomolecules. The immune system involves >1,500 genes/proteins in many interconnected pathways and processes, and a systems-level approach is critical in broadening our understanding of the immune response to vaccination. Changes in molecular pathways can be detected using high-throughput omics datasets (e.g., transcriptomics, proteomics, and metabolomics) by using methods such as pathway enrichment, network analysis, machine learning, etc. Importantly, integration of multiple *omic* datasets is becoming key to revealing novel biological insights. In this perspective article, we highlight the use of protein-protein interaction (PPI) networks as a multi-omics integration approach to unravel information flow and mechanisms during complex biological events, with a focus on the immune system. This involves a combination of tools, including: *InnateDB*, a database of curated interactions between genes and protein products involved in the innate immunity; *NetworkAnalyst*, a visualization and analysis platform for InnateDB interactions; and *MetaBridge*, a tool to integrate metabolite data into PPI networks. The application of these systems techniques is demonstrated for a variety of biological questions, including: the developmental trajectory of neonates during the first week of life, mechanisms in host-pathogen interaction, disease prognosis, biomarker discovery, and drug discovery and repurposing. Overall, systems biology analyses of omics data have been applied to a variety of immunology-related questions, and here we demonstrate the numerous ways in which PPI network analysis can be a powerful tool in contributing to our understanding of the immune system and the study of vaccines.

Keywords: systems biology, multi-omic integration, transcriptomics, innate immunity, immune ontogeny, host-pathogen interaction, drug discovery and repurposing, systems vaccinology

OPEN ACCESS

Edited by:
Jay Evans,
University of Montana, United States

Reviewed by:
Susana Magadan,
University of Vigo, Spain
Geert Leroux-Roels,
Ghent University, Belgium

***Correspondence:**
Robert E. W. Hancock
bob@hancocklab.com

Specialty section:
This article was submitted to Vaccines and Molecular Therapeutics, a section of the journal Frontiers in Immunology

Received: *11 March 2020*
Accepted: *24 June 2020*
Published: *30 July 2020*

Citation:
Dhillon BK, Smith M, Baghela A, Lee AHY and Hancock REW (2020) Systems Biology Approaches to Understanding the Human Immune System. Front. Immunol. 11:1683. doi: 10.3389/fimmu.2020.01683

INTRODUCTION

In the field of immunology, a systems biology approach is necessary to understanding the immune response to vaccination, infection and diseases, since these involve complex interactions between a large number of genetic, epigenetic, physiological and environmental factors. Systems-level strategies can ultimately be applied to better understand the molecular changes in humans upon exposure to a vaccine or an immunotherapeutic, to understand the mechanisms underlying disease

or pathogenesis, and to characterize the effect(s) of specific challenges to the immune system (1–5). Omics technologies offer the ability to measure such aspects in an unbiased way that is high-throughput and cost-effective. Several omics methods have been employed in the context of systems vaccinology (3), including but not limited to, whole genome sequencing (genomics), RNA-Seq for measuring mRNA levels (transcriptomics), high-throughput mass spectrometry for measuring protein levels (proteomics) and metabolite levels (metabolomics), CHiP-Seq for determining transcription factor binding sites, ATAC-Seq to identify DNA modification sites (epigenomics), 16S rRNA sequencing for microbiota profiling (microbiomics), and equivalent omics analyses performed at the single-cell level. Recently, there has also been a growing effort to obtain multiple omics profiles in the same individuals, since shared insights across omics datasets strengthens links between underlying biological mechanisms and responses of interest, and can provide more reliable interpretation of gene function, higher-level changes and novel insights not observed in single-omics studies (6–8). Overall, biological samples can be manipulated to generate numerous omics datasets, and can be applied to study how our immune systems elicit effective, therapeutic and/or pathological responses.

A key challenge in systems biology is building the appropriate bioinformatics tools to integrate omics datasets, ultimately enabling the correlation of global changes with the underlying biological events that drove those changes. Statistical and machine learning approaches have been applied to omics datasets [reviewed previously (9–11)] to identify sets of molecular features that (i) are dysregulated/correlated with observed phenotypes, (ii) can be used as biomarkers to predict observed phenotypes, or (iii) can be targeted by drugs for improved therapies. A wide array of tools are available to run single- or multi-omics analysis pipelines (12), including commercial platforms and more recently published "self-serve" platforms [e.g., OmicsNet (13), OmicsPlayground (14)]. Typically, such methods interrogate information in either a supervised or unsupervised manner; supervised methods identify differences between labeled omics data from different conditions (e.g., responders vs. non-responders or treated vs. untreated) while, unsupervised methods reveal global patterns of gene dysregulation without any labels.

Downstream characterization of dysregulated molecules can further our understanding of underlying biological mechanisms at play. This can be achieved by interrogating curated functional genomics information from databases of gene ontologies (functional descriptions), pathways, known interactors, transcription factor binding sites (TFBS) upstream of dysregulated genes, etc. through various enrichment analyses. However, a large proportion of genes have not been assigned to canonical pathways in pathways databases (such as KEGG or Reactome), so pathway enrichment limits the ability of such approaches to reveal novel insights (15).

Abbreviations: CF, cystic fibrosis; CFTR, cystic fibrosis transmembrane regulator; DE, differentially expressed; DOL, day of life; IDR, innate defense regulator; iNTS, invasive non-typhoidal *Salmonella*; MAP, mitogen-activated; PPI, protein-protein interaction; TFBS, transcription factor binding site.

The use of biological networks is a powerful approach to integrate multi-omics data to identify novel biological insights (15–18). To characterize the role of individual molecular features in larger cellular processes and global changes using networks involves either overlaying omics data on experimentally-derived known networks [e.g., protein-protein interaction (PPI) networks], or by inferring networks directly from the data [e.g., co-expressed genes (19)], the strengths/limitations of which have been reviewed previously (15). A few commonly used biological networks along with related resources and tools are summarized in **Table 1**. The application of PPI networks to interrelate dysregulated genes is a very powerful method for revealing the systems-level flow of information through key hubs (highly connected protein nodes) and subnetworks. Because PPIs include direct, metabolic, and regulatory interactions between proteins, they essentially chart potentially biologically relevant, i.e., functional, interconnections. This can enable the determination of emergent properties, which are essentially new biological insights into the processes driving the observed transcriptional differences. The results from a PPI network analysis are always framed as hypotheses rather than knowledge *per se*, and must be eventually tested using downstream wet lab experiments (15).

In this article, we provide an overview of the philosophies and methodologies that can be employed in the analysis of omics data, especially with regards to integration of omics datasets using an unsupervised network analysis approach. Examples are provided of how such analyses enable novel hypothesis generation for: (a) immune system development, (b) mechanisms of host-pathogen interactions, (c) discovery of mechanism-based biomarkers, and (d) strategies to define prospective new interventions based on drug repurposing. While the methods are somewhat biased toward the study of innate immune and inflammatory responses, it is worth mentioning that "innate immunity instructs adaptive immunity" (63) in that (i) the effectors of adaptive immunity are often innate immune mechanisms, (ii) many of the pathways involved are the same, and (iii) vaccine adjuvants that improve adaptive immune responses boost innate immunity. Therefore, the tools we describe have value in investigating adaptive immunity as well as human genetic diseases/conditions with an underlying inflammatory pathology.

SYSTEMS TOOLS FOR NETWORK-BASED ANALYSES USING PPIS

InnateDB (43, 44) and other International Molecular Exchange (IMEx) consortium databases (42) provide the basis for understanding biological connections in cells according to known interactions between molecular elements, such as proteins. InnateDB is a publicly available database (www.innatedb.com) focused on elucidating the genes, proteins, and molecular "interactome" of the innate immune response, with an emphasis on curation of experimentally-validated PPIs and signaling pathways in human, mouse and bovine. The interactome can be used to understand the interplay between multi-omics datasets that measure different parts of a larger

TABLE 1 | Examples of functional biological information that can be represented using networks, along with corresponding databases/repositories and supplementary data analysis tools that can be used to assess the functional data in high-throughput omics datasets.

Type of functional information	Select databases/ repositories	Supplementary Omic-data analysis tools
Metabolic pathways, reactions and associated enzymes and transporters	Kyoto Encyclopedia of Genes and Genomes (KEGG) (20)	MetaBridge (21)
	Reactome (22)	OmicsPlayground (14)
	Panther pathway database (23)	ReactomePA (24)
	Gene Ontology (25)	SIGORA (26)
	Edinburg Human Metabolic Network (27)	iMAT (28)
	Recon3D (29)	INIT (30)
	iHsa (31)	mCADRE (32)
	BioModels (33)	TIMBR (31)
Gene regulatory networks (interactions between transcription factors and their target genes)	Encyclopedia of DNA elements (ENCODE) (34, 35) JASPAR (36) TRANSFAC (37)	MRNET (38) ARACNE (39) iRegulon (40) dynGENIE3 (41)
Protein-protein interaction (PPI) networks (includes direct, metabolic, and regulatory interactions)	International Molecular Exchange (IMEx) Consortium (42), which includes: InnateDB (43, 44) Biomolecular Interaction Network Database (BIND) (45) Database of Interacting Proteins (DIP) (46) Molecular INTeraction Database (MINT) (47) MIntAct (48) The Biological General Repository for Interaction Datasets (BioGRID) (49)	NetworkAnalyst (50–52) OmicsNet (13) PPIExp (53)
Signaling networks (interactions involved in a cell's response to its environment)	KEGG (20) Reactome (22) STKE (54) TRANSPATH (55)	ReactomePA (24)
Drug targets (interactions between drugs and their cellular targets)	DrugBank (56) Therapeutic target database (TTD) (57) SuperTarget (58) STITCH (59) ChEMBL (60) BindingDB (61) KEGG (20)	DINIES (62)

system of physical, metabolic, and regulatory networks. For example, human TRAF6 and MyD88 are usually defined as having a role in the major TLR4 to NFκB signaling pathway of innate immunity. However, in InnateDB, they are experimentally documented to interact with 398 and 129 proteins, respectively, in humans. This means that there is a massive potential for these proteins to bridge and/or participate in multiple biological pathways when activated by innate immune stimuli.

InnateDB is an important tool in immunology as evidenced by the >6,000,000 hits from more than 55,000 visitors annually. While all known pathways (>3,500) and molecular interactions (318,000 in human) are present, the emphasis on innate immunity is achieved through the contextual review, curation and annotation of molecular interactions and pathways involved in innate immunity. To date, the InnateDB curation team has reviewed more than 5,200 publications annotating >27,000 molecular interactions of >9,400 separate genes in rich detail including annotation of the cell, cell-line and tissue type; the molecules involved; the interaction detection method; etc. By including interaction and pathway data relevant to all biological processes, a much broader perspective of innate immunity can be achieved, especially since an effective innate immune response requires the coordinated efforts of many important processes including the endocrine, circulatory, and nervous systems (64). Additionally, it becomes possible to investigate any biological signaling process of interest beyond the immune system, as well as inflammation and adaptive immunity.

InnateDB facilitates systems-level analyses by enabling the integration, analysis and visualization of user-supplied quantitative data, such as gene expression data, in the context of molecular interaction networks and pathways. This includes the statistically robust analysis of overrepresented pathways, interactomes, ontologies, TFBS, and networks. One can, for example, refine the network to show only molecular interactions between a list of differentially expressed (DE) genes (and their encoded products) or view all potential interactors regardless of whether they are DE. This can aid in the identification of important nodes that may not be regulated transcriptionally or which are expressed at an earlier or later time. Networks derived from InnateDB can be interactively visualized using the Cerebral plug-in for Cytoscape (65) to generate biologically intuitive, pathway-like layouts of networks, or in a more recently developed tool, NetworkAnalyst (50–52). NetworkAnalyst is an extremely fast network analysis and visualization tool for the analysis of gene expression data in the context of PPI networks. In addition, MetaBridge (21) is a tool that can be used for the integration of metabolite-protein interactions into these existing networks. In combination, these tools can be used to perform multi-omics integration of transcriptomics, proteomics, and metabolomics data in an unsupervised manner.

In addition to these outlined methods, there are bioinformatics tools available for performing other types of network analyses specifically for studying the immune system. Examples include immuneExpresso (66), a data mining tool built as part of Immport to capture inter-cell interactions, and Ontogenet (67), a component of the ImmGen database enabling construction of gene regulatory networks based on sets of co-expressed genes. Such tools can be useful in revealing novel inter-cell interactions or regulatory factors, respectively, but ultimately may be too limited in scope for a systems-level analysis.

Thus, we focus here on how PPI-based network analysis tools can be applied to better understand human health and disease.

MECHANISTIC INSIGHTS INTO HUMAN IMMUNE DEVELOPMENT

Most recently, as a part of the EPIC-HIPC consortium, we published a study that revealed a robust developmental trajectory of immune ontogeny during the first week of life in newborns using a multi-omics integration approach (9). Transcriptomic, proteomic, and metabolomic data were derived from <1 ml of blood collected from West African (The Gambia) neonates at two time points: day of life (DOL) 0 and a second DOL, either 1, 3, or 7.

Importantly, through this study, we were able to show that multi-omics integration using PPI networks (through NetworkAnalyst, InnateDB, and MetaBridge) provided similar biological insights, but greater depth, when compared to data-driven supervised integration approaches [namely, DIABLO (68) and Multifactorial Response Network (MMRN) (69, 70)]. Major observations from this study revealed that the first week of life is highly dynamic; DOL0 and DOL1 were quite similar with few DE genes, but by DOL3, 1,125 DE genes were detected, and 1,864 DE genes by DOL7. These represented several key pathways in immune development, mainly centered around interferon signaling, the complement cascade, and neutrophil activity. These have previously been shown to play a role in the newborn immune response to infection, but until this study were not identified as central to ontogeny in the first week of life. Importantly, these pathways and nearly 60% of transcriptomic changes were confirmed in a second independent cohort of neonates from Papua New Guinea/Australasia, revealing that neonatal immune development is not random, but follows a precise and possibly purposeful age-specific path.

An unsupervised PPI network was used to integrate the transcriptomic, metabolomics, and proteomic data to reveal a single functional network, highlighting that individual omics datasets are complementary, reporting different facets of the same biological processes. For example, both the transcriptomic and proteomic data confirmed the increase in type I interferon-related functions and the regulation of complement cascades. Importantly, this integration also revealed novel nodes in the PPI network that were not identified by any single-omics dataset on its own, representing novel biological insights, including changes in cellular replication machinery, creatinine metabolism, fibrin clotting cascade, adaptive immunity markers and phagosome activity.

Thus, these systems biology approaches allowed novel insights into the immune developmental trajectory during the first week of life in newborns. Further studies are being conducted to provide insights into the mechanistic differences in the susceptibility of neonates to infection-related disease or death during this critical phase of life. Also, in the context of vaccinology, an integrative systems biology approach is being used to reveal mechanistic insights into the molecular determinants of vaccination efficacy, while taking into account this developmental trajectory.

MECHANISTIC INSIGHTS INTO HOST-PATHOGEN INTERACTIONS

Systems biology methods have also been leveraged to study host-pathogen interactions (71). One example is of infection by the obligate human intracellular pathogen *Chlamydia trachomatis*, the major cause of bacterial sexually-transmitted diseases (STDs) and preventable blindness worldwide. This involved a study that coupled transcriptomics and proteomics to assess the macrophage responses to infection with *C. trachomatis* (72). Macrophages were derived from human induced pluripotent stem cells (iPSdMs), which share >95% similarity in terms of gene expression with primary human blood monocyte-derived macrophages, and were able to support the growth of *C. trachomatis* intracellularly to mimic infection *in-vitro*.

Pathway analysis of 2,029 DE genes (from transcriptomics) and 307 DE proteins (from proteomics) at 24 h post-infection, revealed strong interferon α, β, and γ responses, and dysregulation of various Toll-like receptor pathways, the endosomal/vacuolar pathway, energy metabolism, and metabolism of amino acids and nucleotides and inhibition of translation. Most significantly upregulated were genes associated with type I interferon signaling, including key transcription factors such as interferon regulatory factors (IRF)-1, 3, and 7, which are known to contribute to the regulation of type I interferons during *Chlamydia* infection.

Importantly, IRF5 and IL-10RA, not previously characterized for their role in *Chlamydia* infection, were identified as key players in limiting infection in macrophages. Indeed, IRF5$^{-/-}$ and IL-10RA$^{-/-}$ mutant iPSDM cells were both shown to have increased susceptibility to *C. trachomatis* infection. These results, along with numerous other published studies [e.g., (73–77)], demonstrate that multi-omics integration using PPI networks can reveal novel insight into the factors that play a significant role in the host immune response to infections.

MECHANISM-BASED BIOMARKERS FOR DISEASE DIAGNOSIS AND PROGNOSIS PREDICTION

Systems biology analyses have also led to insights into mechanisms underlying disease prognosis and prediction of diagnostic biomarkers. One such study of the enteric pathogen *Salmonella enterica sv. Typhimurium* (78) involved the use of transcriptomics to compare gene expression in HIV patients with and without severe invasive non-typhoidal *Salmonella* (iNTS) infections, as well as HIV patients with other acute bacterial infections (including *E. coli* and *Streptococcus pneumoniae*). Initially, 1,200 genes were upregulated in HIV patients with

iNTS and with other acute bacterial infections, compared to HIV patients without a bacterial infection. However, genes upregulated in patients with non-*Salmonella* acute infections showed enrichment for pathways typically associated with innate immune/inflammatory responses, while conversely the gene expression response in patients with iNTS could be explained by upregulation of genes that are associated with suppression of inflammation (NFKBIB, PI3K, REL, SIGIRR, SOCS4, SOCS7). This lack of innate immune response and viral signature, which was subsequently shown to be consistent with increased viral load (79), leading to insights into the poor prognosis of HIV patients with iNTS.

These types of analyses were also used to explore immune manipulation using host defense (antimicrobial) peptides. Such peptides selectively modulate the innate immune response and protect against infection, and are produced by many organisms to defend against infections (80). Furthermore, novel small innate defense regulator (IDR) peptides have been shown to be effective in animal models against antibiotic resistant bacteria, tuberculosis, cerebral malaria, pre-term birth and inflammation (81, 82). To better understand the cellular cascade that occurs after these IDR peptides enter the cell, transcriptional changes were assessed in human monocytes and peripheral blood mononuclear cells (83). The biological relevance of these gene expression changes was assessed using pathway over-representation, TFBS analysis, and network analysis with NetworkAnalyst, implicating 11 pathways including the p38, Erk1/2, and JNK mitogen-activated (MAP)-kinases, NFκB, two Src family kinases, and more than 15 transcription factors [including NFκB (most subunits), Creb, IRF4, AP-1, AP-2, Are, E2F1, SP1, Gre, and STAT3]. NetworkAnalyst showed that some of the top connected hub proteins within networks constructed from dysregulated genes were involved in the functioning of MAP kinases and induction of chemokines, anti-inflammatory pathways particularly TGFβ, and type I interferon responses. These highly connected hubs reveal mechanistic insights and could potentially represent diagnostic or treatment biomarkers. Ultimately, a similar approach can be utilized to evaluate any agent perturbing cellular function, including immunomodulators and vaccines, and can define biomarkers differentiating between responders and non-responders.

DRUG DISCOVERY AND REPURPOSING

Systems biology techniques have been applied to aid in drug discovery and repurposing of existing agents for the treatment of cancers, bacterial and viral infections, and genetic disorders (84). One such study aimed at finding better therapeutics for cystic fibrosis (CF) utilized transcriptomics to study immortalized $CFTR^{-/-}$ (cystic fibrosis transmembrane regulator) epithelial cells stimulated for hyperinflammation, a state known to lead to deterioration of lung function in CF patients (85). Genes differentially expressed between $CFTR^{-/-}$ cells and corrected variants were submitted to InnateDB for analysis and integration with PPI networks. This revealed the interconnectivity of the CFTR and innate immune networks through the PRKAA1 (AMP kinase)/AKT1 and HSPB1 pathways. Genes within this network were then submitted to DrugBank (86), allowing for the identification of the diabetes drug Metformin as an AMP kinase activator, which was then tested *in-vitro* and shown to reduce inflammation by ∼50%. DE genes between $CFTR^{-/-}$ cells and corrected variants also included 54 genes involved in autophagy. In disease states, autophagy is an adaptive response to stress that favors infection survival and resolution (87). Follow up studies confirmed that CFTR mutant cells demonstrated arrested autophagy. It was then demonstrated that the antimicrobial peptide IDR-1018 resolved this arrested autophagy state and reduced inflammation. These genes also revealed a strong upregulation of ER stress and unfolded protein response pathways, through activation of the IRE-1 pathway (88). Follow up studies showed that salubrinal, an inhibitor of negative regulator GADD34, upregulated this pathway and suppressed inflammation. Thus, through these systems biology-based studies, novel pharmaceuticals (IDR-1018) and 2 existing drugs (Metformin and salubrinal) were identified as potential treatments for CF-related hyperinflammation. As such, along with numerous other studies [e.g., (89–92)], it has been shown that integrating omics datasets using resources such as InnateDB and DrugBank can reveal potential drug targets for improved therapies.

DISCUSSION AND THE FUTURE

The analyses outlined in this article merely scratch the surface of what is possible using systems biology and high-throughput omics techniques to study the immune system, e.g., the major tools described here (43, 44, 50–52) have been used and cited more than 1,500 times. The above-described examples highlight that using unbiased multi-omics experiments in conjunction with incisive bioinformatics tools, such as PPI network integration, one can go beyond the hypothesis-testing scientific method to use unbiased omics data to generate fundamentally new hypotheses and develop new biological insights. Ultimately such studies should lead to the development of novel diagnostics, individualized therapies for diseases and vaccines. Furthermore, systems biology approaches can provide invaluable insights to inform the stratification of individuals with the same syndrome but different underlying mechanisms, the diagnosis of disease and/or flare-ups, ongoing development of new vaccines and/or adjuvants as well as immune-based therapeutics providing insights into the optimal strategies for delivery of interventions.

AUTHOR CONTRIBUTIONS

BD, MS, and AB all contributed to writing of the first draft of this article. AL performed data analysis of the ontogeny study and provided valuable feedback through the writing process. RH supervised all authors, edited the manuscript and provided

critical insights and feedback. All authors contributed to the article and approved the submitted version.

FUNDING

Our bioinformatics research is currently supported by a grant from the Canadian Institutes for Health Research FDN-154287, and previously received funding from Genome Canada, Genome BC, and the Foundation for the National Institutes of Health through their Grand Challenges in Global Health Research program. RH holds a Canada Research Chair and a UBC Killam Professorship.

ACKNOWLEDGMENTS

The authors wish to acknowledge collaborators Fiona Brinkman, David Lynn, Jeff Xia, Tamara Munzner, and previous lab members Erin Gill, Chris Fjell, and Jennifer Gardy as well as the InnateDB curation team for their fantastic and critical contributions.

REFERENCES

1. Trautmann L, Sekaly R. Solving vaccine mysteries: a systems biology perspective. *Nat Immunol.* (2011) 12:729. doi: 10.1038/ni.2078
2. Mooney M, McWeeney S, Canderan G, Sékaly R. A systems framework for vaccine design. *Curr Opin Immunol.* (2013) 25:551–5. doi: 10.1016/j.coi.2013.09.014
3. Pulendran B, Li S, Nakaya HI. Systems vaccinology. *Immunity.* (2010) 33:516–29. doi: 10.1016/j.immuni.2010.10.006
4. Oberg AL, Kennedy RB, Li P, Ovsyannikova IG, Poland GA. Systems biology approaches to new vaccine development. *Curr Opin Immunol.* (2011) 23:436–43. doi: 10.1016/j.coi.2011.04.005
5. Kotliarov Y, Sparks R, Martins AJ, Mulè MP, Lu Y, Goswami M, et al. Broad immune activation underlies shared set point signatures for vaccine responsiveness in healthy individuals and disease activity in patients with lupus. *Nat Med.* (2020) 26:618–29. doi: 10.1038/s41591-020-0769-8
6. Ge H, Walhout AJ, Vidal M. Integrating 'omic'information: a bridge between genomics and systems biology. *Trends Genet.* (2003) 19:551–60. doi: 10.1016/j.tig.2003.08.009
7. Lee AH, Shannon CP, Amenyogbe N, Bennike TB, Diray-Arce J, Idoko OT, et al. Dynamic molecular changes during the first week of human life follow a robust developmental trajectory. *Nat Commun.* (2019) 10:1092. doi: 10.1038/s41467-019-08794-x
8. Ebrahim A, Brunk E, Tan J, O'brien EJ, Kim D, Szubin R, et al. Multi-omic data integration enables discovery of hidden biological regularities. *Nat Commun.* (2016) 7:1–9. doi: 10.1038/ncomms13091
9. Tolios A, De Las Rivas J, Hovig E, Trouillas P, Scorilas A, Mohr T. Computational approaches in cancer multidrug resistance research: Identification of potential biomarkers, drug targets and drug-target interactions. *Drug Resist Updates.* (2020) 48:100662. doi: 10.1016/j.drup.2019.100662
10. Kidd BA, Peters LA, Schadt EE, Dudley JT. Unifying immunology with informatics and multiscale biology. *Nat Immunol.* (2014) 15:118–27. doi: 10.1038/ni.2787
11. Tavassoly I, Goldfarb J, Iyengar R. Systems biology primer: the basic methods and approaches. *Essays Biochem.* (2018) 62:487–500. doi: 10.1042/EBC20180003
12. Beale DJ, Karpe AV, Ahmed W. Beyond metabolomics: a review of multi-omics-based approaches. *Microb Metab.* (2016) 289—312. doi: 10.1007/978-3-319-46326-1_10
13. Zhou G, Xia J. OmicsNet: a web-based tool for creation and visual analysis of biological networks in 3D space. *Nucleic Acids Res.* (2018) 46:W514–22. doi: 10.1093/nar/gky510
14. Akhmedov M, Martinelli A, Geiger R, Kwee I. Omics playground: a comprehensive self-service platform for visualization, analytics and exploration of big omics data. *NAR Genom Bioinform.* (2020) 2:lqz019. doi: 10.1093/nargab/lqz019
15. Charitou T, Bryan K, Lynn DJ. Using biological networks to integrate, visualize and analyze genomics data. *Genet Select Evol.* (2016) 48:27. doi: 10.1186/s12711-016-0205-1
16. Barabasi A, Oltvai ZN. Network biology: understanding the cell's functional organization. *Nat Rev Genet.* (2004) 5:101. doi: 10.1038/nrg1272
17. Saint-Antoine MM, Singh A. Network inference in systems biology: recent developments, challenges, and applications. *Curr Opin Biotechnol.* (2020) 63:89–98. doi: 10.1016/j.copbio.2019.12.002
18. Mardinoglu A, Boren J, Smith U, Uhlen M, Nielsen J. Systems biology in hepatology: approaches and applications. *Nat Rev Gastroenterol Hepatol.* (2018) 15:365–77. doi: 10.1038/s41575-018-0007-8
19. Costa RL, Boroni M, Soares MA. Distinct co-expression networks using multi-omic data reveal novel interventional targets in HPV-positive and negative head-and-neck squamous cell cancer. *Sci Rep.* (2018) 8:1–13. doi: 10.1038/s41598-018-33498-5
20. Kanehisa M, Goto S. KEGG: Kyoto encyclopedia of genes and genomes. *Nucleic Acids Res.* (2000) 28:27–30. doi: 10.1093/nar/28.1.27
21. Hinshaw SJ, Lee AHY, Gill EE, Hancock REW. MetaBridge: enabling network-based integrative analysis via direct protein interactors of metabolites. *Bioinformatics.* (2018) 34:3225–7. doi: 10.1093/bioinformatics/bty331
22. Croft D, Mundo AF, Haw R, Milacic M, Weiser J, Wu G. The reactome pathway knowledgebase. *Nucleic Acids Res.* (2014) 42:D472–7. doi: 10.1093/nar/gkt1102
23. Mi H, Thomas P. PANTHER pathway: an ontology-based pathway database coupled with data analysis tools. *Protein Netw Pathw Anal.* (2009) 563:123–40. doi: 10.1007/978-1-60761-175-2_7
24. Yu G, He Q. ReactomePA: an R/bioconductor package for Reactome pathway analysis and visualization. *Mol BioSyst.* (2016) 12:477–9. doi: 10.1039/C5MB00663E
25. Gene Ontology Consortium. The Gene Ontology (GO) database and informatics resource. *Nucleic Acids Res.* (2004) 32 (Suppl_1):D258–61. doi: 10.1093/nar/gkh036
26. Foroushani AB, Brinkman FS, Lynn DJ. Pathway-GPS and SIGORA: identifying relevant pathways based on the over-representation of their gene-pair signatures. *PeerJ.* (2013) 1:e229. doi: 10.7717/peerj.229
27. Ma H, Sorokin A, Mazein A, Selkov A, Selkov E, Demin O, et al. The Edinburgh human metabolic network reconstruction and its functional analysis. *Mol Syst Biol.* (2007) 3:135. doi: 10.1038/msb4100177
28. Zur H, Ruppin E, Shlomi T. iMAT: an integrative metabolic analysis tool. *Bioinformatics.* (2010) 26:3140–2. doi: 10.1093/bioinformatics/btq602
29. Brunk E, Sahoo S, Zielinski DC, Altunkaya A, Dräger A, Mih N, et al. Recon3D enables a three-dimensional view of gene variation in human metabolism. *Nat Biotechnol.* (2018) 36:272. doi: 10.1038/nbt.4072
30. Agren R, Bordel S, Mardinoglu A, Pornputtapong N, Nookaew I, Nielsen J. Reconstruction of genome-scale active metabolic networks for 69 human cell types and 16 cancer types using INIT. *PLoS Comp Biol.* (2012) 8:e1002518. doi: 10.1371/journal.pcbi.1002518
31. Blais EM, Rawls KD, Dougherty BV, Li ZI, Kolling GL, Ye P, et al. Reconciled rat and human metabolic networks for comparative toxicogenomics and biomarker predictions. *Nat Commun.* (2017) 8:1–15. doi: 10.1038/ncomms14250
32. Wang Y, Eddy JA, Price ND. Reconstruction of genome-scale metabolic models for 126 human tissues using mCADRE. *BMC Syst Biol.* (2012) 6:153. doi: 10.1186/1752-0509-6-153
33. Malik-Sheriff RS, Glont M, Nguyen TV, Tiwari K, Roberts MG, Xavier A, et al. BioModels - 15 years of sharing computational models in life science. *Nucleic Acids Res.* (2020) 48:D407–15. doi: 10.1093/nar/gkz1055

34. ENCODE Project Consortium. The ENCODE (ENCyclopedia of DNA elements) project. *Science*. (2004) 306:636–40. doi: 10.1126/science.1105136
35. Ecker JR, Bickmore WA, Barroso I, Pritchard JK, Gilad Y, Segal E. ENCODE explained. *Nature*. (2012) 489:52–4. doi: 10.1038/489052a
36. Mathelier A, Fornes O, Arenillas DJ, Chen CY, Denay G, Lee J, et al. JASPAR 2016: a major expansion and update of the open-access database of transcription factor binding profiles. *Nucleic Acids Res.* (2016) 44:D110–5. doi: 10.1093/nar/gkv1176
37. Matys V, Fricke E, Geffers R, Gößling E, Haubrock M, Hehl R, et al. TRANSFAC®: transcriptional regulation, from patterns to profiles. *Nucleic Acids Res.* (2003) 31:374–8. doi: 10.1093/nar/gkg108
38. Meyer PE, Kontos K, Lafitte F, Bontempi G. Information-theoretic inference of large transcriptional regulatory networks. *EURASIP J Bioinform Syst Biol.* (2007) 2007:1–9. doi: 10.1155/2007/79879
39. Margolin AA, Nemenman I, Basso K, Wiggins C, Stolovitzky G, Dalla Favera R, et al. ARACNE: an algorithm for the reconstruction of gene regulatory networks in a mammalian cellular context. *BMC Bioinform*. (2006) 7:S7. doi: 10.1186/1471-2105-7-S1-S7
40. Verfaillie A, Imrichová H, Van de Sande B, Standaert L, Christiaens V, Hulselmans G, et al. iRegulon: from a gene list to a gene regulatory network using large motif and track collections. *PLoS Comp Biol.* (2014) 10:e1003731. doi: 10.1371/journal.pcbi.1003731
41. Geurts P. dynGENIE3: dynamical GENIE3 for the inference of gene networks from time series expression data. *Sci Rep*. (2018) 8:1–12. doi: 10.1038/s41598-018-21715-0
42. Orchard S, Kerrien S, Abbani S, Aranda B, Bhate J, Bidwell S, et al. Protein interaction data curation: the international molecular exchange (IMEx) consortium. *Nat Methods*. (2012) 9:345–50. doi: 10.1038/nmeth.1931
43. Lynn DJ, Winsor GL, Chan C, Richard N, Laird MR, Barsky A, et al. InnateDB: facilitating systems-level analyses of the mammalian innate immune response. *Mol Syst Biol.* (2008) 4:218. doi: 10.1038/msb.2008.55
44. Breuer K, Foroushani AK, Laird MR, Chen C, Sribnaia A, Lo R, et al. InnateDB: systems biology of innate immunity and beyond—recent updates and continuing curation. *Nucleic Acids Res.* (2012) 41:D1228–33. doi: 10.1093/nar/gks1147
45. Bader GD, Betel D, Hogue CW. BIND: the biomolecular interaction network database. *Nucleic Acids Res.* (2003) 31:248–50. doi: 10.1093/nar/gkg056
46. Salwinski L, Miller CS, Smith AJ, Pettit FK, Bowie JU, Eisenberg D. The database of interacting proteins: 2004 update. *Nucleic Acids Res.* (2004) 32 (Suppl_1):D449–51. doi: 10.1093/nar/gkh086
47. Licata L, Briganti L, Peluso D, Perfetto L, Iannuccelli M, Galeota E, et al. MINT, the molecular interaction database: 2012 update. *Nucleic Acids Res.* (2012) 40:D857–61. doi: 10.1093/nar/gkr930
48. Orchard S, Ammari M, Aranda B, Breuza L, Briganti L, Broackes-Carter F, et al. The MIntAct project - IntAct as a common curation platform for 11 molecular interaction databases. *Nucleic Acids Res.* (2014) 42:D358–63. doi: 10.1093/nar/gkt1115
49. Oughtred R, Stark C, Breitkreutz B, Rust J, Boucher L, Chang C, et al. The BioGRID interaction database: 2019 update. *Nucleic Acids Res.* (2019) 47:D529–41. doi: 10.1093/nar/gky1079
50. Xia J, Benner MJ, Hancock REW. NetworkAnalyst-integrative approaches for protein–protein interaction network analysis and visual exploration. *Nucleic Acids Res.* (2014) 42:W167–74. doi: 10.1093/nar/gku443
51. Xia J, Gill EE, Hancock REW. NetworkAnalyst for statistical, visual and network-based meta-analysis of gene expression data. *Nat Protoc.* (2015) 10:823. doi: 10.1038/nprot.2015.052
52. Zhou G, Soufan O, Ewald J, Hancock REW, Basu N, Xia J. NetworkAnalyst 3.0: a visual analytics platform for comprehensive gene expression profiling and meta-analysis. *Nucleic Acids Res.* (2019) 47:W234–41. doi: 10.1093/nar/gkz240
53. Liu X, Chang C, Han M, Yin R, Zhan Y, Li C, et al. PPIExp: a web-based platform for integration and visualization of Protein-Protein interaction data and spatiotemporal proteomics data. *J Proteome Res.* (2018) 18:633–41. doi: 10.1021/acs.jproteome.8b00713
54. Gough NR. Science's signal transduction knowledge environment: the connections maps database. *Ann N Y Acad Sci.* (2002) 971:585–7. doi: 10.1111/j.1749-6632.2002.tb04532.x
55. Krull M, Pistor S, Voss N, Kel A, Reuter I, Kronenberg D, et al. TRANSPATH®: an information resource for storing and visualizing signaling pathways and their pathological aberrations. *Nucleic Acids Res.* (2006) 34 (Suppl_1):D546–51. doi: 10.1093/nar/gkj107
56. Law V, Knox C, Djoumbou Y, Jewison T, Guo AC, Liu Y, et al. DrugBank 4.0: shedding new light on drug metabolism. *Nucleic Acids Res.* (2014) 42:D1091–7. doi: 10.1093/nar/gkt1068
57. Qin C, Zhang C, Zhu F, Xu F, Chen SY, Zhang P, et al. Therapeutic target database update 2014: a resource for targeted therapeutics. *Nucleic Acids Res.* (2014) 42:D1118–23. doi: 10.1093/nar/gkt1129
58. Hecker N, Ahmed J, von Eichborn J, Dunkel M, Macha K, Eckert A, et al. SuperTarget goes quantitative: update on drug-target interactions. *Nucleic Acids Res.* (2012) 40:D1113–7. doi: 10.1093/nar/gkr912
59. Kuhn M, Szklarczyk D, Pletscher-Frankild S, Blicher TH, Von Mering C, Jensen LJ, et al. STITCH 4: integration of protein-chemical interactions with user data. *Nucleic Acids Res.* (2014) 42:D401–7. doi: 10.1093/nar/gkt1207
60. Gaulton A, Bellis LJ, Bento AP, Chambers J, Davies M, Hersey A, et al. ChEMBL: a large-scale bioactivity database for drug discovery. *Nucleic Acids Res.* (2012) 40:D1100–7. doi: 10.1093/nar/gkr777
61. Liu T, Lin Y, Wen X, Jorissen RN, Gilson MK. BindingDB: a web-accessible database of experimentally determined protein-ligand binding affinities. *Nucleic Acids Res.* (2007) 35 (Suppl_1):D198–201. doi: 10.1093/nar/gkl999
62. Yamanishi Y, Kotera M, Moriya Y, Sawada R, Kanehisa M, Goto S. DINIES: drug-target interaction network inference engine based on supervised analysis. *Nucleic Acids Res.* (2014) 42:W39–45. doi: 10.1093/nar/gku337
63. Jain A, Pasare C. Innate control of adaptive immunity: beyond the three-signal paradigm. *J Immunol.* (2017) 198:3791–800. doi: 10.4049/jimmunol.1602000
64. Gardy JL. Enabling a systems biology approach to immunology: focus on innate immunity. *Trends Immunol.* (2009) 30:249–62. doi: 10.1016/j.it.2009.03.009
65. Barsky A, Gardy JL, Hancock REW, Munzner T. Cerebral: a cytoscape plugin for layout of and interaction with biological networks using subcellular localization annotation. *Bioinformatics*. (2007) 23:1040–2. doi: 10.1093/bioinformatics/btm057
66. Bhattacharya S, Dunn P, Thomas CG, Smith B, Schaefer H, Chen J, et al. ImmPort, toward repurposing of open access immunological assay data for translational and clinical research. *Sci Data*. (2018) 5:180015. doi: 10.1038/sdata.2018.15
67. Shay T, Kang J. Immunological genome project and systems immunology. *Trends Immunol.* (2013) 34:602–9. doi: 10.1016/j.it.2013.03.004
68. Singh A, Shannon CP, Gautier B, Rohart F, Vacher M, Tebbutt SJ, et al. DIABLO: an integrative approach for identifying key molecular drivers from multi-omics assays. *Bioinformatics*. (2019) 35:3055–62. doi: 10.1093/bioinformatics/bty1054
69. Chaussabel D, Baldwin N. Democratizing systems immunology with modular transcriptional repertoire analyses. *Nat Rev Immunol.* (2014) 14:271–80. doi: 10.1038/nri3642
70. Li S, Sullivan NL, Rouphael N, Yu T, Banton S, Maddur MS, et al. Metabolic phenotypes of response to vaccination in humans. *Cell.* (2017) 169:862–77. e17. doi: 10.1016/j.cell.2017.04.026
71. Yeung A, Hale C, Clare S, Palmer S, Scott JB, Baker S, et al. Using a systems biology approach study host-pathogen interactions. *Bacteria Intracell.* (2019) 18:337–47. doi: 10.1128/microbiolspec.BAI-0021-2019
72. Yeung AT, Hale C, Lee AH, Gill EE, Bushell W, Parry-Smith D, et al. Exploiting induced pluripotent stem cell-derived macrophages to unravel host factors influencing chlamydia trachomatis pathogenesis. *Nat Commun.* (2017) 8:1–12. doi: 10.1038/ncomms15013
73. Elmassry MM, Mudaliar NS, Colmer-Hamood JA, et al. New markers for sepsis caused by *Pseudomonas aeruginosa* during burn infection. *Metabolomics*. (2020) 16:1–16. doi: 10.1007/s11306-020-01658-2
74. Baschal EE, Larson ED, Bootpetch Roberts TC, et al. Identification of novel genes and biological pathways that overlap in infectious and nonallergic diseases of the upper and lower airways using network analyses. *Front Genet*. (2020) 10:1352. doi: 10.3389/fgene.2019.01352

75. Sun X, Hua S, Gao C, Blackmer JE, Ouyang Z, Ard K, et al. Immune-profiling of ZIKV-infected patients identifies a distinct function of plasmacytoid dendritic cells for immune cross-regulation. *Nat Commun.* (2020) 11:1–13. doi: 10.1038/s41467-020-16217-5
76. Smith J. Immunological molecular responses of human retinal pigment epithelial cells to infection with *Toxoplasma gondii*. *Front Immunol.* (2019) 10:708. doi: 10.3389/fimmu.2019.00708
77. Mulindwa J, Matovu E, Enyaru J, Clayton C. Blood signatures for second stage human African trypanosomiasis: a transcriptomic approach. *BMC Med Genom.* (2020) 13:1–12. doi: 10.1186/s12920-020-0666-5
78. Schreiber F, Lynn DJ, Houston A, Peters J, Mwafulirwa G, Finlay BB, et al. The human transcriptome during nontyphoid Salmonella and HIV coinfection reveals attenuated NFκB-mediated inflammation and persistent cell cycle disruption. *J Infect Dis.* (2011) 204:1237–45. doi: 10.1093/infdis/jir512
79. Preziosi MJ, Kandel SM, Guiney DG, Browne SH. Microbiological analysis of nontyphoidal Salmonella strains causing distinct syndromes of bacteremia or enteritis in HIV/AIDS patients in San Diego, California. *J Clin Microbiol.* (2012) 50:3598–603. doi: 10.1128/JCM.00795-12
80. Scott MG, Dullaghan E, Mookherjee N, Glavas N, Waldbrook M, Thompson A, et al. An anti-infective peptide that selectively modulates the innate immune response. *Nat Biotechnol.* (2007) 25:465–72. doi: 10.1038/nbt1288
81. Mansour SC, de la Fuente-Núñez C, Hancock REW. Peptide IDR-1018: modulating the immune system and targeting bacterial biofilms to treat antibiotic-resistant bacterial infections. *J Peptide Sci.* (2015) 21:323–9. doi: 10.1002/psc.2708
82. Wu BC, Lee AHY, Hancock REW. Mechanisms of the innate defense regulator peptide-1002 anti-inflammatory activity in a sterile inflammation mouse model. *J Immunol.* (2017) 199:3592–603. doi: 10.4049/jimmunol.1700985
83. Mookherjee N, Hamill P, Gardy J, Blimkie D, Falsafi R, Chikatamarla A, et al. Systems biology evaluation of immune responses induced by human host defence peptide LL-37 in mononuclear cells. *Mol BioSyst.* (2009) 5:483–96. doi: 10.1039/b813787k
84. Hopkins AL. Network pharmacology: the next paradigm in drug discovery. *Nat Chem Biol.* (2008) 4:682. doi: 10.1038/nchembio.118
85. Mayer ML, Blohmke CJ, Falsafi R, Fjell CD, Madera L, Turvey SE, et al. Rescue of dysfunctional autophagy attenuates hyperinflammatory responses from Cystic Fibrosis cells. *J Immunol.* (2013) 190:1227–38. doi: 10.4049/jimmunol.1201404
86. Knox C, Law V, Jewison T, Liu P, Ly S, Frolkis A, et al. DrugBank 3.0: a comprehensive resource for 'omics' research on drugs. *Nucleic Acids Res.* (2010) 39 (Suppl_1):D1035–41. doi: 10.1093/nar/gkq1126
87. Saha S, Panigrahi DP, Patil S, Bhutia SK. Autophagy in health and disease: a comprehensive review. *Biomed Pharmacother.* (2018) 104:485–95. doi: 10.1016/j.biopha.2018.05.007
88. Blohmke CJ, Mayer ML, Tang AC, Hirschfeld AF, Fjell CD, Sze MA, et al. Atypical activation of the unfolded protein response in cystic fibrosis airway cells contributes to p38 MAPK-mediated innate immune responses. *J Immunol.* (2012) 189:5467–75. doi: 10.4049/jimmunol.1103661
89. Cheng F, Desai RJ, Handy DE, Wang R, Schneeweiss S, Barabási AL, et al. Network-based approach to prediction and population-based validation of *in silico* drug repurposing. *Nat Commun.* (2018) 9:1–12. doi: 10.1038/s41467-018-05116-5
90. Cheng F, Murray JL, Zhao J, Sheng J, Zhao Z, Rubin DH. Systems biology-based investigation of cellular antiviral drug targets identified by gene-trap insertional mutagenesis. *PLoS Comp Biol.* (2016) 12:e1005074. doi: 10.1371/journal.pcbi.1005074
91. Han Z, Xue W, Tao L, Zhu F. Identification of novel immune-relevant drug target genes for Alzheimer's disease by combining ontology inference with network analysis. *CNS Neurosci Ther.* (2018) 24:1253–63. doi: 10.1111/cns.13051
92. Abhyankar V, Bland P, Fernandes G. The role of systems biologic approach in cell signaling and drug development responses - a mini review. *Med Sci.* (2018) 6:43. doi: 10.3390/medsci6020043

Conflict of Interest: The authors declare that the research was conducted in the absence of any commercial or financial relationships that could be construed as a potential conflict of interest.

frontiers in Immunology

ORIGINAL RESEARCH
published: 19 August 2020
doi: 10.3389/fimmu.2020.01876

Assessment of Immunogenicity of Adjuvanted Quadrivalent Inactivated Influenza Vaccine in Healthy People and Patients With Common Variable Immune Deficiency

Aristitsa Mikhailovna Kostinova[1], Nelli Kimovna Akhmatova[2], Elena Alexandrovna Latysheva[1], Yulia Alexeevna Dagil[1], Svetlana Valentinovna Klimova[1], Anna Egorovna Vlasenko[3], Ekaterina Alexandrovna Khromova[2], Tatyana Vasilievna Latysheva[1] and Mikhail Petrovich Kostinov[2]*

[1] National Research Center Institute of Immunology Federal Medical-Biological Agency of Russia, Moscow, Russia, [2] Federal State Budgetary Scientific Institution I. Mechnikov Research Institute of Vaccines and Sera, Moscow, Russia, [3] Novokuznetsk State Institute for Advanced Training of Physicians, Branch Campus of the Russian Medical Academy of Continuous Professional Education, Novokuznetsk, Russia

OPEN ACCESS

Edited by:
Simon Daniel Van Haren, Boston Children's Hospital, Harvard Medical School, United States

Reviewed by:
Corey Patrick Mallett, GlaxoSmithKline, Italy
Giuseppe Andrea Sautto, University of Georgia, United States
Esther Blanco, Instituto Nacional de Investigación y Tecnología Agraria y Alimentaria (INIA), Spain

***Correspondence:**
Aristitsa Mikhailovna Kostinova
aristica_kostino@mail.ru

Specialty section:
This article was submitted to Vaccines and Molecular Therapeutics, a section of the journal Frontiers in Immunology

Received: 23 April 2020
Accepted: 13 July 2020
Published: 19 August 2020

Citation:
Kostinova AM, Akhmatova NK, Latysheva EA, Dagil YA, Klimova SV, Vlasenko AE, Khromova EA, Latysheva TV and Kostinov MP (2020) Assessment of Immunogenicity of Adjuvanted Quadrivalent Inactivated Influenza Vaccine in Healthy People and Patients With Common Variable Immune Deficiency. Front. Immunol. 11:1876. doi: 10.3389/fimmu.2020.01876

Background: Recent addition to vaccines of adjuvants has been actively used to enhance the immunogenicity. However, the use of adjuvants for the development of quadrivalent inactivated influenza vaccines (QIV) is currently limited. The aim of this study was to examine immunogenicity of adjuvanted QIV in healthy people and patients with primary immune deficiency—common variable immune deficiency (CVID).

Methods: In total before the flu season 2018–2019 in the study were involved 32 healthy volunteers aged 18–52 years and 6 patients with a confirmed diagnosis of CVID aged 18–45 years. To evaluate antibody titers 21 days after vaccination against the influenza A and B strains a hemagglutination inhibition assay (HI) was used.

Results: In healthy volunteers adjuvanted QIV has proved its immunogenicity to strains A/H1N1, A/H3N2, B/Phuket and B/Colorado in seroprotection (90, 97, 86, and 66%, respectively), seroconversion (50, 60, 52, and 45%, respectively), GMR (6.2, 5.7, 4.2, and 3.4, respectively). Statistically significant differences in the level of all criteria were revealed between groups of healthy and CVID patients regardless of the virus strain. Most patients with CVID showed an increase in post-vaccination antibody titer without reaching conditionally protective antibody levels.

Conclusion: Immunization with single dose of adjuvanted QIV with decreased amount of hemagglutinin protein to all virus strains due to the use of azoximer bromide forms protective immunity in healthy people, but in patients with CVID the search for new vaccination schemes is the subject of further investigations, as well as the effectiveness of boosterization with adjuvant vaccines.

Keywords: adjuvanted QIV, immunogenicity, influenza, vaccination, CVID, azoximer bromide

INTRODUCTION

Influenza virus infection, caused by single-stranded RNA viruses belonging to the Orthomyxoviridae family, is associated with significant morbidity and mortality worldwide, and affects particularly risk groups such as patients with cardiopulmonary conditions, pregnant women and children, old people and immunocompromised patients. It impacts all countries: every year, there are an estimated 1 billion cases, 3–5 million severe cases, and 290–650 000 influenza-related respiratory deaths worldwide (1).

The first vaccine against the influenza virus was created in 1944, included two strains of the influenza virus until in 1978 was developed the first trivalent both inactivated (TIV) and live attenuated influenza vaccine, which was broadly used for immunization (2). The vaccine included two strains of type A influenza virus and one of two genetically distinct type B influenza lineages (Yamagata or Victoria) which WHO annually choose for inclusion in formulation of influenza vaccines in Northern and Southern hemispheres (3). However, an analysis over 10 years in the USA and 8 years in Europe showed a mismatch between the circulating in population seasonal lineage and the vaccine Lineage of type B influenza virus in 25–50% seasons from 2001to 2011 years of analysis (4, 5). The same situation was seen in the Russian Federation in the period from 2006 to 2015, when the mismatch was found in 3 of 9 seasons (6). That is why in 2012 WHO recommended for use new inactivated quadrivalent influenza vaccines which include both B lineages besides both A strains.

Two modeling studies performed in the USA and Germany concluded that QIV could have prevented ∼395,000 infections per year in the world and at least 30,000 cases, 3,500 hospitalizations, and 700 deaths in the USA population caused by B lineage mismatch (7, 8).

In numerous studies conducted both at the preclinical stage and already in vaccinated adults, inactivated QIV was as immunogenic as seasonal TIV, with equivalent efficacy against the shared three strains included in TIV, and a superior immunogenicity against the non-TIV B lineage (9).

In recent decades, addition to vaccines of adjuvants, that allow to reduce the amount of included antigens with the level of post-vaccination IgG which are synthesized in a short time at the same or even higher level than after non-adjuvant vaccines, have been used to enhance the immunogenicity. However, the use of adjuvants for the development of QIV is currently limited.

Adjuvant is a non-specific immunostimulant of inorganic and organic genesis, which increases the specific immune response to antigens. They have been used for over 90 years and currently are the components of more than 30 licensed vaccines, among them influenza vaccines from different manufacturers (10). The inclusion of an adjuvant allows to reduce the amount of virus antigen and the number of immunizations (doses) to create a stable immunity to infectious diseases. For example, in the UK, an influenza vaccine containing 15 strains of the virus is currently being developed, while the dose of antigen in it is reduced by 100 times, due to the remaining danger of a pandemic, according to the WHO (11). Despite different mechanism, almost all adjuvants initially influence on antigen-presenting cell (12, 13). In addition, some of them are able to interact with B-lymphocytes, that also leads to stimulation of the humoral immunity.

In studies conducted in Russia devoted to a trivalent subunit polymer (immuno-adjuvant) influenza vaccine containing 5 μg of antigens of two virus strains type A and one virus strains type B, and azoximer bromide used as an adjuvant, it was shown that specific antibodies were synthesized in values similar to subunit non-adjuvant vaccines (14). It can be assumed that when using the same amount of adjuvant (500 μg of azoximer bromide), but with an increased number of different virus antigens, a similar effect will be obtained.

It is especially important to achieve protection against influenza in patients with defects in the humoral immunity, who respond with a low level of specific antibodies or lack of their synthesis after vaccination. It should be noted that one of the criteria for the diagnosis of common variable immune deficiency (CVID) in a group of patients with primary immunodeficiency (PID) with defects predominantly in the humoral immunity is a poor antibody response to vaccines, i.e., absence of protective levels despite vaccination (15).

To our knowledge, currently only three studies have examined the formation of post-vaccination immune response in a limited number of CVID patients, where are reported data on their ability to synthesize specific antibodies and induce cell immunity in response to influenza vaccines (16–18). Two of them were conducted with the use of adjuvanted influenza pandemic vaccine A/California/7/2009 (H1N1)-like split virus (X179a) adjuvanted with the oil-in-water emulsion AS03. In the study of Pedersen et al. the number of participants with CVID was only 3, while the author reported that two of them responded to the vaccination by a >4-fold rise in haemagglutination inhibition (HI) antibodies (19). In another study of the same vaccine, published in 2018, 48 CVID patients were vaccinated against influenza, and it was detected that 8 (16.7%) patients had reached a ≥1:40 titer of specific antibodies against the pandemic influenza A(H1N1) antigen: 4 after the first vaccination, the other 4—after booster dose 1 month later (67–98.3% of healthy people form protective antibody levels since 21days after a single dose of Pandemrix®) (20). In the third study after immunization with a non-adjuvant influenza vaccine 1 of 8 responded by synthesis if antibodies against at least 1 of the 3 vaccine strains (17).

AIM OF THE STUDY

To examine the formation of humoral immunity after immunization with the quadrivalent inactivated subunit adjuvanted influenza vaccine to virus strains in healthy people and patients with CVID.

MATERIALS AND METHODS

In an open-label, single-center, non-randomized, prospective, cohort, controlled study the effect of influenza tetravalent inactivated subunit adjuvanted vaccine on antibody synthesis in healthy volunteers and patients with CVID was examined.

Patient Description

In total before the flu season 2018–2019 in study were enrolled 32 healthy volunteers aged 18–52 years. The comparison group consisted of 6 patients with a confirmed diagnosis of Common variable immune deficiency aged 18–45 years who met the inclusion criteria.

CVID is one of the most frequently diagnosed primary immunodeficiencies. People with CVID are highly susceptible to bacterial or more rarely viral invaders and often develop recurrent infections, particularly in the lungs, sinuses, and ears. The characteristic laboratory features include low levels of serum immunoglobulins [marked decrease of IgG and marked decrease of IgA with or without low IgM levels (measured at least twice; <2SD of the normal levels for age)], which causes an increased susceptibility to infection (18). Another part of the diagnosis of CVID is a lack of functional antibody in serum against vaccine antigens such as tetanus, diphtheria, pneumococcal polysaccharide (21). They have absence of protective levels despite vaccination. The treatment of CVID is monthly intravenous immunoglobulin (IVIG) replacement therapy during all life period. All the important IgG antibodies presented in normal population are extracted from a large pool of human plasma from donors.

Inclusion Criteria

- Healthy volunteers aged from 18 to 52 years without chronic bronchopulmonary, cardiovascular, rheumatological diseases, hepatic or renal impairment, metabolic disorders confirmed by anamnestic data or objective clinical examination.
- Confirmed diagnosis CVID in accordance with diagnostic criteria established by the European Society for Immunodeficiency Diseases (http://esid.org/WorkingParties/Registry/Diagnosis-criteria) and the American Academy of Allergy, Asthma and Immunology for the diagnosis and treatment of PID.
- IVIG therapy no later than 28 days before vaccination and no earlier than 21 days after it, that is, a break between two subsequent administrations of immunoglobulins for at least 7 weeks.
- Signed informed consent.

Exclusion Criteria

- Symptoms of influenza or flu-like illness in the past 6 months.
- Symptoms of acute infection at the time of vaccination and during 1 month before current vaccination.
- Glucocorticosteroid or other immunosuppressive therapy admission at the time of the study and 3 months before the start.
- Symptoms of enteropathy with protein loss in patients with CVID at the time of the study.

All participants in the previous season (2017–2018) did not receive influenza vaccine and no influenza infection was registered, although in the 2016–2017 season some of the healthy volunteers were immunized against influenza that was not observed among patients with CVID who have not been vaccinated in previous two flu seasons.

Vaccination was conducted in the Department of Immunopathology in the Institute of Immunology of the FMBA of Russia. The laboratory part of the study was carried out in the laboratory of the Mechanisms of immune regulation in Mechnikov Research Institute of Vaccines and Sera in Moscow. The study was conducted according to the Russian Federation National Standard Protocol ГОСТР 52379-2005 Good Clinical Practice≫ and International GCP standards (22). The study was based on the ethical principles and recommendations of the WHO and the Russian Ministry of Health. All patients signed the informed consent for the participation.

Vaccines

First immunization was carried out on the 26 of November 2018 and the last on the 21 of February 2019. Single-dose vaccination was performed according to the manufacturer's instructions. All patients received the Quadrivalent inactivated subunit adjuvanted influenza vaccine Grippol® Quadrivalent (NPO Petrovax Pharm LLC, Russia).

Grippol® Quadrivalent is the first Russian quadrivalent inactivated subunit adjuvanted influenza vaccine manufactured in Russia full-cycle starting from active pharmaceutical ingredient production to the applicable GMP regulations. Grippol Quadrivalent contained four viral strains as recommended by the WHO: A/Michigan/45/2015 (H1N1) pdm09-like virus; A/Singapore/INFIMH-16-0019/2016 (H3N2)-like virus; B/Colorado/06/2017-like virus (B/Victoria/2/87 lineage); B/Phuket/3073/2013-like virus (B/Yamagata/16/88 lineage).

The key benefit of the vaccine is a decreased amount of hemagglutinin protein due to the use of Polyoxidonium (azoximer bromide)—a water-soluble high-molecular immune system adjuvant that enhances the immune response to vaccination and provides for cutting the antigen load three-fold as compared to traditional technologies. This antigen sparing technology is unique; for more than 20 years, it has been used in Russia to produce vaccines that have been successfully administered within the framework of the national immunization schedules in the Russian Federation and other countries. In 1 vaccination dose (0.5 ml) there are 20 μg of antigens (5 μg of hemagglutinin of each strain) and 500 mcg of azoximer bromide.

Blood Samples

Serum intake for determining the level of virus-specific antibodies was performed before vaccination, 21–22 days and 3 months after vaccination. On the 21–22 days after vaccination, the study participants in the group of patients with CVID were scheduled to undergo IVIG therapy in a standard dose of 0.4 g/kg. The next sampling of whole blood was 3 months after vaccination on the background of IVIG therapy.

Laboratory Methods

To evaluate antibody titers against the influenza A and B strains a HI assay was used as recommended by CDC method for evaluating the immunogenicity of influenza vaccines (23). To remove non-specific inhibitors of hemagglutination, test sera were incubated at 37°C overnight (19 ± 1 h) at 1:4 dilution

with receptor-destroying enzyme (RDE; Denka Seiken, Tokyo, Japan) followed by a 30-min inactivation step at 56°C and further dilution to 1:10 with phosphate-buffered saline (PBS). HI assay was performed with 0.5% chicken RBC and 4 hemagglutination units of antigens. Antigens for HI assay were provided by Smorodintsev Research Institute of Influenza (WHO National Influenza Center of Russia, Saint-Petersburg).

To determine specific antibodies were used strains, recommended by WHO for quadrivalent vaccines in 2018–2019 influenza season: A/H1N1/Michigan 45/15, A/H3N2/Singapore/INFMH-16-0019/16, B/Colorado/06/17 (B/Victoria lineage), and B/Phuket/3073/13 (B/Yamagata lineage).

To evaluate immunogenicity of the influenza vaccine according to the Guideline on clinical evaluation of vaccines of the Committee on Human Medicinal Products (CHMP) criteria for adult patients were used (24):

(1) Seroprotection level—percentage of vaccinated patients with a hemagglutinin-inhibiting antibodies titer ≥1:40 on the 21 day after vaccination (reference level—over 70%).
(2) Seroconversion level—percentage of vaccinated patients with either a pre-vaccination HI titer <10 and a post-vaccination HI titer ≥40 or a pre-vaccination HI titer ≥10 and a ≥4-fold increase in HI titer on the 21 day after vaccination (reference level—over 40%)
(3) Geometric mean antibody titers (GMT)
(4) Geometric mean ratio (GMR)—increase in the mean geometric titer of hemagglutinin-inhibiting antibodies on the 21 days after vaccination compared to baseline (reference level—over 2.5-fold).

The efficacy and immunogenicity of the vaccine is considered to be satisfactory if the vaccine meets at least one of these criteria.

Statistical Analysis

For the intergroup comparison of qualitative signs (seroprotection and seroconversion levels) the Chi-Square test was used, in the case of cells in the table with expected frequencies of <5%, the exact Fisher test was used. Comparison of qualitative characteristics in related samples (in the dynamics between control points) was carried out using the McNemar test. Descriptive statistics of qualitative characteristics are represented by the fraction, 95% confidence interval of the fraction calculated by the Clopper-Pearson method, and the absolute number of subjects with the studied characteristic in the total number of group (n/N). Descriptive statistics of quantitative characteristics

TABLE 1 | Seroprotection level in the groups of healthy participants and patients with CVID.

Virus strain	Period	Healthy participants ($n = 32$)			Patients with CVID (n = 6)			Between groups[a]
		People	%	95%CI	People	%	95%CI	
A/H1N1/ Michigan	Before vaccination	20/32	63	[43-79]	2/6	33	[4-78]	$p = 0.22$
	After 3 weeks	27/30	90	[73-98]	2/6	33	[4-78]	**$p = 0.008$**
	After 3 months	8/9	89	[52-100]	3/6	50	[12-88]	$p = 0.24$
Dynamics analysis[b]		**$p^{1-0} = 0.04$,** $p^{3-1} = 1.00$				$p^{1-0} = 1.00$, $p^{3-1} = 1.00$		-
A/H3N2/ Singapore	Before vaccination	22/32	69	[50-84]	2/6	33	[4-78]	$p = 0.17$
	After 3 weeks	29/30	97	[83-100]	3/6	50	[12-88]	**$p = 0.01$**
	After 3 months	7/9	78	[40-97]	4/6	67	[22-96]	$p = 1.00$
Dynamics analysis		**$p^{1-0} = 0.02$,** $p^{3-1} = 0.50$				$p^{1-0} = 1.00$, $p^{3-1} = 1.00$		-
B/Colorado	Before vaccination	7/31	23	[10-41]	0/6	0	[0–46]	$p = 0.57$
	After 3 weeks	19/29	66	[46-82]	0/6	0	[0-46]	**$p = 0.005$**
	After 3 months	6/9	67	[30-93]	0/6	0	[0-46]	**$p = 0.03$**
Dynamics analysis		**$p^{1-0} = 0.002$,** $p^{3-1} = 1.00$				$p^{1-0} = 1.00$, $p^{3-1} = 1.00$		**-**
B/Phuket	Before vaccination	13/31	42	[25-61]	0/6	0	[0–46]	$p = 0.07$
	After 3 weeks	25/29	86	[68-96]	0/6	0	[0-46]	**$p < 0.001$**
	After 3 months	7/9	78	[30-93]	0/6	0	[0-46]	**$p = 0.007$**
Dynamics analysis		**$p^{1-0} < 0.001$,** $p^{3-1} = 1.00$				$p^{1-0} = 1.00$, $p^{3-1} = 1.00$		-

[a]The exact Fisher test was used, [b]the McNemar test with the Holm-Bonferroni correction was used, p-value$^{1-0}$, p-value$^{3-1}$–the statistical significance of the difference between the control point of 3 weeks and the initial level and between the control points of 3 months and 3 weeks, respectively.

Differences in seroprotection levels to strains A/H1N1 and A/H3N2 between groups of healthy control and CVID patients were observed 3 weeks after vaccination. Seroprotection levels to strains B/Colorado and B/Phuket between these groups statistically significant differed both 3 weeks and 3 months after vaccination.

Bold values indicate seroprotection reference levelis over 70%.

are represented by the geometric mean and its 95% confidence interval. To apply the statistical criteria the initial quantitative data were pre-logarithmized and checked for compliance with the normal distribution (the Shapiro-Wilks test was used). The check showed that all the pre-logarithmized data correspond to the normal distribution. To compare two independent groups by quantitative criteria, the Student criterion was used (in the absence of equality of variances, which was checked by the Livin test, the Student criterion with the Welch modification was used). Comparison of quantitative characteristics in related groups (in the dynamics between control points) was carried out by the Student criterion for related samples. Calculation of criteria for quantitative characteristics was carried out on logarithmized data. The analysis assumed a comparison between the values of characteristics at the control point of 1 month and the initial level and control points of 3 months and 1 month; if a statistically significant difference for 1–3 months was detected, the values of characteristics at the control point of 3 months was compared with the initial level. All calculations were carried out in a freely distributed statistical environment R (v.3.6), the "stats" package (v.3.6.2) was used.

RESULTS

Seroprotection Level

Analysis of the results with assessment of the seroprotection level in the groups of healthy participants and CVID patients is presented in **Table 1** and **Figure 1**.

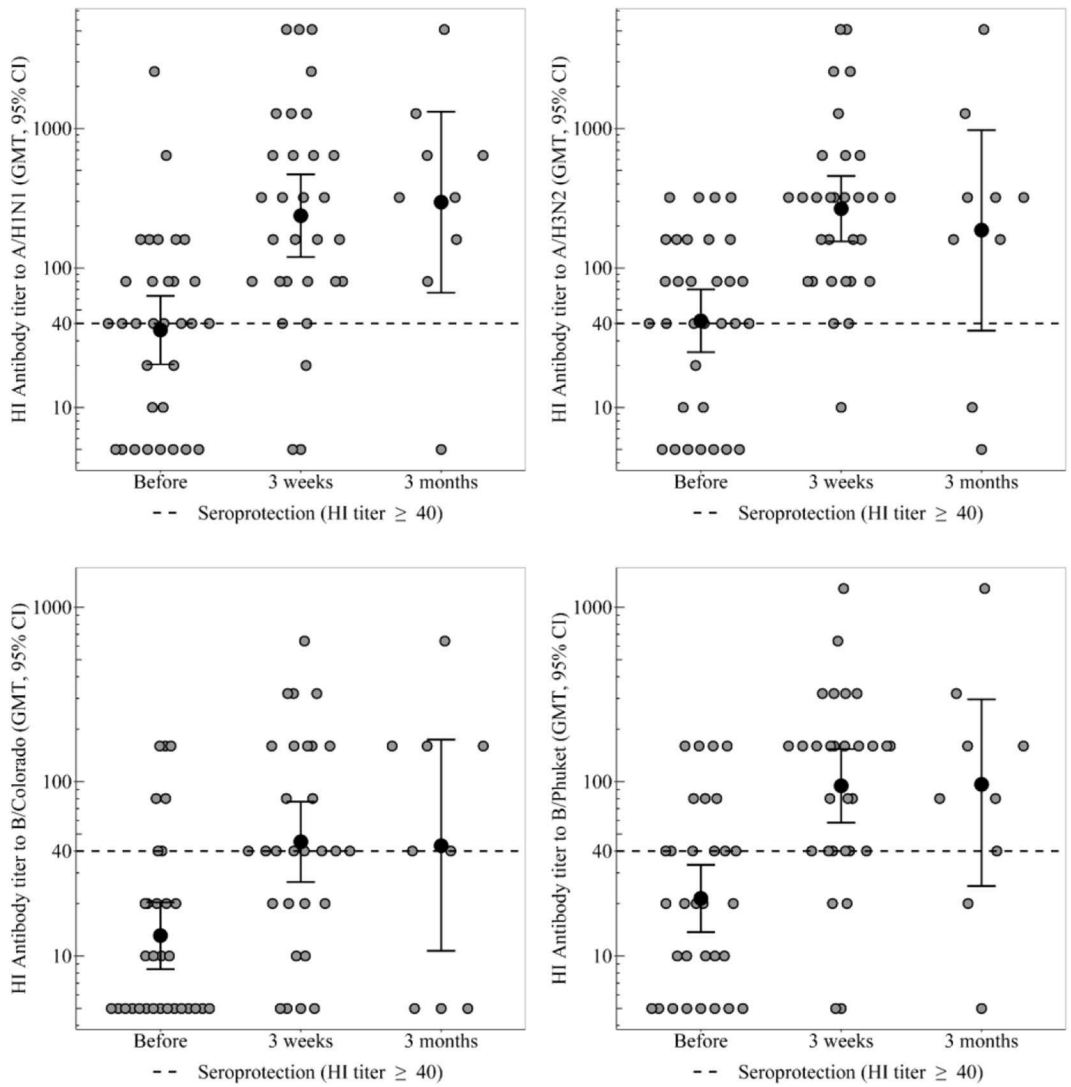

FIGURE 1 | HI antibody titers, which show the individual titers of healthy participants and GMT (95% CI) in the group of healthy participants. In the group of healthy participants, a statistically significant increase in the proportion of seropositive was observed 3 weeks after immunization toward all strains. Three months after vaccination statistically significant decrease in seroprotection level was not detected for any strain. In the group of CVID patients the GMT remains unchanged throughout the whole period, regardless of any strain. In the group of healthy participants a 3 weeks after immunization statistically significant increase in antibody titer was observed for all virus strains.

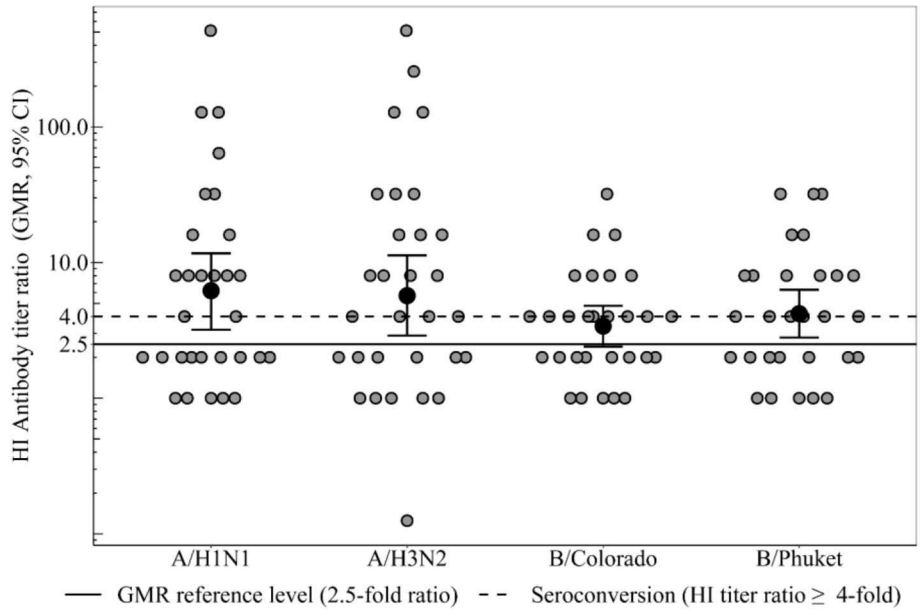

FIGURE 2 | HI antibody titers ratio (3 weeks after immunization), which show the ratio of individual titers of healthy participants and GMR (95% CI) in the group of healthy participants. Seroconversion level in the group of healthy participants 3 weeks after immunization to all vaccine influenza virus strains met the CHMP criterion (not <40%). GMR in the group of healthy participants for all 4 strains meets the CHMP criterion of effectiveness (at least 2.5). In the group of patients with CVID GMR did not reach the threshold minimum for any strain.

In the group of healthy participants, a statistically significant increase in the proportion of seropositive was observed 3 weeks after immunization toward all strains. As a result, seroprotection level to strains A/H1N1, A/H3N2, and B/Phuket meets the criterion of CHMP effectiveness (at least 70%) and is 90, 97, and 86%, respectively. Seroprotection level to strain B/Colorado is 66% that is close to the threshold value. 3 months after vaccination in the group of healthy participants the seroprotection level remains the same or slightly lower than achieved a month after immunization; statistically significant decrease was not detected for any strain.

The proportion of seropositive in the group of CVID patients did not change statistically significant after vaccination, remaining at the level of 0% to strains B/Colorado and B/Phuket, 33–50% to strain A/H1N1 and 33–67% to strain A/H3N2.

Initially, before vaccination, regardless of the strain, the proportion of seropositive between groups of healthy control and CVID patients did not statistically significant differ. Differences in seroprotection levels to strains A/H1N1 and A/H3N2 between groups of healthy control and CVID patients were observed 3 weeks after vaccination. Seroprotection levels to strains B/Colorado and B/Phuket between these groups statistically significant differed both 3 weeks and 3 months after vaccination. Probably no differences were detected after 3 months, due to a slight increase in proportion of seropositive among CVID patients and a small amount of them.

Seroconversion Level

Seroconversion level in the group of healthy participants 3 weeks after immunization (**Figure 2**) to strain A/H1N1 was 50% [95%CI = [31–69%], 15 participants out of 30], to strain A/H3N2−60% [95%CI = [41–77%], 18 out of 30], to strain B/Colorado−45% (95%CI = [26–64%], 13 out of 29], to strain B/Phuket−52% [95%CI = [33–71%], 15 out of 29] that meets the CHMP criterion (not <40%). In the group of CVID patients seroconversion level (**Table 2**) was 0% to all strains except strain A/H3N2−17% (one person out of six). Thus, statistically significant differences in the level of seroconversion were revealed between groups of healthy and CVID patients regardless of the virus strain.

Geometric Mean Rate

GMR in the group of healthy participants (**Figure 2**) for all four strains meets the CHMP criterion of effectiveness (at least 2.5) and amounts to strain A/H1N1 6.2, to strain A/H3N2 5.7, to strain B/Colorado 3.4 and to strain B/Phuket 4.2. In the group of patients with CVID GMR did not reach the threshold minimum for any strain. Thus, GMR is statistically significant higher in the group of healthy participants compared with CVID patients regardless of the virus strain (**Table 2**).

Geometric Mean Antibody Titers

GMT in the groups of healthy and CVID patients are presented in the **Table 3** and **Figure 1**.

In the group of healthy participants a 3 weeks after immunization statistically significant increase in antibody titer was observed for all virus strains. Three months after vaccination the GMT of antibodies remains unchanged relatively to the 3 weeks level.

In the group of CVID patients the GMT remains unchanged throughout the whole period, regardless of any strain. As a result the groups of healthy and CVID patients differ statistically significant throughout the post-vaccination period, regardless of any strain.

TABLE 2 | Individual HI antibody titers, seroconversion level and GMR in the group of CVID patients.

Strains	Patients	HI antibody titers from individual patient			HI Antibody titers ratio (3 weeks)
		Before	3 weeks	3 months	
A/H1N1	1	20	10	10	0.5
	2	20	20	20	1
	3	40	40	40	1
	4	20	20	20	1
	5	20	20	40	1
	6	80	40	40	0.5
	Seroconversion level (3 weeks): 0%, 95%CI = [0–46%], $p = 0.03$—compared to healthy[a]				
	GMR (3 weeks): 0.8, 95%CI = [0.5–1.2], $p < 0.001$—compared to healthy[b]				
A/H3N2	1	10	5	5	0.5
	2	5	5	20	1
	3	40	40	40	1
	4	10	80	40	8
	5	20	20	40	1
	6	80	80	40	1
	Seroconversion level (3 weeks): 17%, 95% CI = [0–64%], $p = 0.05$—compared to healthy				
	GMR (3 weeks): 1.3, 95% CI = [0.5–3.4], $p = 0.014$—compared to healthy				
B/Colorado	1	5	5	5	1
	2	5	5	5	1
	3	10	10	20	1
	4	5	10	20	2
	5	5	5	10	1
	6	20	10	10	0.5
	Seroconversion level (3 weeks): 0%, 95% CI = [0–46%], $p = 0.04$—compared to healthy				
	GMR (3 weeks): 1.0, 95% CI = [0.6–1.6], $p = 0.002$—compared to healthy				
B/Phuket	1	10	5	5	0.5
	2	10	10	10	1
	3	20	10	10	0.5
	4	5	5	10	1
	5	10	10	10	1
	6	20	20	20	1
	Seroconversion level (3 weeks): 0%, 95% CI = [0–46%], $p = 0.03$—compared to healthy				
	GMR (3 weeks): 0.8, 95% CI = [0.5–1.2], $p < 0.001$—compared to healthy				

[a] *The exact Fisher test was used,* [b] *the Mann-Whitney test was used.*

DISCUSSION

What Is Known About Adjuvanted TIV (aTIV)?

Currently, the use of the trivalent adjuvant vaccine against influenza virus in the world is proved in people ≥65 years old compared with QIV and non-adjuvant TIV in accordance with the statement by the Public Health England and Joint Committee on Vaccination and Immunization (25).

Monovalent A(H1N1) influenza vaccine with adjuvant AS03 (Pandemrix®, GlaxoSmithKline, Belgium) was widely used during a pandemic 2009–2010 influenza season in order to form a specific immune response in a short time, both among a healthy adult population and immunocompromised patients (boosted after 1 month), in whom it showed encouraging results.

The European adjuvanted influenza vaccine with MF59C.1® which is composed of 9.75 mg squalene showed significant immunogenicity. Moreover, several meta-analyses have shown a statistical superiority of aTIV, independently from the (sub)type considered, and high immunogenicity against drifted/heterologous strains, especially against A(H3N2) (26).

In numerous investigations conducted in Russia, it was shown that the immunogenicity and protective properties of antigens, attached to the synthetic high molecular weight polymer carrier—azoximer bromide, increase tens of times, enhance both antibody and cell-mediated immune responses, enlarges synthesis of all classes of protective antibodies (IgM, IgG, IgA), except IgE (27). Thus, it is a strong activator of B- and T-lymphocytes and this finding has led for subsequent clinical use in various groups of patients with abnormalities in immune system, as well as for the production of influenza vaccines.

The first adjuvanted influenza vaccine (Grippol) in Russia was introduced into healthcare practice in 1997 and contained in addition to 500 μg of azoximer bromide 5 μg of hemagglutinin each of the influenza viruses type A (A/H1N1 and A/H3N2) and 11 μg of type B (one lineage) influenza virus. Then in 2008 Grippol Plus vaccine was registered with a reduced number of antigens of the influenza virus type B from 11 to 5 μg without losing its immunogenic properties.

At the stage of clinical registration studies among adults of Grippol plus and the tetravalent vaccine (Grippol Quadrivalent—appeared in Russia in 2018), containing 500 μg of azoximer bromide in addition to 5 μg of hemagglutinin from each of 3 or 4 strains of influenza A and B viruses, respectively, their accordance with the immunogenicity criteria for inactivated influenza vaccines was proved for all strains: for TIV the level of seroprotection was 76–95%; in seronegative individuals, the level of seroconversion reached 73–95%, the geometric mean rate (GMR) 6.7–23.6 (28–30); for QIV 1 month after vaccination of healthy volunteers, the seroconversion level to strains A/H1N1, A/H3N2, and B/Yamagata, B/Victoria was 65.8, 69.3, 65.8, and 67.8%, respectively, and the geometric mean rate (GMR)—4.9, 5.3, 5.4, and 4.8 respectively.

Numerous post-registration studies conducted in 2009–2019 were devoted to assessing the safety, immunogenicity, prophylactic and clinical efficacy of the trivalent polymer subunit vaccine against influenza in different risk groups, such as:

TABLE 3 | GMT in the groups of healthy participants and CVID patients.

Strains	Period	Healthy participants		Patients with CVID		Between groups[a]
		GMT	95%CI	GMT	95%CI	
A/H1N1	Before vaccination	35.9	[20.4–63.1]	28.3	[15.4–52.0]	$p = 0.72$
	After 3 weeks	237.0	[119.8–468.7]	22.4	[13.0–38.8]	$\mathbf{p < 0.001}$
	After 3 months	296.3	[66.5–1319.7]	25.2	[13.9–45.6]	$\mathbf{p = 0.01}$
	Dynamics analysis [b,c]	$\mathbf{p^{1-0} < 0.001}$, $p^{3-1} = 0.09$		$p^{1-0} = 0.17$, $p^{3-1} = 0.36$		–
A/H3N2	Before vaccination	41.8	[24.9–70.2]	17.8	[6.1–52.0]	$p = 0.18$
	After 3 weeks	266.0	[155.1–456.1]	22.4	[5.9–85.3]	$\mathbf{p < 0.001}$
	After 3 months	186.8	[35.5–972.6]	25.0	[10.4–60.3]	$\mathbf{p = 0.05}$
	Dynamics analysis	$\mathbf{p^{1-0} < 0.001}$, $p^{3-1} = 0.08$		$p^{1-0} = 0.57$, $p^{3-1} = 0.74$		–
B/Colorado	Before vaccination	13.1	[8.4–20.3]	7.1	[3.8–13.0]	$p = 0.07$
	After 3 weeks	45.2	[26.6–76.7]	7.1	[4.8–10.5]	$\mathbf{p < 0.001}$
	After 3 months	42.9	[10.7–174.2]	10.0	[5.5–19.1]	$\mathbf{p = 0.05}$
	Dynamics analysis	$\mathbf{p^{1-0} < 0.001}$, $p^{3-1} = 0.07$		$p^{1-0} = 1.00$, $p^{3-1} = 0.08$		–
B/Phuket	Before vaccination	21.4	[13.7–33.3]	11.2	[6.5–19.4]	$p = 0.21$
	After 3 weeks	94.6	[58.1–153.8]	8.9	[5.2–15.4]	$\mathbf{p < 0.001}$
	After 3 months	86.4	[25.2–296.7]	10.0	[6.3–15.8]	$\mathbf{p = 0.007}$
	Dynamics analysis	$\mathbf{p^{1-0} < 0.001}$, $p^{3-1} = 0.07$		$p^{1-0} = 0.17$, $p^{3-1} = 0.36$		–

[a] *Student criterion was used,* [b] *Student criterion was used for paired samples,* [c] *all criteria were counted on pre-logarithmized data.*
The groups of healthy and CVID patients differ statistically significant throughout the post-vaccination period, regardless of any strain.
Bold values indicate seroprotection reference levelis over 70%.
p-values $^{1-0,\ 3-1}$*? the statistical significance of the difference between the control point of 3 weeks and the initial level and between the control points of 3 months and 3 weeks, respectively.*

pregnant women (31–38), elderly people aged 60 and over with cardiovascular system diseases (39, 40), children and adults with asthma and other chronic obstructive respiratory tract diseases (41–44), that showed high immunogenicity and good tolerance in all participants from risk groups who are subject to vaccination as part of the Russian national immunization program. Even in patients ≥60 years with diseases of cardiovascular system the level of seroconversion was 49.5–68.5%, GMR was 2.8–5.7, and seroprotection was 83.7–84.8%.

What Is Known About QIV?

According to the results of numerous investigations carried out at the clinical stages of QIV studies and after their use in practice, non-inferiority of antibody responses to QIV comparing with TIV for the matched strains, and its superiority for not corresponding B strain was shown (9). In two phase-III clinical trials totally among 6,224 adult volunteers aged ≥18 years (4,659 in one study and 1,565 in another) in comparison with the TIV, the QIV displayed superior immunogenicity toward the alternative-lineage B strain, without impairing the immune responses to shared strains. Moreover, QIV vaccines proved similar reactogenicity and safety (45, 46).

Some models for influenza virus type B spread in the world were elaborated. According to Eichner et al. with a retrospective analysis over the past 50 years of usage TIV 11.2% of cases type B influenza infection could have been prevented using QIV (8). According to the results of another study during the period 2000–2013 QIV would prevent, on average, about 16% more cases of type B influenza infection than TIV when the vaccine and circulating strains do not match, suggesting that cross-protection is 70% between B lines. It has also been shown that old people (≥65 years old) and adults aged 50–64 years benefited the most from QIV, with a decrease of 21 and 18% of infections, respectively (47). Depending on the levels of vaccine-induced cross-protection between B lineages decrease in cross-protection to 50, 30, and 0% effectiveness of QIV increases up to 25, 30, and 34% relatively B lineage infections.

Vaccination in Patients With CVID

In patients with CVID, belonging to the group of immunocompromised patients, vaccination, despite the regular administration of donor immunoglobulins, is the only way to form a protection against the virus, as well as to prevent infectious complications of influenza. At the same time, there is a study reporting the content of cross-reactive A/H1N1 antibodies in IVIG (48). However, in a study by Gardulf et al. in 48 patients with CVID, despite regular IVIG therapy (1 time per week), this fact is not confirmed (20).

Only this study and the study by Pedersen et al. [2/3 patients with CVID showed protective level of antibodies with a >4-fold increase by seroconversion after double dose of the vaccine at the beginning and boostarization after 3 weeks (7.5 + 3.75 μg)] have presented data from the use of the specific adjuvant X179a in individuals with CVID whereas in healthy population in investigations it has been shown that 67–98.3% produce protective levels of antibodies against the influenza A(H1N1) 21days after injection of a single dose (3.75 μg) of the vaccine Pandemrix® (49, 50).

While Eibl and Wolf believe that vaccination against the influenza virus should follow the same schemes as in healthy individuals (51), data from clinical studies show the need for boosting dose not earlier than 21 days after vaccination, or the introduction of a double dose at the same time with the goal of more active stimulation (19, 20).

In our study we decided to vaccinate patients with CVID with 1 dose of the tetravalent adjuvanted influenza vaccine on the background of absence of IVIG immunotherapy for 7 weeks. An immune response was expected due to the presence of an adjuvant that activates innate immunity factors, as well as an expanded spectrum of antigens in the vaccine, in contrast to the study using the Pandemrix mono-vaccine.

Our Results

In healthy patients vaccinated with a tetravalent adjuvant vaccine with a reduced amount of antigens against all 4 strain-specific surface antigens up to 5 μg, this vaccine has proved its immunogenicity in such criteria as seroprotection (≥70%), seroconversion (≥40%), GMT, and GMR (≥2.5). The level of seroconversion to strain A/H3N2 is statistically significantly higher in the group of initially seronegative (in 2.5 times: 100 vs. 40%).

Based on an individual analysis of the specific antibodies titer in each patient with CVID, it can be noted that 3 out of 6 patients showed ≥2-fold increase in the titer of antibodies to the influenza type B/Victoria lineage (moreover, in 1/6 the antibody growth was 4 times) 3 months after vaccination, that had not been observed in blood sample analysis after 3 weeks. This may indicate the need for a study of post-vaccination antibodies to various infections in such patients not earlier than 4 weeks after immunization. However, protective antibody titer of ≥1:40 to strains of two lines (Yamagata and Victoria) was not achieved at all and was no more than 1:20. Although it should be noted that for patients with CVID, a conditional indicator of the effectiveness of vaccination is an 2–4-fold increase of post-vaccination antibody level in relation to the pre-vaccination.

As for the level of antibodies to A/H3N2, three patients showed an increase in antibody titer to 1:20, 1:40, and 1:80 (by 2, 4, and 8 times respectively); they were also found in 2/6 in blood samples 3 months and in 1/6–3 weeks after immunization.

For A/H1N1 strain only one patient in the post-vaccination period showed an increase in antibody titer by 2 times after 3 months compared with the initial (1:20) and reached a protective level (1:40).

Therefore, the obtained results on the assessment of post-vaccination immunity using a quadrivalent immuno-adjuvant vaccine indicate that in 50% of patients (3/6) with CVID an increase in antibody titer to strain A/H3N2 is observed (at protective level in 2/6 patients, 33.3%); to A/H1N1- in 16.7% (1/6 patients) at the protective level; to B/Victoria—in 50% (3/6 patients) there is an increase in antibody titer without reaching a protective level; to B/Yamagata—increase in titers was not detected.

Considering the fact that only one patient out of 6 with CVID showed a protective level of antibodies in the control blood sample 3 weeks after vaccination, while the rest of the patients had antibodies only 3 months later, we can suggest that patients with CVID should probably conduct a follow-up analysis for greater reliability no earlier than 4 weeks after immunization.

The search for new vaccination schemes is the subject of further investigations, as well as the effectiveness of boosterization with immunoadjuvant vaccines in patients with CVID.

CONCLUSION

A detailed assessment of the immunogenicity of a tetravalent influenza virus vaccine with a reduced concentration of antigens of all four strains with the inclusion of an immunoadjuvant in healthy was made, its immunogenicity similar to that of the non-adjuvant QIV in the world. In patients with CVID the use of this vaccine was also investigated for the first time, and encouraging results were obtained.

DATA AVAILABILITY STATEMENT

All datasets generated for this study are included in the article.

ETHICS STATEMENT

The studies involving human participants were reviewed and approved by Ethical Committee of National Research Center—Institute of Immunology Federal Medical-Biological Agency of Russia. The patients/participants provided their written informed consent to participate in this study.

AUTHOR CONTRIBUTIONS

AK: investigation and writing—original draft. NA: methodology, resources, and data curation. EL: conceptualization and writing—review & editing. AV: visualization and formal analysis. YD and SK: investigation. TL: writing—review & editing. MK: methodology, resources, and project administration. All authors contributed to the article and approved the submitted version.

REFERENCES

1. World Health Organization. *Global Influenza Strategy 2019–2030. World Health Organization.* (2019) Available online at: https://apps.who.int/iris/handle/10665/311184
2. Hannoun C. The evolving history of influenza viruses and influenza vaccines. *Expert Rev Vaccin.* (2013) 12:1085–94. doi: 10.1586/14760584.2013.824709
3. WHO. *Recommended Composition of Influenza Virus Vaccines for Use in the 2015–2016 Northern Hemisphere Influenza Season*. (2015) Available online at: https://www.who.int/influenza/vaccines/virus/recommendations/2015_16_north/en/ (accessed February 26, 2015)
4. Ambrose ChS, Levin MJ. Rationale for quadrivalent infuenza vaccines. *Hum Vaccin Immunother.* (2012) 8:81–8. doi: 10.4161/hv.8.1.17623

5. Caini S, Huang QS, Ciblak MA, Kusznierz G, Owen R, Wangchuk S, et al. Epidemiological and virological characteristics of influenza B: results of the Global Influenza B Study. *Influenza Other Respir Viruses.* (2015) 9(Suppl. 1):3–12. doi: 10.1111/irv.12319
6. Kharit SM, Rudakova AV, Uskov AN, Konovalova LN, Lobzin YuV. The averted costs due to influenza vaccination with trivalent and quadrivalent vaccines. *J Infektologii.* (2017) 2:17–22. doi: 10.22625/2072-6732-2017-9-2-17-22
7. Lee BY, Bartsch SM, Willig AM. The economic value of a quadrivalent versus trivalent influenza vaccine. *Vaccine.* (2012) 30:7443–6. doi: 10.1016/j.vaccine.2012.10.025
8. Eichner M, Schwehm M, Hain J, Uphoff H, Salzberger B, Knuf M, et al. Flu - an individual based simulation tool to study the effects of quadrivalent vaccination on seasonal influenza in Germany. *BMC Infect Dis.* (2014) 14:365. doi: 10.1186/1471-2334-14-365
9. Moa AM, Chughtai AA, Muscatello DJ, Turner RM, MacIntyre CR. Immunogenicity and safety of inactivated quadrivalent influenza vaccine in adults: a systematic review and meta-analysis of randomised controlled trials. *Vaccine*. (2016) 34:4092–102. doi: 10.1016/j.vaccine.2016.06.064
10. Di Pasquale A, Preiss S, Tavares Da Silva F, Garcon N. Vaccine adjuvants: from 1920 to 2015 and beyond. *Vaccines.* (2015) 3:320–43. doi: 10.3390/vaccines3020320
11. Multi strain influenza vaccine. *OraPro-Flu*. Available online at: https://www.stabilitech.com/multi-strain-influenza-vaccine/#
12. Paul WE. *Fundamental Immunology, 6th edition*. Philadelphia, PA: Wolters Kluwer/ Lippincott Williams & Wilkins. (2008). p. 1603
13. Alexia C, Cren M, Louis-Plence P, Vo D-N, El Ahmadi Y, Dufourcq-Lopez E, et al. Polyoxidonium® activates cytotoxic lymphocyte responses through dendritic cell maturation: clinical effects in breast cancer. *Front Immunol.* (2019) 10:2693. doi: 10.3389/fimmu.2019.02693
14. Kostinov MP, Cherdantsev AP, Kuselman AI, Akhmatova NK, Kostinova AM, Deryabina EV, et al. Prospective randomized open-label comparative study of immunogenicity after subunit and polymeric subunit influenza vaccines administration among mothers and infants. *Hum. Vaccin. Immunother.* (2018) 14:2971–78. doi: 10.1080/21645515.2018.1507585
15. ESID Registry – Working Definitions for Clinical Diagnosis of PID. Available online at: https://esid.org/content/download/16628/452872/file/ESIDRegistry_ClinicalCriteria.pdf (accessed January 22, 2019).
16. van Assen S, Holvast A, Telgt DS, Benne CA, de Haan A, Westra J, et al. Patients with humoral primary immunodeficiency do not develop protective anti-influenza antibody titers after vaccination with trivalent subunit influenza vaccine. *Clin Immunol.* (2010) 136:228–35. doi: 10.1016/j.clim.2010.03.430
17. Hanitsch LG, Lobel M, Mieves JF, Bauer S, Babel N, Schweiger B, et al. Cellular and humoral influenza-specific immune response upon vaccination in patients with common variable immunodeficiency and unclassified antibody deficiency. *Vaccine.* (2016) 34:2417–23. doi: 10.1016/j.vaccine.2016.03.091
18. van Assen S, de Haan A, Holvast A, Horst G, Gorter L, Westra J, et al. Cell-mediated immune responses to inactivated trivalent influenza-vaccination are decreased in patients with common variable immunodeficiency. *Clin Immunol.* (2011) 141:161–8. doi: 10.1016/j.clim.2011.07.004
19. Pedersen G, Halstensen A, Sjursen H, Naess A, Kristoffersen EK, Cox RJ. Pandemic influenza vaccination elicits influenza-specific CD4+ Th1-cell responses in hypogammaglobulinaemic patients: four case reports. *Scand J Immunol.* (2011) 74:210–8. doi: 10.1111/j.1365-3083.2011.02561.x
20. Gardulf A, Abolhassani H, Gustafson R, Eriksson LE, Hammarström L. Predictive markers for humoral influenza vaccine response in patients with common variable immunodeficiency. *J Allergy Clin Immunol.* (2018) 142:1922–31.e2. doi: 10.1016/j.jaci.2018.02.052
21. Immune Deficiency Foundation. *CVID Community Center*. https://primaryimmune.org/about-primary-immunodeficiencies/specific-disease-types/common-variable-immune-deficiency
22. Good Clinical Practice. *Russian Federation National Standard, GOSTR 52379-2005/ Moscow.* (2005) Available online at: http://www.medtran.ru/rus/trials/gost/52379-2005.html
23. Antigenic Characterization. *Content source: Centers for Disease Control and Prevention, National Center for Immunization and Respiratory Diseases (NCIRD).* (2019) https://www.cdc.gov/flu/about/professionals/antigenic.htm# (accessed October 15, 2019)
24. European Medicine Agency. *Committee on Human Medicinal Products (CHMP). Guideline on Clinical Evaluation of Vaccines*. (2018) Available online at: https://www.ema.europa.eu/en/clinical-evaluation-new-vaccines (accessed April 26, 2018)
25. Public Health England (PHE). *Guidance. Summary of Data to Support the Choice of Influenza Vaccination for Adults in Primary Care.* (2018) Available online at: https://www.gov.uk/government/publications/flu-vaccination-supporting-data-for-adult-vaccines/summary-of-data-to-support-the-choice-of-influenza-vaccination-for-adults-in-primary-care (accessed September 10, 2018).
26. de Waure C, Boccalini S, Bonanni P, Amicizia D, Poscia A, Bechini A, et al. Adjuvanted influenza vaccine for the Italian elderly in the 2018/19 season: an updated health technology assessment. *Eur J Public Health*. (2019) 29:900–5. doi: 10.1093/eurpub/ckz041
27. Khaitov MR. The results and prospects of researches on the development of artificial vaccines. *Immunologiya.* (1982) 6:35–40.
28. Voitsehovskaya EM, Vakin VS, Vasilieva AA. Results of the analysis of the new vaccine "Grippol® plus" immunogenicity. *Epidemiol Vaccin Prev*. (2009) 44:40–5. (in Russ.)
29. Nekrasov AV, Puchkova NG, Kharit SM. Vaccine grippol® neo: results of clinical investigations on safety and reactogenicity (phase II). *Epidemiol Vaccin Prev.* (2009) 5:54–60. (in Russ.)
30. Romanenko VV, Osipova IV, Lioznov DA, Martsevich *SY,* Ankudinova *AV*, Chebykina *TV*. Clinical study of safety and efficacy of a polymer-subunit adjuvant influenza vaccine applied in combination with an immune modulator in people aged 60 and over. *Epidemiol Vaccin Prev.* (2016) 15:63–71. doi: 10.31631/2073-3046-2016-15-5-63-71
31. Cherdantsev AP, Kuselman AI, Sinitsina MN, Shalyagina ME, Kostinov MP, Tarbaeva DA. A study of the clinical safety of pregnant influenza vaccination. *Med Alman.* (2011) 4:120–2.
32. Kostinov MP, Cherdantsev AP, Savis'ko AA, Tarbaeva DA, Solov'yova IL. True and false reactions in pregnant women to introduction of influenza vaccine. *Problems of Gynecology, Obstetrics and Perinatology*. (2011) 10:44–8. (in Russ.)
33. Kostinov MP, Cherdantsev AP, Shmitko AD, et al. The efficacy of immunoadjuvant-containing influenza vaccines in pregnancy. In: Afrin F, editor. *Hassan Hemeg and Hani Ozbak*. (2017). p. 67–93.
34. Kostinov MP, Cherdantsev AP, Shmitko AD, Praulova DA, A. D. Protasov, U. A. Dagil, et al. Immunogenicity of adjuvant influenza vaccine for pregnant women. *Russ J Infect Immun*. (2017) 7:193–202. (In Russ.) doi: 10.15789/2220-7619-2017-2-193-202
35. Kostinov MP, Cherdantsev AP, Semenova SS, Tarbaeva DA, Savisko AA, Serova OF, et al. Obstetric and perinatal outcomes among pregnant women after influenza vaccination and after transferred respiratory infection. *Gynecology.* (2015) 17:43–6. (In Russ.) doi: 10.26442/2079-5831_17.4.43-46
36. Kostinov MP, Cherdantsev AP. Health state of children born from pregnant women vaccinated against influenza. *Pediatria.* (2016) 1:67–71. (in Russ.)
37. Cherdantsev AP, Kostinov MP, Kuselman AI. Vaccine prevention of influenza in pregnant woman. In: Cherdantsev AP, Kostinov MP, Kuselman AI, editors. *Guidelines for doctors*. 2nd ed., enlarged. Moscow (Russia): MDV Grup Art Studio "Sozvezdie" (2014). p. 112.
38. Zverev VV, Kostinov MP, Cherdantsev AP, Kuselman AI, Kiselev OI, Erofeeva MK, et al. editors. *Vaccination against influenza in pregnancy*. Federal clinical guidelines. Remedium. (2015) p. 42.
39. Boytsov SA, Lukyanov MM, Platonova EV, Gorbunov V, Romanchuk SV, Nazarova OA, et al. Investigation of the efficiency and safety of influenza vaccination in patients with circulatory system diseases. *Russian J Prev Med Public Health.* (2014) 6:13–20. (in Russ.) doi: 10.17116/profmed20141476 13-20
40. Boytsov SA, Lukyanov MM, Platonova EV, Gorbunov V, Romanchuk SV, Nazarova OA, et al. Efficiency of influenza vaccination in patients with circulatory system diseases under dispensary observation in outpatient clinics: prospective followup monitoring data. *Rational Pharmacotherapy Cardiol.* (2016) 12:703–10. (In Russ). doi: 10.20996/1819-6446-2016-12-6-703-710

41. Chebykina AV, Kostinov MP, Magarshak OO. Estimation of Safety and Efficiency of Vaccination From a Flu at Patients with Chronic Obstructive Lung Syndrome. *Epidemiol Vacc Prev*. (2010) 55:50–53. (in Russ.)
42. Kostinov MP, Chuchalin AG, Chebykina AV. Specificities of the formation of post-vaccination immunity to influenza in patients with chronic bronchopulmonary pathologies. *Infecti Dis*. (2011) 9:35–40. (in Russ.)
43. Andreeva NP, Petrova TI, Kostinov MP. The effect of active immunization against influenza and pneumococcal infection in children with bronchial asthma on the course of the disease and the microbial spectrum of sputum. *Russian J Allergy*. (2006) 5:31–5. (in Russ.)
44. Kostinov MP, Akhmatova NK, Khromova EA, Skhodova SA, Stolpnikova VN, Cherdantsev AP, et al. The impact of adjuvanted and non-adjuvanted influenza vaccines on the innate and adaptive immunity effectors. In: *IntechOpen Book Series. Infectious Diseases, Vol. 1. Influenza. Therapeutics and Challenges. Saxena* SK, editor (2018). p. 83–109. doi: 10.5772/intechopen.71939
45. Kieninger D, Sheldon E, Lin WY, Yu CJ, Bayas JM, Gabor JJ, et al. Immunogenicity, reactogenicity and safety of an inactivated quadrivalent influenza vaccine candidate versus inactivated trivalent influenza vaccine: a phase III, randomized trial in adults aged ≥18 years. *BMC Infect Dis*. (2013) 13:343. doi: 10.1186/1471-2334-13-343
46. Pépin S, Donazzolo Y, Jambrecina A, Salamand C, Saville M. Safety and immunogenicity of a quadrivalent inactivated influenza vaccine in adults. *Vaccine*. (2013) 31:5572–8. doi: 10.1016/j.vaccine.2013.08.069
47. Crépey P, de Boer PT, Postma MJ, Pitman R. Retrospective public health impact of a quadrivalent influenza vaccine in the United States. *Influenza Other Respir Viruses*. (2015) 9 (Suppl 1):39–46. doi: 10.1111/irv.12318
48. Hong DK, Tremoulet AH, Burns JC, Lewis DB. Cross-reactive neutralizing antibody against pandemic (2009). *H1N1 Influenza a Virus in Intravenous Immunoglobulin Preparations. Pediatr Infect Dis J*. (2011) 30:67–9. doi: 10.1097/INF.0b013e3181f127be
49. Manuel O, Pascual M, Hoschler K, Giulieri S, Alves D, Ellefsen K, et al. Humoral response to the influenza A H1N1/09 monovalent AS03-adjuvanted vaccine in immunocompromised patients. *Clin Infect Dis*. (2011) 52:248–56. doi: 10.1093/cid/ciq104
50. European Medicines Agency. Pandemrix. Annex I. *Summary of Product Characteristics*. European Medicines Agency, London, United Kingdom. Available online at: http://www.ema.europa.eu/docs/en_GB/document_library/EPAR_-_Product_Information/human/000832/WC500038121.pdf
51. Eibl MM, Wolf HM. Vaccination in patients with primary immune deficiency, secondary immune deficiency and autoimmunity with immune regulatory abnormalities. *Immunotherapy*. (2015) 7:1273–92. doi: 10.2217/IMT.15.74

Conflict of Interest: The authors declare that the research was conducted in the absence of any commercial or financial relationships that could be construed as a potential conflict of interest.

frontiers in Immunology

ORIGINAL RESEARCH
published: 08 September 2020
doi: 10.3389/fimmu.2020.02096

Modulation of Cell Surface Receptor Expression by Modified Vaccinia Virus Ankara in Leukocytes of Healthy and HIV-Infected Individuals

Adrien Leite Pereira[1], Quentin Jouhault[1], Ernesto Marcos Lopez[1], Antonio Cosma[1], Olivier Lambotte[1,2,3], Roger Le Grand[1], Michael H. Lehmann[4] and Nicolas Tchitchek[1]**

[1] INSERM U1184, Immunology of Viral Infections and Autoimmune Diseases, IDMIT Infrastructure, CEA–Université Paris Sud 11, Fontenay-aux-Roses, France, [2] INSERM U1184, Center for Immunology of Viral Infections and Autoimmune Diseases, Le Kremlin-Bicêtre, France, [3] APHP, Service de Médecine Interne et Immunologie Clinique, Hôpitaux Universitaires Paris Saclay, Le Kremlin-Bicêtre, France, [4] Institute for Infectious Diseases and Zoonoses, Ludwig-Maximilians-Universität München, Munich, Germany

OPEN ACCESS

Edited by:
Scott James Tebbutt,
The University of British Columbia,
Canada

Reviewed by:
Amy L. MacNeill,
Colorado State University,
United States
Robert Drillien,
INSERM U964, Institut de Génétique et de Biologie Moléculaire et Cellulaire (IGBMC), France

***Correspondence:**
Michael H. Lehmann
Michael.Lehmann@lmu.de;
Orlataler@web.de
Nicolas Tchitchek
nicolas.tchitchek@sorbonne-universite.fr;
nicolas.tchitchek@gmail.com

Specialty section:
This article was submitted to Vaccines and Molecular Therapeutics, a section of the journal Frontiers in Immunology

Received: 06 May 2020
Accepted: 03 August 2020
Published: 08 September 2020

Citation:
Leite Pereira A, Jouhault Q, Marcos Lopez E, Cosma A, Lambotte O, Le Grand R, Lehmann MH and Tchitchek N (2020) Modulation of Cell Surface Receptor Expression by Modified Vaccinia Virus Ankara in Leukocytes of Healthy and HIV-Infected Individuals. Front. Immunol. 11:2096. doi: 10.3389/fimmu.2020.02096

Viral vectors are increasingly used as delivery means to induce a specific immunity in humans and animals. However, they also impact the immune system, and it depends on the given context whether this is beneficial or not. The attenuated vaccinia virus strain modified vaccinia virus Ankara (MVA) has been used as a viral vector in clinical studies intended to treat and prevent cancer and infectious diseases. The adjuvant property of MVA is thought to be due to its capability to stimulate innate immunity. Here, we confirmed that MVA induces interleukin-8 (IL-8), and this chemokine was upregulated significantly more in monocytes and HLA-DR^{bright} dendritic cells (DCs) of HIV-infected patients on combined antiretroviral therapy (ART) than in cells of healthy persons. The effect of MVA on cell surface receptors is mostly unknown. Using mass cytometry profiling, we investigated the expression of 17 cell surface receptors in leukocytes after *ex vivo* infection of human whole-blood samples with MVA. We found that MVA downregulates most of the characteristic cell surface markers in particular types of leukocytes. In contrast, C-X-C motif chemokine receptor 4 (CXCR4) was significantly upregulated in each leukocyte type of healthy persons. Additionally, we detected a relative higher cell surface expression of the HIV-1 co-receptors C-C motif chemokine receptor 5 (CCR5) and CXCR4 in leukocytes of HIV-ART patients than in healthy persons. Importantly, we showed that MVA infection significantly downregulated CCR5 in CD4+ T cells, CD8+ T cells, B cells, and three different DC populations. CD86, a costimulatory molecule for T cells, was significantly upregulated in HLA-DR^{bright} DCs after MVA infection of whole blood from HIV-ART patients. However, MVA was unable to downregulate cell surface expression of CD11b and CD32 in monocytes and neutrophils of HIV-ART patients to the same extent as in monocytes and neutrophils of healthy persons. In summary, MVA modulates the expression of many different kinds of cell surface receptors in leukocytes, which can vary in cells originating from persons previously infected with other pathogens.

Keywords: AIDS, chemokine, cytokine, mass cytometry, modified vaccinia virus Ankara, poxvirus, surface marker, vaccination

INTRODUCTION

Protection of humans against infectious diseases by vaccination is considered as one of the greatest successes in the history of medicine. In particular, 40 years ago, the world health assembly officially declared smallpox eradicated. Vaccinia virus (VACV) has been successfully used to vaccinate against smallpox, but it can cause severe side effects (1, 2). Therefore, as an effort to attenuate VACV in a way that increases its safety while keeping its immunogenic potential, chorioallantois vaccinia virus Ankara (CVA) was passaged multiple times in chicken embryo fibroblasts (CEFs). This yielded a modified VACV strain, which does not replicate in primary human cells (3). Vaccination of persons with the modified vaccinia virus Ankara (MVA) was well tolerated in more than 120,000 persons (4), and recently, the safety and efficacy of MVA were confirmed in a phase 3 clinical trial designed for the usage of MVA against smallpox (5).

Additionally, MVA has been widely used as a viral vector in clinical studies intended to treat and prevent cancer and infectious diseases (6–9). The safety of virus-vectored vaccines is intensively discussed and regulatory guidelines for their usage are being established (10, 11). The effectiveness of a vaccine depends not only on its specific composition but also on the individual immunological status of a person to be vaccinated (12). The latter point is highly relevant for the development of therapeutic HIV vaccines because HIV-1-infected patients suffer from chronic inflammation even when receiving antiretroviral therapy (ART) (13).

MVA has been applied as a viral vector in several clinical trials that enrolled HIV-1-infected patients (14–18) and healthy persons (19–21). Therein, MVA has indeed proved to be safe, and its ability to stimulate innate immunity has been considered as a beneficial adjuvant effect (22, 23). Although there are some studies about MVA-induced cytokine expression (24–26), only limited information is available about the effect of this virus on cell surface receptors in leukocytes (27–29). However, such information is necessary for a better understanding of the complex immune responses triggered by this virus in vaccinated individuals.

Moreover, it is necessary to reveal potential differences in vaccine responsiveness between infected and healthy persons to improve vaccine design for example for people living with HIV. Therefore, we investigated by mass cytometry the effects of MVA on cytokine expression and the expression levels of some selected cell surface receptors including C-C motif chemokine receptor 5 (CCR5) and C-X-C motif chemokine receptor 4 (CXCR4), the two major co-receptors for HIV entry (30), in leukocytes of HIV-1-infected patients receiving ART in comparison to healthy persons.

MATERIALS AND METHODS

Patients

Whole-blood samples from five HIV-infected patients on combined ART (HIV-ART patients) and five healthy persons were collected in lithium heparin tubes by the Etablissement Français du Sang (EFS, Hôpital Saint Louis, Paris, France) and the Hôpital du Kremlin Bicêtre, respectively. The age (range), infection route, number of $CD4^+$ T cells, viral load, year of HIV detection, year of the beginning of ART, type of ART, and adherence to ART were provided for each HIV-infected patient (**Table 1**). Their age ranged from 45 to 60 years, the CD4 cell counts from 427 to 811 cells/mm^3, and the plasma HIV RNA levels were <40 copies/ml. The age (range) of each healthy subject is provided in **Table 2**.

In this study, viral loads were used to determine whether ARTs were effective. We concluded that the adherence to treatments was correct and the treatments were effective, as the viral loads were <40 copies/ml for all patients.

Virus

MVA clonal isolate F6 was made available to the CEA by Gerd Sutter (LMU Munich, Germany) on the basis of a Material Transfer Agreement with the Ludwig-Maximilians-Universität München (LMU-MTA). MVA was propagated in primary CEFs, which were cultivated in Eagle's minimum essential medium (Sigma-Aldrich) supplemented with 2% fetal calf serum. Afterwards, cells were freeze-thawed three times and the cell debris were removed by centrifugation at a relative centrifugal field (RCF) of 453 × *g* for 15 min. The supernatant was centrifuged again at an average RCF of 22,700 × *g* for 3 h. The resulting pellet was dissolved in 10 mM Tris–HCl, pH 9.0, and stored at −80°C. Titration was performed on CEFs as described (31). MVA preparations were regularly screened for potential mycoplasma and other bacterial contaminations.

Cell Infection, Stimulation, and Storage

Fresh whole-blood samples were infected with MVA at a multiplicity of infection (MOI) of one and incubated at 37°C under 5% CO_2 in six-well plates (BD Biosciences). After 1 h, brefeldin A (BFA), dissolved in dimethyl sulfoxide (Sigma-Aldrich), was added to the cells at a final concentration of 1 μg/ml to perform intracellular cytokine staining as described (32), and cell incubation was continued for 16 h. Then, cells were fixed and erythrocytes were lysed as described previously (33). In detail, the fixation mixture (FM) contained 18.5% glycerol (Sigma-Aldrich, Lyon, France) in 1X Dulbecco's phosphate-buffered saline (DPBS) without $CaCl_2$ or $MgCl_2$, pH 7.4 (Gibco by Life Technologies, Villebon-sur-Yvette, France) and 5% formaldehyde, which was prepared from a 36% paraformaldehyde solution (VWR BDH Prolabo, Fontenay-sous-Bois). Ten-milliliter FM was added to 1 ml blood, which was incubated for 10 min at 4°C and then centrifuged at 800 × *g* for 5 min at room temperature (RT). Red blood cells present in the pellets were lysed by adding 10 ml Milli-Q water. After incubation at RT for 20 min, cells were washed two times with 1X DPBS and centrifuged between washes at 800 × *g* for 5 min at RT. Then, cells were counted, resuspended in FM to 200-μl aliquots containing 3×10^6 cells, and stored at −80°C. This procedure enabled freezing and recovery of all blood leukocytes without damage,

TABLE 1 | Characteristics of HIV-ART patients.

Patients	PAT-1	PAT-2	PAT-3	PAT-4	PAT-5
Current age	45–50	55–60	50–55	50–55	55–60
Infection routes	Sexual	Sexual	Unknown	Unknown	Sexual
Number of $CD4^+$ T cells (cells/mm^3)	559	427	624	758	811
Viral load	<40	<40	<40	<40	<40
Detection	2000	1985	2009	1999	1995
Treatments starting	2015	1990	2009	1999	1995
Treatment	Emtricitabine Rilpivirine Tenofovir	Emtricitabine Rilpivirine Tenofovir	Emtricitabine Rilpivirine Tenofovir	Abacavir Lamivudine Dolutegravir	Emtricitabine Disoproxil fumarate Tenofovir
Adherence to treatment	Yes	Yes	Yes	Yes	Yes

The current age (range), contamination pathway, viral load, year of detection and starting treatment, and ongoing treatment are shown for each HIV-infected patient.

TABLE 2 | Characteristics of healthy persons.

Patients	HEA-1	HEA-2	HEA-3	HEA-4	HEA-5
Current age	45–50	60–65	25–30	30–35	55–60

The age (range) of each healthy subject is shown.

especially polymorphonuclear cells, which are highly labile and cryopreservation-sensitive (34).

Staining and Acquisition

For each sample, 3×10^6 cryopreserved fixed cells were washed twice with staining buffer [PBS-0.5% bovine serum albumin (BSA), Sigma-Aldrich] and labeled with conjugated antibodies according to the following procedures. Cells were incubated at 4°C for 30 min with a mixture of the metal-labeled surface antibodies (Abs) in staining buffer. After two washes with 1X DPBS, cells were incubated in fixation solution [PBS-1.6% paraformaldehyde (PFA), Electron Microscopy Sciences Hartfield] at RT for 20 min, and permeabilized with 1X Perm/Wash buffer (BD Biosciences) at RT for 10 min. Staining with metal-labeled intracellular Abs and an iridium nucleic acid intercalator in 1X Perm/Wash buffer was carried out as for extracellular staining. Cells were stored overnight in 0.1 μM iridium nucleic acid intercalator in a fixation solution. The following day, cells were washed with Milli-Q water, resuspended in 1 ml Milli-Q water, and filtered using a 35-μm nylon mesh cell strainer (BD Biosciences), before the addition of EQ Four-Element Calibration Beads (Fluidigm), according to the manufacturer's instructions. The acquisition of each sample was manually performed two times in succession on a CyTOF-1 instrument (Fluidigm). The metal and clones of all antibodies used in the mass cytometry panel are shown in **Table 3**.

Characterization of Modified Vaccinia Virus Ankara-Specific Immune Responses

Following data acquisition, cells were gated to exclude beads, doublets, and non-specific background (**Supplementary Figure S1A**). A Spanning-tree Progression

TABLE 3 | Mass cytometry panel.

Metal	Antibody	Clone	Provider
Pr141	CD66	TET2	Miltenyi
Nd142	HLA-DR	L243 (G46-6)	Biolegend
Nd143	CD3	UCHT1	BD Bioscience
Nd144	CD64	10.1.1	BD Bioscience
Nd145	CD86	2331 (FUN-1)	BD Bioscience
Nd146	IL-6	MQ2-13A5	Miltenyi
Sm147	IFN-α	LT27:295	Miltenyi
Nd148	IL-1β	H1b-98	Biolegend
Sm149	CD14	M5E2	BD Bioscience
Nd150	CD11b	ICRF44	BD Bioscience
Eu151	CD38	AT1	Clinisciences
Sm152	CD16	B73.1	BD Bioscience
Eu153	CD154	TRAP1	BD Bioscience
Sm154	CD8A	37006	R&D systems
Gd155	CD32	2E1	Miltenyi
Gd156	CCL4	D21-1351	BD Bioscience
Gd158	IP10	6D4	Clinisciences
Tb159	TNF-α	MAb11	BD Bioscience
Gd160	IL-1α	364/3B3-14	eBioscience
Dy161	NKp80	4A4D10	Miltenyi
Dy162	IL-12	C8.6	Miltenyi
Dy163	Perforin	dG9-DTAG9	BD Bioscience
Dy164	CXCR4	12G5	BD Bioscience
Ho165	CD11a	HI111	BD Bioscience
Er166	CCR5	3A9	BD Bioscience
Er167	IL-8	NAPII	eBioscience
Er168	CD11c	B-ly6	BD Bioscience
Tm169	CD4	L200	BD Bioscience
Er170	CCL5	2D5	BD Bioscience
Yb171	IFN-g	25723	R&D systems
Yb172	CD25	BC96	Biolegend
Yb173	CD123	7G3	BD Bioscience
Yb174	CD19	HIB19	BD Bioscience
Yb175	IL-1RA	AS17	BD Bioscience
Yb176	CCL2	5D3-F7	Biolegend
Ir191/Ir193	Intercalator-Ir	–	–

The antibodies used in this study are shown along with the metal isotope and clone for each. CCL, C-C motif chemokine ligand; CCR, C-C motif chemokine receptor; CXCR, C-X-C motif chemokine receptor; IFN, interferon; IL, interleukin; TNF, tumor necrosis factor.

Analysis of Density-normalized Events (SPADE) was performed on the cytometric profiles of the entire dataset (35). The SPADE analysis was parameterized to generate 100 cell clusters using a downsampling of 5%. SPADE clustering was based on the levels of CD3, CD4, CD8, CD11c, CD14, CD16, CD19, CD32, CD64, CD66, CD123, HLA-DR, NKp80, and Perforin (**Supplementary Figures S1B,C**).

T cell, B cell, natural killer (NK) cell, polymorphonuclear neutrophil (PMN), basophil, monocyte, conventional DC (HLA-DR^{high} and HLA-DR^{bright}), and plasmacytoid DC (pDC) populations were identified by annotating clusters generated by the SPADE analysis based on their expression of CD3, CD11c, CD14, CD16, CD19, CD64, CD66, CD123, and HLA-DR (**Supplementary Figures S1B,C**). HLA-DR^{high} and HLA-DR^{bright} DC populations were defined based on the expression of HLA-DR (**Supplementary Figure S1D**). Finally, CD4$^+$ T and CD8$^+$ T-cell populations were split using classical gating (**Supplementary Figure S1E**).

Gating Strategy

T cells were identified as CD3$^+$, B cells as HLADR$^+$ CD19$^+$, NK cells as HLA-DR$^-$ CD16$^+$, PMNs as CD66$^+$, basophils as HLA-DR$^-$ CD123$^+$, monocytes as HLADR$^+$ CD14$^+$ CD64$^+$, conventional DCs as HLA-DR$^+$ CD11c$^+$ CD64$^-$, and plasmacytoid DCs as HLADR$^+$ CD123$^+$ CD11c$^-$. The percentages of each leukocyte population isolated from healthy persons and HIV-ART patients are illustrated in **Supplementary Figure S2**.

Cytometry Data Analysis and Statistics

Cytometry data were normalized using Rachel Finck's MATLAB normalizer based on EQ Four-Element Calibration Beads (36). FCS files were concatenated using the FCS file concatenation tool (Cytobank). SPADE analysis was performed on the Cytobank platform, whereas FlowJo software (TreeStar version 9.9) was used to determine the median signal intensity (MSI) of cell surface receptors (for each cell population) and the percentage number of cells producing cytokines. Phenotypic heatmaps were obtained using Tableau software. Statistical comparisons of cell cluster abundances were performed using the Mann–Whitney test available in R software (R Core Team).

RESULTS

Modified Vaccinia Virus Ankara Induces a Higher Percentage Number of Leukocytes Producing Interleukin-8 in the Blood of HIV-ART Patients

It is well established that MVA induces cytokine production (24–26), but it is mostly unknown whether cells of immunocompromised persons including those of HV-1-infected patients respond to this viral vector equally. Therefore, we investigated whether MVA differentially induces cytokine expression in leukocytes of HIV-ART patients and healthy persons. For that, the expression of C-C motif chemokine ligand (CCL)2, CCL4, interferon (IFN)-α, IL-1α, IL-1β, IL-1RA, IL-6, IL-8, IL-12, and tumor necrosis factor (TNF) was determined for each cell type as classified in **Supplementary Figure S1**.

We found that *ex vivo* infection of whole blood with MVA significantly induced the production of IL-8, CCL2, and CCL4 in monocytes and HLA-DR^{high} DCs of HIV-ART patients and healthy persons (**Figures 1A,B**). The percentage number of IL-8-producing monocytes was significantly higher in MVA-infected blood of HIV-ART patients (67.32%) than in MVA-infected blood of healthy persons (31.16%) (**Figure 1A**). MVA also significantly induced the production of CCL4 in HLA-DR^{bright} DCs of HIV-ART patients and healthy persons, but IL-8 and CCL2 were significantly induced only in HLA-DR^{bright} DCs from MVA-infected blood of HIV-ART patients. Thus, the percentage number of HLA-DR^{bright} DCs producing IL-8 was significantly higher in MVA-infected blood of HIV-ART patients (34.30%) than in MVA-infected blood of healthy persons (20.82%) (**Figure 1C**). No production of cytokines was detected in pDCs (**Figure 1D**) and also not in other cell types.

Modified Vaccinia Virus Ankara Downregulates Cell Surface Markers but Upregulates C-X-C Motif Chemokine Receptor 4 in Leukocytes of Healthy Persons

Studies about the effect of MVA on the expression of cell surface markers are rare (27, 28). However, such information would be very valuable to better understand the intrinsic adjuvant properties of MVA when used as a viral vector in vaccine development (8, 22). Therefore, using mass cytometry, we simultaneously investigated the expression of 17 characteristic cell surface markers (CD3, CD4, CD8, CD11a, CD11b, CD11c, CD14, CD16, CD19, CD32, CD64, CD66, CD86, CD123, CCR5, CXCR4, and HLA-DR) in leukocytes of healthy persons and HIV-ART patients after *ex vivo* infection of whole blood with MVA (**Figure 2**). MVA downregulated most of the characteristic cell surface markers expressed in the different leukocyte cell types from healthy persons, except for CXCR4, which was upregulated in each cell type investigated (**Figures 2A**, **3B**).

Chronic HIV-1 Infection Impacts the Expression of Cell Surface Receptors

Previously, it was shown that leukocytes of HIV-infected patients display increased cell surface levels of CCR5 (37, 38). Here, we confirmed by using mass cytometry that CCR5 is significantly upregulated in monocytes, CD4$^+$ T cells, CD8$^+$ T cells, and B cells of HIV-ART patients as compared with cells of healthy persons (**Figures 2A–C**, left panels). We also found high CCR5 cell surface expression in all three DC populations but not in natural killer cells. Monocytes of HIV-ART patients additionally had increased cell surface expression of CD14 and decreased cell surface expression of CD64 and CD11b.

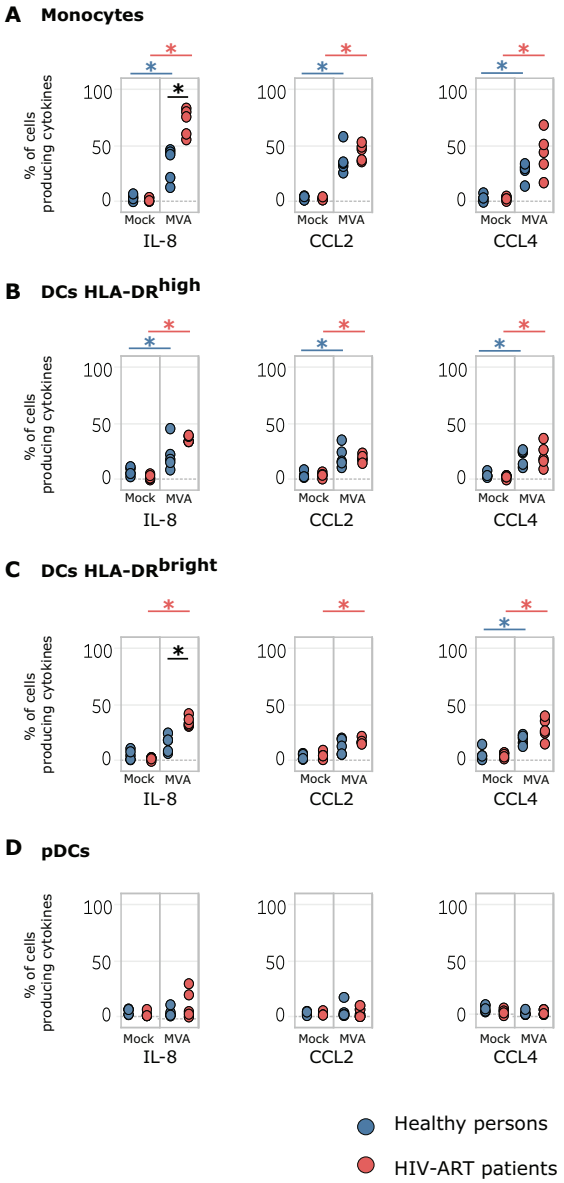

FIGURE 1 | Modified vaccinia virus Ankara (MVA) induces chemokine expression in cells of whole blood from healthy persons and HIV-ART patients. Whole-blood samples of healthy persons and HIV-ART patients were infected with MVA for 16 h or left non-infected. Phosphate-buffered saline (PBS) served as a control. Monocytes, $HLADR^{high}$ dendritic cell (DC), $HLADR^{bright}$ DC, and plasmacytoid DC (pDC) populations were computationally isolated. The percentage numbers of **(A)** monocytes, **(B)** $HLADR^{high}$ DCs, **(C)** $HLADR^{bright}$ DCs, and **(D)** pDCs producing interleukin (IL)-8, C-C motif chemokine ligand (CCL)2, and CCL4 are presented. Blue points correspond to the percentage number of cells obtained from healthy persons; red points to those from HIV-ART patients. Significant differences ($p < 0.05$) between samples are indicated by an asterisk.

CXCR4 cell surface expression was upregulated in each leukocyte type of HIV-ART patients except in basophils, which had the same level as observed in samples of healthy persons. Neutrophils of HIV-ART patients additionally had increased cell surface expression of CD66 and decreased cell surface expression of CD11b (**Figure 2C**, left panel).

Modified Vaccinia Virus Ankara Differentially Affects Cell Surface Expression of C-C Motif Chemokine Receptor 5 and C-X-C Motif Chemokine Receptor 4

Since MVA is applied as a viral vector in several clinical trials that enrolled HIV-infected patients (14–17), knowledge about the potential effects of MVA on HIV/AIDS progression would be of great interest. Here we found that infection of whole blood of HIV-ART patients with MVA significantly downregulated CCR5 in B cells ($p = 0.001$), $HLA\text{-}DR^{bright}$ DCs ($p = 0.012$), $HLA\text{-}DR^{high}$ DCs ($p = 0.016$), pDCs ($p = 0.008$), $CD4^+$ T cells ($p = 0.008$), and $CD8^+$ T cells ($p = 0.008$) (**Figure 3A**). In healthy persons, CCR5 expression was significantly downregulated by MVA only in neutrophils (**Figure 3B**).

In contrast, MVA significantly increased cell surface expression of CXCR4 in B cells ($p = 0.015$), monocytes ($p = 0.012$), NK cells ($p = 0.008$), neutrophils ($p = 0.008$), and $CD8^+$ T cells ($p = 0.008$) of HIV-ART patients (**Figure 3A**) and in each leukocyte population of healthy persons (**Figure 3B**).

Modified Vaccinia Virus Ankara Differentially Affects Cell Surface Expression of CD86, CD32, and CD11b

Previously, it was shown in human monocyte-derived DCs that MVA increases cell surface expression of CD86/B7-2 (27), a co-stimulatory molecule for T-cell activation expressed by antigen-presenting cells (39). Here, we observed a slight upregulation of CD86 in $HLA\text{-}DR^{bright}$ DCs from MVA-infected blood samples of healthy persons, but this was not statistically different from non-infected cells of healthy persons (**Figure 2A**). However, CD86 cell surface expression was significantly upregulated by MVA in $HLA\text{-}DR^{bright}$ DCs of HIV-ART patients as compared to non-infected cells of HIV-ART patients (**Figure 2B**). We also observed higher levels of CD86 in monocytes from MVA-infected blood samples of HIV-ART patients as compared to non-infected cells of HIV-ART patients, but, most probably due to the low number of samples, the difference was not significant.

CD32 cell surface expression was significantly downregulated in monocytes and neutrophils of healthy persons (**Figure 2A**) and HIV-ART patients (**Figure 2B**) after infection of whole blood with MVA. However, the decrease of CD32 was less in monocytes and neutrophils from MVA-infected blood samples of HIV-ART patients, resulting in significantly higher CD32 levels as compared with cells from MVA-infected blood samples of healthy persons (**Figure 2C**, right panel).

Modified vaccinia virus Ankara abrogated CD11b surface expression in cells of healthy persons (**Figure 2A**) but had no significant effect on CD11b surface expression in monocytes and neutrophils of HIV-ART patients (**Figure 2B**). This resulted in significantly higher surface expression of CD11b in monocytes

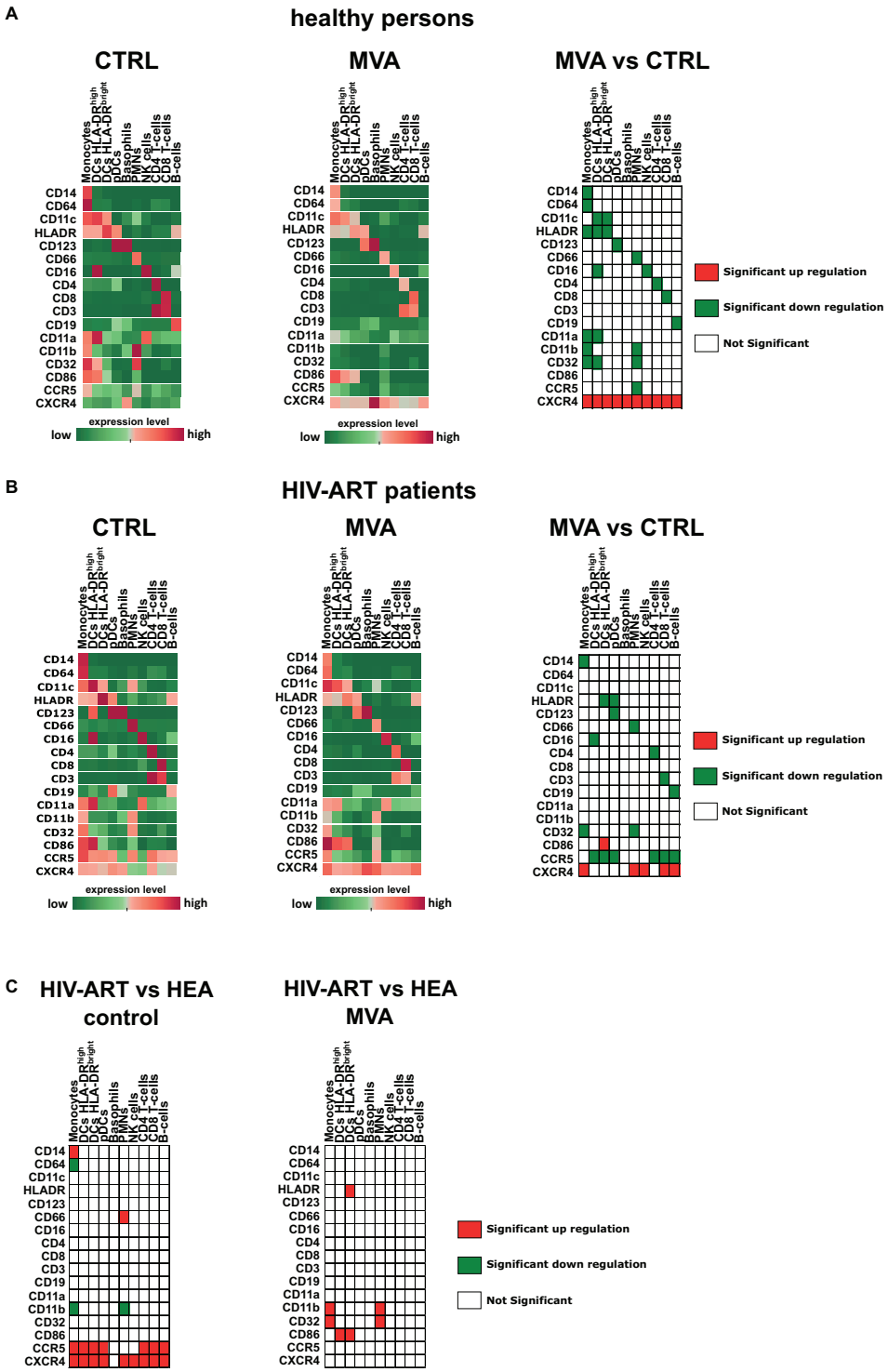

FIGURE 2 | Modulation of cell surface receptor expression by modified vaccinia virus Ankara (MVA) in healthy persons and HIV-ART patients. Whole-blood samples of healthy persons **(A)** and HIV-ART patients **(B)** were infected with MVA for 16 h or left non-infected. Cells were stained with a panel of 35 cell markers and analyzed with Tableau and R software as described in the section "Materials and Methods." The median expression level [median signal intensity (MSI)] of each cell surface receptor of each cell population is illustrated by an individual heatmap. The expression level ranges from dark green (lowest expression) to dark red (highest expression). Significant differences in the level of cell surface receptor expression between non-infected [**(A,B)** left panel] and MVA-infected [**(A,B)** middle panel] cell populations are indicated for healthy persons [**(A)**, right table] and HIV-ART patients [**(B)**, right table]. **(C)** Significant differences in the level of cell surface receptor expression between healthy persons and HIV-ART patients are indicated for non-infected [**(C)**, left table] and MVA-infected [**(C)**, right table] cell populations. Differences with $p < 0.05$ were considered significant.

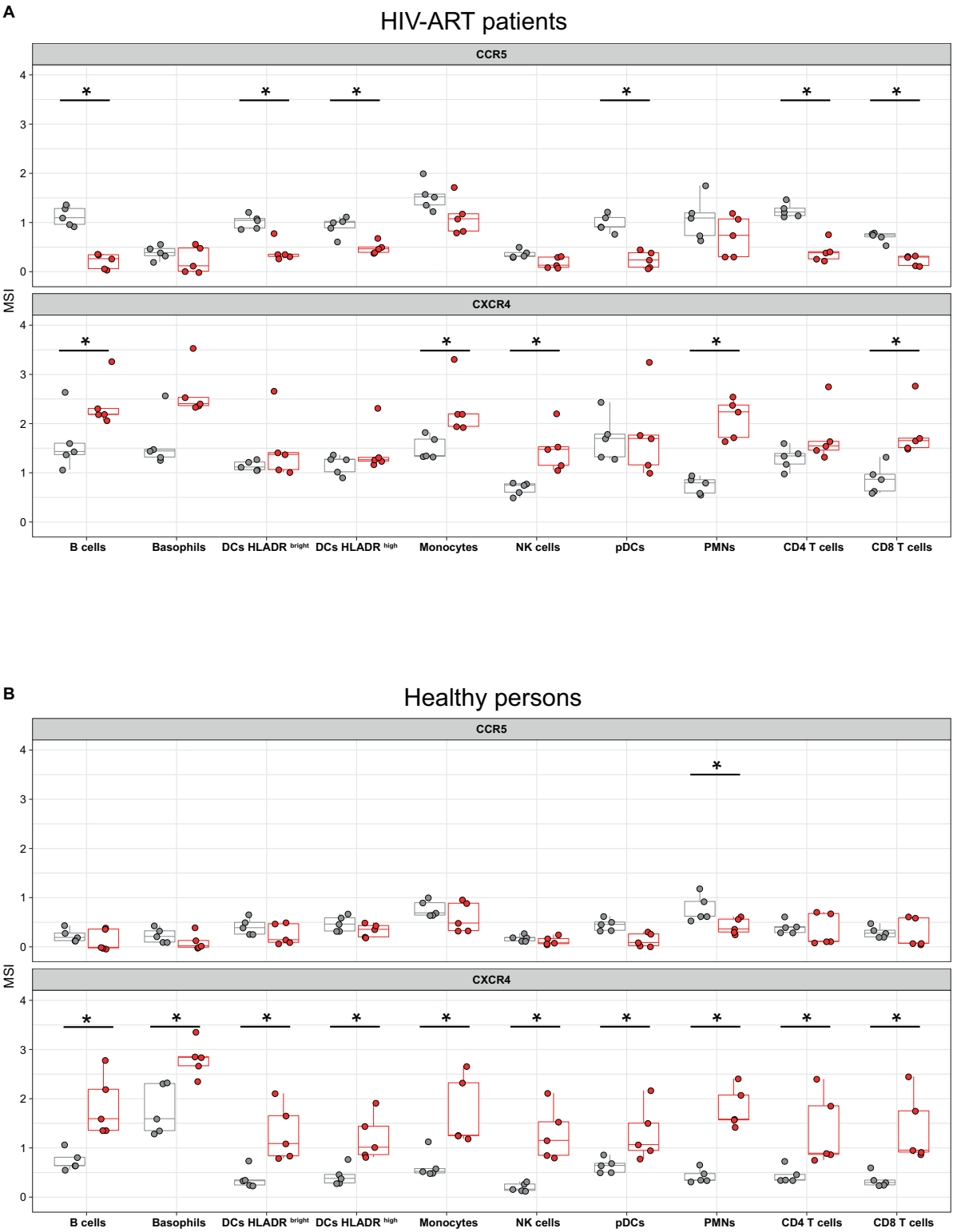

FIGURE 3 | Modified vaccinia virus Ankara (MVA) affects cell surface expression of C-C motif chemokine receptor (CCR5) and C-X-C motif chemokine receptor 4 (CXCR4) in leukocytes of HIV-ART patients and healthy persons. Whole-blood samples of HIV-ART patients **(A)** and healthy persons **(B)** were infected with MVA (red boxes) for 16 h or left non-infected (gray boxes). Cells were stained with a panel of 35 cell markers and analyzed with R software as described in the section "Materials and Methods." CCR5 and CXCR4 expression levels [median signal intensity (MSI)] of each sample are blotted in the respective jitter plot representations. Significant differences ($p < 0.05$) between samples are indicated by an asterisk.

and neutrophils from MVA-infected blood samples of HIV-ART patients as compared to cells from MVA-infected blood samples of healthy persons (**Figure 2C**, right panel).

DISCUSSION

Cell surface receptors enable intercellular communication and thereby they regulate cell proliferation, differentiation, migration, and death. Additionally, cell surface receptors mediate intracellular signaling leading to gene expression and the exchange of molecules with the cell environment. Obligate intracellular pathogens such as viruses can use cell surface molecules to get access to necessary resources, which enable their replication. It depends on the nature of the virus how this works in detail and whether this process is highly specific as in HIV-1 or promiscuous as in orthopoxviruses (40, 41).

In the present study, we confirmed previous findings that CCR5 expression is low in leukocytes of healthy persons and significantly increased in HIV-1-infected patients (37, 38). CCR5 is the main co-receptor of HIV-1 and expressed in many different hematopoietic and non-hematopoietic cell types. Decreased CCR5 surface expression delays AIDS progression and can prevent infection of cells with an R5-tropic HIV strain. It seems even possible to cure HIV-infected patients by transplantation of stem cells having a homozygous CCR5 gene with a 32-bp deletion that causes the total absence of CCR5 at the cell surface (42, 43). Consequently, CCR5 has been recognized as a key drug target against HIV (44), and here we discovered that infection of whole-blood samples with MVA downregulates cell surface expression of CCR5 in DCs, $CD4^+$ T cells, $CD8^+$ T cells, and B cells of HIV-1-infected patients. This result is in agreement with the finding of Guerra et al. (45) who detected by an RNA microarray that MVA downregulates CCR5 mRNA levels in human monocyte-derived DCs.

Modified vaccinia virus Ankara-infected cells were found in the blood and draining lymph node of cynomolgus macaques, which were inoculated intramuscularly with MVA (46). Systemic spread of MVA was also detected in mice and ferrets although MVA is unable to replicate in most mammalian cells (47–50), suggesting that MVA-infected cells acquire the ability to migrate to lymph nodes and other locations distant from the site of inoculation. Here, we found by mass cytometry that MVA increases cell surface expression of CXCR4 in each cell type of healthy persons but does not further increase the high level of CXCR4 surface expression in DCs, basophils, and $CD4^+$ T cells of HIV-ART patients. Thus, MVA-infected cells should migrate into organs, which express C-X-C motif chemokine ligand 12 (51), the only natural agonist for CXCR4 (52). Indeed, this was shown previously for neutrophils, which migrated into the draining lymph node and bone marrow after being infected with MVA in the skin (53). CXCR4 surface expression in leukocytes of HIV-ART patients was increased, which is in accordance with a recent study (54) but in contrast to previous findings in HIV-1-infected patients (38) and simian immunodeficiency virus (SIV)-infected cynomolgus macaques (55).

On the other hand, we could not confirm the upregulation of CD11b, CD32, and CD64 surface expression in monocytes and neutrophils of HIV-ART patients as reported (54). We even detected less CD11b surface expression in monocytes and neutrophils of HIV-ART patients as compared to cells of healthy persons. Upregulation of CD11b surface expression in human monocytes and neutrophils was reported for the reverse transcriptase inhibitor abacavir but not for tenofovir (56). Tenofovir in combination with emtricitabine and rilpivirine was used to treat patients in the present study except for patient number 4, who received abacavir in combination with lamivudine and dolutegravir. Probably, the potential stimulating effect of abacavir on CD11b surface expression was blocked by dolutegravir, which inhibits activation of nuclear factor (NF)-κB (57), an essential transcription factor for CD11b expression in neutrophils (58) and monocytes (59).

It was shown that MVA increases cell surface expression of CD86 in human monocyte-derived DCs (27). Here, we confirmed the upregulation of CD86 by MVA in DCs of HIV-ART patients, and the level of CD86 cell surface expression was even higher than in MVA-infected DCs of healthy persons. There is evidence that MVA increases the expression of CD86 in human monocyte-derived DCs mainly in non-infected bystander cells (60). Thus, we have to state that the effects of MVA on cell surface receptors as well as on chemokine expression that we observed cannot clearly be assigned to either infected cells or non-infected bystander cells. Consequently, that means that there could be a much higher number of cells affected by MVA than MVA-infected cells are virtually present in a system. This feature of MVA together with its ability to spread *in vivo* might have a systemic effect on the expression of cell surface receptors including CCR5.

Additionally, there is a consensus that cells of the monocyte/macrophage lineage are primarily infected by MVA *in vitro* and *in vivo* (29, 46, 61), and monocyte-derived tissue macrophages have a life span of months to years (62). Taken together, it could be possible that locally administered MVA modulates some systemic immune parameters for weeks or even months, which fits well in the concept of trained immunity (63, 64). In summary, here we found that MVA modulates the expression of many cell surface receptors, which can be different in healthy persons and HIV-ART patients in terms of quality and quantity. Moreover, we confirmed the ability of MVA to mature DCs and to induce chemokine expression in whole blood of HIV-ART patients and healthy persons. However, since many essential surface receptors were downregulated by MVA, it remains an open question whether the immunostimulatory activity of MVA is based only on the paracrine effects of MVA-induced cytokines or perhaps also on a not yet identified surface molecule, which is upregulated in MVA-infected cells.

DATA AVAILABILITY STATEMENT

Cytometric profiles collected in this study are available in the FlowRepository database under accession number FR-FCM-ZYVA.

ETHICS STATEMENT

The studies involving human participants were reviewed and approved by the Comité de Protection des Personnes (CPP) Ile de France VII, under protocol number PP 14-003. The patients/participants provided their written informed consent to participate in this study.

AUTHOR CONTRIBUTIONS

AC, AL, and NT contributed to the conceptualization and methodology. AC, AL, EM, QJ, OL, RL, and NT contributed to the validation. AL, QJ, and NT contributed to the formal analysis. AC, AL, QJ, and NT contributed to the investigation. AL and OL contributed to the resources. AL, ML, and NT contributed to the writing of the original draft. AC and RL contributed to the acquisition of funding. AC, OL, RL, and NT contributed to the supervision. All authors contributed to the writing, reviewing, and editing.

FUNDING

The IDMIT infrastructure was supported by the French Government "Programme d'Investissements d'Avenir" (PIA) under Grant ANR-11-INBS-0008 and grant ANR-10-EQPX-02-01 (FlowCyTech facility). NT was supported by fellowships from the ANRS (France Recherche Nord & Sud Sida-hiv Hépatites).

ACKNOWLEDGMENTS

We warmly thank the patients and healthy donors. We are grateful to the physicians at the Bicêtre Hospital.

SUPPLEMENTARY MATERIAL

The Supplementary Material for this article can be found online at: https://www.frontiersin.org/articles/10.3389/fimmu.2020.02096/full#supplementary-material

REFERENCES

1. Kretzschmar M, Wallinga J, Teunis P, Xing S, Mikolajczyk R. Frequency of adverse events after vaccination with different vaccinia strains. *PLoS Med*. (2006) 3:e272. doi: 10.1371/journal.pmed.0030272
2. Casey CG, Iskander JK, Roper MH, Mast EE, Wen XJ, Török TJ, et al. Adverse events associated with smallpox vaccination in the United States, January-October 2003. *J Am Med Assoc*. (2005) 294:2734–43. doi: 10.1001/jama.294.21.2734
3. Mayr A, Munz E. [Changes in the vaccinia virus through continuing passages in chick embryo fibroblast cultures]. *Zentralbl Bakteriol Orig*. (1964) 195:24–35.
4. Mahnel H, Mayr A. Experiences with immunization against orthopox viruses of humans and animals using vaccine strain MVA. *Berl Munch Tierarztl Wochenschr*. (1994) 107:253–6.
5. Pittman PR, Hahn M, Lee HS, Koca C, Samy N, Schmidt D, et al. Phase 3 efficacy trial of modified vaccinia ankara as a vaccine against smallpox. *N Engl J Med*. (2019) 381:1897–908. doi: 10.1056/NEJMoa1817307
6. Amato RJ, Stepankiw M. Evaluation of MVA-5T4 as a novel immunotherapeutic vaccine in colorectal, renal and prostate cancer. *Future Oncol*. (2012) 8:231–7. doi: 10.2217/fon.12.7
7. Medina-Echeverz J, Hinterberger M, Testori M, Geiger M, Giessel R, Bathke B, et al. Synergistic cancer immunotherapy combines MVA-CD40L induced innate and adaptive immunity with tumor targeting antibodies. *Nat Commun*. (2019) 10:5041. doi: 10.1038/s41467-019-12998-6
8. Gilbert SC. Clinical development of modified vaccinia virus Ankara vaccines. *Vaccine*. (2013) 31:4241–6. doi: 10.1016/j.vaccine.2013.03.020
9. Kreijtz JHCM, Goeijenbier M, Moesker FM, van den Dries L, Goeijenbier S, De Gruyter HLM, et al. Safety and immunogenicity of a modified-vaccinia-virus-Ankara-based influenza A H5N1 vaccine: a randomised, double-blind phase 1/2a clinical trial. *Lancet Infect Dis*. (2014) 14:1196–207. doi: 10.1016/S1473-3099(14)70963-6
10. Condit RC, Williamson A, Sheets R, Seligman SJ, Monath TP, Excler J, et al. Unique safety issues associated with virus vectored vaccines: potential for and theoretical consequences of recombination with wild type virus strains. *Vaccine*. (2017) 34:6610–6. doi: 10.1016/j.vaccine.2016.04.060
11. Kochhar S, Excler J, Bok K, Gurwith M, Mcneil MM, Seligman SJ, et al. Defining the interval for monitoring potential adverse events following immunization (AEFIs) after receipt of live viral vectored vaccines. *Vaccine*. (2018) 37:5796–802. doi: 10.1016/j.vaccine.2018.08.085
12. Routy JP, Mehraj V. Potential contribution of gut microbiota and systemic inflammation on HIV vaccine effectiveness and vaccine design. *AIDS Res Ther*. (2017) 14:1–6. doi: 10.1186/s12981-017-0164-9
13. Zicari S, Sessa L, Cotugno N, Ruggiero A, Morrocchi E, Concato C, et al. Immune activation, inflammation, and Non-AIDS co-morbidities in HIV-infected patients under long-term ART. *Viruses*. (2019) 11:200. doi: 10.3390/v11030200
14. Iyer SS, Amara RR. DNA/MVA vaccines for HIV/AIDS. *Vaccines*. (2014) 2:160–78. doi: 10.3390/vaccines2010160
15. Kutscher S, Allgayer S, Dembek CJ, Bogner JR, Protzer U, Goebel FD, et al. MVA- nef induces HIV-1-specific polyfunctional and proliferative T-cell responses revealed by the combination of short- and long-term immune assays. *Gene Ther*. (2010) 17:1372–83. doi: 10.1038/gt.2010.90
16. Gómez CE, Perdiguero B, García-arriaza J, Cepeda V, Sánchez-sorzano CÓ, Mothe B, et al. A phase I randomized therapeutic MVA-B vaccination improves the magnitude and quality of the T cell immune responses in HIV-1-infected subjects on HAART. *PLoS One*. (2015) 10:e0141456. doi: 10.1371/journal.pone.0141456
17. Greenough TC, Cunningham CK, Muresan P, McManus M, Persaud D, Fenton T, et al. Safety and immunogenicity of recombinant poxvirus HIV-1 vaccines in young adults on highly active antiretroviral therapy. *Vaccine*. (2008) 26:6883–93. doi: 10.1016/j.vaccine.2008.09.084
18. Cosma A, Nagaraj R, Bühler S, Hinkula J, Busch DH, Sutter G, et al. Therapeutic vaccination with MVA-HIV-1 nef elicits Nef-specific T-helper cell responses in chronically HIV-1 infected individuals. *Vaccine*. (2003) 22:21–9. doi: 10.1016/s0264-410x(03)00538-3
19. Ponnan SM, Pattabiram S, Thiruvengadam K, Goyal R, Singla N, Mukherjee J, et al. Induction and maintenance of bi-functional (IFN-γ + IL-2+ and IL-2+ TNF-α+) T cell responses by DNA prime MVA boosted subtype C prophylactic vaccine tested in a phase I trial in India. *PLoS One*. (2019) 14:e0213911. doi: 10.1371/journal.pone.0213911
20. Viegas EO, Kroidl A, Munseri PJ, Missanga M, Nilsson C, Tembe N, et al. Optimizing the immunogenicity of HIV prime- boost DNA-MVA-rgp140 / GLA vaccines in a phase II randomized factorial trial design. *PLoS One*. (2018) 12:e0206838. doi: 10.1371/journal.pone.0206838
21. Baden LR, Walsh SR, Seaman MS, Cohen YZ, Johnson JA, Licona JH, et al. First-in-human randomized, controlled trial of mosaic HIV-1 immunogens delivered via a modified vaccinia Ankara vector. *J Infect Dis*. (2018) 218:633–44. doi: 10.1093/infdis/jiy212
22. Philip JRP, Torres-Domínguez LE, Brandmüller C, Sutter G, Lehmann MH. Modified vaccinia virus Ankara: innate immune activation and induction of

cellular signalling. *Vaccine*. (2013) 31:4231–4. doi: 10.1016/j.vaccine.2013.03.017
23. Nörder M, Becker P, Drexler I, Link C, Erfle V, Guzma C. Modified vaccinia virus Ankara exerts potent immune modulatory activities in a murine model. *PLoS One*. (2010) 5:e11400. doi: 10.1371/journal.pone.0011400
24. Lehmann MH, Price PJR, Brandmüller C, Sutter G. Modified vaccinia virus Ankara but not vaccinia virus induces chemokine expression in cells of the monocyte / macrophage lineage. *Virol J*. (2015) 12:1–6. doi: 10.1186/s12985-015-0252-1
25. Royo S, Sainz B, Hernandez-Jimenez E, Reyburn H, Lopez-Collazo E, Guerra S. Differential induction of apoptosis, interferon signaling, and phagocytosis in macrophages infected with a panel of attenuated and nonattenuated poxviruses. *J Virol*. (2014) 88:5511–23. doi: 10.1128/JVI.00468-14
26. Lehmann MH, Kastenmuller W, Kandemir JD, Brandt F, Suezer Y, Sutter G. Modified vaccinia virus Ankara triggers chemotaxis of monocytes and early respiratory immigration of leukocytes by induction of CCL2 expression. *J Virol*. (2009) 83:2540–52. doi: 10.1128/JVI.01884-08
27. Drillien R, Spehner D, Hanau D. Modified vaccinia virus Ankara induces moderate activation of human dendritic cells. *J Gen Virol*. (2004) 85:2167–75. doi: 10.1099/vir.0.79998-0
28. Kastenmuller W, Drexler I, Ludwig H, Erfle V, Peschel C, Bernhard H, et al. Infection of human dendritic cells with recombinant vaccinia virus MVA reveals general persistence of viral early transcription but distinct maturation-dependent cytopathogenicity. *Virology*. (2006) 350:276–88. doi: 10.1016/j.virol.2006.02.039
29. Brandler S, Lepelley A, Desdouits M, Guivel-Benhassine F, Ceccaldi PE, Levy Y, et al. Preclinical studies of a modified vaccinia virus Ankara-based HIV candidate vaccine: antigen presentation and antiviral effect. *J Virol*. (2010) 84:5314–28. doi: 10.1128/jvi.02329-09
30. Chen B. Molecular mechanism of HIV-1 Entry. *Trends Microbiol*. (2019) 27:878–91. doi: 10.1016/j.tim.2019.06.002
31. Kremer M, Volz A, Kreijtz JHCM, Fux R, Lehmann MH, Sutter G. Easy and efficient protocols for working with recombinant vaccinia virus MVA. *Methods Mol Biol*. (2012) 890:59–92. doi: 10.1007/978-1-61779-876-4_4
32. Leite Pereira A, Tchitchek N, Marcos Lopez E, Lambotte O, Le Grand R, Cosma A. A high-resolution mass cytometry analysis reveals a delay of cytokines production after TLR4 or TLR7/8 engagements in HIV-1 infected humans. *Cytokine*. (2018) 111:97–105. doi: 10.1016/j.cyto.2018.08.018
33. Palgen JL, Tchitchek N, Rodriguez-Pozo A, Jouhault Q, Abdelhouahab H, Dereuddre-Bosquet N, et al. Innate and secondary humoral responses are improved by increasing the time between MVA vaccine immunizations. *NPJ Vaccines*. (2020) 5:24. doi: 10.1038/s41541-020-0175-8
34. Elhmouzi-younes J, Palgen J, Tchitchek N, Delandre S, Namet I, Bodinham CL, et al. In depth comparative phenotyping of blood innate myeloid leukocytes from healthy humans and macaques using mass cytometry. *Cytom A*. (2017) 91:969–82. doi: 10.1002/cyto.a.23107
35. Qiu P, Simonds EF, Bendall SC, Gibbs KD, Bruggner RV, Linderman MD, et al. Extracting a cellular hierarchy from high-dimensional cytometry data with SPADE. *Nat Biotechnol*. (2011) 29:886–91. doi: 10.1038/nbt.1991
36. Finck R, Simonds EF, Jager A, Krishnaswamy S, Sachs K, Fantl W, et al. Normalization of mass cytometry data with bead standards. *Cytom Part A*. (2013) 83:483–94. doi: 10.1002/cyto.a.22271
37. Rosati M, Valentin A, Patenaude DJ, Pavlakis GN. Lymphocytes from HIV-1-infected individuals. *J Immunol*. (2001) 167:1654–62. doi: 10.4049/jimmunol.167.3.1654
38. Shalekoff S, Pendle S, Johnson D, Martin DJ, Tiemessen CT. Distribution of the human immunodeficiency virus coreceptors CXCR4 and CCR5 on leukocytes of persons with human immunodeficiency virus type 1 infection and pulmonary tuberculosis: implications for pathogenesis. *J Clin Immunol*. (2001) 21:390–401. doi: 10.1023/a:1013121625962
39. Chen L, Flies DB. Molecular mechanisms of T cell co-stimulation and co-inhibition. *Nat Rev Immunol*. (2013) 13:227–42. doi: 10.1038/nri3405
40. Wilen CB, Tilton JC, Doms RW. HIV: cell binding and entry. *Cold Spring Harb Perspect Med*. (2012) 2:1–13. doi: 10.1101/cshperspect.a006866
41. McFadden G. Poxvirus tropism. *Nat Rev Microbiol*. (2005) 3:201–13. doi: 10.1038/nrmicro1099
42. Gupta RK, Abdul-Jawad S, McCoy LE, Mok HP, Peppa D, Salgado M, et al. HIV-1 remission following CCR5Δ32/Δ32 haematopoietic stem-cell transplantation. *Nature*. (2019) 568:244–8. doi: 10.1038/s41586-019-1027-4
43. Hütter G, Nowak D, Mossner M, Ganepola S, Müssig A, Allers K, et al. Long-term control of HIV by CCR5 Delta32/Delta32 stem-cell transplantation. *N Engl J Med*. (2009) 360:692–8. doi: 10.1056/NEJMoa0802905
44. Lopalco L. CCR5: from natural resistance to a new anti-HIV strategy. *Viruses*. (2010) 2:574–600. doi: 10.3390/v2020574
45. Guerra S, Na L, Gonza M, Lo LA, Climent N, Gatell M, et al. Distinct gene expression profiling after infection of immature human monocyte-derived dendritic cells by the attenuated poxvirus vectors MVA and NYVAC. *J Virol*. (2007) 81:8707–21. doi: 10.1128/JVI.00444-07
46. Altenburg AF, Van De Sandt CE, Li BWS, Macloughlin RJ, Fouchier RAM, Van Amerongen G, et al. Modified vaccinia virus ankara preferentially targets antigen presenting cells in vitro, ex vivo and in vivo. *Sci Rep*. (2017) 7:1–14. doi: 10.1038/s41598-017-08719-y
47. Blanchard TJ, Alcami A, Andrea P, Smith GL. Modified vaccinia virus Ankara undergoes limited replication in human cells and lacks several immunomodulatory proteins:implications for use as a human vaccine. *J Gen Virol*. (1998) 79:1159–67. doi: 10.1099/0022-1317-79-5-1159
48. Drexler I, Heller K, Wahren B, Erfle V, Sutter G. Highly attenuated modified vaccinia virus Ankara replicates in baby hamster kidney cells, a potential host for virus propagation, but not in various human transformed and primary cells. *J Gen Virol*. (1998) 79:347–52. doi: 10.1099/0022-1317-79-2-347
49. Moss B, Carroll MW, Wyatt LS, Bennink JR, Hirsch VM, Goldstein S, et al. Host range restricted, non-replicating vaccinia virus vectors as vaccine candidates. *Adv Exp Med Biol*. (1996) 397:7–13. doi: 10.1007/978-1-4899-1382-1_2
50. Wyatt LS, Moss B, Rozenblatt S. Replication-deficient vaccinia virus encoding bacteriophage T7 RNA polymerase for transient gene expression in mammalian cells. *Virology*. (1995) 210:202–5. doi: 10.1006/viro.1995.1332
51. Müller A, Homey B, Soto H, Ge N, Catron D, Buchanan ME, et al. Involvement of chemokine receptors in breast cancer metastasis. *Nature*. (2001) 410:50–6. doi: 10.1038/35065016
52. Bachelerie F, Ben-baruch A, Burkhardt AM, Combadiere C, Farber JM, Graham GJ, et al. Update on the extended family of chemokine receptors and introducing a new nomenclature for atypical chemokine receptors. *Pharmacol Rev*. (2014) 66:1–79. doi: 10.1124/pr.113.007724
53. Duffy D, Perrin H, Abadie V, Benhabiles N, Boissonnas A, Liard C, et al. Neutrophils transport antigen from the dermis to the bone marrow, initiating a source of memory CD8+ T cells. *Immunity*. (2012) 37:917–29. doi: 10.1016/j.immuni.2012.07.015
54. Leite Pereira A, Tchitchek N, Lambotte O, Le Grand R, Cosma A. Characterization of leukocytes from HIV-ART patients using combined cytometric profiles of 72 cell markers. *Front Immunol*. (2019) 10:1777. doi: 10.3389/fimmu.2019.01777
55. Lemaitre J, Cosma A, Desjardins D, Lambotte O, Le Grand R. Mass cytometry reveals the immaturity of circulating neutrophils during SIV infection. *J Innate Immun*. (2019) 12:170–81. doi: 10.1159/000499841
56. De Pablo C, Orden S, Calatayud S, Martí-Cabrera M, Esplugues JV, Álvarez Á. Differential effects of tenofovir/emtricitabine and abacavir/lamivudine on human leukocyte recruitment. *Antivir Ther*. (2012) 17:1615–9. doi: 10.3851/IMP2357
57. Afonso P, Auclair M, Caron-Debarle M, Capeau J. Impact of CCR5, integrase and protease inhibitors on human endothelial cell function, stress, inflammation and senescence. *Antivir Ther*. (2017) 22:645–57. doi: 10.3851/IMP3160
58. Sokoloski JA, Sartorelli AC, Rosen CA, Narayanan R. Antisense oligonucleotides to the p65 subunit of NF-kB block CD11b expression and alter adhesion properties of differentiated HL-60 granulocytes. *Blood*. (1993) 82:625–32. doi: 10.1182/blood.v82.2.625.bloodjournal822625
59. Dai Y, Rahmani M, Grant S. An intact NF-kappaB pathway is required for histone deacetylase inhibitor-induced G1 arrest and maturation in U937 human myeloid leukemia cells. *Cell Cycle*. (2003) 2:467–72. doi: 10.4161/cc.2.5.465

60. Pascutti MF, Rodríguez AM, Falivene J, Giavedoni L, Drexler I, Gherardi MM. Interplay between modified vaccinia virus ankara and dendritic cells: phenotypic and functional maturation of bystander dendritic cells. *J Virol*. (2011) 85:5532–45. doi: 10.1128/JVI.02267-10
61. Liu L, Chavan R, Feinberg MB. Dendritic cells are preferentially targeted among hematolymphocytes by modified vaccinia virus Ankara and play a key role in the induction of virus-specific T cell responses in vivo. *BMC Immunol*. (2008) 9:15. doi: 10.1186/1471-2172-9-15
62. Röszer T. Understanding the biology of self-renewing macrophages. *Cells*. (2018) 7:103. doi: 10.3390/cells7080103
63. Töpfer E, Boraschi D, Italiani P. Innate immune memory: the latest frontier of adjuvanticity. *J Immunol Res*. (2015) 2015:478408. doi: 10.1155/2015/478408
64. Sánchez-Ramón S, Conejero L, Netea MG, Sancho D, Palomares Ó, Subiza JL. Trained immunity-based vaccines: a new paradigm for the development of broad-spectrum anti-infectious formulations. *Front Immunol*. (2018) 9:2936. doi: 10.3389/fimmu.2018.02936

Conflict of Interest: The authors declare that the research was conducted in the absence of any commercial or financial relationships that could be construed as a potential conflict of interest.

frontiers in Immunology

ORIGINAL RESEARCH
published: 23 September 2020
doi: 10.3389/fimmu.2020.579761

Vaccine Adjuvants Differentially Affect Kinetics of Antibody and Germinal Center Responses

Gabriel Kristian Pedersen[1], *Katharina Wørzner*[1], *Peter Andersen*[1,2] *and Dennis Christensen*[1]*

[1] Center for Vaccine Research, Statens Serum Institut, Copenhagen, Denmark, [2] Department of Immunology and Microbiology, University of Copenhagen, Copenhagen, Denmark

Aluminum salts and squalene based oil-in-water emulsions (SE) are widely used adjuvants in licensed vaccines, yet their mechanisms are not fully known. Here we report that induction of antibody responses displays different kinetics dependent on the adjuvant used. SE facilitated a rapid antibody response in contrast to aluminum hydroxide (AH) and the depot-forming cationic liposome-based adjuvant (CAF01). Antigen given with the SE adjuvant rapidly reached follicular B cells in the draining lymph node, whereas antigen formulated in AH or CAF01 remained at the site of injection as a depot. Removal of the injection site early after immunization abrogated antibody responses only when antigen was given in the depot-forming adjuvants. Despite initial delays in B cell activation and germinal center (GC) formation when antigen was given in depot-forming adjuvants, the antibody levels reached higher magnitudes than when the antigen was formulated in SE. This study demonstrates that the kinetic aspect of antibody responses is critical in adjuvant benchmarking and suggests that the optimal vaccination regime depends on the adjuvant used.

Keywords: adjuvant, vaccine, antibody, kinetics, germinal center (GC), alum, squalene emulsion, CAF01

OPEN ACCESS

Edited by:
Scott James Tebbutt, The University of British Columbia, Canada

Reviewed by:
Ugo D'Oro, GlaxoSmithKline, Italy
Oliver W. Gramlich, The University of Iowa, United States

***Correspondence:**
Dennis Christensen
den@ssi.dk

Specialty section:
This article was submitted to Vaccines and Molecular Therapeutics, a section of the journal Frontiers in Immunology

Received: *03 July 2020*
Accepted: *24 August 2020*
Published: *23 September 2020*

Citation:
Pedersen GK, Wørzner K, Andersen P and Christensen D (2020) Vaccine Adjuvants Differentially Affect Kinetics of Antibody and Germinal Center Responses. Front. Immunol. 11:579761. doi: 10.3389/fimmu.2020.579761

INTRODUCTION

Antibody responses are the best correlate of protection against many infectious diseases and vaccines inducing optimal antibody responses are therefore desired (1). Adjuvants are used to augment or modify immune responses and the choice of adjuvant can impact both the affinity, specificity, and functional profile of the elicited antibody response (2, 3). The mechanism of action for adjuvants is becoming increasingly well-defined, particularly for those that ligate pathogen recognition receptors, such as toll-like receptors (4). However, for many adjuvants, such as Aluminum-based (e.g., Aluminum hydroxide (AH), often referred to as "Alum") and squalene based oil-in-water emulsions (e.g., MF59^{TM}), the mechanism of action is less clear and may be a combinational effect [e.g., induction of apoptosis and DAMP signaling (4–6)]. Some adjuvants also retain antigen at the site of injection and the ability of aluminum salts to induce an antigen depot was long believed to be essential for the adjuvant effect, although this has lately been questioned (7, 8). With an increasing number of adjuvants going from pre-clinical to clinical development, there is an unmet need for adjuvant benchmarking studies (9).

Optimal elicitation of antibody responses requires a number of ordered events. Priming of antibody responses against T-dependent antigens predominantly occurs in lymph nodes (LN) draining the site of injection (10) upon acquisition of antigen by follicular B cells (11). After

interacting with T helper cells at the T/B border, responding B cell clones can initiate a germinal center (GC) reaction, in which the B cells proliferate, mature their B cell receptors to increase affinity and perform class-switching (12). A prerequisite to GC formation is transport of unprocessed antigen to lymphoid organs, which may occur *via* active cellular transport or lymphatic drainage (13, 14). Strategies to promote transport to follicular B cells, such as antigen acquisition by innate immune cells at the site of injection (15), their migration to LNs and delivery of antigen to follicular dendritic cells and B cells (16), therefore hold the potential to favor germinal center reactions, induce class-switching and promote high-affinity antibody responses. On the contrary, adjuvants that sequester antigen at the site of injection may cause a limited antigen presentation to follicular dendritic cells and B cells, which could manifest as reduced or delayed B cell activation, germinal center formation and resulting antibody responses. Notably, slow-release of antigen could also be of advantage, since a constant feeding of antigen to existing germinal centers may aid in sustaining these, possibly promoting affinity maturation (17–19). Data supporting this theory have been generated using continuous antigen delivery either by repeated boosting, mini-pellets, microneedles or *via* osmotic sustained release pumps (17, 20–23). However, studies addressing how vaccine depot formation influences immune response kinetics are lacking.

In previous studies comparing clinically tested adjuvants, emulsion-based adjuvants (e.g., MF59^{TM} and GLA-SE) promoted a rapid increase in antibody titers, whilst adjuvants which have been suggested to form a vaccine depot [e.g., CAF01 and AH (5, 24), gave distinctly low responses early after immunization (9, 25–27)]. We hypothesized that antibody response kinetics depend on the type of adjuvant applied, and since these studies investigated responses only 7–14 days post immunization, it was possible that the adaptive immunity had not fully matured at these early time points. We therefore performed a study to follow kinetics of GC formation and antibody responses after a single immunization with antigen formulated in adjuvants. We compared adjuvants reported to retain antigen at the site of injection [CAF01 (24, 28) and AH (5)], to emulsions [MF59^{TM}-like squalene emulsion AddaVax^{TM} (SE)] that are reported not to retain antigen (29). Antigen tracking studies revealed that CAF01 and AH indeed facilitated retention of antigen at the site of injection, whilst antigen formulated in SE rapidly associated with follicular B cells in draining LNs. Moreover, we found that GC's appeared earlier in mice immunized with antigen formulated in SE adjuvant than with the CAF01 and AH adjuvants and that this was paralleled by a faster antibody response. However, at later time points the depot-forming adjuvants resulted in higher magnitude antibody responses than the non-depot-forming adjuvant. This study shows that adjuvants differentially affect GC kinetics, which may influence the optimal timing for booster vaccinations and is essential to take in to account when comparing different adjuvants.

MATERIALS AND METHODS

Mice

Female CB6F1 (CB6F1/OlaHsD) wild type mice, 6–8 weeks old, were ordered from Harlan Laboratories (The Netherlands) and housed in the animal facilities at Statens Serum Institut, Denmark. Mouse studies were conducted in accordance with the regulations set forth by the national animal protection committee and in accordance with European Community Directive 86/609. The experiments performed have been approved by the governmental Animal Experiments Inspectorate under licenses 2014-15-2934-01065 and 2017-15-0201-01363.

Antigens and Adjuvants

Chlamydia trachomatis antigen CTH522 (MOMPextVD4) and *M. tuberculosis* H56 antigens were recombinantly produced in *E. coli* K12 as described previously (9, 30). OVA-AF647 was from Invitrogen and NP_{20}-OVA (4-Hydroxy-3-nitrophenylacetyl-OVA) from Biosearch technologies. CAF01 (DDA/TDB) was produced in house (Statens Serum Institut, Copenhagen, Denmark) (31), The AddaVax^{TM} oil-in-water squalene emulsion (SE) was from Invivogen (Toulouse, France) and aluminum oxyhydroxide (AH) (2% Alhydrogel®) was from Brenntag Biosector (Frederikssund, Denmark).

Immunizations

Mice were given a single immunization subcutaneously (s.c.) at the base of the tail with 5 μg recombinant CTH522 antigen (SSI) or NP-OVA (Biosearch Technologies) in a volume of 200 μl TRIS buffer (pH 7.4) per immunization. Adjuvant doses were according to manufacturer's instructions: CAF01 (dose 250 μg/50 μg (DDA/TDB), SE (dose of 100 μl 4.3% w/v squalene, 0.5% w/v Tween 80, 0.5% w/v Span 85 mixed 1:1 with antigen/PBS) and AH (dose of 500 μg Aluminum content). Control mice (antigen alone) received 5 μg recombinant antigen in 200 μL PBS.

Surgery for Injection Site Removal

Mice were injected intradermally (i.d.) at the back (after cutting the hair with electric clippers) with CTH522 (5 μg) in CAF01 (125 μg DDA/25 μg TDB), SE (mixed 1:1 with antigen/PBS) or AH (dose of 125–250 μg Aluminum content) in a total volume of 25–50 μl. Antigen depots were removed at various time points after vaccine administration. Mice were anesthetized using Zoletil-mix (tiletaminhydrochloride/zolazepamhydrochloride/xylazin/butorphanol) and a small incision was made in the skin to remove the antigen depot. The incision was closed with tissue adhesive (3M Vetbond) and/or surgical silk-thread (Vicryl 6-9, Ethicon) and Carprofen analgesia was administered for 4 days post-surgery. All mice, including the control group, were anesthetized and received analgesic treatment.

Organ Preparation

LNs and spleens were filtered through a 70 μm nylon mesh (BD Biosciences). Muscle tissue was treated with enzymes A, D, and P of the Skeletal Muscle Dissociation Kit (Miltenyi Biotec GmbH,

Bergisch Gladbach, Germany) according to the manufacturer's instructions. Muscle tissues were then prepared for single cell suspensions using the GentleMACS system (Miltenyi Biotec GmbH, Bergisch Gladbach, Germany). Muscle supernatants were used for cytokine profiling (see below). The cells were washed and prepared as previously described (9) and re-suspended in cell culture medium (RPMI-1640 supplemented with $5 \times 10\text{-}^5$ M 2-mercaptoethanol, 1% pyruvate, 1% HEPES, 1% (v/v) premixed penicillin-streptomycin solution (Invitrogen Life Technologies), 1 mM glutamine, and 10% (v/v) fetal calve serum (FCS). The cells were adjusted to 2×10^5 cells/well (MSD/ cytokine ELISA) or 1–2 $\times 10^6$ cells/well (Flow cytometry).

In vivo Tracking Studies

OVA coupled to AlexaFluor (AF) 647 (Thermo Scientific) was mixed with TRIS buffer (pH 7.4) and administered alone or with the indicated adjuvant at a dose of 5 μg either intramuscularly (i.m.) (50 μl) in the thigh muscle or s.c. (200 μl) at the base of tail as stated. Mice were euthanized 6, 24, 48 h or 7 days after the injection. Muscle tissue and draining LNs (inguinal) were isolated and used for flow cytometry.

Cytokine Profiling

The Mouse U-plex (custom cytokine: MIP-1α, IL-12p70, IL-1β, IL-6, TNF-α, MCP-1, IL-5, and IL-10) was performed according to the manufacturer's instructions (Meso Scale Discovery) to measure cytokine concentrations in muscle supernatants. The plates were read on the Sector Imager 2400 system (Meso Scale Discovery) and calculation of cytokine concentrations in unknown samples was determined by 4-parameter logistic non-linear regression analysis of the standard curve. IFN-γ and IL-17 responses were measured by ELISA as described previously, using supernatants from splenocyte cultures stimulated *in vitro* with CTH522 antigen (2 μg/ml) in cell culture medium for 72 h at 37°C and 5% CO_2 (30).

Immunohistology

Mice were injected into the thigh muscle with CTH522 alone or in the presence of the indicated adjuvant. At 6, 24, and 48 h and at 7 and 60 days post injection, muscles were collected and fixed in formalin. Tissues were embedded into paraffin and sectioned to 4 μm thickness. Hematoxylin (HE) (Histolab Ab) and Immunoperoxidase staining followed by rabbit anti-CD64 (Sino Biologicals) and HRP-polymer anti-rabbit antibody (Nordic Biosite) was performed. Tissues were scored for CD64 positive cells as <100 (0), 100–1,000 (1), 1,000–2,000 (2), 2,000–5,000 (3) or >5,000 cells (4) per muscle.

Inguinal LNs were isolated following subcutaneous injection at the base of tail with CTH522 alone or in the presence of the indicated adjuvant and at various time points after administration assessed for germinal centers. 4 μm thick paraffin-embedded tissue sections were stained with HE and rabbit anti-Ki67 (Sp6) followed by HRP-polymer anti-rabbit antibody (Nordic Biosite). Germinal centers were identified as clusters of Ki67 positive cells and the surface areas of the germinal centers were measured. Slide quality was controlled utilizing an Olympus BX-60 microscope and an integrated Scion color digital camera. Slides were digitalized utilizing a 3D-Histech Panoramic MIDI and HV-F22 Hitatchi camera and interpreted with Case Viewer software. Stainings and interpretation of slides were assessed by a pathologist who was blinded to the treatment groups.

ELISA for Antibody Responses

Maxisorb Plates (Nunc) were coated with 0.05 μg/well CTH522 overnight at 4°C. Individual mouse sera were analyzed in duplicate. After blocking, serum was added in PBS with 2% BSA, starting with a 30-fold dilution for antigen-specific IgM, IgG or IgG subclasses. HRP-conjugated secondary antibody [rabbit anti-mouse IgG (Zymed), Goat anti-mouse IgG1 (Southern Biotech) or IgG2c (Thermofischer)] was diluted in PBS with 1% BSA. For detection of IgM, serum was added in PBS with 5% skimmed milk and detection was done using biotin conjugated anti-mouse IgM (Southern Biotech) for 1 h followed by streptavidin-HRP (BD Biosciences). After 1 h of incubation, antigen-specific antibodies were detected using TMB substrate as described by the manufacturer (Kem-En-Tec Diagnostics). The absorbance values were plotted as a function of the reciprocal dilution of serum samples. Antibody titers were determined as the highest serum dilution corresponding to a cut-off of ≥0.2 OD450. To measure anti-NP antibody responses, ELISA plates were coated with 0.1 μg/well of BSA coupled with different ratios of NP (NP2-BSA and NP13-BSA) (Biosearch Technologies).

Flow Cytometry

One million cells were stained in PBS+1% FBS. Cocktails of antibodies against the following surface proteins were used: B220 PerCP-Cy5.5 (RA3-6B2), B220 FITC (RA3-6B2), GL7 BV421 (GL7), IgD BV786 (11-26c.2a), Ly6G PE (1A8), CD11b PerCP-Cy5.5 (M1/70), CD11b PE-Cy7 (M1/70), CD4 APC (RM4-5), CxCR5 BV421 (2G8), CD11c BV421 (HL3) (All BD) CD38 PE-Cy7 (90), F4/80 PE-Cy7 (BM8), F4/80 APC-EF780 (eBioscience), CD11c APC-Cy7 (N418), and PD-1 BV605 (29F.1A12) (Biolegend). A live/dead marker was used to exclude dead cells in the GC B and TFH cell panels (Fixable Viability Dye eFluor™ 780, eBioscience). AF647-labeled ovalbumin (OVA-AF647) was from Invitrogen. Antigen-specific germinal center B cells were measured by including CTH522 coupled to AF488 as probe (conjugated by Life technologies at a coupling ratio of 3 moles dye/mole). Cells were analyzed on a BD Fortessa or FACSCanto flow cytometer.

Statistical Analysis

Differences between adjuvanted groups were analyzed by Kruskal-Wallis test (antibody titres), using the SE group as reference, and Dunn's test for multiple comparisons or One-way ANOVA, using the SE group as reference, and Dunnett's test for multiple comparisons. Prism 8 software (GraphPad v8.2.1) was used for all statistical analyses.

RESULTS

Adjuvants Differentially Influence Kinetics of Antibody Responses

To investigate kinetics of antibody responses, we performed subcutaneous immunizations with the clinically tested *Chlamydia trachomatis* protein antigen CTH522 (32) formulated in either CAF01, SE or AH and analyzed antigen-specific IgM and IgG antibody responses. SE facilitated a rapid increase in IgM antibody at 7 days following immunization (significantly higher than in the CAF01 ($p = 0.041$) and AH ($p = 0.003$) groups, whilst in the AH and CAF01 groups IgM responses remained low until day 14 (**Figure 1A**). Antigen-specific IgG responses were also highest in the SE group at day 7 [Significant compared to the CAF01 group ($p = 0.014$) (**Figure 1B**)], whilst at day 14 IgG responses were similar in all groups. At days 21 and 42 IgG titers were higher in mice that had received AH (significant, $p =$ 0.002–0.031) and CAF01 (not significant $p = 0.34$) as compared to the SE adjuvant. The IgG responses consisted predominantly of IgG1 in all adjuvanted groups, whereas IgG2c responses were low after a single immunization (**Supplementary Figure 1**). Similar kinetics of antibody responses were seen when using the *Mycobacterium tuberculosis* fusion protein H56 (33) (**Figure 1C**), for which SE facilitated significantly higher responses at 7 days post immunization than CAF01 and AH ($p = 0.0007$), whilst the opposite was found at day 42, where both CAF01 and AH performed better than the SE group ($p = 0.014$–0.026).

To measure how the different adjuvants affected affinity maturation, we immunized mice with the model-antigen NP-OVA and measured circulating total NP-binding (NP_{13}-binding) and high affinity (NP_2-binding) IgG antibodies at various time points (34). Early after immunization (day 7), significantly higher total NP-binding antibody responses were found in the SE group compared to in the CAF01 ($p = 0.0009$) and AH ($p = 0.003$) groups (**Figure 1D**). However, whilst circulating anti-NP antibody levels plateaued in mice that had received SE adjuvanted vaccine at days 21 and 42 post immunization, responses continued to increase in those that had received CAF01 or AH. Thus, at day 42 post immunization, responses were 10–20 fold higher in the CAF01 ($p < 0.0001$) and AH ($p = 0.0004$) groups compared to the SE group. Similarly, high-affinity (NP_2-binding) antibody titers were significantly higher in the SE group than in both the CAF01 ($p = 0.0006$) and AH ($p = 0.032$) groups at day 7 post immunization (**Figure 1D**), whereas the CAF01 and AH induced high-affinity IgG titers reached significantly higher levels than in the SE group at day 42 ($p = 0.0001$–0.002). Despite the higher titers of high affinity (NP_2-binding) antibodies in the CAF01 and AH groups, the relative binding affinity, as indicated by the ratio of NP_2-binding and NP_{13}-binding antibodies, was similar in all the adjuvanted groups. Overall, these data demonstrate that adjuvants differentially influence the kinetics of antibody induction both qualitatively and quantitatively. We hypothesized that the delayed antibody response observed when antigen was formulated in the AH and CAF01 adjuvants was due to impaired antigen transport to LNs and therefore studied how the different adjuvants affected antigen retention at the site of injection and lymph node drainage.

CAF01 and AH Retain Antigen at the Site-of-Injection

To investigate antigen pharmacokinetics and uptake by innate cells, we performed injections of fluorescently labeled ovalbumin (OVA-AF647) alone or adjuvanted with CAF01, SE or AH. When administered intramuscularly, all adjuvants increased influx of cells to the muscle compared to antigen alone, with cell numbers peaking at 48 h after injection (**Figure 2A**). At 7 days post injection, cell numbers in the SE group had declined to levels similar to the antigen-alone group, whilst there were still 2-3-fold higher numbers in the other adjuvanted groups. We used the following gating strategy, modified from (15) to investigate the influx of immune cells into the injected muscle: neutrophils ($CD11b^+CD11c^-Ly6G^{high}$), eosinophils ($Ly6G^{int}$, $F4/80^{int}$), macrophages ($CD11b^+$, $F4/80^{high}$), monocytes ($CD11b^{high}$, F4/80-, $CD11c^-$), DCs ($CD11c^+$, $CD11b^{+/-}$), and B cells ($B220^+$) (**Supplementary Figure 2**). There was a rapid influx of neutrophils and eosinophils to the site of injection, whilst monocytes, macrophages and dendritic cells appeared later (**Figure 2A**, **Supplementary Figure 2**). When antigen was given in CAF01, higher numbers of neutrophils were recruited than with the other adjuvants (significant compared to the SE group at the 48-h time point, $p = 0.001$) (**Figure 2A**). In contrast, we observed more eosinophils and macrophages when OVA was injected with SE compared to CAF01 and AH (**Figure 2A**). Examining cells in the injected muscle that had acquired antigen (OVA^+), we found similar numbers in the group injected with antigen in SE and the antigen-alone group (**Figure 2B**), whilst numbers were higher in the CAF01 and AH groups (significant at the 48-h time point, $p = 0.007$–0.009).

Adjuvants increase the levels of pro-inflammatory cytokines at the site of injection and we investigated if the depot-effect would correlate with persistence of cytokine responses. We measured a panel of cytokines (MIP-1a, Il-1B, TNF-a, IL-6, KC/GRO, IL-10, IL-12p70, and IL-5) in the muscle supernatant at various time points after injection using electrochemiluminiscence (MSD). When antigen was formulated in SE, the highest cytokine levels were observed already 6 h after administration and the cytokine response then decreased to reach levels comparable to the antigen-alone group at 7 days post administration (**Figure 2C**, **Supplementary Figure 1**). For the CAF01 and AH groups, responses were first detected at 24 h after administration and remained relatively constant throughout the study, although cytokine levels in the AH group remained relatively low until day 7. We measured how the different adjuvants influenced persistence of innate immune cells at the site of injection, by injecting antigen (CTH522) alone or formulated with the three adjuvants and performing HE staining at different time points after administration. The injected muscles were scored for presence of mononuclear cells and stained by anti-CD64 as a marker for innate cell infiltration. All adjuvants increased mono- and multinuclear cell numbers (**Figure 2D**), but at the 7-days-time-point muscles injected with SE scored negative for

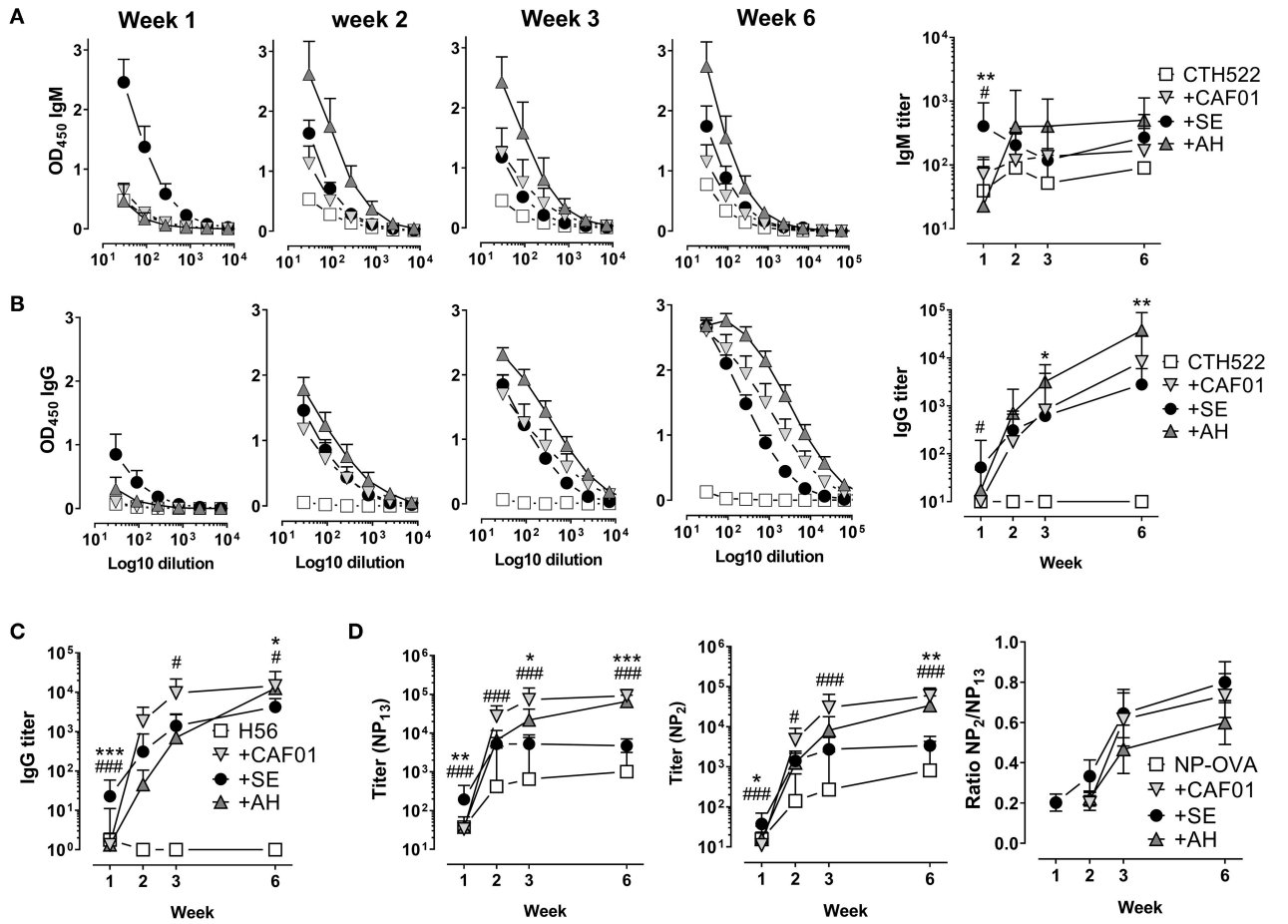

FIGURE 1 | Distinct kinetics of antibody responses dependent on the adjuvant. Mice were vaccinated subcutaneously with 5 μg of the recombinant protein antigen **(A,B)** CTH522 or **(C)** H56 either alone or in the presence of CAF01, SE (squalene emulsion), or AH (aluminum hydroxide). Antigen-specific IgG antibody responses were measured at the indicated time points. **(C)** Antibody response kinetics to immunization with NP-OVA. Mice were immunized s.c. with NP-OVA (5 μg) alone or in the presence of the indicated adjuvant and total and high affinity NP-specific IgG antibodies were measured by coating with NP_{13}-BSA or NP_2-BSA, respectively. Data show titers expressed as geometric mean+95% CI or ratios of NP_2/NP_{13} titers+SEM of four mice in the non-adjuvanted groups or eight **(A–C)** to 10 **(D)** mice in the adjuvanted groups. Statistically significant differences between the SE and AH groups are indicated by *, **, and ***, whilst significant differences between the SE and CAF01 groups are indicated by # and ### (Kruskal Wallis test, using the SE group as reference and significance levels of $p < 0.05$ and $p < 0.001$, respectively). Data are representative of one **(C)** or two **(A,B,D)** experiments.

the presence of these cells, whilst they were still observed in the CAF01 and AH groups. Similar kinetics were found for CD64 expression, which was higher in tissue samples from the CAF01 and AH groups compared with the SE group at 7 days post administration. Notably, muscles injected with either CAF01 or AH, had $CD64^+$ cells present even 60 days post administration. Thus, in contrast to SE, CAF01, and AH facilitated vaccine depot formation with persistent infiltration of innate immune cells.

Depot Formation Is Associated With Reduced Antigen Drainage to Proximal Lymph Nodes

B cell priming predominantly occurs in the follicle of the draining LN, which requires active or passive transport of antigen to this site. To investigate influence of the different adjuvants on antigen transport to the draining LN, we characterized LN cell association with fluorescently labeled antigen (OVA-AF647) injected s.c. Overall fewer $antigen^+$ cells were found in draining LNs of mice having received CAF01 or AH adjuvanted vaccines compared to in the SE group or in mice immunized with antigen alone (**Figure 3A**). In the SE group a significant number of $CD11b^+F4/80^+$ macrophages were $antigen^+$ already 6 h after administration (**Figure 3A**, **Supplementary Figure 3**). OVA^+ $Ly6G^+$ neutrophils, were also present in the group adjuvanted with SE, as reported previously for MF59™ (15). At the 24-h-time point, increased numbers of OVA^+ $CD11c^+$ DCs appeared in the SE and antigen-alone groups. The cell type distribution of $antigen^+$ cells varied between the different vaccine

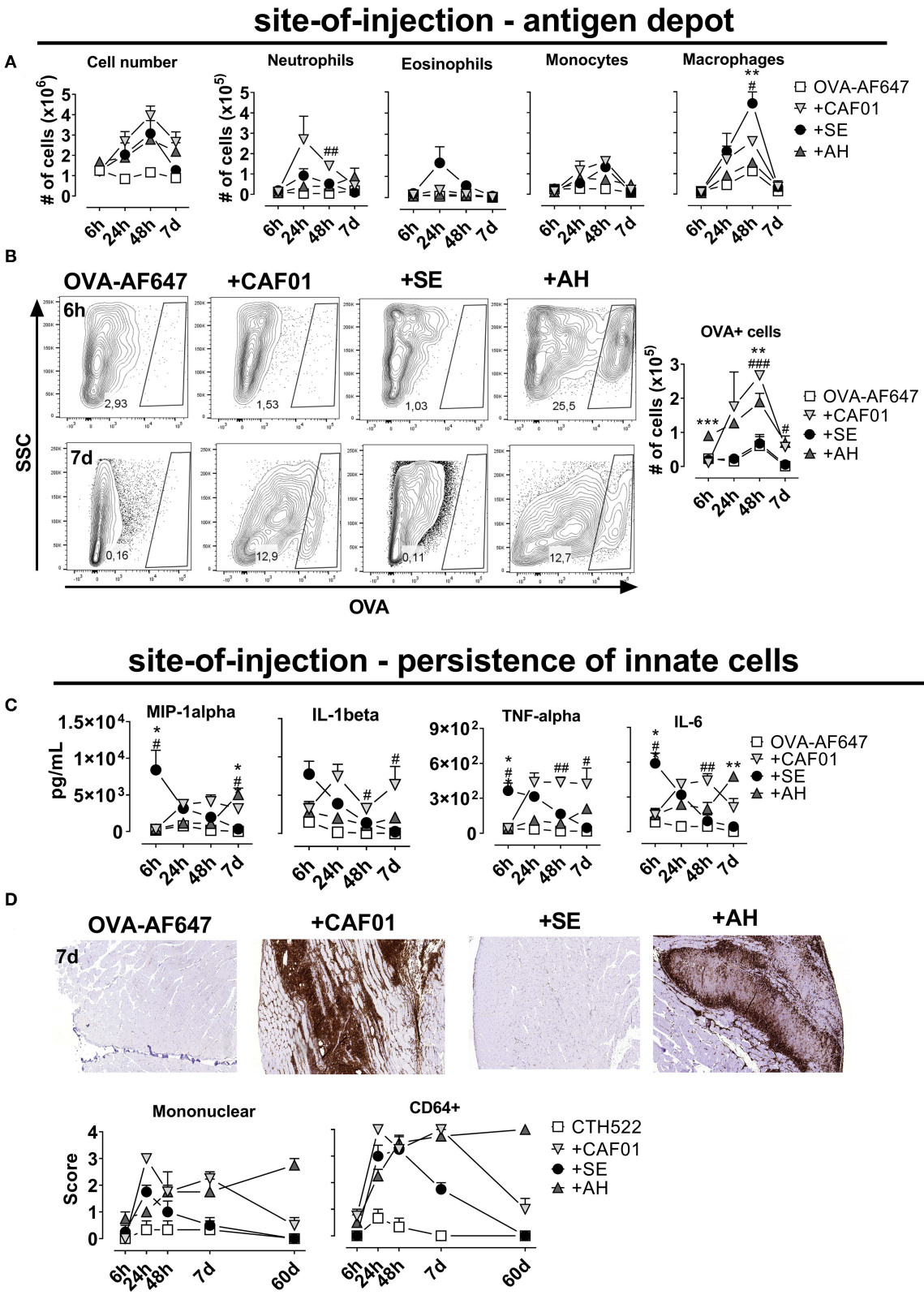

FIGURE 2 | Persistence of antigen at the site of injection is influenced by adjuvant system. Mice were injected into the quadriceps muscle with ovalbumin (OVA) coupled to AF647 either alone or in the presence of the indicated adjuvant. **(A)** Total cell number (left panel) and the numbers of the indicated cell subsets (right

(Continued)

FIGURE 2 | panels) in the injected muscles at various time points after injection. **(B)** OVA-positive cells after injection. **(C)** Quantity of the indicated cytokines at various time points after injection. Mouse groups consisted of 12 mice per group with 3 mice per group sacrificed at each time point. Each point represents mean+ SEM. Statistically significant differences between the SE and AH groups are indicated by *, **, and ***, whilst significant differences between the SE and CAF01 groups are indicated by #,##, and ### (One-way ANOVA with Tukey's correction for multiple group comparison, using the SE group as reference and significance levels of $p < 0.05$, $p < 0.01$, and $p < 0.001$, respectively). **(D)** Mice were vaccinated with CTH522 in the presence of the indicated adjuvants. The mice were scored by HE histology and immunofluorescent staining for mononuclear and inflammatory ($CD64^+$) cells infiltrating the muscle at various time points after immunization. Representative plots display the 7 day time point. Three (antigen alone) or 8 mice (adjuvanted groups) were sacrificed at each time point.

groups (**Figure 3B**). Thus, at 6 h post administration, $antigen^+$ cells were mainly found amongst monocytes in the antigen alone group and DCs in the CAF01-adjuvanted group. In contrast, a substantial fraction of $antigen^+$ cells in mice having received SE were macrophages. After 24 h the cell type distribution amongst $antigen^+$ cells in the DLN was more similar between the different adjuvanted groups. Whilst few DLN B cells had bound OVA at 6 h post administration, high numbers of $antigen^+$ B cells were found in the DLN after 24 h (**Figure 3C**). Up to 1×10^4 $antigen^+$ B cells were observed in the draining LNs of mice in the OVA-alone and the OVA in SE groups, whereas 10-50-fold lower numbers were detected in mice immunized with OVA in CAF01 or AH (significant, $p = 0.0001$). Similar results were observed when injecting the OVA-adjuvant combinations intramuscularly (data not shown). Activation of B cells in the draining LN following vaccination leads to expansion of these cells. All the tested adjuvants increased overall and B cell numbers in the draining LN (**Figure 3D**). The expansion occurred with different kinetics though, with the highest cell numbers found in the SE group at 48 h post injection, and after 8 days in the CAF01 and AH groups. Overall, administering antigen in the depot-inducing adjuvants CAF01 and AH led to reduced antigen drainage to proximal LNs and delayed B cell expansion, compared to when administered in SE adjuvant.

Germinal Center Formation Is Delayed When Using Depot-Forming Adjuvants

Antibodies to protein antigens are predominantly produced from GC-derived plasma cells (11), although some of the antibody secreting cells can also be of extrafollicular origin (35). To test if the reduced amount of antigen delivered in draining LNs associated with administration in depot-forming adjuvants would lead to delayed GC formation, we compared the kinetics of GC B cell responses using antigen formulated in the depot- and non-depot-forming adjuvants. We used the CTH522 antigen for immunization and a fluorophore-labeled version of the antigen as a probe to evaluate antigen-specific GC B cell kinetics. Antigen alone did not induce any detectable antigen-specific GC B cells (**Figure 4A**). We also did not detect any GCs at the day 4 time point for any of the groups. At day 7 post immunization, a clear population of $B220^+CD38_{lo}GL7^+$ GC B cells appeared in the SE group, of which on average 20% bound the labeled CTH522 probe. In contrast, GC B cells were not detected in the AH and CAF01 groups before at days 10 and 14, respectively (**Figure 4A**). The frequency of GC B cells declined at days 21 and day 28 in all groups, but was significantly higher in the CAF01 group compared to the SE group at day 28 ($p = 0.020$).

To confirm that the single cell stainings of GC B cells reflected germinal center formation, we evaluated Ki67 in H&E stained sections of draining LNs (**Figure 4B**). At 7 days post immunization, germinal centers indicated by clusters of $Ki67^+$ cells could easily be observed in most of the mice that had received CTH522 antigen formulated in SE. In contrast, very few germinal centers were detected in the CAF01 and AH-adjuvanted groups and the germinal center area was significantly lower than in the SE group ($p = 0.028$–0.033). At 14 days post immunization, there were no significant differences in GC area between the adjuvanted groups, although there was a tendency toward lower GC responses in the AH group. At day 42 post immunization, similar high levels of GCs could still be detected in some of the mice that had received CAF01-adjuvanted vaccine, whilst GC levels were lower in the SE (not significant, $p = 0.09$) and AH groups. Thus, GCs appeared earlier when antigen was administered in SE than when formulated with CAF01 or AH.

Removal of the Injection Site Abrogates Antibody Responses When Antigen Is Formulated in Depot-Inducing Adjuvants

Recent studies have questioned the role of the AH-induced antigen depot in elicitation of immune responses (8). We therefore investigated how removing the vaccine depot would affect antibody responses for depot vs. non-depot inducing adjuvants. For the surgery to be minimally invasive, we used intradermal (i.d.) immunizations. Injecting the CTH522 antigen in the various adjuvants confirmed that this administration route gave similar antibody kinetic profiles for the tested adjuvants as after s.c. immunization (**Figure 5A**). Removal of the vaccine depot at 6 and 24 h post administration completely abrogated antibody responses in mice having received AH and CAF01 adjuvanted vaccine (**Figure 5B**). In contrast, for the SE group, antibody responses were observed despite injection site ablation. Even when removing the antigen depot at 72 h post administration, antibody responses were still reduced in the CAF01 group and completely abrogated in the AH group. These data confirm that most antigen formulated in AH and CAF01 remains at the site of injection, at least for the first 24–72 h post i.d. administration, and it is possible that this depot effect may be responsible for the slower onset of GC formation and antibody responses.

DISCUSSION

Germinal centers (GCs) form in secondary lymphoid organs in response to immunization with T-cell-dependent antigens. Upon acquiring antigen an immune cascade is elicited where

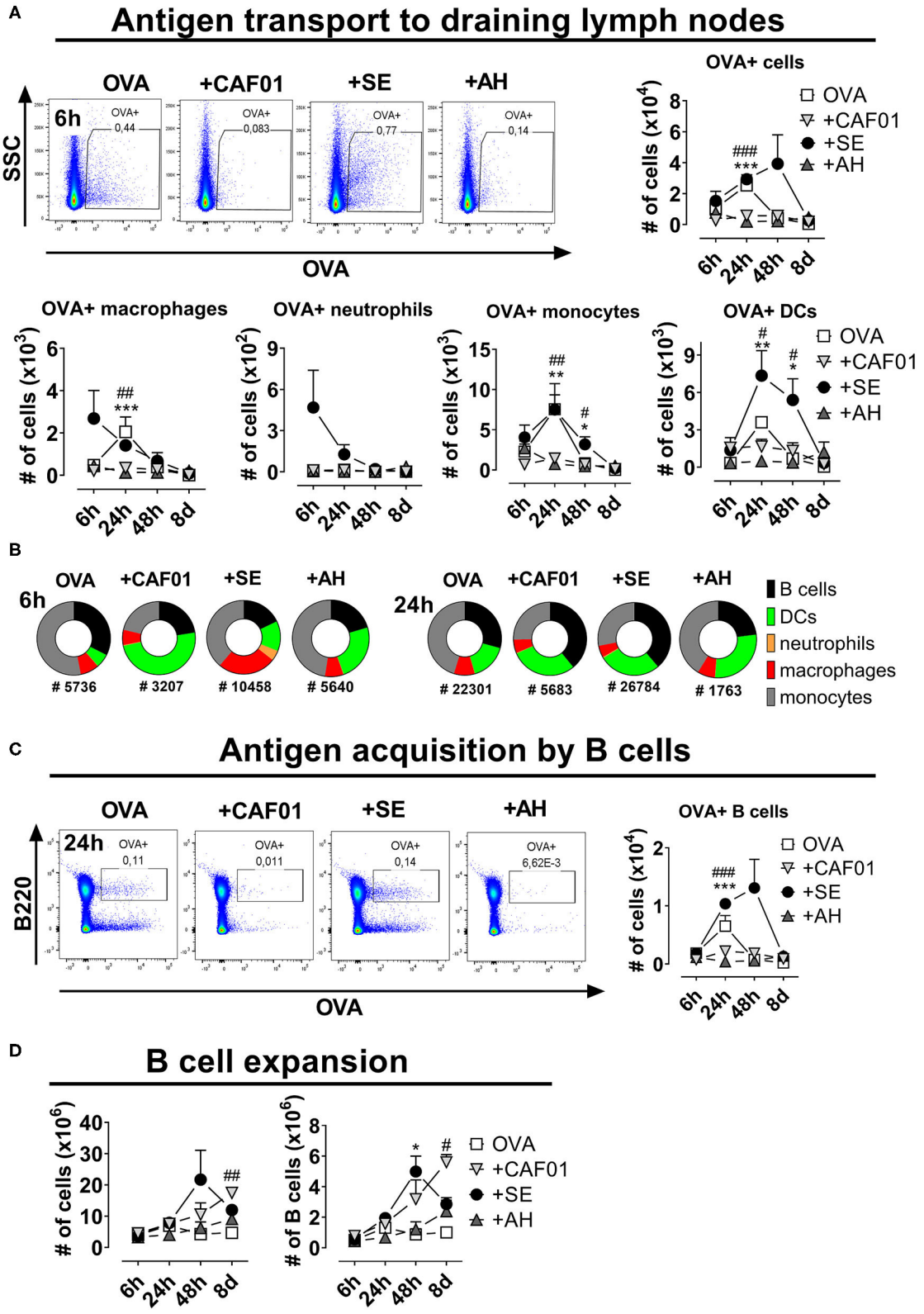

FIGURE 3 | Reduced antigen drainage to proximal lymph nodes in the presence of depot-inducing adjuvants. Mice were injected subcutaneously at the base of tail with ovalbumin (OVA) coupled to AF647 either alone or in the presence of the indicated adjuvant and the draining inguinal lymph nodes were collected at various time points thereafter. **(A)** Cells binding to OVA in the draining lymph nodes. Representative plots display the 6-h-time-point (upper panels). Lower panels display the

(Continued)

FIGURE 3 | numbers of cells within the indicated subsets binding to OVA. **(B)** Fraction of cells within the indicated subsets binding to OVA at 6 and 24 h post administration. The total numbers of OVA^+ cells (surface-adsorbed or internalized) are displayed below the pies. **(C)** Representative plots of B cells binding to OVA at 24 h post injection (left panel) and summarized for the different time points (right panel). **(D)** The total cell number (left panel) and the percentage and numbers of $B220^+$ B cells (right panels) at the indicated time points after injection. Each group consisted of 3 (naïve and antigen alone) or 4 (for each adjuvant) mice evaluated at each time point. Each point represents mean+ SEM. Statistically significant differences between the SE and AH groups are indicated by *, **, and *** whilst significant differences between the SE and CAF01 groups are indicated by $^{\#,\#\#,}$ and $^{\#\#\#}$ (One-way ANOVA with Tukey's correction for multiple group comparison, using the SE group as reference and significance levels of $p < 0.05$, $p < 0.01$, and $p < 0.001$, respectively).

responding B cells form GCs to undergo proliferation, affinity maturation and class-switching and obtain one of two productive fates; memory B cells or plasma cells (36). During acute infections, microorganisms may replicate for weeks, thus providing continuous supply of antigen that may enter and sustain germinal center reactions. Soluble protein from subunit vaccines can be detected in the draining LNs already a few hours post immunization and is cleared much more rapidly, with intact antigen being non-detectable at 24–72 h later (11, 37). Mature naïve B cells are not found in muscle tissue, a common site for vaccine injection, but are circulating between follicles of secondary lymphoid organs. Initiation of T-cell dependent antibody responses requires that B cells in draining LN follicles encounter the injected cognate antigen (13). Inspired by studies indicating that particularly depot-inducing adjuvants elicit poor antibody responses early after a priming immunization (9, 27, 38), we hypothesized that slow release of vaccine from the site of injection, when antigen is formulated in depot-forming adjuvants, would lead to a delay in elicitation of B cell responses. It was previously demonstrated that more antigen-binding cells can be observed in the draining LNs of mice vaccinated with antigen formulated in MF59^{TM} or AS03 compared to in AH (15, 25). We confirmed these data and found that formulation in CAF01 also led to significantly reduced numbers of antigen-positive cells in draining LNs compared to when antigen was given alone or in an MF59^{TM}-like SE adjuvant. Thus, whilst SE facilitated delivery to follicular B cells in the proximal LN (**Figure 3**), most antigen formulated in CAF01 or AH remained at the site of injection, which correlated with a delay in GC formation and antibody responses. In a recent study using osmotic pumps to facilitate slow delivery immunization, GC responses were also delayed compared to a bolus vaccine (23). Overall this suggests that antigen delivered slowly (e.g., by osmotic pumps or depot-inducing adjuvants, limits the amounts of antigen available for naïve B cells in proximal LNs, which reduces the chances of early B cell activation and formation of GCs).

The tested adjuvants induced marked differences in the cell types recruited to the site of injection after i.m. imunization. SE induced the highest influx of eosinophils and F4/80+ macrophages, whilst CAF01 induced the highest influx of neutrophils. It has been proposed that Trehalose 6,6′-dimycolate (TDM), of which the immunostimulatory component of CAF01 (TDB) is a synthetic analog, can function as a neutrophil chemoattractant (39). Notably, although AH induced the lowest influx of $Ly6G^+$ neutrophils and $F4/80^+$ macrophages of the adjuvants when measured by flow cytometry, immunohistology revealed many $CD64^+$ cells in the injected muscle, which could be macrophages or inflammatory monocytes. In a previous study, AH was also demonstrated to attract $F4/80^+$ macrophages to the site of injection (40). However, in the current study more $F4/80^+$ macrophages were detected in the other adjuvanted groups, suggesting that at least relatively to SE and CAF01, AH induces little influx of $F4/80^+$ macrophages. The infiltrating innate cells persisted at the site of injection long-term post injection of CAF01 and AH, whilst there was a more rapid decline in these cells in the SE group. We also observed striking differences in the distribution of immune cells acquiring antigen in the draining LN amongst the different adjuvanted groups. Despite CAF01 recruiting neutrophils to the site of injection, few antigen-positive neutrophils were seen in the draining LN. In contrast, SE induced limited recruitment of neutrophils to the site of injection, yet facilitated a rapid increase in antigen$^+$ neutrophils in the draining LN 6 h post injection, as described previously (15). It is possible that SE adjuvant facilitates neutrophil-mediated transport of antigen from the site of injection to the draining LN, however neutrophil depletion experiments demonstrated that these cells are redundant for the ability of MF59^{TM} to promote antibody responses (15).

Sustained antigen delivery [e.g., *via* osmotic pumps or repeated injections can greatly increase the magnitude of antibody responses (17, 23)]. Theoretically, adjuvants forming antigen depots hold the promise to also promote sustained delivery of antigen. In the present studies the depot-forming adjuvants CAF01 and AH, despite initially delaying germinal center formation, promoted antibody responses, which were of higher magnitude than the non-depot forming SE adjuvant later on (**Figures 1**, **5** and summarized in **Figure 6**). Although we found that adjuvants differentially influenced antigen drainage to proximal LNs and that this correlated with the kinetics of germinal center formation and antibody responses, it is difficult to ascertain that these events are directly connected. Thus, it is possible that the different immune profile stimulated by the non-depot-inducing adjuvant SE compared to CAF01/AH is responsible for the different kinetics of antibody responses, rather than the differences in drainage patters. Along these lines, Hutchison et al. showed that injection site ablation as early as 2 h post injection had no impact on antibody responses to Alum-adjuvanted vaccine, suggesting little if any role of an antigen depot (8). Whilst this study used ear ablation for injection site removal, we used another more clinically relevant i.d. route. Although it would have been relevant to study injection site removal after s.c. immunization to directly compare with studies of antibody response kinetics (**Figure 1**), we chose to perform the surgery after i.d. immunization to make it less invasive. However, we found that although different routes of

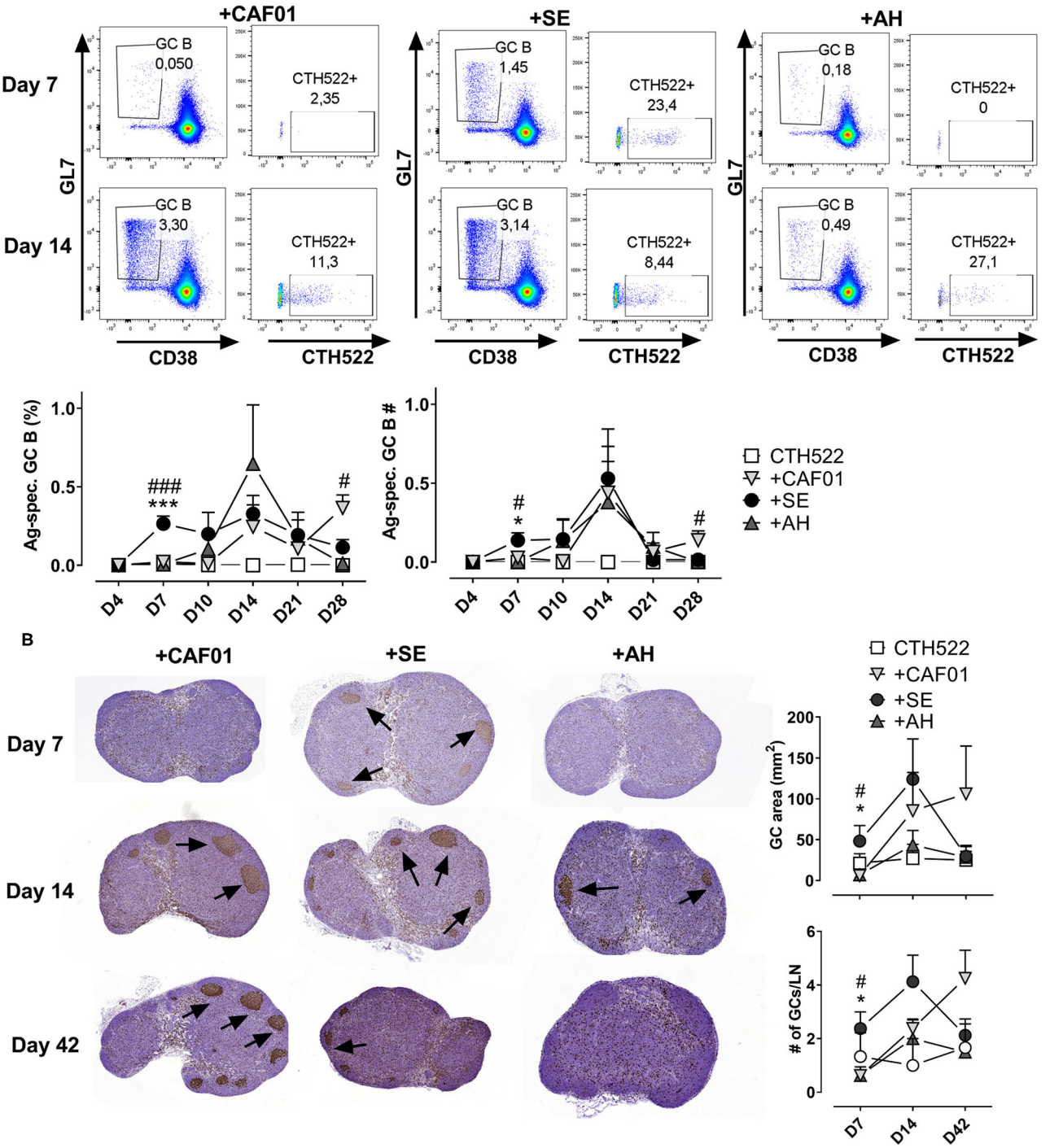

FIGURE 4 | Adjuvants differentially influence germinal center kinetics. Mice were immunized subcutaneously with CTH522 protein antigen either alone or in the presence of the indicated adjuvant. **(A)** Representative plots of antigen-specific germinal center (GC) B cells ($B220^+CD38\text{-}GL7^+$ cells binding CTH522 coupled to AF488) in the draining inguinal lymph nodes at days 7 and 14 post immunization. Lower panels: percentages (of B220+) and numbers of antigen-specific germinal center B cells. Each group consisted of 2 (antigen alone) or 4 (antigen +adjuvants) mice. Data are representative of two independent experiments. **(B)** Draining lymph node GC areas (upper panel) and number of GCs as indicated by clusters of $Ki67^+$ cells. Groups consisted of 3 (antigen alone) or 8 (antigen +adjuvants) mice. The experiment was performed once. Each point represents mean+ SEM. Statistically significant differences between the SE and AH groups are indicated by * and *** whilst significant differences between the SE and CAF01 groups are indicated by # and ### (One-way ANOVA with Tukey's correction for multiple group comparison, using the SE group as reference and significance levels of $p < 0.05$ and $p < 0.001$, respectively).

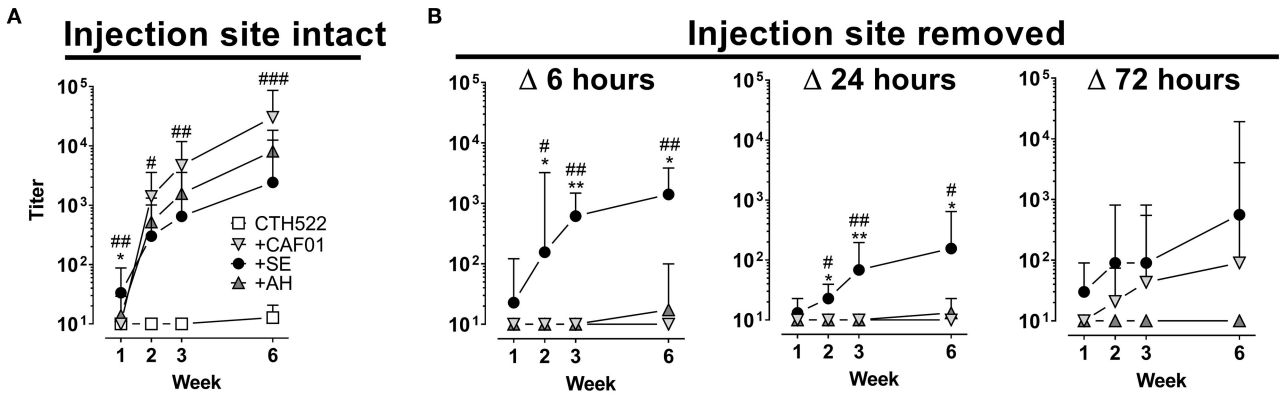

FIGURE 5 | Removal of the injection site impairs antibody responses when antigen is formulated in depot-inducing adjuvants. Mice were immunized intradermally (i.d.) with CTH522 protein antigen either alone or in the presence of the indicated adjuvant. At various time points after injection, mice were anesthetized and the injection site either surgically removed or left intact. **(A,B)** Antigen-specific IgG antibody responses were measured at the indicated time points. Each vaccine group consisted of three to four mice and data are displayed as geometric mean+95% CI. Data in which the injection site was left intact (left panels) were compiled from three experiments. Statistically significant differences between the SE and AH groups are indicated by * and ** whilst significant differences between the SE and CAF01 groups are indicated by #, ##, and ### (One-way ANOVA with Tukey's correction for multiple group comparison, using the SE group as reference and significance levels of $p < 0.05$, $p < 0.01$, and $p < 0.001$ respectively).

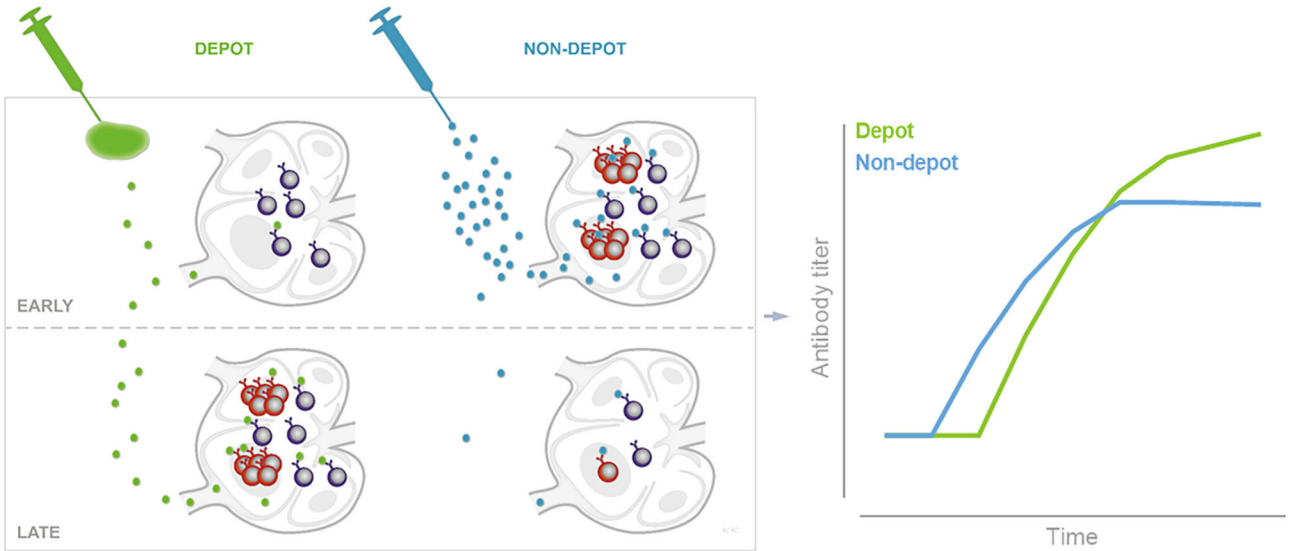

FIGURE 6 | Schematic of depot formation affecting induction and persistence of germinal centers. Depot-forming adjuvants sequester antigen at the site of injection. Early after immunization this leads to reduced B cell activation and GC formation in the draining LNs, compared to when antigen is given in an adjuvant which does not form an antigen depot. The slow release of antigen from the depot may help sustain germinal centers to promote a higher magnitude long-term antibody response as illustrated by data adapted from **Figure 1** (right panel).

immunization may influence kinetics of the immune response, similar kinetics of antibody responses were observed after s.c. and i.d. administration (**Figures 1**, **5**), which included the pattern that SE facilitated a rapid IgG antibody response, whilst AH and CAF01 gave delayed antibody responses, ultimately reaching higher magnitudes. Removing the injection site within 24 h post administration of CTH522 in AH or CAF01 completely abrogated antibody responses (**Figure 5**), suggesting that most antigen formulated in AH or CAF01 remained at the site of injection for this period of time. The discrepancy between the study by Hutchison et al. and ours may be due to the differences in route (8) or antigens used (CTH522 vs. OVA). Antigens may adsorb to cationic liposomes and AH mainly by electrostatic, ligand exchange and hydrophobic interactions (41, 42). Thus, the degree of antigen depot and kinetics of antigen drainage are expected to be different for antigens with other physicochemical characteristics than those used in the present study [e.g., positively charged proteins (The antigens used here were 43–50 kDa proteins with pIs of 4.5–5.2)] (43, 44). However, although many antigens rapidly elute from AH after injection

(45–47), we found high numbers of OVA^+ cells at the injection site, even 7 days post administration of OVA in AH (**Figure 2**).

In the present study the depot-inducing adjuvants (CAF01 and AH) elicited IgG responses of similar kinetics and, for both, IgG titers continued to rise until the last time point 6 weeks post immunization. In a recent clinical trial evaluating a *Chlamydia trachomatis* vaccine, CAF01 elicited significantly higher IgG antibody responses than AH following a prime-boost regimen with the CTH522 antigen (32). Notably in that study, the IgG responses were boosted to much higher levels by the second booster (at 16 weeks) compared to after the first booster (at 4 weeks). It is generally believed that booster immunizations are most effective when administered after antibody responses have peaked (48). Given the data of the current study demonstrating that antibody responses mature slowly, with the highest IgG titers not observed before the end of the study (week 6), it seems possible that higher antibody responses would be obtained if the first booster vaccine was given later than 4 weeks after priming. For certain vaccines, limited spacing between immunizations has even been suggested to promote reduced responses to later administered booster doses [e.g., for the serogroup C meningococcal (Men-C)-conjugate vaccine], a single dose rather than a two-dose regime (spaced 1 month apart) primed for higher antibody responses to later boosting at 12 months of age (49). Thus, kinetics of antibody responses after prime immunization, and how these are modulated by adjuvants, warrants further study, in particular for designing prime-boost regimes.

We demonstrated that the antibody responses mature with different kinetics dependent on the adjuvant used. Specifically, two adjuvants (CAF01 and AH) which formed antigen depots at the site of injection induced delayed germinal center formation but promoted higher antibody responses than a non-depot-inducing adjuvant (SE) after a single immunization. These results are important for several reasons. First, considering adjuvant-dependent immune response kinetics is important in adjuvant comparison studies; second, the optimal time point for booster immunization, which is after contraction of germinal centers (48), may be dependent on the adjuvant used and third, by carefully considering antigen and adjuvant compatibility, and through rationally designing adjuvants to release antigen in a controlled manner, it may be possible to further promote antibody responses to protect against diseases where high magnitude somatically mutated antibodies are required. Understanding the immune kinetics controlled by the adjuvant is therefore of highest importance when comparing vaccines both pre-clinically and clinically.

DATA AVAILABILITY STATEMENT

The raw data supporting the conclusions of this article will be made available by the authors, without undue reservation.

ETHICS STATEMENT

Mouse studies were conducted in accordance with the regulations set forth by the National Danish animal protection committee and in accordance with European Community Directive 86/609. The experiments performed have been approved by the Governmental Danish Animal Experiments Inspectorate under licenses 2014-15-2934-01065 and 2017-15-0201-01363.

AUTHOR CONTRIBUTIONS

GP, PA, and DC designed research and wrote the paper. GP and KW performed experiments. GP and DC analyzed data. All authors contributed to the article and approved the submitted version.

FUNDING

This work was supported by the European Commission through contract FP7-HEALTH-2011.1.4-4-280873 (ADITEC).

ACKNOWLEDGMENTS

We appreciate the expert technical assistance provided by Janne Rahbech, Rune Fledelius Jensen, Julia Sid Hansen, and the staff at the experimental animal facilities at Statens Serum Institut. We thank Louise Krag Isling for help with analyzing the histology data and Karen S. Korsholm for the graphical illustration.

SUPPLEMENTARY MATERIAL

The Supplementary Material for this article can be found online at: https://www.frontiersin.org/articles/10.3389/fimmu.2020.579761/full#supplementary-material

REFERENCES

1. Plotkin SA. Correlates of protection induced by vaccination. *Clin Vaccine Immunol.* (2010) 17:1055–65. doi: 10.1128/CVI.00131-10
2. Khurana S, Verma N, Yewdell JW, Hilbert AK, Castellino F, Lattanzi M, et al. MF59 adjuvant enhances diversity and affinity of antibody-mediated immune response to pandemic influenza vaccines. *Sci Transl Med.* (2011) 3:85ra48. doi: 10.1126/scitranslmed.3002336
3. Del Giudice G, Rappuoli R, Didierlaurent AM. Correlates of adjuvanticity: a review on adjuvants in licensed vaccines. *Semin Immunol.* (2018) 39:14–21. doi: 10.1016/j.smim.2018.05.001
4. Reed SG, Orr MT, Fox CB. Key roles of adjuvants in modern vaccines. *Nat Med.* (2013) 19:1597–608. doi: 10.1038/nm.3409
5. Oleszycka E, Lavelle EC. Immunomodulatory properties of the vaccine adjuvant alum. *Curr Opin Immunol.* (2014) 28:1–5. doi: 10.1016/j.coi.2013.12.007
6. McKee AS, Marrack P. Old and new adjuvants. *Curr Opin Immunol.* (2017) 47:44–51. doi: 10.1016/j.coi.2017.06.005
7. Noe SM, Green MA, HogenEsch H, Hem SL. Mechanism of immunopotentiation by aluminum-containing adjuvants elucidated by the relationship between antigen retention at the inoculation site and the immune response. *Vaccine.* (2010) 28:3588–94. doi: 10.1016/j.vaccine.2010.02.085
8. Hutchison S, Benson RA, Gibson VB, Pollock AH, Garside P, Brewer JM. Antigen depot is not required for alum adjuvanticity. *FASEB J.* (2012) 26:1272–9. doi: 10.1096/fj.11-184556

9. Knudsen NPH, Olsen A, Buonsanti C, Follmann F, Zhang Y, Coler RN, et al. Different human vaccine adjuvants promote distinct antigen-independent immunological signatures tailored to different pathogens. *Sci Rep.* (2016) 6:19570. doi: 10.1038/srep19570
10. Liang F, Lindgren G, Sandgren KJ, Thompson EA, Francica JR, Seubert A, et al. Vaccine priming is restricted to draining lymph nodes and controlled by adjuvant-mediated antigen uptake. *Sci Transl Med.* (2017) 9:aal2094. doi: 10.1126/scitranslmed.aal2094
11. Pape KA, Catron DM, Itano AA, Jenkins MK. The humoral immune response is initiated in lymph nodes by B cells that acquire soluble antigen directly in the follicles. *Immunity.* (2007) 26:491–502. doi: 10.1016/j.immuni.2007.02.011
12. De Silva NS, Klein U. Dynamics of B cells in germinal centres. *Nat Rev Immunol.* (2015) 15:137–48. doi: 10.1038/nri3804
13. Carrasco YR, Batista FD. B cells acquire particulate antigen in a macrophage-rich area at the boundary between the follicle and the subcapsular sinus of the lymph node. *Immunity.* (2007) 27:160–71. doi: 10.1016/j.immuni.2007.06.007
14. Heesters BA, van der Poel CE, Das A, Carroll MC. Antigen presentation to B cells. *Trends Immunol.* (2016) 37:844–54. doi: 10.1016/j.it.2016.10.003
15. Calabro S, Tortoli M, Baudner BC, Pacitto A, Cortese M, O'Hagan DT, et al. Vaccine adjuvants alum and MF59 induce rapid recruitment of neutrophils and monocytes that participate in antigen transport to draining lymph nodes. *Vaccine.* (2011) 29:1812–23. doi: 10.1016/j.vaccine.2010.12.090
16. Phan TG, Green JA, Gray EE, Xu Y, Cyster JG. Immune complex relay by subcapsular sinus macrophages and noncognate B cells drives antibody affinity maturation. *Nat Immunol.* (2009) 10:786–93. doi: 10.1038/ni.1745
17. Tam HH, Melo MB, Kang M, Pelet JM, Ruda VM, Foley MH, et al. Sustained antigen availability during germinal center initiation enhances antibody responses to vaccination. *Proc Natl Acad Sci USA.* (2016) 113:E6639–48. doi: 10.1073/pnas.1606050113
18. Cirelli KM, Crotty S. Germinal center enhancement by extended antigen availability. *Curr Opin Immunol.* (2017) 47:64–9. doi: 10.1016/j.coi.2017.06.008
19. Turner JS, Benet ZL, Grigorova IL. Antigen acquisition enables newly arriving B cells to enter ongoing immunization-induced germinal centers. *J Immunol.* (2017) 199:1301–7. doi: 10.4049/jimmunol.1700267
20. Higaki M, Azechi Y, Takase T, Igarashi R, Nagahara S, Sano A, et al. Collagen minipellet as a controlled release delivery system for tetanus and diphtheria toxoid. *Vaccine.* (2001) 19:3091–6. doi: 10.1016/S0264-410X(01)00039-1
21. Kemp JM, Kajihara M, Nagahara S, Sano A, Brandon M, Lofthouse S. Continuous antigen delivery from controlled release implants induces significant and anamnestic immune responses. *Vaccine.* (2002) 20:1089–98. doi: 10.1016/S0264-410X(01)00444-3
22. Boopathy AV, Mandal A, Kulp DW, Menis S, Bennett NR, Watkins HC, et al. Enhancing humoral immunity via sustained-release implantable microneedle patch vaccination. *Proc Natl Acad Sci USA.* (2019) 116:16473–8. doi: 10.1073/pnas.1902179116
23. Cirelli KM, Carnathan DG, Nogal B, Martin JT, Rodriguez OL, Upadhyay AA, et al. Slow delivery immunization enhances HIV neutralizing antibody and germinal center responses via modulation of immunodominance. *Cell.* (2019) 177:1153–71 e1128. doi: 10.1016/j.cell.2019.04.012
24. Henriksen-Lacey M, Bramwell VW, Christensen D, Agger E-M, Andersen P, Perrie Y. Liposomes based on dimethyldioctadecylammonium promote a depot effect and enhance immunogenicity of soluble antigen. *J Control Release.* (2010) 142:180–6. doi: 10.1016/j.jconrel.2009.10.022
25. Morel S, Didierlaurent A, Bourguignon P, Delhaye S, Baras B, Jacob V, et al. Adjuvant System AS03 containing alpha-tocopherol modulates innate immune response and leads to improved adaptive immunity. *Vaccine.* (2011) 29:2461–73. doi: 10.1016/j.vaccine.2011.01.011
26. Lofano G, Mancini F, Salvatore G, Cantisani R, Monaci E, Carrisi C, et al. Oil-in-water emulsion MF59 increases germinal center B cell differentiation and persistence in response to vaccination. *J Immunol.* (2015) 195:1617–27. doi: 10.4049/jimmunol.1402604
27. Ciabattini A, Pettini E, Fiorino F, Pastore G, Andersen P, Pozzi G, et al. Modulation of primary immune response by different vaccine adjuvants. *Front Immunol.* (2016) 7:427. doi: 10.3389/fimmu.2016.00427
28. Henriksen-Lacey M, Christensen D, Bramwell VW, Lindenstrom T, Agger EM, Andersen P, et al. Comparison of the depot effect and immunogenicity of liposomes based on dimethyldioctadecylammonium (DDA), 3beta-[N-(N',N'-Dimethylaminoethane)carbomyl] cholesterol (DC-Chol), and 1,2-Dioleoyl-3-trimethylammonium propane (DOTAP): prolonged liposome retention mediates stronger Th1 responses. *Mol Pharmaceutics.* (2011) 8:153–61. doi: 10.1021/mp100208f
29. O'Hagan DT, Ott GS, De Gregorio E, Seubert A. The mechanism of action of MF59—an innately attractive adjuvant formulation. *Vaccine.* (2012) 30:4341–8. doi: 10.1016/j.vaccine.2011.09.061
30. Olsen AW, Follmann F, Erneholm K, Rosenkrands I, Andersen P. Protection against chlamydia trachomatis infection and upper genital tract pathological changes by vaccine-promoted neutralizing antibodies directed to the VD4 of the major outer membrane protein. *J Infect Dis.* (2015) 212:978–89. doi: 10.1093/infdis/jiv137
31. Davidsen J, Rosenkrands I, Christensen D, Vangala A, Kirby D, Perrie Y, et al. Characterization of cationic liposomes based on dimethyldioctadecylammonium and synthetic cord factor from *M. tuberculosis* (trehalose 6,6 '-dibehenate)—A novel adjuvant inducing both strong CMI and antibody responses. *Biochim Biophys Acta Biomembranes.* (2005) 1718:22–31. doi: 10.1016/j.bbamem.2005.10.011
32. Abraham S, Juel HB, Bang P, Cheeseman HM, Dohn RB, Cole T, et al. Safety and immunogenicity of the chlamydia vaccine candidate CTH522 adjuvanted with CAF01 liposomes or aluminium hydroxide: a first-in-human, randomised, double-blind, placebo-controlled, phase 1 trial. *Lancet Infect Dis.* (2019) 19:1091–1100. doi: 10.1016/S1473-3099(19)30279-8
33. Luabeya AK, Kagina BM, Tameris MD, Geldenhuys H, Hoff ST, Shi Z, et al. First-in-human trial of the post-exposure tuberculosis vaccine H56:IC31 in *Mycobacterium tuberculosis* infected and non-infected healthy adults. *Vaccine.* (2015) 33:4130–40. doi: 10.1016/j.vaccine.2015.06.051
34. Ersching J, Efeyan A, Mesin L, Jacobsen JT, Pasqual G, Grabiner BC, et al. Germinal center selection and affinity maturation require dynamic regulation of mTORC1 kinase. *Immunity.* (2017) 46:1045. doi: 10.1016/j.immuni.2017.06.005
35. MacLennan IC, Toellner KM, Cunningham AF, Serre K, Sze DM, Zuniga E, et al. Extrafollicular antibody responses. *Immunol Rev.* (2003) 194:8–18. doi: 10.1034/j.1600-065X.2003.00058.x
36. Mesin L, Ersching J, Victora GD. Germinal center B cell dynamics. *Immunity.* (2016) 45:471–82. doi: 10.1016/j.immuni.2016.09.001
37. Li C, Buckwalter MR, Basu S, Garg M, Chang J, Srivastava PK. Dendritic cells sequester antigenic epitopes for prolonged periods in the absence of antigen-encoding genetic information. *Proc Natl Acad Sci USA.* (2012) 109:17543–8. doi: 10.1073/pnas.1205867109
38. Demento SL, Cui W, Criscione JM, Stern E, Tulipan J, Kaech SM, et al. Role of sustained antigen release from nanoparticle vaccines in shaping the T cell memory phenotype. *Biomaterials.* (2012) 33:4957–64. doi: 10.1016/j.biomaterials.2012.03.041
39. Lee WB, Yan JJ, Kang JS, Zhang Q, Choi WY, Kim LK, et al. Mincle activation enhances neutrophil migration and resistance to polymicrobial septic peritonitis. *Sci Rep.* (2017) 7:41106. doi: 10.1038/srep41106
40. Lu F, Hogenesch H. Kinetics of the inflammatory response following intramuscular injection of aluminum adjuvant. *Vaccine.* (2013) 31:3979–86. doi: 10.1016/j.vaccine.2013.05.107
41. al-Shakhshir RH, Regnier FE, White JL, Hem SL. Contribution of electrostatic and hydrophobic interactions to the adsorption of proteins by aluminium-containing adjuvants. *Vaccine.* (1995) 13:41–4. doi: 10.1016/0264-410X(95)80009-3
42. Hamborg M, Rose F, Jorgensen L, Bjorklund K, Pedersen HB, Christensen D, et al. Elucidating the mechanisms of protein antigen adsorption to the CAF/NAF liposomal vaccine adjuvant systems: effect of charge, fluidity and antigen-to-lipid ratio. *Biochim Biophys Acta.* (2014) 1838:2001–10. doi: 10.1016/j.bbamem.2014.04.013

43. HogenEsch H, O'Hagan DT, Fox CB. Optimizing the utilization of aluminum adjuvants in vaccines: you might just get what you want. *Npj Vaccines.* (2018) 3:51. doi: 10.1038/s41541-018-0089-x
44. Moyer TJ, Kato Y, Abraham W, Chang JYH, Kulp DW, Watson N, et al. Engineered immunogen binding to alum adjuvant enhances humoral immunity. *Nat Med.* (2020) 26:430–40. doi: 10.1038/s41591-020-0753-3
45. Weissburg RP, Berman PW, Cleland JL, Eastman D, Farina F, Frie S, et al. Characterization of the MN gp120 HIV-1 vaccine: antigen binding to alum (vol 12, pg 1439, 1995). *Pharmaceut Res.* (1996) 13:183. doi: 10.1023/A:1016266916893
46. Hansen B, Sokolovska A, HogenEsch H, Hem SL. Relationship between the strength of antigen adsorption to an aluminum-containing adjuvant and the immune response. *Vaccine.* (2007) 25:6618–24. doi: 10.1016/j.vaccine.2007.06.049
47. HogenEsch H. Mechanism of immunopotentiation and safety of aluminum adjuvants. *Front Immunol.* (2013) 3:406. doi: 10.3389/fimmu.2012.00406
48. Siegrist CA. Vaccine immunology. In: SA Plotkin, editor. *Plotkin's Vaccines*. 7th ed. Philadelphia, PA: Elsevier (2018). p. 16–34.e17. doi: 10.1016/B978-0-323-35761-6.00002-X
49. Pace D, Khatami A, McKenna J, Campbell D, Attard-Montalto S, Birks J, et al. Immunogenicity of reduced dose priming schedules of serogroup C meningococcal conjugate vaccine followed by booster at 12 months in infants: open label randomised controlled trial. *BMJ.* (2015) 350:1554. doi: 10.1136/bmj.h1554

Conflict of Interest: PA and DC are co-inventors on patents on the cationic adjuvant formulations (CAF). All rights have been turned over to Statens Serum Institut, which is a non-profit government research facility.

The remaining authors declare that the research was conducted in the absence of any commercial or financial relationships that could be construed as a potential conflict of interest.

frontiers in Immunology

ORIGINAL RESEARCH
published: 23 September 2020
doi: 10.3389/fimmu.2020.569988

Investigating Immunization With Nucleotide Enzymes of *Schistosoma mansoni*: Nucleoside Diphosphate Kinase and Adenylosuccinate Lyase as New Antigenic Targets Against Schistosomiasis

Túlio di Orlando Cagnazzo[1], Camila Tita Nogueira[1], Cynthia Aparecida de Castro[1], Débora Meira Neris[1], Ana Carolina Maragno Fattori[1], Ricardo de Oliveira Correia[1], Yulli Roxenne Albuquerque[1], Bruna Dias de Lima Fragelli[1], Tiago Manuel Fernandes Mendes[2], Silmara Marques Allegretti[2], Edson Garcia Soares[3], Larissa Romanello[4], Juliana Roberta Torini[4], Humberto D'Muniz Pereira[4] and Fernanda de Freitas Anibal[1]**

[1] Laboratório de Inflamação e Doenças Infecciosas, Departamento de Morfologia e Patologia, Universidade Federal de São Carlos – UFSCar, São Carlos, Brazil, [2] Departamento de Biologia Animal, Instituto de Biologia, Universidade Estadual de Campinas, Campinas, Brazil, [3] Laboratório de Citopatologia, Departamento de Patologia e Medicina Legal, Universidade de São Paulo, Ribeirão Preto, Brazil, [4] Laboratório de Biologia Estrutural, Instituto de Física de São Carlos, Universidade de São Paulo, São Carlos, Brazil

Schistosomiasis, caused by *Schistosoma mansoni* trematode worm, affects more than 1.5 million people in Brazil. The current treatment consists in the administration of Praziquantel, the only medicine used for treatment for more than 40 years. Some of the limitations of this drug consist in its inactivity against schistosomula and parasite eggs, the appearance of resistant strains and non-prevention against reinfection. Thus, the objective of this study was to evaluate the effect of immunization with recombinant functional enzymes of the purine salvage pathway of *S. mansoni*, Nucleoside Diphosphate Kinase (NDPK) and Adenylosuccinate Lyase (ADSL), to evaluate the host immune response, as well as the parasite load after vaccination. For this, Balb/c mice were divided into 5 groups: control (uninfected and untreated), non-immunized/infected, NDPK infected, ADSL infected, and NDPK + ADSL infected. Immunized groups received three enzyme dosages, with a 15-day interval between each dose, and after 15 days of the last application the animals were infected with 80 cercariae of *S. mansoni*. On the 47th day after the infection, fecal eggs were counted and, on the 48th day after the infection, the evaluation of leukocyte response, parasite load, antibody production, cytokines quantification, and histopathological analysis were performed. The results showed that immunizations with NDPK, ADSL or NDPK + ADSL promoted a discreet reduction in eosinophil counts in lavage of peritoneal cavity. All immunized animals showed increased production and secretion of IgG1, IgG2a, and IgE antibodies. Increased production of IL-4 was observed in the group immunized with the combination of both enzymes (NDPK + ADSL). In addition, in all immunized

OPEN ACCESS

Edited by:
Simon Daniel Van Haren, Boston Children's Hospital and Harvard Medical School, United States

Reviewed by:
Olfat Ali Hammam, Theodor Bilharz Research Institute, Egypt
Norman Nausch, University Hospital of Düsseldorf, Germany

***Correspondence:**
Cynthia Aparecida de Castro
cynthiaefi2004@yahoo.com.br
Fernanda de Freitas Anibal
ffanibal@ufscar.br;
feranibal@yahoo.com

Specialty section:
This article was submitted to Vaccines and Molecular Therapeutics, a section of the journal Frontiers in Immunology

Received: *05 June 2020*
Accepted: *20 August 2020*
Published: *23 September 2020*

Citation:
Cagnazzo TO, Nogueira CT, Castro CA, Neris DM, Fattori ACM, Correia RO, Albuquerque YR, Fragelli BDL, Mendes TMF, Allegretti SM, Soares EG, Romanello L, Torini JR, Pereira HD'M and Anibal FF (2020) Investigating Immunization With Nucleotide Enzymes of Schistosoma mansoni: Nucleoside Diphosphate Kinase and Adenylosuccinate Lyase as New Antigenic Targets Against Schistosomiasis. Front. Immunol. 11:569988. doi: 10.3389/fimmu.2020.569988

groups there were reductions in egg counts in the liver and intestine, such as reductions in liver granulomas. Thus, we suggest that immunizations with these enzymes could contribute to the reduction of schistosomiasis transmission, besides being important in immunopathogenesis control of the disease.

Keywords: schistosomiasis, *Schistosoma mansoni*, Nucleoside Diphosphate Kinase, Adenylosuccinate Lyase, immunization

INTRODUCTION

According to the World Health Organization (WHO), a group of diseases called Neglected Tropical Diseases (NTD) affects approximately 1 billion people in regions with high rates of tropical and subtropical climate poverty, and costs developing countries' economies billions of dollars every year (1). An important highlight within this group of diseases is schistosomiasis, which affects over 200 million people worldwide, with an estimated at-risk population of 700 million (2). Five species of the schistosoma-genus trematode worm are capable of infecting humans; in Brazil, the species *Schistosoma mansoni* is present, causing the well-known mansonic schistosomiasis. With approximately 1.5 million people living in areas of risk for contamination by the parasite (3), mansonic schistosomiasis represents great importance in socioeconomic terms and impact on public health in the country, since influences from the cognitive response of school-age children to the economic production of the country and its consequent development.

The strategy preconized by WHO (4) for schistosomiasis control aims to prevent morbidity in later life through regular treatment with Praziquantel (PZQ), which is currently the only recommended drug for treatment of the species of schistosome infecting humans. The main control strategy is the mass administration of the drug, however, data from the institution itself show that the population that is at risk of acquiring the disease is not fully achieved (4). Added to this, the fact that the drug is not effective against schistosomula or eggs of *S. mansoni* makes its use restricted (5). Another limiting factor for the indiscriminate use of the drug is the emergence of resistant strains over the years (6). Finally, one of the most important aspects of drug failure is its use as a control method, since it does not prevent reinfection (5, 7, 8).

Due to the inadequacies and limitations of the approaches to control schistosomiasis centered on treatment with PZQ, it is necessary to develop a vaccine for this parasitosis (9). The immune response to *S. mansoni* infection has been extensively studied with the objective of identifying antigens that can elucidate the protective response in immunized individuals. Although there are no vaccines available for human use against schistosomiasis, a study with potential candidates in the clinical phase and in experimental models supports the feasibility of developing an effective vaccine (9).

To characterize new targets for vaccine development, we decided to perform a pre-clinical study using the Nucleosides Diphosphate Kinase (NDPK) and Adenylosuccinate Lyase (ADSL) enzymes. These enzymes are involved in the purine rescue pathway of *S. mansoni*. The parasite does not have the purine synthesis pathway, therefore, the purine rescue pathway is the only way to obtain these molecule (10). The biosynthesis of puric and pyrimidic bases is one of the main pathways studied for the development of drugs and vaccines, because they are directly related to the maintenance of DNA and RNA synthesis (11). Besides that, studies have been using these recombinant enzymes to identify new therapeutic targets (12, 13). Such works show that the enzymes of the purine rescue pathway seem to modulate the infection by *Schistosoma* sp. in different species, but this remains an unclear mechanism.

In this pathway, NDPK enzyme, in addition to being very active, is responsible for converting nucleotide diphosphate into triphosphates, while the enzyme ADSL is responsible for the cleavage of adenylosuccinate to adenosine 5′-monophosphate and fumarat (14, 15). In addition, another possible action of NDPK is to aid in the digestion of the host's blood, since this protein was found in regurgitation and in the anterior esophagus of adult worms coming into direct contact with the host's blood (15, 16). There is little information on ADSL in *S. mansoni*, but some studies suggest this is a potential chemotherapeutic target (17, 18). In humans, this enzyme can act in the two purine pathways; on the other hand, in *S. mansoni* it is involved only in the purine rescue pathway. This fact may have caused differences in the enzyme structure between the two species, thus enabling the worm's ADSL to be a candidate for the vaccine or a target for drugs against schistosomiasis (17). On the other hand, studies with enzymes from the purine rescue pathway as candidates for vaccine against *S. mansoni* are scarce. However, Neris et al. (19) demonstrated an increase in the specific immune response after immunization with enzymes from the *S. mansoni* purine rescue pathway (PNP1, HGPRT, and ADK1).

Therefore, the need for new candidates for vaccines and the influence of the essential metabolic pathways of *S. mansoni* on the survival of the parasite motivated the performance of the present study. The vaccine formulation using the recombinant nucleoid enzymes NDPK and ADSL from the route of purines salvation of *S. mansoni* aimed to evaluate the immunological response developed against the parasite, in addition to improving understanding about infection and, consequently, better understanding about the control and prevention of mansonic schistosomiasis.

METHODOLOGY

Recombinant Enzymes of *S. mansoni*

The recombinant enzymes of *S. mansoni* (ADSL – code Smp_038030) and (NDPK – code Smp_092750) were produced

by insertion of plasmids into bacterial cultures using the protein expression methodology and purified by the affinity chromatography method at the Crystallography Laboratory in the Institute of Physics of São Carlos (IFSC – USP) as previously described (15, 17).

Animals

Female Balb / c mice, weighing between 15 and 18 *g*, with 4 to 6 weeks of age, were used, from the Animal House Unit II from the Faculty of Pharmaceutical Sciences of Ribeirão Preto, University of São Paulo (FCFRP-USP). The animals have the SPF certificate and the entire experimental design was based on the recommendations of the Ethical Principles for Animal Experimentation and was authorized by the Ethics Committee on the Use of Animals (CEUA) of the Federal University of São Carlos – UFSCar, under the protocol number 2-022/2014.

Immunization

Following the experimental design shown in **Figure 1**, two independent experiments were carried out with n = 6–7 animals/group/experiment. The animals were divided into the following experimental groups: (1) Control group (CTRL): not immunized and not infected; (2) Infected group (INF): not immunized and infected with *S. mansoni*; (3) NDPK group: immunized with the NDPK enzyme and later infected with *S. mansoni*; (4) ADSL group: immunized with the ADSL enzyme and later infected with *S. mansoni* and (5) NDPK + ADSL group: immunized with the mix of enzymes NDPK + ADSL and later infected with *S. mansoni*. The immunization was performed with the application of three doses, with an interval of 15 days between doses. All immunizations were performed intraperitoneally. The groups NDPK and ADSL were immunized with 100 μg of the enzyme, NDPK, and ADSL, respectively, with 100 μg of the adjuvant aluminum hydroxide, solubilized in 1x PBS, totalling 200 μL of final solution per animal. The NDPK + ADSL group was immunized with 100 μg of enzyme (50 μg of NDPK + 50 μg of ADSL), with 100 μg of the adjuvant aluminum hydroxide, solubilized in PBS 1x, totalling 200 μL of final solution per animal.

Infection of Animals With *S. mansoni*

After 15 days of the last immunization, the animals of the groups INF, NDPK, ADSL, and NDPK + ADSL were challenged with 80 cercariae of *S. mansoni* per animal. Infectious larvae (cercariae) from Belo Horizonte strain (Minas Gerais – Brazil) maintained in the Department of Animal Biology from the Institute of Biology (IB) of the State University of Campinas – UNICAMP, Campinas – SP were used. The procedure was performed by caudal immersion in order to mimic the natural infection promoted by the parasite, as previously described (20).

Evaluation of Parasitic Load

Fecal Egg Count and Adult Worms' Recovery

Fecal egg count was performed using the Kato-Katz method (21), where the kit used was HELM TEST – Bio-Manguinhos, Fundação Oswaldo Cruz – FIOCRUZ.

The feces of each animal were individually sieved in a filter and mounted on microscopic slides, with a standardized amount of feces through a hole with a known diameter in the plate and covered with cellophane paper impregnated with malachite green, aiming to the conservation of feces and the clearing of eggs of *S. mansoni*. Subsequently, the eggs were counted and the number of eggs per gram of feces was calculated according to the following standardized formula by the kit: number of eggs in the sample per gram of feces = number of eggs found in the slide × factor 24.

Adult worms were recovered through perfusion of the portal system and intestinal mesentery (22). Percentage (%) reduction of the parasitic load was calculated comparing the average of worms recovered from each experimental group and the respective control, according to the following formula (23):

$$\%\mathrm{RPL} = \frac{\mathrm{RCG} - \mathrm{REG}}{\mathrm{RCG}} \times 100$$

where %RPL is the Reduction in the Parasitic Load, RCG is Recovery in the Control Group and REG is Recovery in the Experimental Group.

Immunological Profile: Eosinophils

Peritoneal Cavity Lavage and Blood

The eosinophils from the peritoneal cavity lavage (PCL) and blood were analyzed by extracting tissues from animals in all experimental groups on the 48th day after infection. The animals' blood was obtained by puncture of the left brachial vein using Ethylenediamine Tetra-acetic Acid (EDTA – from Ethylenediamine tetra acetic acid) as an anticoagulant. To perform the LCP, 3 mL of 1x PBS, pH 7.4, containing 0.5% sodium citrate (citrated PBS) were used. The solution was injected into the peritoneum with a syringe and needle, the region was homogenized, and the cells of the peritoneal region were subsequently recovered. The total number of eosinophils/mm^2 in both compartments (blood and PCL) were determined using Turk's solution. at 1:20 dilution. Each sample was counted in a Neubauer chamber. Blood smears were used for the differential counting of blood cells and slides were made in cytocentrifuge for the differential counting of cells of the PCL. Blood and PCL slides were stained using the Rapid Panoptic dye and 100 cells were counted, being differentiated into eosinophils, by optical microscopy, with an increase of 1000.

Immunoenzymatic Assay

Antibodies and cytokines were investigated from the animals' total plasma pool by ELISA immunoenzymatic assay (Enzyme Linked Immuno Sorbent Assay), following manufacturer's instructions for IgG1 (anti-Mouse IgG1 Antibody HRP Conjugated, Bethyl Laboratories, Inc.), IgG2a, IgE, IL-4, and IFN-γ kits (Kit OptEIA^{TM}, BD Biosciences), briefly described: in 96-well microtiter plates, 2 μg/well of the enzymes (NDPK, ADSL, and NDPK+ADSL) were applied for sensitization to IgE and IgG2a and 12 μg/well to IgG1 diluted in 0.1 M carbonate buffer – pH 9.5, totalling 100 μL/well, for 16 h at 4°C. For the IL-4 and IFN-γ cytokines, sensitization was performed with

the respective primary monoclonal antibody diluted in 0.1 M carbonate buffer – pH 9.5, totalling 100 μL/well, for 16 h at 4°C. After sensitization, the plates were washed with 300 μL/well of 1x PBS + 0.05% Tween 20, pH 7.4 (washing solution). After washing, 200 μL/well of blocking solution (PBS 1x + BSA – Bovine Serum Albumin 1%) were added and the plates were incubated for 1 h. After this period, the plates were washed again. Before applying the samples to the plates, the animals' plasma was divided into pools of 2 individuals from each experimental group, for each experiment. The samples were applied and incubated for 2 h. The samples were diluted in 1:10 carbonate buffer for the of antibodies analysis (100 μL/well) and for the cytokines were used pure samples (50 μL/well). After the incubation period, the plates were washed. The secondary antibody conjugated with peroxidase enzyme was added, diluted in PBS 1x + 1% BSA, in different proportions for each antibody and cytokine according to the manufacturer and 100 μL/well was added. The plates were then incubated for 1 h and 30 min in the dark. After this period, the plates were washed and 100 μL/well of the TMB substrate (3.3', 5.5' – Tetramethylbenzidine) and the plates were incubated, still protected from light, by approximately 30 min. Then, the reaction was blocked with the application of 50 μL/well of 2N sulfuric acid. The plates were read at a wavelength of 450 nm by the ELISA plate reader.

Histology of Liver and Intestines

Liver and intestines were collected 48 days after infection and fixed in buffered formaldehyde. The samples were embedded in paraffin blocks, sectioned in 5 μm sections and stained with Haematoxylin-Eosin (H.E.) and Masson's Trichrome. The slides were prepared at the Laboratory of Cytopathology, Department of Pathology and Legal Medicine, Faculty of Medicine of Ribeirão Preto – FMRP – USP. The slides were scanned at the 3DHistech Panoramic Desk in the Applied Immunology Laboratory, Department of Genetics and Evolution – DGE, at the Federal University of São Carlos – UFSCar. The images were made using 3DHistech's Pannoramic Viewer 1.15.4 program.

Statistical Analysis

The results were expressed as mean ± standard deviation (SD) and analyzed using GraphPad Prism 7.0 (San Diego, CA, United States). Shapiro–Wilk test was used to assess normality. The ANOVA test (unidirectional analysis of variance) was applied to the parametric data and the post-test was performed using the Tukey multiple comparison test. For non-parametric data, the Kruskal–Wallis test was used, and the post-test was performed using Dunn's multiple comparison test. The statistical significance considered was $p < 0.05$.

RESULTS

Evaluation of the Parasitic Load

Figure 2 represents the number of eggs in feces and worms recovered from the mice's hepatic vein. There was no statistical difference between the immunized groups and the INF group. The INF immunized with both recombinant enzymes (NDPK + ADSL), showed the highest values when compared to the other groups, in addition to the data of eggs/feces found in each animal being more dispersed in this group.

Quantification of Eosinophils in the Blood and in the Peritoneal Cavity Lavage

The **Figure 3** represents the number of eosinophils in the blood and PCL of animals in the CTRL group and animals infected and immunized or not with NDPK, ADSL, and the association between NDPK and ADSL. In the blood (**Figure 3A**), there was no statistically significant difference in the number of eosinophils between the groups. In the PCL (**Figure 3B**) there was a significant increase in the number of eosinophils in all groups when compared to the CTRL group. However, the number of eosinophils in all immunized groups was lower than that of the INF group, but without statistical significance.

Quantification of Cytokines in Plasma

The concentrations of IFN-γ and IL-4 present in the animals' plasma pool are shown in **Figure 4**. IFN-γ did not differ statistically between groups, despite being more present in the INF group (**Figure 4A**). The plasma concentrations of IL-4 were higher in the NDPK + ADSL group when compared to the CTRL group (**Figure 4B**).

Detection of Antibodies Present in Plasma

The evaluation of the production of IgG1, IgG2a, and IgE antibodies in a plate sensitized with recombinant NDPK protein from *S. mansoni*, caused a significant increase in IgG1 production in the INFs, NDPK, ADSL, and NDPK + ADSL immunized, compared to the group CTRL and INF (**Figure 5A**). In the production of IgE, the behavior was similar in that, only the groups NDPK and NDPK + ADSL had higher values compared to the group CTRL and INF (**Figure 5G**), but IgG2a showed no difference between the groups (**Figure 5D**).

Considering the levels of IgG1, IgG2a, and IgE antibodies in a plate sensitized with the recombinant enzyme ADSL from *S. mansoni*, there was an increase in the production of IgG1 in the ADSL and NDPK + ADSL groups compared to the INF (**Figure 5B**). In the production of IgG2a, the ADSL, and NDPK + ADSL groups also showed higher values when compared to the INF (**Figure 4E**). IgE production did not differ between groups (**Figure 5F**). When there was sensitization with the recombinant protein NDPK + ADSL from *S. mansoni*, a significant increase in IgG1 production was observed in the group immunized with ADSL compared to the IFN group (**Figure 5C**). IgG2a was higher in the ADSL and NDPK + ADSL groups compared to the IFN and CTRL controls. IgE production was higher in the three immunized groups (NDPK, ADSL, and NDPK + ADSL) compared to INF (**Figure 5I**).

Histopathology of the Liver

Mice livers were analyzed through histology using HE staining to assess the presence and quantification of granulomas (24)

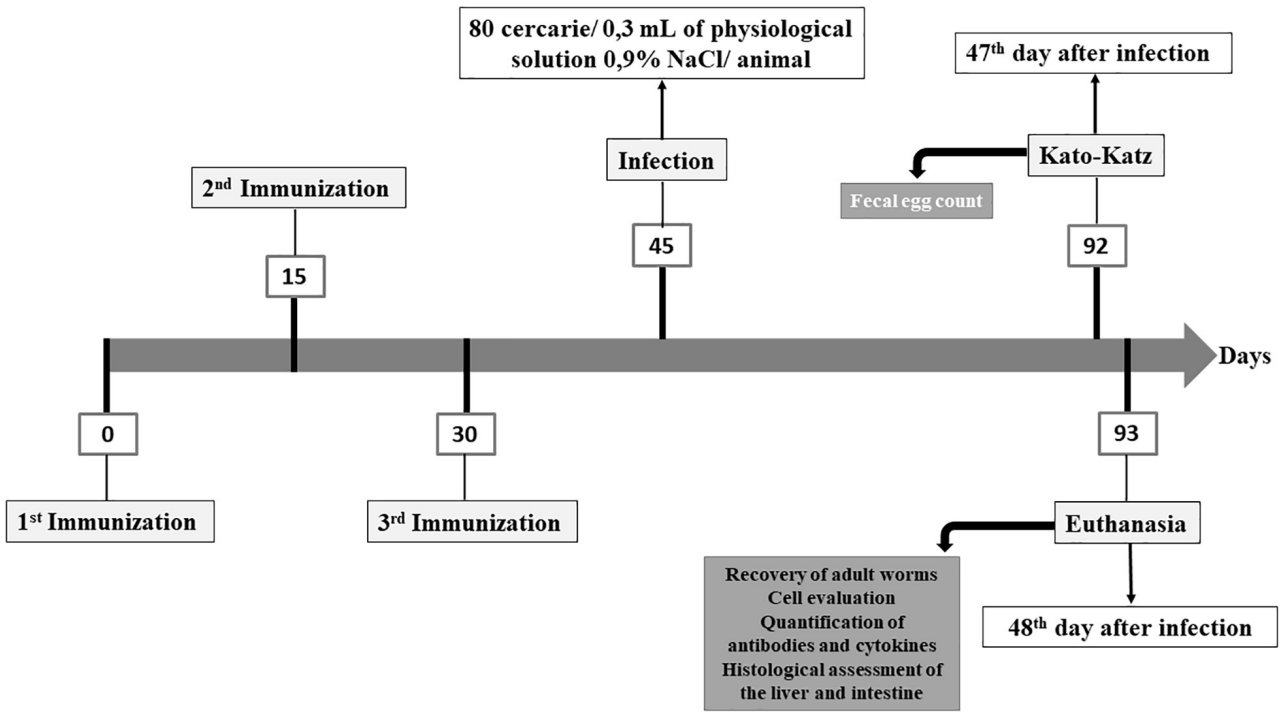

FIGURE 1 | Experimental design for immunization of the animals with the recombinant proteins NDPK and ADSL.

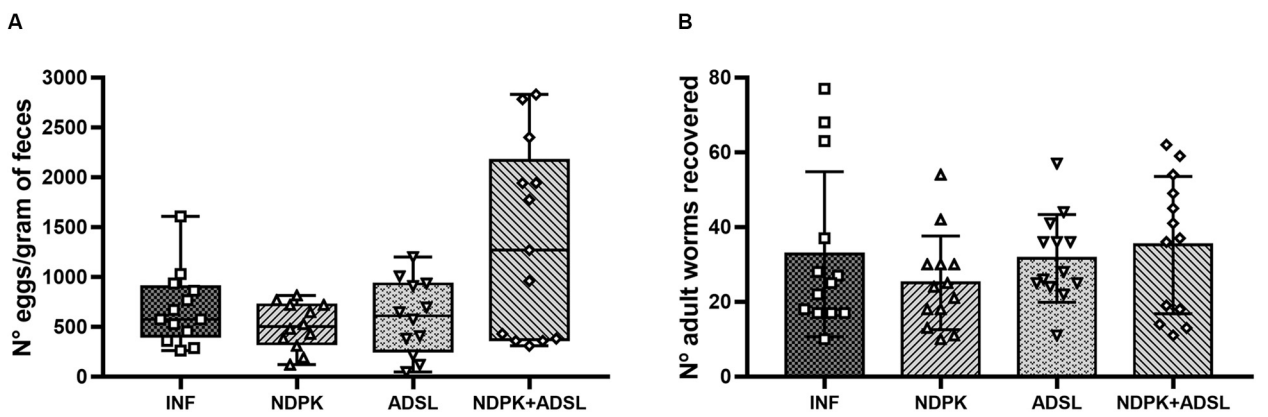

FIGURE 2 | Number of eggs in feces **(A)** and adult worms recovered from the hepatic portal system **(B)** from two independent experiments (n = 6–7 animals/group/experiment). The numbers of eggs/gram of feces data represent the first and third quartiles at the top and bottom of the box plot graph, the middle line represents the median value and the minimum and maximum values are represented by the error bars (whiskers). The numbers of adult worms recovered data represent the mean ± SD. There was no statistical difference between the results of the immunized groups when compared with the INF group. The geometric figures represent the dispersion of the data for each group.

and the appearance of cell infiltrate, and Masson trichrome (MT) to assess the collagen deposit (**Figure 6**). The animals in the CTRL group had well-structured and preserved liver tissue (**Figure 6A**). On the other hand, it was possible to observe the formation of periovular granulomas formed by lymphocytes, eosinophils, neutrophils, and epithelioid cells in all groups infected with *S. mansoni*, immunized or not (**Figures 6C,E,G,I**). The tissue showed structures preserved in places where there was no egg deposition.

The hepatic tissue of the CTRL group (**Figure 6B**) presented thin pericanalicular and perivascular collagen. The livers of all groups that were infected with *S. mansoni*, immunized or not, in addition to the presence of pericanalicular and perivascular collagen, it was possible to observe the formation of collagenous material around the eggs, along with granulomas (**Figures 6B,D,F,H,J**).

Table 1 shows that egg counts in the liver of animals in the NDPK and ADSL groups had a significant reduction

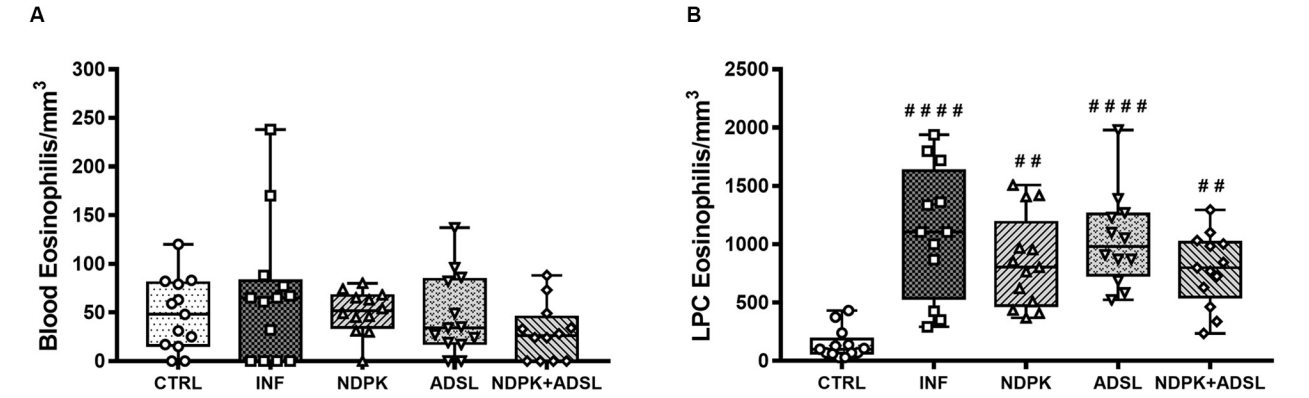

FIGURE 3 | Number of eosinophils in the blood **(A)** and in the PCL **(B)** 48 days after infection with *S. mansoni* and 93 days after the first immunization. The upper and lower part of the Box plot graph represents the first and third quartiles, the middle line represents the median value and the minimum and maximum values are represented by the error bars (whiskers). (#) Represents a statistically significant difference from two independent experiments (n = 6–7 animals) using the Kruskal–Wallis non-parametric test followed by Dunn's post-test between the results of the experimental groups when compared with the CTRL group; ##$p < 0.01$; ####$p < 0.0001$. The geometric figures represent the dispersion of the data for each group.

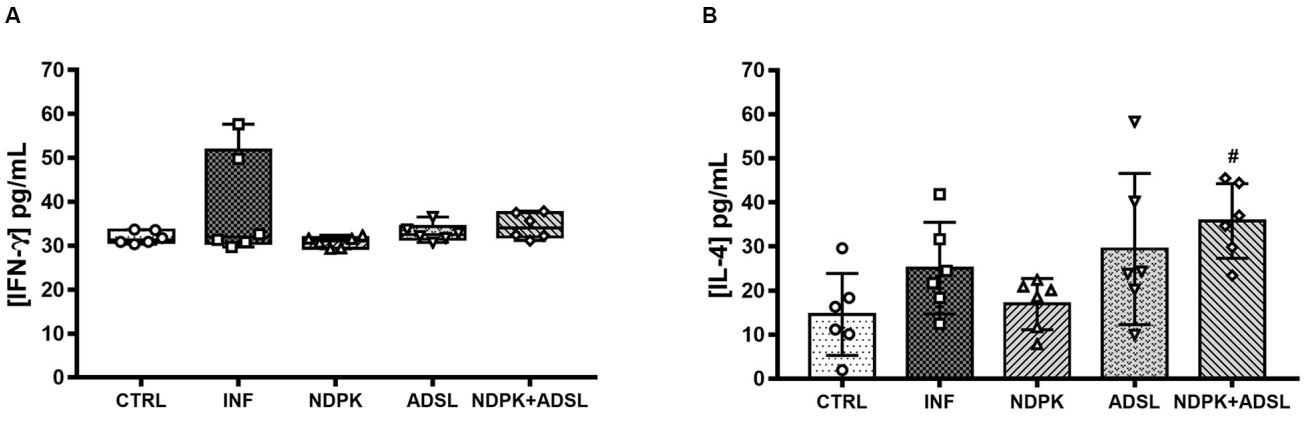

FIGURE 4 | Concentrations of IFN-γ **(A)** and IL-4 **(B)** cytokines in plasma pool 48 days after infection with *S. mansoni* and 93 days after the first immunization of two independent experiments (n = 6–7 animals). The IFN-γ cytokine data represent the first and third quartiles at the top and bottom of the box plot graph, the middle line represents the median value and the minimum and maximum values are represented by the error bars (whiskers). The IL-4 cytokine data represent the mean ± SD. (#) represents statistically significant difference using the One-Way ANOVA parametric test followed by the Tukey's post-test between the results of the experimental groups when compared with the CTRL group; $^{\#}p < 0.05$. The geometric figures represent the dispersion of the data for each group.

when compared to the INF group, promoting a reduction of 49.01% and 43.48%, respectively, indicating a greater reduction in the group immunized with the recombinant enzyme NDPK. Regarding the counts of granulomas in the liver tissue, the reductions of the NDPK and ADSL groups in relation to the INF group reached 45.83% and 32.55%, respectively. Clearly, immunization with the recombinant enzyme NDPK was responsible for the greatest efficiency in reducing liver tissue granulomas in animals with experimental mansonic schistosomiasis.

In the evaluation of egg count in mesenteric tissue, the group with the highest rate of egg reduction in the intestine was NDPK + ADSL, with 53.15%, followed by the ADSL groups, with 50.45%, and NDPK, with 38.84%. Although there is no statistical difference, immunizations with recombinant enzymes (NDPK and ADSL) were shown to be important in reducing the amount of *S. mansoni* eggs in the animals' intestines.

DISCUSSION

Schistosomiasis affects almost 240 million people worldwide, and more than 700 million people live in endemic areas. The infection is prevalent in tropical and sub-tropical areas, in poor communities without potable water and adequate sanitation (25).

The morbidity triggered by this disease is related to the pathology caused by the host's own granulomatous immune response. Due to the retention of eggs in the liver, intestine and spleen, there is the occurrence of fibrosis and organ calcification, in addition to hepatosplenomegaly (26, 27). There are still no vaccines available for schistosomiasis and there are few potential

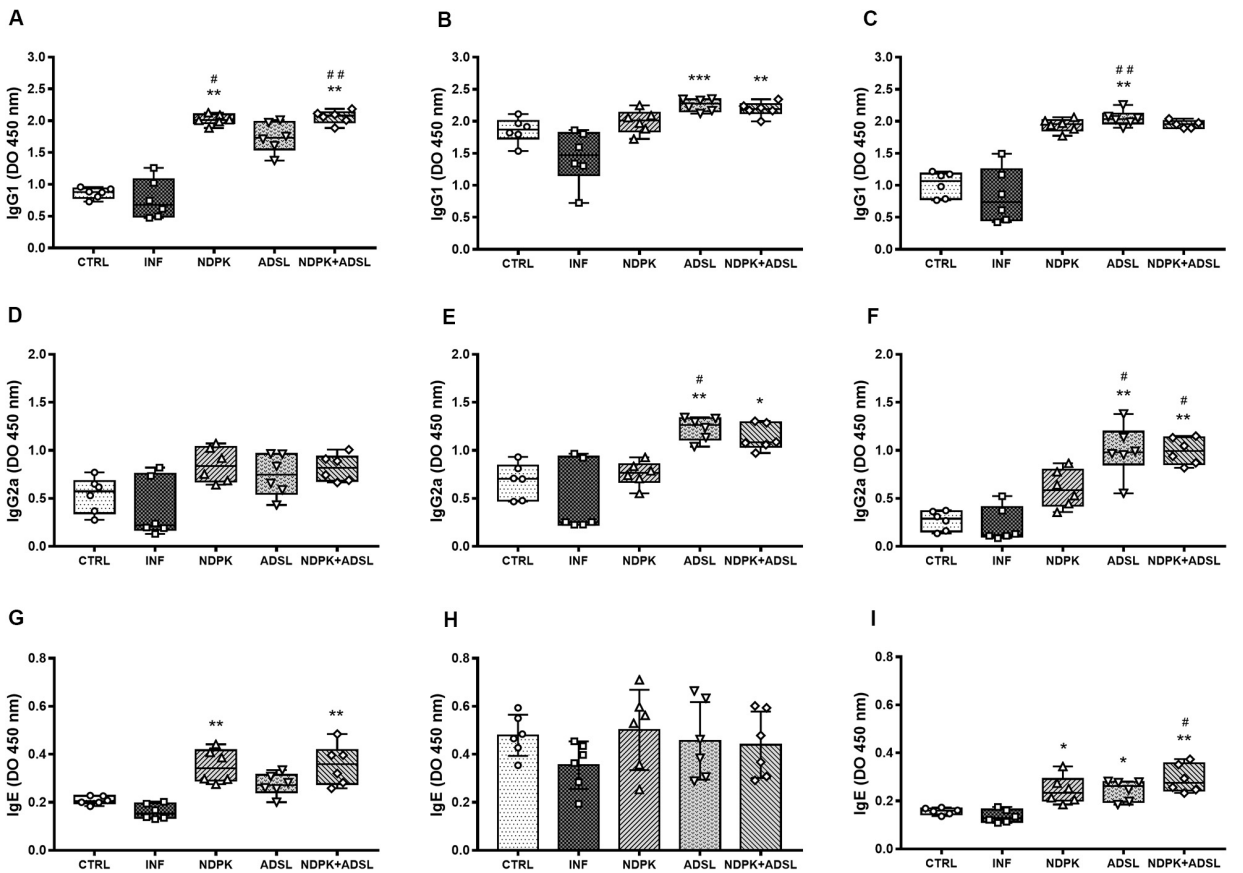

FIGURE 5 | Detection of IgG1 **(A–C)**, IgG2a **(D–F)**, and IgE **(G–I)** antibodies in a plate sensitized with NDPK, ADSL, and NDPK+ADSL in the plasma pool of mice 48 days after infection with S. *mansoni,* and 93 days after the first immunization of two independent experiments (n = 6–7 animals). Nonparametric data were analyzed using the Kruskal–Wallis test followed by Dunn's post-test and are represented in Box plot, with the lower and upper lines being the first and third quartiles, the middle line being the median value and the minimum and maximum values are represented by error bars (whiskers). Parametric data were analyzed by the One-Way ANOVA test followed by the Tukey's post-test and are represented in the bar graph through the mean ± SD. (#) represents a statistically significant difference between the results of the experimental groups when compared with the CTRL group; $^{\#}p < 0.05$; $^{\#\#}p < 0.01$. (*) It represents a statistically significant difference between the results of the experimental groups when compared with the INF group; $^{*}p < 0.05$; $^{**}p < 0.01$; $^{***}p < 0.001$. The geometric figures represent the dispersion of the data for each group.

vaccine agents that have advanced to clinical tests (Sm-TSP-2, Sm-p80, and Sm14) (9). Thus, studies that seek to identify new immunogens for this disease, such as the recombinant enzymes NDPK and ADSL of *S. mansoni*, remain an urgent need for the development of a vaccine formulation.

A vaccine against schistosomiasis does not necessarily need to have sterilizing immunity, as long as it acts by limiting the parasitic burden and/or the maturation of the worms. This last attribute is important to induce a reduction in the fertility of females and, consequently, in reducing the release of eggs, which is mainly responsible for the disease morbidity (28–31).

In our study, after three immunizations with the recombinant enzymes of *S. mansoni* NDPK and ADSL, it was not possible to observe a significant reduction in the number of adult worms or in the number of eggs present in the feces and intestine. Immunization with both enzymes associated (NDPK + ADSL), has not been shown to reduce the number of adult worms or eggs in the stool. Furthermore, there was no significant reduction in the number of eggs in the liver (16.60%) and intestines (53.15%) and in granulomas in the liver (23.18%). One possible explanation is that the concentration of each recombinant enzyme used in the NDPK + ADSL group (50 μg) is half the concentration used in the groups immunized with each enzyme individually (100 μg), which may not have been sufficient to induce a significant protective effect in the analyzed parameters.

The parasite's eggs, when established in the liver, lead to the recruitment of various inflammatory cells to the injury site, such as eosinophils, neutrophils and macrophages, to form the granuloma (32). The granulomatous response around eggs trapped in the liver tissue is initially orchestrated by CD4 + T lymphocytes, but CD8 + T cells, B cells, and macrophages have also been shown to be important in this formation. In addition

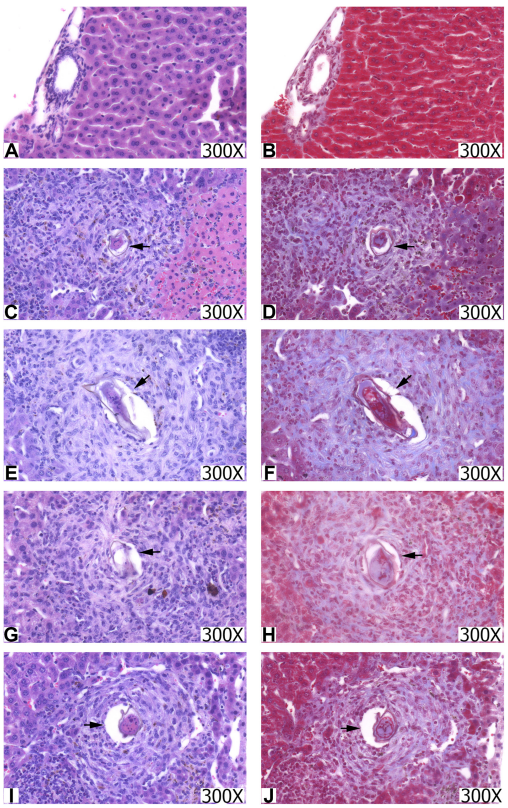

FIGURE 6 | Histopathological sections of the liver from the groups CTRL **(A,B)**, INF **(C,D)**, NDPK **(E,F)**, ADSL **(G,H)**, and NDPK + ADSL **(I,J)**. The images on the left were stained with hematoxylin-eosin (HE) and those on the right with Masson trichrome (TM). Increase: 300X. The arrows indicate the presence of the granuloma around the egg.

TABLE 1 | Counting of granulomas and eggs in the liver and intestine of the animals on the 48th day after infection.

	INF	NDPK	ADSL	NDPK+ADSL
Granulomas in the liver/slide	32.00 ± 5,63	17.33 ± 4.56**	21.58 ± 5.28*	24.58 ± 10.66
Reduction (%)	–	45.83%	32.55%	23.18%
Eggs in the liver/slide	21.08 ± 6.17	10.75 ± 4.01**	11.92 ± 4.83*	17.58 ± 8.87
Reduction (%)	–	49.01%	43.48%	16,60%
Eggs in the intestines/slide	18.50 ± 13.80	11.50 ± 8.58	9.17 ± 4.77	8.67 ± 4.72
Reduction (%)	–	38.84%	50.45%	53.15%

*The data represent the mean ± SD (n = 7 animals) of two independent experiments using the parametric One-Way ANOVA test and Tukey post-test. (*) represents a statistically significant difference between the results of the experimental groups when compared with the INF group; *p < 0.05 and **p < 0.01.*

to these cells, the eosinophil proved to be the main constituent of granuloma (33). Eosinophils are known for their functions as effector cells against helminth infections, although there are still discussions about their exact function (34, 35). To act on the sites of inflammation/infection, eosinophils are recruited to these sites, which can contribute to the decline of circulating eosinophils (36). In our results, there was an increase in eosinophils in the PCL of the infected animals (INF, NDPK, ADSL, and NDPK + ADSL) when compared to the CTRL group. There was no reduction in the number of eosinophils in both peripheral blood and PCL in the NDPK, ADSL, and NDPK + ADSL groups in relation to the CTRL and INF groups. On the other hand, it is noteworthy that, although there is no significant difference, the immunized groups have less eosinophils compared to INF, which may be an indication of an onset of eosinophilia modulation.

Additionally, in our results it is possible to observe that the animals' immunization with the NDPK and ADSL enzyme within 48 days after infection showed a decrease in the percentage of granulomas in the liver and the number of eggs in the liver, when compared to the infected/untreated group, showing higher percentages of reduction to NDPK. The decrease in the number of eggs is very important, once granulomas are caused mainly by immune responses against soluble egg antigens (SEAs) (37), and even a smaller number of eggs being deposited in the tissues can lead to a reduction in the process granulomatous (38), consequently considering a possible decrease in the morbidity of this pathogenesis. Our findings are in accordance with the study by Neris et al. (39), where the authors observed that PNP and HGPRT, enzymes of the metabolic pathways of nucleotides, were able to modulate the infection by reducing the parasitic load on the liver, intestine and feces from animals infected with *S. mansoni* after 48 days of infection. Immunization with the union of NDPK and ADSL did not show a significant decrease in the reduction of granulomas, eggs in the liver or in the intestines when compared to the immunized group, suggesting that other factors may be interfering in the control of mansonic schistosomiasis.

The results obtained suggest that immunizations with recombinant enzymes evaluated individually, mainly NDPK, may be acting in the regulation of the host's immune response against the parasite and its immunopathology associated with the development of granuloma. Immunization with the Smteg recombinant integument protein also induced a decrease in the egg count in the animals' liver, with the rate being of 65% (40). Other recombinant proteins of *S. mansoni* also showed a reduction in the number of eggs (immunization by SmRho) and in the formation of granuloma (immunization by rP22) (41, 42).

The data presented here for NDPK seem promising, but it is worth noting that the immunological interactions necessary to eradicate invasive parasites are extremely complex and require components of both the humoral and cell-mediated immune mechanisms (43). A study with knockout mice for B cells showed the fundamental role of antibodies in inducing resistance to schistosomiasis (44). In this way, the different functional properties of antibodies make them interesting to study as they could provide important information about the progression of the disease and the effectiveness of vaccination.

In our work, the response of antibodies in the host after immunizations with the recombinant enzymes NDPK and ADSL, showed a significant increase in the production of IgG1 antibody in the groups that were previously immunized (NDPK, ADSL, and NDPK + ADSL) when compared to the CTRL and INF group, subject to sensitization of the respective enzyme. As for

the IgG2a concentration, the ADSL to NDPK + ADSL groups showed increased levels when compared to the INF group. Thus, since there was an increase in the production of antibodies, both IgG1 and IgG2a, we can infer that recombinant enzymes were capable to induce specific immunity in animals against antigens of the parasite. In addition, we can observe that the concentration of antibodies of type IgG1 is higher than the concentration of antibodies of type IgG2a. The predominance of plasma IgG1 levels over IgG2a indicates that the immune response present in animals is a Th2 pattern, which is observed in the chronic phase of the disease, largely due to the presence of parasite eggs in the tissue (45, 46). The decrease in the Th2 response results in tissue damage and host mortality due to the Th1-like pro-inflammatory response. Thus, the Th2 response also acts as a protective function in the host, which is extremely important, since its appropriate regulation minimizes the damage caused by the pathology (26). A study with immunizations of the recombinant proteins Sm29 and TSP also showed an increase in IgG1, in addition to IgG3, indicating the role of these immunoglobulins in acting in the elimination of the parasite and eggs, in addition of stimulating the immune system to produce antibodies against them (47, 48). The alleged resistance to reinfection is also seen in other studies using recombinant proteins such as SmStoLP-2 (49) and Sm14-FABP (50).

Helminth infection induces a Th2 response in the host characterized by high synthesis of IgE and eosinophilia. *S. mansoni* represents a particularly potent inducer of this type of immune response, resulting in a disease characterized by high levels of IgE, IgG1, and IgG4 (51). In the Th2 type response, during the chronic phase of the disease, IgE works largely through its ability to bind to eosinophils and mast cells, both important in the response to tissue damage (52). Numerous studies of human schistosomiasis show that levels of antiparasitic IgE are related to resistance to reinfection (53–55).

In our work, a significant increase in IgE levels in responses to NDPK protein can be observed in the NDPK and NDPK + ADSL groups, in addition to an increase in IgE in response to NDPK + ADSL in all immunized groups. No increase in IgE was observed in response to the ADSL protein. Similar to our analysis, other studies have also sought to induce an increase in the protective immune response through increased production of IgE by the host, as is the case of the study conducted using Paramiosin (54) and cysteine protease cathepsin B1 (SmCB1) (56) as targets, resulting in increased protection against reinfection.

In an infection with *S. mansoni*, helper T cells are divided into two subsets. The cells of the first subset, Th1, produce IFN-γ and preferentially promote the cell-mediated immune response provided by the activation of macrophages; meanwhile, the cells of the second subset, Th2, produce interleukins IL-4 and IL-5, which promote the production of IgE and the production and activation of eosinophils, respectively, (57, 58). In the work carried out by Henri et al. (59), the authors showed that low IFN-γ production is associated with severe periportal fibrosis, indicating that the decrease in this cytokine increases the severity of the disease. In our study, we observe that there were no statistically significant changes in the measurement of the IFN-γ cytokine.

When it comes to the Th2 response, one of the main cytokines involved in regulating the response is IL-4. This cytokine has been shown to be the main regulatory molecule in Th2 cell differentiation and in the cytokine response of this response pattern. In addition, the protective function of IL-4 in this response pattern is also notable (60, 61). In fact, the Th2 response is essential for the host's survival against *S. mansoni*. Brunet et al. (62) observed that IL-4 deficient mice had an impaired Th2 response and died earlier due to massive intestinal inflammation. When we analyzed the concentration of IL-4 in the plasma of animals in our experimental groups, we could see that there was no difference between groups when compared to INF. This stimulus is consistent with the results of eosinophils, which also did not show any difference between groups.

Our results indicate that the recombinant proteins NDPK and ADSL from the purine salvage pathway of *S. mansoni* have the potential for a possible formulation of a vaccine against mansonic schistosomiasis. Further studies are still needed to better understand the role of these proteins during the host's immune response and how the enzymes NDPK and ADSL are acting to modulate the immune response in order to promote control and induce protection in the host against the parasite. Furthermore, we conclude that the protein with the greatest immunogenic potential for further studies is NDPK in its simple formulation.

DATA AVAILABILITY STATEMENT

All datasets presented in this study are included in the article/supplementary material.

ETHICS STATEMENT

The animal study was reviewed and approved by Ethics Committee on the Use of Animals (CEUA) of the Federal University of São Carlos – UFSCar, under the protocol no. 2-022/2014.

AUTHOR CONTRIBUTIONS

DN, AF, RC, TC, LR, JT, BF, and TM participated in the performance of assays. CC, CN, and YA participated in data analysis. SA, ES, and HP were responsible for materials acquisition, analysis, or interpretation of data. FA participated in the production of the manuscript, acquisition of funding, and coordination of the project. All authors contributed to writing or critical review of the work for intellectual content and approved the final version.

FUNDING

FAPESP 2014/07331-5; FAPESP 2012/14223-9; FAPESP 2012/05532-8; and FAPESP 202/10213-9. TM was financed partially by the Coordenação de Aperfeiçoamento de Pessoal de Nível Superior – Brasil (CAPES) – Finance Code 001.

ACKNOWLEDGMENTS

The authors would like thank all the people who directly or indirectly contributed to the development of this research, collaborators from the Federal University of São Carlos (UFSCar), the Institute of Physics of São Carlos, University of São Paulo (IFSC – USP), Faculty of Pharmaceutical Sciences of Ribeirão Preto, University of São Paulo (FCFRP-USP) and for the funding.

REFERENCES

1. World Health Organisation. *Neglected Tropical Diseases*. Geneva: World Health Organisation (2019).
2. Vos T, Abajobir AA, Abbafati C, Abbas KM, Abate KH, Abd-Allah F, et al. Global, regional, and national incidence, prevalence, and years lived with disability for 328 diseases and injuries for 195 countries, 1990-2016: a systematic analysis for the Global Burden of disease study 2016. *Lancet*. (2017) 390:1211–59. doi: 10.1016/S0140-6736(17)32154-2
3. Ministério da Saúde. *Esquistossomose: Causas, Sintomas, Tratamento, Diagnóstico e Prevenção*. Brazil: Ministério da Saúde (2019).
4. World Health Organization. *Schistosomiasis*. Geneva: World Health Organization (2019).
5. Othman AA, Soliman RH. Schistosomiasis in Egypt: a never-ending story? *Acta Trop*. (2015) 148:179–90. doi: 10.1016/j.actatropica.2015.04.016
6. Cioli D, Botros SS, Wheatcroft-Francklow K, Mbaye A, Southgate V, Tchuenté LAT, et al. Determination of ED50 values for praziquantel in praziquantel-resistant and -susceptible *Schistosoma mansoni* isolates. *Int J Parasitol*. (2004) 34:979–987. doi: 10.1016/j.ijpara.2004.05.001
7. Olveda DU. Bilharzia: pathology, diagnosis, management and control. *Trop Med Surg*. (2013) 1:135. doi: 10.4172/2329-9088.1000135
8. Gryseels B. Schistosomiasis. *Infect Dis Clin North Am*. (2012) 26:383–97. doi: 10.1016/j.idc.2012.03.004
9. Molehin AJ. Schistosomiasis vaccine development: update on human clinical trials. *J Biomed Sci*. (2020) 27:28. doi: 10.1186/s12929-020-0621-y
10. Dovey HF, McKerrow JH, Wang CC. Purine salvage in *Schistosoma mansoni* schistosomules. *Mol Biochem Parasitol*. (1984) 11:157–67. doi: 10.1016/0166-6851(84)90062-8
11. Senft AW, Miech RP, Brown PR, Senft DG. Purine metabolism in *Schistosoma mansoni*. *Int J Parasitol*. (1972) 2:249–60. doi: 10.1016/0020-7519(72)90013-6
12. Peng HJ, Chen XG, Li H, Wang CM. Expression of adenylate kinase of *Schistosoma japonicum* and evaluation on the immunoreactivity of the recombinant protein. *Zhongguo Ji Sheng Chong Xue Yu Ji Sheng Chong Bing Za Zhi*. (2004) 22:46–9.
13. Pereira TC, Pascoal VDB, Marchesini RB, Maia IG, Magalhães LA, Zanotti-Magalhães EM, et al. Schistosoma mansoni: evaluation of an RNAi-based treatment targeting HGPRTase gene. *Exp Parasitol*. (2008) 118:619–23. doi: 10.1016/j.exppara.2007.11.017
14. Kmoch S. Human adenylosuccinate lyase (ADSL), cloning and characterization of full-length cDNA and its isoform, gene structure and molecular basis for ADSL deficiency in six patients. *Hum Mol Genet*. (2000) 9:1501–13. doi: 10.1093/hmg/9.10.1501
15. Torini JR, de Freitas Fernandes A, Balasco Serrão VH, Romanello L, Bird LE, Nettleship JE, et al. Characterization of a Schistosoma mansoni NDPK expressed in sexual and digestive organs. *Mol Biochem Parasitol*. (2019) 231:111187. doi: 10.1016/j.molbiopara.2019.111187
16. Hall SL, Braschi S, Truscott M, Mathieson W, Cesari IM, Wilson RA. Insights into blood feeding by schistosomes from a proteomic analysis of worm vomitus. *Mol Biochem Parasitol*. (2011) 179:18–29. doi: 10.1016/j.molbiopara.2011.05.002
17. Romanello L, Serrão VHB, Torini JR, Bird LE, Nettleship JE, Rada H, et al. Structural and kinetic analysis of *Schistosoma mansoni* adenylosuccinate lyase (SmADSL). *Mol Biochem Parasitol*. (2017) 214:27–35. doi: 10.1016/j.molbiopara.2017.03.006
18. Foulk BW, Pappas G, Hirai Y, Hirai H, Williams DL. Adenylosuccinate lyase of *Schistosoma mansoni*: gene structure, mRNA expression, and analysis of the predicted peptide structure of a potential chemotherapeutic target. *Int J Parasitol*. (2002) 32:1487–95. doi: 10.1016/S0020-7519(02)00161-3
19. Neris DM, Pereira HD, de Souza LC, de Correia RO, de Rodolpho JMA, de Oliveira SRP, et al. Immunization with purine salvation pathway recombinant enzymes induces the production of anti- *Schistosoma mansoni* immunoglobulines. *Int Trends Immun*. (2013) 1:49–56.
20. Olivier L, Stirewalt MA. An efficient method for exposure of mice to cercariae of *Schistosoma mansoni*. *J Parasitol*. (1952) 38:19–23. doi: 10.2307/3274166
21. Katz N, Chaves A, Pellegrino J. A simple device for quantitative stool thick smear technique in *Schistosomiasis mansoni*. *Rev Soc Bras Med Trop*. (1972) 14:397–400.
22. Pellegrino J, Siqueira AF. Tecnica de perfusâo para colheita de Schistosoma mansoni em cobaias experimentalmente infestadas. *Rev Bras Malariol Doencas Trop*. (1956) 8:589–97.
23. Delgado VS, Suarez DP, Cesari IM, Incani RN. Experimental chemotherapy ofSchistosoma mansoni with praziquantel and oxamniquine: differential effect of single or combined formulations of drugs on various strains and on both sexes of the parasite. *Parasitol Res*. (1992) 78:648–54. doi: 10.1007/BF00931515
24. Feitosa KA, Zaia MG, Rodrigues V, Castro CA, de Correia RO, Pinto FG, et al. Menthol and menthone associated with acetylsalicylic acid and their relation to the hepatic fibrosis in *Schistosoma mansoni* infected mice. *Front Pharmacol*. (2018) 8:1000. doi: 10.3389/fphar.2017.01000
25. World Health Organization. *What is Schistosomiasis??*. Geneva: World Health Organisation (2020).
26. Colley DG, Secor WE. Immunology of human schistosomiasis. *Parasite Immunol*. (2014) 36:347–57. doi: 10.1111/pim.12087
27. Schwartz C, Fallon PG. Schistosoma "Eggs-iting" the host: granuloma formation and egg excretion. *Front Immunol*. (2018) 9:2492. doi: 10.3389/fimmu.2018.02492
28. Wilson RA, Coulson PS. Schistosome vaccines: a critical appraisal. *Mem Inst Oswaldo Cruz*. (2006) 101:13–20. doi: 10.1590/S0074-02762006000900004
29. Rofatto HK, Cezar L, Leite DC, Aparecida C, Kanno AI, Omar B, et al. Antígenos vacinais contra esquistossomose mansônica?: passado e presente vaccine antigens against schistosomiasis?: past and present. *Biologia (Bratisl)*. (2011) 6b:54–9.
30. Siddiqui AA, Siddiqui BA, Ganley-Leal L. Schistosomiasis vaccines. *Hum Vaccin*. (2011) 7:1192–7. doi: 10.4161/hv.7.11.17017
31. Merrifield M, Hotez PJ, Beaumier CM, Gillespie P, Strych U, Hayward T, et al. Advancing a vaccine to prevent human schistosomiasis. *Vaccine*. (2016) 34:2988–91. doi: 10.1016/j.vaccine.2016.03.079
32. McCormick ML, Metwali A, Railsback MA, Weinstock JV, Britigan BE. Eosinophils from schistosome-induced hepatic granulomas produce superoxide and hydroxyl radical. *J Immunol*. (1996) 157:5009–15.
33. Hams E, Aviello G, Fallon PG. The *Schistosoma* granuloma: friend or foe? *Front Immunol*. (2013) 4:89. doi: 10.3389/fimmu.2013.00089
34. Tweyongyere R, Namanya H, Naniima P, Cose S, Tukahebwa EM, Elliott AM, et al. Human eosinophils modulate peripheral blood mononuclear cell response to Schistosoma mansoni adult worm antigen in vitro. *Parasite Immunol*. (2016) 38:516–22. doi: 10.1111/pim.12336
35. Swartz JM, Dyer KD, Cheever AW, Ramalingam T, Pesnicak L, Domachowske JB, et al. *Schistosoma mansoni* infection in eosinophil lineage – ablated mice. *Blood*. (2006) 108:2420–7. doi: 10.1182/blood-2006-04-015933.Supported
36. Hogan SP, Waddell A, Fulkerson PC. Eosinophils in infection and intestinal immunity. *Curr Opin Gastroenterol*. (2013) 29:7–14. doi: 10.1097/MOG.0b013e32835ab29a
37. Zheng B, Zhang J, Chen H, Nie H, Miller H, Gong Q. T lymphocyte-mediated liver immunopathology of schistosomiasis. *Front Immunol*. (2020) 11:61. doi: 10.3389/fimmu.2020.00061
38. Helmy MMF, Mahmoud SS, Fahmy ZH. Experimental parasitology *Schistosoma mansoni?*: effect of dietary zinc supplement on egg granuloma in Swiss mice treated with praziqantel. *Exp Parasitol*. (2009) 122:310–7. doi: 10.1016/j.exppara.2009.04.006

39. Neris DM. *Efeito da Imunização com Enzimas Recombinantes do Metabolismo de Nucleotídeos de Schistosoma mansoni sobre o Desenvolvimento da Esquistossomose Mansônica Experimental*. Brazil: Federal University of São Carlos (2012).
40. Teixeira De Melo T, Michel De Araujo J, Do Valle Durães F, Caliari MV, Oliveira SC, Coelho PMZ, et al. Immunization with newly transformed Schistosoma mansoni schistosomula tegument elicits tegument damage, reduction in egg and parasite burden. *Parasite Immunol*. (2010) 32:749–59. doi: 10.1111/j.1365-3024.2010.01244.x
41. Rezende CMF, Silva MR, Santos IGD, Silva GAB, Gomes DA, Goes AM. Immunization with rP22 induces protective immunity against *Schistosoma mansoni*: effects on granuloma down-modulation and cytokine production. *Immunol Lett*. (2011) 141:123–33. doi: 10.1016/j.imlet.2011.09.003
42. Oliveira CR, Rezende CMF, Silva MR, Pêgo AP, Borges O, Goes AM. A new strategy based on smrho protein loaded chitosan nanoparticles as a candidate oral vaccine against schistosomiasis. *PLoS Negl Trop Dis*. (2012) 6:e1894. doi: 10.1371/journal.pntd.0001894
43. Wynn TA, Hoffmann KF. Defining a schistosomiasis vaccination strategy – is it really Th1 versus Th2? *Parasitol Today*. (2000) 16:497–501. doi: 10.1016/S0169-4758(00)01788-9
44. Jankovic D, Wynn TA, Kullberg MC, Hieny S, Caspar P, James S, et al. Optimal vaccination against Schistosoma mansoni requires the induction of both B cell- and IFN-gamma-dependent effector mechanisms. *J Immunol*. (1999) 162:345–51.
45. Abreu PAE, Miyasato PA, Vilar MM, Dias WO, Ho PL, Tendler M, et al. Sm14 of *Schistosoma mansoni* in fusion with tetanus toxin fragment C induces immunoprotection against tetanus and schistosomiasis in mice. *Infect Immun*. (2004) 72:5931–7. doi: 10.1128/IAI.72.10.5931-5937.2004
46. Yan Y, Liu S, Song G, Xu Y, Dissous C. Characterization of a novel vaccine candidate and serine proteinase inhibitor from *Schistosoma japonicum* (Sj serpin). *Vet Parasitol*. (2005) 131:53–60. doi: 10.1016/j.vetpar.2005.04.038
47. Tran MH, Pearson MS, Bethony JM, Smyth DJ, Jones MK, Duke M, et al. Tetraspanins on the surface of *Schistosoma mansoni* are protective antigens against schistosomiasis. *Nat Med*. (2006) 12:835–40. doi: 10.1038/nm1430
48. Cardoso FC, Pacífico RNA, Mortara RA, Oliveira SC. Human antibody responses of patients living in endemic areas for schistosomiasis to the tegumental protein Sm29 identified through genomic studies. *Clin Exp Immunol*. (2006) 144:382–91. doi: 10.1111/j.1365-2249.2006.03081.x
49. Farias LP, Cardoso FC, Miyasato PA, Montoya BO, Tararam CA, Roffato HK, et al. *Schistosoma mansoni* stomatin like protein-2 is located in the tegument and induces partial protection against challenge infection. *PLoS Negl Trop Dis*. (2010) 4:e597. doi: 10.1371/journal.pntd.0000597
50. Al-Sherbiny M, Osman A, Barakat R, El Morshedy H, Bergquist R, Olds R. In vitro cellular and humoral responses to *Schistosoma mansoni* vaccine candidate antigens. *Acta Trop*. (2003) 88:117–30. doi: 10.1016/S0001-706X(03)00195-5
51. Schramm G, Haas H. Th2 immune response against *Schistosoma mansoni* infection. *Microbes Infect*. (2010) 12:881–8. doi: 10.1016/j.micinf.2010.06.001
52. Allen JE, Maizels RM. Diversity and dialogue in immunity to helminths. *Nat Rev Immunol*. (2011) 11:375–88. doi: 10.1038/nri2992
53. Fitzsimmons CM, Falcone FH, Dunne DW. Helminth allergens, parasite-specific IgE, and its protective role in human immunity. *Front Immunol*. (2014) 5:61. doi: 10.3389/fimmu.2014.00061
54. Jiz M, Friedman JF, Leenstra T, Jarilla B, Pablo A, Langdon G, et al. Immunoglobulin E (IgE) responses to paramyosin predict resistance to reinfection with *Schistosoma japonicum* and are attenuated by IgG4. *Infect Immun*. (2009) 77:2051–8. doi: 10.1128/IAI.00012-09
55. de Moira AP, Fulford AJC, Kabatereine NB, Ouma JH, Booth M, Dunne DW. Analysis of complex patterns of human exposure and immunity to *Schistosomiasis mansoni*: the influence of age, sex, ethnicity and IgE. *PLoS Negl Trop Dis*. (2010) 4:e820. doi: 10.1371/journal.pntd.0000820
56. de Oliveira Fraga LA, Lamb EW, Moreno EC, Chatterjee M, Dvoøák J, Delcroix M, et al. Rapid induction of IgE responses to a worm cysteine protease during murine pre-patent schistosome infection. *BMC Immunol*. (2010) 11:56. doi: 10.1186/1471-2172-11-56
57. Butterworth AE. Immunological aspects of human schistosomiasis. *Br Med Bull*. (1998) 54:357–68.
58. Alebie G. Immune modulation by *Schistosoma mansoni* infection and its implication in auto immune disorders and allergic diseases. *J Bacteriol Parasitol*. (2014) 5:3. doi: 10.4172/2155-9597.1000189
59. Henri S, Chevillard C, Mergani A, Paris P, Gaudart J, Camilla C, et al. Cytokine regulation of periportal fibrosis in humans infected with *Schistosoma mansoni*: IFN- is associated with protection against fibrosis and TNF- with aggravation of disease. *J Immunol*. (2002) 169:929–36. doi: 10.4049/jimmunol.169.2.929
60. Paul WE, Zhu J. How are T(H)2-type immune responses initiated and amplified? *Nat Rev Immunol*. (2010) 10:225–35. doi: 10.1038/nri2735
61. Gause WC, Wynn TA, Allen JE. Type 2 immunity and wound healing: evolutionary refinement of adaptive immunity by helminths. *Nat Rev Immunol*. (2013) 13:607–14. doi: 10.1038/nri3476
62. Brunet LR, Finkelman FD, Cheever AW, Kopf MA, Pearce EJ. IL-4 protects against TNF-alpha-mediated cachexia and death during acute schistosomiasis. *J Immunol*. (1997) 159:777–85.

Conflict of Interest: The authors declare that the research was conducted in the absence of any commercial or financial relationships that could be construed as a potential conflict of interest.

frontiers in Immunology

ORIGINAL RESEARCH
published: 30 September 2020
doi: 10.3389/fimmu.2020.575504

Combinational PRR Agonists in Liposomal Adjuvant Enhances Immunogenicity and Protective Efficacy in a Tuberculosis Subunit Vaccine

*Ling Hao, Yaqi Wu, Yandi Zhang, Zijie Zhou, Qing Lei, Nadeem Ullah, Jo-Lewis Banga Ndzouboukou, Xiaosong Lin and Xionglin Fan**

Department of Pathogen Biology, School of Basic Medicine, Tongji Medical College, Huazhong University of Science and Technology, Wuhan, China

OPEN ACCESS

Edited by:
Francesco Borriello, Harvard Medical School, United States

Reviewed by:
Bernd Lepenies, University of Veterinary Medicine Hannover, Germany
Diana Quan-Le, Centenary Institute, Australia

***Correspondence:**
Xionglin Fan
xlfan@hust.edu.cn

Specialty section:
This article was submitted to Vaccines and Molecular Therapeutics, a section of the journal Frontiers in Immunology

Received: *23 June 2020*
Accepted: *15 September 2020*
Published: *30 September 2020*

Citation:
Hao L, Wu Y, Zhang Y, Zhou Z, Lei Q, Ullah N, Banga Ndzouboukou J-L, Lin X and Fan X (2020) Combinational PRR Agonists in Liposomal Adjuvant Enhances Immunogenicity and Protective Efficacy in a Tuberculosis Subunit Vaccine. Front. Immunol. 11:575504. doi: 10.3389/fimmu.2020.575504

Bacillus Calmette-Guerin (BCG) is the only licensed vaccine to prevent children from tuberculosis (TB), whereas it cannot provide effective protection for adults. Our previous work showed a novel vaccine candidate, liposomal adjuvant DMT emulsified with a multistage antigen CMFO, could protect mice against primary progressive TB, latency, and reactivation. To develop a more effective vaccine against adult TB, we aimed to further understand the role of pattern recognition receptor (PRR) agonists monophosphoryl lipid A (MPLA) and trehalose-6,6'-dibehenate (TDB) of the liposomal adjuvant DMT in the CMFO subunit vaccine-induced protection. Using C57BL/6 mouse models, the current study prepared different dimethyldioctadecylammonium (DDA)–based liposomal adjuvants with MPLA, TDB, or both (DMT), and then compared the immunogenicity and the protective efficacy among different liposomal adjuvanted CMFO subunit vaccines. Our study demonstrated that CMFO/DMT provided stronger and longer-lasting protective efficacy than the CMFO emulsified with adjuvants DDA or DDA/TDB. In addition, DDA/MPLA adjuvanted CMFO conferred a comparable protection in the lung as CMFO/DMT did. Higher levels of IFN-γ, IL-2, TNF-α, and IL-17A secreted by splenocytes were related with a more powerful and durable protection induced by CMFO/DMT through a putative synergistic effect of both MPLA and TDB *via* binding to TLR4 and Mincle. IL-2^+ $CD4^+$ T cells, especially IL-2^+ $CD4^+$ T_{CM} cells, in the lung after infection were significantly associated with the vaccine-induced protection, whereas stronger IL-10 response and lower IL-2^+ $CD4^+$ T cells also contributed to the inferior protection of the DDA/TDB adjuvanted CMFO subunit vaccine. Given their crucial roles in vaccine-induced protection, combinational different PRR agonists in adjuvant formulation represent a promising strategy for the development of next-generation TB vaccine.

Keywords: tuberculosis, subunit vaccine, Bacillus Calmette-Guerin, adjuvant, primary infection, pattern-recognition receptor agonist, monophosphoryl lipid A, trehalose-6,6'-dibehenate

INTRODUCTION

Despite the only licensed vaccine to prevent children from tuberculosis (TB), Bacillus Calmette-Guerin (BCG) vaccine cannot generate lifelong immunity, which has a limited protection period of no more than 15 years (1). Currently, adult is a major target population in pulmonary TB epidemics, which accounts for about 90% of the global TB burden (2). Moreover, about one-fourth of the world population has been estimated to be a status of latent TB infection (LTBI) and 5%–10% of them would progress to active TB disease during lifetime (3). Such a situation is currently being exacerbated by the emergence of multidrug-resistant TB (MDR-TB) and extensively drug-resistant TB (XDR-TB), and co-infection with HIV, respectively. As a major threat on global public health, a more effective vaccine is urgently needed to control adult TB.

Attempts have been made to develop novel TB vaccines, such as subunit vaccines, recombinant BCG vaccines, recombinant viral vectors, and attenuated strains, etc. (4). Among them, TB subunit vaccine has attracted increasing attention owing to its definite components and good safety. To produce a robust immune response to reduce the burden of *Mycobacterium tuberculosis* strains under various metabolic states *in vivo*, we and others constructed multistage subunit vaccines, such as A1D4 (Rv1813-Rv2660c-Ag85B-Rv2623-HspX) (5), WH121 (Rv3407-PhoY2-Ag85A-Rv2626c-RpfB) (6), CMFO (Rv2875-Rv3044-Rv2073c-Rv0577) (7), ID93 (Rv3619-Rv1813-Rv3620-Rv2608) (8), and H56 (Ag85B-ESAT-6-Rv2660c) (9), through combining antigens expressed by logarithmically growing and dormant *M. tuberculosis* strains. However, only the antigen CMFO emulsified with the novel liposome adjuvant DMT was validated to be an effective booster of the BCG vaccine (7, 10). Recent clinical trials showed that the efficacy of subunit vaccine candidates M72/AS01$_E$ (11) and H4:IC31 (12) to protect against adult TB was only 49.7% and 30.5%, respectively. The imperfect efficacy of clinical trials spurs us on to greater efforts to understand the action mechanism of these candidates.

A significant proportion of adults have already received the BCG vaccination or have been latently infected with *M. tuberculosis* worldwide (3, 13). Under this context, cell-mediated immunity might be more required to play a critical role in the vaccine-induced protection. However, there is still a lack of effective adjuvants to induce appropriate cellular immune responses. The role of adjuvant as a decisive factor affecting the efficacy of TB subunit vaccine is often overlooked. The adjuvant DMT is formulated through the incorporation of dimethyldioctadecylammonium (DDA) liposome by toll-like receptor 4 (TLR4) and Mincle agonists, monophosphoryl lipid A (MPLA) and trehalose-6,6'-dibehenate (TDB) (14–16). The liposomal adjuvant AS01$_E$ is composed of MPLA together with QS-21 (a triterpene saponin purified from *Quillaja saponaria*) (11). Another liposome-based adjuvant CAF01 also makes advantage of similar components such as DDA and TDB (17). The common component MPLA, a detoxified version of lipopolysaccharides, can be recognized by pattern recognition receptor (PRR) TLR4 expressing on the surface of antigen-presenting cells (APCs), which activates NF-κB through MyD88 and TRIF-dependent pathways and thus induces a Th1 biased response (14, 18–20). The other ingredient TDB, a synthetic analogue of mycobacterial cord factor, binds to the C-type lectin receptors Mincle and Mcl to activate macrophages (21) and could induce MyD88 and Card9-dependent Th1/Th17 responses *in vivo* against *M. tuberculosis* challenge (22, 23). In particular, these adjuvants and their ingredients have been demonstrated to be safe and tolerable in clinical trials (11, 17, 24). We assumed that different PRR agonists might modulate the adjuvant effects of the liposomes and thus affect the efficacy of TB subunit vaccines. To develop a more effective vaccine against TB, we aimed to further understand the role of both PRR agonists of the adjuvant DMT in vaccine-induced protection. In this study, we prepared different DDA-based liposomal adjuvants with MPLA, TDB, or both in this study, and then compared the immunogenicity and the protective efficacy among different liposomal adjuvanted CMFO subunit vaccines in C57BL/6 mouse models.

Abbreviations: TB, tuberculosis; BCG, Bacillus Calmette-Guerin; DDA, dimethyldioctadecylammonium; MPLA, monophosphoryl lipid A; TDB, trehalose-6,6'-dibehenate; DM, DDA/MPLA; DT, DDA/TDB; DMT, DDA/MPLA/TDB; LTBI, latent TB infection; MDR-TB, multidrug resistant TB; XDR-TB, extensively drug resistant TB; A1D4, Rv1813-Rv2660c-Ag85B-Rv2623-HspX; WH121, Rv3407-PhoY2-Ag85A-Rv2626c-RpfB; CMFO, Rv2875-Rv3044-Rv2073c-Rv0577; ID93, Rv3619-Rv1813-Rv3620-Rv2608; H56, Ag85B-ESAT-6-Rv2660c; PRR, pattern-recognition receptor; TLR4, toll-like receptor 4; antigen-presenting cells, APCs; PDI, polydispersity index; s.c., subcutaneously; i.n., intranasally; CBA, cytometric bead array; FACS, fluorescence activated cell sorting; T_{CM}, central memory T cell; T_{EM}, effector memory T cell.

MATERIALS AND METHODS

Preparation of Liposomal Adjuvants and Vaccines

Four liposomal formulations (**Table S1**), namely, DDA, DDA/MPLA (DM), DDA/TDB (DT), and DMT, were prepared using the lipid film hydration method as previously described (25). Briefly, weighed amounts of DDA (Avanti Polar Lipids Inc., AL, USA), MPLA (Avanti), or TDB (Avanti) were first dissolved in chloroform/methanol (9:1 in volume). The solvent was then blow-dried with N_2 to form a thin lipid film by using a roto-evaporator. Samples were further dried under hypobaric condition overnight. Unilamellar vesicles were formed by hydrating the lipid film in sterile Tris-buffer (10 mM, pH 7.4) at 60°C for 60 min, followed by vortex every 10 min. Recombinant CMFO protein was expressed by a genetically engineered expression system in *E. coli* and purified using nitrilotriacetic acidmetal ion affinity chromatography (GE Healthcare, NJ, USA) (7). The endotoxin in each purified products was removed (<0.1 EU/ml) by ToxinEraser™ Endotoxin Removal Kit (Genscript, Nanjing, China). Different vaccines were prepared by mixing 100 μl of CMFO solution (0.2 mg/ml) with 100 μl liposomes (**Table S1**). Physicochemical property analysis of both liposomes and vaccine formulations were performed as our previously described (25). The results of the particle size, polydispersity index (PDI), and zeta potential from three batches of samples were presented as mean ± SD.

Mice and Immunization

Specific-pathogen-free female C57BL/6 mice, 6–8 weeks old, were obtained from the Charles River Company (Beijing, China) and maintained in animal feeding cabinet (VentiRack, CA, USA) in an ABSL-3 biosafety laboratory. Mice were randomly divided into different groups and immunized subcutaneously (s.c.) with different vaccine formulations (200 μl/dose) twice in a 3-week interval. PBS, different liposomal adjuvants DDA, DM, DT, and DMT alone were used as controls. Approximately, 1×10^6 CFU of BCG China strain was vaccinated once as a positive control. All experiments were repeated twice.

Challenge With Virulent *M. tuberculosis* H37Rv Strain

To evaluate the short-term and long-term protective efficacy, mice vaccinated with different formulations were challenged intranasally (i.n.) with ~100 CFU of virulent *M. tuberculosis* H37Rv strain at the 10^{th} and 20^{th} weeks. Four weeks post-challenge, the protective efficacy among different groups was assessed by comparing bacterial loads in both spleen and lung (n = 6), and by scoring the lung histopathological changes as previously described (n = 3) (5). Briefly, bacterial load per organ was enumerated by plating 10-fold continuous dilutions of whole organ homogenates on 7H11 agar plates (Cat#212203, BD Biosciences, NJ, USA). In addition, 2 μg/ml of 2-thiophenecarboxylic acid hydrazide (Beijing Luqiao Corp, China) was selectively added to inhibit the residual BCG growth. The results were shown as Log_{10} CFU/organ of individual animals (n = 6). The score was obtained by measuring the percentage of the consolidation area of the whole field of vision (magnification ×40) and expressed as mean ± SD of five fields of vision from each group (n = 3).

Antibody Titer Determination of Antigen-Specific IgG and Its Subclasses

Nine weeks after immunization, CMFO-specific endpoint titers for IgG, IgG1, and IgG2a (Cat#151276, 133045, and 157720; Abcam, Cambridge, MA, USA) were detected in sera from each mouse by ELISA as previously described (7). The results were shown as Log_{10} (endpoint titer) of individual animals (n = 6).

Determination of Cytokines Secreted by Splenocytes

Nine weeks after immunization or 4 weeks after infection, splenocytes from each mouse were aseptically seeded in triplicate in 24-well plates at the density of 5×10^6 cells/well. The cells were re-stimulated with 10 μg CMFO for 72 h. Culture supernatant was then collected and the cytokines secreted by splenocytes were detected using Mouse Th1 (IFN-γ, IL-2, and TNF-α), Th2 (IL-4), Th17 (IL-17A), regulatory (IL-10 and IL-6) Cytokine Kit (BD Biosciences) based on cytometric bead array (CBA) technology (25).

Detection of CMFO-Specific T Cells

Nine weeks after immunization or four weeks after infection, intracellular flow cytometry was performed as previously described (7). Briefly, 5×10^6 splenocytes or lung cells from each mouse were seeded in triplicate in 24-well plates and incubated with CMFO (10 μg) and anti-CD28/CD49d (1 μg, eBioscience CA, USA) for 4 h. Then, Brefeldin A (3 μg) and monensin solution (2 μM, eBioscience) were added for further incubation for 12 h. RPMI 1640 medium (Hyclone, USA) was used as a negative control. Cell stimulation cocktail (1 μg, eBioscience) was used to monitor cell responses. Then, cells were collected and stained for 30 min at room temperature in the dark with surface markers, including anti-CD4-APC-Cy7 (Cat#552051, BD Pharmingen™), anti-CD8α-BV510 (Cat#563068, BD Horizon™), anti-CD44-FITC (Cat#561859, BD Pharmingen™), and anti-CD62L-PerCP-Cy5.5 (Cat#560513, BD Pharmingen™). After permeabilization using a Fixation/Permeabilization Solution Kit (Cat#555028, BD Cytofix/Cytoperm™ Plus), cells were stained with intracellular markers, anti-IFN-γ-PE (Cat#554412, BD Pharmingen™) and anti-IL-2-APC (Cat#554429, BD Pharmingen™), for 30 min at room temperature in the dark. Stained cells (5×10^5) were collected and examined by an LSRII multicolor flow cytometry (BD Biosciences). FlowJo software (Tree Star Inc., OH, USA) was used to analyze the proportion of CMFO-specific IFN-γ^+ (or IL-2^+) T cells, central memory T cells (T_{CM}, $CD62L^{hi}CD44^{hi}$), and effector memory T cells (T_{EM}, $CD62L^{lo}CD44^{hi}$) per organ. The absolute number of each T cell subpopulation was obtained by multiplying its proportion by the total number of the organ cells.

Statistical Analyses

Statistical analyses were performed using GraphPad Prism 5.0 (San Diego, CA, USA). Two-tailed student's *t*-test was used for two-group comparison. Multigroup analyses were carried out by one-way ANOVA test, and Tukey's multiple comparison test was used for further pair-wise comparison. A significant difference was considered when a p value was less than 0.05.

RESULTS

Physicochemical Characteristics of Both Liposomes and CMFO-Liposome Complexes

Different liposomes had a similar morphology and formed nearly spherical vesicles as our previous demonstrated by transmission electron microscopy (data not shown) (25). Compared with the DDA liposome, an addition of TDB and/or MPLA into the DDA liposome did not result in the change of particle size and PDI (**Figure 1**). In line with previous studies (25, 26), the incorporation of MPLA into DDA vesicles resulted in a significant decrease of the surface charge, as demonstrated by the lower Zeta potential values of DM and DMT. The antigen CMFO, emulsified with different liposomes, resulted in a general trend of increased particle size and PDI while reduced zeta potential across all four formulations. In particular, the particle sizes of CMFO/DM, CMFO/DT, and CMFO/DMT were

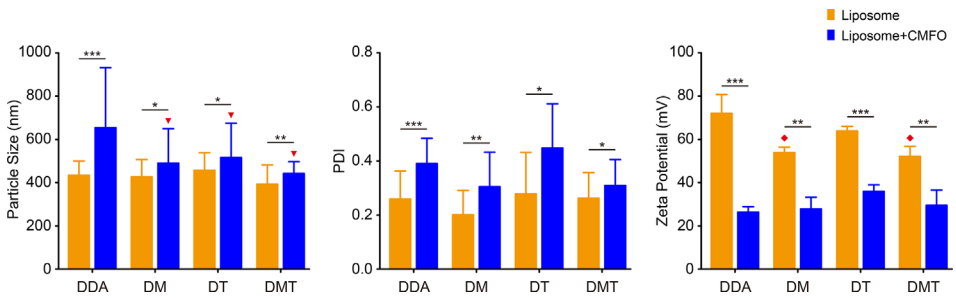

FIGURE 1 | The particle size, PDI, and zeta potential of both liposomes and CMFO-liposome complexes. Results were shown as mean ± SD of three independent liposome batches. $^{*}p < 0.05$, $^{**}p < 0.01$, $^{***}p < 0.001$, $^{\blacktriangledown}p < 0.01$ vs. CMFO/DDA, and $^{\blacklozenge}p < 0.05$ vs. DDA.

significantly smaller than that of CMFO/DDA, respectively. However, all CMFO-liposome complexes remained cationic.

Short- and Long-Term Protection Among Liposomal Adjuvanted Subunit Vaccines

To confirm the effect of different adjuvants on the short-term protective efficacy, C57BL/6 mice were vaccinated with different vaccines as described in **Figure 2A** and then challenged with *M. tuberculosis* at the 10th week after immunization. All of liposomal adjuvanted CMFO subunit vaccines resulted in a lower organ bacterial load than their respective adjuvant alone treated controls (**Figures 2B, C**). Notably, CMFO/DMT showed the strongest protection among liposomal adjuvanted CMFO subunit vaccines, as demonstrated by bacterial load in both lung and spleen, lung histopathological changes and scores (**Figures 2B–E**). Consistent with our previous findings (7), there was no statistical difference of bacterial loads in the lung or spleen between CMFO/DMT and BCG groups. Interestingly, when compared with the CMFO/DDA group, CMFO/DMT exhibited a stronger ability to inhibit the growth of *M. tuberculosis* in both lung and spleen, respectively. However, mice vaccinated with CMFO/DMT only had a lower bacterial load in their spleen than CMFO/DM or CMFO/DT did (**Figure 2C**).

At the 20th week, vaccinated mice were further challenged with *M. tuberculosis* to examine long-term protective efficacy (**Figure 3A**). Of the all groups, PBS control group still had the highest organ bacterial loads and lung pathological scores. Surprisingly, mice vaccinated with CMFO/DMT had more significantly decreased bacterial load than did with DDA or DT adjuvanted CMFO vaccines (**Figures 3B, C**). In comparison with the CMFO/DM vaccine, CMFO/DMT had milder lung histopathological change and lower score (**Figures 3D, E**). However, both groups had no statistical difference in terms of bacterial load in lung and spleen (**Figures 3B, C**).

Similar Patterns of Antibody Response Elicited by Liposomal Adjuvanted Subunit Vaccines

To analyze the effect of different adjuvants on antibody production, CMFO-specific antibodies, including IgG, IgG2a, and IgG1, in the sera of different vaccinated mice were tested by ELISA. As expected, PBS and adjuvant control groups did not produce any antigen-specific antibodies (data not shown). When compared with the CMFO/DDA group, CMFO/DMT induced much higher levels of CMFO-specific IgG, IgG2a, and IgG1, while CMFO/DM elicited stronger anti-CMFO IgG and IgG2a responses (**Figures 4A–C**). Interestingly, four liposome–based CMFO subunit vaccinated groups induced similar antibody responses, as evidenced by the ratio of IgG2a/IgG1 response to CMFO (**Figure 4D**).

Differential Cytokine Profiles Among Liposomal Adjuvanted Subunit Vaccines

CMFO-specific cytokine profiles in the supernatant of splenocytes from different vaccination groups before and after challenge were detected by using a CBA kit. Prior to the exposure, splenocytes from BCG vaccinated mice secreted the higher levels of CMFO-specific IFN-γ, IL-2, IL-6, IL-17A, and TNF-α than those from the PBS control group (**Figure 5**). When compared with DDA alone, DMT alone significantly increased the levels of CMFO-specific IFN-γ, IL-6, IL-17A, or TNF-α, while DM alone enhanced the secretion of IFN-γ, IL-6, and TNF-α. Different liposomal adjuvanted CMFO vaccinated mice elicited higher levels of IFN-γ, IL-2, IL-6, IL-17A, and TNF-α than their respective adjuvant alone controls. In particular, CMFO/DMT induced the highest levels of IFN-γ, IL-2, IL-17A, and TNF-α of all groups. In addition, mice vaccinated with either CMFO/DM or CMFO/DT also produced more IFN-γ, IL-2, IL-6, TNF-α, and IL-17A than CMFO/DDA did. Only IL-2 response to CMFO in the CMFO/DM group was stronger than that in the CMFO/DT group (**Figure 5B**), while splenocytes from the CMFO/DT vaccinated mice secreted more CMFO-specific IL-6, IL-10, and IL17A than those of the CMFO/DM vaccinated mice (**Figures 5C–E**). Interestingly, CMFO/DT induced the highest level of IL-10 among all liposomal adjvanted CMFO vaccinated mice (**Figure 5D**).

After exposure, the levels of CMFO-specific IL-10 and IL-17A were decreased significantly, whereas IL-2 secretion from splenocytes of different groups had a marked increase (**Figure 6**). Mainly, the results of different groups post-exposure were

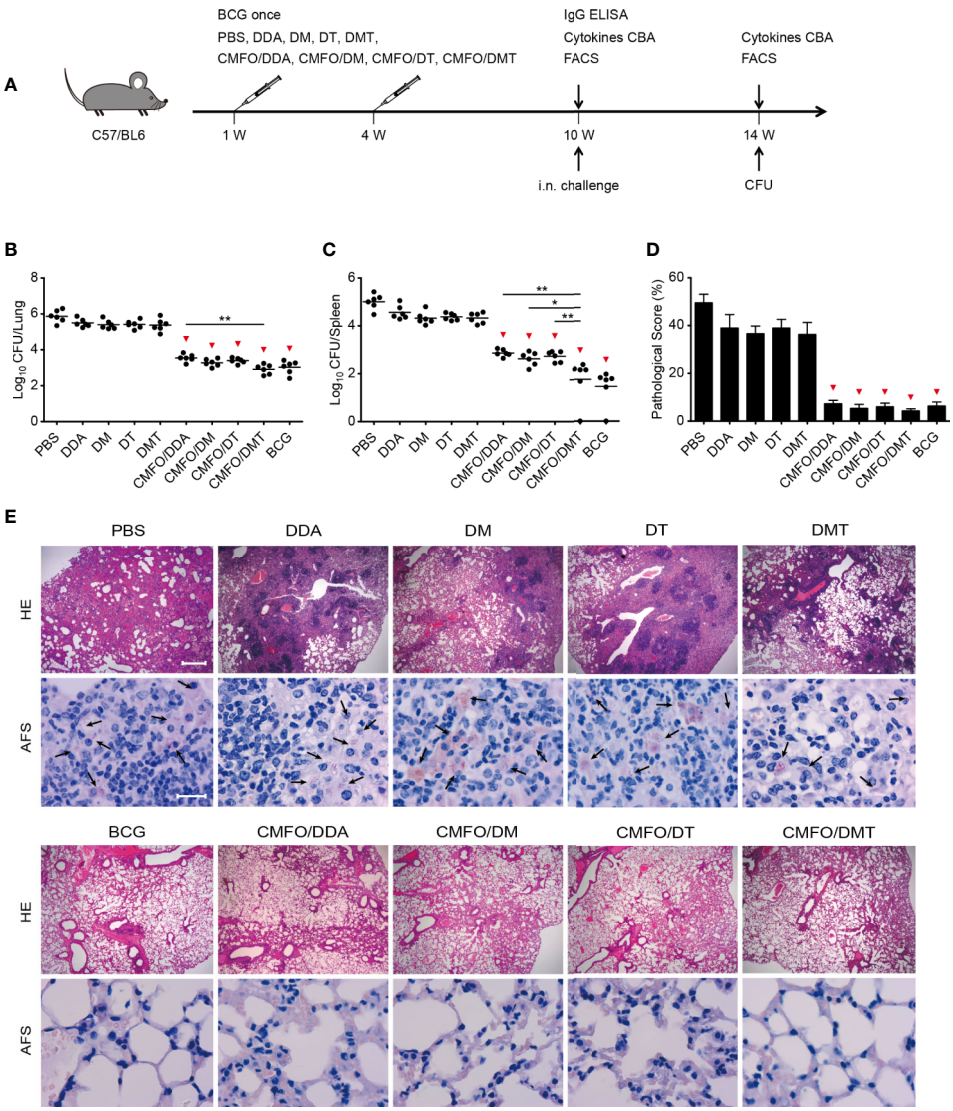

FIGURE 2 | Comparison of the short-term protective efficacy against primary TB infection among different regimens. **(A)** Vaccination and challenge schedule. At the 14th week, bacterial load in the lung **(B)** and the spleen **(C)** of different groups was enumerated and shown as Log_{10} CFU/organ of individual animals (n = 6). The line in each group represented mean value. **(D)** The lung pathological scores of different groups. $^{*}p < 0.05$, $^{**}p < 0.01$, and $^{▼}p < 0.05$ vs. respective controls. **(E)** The representative lung pathological changes were shown for HE and AF staining (n = 3). HE, hematoxylin-eosin; AFS, acid-fast staining. Scar bar: 400 μm for HE staining, 20 μm for AF staining. Arrows indicated AF-positive bacteria. All experiments were repeated twice and similar results were obtained.

consistent with those pre-exposure, in addition to the splenocytes from the CMFO/DT vaccinated mice secreted more CMFO-specific IFN-γ, IL-6, IL-10, and IL-17A than those of the CMFO/DM vaccinated mice. Whatever before and after exposure, the level of IL-4 in all groups was very low, less than 1 pg/ml (data not shown).

Differential T Cell Responses Induced in Spleens Before and After Infection

To investigate immunological effects related with the protection against primary infection, the numbers of CMFO-specific IFN-γ^+ (or IL-2^+) T cells, IL-2^+ T_{CM} ($CD62L^{hi}CD44^{hi}$) cells, and IFN-γ^+ T_{EM} ($CD62L^{lo}CD44^{hi}$) cells in splenocytes from different vaccinated mice were determined by fluorescence activated cell sorting (FACS) before (**Figures 7A, B**) and after infection (**Figure 8**). CMFO-specific IFN-γ^+ $CD4^+$ T cells and IFN-γ^+ $CD4^+$ T_{EM} cells were dominated in the spleen of all vaccinated mice before the exposure (**Figure 7B**). As expected, the BCG group had higher numbers of CMFO-specific T cells than that from the PBS control. Liposomal adjuvants alone did not induce any of these T cells at the 10th week. Interestingly, CMFO/DMT induced the highest levels of IFN-γ^+ or IL-2^+

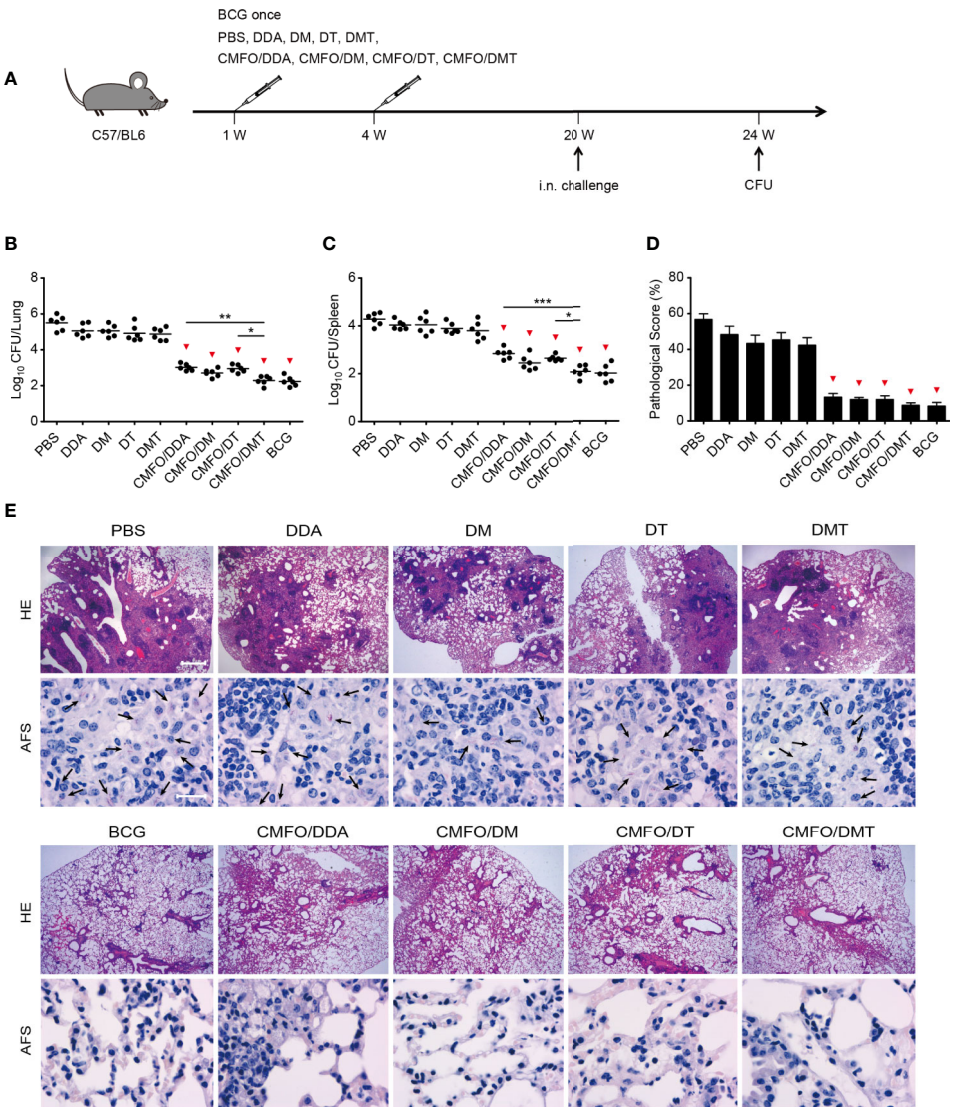

FIGURE 3 | Comparison of the long-term protective efficacy against primary TB infection among different regimens. **(A)** Vaccination and challenge schedule. At the 24th week, bacterial load in the lung **(B)** and the spleen **(C)** of different groups was enumerated and shown as Log_{10} CFU/organ of individual animals (n = 6). The line in each group represented mean value. **(D)** The lung pathological scores of different groups. $^{*}p < 0.05$, $^{**}p < 0.01$, $^{***}p < 0.001$, and $^{\blacktriangledown}p < 0.05$ vs. respective controls. **(E)** The representative lung pathological changes were shown for HE and AF staining (n = 3). HE, hematoxylin-eosin; AFS, acid-fast staining. Scar bar: 400 μm for HE staining, 20 μm for AF staining. Arrows indicated AF-positive bacteria. All experiments were repeated twice and similar results were obtained.

$CD4^+$ T cells, IFN-γ^+ $CD4^+$ T_{EM} cells, and IL-2^+ $CD4^+$ T_{CM} cells in the spleen of all groups. When compared with the CMFO/DDA group, CMFO/DM induced more IL-2^+ $CD4^+$ T cells and IL-2^+ T_{CM} cells, while CMFO/DT induced more IFN-γ^+ or IL-2^+ $CD4^+$ T cells and IFN-γ^+ $CD4^+$ T_{EM} cells. More importantly, both DM and DMT adjuvanted CMFO vaccines elicited more IL-2^+ $CD8^+$ T_{CM} cells than CMFO/DDA or CMFO/DT did.

After infection, IL-2^+ $CD4^+$ T cells and T_{CM} cells were dominant in the spleen of all groups (**Figure 8**). Among all groups, CMFO/DMT induced the highest levels of CMFO-specific IFN-γ^+ T cells, IFN-γ^+ $CD4^+$ T_{EM} cells, and IL-2^+ $CD4^+$ T cells or T_{CM} cells. When compared with the CMFO/DDA group, CMFO/DM induced more IFN-γ^+ $CD4^+$ T_{EM} cells, IL-2^+ $CD4^+$ T cells, and IL-2^+ $CD4^+$ T_{CM} cells, while CMFO/DT induced more IFN-γ^+ T cells, IFN-γ^+ $CD4^+$ T_{EM} cells, IL-2^+ $CD8^+$ T cells, and IL-2^+ T_{CM} cells.

Differential T Cell Responses Elicited in Lungs After Infection

T cell responses to the antigen CMFO were also detected in the lung by FACS (**Figures 9**, **10**). At the 10th week after

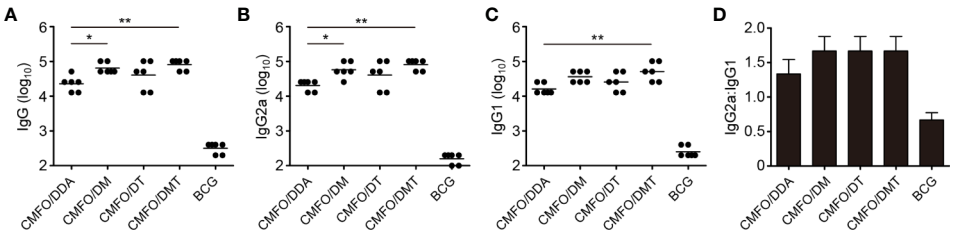

FIGURE 4 | Sera antigen-specific antibody responses (n = 6). Nine weeks after immunization, CMFO-specific endpoint titers for IgG **(A)**, IgG2a **(B),** and IgG1 **(C)** in sera of mice were detected by ELISA. All results were shown as Log_{10} endpoint titer of individual animals and the line in each group represented mean value. $^{*}p < 0.05$ and $^{**}p < 0.01$. **(D)** The ratio of IgG2a/IgG1 in different vaccinated mice. All experiments were repeated twice and similar results were obtained.

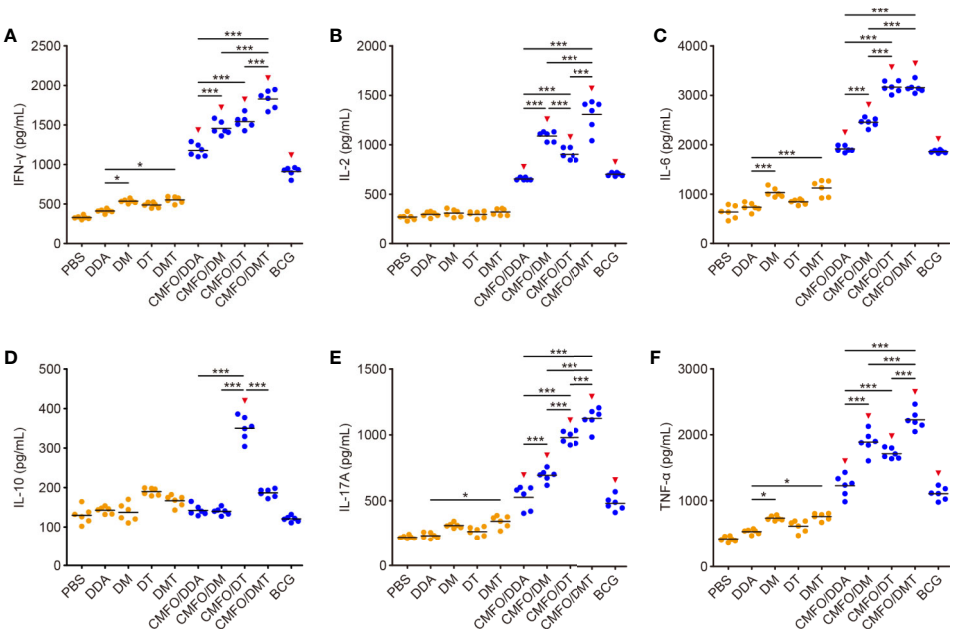

FIGURE 5 | CMFO-specific cytokine responses before exposure (n = 6). Nine weeks after immunization, CMFO-specific Th1/Th2/Th17 cytokines including IFN-γ **(A)**, IL-2 **(B)**, IL-6 **(C)**, IL-10 **(D)**, IL-17 **(E)**, and TNF-α **(F)** in the supernatant of splenocytes from different vaccinated mice were detected by a CBA kit. All experiments were repeated twice and similar results were obtained. The line in each group represented mean value. $^{*}p < 0.05$, $^{***}p < 0.001$, and $^{\blacktriangledown}p < 0.05$ vs. respective controls.

immunization, IL-2^+ $CD4^+$ T cells were dominated in all vaccinated mice (**Figure 9**). Different adjuvanted CMFO vaccines elicited higher levels of IL-2^+ $CD4^+$ T cells than their respective adjuvant controls. However, the levels of CMFO-specific IFN-γ^+ T cells or T_{EM} cells, IL-2^+ $CD8^+$ T cells and IL-2^+ T_{CM} cells in the lung of all groups were very low, only less than 10^4.

After infection, IL-2^+ $CD4^+$ T cells or T_{CM} cells were still dominated in the lung of all vaccinated groups (**Figure 10**). Notably, CMFO/DMT elicited the highest levels of IFN-γ^+ or IL-2^+ $CD4^+$ T cells, IFN-γ^+ T_{EM} cells, and IL-2^+ $CD4^+$ T_{CM} cells in the lung of all groups. When compared with the CMFO/DDA group, CMFO/DM induced more IFN-γ^+ or IL-2^+ T cells, IFN-γ^+ $CD4^+$ T_{EM} cells, and IL-2^+ T_{CM} cells, while CMFO/DT induced more IFN-γ^+ or IL-2^+ $CD8^+$ T cells, IFN-γ^+ $CD4^+$ T_{EM} cells, and IL-2^+ T_{CM} cells. In addition, the similar levels of IFN-γ^+ or IL-2^+ $CD8^+$ T cells were observed in DM, DT, and DMT adjuvanted CMFO vaccinated groups.

DISCUSSION

Currently, only a few subunit vaccine candidates with or without prime-boost strategies could exert superior effects than the BCG vaccine does against adult TB in preclinical or clinical trials (27, 28). To develop more effective vaccines, it is

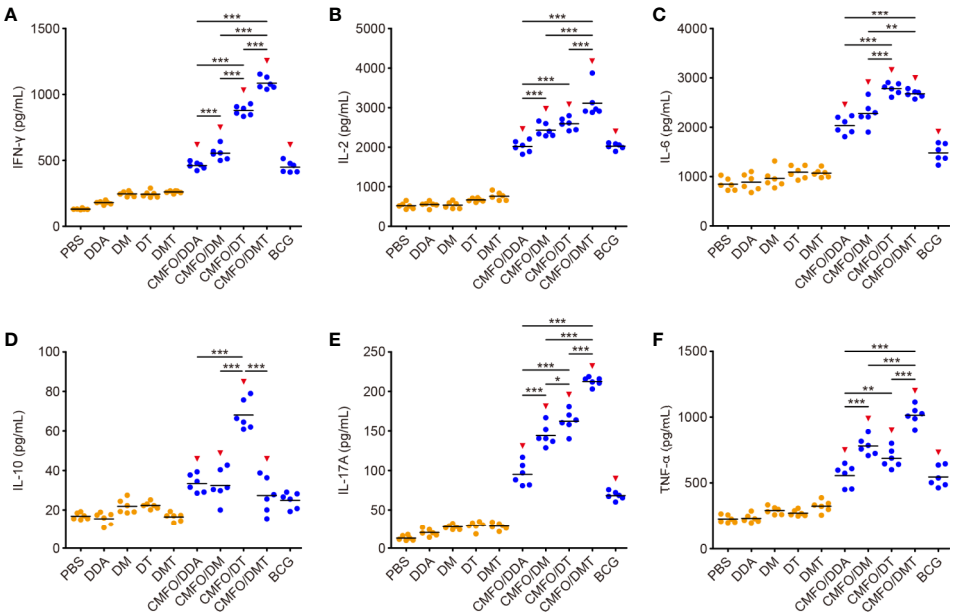

FIGURE 6 | CMFO-specific cytokine responses after exposure (n = 6). Nine weeks after immunization, C57BL/6 mice were challenged with *M. tuberculosis*. Four weeks after infection, CMFO-specific Th1/Th2/Th17 cytokines including IFN-γ **(A)**, IL-2 **(B)**, IL-6 **(C)**, IL-10 **(D)**, IL-17 **(E)**, and TNF-α **(F)** in the supernatant of splenocytes from different vaccinated mice were detected by a CBA kit. All experiments were repeated twice and similar results were obtained. The line in each group represented mean value. $^{*}p < 0.05$, $^{**}p < 0.01$, $^{***}p < 0.001$, and $^{▾}p < 0.05$ vs. respective controls.

significant to understand the role of adjuvants on the efficacy of subunit vaccines. In this study, we investigated the effects of each components of the adjuvant DMT on the protection against primary TB infection in CMFO/DMT subunit vaccinated mice. Our study demonstrated a comparable efficiency between CMFO/DMT and BCG vaccines in terms of their short- and long-term protection. CMFO/DMT achieved a stronger and longer-lasting protection than that from CMFO emulsified with adjuvants DDA or DDA/TDB. Interestingly, DDA/MPLA adjuvanted CMFO could confer to a similar protection in the lung as did with CMFO/DMT. Adjuvants DDA/MPLA, DDA/TDB, and DMT induce similar antibody responses and all are strong inducers of Th1/Th17 cytokine responses. Compared with DMT and DDA/MPLA, the induction of strong IL-10 response and low IL-2^{+} $CD4^{+}$ T cells was relevant to the reduced protection of DDA/TDB adjuvanted CMFO subunit vaccine. Therefore, our findings confirmed that different PRR agonists could modulate the immune responses, especially cellular immune responses in subunit vaccinated mice. The DMT might be a very promising adjuvant for TB subunit vaccines.

Differential protective efficacy among liposomal adjuvanted CMFO subunit vaccines provides us opportunities to elucidate immunological mechanisms of different subcomponents in liposomal adjuvants. In this study, the introduction of the negatively charged MPLA into the DDA liposome significantly decreased the surface charge of the liposome, which might improve the stability of DDA-based liposomes as demonstrated in previous studies (25, 26). Cationic adjuvant systems, such as IC31 and CAF01, have been proved to be crucial for the formation of an antigen depot at the site-of-injection, the prolonged uptake of antigens by APCs, and the ability of a vaccine to induce adaptive immune responses (29–31). Our previous study also confirmed that the cationic adjuvant DMT had a slower and longer-lasting release effect on antigens and agonists than the DDA liposome (25). The recombinant antigen CMFO was negative charge, which could be readily adsorbed by the positively charged DMT liposome. The controlled release effect of the DMT adjuvant on antigens and agonists might result in the long-term deposition of the vaccine antigen at the injection site for APCs uptaking, increase the time of vaccine exposure to the immune cells, and thus facilitate the sustained Th1 responses. In the current study, both DM and DMT adjuvanted CMFO subunit vaccines potentiated the production of serum IgG and IgG2b antibodies than the antigen complexed with DDA alone, indicating that antibody-mediated immunity might also play roles in the protection against TB, as previously reported (32–35). The multifaceted functions of the antibody have been proposed as mediating opsonic killing, removing immunomodulatory antigens of *M. tuberculosis* and modulating inflammation (36). Low-antibody titers and defective humoral immunity may increase the risk of *M. tuberculosis* infection and dissemination (37–39). More importantly, different liposomal adjuvanted CMFO vaccines also elicited differential cytokine profiles and T cell responses in the spleen and lung before and

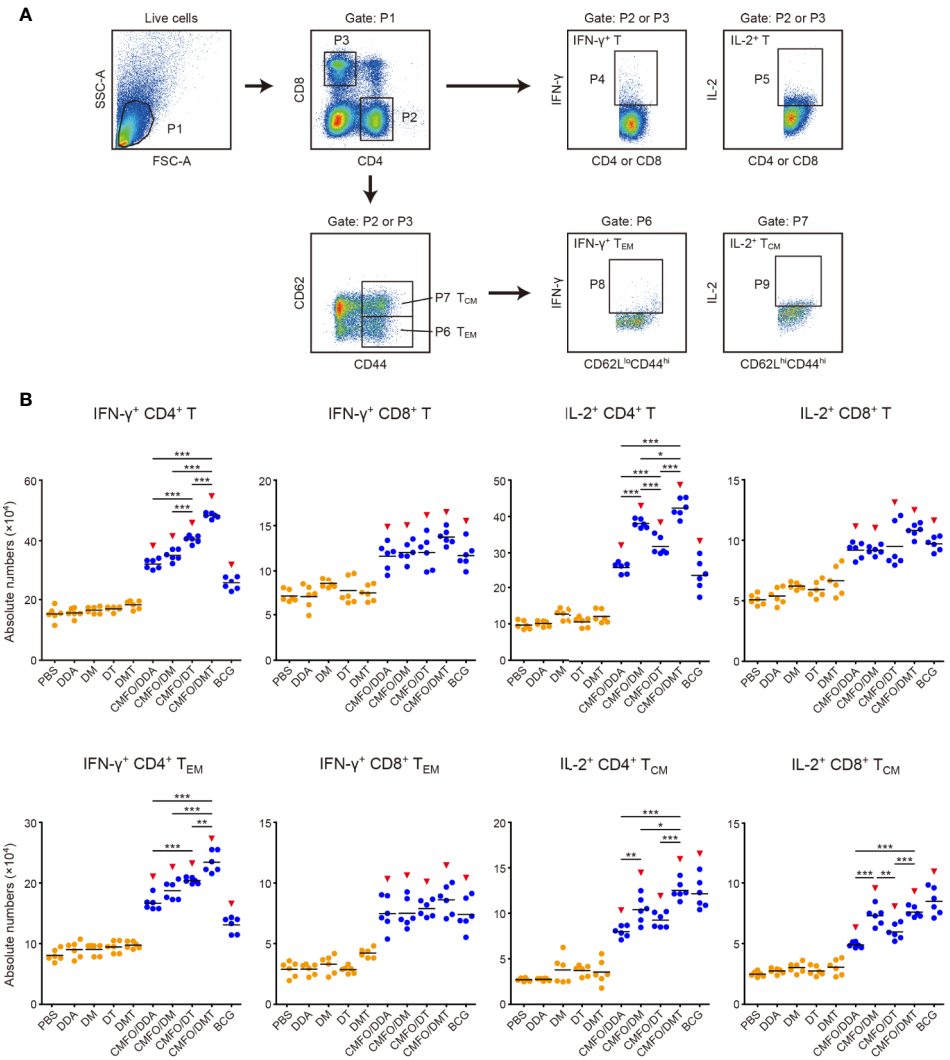

FIGURE 7 | Comparison of the levels of CMFO-specific T cells in the spleen of different immunized mice before exposure (n = 6). Nine weeks after immunization, splenocytes of different groups were collected and stained with different markers for FACS analysis. **(A)** Gating strategy to identify CMFO-specific T cell sub-populations. **(B)** The absolute numbers of CMFO-specific IFN-γ+ $CD4^+$ (or $CD8^+$) T cells, IL-2^+ $CD4^+$ (or $CD8^+$) T cells, IFN-γ^+ $CD4^+$ (or $CD8^+$) T_{EM} cells, and IL-2^+ $CD4^+$ (or $CD8^+$) T_{CM} cells per spleen of individual animals were shown. All experiments were repeated twice and similar results were obtained. The line in each group represented mean value. $^*p < 0.05$, $^{**}p < 0.01$, $^{***}p < 0.001$, and $^▾p < 0.05$ vs. respective controls. Representative FACS plots were shown in **Figure S1**.

after exposure. In line with previous reports (9, 22, 23, 40), the adjuvant DDA/MPLA is a strong inducer of antigen-specific IFN-γ and IL-2 responses, while the adjuvant DDA/TDB stimulated high levels of antigen-specific IFN-γ and IL-17A. However, DDA/TDB also induced the highest level of IL-10 responses to the antigen CMFO before and after infection of all groups. IL-10 suppresses the functions of macrophages and dendritic cells (41, 42), and thus might play a suppressive role in the efficacy of DDA/TDB emulsified CMFO subunit vaccine. Among all groups, DMT adjuvanted CMFO elicited the highest levels of IFN-γ, IL-2, TNF-α, and IL-17A. IFN-γ can trigger the activation of alveolar macrophage, thus killing engulfed *M. tuberculosis* (43–45). TNF-α triggers cytotoxic T cells to directly kill intracellular pathogen, and recruits monocytes and circulate antigen-specific T lymphocytes to the infection site (46, 47). IL-2 is secreted by activated T cells, which can promote the differentiation and proliferation of lymphoid cells, further enhancing the cell-mediated anti-infective immune responses (48). IL-17A plays a critical role in the formation of mature granuloma for pathogen containment at early disease stage (49–51). In addition, IL-6 could induce early IFN-γ expression to inhibit *M. tuberculosis* growth, however it is not necessary for the development of protective immunity (52). Therefore, the CMFO/DMT induced protection correlates with the levels of IFN-γ, IL-2, TNF-α, and IL-17A secreted by splenocytes, which might be a synergistic effect of

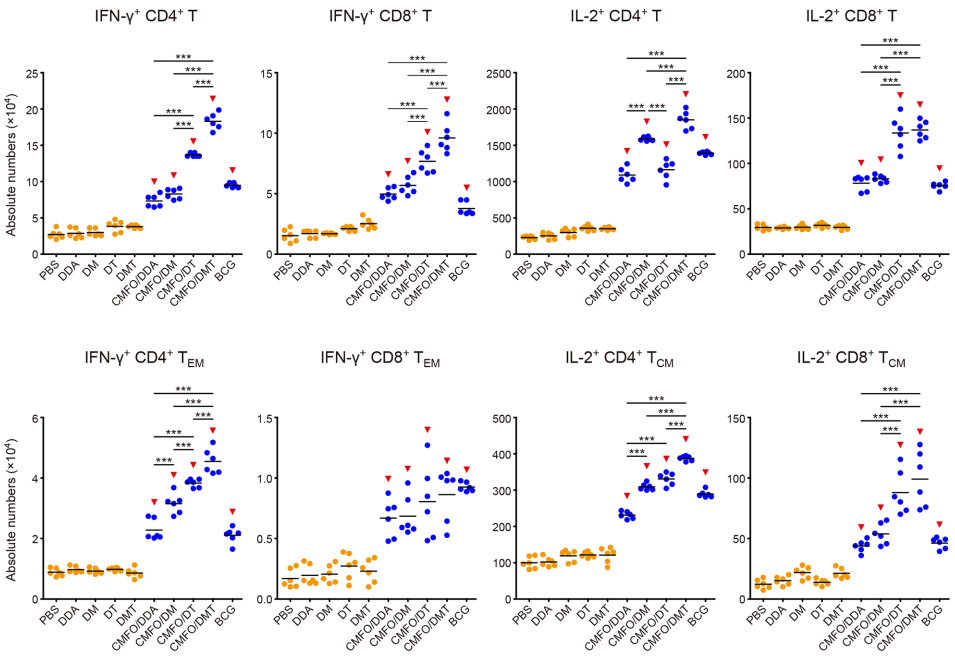

FIGURE 8 | Comparison of the levels of CMFO-specific T cells in the spleen of different immunized mice after exposure (n = 6). Nine weeks after immunization, C57BL/6 mice were challenged with *M. tuberculosis*. Four weeks after infection, the absolute numbers of CMFO-specific IFN-γ+ CD4+ (or CD8+) T cells, IFN-γ+ CD4+ (or CD8+) T_{EM} cells, IL-2+ CD4+ (or CD8+) T cells, and IL-2+ CD4+ (or CD8+) T_{CM} cells per spleen were detected. The experiments were repeated twice and similar results were obtained. The line in each group represented mean value. ***$p < 0.001$ and ▾$p < 0.05$ vs. respective controls. Representative FACS plots were shown in **Figure S2**.

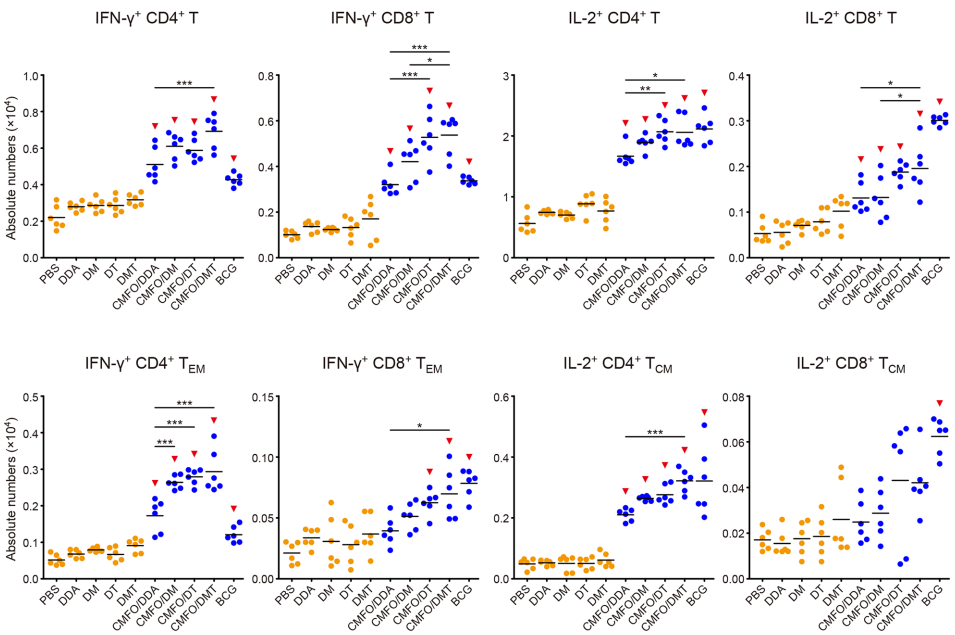

FIGURE 9 | Comparison of the levels of CMFO-specific T cells in the lung of different immunized mice before exposure (n = 6). Nine weeks after immunization, the absolute numbers of CMFO-specific IFN-γ+ CD4+ (or CD8+) T cells, IFN-γ+ CD4+ (or CD8+) T_{EM} cells, IL-2+ CD4+ (or CD8+) T cells, and IL-2+ CD4+ (or CD8+) T_{CM} cells per lung were detected. The experiments were repeated twice and similar results were obtained. The line in each group represented mean value. *$p < 0.05$, **$p < 0.01$, ***$p < 0.001$, and ▾$p < 0.05$ vs. respective controls. Representative FACS plots were shown in **Figure S3**.

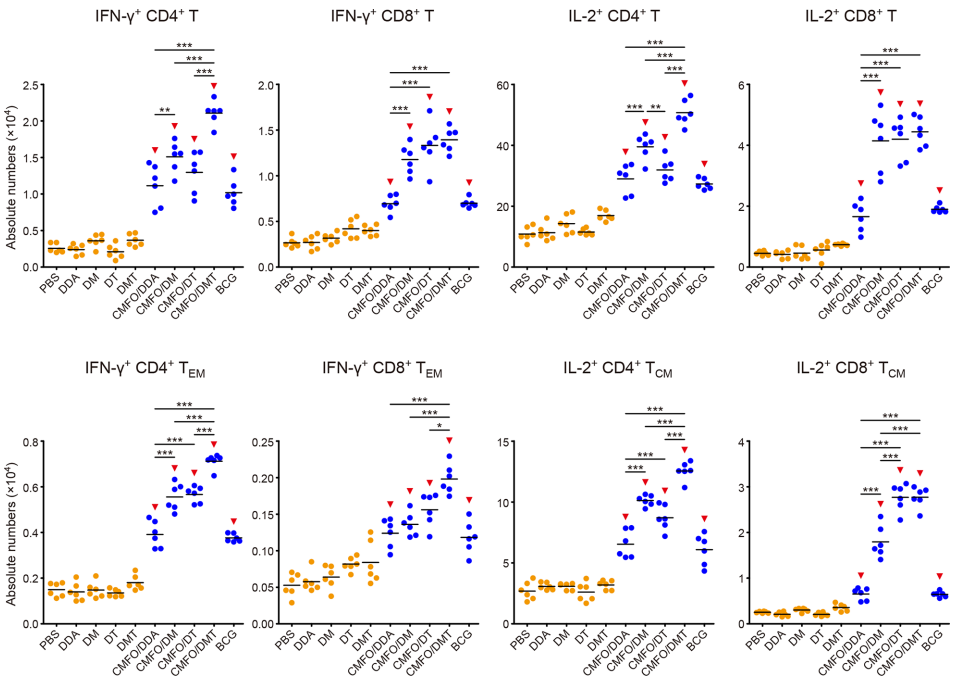

FIGURE 10 | Comparison of the levels of CMFO-specific T cells in the lung of different immunized mice after exposure (n = 6). Nine weeks after immunization, C57BL/6 mice were challenged with *M. tuberculosis*. Four weeks after infection, the absolute numbers of CMFO-specific IFN-γ+ $CD4^+$ (or $CD8^+$) T cells, IFN-γ+ $CD4^+$ (or $CD8^+$) T_{EM} cells, IL-2^+ $CD4^+$ (or $CD8^+$) T cells, and IL-2^+ $CD4^+$ (or $CD8^+$) T_{CM} cells per lung were detected. All experiments were repeated twice and similar results were obtained. The line in each group represented mean value. $^*p < 0.05$, $^{**}p < 0.01$, $^{***}p < 0.001$, and $^▼p < 0.05$ vs. respective controls. Representative FACS plots were shown in **Figure S4**.

MPLA and TDB *via* binding to TLR4 and Mincle (**Figure 11**). Most importantly, higher levels of effector and central memory T cells correspond to the better vaccine-induced protection against TB as demonstrated in previous studies (7, 17, 53). Differential T cell responses in the spleen and lung before and after exposure were also induced by different subunit vaccines in this study. $CD4^+$ T cells play a central role in adaptive immune responses for TB control and even clearance. Vaccine-induced immunological memory is the key to provide lifelong protection. Memory T cells exist in at least two sub-populations, namely, T_{EM} and T_{CM} cells (54, 55). T_{EM} cells express receptors needed for the migration into non-lymphoid organs, which immediately produce microbicidal lymphokines upon reactivation (54, 55). T_{CM} cells express high levels of CCR7, which direct recirculation through lymph nodes and proliferate to produce new antigen-specific $CD4^+$ T cells (54, 55). IL-2^+ $CD4^+$ T cells, especially IL-2^+ $CD4^+$ T_{CM} cells might play a pivotal role in vaccine-induced protection as these cells were dominated in the lung of CMFO/DMT vaccinated mice after *M. tuberculosis* infection. In addition, the adjuvants DDA/MPLA and DDA/TDB could elicit different kinds of T cells in the spleen and lung. Depending on the mechanisms of the required protective immunity, these adjuvants can be utilized to develop subunit vaccines for preventing against different infectious diseases.

Taken together, our findings have illustrated a synergistic effect among subcomponents MPLA and TDB of the adjuvant DMT, which together contribute an enhanced immunogenicity and better longer-lasting protection of the CMFO/DMT vaccine against primary progressive TB. Therefore, the current work is an important extension of the CMFO/DMT vaccine. Given a crucial role of adjuvants in vaccine-induced protection, a combinational strategy with different PRR agonists might be a direction deserved for further investigation toward a next-generation TB vaccine.

DATA AVAILABILITY STATEMENT

The raw data supporting the conclusions of this article will be made available by the authors, without undue reservation.

ETHICS STATEMENT

The animal study was reviewed and approved by the Committee on the Ethics of Animal Experiments and the School Committee on Biosafety of Tongji Medical College, Huazhong University of Science and Technology.

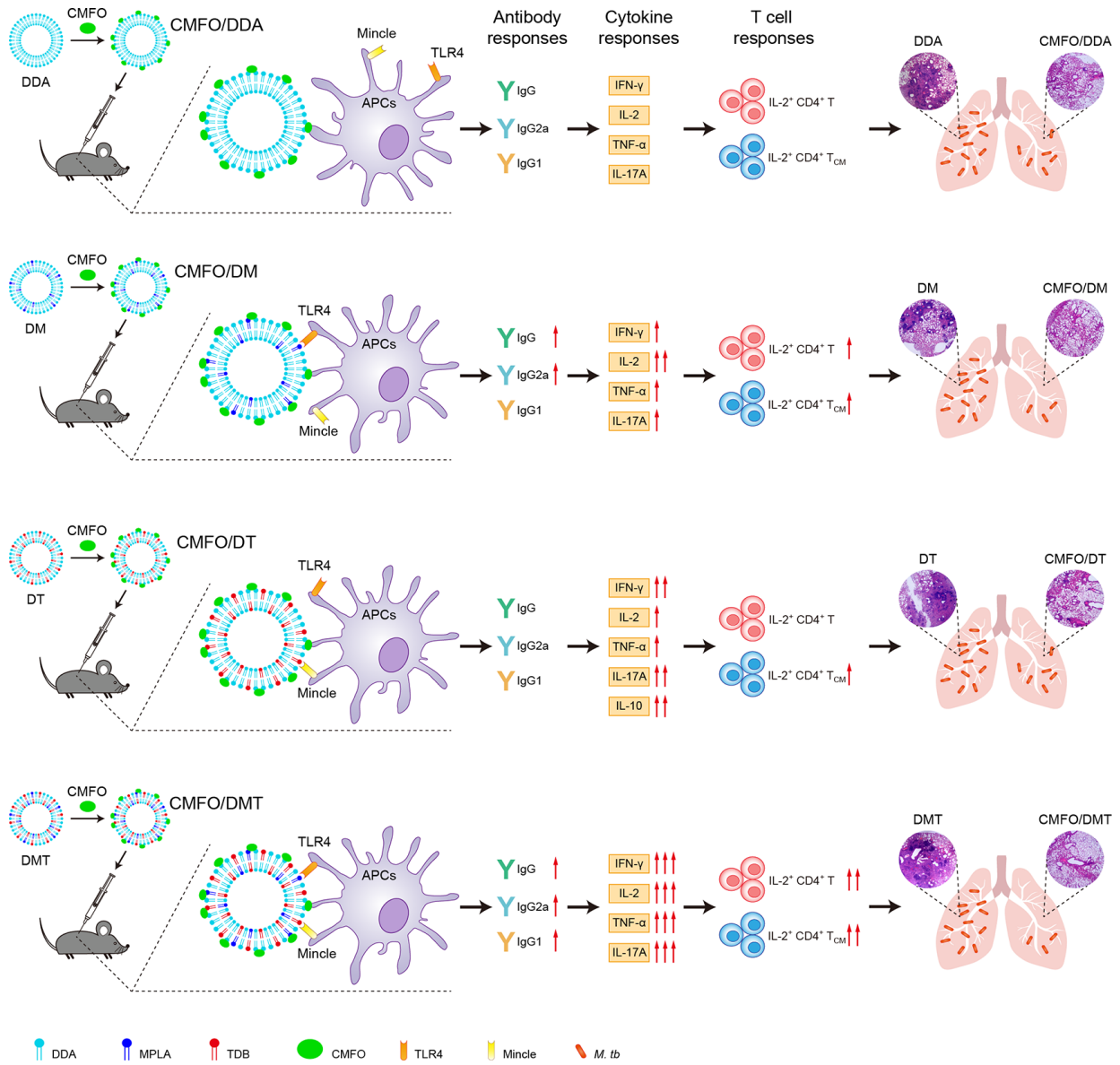

FIGURE 11 | Overview of the mechanism of different liposomal adjuvanted CMFO subunit vaccines.

AUTHOR CONTRIBUTIONS

This project was designed by XF. LH, YW, ZZ, QL, YZ, NU, J-LBN, and XL performed the experiments. LH, XF, YW, ZZ, and QL analyzed the data. LH wrote the manuscript and the final manuscript was revised thoroughly by XF.

FUNDING

This work was supported by grants from the National Mega-Projects of Science Research for the 13th Five-year Plan of China (No. 2018ZX10302302002-001), the Natural Science Foundation of China (No. 81772147, 81971909), the Fundamental Research Funds for the Central Universities (HUST COVID-19 Rapid Response Call No. 2020kfyXGYJ040), and the R&D program of Wuhan Bureau of Science and Technology (No. 2020020601012218).

SUPPLEMENTARY MATERIAL

The Supplementary Material for this article can be found online at: https://www.frontiersin.org/articles/10.3389/fimmu.2020.575504/full#supplementary-material

REFERENCES

1. Mangtani P, Abubakar I, Ariti C, Beynon R, Pimpin L, Fine PE, et al. Protection by BCG vaccine against tuberculosis: a systematic review of randomized controlled trials. *Clin Infect Dis* (2014) 58(4):470–80. doi: 10.1093/cid/cit790
2. WHO. *Global Tuberculosis Report 2019*. Geneva, Switzerland: United Nations, World Health Organization (WHO (2019). Available at: http://www.who.int/tb/publications/global_report/en/.
3. WHO. *Latent TB infection: updated and consolidated guidelines for programmatic management*. Geneva: World Health Organization (2018).
4. Andersen P, Scriba TJ. Moving tuberculosis vaccines from theory to practice. *Nat Rev Immunol* (2019) 19(9):550–62. doi: 10.1038/s41577-019-0174-z
5. Wang X, Zhang J, Liang J, Zhang Y, Teng X, Yuan X, et al. Protection against Mycobacterium tuberculosis infection offered by a new multistage subunit vaccine correlates with increased number of IFN-γ+ IL-2+ CD4+ and IFN-γ+ CD8+ T cells. *PLoS One* (2015) 10(3):e0122560. doi: 10.1371/journal.pone.0122560
6. Yu Q, Wang X, Fan X. A New Adjuvant MTOM Mediates *Mycobacterium tuberculosis* Subunit Vaccine to Enhance Th1-Type T Cell Immune Responses and IL-2^+ T Cells. *Front Immunol* (2017) 8:585. doi: 10.3389/fimmu.2017.00585
7. Ma J, Teng X, Wang X, Fan X, Wu Y, Tian M, et al. A Multistage Subunit Vaccine Effectively Protects Mice Against Primary Progressive Tuberculosis, Latency and Reactivation. *EBioMedicine* (2017) 22:143–54. doi: 10.1016/j.ebiom.2017.07.005
8. Bertholet S, Ireton GC, Ordway DJ, Windish HP, Pine SO, Kahn M, et al. A defined tuberculosis vaccine candidate boosts BCG and protects against multidrug-resistant Mycobacterium tuberculosis. *Sci Transl Med* (2010) 2 (53):53ra74. doi: 10.1126/scitranslmed.3001094
9. Aagaard C, Hoang T, Dietrich J, Cardona PJ, Izzo A, Dolganov G, et al. A multistage tuberculosis vaccine that confers efficient protection before and after exposure. *Nat Med* (2011) 17(2):189–94. doi: 10.1038/nm.2285
10. Darrah PA, DiFazio RM, Maiello P, Gideon HP, Myers AJ, Rodgers MA, et al. Boosting BCG with proteins or rAd5 does not enhance protection against tuberculosis in rhesus macaques. *NPJ Vaccines* (2019) 4:21. doi: 10.1038/s41541-019-0113-9
11. Tait DR, Hatherill M, Van Der Meeren O, Ginsberg AM, Van Brakel E, Salaun B, et al. Final Analysis of a Trial of M72/AS01E Vaccine to Prevent Tuberculosis. *N Engl J Med* (2019) 381(25):2429–39. doi: 10.1056/NEJMoa1909953
12. Nemes E, Geldenhuys H, Rozot V, Rutkowski KT, Ratangee F, Bilek N, et al. Prevention of M. tuberculosis Infection with H4:IC31 Vaccine or BCG Revaccination. *N Engl J Med* (2018) 379(2):138–49. doi: 10.1056/NEJMoa1714021
13. Harris RC, Dodd PJ, White RG. The potential impact of BCG vaccine supply shortages on global paediatric tuberculosis mortality. *BMC Med* (2016) 14 (1):138. doi: 10.1186/s12916-016-0685-4
14. Mata-Haro V, Cekic C, Martin M, Chilton PM, Casella CR, Mitchell TC. The vaccine adjuvant monophosphoryl lipid A as a TRIF-biased agonist of TLR4. *Science* (2007) 316(5831):1628–32. doi: 10.1126/science.1138963
15. Schoenen H, Bodendorfer B, Hitchens K, Manzanero S, Werninghaus K, Nimmerjahn F, et al. Cutting edge: mincle is essential for recognition and adjuvanticity of the mycobacterial cord factor and its synthetic analog trehalose-dibehenate. *J Immunol* (2010) 184(6):2756–60. doi: 10.4049/jimmunol.0904013
16. Teng X, Tian M, Li J, Tan S, Yuan X, Yu Q, et al. Immunogenicity and protective efficacy of DMT liposome-adjuvanted tuberculosis subunit CTT3H vaccine. *Hum Vaccin Immunother* (2015) 11(6):1456–64. doi: 10.1080/21645515.2015.1037057
17. van Dissel JT, Joosten SA, Hoff ST, Soonawala D, Prins C, Hokey DA, et al. A novel liposomal adjuvant system, CAF01, promotes long-lived Mycobacterium tuberculosis-specific T-cell responses in human. *Vaccine* (2014) 32(52):7098–107. doi: 10.1016/j.vaccine.2014.10.036
18. Kolanowski ST, Dieker MC, Lissenberg-Thunnissen SN, van Schijndel GM, van Ham SM, ten Brinke A. TLR4-mediated pro-inflammatory dendritic cell differentiation in humans requires the combined action of MyD88 and TRIF. *Innate Immun* (2014) 20(4):423–30. doi: 10.1177/1753425913498626
19. Dendouga N, Fochesato M, Lockman L, Mossman S, Giannini SL. Cell-mediated immune responses to a varicella-zoster virus glycoprotein E vaccine using both a TLR agonist and QS21 in mice. *Vaccine* (2012) 30(20):3126–35. doi: 10.1016/j.vaccine.2012.01.088
20. Casella CR, Mitchell TC. Putting endotoxin to work for us: monophosphoryl lipid A as a safe and effective vaccine adjuvant. *Cell Mol Life Sci* (2008) 65 (20):3231–40. doi: 10.1007/s00018-008-8228-6
21. Ishikawa E, Ishikawa T, Morita YS, Toyonaga K, Yamada H, Takeuchi O, et al. Direct recognition of the mycobacterial glycolipid, trehalose dimycolate, by C-type lectin Mincle. *J Exp Med* (2009) 206(13):2879–88. doi: 10.1084/jem.20091750
22. Desel C, Werninghaus K, Ritter M, Jozefowski K, Wenzel J, Russkamp N, et al. The Mincle-activating adjuvant TDB induces MyD88-dependent Th1 and Th17 responses through IL-1R signaling. *PLoS One* (2013) 8(1):e53531. doi: 10.1371/journal.pone.0053531
23. Werninghaus K, Babiak A, Gross O, Hölscher C, Dietrich H, Agger EM, et al. Adjuvanticity of a synthetic cord factor analogue for subunit Mycobacterium tuberculosis vaccination requires FcRgamma-Syk-Card9-dependent innate immune activation. *J Exp Med* (2009) 206(1):89–97. doi: 10.1084/jem.20081445
24. Idoko OT, Owolabi OA, Owiafe PK, Moris P, Odutola A, Bollaerts A, et al. Safety and immunogenicity of the M72/AS01 candidate tuberculosis vaccine when given as a booster to BCG in Gambian infants: an open-label randomized controlled trial. *Tuberculosis (Edinb)* (2014) 94(6):564–78. doi: 10.1016/j.tube.2014.07.001
25. Tian M, Zhou Z, Tan S, Fan X, Li L, Ullah N. Formulation in DDA-MPLA-TDB Liposome Enhances the Immunogenicity and Protective Efficacy of a DNA Vaccine against Mycobacterium tuberculosis Infection. *Front Immunol* (2018) 9:310. doi: 10.3389/fimmu.2018.00310
26. Nordly P, Agger EM, Andersen P, Nielsen HM, Foged C. Incorporation of the TLR4 agonist monophosphoryl lipid A into the bilayer of DDA/TDB liposomes: physico-chemical characterization and induction of CD8+ T-cell responses in vivo. *Pharm Res* (2011) 28(3):553–62. doi: 10.1007/s11095-010-0301-9
27. Brennan MJ, Clagett B, Fitzgerald H, Chen V, Williams A, Izzo AA, et al. Preclinical evidence for implementing a prime-boost vaccine strategy for tuberculosis. *Vaccine* (2012) 30:2811–23. doi: 10.1016/j.vaccine.2012.02.036
28. Nieuwenhuizen NE, Kaufmann SHE. Next-generation vaccines based on Bacille Calmette-Guerin. *Front Immunol* (2018) 9:121. doi: 10.3389/fimmu.2018.00121
29. Schellack C, Prinz K, Egyed A, Fritz JH, Wittmann B, Ginzler M, et al. IC31, a novel adjuvant signaling via TLR9, induces potent cellular and humoral immune responses. *Vaccine* (2006) 24(26):5461–72. doi: 10.1016/j.vaccine.2006.03.071
30. Henriksen-Lacey M, Christensen D, Bramwell VW, Lindenstrøm T, Agger EM, Andersen P, et al. Liposomal cationic charge and antigen adsorption are important properties for the efficient deposition of antigen at the injection site and ability of the vaccine to induce a CMI response. *J Control Release* (2010) 145(2):102–8. doi: 10.1016/j.jconrel.2010.03.027
31. Henriksen-Lacey M, Bramwell VW, Christensen D, Agger EM, Andersen P, Perrie Y. Liposomes based on dimethyldioctadecylammonium promote a depot effect and enhance immunogenicity of soluble antigen. *J Control Release* (2010) 142(2):180–6. doi: 10.1016/j.jconrel.2009.10.022
32. Ciurana CL, Zwart B, van Mierlo G, Hack CE. Complement activation by necrotic cells in normal plasma environment compares to that by late apoptotic cells and involves predominantly IgM. *Eur J Immunol* (2004) 34 (9):2609–19. doi: 10.1002/eji.200425045
33. Williams A, Reljic R, Naylor I, Clark SO, Falero-Diaz G, Singh M, et al. Passive protection with immunoglobulin A antibodies against tuberculous early infection of the lungs. *Immunology* (2004) 111(3):328–33. doi: 10.1111/j.1365-2567.2004.01809.x
34. Guirado E, Amat I, Gil O, Díaz J, Arcos V, Caceres N, et al. Passive serum therapy with polyclonal antibodies against Mycobacterium tuberculosis protects against post-chemotherapy relapse of tuberculosis infection in SCID mice. *Microbes Infect* (2006) 8(5):1252–9. doi: 10.1016/j.micinf.2005.12.004

35. Huygen K, Content J, Denis O, Montgomery DL, Yawman AM, Deck RR, et al. Immunogenicity and protective efficacy of a tuberculosis DNA vaccine. *Nat Med* (1996) 2(8):893–8. doi: 10.1038/nm0896-893
36. Achkar JM, Casadevall A. Antibody-mediated immunity against tuberculosis: implications for vaccine development. *Cell Host Microbe* (2013) 13(3):250–62. doi: 10.1016/j.chom.2013.02.009
37. Logan E, Luabeya AKK, Mulenga H, Mrdjen D, Ontong C, Cunningham AF, et al. Elevated IgG Responses in Infants Are Associated With Reduced Prevalence of Mycobacterium tuberculosis Infection. *Front Immunol* (2018) 9:1529. doi: 10.3389/fimmu.2018.01529
38. Donald PR, Marais BJ, Barry CE3. Age and the epidemiology and pathogenesis of tuberculosis. *Lancet* (2010) 375(9729):1852–4. doi: 10.1016/S0140-6736(10)60580-6
39. Maglione PJ, Xu J, Chan J. B cells moderate inflammatory progression and enhance bacterial containment upon pulmonary challenge with Mycobacterium tuberculosis. *J Immunol* (2007) 178(11):7222–34. doi: 10.4049/jimmunol.178.11.7222
40. Agger EM, Cassidy JP, Brady J, Korsholm KS, Vingsbo-Lundberg C, Andersen P. Adjuvant modulation of the cytokine balance in Mycobacterium tuberculosis subunit vaccines; immunity, pathology and protection. *Immunology* (2008) 124(2):175–85. doi: 10.1111/j.1365-2567.2007.02751.x
41. Redford PS, Murray PJ, O'Garra A. The role of IL-10 in immune regulation during M. tuberculosis infection. *Mucosal Immunol* (2011) 4(3):261–70. doi: 10.1038/mi.2011.7
42. Gesser B, Leffers H, Jinquan T, Vestergaard C, Kirstein N, Sindet-Pedersen S, et al. Identification of functional domains on human interleukin 10. *Proc Natl Acad Sci U S A* (1997) 94(26):14620–5. doi: 10.1073/pnas.94.26.14620
43. Flynn JL, Chan J, Lin PL. Macrophages and control of granulomatous inflammation in tuberculosis. *Mucosal Immunol* (2011) 4(3):271–8. doi: 10.1038/mi.2011.14
44. Weiss G, Schaible UE. Macrophage defense mechanisms against intracellular bacteria. *Immunol Rev* (2015) 264(1):182–203. doi: 10.1111/imr.12266
45. Cooper AM, Dalton DK, Stewart TA, Griffin JP, Russell DG, Orme IM. Disseminated tuberculosis in interferon gamma gene-disrupted mice. *J Exp Med* (1993) 178(6):2243–7. doi: 10.1084/jem.178.6.2243
46. Harris J, Keane J. How tumour necrosis factor blockers interfere with tuberculosis immunity. *Clin Exp Immunol* (2010) 161(1):1–9. doi: 10.1111/j.1365-2249.2010.04146.x
47. Roach DR, Bean AG, Demangel C, France MP, Briscoe H, Britton WJ. TNF regulates chemokine induction essential for cell recruitment, granuloma formation, and clearance of mycobacterial infection. *J Immunol* (2002) 168 (9):4620–7. doi: 10.4049/jimmunol.168.9.4620
48. Kelso A, MacDonald HR, Smith KA, Cerottini JC, Brunner KT. Interleukin 2 enhancement of lymphokine secretion by T lymphocytes: analysis of established clones and primary limiting dilution microcultures. *J Immunol* (1984) 132(6):2932–8. doi: 10.1002/cber.19190520306
49. Yoshida YO, Umemura M, Yahagi A, O'Brien RL, Ikuta K, Kishihara K, et al. Essential role of IL-17A in the formation of a mycobacterial infection-induced granuloma in the lung. *J Immunol* (2010) 184(8):4414–22. doi: 10.4049/jimmunol.0903332
50. Umemura M, Yahagi A, Hamada S, Begum MD, Watanabe H, Kawakami K, et al. IL-17-mediated regulation of innate and acquired immune response against pulmonary Mycobacterium bovis bacille Calmette-Guerin infection. *J Immunol* (2007) 178(6):3786–96. doi: 10.4049/jimmunol.178.6.3786
51. Fogli LK, Sundrud MS, Goel S, Bajwa S, Jensen K, Derudder E, et al. T cell-derived IL-17 mediates epithelial changes in the airway and drives pulmonary neutrophilia. *J Immunol* (2013) 191(6):3100–11. doi: 10.4049/jimmunol.1301360
52. Saunders BM, Frank AA, Orme IM, Cooper AM. Interleukin-6 induces early gamma interferon production in the infected lung but is not required for generation of specific immunity to Mycobacterium tuberculosis infection. *Infect Immun* (2000) 68(6):3322–6. doi: 10.1128/IAI.68.6.3322-3326.2000
53. Ma J, Tian M, Fan X, Yu Q, Jing Y, Wang W, et al. Mycobacterium tuberculosis multistage antigens confer comprehensive protection against pre- and post-exposure infections by driving Th1-type T cell immunity. *Oncotarget* (2016) 7(39):63804–15. doi: 10.18632/oncotarget.11542
54. Sallusto F, Geginat J, Lanzavecchia A. Central memory and effector memory T cell subsets: function, generation, and maintenance. *Annu Rev Immunol* (2004) 22:745–63. doi: 10.1146/annurev.immunol.22.012703.104702
55. Reinhardt RL, Khoruts A, Merica R, Zell T, Jenkins MK. Visualizing the generation of memory CD4 T cells in the whole body. *Nature* (2001) 410 (6824):101–5. doi: 10.1038/35065111

Conflict of Interest: The authors declare that the research was conducted in the absence of any commercial or financial relationships that could be construed as a potential conflict of interest.

frontiers in Immunology

ORIGINAL RESEARCH
published: 05 October 2020
doi: 10.3389/fimmu.2020.559590

Artificial Intelligence Applied to *in vitro* Gene Expression Testing (IVIGET) to Predict Trivalent Inactivated Influenza Vaccine Immunogenicity in HIV Infected Children

Nicola Cotugno[1,2], Veronica Santilli[1], Giuseppe Rubens Pascucci[1], Emma Concetta Manno[1], Lesley De Armas[3], Suresh Pallikkuth[3], Annalisa Deodati[4], Donato Amodio[1,2], Paola Zangari[1], Sonia Zicari[1], Alessandra Ruggiero[1], Martina Fortin[5], Christina Bromley[5], Rajendra Pahwa[3], Paolo Rossi[1,2], Savita Pahwa[3] and Paolo Palma[1,2]*

[1] Academic Department of Pediatrics (DPUO), Research Unit of Congenital and Perinatal Infections, Bambino Gesù Children's Hospital, Rome, Italy, [2] Chair of Pediatrics, Department of Systems Medicine, University of Rome "Tor Vergata", Rome, Italy, [3] Miami Center for AIDS Research, Department of Microbiology and Immunology, Miller School of Medicine, University of Miami, Miami, FL, United States, [4] Academic Department of Pediatrics (DPUO), Research Unit of Growth Disorders, Bambino Gesù Children's Hospital, Rome, Italy, [5] BioStat Solutions, Inc., Frederick, MD, United States

OPEN ACCESS

Edited by:
Francesco Borriello, Boston Children's Hospital and Harvard Medical School, United States

Reviewed by:
Brett McKinney, University of Tulsa, United States
Paulo Bettencourt, University of Oxford, United Kingdom

***Correspondence:**
Savita Pahwa
spahwa@med.miami.edu
Paolo Palma
paolo.palma@opbg.net

Specialty section:
This article was submitted to Vaccines and Molecular Therapeutics, a section of the journal Frontiers in Immunology

Received: 06 May 2020
Accepted: 18 August 2020
Published: 05 October 2020

Citation:
Cotugno N, Santilli V, Pascucci GR, Manno EC, De Armas L, Pallikkuth S, Deodati A, Amodio D, Zangari P, Zicari S, Ruggiero A, Fortin M, Bromley C, Pahwa R, Rossi P, Pahwa S and Palma P (2020) Artificial Intelligence Applied to in vitro Gene Expression Testing (IVIGET) to Predict Trivalent Inactivated Influenza Vaccine Immunogenicity in HIV Infected Children. Front. Immunol. 11:559590. doi: 10.3389/fimmu.2020.559590

The number of patients affected by chronic diseases with special vaccination needs is burgeoning. In this scenario, predictive markers of immunogenicity, as well as signatures of immune responses are typically missing even though it would especially improve the identification of personalized immunization practices in these populations. We aimed to develop a predictive score of immunogenicity to Influenza Trivalent Inactivated Vaccination (TIV) by applying deep machine learning algorithms using transcriptional data from sort-purified lymphocyte subsets after *in vitro* stimulation. Peripheral blood mononuclear cells (PBMCs) collected before TIV from 23 vertically HIV infected children under ART and virally controlled were stimulated *in vitro* with p09/H1N1 peptides (stim) or left unstimulated (med). A multiplexed-qPCR for 96 genes was made on fixed numbers of 3 B cell subsets, 3 T cell subsets and total PBMCs. The ability to respond to TIV was assessed through hemagglutination Inhibition Assay (HIV) and ELIspot and patients were classified as Responders (R) and Non Responders (NR). A predictive modeling framework was applied to the data set in order to define genes and conditions with the higher predicted probability able to inform the final score. Twelve NR and 11 R were analyzed for gene expression differences in all subsets and 3 conditions [med, stim or Δ (stim-med)]. Differentially expressed genes between R and NR were selected and tested with the Adaptive Boosting Model to build a prediction score. The score obtained from subsets revealed the best prediction score from 46 genes from 5 different subsets and conditions. Calculating a combined score based on these 5 categories, we achieved a model accuracy of 95.6% and only one misclassified patient. These data show how a predictive bioinformatic model applied to transcriptional analysis deriving from

in-vitro stimulated lymphocytes subsets may predict poor or protective vaccination immune response in vulnerable populations, such as HIV-infected individuals. Future studies on larger cohorts are needed to validate such strategy in the context of vaccination trials.

Keywords: gene expression, predictive biomarkers, artificial intelligence, deep learning, influenza vaccine, HIV, vaccinomics

INTRODUCTION

The advent of vaccinations has reshaped the history of medicine and across the twenty-first century has led to a decrease in morbidity of previously fatal diseases (1, 2). However, with steadily improving survival rates due to the availability of novel therapeutic tools, the vulnerable populations with special vaccination needs is burgeoning (3–5). Nowadays vaccine development programs mainly focus on otherwise healthy populations; as such, vaccine indications are based on data arising from healthy study participants. Accordingly, most vaccine indications in vulnerable groups (VPs), elderly, pregnant women and patients affected by chronic conditions (i.e., HIV infected patients), are derived from extrapolations, assumptions, or post-licensure studies (5). Thus, limited data are currently available to tailor vaccine interventions in these populations. Since the seasonal flu vaccine is well-established in routine use in HIV, it may represent the paradigm vaccine to illustrate many of the issues that affect most or all vaccines in VPs. Despite recommendations on seasonal influenza vaccination for targeted or at-risk groups (i.e., HIV, elderly, comorbidities etc.), such populations are at increased risk of acquiring vaccine-preventable infections and suffer higher infectious morbidity and mortality than healthy individuals (6, 7). This represents a major health and economic burden to society, which will become increasingly difficult to manage given limited public resources (8). In parallel, many uncertainties remain about the optimal strategies for identifying susceptible individuals, and for offering them sustained protection through a personalized immunization schedule. Novel biomarkers of protective immune responses to vaccines are needed. Vaccinology, based on the immune response network theory (9), which utilizes immunogenetics, immunogenomics and systems biology approaches to understand the basis for inter-individual variations in vaccine induced immune responses can provide such biomarkers (10, 11). In particular, vaccinomics utilize high-throughput, high-dimensional systems biology approaches, which aims to predict differences in protective or suboptimal immune responses to vaccines (12). In this regard, the basis of personalized and predictive vaccinology is the assessment of an individual's genetic background that may impact vaccine immunogenicity and efficacy. Thus, far this approach has been mostly conducted in healthy subjects leading to important findings (13). However, these data can only be partially translated in to specific populations. We recently described distinct transcriptional signatures of purified B and T cell subsets in vertically HIV infected children that was able to distinguish between patients able to respond to Trivalent Inactivated Vaccination (TIV) compared vs. non-responders (14, 15). In addition, purified H1N1 specific B cells showed significant differences in P-TEN/PI3KC2B pathway between responders and non-responders (16, 17).

Following the idea that a single vaccine cannot "fit all" (9), we here aimed at developing a predictive score of poor or protective vaccination immune response to seasonal flu vaccination through an artificial intelligence approach fed by data deriving from a novel *in vitro* gene expression testing approach (IVIGET) in HIV infected patients differentially responding to TIV. We here showed that a multiplexed gene expression analysis from sorted lymphocites subsets in different *in vitro* conditions was able to feed an artificial inteligence model able to select predictive features of influenza vaccination immunogenicity in a pediatric population with suboptimal immune response upon the influenza vaccination.

METHODS

Study Subjects

Twenty-three subjects vertically infected with HIV-1 (abbreviated as HIV) and on suppressive anti-retroviral therapy (ART) were enrolled between September and November 2012 at Bambino Gesù Children's Hospital, Rome, Italy. Written informed consent was obtained from all subjects or parents/legal guardians upon enrolment and the study was approved by the Institutional review board of the Bambino Gesù Children's Hospital. PBMCs and plasma were isolated by density gradient isolation [46] collected pre (T0) and 21 days post vaccination (T1) and cryopreserved and processed for study at a later date. Serum samples were stored at −80°C.

Immunization and Sample Collection

Patients were immunized with a single dose of Inactivated Influenza Vaccine Trivalent Types A and B (Split Virion) VAXIGRIP® (sanofi pasteur). The strains for the 2012–2013 season were: A/California/7/2009 (H1N1) pdm09-like strain (abbreviated as H1N1), A/Victoria/361/2011 (H3N2)-like strain (abbreviated as H3N2) and B/Wisconsin/1/2010-like strain (abbreviated as B).

Hemagglutination Inhibition (HI) Assay

The antibody titers to the H1N1, H3N2 and B influenza strains in sera from HIV and HC were evaluated separately by HI assay (18). The virus strains used in the HI assay were A/California/7/2009 (H1N1) pdm09-like strain, A/Victoria/361/2011 (H3N2)-like strain and B/Wisconsin/1/2010-like strain according to the 2012–2013

influenza vaccine formulation. The HI assay was performed as previously described (18). The HI antibody titers were expressed as the reciprocal of the highest serum dilution at which hemagglutination was prevented. (http://www.gmp-compliance.org/guidemgr/files/021496EN.PDF).

ELISPot

PBMCs collected at T0 and T1 from HIV and HC were thawed and policlonally activated *in vitro* in complete RPMI medium (Invitrogen) supplemented with 2.5 μg/mL CpG type B (Hycult biotech), 20 ng/mL IL-4 (Peprotech) and 20 ng/mL IL-21 (ProSpec). Cells were harvested after 5 days of culture at 37°C. ELISpot 96-well filtration plates (Millipore) were coated with the addition of purified H1N1, H3N2, and B influenza inactivated virus particles and subsequently loaded with 2×10^5 cells/well. Membranes were punched out with an Eli.Punch device and developed spots were scanned with an Eli.Scan and counted with the ELISpot Analysis Software V5.1 (all from A.EL.VIS).

Determining Vaccine Response Status

T0 and T1 samples were employed to evaluate patient's ability to respond to the vaccination as previously described (17). Response to vaccinations was determined both by ELISPot for the 3 strains of Flu vaccines (H1N1, H3N2, B) and by Haemagglutination-Inhibition assay (HIA) detected at the time of immunization and 21 days after vaccination as previously described (14, 15). In order to compare patients with differential ability to respond to the vaccination, patients were first selected according to their seroconversion to H1N1 21 days after the immunization resulting in 2 groups, Seroconverter (HIA fold increase $\geq = 4$) and Non Seroconverter (HIA fold increase < 4). As additional criteria, patients were selected according to the ELISpot responses for H1N1 at 21 days after immunization as ELISpot negative (<80 H1N1 specific spots/106 PBMCs) and ELISpot positive (>80 H1N1 specific spots/106 PBMCs). According to these 2 criteria we could select among the HIV infected children 12 non responders (NR; HIA fold increase <4 AND H1N1 specific spots <80/106 PBMCs), 11 responders (R; HIA fold increase >= 4 AND H1N1 specific spots >80/106 PBMCs).

In vitro Stimulation, Cell Sorting, and RNA Extraction

T0 PBMC were thawed and cells were counted with Countess Automated Cell counter (Life technology). Cells were resuspended in complete RPMI medium at a concentration of 5×10^6 PBMCs/mL and left at 37°C for 16 h in the presence or absence of H1N1 A/California /09 HA peptides in a final concentration 20 μL/mL. PMBCs were stained for surface markers, Vivid (Pacific Blue), CD10 (PECy7), CD20 (PE), CD27 (APC), IgD (FITC), CD21 (PECy5) for the B cell panel for 15 min and for CD3 (AmCyan), CD4 (PerCP Cy5.5), CD45RO (ECD), CCR7 (Alexa Fluor 700), and CXCR5 (Alexa Fluor 647) and a live/dead marker (ViViD; Molecular Probes) for the T cell panel for 15 min. Subsequently, stained PBMCs were washed twice in PBS, finally filtered with a 40 uM mesh and sorted by FACSAriaII (BD Biosciences). The purity of the sorted cell populations were typically >99%. All antibodies were previously titrated. Viable lymphocytes were identified as live dead amine dye negative (ViViD-) cells (Invitrogen).

Five-Hundred live cells per B and T cell subset were sorted into tubes previously loaded with 9 μL of PCR buffer (see also **Figure 1** for gating strategy). After sorting, cells were immediately centrifuged (3000RPM for 3 min) and kept on ice. Samples were subsequently transferred in PCR tubes and 18 PCR cycles were performed on a C1000 Thermal Cycler (Bio Rad) with the following scheme (50°C for 20′, 95°C for 2′, 95°C 15″, 60°C for 4′. Last step repeated 18 times). Cells were finally kept at −20 until further analysis. PCR buffer premix for cell sorting contained the following: Cells Direct Reaction mix 5 μL, DEPC water 1,4, Superscript III + Taq 1 μl, 0.2x diluted assay (96 primer mix) 2.5 μL, Superasein 0,1 μL.

Multiplexed RT-PCR

Previously amplified samples were loaded on a Fluidigm 96.96 standard chip following manufacturer's instructions. Briefly, assay pre-mix was prepared 1:1 20X TaqMan Gene Expression Assay (Applied Biosystems) and Assay Loading Reagent (Fluidigm, Biomark®). The sample pre-mix was prepared with TaqMan Universal PCR Master Mix (2X)(Applied Biosystems), 20XGE Sample Loading Reagent (Fluidigm), and cDNA. Full list of the two panels of gene probes (B subsets and T subsets is shown in **Supplemental Table 1** and **2**). 5 μl of Assay and Sample mix were loaded into the chip according to manufacturers instructions. Genes' selection has been made according to previous analysis on RNA Sequencing on HIV infected children from a different cohort (data not shown), the literature and online gene banks and biological queries.

Cycle threshold value (Ct) deriving from exported files was corrected according to number of cells sorted if lower than 500. Calculations were made following the expression 67, 5/500 = Y/X where X is the number of cells sorted and Y is the cells equivalent cDNA of cell sorted. The dilution factor (n) was calculated as $n = 67$, 5/Y, and base 2 log of n was subsequently subtracted to Ct value in order to get Corrected Cycle Threshold (c-Ct). Expression threshold (Et), which was used for the main analysis was finally obtained with 40-cCT. Once exported and corrected, data were analyzed through Fluidigm SingluaR (SingulaR analysis toolset 3.0) package, loaded on R (software R 3.0.2 GUI 1.62). As previously described (De Armas, 2017) gene expression differences between different groups within same subset and condition were used to identify Differentially Expressed Genes (DEGs). Alternatively, paired gene expression differences between stimulated (stim) and unstimulated samples (med) (stim-med) within the same subset were used to define Differentially Induced Genes (DIGs). All raw data on gene expression analysis used for the present project are available on the Gene Expression Omnibus: NCBI gene expression and hybridization array data repository (GEO) (GSE155730).

Bioinformatics and Statistical Analysis

Predictive Modeling Framework

We propose a workflow (**Figure 2**) used for gene selection and model building that use the 96 genes with age and sex as covariates. This method was applied to each subset of B cells (AM,

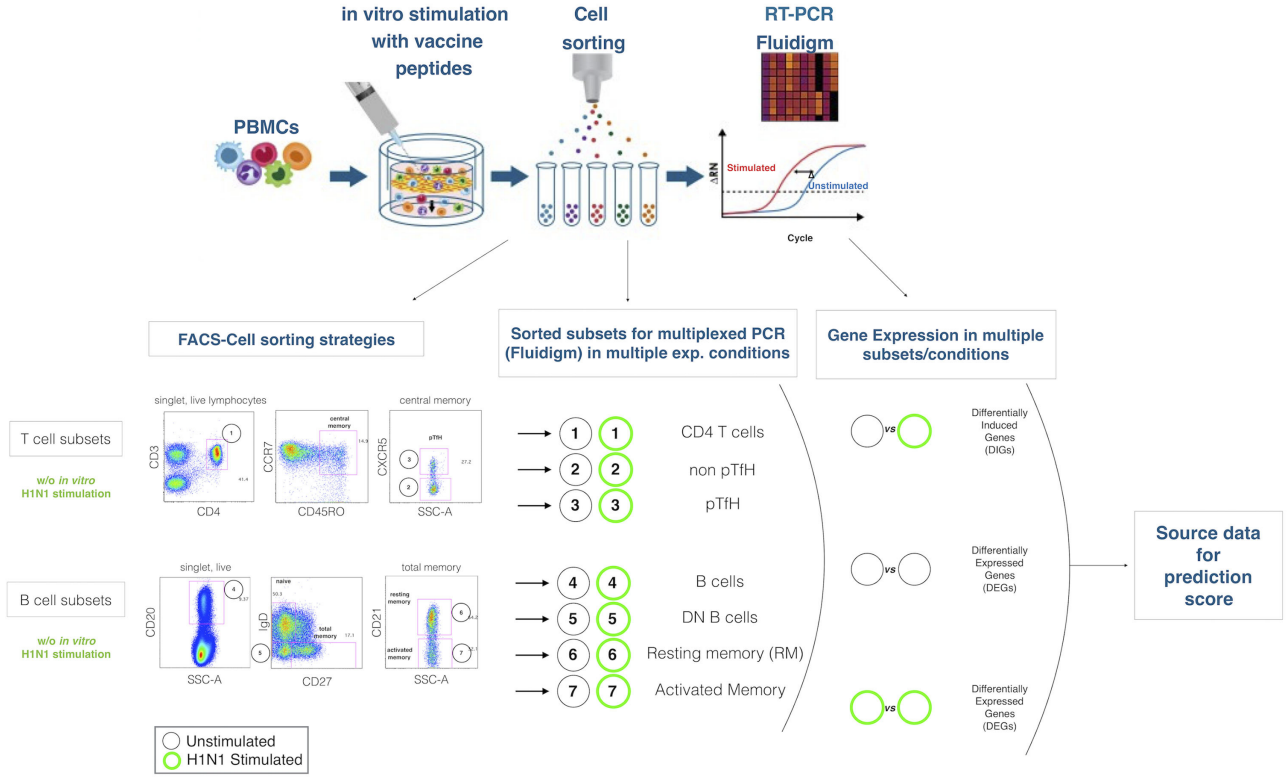

FIGURE 1 | Experimental design. The cartoon on the top panel depicts the experimental procedure. Briefly, total PBMCs are in 2 aliquotes, one stimulated and the latter unstimulated. After sorting lymphocite subsets, gene expression is analyzed by Fluidigm Biomark. Bottom panel describes the gating strategies and the lymphocites subsets selected for sorting and gene expression analysis. Mathematical analysis applied on the subsets in order to obtain differentially expressed genes (DEGs) and differentially induced genes (DIGs) are described.

DN, REM) and T cells (CD4, NT, PBMC, TFH), further divided into two conditions, namely stimulated (stim), unstimulated (med) and the derived data of the stim-med, for 23 patients. In addition, this workflow has also been applied to the entire dataset (B and T cells) to obtain a predicted probability score. Due to the small sample size and high dimensional data, the Wilcoxon Rank Sum Test was used to select genes whose expression levels are different between responders and non-responders. As compared to other feature selection methods, this test outperforms others in terms of accuracy and robustness (19) Using the two-sided test to evaluate whether these two subpopulations had different gene levels, *p*-values were derived to assess significance at $\alpha = 0.05$. Genes with significantly different expression levels were used in the next step of the analysis framework. The feature selection process was applied to each dataset to select those genes that are predictive of response to vaccine. Applying multiple machine learning methods, each using a different approach, increased the confidence in selecting the best genes for the model.

The machine learning methods used were Elastic Net (glmnet function in R) (20), Support Vector Machines (svm.fs function in R) (21) and Random Forests (randomForest function in R) using 3-fold cross validation repeated 8 times (22). Variable importance was also calculated by Random Forests and used to define the gene importance ranking as previously described (22). If a gene or feature was selected at least 10 times in total throughout the process, then it was considered for further analysis in the prediction model.

After selecting a subset of features by using the Wilcoxon Rank Sum Test and machine learning, an Adaptive Boosting model using continuous predictors and generating predicted probabilities of response was used as the final predictive model. The Adaptive Boosting model (http://rob.schapire.net/papers/explaining-adaboost.pdf) was used as it is less susceptible to overfitting and attempts to combine rules to create a more accurate prediction. This model was implemented in R using the caret (http://topepo.github.io/caret/index.html) package. The ADA Boost method uses a training set, a subset of the data that is set aside, and assigns a ± 1 as classifier values. A classifier value indicates how important a feature is for the model. The classifiers are then weighted based on the training set, and the prediction is recalculated. Using the data, the program will assign weights to features beyond the ± 1 classifier at every stage. To obtain the final results of the model, ADA Boost uses the sum of every weight and classifier combination to provide a probability of response. The result of the model is a predicted probability of response for each patient (**Figures 3**, **4**). Considering both the Wilcoxon and

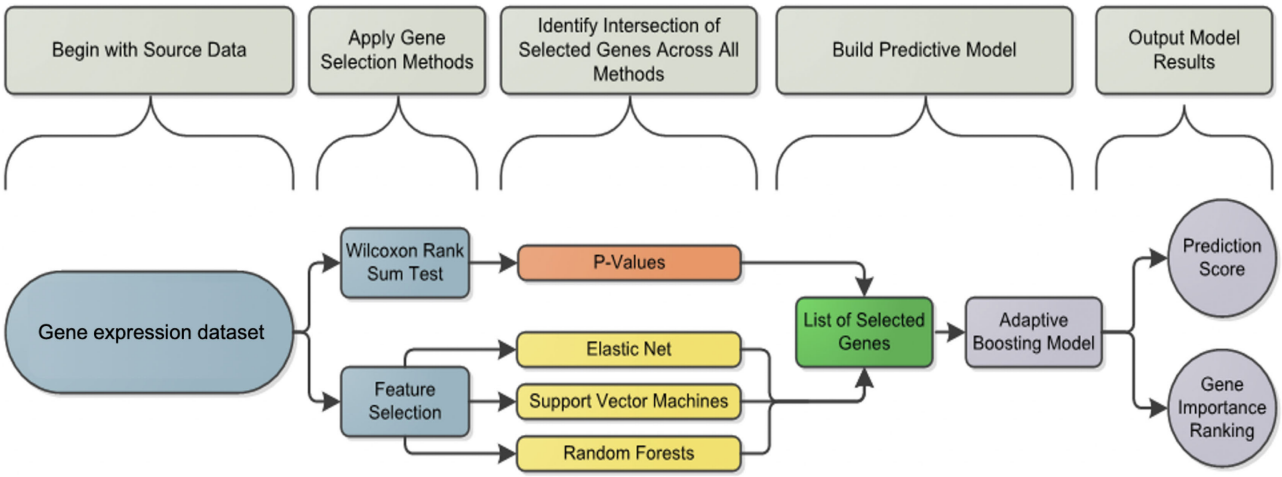

FIGURE 2 | Analysis framework flowchart: pipeline workflow for predicting the vaccine response. Differentially induced genes between responders and non-responders were selected using a machine learning feature selection based on three different algorithms and the Wilcoxon test for each cell subset and condition. The list of selected genes was used by the Adaptive Boosting algorithm to build the predictive model and calculate the prediction score.

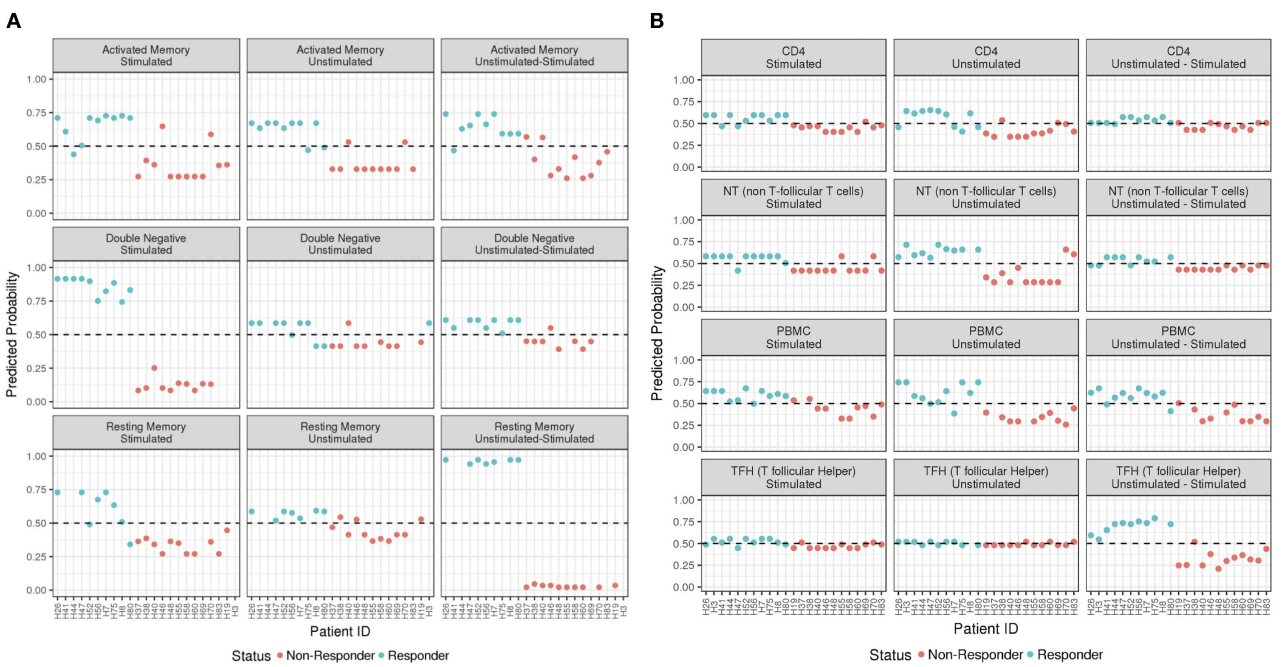

FIGURE 3 | ADA Boost Probability Scores for T Cells **(A)** and B cell subsets **(B)**. The probabilities of prediction are shown for each patient (the non-responder in red and responder in blue). If the probability is >0.50 the patient has been classified as responder, on the contrary if <0.50.

feature selection significant genes, the final model uses the intersection (B cells) or union (T cells) of the genes across subsets. The R statistical software version 3.0.3 was used for all analyses (www.r-project.org).

The R package "enrichR" v2.1 was used to perform functional annotation and pathway enrichment analysis on the genes selected to build the five models with the best prediction precision.

RESULTS

Patients' Characteristics and H1N1 Response to Influenza Vaccination

To define the ability to elicit memory response upon H1N1 of the trivalent inactivated Influenza vaccination 2012/2013 (TIV) we investigated hemoagglutination inhibition assay in 65 HIV infected children under stable and highly active antiretroviral

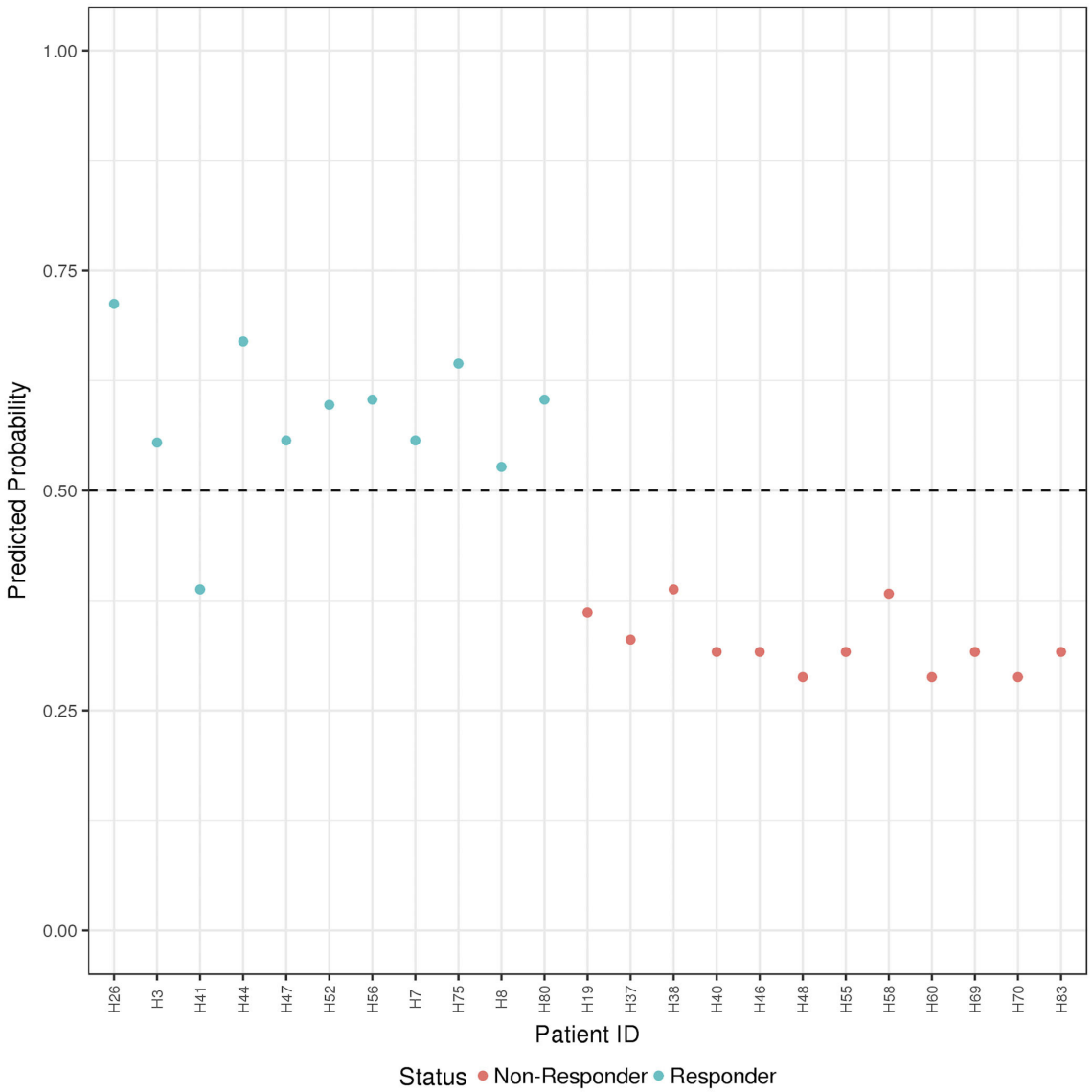

FIGURE 4 | ADA Boost Probability Scores (B and T Cells): the combined prediction score between B and T cells are shown for each patient (the non-responder in red and responder in blue). If the probability is >0.50 the patient has been classified as responder, on the contrary if <0.50.

treatment (HAART) and viral control at the time of vaccination. Clinical characteristics are listed in **Table 1**. Study participants were classified as vaccine responders (R) and vaccine non-responders (NR) according to the criteria established by Food and Drug Administration Guidance for Industry as previously described (14). R were characterized by HAI titer to H1N1 antigen (Ag) at T1 of >1:40 and > four-fold increase compared to baseline. In order to validate our criteria of selection, even considering the lower reliability of serological correlates in such patients, we applied an additional measure of vaccine responsiveness in our study population performing the B cell ELISpot response to H1N1 Ag (≥ or < 80 spots /106 PBMCs in responders (R) and non-responders (NR), respectively).

Features Selection and Identification of Predictive Score Through Artificial Intelligence

In order to predict the vaccination response based on the expression levels of 96 genes, we have implemented a bioinformatic pipeline that was tested on six sorted subsets of B and T cells, as reported in **Figure 1** and PBMC in 23 patients. For each subset, the conditions of stimulation (stim), non-stimulation (med) and the difference between the two (stim-med) have been considered. For each of these subset/condition, the algorithm, reported in **Figure 2**, selects the Differentially Induced Genes (DIGs) and Differentially Expressed Genes (DEGs) whose expression levels can, better than others, discriminate responding

TABLE 1 | Study subjects' characteristics.

Baseline characteristics	HIV NR	HIV R
Age years, mean (SEM)	15.16 (2.1)	13.72 (2.3)
n (female)	12 (7)	11 (5)
%CD4+ T cells, mean (SEM)	37.97 (4.9)	32.49 (6.0)
HIV RNA <50cp/mL, n	11	10
IgG (mg/dL) (mean)	1387.4	1,356
IgM (mg/dL) (mean)	135.1	118.9
IgA (mg/dL) (mean)	210.7	225.1
CDC (A/B/C) (1/2/3)	(3/4/5) (3/4/5)	(2/5/4) (4/3/4)
Lymphocites/mm^3 mean (SEM)	2494 (278,9)	3109 (363,1)
WBC 10^3/uL, mean (SEM)	7.6 (1.5)	7.3 (0.7)
ART regimen (2 NRTI+PI-r/2 nNRTI+ NRTI/2 NRTI+ii)	(5/5/2)	(5/4/2)

SEM, standard error of the mean; CRP, C-reactive protein; CDC, Center for Disease Control classification of AIDS. WBC, white blood cells. ART, antiretroviral treatment; NRTI, Nucleoside and Nucleotide Analog Reverse Transcriptase Inhibitors; PI, Protease Inhibitors; nNRTI, Non-Nucleoside Analog Reverse Transcriptase Inhibitors; ii, Integrase Inhibitors.

TABLE 2 | Selected genes and conditions.

		Condition		
Cell type	Cell subset	Med	stim	Med-stim
B	AM	1	2	5
	DN	5	9	5
	REM	8	8	3
T	CD4	7	9	12
	NT	12	14	12
	PBMC	18	9	12
	TFH	4	11	13
Total		55	62	62

individuals from non-responders upon TIV. A total of 179 genes/conditions were initially selected among the different subsets and conditions (**Table 2**). As shown in **Table 2**, a specific number of genes were respectively, selected for the med (55 genes), stim (62 genes), and med-stim conditions (62 genes). Subsequently, these genes were then used to build statistical models. The ADA Boost models generated for each category returned a probability score that estimates the classification of each patient in responder (R) and non-responder (NR). Assuming a predicted probability >0.50 classified as a responder, the ADA Boost model was able to predict R and NR in specific subsets and conditions according to the previously selected genes. Indeed, the Resting Memory (REM) med-stim, Double Negative (DN) stim, TFH med-stim and PBMC med datasets showed the best results in terms of predicted probability as shown in **Figure 3**. No mispredictions were found in REM med-stim, DN stim and PBMC unstim, whereas only one misprediction was found according the ADA boost of TFH med-stim.

In order to provide a comprehensive description of gene expression with higher accuracy in terms of prediction probability, all gene expression analyses, from multiple subsets and conditions were ranked.

Table 3 summarizes the classification accuracy and a relative ranking for each category. Rankings were used to identify the cell subsets and conditions that yielded high prediction accuracy as well as a wider range of predicted probability values. Correct prediction ranged from 68% up to 100% when tested on the cohort. Following these criteria, five cell subsets/conditions providing the highest classification accuracy combined with the highest predicted probability were highlighted (**Table 3**).

Finally, the B and T cells subsets/conditions were used to calculate a combined score. The score, was then tested in our cohort of patients which were blindly predicted as responders and non-responders. In this case, as shown in **Figure 4** and **Table 4**, only one patient out of the entire cohort was misclassified providing a prediction accuracy of 95.6%.

Due to the small sample size, in order to overcome the unfeasibility to perform a nested cross valitation, we confirmed the stability of the accuracy in features' selection of the top 5 B/T subsets/conditions resampling the dataset according to these 5 subset/condition. This re-analysis confirmed the stability in feature's selection of the initial model. Indeed, all subset models out of the 5 selected cell subsets/ condition feature displayed between 80 and 100% accuracy according to the bootstrap replications (**Supplementary Table 3**). The best performing subset by this metric was the B DN med_stim subset with a confidence interval ranging from 94 to 100%. All genes from the subset models had 50–90% selection rates in bootstrap replicates.

Functional Analysis of Genes Selected by Artificial Intelligence

In order to characterize the biological functions of the genes used to build the five models with the highest prediction accuracy, we performed a functional enrichment analysis on the five sets of genes shown in **Table 5**. According to gene set enrichment analysis, the REM med_stim selected genes associated with transcription pathways of chemokine expression and T cell-oriented proliferation (**Figure 5**). These results are in line with ontologies which were particularly enriched in the positive regulation of T helper I type immune responses (**Figure 5**). In the T cell counterpart, pTFH cells, several genes involved in cytokine-cytokine mediated signaling were enriched. Also JAK-STAT signaling and TLR oriented stimulation pathways were upregulated (**Figure 5**) in patients able to respond to TIV. It is important to mention that other genes, such as *IL21* and *TNSF13* (APRIL), previously reported to be crucial in the T-B cell interaction (23, 24), resulted informative after *in vitro* stimulation to define responders. According to our previous analysis (15) these data may suggest that the functional expression of these genes after *in vitro* stimulation is able to predict the ability of these cells to activate a functional cascade which sustain an effective humoral response after vaccination.

Gene ontology analysis also revealed the expression of chemokine receptors with complementary activity between IgD-

TABLE 3 | Subsets and conditions importance ranking.

	Correct classification			Predicted probability of response			
Cell type, subset, Condition	**No. Patients**	**Correct (%)**	**Rank**	**Minimum**	**Maximum**	**Range**	**Rank**
B_REM_med_stim	17	100%	2	0.022	0.972	0.950	1
B_DN_stim	20	100%	1	0.084	0.916	0.832	2
T_TFH_med_stim	22	95%	3	0.210	0.790	0.580	3
T_PBMC_med	21	90%	6	0.258	0.742	0.484	4
B_AM_med_stim	21	86%	12	0.261	0.739	0.479	5
B_REM_stim	19	89%	7	0.271	0.729	0.459	6
B_AM_stim	22	86%	10	0.273	0.727	0.453	7
T_NT_med	22	91%	5	0.286	0.714	0.429	8
T_PBMC_med_stim	21	86%	13	0.296	0.673	0.377	9
T_PBMC_stim	21	86%	14	0.326	0.674	0.347	10
B_AM_med	21	81%	16	0.329	0.671	0.343	11
T_CD4_med	23	74%	20	0.347	0.653	0.305	12
B_REM_med	18	83%	15	0.366	0.593	0.227	13
B_DN_med_stim	17	94%	4	0.392	0.608	0.217	14
T_CD4_stim	23	87%	8	0.404	0.596	0.192	15
B_DN_med	19	79%	17	0.414	0.586	0.172	16
T_NT_stim	23	87%	9	0.418	0.582	0.164	17
T_CD4_med_stim	23	78%	18	0.427	0.573	0.146	18
T_NT_med_stim	22	86%	11	0.429	0.571	0.142	19
T_TFH_stim	23	78%	19	0.447	0.553	0.106	20
T_TFH_med	22	68%	21	0.481	0.519	0.038	21

All subsets and conditions were ranked both for the accuracy of classification and for the expected probability range. According to both rankings, the categories with the best classification capacity, highlighted in red, were selected for the final score.

CD27- Double Negative (DN) B cells and pTFH. Importantly *IL2* and *IL2RA* were both selected in the pTFH and DN, respectively. These data may suggest how activation of this pathway after *in vitro* stimulation represents a functional correlate of plasma cell lineage commitment after *in vitro* stimulation as previously reported in mice (25).

DISCUSSION

Definitive and predictive biomarkers of vaccination efficacy are still largely unknown and may provide crucial information in the design or improvement of existing vaccines. This gap further applies to specific groups of patients presenting with underlying immunological conditions which increase their risk of suboptimal responses to vaccinations (4, 5). In the present study we developed a predictive score of immunogenicity to seasonal flu vaccination through an artificial intelligence approach fed by data deriving from a novel *in vitro* gene expression testing approach (IVIGET) performed prior to the immunization in a cohort of HIV infected patients.

Systems biology has helped to develop specific predictive assays in the oncology field. Also, targeted molecular assays have played an increasingly important role in identifying prognostic outcomes or predicting response to chemotherapy, starting from tumor biopsies (26). Indeed, these assays, which are now routinely performed in local pathology labs to help guide treatment decisions in breast cancer (27) lung cancer (28), and colorectal cancer (29), have been tested and validated on tumor biopsies.

On the other hand, systems vaccinology has been often analyzed in total blood or cell suspensions (e.g., PMBCs) which present an high intrinsic variability due to transitory confounding effects (e.g., concomitant infections or vaccination, inflammation, systemic immune deficiency, etc.) which may represent important variables making the aim of systems biology even more challenging. In addition, specific changes in cell frequency due to underlying immune defects or to physiologic conditions (i.e., age, pregnancy) may importantly interfere with the analysis of functional correlates of vaccine efficacy (11, 30).

Additional confounding effects are represented by inter-individual differences such as gender, age, pre-existing immunity, microbiota or systemic conditions which may further affect data analysis and their interpretation (31–33).

Following this idea, over the last few years we have described trancriptional signatures of vaccine response from purified lymphocyte subsets or single Ag specific cells in VPs (14, 16, 17). Our data demonstrated how the analysis of purified cell subpopulations may provide additional information compared to total PBMCs, and how gene expression analysis after *in vitro* stimulation may provide distinct predictive correlates of Ab and cellular response upon TIV (16) in VPs. In the present study,

TABLE 4 | Cross validation of the model.

ID	Non responder	Responder	Predicted	Observed
H19	0.639	0.361	Non.Responder	Non.Responder
H26	0.288	0.712	Responder	Responder
H3	0.445	0.555	Responder	Responder
H37	0.669	0.331	Non.Responder	Non.Responder
H38	0.613	0.387	Non.Responder	Non.Responder
H40	0.683	0.317	Non.Responder	Non.Responder
H41	0.613	0.387	Non.Responder	Responder
H44	0.331	0.669	Responder	Responder
H46	0.683	0.317	Non.Responder	Non.Responder
H47	0.443	0.557	Responder	Responder
H48	0.712	0.288	Non.Responder	Non.Responder
H52	0.403	0.597	Responder	Responder
H55	0.683	0.317	Non.Responder	Non.Responder
H56	0.397	0.603	Responder	Responder
H58	0.617	0.383	Non.Responder	Non.Responder
H60	0.712	0.288	Non.Responder	Non.Responder
H69	0.683	0.317	Non.Responder	Non.Responder
H7	0.443	0.557	Responder	Responder
H70	0.712	0.288	Non.Responder	Non.Responder
H75	0.356	0.644	Responder	Responder
H8	0.473	0.527	Responder	Responder
H80	0.397	0.603	Responder	Responder
H83	0.683	0.317	Non.Responder	Non.Responder

Predicted and observed outcome are listed for all patients.

TABLE 5 | List of the genes used to build the five models with the highest prediction accuracy.

Subset/condition	Gene name
REM med_stim	BATF, CCR2, CD69
DN stim	DUSP4, HAVCR2, IL2RA, PDL1, PPP3CA, SAMHD1, SELPLG, STAT3, TLR9
TFH med_stim	ABCB1, DUSP4,FOXP3, ICOS, IFNG, IL2, IL21, LAG3, MAPK3, PDCD1, PDL1, SOCS1, TNFSF13
PBMC med	ADAM17, BCL6, CAV1,CCR6, GATA3, IL6RA, IL6ST, PKC.A, BST2, CD3D, CXCR4, ICOS,ID2, IFNG, IL21R,IRF4,MAF, PTX3
DN med_stim	CAMK4, MX1, SELPLG, SOCS1, TLR9

In red are shown the up-regulated genes for the med and stim categories (DN stim, PBMC med) and the genes with the highest Δ (stim-med) value in the Responders for the med-stim categories (REM med-stim, TFH med- stim, DN med-stim. In blue are shown the down-regulated genes for the med and stim categories and the genes with the lowest Δ (stim-med) in the Responders for the med-stim categories (REM med-stim, TFH med-stim, DN med-stim.

our analysis approach complement the evidence produced on single subsets applying state-of- the-art machine learning and methodology to the *in vitro* gene expression testing (IVIGET) which is focused on cell subsets directly involved in the immune responses upon Influenza vaccination. After multiple gene selection methods were applied for all subsets and conditions the score was interrogated at the time of vaccination on the ability to predict immune response to TIV in a previously investigated cohort of HIV infected patients (14). Albeit limited by the small sample size, which made the nested cross validation unfeasible, our analysis was able to perform a selection of genes and conditions able to predict vaccination response in specific B and T cell subsets. Conditions with higher prediction probability and correct classification were further ranked and selected to produce the final score which was blindly tested on the cohort. To further overcome the contamination of the test set, the 5 top ranked subsets after single-model re-analysis confirmed the stability of the accuracy and suggests how the model is able to build a predictive score for vaccination response by selecting important subset/condition to be validated in larger scale studies. Four out of five of the subset/condition selected for the final score included the stimulated condition and more precisely three out of the five refer to data derived from the difference in gene expression between the stimulated and unstimulated condition. Overall these results suggest that this *in vitro* stimulation approach in combination with others *in vitro* tests recently described (34) may provide important information in term of prediction of vaccine responsiveness and early pre-clinical selection of effective vaccine candidates for VPs. Our data may thus confirm that gene expression after a relatively short (16 h) *in vitro* stimulation may emulate early transcriptional changes that were analyzed *in vivo* both in mice (35) and in humans (36, 37). Early transcriptional changes, derived from whole transcriptome sequencing from blood samples collected at day 0, 1, 3, and 7 after immunization were shown to be informative in predicting long-term humoral and cell mediated responses to Hepatitis B, Ebola (38) and yellow fever (36) vaccinations. Interestingly the majority of differentially expressed genes (DEGs) resulted from the analyis between day 1 or day 3 and day 0 suggesting that early signatures were able to orchestrate and correlate with long term memory responses. In line with this, our analysis revealed how the majority of selected features were among Differentially Induced Genes (DIGs) after a peptide mix stimulation of 16 h). Following these evidence we also recently reported how early signatures after *in vitro* stimulation in Ag specific B cells were able to define the B cell fate after re-encountering of the antigen (39). Overall these findings suggest that both the analysis of purified cells, directly involved in the immune response triggered by a peptide-specific stimulation may provide distinct signatures of immunogenicity that may be useful to implement vaccination predictive tools.

It is important to consider as a limit of the tools presented here, that effectiveness of the score may be specific to the seasonal influenza vaccination (e.g., 2009) and may not apply to other viral strains that make up the vaccine as it continuously changes over the years. It was noted by Nakaya et al. that transcriptional differences differed between the Live Attenuated Influenza Vaccine and the TIV with respect to both classes of genes and cell subsets orchestrating the early immune response (40). Indeed, in a targeted microarray confirmatory analysis on sorted subsets, B cells showed higher DEGs in TIV vaccinee compared to LAIV with a peculiar enrichment in Antibody secreting cells genes (39, 40). Additional studies will be needed to cross validate the score in yearly vaccinated patients and in a vaccine-type/year specific manner. The overfitting caused by the model may represent another limit of the study (41). To

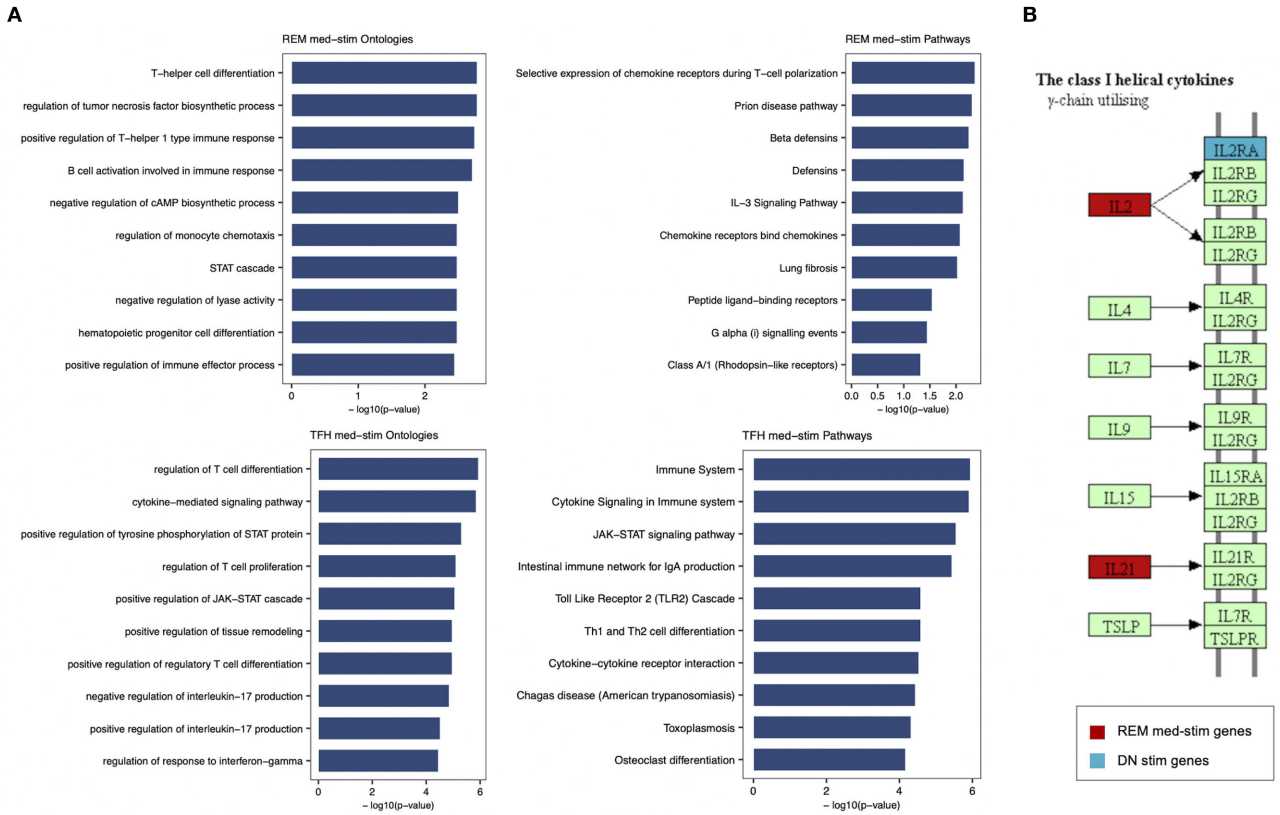

FIGURE 5 | Enrichment analysis performed for REM med-stim and TFH med-stim genes on GO terms and pathways. **(A)** Bar plots with the top 10 terms sorted by *p*-value. **(B)** Cytokine-cytokine receptor Kegg map that shows in red the REM med-stim genes and in blue the DN stim gene.

reduce this potential problem, we adopted the Adaptive Boosting algorithm which is less susceptible to overfitting through implicit regularization and attempts to combine rules to create a more accurate prediction (http://rob.schapire.net/papers/explaining-adaboost.pdf). Moreover, we have implemented a robust feature selection based on four different methods and we used a dataset balanced between responders and non-responders. To further reduce the risk of overfitting and to increase the accuracy of the models, it would be necessary to increase the sample size and possibly use two independent datasets for the testing and training phases (42).

As previously discussed, the score applies on a relatively limited and curated panel of genes that cannot provide a complete mechanistic insight on the biology orchestrating the immune response upon TIV. However, the genes selected by the score confirm the accumulating evidence on B and T lymphocytes functional data which have been produced in the last few years in patients differentially responding to TIV. Indeed, previous results in pTFH after *in vitro* stimulation highlight the importance of IL21, found upregulated in R (43), confirming previous report in children, adults and elderly able to respond to TIV (44). Also the IL2 pathway, in line with previous evidence (42, 43), seems negatively correlated to the ability to respond to the vaccination when over expressed by pTFH. Overall, these data suggest how IL2 expression triggers a Th1 oriented immune response, rather than long term memory, which was confirmed in another study investigating the correlation between circulating TfH and immunogenicity upon Ebola virus vaccination (44). Our data further add information about the IL2 pathway in the B cell compartment as it was noted that IL2RA was included by the gene selection of DN after *in vitro* stimulation. The IL2 effect on human naïve B cells was recently investigated for the ability to induce plasmacell differentiation through ERK signaling after BACH2 silencing (25). For the first time, we showed that in TIV non responders, IL2RA receptor was upregulated in the so called "double negative" B-cell subset (expressing neither CD27 nor IgD), recently reported to be accumulated in aging populations (45). Overall, these data may suggest how the lack of downregulation in the B cell counterpart after IL2 production from the circulating TFH may interfere with an adequate memory response. Additional studies on this subset will be needed in order to define whether a manipulation or an adjuvanted vaccination specifically targeting the IL21/IL2 molecule production and receptors expression may increase vaccine immunogenicity.

Also Resting memory after *in vitro* stimulation were selected by the score as an informative subset of TIV response. BATF, a transcription factor which was recently showed to induce plasmacell differentiation of memory B cells after CD40L/CD40 signaling (46) was upregulated after H1N1 peptides *in vitro*

stimulation of TIV responders. Also CD69 and CCR2 genes emerging from the score in the Resting memory subset confirm the importance of a T cell mediated response.

Although this analysis cannot provide a full mechanistic insight of the molecular mechanisms underlying the immune response since it is performed on a curated and limited panel of genes rather than the full transcriptome, it is promising in providing functional correlates to be used in a prediction score. Additional mechanistic analysis with deeper transcriptional analysis should confirm findings from these data.

In conclusion our analysis suggest that the *in vitro* stimulation and gene expression analysis on purified cell subsets that are involved in the immune responses upon vaccination, may represent valuable information to build a predictive score of immunogenicity. These analyses should be supported by future studies with larger sample size in order to validate this score in HIV infected children. These results may inform novel and more effective immunization strategies in HIV infected children and in other vulnerable population presenting with suboptimal immune responses.

Future studies, beyond the current approach, to evaluate protective immune responses remains an important goal to facilitate the interpretation of response to existing and emerging vaccines, particularly in VPs.

DATA AVAILABILITY STATEMENT

The original contributions presented in the study are included in the article/**Supplementary Materials**, further inquiries can be directed to the corresponding author/s.

ETHICS STATEMENT

The studies involving human participants were reviewed and approved by Coordinamento Amminstrativo Studi Clinici e Comitato Etico Presidenza IRCCS Ospedale Pediatrico Bambino Gesù. Written informed consent to participate in this study was provided by the participants' legal guardian/next of kin.

AUTHOR CONTRIBUTIONS

NC, LD, PP, and SaP conceived the study and designed the experiments. NC and LD performed the experimental procedures. NC and GP drafted the first version of the article. CB, MF, and NC performed statistical analysis and bioinformatics. VS, EM and PZ provided samples and participated to the design of the study. Supervision and resources were provided by PR, PP, and SP. All authors participated in writing, review and editing of the article.

FUNDING

This work was made possible by support from a Miami CFAR pilot award to NC, from Children's Hospital Bambino Gesù, ricerca corrente 2020 to NC and ricerca corrente 2019 to PP. We also received support from grants AI108472 and AI127347 to SP and the Laboratory Sciences Core of the Miami CFAR (P30AI073961) from the National Institutes of Health (NIH), which was supported by the following NIH Co-Funding and Participating Institutes and Centers: NIAID, NCI, NICHD, NHLBI, NIDA, NIMH, NIA, NIDDK, NIGMS, FIC, and OAR.

ACKNOWLEDGMENTS

We would like to acknowledge all patients and guardians who decided to participate to the study. We thank Celeste Sanchez, Varghese George, Sara Alfieri. We acknowledge Timothy Ambrose from Biostat Solution who worked on the data analysis over the revision process. We thank Jennifer Faudella for her administrative assistance. We thank Andrea Rosati for discussions and suggestions during the preliminary phase of the study.

SUPPLEMENTARY MATERIAL

The Supplementary Material for this article can be found online at: https://www.frontiersin.org/articles/10.3389/fimmu.2020.559590/full#supplementary-material

Supplementary Figure 1 | ELISpot analysis. **(A)** Shows representative plates for ELIspot. Dot plot in panel B shows H1N1 specific B cells per million PBMCs from samples collected 21 days after TIV.

Supplementary Table 1 | Gene panels with probe list for B cells.

Supplementary Table 2 | Gene panels with probe list for T cells.

Supplementary Table 3 | Single model re-analysis on top 5 ranked subsets/conditions.

REFERENCES

1. Roush SW, Murphy TV, Vaccine-Preventable Disease Table Working G. Historical comparisons of morbidity and mortality for vaccine-preventable diseases in the United States. *JAMA*. (2007) 298:2155–63. doi: 10.1001/jama.298.18.2155
2. Centers for Diseas and Prevention. Local health department costs associated with response to a school-based pertussis outbreak — Omaha, Nebraska, September-November 2008. *MMWR Morb Mortal Wkly Rep*. (2011) 60:5–9. Available online at: https://www.cdc.gov/mmwr/preview/mmwrhtml/mm6001a2.htm
3. Cagigi A, Cotugno N, Giaquinto C, Nicolosi L, Bernardi S, Rossi P, et al. Immune reconstitution and vaccination outcome in HIV-1 infected children: present knowledge and future directions. *Hum Vaccin Immunother*. (2012) 8:1784–94. doi: 10.4161/hv.21827
4. Cotugno N, Douagi I, Rossi P, Palma P. Suboptimal immune reconstitution in vertically HIV infected children: a view on how HIV replication and timing of HAART initiation can impact on T and B-cell compartment. *Clin Dev Immunol*. (2012) 2012:805151. doi: 10.1155/2012/805151
5. Cotugno N, Ruggiero A, Santilli V, Manno EC, Rocca S, Zicari S, et al. OMIC technologies and vaccine development: from the identification of vulnerable individuals to the formulation of invulnerable vaccines. *J Immunol Res*. (2019) 2019:8732191. doi: 10.1155/2019/8732191
6. Sutcliffe CG, Moss WJ. Do children infected with HIV receiving HAART need to be revaccinated? *Lancet Infect Dis*. (2010) 10:630–42. doi: 10.1016/S1473-3099(10)70116-X

7. Dube E, Leask J, Wolff B, Hickler B, Balaban V, Hosein E, et al. The WHO Tailoring Immunization Programmes (TIP) approach: review of implementation to date. *Vaccine*. (2018) 36:1509–15. doi: 10.1016/j.vaccine.2017.12.012
8. Doherty M, Buchy P, Standaert B, Giaquinto C, Prado-Cohrs D. Vaccine impact: benefits for human health. *Vaccine*. (2016) 34:6707–14. doi: 10.1016/j.vaccine.2016.10.025
9. Poland GA, Kennedy RB, Mckinney BA, Ovsyannikova IG, Lambert ND, Jacobson RM, et al. Vaccinomics, adversomics, and the immune response network theory: individualized vaccinology in the 21st century. *Semin Immunol*. (2013) 25:89–103. doi: 10.1016/j.smim.2013.04.007
10. Poland GA. Pharmacology, vaccinomics, and the second golden age of vaccinology. *Clin Pharmacol Ther*. (2007) 82:623–6. doi: 10.1038/sj.clpt.6100379
11. Lee AH, Shannon CP, Amenyogbe N, Bennike TB, Diray-Arce J, Idoko OT, et al. Dynamic molecular changes during the first week of human life follow a robust developmental trajectory. *Nat Commun*. (2019) 10:1092. doi: 10.1038/s41467-019-08794-x
12. Poland GA, Ovsyannikova IG, Kennedy RB, Lambert ND, Kirkland JL. A systems biology approach to the effect of aging, immunosenescence and vaccine response. *Curr Opin Immunol*. (2014) 29:62–8. doi: 10.1016/j.coi.2014.04.005
13. Pulendran B. Immunology taught by vaccines. *Science*. (2019) 366:1074–5. doi: 10.1126/science.aau6975
14. Cotugno N, De Armas L, Pallikkuth S, Rinaldi S, Issac B, Cagigi A, et al. Perturbation of B cell gene expression persists in HIV-infected children despite effective antiretroviral therapy and predicts H1N1 response. *Front Immunol*. (2017) 8:1083. doi: 10.3389/fimmu.2017.01083
15. De Armas LR, Cotugno N, Pallikkuth S, Pan L, Rinaldi S, Sanchez MC, et al. Induction of IL21 in Peripheral T follicular helper cells is an indicator of influenza vaccine response in a previously vaccinated HIV-infected pediatric cohort. *J Immunol*. (2017) 198:1995–2005. doi: 10.4049/jimmunol.1601425
16. De Armas LR, Pallikkuth S, Pan L, Rinaldi S, Cotugno N, Andrews S, et al. Single cell profiling reveals PTEN overexpression in influenza-specific B cells in aging HIV-infected individuals on Anti-retroviral Therapy. *Sci Rep*. (2019) 9:2482. doi: 10.1038/s41598-019-38906-y
17. Cotugno N, Zicari S, Morrocchi E, De Armas LR, Pallikkuth S, Rinaldi S, et al. Higher PIK3C2B gene expression of H1N1+ specific B-cells is associated with lower H1N1 immunogenicity after trivalent influenza vaccination in HIV infected children. *Clin Immunol*. (2020) 215:108440. doi: 10.1016/j.clim.2020.108440
18. Cagigi A, Rinaldi S, Di Martino A, Manno EC, Zangari P, Aquilani A, et al. Premature immune senescence during HIV-1 vertical infection relates with response to influenza vaccination. *J Allergy Clin Immunol*. (2014) 133:592–4. doi: 10.1016/j.jaci.2013.10.003
19. Haury AC, Gestraud P, Vert JP. The influence of feature selection methods on accuracy, stability and interpretability of molecular signatures. *PLoS ONE*. (2011) 6:e28210. doi: 10.1371/journal.pone.0028210
20. Friedman J, Hastie T, Tibshirani R. Regularization paths for generalized linear models via coordinate descent. *J Stat Softw*. (2010) 33:1–22. doi: 10.18637/jss.v033.i01
21. Zhang HH, Ahn J, Lin X, Park C. Gene selection using support vector machines with non-convex penalty. *Bioinformatics*. (2006) 22:88–95. doi: 10.1093/bioinformatics/bti736
22. Ishwaran H, Lu M. Standard errors and confidence intervals for variable importance in random forest regression, classification, and survival. *Stat Med*. (2019) 38:558–82. doi: 10.1002/sim.7803
23. Pallikkuth S, Pilakka Kanthikeel S, Silva SY, Fischl M, Pahwa R, Pahwa S. Upregulation of IL-21 receptor on B cells and IL-21 secretion distinguishes novel 2009 H1N1 vaccine responders from nonresponders among HIV-infected persons on combination antiretroviral therapy. *J Immunol*. (2011) 186:6173–81. doi: 10.4049/jimmunol.1100264
24. Matsuda Y, Haneda M, Kadomatsu K, Kobayashi T. A proliferation-inducing ligand sustains the proliferation of human naive (CD27(-)) B cells and mediates their differentiation into long-lived plasma cells *in vitro* via transmembrane activator and calcium modulator and cyclophilin ligand interactor and B-cell mature antigen. *Cell Immunol*. (2015) 295:127–36. doi: 10.1016/j.cellimm.2015.02.011
25. Hipp N, Symington H, Pastoret C, Caron G, Monvoisin C, Tarte K, et al. IL-2 imprints human naive B cell fate towards plasma cell through ERK/ELK1-mediated BACH2 repression. *Nat Commun*. (2017) 8:1443. doi: 10.1038/s41467-017-01475-7
26. Nielsen T, Wallden B, Schaper C, Ferree S, Liu S, Gao D, et al. Analytical validation of the PAM50-based prosigna breast cancer prognostic gene signature assay and ncounter analysis system using formalin-fixed paraffin-embedded breast tumor specimens. *BMC Cancer*. (2014) 14:177. doi: 10.1186/1471-2407-14-177
27. Selinka HC, Bosing-Schneider R. xid mice fail to express an anti-dextran immune response but carry alpha(1-3)dextran-specific lymphocytes in their potential repertoire. *Eur J Immunol*. (1988) 18:1727–32. doi: 10.1002/eji.1830181111
28. Li R, Li H, Ge C, Fu Q, Li Z, Jin Y, et al. Increased expression of the RNA-binding motif protein 47 predicts poor prognosis in non-small-cell lung cancer. *Oncol Lett*. (2020) 19:3111–22. doi: 10.3892/ol.2020.11417
29. Huang R, Zhou L, Chi Y, Wu H, Shi L. LncRNA profile study reveals a seven-lncRNA signature predicts the prognosis of patients with colorectal cancer. *Biomark Res*. (2020) 8:8. doi: 10.1186/s40364-020-00187-3
30. Cotugno N, De Armas L, Pallikkuth S, Rossi P, Palma P, Pahwa S. Paediatric HIV infection in the 'omics era: defining transcriptional signatures of viral control and vaccine responses. *J Virus Erad*. (2015) 1:153–8. doi: 10.1016/S2055-6640(20)30507-0
31. Furman D, Hejblum BP, Simon N, Jojic V, Dekker CL, Thiebaut R, et al. Systems analysis of sex differences reveals an immunosuppressive role for testosterone in the response to influenza vaccination. *Proc Natl Acad Sci USA*. (2014) 111:869–74. doi: 10.1073/pnas.1321060111
32. Nakaya HI, Bruna-Romero O. Is the gut microbiome key to modulating vaccine efficacy? *Expert Rev Vaccines*. (2015) 14:777–9. doi: 10.1586/14760584.2015.1040395
33. Zimmermann P, Curtis N. Factors that influence the immune response to vaccination. *Clin Microbiol Rev*. (2019) 32:18. doi: 10.1128/CMR.00084-18
34. Sanchez-Schmitz G, Stevens CR, Bettencourt IA, Flynn PJ, Schmitz-Abe K, Metser G, et al. Microphysiologic human tissue constructs reproduce autologous age-specific BCG and HBV primary immunization *in vitro*. *Front Immunol*. (2018) 9:2634. doi: 10.3389/fimmu.2018.02634
35. Derian N, Bellier B, Pham HP, Tsitoura E, Kazazi D, Huret C, et al. Early transcriptome signatures from immunized mouse dendritic cells predict late vaccine-induced T-cell responses. *PLoS Comput Biol*. (2016) 12:e1004801. doi: 10.1371/journal.pcbi.1004801
36. Querec TD, Akondy RS, Lee EK, Cao W, Nakaya HI, Teuwen D, et al. Systems biology approach predicts immunogenicity of the yellow fever vaccine in humans. *Nat Immunol*. (2009) 10:116–25. doi: 10.1038/ni.1688
37. Bartholomeus E, De Neuter N, Meysman P, Suls A, Keersmaekers N, Elias G, et al. Transcriptome profiling in blood before and after hepatitis B vaccination shows significant differences in gene expression between responders and non-responders. *Vaccine*. (2018) 36:6282–9. doi: 10.1016/j.vaccine.2018.09.001
38. Rechtien A, Richert L, Lorenzo H, Martrus G, Hejblum B, Dahlke C, et al. Systems vaccinology identifies an early innate immune signature as a correlate of antibody responses to the ebola vaccine rVSV-ZEBOV. *Cell Rep*. (2017) 20:2251–61. doi: 10.1016/j.celrep.2017.08.023
39. Cotugno N, Morrocchi E, Rinaldi S, Rocca S, Pepponi I, Di Cesare S, et al. Early antiretroviral therapy-treated perinatally HIV-infected seronegative children demonstrate distinct long-term persistence of HIV-specific T-cell and B-cell memory. *AIDS*. (2020) 34:669–80. doi: 10.1097/QAD.0000000000002485
40. Nakaya HI, Wrammert J, Lee EK, Racioppi L, Marie-Kunze S, Haining WN, et al. Systems biology of vaccination for seasonal influenza in humans. *Nat Immunol*. (2011) 12:786–95. doi: 10.1038/ni.2067
41. Camacho DM, Collins KM, Powers RK, Costello JC, Collins JJ. Next-generation machine learning for biological networks. *Cell*. (2018) 173:1581–92. doi: 10.1016/j.cell.2018.05.015
42. Gonzalez-Dias P, Lee EK, Sorgi S, De Lima DS, Urbanski AH, Silveira EL, et al. Methods for predicting vaccine immunogenicity and reactogenicity. *Hum Vaccin Immunother*. (2020) 16:269–76. doi: 10.1080/21645515.2019.1697110

43. Pallikkuth S, De Armas LR, Rinaldi S, George VK, Pan L, Arheart KL, et al. Dysfunctional peripheral T follicular helper cells dominate in people with impaired influenza vaccine responses: results from the FLORAH study. *PLoS Biol*. (2019) 17:e3000257. doi: 10.1371/journal.pbio.3000257
44. Cubas R, Van Grevenynghe J, Wills S, Kardava L, Santich BH, Buckner CM, et al. Reversible reprogramming of circulating memory T follicular helper cell function during chronic HIV infection. *J Immunol*. (2015) 195:5625–36. doi: 10.4049/jimmunol.1501524
45. Rinaldi S, Pallikkuth S, George VK, De Armas LR, Pahwa R, Sanchez CM, et al. Paradoxical aging in HIV: immune senescence of B Cells is most prominent in young age. *Aging*. (2017) 9:1307–25. doi: 10.18632/aging.101229
46. Koike T, Harada K, Horiuchi S, Kitamura D. The quantity of CD40 signaling determines the differentiation of B cells into functionally distinct memory cell subsets. *Elife*. (2019) 8:e44245. doi: 10.7554/eLife.44245.028

Conflict of Interest: MF, and CB were employed by BioStat Solutions, Inc.

The remaining authors declare that the research was conducted in the absence of any commercial or financial relationships that could be construed as a potential conflict of interest.

frontiers in Immunology

ORIGINAL RESEARCH
published: 08 October 2020
doi: 10.3389/fimmu.2020.577751

Serological Protection 5–6 Years Post Vaccination Against Yellow Fever in African Infants Vaccinated in Routine Programmes

Olubukola T. Idoko[1,2], Cristina Domingo[3], Milagritos D. Tapia[4], Samba O. Sow[4], Christof Geldmacher[5,6], Elmar Saathoff[5,6] and Beate Kampmann[1,7]*

[1] Vaccines and Immunity Theme, Medical Research Council Unit The Gambia at the London School of Hygiene and Tropical Medicine, Fajara, Gambia, [2] CIH[LMU] Center for International Health, Medical Center of the University of Munich (Ludwig-Maximilians-Universität München), Munich, Germany, [3] Centre for Biological Threats and Special Pathogens, Robert Koch Institute, Berlin, Germany, [4] Centre pour le Développement des Vaccins, University of Maryland, Bamako, Mali, [5] Division of Infectious Diseases and Tropical Medicine, University Hospital, Ludwig-Maximilians-Universität München Munich, Munich, Germany, [6] German Centre for Infection Research (Deutsches Zentrum für Infektionsforschung), Munich, Germany, [7] The Vaccine Centre, Faculty of Infectious and Tropical Diseases, London School of Hygiene and Tropical Medicine, London, United Kingdom

OPEN ACCESS

Edited by:
Jay Evans, University of Montana, United States

Reviewed by:
Christine Wong, Charité – Universitätsmedizin Berlin, Germany
Galileo Escobedo, General Hospital of Mexico, Mexico

***Correspondence:**
Olubukola T. Idoko
Olubukola.Idoko@lshtm.ac.uk; bukkyidoko@gmail.com

Specialty section:
This article was submitted to Vaccines and Molecular Therapeutics, a section of the journal Frontiers in Immunology

Received: *29 June 2020*
Accepted: *03 September 2020*
Published: *08 October 2020*

Citation:
Idoko OT, Domingo C, Tapia MD, Sow SO, Geldmacher C, Saathoff E and Kampmann B (2020) Serological Protection 5–6 Years Post Vaccination Against Yellow Fever in African Infants Vaccinated in Routine Programmes. Front. Immunol. 11:577751. doi: 10.3389/fimmu.2020.577751

Introduction: Although effective live attenuated yellow fever (YF) vaccines have been available for over 9 decades sporadic outbreaks continue to occur in endemic regions. These may be linked to several factors including epidemiological factors such as vector and intermediate host distribution or vaccine coverage and efficacy. The World Health Organization's research priorities include gathering systematic evidence around the potential need for booster vaccination with YF vaccine whether this follows full or fractional doses in children. Knowledge on the longevity of response to YF vaccine and the implications of this response needs to be consolidated to guide future vaccination policy.

Methods: We measured anti-YF IgG by microneutralization assay in a group of 481 African infants who had received YF vaccine as part of routine EPI programmes, to explore serological protection from YF 5–6 years post YF vaccination, as well as the effect of co variates.

Findings: Notably, 22.2% of the cohort had undetectable antibody concentrations, with another 7.5% revealing concentrations below the threshold of seropositivity of 0.5 IU/mL. Sex, season, country and time since vaccination did not affect the longevity of antibody concentration or having antibody concentrations above a defined threshold.

Conclusion: Roughly 30% of children in this cohort did not demonstrate anti-yellow fever antibody concentrations above the defined threshold of protection, with 20% having no demonstrable antibody. Knowledge on the longevity of response to YF vaccine and the implications needs to be consolidated to guide future vaccination policy.

Keywords: serologic, protection, 5-6 years post vaccination, yellow fever, routine immunizations

BACKGROUND

Effective vaccines against yellow fever (YF) virus have been available for over nine decades (1). In endemic regions of the world, these vaccines are generally used as part of the routine Expanded Programme on Immunization (EPI) vaccines given to children in infancy (2). The currently available YF vaccines are live attenuated vaccines shown to be highly immunogenic and to provide long term protection after a single dose (1).The primary correlate of protection is neutralizing antibody, though cell mediated and innate immune responses have also been proposed to play a role (3).

In 2014 the World Health Organization (WHO) changed its recommendation of 10-yearly vaccination against YF to a single dose for life. Fractional doses are also in use during epidemics when vaccine supplies are limited. However, WHO has recognized the need for studies that establish the longevity of response to a single YF vaccine dose as a priority, particularly in special groups such as infants, immunocompromised individuals and those who received fractional doses of the vaccine (4–6). Establishing the longevity of response following single dose YF vaccination is key to guide future policy on the use of the vaccine, particularly in endemic settings. If the longevity of response is found to be sub optimal in these groups, millions may be vulnerable to infection in these endemic areas. The current projections of population coverage under the 2017–2026 Eliminating YF Epidemics (EYE) strategy, which implements YF vaccination in infants as part of the EPI in endemic countries (7), could be off-target if serological and possibly clinical protection from disease is short-lived.

The proportion of individuals with protective anti-yellow fever antibody reported in the literature ranges from 69 to 98% up to 11 years post vaccination (8–12). Data from children remains limited but are of particular importance, given that in endemic settings a single dose for life given in infancy would be the only YF vaccine administration. It is also possible that immune responses to YF differ between adults and children and data from children showing both production and longevity of protective antibody need to be generated, especially since it has already been demonstrated that infants show poorer and sometimes varied seroconversion rates following YF vaccination (13–16) in different settings. This finding is likely to impact on the longevity of antibody response.

To our knowledge there are limited data on longevity of YF antibody available from the African continent. One previous study by Domingo et al. involving children from Ghana and Mali examined longevity of antibody response to YF vaccine in African infants who had received the vaccines according to EPI schedules but as part of large randomized controlled trials (ideal settings). In these circumstances, "real life" factors such as cold chain maintenance and other programmatic limitations are less likely to affect overall outcome given the influence of full time study teams (17). Generating data on the antibody concentrations to YF several years post vaccination under routine EPI program conditions therefore remains important to inform the WHO guidelines with a view to assess need for booster doses if the only dose of YF vaccine is administered in infancy.

We measured anti-YF IgG by microneutralization assay in a group of African infants who had received YF vaccine as part of routine EPI programmes, to explore serological protection from YF 5–6 years post YF vaccination.

We also explored the impact of cofactors such as sex, season of vaccination, country and time since vaccination on the concentration of anti-YF IgG neutralizing antibodies.

ROLE OF FUNDING SOURCE

The funders had no role in the study design, data collection, data analysis, data interpretation, or manuscript write up.

ETHICAL APPROVALS

Written informed consent according Good Clinical Practice guidelines and the Declaration of Helsinki was obtained from a parent of each participant. The initial and current studies were approved by the ethics committees at the host institutions and Programme for Appropriate Technology in Health (PATH).

METHODS

Population and Samples

We assayed YF antibody responses in a cohort of African children from The Gambia ($N = 243$) and Mali ($N = 238$) using banked serum samples which were originally collected as part of an antibody persistence study to assess persistence of antibodies to MenAfriVac 4–5 years after the children had originally received MenAfriVac at 12–23 months of age. With these 481 samples we would have a power of 1.0 to detect a 10% difference in the proportion of individuals attaining protective titres assuming that one vaccine dose would result in 98% of children having protective anti-YF antibody titres 5–6 years post vaccination at a 5% alpha.

These blood samples were collected between October 2011 and April 2012 and included samples from all children who could be traced 4–5 years post MenAfriVac vaccination. Left over banked serum was accessed for this analysis (18) and current assays were conducted between January and March 2019.

Records of YF Vaccination

As a prerequisite to enrolment into the MenAfrivac trial at age 12–23 months, the infants were required to have documentation showing that they received all recommended vaccinations for age which included one dose of YF vaccine received up to 1-year pre enrolment. The EPI program in Mali utilized yellow fever vaccines from Institute Pasteur, SANOFI Pasteur and BIOMANGUINHOS. The Gambia EPI utilized vaccines from vaccines from Institute Pasteur only. All blood samples assayed in this study were collected between 5- and 6-years post YF vaccination (corresponding to 4–5 years post study enrolment) and remaining aliquots had been stored at −70°C at the University of Siena Sera Bank in Italy. Samples were maintained at this temperature while stored at and during transport form the clinical sites and during transport to the assay lab.

Lab Assays

The concentrations of neutralizing antibodies to YF virus were tested at the Robert Koch Institute in Berlin using a microneutralization assay (17). Briefly, 100 TCDI50 infectious doses of a YF virus 17-D (Stamaril, Sanofi Pasteur, Val de Reuil, France) were incubated with serial 2-fold dilutions of sera before inoculation into Vero cells cultured in 96-well plates. The cells were then microscopically examined for cytopathic effect 7 days later. Reference serum samples were run with each plate to minimize batch effects and ensure suitability of assay.

Cut Offs

Although neutralizing titres of ≥1:5 or 1:10 (17, 19) are considered a surrogate of protection (seroprotection), difference in in assay methods may limit comparability of results from different laboratories. The titres were thus standardized by conversion into antibody concentrations in IU/mL using a WHO international standard (WHO International Standard, NISBC 99/616 reconstituted at 143 IU/ml) to allow for comparability with other available data. This was done by comparison with two positive controls for yellow fever neutralizing antibodies included with every assay. These controls were calibrated at 426.82 and 106.7 IU/ml, respectively. Based on earlier studies (20–22), we applied a concentration threshold of ≥0·5 IU/ml to discriminate seropositivity.

Data Analysis

Where applicable, antibody concentrations were normalized by log 2 transformation. Uni- and multivariable mixed effects models were applied, adjusting for sex, season of vaccination and time since vaccination. Separate models were run for seropositivity (binary outcome) and raw post-vaccination antibody titres (continuous). Means, median, proportions and odds ratios were calculated along with their corresponding 95% confidence intervals. An alpha error level of 5% was used to judge significance. All analyses were performed using Stata version 14·2 (23).

RESULTS

Sera from 481 children (238 from Mali and 243 from The Gambia) were available of which 224 were male and 256 were female. Sex was missing for one participant.

Participants Demonstrating Seropositivity 5–6 Years Post Vaccination

The median antibody concentration was 1.2 [interquartile range (0.4–2.4)]. Notably, 22.2% of the cohort had undetectable antibody concentrations, with another 7.5% revealing concentrations below the threshold of seropositivity of 0.5 IU/mL. **Table 1** summarizes antibody concentrations by country.

The antibody concentrations did not differ significantly by country ($p = 0.13$) with a trend to higher concentrations in the Malian cohort.

TABLE 1 | Anti-YF antibody concentrations (UI/mL).

	Mean (95% CI)	Percentage with undetectable antibody (% 95% CI)	Percentage with antibody below protective threshold (% 95% CI)
Overall ($N = 481$)	2.9 (2.3–3.5)	22.2 (18.6–26.2)	29.7 (25.7–34.0)
Mali (N =238)	3.4 (2.3–4.4)	25.6 (20.2–31.7)	31.5 (25.7–37.8)
Gambia ($N = 243$)	2.5 (1.9–3.0)	18.9 (14.2–24.4)	28.0 (22.4–34.1)

95% CI, 95% confidence interval; IQR, interquartile range; YF Ab, YF antibody; N, number of observations; NB, Percentage with concentrations below the protective threshold includes individuals with undetectable concentrations.

Participants With Defined Protective Antibody Titer

The median antibody titer was 1:12.0 [interquartile range (1:4.0–1:22.0)]. Of the cohort, 21.8% had undetectable antibody titres at this time point, with another 5% revealing concentrations below the defined titer for protection of 1:5.

Distribution of Antibody Concentrations

Antibody concentration distribution was non- significantly higher concentrations in Mali ($t = 1.51$; $p = 0.13$) and showing generally low antibody tires 5–6 years post vaccination following a single dose of YF vaccine (**Supplementary Figure 1**).

Effect of Covariates on Antibody Concentration

Sex, season, country and time since vaccination did not affect the longevity of antibody concentration in uni- or multivariable regression models for antibody concentration as a continuous variable (**Table 2**).

The odds of maintaining an antibody concentration above 0.5 UI/mL was also unaffected by the sex, season of vaccination, country or time since vaccination (**Table 3**).

Similar findings were noted when the cut off for titres of ≥1:5 or 1:10 was applied.

DISCUSSION

The analysis of serum samples from 481 children vaccinated with one dose of YF vaccine in infancy showed that roughly 30% did not have protective antibody concentrations of 0.5 UI/ml (17) 5–6 years after vaccination. Most of this group had undetectable antibody concentrations (seronegative) and even where detectable, concentrations were below 0.1 IU/mL. This finding is concerning and may have significant implications for long term protection from YF in individuals who have received the YF vaccine as a single dose in the first year of life within EPI programs and in line with the current WHO recommendations.

By comparison, a small study in adults from the Netherlands who had received a fractional dose of YF vaccine demonstrated that 98% of the individuals vaccinated were still protected 10 years later (10), but the sample size of 40 individuals was small and represented only 48% of the original recipients of the vaccine (10). A more recent report followed up 349 Chinese adults

TABLE 2 | Association of covariates at time of vaccination with log2 anti-YF antibody concentrations.

		Univariable (crude)		Multivariable (adjusted)	
Covariate	**N**	**Coef. (95% CI)**	**p-value**	**Coef. (95% CI)**	**p-value**
Sex					
Male*	256	0.00 - -	–	0.00 - -	–
Female	224	0.02 (−0.15 to 0.20)	0.7767	0.03 (−0.15 to 0.20)	0.7590
Season					
Dry*	311	0.00 - -	–	1.00 - -	–
Rainy	170	0.02 (−0.16 to 0.20)	0.8479	0.02 (−0.16 to 0.20)	0.8239
Country					
Mali*	232	0.00 - -	–	0.00 - -	–
Gambia	179	−0.04 (−0.21 to 0.13)	0.6343	−0.04 (−0.21 to 0.13)	0.6270
Time since vaccination	–	0.07 (−0.19 to 0.34)	0.5798	0.08 (−0.18 to 0.34)	0.5656

*NB, Sex missing for 1 participant. *Reference stratum. N, number of observations; Coef, coeficient; 95% CI, 95% confidence interval. Results of separate uni- and multi-variable linear regression. Multi-variable model adjusted for, sex and season of vaccination and time since vaccination.*

TABLE 3 | Association of covariates at time of vaccination with recording a threshold of anti-YF antibody concentrations of 0.5 or more.

			Univariable (crude)		Multivariable (adjusted)	
Covariate	**N**	**Mean**	**OR (95% CI)**	***p*-value**	**OR (95% CI)**	**p-value**
Sex						
Male*	256	2.8	1.00 - -	–	1.00 - -	–
Female	224	3.0	1.12 (076–1.66)	0.5632	1.12 (0.75–1.65)	0.5846
Season						
Dry*	311	3.0	1.00 - -	–	1.00 - -	–
Rainy	170	2.8	0.21 (0.66–1.51)	0.9992	1.02 (0.68–1.54)	0.9102
Country						
Mali*	232	3.4	1.00 - -	–	1.00 - -	–
Gambia	179	2.5	1.20 (0.81–1.77)	0.3708	1.20 (0.81–1.77)	0.3652
Time since vaccination	–	–	1.05 (0.57–1.91)	0.8853	1.06 (0.58–1.92)	0.8510

*NB, Sex missing for 1 participant. *Reference stratum. N, number of observations; Coef, coeficient; 95% CI, 95% confidence interval. Results of separate uni- and multi-variable logistic regression. Multi-variable model adjusted for, sex and season of vaccination and time since vaccination.*

who had received YF vaccine prior to deployment to Africa and reported negligible concentrations 11 years post vaccination (12). Several other studies have demonstrated similar decline in antibody in adults at varied time points post vaccination (9, 11, 24–26). The findings following a fractional dose of YF vaccine in The Netherlands differ from ours with a larger proportion retaining protective concentration but are in keeping with other reports of declining antibody from adults. All of these data are generated from studies in adults, unlike the pediatric data presented here. In addition, the different geographical settings (Europe, Asia vs. YF endemic Africa) have no or different prior exposure and other environmental differences which could also play a role in acquisition and persistence of antibody. Natural exposure differs between non-endemic and endemic settings and potentially also between age groups.

Following a full dose of YF vaccine in US adults all individuals who received multiple doses of YF vaccine had protective concentrations, irrespective of the time since vaccination. When only one dose had been received however, 94% had protective concentrations if that dose was <10 years from testing. When tested 10 or more years later however, only 82% had protective concentrations (11). These findings would suggest that even in adults, booster vaccinations may be warranted in certain populations. This view was published in a recent opinion piece (8).

Only 69% of children in Brazil maintained protective concentrations 10 years after receiving a full vaccine dose (8, 9). To our knowledge there has only been one study on the African continent assessing antibody longevity in children. This recent study assessed longevity in children who had received YF vaccine as part of 2 randomized controlled clinical trials. The study similarly demonstrated a drastic decline of YF immunity in children vaccinated as infants even within the ideal clinical trial settings with 50.4% (4.5 years post vaccination) and 43.1% (6 years post vaccination) retaining seropositivity in Mali and Ghana, respectively (17). These findings may be compounded by several factors including natural disease exposure but in keeping with ours suggest a population of children vulnerable to YF infection several years post vaccination irrespective of setting where vaccine was received.

Given the limited data available on persistence of antibody to YF in children and previous similar findings, our findings are timely and have the potential to inform future discussions regarding policy for YF vaccine use. The data from Brazil however does not state the vaccine used and this information may be an important consideration for the longevity of vaccine response. Our cohorts received similar vaccines although we do not have data per individual for vaccines received.

The sex, season of vaccination and time since vaccination did not impact the longevity of anti-YF antibody concentration 5–6 years post vaccination. This is similar to findings from a US cohort of adult travelers 3–4 years post vaccination with YF vaccine prior to travel to endemic regions. The only factors associated with higher antibody concentrations 3–4 years post vaccination were early onset of detection and higher antibody concentration 1-month post vaccination (27). These were not variables available for our analysis. In African studies sex was also not found to contribute to seropositivity (17).

LIMITATIONS

The precise age at vaccination of our cohort (no date of birth records available) and anthropometric measures at time of vaccination were unknown and could have impact on the longevity of antibody. There may also be limitations within the EPI system ranging from cold chain maintenance to vaccine delivery methods that could have affected our results. Given the similarity of our findings with those from children vaccinated in ideal clinical trial settings however (17), this is unlikely.

CONCLUSION

As identified by WHO there is a need to gather evidence around the potential need for booster vaccination with YF vaccine whether this follows full or fractional doses in children and adults (4, 5, 28). This knowledge needs to be consolidated to guide future vaccination policy. Our findings suggest that children in this region of sub-Saharan Africa may require booster doses due at least by school entry age. Additional studies that explore antibody functionality and not just quantity would also be warranted as the function and not just the quantity of antibody is likely to mediate protection.

DATA AVAILABILITY STATEMENT

All datasets generated for this study are included in the article/**Supplementary Material**.

ETHICS STATEMENT

The initial and current studies involving human participants were reviewed and approved by Medical Research Council Unit The Gambia/Gambian Government Joint ethics Committee and Comité d'éthique de la Faculté de médecine de pharmacie et d'odonto-stomatologie (FMPOS), Bamako, Mali. Written informed consent to participate in the the original study as well as consent for future use of banked samples was provided by the participants' legal guardian/parent.

AUTHOR CONTRIBUTIONS

OI conceived the study and performed the statistical analysis and drafted the manuscript. CD led the performance of the laboratory assays and critically reviewed the manuscript content. OI, BK, SS, and MT led recruitment of participants for the original studies and reviewed the manuscript. ES provided support for statistical analysis and critically reviewed manuscript content. CG and BK supported analysis and critically reviewed the manuscript. All authors contributed to the article and approved the submitted version.

FUNDING

Funding for the analysis of YF titres in the stored sera was received from the Wellcome Trust Institutional Strategic Support Fund to OI under the Imperial College Global Health Clinical Fellowship Scheme (Grant Ref PS2874_WMNP). The original MenAfriVac clinical trials in which these samples were collected were funded by grants to Program for Appropriate Technology in Health (PATH) from the Bill and Melinda Gates Foundation. The funders played no role in study design, data collection, data analysis, data interpretation or manuscript preparation. This MRCUG at LSHTM is jointly funded by the UK Medical Research Council (MRC) and the UK Department for International Development (DFID) under the MRC/DFID Concordat agreement and is also part of the EDCTP2 programme supported by the European Union. BK was supported by grants from UKRI (MC_UP_A900/1122, MC_UP_A900/115) and the IMmunising PRegnant women and INfants neTwork (IMPRINT) funded by the GCRF Networks in Vaccines Research and Development which was co-funded by the MRC and BBSRC.

ACKNOWLEDGMENTS

The authors acknowledge the study participants and communities as well as all staff of the original trials. The authors are grateful to the Meningitis Vaccine Project for its guidance and administrative support in facilitating access to the biological samples and accompanying data in agreement with PATH. The samples and previous data were collected in the course of the MenAfriVac trials supported by grants from the Bill and Melinda Gates Foundation (to PATH). We are also grateful to the Wellcome Trust Institutional Strategic Support fund to OI for funding this analysis.

SUPPLEMENTARY MATERIAL

The Supplementary Material for this article can be found online at: https://www.frontiersin.org/articles/10.3389/fimmu.2020.577751/full#supplementary-material

Supplementary Figure 1 | Distribution if anti-YF antibody concentration by Country. Kernel density: non-parametric estimation of probability density function of anti-YF concentration. NB: *P*-value for difference in antibody concentration between countries = 0.1348.

REFERENCES

1. SAGE Working Group. *Background Paper on Yellow Fever Vaccine* (2013). Available online at: https://www.mesvaccins.net/textes/1_Background_Paper_Yellow_Fever_Vaccines.pdf
2. WHO. *Recommended Routine Immunizations for Children* (2020). Available online at: https://www.who.int/immunization/policy/immunization_tables/en/
3. Kollmann TR, Marchant A. Towards predicting protective vaccine responses in the very young. *Trends Immunol.* (2016) 37:523–34. doi: 10.1016/j.it.2016.05.005
4. WHO. Vaccines and vaccination against yellow fever: WHO Position Paper, June 2013–recommendations. *Vaccine.* (2015) 33:76–7. doi: 10.1016/j.vaccine.2014.05.040
5. World Health O. WHO position on the use of fractional doses - June 2017, addendum to vaccines and vaccination against yellow fever WHO: Position paper - June 2013. *Vaccine.* (2017) 35:5751–2. doi: 10.1016/j.vaccine.2017.06.087
6. WHO. Vaccines and vaccination against yellow fever. *Wkly Epidemiol Rec.* (2013) 88(27):269-83.
7. WHO. Eliminate Yellow fever Epidemics (EYE): a global strategy, 2017-2026. *Wkly Epidemiol Rec.* (2017) 92:193–204.
8. Plotkin SA. Ten yearly yellow fever booster vaccinations may still be justified. *J Travel Med.* (2018) 25:1–2. doi: 10.1093/jtm/tay130
9. de Melo AB, da Silva Mda P, Magalhaes MC, Gonzales Gil LH, Freese de Carvalho EM, Braga-Neto UM, et al. Description of a prospective 17DD yellow fever vaccine cohort in Recife, Brazil. *Am J Trop Med Hyg.* (2011) 85:739–47. doi: 10.4269/ajtmh.2011.10-0496
10. Roukens AHE, van Halem K, de Visser AW, Visser LG. Long-term protection after fractional-dose yellow fever vaccination: follow-up study of a randomized, controlled, noninferiority trial. *Ann Intern Med.* (2018) 169:761–5. doi: 10.7326/M18-1529
11. Lindsey NP, Horiuchi KA, Fulton C, Panella AJ, Kosoy OI, Velez JO, et al. Persistence of yellow fever virus-specific neutralizing antibodies after vaccination among US travellers. *J Travel Med.* (2018) 25:1–12. doi: 10.1093/jtm/tay108
12. Jia Q, Jia C, Liu Y, Yang Y, Qi J, Tong L, et al. Clinical evidence for the immunogenicity and immune persistence of vaccination with yellow fever virus strain 17D in Chinese peacekeepers deployed to Africa. *Antiviral Res.* (2019) 162:1–4. doi: 10.1016/j.antiviral.2018.12.001
13. Idoko OT, Mohammed N, Ansah P, Hodgson A, Tapia MD, Sow SO, et al. Antibody responses to yellow fever vaccine in 9 to 11-month-old Malian and Ghanaian children. *Exp Rev Vaccines.* (2019) 18:867–75. doi: 10.1080/14760584.2019.1640118
14. Collaborative Group for Studies of Yellow Fever Vaccines. A randomised double-blind clinical trial of two yellow fever vaccines prepared with substrains 17DD and 17D-213/77 in children nine-23 months old. *Mem Inst Oswaldo Cruz.* (2015) 110:771–80. doi: 10.1590/0074-02760150176
15. Nascimento Silva JR, Camacho LA, Siqueira MM, Freire Mde S, Castro YP, Maia Mde L, et al. Mutual interference on the immune response to yellow fever vaccine and a combined vaccine against measles, mumps and rubella. *Vaccine.* (2011) 29:6327–34. doi: 10.1016/j.vaccine.2011.05.019
16. Roy Chowdhury P, Meier C, Laraway H, Tang Y, Hodgson A, Sow SO, et al. Immunogenicity of yellow fever vaccine coadministered with menafrivac in healthy infants in Ghana and Mali. *Clin Infect Dis.* (2015) 61 (Suppl. 5):S586–93. doi: 10.1093/cid/civ603
17. Domingo C, Fraissinet J, Ansah PO, Kelly C, Bhat N, Sow SO, et al. Long-term immunity against yellow fever in children vaccinated during infancy: a longitudinal cohort study. *Lancet Infect Dis.* (2019) 19:1363–70. doi: 10.2139/ssrn.3346514
18. Sow SO, Okoko BJ, Diallo A, Viviani S, Borrow R, Carlone G, et al. Immunogenicity and safety of a meningococcal A conjugate vaccine in Africans. *N Engl J Med.* (2011) 364:2293–304. doi: 10.1056/NEJMoa1003812
19. Plotkin SA. Correlates of protection induced by vaccination. *Clin Vaccine Immunol.* (2010) 17:1055–65. doi: 10.1128/CVI.00131-10
20. Wieten RW, Jonker EF, van Leeuwen EM, Remmerswaal EB, Ten Berge IJ, de Visser AW, et al. A single 17D yellow fever vaccination provides lifelong immunity; characterization of yellow-fever-specific neutralizing antibody and T-cell responses after vaccination. *PLoS ONE.* (2016) 11:e0149871. doi: 10.1371/journal.pone.0149871
21. de Menezes Martins R, Maia MLS, de Lima SMB, de Noronha TG, Xavier JR, Camacho LAB, et al. Duration of post-vaccination immunity to yellow fever in volunteers eight years after a dose-response study. *Vaccine.* (2018) 36:4112–7. doi: 10.1016/j.vaccine.2018.05.041
22. Campi-Azevedo AC, de Almeida Estevam P, Coelho-Dos-Reis JG, Peruhype-Magalhaes V, Villela-Rezende G, Quaresma PF, et al. Subdoses of 17DD yellow fever vaccine elicit equivalent virological/immunological kinetics timeline. *BMC Infect Dis.* (2014) 14:391. doi: 10.1186/1471-2334-14-391
23. StataCorp. *Stata Statistical Software: Release 14.* College Station, TX: StataCorp LP (2015).
24. Niedrig M, Lademann M, Emmerich P, Lafrenz M. Assessment of IgG antibodies against yellow fever virus after vaccination with 17D by different assays: neutralization test, haemagglutination inhibition test, immunofluorescence assay and ELISA. *Trop Med Int Health.* (1999) 4:867–71. doi: 10.1046/j.1365-3156.1999.00496.x
25. Groot H, Riberiro RB. Neutralizing and haemagglutination-inhibiting antibodies to yellow fever 17 years after vaccination with 17D vaccine. *Bull World Health Organ.* (1962) 27:699–707.
26. Collaborative Group for Studies on Yellow Fever Vaccines. Duration of post-vaccination immunity against yellow fever in adults. *Vaccine.* (2014) 32:4977–84. doi: 10.1016/j.vaccine.2014.07.021
27. Gibney KB, Edupuganti S, Panella AJ, Kosoy OI, Delorey MJ, Lanciotti RS, et al. Detection of anti-yellow fever virus immunoglobulin m antibodies at 3-4 years following yellow fever vaccination. *Am J Trop Med Hyg.* (2012) 87:1112–5. doi: 10.4269/ajtmh.2012.12-0182
28. Vannice KS, Keita M, Sow SO, Durbin AP, Omer SB, Moulton LH, et al. Active Surveillance for adverse events after a mass vaccination campaign with a group A Meningococcal Conjugate Vaccine (PsA-TT) in Mali. *Clin Infect Dis.* (2015) 61 (Suppl. 5):S493–500. doi: 10.1093/cid/civ497

Conflict of Interest: The authors declare that the research was conducted in the absence of any commercial or financial relationships that could be construed as a potential conflict of interest.

frontiers in Immunology

REVIEW
published: 15 October 2020
doi: 10.3389/fimmu.2020.590373

Towards Precision Vaccines: Lessons From the Second International Precision Vaccines Conference

Dheeraj Soni[1,2], *Simon D. Van Haren*[1,2], *Olubukola T. Idoko*[1,3], *Jay T. Evans*[4], *Joann Diray-Arce*[1,2,5], *David J. Dowling*[1,2] *and Ofer Levy*[1,2,5]*

[1] Precision Vaccines Program, Division of Infectious Diseases, Boston Children's Hospital, Boston, MA, United States, [2] Department of Pediatrics, Harvard Medical School, Boston, MA, United States, [3] Vaccine Centre, London School of Hygiene and Tropical Medicine, London, United Kingdom, [4] Center for Translational Medicine, University of Montana, Missoula, MT, United States, [5] Broad Institute of MIT & Harvard, Cambridge, MA, United States

OPEN ACCESS

Edited by:
Urszula Krzych,
Walter Reed Army Institute of Research, United States

Reviewed by:
Geert Leroux-Roels,
Ghent University, Belgium
Mariusz Skwarczynski,
The University of Queensland, Australia
Benjamin Mordmüller,
Tübingen University Hospital, Germany

***Correspondence:**
Ofer Levy
ofer.levy@childrens.harvard.edu

Specialty section:
This article was submitted to Vaccines and Molecular Therapeutics, a section of the journal Frontiers in Immunology

Received: 01 August 2020
Accepted: 23 September 2020
Published: 15 October 2020

Citation:
Soni D, Van Haren SD, Idoko OT, Evans JT, Diray-Arce J, Dowling DJ and Levy O (2020) Towards Precision Vaccines: Lessons From the Second International Precision Vaccines Conference. Front. Immunol. 11:590373. doi: 10.3389/fimmu.2020.590373

Other than clean drinking water, vaccines have been the most effective public health intervention in human history, yet their full potential is still untapped. To date, vaccine development has been largely limited to empirical approaches focused on infectious diseases and has targeted entire populations, potentially disregarding distinct immunity in vulnerable populations such as infants, elders, and the immunocompromised. Over the past few decades innovations in genetic engineering, adjuvant discovery, formulation science, and systems biology have fueled rapid advances in vaccine research poised to consider demographic factors (*e.g.*, age, sex, genetics, and epigenetics) in vaccine discovery and development. Current efforts are focused on leveraging novel approaches to vaccine discovery and development to optimize vaccinal antigen and, as needed, adjuvant systems to enhance vaccine immunogenicity while maintaining safety. These approaches are ushering in an era of precision vaccinology aimed at tailoring immunization for vulnerable populations with distinct immunity. To foster collaboration among leading vaccinologists, government, policy makers, industry partners, and funders from around the world, the *Precision Vaccines Program* at Boston Children's Hospital hosted the 2nd International Precision Vaccines Conference (IPVC) at Harvard Medical School on the 17th–18th October 2019. The conference convened experts in vaccinology, including vaccine formulation and adjuvantation, immunology, cell signaling, systems biology, biostatistics, bioinformatics, as well as vaccines for non-infectious indications such as cancer and opioid use disorder. Herein we review highlights from the 2nd IPVC and discuss key concepts in the field of precision vaccines.

Keywords: precision vaccines, systems biology, International Precision Vaccines Conference, vaccinologists, non-infectious diseases, adjuvants, formulations, vulnerable populations

INTRODUCTION

Vaccines remain the most effective public health intervention to reduce the burden of infectious diseases. However, several factors can influence and ultimately alter the efficacy of vaccines. These include differences in immune status (*e.g.* healthy *vs* immunocompromised individuals), sex, and age (*e.g.* newborn/infant *vs* adult *vs* elderly) (1). The significance of this disparity is illustrated by the relatively high burden of infections at the young and the elderly compared with middle-aged adults. Furthermore, newborn and young infants (<6 months of age) display distinctions in immune cell functionality that creates a "window of vulnerability", making some vaccines less effective in this group as compared to the same strategies used later in life (2, 3). In addition, there are numerous other factors which may influence immune responses and consequently affect vaccine efficacy. These can be circadian and circannual rhythms as well as geographical location which can correspond to individuals with distinct genetic and epigenetic backgrounds (4). It is imperative to consider this multitude of factors for developing vaccines that target pathogens endemic to specific geographical area. Finally, in considering vaccine (self-) adjuvantation, whole, live microorganisms activate distinct immune responses that are typically more robust than those induced by individual adjuvants (5, 6). The use of optimized adjuvanted vaccine formulations targeted to a given population may overcome barriers in vaccine development and match or even exceed pathogens in eliciting effective immune responses (7).

To discuss strategies and foster synergies in vaccine development, a community of experts from a range of fields, including immunology, pediatrics, vaccinology, systems biology utilizing powerful big data ("OMIC") approaches, as well as vaccine adjuvantation and formulation, gathered at the Joseph B. Martin Conference Center at Harvard Medical School (Boston, MA, USA) on the 17th and 18th October 2019 for the 2nd biennial International Precision Vaccines Conference (IPVC) (**Figure 1**). The following sections report highlights from the conference followed by key concepts in the field of precision vaccines.

Precision Vaccines Program

After brief welcoming remarks from Dr. Gary R. Fleisher (Department of Medicine, Boston Children's Hospital and Harvard Medical School, Boston, MA, USA), Dr. Ofer Levy (*Precision Vaccines Program*, Boston Children's Hospital and Harvard Medical School, Boston, MA, USA) introduced the *Precision Vaccines Program* (PVP) that sponsored the conference (http://www.childrenshospital.org/research-and-innovation/research/departments/medicine/precision-vaccines-program). Based in the Division of Infectious Diseases at Boston Children's Hospital, the PVP fosters international collaboration to characterize distinct vaccine-induced immune responses of vulnerable populations such as the very young and the elderly to inform development of novel vaccines tailored to protect them. Program members have domain expertise in vaccinology, clinical trials, immunology, molecular biology, biostatistics, bioinformatics, and powerful big data ("OMIC") approaches.

Recent advances in genetics, molecular and systems biology, as well as in translational medicine have informed a precision medicine strategy for defining subpopulations of patients sharing similar characteristics and tailoring medical interventions

FIGURE 1 | Attendees of the 2nd biennial International Precision Vaccines Conference. The 2nd biennial IPVC (17th and 18th October 2019), sponsored by the Boston Children's Hospital *Precision Vaccines Program*, was held at the Joseph B. Martin Conference Center at Harvard Medical School (Boston, MA, USA).

according to a patient's responsiveness. The use of this approach in vaccinology, further enhanced by advances in immune ontogeny studies and human *in vitro* culture systems, as well as in adjuvantation and formulation science, is paving the way for the development of precision vaccines. These are defined as vaccines that (i) consider the target population; (ii) are formulated to selectively activate the immune system by targeting specific anatomic sites, cells, and pathways that generate a protective response; and (iii) may, as needed, contain adjuvantation systems known to optimally enhance immunogenicity in a target population. In order to accomplish this complex and crucial task, systems biology methodologies such as transcriptomics, proteomics, and metabolomics as well as preclinical human *in vitro* models that consider age- and sex-specific differences can be leveraged to generate hypotheses to be tested in appropriate animal models and eventually in targeted clinical trials. Key to the success of this approach is interdisciplinary collaboration such as that catalyzed by the PVP and IPVC.

Since the 1st IPVC held in 2017 (8), PVP has experienced a marked growth, including (a) a robust Precision Vaccines Network now >400 individuals from academia, government, and industry, (b) growth in the scope of our collaborative systems biology and immune ontogeny studies on vaccines against hepatitis B, influenza, HIV, RSV and pertussis as well as opioid overdose, and (c) a growing stream of innovation in discovery and development of adjuvants and adjuvanted vaccines.

This 2nd Biennial Precision Vaccines Conference served as a platform to foster international collaboration for developing vaccines tailored to distinct and vulnerable populations such as the young and elderly. The target audience included academic-, government-, and industry-based physicians, scientists, and trainees interested in developing vaccines for vulnerable populations.

Horizon for New Vaccine Development

Dr. Stanley A. Plotkin (University of Pennsylvania, Philadelphia, USA) opened the conference by emphasizing the need for precision vaccinology. Dr. Plotkin highlighted widely used approaches for developing attenuated (*i.e.* physical changes or passage in animals/eggs/cell culture) and inactivated (killed whole organisms and utilizing polysaccharides or purified proteins) vaccines (9). However, growing knowledge in the field of vaccinology has established that host genetics also plays a vital role in vaccine responses, therefore, to tackle new complex problems we need to utilize innovative strategies. Attenuated vaccines include temperature-sensitive mutations and reassortment, viral recombinants and deletion mutants, codon de-optimization, microRNA insertion, and replication vectors that present genes from pathogens. Novel strategies for developing inactivated vaccines include DNA plasmids, mRNA, reverse vaccinology, antigen identification by transcriptomics and proteomics, structural analysis, adjuvants, and induction of innate immunity. Dr. Plotkin highlighted the importance of systems biology approach for a rational vaccine design (10). In addition, he identified currently unsolved problems in vaccinology including (a) immune memory; (b) multiplicity of virulence antigens in complex pathogens; (c) multiple HLA types; (d) conserved epitopes; (e) finding correlates of protection; (f) immaturity and post-maturity of the immune system; (g) mucosal immunization with non-replicating antigens; (h) adjuvants capable of selectively expanding cell types; and (i) the challenge of generating T-cell immunity without replicating vaccines. The possible solutions include (a) enhancing stimulation Tfh cells and induction of innate immunity by TLR agonists; (b) analysis of natural immune responses *i.e.*, "antigenomics"; (c) developing polyepitope vaccines; (d) utilizing structural biology; (e) systems biological approaches; (f) cytokine modulation; (g) formulation approaches, specifically nanoemulsions; (h) using single or combined TLR ligands; and (i) utilizing toolbox of adjuvants; respectively (11). Many of these problems along with their potential solutions were discussed in detail during the conference.

Dr. Dan Barouch (Center for Virology and Vaccine Research at Beth Israel Deaconess Medical Center; Harvard Medical School) provided an overview of the recent progress in preclinical to clinical development of HIV vaccines. Although significant progress has been made with dozens of highly effective anti-HIV drugs available to control the infection, there is an unmet need for an HIV vaccine to effectively address the growing HIV/AIDS pandemic (12). Dr. Barouch provided an update on currently ongoing efficacy trials for two HIV-1 vaccine candidates and a broadly neutralizing mAb. The strategy for a global prophylactic HIV-1 vaccine includes the use of: a) vectors that elicit potent immune responses in individuals irrespective of their spatial location, b) bioinformatically engineered antigens (a.k.a mosaic antigens) to improve immunologic coverage of global virus diversity, and c) envelope proteins to increase humoral immunity. These trials are based on the foundation of precision vaccines, with the ultimate aim of identifying immune responses which would aid in protection against the infection (13). He presented work on mosaic HIV-1 vaccines (*i.e.* Ad26/Env) which provided up to 40–67% protection against SIVmac251 and SHIV-SF162P3 challenges in non-human primates (NHPs). In addition, adoptive transfer of purified IgG from Ad26/Env vaccinated NHPs provided protective efficacy against SIVmac251 challenges (13, 14). Since these data suggest that functional antiviral antibodies are responsible for protection against SIVmac251 in NHPs, current ongoing studies involving phase-2b/3 clinical efficacy trials are aimed at evaluating the efficacy of functional antiviral antibodies for protection in humans against HIV-1.

Vaccines for Vulnerable Populations: Ontogeny and Immunodeficiency

Dr. Richard Malley (Boston Children's Hospital; Harvard Medical School; Affinivax) provided an overview of the novel vaccine platform named multiple antigen presenting system (MAPS) and highlighted an example of it's application to develop vaccines against *Staphylococcus aureus*. His earlier research focused on developing broad serotype-independent protection against pneumococcal disease identified three key challenges: a) serotype replacement, b) cost (complex and

difficult to manufacture vaccine), and c) immunogenicity does not always imply clinical efficacy (15). Although killed whole cell vaccine (WCV) is cheaper to manufacture and addresses serotype replacement, it comes with distinct challenges such as a) growing hesitancy for WCVs in vulnerable populations (*i.e.* infants), b) inapplicability to a variety of pathogens, and c) high immunogenicity due to particulate nature of WCVs. Therefore, Dr. Malley et al. have developed MAPS which induces broader responses (both B-cell and T-cell) with several potential immunological, technological, and financial advantages (16). MAPS enables the creation of a macromolecular complex that mimics the properties of WCVs by integrating various antigen components (including proteins and polysaccharides) within the same construct to aid in inducing multipronged immune responses including, Th1 and Th17 responses (16).

Dr. Paolo Palma (Bambino Gesù Children's Hospital, Rome, Italy) highlighted how vaccination coverage is lower in vulnerable populations (VPs) and/or individuals with chronic conditions, particularly due to lack of safety and immunogenicity data in the specific populations. However, research in the past decade has led to the switching of vaccine development from empirical to a personalized vaccinology approach, which promises to advance effective treatments for VPs. Dr. Palma's laboratory has made several observations emphasizing that correlates of protection in individuals with transplants (17) or chronic conditions (such as HIV-infection) are significantly different from the healthy individuals (18–20). In conclusion, he highlighted the virtuous circle of precision vaccinology which involves data collection from existing cohorts, data modeling of VPs, development of a harmonized OMICs platform, vaccine trials in VPs and identification of novel biomarkers of immunogenicity and safety to tailor vaccine intervention to those who may most benefit from its considerable promise (21).

Trained/Heterologous Immunity

Dr. Christine Benn (Statens Serum Institut; Denmark) discussed research activities from the Bandim Health Project in Guinea-Bissau and the Danish Institute for Advanced Studies, University of Southern Denmark (22). This included the non-specific (heterologous) effects of vaccines in Africa and Europe (23). She discussed how non-specific effects of vaccines on other diseases may impact overall health and the differences between these effects apparently related to the differential effects of live (*e.g.*, BCG) *vs* non-live [*e.g.*, diphtheria–tetanus–pertussis (DTP)] vaccines. Her studies have suggested that live vaccines tend to induce beneficial overall non-specific effects, whereas non-live vaccines tend to induce negative non-specific effects, especially in girls. She emphasized the urgent need for a better understanding of the mechanisms underlying non-specific vaccine effects (24). She highlighted that current vaccines are largely understood within the framework of their specific effects and that a real-life assessment of overall effects of vaccines is urgently needed. She viewed the following as key to developing new vaccines: a) test vaccines *vs* true placebo and studying overall health effects pre-licensure b) randomized implementation, c) developing methods for post-licensure evaluation, d) developing live vaccines or artificially mimicking effect of live vaccines; and e) changing focus from preventing single diseases towards enhancing overall host health.

Dr. David J. Dowling (PVP, Boston Children's Hospital; Harvard Medical School) presented an overview of ongoing work within the PVP to exploit the concepts of trained/heterologous immunity into next generation adjuvanted vaccine formulations (25, 26). Adjuvantation is a key approach to enhancing vaccine immunogenicity (27). For example, Dr. Dowling highlighted the need to characterize the mechanisms underlying heterologous immunological responses elicited by the BCG vaccine (28) to inform rational design of synthetic formulations that mimic BCG's heterologous beneficial effects while avoiding and improving upon its shortcomings (29). Both the immunological pathways and duration of immunostimulation elicited by BCG vaccination have been linked to its efficacy as a neonatal vaccine. As such, study of BCG-induced innate memory may inform discovery and development of novel vaccine adjuvants. In addition, he reviewed prior work from the PVP in which a) BCG was shown to act as an adjuvant, in an age- and formulation-specific fashion (30), b) BCG formulations are not uniform (31) and c) TLR8 may mediate BCG vaccine-induced protection, and TLR8 agonist-containing nanoparticle delivery systems designed to mimic BCG efficiently induce trained immunity in newborn mice (32).

Clinical Aspects

This session included discussions on clinical considerations in vaccinology and highlighted research activities from the speakers from their research studies across the globe.

Dr. Lindsey Baden (Brigham and Women's Hospital; Dana Farber Cancer Institute; Harvard Medical School; Ragon Institute of MGH, MIT and Harvard) highlighted the challenges in vaccine development for various vaccines currently in trials. These challenges include inadequate knowledge of correlates of protection for novel vaccines, the need to optimize a range of factors for optimal immunogenicity, including dose, schedule, route, delivery system, and adjuvants to elicit potent immune responses, as well as global diversity and vaccine manufacturing. He highlighted how several HIV vaccine trials to date have failed to demonstrate beneficial efficacy (33, 34). In addition, he discussed the development of Mosaic Ad26/Env HIV-1 vaccine which is a multi-year study in collaboration with Dr. Dan Barouch and is currently advanced to Phase 3 trial (13). Dr. Baden also shared data from multiple studies including CMV (35) and cholera (36) vaccines, to highlight the need for leveraging a proper model for vaccine developing since: a) different pathogens pose very different challenges, b) both science and product development can occur simultaneously, and c) developing proper models or surrogates with clinical meaning facilitates rapid iteration along with informing the meaning of immunologic parameters measured.

Dr. Nadine Rouphael (Emory University, Atlanta, USA) highlighted the research conducted at Hope Clinic Mission of Emory University aimed at translating basic research discoveries to clinical advances. This included research targeted at unravelling the differences in vaccine responses based on age, environmental conditions (*e.g.*, role of stress, diet, infection, microbiome) and genetic differences (37). In addition, she

highlighted the potential of systems vaccinology in probing diversity among human immune systems, by delineating the impact of the genes, the environment, and the microbiome on vaccination-induced protective immunity. Such insights are crucial, for example, for optimizing vaccines for immune-compromised populations (38).

Dr. Olubukola Idoko (PVP; Medical Research Council, The Gambia) highlighted research from the Medical Research Council Unit at the London School of Hygiene and Tropical Medicine in The Gambia (West Africa), including the long-standing contributions to pneumococcal vaccine and epidemiology research, spanning 40 years. She highlighted some challenges with conducting trials in the developing world including the challenges of obtaining informed consent on account of linguistic diversity and the limited clinical and trial facilities, while stressing the need for trials in these settings particularly as evidence indicates that vaccines work differently in different settings. She presented an example of markedly varied responses to yellow fever vaccine in two West African settings and the absence of any demonstrable antibodies to yellow fever 5–6 years post vaccination in 20% of a cohort of African infants (39).

Approaches to Enhance Vaccinology

Systems Biology

For the past decades, systems biology approaches have increased our understanding of molecular interactions in biological systems (40). High throughput technologies such as different 'omics' modalities have enabled interrogation of vital biological processes within the immune system and holistic prediction of system behaviors (41, 42). Systems vaccinology alludes to the application of systems biology to study vaccine discovery, development, and immunogenicity. Immune signatures measured prior to and after vaccination enable predicting modulated targets and inform optimized vaccination strategies (43). Systems biology experts at the IPVC elucidated how this approach can provide insight into the mechanisms of vaccine immunogenicity.

Dr John Tsang (NIH Center of Human Immunology and Multiscale Systems Biology Section NIAID, NIH, Bethesda, USA) presented the relationship of pre-*vs* post-vaccination neutralizing antibody titers as a variable characteristic in human immune responses (44, 45). He explained that while genetics could partially explain phenotypic variability in early life, additional non-genetic factors contribute to the complex state of individual human immunity. Machine learning techniques can be applied to build predictive models and uncover biologically relevant parameters such as the quality and quantity of an immune response following an intervention such as immunization. Dr. Tsang reiterated that one distinct advantage of the human model is having substantial population variations to power correlation analyses (46). His work on global analyses of human immune variation found that baseline predicts antibody responses independent of age and pre-existing antibody titers using pre-perturbation cell populations (44). These findings suggest that baseline differences between individuals may be a key determinant of distinct individual responses to an intervention providing a resource for studying human immunity in health and disease.

Dr. Scott Tebbutt (University of British Columbia; PROOF Center, Vancouver, BC, Canada) introduced the concept of multivariate methods for single and integrative multi-omics supervised analyses. He outlined his team's involvement with the Human Vaccine Project for Hepatitis B vaccination and Varicella Zoster vaccination study in adults using multiple systems biology techniques. Since the scale of these studies is enormous, combining datasets enables identification of systems biology features that are broadly predictive of antibody response. He found that combined datasets without scaling and batch correction resulted only in modest performance, while scaled/ComBat-corrected concatenated datasets were ten times improved with performance. The study revealed genes relating to T-cell regulated biology as the top enriched pathway. A single gene feature RAB11 Family interacting protein 5 (RAB11FIP5) was identified as important for induction of broadly neutralizing antibodies by the *Shingrix* zoster vaccine. Their work on multi-integration models may help identify predictors of antibody responses to multiple vaccines.

Dr. Al Ozonoff (PVP, Boston Children's Hospital; Harvard Medical School) presented practical issues and solutions to digital infrastructure for systems biology. He outlined that responsibilities of the PVP-Data Management Core (PVP-DMC), which he leads, includes accurate and reliable data capture, secure project data management and analytic computing, and quality assurance. In addition to the importance of these approaches to achieving project's scientific goals, a successful computing infrastructure also enables a collaborative and integrative environment balancing centralized and de-centralized structures and processes. Data security is strictly ensured while striking a balance with data access to both computational savvy researchers and biologists without compromising data integrity. While cloud-based collaborative science is an attractive approach to collaborative systems biology studies, challenges and trade-offs should be discussed with collaborators early during project design.

Dr Madeleine Jennewein (Ragon Institute of MGH, MIT and Harvard) reported how systems serology is a powerful approach to dissect maternal antibody transfer to a newborn. Systems serology platform describes how biological samples lead to biophysical measurements of antigen-specific analyses as well as profiling the functional activities of numerous immune cells. Maternal vaccination protects neonates during the first year of life due to specialized antibody transfer across the placenta (47). The neonatal Fc receptor, FcRn, doesn't fully account for antibody transfer. Indeed, the placenta selectively transfers NK cell-activating antibodies to neonates to access functional neonatal innate immune cells. Differential antibody Fc-glycosylation controls antibody transfer across the placenta and neonatal NK cells appear to be highly responsive to immune complexes. These findings may inform vaccination strategies to control antibody glycosylation to optimize the beneficial impact of maternal vaccination.

Dr. Robert Hancock (University of British Columbia, Vancouver, BC, Canada) illustrated how systems immunology approaches such as protein–protein interactions can infer functional links to understand inflammation, immunity, and sepsis. He presented the massive gene expression changes that occur in the first week of life in Gambian newborns. His team developed a web-based tool *NetworkAnalyst* to comprehensively allow researchers to determine features and functions leading to generation of biological hypotheses (48). With this tool, the same themes and pathways relating to interferon signaling, complement, and neutrophil activity are present in Gambian and Papua New Guinean newborns in the first week of life. They also applied this tool to a transcriptomics study of pediatric appendicitis, discovering a large number of significant differentially expressed genes between perforated and simple appendicitis involved in immunoregulatory interactions between a lymphoid and non-lymphoid cell, neutrophil degranulation as well as interleukin and interferon signaling. Dr. Hancock highlighted his group's work on meta-analysis of sepsis biomarkers from 10 studies and found that early sepsis is associated with a diagnostic immune non-responsiveness gene expression signature related to immune cell reprogramming or endotoxin tolerance (49).

Dr. Jessica Lasky-Su (Channing Network Medicine, Brigham and Women's Hospital; Harvard Medical School) presented how the plasma metabolome affects asthma pathophysiology. She presented the Maternal Vitamin D Supplementation to Prevent Childhood Asthma (VDAART) trial that is assessing whether vitamin D supplementation in pregnant women can prevent the development of asthma and allergies in offspring (50). Vitamin D plays a critical role in immune responses that may reduce inflammation in the airways and the likelihood of developing an infection (51). The VDAART study follows pregnant women from 10 to 18 weeks and their offspring through 6 years of age specifically assessing asthma related outcomes. Her group is also participating in the Copenhagen Prospective Studies on Asthma in Childhood (COPSAC) study that found that maternal vitamin D reduces the risk of asthma and wheezes. From these studies they have identified maternal metabolites associated with asthma in offspring at ages 3 and 4 years including the asthma bronchodilator theophylline. The presence of caffeine was associated with lower odds of asthma at 3 years of age. Her group found that high concentrations of polyunsaturated fatty acid (PUFA) and Vitamin D were associated with a large reduction in asthma risk (52). They also identified a potential role in asthma of the sphingolipid biosynthesis regulator ORMDL3. A combination of absence of a high risk ORMDL3 allele together with vitamin D supplementation was associated with the lowest risk of asthma suggesting that ORMDL3 is a key regulator of sphingolipid biosynthesis.

Dr. Hanno Steen (PVP, Boston Children's Hospital; Harvard Medical School) reported on powerful sample sparing proteomic technologies that enable extraction of a deep proteome from sub-microliter volumes of plasma or serum. He outlined the objective to develop a plasma proteomics platform that is applicable to small samples, provides high throughput, and is cost efficient. He described a mass spectrometry-based workflow wherein as little as 0.3 µl of plasma or serum enables analysis to a robust analytical depth (53). He presented studies employing these methods to study small sample volumes in the context of immune ontogeny across the first week of life, Lyme Disease biomarker discovery as well as systems vaccinology to characterize responses to hepatitis B and influenza vaccines. This powerful and efficient approach is poised to make a positive impact across a wide range of studies in infectious diseases and vaccinology.

Vaccine Adjuvantation and Formulation

Vaccine adjuvants and formulation/delivery technologies have been a key driver in the advancement of modern vaccinology. For nearly 80 years aluminum salts were the only adjuvant included in FDA approved vaccines. This has changed in recent years with multiple vaccines containing new adjuvants approved including those with oil in water emulsions, such as MF59 and AS03 (54, 55), TLR agonists monophosphoryl lipid A and CpG (56, 57) and innovative adjuvant combinations including AS01 and AS04 (58, 59). Recent successes in the development and approval of new safe and effective adjuvants have changed the playing field and opened new doors for precision vaccines targeting vulnerable groups such as infants, elders, and immunocompromised populations. Experts at the 2nd biennial IPVC highlighted a number of new adjuvant and formulation systems being developed in laboratories across the world.

Dr. Dennis Christensen (Statens Serum Institut, Denmark) presented on the role of depot formulations in the induction of systemic and mucosal immunity (60). Dr. Christensen and colleagues previously reported the utility of "prime-pul" vaccination (IM prime followed by intrapulmonary boost) in generating both systemic and mucosal responses to a TB subunit vaccine (H56) in combination with CAF01 adjuvant (trehalose-6,6-dibehenate (TDB) liposomes) (61, 62). The mechanisms for this enhanced immunity have been further elucidated by evaluating the uptake of H56/CAF01 by APCs and lung epithelial/endothelial cells after prime-pull vaccination or prime (IM or intrapulmonary) vaccination alone. Compared to single vaccinations by either route, prime-pul vaccination enhanced vaccine uptake by pulmonary endothelial and epithelial cells as well as pulmonary and splenic APCs leading to stronger activation of lung-draining lymph node DCs. Thus, innate and adaptive responses can be differently controlled through the priming and booster route of vaccination, timing of vaccinations, and use of adjuvants. These observations suggest that both innate myeloid APCs and immune memory play a role in prime-boost vaccine responses, and different immunization strategies can be employed to alter vaccine-induced immunity.

Dr. Christopher Fox (Infectious Disease Research Institute, Seattle, USA) highlighted the identification, characterization and testing of conifer-derived polyprenols as an alternative to squalene in oil-in-water nanoemulsions. Oil-in-water emulsions (AS01 and MF59) have been widely used to enhance immunity in the elderly and young children with >200 million

doses administered to date. Squalene (derived from shark liver) is a major component in many oil-in-water nanoemulsions, including both AS01 and MF59 (54, 55), but very little is known about the structure–activity-relationship (SAR) for this important emulsifier. Dr. Fox reported that polyprenols derived from Siberian fir demonstrated favorable physiochemical properties in comparison to squalene and enhance immunity to an influenza virus vaccine in mice, ferrets, and pigs. Vaccine immunity was further enhanced in mice and ferrets with the addition of a synthetic TLR4-based adjuvant, GLA, to the polyprenol emulsion.

Dr. Simon van Haren (PVP; Boston Children's Hospital; Harvard Medical School) provided an update on the induction of neonatal Th1 and CD8 immunity to respiratory syncytial virus (RSV) using age-specific synergistic adjuvant combinations. Dr. Haren and the PVP team previously reported that newborn DCs are highly responsive to dual activation with trehalose-6,6-dibehenate (TDB), a Mincle receptor ligand and R848, and TLR7/8 ligand, driving a Th1 polarizing cytokine response (63). Dr. van Haren extended these published studies demonstrating that human cord blood derived DCs activated with R848 plus TDB synergistically activated signaling pathways that lead to antigen cross-presentation on MHC class I. The combination adjuvant (3M-052+TDB liposomes) was evaluated for adjuvant activity *in vivo* using the RSV pre-fusion F antigen. Administration of a vaccine including this dual-adjuvant liposome delivery system enhanced generation of antigen-specific Th1 cells and CD8+ T cells in newborn mice.

Signaling Pathways and *In Vitro* Modeling

Recent advances in the field of innate immunity have led to our increased understanding of mechanisms involved in vaccine-induced immunity, which has informed rational vaccine design (64, 65). Accordingly, dissecting innate immune signaling pathways along with improving *in vitro* models are crucial for characterization and evaluation of novel antigen and adjuvants.

Dr. Ivan Zanoni (Boston Children's Hospital; Harvard Medical School) presented work on how the physical properties of PAMPs govern the immune response. The activation of PRRs in innate immune cells by PAMPs or DAMPs is regarded as a crucial step for induction of adaptive immunity. Migratory dendritic cells (DCs) play an essential role in initiating antigen-dependent adaptive immune response. Dendritic cells dispersed throughout peripheral tissues sense the presence of microbial clues released during an infection, are activated, and migrate to the draining lymph node (dLN)—enabling a transfer of "information" from peripheral tissue to the dLN—where an antigen-dependent adaptive immune response against the pathogen is initiated. Activation of PRRs allows migration of DCs from the periphery into the draining lymph node (dLN) where they transfer the information from the inflamed/infected tissue into the dLN and thus trigger activation of T-cell and B-cell responses. In last few years, beside this antigen-dependent response in dLN, another event antigen-independent innate response in LN has been discovered. Several groups have shown that inflammation in the periphery enables migration of DCs that interact with stromal cells which allows for lymph node expansion to create physical space for T- and B-cells to proliferate and establishment of a pro-inflammatory milieu, sustain and allow a potent adaptive innate response. Dr. Zanoni's laboratory made the observation that although soluble fungal polysaccharides remain immune-silent in the periphery, they become potent immunogens in the dLN. These fungal moieties activate an immune response similar to viral infection, without any requirement for phagocyte migration. These observations highlight how the physical form of certain PAMPs impacts innate and adaptive immunity (66).

Dr. Leif Erik Sander (Charité University Hospital, Berlin, Germany) highlighted how recognition of microbial viability serves as a key driver of vaccine responses. Previous work by Dr. Sander established how murine antigen-presenting cells can discriminate living from dead bacteria (67, 68). In particular, microbial RNA can mimic microbial infections therefore highlighting the need to target nucleic acid sensing receptors to promote robust T-cell dependent immunity (69). Because these mRNAs are not found in dead bacteria, they belong to a special class of PAMPs, which have been termed "vita-PAMPs". Accordingly, live microbes activate multifaceted immune responses that facilitate long-lasting protective immunity. Future vaccine development pipelines may integrate vita-PAMP activation strategies to enhance immunization, especially for infectious diseases for which no current vaccine exists.

Vaccines for Non-infectious Indications

Dr. Joost Oppenheim (Center for Cancer Research, National Cancer Institute, NIH, USA) presented work on therapeutic vaccination for tumors in mice. Over the last 15 years, research from Dr. Oppenheim's lab and other groups have identified numerous cytokine-like products of cell which are constitutively present and, apart from functioning as danger signals, are involved in host defense, inflammation as well as repair mechanism, called pathogen-associated molecular pattern molecules (PAMPs) and damage-associated molecular pattern molecules (DAMPs). Both innate and adaptive immune responses are engaged by the alarmins' (PAMPs and DAMPs) activation of the dendritic cells (70). In particular, the alarmin HMGN1 (High Mobility Group Nucleosome Binding Domain 1) which intracellularly acts as non-histone chromosome protein that regulates chromatin remodeling and transcription of certain genes, on the contrary, extracellularly acts as antimicrobial and Th1-polarizing signal. HMGN1, which acts on TLR4 to induce DC migration and maturation, is therefore crucial for host defense mechanisms. Multiple studies from Dr. Oppenheim's group have shown how HMGN1 contributes to the generation of antitumor immunity and has therefore drawn interest as a potential target for antitumor therapy (71). They made the observation that synergistic effect of R848 (TLR7/8 agonist) along with HMGN1 (TLR4 agonist) leads to augmented IL-12 responses and phenotypic maturation of mouse bone marrow derived dendritic cells (BMDCs) (72). This led to the development of a therapeutic vaccine (TheraVac) combining HMGN1 and R848 plus a checkpoint inhibitor (Cytoxan), which is effective on large tumors in mice without use of exogenous tumor-associated antigen(s) (73).

Dr. Thomas Kosten (University of Houston, Texas) summarized his more than two decades of work on anti-addiction vaccines (74, 75). According to a 2018 substance use survey, ~165 million people aged ≥12 years in the USA (~60% of the population) were past month substance users (*e.g.*, tobacco, alcohol, or illicit drugs such as opioids). Substance use disorder (SUD) is a growing problem with severe outcomes such as overdose-related death, yet there are limited options presently available to overcome this issue. Anti-addiction vaccines are aimed at inducing antibodies against a given drug (*e.g.*, opioid) and trap it in the blood stream. These antibody–drug complexes are unable to enter the blood–brain barrier and are subsequently removed from the circulation, thereby making drugs non-reinforcing and also preventing overdose-related death due to respiratory suppression. Although there are no currently approved anti-addiction vaccines, limited safety concerns and advances in efficacy make anti-addiction vaccines a promising therapeutic strategy to counteract the increasing clinical burden of SUDs.

FUNDING PERSPECTIVES

A panel discussion regarding funding perspectives moderated by Dr. Ofer Levy included representatives from institutions that support vaccine research. Dr. Mary Marovich (Director of Vaccine Research Program; Division of AIDS, NIH) discussed NIH's current perspective on HIV vaccine development. This included NIH's current interest in potential vaccines which induce broadly neutralizing antibodies to target HIV, funded by the Pre-clinical Research and Development Branch (PRDB) and Vaccine Translational Research Branch (VTRB) portfolios.

Dr. Mercy PrabhuDas (Program Officer in the Division of Allergy, Immunology and Transplantation at NIAID, NIH) discussed the interest at NIAID in vaccine research tailored for vulnerable populations, including the Immunity in Neonates and Infants and the Immunity in the Elderly programs at NIAID.

Dr. David Kaufman (Chief Medical Officer at the Bill & Melinda Gates Medical Research Institute) discussed innovative approaches to accelerate discovery and development of vaccines for global populations in need, including utilizing systems immunology tools, molecular epidemiology studies, controlled human infection models, and adaptive trial designs to optimize vaccine dosing, as well as creation of more stringent and accurate go/no-go decision points.

TOWARDS PRECISION VACCINOLOGY

Vaccinology has largely been driven by an empiric paradigm that assumes that a given vaccine will work equally in all individuals. Accordingly, until recently, few vaccines had been specifically tailored to overcome the immunosenescence of aging or altered efficacy in immunocompromised individuals (76). Recent innovations in genetic engineering, human *in vitro* modeling, formulation science, and systems biology have fueled rapid advances in vaccine research that accounts for demographic factors (*e.g.*, age, sex, genetics, and epigenetics) in vaccine discovery and development. These novel approaches are being leveraged to discover and develop vaccinal antigens and, as needed, adjuvant systems to enhance vaccine immunogenicity while maintaining safety. The potential benefits of these research efforts can only be fully utilized if they also help promote vaccine confidence and are coupled with universal vaccine coverage (77). These approaches are ushering in an era of precision vaccinology aimed at tailoring immunization for vulnerable populations with distinct immunity (**Figure 2**). In 2004 Dr. Stanley Plotkin, referred to as the 'Godfather of Vaccinology', outlined the history of the first five revolutions in vaccinology and outlined some predictions for the next candidate "sixth revolution" (9). In the past two decades, advancements in novel *delivery systems* have led to remarkable improvements in vaccine translation, positioning it as a sixth revolution in vaccinology (26). During the conference's conclusion panel, he emphasized how the concept of precision vaccines represents the "seventh revolution" in vaccinology wherein the attention of vaccine development is focused on the individual (or group) rather than the herd. Specifically, instead of focusing on development of vaccines for use in large populations to control epidemic diseases the focus has now shifted to the individual characteristics of each vaccinee, including assessment of efficacy and safety of the vaccine on an individual basis. Indeed, some of the currently administered vaccines are not fully protective in specific populations (*e.g.*, influenza and mumps vaccine) (27, 78). An individual's characteristics such as prior exposure, priming, immune status (for live vaccines) are critical for efficacy of influenza vaccines. Additionally, multiple recent mumps outbreaks in colleges and closed-knit communities, including among vaccinated individuals (79), and lack of appropriate correlates of protection (80) have highlighted the need to develop vaccines in an individualistic manner. In regard to safety, rare severe reactions, such as Guillan–Barré Syndrome after exposure to influenza vaccine or virus and intussusception after rotavirus vaccination, still need to be addressed (78). Therefore, under rare circumstances, certain vaccines (*e.g.*, live vaccines) may be contraindicated in certain individuals, depending upon their immune disposition. He also highlighted the need to individualize adjuvants, referring to a recent example where an adjuvant system-03 (AS03; an oil-in-water emulsion adjuvant)-adjuvanted influenza vaccine was associated with increased risk for narcolepsy only for vaccinated populations in Scandinavia, suggesting population-specific vaccine effects (78). The Center for Disease Control (CDC) recently assessed safety data on adjuvanted pH1N1 vaccines (*arepanrix*-AS03, *Focetria*-MF59, and *Pandemrix*-AS03) from 10 global study sites and confirmed, other than the association for *arepanrix* in Scandinavia, lack of any detectable associations between the vaccines and narcolepsy (81). However, the phenomena observed in a particular population (Scandinavian study subjects) further emphasized the need for evaluation of adjuvanted vaccines in a population-specific manner to enhance safety and efficacy.

In conclusion, the second biennial IPVC 2019 reviewed and incorporated contemporary topics guiding the field of precision vaccines. As with any conference, there were areas that were important but not covered which may be potential topics for

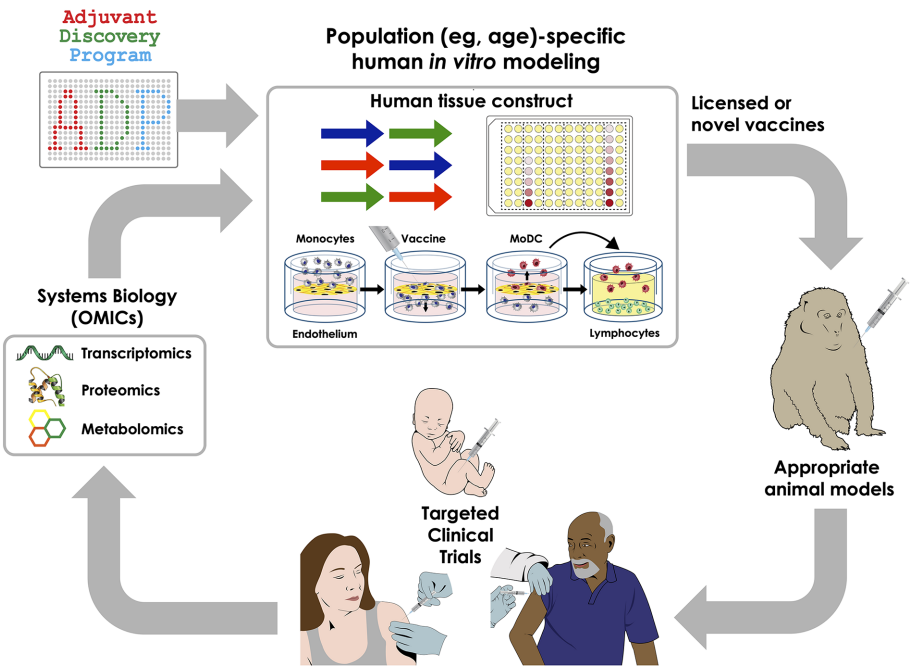

FIGURE 2 | Integrated approaches to precision vaccinology. Discovery and development of precision vaccines may include a series of sequential approaches including system biology analysis of biosamples from clinical trials to define vaccine-induced cellular and molecular signatures that correlate with immunogenicity, thereby generating new mechanistic hypotheses; use of human *in vitro* systems for hypothesis testing and targeted adjuvant discovery employing population-specific biosamples, selection of appropriate animal models and clinical trials in specific vulnerable populations.

discussion at the next IPVC (2021), including: A) measuring vaccine efficacy: despite our increased understanding of immune responses to infection, there is incomplete understanding of the immune responses specifically required for protection; B) implementation research that focuses on technical, managerial, financial, systems, socio-behavioral, and communication aspects to inform evidence-based policies and practices important for introduction of new vaccines and maintaining/expanding coverage for currently approved vaccines; C) vaccine access: wider global availability of affordable vaccines is required to curb preventable diseases; and D) vaccines for allergy: there is growing interest in utilizing vaccines for allergen-specific immunotherapy and for disease-modifying allergy therapy (82). The third International Precision Vaccines Conference, to be held on September 22nd and 23rd of 2021 at Harvard Medical School (Boston, MA, USA), will consider these and other areas by gathering a multidisciplinary community of scientists to review progress and encourage partnerships focused on the most current challenges and opportunities in precision vaccines research.

AUTHOR CONTRIBUTIONS

DS, SVH, OTI, JTE, JD-A, DD, and OL wrote the manuscript. OL edited the manuscript. All authors contributed to the article and approved the submitted version.

FUNDING

The PVP is supported in part by US National Institutes of Health (NIH)/National Institutes of Allergy and Infectious Diseases (NIAID) awards including Molecular Mechanisms of Combination Adjuvants (1U01AI124284-01), Adjuvant Discovery (HHSN272201400052C and 75N93019C00044) and Development (HHSN272201800047C) Program Contracts, and Human Immunology Project Consortium (HIPC) U19AI118608-01A1 to OL. DD's laboratory is supported by NIH grant 1R21AI137932-01A1 and Adjuvant Discovery Program contract 75N93019C00044 as well as by the BCH Department of Pediatrics and the Chief Scientific Office.

ACKNOWLEDGMENTS

We thank our fellow members of the Precision Vaccines Conference organizing committee, including Diana Vo and Bianca Dy, and all the members of the PVP for helpful discussions. The 2nd IPVC was supported in part by sponsorship from Pfizer, GlaxoSmithKline, Inimmune, Metabolon, Takeda, and Adjuvance as well as by an internal award from the Boston Children's Hospital Department of Pediatrics to the PVP. We are grateful to Kristin Johnson for the artwork depicted in **Figure 2**.

REFERENCES

1. Kollmann TR, Kampmann B, Mazmanian SK, Marchant A, Levy O. Protecting the Newborn and Young Infant from Infectious Diseases: Lessons from Immune Ontogeny. *Immunity* (2017) 46(3):350–63. doi: 10.1016/j.immuni.2017.03.009
2. Dowling DJ, Levy O. Ontogeny of early life immunity. *Trends Immunol* (2014) 35(7):299–310. doi: 10.1016/j.it.2014.04.007
3. Torow N, Hornef MW. The Neonatal Window of Opportunity: Setting the Stage for Life-Long Host-Microbial Interaction and Immune Homeostasis. *J Immunol* (2017) 198(2):557–63. doi: 10.4049/jimmunol.1601253
4. Kampmann B, Jones CE. Factors influencing innate immunity and vaccine responses in infancy. *Philos Trans R Soc Lond B Biol Sci* (2015) 370(1671). doi: 10.1098/rstb.2014.0148
5. Blander JM, Barbet G. Exploiting vita-PAMPs in vaccines. *Curr Opin Pharmacol* (2018) 41:128–36. doi: 10.1016/j.coph.2018.05.012
6. Ugolini M, Sander LE. Dead or alive: how the immune system detects microbial viability. *Curr Opin Immunol* (2019) 56:60–6. doi: 10.1016/j.coi.2018.09.018
7. Dowling DJ, Levy O. Pediatric Vaccine Adjuvants: Components of the Modern Vaccinologist's Toolbox. *Pediatr Infect Dis J* (2015) 34(12):1395–8. doi: 10.1097/INF.0000000000000893
8. Borriello F, van Haren SD, Levy O. First International Precision Vaccines Conference: Multidisciplinary Approaches to Next-Generation Vaccines. *mSphere* (2018) 3(4):e00214-18. doi: 10.1128/mSphere.00214-18
9. Plotkin SA. Six revolutions in vaccinology. *Pediatr Infect Dis J* (2005) 24(1):1–9. doi: 10.1097/01.inf.0000148933.08301.02
10. Koff WC, Burton DR, Johnson PR, Walker BD, King CR, Nabel GJ, et al. Accelerating next-generation vaccine development for global disease prevention. *Science* (2013) 340(6136):1232910. doi: 10.1126/science.1232910
11. Plotkin SA. Increasing Complexity of Vaccine Development. *J Infect Dis* (2015) 212 Suppl 1:S12–16. doi: 10.1093/infdis/jiu568
12. Fauci AS. An HIV Vaccine Is Essential for Ending the HIV/AIDS Pandemic. *JAMA* (2017) 318(16):1535–6. doi: 10.1001/jama.2017.13505
13. Barouch DH, Tomaka FL, Wegmann F, Stieh DJ, Alter G, Robb ML, et al. Evaluation of a mosaic HIV-1 vaccine in a multicentre, randomised, double-blind, placebo-controlled, phase 1/2a clinical trial (APPROACH) and in rhesus monkeys (NHP 13-19). *Lancet* (2018) 392(10143):232–43. doi: 10.1016/S0140-6736(18)31364-3
14. Barouch DH, Alter G, Broge T, Linde C, Ackerman ME, Brown EP, et al. Protective efficacy of adenovirus/protein vaccines against SIV challenges in rhesus monkeys. *Science* (2015) 349(6245):320–4. doi: 10.1126/science.aab3886
15. Moffitt KL, Malley R. Next generation pneumococcal vaccines. *Curr Opin Immunol* (2011) 23(3):407–13. doi: 10.1016/j.coi.2011.04.002
16. Zhang F, Lu YJ, Malley R. Multiple antigen-presenting system (MAPS) to induce comprehensive B- and T-cell immunity. *Proc Natl Acad Sci USA* (2013) 110(33):13564–9. doi: 10.1073/pnas.1307228110
17. Rocca S, Santilli V, Cotugno N, Concato C, Manno EC, Nocentini G, et al. Waning of vaccine-induced immunity to measles in kidney transplanted children. *Med (Baltimore)* (2016) 95(37):e4738. doi: 10.1097/MD.0000000000004738
18. Cagigi A, Rinaldi S, Di Martino A, Manno EC, Zangari P, Aquilani A, et al. Premature immune senescence during HIV-1 vertical infection relates with response to influenza vaccination. *J Allergy Clin Immunol* (2014) 133(2):592–4. doi: 10.1016/j.jaci.2013.10.003
19. Sessa L, Reddel S, Manno E, Quagliariello A, Cotugno N, Del Chierico F, et al. Distinct gut microbiota profile in antiretroviral therapy-treated perinatally HIV-infected patients associated with cardiac and inflammatory biomarkers. *AIDS* (2019) 33(6):1001–11. doi: 10.1097/QAD.0000000000002131
20. Zicari S, Sessa L, Cotugno N, Ruggiero A, Morrocchi E, Concato C, et al. Immune Activation, Inflammation, and Non-AIDS Co-Morbidities in HIV-Infected Patients under Long-Term ART. *Viruses* (2019) 11(3):200. doi: 10.3390/v11030200
21. Cotugno N, Ruggiero A, Santilli V, Manno EC, Rocca S, Zicari S, et al. OMIC Technologies and Vaccine Development: From the Identification of Vulnerable Individuals to the Formulation of Invulnerable Vaccines. *J Immunol Res* (2019) 2019:8732191. doi: 10.1155/2019/8732191
22. Thysen SM, Fernandes M, Benn CS, Aaby P, Fisker AB. Cohort profile : Bandim Health Project's (BHP) rural Health and Demographic Surveillance System (HDSS)-a nationally representative HDSS in Guinea-Bissau. *BMJ Open* (2019) 9(6):e028775. doi: 10.1136/bmjopen-2018-028775
23. Aaby P, Benn CS, Flanagan KL, Klein SL, Kollmann TR, Lynn DJ, et al. The non-specific and sex-differential effects of vaccines. *Nat Rev Immunol* (2020) 20(8):464–70. doi: 10.1038/s41577-020-0338-x
24. de Bree LCJ, Koeken V, Joosten LAB, Aaby P, Benn CS, van Crevel R, et al. Non-specific effects of vaccines: Current evidence and potential implications. *Semin Immunol* (2018) 39:35–43. doi: 10.1016/j.smim.2018.06.002
25. Goodridge HS, Ahmed SS, Curtis N, Kollmann TR, Levy O, Netea MG, et al. Harnessing the beneficial heterologous effects of vaccination. *Nat Rev Immunol* (2016) 16(6):392–400. doi: 10.1038/nri.2016.43
26. Soni D, Bobbala S, Li S, Scott EA, Dowling DJ. The sixth revolution in pediatric vaccinology: immunoengineering and delivery systems. *Pediatr Res* (2020). doi: 10.1038/s41390-020-01112-y
27. Nanishi E, Dowling DJ, Levy O. Toward precision adjuvants: optimizing science and safety. *Curr Opin Pediatr* (2020) 32(1):125–38. doi: 10.1097/MOP.0000000000000868
28. Angelidou A, Diray-Arce J, Conti MG, Smolen KK, van Haren SD, Dowling DJ, et al. BCG as a Case Study for Precision Vaccine Development: Lessons From Vaccine Heterogeneity, Trained Immunity, and Immune Ontogeny. *Front Microbiol* (2020) 11:332. doi: 10.3389/fmicb.2020.00332
29. Dowling DJ. Recent Advances in the Discovery and Delivery of TLR7/8 Agonists as Vaccine Adjuvants. *Immunohorizons* (2018) 2(6):185–97. doi: 10.4049/immunohorizons.1700063
30. Scheid A, Borriello F, Pietrasanta C, Christou H, Diray-Arce J, Pettengill MA, et al. Adjuvant Effect of Bacille Calmette-Guerin on Hepatitis B Vaccine Immunogenicity in the Preterm and Term Newborn. *Front Immunol* (2018) 9:29. doi: 10.3389/fimmu.2018.00029
31. Angelidou A, Conti MG, Diray-Arce J, Benn CS, Shann F, Netea MG, et al. Licensed Bacille Calmette-Guerin (BCG) formulations differ markedly in bacterial viability, RNA content and innate immune activation. *Vaccine* (2020) 38(9):2229–40. doi: 10.1016/j.vaccine.2019.11.060
32. Dowling DJ, Scott EA, Scheid A, Bergelson I, Joshi S, Pietrasanta C, et al. Toll-like receptor 8 agonist nanoparticles mimic immunomodulating effects of the live BCG vaccine and enhance neonatal innate and adaptive immune responses. *J Allergy Clin Immunol* (2017) 140(5):1339–50. doi: 10.1016/j.jaci.2016.12.985
33. Rerks-Ngarm S, Pitisuttithum P, Nitayaphan S, Kaewkungwal J, Chiu J, Paris R, et al. Vaccination with ALVAC and AIDSVAX to prevent HIV-1 infection in Thailand. *N Engl J Med* (2009) 361(23):2209–20. doi: 10.1056/NEJMoa0908492
34. Hammer SM, Sobieszczyk ME, Janes H, Karuna ST, Mulligan MJ, Grove D, et al. Efficacy trial of a DNA/rAd5 HIV-1 preventive vaccine. *N Engl J Med* (2013) 369(22):2083–92. doi: 10.1056/NEJMoa1310566
35. Aldoss I, La Rosa C, Baden LR, Longmate J, Ariza-Heredia EJ, Rida WN, et al. Poxvirus Vectored Cytomegalovirus Vaccine to Prevent Cytomegalovirus Viremia in Transplant Recipients: A Phase 2, Randomized Clinical Trial. *Ann Intern Med* (2020) 172(5):306–16. doi: 10.7326/M19-2511
36. Chen WH, Cohen MB, Kirkpatrick BD, Brady RC, Galloway D, Gurwith M, et al. Single-dose Live Oral Cholera Vaccine CVD 103-HgR Protects Against Human Experimental Infection With Vibrio cholerae O1 El Tor. *Clin Infect Dis* (2016) 62(11):1329–35. doi: 10.1093/cid/ciw145
37. Hagan T, Cortese M, Rouphael N, Boudreau C, Linde C, Maddur MS, et al. Antibiotics-Driven Gut Microbiome Perturbation Alters Immunity to Vaccines in Humans. *Cell* (2019) 178(6):1313–28.e1313. doi: 10.1016/j.cell.2019.08.010
38. Pulendran B. Systems vaccinology: probing humanity's diverse immune systems with vaccines. *Proc Natl Acad Sci USA* (2014) 111(34):12300–6. doi: 10.1073/pnas.1400476111
39. Idoko OT, Mohammed N, Ansah P, Hodgson A, Tapia MD, Sow SO, et al. Antibody responses to yellow fever vaccine in 9 to 11-month-old Malian and Ghanaian children. *Expert Rev Vaccines* (2019) 18(8):867–75. doi: 10.1080/14760584.2019.1640118
40. Pulendran B, Li S, Nakaya HI. Systems vaccinology. *Immunity* (2010) 33(4):516–29. doi: 10.1016/j.immuni.2010.10.006

41. Hagan T, Nakaya HI, Subramaniam S, Pulendran B. Systems vaccinology: Enabling rational vaccine design with systems biological approaches. *Vaccine* (2015) 33(40):5294–301. doi: 10.1016/j.vaccine.2015.03.072
42. Raeven RHM, van Riet E, Meiring HD, Metz B, Kersten GFA. Systems vaccinology and big data in the vaccine development chain. *Immunology* (2019) 156(1):33–46. doi: 10.1111/imm.13012
43. Tsang JS, Dobano C, VanDamme P, Moncunill G, Marchant A, Othman RB, et al. Improving Vaccine-Induced Immunity: Can Baseline Predict Outcome? *Trends Immunol* (2020) 41(6):457–65. doi: 10.1016/j.it.2020.04.001
44. Tsang JS, Schwartzberg PL, Kotliarov Y, Biancotto A, Xie Z, Germain RN, et al. Global analyses of human immune variation reveal baseline predictors of postvaccination responses. *Cell* (2014) 157(2):499–513. doi: 10.1016/j.cell.2014.03.031
45. Team H.-C.S.P., Consortium H-I. Multicohort analysis reveals baseline transcriptional predictors of influenza vaccination responses. *Sci Immunol* (2017) 2(14):eaal4656. doi: 10.1126/sciimmunol.aal4656
46. Tsang JS. Utilizing population variation, vaccination, and systems biology to study human immunology. *Trends Immunol* (2015) 36(8):479–93. doi: 10.1016/j.it.2015.06.005
47. Jennewein MF, Goldfarb I, Dolatshahi S, Cosgrove C, Noelette FJ, Krykbaeva M, et al. Fc Glycan-Mediated Regulation of Placental Antibody Transfer. *Cell* (2019) 178(1):202–215 e214. doi: 10.1016/j.cell.2019.05.044
48. Xia J, Benner MJ, Hancock RE. NetworkAnalyst–integrative approaches for protein-protein interaction network analysis and visual exploration. *Nucleic Acids Res* (2014) 42(Web Server issue):W167–174. doi: 10.1093/nar/gku443
49. Pena OM, Hancock DG, Lyle NH, Linder A, Russell JA, Xia J, et al. An Endotoxin Tolerance Signature Predicts Sepsis and Organ Dysfunction at Initial Clinical Presentation. *EBioMedicine* (2014) 1(1):64–71. doi: 10.1016/j.ebiom.2014.10.003
50. Litonjua AA, Lange NE, Carey VJ, Brown S, Laranjo N, Harshfield BJ, et al. The Vitamin D Antenatal Asthma Reduction Trial (VDAART): rationale, design, and methods of a randomized, controlled trial of vitamin D supplementation in pregnancy for the primary prevention of asthma and allergies in children. *Contemp Clin Trials* (2014) 38(1):37–50. doi: 10.1016/j.cct.2014.02.006
51. Wolsk HM, Chawes BL, Litonjua AA, Hollis BW, Waage J, Stokholm J, et al. Prenatal vitamin D supplementation reduces risk of asthma/recurrent wheeze in early childhood: A combined analysis of two randomized controlled trials. *PloS One* (2017) 12(10):e0186657. doi: 10.1371/journal.pone.0186657
52. Lee-Sarwar K, Kelly RS, Lasky-Su J, Kachroo P, Zeiger RS, O'Connor GT, et al. Dietary and Plasma Polyunsaturated Fatty Acids Are Inversely Associated with Asthma and Atopy in Early Childhood. *J Allergy Clin Immunol Pract* (2019) 7(2):529–.e528. doi: 10.1016/j.jaip.2018.07.039
53. Bennike TB, Bellin MD, Xuan Y, Stensballe A, Moller FT, Beilman GJ, et al. A Cost-Effective High-Throughput Plasma and Serum Proteomics Workflow Enables Mapping of the Molecular Impact of Total Pancreatectomy with Islet Autotransplantation. *J Proteome Res* (2018) 17(5):1983–92. doi: 10.1021/acs.jproteome.8b00111
54. Garcon N, Vaughn DW, Didierlaurent AM. Development and evaluation of AS03, an Adjuvant System containing alpha-tocopherol and squalene in an oil-in-water emulsion. *Expert Rev Vaccines* (2012) 11(3):349–66. doi: 10.1586/erv.11.192
55. O'Hagan DT, Ott GS, De Gregorio E, Seubert A. The mechanism of action of MF59 - an innately attractive adjuvant formulation. *Vaccine* (2012) 30 (29):4341–8. doi: 10.1016/j.vaccine.2011.09.061
56. Rosewich M, Lee D, Zielen S. Pollinex Quattro: an innovative four injections immunotherapy in allergic rhinitis. *Hum Vaccin Immunother* (2013) 9 (7):1523–31. doi: 10.4161/hv.24631
57. A Two-Dose Hepatitis B Vaccine for Adults (Heplisav-B). *JAMA* (2018) 319 (8):822–3. doi: 10.1001/jama.2018.1097
58. Garcon N, Segal L, Tavares F, Van Mechelen M. The safety evaluation of adjuvants during vaccine development: the AS04 experience. *Vaccine* (2011) 29(27):4453–9. doi: 10.1016/j.vaccine.2011.04.046
59. Coccia M, Collignon C, Herve C, Chalon A, Welsby I, Detienne S, et al. Cellular and molecular synergy in AS01-adjuvanted vaccines results in an early IFNgamma response promoting vaccine immunogenicity. *NPJ Vaccines* (2017) 2:25. doi: 10.1038/s41541-017-0027-3
60. Henriksen-Lacey M, Bramwell VW, Christensen D, Agger EM, Andersen P, Perrie Y. Liposomes based on dimethyldioctadecylammonium promote a depot effect and enhance immunogenicity of soluble antigen. *J Control Release* (2010) 142(2):180–6. doi: 10.1016/j.jconrel.2009.10.022
61. van Dissel JT, Joosten SA, Hoff ST, Soonawala D, Prins C, Hokey DA, et al. A novel liposomal adjuvant system, CAF01, promotes long-lived Mycobacterium tuberculosis-specific T-cell responses in human. *Vaccine* (2014) 32(52):7098–107. doi: 10.1016/j.vaccine.2014.10.036
62. Thakur A, Rodriguez-Rodriguez C, Saatchi K, Rose F, Esposito T, Nosrati Z, et al. Dual-Isotope SPECT/CT Imaging of the Tuberculosis Subunit Vaccine H56/CAF01: Induction of Strong Systemic and Mucosal IgA and T-Cell Responses in Mice Upon Subcutaneous Prime and Intrapulmonary Boost Immunization. *Front Immunol* (2018) 9:2825. doi: 10.3389/fimmu.2018.02825
63. van Haren SD, Dowling DJ, Foppen W, Christensen D, Andersen P, Reed SG, et al. Age-Specific Adjuvant Synergy: Dual TLR7/8 and Mincle Activation of Human Newborn Dendritic Cells Enables Th1 Polarization. *J Immunol* (2016) 197(11):4413–24. doi: 10.4049/jimmunol.1600282
64. Pulendran B, Ahmed R. Immunological mechanisms of vaccination. *Nat Immunol* (2011) 12(6):509–17. doi: 10.1038/ni.2039
65. Levitz SM, Golenbock DT. Beyond empiricism: informing vaccine development through innate immunity research. *Cell* (2012) 148(6):1284–92. doi: 10.1016/j.cell.2012.02.012
66. Borriello F, Spreafico R, Poli V, Chou J, Barrett NA, Lacanfora L, et al. The physical form of microbial ligands bypasses the need for dendritic cell migration to stimulate adaptive immunity. *bioRxiv* (2020). doi: 10.1101/2020.03.03.973727
67. Sander LE, Davis MJ, Boekschoten MV, Amsen D, Dascher CC, Ryffel B, et al. Detection of prokaryotic mRNA signifies microbial viability and promotes immunity. *Nature* (2011) 474(7351):385–9. doi: 10.1038/nature10072
68. Blander JM, Sander LE. Beyond pattern recognition: five immune checkpoints for scaling the microbial threat. *Nat Rev Immunol* (2012) 12(3):215–25. doi: 10.1038/nri3167
69. Georg P, Sander LE. Innate sensors that regulate vaccine responses. *Curr Opin Immunol* (2019) 59:31–41. doi: 10.1016/j.coi.2019.02.006
70. Yang D, Han Z, Oppenheim JJ. Alarmins and immunity. *Immunol Rev* (2017) 280(1):41–56. doi: 10.1111/imr.12577
71. Yang D, Han Z, Alam MM, Oppenheim JJ. High-mobility group nucleosome binding domain 1 (HMGN1) functions as a Th1-polarizing alarmin. *Semin Immunol* (2018) 38:49–53. doi: 10.1016/j.smim.2018.02.012
72. Alam MM, Yang D, Trivett A, Meyer TJ, Oppenheim JJ. HMGN1 and R848 Synergistically Activate Dendritic Cells Using Multiple Signaling Pathways. *Front Immunol* (2018) 9:2982:2982. doi: 10.3389/fimmu.2018.02982
73. Nie Y, Yang D, Trivett A, Han Z, Xin H, Chen X, et al. Development of a Curative Therapeutic Vaccine (TheraVac) for the Treatment of Large Established Tumors. *Sci Rep* (2017) 7(1):14186. doi: 10.1038/s41598-017-14655-8
74. Ohia-Nwoko O, Kosten TA, Haile CN. Animal Models and the Development of Vaccines to Treat Substance Use Disorders. *Int Rev Neurobiol* (2016) 126:263–91. doi: 10.1016/bs.irn.2016.02.009
75. Heekin RD, Shorter D, Kosten TR. Current status and future prospects for the development of substance abuse vaccines. *Expert Rev Vaccines* (2017) 16 (11):1067–77. doi: 10.1080/14760584.2017.1378577
76. Poland GA, Ovsyannikova IG, Kennedy RB. Personalized vaccinology: A review. *Vaccine* (2018) 36(36):5350–7. doi: 10.1016/j.vaccine.2017.07.062
77. Piot P, Larson HJ, O'Brien KL, N'Kengasong J, Ng E, Sow S, et al. Immunization: vital progress, unfinished agenda. *Nature* (2019) 575 (7781):119–29. doi: 10.1038/s41586-019-1656-7
78. Plotkin SA, Offit PA, DeStefano F, Larson HJ, Arora NK, Zuber PLF, et al. The science of vaccine safety: Summary of meeting at Wellcome Trust. *Vaccine* (2020) 38(8):1869–80. doi: 10.1016/j.vaccine.2020.01.024
79. Donahue M, Hendrickson B, Julian D, Hill N, Rother J, Koirala S, et al. Multistate Mumps Outbreak Originating from Asymptomatic Transmission at a Nebraska Wedding - Six States, August-October 2019. *MMWR Morb Mortal Wkly Rep* (2020) 69(22):666–9. doi: 10.15585/mmwr.mm6922a2
80. Plotkin SA. Correlates of protection induced by vaccination. *Clin Vaccine Immunol* (2010) 17(7):1055–65. doi: 10.1128/CVI.00131-10
81. Weibel D, Sturkenboom M, Black S, de Ridder M, Dodd C, Bonhoeffer J, et al. Narcolepsy and adjuvanted pandemic influenza A (H1N1) 2009 vaccines -

Multi-country assessment. *Vaccine* (2018) 36(41):6202–11. doi: 10.1016/j.vaccine.2018.08.008

82. Storni F, Zeltins A, Balke I, Heath MD, Kramer MF, Skinner MA, et al. Vaccine against peanut allergy based on engineered virus-like particles displaying single major peanut allergens. *J Allergy Clin Immunol* (2020) 145 (4):1240–53 e1243. doi: 10.1016/j.jaci.2019.12.007

Conflict of Interest: DD, OL, and JTE are named inventors on several patent applications related to vaccine adjuvants. JTE is currently employed by Inimmune corporation. OTI is currently employed by Sanofi Pasteur but was not at the time of gathering this data.

The remaining authors declare that the research was conducted in the absence of any commercial or financial relationships that could be construed as a potential conflict of interest.

frontiers in Immunology

ORIGINAL RESEARCH
published: 16 October 2020
doi: 10.3389/fimmu.2020.577823

MPL Adjuvant Contains Competitive Antagonists of Human TLR4

Yi-Qi Wang[1], *Hélène Bazin-Lee*[2], *Jay T. Evans*[2], *Carolyn R. Casella*[3] *and Thomas C. Mitchell*[3]*

[1] School of Pharmaceutical Science, Zhejiang Chinese Medical University, Hangzhou, China, [2] Center for Translational Medicine, University of Montana, Missoula, MT, United States, [3] Department of Microbiology and Immunology, School of Medicine, University of Louisville, Louisville, KY, United States

Monophosphoryl lipid A (MPL®) is the first non-alum vaccine adjuvant to achieve widespread clinical and market acceptance, a remarkable achievement given that it is manufactured from a *Salmonella enterica* endotoxin. To understand how MPL® successfully balanced the dual mandate of vaccine design—low reactogenicity with high efficacy—clinical- and research-grade MPL was evaluated in human and mouse cell systems. Stimulatory dose response curves revealed that most preparations of MPL are much more active in mouse than in human cell systems, and that the limited efficacy observed in human cells correlated with TLR4 inhibitory activity that resulted in a partial agonist profile. Further analysis of the major components of MPL® adjuvant prepared synthetically identified two structural variants that functioned as competitive antagonists of human TLR4. A partial agonist profile could be recapitulated and manipulated by spiking synthetic agonists with synthetic antagonists to achieve a broad dose range over which TLR4 stimulation could be constrained below a desired threshold. This report thus identifies mixed agonist–antagonist activity as an additional mechanism by which MPL® adjuvant is detoxified, relative to its parental LPS, to render it safe for use in prophylactic vaccines.

Keywords: monophosphoryl lipid A (MPL), Toll-like receptor 4 (TLR4), partial agonist, vaccine adjuvant, reactogenicity, safety

OPEN ACCESS

Edited by:
Lee Mark Wetzler, Boston University, United States

Reviewed by:
Srijayaprakash Babu Uppada, University of Nebraska Medical Center, United States
Axel T. Lehrer, University of Hawaii at Manoa, United States

***Correspondence:**
Thomas C. Mitchell
tom.mitchell@louisville.edu

Specialty section:
This article was submitted to Vaccines and Molecular Therapeutics, a section of the journal Frontiers in Immunology

Received: *30 June 2020*
Accepted: *28 September 2020*
Published: *16 October 2020*

Citation:
Wang Y-Q, Bazin-Lee H, Evans JT, Casella CR and Mitchell TC (2020) MPL Adjuvant Contains Competitive Antagonists of Human TLR4. Front. Immunol. 11:577823. doi: 10.3389/fimmu.2020.577823

INTRODUCTION

Monophosphoryl lipid A (MPL®) is the first vaccine adjuvant to achieve clinical and market success since the advent of aluminum salts in the early 20th century. It was first authorized as a component of adjuvant system 4 [AS04 (1)], aluminum hydroxide semi-crystalline gels adsorbed hydrostatically with MPL, in the HBV vaccine Fendrix (2) for use in patients with renal insufficiency and then for broader use in the HPV vaccine Cervarix (3, 4). Formulations that lack alum completely, such as adjuvant system 1 [AS01 (5)] that contain MPL and QS-21 in liposomal complexes similarly achieved success as the adjuvant component of the varicella zoster vaccine Shingrix (6, 7). Because MPL® is a highly purified derivative of the lipopolysaccharide (LPS) component of the cell-wall of *Salmonella enterica* its success as an adjuvant has been understood primarily in the context of its activity as an agonist of TLR4 that directly activates dendritic cells (8). TLR4-mediated activation of antigen-presenting and innate immune cells leads to mildly inflammatory conditions (9) that favor

Th1 differentiation and production of Th1-associated humoral responses (10). MPL® adjuvant therefore provides a counterbalance to the Th2-differentiating properties of alum (11) by harnessing the immunostimulatory power of TLR4 activation. The clinical success of MPL® adjuvant in the context of prophylactic immunization is a benchmark achievement that bodes well for further use of TLR agonists as vaccine adjuvants, provided we can learn to deploy them safely.

Edgar Ribi's goal in creating MPL® adjuvant was to generate a compound that retained the tumoricidal properties of LPS while lacking its dangerous endotoxicity (12). In collaboration with Kuni Takayama an acid hydrolysis method was developed to convert the LPS of *Salmonella enterica* serovar Minnesota Re595 into a low toxicity, monophosphoryl lipid A (13–15). An additional base hydrolysis modification was added by Kent Myers and colleagues in order to remove one specific fatty acid and further decrease residual endotoxicity (10, 16). Clinical-grade MPL® is manufactured exclusively by GlaxoSmithKline for use as an adjuvant in its vaccine portfolio whereas 'generic' forms of it, which will be designated as MPLA hereafter, are readily available from a variety of commercial suppliers. These research-grade MPLA preparations are also derived from the LPS of *Salmonella enterica* serovar Minnesota Re595 but are made without application of the base hydrolysis step and therefore differ from MPL® in ways that make it harder to investigate which properties make it a successful adjuvant.

The complexity of the process used to manufacture MPL® from LPS, needed to ensure it is both safety and functionality, generates multiple congeneric forms with anywhere from three to six acyl chains (10, 13, 14, 17–20). The hexa-acylated species is generally highlighted when structures of MPL® are published (21), even though it is not the most abundant (17) and the penta-acylated species is fully functional as an adjuvant in mice (17). The focus on the hexa-acylated species was driven in part by a view of the hexa-acyl Lipid A of *Escherichia coli* as representing the optimal structure for activation of TLR4 (10), which has led to use of synthetic hexa-acylated structures corresponding to the *E. coli* chemotype (22, 23) or hexa-acylated monosaccharide mimetics in pre-clinical and clinical vaccine trials (24–26). Notably, tetra-acylated Lipid IVa is an agonist of mouse TLR4 but a competitive antagonist of human TLR4 (27), part of a broader theme that emerged in which human TLR4 is better able to discriminate amongst different LPS and Lipid A structures, relative to mouse (28). Hence, the multiple, congeneric Lipid A species in MPL® adjuvant may cause its activity in pre-clinical animal models, such as mice, to be very different from that observed in human cell systems.

In this study we sought to evaluate differences in stimulation of human and mouse immune cells by first using research-grade MPLA preparations and then turning to vaccine suspensions containing clinical-grade MPL® adjuvant in the form of AS01 and AS04 (Shingrix and Cervarix, respectively). We also obtained and tested synthetic preparations of the major components of MPL® adjuvant and report for the first time the presence of competitive antagonists of human TLR4, which may impose an upper limit on the extent to which the MPL® mixture can activate inflammatory side effects.

MATERIALS AND METHODS

TLR4 Reagents

Research-grade MPLA (4′-monophosphoryl lipid A) prepared from *Salmonella enterica* serovar Minnesota Re595 LPS by acid hydrolysis was purchased from Avanti Polar Lipids (A-MPLA), Enzo Life Sciences (cat.no. ALX-581-202, E-MPLA), Invivogen (I-MPLA) and Sigma-Aldrich (S-MPLA) all of which are heterogeneous mixtures estimated to average ~MW 1,700 g/mol. Clinical-grade MPL adjuvant® manufactured from *Salmonella minnesota* Re595 LPS by acid and base hydrolysis (resulting in a mixture of 3-*O*-desacyl-4′-monophosphoryl lipid A congeners with three to six acyl chains) was tested in the form of Cervarix vaccine, an aluminum hydroxide-adsorbed suspension containing 100 μg/ml MPL adjuvant (AS04) plus recombinant HPV virus-like particles, and the adjuvant vial from Shingrix vaccine (*i.e.*, without mixing in lyophilized glycoprotein E from the separate antigen vial), a dioleoyl phosphatidylcholine (DOPC) liposomal formulation containing 100 μg/ml MPL® adjuvant, the immunostimulatory saponin QS-21, and cholesterol ($AS01_B$).

Tandem mass spectrometry was performed through the Analytical Services Division of Avanti Polar Lipids, Inc. (Alabaster, AL) to evaluate the composition of research-grade MPLA preparations. Briefly, samples of each preparation, 100 μg, were dissolved in 1 ml of 70:28: methanol:dichloromethane: water and assayed by LC/MS/MS to determine the relative abundance of MPLA molecular species with four to seven acyl chains using the same Q1/Q3 precursor ion/product ion analytic method Avanti employs in analysis of its *S. minnesota* Re595 MPLA product (A-MPLA).

Reference TLR4 agonists included LPS from *Salmonella enterica* serovar Minnesota Re595 (MW ~2,300 g/mol, Enzo Life Sciences cat. no. ALX-581-008); synthetic Lipid A (MW 1,797.2 g/mol, Peptides International cat.no. CLP-24005-s) with 1,4′ phosphates and six acyl chains in a 2:2:1:1 configuration corresponding to the *E. coli* chemotype (aka LA-15-PP or compound 506); phosphorylated hexa-acyl disaccharide (PHAD, MW 1,763.5 g/mol, Avanti Polar Lipids cat. no. 699800P), a synthetic MPLA with a 4′ phosphate and six acyl chains corresponding to the *E. coli* chemotype; and 3D(6-acyl) PHAD (3D-6A-PHAD, MW 1,747.5 g/mol, Avanti Polar Lipids cat. no. 699855P) a synthetic variant of PHAD with acyl chains in a 2:2:0:2 configuration corresponding to the hexa-acylated component of clinical-grade MPL adjuvant®. Acyl chains in the PHAD synthetics are uniformly C14 in length, whereas the Lipid A synthetic has one secondary acyl chain that is C12.

Individual components of MPL adjuvant® were synthesized as described previously (18, 19) as 3-*O*-desacyl-4′-monophosphoryl lipid A congeners with varying numbers of acyl chains corresponding to the major components found in clinical-grade MPL adjuvant®: hexa-acylated (hereafter referred to as ML6, 2:2:0:2 acyl chain configuration), penta-acylated (ML5A and ML5B, 2:2:0:1 and 1:2:0:2 acyl chain configurations, respectively), tetra-acylated (ML4A and ML4B, 1:2:0:1 and 0:2:0:2 acyl chain configurations, respectively), and

tri-acylated (ML3, 0:2:0:1 acyl chain configuration) monophosphoryl lipid A. The MPL® adjuvant synthetics reflect differences in acyl chain lengths of *S. enterica* Minnesota LPS in which the 2′-secondary acyl chain is C12, and the 2-secondary acyl chain is C16 in length.

LPS, Lipid A, and monophosphoryl Lipid A reagents other than Cervarix and the adjuvant vial of Shingrix were suspended in endotoxin-free water containing 2% glycerol by sonication at 80 kHz in an Avanti Sonicator (model G112SP1TB) until clear.

Cells

Human and mouse HEK-Blue reporter cells express human or mouse CD14, MD2, and TLR4 and secreted embryonic alkaline phosphatase (SEAP) under control of a promoter with binding sites for NFκB and AP-1 transcription factors (InvivoGen cat. nos. hkb-htlr4 and hkb-mtlr4). Cells were cultured as directed by the supplier, with the exception that Glutamax (ThermoFisher cat. no. 10569010) was used in place of L-glutamine, and TrypLE Express (ThermoFisher cat. no. 12605010) was used to release adherent cells for each passage. BALB/c mouse RAW264.7 and human THP-1 cells (ATCC® cat. nos. TIB-71 and TIB-202) were cultured in DMEM (4.5 g/L D-Glucose with 2 mM L-glutamine, 1 mM sodium pyruvate, 100 U/ml penicillin and 100 μg/ml streptomycin) supplemented with 10% heat-inactivated FBS. THP-1 cells were exposed to phorbol-12-myristate-13-acetate (PMA, InvivoGen cat no. tlrl-pma), 5 ng/ml, for 48 h prior to treatment with TLR4 agonists. Bone marrow-derived dendritic cells (BMDCs) were generated using C57BL/6 mouse femurs following the exact method published by Lutz et al. (29) except that 5 rather than 20 ng/ml recombinant GM-CSF was used to differentiate the DC. Human peripheral blood monocytes (PBMCs) were prepared from venous blood of healthy volunteers that had been collected using sodium citrate as anti-coagulant, 20 ml of which was mixed with 15 ml calcium- and magnesium-free Hank's Balanced Saline Solution (HBSS) and then laid over 6 ml Histopaque®-1077 (1.077 g/ml, Sigma-Aldrich cat no. 10771) for density gradient centrifugation. The buffy coat layer was collected by pipette, washed once in HBSS, once in serum-free RPMI-1640, and then the PBMCs were resuspended in RPMI-1640 supplemented with 100 U/ml penicillin, 100 g/ml streptomycin, 1 mM Na-Pyruvate, 2 mM L-glutamine, 50 μM βME and 10% heat-inactivated, male AB human serum for culture.

Assays

SEAP assays were performed to evaluate the extent to which TLR4 signaling was activated in HEK-Blue reporter cells expressing mouse or human receptors (CD14, MD2 and TLR4). Reporter cells were harvested when 70–80% confluent and plated in 96-well, flat-bottom microtiter plates either 1 h, one day or two days (5×10^4, 4×10^4 or 2×10^4 cells/well, respectively) before addition of TLR4 agonists for 18–24 h. Culture supernatants were transferred to U-bottom microtiter plates, centrifuged and transferred again to microtiter plates to ensure reporter cells were not present. The culture supernatants were added to QUANTI-BLUE substrate following instructions provided by the manufacturer (InvivoGen cat. nos. rep-qbl or rep-qbs) and incubated at 37°C in a tissue culture incubator. At successive intervals beginning 10 min after mixing the supernatants and substrate, the plates were placed in an Emax plate reader (Molecular Devices LLC) and optical density was measured at visible light wavelength 650 nM (OD_{650}). The shortest incubations at which dose response curve fits produced maximal R^2 'goodness of fit' values, as determined by GraphPad Prism software, were used for analysis.

ELISA was performed to measure TNFα secretion by cell-lines and primary cells exposed to TLR4 reagents as a measure of receptor activation. Human PBMC, 5×10^5/well, or THP-1 cells, 5×10^4/well, and mouse BMDC or RAW264.7, 10^5/well, were plated in microtiter plates to which TLR4 reagents were added for 18–24 h. Culture supernatants were transferred to U-bottom microtiter plates, centrifuged, transferred again to fresh microtiter plates to ensure cells were no longer present and then frozen until needed. Human or mouse TNα was quantified using ELISA kits as directed by the kit supplier (eBioscience cat. nos. 88-7324-77 and 88-7324-88, respectively) using an Emax plate reader and SoftMax Pro analytical software (Molecular Devices, LLC). Culture supernatants from replicate freezing were diluted as needed to ensure unknown sample values were within the range observed in the standard curves.

Pharmacological Dose Response Curves

Pharmacological profiles of the TLR4 reagents were generated by performing dose response curves in one of four formats. **1**) Agonist potency and efficacy (EC50 and height of dose plateau, respectively) were measured by diluting TLR4 reagents successively in complete culture medium [DMEM or RPMI supplemented with fetal bovine serum (FBS) or RPMI supplemented with human serum, depending on cell-type]. Half-log step dilutions were performed in 96-well, U-bottom microtiter plates using a multichannel pipette to transfer and mix the suspensions, with fresh tips used for each dilution step. One-tenth (20 μl) volumes from wells of the dilution plate were then transferred to wells containing cells that had been plated in nine-tenth volumes (180 μl) of culture medium. **2**) Mixed agonist–antagonist potency and efficacy were measured by mixing a TLR4 agonist with a candidate antagonist at a fixed ratio and then performing half-log step dilutions before treating HEK reporter cells. Analysis of values obtained from SEAP assays of culture supernatants was then performed as described for preparations containing agonist alone, above. **3**) Competitive *vs* allosteric or non-competitive antagonist type was evaluated by diluting a reference agonist within a fixed concentration of a candidate inhibitor in half-log steps, treating HEK reporter cells, performing SEAP assays and then analyzing the data as described for agonist assays, above. Competitive antagonists are characterized by values that reach the same dose plateau as for a reference, full agonist, while shifting potency to higher EC50 values. Non-competitive antagonists are characterized by values that do not reach the same dose plateau as a full agonist, indicating that overabundance alone of the antagonist cannot compete with the agonist for binding to activation sites. **4**) Inhibitory potency (IC50) was measured by diluting antagonists within a fixed concentration of a reference agonist,

treating HEK reporter cells and performing SEAP assays as described.

Statistical Analysis

All statistical tests were performed using GraphPad Prism version 8.4.3 for Windows, GraphPad Software, San Diego, California USA, www.graphpad.com. Assay results were graphed as means ± standard deviations (SD) pooled from multiple independent experiments and replicate treatment groups as specified in each figure legend. Dose stimulation and IC50 assay results were additionally fit by regression curves using the Prism log(agonist) *vs.* response—variable slope (four parameters) and the log(inhibitor) *vs.* response—variable slope (four parameters) equations, respectively. Each curve fit is depicted as a solid line with shaded boundaries representing 99% confidence intervals, or the space that would describe the true value of the population mean in 99% of experimental repetitions. These 99% confidence intervals are equivalent to p values ≤ 0.01 for curves whose shaded boundaries do not overlap. In **Figure S1** the relationship between abundance of a given MPLA component and the top dose plateau (apparent efficacy) was evaluated using Prism multiple variable tables to calculate non-parametric Spearman coefficients with P values computed from two-tailed tests of significance of the correlations.

RESULTS

Heterogeneity of Research-Grade MPLA

Research-grade MPLA is often used in pre-clinical mouse studies as a surrogate for MPL® adjuvant. We decided to compare the relative activities of one commercial preparation of MPLA, denoted here as E-MPLA, that we have used in previous mouse studies in mouse *versus* human systems. For these first experiments, we deployed matched pairs of cell types to evaluate species-specific differences: human or mouse TLR4 HEK-Blue reporter cells, human THP-1 or mouse RAW264.7 cell-lines, and primary PBMC from healthy blood donors or bone marrow-derived dendritic cells from mice (**Figures 1A–F**). In each comparison synthetic Lipid A was the most potent of the

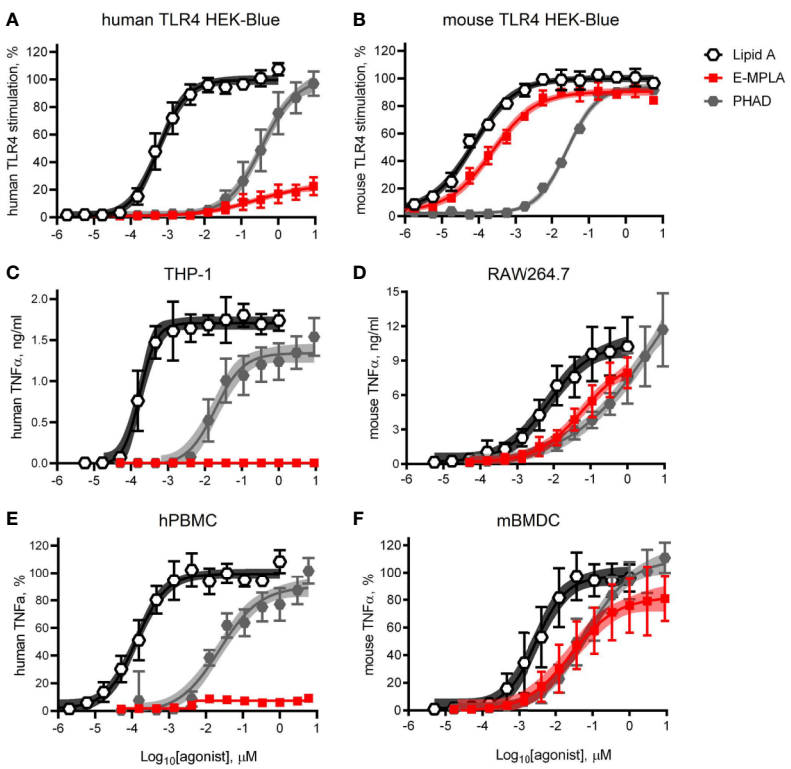

FIGURE 1 | Partial agonism of TLR4 by research-grade MPL adjuvant is species-specific. HEK-Blue reporter cells, monocytic cell-lines, and primary cells of mouse and human origin were exposed to research-grade E-MPLA to compare dose response profiles. Dose curves were performed as half-log step dilutions from a peak concentration of 10 μM with exposure of cells for 18–24 h to synthetic *E. coli* chemotype Lipid A, its monophosphoryl counterpart PHAD, or MPLA from Enzo Life Sciences (E-MPLA). **(A, B)** show normalized responses of HEK-Blue reporter cells engineered to express human TLR4 or mouse TLR4 respectively; 100% = top dose plateau of the full agonist Lipid A. **(C, D)** show TNFα production by human monocytic THP-1 or mouse RAW264.7 cells, respectively. **(E, F)** show normalized TNFα production by human PBMC or mouse BMDC, respectively; 100% = top dose plateau of the full agonist Lipid A Average values ± SD combined from three **(A, B, D, F)** or two **(C, E)** independent experiments, each performed in triplicate, are shown along with shaded regions that indicate the 99% confidence intervals within which the true population means should occur 99% of the time. In each paired comparison research-grade MPLA-E scored as a partial agonist of human TLR4 not mouse TLR4, relative to the full agonists Lipid A (full/potent) and PHAD (full/weak).

agonists tested and reached dose curve plateaus that provided a benchmark for the upper limit of TLR4 signaling capacity for each cell type. The monophosphorylated counterpart to Lipid A, PHAD, was consistently less potent than Lipid A but had the same potential to saturate TLR4 signaling capacity at high doses, whether human or mouse. Monophosphoryl PHAD is thus a weak yet full agonist of both mouse and human TLR4. E-MPLA, however, revealed markedly different activities as a function of species: in each of the mouse TLR4 cell systems (**Figures 1B, D, F**) it was a robust agonist that stimulated very close to the maximal activity seen with Lipid A, whereas in human TLR4 cell systems (**Figures 1A, C, E**) its peak activity was severely limited and behaved more like a partial than a full agonist. The same limited peak activity in human *versus* mouse cells was observed in reporter cells (**Figures 1A, B**), monocytic cell-lines (**Figures 1C, D**) and primary cells (**Figures 1D, E**) suggesting the pattern is likely to be true *in vivo* in humans as well.

To determine whether partial agonism of human TLR4 was specific to E-MPLA, we tested four other commercial preparations using human TLR4 and mouse TLR4 reporter cells. Two of the preparations, S- and I-MPLA, showed the same limited plateau as E-MPLA in human cells, whereas A-MPLA and L-MPLA were more effective. All preparations, however, were robust agonists of mouse TLR4 signaling as compared to the full (if weak) agonist PHAD (**Figure 2B**). THP-1 response patterns (**Figure 2C**) showed a similar rank order of efficacies amongst the MPLA preparations as did the human TLR4 reporter cells, A-MPLA > L-MPLA >> E-MPLA > S- and I-MPLA, although the responses were even more muted relative to PHAD in THP-1 cell cultures. Given the known heterogeneity of MPL® adjuvant we decided to test the MPLA preparations for evidence of inhibitory activity by serially diluting each of them in a fixed concentration of LPS and testing human TLR4 HEK-Blue cells for responsiveness (**Figure 2D**). The same three MPLA preparations with limited efficacy in THP-1 and human TLR4 reporter cells were also inhibitors of LPS, while the remaining two were not. Hence, only the low efficacy preparations of MPLA demonstrated a hallmark of partial agonists—inhibition of full agonists—but the pattern was not uniformly seen among the different preparations, presumably due to differences in manufacturing.

The various MPLA preparations were evaluated by tandem mass spectrometry to determine which, if any, components were correlated with low dose plateaus. The results of this analysis (**Figure S1**) showed that one component, a tetra-acylated structure designated 4c, was significantly and inversely correlated with the height of the top dose plateau. However, the analysis also revealed the absence of structures de-acylated at the 3-O-position, which highlighted the lack of base hydrolysis used in preparation of the commercial MPLAs. Because clinical MPL® adjuvant is base hydrolyzed and therefore uniformly 3-O-desacylated (10, 16) the partial agonist activity observed in some of the MPLA preparations did not necessarily mean that MPL® adjuvant must also behave as a partial agonist of human TLR4.

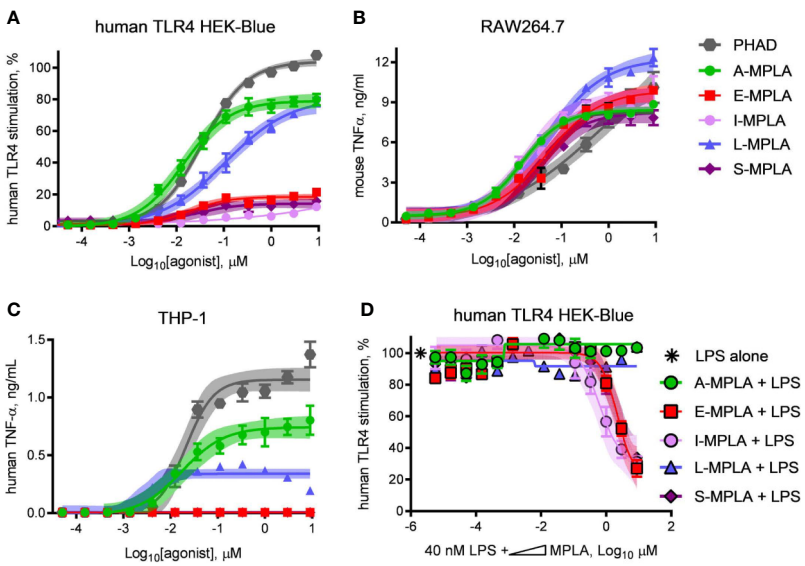

FIGURE 2 | Partial agonist activity of MPLA preparations correlates with presence of TLR4 inhibitors. Research-grade MPLA preparations from five commercial sources were tested for mouse *vs* human TLR4 stimulatory activity. Secretion of alkaline phosphatase by **(A)** human TLR4 HEK-Blue reporter cells was used as a marker of receptor stimulation after exposure to increasing doses of MPLA. TNFα production was used as a marker of TLR4 stimulation by **(B)** RAW264.7 mouse monocytic cells and **(C)** THP-1 human monocytic cells. Inhibition curves were performed with **(D)** human TLR4 HEK-Blue cells exposed to a fixed concentration of LPS alone or in combination with increasing amounts of each MPLA. Symbols and error bars show the average ± SD of **(A, B)** normalized values (100% = top dose plateau of Lipid A from three independent experiments or of **(C, D)** cytokine abundance measured in two independent experiment each performed in triplicate. Shaded regions indicate 99% confidence intervals within which the true population means should occur 99% of the time. MPLA preparations with the lowest dose plateaus for stimulation of human TLR4 [E-, I-, and S-MPLA in **(A)**] were the same as those that inhibited TLR4 stimulation when combined with LPS in **(B)**.

Species-Specific Activity of MPL® Adjuvant

We obtained clinical preparations of Shingrix and Cervarix vaccines, which contain MPL® adjuvant in the forms of AS01 and AS04, respectively, and tested their activities as agonists of mouse *versus* human TLR4. Exposure of hTLR4 HEK-Blue reporter cells to serially diluted Cervarix vaccine and contents of the adjuvant vial from Shingrix vaccine resulted in very weak and very low efficacy stimulation of human TLR4 relative to Lipid A (**Figure 3A**). Both clinical preparations were markedly more effective as agonists of mouse TLR4 (**Figure 3B**), with high doses of Cervarix reaching the same dose plateau as Lipid A and high doses of Shingrix adjuvant (*i.e.*, $AS01_B$) approaching 70% the efficacy of Lipid A. Relative to Lipid A, the full stimulation benchmark, Cervarix was 27% (95% confidence interval, CI, 23–39%) as effective an agonist of human TLR4 but 100% (CI 97–105%) as effective an agonist of mouse TLR4. Similarly, Shingrix $AS01_B$ was 7.2% (CI 6.4–8.0%) *versus* 68% (CI 66–71%) as effective an agonist of human *versus* mouse TLR4, respectively, using Lipid A as the full agonist benchmark. Stimulatory potencies of AS04 and $AS01_B$ for mouse TLR4 were 6- to 20-fold higher than for human TLR4 (**Figure 3C**), whereas that of Lipid A was about the same in both. Together, these higher potency and efficacy patterns in **Figure 3B** demonstrate that the low activity in **Figure 3A** was not due to MPL® adjuvant being impaired or unavailable in the HEK-Blue reporter system.

It is formally possible that adsorption of MPL® adjuvant on aluminum hydroxide could be responsible for the limited efficacy of Cervarix in the human TLR4 reporter cell assay, despite the high activity for mouse TLR4 and the fact that the Shingrix $AS01_B$ suspension does not contain alum. We did not have access to pure MPL® adjuvant nor was it possible to retrieve it in pure form from the Cervarix suspension so we addressed this possibility by evaluating the effect that alum adsorption had on the efficacies of MPLA preparations. As shown in **Figure 3D**, neither adsorption of high efficacy A-MPLA nor low efficacy S-MPLA on aluminum hydroxide resulted in lower dose plateaus although potencies were reduced, suggesting that alum adsorption reduces the available concentration of MPL® adjuvant but not its maximal activity at high doses. This observation along with the different pharmacological profiles of MPL®-adjuvanted vaccines in human *vs* mouse cell systems led us to conclude that research-grade MPLA (**Figures 1** and **2**) and clinical-grade MPL® adjuvant function as partial agonists of TLR4, despite being prepared by distinct manufacturing methods.

MPL® adjuvant is a heterogeneous mixture of congeneric lipid A with 4′-phophoryl groups and varying numbers of acyl chains (10, 13, 14, 17–19), as summarized in **Figure 4A**. **Figure 4B** shows other synthetic Lipid A preparations used in our study, including *E. coli* chemotype PHAD and 3D-6A-PHAD, the latter of which is almost identical to the best known component of MPL®, hexa-acyl ML6, by virtue of lacking a fatty acid at position 3 of the reducing half of the diglucosamine headgroup. However, 3D-6A-PHAD differs in having uniformly C14-length acyl chains rather than C12 and C16 secondary acyl chains attached at positions 2′ and 2 of the diglucosamine headgroup,

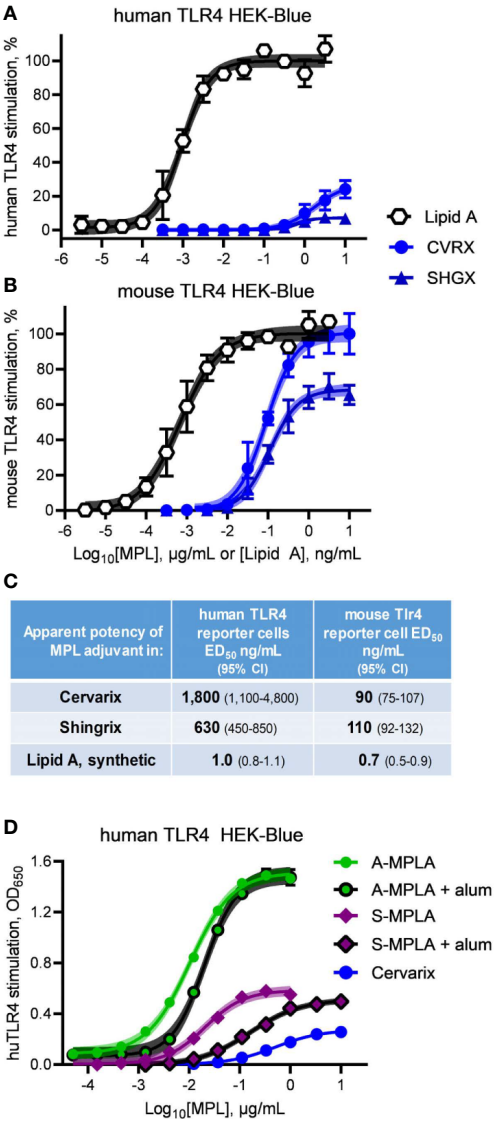

Apparent potency of MPL adjuvant in:	human TLR4 reporter cells ED_{50} ng/mL (95% CI)	mouse Tlr4 reporter cell ED_{50} ng/mL (95% CI)
Cervarix	**1,800** (1,100-4,800)	**90** (75-107)
Shingrix	**630** (450-850)	**110** (92-132)
Lipid A, synthetic	**1.0** (0.8-1.1)	**0.7** (0.5-0.9)

FIGURE 3 | Clinical-grade MPL adjuvant is a partial agonist of human TLR4. Clinical-grade MPL adjuvant® was evaluated for human *vs* mouse TLR4 dose response profiles by exposing **(A)** human TLR4 and **(B)** mTLR4 HEK-Blue reporter cells to Cervarix vaccine (CVRX) or the AS01 adjuvant component of Shingrix vaccine (SHGX) for 24 h. 100% = the top dose plateau for Lipid A-induced secretion of alkaline phosphatase, which was used to normalize TLR4 stimulatory activity between the two reporter cell-lines for a combined total of three independent experiments. **(C)** MPL adjuvant® was 5–16% as potent an agonist of human TLR4 than it was of mouse TLR4 as determined by stimulatory curve fitting to calculate ED50 for the curves shown in **(A, B)**. Low dose plateaus of human TLR4 responses to MPL adjuvant® relative to Lipid A and mouse TLR4 responses, indicate it is a partial agonist of human TLR4. **(D)** human TLR4 HEK-Blue cells were treated with MPLA adsorbed on alum and compared to MPLA alone; alum adsorption did not decrease efficacy of two MPLA preparations. Curve fitting to calculate the top dose plateaus with and without alum produced the following values (with 95% confidence intervals): A-MPLA, 1.51 (1.49–1.53) *vs* A-MPLA + alum, 1.49 (1.47–1.52); S-MPLA, 0.59 (0.57–0.60) *vs* S-MPLA + alum, 0.51 (0.50–0.53). Shaded regions indicate 99% confidence intervals within which the true population means should occur 99% of the time.

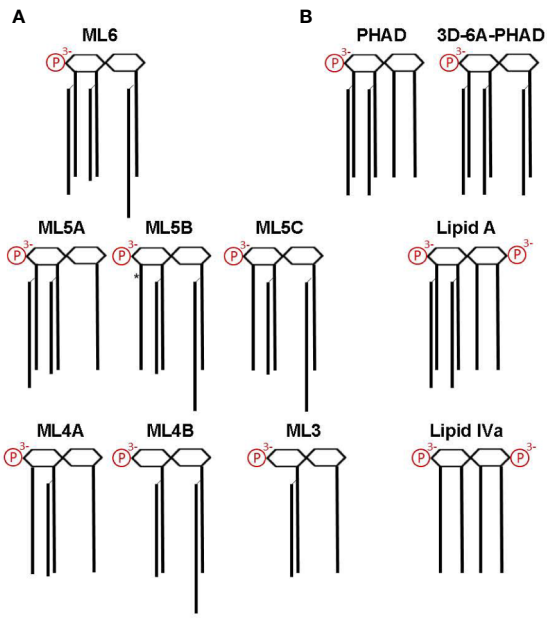

FIGURE 4 | Structures of MPL components and other Lipid A used in this study. Lipid A structures are shown as simplified diagrams representing a β-(1→6) di-glucosamine backbone with varying numbers of acyl chains and phosphates; 1- and 4′ phosphorylation sites are depicted on the right and left, respectively. Amino, ether, ester, and hydroxide linkages are omitted. **(A)** The major components of MPL adjuvant® are congeners that differ primarily at the level of acyl chain attachment sites and lengths. All MPL® adjuvant components lack an acyl chain at the 3-position (*i.e.*, are 3-O-deacylated) due to an alkaline hydrolysis processing step. *, denotes location of an unsaturated acyl group that represents the sole difference between ML5B and ML5C. Note that the 2′-position secondary acyl chains are slightly shorter, C12, than the other C14 chains and that the 2-position secondary acyl chain is slightly longer, C16. **(B)** Structures of synthetic Lipid A used in this study. PHAD (phosphorylated hexa-acyl disaccharide) is a synthetic 4′-monophosphorylated lipid A with six C14 acyl chains in the *E. coli* configuration (2:2:1:1); 3D-6A-PHAD is a synthetic 3-O-desacylated variant in the same configuration as ML6 (2:2:0:2) but with uniform acyl chain lengths. Lipid A, synthesized with six acyl chains and 1-, 4′-phosphates, is highly potent agonist of both mouse and human TLR4; Lipid IVa, synthesized with four primary acyl chains and 1-, 4′-phosphates, is an agonist of mouse TLR4 but a potent antagonist of human TLR4.

respectively. We obtained synthetically prepared versions of most of the major MPL® components and tested them for activity as agonists of mouse *versus* human TLR4.

Dose response curves were generated using MPL® components ML6, ML5A, ML5B, ML4A, ML4B, and ML3 to treat human *versus* mouse TLR4 HEK-Blue reporter cells and THP-1 *versus* RAW264.7 cell-lines (**Figure 5**). Curves generated with the full but weak agonist PHAD were used as benchmarks for maximal stimulation of TLR4 in each cell system. The most evident species-specific difference was observed with component ML4A, which was all but inactive when testing human TLR4 HEK-Blue (**Figure 5A**) cells but approached 80% of the efficacy of the full agonist PHAD when testing the mouse counterpart, mouse TLR4 HEK-Blue (**Figure 5B**). A similar pattern was evident when comparing the activity of ML4A in THP-1 and RAW264.7 cultures (**Figures 5C, D**). The other tetra-acylated component we tested, ML4B was largely inactive in all stimulation assays, as was ML3.

ML5A was the most consistently active in human cell systems, even when compared to ML6, whereas both were similarly active in mouse TLR4 HEK-Blue and RAW264.7 cells. Generally speaking, mouse TLR4 seemed unable to distinguish ML4A, ML5A and ML6 from one another while human TLR4 was much more sensitive to acyl chain variation.

Inhibitory Components in MPL® Adjuvant Mixtures

The limited efficacy of some research-grade MPLA preparations were correlated with their ability to inhibit a full agonist of human TLR4 (**Figures 2A, C, D**). This observation led us next to test the synthesized components of MPL® adjuvant for inhibitory activity. To do this, we diluted components ML3, ML4A and B, ML5A and ML6 in a solution containing a fixed concentration of the full agonist PHAD, 1 μM, and plotted the results in the form of an IC50 curve (**Figure 6A**). Of the five components tested, only ML3 and ML4A showed inhibitory potential. These components were tested again but this time using a fixed concentration of PHAD that corresponded to its EC50 in the same cell system, 30 nM (**Figure 6B**). Here, a more complete inhibition curve was generated in which ML3 completed blocked PHAD at a sufficiently high dose. Calculation of its IC50 under these conditions indicated that its inhibitory potency was almost four orders of magnitude weaker than a control antagonist of human TLR4, Lipid IVa. Component ML4A was a slightly more potent inhibitor of PHAD but at high doses the curve appeared to approach a bottom plateau rather than achieving full inhibition. We also tested ML3 and ML4A for inhibitory effects on a PHAD variant, 3D-6A-PHAD, that is similar in structure to that of ML6 in lacking an acyl chain at the 3-position of the diglucosamine headgroup (**Figure 3**) and, as a commercial reagent, is available in more abundant quantities than ML6. We measured the EC50 of 3D-6A-PHAD for stimulation of human TLR4 HEK-Blue reporter cells and used this concentration, 300 nM, as a fixed diluent in which to serially dilute ML3, ML4A, or Lipid IVa (**Figure 6C**). Treatment of human TLR4 reporter cells with these dilution series again showed that all functioned as inhibitors of a reference agonist, 3D-6A-PHAD, that also served as a more accurate surrogate for one of the agonists present in the MPL® adjuvant mixture of congeners.

We next evaluated the antagonist type, competitive or non-competitive, of the ML3 and ML4A components by using them as fixed concentration diluents in dilution series of PHAD (**Figure 7A**) or 3D-6A-PHAD (**Figure 7B**). Both ML3 and ML4A shifted the potency curves of the agonists without preventing either PHAD or 3D-6A-PHAD from fully stimulating the human TLR4 reporter cells as the agonist concentrations rose, the hallmark of a competitive antagonist that can be out-competed by sufficiently high concentrations of agonist. The Lipid IVa control produced a competitive antagonist curve when mixed with PHAD, as expected, but its

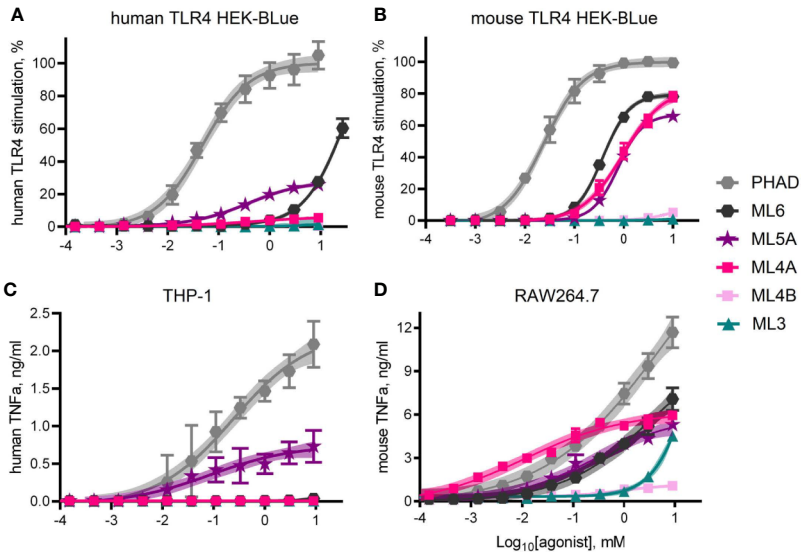

FIGURE 5 | TLR4 stimulatory activity of synthetic MPL adjuvant® components. Synthetic versions of several of the major components of MPL adjuvant® were tested for TLR4 stimulatory activity using HEK-Blue reporter cells that expressed either **(A)** human TLR4 or **(B)** mouse TLR4. Values shown are averages ± SD from three **(A)** or two **(B)** independent experiments normalized by setting 100% = top dose plateau of PHAD in each experiment. Shaded regions indicate 99% confidence intervals within which the true population means should occur 99% of the time. TNFα secretion by **(C)** human THP-1 and **(D)** mouse RAW264.7 cells as measured by ELISA 24 hrs after exposure to agonists in triplicate pooled from two or three independent experiments, respectively, with the exception of ML4A, ML4B and ML3 which were tested in triplicate in one experiment with RAW264.7 cells. Overall, ML5A and ML6 are weaker agonists of human TLR4 than of mouse TLR4, relative to the full agonist PHAD, whereas ML4A is an agonist only of mouse TLR4.

inhibitory effect could not be overcome by the concentrations we used when testing 3D-6A-PHAD, highlighting the weakness of the 3-O-deacylated derivative as an agonist of human TLR4. Overall, the patterns observed in **Figures 6** and **7** showed that two of the major MPL® components, tri-acylated ML3 and tetra-acylated ML4A, were competitive antagonists of human TLR4.

Mixed Agonist–Antagonist Preparations

MPL® adjuvant, in the form of intact Cervarix vaccine or the adjuvant vial of Shingrix, appeared to function as a partial agonist of human TLR4, with a limited dose plateau even at high doses (**Figures 3A, D**). However it was possible this pattern was attributable to the other compounds present, such as viral antigen in Cervarix or the saponin QS-21 in $AS01_B$. To determine if we could re-capitulate partial agonism of human TLR4 without these other compounds, we mixed 3D-6A-PHAD with either ML3, ML4A or ML3+ML4A at a 5:1 ratio, prepared serial dilutions at this fixed ratio and compared the TLR4 stimulatory activities of the mixtures to that of 3D-6A-PHAD alone (**Figure 8A**). Although the weakness of the 3D-6A-PHAD agonist made it difficult to achieve a clear dose plateau, the addition of ML3 and ML4A appeared to limit its activity in a manner that was reminiscent of the curves observed for Cervarix or the Shingrix $AS01_B$ adjuvant.

Repetition of this experiment using the comparatively stronger agonist PHAD (**Figure 8B**) generated curves in which ML3 and ML4A very modestly reduced TLR4 stimulatory activity without establishing a flattened dose plateau, even when ML4A and PHAD were mixed at fixed ratios of 30:1 and 60:1 antagonist:agonist. To determine whether or not this failure to convert PHAD from a full agonist to a partial agonist (in the form of a mixed agonist-antagonist formulation) was due to the weakness of ML3 and ML4A inhibitory effects we then performed mixed agonist-antagonist assays using the potent antagonist Lipid IVa in place of ML3 and ML4A (**Figure 8C**). In this case, the PHAD dose response curve was trending to a flattened curve with as little as one part Lipid IVa to 180 parts PHAD and was clearly flatted when using lower ratios of agonist, 1:60 or 1:20 antagonist:agonist. Collectively, the patterns observed in **Figures 8A–C** indicated that a full agonist of TLR4 could be made to function as if it were a partial agonist by adding an antagonist at a fixed ratio, provided the antagonist was of sufficient inhibitory potency relative to the agonist being tested. We concluded, therefore, that the partial agonism of human TLR4 by MPL® adjuvant preparations AS01B and AS04 could be explained by the presence of a mixture of agonists and antagonists of the receptor.

DISCUSSION

We identified two antagonists of human TLR4 in clinical-grade MPL® adjuvant, components ML3 and ML4A which are tri- and tetra-acylated, respectively. We propose their presence is an additional mechanism by which chemical processing detoxifies *S. enterica* serovar Minnesota Re595 LPS for therapeutic use. The structural determinants of therapeutic detoxification that have been documented in the literature include i) loss of inner core

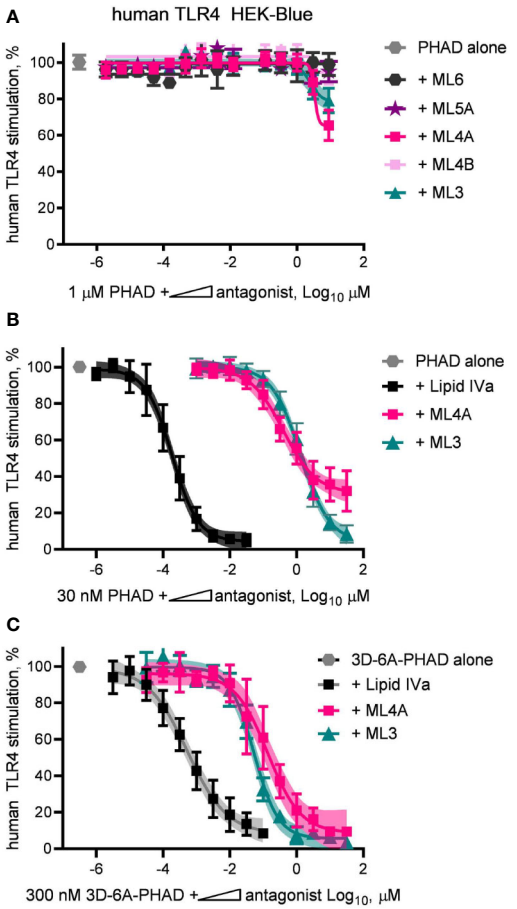

FIGURE 6 | Inhibition of human TLR4 by tetra- and tri-acylated components of MPL adjuvant. Synthetic versions of several major components of MPL adjuvant® were tested for inhibitory activity using human TLR4 HEK-Blue reporter cells. **(A)** MPL adjuvant® components ML3, ML4A, ML4B, ML5A and ML6 were diluted in half-log steps in a mixture containing a fixed concentration of PHAD (1 μM) and added to human TLR4 HEK-Blue reporter cells for 22 h. Values shown are averages ± SD of secreted alkaline phosphatase from two independent experiments, each performed in triplicate and normalized by setting 100% = PHAD alone (1 μM). **(B, C)** MPL adjuvant® components ML3 and ML4A were diluted from a peak dose of 31.6 μM (or a peak dose of 0.03 μM Lipid IVa as antagonist control) in half-log steps in a mixture containing a fixed concentration of PHAD (30 nM) or 3D-6A-PHAD (300 nM), respectively. Values shown are averages ± SD of secreted alkaline phosphatase from two independent experiments normalized by setting 100% = PHAD or 3D-6A-PHAD alone, respectively. Shaded regions indicate 99% confidence intervals within which the true population means should occur 99% of the time. Calculated $IC50^{PHAD}$ values (95% CI) were: ML3, 1.32 μM (1.08–1.67); ML4A, 0.40 μM (0.27–0.62); and Lipid IVa: 0.19 nM (0.15–0.23).

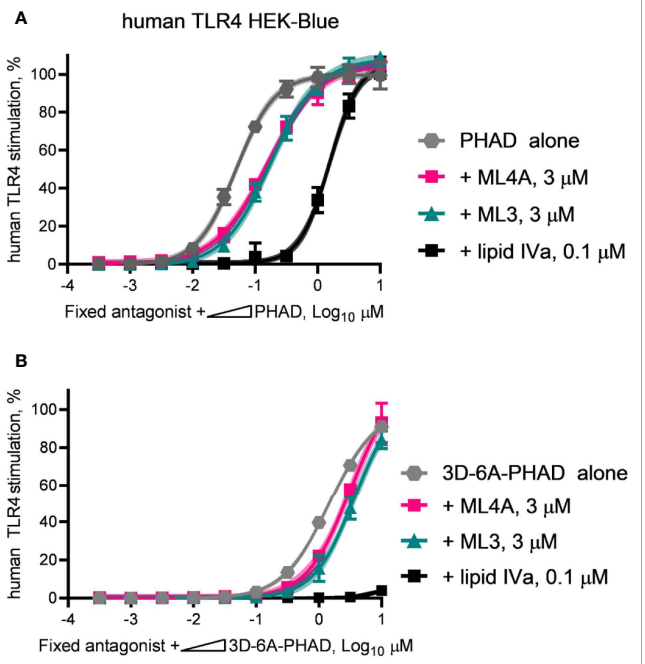

FIGURE 7 | ML3 and ML4A function as competitive antagonists of human TLR4. MPL adjuvant® components ML3 and ML4A were tested for competitive antagonism of human TLR4 using reporter cells. The agonists **(A)** PHAD and **(B)** 3D-6A-PHAD were diluted in half-log steps from a peak concentration of 10 μM in a mixture containing a fixed concentration of ML3 (3 μM), ML4A (3 μM) or Lipid IVa (0.1 μM). Values shown are averages ± SD of secreted alkaline phosphatase from two independent experiments, each performed in duplicate or triplicate and normalized by setting 100% = PHAD or 3D-6A-PHAD alone (3 μM). Shaded regions indicate 99% confidence intervals within which the true population means should occur 99% of the time. Agonist curves in the presence of a fixed amount of ML3 or ML4A reached the same top dose plateaus as for agonist alone indicating both are competitive antagonists of human TLR4.

saccharides (30), ii) loss of the 1-phosphate (14)., iii) loss of the 3-O-acyl chain (10) and now, we suggest, iv) the presence of antagonists that prevent full occupancy of TLR4 such that the overall mixture behaves as a partial agonist.

Our finding that component ML4A is an agonist of mouse TLR4 (**Figures 5B, D**) but an antagonist of human TLR4 (**Figure 6**) is consistent with the behavior of another tetra-acylated structure, Lipid IVa. The known presence of tetra-acylated congeners in MPL® adjuvant was in fact one of the rationales for our decision to evaluate the species specificity effects of both the clinical-grade and the research-grade versions of the adjuvant mixture. Product information provided by the manufacturers of the various MPLA preparations indicates that none of the sources we used, or could find, included the alkaline hydrolysis step described by Myers and colleagues (10, 16). Omission of this step, which specifically releases the 3-O-acyl chain of Lipid A, means that the structure of the tetra-acylated component that appears to be present in some of the MPLA preparations we tested (E-, I-, and S-MPLA; **Figure 2D**) is not likely to be identical to ML4A. A likely candidate is a monophosphorylated version of Lipid IVa that would retain a 3-O-acyl chain in a 1:1:1:1 configuration (four primary acyl chains). Confirmation that this is true would require detailed analysis of the structures present in the various MPLA preparations.

A somewhat more surprising finding than the presence of a tetra-acylated antagonist of human TLR4 in MPL® adjuvant is the existence of a tri-acylated antagonist, component ML3. A search of the literature revealed that this structure–activity relationship is not unprecedented because synthetic

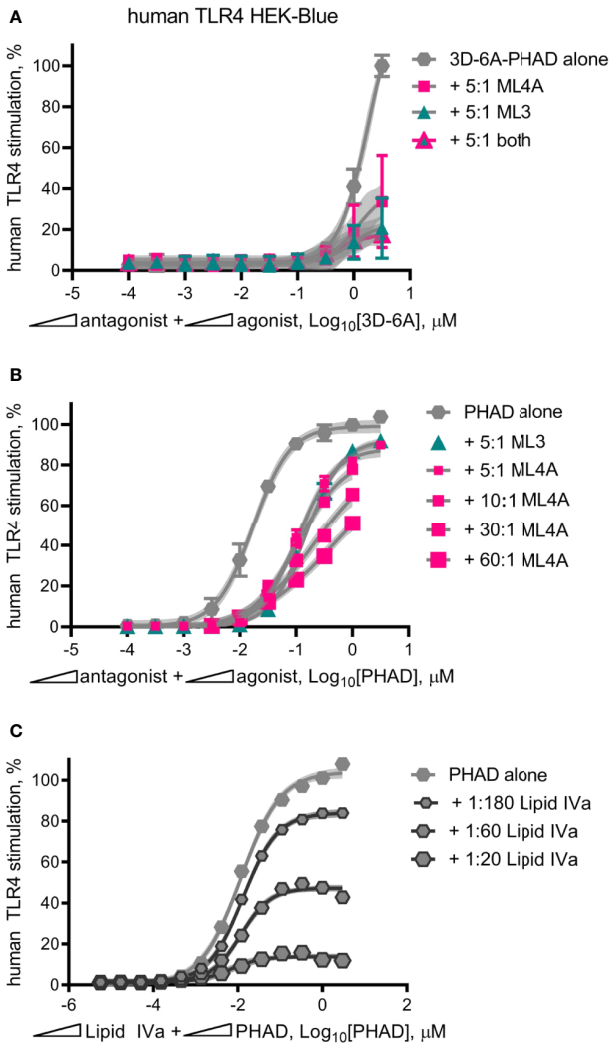

FIGURE 8 | Mixed agonist–antagonist dose profiles replicate the low dose plateau of MPL adjuvant®. Dose curve profiles of agonist-antagonist mixtures at fixed ratios were generated using human TLR4 reporter cells to determine whether the suppressed dose plateau of MPL adjuvant® could be recapitulated with synthetic components. **(A)** 3D-6A-PHAD, as a surrogate for ML6, was mixed with either ML3, ML4A or both at a ratio of 5:1 antagonist: agonist and diluted in half-log steps from peak concentrations of [3.16 μM 3D-6A-PHAD + 15.8 μM antagonist]. Values ± SD shown are of secreted alkaline phosphatase from three independent experiments performed in duplicate and normalized by setting 100% = max value for 3D-6A-PHAD alone. **(B)** PHAD was mixed with ML4A at ratios of 5:1, 10:1, 30:1 or 60:1 antagonist:agonist and diluted in half-log steps from peak concentrations of either 3.16 μM (5:1) or 1 μM (10:1, 30:1, 60:1) PHAD; two experiments were normalized by setting 100% = top dose plateau for PHAD alone. **(C)** PHAD was mixed with Lipid IVa at ratios of 1:20, 1:60 or 1:180 antagonist:agonist and diluted in half-log steps from a peak concentration of 3.16 μM PHAD; Values ± SD are from three independent experiments, each in triplicate, normalized by setting 100% = top dose plateau for PHAD alone. Shaded regions indicate 99% confidence intervals within which the true population means should occur 99% of the time. Mixed agonist:antagonist preparations containing synthetic PHAD and Lipid IVa generated the largest dose range across which a suppressed plateau of human TLR4 stimulation could be maintained.

compounds similar in structure to ML3 but with two phosphates, or one phosphate and non-physiological R groups placed at the 1-position, were reported to inhibit human TLR4 several years ago (31). Although the abundance of ML3 in MPL® adjuvant preparations is unclear because studies of MPL® composition were generally focused on analysis of structures with four or more acyl chains (10, 13, 14, 17, 20), its inhibitory activity likely overlaps with that of the more abundant ML4A structure to form a mixture of TLR4 agonists and antagonists whose combined activity is typical of partial agonism, ie, partial stimulation of a signaling system through non-saturating engagement of its upstream receptors or downstream effector molecules. In the case of ML3 and ML4A, it is probable that upstream receptor occupancy is affected due to their behavior as competitive antagonists in the potency shift assays we performed (**Figure 7**).

We also report a technique whereby the partial agonism of human TLR4 by MPL® adjuvant can be replicated with a far simpler mixture of components. In the example provided (**Figure 8C**), mixtures of the full agonist PHAD with the antagonist Lipid IVa generated dose response curves in the human TLR4 HEK-Blue system whose top dose plateau could be manipulated by adjusting and then fixing the relative proportions of the two compounds. This 'antagonist spiking' approach has the advantages of simplifying the number of components to be monitored in production of vaccine lots, relative to the half-dozen present in MPL® adjuvant whose proportions are sensitive to minor differences in temperature and acid and alkaline hydrolysis conditions (10) and reducing the amount of material needed to achieve a desired threshold of TLR4 receptor occupancy and stimulation (**Figure 8C**).

It remains to be determined whether or not partial agonism of TLR4 by a mixed agonist-antagonist preparation is actually beneficial. Consideration of the frequency of reactogenic side effects reported in clinical trials of vaccines containing MPL® adjuvant, however, suggest that it may be critically important at the level of maintaining tolerability in healthy human subjects. A review of clinical trial data from head-to-head comparisons of vaccines that differed solely or primarily in having MPL® adjuvant or not (*i.e.*, alum alone *versus* AS04 formulations) revealed that intramuscular immunizations produced painful inflammatory reactions in nearly 90% of study participants when the vaccine included MPL® adjuvant *versus* 40–60% when it did not (32). This pattern was surprisingly uniform across differing demographics that included girls age 9–14 (33), women aged 18–45 (34), or men and women aged 18–45 (35). Removal of adjuvant components such as ML3 and ML4A that moderate the extent to which TLR4 is activated could potentially exacerbate painful injection sites and other indices of local inflammatory reactions. Hence, it is possible that the current composition of MPL® adjuvant is approaching the asymptote of tolerability that influences when a vaccine is considered to be safe such that increases in its TLR4 stimulatory function could be counterproductive.

Interindividual human variability of TLR4 responses further complicates the safe use of an endotoxin-derived material in vaccines. Cervarix and Shingrix injections deliver MPL® adjuvant at an initial concentration of 100 μg/ml, which could

theoretically be decreased if endogenous antagonists were somehow removed. A low dose of a full TLR4 agonist presumably could be used to achieve therapeutic effects below the threshold for endotoxic effects in some individuals, but achieving the same outcome consistently in large numbers of diverse people, as is the case with prophylactic immunization seems problematic. This is because some individuals appear to be more sensitive to endotoxin signaling than others. For example, in a study of 102 healthy blood donors whose cells were exposed to 10 ng/ml LPS for 6 h the amount of TNFα produced varied by three orders of magnitude (36). This enormous range of sensitivities suggests that methods by which TLR4 receptor occupancy is minimized, fortuitously or by design, could be beneficial by putting an upper limit on the extent to which the signaling system can be activated. Our study thus identifies mixed agonist-antagonist activity as an additional mechanism by which MPL® adjuvant is detoxified to render it safe for widespread use in the vast populations of individuals in need of immune protection from infectious disease.

DATA AVAILABILITY STATEMENT

All datasets presented in this study are included in the article/ **Supplementary Material**.

ETHICS STATEMENT

The studies involving human participants were reviewed and approved by University of Louisville Institutional Review Board. The patients/participants provided their written informed consent to participate in this study. The use of mice as a source of bone marrow was reviewed and approved by Institutional Animal Use and Care Committee.

AUTHOR CONTRIBUTIONS

TM, CC, JE, and HB-L conceived of the project. Y-QW wrote sections of the manuscript with finalization of it by TM and CC. Y-QW, CC, and TM performed experiments as described in the text. All authors contributed to the article and approved the submitted version.

FUNDING

Research reported in this publication was supported by the National Institute of Allergy and Infectious Diseases of the National Institutes of Health under Award Number R01AI127970. The content is solely the responsibility of the authors and does not necessarily represent the official views of the National Institutes of Health. Additional funding was provided by the Barnstable-Brown Foundation and the Commonwealth of Kentucky Research Challenge Trust Fund.

ACKNOWLEDGMENTS

The authors gratefully acknowledge Dr. David Johnson and Mark M. Livesay for providing synthetic versions of MPL® components, and Ikenna Chukwudolue, Caryl Conklin and Dr. Joseph P. Kolb for assistance in preparing and testing the components.

SUPPLEMENTARY MATERIAL

The Supplementary Material for this article can be found online at: https://www.frontiersin.org/articles/10.3389/fimmu.2020.577823/full#supplementary-material

REFERENCES

1. Garçon N, Van Mechelen M, Wettendorff M. Development and evaluation of AS04, a novel and improved adjuvant system containing MPL and aluminum salt. In: VEJC Schijns, DT O'Hagan, editors. *Immunopotentiators in Modern Vaccines*. London: Academic Press (2006). p. 161–77.
2. European Medicines Agency: Committee for Medicinal Products for Human Use - Fendrix: EPAR - Scientific Discussion. (2005). Available at: https://www.ema.europa.eu/documents/scientific-discussion/fendrix-epar-scientific-discussion_en.pdf, June 2020.
3. European Medicines Agency: Committee for Medicinal Products for Human Use - Cervarix: EPAR - Procedural steps taken before authorisation. (2007). Available at: https://www.ema.europa.eu/documents/procedural-steps/cervarix-epar-procedural-steps-taken-authorisation_en.pdf, June 2020.
4. Centers for Disease Control (CDC). FDA licensure of bivalent human papillomavirus vaccine (HPV2, Cervarix) for use in females and updated HPV vaccination recommendations from the Advisory Committee on Immunization Practices (ACIP). *MMWR Morb Mortal Wkly Rep* (2010) 59 (20):626–9.
5. Didierlaurent AM, Laupeze B, Di Pasquale A, Hergli N, Collignon C, Garcon N. Adjuvant system AS01: helping to overcome the challenges of modern vaccines. *Expert Rev Vaccines* (2017) 16(1):55–63. doi: 10.1080/14760584.2016.1213632
6. Dooling K, Guo A, Patel M, Lee G, Moore K, Belongia E, et al. Recommendations of the Advisory Committee on Immunization Practices for Use of Herpes Zoster Vaccines. *MMWR Morb Mortal Wkly Rep* (2018) 67:103–8. doi: 10.15585/mmwr.mm6703a5
7. European Medicines Agency: Committee for Medicinal Products for Human Use - European public assessment report for Shingrix. (2018). Available at: https://www.ema.europa.eu/documents/assessment-report/shingrix-epar-public-assessment-report_en.pdf, June 2020.
8. Didierlaurent AM, Collignon C, Bourguignon P, Wouters S, Fierens K, Fochesato M, et al. Enhancement of adaptive immunity by the human vaccine adjuvant AS01 depends on activated dendritic cells. *J Immunol* (2014) 193(4):1920–30. doi: 10.4049/jimmunol.1400948
9. Didierlaurent AM, Morel S, Lockman L, Giannini SL, Bisteau M, Carlsen H, et al. AS04, an aluminum salt- and TLR4 agonist-based adjuvant system, induces a transient localized innate immune response leading to enhanced adaptive immunity. *J Immunol* (2009) 183(10):6186–97. doi: 10.4049/jimmunol.0901474
10. Ulrich JT, Myers KR. Monophosphoryl Lipid A as an Adjuvant. In: MF Powell, MJ Newman, editors. *Vaccine Design: The Subunit and Adjuvant Approach*. New York: Plenum Press (1995). p. 495–524.
11. McKee AS, Munks MW, MacLeod MKL, Fleenor CJ, Van Rooijen N, Kappler JW, et al. Alum Induces Innate Immune Responses through Macrophage and Mast Cell Sensors, But These Sensors Are Not Required for Alum to Act As an

Adjuvant for Specific Immunity. *J Immunol* (2009) 183(7):4403. doi: 10.4049/jimmunol.0900164
12. Ribi E, Parker R, Strain SM, Mizuno Y, Nowotny A, Von Eschen KB, et al. Peptides as requirement for immunotherapy of the guinea-pig line-10 tumor with endotoxins. *Cancer Immunol Immunother* (1979) 7(1):43–58. doi: 10.1007/BF00205409
13. Qureshi N, Takayama K, Ribi E. Purification and Structural Determination of Nontoxic Lipid A Obtained from the Lipopolysaccharide of Salmonella-Typhimurium. *J Biol Chem* (1982) 257(19):1808–15.
14. Ribi E, Cantrell JL, Takayama K, Qureshi N, Peterson J, Ribi HO. Lipid A and immunotherapy. *Rev Infect Dis* (1984) 6(4):567–72. doi: 10.1093/clinids/6.4.567
15. Takayama K, Ribi E, Cantrell JL. Isolation of a Nontoxic Lipid A Fraction Containing Tumor Regression Activity. *Cancer Res* (1981) 41(7):2654–7.
16. KR Myers, AT Truchot, J Ward, Y Hudson, JT Ulrich eds. *A Critical Determinant of Lipid A Endotoxic Activity. Int Congr Ser*. San Diego, CA: Elsevier Science Publishers (1990). p. 1990.
17. Hagen SR, Thompson JD, Snyder DS, Myers KR. Analysis of a monophosphoryl lipid A immunostimulant preparation from Salmonella minnesota R595 by high-performance liquid chromatography. *J Chromatogr A* (1997) 767(1-2):53–61. doi: 10.1016/s0021-9673(97)00041-1
18. Johnson DA, Keegan DS, Sowell CG, Livesay MT, Johnson CL, Taubner LM, et al. 3-O-Desacyl monophosphoryl lipid A derivatives: synthesis and immunostimulant activities. *J Med Chem* (1999) 42(22):4640–9. doi: 10.1021/jm990222b
19. Johnson DA, Sowell CG, Keegan DS, Livesay MT. Chemical synthesis of the major constituents of Salmonella minnesota monophosphoryl lipid A. *J Carbohyd Chem* (1998) 17(9):1421–6. doi: 10.1080/07328309808002363
20. Garçon N, Tavares Da Silva F. "Chapter 15 - Development and Evaluation of AS04, a Novel and Improved Adjuvant System Containing 3-O-Desacyl-4′-Monophosphoryl Lipid A and Aluminum Salt". In: VEJC Schijns, DTO'Hagan, editors. *Immunopotentiators Modern Vaccines* (Second Edition). Academic Press (2017). p. 287–309. doi: 10.1016/B978-0-12-804019-5.00015-3
21. Garçon N, Friede M. Evolution of Adjuvants Across the Centuries. In: SA Plotkin, WA Orenstein, PA Offit, KM Edwards, editors. *Plotkin's Vaccines, Seventh Edition*. Elsevier (2018). p. 61–74.e4.
22. Coler RN, Bertholet S, Moutaftsi M, Guderian JA, Windish HP, Baldwin SL, et al. Development and characterization of synthetic glucopyranosyl lipid adjuvant system as a vaccine adjuvant. *PLoS One* (2011) 6(1):e16333. doi: 10.1371/journal.pone.0016333
23. Reed SG, Carter D, Casper C, Duthie MS, Fox CB. Correlates of GLA family adjuvants' activities. *Semin Immunol* (2018) 39:22–9. doi: 10.1016/j.smim.2018.10.004
24. Evans JT, Cluff CW, Johnson DA, Lacy MJ, Persing DH, Baldridge JR. Enhancement of antigen-specific immunity via the TLR4 ligands MPL™ adjuvant and Ribi.529. *Expert Rev Vaccines* (Second Edition) (2003) 2 (2):219–29. doi: 10.1586/14760584.2.2.219
25. Fox CB, Carter D, Kramer RM, Beckmann AM, Reed SG. Current Status of Toll-Like Receptor 4 Ligand Vaccine Adjuvants. In: VEJC Schijns, DT O'Hagan, editors. *Immunopotentiators in Modern Vaccines (Second Edition)*. Academic Press (2017). p. 105–27.
26. Johnson D. Synthetic TLR4-active Glycolipids as Vaccine Adjuvants and Stand-alone Immunotherapeutics. *Curr Topics Med Chem* (2008) 8:64–79. doi: 10.2174/156802608783378882
27. Golenbock DT, Hampton RY, Qureshi N, Takayama K, Raetz CR. Lipid A-like molecules that antagonize the effects of endotoxins on human monocytes. *J Biol Chem* (1991) 266(29):19490–8.
28. Hajjar AM, Ernst RK, Tsai JH, Wilson CB, Miller SI. Human Toll-like receptor 4 recognizes host-specific LPS modifications. *Nat Immunol* (2002) 3(4):354–9. doi: 10.1038/ni777
29. Lutz MB, Kukutsch N, Ogilvie ALJ, Rößner S, Koch F, Romani N, et al. An advanced culture method for generating large quantities of highly pure dendritic cells from mouse bone marrow. *J Immunol Methods* (1999) 223 (1):77–92. doi: 10.1016/S0022-1759(98)00204-X
30. Cochet F, Peri F. The Role of Carbohydrates in the Lipopolysaccharide (LPS)/Toll-Like Receptor 4 (TLR4) Signalling. *Int J Mol Sci* (2017) 18(11):2318. doi: 10.3390/ijms18112318
31. Dunn-Siegrist I, Tissieres P, Drifte G, Bauer J, Moutel S, Pugin J. Toll-like receptor activation of human cells by synthetic triacylated lipid A-like molecules. *J Biol Chem* (2012) 287(20):16121–31. doi: 10.1074/jbc.M112.348383
32. Mitchell TC, Casella CR. No pain no gain? Adjuvant effects of alum and monophosphoryl lipid A in pertussis and HPV vaccines. *Curr Opin Immunol* (2017) 47:17–25. doi: 10.1016/j.coi.2017.06.009
33. Leung TF, Liu AP-Y, Lim FS, Thollot F, Oh HML, Lee BW, et al. Comparative immunogenicity and safety of human papillomavirus (HPV)-16/18 AS04-adjuvanted vaccine and HPV-6/11/16/18 vaccine administered according to 2- and 3-dose schedules in girls aged 9–14 years: Results to month 12 from a randomized trial. *Hum Vaccines Immunother* (2015) 11(7):1689–702. doi: 10.1080/21645515.2015.1050570
34. Einstein MH, Baron M, Levin MJ, Chatterjee A, Fox B, Scholar S, et al. Comparative immunogenicity and safety of human papillomavirus (HPV)-16/18 vaccine and HPV-6/11/16/18 vaccine: follow-up from months 12-24 in a Phase III randomized study of healthy women aged 18-45 years. *Hum Vaccin* (2011) 7(12):1343–58. doi: 10.4161/hv.7.12.18281
35. Leroux-Roels G, Marchant A, Levy J, Van Damme P, Schwarz TF, Horsmans Y, et al. Impact of adjuvants on CD4(+) T cell and B cell responses to a protein antigen vaccine: Results from a phase II, randomized, multicenter trial. *Clin Immunol* (2016) 169:16–27. doi: 10.1016/j.clim.2016.05.007
36. Wurfel MM, Park WY, Radella F, Ruzinski J, Sandstrom A, Strout J, et al. Identification of high and low responders to lipopolysaccharide in normal subjects: an unbiased approach to identify modulators of innate immunity. *J Immunol* (2005) 175(4):2570–8. doi: 10.4049/jimmunol.175.4.2570

Conflict of Interest: The authors declare that the research was conducted in the absence of any commercial or financial relationships that could be construed as a potential conflict of interest.

frontiers in Immunology

ORIGINAL RESEARCH
published: 20 October 2020
doi: 10.3389/fimmu.2020.578505

Preparing for Life: Plasma Proteome Changes and Immune System Development During the First Week of Human Life

Tue Bjerg Bennike[1,2,3,4†‡], Benoit Fatou[1,2,3‡], Asimenia Angelidou[2,3,5†], Joann Diray-Arce[2,3], Reza Falsafi[6], Rebecca Ford[7], Erin E. Gill[6], Simon D. van Haren[2,3†], Olubukola T. Idoko[8], Amy H. Lee[6,9], Rym Ben-Othman[10], William S. Pomat[7], Casey P. Shannon[11†], Kinga K. Smolen[2,3†], on behalf of The EPIC Consortium, Scott J. Tebbutt[11,12,13†], Al Ozonoff[2,3†], Peter C. Richmond[14], Anita H. J. van den Biggelaar[14†], Robert E. W. Hancock[6], Beate Kampmann[8,15†], Tobias R. Kollmann[10,16†], Ofer Levy[2,3,17†] and Hanno Steen[1,2,3†]*

[1] Department of Pathology, Boston Children's Hospital, Boston, MA, United States, [2] Precision Vaccines Program, Boston Children's Hospital, Boston, MA, United States, [3] Harvard Medical School, Boston, MA, United States, [4] Department of Health Science and Technology, Aalborg University, Aalborg, Denmark, [5] Department of Neonatology, Beth Israel Deaconess Medical Center, Boston, MA, United States, [6] Department of Microbiology and Immunology, University of British Columbia, Vancouver, BC, Canada, [7] Papua New Guinea Institute of Medical Research, Goroka, Papua New Guinea, [8] Vaccines and Immunity Theme, Medical Research Council Unit, The Gambia at the London School of Hygiene and Tropical Medicine, Banjul, Gambia, [9] Department of Molecular Biology and Biochemistry, Simon Fraser University, Burnaby, BC, Canada, [10] Department of Pediatrics, University of British Columbia, and BC Children's Hospital, Vancouver, BC, Canada, [11] PROOF Centre of Excellence, Vancouver, BC, Canada, [12] UBC Centre for Heart Lung Innovation, St. Paul's Hospital, Vancouver, BC, Canada, [13] Department of Medicine, Division of Respiratory Medicine, University of British Columbia, Vancouver, BC, Canada, [14] Telethon Kids Institute, Perth, WA, Australia, [15] Vaccine Centre, Faculty of Infectious and Tropical Diseases, London School of Hygiene and Tropical Medicine, London, United Kingdom, [16] Department of Experimental Medicine, University of British Columbia, Vancouver, BC, Canada, [17] Broad Institute of MIT & Harvard, Cambridge, MA, United States

Neonates have heightened susceptibility to infections. The biological mechanisms are incompletely understood but thought to be related to age-specific adaptations in immunity due to resource constraints during immune system development and growth. We present here an extended analysis of our proteomics study of peripheral blood-plasma from a study of healthy full-term newborns delivered vaginally, collected at the day of birth and on day of life (DOL) 1, 3, or 7, to cover the first week of life. The plasma proteome was characterized by LC-MS using our established 96-well plate format plasma proteomics platform. We found increasing acute phase proteins and a reduction of respective inhibitors on DOL1. Focusing on the complement system, we found increased plasma concentrations of all major components of the classical complement pathway and the membrane attack complex (MAC) from birth onward, except C7 which seems to have near adult levels at birth. In contrast, components of the lectin and alternative complement pathways mainly decreased. A comparison to whole blood messenger RNA (mRNA) levels enabled characterization of mRNA and protein levels in parallel, and for 23 of the 30 monitored complement proteins, the whole blood transcript information by itself was not reflective of the plasma protein levels or dynamics during the first week of life. Analysis of

OPEN ACCESS

Edited by:
Christoph T. Berger,
University of Basel, Switzerland

Reviewed by:
Glenn Robert Burgner Bantug,
University of Basel, Switzerland
Axel Olin,
Stanford University, United States

***Correspondence:**
Hanno Steen
hanno.steen@childrens.harvard.edu

†ORCID:
Casey P. Shannon
orcid.org/0000-0002-5687-3156
Tue Bjerg Bennike
orcid.org/0000-0003-4354-1731
Scott Tebbutt
orcid.org/0000-0002-7908-1581
Simon Van Haren
orcid.org/0000-0002-1791-0161
Kinga Smolen
orcid.org/0000-0001-8650-3693
Anita Van Den Biggelaar
orcid.org/0000-0002-3323-7261
Beate Kampmann
orcid.org/0000-0002-6546-4709
Tobias Kollmann
orcid.org/0000-0003-2403-976
Al Ozonoff
orcid.org/0000-0003-4233-5899
Asimenia Angelidou
orcid.org/0000-0002-6716-6561
Ofer Levy
orcid.org/0000-0002-5859-1945
Hanno Steen
orcid.org/0000-0003-0179-6648

‡These authors have contributed equally to this work

Specialty section:
This article was submitted to Vaccines and Molecular Therapeutics, a section of the journal Frontiers in Immunology

Received: 30 June 2020
Accepted: 22 September 2020
Published: 20 October 2020

immunoglobulin (Ig) mRNA and protein levels revealed that IgM levels and synthesis increased, while the plasma concentrations of maternally transferred IgG1-4 decreased in accordance with their *in vivo* half-lives. The neonatal plasma ratio of IgG1 to IgG2-4 was increased compared to adult values, demonstrating a highly efficient IgG1 transplacental transfer process. Partial compensation for maternal IgG degradation was achieved by endogenous synthesis of the IgG1 subtype which increased with DOL. The findings were validated in a geographically distinct cohort, demonstrating a consistent developmental trajectory of the newborn's immune system over the first week of human life across continents. Our findings indicate that the classical complement pathway is central for newborn immunity and our approach to characterize the plasma proteome in parallel with the transcriptome will provide crucial insight in immune ontogeny and inform new approaches to prevent and treat diseases.

Keywords: ontogeny, complement, innate immune system, immunoglobulin, proteomics, inhibitors, membrane attack complex (MAC), terminal complement complex (SC5b-9)

INTRODUCTION

Bacteria and viruses that cause mild to no disease in adults can be life-threatening in newborns and infants (1). Neonatal infections cause 700,000 annual casualties, corresponding to 40% of deaths in children under 5 years of age (2). The biological mechanisms responsible for the early age-specific susceptibility are thought to be related to immune system development and age-specific adaptations in immunity due to resource constraints (1–3). This results in heightened vulnerability in early life where immune protection primarily relies on the innate immune system including leukocytes, cytokines, and the complement system, and the added protection from maternal factors including IgG antibodies transferred to the fetus over the placenta and IgA from breast milk (4–6). The complement system is a central element in the innate immune system and activation initiates several defense mechanisms, including enhancing circulating immunoglobulins, opsonization, immune cell recruitment, regulation of adaptive immunity, and the direct disruption of cell membranes (5).

The developmental trajectory of the immune system is increasingly recognized as a major determinant for overall health throughout life (7). However, our knowledge of the early life immune ontogeny and molecular mechanisms involved remains limited. We recently published the most comprehensive systems biology study of the first week of human life to date, using high-dimensional analytic platforms (7). Systems biology studies, including proteomics and transcriptomics, generate inherently comprehensive data that can be analyzed on many levels. Herein we present an extended analysis of the proteomics data of blood plasma from newborns using an improved bioinformatic pipeline. The high-dimensional molecular measurements together with unbiased analytic approaches, enable a deep data-driven analysis. The aim was to identify and characterize molecular networks and signatures related to immune system changes during the first week of life. Given the importance for newborn immunity, we focused our analysis on the complement system and maternally transferred antibodies.

This deep data analysis has greatly expanded on our original findings, indicating a highly dynamic biological state during the first week of life, compared to a relatively steady state in healthy adults (8). Findings in our study's main cohort from West Africa (The Gambia) were validated in an independent cohort from Australasia (Papua New Guinea, PNG). Even though dramatic changes occur in the first week of life, ontogeny follows a robust trajectory that is consistent even in geographically and ethnically distinct populations.

MATERIALS AND METHODS

Study Cohort and Ethics

Thirty and nineteen healthy, term newborns were enrolled at the Medical Research Council (MRC) Unit The Gambia at London School of Hygiene and Tropical Medicine and at the Institute for Medical Research (IMR) in Goroka, Papua New Guinea in accordance, with a local Ethics Committee-approved protocol (MRC SCC 1436 and IMR IRB#1515 and MRAC #16.14). A detailed description of the protocol has been published (9).

Following informed consent, mothers were screened for HIV-I and -II and hepatitis B. Positivity for either virus represented an exclusion criterion. Inclusion criteria were a healthy appearing infant as determined by physical examination, born by vaginal delivery at gestational age of >36 weeks, with a 5-min Apgar score > 8, and a birth weight of >2.5 kg. Peripheral blood samples were obtained from all infants on the day of birth (DOL0) and then again either at DOL1, DOL3, or DOL7 to limit phlebotomy to a maximum of twice in the first week of life (**Figure 1** and **Supplementary Figure 1**). Peripheral venous blood was drawn from infants *via* sterile venipuncture directly into heparinized collection tubes [Becton Dickinson (BD) Biosciences; San Jose, CA, USA]. Aliquots (200 µl) were immediately placed in RNA-later (Ambion Thermo Fisher; Waltham, MA, USA) for RNAseq analysis with the remaining blood kept in the collection tubes at room temperature. Within 4 h, the whole blood was centrifuged

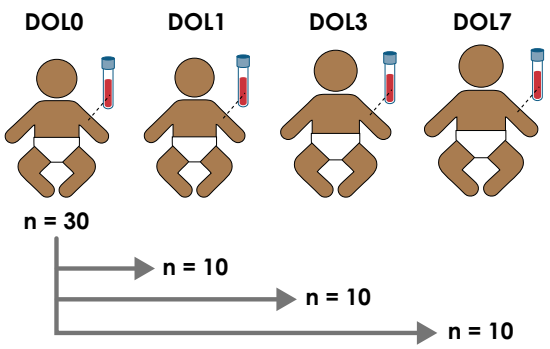

FIGURE 1 | Study design and number of enrolled newborns in the main cohort enrolled in The Gambia.

on site at 500 × g for 10 min at room temp and the plasma was stored at −80°C. All samples were shipped on dry ice (World Courier; New Hyde Park, NY, USA).

Plasma cytokine profiles were determined using a custom designed multi-analyte Cytokine Human Magnetic Panel Bead Array (Invitrogen/Life Technologies; Carlsbad, CA). Metabolite profiles were determined by metabolomics (Metabolon, Durham, NC, USA). Data was downloaded from the original publication (7) and re-analyzed.

Proteomics Sample Preparation

For the original study (7), plasma samples from newborns were prepared for proteome analysis using the in-house developed plasma and serum proteomics workflow, based on the MStern blotting sample processing and trypsinization protocol (10, 11). To this end, 5 µL plasma were diluted in 100 µL sample buffer (8 M urea in TRIS-HCl, pH 8.5). Protein disulfide bonds were reduced with dithiothreitol (10 mM final concentration) and alkylated with iodoacetamide (50 mM final concentration). An aliquot with 10 µg protein was transferred to a 96 well plate with a polyvinylidene fluoride (PVDF) membrane bottom (MSIPS4510, Millipore, MA, USA). Protein digestion was performed with sequencing-grade modified trypsin (V5111, Promega, Madison, WI, USA) at a nominal protease to protein ratio of 1:25 w/w. After incubation for 2 h at 37°C, the peptides were eluted and concentrated to dryness in a vacuum centrifuge. To monitor retention time stability and system performance, iRT peptides (Biognosys, Schlieren, Switzerland) were spiked into all samples.

Mass Spectrometry Analysis

The samples were analyzed using a nanoLC system (Eksigent, Dublin, CA) equipped with a LCchip system (cHiPLC nanoflex, Eksigent, CA, USA) coupled online to a Q Exactive Mass Spectrometer (Thermo Scientific, Bremen, Germany). From each sample, 0.2 µg peptide material was separated using a linear gradient from 93% solvent A (0.1% formic acid in water), 7% solvent B (0.1% formic acid in acetonitrile) which was increased to 32% solvent B over 60 min. The mass spectrometer was operated in data-dependent mode, selecting up to the 12 most intense precursors for fragmentation from each precursor scan.

Proteomics Data Analysis

Unbiased data-driven analytical approaches have the advantage that the data can be repeatedly interrogated based on varying starting hypotheses. Using the proteomics raw data from the original study (7), we performed a label-free protein quantitation (LFQ) analysis in the newest version of MaxQuant (v 1.6.2.5) using standard settings with quantitation by razor (protein-group shared) and unique peptides and LFQ normalization (12). Proteins were identified using the built-in Andromeda search engine and an updated reviewed UniProt Human Reference Proteome (13). Standard search settings were employed with matching between runs on and the following abundant modifications: max three tryptic missed cleavages, methionine oxidation as variable modification, and cysteine carbamidomethylation as fixed modification (11). The revert decoy search strategy in MaxQuant was used to filter all reported proteins and peptides to <1% false discovery rate (FDR) (14).

The lists of identified protein groups (henceforth referred to as proteins) and relative protein LFQ quantities were imported into R using Rstudio (15, 16), prior to application of an analytical workflow beyond that commonly applied to proteomics. The following additional filtering criteria were applied for quantifiable proteins: removal of i) proteins, which are commonly introduced during the handling, preparation and processing of the samples, tagged as likely contaminants by MaxQuant (e.g., keratins, trypsin, etc.), ii) proteins only identified by peptides containing variable modifications, and iii) proteins that were quantifiable in less than 50% of DOL0 and DOL1, 3, or 7 study participants. The strict filtering strategy enabled us to avoid the need to impute missing datapoints, and only use actual data, except for conducting principal component analysis (PCA) where missing values were replaced with values from a Gaussian distribution (q = 0.01, tune.sigma = 0.3) to simulate signals from low abundant proteins (17). ComBat R-package was used to correct for batch effects for samples run on different LC-MS columns and MStern plates (18). Quantro R-package was used to analyze for global differences in the protein abundances between the different DOLs (10,000 simulations), which could point to methodological problems (19). Additionally, ggplot2 was used for visualizations, MixOmics for analysis, and dplyr for data matrix formatting (20–22). All data is publicly available and can be accessed through this publication. The mass spectrometry RAW data and search results have been deposited to the ProteomeXchange consortium *via* the PRIDE partner repository and are available with the data set identifier PXD019817, as well as archived on ImmPort (https://immport.niaid.nih.gov/home) under accession numbers SDY1256 and SDY1412 (23, 24).

Differential Protein Expression Analysis and Bioinformatics

We fitted a linear mixed-effects regression model of intensity, with fixed effects of DOL, sex, LC column/MStern plate, and a

random participant effect, using the lmer function from the lme4 R package (25). Proteins that were quantifiable in less than 50% of DOL0 and DOL1, 3, or 7 study participants were removed, and remaining missing values were not included in the analysis. P-values and fold changes were calculated DOL-wise using the paired experimental design, with a null-model without DOL using the ANOVA-function, and we controlled the FDR by applying the Benjamini–Hochberg correction method (26). Proteins were considered to be significantly differentially regulated at 5% FDR and +/− 0.2 log2 foldchange. Additionally, we performed a missing-value analysis based on Fisher's exact testing on the data matrix prior to filtering, as the strict valid value filtering scheme would have removed DOL-unique proteins. Significant proteins were further analyzed using WebGestaltR for pathway analysis, StringDB for obtaining protein-protein interaction networks, and Cytoscape for visualization (27–29). Boxplot center lines show the medians, box limits indicate the 25th and 75th percentiles, whiskers extend 1.5 times the interquartile range from the 25th and 75th percentiles, outliers are represented by dots. FDR adjusted p-values (q-values) from the statistical models are reported on the boxplots, unless otherwise stated.

Immunoglobulin G Subclass Ratio Analysis

The relative inter-abundances of the IgG subclasses were estimated using the intensity-based absolute quantitation (iBAQ) values from MaxQuant, calculated from unique peptide abundances only (uploaded to the PRIDE repository PXD019817). To enable a comparison to the adult state, we used data from a previously published proteomics study of plasma from 30 healthy adult Danes (10). To compensate for the different experimental designs, we normalized the IgG ratios to IgG2 (of note, normalization to IgG3 yielded similar results) in each dataset. Significantly different Ig-ratios were calculated using two-sample t-tests.

RNA Sample Preparation and Sequencing

For RNA sequencing, total RNA was extracted from whole blood using the RiboPure RNA Purification Kit. Quantification and quality assessment of total RNA was performed on an Agilent 2100 Bioanalyzer. Samples with sufficiently high RNA integrity number were considered for sequencing. Poly-adenylated RNA was captured using the NEBNext Poly(A) mRNA Magnetic Isolation Module. Strand-specific cDNA libraries were generated from poly-adenylated RNA using the KAPA Stranded RNA-Seq Library Preparation Kit and sequenced on a HiSeq 2500 (Illumina; San Diego, CA, USA). Sequence quality was assessed using FastQC and MultiQC1.8.1 (30). The FASTQ sequence reads were aligned to the human genome (Ensembl GRCh38.98) using STAR v2.7 and mapped to Ensembl GRCh38 transcripts (31). Read-counts were generated using htseq-count (HTSeq 0.11.2-1) (32). Data processing and subsequent differential gene expression (DGE) analyses were performed using the latest versions of R and DESeq2 using the Wald statistics and paired analysis (33). Genes with very low counts (with less than 10 counts in nine or more samples, or the smallest number of biological replicates within each treatment group) and globin transcripts were filtered out prior to DGE analysis.

RESULTS AND DISCUSSION

Enrolled Participants

Blood samples were collected employing a sample-sparing protocol, which enabled characterization of the plasma proteome, plasma metabolome, cytokine/chemokine profile, whole blood transcriptome, and single cell immunophenotype in the same sample (7). We utilized a paired study design with a blood sample collected from all newborns on the day of life (DOL) 0, and a matching follow-up sample either at DOL1, 3, or 7 (**Figure 1**). The main cohort included 60 samples collected from 30 newborns in The Gambia/West Africa and the smaller validation cohort comprised 38 samples collected from 19 newborns in Papua New Guinea (PNG)/Australasia using a similar experimental design (**Supplementary Figure 1**).

Having access to peripheral blood samples rather than cord blood for the DOL0 sample, provided each subject with an ideal specific baseline-sample. This would not have been the case with cord-blood as differences between peripheral and cord-blood have been reported (34). Findings in this study are limited to healthy babies born by vaginal delivery.

Quantifiable Proteins in Newborn Blood Plasma Cluster by Day of Life

We analyzed plasma samples using our published plasma proteomics workflow in a 96-well plate format, and identified 382 plasma proteins (FDR<1%), of which 197 passed our criteria for quantifiable proteins (10, 11). These numbers are comparable to those reported in similar plasma- and serum studies (10, 35, 36). Depletion of high-abundant proteins prior to analysis, such as albumin, complement component proteins, and immunoglobulins, could increase the number of monitored plasma proteins (10), but could also interfere with the abundance of other proteins, since e.g., albumin functions as a protein carrier (37). Therefore, to ensure the highest quality of data, we chose not to deplete the high-abundant plasma-proteins prior to proteomics analysis, which also enables us to characterize the levels of these, many of which are involved in modulating the immune system, and were as such relevant to our study.

Principal component analysis (PCA) of quantifiable proteins in newborn blood plasma revealed consistent changes over the first week in both the main cohort (**Figure 2**) and the validation cohort (**Supplementary Figure 2**), demonstrating a common developmental trajectory of the newborn plasma proteome during the first week of life across continents.

The Number of Changed Plasma-Proteins Increases With Age

This study aimed to identify differentiating proteins over the first week of life. For this purpose, we performed a linear regression analysis of the protein abundance data. Our statistical model allowed us to identify an increasing number of proteins that showed statistically significant DOL-dependent abundance differences (**Figures 3A, B**, **Supplementary Tables 1–3**). A similar trajectory was seen in the validation cohort (**Supplementary Figures 3-5**, **Supplementary Tables 4–6**).

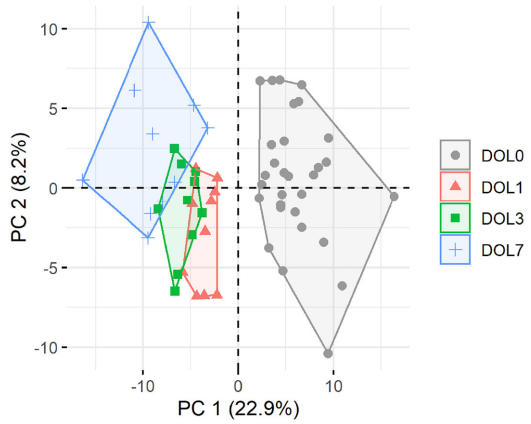

FIGURE 2 | Principal component analysis (PCA) plot of all quantifiable proteins separates samples by day of life (DOL). PC, principal component. Explained variance given in percentages.

The use of linear regression analysis yielded increased sensitivity compared to analysis using t-tests, as evidenced by identification of twice the number of differentiating proteins (7), likely by achieving higher statistical power (38, 39).

The proteins with the largest abundance increase at DOL1 compared to DOL0 were the acute phase proteins haptoglobin (HP) and serum amyloid A-1 (SAA1) (**Figures 3C, D**). SAA2 was also increased but did not pass multiple hypothesis testing (q-value: 0.11, p-value 0.03) (**Supplementary Table 7**). HP, SAA1, and SAA2 were the top three most increased proteins in the validation cohort at DOL1 when disregarding statistical significance as the number of samples in the validation cohort was smaller (**Supplementary Table 8**). This demonstrates a consistent observation across geographically distinct cohorts and experiments.

A correlation analysis of all protein level change relative to DOL0 (**Figure 4**) revealed several clusters of proteins with similar trajectories, including a hemoglobin (Hb) cluster and an acute phase response cluster with SAA1, SAA2, and complement component C6. The expression of the various globin genes is strictly balanced and coordinated, and the positive correlation of the Hb subunits is expected and validates the applied methodology (40).

Low Levels of Haptoglobin in the Hours After Birth

Several studies have failed to consistently measure HP in neonates and in particular at birth when concentrations are low, likely because of insufficient assay sensitivity (41). The reliable identification of HP at DOL0 demonstrates the high sensitivity of the applied methodology. The finding of increased HP after birth is in agreement with previous studies, where a significant increase in HP was measured at DOL2-4 compared to DOL0 (41), and in adults compared to neonates and children (42). Our study demonstrates that the increased HP can be measured as early as 24 h after birth.

The main physiological function of HP is to sequester free (extracellular) hemoglobin (Hb) released from destroyed red blood cells (43). The HP-Hb complex is quickly cleared from the circulation through monocytes and tissue macrophages *via* CD163 receptors, and degraded in lysosomes rather than being recycled which can lead to HP depletion (44). The gradual increase of HP at DOL1, 3, and 7 relative to DOL0, may reflect a physiologic rise of HP in neonatal plasma levels in these healthy newborn cohorts, preceding the need for clearance of the fetal hemoglobin HbF ($\alpha_2\gamma_2$) from the neonatal circulation as it is gradually replaced by the adult type HbA ($\alpha_2\beta_2$) over the first 6 months of life.

By binding excessive free Hb, HP exerts anti-inflammatory and anti-oxidant effects (43). Newborns and infants with a bacterial infection have increased HP-levels, and HP appears to regulate some adverse effects of inflammation (41) but the role of HP in neonatal sepsis is not yet fully understood. A study with a higher time-resolution could provide additional insights into the perinatal physiologic fluctuations of HP.

Acute Phase Response Proteins Transiently Increase on Day of Life 1

SAA1 is an acute phase protein with antimicrobial activity (45) mainly produced in response to infections (46), and was significantly increased at DOL1 and returned to DOL0 levels at DOL3 and DOL7.

SAA1 is mainly synthesized in the liver, but can also be synthesized by stimulated monocytes and monocyte-derived macrophages (47). We were unable to identify the corresponding mRNA in the whole blood, which indicated that during the first week of life SAA synthesis might be limited to the hepatocytes rather than stimulated immune cells in circulation.

Increased SAA1-levels could indicate the presence of an acute phase response at DOL1. To identify proteins with a similar trajectory, we performed a correlation analysis of SAA1 against all proteins (**Table 1**). Most proteins correlating positively with SAA1 were involved in the acute phase response. The protein with the most negative correlation to SAA1, alpha-2-macroglobulin (A2M), is involved in inhibiting the complement system response. Additionally, clusterin (CLU), another central inhibitor of the complement cascades, correlated negatively with SAA1.

Altogether these findings demonstrate the presence of an acute-phase response 24 h after birth, driven by an increase of several acute-phase proteins and a simultaneous reduction of inhibitory proteins. Our findings are in line with a previous publication, where SAA1 levels in newborns in Sweden were increased at DOL1 and subsequently decreased at DOL2 and DOL3 (48), and an acute phase response was evident shortly after birth (49, 50). Our study further expands on the molecular mediators of the acute phase response, demonstrating the involvement of the complement system and simultaneous reduction of inhibitors. The relatively short *in vivo* half-life of SAA1 (51, 52) in the 90-min range makes it unlikely that the increase on DOL1 was directly caused by immune cell activation during vaginal delivery. This is supported by the lack of corresponding whole blood mRNA, indicating that hepatocytes rather than activated immune cells are the likely point of synthesis.

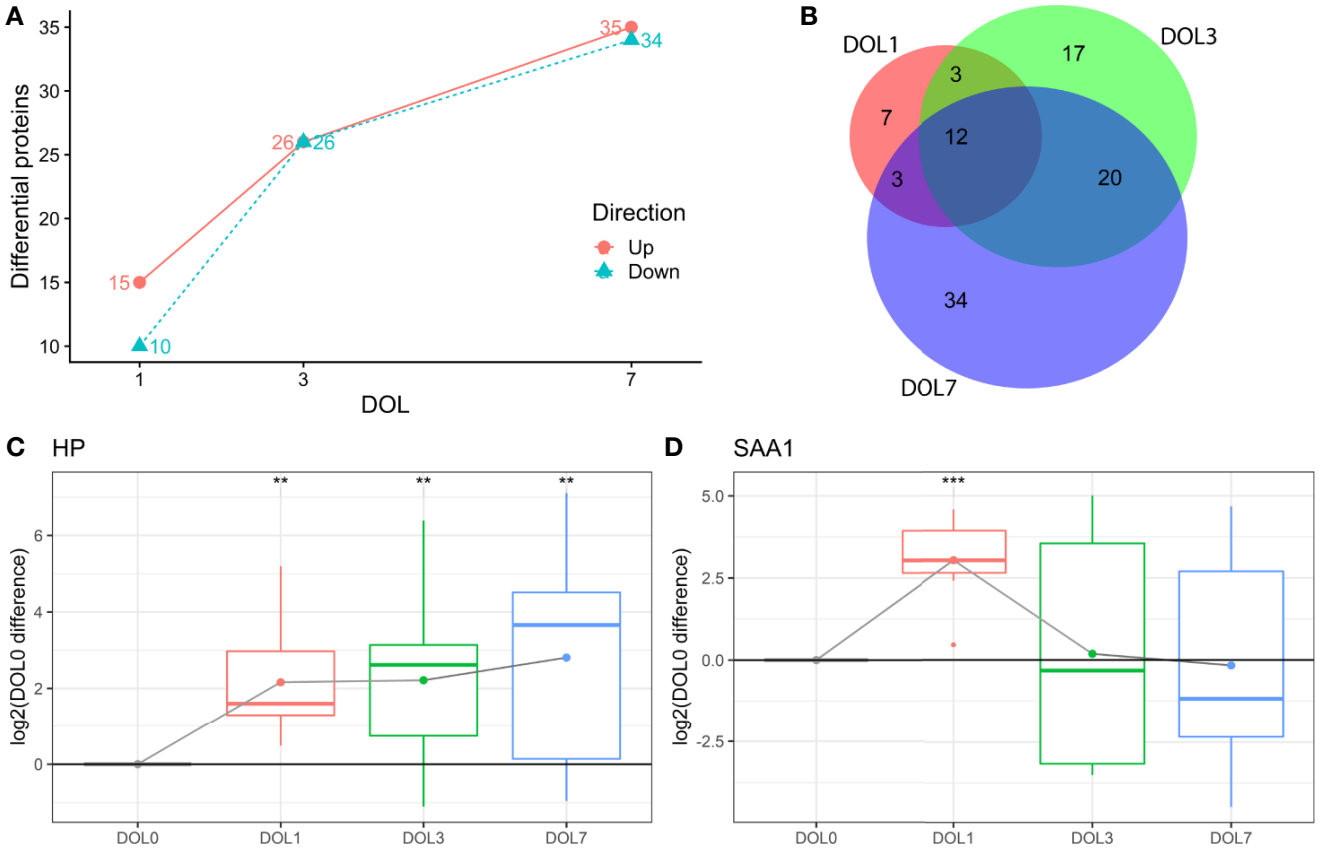

FIGURE 3 | Differentially abundant plasma proteins (q-value < 0.05) compared to day of life (DOL) 0. **(A)** We identified a robust trajectory of differentially expressed proteins over the first week of life. **(B)** Overlap of regulated proteins. Protein regulations of **(C)** Haptoglobin (HP). **(D)** Serum amyloid A1 (SAA1) normalized to DOL0, with mean abundance difference indicated by dots connected with a line. q-value * <0.05, **: <0.01, ***: <0.001.

Interleukin-6 (IL-6) is an inducer of hepatic acute phase protein synthesis (53), and of adrenal gland production of cortisol, a metabolite that enhances the acute phase response in part *via* increasing IL-6 receptor expression on hepatocytes (18). To further characterize molecular drivers of the acute phase response in early life, we investigated plasma IL-6 and cortisol concentrations, as determined by multi-plex assay and metabolomics, respectively. Likely reflecting recent labor (50), both IL-6 and cortisol levels were highest at DOL0 (7) (**Supplementary Table 9**), and likely initiate the subsequent physiologic acute phase response of the newborn (18, 50). Altered neonatal blood circulation and increased oxygen levels, as well as decreasing levels of circulating maternal factors in the newborn may also contribute to these early proteomic shifts. Speculatively, this first newborn inflammatory acute phase response could be a means of immune system development activation, in response to the extrauterine transition and anticipation of encounters with various microorganisms.

Complement System Development Is Central Over the First Week of Life

To identify underlying biological themes in addition to the early acute phase response, we performed a protein-protein interaction analysis of the increasing number of proteins showing ontogenic changes during the first week of life. The analysis revealed that many of the differentiating proteins were functionally related, and especially a cluster of proteins involved in the complement system increased with DOL (**Figure 5**, boxed area).

Activation of the complement system through the classical, lectin, or alternative complement pathways culminates in the common terminal pathway, which results in the formation of the membrane-lysing pore-structure termed the membrane attack complex (MAC) also known as the terminal component complex (TCC) (**Figure 6**) (54).

Although several studies have investigated circulating complement components in neonates (5), each of them have only partially characterized the complement system. Our study represents the first to characterize the development of the circulating complement system trajectories as a whole over the first week of life in two independent cohorts (**Table 2**, **Supplementary Table 9**) including whole blood transcriptomics. Neonates are relatively deficient in complement components, which increases their susceptibility to infections during the first months of life (5). The current consensus is that complement components are not able to cross the placental membrane under physiological conditions, and that all complement proteins identified in newborn blood therefore are synthesized by the fetus/newborn, and mainly by hepatocytes

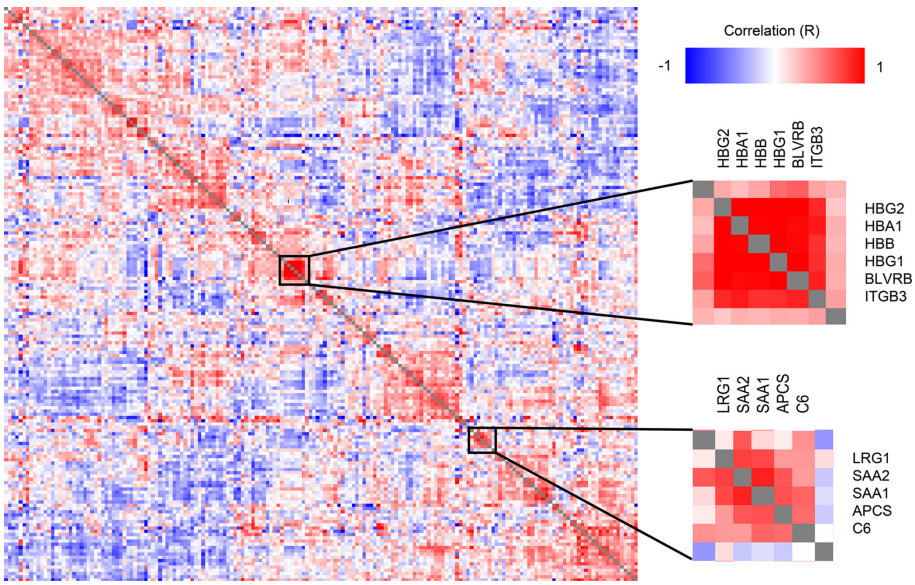

FIGURE 4 | Clustered Pearson's protein-protein correlation matrix of protein changes during the first week of life, of all quantifiable proteins (on the x- and y-axis) which allows for identifying proteins with similar trajectories across all samples. Several clusters of correlating proteins were identified, including a cluster centered around hemoglobin and an acute phase response cluster including SAA1 and SAA2.

TABLE 1 | Proteins with abundance differences significantly correlating (p-value < 0.05) with serum amyloid A-1 protein (SAA1) demonstrated an acute-phase response at DOL1.

R	P-value	Protein name	Gene name	Description	UPID
1.000	<2.2E–16	Serum amyloid A-1 protein	SAA1	Acute-phase response	P0DJI8
0.821	5.78E–04	Serum amyloid A-2 protein	SAA2	Acute-phase response	P0DJI9
0.672	3.16E–03	Leucine-rich alpha-2-glycoprotein	LRG1	Brown fat cell differentiation/bacterial response	P02750
0.642	3.06E–04	Serum amyloid P-component	APCS	Acute-phase response	P02743
0.587	1.28E–03	Fibrinogen alpha chain	FGA	Blood clotting/associated with infection	P02671
0.566	2.10E–03	Complement component C6	C6	Complement activation	P13671
0.512	6.27E–03	Alpha-1-antichymotrypsin	SERPINA3	Acute-phase response	P01011
0.459	1.60E–02	Haptoglobin	HP	Acute-phase response	P00738
0.413	3.21E–02	Alpha-1-acid glycoprotein 1	ORM1	Acute-phase response	P02763
0.405	3.59E–02	Fibrinogen beta chain	FGB	Blood clotting/associated with infection	P02675
0.389	4.51E–02	Neutrophil defensin 3	DEFA3	Antibacterial activities	P59666
–0.389	4.48E–02	Complement C1q subunit C	C1QC	Complement system	P02747
–0.423	2.81E–02	Plasma kallikrein	KLKB1	Convert prorenin into renin	P03952
–0.450	3.14E–02	Flavin reductase (NADPH)	BLVRB	Oxidoreductase	P30043
–0.458	1.63E–02	Clusterin	CLU	Inhibitor of complement	P10909
–0.484	1.05E–02	Inter-alpha-trypsin inhibitor heavy chain H2	ITIH2	Protease inhibitor	P19823
–0.509	6.73E–03	Apolipoprotein M	APOM	Cholesterol homeostasis	O95445
–0.751	6.41E–06	Alpha-2-macroglobulin	A2M	Inhibitor of complement	P01023

(55). It should be noted that C3 and C7 may be transferred from the fetus to the mother, while C1RL may be a tissue (placenta) leakage protein detected in newborn plasma (56).

The Classical Complement Pathway Components Increase Over the First Week of Life

The classical pathway is activated, primarily on mucosal surfaces, by binding of the C1 complex (C1q, C1r, and C1s) to surface-bound immune complexes, mainly IgG or IgM (57). C1 activation initiates the terminal pathway and the formation of the MAC transmembrane pore-structure on the target membrane.

We identified C1q (chains A, B, and C), C1r, C1s, C4 (isotype B), and C2 components. While the data sufficed for the identification of C1q chain A, they did not meet our stringent requirements for robust quantification, i.e., quantitative analysis of C1qA was omitted. Plasma concentrations of the C1 complex (C1qB, C1qC, C1r, and C1s), C4B, and C2 from the classical component pathway increased over the first week of life (**Figure 7A**, **Table 2**). C1r and C1s were significantly increased on DOL3, and C1qB on DOL7

compared to DOL0. Highly similar changes were seen in the validation cohort (**Supplementary Tables 8**, **9**).

While the trajectories of C1q chain B and C demonstrated a similar increase, only C1qB was significantly increased at DOL7 with C1qC at near significance levels (p-value 0.026, q-value 0.060). C1q is predominantly synthesized by blood-cells, whereas C1r and C1s, like most complement components, are synthesized mainly by hepatocytes (58). The difference in synthesis location likely explains the slightly different abundance pattern of C1q lacking a significant increase on DOL3. The increased concentration of C1q is in good agreement with previous reports (5). Our study is the first to report the increased concentration of the individual B and C subunits.

Our findings demonstrate the increased levels of the components activating the classical complement pathway, which is supported by the finding of increasing levels of C4B rather than C4A. In humans, C4 exists in isotypes A and B, and following activation of the C1 complex, both isotypes are cleaved into alpha and beta-chains (59). C4A beta forms an amide bond which has good efficiency in binding amino group-rich immune complexes whereas C4B beta forms an ester bond which has good efficiency in binding carbohydrate-rich cellular surfaces (60). This makes C4B the more functionally active isotype to activate C3 through the classical- and lectin pathway (61). As a result, a deficiency of C4B increases vulnerability to bacterial and viral infections, whereas C4A deficiency is linked to autoimmune diseases (61).

Overall, the average plasma concentration of classical pathway components was significantly increased over the first week of life, and as early as 24 h after birth.

The Lectin Complement Pathway Components Decrease Over the First Week of Life

In contrast to the increase in components of the classical complement pathway, plasma concentrations of complement components involved in initiating the lectin complement pathway decrease over the first week of life. The lectin pathway is initiated by binding of mannose-binding lectin (MBL), collectin 11, and ficolins (FCN1, FCN2, and FCN3) to oligosaccharides and acetylated residues on the surface of bacteria, viruses, and dying cells. Following binding, mannan-binding lectin serine protease 1 (MASP-1) or 2 is recruited into the MBL complex, which similarly to the classical complement

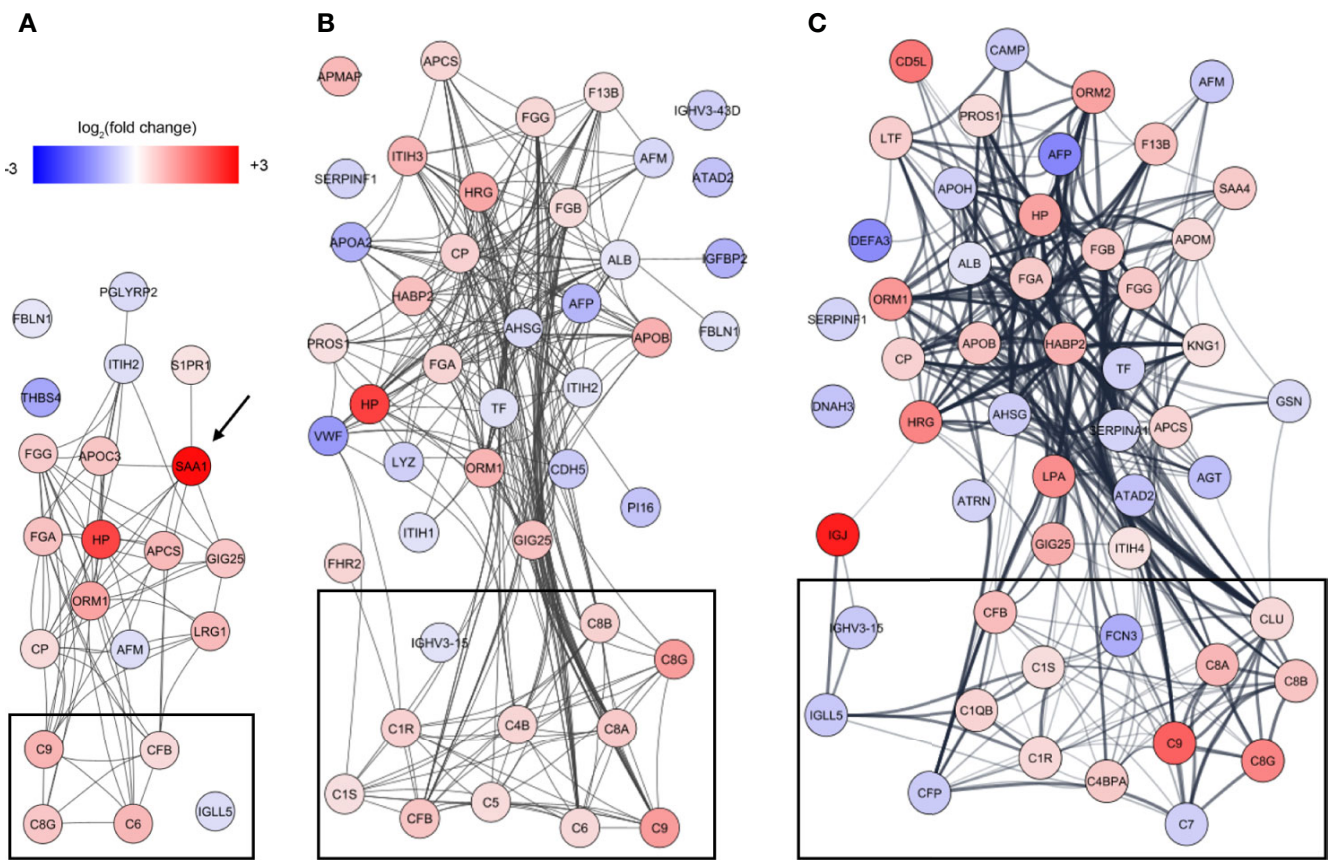

FIGURE 5 | Analysis of protein-protein interactions of the differentiating proteins at **(A)** DOL1, **(B)** DOL3, and **(C)** DOL7 compared to DOL0 (at birth). SAA1 which was regulated at DOL1 only is indicated with an arrow, and lines indicate interacting proteins. Proteins tagged as complement system in Gene Ontology are indicated with black boxes without further curation.

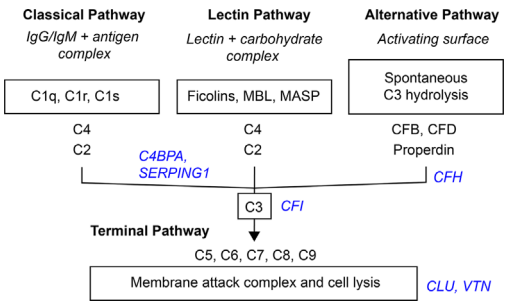

FIGURE 6 | Simplified scheme of the three activation- and terminal complement pathway. Inhibitors in blue italic.

pathway results in cleavage of C2 and C4 and formation of the C4bC2b complex. MASP-1 is required for activation of MASP-2, and of the two only MASP-2 can cleave C4 (62). The resulting C4bC2b complex triggers the enzymatic cleavage of C3 into C3a and C3b, and initiates the terminal complement pathway (62).

Of the six lectin complement pathway pattern-recognition proteins, we identified three in our plasma proteomics dataset: FCN-2, FCN-3, and MASP1. While the data sufficed for the identification of MASP1, they did not meet our stringent requirements for robust quantification, i.e., quantitative analysis of MASP1 was omitted. FCN-3 showed a downward trend during the first week of life and was significantly reduced at DOL7 (**Figure 7B**) in the main cohort, whereas the reduced levels at DOL7 were not statistically significant in the validation cohort (**Supplementary Table 10**). Since neither of the two underlying genes are transcribed/translated in blood cells, no corresponding mRNA information was obtained (63). The lack of feasibility to detect and/or solidly quantify lectin complement pathway proteins, might be explained by a presumed low plasma concentration, and warrants targeted follow-up studies.

Serum concentrations of lectin pathway factors FCN-1, FCN-2, FCN-3, MASP-2 (64), and MBL (65, 66) are reportedly low in newborns compared to infants, children, and adults (67). Ficolins are reportedly lower in neonates than in older children (68). This is the first study to report on the FCN-3 concentration trajectory during the first week of life. The measured decreased plasma concentrations of FCN-3 through the first week of life would be expected to further be associated with impaired activation of the lectin complement pathway in early life, and indicates that the increase of lectin pathway component levels takes place after the first week of life.

Overall, our findings indicate that the levels of activating components in the lectin complement pathway remain relatively deficient in the first week of life, a finding supported by negligible protein synthesis.

The Alternative Complement Pathway Components Display a Binomial Distribution

Compared to classical- and lectin complement pathways, changes in components of the alternative complement pathway displayed a binomial distribution. Our plasma proteomic workflow provided us with identification and quantification of three proteins associated with activation of the alternative complement pathway (69) (**Figure 7C**). We measured a statistically significant decrease of properdin (aka complement factor P/CFP) at DOL7, and an overall decreasing trend during the first week of life, whereas complement factor B (CFB) continuously increased from DOL1 onward to DOL7. A similar protein trajectory was found in the validation cohort for CFB, whereas the levels of CFP did not achieve statistical significance (**Supplementary Table 9**).

CFB and CFP are essential for activation of the alternative complement pathway, and newborns have reduced plasma concentration compared to adults (5). Adult levels of CFB are reportedly achieved within 6 months after birth, in contrast to CFP-levels that remain low at 6 months of age (5). Here we demonstrated for the first time that these trajectories are established as early as 24 h after birth. CFP is the only complement regulator that enhances complement activation, by stabilizing the C3bBb-complex. It is mainly synthesized outside the liver by neutrophils, monocytes, and primary T cells, and can be secreted upon stimulation (70, 71). The CFP mRNA levels did not show any significant change during the first week of life (fold-change < 0.2, p-value > 0.05) (7), indicating insufficient CFP synthesis to maintain the DOL0-plasma levels, a lack of compensatory protein synthesis, and a presumed absence of leukocyte stimulation.

Overall, our findings indicate that the levels of activating components in the alternative complement pathway remain low with negligible synthesis in the first week of life.

The Terminal Complement Pathway Components Increase Over the First Week of Life

The MAC is the terminal point of the terminal complement pathway and complement activation, and the transmembrane pore-structure which causes cell lysis and ultimately cell death (54).

Our plasma platform allowed us, for the first time, to quantify all major MAC components, C5-9 (**Figure 7D**). At DOL3 and DOL7, all but one of the major components of MAC showed significant abundance increases (C5, C6, C8, and C9). The notable exception was C7, which showed a significant decrease in plasma levels during the first week of life. Again, similar protein trajectories were found in the validation cohort (**Supplementary Table 9**).

The MAC components are mainly synthesized by hepatocytes. In this regard, C7 is unique in being synthesized by blood cells in addition to hepatocytes (72–74). Newborns demonstrate near-adult levels of C7, as opposed to low levels of the remainder of MAC components (5, 75). C7 is often the rate-limiting step in MAC-formation and a decrease of C7 would potentially inhibit MAC formation, while local C7 synthesis at the site of inflammation might enhance MAC formation (72). The decrease of C7 from DOL3 onward is also noteworthy as we were unable to even detect the corresponding mRNA in whole blood.

TABLE 2 | Change of central complement system proteins at DOL-1, 3, and 7 (0% equals no change relative to at birth).

Protein names	GN	DOL1	DOL3	DOL7	Protein level	Function	UPID
Complement C1q subcomponent B	C1QB	*–1.3%*	13.7%	**34.7%**		C	P02746
Complement C1q subcomponent C	C1QC	*6.2%*	18.9%	26.0%		C	P02747
Complement C1r subcomponent	C1R	*12.4%*	**37.1%**	**30.6%**		C	P00736
Complement C1s subcomponent	C1S	*4.1%*	**22.1%**	**24.1%**		C	P09871
Complement C2	C2	*12.9%*	18.5%	*18.3%*		C	P06681
Complement C3	C3	*4.1%*	*2.3%*	*7.4%*	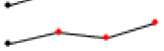	C, L, A	P01024
Complement C4-B	C4B	*6.7%*	**32.1%**	22.7%	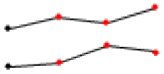	C	P0C0L5
Complement factor B	CFB	**27.4%**	**50.5%**	**63.1%**	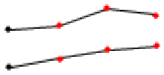	A	P00751
Complement factor D	CFD	*–16.8%*	–17.7%	–20.2%	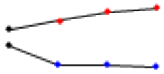	A	P00746
Properdin	CFP	*9.6%*	*–15.7%*	**–31.0%**	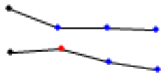	A	P27918
Prothrombin	F2	*–1.0%*	*7.8%*	*2.6%*	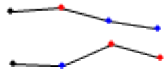	C, L, A	P00734
Ficolin-2	FCN2	*–28.7%*	*–1.5%*	*–21.5%*	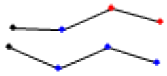	L	Q15485
Ficolin-3	FCN3	*–20.7%*	*–43.5%*	**–46.5%**		L	O75636
Complement C5	C5	*6.6%*	**26.4%**	*18.8%*		MAC	P01031
Complement component C6	C6	**69.7%**	**28.8%**	23.3%		MAC	P13671
Complement component C7	C7	*3.5%*	**–12.1%**	**–28.3%**	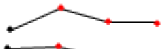	MAC	P10643
Complement component C8 alpha	C8A	*11.2%*	**46.4%**	**72.9%**	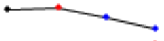	MAC	P07357
Complement component C8 beta	C8B	*22.0%*	**37.4%**	**53.6%**		MAC	P07358
Complement component C8 gamma	C8G	**49.9%**	**113.2%**	**162.0%**		MAC	P07360
Complement component C9	C9	**75.8%**	**115.2%**	**253.2%**		MAC	P02748
Alpha-2-macroglobulin	A2M	**–5.8%**	*–1.3%*	*0.5%*		I	P01023
C4b-binding protein alpha chain	C4BPA	*1.8%*	*17.3%*	**44.8%**		I	P04003
Complement factor H	CFH	*–4.7%*	*0.3%*	10.9%	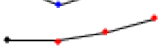	I	P08603
Complement factor I	CFI	*2.7%*	*–3.9%*	*14.1%*	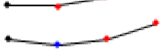	I	P05156
Clusterin	CLU	*–12.9%*	*5.8%*	**29.5%**		I	P10909
Carboxypeptidase B2	CPB2	*–4.0%*	*–0.5%*	*4.2%*	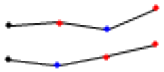	I	Q96IY4
Carboxypeptidase N catalytic chain	CPN1	*22.8%*	*0.3%*	*–1.2%*	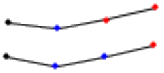	I	P15169
Vitamin K-dependent protein S	PROS1	*–6.1%*	**21.2%**	**26.4%**	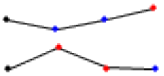	I	P07225
Plasma protease C1 inhibitor	SERPING1	*–10.2%*	*8.2%*	*–25.9%*		I	P05155
Vitronectin	VTN	*–5.7%*	*0.9%*	13.5%	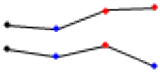	I	P04004

Gray italic: p-value > 0.05, black: p-value < 0.05, black bold: q-value < 0.05. Trend marker red (blue): positive (negative) change compared to DOL0. Pathways from Gene Ontology without further curation: C, classical; L, lectin; A, alternative; I, complement inhibitor; MAC, membrane attack complex.

Low levels of the MAC components at baseline followed by their increase, apart from C7, could indicate MAC maturation to support innate immunity.

The Complement Inhibitors

Inhibitors are central in controlling complement system activity in order to limit damage to the site of inflammation and protect healthy host-cells.

Out of the 10 complement system inhibitors identified in our analysis, A2M was reduced on DOL1. From DOL1 onward, five showed a subsequent increase (**Figure 7E**) based on adjusted (CLU, vitamin K-dependent protein S/PROS1, and C4b-binding protein alpha-chain/C4BPA) or unadjusted (CFH and vitronectin/VTN) p-values at DOL7 compared to DOL0. A similar trajectory of PROS1, C4BPA, and CFH was seen in the validation cohort (**Supplementary Table 9**).

The general decrease of complement inhibitors 24 h after birth supports our finding of an acute phase response on DOL1, driven by an increase of acute phase proteins and complement proteins, and the decrease of several complement system inhibitors. A2M is a protease inhibitor and it has been reported that A2M binds covalently to and inhibits MASP (73), although the inhibitory functions of A2M on the complement system are still debated (74). In our study the decreased A2M-levels at DOL1 returned to baseline levels at DOL3. This is the first study to report on the A2M levels in the

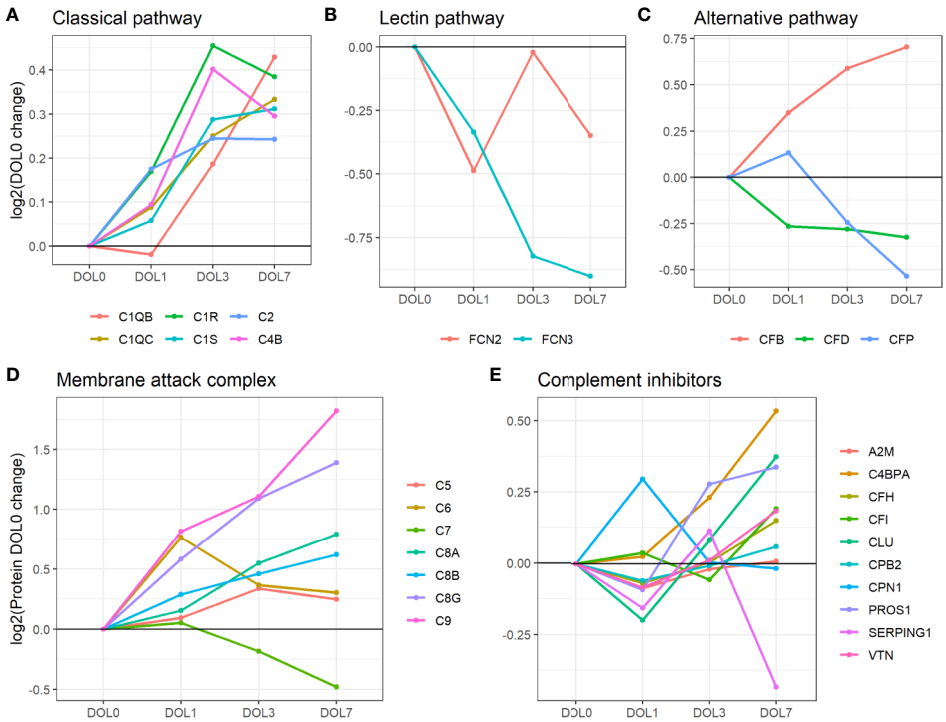

FIGURE 7 | Average change of complement proteins grouped by their function across the first week of life compared to DOL0. **(A)** classical pathway, **(B)** lectin pathway, and **(C)** alternative pathway. **(D)** Membrane attack complex (MAC) proteins, **(E)** complement inhibitors. Pathway activations from Gene Ontology without further curation.

first week of life, and reportedly infants and children have increased A2M-levels compared to adults, indicating that the increased trajectory of A2M likely continues past DOL7 (42).

CLU and VTN inhibit formation of the MAC (76), and newborns have lower levels when compared to adults (42, 77). The increased MAC inhibitor and the increasing abundances of the MAC components therefore clearly indicate a readying of the MAC for the postnatal period during the first week of life.

Newborns have low levels of CFH compared to adults (5), and the steady levels of CFH and sudden increase at DOL7 could indicate the early preparation for the alternative complement pathway, in line with the detected increase of CFB at DOL7 (**Supplementary Table 9**).

The function of PROS1 in the complement system remains incompletely understood. However, PROS1 has been suggested to redirect C4BP to the surface of apoptotic cells to control activation of the classical complement pathway. PROS1 has high affinity for negatively charged phospholipid phosphatidylserine, which is expressed and exposed on cells in the initial stage of apoptosis. In human plasma, 60–70% of PROS1 circulates bound in a complex with C4B. It is reported that PROS1 mediates binding of C4BP to apoptotic cells, thereby controlling complement activation (78). Newborn levels of PROS1 and C4BP are lower than adult levels (78). PROS1 also has anticoagulant effects lost upon binding to C4BP. The similar increase of PROS1 and C4BP makes it possible that the increased level of PROS1 is related to regulating the increase of complement system components. However, further studies are required.

Altogether, our findings demonstrated the consistent and robust increase of complement components in the classical activation pathway over the first week of life, while components of the lectin- and alternative pathway lacked a clear developmental trajectory. Additionally, all components of the MAC except the rate-limiting C7 were increased at DOL7. The absence of blood cell expression of C7, SAA1, and CFP indicates that blood cell stimulation is not a main initiator of the protein synthesis in the first week of life, and that the maturation of the complement components is therefore mainly driven by ontogeny rather than bacterial stimulation. Finally, we measured a decrease of most complement system inhibitors at DOL1 and subsequent recovery and increase at DOL7. Newborns are deficient in most complement components and the increasing plasma-levels indicate that the complement system components are approaching adult levels and maturation. However, future studies should be performed to investigate if the complement system activity follows the measured concentrations of complement system components. Speculatively, the apparent prioritization of synthesis of components related to the classical and terminal complement pathway, could be a means of obtaining a first complete complement response to pathogens as quickly as possible during a resource constrained immune system development.

Whole Blood Messenger RNA Levels of the Complement System Poorly Reflect Protein Plasma Levels

The inconsistency between protein and mRNA levels for several complement components, led us to perform a correlation analysis for the complement pathway data. We extracted all complement proteins for which we had corresponding whole blood mRNA information.

While the majority of the complement proteins with corresponding whole blood transcripts increased with age (**Figure 8**), the corresponding mRNA levels had a binominal distribution, with one group increasing from DOL0 to DOL3 and subsequent leveling off at DOL7, while the other group showing little abundance differences during the first week of life (**Figure 8**). Accordingly, there was a weak correlation between the change in protein plasma levels and change in whole blood mRNA levels (all pairs $R < 0.3$, p-value > 0.05). Of note, when we performed the correlation analysis using DOL average rather than individual participant data, we achieved much higher (R −0.67 to 0.88) yet still statistically insignificant (p-value > 0.05) correlation coefficients. This observation suggests large protein-to-RNA level variations between participants, or could represent concordance of mRNA and protein level data for only a small subset of complement protein. Indeed, of the 30 monitored complement proteins, the mRNA levels reflected the protein level changes for the following seven complement proteins (average $R > 0.3$): C1QB ($R = 0.88$), C1QC ($R = 0.86$), C2 ($R = 0.90$), C3 ($R = 0.85$), CLU ($R = 0.74$), SERPING1 ($R = 0.79$), and complement factor D/CFD ($R = 0.49$).

Differences between the mRNA/transcriptomics and proteins/proteomics information highlight the fact that there is no transcriptomics equivalent to the plasma proteome. The plasma proteome is a systemic body fluid integrating protein reflecting dynamic processes of protein expression and degradation across different organ systems and body compartments, while the whole blood transcriptome provides transcriptomic information from whole white blood cell fraction only (non-nucleated red blood cells having proteins but no transcripts), with neutrophils having lower transcript abundance making a more minor contribution. As the white blood cells are removed during the plasma preparation, whole blood transcriptomics and plasma proteomics map the two complementary, mutually exclusive blood fractions. Indeed, integration of the transcriptome and proteome is key to elucidate meaningful physiologic changes and generate mechanistic hypotheses to study the immune ontogeny of the newborn.

Increased Immunoglobulin M and J Chain Synthesis

The increased levels of components related to the classical complement activation pathway prompted us to investigate IgM and IgG, the main target molecules for the C1-complex and thereby activators of the classical complement pathway. IgM cannot cross the placental barrier and is the first antibody synthesized by peripheral blood lymphocytes during primary infections, thereby highlighting its central role in the initial immune response (79, 80). IgM is a pentamer connected with joining chains (J chain), which regulates the polymerization of the molecule for efficient secretion (79, 81).

Plasma levels of IgM increased over the first week of life (**Figure 9A**), a finding confirmed in the validation cohort (**Supplementary Figures 6A, B**). J chain levels also increased, mirroring the IgM concentration trajectories (**Figure 9B**), with a strong positive Pearson's correlation that was statistically significant ($R = 0.73$, p-value = 2.44E−5). In accordance with plasma concentrations, we measured similar increased mRNA level trajectories for the IgM and J chain when compared to the plasma proteins and found a significant positive correlation between plasma and mRNA levels (**Figures 9A, B** dotted line).

The physiologic average serum level of IgM is reportedly 18.5 mg/dl (15% of adult levels) in the first month of life, and this increases 3-fold in months 1–5 of life reaching adult levels by 1–2 years of age (82). The present study demonstrated that IgM levels increased from DOL3 onward in the first week of life, and based on the data an incant at DOL7 can be expected to have IgM concentrations of 38 to 54 mg/dl, when assuming average IgM concentrations at DOL0. J chain is required for Ig-transport across the mucosal epithelium, e.g., for secretion. Whether J chain regulation occurs at the protein level remains to be determined, and there are conflicting views on the origins of some of the J chain secreting cells (81). Based on our findings, there was J chain expression in whole blood and there were ontogeny-induced increases at both the cell transcriptional and plasma-protein levels.

Insufficient Immunoglobulin G Synthesis

IgG antibodies are the most abundant Ig-class in the circulation, especially in the fetus through placental transfer mediated by the FcRn receptors (82). Placentally transferred IgG provide protection in the first weeks of life due to the relatively long *in vivo* half-life of IgG (~3 weeks) (83). Of the four IgG subclasses, IgG1 can primarily be induced by soluble protein antigens and membrane proteins, IgG2 by bacterial capsular polysaccharides, IgG3 by viral antigens (like IgG1) and induce pro-inflammatory effects, and IgG4 by repeated exposure to a non-infectious antigen (84).

We measured significantly decreasing plasma concentrations of all four IgG subclasses over the first week of life, and IgG1 was significantly decreasing as early as 24 h after birth (**Figures 9C**, **10A–D**). A similar trajectory of IgG plasma-levels was seen in the validation cohort (**Supplementary Figures 7A–D**).

Serum levels of IgG1-4 are reportedly decreased in 1–5 month old infants compared to 0–30 day old newborns (82). Our study adds to the existing literature by providing granularity in the IgG1-4 plasma level trajectory over the first week of life. The measured decreases in IgG levels from birth to 5 months of age are consistent with a drop of maternal IgG levels in the newborn circulation, on top of low endogenous production. This physiologic transient hypogammaglobulinemia is a well-described phenomenon and is typically not clinically significant. Adult concentrations of most IgG-subclasses are eventually reached by 4–6 years of age (82).

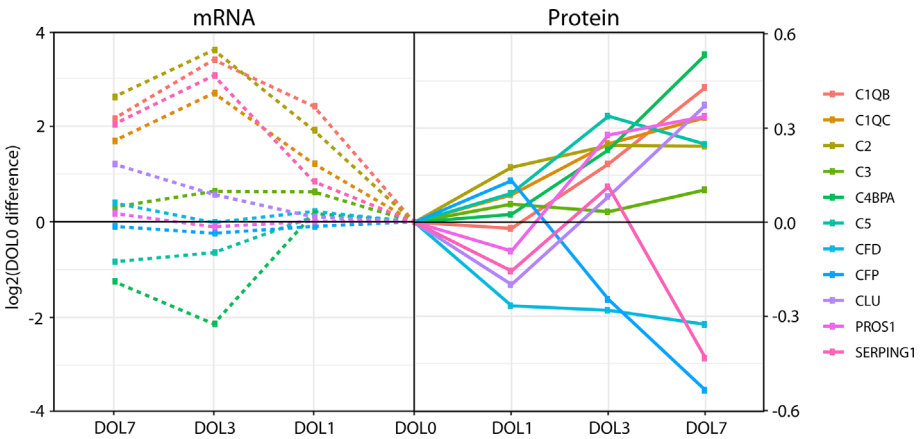

FIGURE 8 | Divergence of complement plasma protein and whole blood messenger RNA (mRNA) levels, as compared to DOL0, of the 11 complement proteins with detected whole blood mRNA.

We were interested in determining the timing of initiation for endogenous IgG synthesis from newborn plasma cells. We thus measured mRNA levels of IgG subclasses from DOL0, and found IGHG1 mRNA transcripts in 26 of the 30 newborns at DOL0 (validation cohort 13 of 19 newborns), indicative of endogenous IgG1 synthesis as early as DOL0. Additionally, we observed that IGHG1 mRNA levels were significantly increased on DOL3 and DOL7 (**Figure 9C**), while no mRNA was detected for IGHG2-4 in either cohort. The protein levels and mRNA levels of IGHG1 were negatively correlated ($R = -0.42$, p-value = 0.037), indicating that despite endogenous IgG1 synthesis as early as DOL0, plasma levels decreased over the first week of life, likely because of dominance of the *in vivo* degradation process. These findings were reproduced in the validation cohort (**Supplementary Figure 6C**).

To investigate the impact of the IgG1 synthesis on the plasma concentration, we calculated the apparent IgG1 plasma concentration half-time in our dataset to 21.1 days. This is comparable to the reported IgG1 *in vivo* half-life of 21–25.8 days (85, 86). The decline in IgG1 plasma concentration in newborns is thereby explained by the reported IgG1 *in vivo* half-life (with no synthesis). This demonstrates that IgG1 synthesis remains insignificant in the first week of life.

We performed an analysis of the inter IgG-subclass ratios. As different proteins were compared, we estimated the IgG-subclass abundances using intensity-based absolute quantitation (iBAQ) values. To enable a comparison to adult levels, we included data from a previously published proteomics study of plasma from 30 healthy adult Danes (10). To compensate for the different experimental designs, we normalized the IgG ratios to IgG2 in each dataset. Of note, normalization to IgG3 yielded similar results.

The analysis revealed that IgG1 was the most abundant IgG throughout the first week of life followed by IgG2, IgG3, and IgG4 (**Figures 10E, F**), in agreement with published literature from newborns within the first 30 days of life (82).

Of the four IgG subclasses, there is a preferential placental transport of IgG1, followed by IgG4, and to a lesser extend of IgG3 and IgG2, based on FcRn receptor affinity (55, 87). Healthy term newborns are born with similar to increased IgG-concentrations compared to the mother (88). Because we did not have access to the maternal IgG-levels, we obtained a previously published proteomics dataset of plasma from 30 healthy adult Danes (**Figures 10E, F**). Newborns had a significantly increased IgG1 to IgG2-4 ratio, when compared to adults. The findings were reproduced in the validation cohort (**Supplementary Figures 7E, F**).

IgM, IgG1, and IgG3 antibodies are efficient activators of the complement system through the classical pathway, whereas a high epitope density is needed of IgG2, and IgG4 is ineffective (89, 90). The relatively elevated concentration of IgG1 in the newborns compared to adults, combined with the specific synthesis of this subclass, and the increase in IgM, suggest a central role of the classical pathway of complement activation for newborn immunity.

CONCLUSION

Our study presented a mapping of the plasma proteome across the first week of human life in a paired African cohort with an independent geographically distinct validation cohort in Australasia. Newborns are primarily dependent on innate immunity to shield them from infection, and we characterized the ontogeny of several innate immune components over the first week of life. Specifically, we found increased plasma and mRNA levels of all major components related to the classical and terminal complement pathways, including the C1 complex and the target molecule IgM, as early as 24 h after birth. All components of the MAC, except C7 which is at near-adult levels at birth, increased by DOL7, as well as most complement system inhibitors, suggesting a central role for the classical complement pathway for neonatal

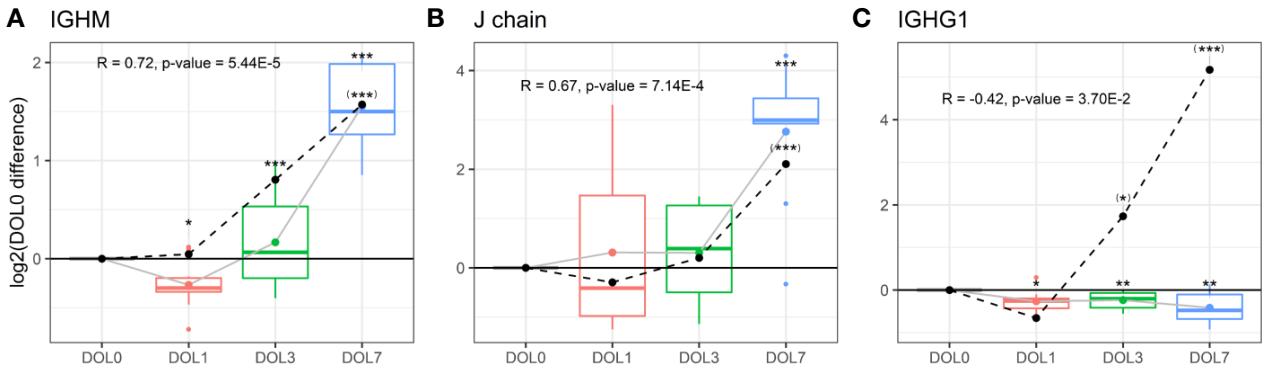

FIGURE 9 | Protein and messenger RNA (mRNA) levels (dotted line) of **(A)** IgM, **(B)** J chain, **(C)** IgG1 across the first week of life compared to DOL0, with mean abundance difference indicated by dots connected by lines. Protein to RNA correlation and p-value given. Statistics compared to DOL0: q-value protein (mRNA) <0.05: *(*), <0.01: **(**), <0.001: ***(***).

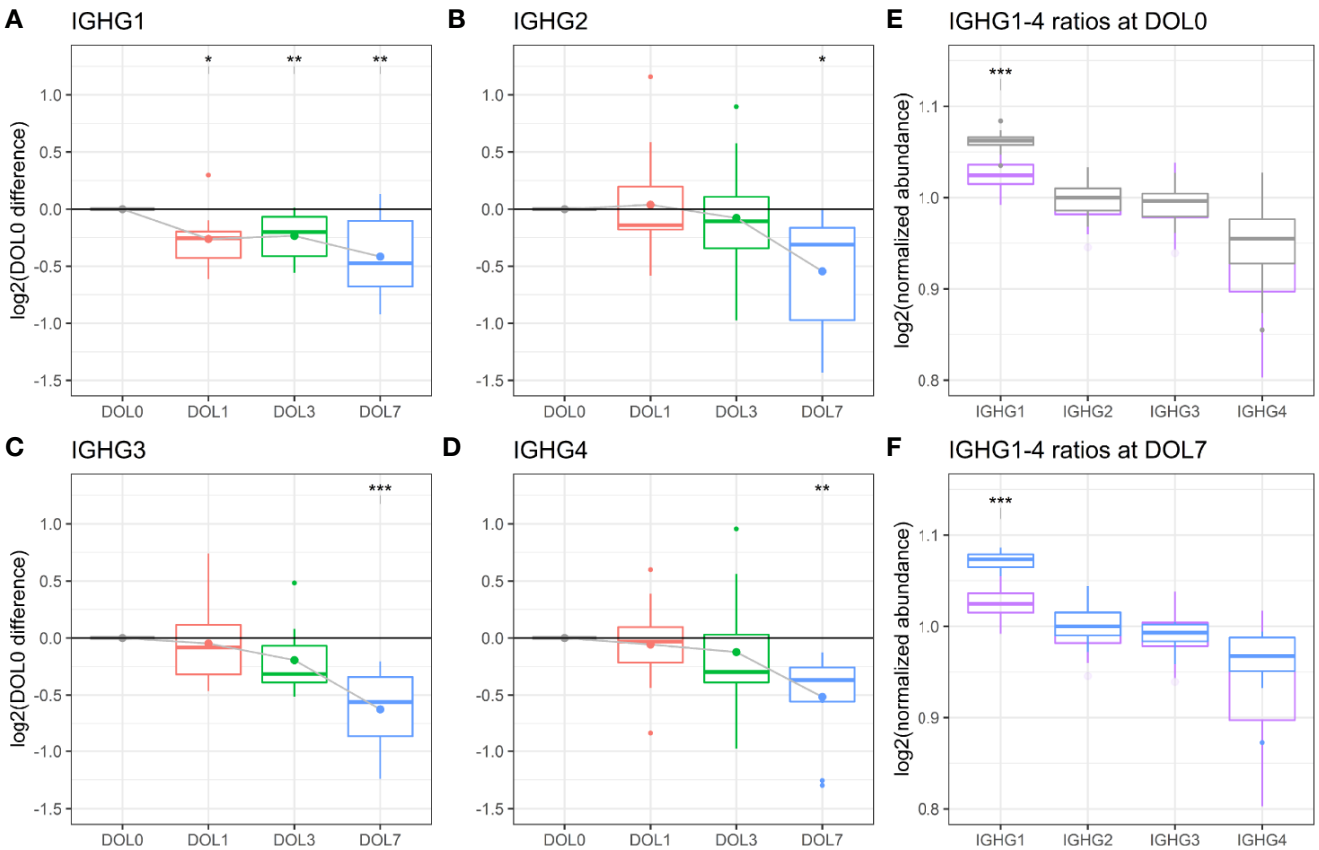

FIGURE 10 | Protein levels of **(A–D)** IgG1-4 across the first week of life as compared to DOL0, with mean abundance difference indicated by dots connected by solid line. **(E)** Comparison of the ratios of IgG1-4 normalized to IgG2 between adult-levels (purple) and newborn-levels at DOL0 (gray), or **(F)** DOL7 (blue). Statistics A–D **(E, F)**: q-value <0.05: *, <0.01: **, <0.001: ***.

immunitysuggesting a central role for the classical complement pathway for neonatal immunity (91–93). With respect to complement components, we noted significant differences between plasma protein concentrations and whole blood mRNA counts, highlighting the value of multi-OMICS integration to gain biologic insights and generate well-informed hypotheses.

We were able to provide granularity around the trajectory of different immunoglobulin subtypes during the first week of life. We detected endogenous synthesis of the IgG1 isotype, but not IgG2-4 and the ratio of IgG1 to IgG2-4 was elevated compared to adults, highlighting the importance of IgG1 for early immunity. Levels of the maternally transferred IgG1-4 declined over the first week of life. We also detected an acute phase response accompanied by a surge in levels of acute phase proteins on the first day of life and an overall reduction of inhibitors. The functional consequences of the differences between the timepoints could not be assessed *in vitro* due to sample size restrictions, and should be investigated in further studies. Additionally, studies involving a higher number of samples, pairing with maternal samples, and higher time resolutions are needed to identify the drivers of this response.

The main strength of our study is the performance of deep proteomics analysis with small volumes of blood plasma. Even though most of our findings are not surprising, this study's main contribution to the literature is a new conceptual framework of neonatal immune ontogeny based on a consistent developmental trajectory of the newborn's immune system over the first week of human life across continents, as evidenced by highly similar trajectories in two geographically distinct newborn cohorts. This study is also proof of concept that high quality, reproducible systems biology research is feasible even in low resource settings.

In summary, our findings have shed additional light on functionally distinct immunobiological processes occurring in the human neonate during the first week of life and can serve as a crucial overview and hypothesis-generating resource for researchers in the field of immune ontogeny. Interpretation of our observations in the context of perinatal physiology will be key to understanding the delicately balanced regulation of the neonatal immune response.

DATA AVAILABILITY STATEMENT

The datasets presented in this study can be found in online repositories. The names of the repository/repositories and accession number(s) can be found in the article/**Supplementary Material**.

ETHICS STATEMENT

The studies involving human participants were reviewed and approved by Local Ethics Committee-approved protocol (MRC SCC 1436 and IMR IRB#1515 and MRAC #16.14). Written informed consent to participate in this study was provided by the participants' legal guardian/next of kin.

THE EPIC CONSORTIUM IN ALPHABETICAL ORDER

Nelly Amenyogbe, Asimenia Angelidou, Tue Bjerg Bennike, Anita H.J. van den Biggelaar, Cai Bing, Ryan R. Brinkman, Kim-Anh Lê Cao, Momoudou Cox, Alansana Darboe, Joann Diray-Arce, Reza Falsafi, Benoit Fatou, Davide Ferrari, Rebecca Ford, Erin E. Gill, Robert E.W. Hancock, Daniel J. Harbeson, Simon D. van Haren, Daniel He, Samuel J. Hinshaw, Olubukola T. Idoko, Beate Kampmann, Ken Kraft, Wendy Kirarock, Tobias R. Kollmann, Amy H. Lee, Ofer Levy, Mehrnoush Malek, Geraldine Masiria, John Paul Matlam, Jorjoh Ndure, Jainaba Njie-Jobe, Oludare Olumade, Rym Ben-Othman, Al Ozonoff, Matthew A. Pettengill, William S. Pomat, Peter C. Richmond, Elishia Roberts, Gerard Saleu, Guzmán Sanchez-Schmitz, Casey P. Shannon, Amrit Singh, Kinga K. Smolen, Hanno Steen, Scott J. Tebbutt, Diana Vo.

AUTHOR CONTRIBUTIONS

OL, TK, HS, RH, ST, AO, AB, and BK were the overall project and core leads. OI and BK established the main cohort. WP and AB established the validation cohort. JD-A, SH, RB-O, and KS processed the samples. TB and BF generated the proteomics data. TB analyzed the proteomics data. RFa, RFo, EG, AL, and RH generated and analyzed the RNA seq data. TB, BF, and HS interpreted the results. TB wrote the manuscript draft with BF and HS. Substantial help was received from the entire EPIC-HIPC. All authors contributed to the article and approved the submitted version.

FUNDING

TK's laboratory is supported by a Michael Smith Foundation for Health Research Career Investigator Award. OL's laboratory is supported by the following U.S. NIH/NIAID awards: Molecular Mechanisms of Combination Adjuvants (1U01AI124284-01), Adjuvant Discovery Program Contract No. HHSN272201400052C and Human Immunology Project Consortium (U19AI118608) as well as an internal Boston Children's Hospital award to the *Precision Vaccines Program*. BK is supported by grants from the MRC/UKRI (MC_UP_A900/1122, MC_UP_A900/115, MR/R005990/1), and the additional field team and laboratory staff at the MRC Unit in The Gambia. Recruitment of the cohort of newborns in Papua New Guinea was funded by seed funding awarded to AB from the Wesfarmers Centre of Vaccines and Infectious Diseases, Telethon Kids Institute. The work in RH's lab was initially supported by the Canadian Institutes for Health Research grant #FDN-154287 and he holds a Canada Research Chair in Health and Genomics and a UBC Killam Professorship. RRB's laboratory is supported by an award from Natural Sciences and Engineering Research Council of Canada. The Lundbeck Foundation (R181-2014-3372), The Carlsberg Foundation (CF14-0561), and A.P. Møller Foundation are acknowledged for grants enabling TB's work. K-ALC is supported in part by the National Health and Medical Research Council (NHMRC) Career Development fellowship (GNT1087415).

ACKNOWLEDGMENTS

We would like to thank all the participants and their parents for their time and willingness to support this study. Research reported in this publication was supported by the National Institute of Allergy and Infectious Diseases (NIAID) of the National Institutes of Health (NIH) as part of the Human Immunology Project consortium under 5U19AI118608-02. The content is solely the responsibility of the authors and does not necessarily represent the official views of the National Institutes of Health. We gratefully acknowledge the support from Drs. Gary Fleisher, Michael Wessels and Ken Kraft as well as Maria Crenshaw, Mark Liu, Kerry McEnaney and Diana Vo (all BCH); Susan Farmer, Manish Sadarangani, Aaron Liu, Gordean Bjornson (all UBC). The Expanded Program on Immunization Consortium (EPIC) contributed collectively to this study. EPIC is an association of academic centers partnering to conduct systems biology studies in newborns and infants, comprised of the investigators listed above at Boston Children's Hospital (BCH), University of British Columbia (UBC), Medical Research Council Unit The Gambia (MRCG), Université libre de Bruxelles, Telethon Kids Institute and University of Western Australia, and the Papua New Guinea Institute for Medical Research (PNG-IMR).

SUPPLEMENTARY MATERIAL

The Supplementary Material for this article can be found online at: https://www.frontiersin.org/articles/10.3389/fimmu.2020.578505/full#supplementary-material

REFERENCES

1. Zhang X, Zhivaki D, Lo-Man R. Unique aspects of the perinatal immune system. *Nat Rev Immunol* (2017) 17(8):495–507. doi: 10.1038/nri.2017.54
2. Kollmann TR, Kampmann B, Mazmanian SK, Marchant A, Levy O. Protecting the Newborn and Young Infant from Infectious Diseases: Lessons from Immune Ontogeny. *Immunity* (2017) 2146(3):350–63. doi: 10.1016/j.immuni.2017.03.009
3. Balbus JM, Barouki R, Birnbaum LS, Etzel RA, Gluckman SPD, Grandjean P, et al. Early-life prevention of non-communicable diseases. *Lancet* (2013) 381:3–4. doi: 10.1016/S0140-6736(12)61609-2
4. Zinkernagel RM. Maternal antibodies, childhood infections, and autoimmune diseases. *N Engl J Med* (2001) 345(18):1331–5. doi: 10.1056/NEJMra012493
5. McGreal EP, Hearne K, Spiller OB. Off to a slow start: Under-development of the complement system in term newborns is more substantial following premature birth. *Immunobiology* (2012) 217(2):176–86. doi: 10.1016/j.imbio.2011.07.027
6. Maródi L. Neonatal Innate Immunity to Infectious Agents. *Infect Immun* (2006) 74(4):1999–2006. doi: 10.1128/IAI.74.4.1999-2006.2006
7. Lee AH, Shannon CP, Amenyogbe N, Bennike TB, Diray-Arce J, Idoko OT, et al. Dynamic molecular changes during the first week of human life follow a robust developmental trajectory. *Nat Commun* (2019) 10(1):1092. doi: 10.1038/s41467-019-08794-x
8. Carr EJ, Dooley J, Garcia-Perez JE, Lagou V, Lee JC, Wouters C, et al. The cellular composition of the human immune system is shaped by age and cohabitation. *Nat Immunol* (2016) 17(4):461–8. doi: 10.1038/ni.3371
9. Idoko OT, Smolen KK, Wariri O, Imam A, Shannon CP, Dibassey T, et al. Clinical Protocol for a Longitudinal Cohort Study Employing Systems Biology to Identify Markers of Vaccine Immunogenicity in Newborn Infants in The Gambia and Papua New Guinea. *Front Pediatr* (2020) 8:197. doi: 10.3389/fped.2020.00197
10. Bennike TB, Bellin MD, Xuan Y, Stensballe A, Møller FT, Beilman GJ, et al. A Cost-Effective High-Throughput Plasma and Serum Proteomics Workflow Enables Mapping of the Molecular Impact of Total Pancreatectomy with Islet Autotransplantation. *J Proteome Res* (2018) 0417(5):1983–92. doi: 10.1021/acs.jproteome.8b00111
11. Bennike TB, Steen H. High-Throughput Parallel Proteomic Sample Preparation Using 96-Well Polyvinylidene Fluoride (PVDF) Membranes and C18 Purification Plates. In: DW Greening, RJ Simpson, editors. *Serum/Plasma Proteomics*. New York, NY: Springer New York (2017). p. 395–402. doi: 10.1074/mcp.O115.049650
12. Cox J, Hein MY, Luber CA, Paron I, Nagaraj N, Mann M. Accurate Proteome-wide Label-free Quantification by Delayed Normalization and Maximal Peptide Ratio Extraction, Termed MaxLFQ. *Mol Cell Proteomics MCP* (2014) 13(9):2513–26. doi: 10.1074/mcp.M113.031591
13. Cox J, Neuhauser N, Michalski A, Scheltema RA, Olsen JV, Mann M. Andromeda: A Peptide Search Engine Integrated into the MaxQuant Environment. *J Proteome Res* (2011) 10(4):1794–805. doi: 10.1021/pr101065j
14. Gupta N, Pevzner PA. False Discovery Rates of Protein Identifications: A Strike against the Two-Peptide Rule. *J Proteome Res* (2009) 8(9):4173–81. doi: 10.1021/pr9004794
15. RStudio Team. *RStudio: Integrated Development Environment for R*. Boston, MA: RStudio, Inc (2015). Available at: http://www.rstudio.com/.
16. R Core Team. *R: A Language and Environment for Statistical Computing*. Vienna, Austria: R Foundation for Statistical Computing (2015). Available at: https://www.R-project.org.
17. Lazar C, Gatto L, Ferro M, Bruley C, Burger T. Accounting for the Multiple Natures of Missing Values in Label-Free Quantitative Proteomics Data Sets to Compare Imputation Strategies. *J Proteome Res* (2016) 15(4):1116–25. doi: 10.1021/acs.jproteome.5b00981
18. Johnson WE, Li C, Rabinovic A. Adjusting batch effects in microarray expression data using empirical Bayes methods. *Biostatistics* (2007) 8(1):118–27. doi: 10.1093/biostatistics/kxj037
19. Hicks SC, Irizarry RA. quantro: a data-driven approach to guide the choice of an appropriate normalization method. *Genome Biol* (2015) 16:117. doi: 10.1186/s13059-015-0679-0
20. Wickham H. *ggplot2: Elegant Graphics for Data Analysis*. New York: Springer-Verlag (2009). 266 p. doi: 10.1007/978-0-387-98141-3
21. Wickham H, François R, Henry L, Müller K. *dplyr: A Grammar of Data Manipulation. R package version 0.7.6*. Boston, MA (2018). Available at: https://CRAN.R-project.org/package=dplyr.
22. Rohart F, Gautier B, Singh A, Lê Cao K-A. mixOmics: An R package for 'omics feature selection and multiple data integration. *PloS Comput Biol* (2017) 13(11):e1005752. doi: 10.1371/journal.pcbi.1005752
23. Vizcaíno JA, Deutsch EW, Wang R, Csordas A, Reisinger F, Ríos D, et al. ProteomeXchange provides globally coordinated proteomics data submission and dissemination. *Nat Biotechnol* (2014) 32:223–6. doi: 10.1038/nbt.2839
24. Vizcaíno JA, Csordas A, del-Toro N, Dianes JA, Griss J, Lavidas I, et al. update of the PRIDE database and its related tools. *Nucleic Acids Res* (2016) 44:D447–56. doi: 10.1093/nar/gkv1145
25. Bates D, Mächler M, Bolker B, Walker S. Fitting Linear Mixed-Effects Models Using lme4. *J Stat Software* (2015) 67(1):1–48. doi: 10.18637/jss.v067.i01
26. Benjamini Y, Krieger AM, Yekutieli D. Adaptive linear step-up procedures that control the false discovery rate. *Biometrika* (2006) 93(3):491–507. doi: 10.1093/biomet/93.3.491
27. Shannon P, Markiel A, Ozier O, Baliga NS, Wang JT, Ramage D, et al. Cytoscape: a software environment for integrated models of biomolecular interaction networks. *Genome Res* (2003) 13(11):2498–504. doi: 10.1101/gr.1239303
28. Liao Y, Wang J, Jaehnig EJ, Shi Z, Zhang B. WebGestalt 2019: gene set analysis toolkit with revamped UIs and APIs. *Nucleic Acids Res* (2019) 47(W1):W199–205. doi: 10.1093/nar/gkz401
29. Szklarczyk D, Franceschini A, Wyder S, Forslund K, Heller D, Huerta-Cepas J, et al. STRING v10: protein-protein interaction networks, integrated over the

tree of life. *Nucleic Acids Res* (2015) 43(D1):D447–52. doi: 10.1093/nar/gku1003
30. Ewels P, Magnusson M, Lundin S, Käller M. MultiQC: summarize analysis results for multiple tools and samples in a single report. *Bioinformatics* (2016) 32(19):3047–8. doi: 10.1093/bioinformatics/btw354
31. Dobin A, Davis CA, Schlesinger F, Drenkow J, Zaleski C, Jha S, et al. STAR: ultrafast universal RNA-seq aligner. *Bioinformatics* (2013) 29(1):15–21. doi: 10.1093/bioinformatics/bts635
32. Anders S, Pyl PT, Huber W. HTSeq—a Python framework to work with high-throughput sequencing data. *Bioinformatics* (2015) 31(2):166–9. doi: 10.1093/bioinformatics/btu638
33. Love MI, Huber W, Anders S. Moderated estimation of fold change and dispersion for RNA-seq data with DESeq2. *Genome Biol* (2014) 15(12):550. doi: 10.1186/s13059-014-0550-8
34. Yasui K, Matsumoto K, Hirayama F, Tani Y, Nakano T. Differences Between Peripheral Blood and Cord Blood in the Kinetics of Lineage-Restricted Hematopoietic Cells: Implications for Delayed Platelet Recovery Following Cord Blood Transplantation. *Stem Cells* (2003) 21(2):143–51. doi: 10.1634/stemcells.21-2-143
35. Bennike T, Ayturk U, Haslauer CM, Froehlich JW, Proffen BL, Barnaby O, et al. A normative study of the synovial fluid proteome from healthy porcine knee joints. *J Proteome Res* (2014) 13(10):4377–87. doi: 10.1021/pr500587x
36. Bennike TB, Barnaby O, Steen H, Stensballe A. Characterization of the porcine synovial fluid proteome and a comparison to the plasma proteome. *Data Brief* (2015) Dec5:241–7. doi: 10.1016/j.dib.2015.08.028
37. Zhou M, Lucas DA, Chan KC, Issaq HJ, Petricoin EF, Liotta LA, et al. An investigation into the human serum "interactome." *ELECTROPHORESIS* (2004) 25(9):1289–98. doi: 10.1002/elps.200405866
38. Kirov S, Sasson A, Zhang C, Chasalow S, Dongre A, Steen H, et al. Degradation of the extracellular matrix is part of the pathology of ulcerative colitis. *Mol Omics* (2019) 15(1):67–76. doi: 10.1039/c8mo00239h
39. Jeanmougin M, de Reynies A, Marisa L, Paccard C, Nuel G, Guedj M. Should We Abandon the t-Test in the Analysis of Gene Expression Microarray Data: A Comparison of Variance Modeling Strategies. *PloS One* (2010) 5(9):e12336. doi: 10.1371/journal.pone.0012336
40. Peri KG, Gagnon C, Bard H. Quantitative Correlation between Globin mRNAs and Synthesis of Fetal and Adult Hemoglobins during Hemoglobin Switchover in the Perinatal Period. *Pediatr Res* (1998) 43(4):504–8. doi: 10.1203/00006450-199804000-00011
41. Chavez-Bueno S, Beasley JA, Goldbeck JM, Bright BC, Morton DJ, Whitby PW, et al. Haptoglobin concentrations in preterm and term newborns. *J Perinatol: Official Journal of the California Perinatal Association* (2011) 31(7):500–3. doi: 10.1038/jp.2010.197
42. Ignjatovic V, Lai C, Summerhayes R, Mathesius U, Tawfilis S, Perugini MA, et al. Age-Related Differences in Plasma Proteins: How Plasma Proteins Change from Neonates to Adults. Uversky V, editor. *PloS One* (2011) 6(2):e17213. doi: 10.1371/journal.pone.0017213
43. Schaer DJ, Buehler PW, Alayash AI, Belcher JD, Vercellotti GM. Hemolysis and free hemoglobin revisited: exploring hemoglobin and hemin scavengers as a novel class of therapeutic proteins. *Blood* (2013) 121(8):1276–84. doi: 10.1182/blood-2012-11-451229
44. Kristiansen M, Graversen JH, Jacobsen C, Sonne O, Hoffman HJ, Law SK, et al. Identification of the haemoglobin scavenger receptor. *Nature* (2001) 409(6817):198–201. doi: 10.1038/35051594
45. Li W, Wang W, Zuo R, Liu C, Shu Q, Ying H, et al. Induction of pro-inflammatory genes by serum amyloid A1 in human amnion fibroblasts. *Sci Rep* (2017) 7:693. doi: 10.1038/s41598-017-00782-9
46. Sack GH. Serum amyloid A – a review. *Mol Med* (2018) 24:46. doi: 10.1186/s10020-018-0047-0
47. Jumeau C, Awad F, Assrawi E, Cobret L, Duquesnoy P, Giurgea I, et al. Expression of SAA1, SAA2 and SAA4 genes in human primary monocytes and monocyte-derived macrophages. *PloS One* (2019) 14:e0217005. doi: 10.1371/journal.pone.0217005
48. Marchini G, Berggren V, Djilali-Merzoug R, Hansson L-O. The birth process initiates an acute phase reaction in the fetus-newborn infant. *Acta Paediatr* (2000) 89(9):1082–6. doi: 10.1111/j.1651-2227.2000.tb03355.x
49. Pettengill MA, van Haren SD, Levy O. Soluble mediators regulating immunity in early life. *Front Immunol* (2014) 5:457. doi: 10.3389/fimmu.2014.00457
50. Levy O. Innate immunity of the newborn: basic mechanisms and clinical correlates. *Nat Rev Immunol* (2007) 7(5):379–90. doi: 10.1038/nri2075
51. Gorevic PD. Amyloid and inflammation. *Proc Natl Acad Sci* (2013) 110(41):16291–2. doi: 10.1073/pnas.1315112110
52. Tape C, Tan R, Neshejm M, Kisilevsky R. Direct Evidence for Circulating apoSAA as the Precursor of Tissue AA Amyloid Deposits. *Scand J Immunol* (1988) 28(3):317–24. doi: 10.1111/j.1365-3083.1988.tb01455.x
53. Castell JV, Gómez-Lechón MJ, David M, Andus T, Geiger T, Trullenque R, et al. Interleukin-6 is the major regulator of acute phase protein synthesis in adult human hepatocytes. *FEBS Lett* (1989) 242(2):237–9. doi: 10.1016/0014-5793(89)80476-4
54. Merle NS, Church SE, Fremeaux-Bacchi V, Roumenina LT. Complement System Part I – Molecular Mechanisms of Activation and Regulation. *Front Immunol* (2015) 6:262. doi: 10.3389/fimmu.2015.00262
55. Palmeira P, Quinello C, Silveira-Lessa AL, Zago CA, Carneiro-Sampaio M. IgG Placental Transfer in Healthy and Pathological Pregnancies. *Clin Dev Immunol* (2012) 2012:985646. doi: 10.1155/2012/985646
56. Pernemalm M, Sandberg A, Zhu Y, Boekel J, Tamburro D, Schwenk JM, et al. In-depth human plasma proteome analysis captures tissue proteins and transfer of protein variants across the placenta. *eLife* (2019) 8. doi: 10.7554/eLife.41608
57. Ferguson JS, Weis JJ, Martin JL, Schlesinger LS. Complement Protein C3 Binding to Mycobacterium tuberculosis Is Initiated by the Classical Pathway in Human Bronchoalveolar Lavage Fluid. *Infect Immun* (2004) 72(5):2564–73. doi: 10.1128/IAI.72.5.2564-2573.2004
58. Lubbers R, van Essen MF, van Kooten C, Trouw LA. Production of complement components by cells of the immune system. *Clin Exp Immunol* (2017) 188(2):183–94. doi: 10.1111/cei.12952
59. Roos MH, Mollenhauer E, Démant P, Rittner C. A molecular basis for the two locus model of human complement component C4. *Nature* (1982) 298(5877):854–6. doi: 10.1038/298854a0
60. Law SK, Dodds AW, Porter RR. A comparison of the properties of two classes, C4A and C4B, of the human complement component C4. *EMBO J* (1984) 3(8):1819–23. doi: 10.1002/j.1460-2075.1984.tb02052.x
61. Rupert KL, Moulds JM, Yang Y, Arnett FC, Warren RW, Reveille JD, et al. The Molecular Basis of Complete Complement C4A and C4B Deficiencies in a Systemic Lupus Erythematosus Patient with Homozygous C4A and C4B Mutant Genes. *J Immunol* (2002) 169(3):1570–8. doi: 10.4049/jimmunol.169.3.1570
62. Beltrame MH, Catarino SJ, Goeldner I, Boldt ABW, de Messias-Reason IJ. The Lectin Pathway of Complement and Rheumatic Heart Disease. *Front Pediatr* (2015) 2:148. doi: 10.3389/fped.2014.00148
63. Szala A, Sawicki S, Swierzko AST, Szemraj J, Sniadecki M, Michalski M, et al. Ficolin-2 and ficolin-3 in women with malignant and benign ovarian tumours. *Cancer Immunol Immunother* (2013) 62(8):1411–9. doi: 10.1007/s00262-013-1445-3
64. Sallenbach S, Thiel S, Aebi C, Otth M, Bigler S, Jensenius JC, et al. Serum concentrations of lectin-pathway components in healthy neonates, children and adults: mannan-binding lectin (MBL), M-, L-, and H-ficolin, and MBL-associated serine protease-2 (MASP-2). *Pediatr Allergy Immunol* (2011) 22(4):424–30. doi: 10.1111/j.1399-3038.2010.01104.x
65. Frakking FNJ, Brouwer N, Zweers D, Merkus MP, Kuijpers TW, Offringa M, et al. High prevalence of mannose-binding lectin (MBL) deficiency in premature neonates. *Clin Exp Immunol* (2006) 145(1):5–12. doi: 10.1111/j.1365-2249.2006.03093.x
66. Kilpatrick DC, Liston WA, Midgley PC. Mannan-binding protein in human umbilical cord blood. *Nat Immun 1996* (1997) 15(5):234–40. doi: 10.1111/j.1365-2249.2006.03093.x
67. Michalski M, Szala A, St. Swierzko A, Lukasiewicz J, Maciejewska A, Kilpatrick DC, et al. H-ficolin (ficolin-3) concentrations and FCN3 gene polymorphism in neonates. *Immunobiology* (2012) 217(7):730–7. doi: 10.1016/j.imbio.2011.12.004
68. Cedzynski M, Swierzko AST, Kilpatrick DC. Factors of the Lectin Pathway of Complement Activation and Their Clinical Associations in Neonates. *J BioMed Biotechnol* (2012) 2012:363246. doi: 10.1155/2012/363246
69. Medicus RG, Götze O, Müller-Eberhard HJ. Alternative pathway of complement: recruitment of precursor properdin by the labile C3/C5

convertase and the potentiation of the pathway. *J Exp Med* (1976) 144 (4):1076–93. doi: 10.1084/jem.144.4.1076
70. Camous L, Roumenina L, Bigot S, Brachemi S, Frémeaux-Bacchi V, Lesavre P, et al. Complement alternative pathway acts as a positive feedback amplification of neutrophil activation. *Blood* (2011) 117(4):1340–9. doi: 10.1182/blood-2010-05-283564
71. Wirthmueller U, Dewald B, Thelen M, Schäfer MK, Stover C, Whaley K, et al. Properdin, a positive regulator of complement activation, is released from secondary granules of stimulated peripheral blood neutrophils. *J Immunol Baltim Md 1950* (1997) 158(9):4444–51.
72. Lachmann PJ, Thompson RA. Reactive lysis: the complement-mediated lysis of unsensitized cells. II. The characterization of activated reactor as C56 and the participation of C8 and C9. *J Exp Med* (1970) 131(4):643–57. doi: 10.1084/jem.131.4.643
73. Terai I, Kobayashi K, Matsushita M, Fujita T, Matsuno K. alpha 2-Macroglobulin binds to and inhibits mannose-binding protein-associated serine protease. *Int Immunol* (1995) 7(10):1579–84. doi: 10.1093/intimm/7.10.1579
74. Paréj K, Dobó J, Závodszky P, Gál P. The control of the complement lectin pathway activation revisited: both C1-inhibitor and antithrombin are likely physiological inhibitors, while α2-macroglobulin is not. *Mol Immunol* (2013) 54(3–4):415–22. doi: 10.1016/j.molimm.2013.01.009
75. Adinolfi M, Beck SE. Human complement C7 and C9 in fetal and newborn sera. *Arch Dis Child* (1975) 50(7):562–4. doi: 10.1136/adc.50.7.562
76. Väkevä A, Laurila P, Meri S. Co-deposition of clusterin with the complement membrane attack complex in myocardial infarction. *Immunology* (1993) 80 (2):177–82.
77. Dahlbäck K, Löfberg H, Alumets J, Dahlbäck B. Immunohistochemical demonstration of age-related deposition of vitronectin (S-protein of complement) and terminal complement complex on dermal elastic fibers. *J Invest Dermatol* (1989) 92(5):727–33. doi: 10.1111/1523-1747.ep12721619
78. Webb JH, Blom AM, Dahlbäck B. Vitamin K-Dependent Protein S Localizing Complement Regulator C4b-Binding Protein to the Surface of Apoptotic Cells. *J Immunol* (2002) 169(5):2580–6. doi: 10.4049/jimmunol.169.5.2580
79. Charles A Janeway J, Travers P, Walport M, Shlomchik MJ. The distribution and functions of immunoglobulin isotypes. In: *Immunobiol Immune Syst Health Dis, 5th Ed*. New York: Garland Science (2001).
80. Kutteh WH, Moldoveanu Z, Prince SJ, Kulhavy R, Alonso F, Mestecky J. Biosynthesis of J-chain in human lymphoid cells producing immunoglobulins of various isotypes. *Mol Immunol* (1983) 20(9):967–76. doi: 10.1016/0161-5890(83)90037-8
81. Castro CD, Flajnik MF. Putting J Chain Back on the Map: How Might Its Expression Define Plasma Cell Development? *J Immunol* (2014) 193(7):3248–55. doi: 10.4049/jimmunol.1400531
82. Aksu G, Genel F, Koturoğlu G, Kurugöl Z, Kütükçüler N. Serum immunoglobulin (IgG, IgM, IgA) and IgG subclass concentrations in healthy children: a study using nephelometric technique. *Turk J Pediatr* (2006) 48(1):19–24.
83. Seijsing J, Yu S, Frejd FY, Höiden-Guthenberg I, Gräslund T. In vivo depletion of serum IgG by an affibody molecule binding the neonatal Fc receptor. *Sci Rep* (2018) 8(1):5141. doi: 10.1038/s41598-018-23481-5
84. Vidarsson G, Dekkers G, Rispens T. IgG Subclasses and Allotypes: From Structure to Effector Functions. *Front Immunol* (2014) 5:520. doi: 10.3389/fimmu.2014.00520
85. Mankarious S, Lee M, Fischer S, Pyun KH, Ochs HD, Oxelius VA, et al. The half-lives of IgG subclasses and specific antibodies in patients with primary immunodeficiency who are receiving intravenously administered immunoglobulin. *J Lab Clin Med* (1988) 112(5):634–40.
86. Morell A, Terry WD, Waldmann TA. Metabolic properties of IgG subclasses in man. *J Clin Invest* (1970) 49(4):673–80. doi: 10.1172/JCI106279
87. Fouda GG, Martinez DR, Swamy GK, Permar SR. The Impact of IgG transplacental transfer on early life immunity. *ImmunoHorizons* (2018) 2 (1):14–25. doi: 10.4049/immunohorizons.1700057
88. Salimonu LS, Ladipo OA, Adeniran SO, Osukoya BO. Serum Immunoglobulin Levels in Normal, Premature and Postmature Newborns and Their Mothers. *Int J Gynecol Obstet* (1978) 16(2):119–23. doi: 10.1002/j.1879-3479.1978.tb00410.x
89. Garred P, Michaelsen TE, Aase A. The IgG subclass pattern of complement activation depends on epitope density and antibody and complement concentration. *Scand J Immunol* (1989) 30(3):379–82. doi: 10.1111/j.1365-3083.1989.tb01225.x
90. Michaelsen TE, Garred P, Aase A. Human IgG subclass pattern of inducing complement-mediated cytolysis depends on antigen concentration and to a lesser extent on epitope patchiness, antibody affinity and complement concentration. *Eur J Immunol* (1991) 21(1):11–6. doi: 10.1002/eji.1830210103
91. Naughton MA, Walport MJ, Würzner R, Carter MJ, Alexander GJ, Goldman JM, et al. Organ-specific contribution to circulating C7 levels by the bone marrow and liver in humans. *Eur J Immunol* (1996) Sep26(9):2108–12. doi: 10.1002/eji.1830260922
92. Würzner R, Joysey VC, Lachmann PJ. Complement component C7. Assessment of in vivo synthesis after liver transplantation reveals that hepatocytes do not synthesize the majority of human C7. *J Immunol* (1994) 152(9):4624–9.
93. Høgåsen AK, Würzner R, Abrahamsen TG, Dierich MP. Human polymorphonuclear leukocytes store large amounts of terminal complement components C7 and C6, which may be released on stimulation. *J Immunol Baltim Md 1950* (1995) 154(9):4734–40.

Conflict of Interest: OL is a named inventor on patents regarding bactericidal/permeability increasing protein (BPI), including "Therapeutic uses of BPI protein products in BPI-deficient humans" (WO2000059531A3) and "BPI and its congeners as radiation mitigators and radiation protectors" (WO2012138839A1). RRB has ownership interest in Cytapex Bioinformatics Inc.

The remaining authors declare that the research was conducted in the absence of any commercial or financial relationships that could be construed as a potential conflict of interest.

Citation: *Bennike TB, Fatou B, Angelidou A, Diray-Arce J, Falsafi R, Ford R, Gill EE, van Haren SD, Idoko OT, Lee AH, Ben-Othman R, Pomat WS, Shannon CP, Smolen KK, Tebbutt SJ, Ozonoff A, Richmond PC, Biggelaar AHJvd, Hancock REW, Kampmann B, Kollmann TR, Levy O and Steen H (2020) Preparing for Life: Plasma Proteome Changes and Immune System Development During the First Week of Human Life.*
Front. Immunol. 11:578505. doi: 10.3389/fimmu.2020.578505

frontiers in Immunology

METHODS
published: 04 November 2020
doi: 10.3389/fimmu.2020.580373

Systems Biology Methods Applied to Blood and Tissue for a Comprehensive Analysis of Immune Response to Hepatitis B Vaccine in Adults

*Rym Ben-Othman[1,2], Bing Cai[1], Aaron C. Liu[1], Natallia Varankovich[1], Daniel He[1], Travis M. Blimkie[3], Amy H. Lee[4], Erin E. Gill[3], Mark Novotny[5], Brian Aevermann[5], Sibyl Drissler[6], Casey P. Shannon[7], Sarah McCann[1], Kim Marty[1], Gordean Bjornson[1], Rachel D. Edgar[8], David Tse Shen Lin[8], Nicole Gladish[8], Julia MacIsaac[8], Nelly Amenyogbe[2], Queenie Chan[9], Alba Llibre[10], Joyce Collin[11], Elise Landais[11,12], Khoa Le[11,12], Samantha M. Reiss[13], Wayne C. Koff[14], Colin Havenar-Daughton[13], Manraj Heran[15], Bippan Sangha[15], David Walt[16], Mel Krajden[17], Shane Crotty[13], Devin Sok[11,12], Bryan Briney[11], Dennis R. Burton[11], Darragh Duffy[10], Leonard J. Foster[9], William W. Mohn[18], Michael S. Kobor[8], Scott J. Tebbutt[7,19], Ryan R. Brinkman[6,20], Richard H. Scheuermann[5,13], Robert E. W. Hancock[3], Tobias R. Kollmann[1,2] and Manish Sadarangani[1]**

[1] Vaccine Evaluation Center, BC Children's Hospital Research Institute, Vancouver, BC, Canada, [2] Telethon Kids Institute, University of Western Australia, Nedlands, WA, Australia, [3] Centre for Microbial Diseases and Immunity Research, University of British Columbia, Vancouver, BC, Canada, [4] Simon Fraser University, Burnaby, BC, Canada, [5] Department of Informatics, J. Craig Venter Institute (La Jolla), La Jolla, CA, United States, [6] Terry Fox Laboratory, Vancouver, BC, Canada, [7] Prevention of Organ Failure (PROOF) Centre of Excellence and Centre for Heart Lung Innovation, St. Paul's Hospital, Vancouver, BC, Canada, [8] Centre for Molecular Medicine and Therapeutics, Department of Medical Genetics, University of British Columbia, Vancouver, BC, Canada, [9] Department of Biochemistry and Molecular Biology, Faculty of Medicine, University of British Columbia, Vancouver, BC, Canada, [10] Translational Immunology Lab, Institut Pasteur, Paris, France, [11] Department of Immunology and Microbiology, The Scripps Research Institute, La Jolla, CA, United States, [12] IAVI Neutralizing Antibody Center, The Scripps Research Institute, La Jolla, CA, United States, [13] Center for Infectious Disease and Vaccine Research, La Jolla Institute for Immunology (LJI), La Jolla, CA, United States, [14] Human Vaccines Project, New York, NY, United States, [15] Department of Radiology, BC Children's Hospital, Vancouver, BC, Canada, [16] Wyss Institute at Harvard University, Department of Pathology, Brigham and Women's Hospital, Harvard Medical School, Boston, MA, United States, [17] British Columbia Centre for Disease Control, Vancouver, BC, Canada, [18] Department of Microbiology and Immunology, Life Sciences Institute, University of British Columbia, Vancouver, BC, Canada, [19] Department of Medicine, Division of Respiratory Medicine, University of British Columbia, Vancouver, BC, Canada, [20] Department of Medical Genetics, University of British Columbia, Vancouver, BC, Canada

OPEN ACCESS

Edited by:
Fabiano Oliveira,
National Institutes of Health (NIH),
United States

Reviewed by:
Joshua Lacsina,
National Institutes of Health (NIH),
United States
Victor Greiff,
University of Oslo, Norway

***Correspondence:**
Manish Sadarangani
msadarangani@bcchr.ubc.ca

Specialty section:
This article was submitted to Vaccines and Molecular Therapeutics, a section of the journal Frontiers in Immunology

Received: 05 July 2020
Accepted: 24 September 2020
Published: 04 November 2020

Citation:
Ben-Othman R, Cai B, Liu AC, Varankovich N, He D, Blimkie TM, Lee AH, Gill EE, Novotny M, Aevermann B, Drissler S, Shannon CP, McCann S, Marty K, Bjornson G, Edgar RD, Lin DTS, Gladish N, MacIsaac J, Amenyogbe N, Chan Q, Llibre A, Collin J, Landais E, Le K, Reiss SM, Koff WC, Havenar-Daughton C, Heran M, Sangha B, Walt D, Krajden M, Crotty S, Sok D, Briney B, Burton DR, Duffy D, Foster LJ, Mohn WW, Kobor MS, Tebbutt SJ, Brinkman RR, Scheuermann RH, Hancock REW, Kollmann TR and Sadarangani M (2020) Systems Biology Methods Applied to Blood and Tissue for a Comprehensive Analysis of Immune Response to Hepatitis B Vaccine in Adults. Front. Immunol. 11:580373. doi: 10.3389/fimmu.2020.580373

Conventional vaccine design has been based on trial-and-error approaches, which have been generally successful. However, there have been some major failures in vaccine development and we still do not have highly effective licensed vaccines for tuberculosis, HIV, respiratory syncytial virus, and other major infections of global significance. Approaches at rational vaccine design have been limited by our understanding of the immune response to vaccination at the molecular level. Tools now exist to undertake in-depth analysis using systems biology approaches, but to be fully realized, studies are required in humans with intensive blood and tissue sampling. Methods that support this intensive sampling need to be developed and validated as feasible. To this end, we

describe here a detailed approach that was applied in a study of 15 healthy adults, who were immunized with hepatitis B vaccine. Sampling included ~350 mL of blood, 12 microbiome samples, and lymph node fine needle aspirates obtained over a ~7-month period, enabling comprehensive analysis of the immune response at the molecular level, including single cell and tissue sample analysis. Samples were collected for analysis of immune phenotyping, whole blood and single cell gene expression, proteomics, lipidomics, epigenetics, whole blood response to key immune stimuli, cytokine responses, *in vitro* T cell responses, antibody repertoire analysis and the microbiome. Data integration was undertaken using different approaches—NetworkAnalyst and DIABLO. Our results demonstrate that such intensive sampling studies are feasible in healthy adults, and data integration tools exist to analyze the vast amount of data generated from a multi-omics systems biology approach. This will provide the basis for a better understanding of vaccine-induced immunity and accelerate future rational vaccine design.

Keywords: multi-omic, single cell, lymph node, gene expression, bio-informatic, immunimonitoring, vaccine

INTRODUCTION

Human vaccination is one of the greatest achievements in medical history. However, failure to develop highly effective vaccines for tuberculosis, HIV, malaria, or cancers emphasizes that the traditional trial-and-error approach is limited, and our incomplete understanding of how vaccines work does not yet enable successful rational vaccine design (1). An ideal vaccine would provide significant protection for a long (lifelong) time following only a single dose (1, 2). Few current vaccines reach this ideal, but some successes show that it is possible. New technologies including multi-omic systems biology offer powerful solutions but its potential has not yet been fully realized.

One of the main reasons for the lack of insight into the mechanisms underlying vaccine-induced protection is that human clinical studies have typically studied the response to vaccines in blood only, collected over few time points after vaccination. While blood sampling coupled with systems biology is a practical and a potentially informative proxy for the tissue-resident host response to vaccination, it likely does not capture the full range of cellular and molecular interactions in the tissue, most importantly the draining lymph node (LN), which is the site of the primary immune response to vaccination. This is due to practical limitations in obtaining relevant tissue samples in humans, necessitating assumptions based on animal, *in vitro* and/or *ex vivo* models (3–5). A complete understanding of human immune responses to vaccination will only be possible with collection of tissue samples, in addition to blood, during clinical trials.

The aim of this study was to demonstrate feasibility of a comprehensive blood- and tissue-based systems biology vaccine study in humans, establish the necessary infrastructure, and undertake analysis of pre- and post-vaccine samples to identify markers of a protective immune response. In this article we will describe in detail the methods utilized in the study for sample collection, sample processing and data analysis. A set of the data generated are included in the companion manuscript ("Multi-omic data integration allows baseline immune signatures to predict hepatitis B vaccine response in a small cohort") and were used for multi-omic data integration to identify baseline signatures that can predict vaccine response.

Abbreviations: Anti HBs, Anti Hepatitis B surface antigen; bcDNA, Bisulfate converted DNA; cDNA, Complementary Deoxyribonucleic Acid; CMV, cytomegalovirus; DC, Dendritic Cells; DE, Differentially Expressed; DIABLO, Data Integration Analysis for Biomarker discovery using Latent component method for Omics studies; DNAm, DNA Methylation; dNTP, deoxynucleotide Triphosphate; ELISA, enzyme Linked Immunosorbent Assay; ERCC, External RNA Controls Consortium; FSC-A, Forward SCatter Area; gDNA, genomic DNA; HBV, Hepatitis B Vaccine; HIV, Human Immunodeficiency Virus; IgG, Immunoglobin G; IU, International Units; LN, Lymph Node; mRNA, Messenger Ribonucleic Acid; NGS, Next-Generation Sequencing; NK, Natural Killer; PBMC, Peripheral Blood Mononuclear Cells; PBS, Phosphate Buffered Saline; PCA, Principal Component Analysis; PCR, Polymerase Chain Reaction; PPI, Protein Protein Interactions; RNA, Ribonucleic Acid; RNAseq, Ribonucleic Acid Sequencing; SEB, Staphylococcal enterotoxin B; SiMoA, single Molecular Array; SNP, Single Nucleotide Polymorphism; SSC-A, Side SCatter Area; UMI, Inique Molecular Identifiers; VDJ, Variable Diversity and Joining genes; VEC, Vaccine Evaluation Center; WBC, White Blood Cells.

METHODS

Study Locations and Participants

This was a prospective, observational study (ClinicalTrials.gov; NCT03083158) of immune responses to hepatitis B virus (HBV) vaccine, with recruitment occurring at the Vaccine Evaluation Center (VEC), BC Children's Hospital, Vancouver, Canada in accordance with a local ethics committee-approved protocol (Ethics Ref: H17-00175). All initial sample processing was undertaken at the VEC laboratory. Other laboratory work occurred at various institutions in Vancouver, La Jolla, Boston, and Paris. Participants were healthy adults, aged 40–80 years, who were seronegative to HBV at the time of enrolment. Eligibility criteria are shown in **Table 1**. Participants were

TABLE 1 | Study inclusion and exclusion criteria.

Inclusion criteria	Exclusion criteria
• Healthy adult aged 40–80 years • No history of hepatitis B disease • No prior receipt of any hepatitis B-containing vaccine • Undetectable level of anti-HBs and anti-HBV core (HBc) antibody and HBs antigen at study enrolment • Generally good health (stable chronic conditions acceptable) • Living independently or with minimal assistance (clinical frailty score 1–5)[78] and able to attend all study visits • Willing and able to comply with the requirements of the protocol • Provided informed consent for participation in the study	• Individual on the study delegation log • History of being a household contact of a known hepatitis B-infected individual • Planned administration of any vaccine not specified in the study protocol from 1 month pre- to the 1 month post-1st dose of vaccine • Planned receipt of any investigational drug during the study • Confirmed or suspected immunodeficiency • Family history of congenital or hereditary immunodeficiency • Receipt of >1 week of systemic immunosuppressants or immune modifying drugs in the 3 months prior to dose 1 of vaccine • Taking any anti-platelet or anti-coagulant medications (excluding daily low-dose aspirin) • Bleeding disorder or thrombocytopenia, that contraindicates intramuscular injection, blood collection and/or lymph node fine needle aspiration • Administration of immunoglobulins within the prior 12 months and/or any other blood products within the prior 3 months or planned during the study period • Current pregnancy or planning to become pregnant in the 6 months post-dose 1 vaccination • History of allergy to any component of the vaccine • Unstable medical condition, as indicated by a requirement for hospitalization or a substantial medication change to stabilize said condition within previous 3 months • History of any neurologic disorders or seizures, including a history of Guillain-Barré syndrome • Clinical Frailty score of 6–7 (moderately frail or severely frail)[78] • Scheduled elective surgery or other procedures requiring general anaesthesia from 1 month pre- to the 1 month post-1st dose of vaccine • Any other significant disease or disorder which, in the opinion of the Investigator, may either put the participants at risk because of participation in the study, or may influence the result of the study, or the participant's ability to participate in the study.

recruited by e-mail, mail and telephone *via* an existing "permission to contact for research" database held at the VEC (**Figure 1**).

Biospecimen Collection

Peripheral blood samples, LN aspirates and microbiome samples were obtained for the investigation of host responses associated with HBV vaccine (**Table 2** and **Figure 2**).

Blood Sample Collection

Peripheral blood was obtained from an easily accessible vein (e.g., back of the hand and elbow crease) by experienced staff at the study site. Blood was drawn in three distinct collection tubes, each one appropriate for the downstream protocol. A large bore butterfly needle (19-21G) was used and the collection tubes inserted into the device as follows: an EDTA-treated vacutainer tube (BD, cat #366643) for complete blood counts (3 ml) then an IVD PAXgene blood collection tube (BD, Cat. No. 762165) for RNA samples (2.5 ml) and finally a pre- heparinized 60-ml syringe for the rest of the samples (~50 ml).

Lymph Node Aspirate Collection

Cells from the vaccine-draining axillary LN were obtained *via* fine needle aspiration (FNA) conducted by an interventional radiologist at the study site. A 22-gauge needle attached to a 5- to 10-ml syringe was passed into the LN *via* ultrasound guidance. The needle was moved back and forth within the LN for 30 s under negative pressure, whereby a 2-ml suction was applied by pulling back the syringe plunger. The needle was then withdrawn, and the contents were immediately expelled into 5 ml of cold sterile complete medium containing 2 mM L-glutamine (RPMI, Gibco cat #72400-047). The needle was rinsed in cold medium 3 to 4 times to collect as many cells as possible. The cells were then placed on ice and immediately transported to the laboratory for further processing.

Microbiome Sample Collection

Microbiome samples were obtained prior and post vaccination using EZ II culture swabs (BD, cat #220145) for fecal samples and EZ I culture swabs (BD cat #220144) for nasal, oral and skin samples. The microbiome samples were chosen to be taken at those two time points to address two aspects: whether the vaccine will change the microbiome and whether the microbiome a person has prior to vaccination correlates with the individual's response to vaccination. All swabs except the fecal swabs were collected by study staff at the study visits.

Fecal Sample Collection

Fecal samples were collected by the study participants at home the day before their study visit. The participants were given a collection kit containing a pair of gloves, a sealed swab, a biohazard bag for transport, and clearly illustrated instructions detailing the collection process. The amount of biomass required was small, saturating only half of the swab to allow optimal downstream processing. The biohazard bags with the fecal samples were kept at 4°C in the participant's refrigerator and brought to the clinic visit by study participants within 20 h of collection. Upon arrival to the clinic, the swabs were transferred to the lab and saved without further processing at −80°C for microbiome analysis.

Skin Samples Collection

The participants were asked not to wash their faces for at least 2 h prior to sample collection. Prior to sampling, a sterile swab was

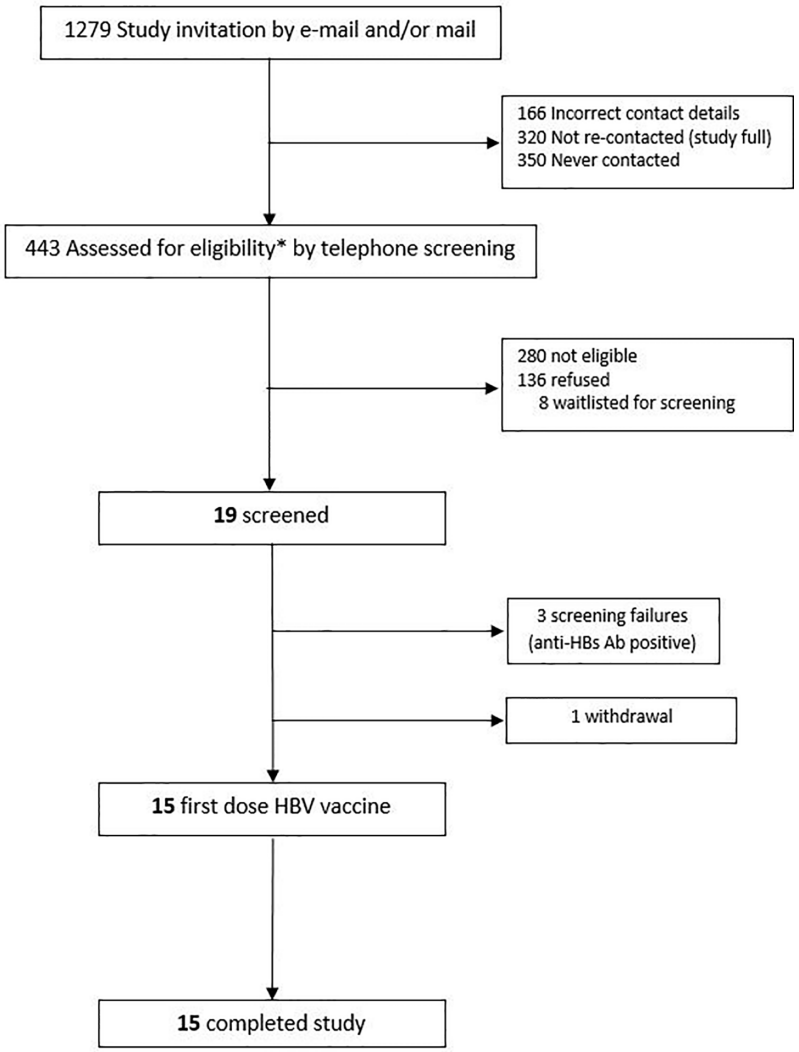

FIGURE 1 | Study participants recruitment strategy.

TABLE 2 | Sample collection details per omic assay and study visits.

	Study Visits											
Assay or Sample Type	**V1**	**V2**	**V3**	**V4**	**V5**	**V6**	**V7**	**V8**	**V9**	**V10**	**V11**	**V12**
Complete blood count	√	√	√	√	√	√	√	√	√	√	√	√
Hepatitis B Serology	√							√		√		√
CMV Serology			√									
Lymph node biopsy		√					√					
Microbiome samples		√	√				√					
Whole blood RNA-seq			√	√	√	√	√					
Epigenetics			√	√	√	√	√					
Proteomics & lipidomics			√	√	√	√	√					
Immune phenotyping			√	√	√	√	√					
Cell mediated Immunity		√						√		√		√
Single cell RNA-seq			√	√	√	√	√					
Milieu interieur			√									
Antibody repertoire			√									
Cytokine Expression			√				√			√		√

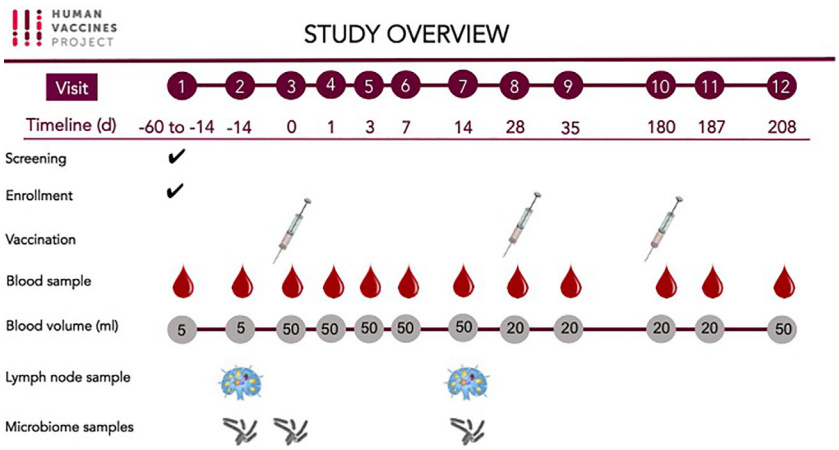

FIGURE 2 | Study Overview.

moistened in an SCF-1 vial. Wearing gloves, the study staff stretched the skin site taut with one hand and with the other hand held the swab so the shaft was parallel to the skin surface and rubbed the swab over the skin surface. Both sides of the cotton tips were firmly rubbed back and forth about 50 times over the skin surface by applying firm pressure. The swab was then sealed and transported to the laboratory to be stored at −80° C until microbiome analysis.

Nasal Sample Collection

The nasal samples were collected using a sterile fresh, dry swab. The swab was inserted approximately 0.5 cm into the nasal cavity. The inside of both nares were swabbed by rubbing the swab along the walls of the nares 5 time. The collection tube was then sealed, place in a biohazard bag and transported within 4 h of collection to the laboratory where it was stored at −80°C until further microbiome analysis.

Oral Sample Collection

The oral swabs were collected using a fresh sterile dry swab. Both sides of the cotton tips were firmly rubbed on the surface of the tongue without touching the inside of the cheeks, teeth or lips. The collection tube was then sealed and placed in a biohazard bag before being transported to the lab and stored within 4 h at −80°C for future microbiome analysis

BLOOD AND LYMPH NODE SAMPLE PRE-PROCESSING FOR MULTI-OMIC ANALYSIS

Lymph Node Cell Processing and Cryopreservation

Freshly collected LN cells were separated by centrifugation at 450 × *g* for 5 min in a pre-cooled centrifuge and resuspended in cold 0.5 ml of heat inactivated fetal bovine serum (HIFBS) (Hyclone, cat #SH30071.0). If red blood cell contamination was observed, we planned to add 2 ml of ACK RBC lysis buffer (Thermo Fisher Gibco cat #A1049201) for 3 min to the cell suspension. To stop the reaction, 10 ml of phosphate buffer saline (PBS) with 2% HIFBS is to be added and the cells separated by centrifugation in the same conditions. In this particular cohort, due to a relatively small number of cells obtained, no RBC lysis was performed on the fine needle aspirate samples collected. The cells were then counted with a hemocytometer using a trypan blue dye, resuspended in a solution containing 90% FBS and 10% DMSO (Hybrimax, Sigma, cat #D2650) and transferred to a pre-labeled chilled cryovial. The LN aspirate samples were stored in liquid nitrogen for future flow cytometry analysis.

Blood Sample Pre-Processing and Storage

Blood samples were processed as shown in **Figure 3**. The goal was to determine changes in cell composition, transcriptome (whole blood and single cell), white blood cell (WBC) and plasma proteome, metabolome, as well as WBC epigenome and next-generation sequencing (NGS) of VDJ regions in antigen-specific B cells clones obtained from peripheral blood mononuclear cells (PBMCs). Pre-vaccine samples were also assessed for the immune response to generic stimuli using Milieu Interieur's TruCulture platform. RNA, proteins, and certain metabolites are susceptible to time and temperature dependent changes; thus, care was taken to process samples as fast as possible. The order of sample processing is dependent on the sample type sensitivity to degradation and changes over time. In this study, the samples were processed in order below.

Blood RNA Samples

Shortly after collection, the blood PAXgene tubes were inverted 10 times and kept at room temperature for a minimum of 2 h for complete lysis of blood cells. The tubes were then stored at −80°C for further transcriptomics analysis.

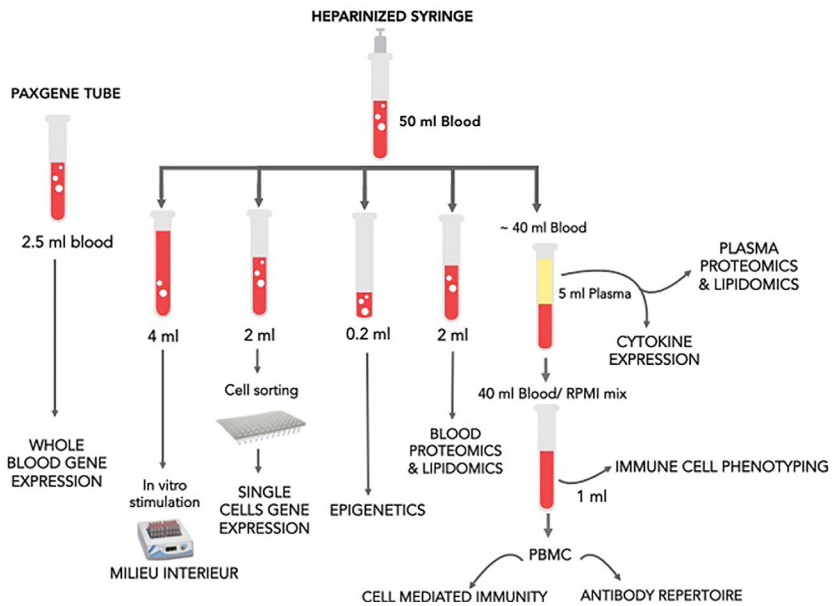

FIGURE 3 | Omic sample processing overview.

Single Cell RNA Samples

A total of 1.5 ml of blood sample was used to stain, single sort the cell populations of interest and perform subsequent single cell sequencing. Initially, 20 mM of EDTA (Fisher #BP120-500) was first diluted 10 times in the blood sample and red blood cells were lysed by adding RBC lysis buffer (eBiosciences, cat #00-4333-57) per manufacture's recommendations. The mix was then resuspended with a sterile pipette and incubated at RT for 10 min, with gentle vortexing every 3 min. To stop the reaction, PBS was added, and the cell suspension separated by centrifugation at 500 × *g* for 5 min. The supernatant was then gently aspirated, and the red blood cell free suspension was resuspended in 3 ml of PBS. Before proceeding to cell staining, 100 µlS cells that served as a negative control for the flow cytometry sorting were set aside for machine calibration. The cells were then were separated by centrifugation at 600 × *g* for 10 min and the cell pellet resuspended in an antibody cocktail mixture (**Table 3**) diluted in PBS and 0.5% BSA (Bovine serum Albumine Sigma Aldrich, cat #A7906) according to the manufacture's recommendations. A fixable viability dye (APC-eFluor 780 cat #65-0865-14) was also added to the cells prior to staining to allow sorting only viable cells. The cell mixture was incubated at RT protected for light for 30 min then washed once in PBS and resuspend in 3 ml of PBS for immediate sorting. The cell types of interest (neutrophils, plasmacytoid DCs, myeloid DCs, NK cells, and monocytes) were single sorted BD FACS Aria chilled chambers. The efficiency of single cell sorting was assessed by microscopy using fluorescent beads. Single cells were sorted into 96-well plates chilled on ice, pre-loaded with 2-µl lysis buffer (0.2% Triton X-100, (Sigma Aldrich, cat #9002-93-1), 2 Units/µl RNase inhibitor (Applied Biosystems, cat #N8080119), 1:2,000,000 dilution of ERCC spike-in RNAs (Life technologies, cat #4456740) and spun down at 300 × *g* at 4°C for 1 min before sorting. Negative and positive samples consisting of no cells per

TABLE 3 | Antibody panel for cell sorting for single cell RNA sequencing.

Marker	Target	Fluorochrome	Clone	Catalog number
CD11c	Myeloid dendritic cells (mDC)	APC	Bu15	BD #340544
CD123	Plasmacytoid dendritic cells (pDC)	PE-Cy7	6H6	ebio #25-1239-42
CD3	T cell lineage	PE-CF-594	UCHT1	BD #562280
CD56	NK cells	PerCP Cy5	HCD56	BioLegend # 318343
CD11b	Mature and Immature Neutrophils	PE	ICRF44	Biolegend #301346
CD66	Neutrophils	PerCP Cy5	ASL-32	Biolegend #92719
CD16	Neutrophils, pro-inflammatory and transitional monocytes and NK cell subsets	FITC	3G8	Pharmingen #560996
HLA-DR	Dendritic cells, monocytes and B cells	eFlour605	LN3	ebio # 83-9956
CD14	Classical and intermediate monocytes	V500	M5E2	BD #561391
CD45	Pan leukocyte antigen	V450	HI30	BD #560367

well and 100 cells per well were included in the plate design to use as controls in the Smart-seq library prep and sequencing. After sorting, each plate containing the single cell lysates was immediately sealed, placed on dry ice, and stored at −80°C.

Epigenetic Whole Blood Samples

Two hundred microliters of heparinized blood was transferred in a cryovial and saved at −80°C without any further processing to allow subsequent epigenetic analysis.

White Blood Cell Proteomic Samples

Two milliliters of 10× RBC lysis buffer (eBiosciences, cat #00-433-57) was diluted in 18 ml of ultrapure water and added to 2 ml heparinized whole blood to lyse red blood cells according to manufacturer's instructions. Briefly, the cell suspension was incubated at room temperature for 15 min with gentle vortexing during the incubation time. Warm PBS was then added to mix to stop the reaction and the cells were separated by centrifugation at 600 × *g* for 10 min to collect the red blood cell free pellet. After an additional wash in PBS, the supernatant was carefully aspirated without disrupting the pellet and the WBC pellet was saved at −80°C to allow subsequent proteomic analysis.

Milieu Interieur Samples

The goal was to stimulate whole blood *in vitro* in a standardized stimulation system. Three core stimuli, plus a null control, were selected to best capture diverse immune responses: LPS; Poly(I:C) and SEB. One milliliter of heparinized whole blood was transferred into TruCulture tubes (with 2 ml media) within 15 min of blood collection, inserted into a dry block incubator, and maintained at 37°C (± 1°C) in room air for 22 h as previously described (6). At the end of the incubation period, tubes were opened, and a valve was inserted to separate the sedimented cells from the supernatant, stopping the stimulation reaction. Supernatants were saved for later Luminex testing at −80°C. For stabilization of RNA, 2 ml of Trizol LS (Sigma) was added to the cell pellet, vigorously vortexed and frozen at −80°C until analysis.

Plasma Samples

The remaining volume of heparinized blood (~30 ml) was placed in 50 ml conical tubes and underwent centrifugation at 1,000 × *g* for 10 min. The entire plasma component was then placed into new 50 ml conical tube and the mix inverted 4 times. The plasma was immediately aliquoted and saved at −80°C for subsequent analysis of the plasma proteome, lipidome and metabolome.

Immune Phenotyping Samples

The remaining cellular blood fraction left over after plasma collection was diluted twice in RPMI, mixed up and down and the cells/RPMI mixture was kept on wet ice. A total of 900 µl of the mix was stored for subsequent flow cytometry analysis. Whole blood cells were processed as previously described (7) using Smart tube lysing and fixing solutions as per manufacture's recommendations. Briefly, 225 µl of diluted heparinized blood was added to four cryovials and mixed with 22 µl of 20 mM EDTA. The cell suspensions were mixed up and down with gentle pipetting, and 2 µl of fixable viability dye (eBioscience #65-0865-14) was added to each vial and the cells incubated for 30 min at 4°C protected from light. Red blood cells were then lysed by adding 350 µl of Smart lysis buffer (SmartTube Stable-Lyse V2) to each vial, incubated for 15 min at RT and the stained cells fixed with 1 ml Smart store buffer (SmartTube Stable-Store V2) for an additional 15 min. The fixed cells were then transferred to −80°C and stored until flow cytometry analysis were performed. Complete blood counts were undertaken shortly after blood draw from fresh samples by BC Children's Hospital clinical laboratory to enumerate total WBC count, plus a differential count of neutrophils, lymphocytes and monocytes using a Sysmex XN-1000 Hematology Analyzer.

PBMC Samples

The remainder of the blood-RPMI mix was used for cryopreservation in order to allow T cell mediated immunity analysis by flow cytometry and NGS of VDJ regions in antigen-specific B cells. The blood was diluted twice in warm RPMI and the mixture gently flowed down the side of a tube, layered onto an identical volume of ficoll-paque (Amersham-Pharmacia, cat #17-1440-02) without breaking the surface plane. The tubes were then subjected to centrifugation at 900 × *g* for 20 min with no brake to allow the gradient to form. At the end of the centrifugation time, the cloudy interface containing the mononuclear cells were transferred to PBS and washed twice in the same medium. Every 10 million PBMCs were then resuspended in cold 0.5 ml of 12.5% human serum albumin (Sigma, cat #A5843) and 2× cold freezing buffer (90% HSA at 12.5%, 20 DMSO). The PBMC vials were saved at −80°C overnight in a freezing container (Mr Frosty Nalgene, cat #5100-000) and then transferred to liquid nitrogen until analysis.

MULTI-OMIC ANALYSIS

Whole Blood Gene Expression

RNA extraction was performed on blood collected in PAXGene tubes using the PAXGene RNA purification kit (QIAGEN), following the manufacturer's protocol. The Agilent 2100 Bioanalyzer (Santa Clara, CA, USA) was used to quantify and assess quality of total RNA. Poly-adenylated RNA was isolated using the NEBNext Poly(A) mRNA Magnetic Isolation Module (NEB, Ipswich, MA, USA). cDNA libraries were created from poly-adenylated RNA using the KAPA Stranded RNA-Seq library preparation kit (Roche, Basel, Switzerland). Samples were sequenced on the HiSeq2500 with single end reads of length 100 bp. Samples were checked for batch effects *via* heatmap analysis of normalized gene counts and none were found. Sequence quality of fastq files was assessed using FastQC v0.11.7 (https://www.bioinformatics.babraham.ac.uk/projects/fastqc/). Alignment of the raw reads to the reference genome was done using STAR v2.5.4b (8) to generate position-sorted BAM files. The genomic index required by STAR was created using the human genome downloaded from Ensembl (9), build

GRCh38 v91, primary assembly. Gene counts were generated using the htseq-count function from HTSeq v0.10.0 (10). Results from the above programs (FastQC, STAR, and HTSeq) were compiled into a single report using MultiQC v1.0 (11). Analysis of RNA-Seq data was conducted using R v3.5.0 (https://www.R-project.org/) and RStudio v1.1.453 (http://www.rstudio.com/). Count files were filtered to remove genes with fewer than 10 counts across 15 samples (the number of biological replicates). Known globin genes were removed corresponding to the following six Ensembl IDs: ENSG00000206172, ENSG00000188536, ENSG00000244734, ENSG00000223609, ENSG00000213934, and ENSG00000196565. After filtering and globin removal, samples had a median library size of 4,842,497, with a minimum of 2,217,471 and maximum of 14,755,180. DESeq2 v1.20.0 (12) was used to identify differentially expressed (DE) genes. DE genes were identified using the Wald statistics test, followed by filtering for significance using a combined threshold of adjusted p-value ≤ 0.05 and absolute fold-changes ≥ 1.5. For pathway enrichment analysis, Sigora v2.0.1 (13) was used with the Reactome database at a hierarchy level of four. Correction for multiple comparisons was done using the Bonferroni method, filtering results based on a value of ≤0.001.

Whole Blood Epigenetic Analysis

Genomic DNA (gDNA) was extracted from 200 µl whole blood samples using DNeasy Blood & Tissue Kit (Qiagen, Hilden, Germany) following manufacturer's instructions. Seven hundred fifty nanograms of resulting gDNA samples were subjected to overnight bisulfite conversions with EZ DNA Methylation kit (ZymoResearch, Irvine, CA) in a PCR thermal cycler (16 cycles of 95°C for 30 s, and 50°C for 60 min). To perform global DNA methylation profiling on the Illumina MethylationEPIC beadchips, 160 ng of the bisulfite converted DNA (bcDNA) samples were used. The array procedure started with an overnight whole-genome amplification at 37°C. The amplified products were then enzymatically fragmented, precipitated with isopropanol, then resuspended in hybridization buffer. Following heat denaturation, processed bcDNA samples were hybridized onto MethylationEPIC BeadChips in an overnight incubation at 48°C. The next day, unbound bcDNA were washed off the chips, then single-base extension was performed with the provided DNP-labeled and biotin-labeled dNTPs. After neutralization, labeled extended primers on each array were stained at 32°C in the chamber rack with Cy5 labeled anti-DNP antibodies and Cy3 labeled streptavidin as per manufacturer's protocol in a 90-min staining procedure. Stained EPIC chips were then sealed, dried, and scanned with the Illumina iScan on a two-color channel to detect Cy3 labeled probes on the green channel and Cy5 labeled probes on the red channel. Using the Illumina GenomeStudio software package, average beta values were calculated by dividing the methylated probe signal intensity by the sum of methylated and unmethylated probe signal intensities. Average beta values range from 0 (completely unmethylated) to 1 (fully methylated) and provided a quantitative readout of relative DNA methylation for each CpG site within the cell population being interrogated. The DNA methylation (DNAm) data were first processed by checking their beta value distributions in R statistical software. The EPIC array beta values were the used to perform hierarchical clustering using either the entire EPIC array or 58 SNP probe's beta values. The DNAm data quality was assessed by filtering of the EPIC was performed according to this criteria: if probes were interrogated a SNP, had evidence of cross hybridizing to a region of the genome other than the designed target (14), had a SNP present at the CpG target or single base extension of the probe (polymorphic probes) (14). Probes were removed if they had a beadcount <3 in 5% of samples, or had 1% of samples with a bad detection p-value > 0.05. Samples were then normalized using the dasen method (15) bringing the beta value closer together. Correction of blood cell composition was performed to in whole blood samples using linear regression of counts from the complete blood count (16). Batch effects between Sentrix IDs were observed using Principal Component Analysis (PCA) and ComBat (17) was used to correct for for Sentrix ID. Data from technical replicates were also assessed. In order to improve computational efficiency and reduce multiple test correction, 101,864 non-variable CpGs were removed as previously described (18). To analyze the data looking at the effect of vaccination, age or sex in the cohort, a linear mixed effects model was ran with DNAm value as outcome, the other factors as main effects with a covariate of the subject ID as a random effects.

Proteomic and Lipidomic Analysis

WBC samples were lysed using published methods (19). Proteins were measured using the Pierce™ Bradford Assay and 10 µg per sample was digested as previously described (20). Peptides were desalted using STop-And-Go Extraction tips (STAGE tips) (21), dried using the Vacufuge Plus (Eppendorf) for 45 min, then chemically dimethylated with light, medium, and heavy formaldehyde (22) for triplex analysis of each time point per individual (i.e., two triplex samples were prepared for each individual, with sample from one of the time points spiked into both triplexed samples to use as a reference). After labeling, samples for each triplex were combined, desalted and dried again using STAGE tips and the Vacufuge Plus. Peptides were resuspended in 30 µl of 0.1% formic acid for liquid chromatography and mass spectrometry analysis (LC-MS). Two micrograms per sample was injected into the EasynLC-1000 chromatography system (Thermo) with a 50-cm analytical column, packed in-house with C18, coupled to an Impact II Q-TOF mass spectrometer (Bruker Daltonics, Bremen, Germany), with detailed parameters as previously described (23). Data was analysed using MaxQuant (v1.5.5.1) with default values and "Match Between Runs" activated, searched against the human Uniprot database (downloaded on 15 July, 2017). The mass spectrometry proteomics data have been deposited to the ProteomeXchange Consortium *via* the PRIDE (24) partner repository with the dataset identifier PXD020474.

Plasma lipidomics samples were prepared using a variation of a published protocol (25). Aliquots of 10 µl of plasma were mixed with 180 µl of ammonium bicarbonate (150 mM), followed by extraction with 790 µl of a 7:2 mixture of methyl

TABLE 4 | Composition of standards used for analysis of plasma lipidomics.

Lipid name	Quantity in standard
lysophosphatidylglycerol 17:1	50 pmol
lysophosphatic acid 17:0	50 pmol
phosphatidylcholine 17:0/17:0	500 pmol
hexosylceramide 18:1;2/12:0	30 pmol
phosphatidylserine 17:0/17:0	50 pmol
phosphatidylglycerol 17:0/17:0	50 pmol
phosphatidic acid 17:0/17:0	50 pmol
lysophposphatidylinositol	50 pmol
lysophosphatidylserine 17:1	50 pmol
cholesterol D6	1 nmol
diacylglycerol 17:0/17:0	100 pmol
triacylglycerol 17:0/17:0/17:0	50 pmol
ceramide 18:1;2/17:0	50 pmol
sphingomyelin 18:1;2/12:0	200 pmol
lysophosphatidylcholine 12:0	50 pmol
lysophosphatidylethanolamine 17:1	30 pmol
phosphatidylethanolamine 17:0/17:0	50 pmol
cholesterol ester 20:0	100 pmol
phosphatidylinositol 16:0/16:0	50 pmol

tert-butyl ether and methanol, respectively. Samples were spiked with 21 µl of internal standard (**Table 4**). Samples were shaken for 15 min at 4°C, and then underwent centrifugation at 3000 × *g* for 5 min, from which 100 µl of the organic portion was taken and dried on a 96-well plate; each was resuspended in 20 µl of ammonium acetate (7.5 mM) in a 1:2:4 mixture of chloroform, methanol, and isopropanol, respectively. The samples were loaded using the TriVersa NanoMate (Advion, Ithaca, NY, USA) infusion robot and a 4-mm infusion chip, and analyzed by the Impact II Q-TOF mass spectrometer (Bruker Daltonics, Bremen, Germany) in positive and negative ionization mode. Raw data were processed using an in-house script. Batch correction was performed on log2-transformed data using ComBat from the "sva" R package (26). A paired *t*-test was used to test for differentially abundant proteins at each post-vaccination time point (Days 1, 3, 7, and 14) compared to the pre-vaccine time point (Day 0). For comparison of non-responders and responders, a *t*-test and multiple-testing correction were applied *via* a custom script in R. For all tests, proteins were filtered for significance using an adjust p-value of 0.05.

Immune Cell Phenotyping

Fixed cells were stained per manufacturer recommendations with different labeled antibodies (**Table 5**) to identify specific cell populations. Flow cytometry data were acquired on a LSRII flow cytometer (BD Biosciences). Flow cytometry raw data were analyzed manually using Flowjo software (version 9.9). In addition, immunophenotyping using automated gating was undertaken on the same samples. This has advantages over manual gating, including increased throughput and identification of specific cell populations with up to 50-dimensional datasets (27). Pre- processing to detect anomalous events obtained during data acquisition was done using the flowCut algorithm (https://rdrr.io/github/jmeskas/flowCut/man/flowCut.htmL). In brief, this approach detects and removes events within time segments for which the fluorescence intensities deviate from the norm. Next, events with either the minimum or maximum value in any of the scatter channels were removed. Singlets were selected using the FSC-A and FCS-W channels. Finally, the data were compensated and transformed using a logical transformation. For each sample, flowDensity (a supervised gating algorithm) (28) was used to determine the thresholds for each marker in each of the biaxial plots in a data-driven manner based on the density distribution of the fluorescence signal. If there were two peaks in the density distribution, the split was located at the minimum between the two peaks. In the case of more than two peaks, the peak-to-peak distance and valley heights was used to determine which split gave the most distinct cut. Otherwise, the algorithm used inflection points. Five challenging populations (live cells, myeloid and plasmacytoid DCs, gamma delta T cells and $CD56^{bri}CD16^{lo}$ NK cells) required a second gating step using flowPeaks, an unsupervised clustering algorithm (29). These included populations which were difficult to separate from the background and which could not easily be defined by polygons with sides at pre-defined angles. We defined these cell populations as the union of all of the clusters with centroids inside of the flowDensity-determined boundaries. Cell counts for each of the populations in the gating strategy were obtained and normalized to the bead count, yielding cell counts for a total of 24 immune cell populations (**Figure 4**). Correlation analysis between antibody titres and cell composition were performed. A Spearman correlation was utilized where antibody data were normally distributed and a Wilcoxon rank sum test when antibody data were skewed.

Single Cell Gene Expression

Processing of the frozen 96-well plates containing single cell lysates was performed as previously described (30) with modifications to accommodate an Agilent BioCel automated liquid handling platform (31). Briefly, single cell lysates contained in the 96-well sorted plates were processed in batches of eight plates, with each plate containing wells reserved for 10 pg Universal Human RNA (Clontech) as a positive control, an ERCC-only control (Thermo Fisher), and water as a negative control. cDNA synthesis, lysis, reverse transcription with Smart-seq2, and PCR were carried out in a reduced volume (12.5 µl) and with ERCC internal controls spiked-in at a reduced concentration using a 55 million-fold dilution of the ERCC stock in the first strand cDNA synthesis step. Amplified cDNAs from the eight 96-well plates were consolidated to two 384-well plates and purified with Ampure magnetic particles. A 10-fold diluted portion of each cDNAs was assessed for expression of the Beta-Actin housekeeping gene by qPCR for quality control of the amplified cDNAs.

A cycle threshold (Ct) of ≤35 was used as a cutoff for the selection of 3,072 cDNAs for library preparation and sequencing. A Star liquid handling platform (Hamilton) was used to consolidate cDNAs selected for Illumina Nextera XT library

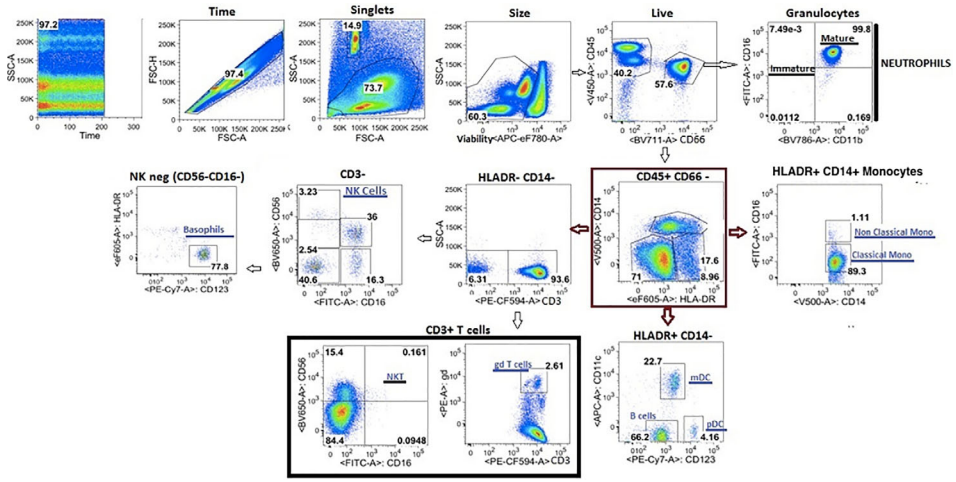

FIGURE 4 | Flow cytometry gating strategy of immune cells in whole blood.

preps into 384-well plates. An automated 1/8th Nextera XT reaction was carried out on 125 pg of the selected cDNAs for the Tn5 tagmentation step, with limited 15-cycle PCR followed by AmPure bead purification. Nextera XT PCR was carried out with a combination of 384 barcode pairs using Nextera barcode sets A and D. Concentrations of the purified Nextera XT reactions were normalized to 1 ng/µl and combined into a 2-ng pool of 384 dual-barcoded samples. RNA-seq was carried out with a total of eight 384 barcoded pools loaded across 16 lanes of an Illumina HiSeq 2500 according to manufacturer's specifications for a total of 3,072 samples sequenced, including controls. A Hiseq SBS V4 250cycle kit and a Paired End V4 Cluster Kit were used for an estimated 2 million reads per sample.

Single cell RNA-seq data was processed according to published methods (30). Briefly, raw sequencing files were demultiplexing using Illumina barcodes, while sequencing primers and low-quality bases were removed using the Trimmomatic software package (32). Trimmed reads were then aligned using HISAT (33) in two steps: first to a reference of ERCC sequences, and then to GRCh38 (Ensembl). StringTie (33) was used to assemble the resulting alignments into transcript structures and gene expression values (TPM) estimated using GENCODE v25 annotation (Ensembl 87; 10-2016); HTSeq-count (10) was used to generate raw gene alignment counts.

Quality control analysis was performed using sequencing and laboratory metrics, including average Phred score, read complexity, and sample concentration, to classify cell samples as pass or fail using a Random Forest quality control classification model as previously described (34). Expression values for cell samples that passed quality control classification were fed into the Scater and SC3 algorithms for PCA, t-distributed stochastic neighbor embedding (tSNE) visualization, and cluster analysis (35, 36). Unsupervised clustering was performed for the entire dataset, while additional supervised clustering guided by flow cytometry marker panels was performed to investigate within cell type variation. Lastly, cell type marker determination was performed using the SC3 unsupervised clustering results and the NS-Forest algorithm (37). The end result of this computational pipeline produces a set of specimen-specific unbiased cell type clusters, a gene expression matrix with the expression levels of genes in individual single cells grouped into cell type clusters, and a set of sensitive and specific marker genes for each cell type cluster to be used for downstream assays (e.g., quantitative PCR) and semantic representations (38).

Cell Mediated Immunity

Cryopreserved PBMCs were thawed at 37°C and rested overnight in AIMV serum free medium (MAfisher, MA, USA). Viable cells were counted using an automated cell counter (Nexcelom, Lawrence, MA, USA). Up to 10^6 PBMCs were plated per well in 96-well plates and either left unstimulated or stimulated with either Staphylococcal enterotoxin B (positive control) or a HB peptide pool (AA labs, San Diego) to assess T cell activation in response to HBV re-stimulation. At 44-h post-stimulation, cells were detached from the wells using 20 µM EDTA (Invitrogen), washed in PBS, and stained with viability dye and antibodies specific to T cell activation markers (**Table 6**). At the end of the incubation, the stained cells were washed and flow data acquired on a LSRII flow cytometer (BD Biosciences). Flow cytomtery data were analyzed using Flowjo software using the gating strategy shown in **Figure 5** (version 9.9, LLC, USA).

Response to Innate and Adaptive Immune Stimuli

The TruCulture® systems were developed to provide robust induction of innate and adaptive immune responses (6) and have previously been shown to be more reproducible than conventional PBMC-based stimulations (39). In this context,

TABLE 5 | Antibody panel for single cell immunophenotyping.

Marker	Target	Fluorochrome	Clone	Catalog Number
CD64	Activated leukocytes	Alex 700	10.1	BD #561188
CD11c	Myeloid dendritic cells (mDC)	APC	Bu15	BD #340544
CD123	Plasmacytoid dendritic cells (pDC)	PE-Cy7	6H6	ebio #25-1239-42
CD3	T cell lineage	PE-CF-594	UCHT1	BD #562280
gd TCR	gamma delta T cells (γδ T cells)	PE	B1.1	ebio #12-9959-42
CD56	NK cells	BV650	HCD56	Biolegend #318343
CD11b	Mature and Immature Neutrophils	BV786	ICRF44	Biolegend #301346
CD66	Neutrophils	Biotin/BV711 Streptavidin	ASL-32	Biolegend #92716/BD563262
CD16	Neutrophils, pro-inflammatory and transitional monocytes and NK cell subsets	FITC	3G8	Pharmingen #560996
HLA-DR	Dendritic cells, monocytes and B cells	eFlour605	LN3	ebio #83-9956
CD14	Classical and intermediate monocytes	V500	M5E2	BD #561391
CD45	Pan leukocyte antigen	V450	HI30	BD #560367

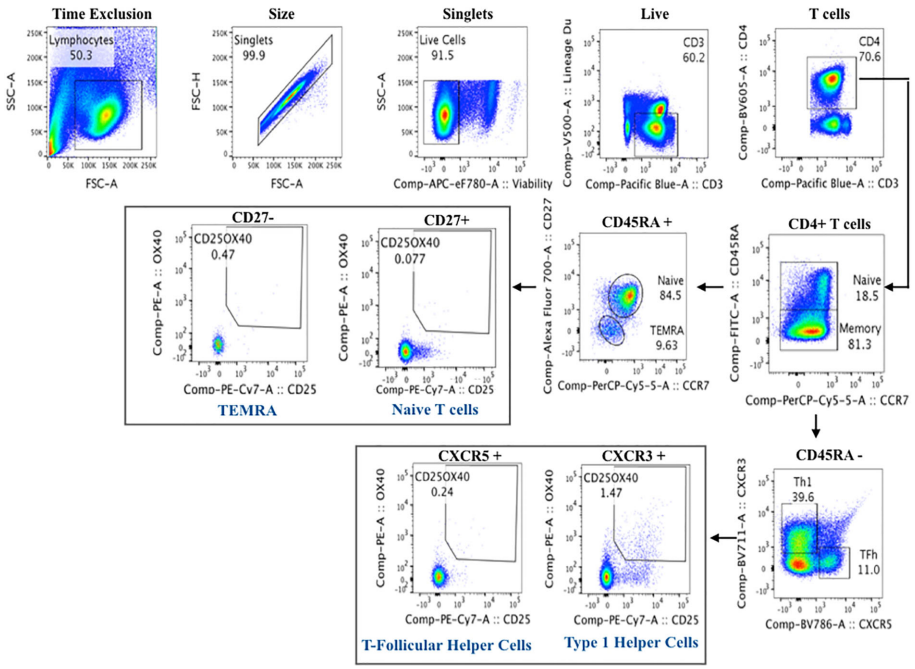

FIGURE 5 | Flow cytometry gating strategy of activated T cells for cell mediated immunity assay to Hepatitis B.

only pre-vaccine samples were tested with the *Milieu Interieur* (40) platform. RNA was isolated from Trizol whole blood cell samples using the NucleoSpin 96 RNA tissue kit protocol (Macherey-Nagel) with some modifications as previously described[4]. RNA yield, integrity (RIN), and quality (RQS) scores were estimated, quality control validated and pristine samples with an RQS > 4 were processed for gene expression analysis. The NanoString nCounter system was used for the digital counting of transcripts. One hundred nanograms of total RNA were hybridized with the Human Immunology v2 Gene Expression CodeSet according to the manufacturer's instructions (41). Samples were processed in two batches, within which the samples were randomized. All samples were normalized together following background subtraction of the negative control probes, using positive control probes and housekeeping genes selected by the GNorm method as previously described (42). Quality control for our data involved checking the following metrics: fields of view ≥0.75; binding density 0.05–2.75, linearity of positive controls (R2 ≥ 0.9), and limit of detection for 0.5 fM positive control ≥2 standard deviations above the mean of the negative controls.

Supernatants from TruCulture tubes were thawed on ice and tested by Luminex xMAP technology for a total of 32 proteins including cytokines, chemokines and growth factors as previously described (6). Samples were measured on the Myriad RBM Inc platform (Austen, Texas) according to CLIA guidelines (set forth by the USA Clinical and Laboratory Standards Institute). The least detectable dose for each assay was derived by averaging the values obtained from 200 runs with the matrix diluent and adding 3 standard deviations to the mean.

TABLE 6 | Antibody panel for in vitro T cell mediated immune responses to hepatitis B.

Marker	Target	Fluorochrome	Clone	Catalog number
CD14	Classical and intermediate monocytes	V500	M5E2	BD #561391
CD19	B cells	V500	HIB19	BD # 561121
CD8	CD8 T cells	BV510	RPA-T8	BD # 563256
CD3	T cell lineage	PacBlue	UCHT1	BD # 558117
CD4	CD4 T cells	BV605	SK3	BD #565998
CD45RA	Naive T cells	FITC	HI100	Biolegend # 304106
CCR7	Naive and regulatory T cells	PerCP-Cy5.5	G043H7	Biolegend # 353220
CD27	T and B cell subsets, NK cells	AF700	M-T271	Biolegend # 356416
CD25	Activated T cells	PE-Cy7	M-A251	BD # 557741
OX40 (CD134)	Activated T cells	PE	L106	BD #340420
PDL1 (CD274)	Activated T cells	APC	29E2A3	Biolegend #329708
CXCR5 (CD185)**	T-Follicular Helper Cells	BV785	J252D4	Biolegend #359132
CXCR3 (CD183)**	Type 1 Helper Cells	BV711	G025H7	Biolegend #353732

***Spiked in the cells during incubation and re-stain.*

The lower limit of quantification was determined based on the standard curve for each assay and is the lowest concentration of an analyte in a sample that can be reliably detected and at which the total error meets CLIA requirements for laboratory accuracy.

Anti-HBV Antibody Repertoire Analysis

The repertoire of anti-HBV IgG antibodies was analyzed by isolation of IgG from single-sorted B cells and IgG NGS. For antibody isolation, single IgG+ antigen-specific CD19+ CD20+ B cells were sorted from PBMC samples in 96-well plates using HBV virus-like particles fluorescently labeled with Alexa Fluor-488 and Alexa Fluor-647 dyes. The sort density was one cell per well to enable later antibody chain pairing. Reverse transcription and PCR amplification of heavy and light chain variable genes were performed, and the antibodies were assembled for each source cell. Post-vaccination antibody clonality was compared between different participants. Antibody NGS was undertaken on samples collected before and after the third vaccine dose. For each sample, antibody heavy chains were amplified from mRNA isolated from total PBMCs. Reverse transcription of the RNA was performed using barcoding primers containing unique molecular identifiers (UMIs), as previously described (43). The resulting cDNA was used to amplify antibody heavy chains. Antibody sequence annotation, including VDJ assignment was performed using AbStar (https://github.com/briney/abstar). Error correction of sequencing data was done by UMI-based correction using AbCorrect (https://github.com/briney/abtools/blob/master/docs/source/abcorrect.rst). This combination of AbStar and AbCorrect allows clustering and consensus/centroid generation on just the VDJ region of the antibody sequence in the proper orientation. For clonal lineage assignment, sequences were assigned to clonal lineages using Clonify, as previously described (43). Clonify uses an antibody-specific distance metric, incorporating length-normalized CDR3 edit distance, V and J gene usage, and shared somatic mutations to determine the relatedness of each antibody sequence pair.

Cytokine Analysis

Single molecule array (Simoa) is an ultra-sensitive single molecule array which is able to detect cytokines at extremely low levels, below the detection methods of conventional immunoassays (44–50). This method integrates conventional bead-based ELISA with microwell-array technology and has limits of detection approaching the attomolar to femtomolar range. Analysis was undertaken for a panel of 15 cytokines (IFN-α, IFN-β, IFN-γ, IFN-ω, IL-1β, IL-2, IL-6, IL-7, IL-8, IL-10, IL-12p40, IL-12p70, IL-15, GM-CSF, and TNF-α), using published methods (48). Briefly, multiplex capture beads were purchased with pre-encoded fluorescent dyes to generate multiple distinct bead populations. Capture antibodies were then coupled onto the paramagnetic beads. Detection antibodies were either purchased with biotin conjugates or biotin conjugated in-house. All reagent solutions (5×10^6 capture antibody-coated paramagnetic beads, biotin-conjugated detection antibodies, 150 pmol/L streptavidin-β-galactosidase reagent, 1× PBS buffer, 100 µmol/L resorufin β-d-galactopyranoside substrate, wash buffers and fluorocarbon oil) were loaded onto the Simoa HD-1 Analyzer (Quanterix, Lexington, MA, USA). Cytokine controls were prepared in 1× PBS containing 25% newborn calf serum. Controls (serial dilutions) and samples fourfold diluted in 1× PBS) were loaded into a 96-well plate and analyzed in triplicate. The samples were screened for 15 cytokines using a total of seven Simoa assays (four 3-plex and three single-plex). Cytokine concentrations were determined *via* hydrolysis of the resorufin β-d-galactopyranoside substrate to generate the fluorescent product resorufin, which was detected *via* excitation/emission of 574 nm/615 nm taken at a 30-s interval, with a threshold of ≥20% increase in fluorescent intensity against the random fluorescent background. Subsequent fluorescent images were taken at excitation/emission wavelengths for the different bead types, as previously described. A four-parameter logistical curve was applied for the average enzymes per bead as a function of cytokine concentration curve fitting.

Microbiome

Bacterial community composition was analyzed in rectal, skin, oral and nasal samples. The data were generated *via* high-throughput sequencing of bacterial V4-16S rRNA amplicons, using the Illumina MiSeq platform using a refined version of an established analysis pipeline, which has been described previously

(51). To identify and remove contaminating sequences, three extraction blanks were included. These were generated by first performing three extraction blanks, then using the eluate from these as a template for PCR amplification, and then sequencing in the same run as the biospecimens. Two positive controls, consisting of cloned SUP05 DNA, were also included (number of copies = 2*10^6). OTUs present in blanks are either introduced from extraction reagents, PCR reagents, or from neighboring samples during either the extraction or the PCR amplification process. Contaminating OTUs were identified as being present in at least 50% of blanks, with count geometric mean plus one standard deviation was greater than the samples, reflecting previously described properties of contaminants arising from extraction or PCR reagents. This approach also avoids removing common contaminating OTUs from neighboring samples either during the extraction or PCR amplification steps, as these are of high relative abundance in the samples but low relative abundance or sporadic presence in the blanks. Contaminating OTUs were removed from the dataset. Samples with total read counts under 1,000 after contaminant removal were also removed from further analysis. The analyses address analytical challenges inherent to microbiome data. First, community composition data are in the form of relative abundance of populations, which do not vary independently, and are not suited to univariate methods. Second, the data are sparse, typically with a large proportion of populations at zero relative abundance in any particular sample. Analysis is robust to sparsity, because rare populations may be functionally important. Third, because whole microbial communities often modulate biological pathways, testing individual populations, which overlooks interactions or correlations among them, may not adequately capture microbiome effects on host responses. To relate microbiome composition to immune responses, multivariate methods were employed, including a workflow for microbiome data analysis in the *mixOmics R* package. To maximize the correlated information between multiple datasets and optimally identify the key microbiome features that explain and reliably classify immune phenotypes, multivariate dimension reduction discriminant analysis was used. This method was extended to allow for exploration of non-linear relationships between features, through the use of kernel methods (52) and other approaches. Additional machine learning approaches (e.g., random forests) were used to develop models predictive of anti-HBs antibody

Lymph Node Cells Analysis

Fluid from LN aspirates was inoculated into ice cold RPMI and transported immediately to the laboratory on ice, before cells were separated by centrifugation at 700 × *g* for 5 min at 4°C. Cells were resuspended in PBS, 2% fetal bovine serum (FBS), counted using crystal violet, and cryopreserved in 80% FBS, 20% DMSO in liquid nitrogen awaiting further analysis. Germinal center (GC) B cells were identified by co-expression of Bcl6 and Ki67, and GC Tfh cells were identified as $CXCR5^{hi}PD1^{hi}$ CD4 T cells (4, 53–55). In general, eight (of 31) LN FNA samples were deemed acceptable for analysis using the established criteria of flow cytometry acquisition of >30,000 total cells and >5,000 B cells. In this study, we analyzed all cells present in the CD20+ B cells or CD4 T cell gates

CONCLUSIONS

In this study, we have determined the feasibility of recruiting healthy adults to a study involving multiple blood and tissue sampling, with multiple vaccine doses and 100% retention. Few studies included the immune responses in solid tissues, particularly lymphoid organs with other omics analysis which will certainly lead to a better understanding of the vaccine-induced protective antibody response (56). The choice of bio-sampling time points to perform multi-omic assay was at some degree based on previous vaccine studies; however, a more frequent sampling scheme could be considered for future studies if no budgetary constraints or burden on the participant is not limiting. Laboratory processing of the large number of sample types from such a study is achievable, and data integration tools are available to analyze and interpret the data. Indeed, a subset of the omics analysis performed on the biospecimen collected were integrated and led us to unique insights in regard to adults response to Hepatitis B vaccine (described in "Multi-omic data integration allows baseline immune signatures to predict hepatitis B vaccine response in a small cohort" manuscript). Similar future studies will be needed with different vaccines, in different age groups, and in high-income and low-to-middle-income countries to enable design of future vaccines which are suitable for all populations. As highlighted in this study, large collaborations will be required to ensure the success of these studies.

DATA AVAILABILITY STATEMENT

The raw data supporting the conclusions of this article will be made available by the authors, without undue reservation.

ETHICS STATEMENT

The studies involving human participants were reviewed and approved by University of British Columbia Clinical Research ethics Board. The patients/participants provided their written informed consent to participate in this study.

AUTHOR CONTRIBUTIONS

RB-O, MS, and TK contributed to the design of the study and writing the clinical and lab protocols SM, KM, GB, and MS contributed to the study participant recruitment, biospecimen collection, financial aspects, and clinical data management RB-O, BC, DH, ACL, and NV contributed in processing the biological samples, performed quality control. MH and BS contributed to lymph node aspirate collection from participants. RB-O, BC, ACL and all other authors (not listed above) performed all the

multi-omic analysis listed in this method paper. WK was extensively involved in the conceptualization/design of the study, and together with other co-authors in the other aspects from concept through manuscript preparation. All authors contributed to the article and approved the submitted version.

FUNDING

DD acknowledges support from the Laboratoire d'Excellence Milieu Intérieur Consortium (grant no. ANR-10-LABX-69-01). MS is supported *via* salary awards from the BC Children's Hospital Foundation, the Canadian Child Health Clinician Scientist Program, and the Michael Smith Foundation for Health Research. This work was funded by the Human Vaccines Project.

ACKNOWLEDGMENTS

We would like to thank the study participants, the research nurses, research assistants, and members of the data team at the Vaccine Evaluation Center who assisted in participants' recruitment.

REFERENCES

1. Koff WC, Burton DR, Johnson PR, Walker BD, King CR, Nabel GJ, et al. Accelerating next-generation vaccine development for global disease prevention. *Science* (2013) 340(6136):1232910. doi: 10.1126/science.1232910
2. Levine MM. "IDEAL" vaccines for resource poor settings. *Vaccine* (2011) 29 Suppl 4:D116–25. doi: 10.1016/j.vaccine.2011.11.090
3. Pauthner M, Havenar-Daughton C, Sok D, Nkolola JP, Bastidas R, Boopathy AV, et al. Elicitation of Robust Tier 2 Neutralizing Antibody Responses in Nonhuman Primates by HIV Envelope Trimer Immunization Using Optimized Approaches. *Immunity* (2017) 46(6):1073–88.e6. doi: 10.1016/j.immuni.2017.05.007
4. Havenar-Daughton C, Carnathan DG, Torrents de la Pena A, Pauthner M, Briney B, Reiss SM, et al. Direct Probing of Germinal Center Responses Reveals Immunological Features and Bottlenecks for Neutralizing Antibody Responses to HIV Env Trimer. *Cell Rep* (2016) 17(9):2195–209. doi: 10.1016/j.celrep.2016.10.085
5. Havenar-Daughton C, Lee JH, Crotty S. Tfh cells and HIV bnAbs, an immunodominance model of the HIV neutralizing antibody generation problem. *Immunol Rev* (2017) 275(1):49–61. doi: 10.1111/imr.12512
6. Duffy D, Rouilly V, Libri V, Hasan M, Beitz B, David M, et al. Functional analysis via standardized whole-blood stimulation systems defines the boundaries of a healthy immune response to complex stimuli. *Immunity* (2014) 40(3):436–50. doi: 10.1016/j.immuni.2014.03.002
7. Lee AH, Shannon CP, Amenyogbe N, Bennike TB, Diray-Arce J, Idoko OT, et al. Dynamic molecular changes during the first week of human life follow a robust developmental trajectory. *Nat Commun* (2019) 10(1):1092. doi: 10.1038/s41467-019-08794-x
8. Dobin A, Davis CA, Schlesinger F, Drenkow J, Zaleski C, Jha S, et al. STAR: ultrafast universal RNA-seq aligner. *Bioinformatics* (2013) 29(1):15–21. doi: 10.1093/bioinformatics/bts635
9. Zerbino DR, Achuthan P, Akanni W, Amode MR, Barrell D, Bhai J, et al. Ensembl 2018. *Nucleic Acids Res* (2018) 46(D1):D754–D61. doi: 10.1093/nar/gkx1098
10. Anders S, Pyl PT, Huber W. HTSeq–a Python framework to work with high-throughput sequencing data. *Bioinformatics* (2015) 31(2):166–9. doi: 10.1093/bioinformatics/btu638
11. Ewels P, Magnusson M, Lundin S, Kaller M. MultiQC: summarize analysis results for multiple tools and samples in a single report. *Bioinformatics* (2016) 32(19):3047–8. doi: 10.1093/bioinformatics/btw354
12. Love MI, Huber W, Anders S. Moderated estimation of fold change and dispersion for RNA-seq data with DESeq2. *Genome Biol* (2014) 15(12):550. doi: 10.1186/s13059-014-0550-8
13. Foroushani AB, Brinkman FS, Lynn DJ. Pathway-GPS and SIGORA: identifying relevant pathways based on the over-representation of their gene-pair signatures. *PeerJ* (2013) 1:e229. doi: 10.7717/peerj.229
14. Pidsley R, Zotenko E, Peters TJ, Lawrence MG, Risbridger GP, Molloy P, et al. Critical evaluation of the Illumina MethylationEPIC BeadChip microarray for whole-genome DNA methylation profiling. *Genome Biol* (2016) 17(1):208. doi: 10.1186/s13059-016-1066-1
15. Pidsley R, Wong CCY, Volta M, Lunnon K, Mill J, Schalkwyk LC. A data-driven approach to preprocessing Illumina 450K methylation array data. *BMC Genomics* (2013) 14:293. doi: 10.1186/1471-2164-14-293
16. Jones MJ, Islam SA, Edgar RD, Kobor MS. Adjusting for Cell Type Composition in DNA Methylation Data Using a Regression-Based Approach. *Methods Mol Biol* (2017) 1589:99–106. doi: 10.1007/7651_2015_262
17. Johnson WE, Li C, Rabinovic A. Adjusting batch effects in microarray expression data using empirical Bayes methods. *Biostatistics* (2007) 8 (1):118–27. doi: 10.1093/biostatistics/kxj037
18. Edgar RD, Jones MJ, Meaney MJ, Turecki G, Kobor MS. BECon: a tool for interpreting DNA methylation findings from blood in the context of brain. *Transl Psychiatry* (2017) 7(8):e1187. doi: 10.1038/tp.2017.171
19. Beck S, Michalski A, Raether O, Lubeck M, Kaspar S, Goedecke N, et al. a Very High-Resolution Quadrupole Time-of-Flight Instrument (QTOF) for Deep Shotgun Proteomics. *Mol Cell Proteomics* (2015) 14(7):2014–29. doi: 10.1074/mcp.M114.047407
20. Chan QW, Melathopoulos AP, Pernal SF, Foster LJ. The innate immune and systemic response in honey bees to a bacterial pathogen, Paenibacillus larvae. *BMC Genomics* (2009) 10:387. doi: 10.1186/1471-2164-10-387
21. Rappsilber J, Ishihama Y, Mann M. Stop and go extraction tips for matrix-assisted laser desorption/ionization, nanoelectrospray, and LC/MS sample pretreatment in proteomics. *Anal Chem* (2003) 75(3):663–70. doi: 10.1021/ac026117i
22. Boersema PJ, Aye TT, van Veen TA, Heck AJ, Mohammed S. Triplex protein quantification based on stable isotope labeling by peptide dimethylation applied to cell and tissue lysates. *Proteomics* (2008) 8(22):4624–32. doi: 10.1002/pmic.200800297
23. McAfee A, Chan QWT, Evans J, Foster LJ. A Varroa destructor protein atlas reveals molecular underpinnings of developmental transitions and sexual differentiation. *Mol Cell Proteomics* (2017) 16(12):2125–37. doi: 10.1074/mcp.RA117.000104
24. Perez-Riverol Y, Csordas A, Bai J, Bernal-Llinares M, Hewapathirana S, Kundu DJ, et al. The PRIDE database and related tools and resources in 2019: improving support for quantification data. *Nucleic Acids Res* (2019) 47 (D1):D442–D50. doi: 10.1093/nar/gky1106
25. Surma MA, Herzog R, Vasilj A, Klose C, Christinat N, Morin-Rivron D, et al. An automated shotgun lipidomics platform for high throughput, comprehensive, and quantitative analysis of blood plasma intact lipids. *Eur J Lipid Sci Technol* (2015) 117(10):1540–9. doi: 10.1002/ejlt.201500145
26. Leek JT, Johnson WE, Parker HS, Jaffe AE, Storey JD. The sva package for removing batch effects and other unwanted variation in high-throughput experiments. *Bioinformatics* (2012) 28(6):882–3. doi: 10.1093/bioinformatics/bts034
27. Rahim A, Meskas J, Drissler S, Yue A, Lorenc A, Laing A, et al. High throughput automated analysis of big flow cytometry data. *Methods* (2018) 134-135:164–76. doi: 10.1016/j.ymeth.2017.12.015
28. Malek M, Taghiyar MJ, Chong L, Finak G, Gottardo R, Brinkman RR. flowDensity: reproducing manual gating of flow cytometry data by automated density-based cell population identification. *Bioinformatics* (2015) 31(4):606–7. doi: 10.1093/bioinformatics/btu677
29. Ge Y, Sealfon SC. flowPeaks: a fast unsupervised clustering for flow cytometry data via K-means and density peak finding. *Bioinformatics* (2012) 28 (15):2052–8. doi: 10.1093/bioinformatics/bts300
30. Krishnaswami SR, Grindberg RV, Novotny M, Venepally P, Lacar B, Bhutani K, et al. Using single nuclei for RNA-seq to capture the transcriptome of

postmortem neurons. *Nat Protoc* (2016) 11(3):499–524. doi: 10.1038/nprot.2016.015
31. McLean JS, Lombardo MJ, Ziegler MG, Novotny M, Yee-Greenbaum J, Badger JH, et al. Genome of the pathogen Porphyromonas gingivalis recovered from a biofilm in a hospital sink using a high-throughput single-cell genomics platform. *Genome Res* (2013) 23(5):867–77. doi: 10.1101/gr.150433.112
32. Bolger AM, Lohse M, Usadel B. Trimmomatic: a flexible trimmer for Illumina sequence data. *Bioinformatics* (2014) 30(15):2114–20. doi: 10.1093/bioinformatics/btu170
33. Pertea M, Kim D, Pertea GM, Leek JT, Salzberg SL. Transcript-level expression analysis of RNA-seq experiments with HISAT, StringTie and Ballgown. *Nat Protoc* (2016) 11(9):1650–67. doi: 10.1038/nprot.2016.095
34. Aevermann B, McCorrison J, Venepally P, Hodge R, Bakken T, Miller J, et al. Production of a Preliminary Quality Control Pipeline for Single Nuclei Rna-Seq and Its Application in the Analysis of Cell Type Diversity of Post-Mortem Human Brain Neocortex. *Pac Symp Biocomput* (2017) 22:564–75. doi: 10.1142/9789813207813_0052
35. McCarthy DJ, Campbell KR, Lun AT, Wills QF. Scater: pre-processing, quality control, normalization and visualization of single-cell RNA-seq data in R. *Bioinformatics* (2017) 33(8):1179–86. doi: 10.1093/bioinformatics/btw777
36. Kiselev VY, Kirschner K, Schaub MT, Andrews T, Yiu A, Chandra T, et al. SC3: consensus clustering of single-cell RNA-seq data. *Nat Methods* (2017) 14(5):483–6. doi: 10.1038/nmeth.4236
37. Aevermann BD, Novotny M, Bakken T, Miller JA, Diehl AD, Osumi-Sutherland D, et al. Cell type discovery using single-cell transcriptomics: implications for ontological representation. *Hum Mol Genet* (2018) 27(R1):R40–R7. doi: 10.1093/hmg/ddy100
38. Bakken T, Cowell L, Aevermann BD, Novotny M, Hodge R, Miller JA, et al. Cell type discovery and representation in the era of high-content single cell phenotyping. *BMC Bioinf* (2017) 18(Suppl 17):559. doi: 10.1186/s12859-017-1977-1
39. Duffy D, Rouilly V, Braudeau C, Corbiere V, Djebali R, Ungeheuer MN, et al. Standardized whole blood stimulation improves immunomonitoring of induced immune responses in multi-center study. *Clin Immunol* (2017) 183:325–35. doi: 10.1016/j.clim.2017.09.019
40. Thomas S, Rouilly V, Patin E, Alanio C, Dubois A, Delval C, et al. The Milieu Interieur study - an integrative approach for study of human immunological variance. *Clin Immunol* (2015) 157(2):277–93. doi: 10.1016/j.clim.2014.12.004
41. Urrutia A, Duffy D, Rouilly V, Posseme C, Djebali R, Illanes G, et al. Standardized Whole-Blood Transcriptional Profiling Enables the Deconvolution of Complex Induced Immune Responses. *Cell Rep* (2016) 16(10):2777–91. doi: 10.1016/j.celrep.2016.08.011
42. Piasecka B, Duffy D, Urrutia A, Quach H, Patin E, Posseme C, et al. Distinctive roles of age, sex, and genetics in shaping transcriptional variation of human immune responses to microbial challenges. *Proc Natl Acad Sci U.S.A.* (2018) 115(3):E488–E97. doi: 10.1073/pnas.1714765115
43. Briney B, Le K, Zhu J, Burton DR. Clonify: unseeded antibody lineage assignment from next-generation sequencing data. *Sci Rep* (2016) 6:23901. doi: 10.1038/srep23901
44. Gaylord ST, Abdul-Aziz S, Walt DR. Single-molecule arrays for ultrasensitive detection of host immune response to dengue virus infection. *J Clin Microbiol* (2015) 53(5):1722–4. doi: 10.1128/JCM.03487-14
45. Gaylord ST, Dinh TL, Goldman ER, Anderson GP, Ngan KC, Walt DR. Ultrasensitive Detection of Ricin Toxin in Multiple Sample Matrixes Using Single-Domain Antibodies. *Anal Chem* (2015) 87(13):6570–7. doi: 10.1021/acs.analchem.5b00322
46. Rissin DM, Kan CW, Campbell TG, Howes SC, Fournier DR, Song L, et al. Single-molecule enzyme-linked immunosorbent assay detects serum proteins at subfemtomolar concentrations. *Nat Biotechnol* (2010) 28(6):595–9. doi: 10.1038/nbt.1641
47. Song L, Shan D, Zhao M, Pink BA, Minnehan KA, York L, et al. Direct detection of bacterial genomic DNA at sub-femtomolar concentrations using single molecule arrays. *Anal Chem* (2013) 85(3):1932–9. doi: 10.1021/ac303426b
48. Wu D, Dinh TL, Bausk BP, Walt DR. Long-Term Measurements of Human Inflammatory Cytokines Reveal Complex Baseline Variations between Individuals. *Am J Pathol* (2017) 187(12):2620–6. doi: 10.1016/j.ajpath.2017.08.007
49. Wu D, Katilius E, Olivas E, Dumont Milutinovic M, Walt DR. Incorporation of Slow Off-Rate Modified Aptamers Reagents in Single Molecule Array Assays for Cytokine Detection with Ultrahigh Sensitivity. *Anal Chem* (2016) 88(17):8385–9. doi: 10.1021/acs.analchem.6b02451
50. Zetterberg H, Wilson D, Andreasson U, Minthon L, Blennow K, Randall J, et al. Plasma tau levels in Alzheimer's disease. *Alzheimers Res Ther* (2013) 5(2):9. doi: 10.1186/alzrt163
51. Havenar-Daughton C, Newton I, Zare S, Reiss S, Schwan B, Suh M, et al. (2020). Normal human lymph node T follicular helper cells and germinal center B cells accessed via fine needle aspirations. *J Immunol Methods* 479:112746. doi: 10.1016/j.jim.2020.112746
52. Tenenhaus A, Philippe C, Frouin V. Kernel Generalized Canonical Correlation Analysis. *Comput Stat Data Anal* (2015) 90(C):114–31. doi: 10.1016/j.csda.2015.04.004
53. Havenar-Daughton C, Lindqvist M, Heit A, Wu JE, Reiss SM, Kendric K, et al. CXCL13 is a plasma biomarker of germinal center activity. *Proc Natl Acad Sci U.S.A.* (2016) 113(10):2702–7. doi: 10.1073/pnas.1520112113
54. Hong JJ, Amancha PK, Rogers KA, Courtney CL, Havenar-Daughton C, Crotty S, et al. Early lymphoid responses and germinal center formation correlate with lower viral load set points and better prognosis of simian immunodeficiency virus infection. *J Immunol* (2014) 193(2):797–806. doi: 10.4049/jimmunol.1400749
55. Petrovas C, Yamamoto T, Gerner MY, Boswell KL, Wloka K, Smith EC, et al. CD4 T follicular helper cell dynamics during SIV infection. *J Clin Invest* (2012) 122(9):3281–94. doi: 10.1172/JCI63039
56. Turner JS, Zhou JQ, Han J, Schmitz AJ, Rizk AA, Alsoussi WB, et al. Human germinal centres engage memory and naive B cells after influenza vaccination. *Nature* (2020) 586(7827):127–32. doi: 10.1038/s41586-020-2711-0

Conflict of Interest: MS has been an investigator on projects funded by GlaxoSmithKline, Symvivo, Sanofi Pasteur, Seqirus, Pfizer, Merck and VBI Vaccines. All funds have been paid to his institution and he has received no personal payments. DW is a board member and equity holder of Quanterix Corporation.

The remaining authors declare that the research was conducted in the absence of any commercial or financial relationships that could be construed as a potential conflict of interest.

frontiers in Immunology

REVIEW
published: 25 November 2020
doi: 10.3389/fimmu.2020.582201

The Role of Systems Vaccinology in Understanding the Immune Defects to Vaccination in Solid Organ Transplant Recipients

Nicholas Scanlon[1,2]*, *Youssef Saklawi*[2] *and Nadine Rouphael*[1,2]

[1] Department of Medicine, School of Medicine, Emory University, Atlanta, GA, United States, [2] The Hope Clinic of the Emory Vaccine Center, Division of Infectious Diseases, Emory University, Decatur, GA, United States

Solid organ transplant recipients (SOTRs) are at increased risk for many infections, whether viral, bacterial, or fungal, due to immunosuppressive therapy to prevent organ rejection. The same immune defects that render transplanted patients susceptible to infection dampen their immune response to vaccination. Therefore, it is vital to identify immune defects to vaccination in transplant recipients and methods to obviate them. These methods can include alternative vaccine composition, dosage, adjuvants, route of administration, timing, and re-vaccination strategies. Systems biology is a relatively new field of study, which utilizes high throughput means to better understand biological systems and predict outcomes. Systems biology approaches have been used to help obtain a global picture of immune responses to infections and vaccination (i.e. systems vaccinology), but little work has been done to use systems biology to improve vaccine efficacy in immunocompromised patients, particularly SOTRs, thus far. Systems vaccinology approaches may hold key insights to vaccination in this vulnerable population.

Keywords: vaccine, transplant, systems biology, systems immunology, systems vaccinology, immunocompromised, immunization

OPEN ACCESS

Edited by:
Simon Daniel Van Haren, Boston Children's Hospital and Harvard Medical School, United States

Reviewed by:
Selidji Todagbe Agnandji, Centre de Recherche Médicales de Lambaréné, Gabon
Casey Patrick Shannon, Prevention of Organ Failure (PROOF), Canada

***Correspondence:**
Nicholas Scanlon
nicholas.scanlon@emory.edu

Specialty section:
This article was submitted to Vaccines and Molecular Therapeutics, a section of the journal Frontiers in Immunology

Received: *10 July 2020*
Accepted: *19 October 2020*
Published: *25 November 2020*

Citation:
Scanlon N, Saklawi Y and Rouphael N (2020) The Role of Systems Vaccinology in Understanding the Immune Defects to Vaccination in Solid Organ Transplant Recipients. Front. Immunol. 11:582201. doi: 10.3389/fimmu.2020.582201

INTRODUCTION

Systems biology was described by Alan Aderem as a "comprehensive quantitative analysis of the manner in which all components of the biological system interact functionally over time and space that is executed by an interdisciplinary team of investigators" (1). Systems biology uses high throughput "-omics" technologies to investigate the structure and dynamics of the entire system to predict outcomes (2). In a systems biology approach, the system is perturbed as a result of an infection or immunization; genes, proteins, lipids, sugars, and molecular pathways are monitored; data are collected, analyzed, and integrated; and mathematical models are formulated to describe or predict how the system may respond to specific perturbations (3). Systems immunology takes advantage of the many ways the immune system can be manipulated to better understand signaling pathways in the immune system and how the innate and adaptive immune systems interact to protect against various pathogens (4). When applied to vaccines, systems biology can give us a better understanding of the immune system in general and the optimal immunological response needed for protection. Systems vaccinology utilizes immunization as a way to probe the immune system in a

synchronized fashion and effects on the immune system are studied at various timepoints after. This approach can identify early signatures associated with protection, separate vaccinees into responders and non-responders, and can reveal important mechanistic insights through translational human vaccine trials to aid in the expedited design of future vaccines to disease where no effective vaccine exists (e.g. HIV) or to protect vulnerable populations (e.g. elderly, HIV infected and SOTRs) (5). While a number of studies have implemented a systems vaccinology approach to better understand the immune response to various immunizations, very little is published regarding systems vaccinology in immunocompromised patients, particularly solid organ transplant recipients (SOTRs). It is well known that individuals are at risk for infection following solid organ transplant, but little is known about the immune defects to vaccination in these patients. Systems vaccinology has allowed us to have a better understanding of how successful vaccines induce adequate immune responses in healthy subjects and how immune defects are uncovered in other vulnerable populations (e.g., the elderly). This blueprint may offer a personalized approach to vaccination in SOTR.

SYSTEMS VACCINOLOGY IN IMMUNOCOMPETENT HOSTS

Early studies in systems vaccinology have used a systems biology approach to obtain a global picture of the molecular networks driving vaccine immunity in immunocompetent hosts as opposed to immunocompromised hosts. The yellow fever vaccine 17D, trivalent inactivated (TIV) and live attenuated (LAIV) influenza vaccines, and meningococcal quadrivalent polysaccharide (MPSV4) and meningococcal quadrivalent conjugate vaccines (MCV4) were among the first to be studied in-depth using this approach. The hepatitis B virus (HBV) vaccine has also been studied utilizing a systems biology approach.

Yellow Fever Vaccine 17D

The first studies to utilize a systems biology approach analyzed the immune responses to the yellow fever vaccine 17D (YF-17D), a live attenuated vaccine highly effective with close to 90% rate of protection (6, 7). The study noted a difference in the magnitude of neutralizing antibody titers and antigen-specific cytotoxic T lymphocyte (CTL) responses at days 15 and 60 between different individuals. Two genes were predictive up to 90% of a high magnitude adaptive immune response: *EIF2AK4* (a critical player in the integrated stress response, resulting in a shutdown of translation of most proteins in the cell) and *TNFRSF17* (which encodes the receptor for B-cell growth factor BLyS-BAFF and plays a role in the differentiation of plasma cells) (7). The authors were able to predict the immunogenicity of YF-17D with innate immune signatures. Thereby, the study laid the groundwork for using a systems biology approach to predict the magnitude of the adaptive immune response to vaccine early on.

Trivalent Inactivated (TIV) and Live Attenuated (LAIV) Influenza Vaccine

Nakaya et al. in 2011 extended a systems biology approach to investigate the innate and adaptive immune responses to the TIV and live attenuated influenza vaccines in humans. Their objective was to determine whether similar signatures, which were predictive of the adaptive immune response in YF-17D were present with TIV and LAIV. They found that LAIV induced a robust type I IFN antiviral transcriptomic signatures. TIV also induced the expression of genes encoding type I IFNs as well as pro-inflammatory mediators and genes involved in the innate sensing of viruses 1–3 days after vaccination and then genes such as *TNRSF17* and others known to be involved in the differentiation of plasmablasts; these correlated well with the magnitude of hemagglutinin titers 28 days after immunization. Another gene, calmodulin-dependent protein kinase IV (*CaMKIV)* was shown to have an expression profile inversely proportional to later antibody titers. LAIV did not induce as robust of an antibody response as TIV. Ultimately, the clinical effectiveness of these two vaccines is known to be similar despite the difference in antibody response. The authors suggested the similar clinical effectiveness may be related to the hypothesized mechanism by which LAIV primes immune cells in the nasal mucosa, which then circulate in the blood to activate other immune cells (8). Delivery method may play an important role in vaccine efficacy. The Human Immunology Project Consortium (HIPC) and the Center for Human Immunology were able to identify transcriptional signatures predictive of response to influenza vaccination. They showed the presence of inflammatory gene signatures was associated with more robust antibody responses in younger individuals, but worse antibody responses in older individuals (9). Ultimately, these studies confirmed that predicting vaccine responses through a systems biology approach was possible in the context of influenza and that baseline immunological status is a potential mechanism by which to understand poor vaccination outcomes in older individuals.

Meningococcal Quadrivalent Polysaccharide Vaccine (MPSV4) and Meningococcal Quadrivalent Conjugate Vaccine (MCV4)

Another study by Li et al. in 2014, utilized a systems vaccinology approach to investigate the immune response to meningococcal polysaccharide (MPSV4) and meningococcal conjugate vaccine (MCV4) as it compares with that of YF-17D, TIV, and LAIV. Both MPSV4 and MCV4 are capable of inducing high antibody titers post-vaccination, but MPSV4 is thought to induce T-cell independent antibody responses, resulting in waning humoral immunity and memory. The authors analyzed data by merging 32,000 peripheral blood mononuclear cell (PBMC) gene expression profiles from 540 published studies and were able to identify 334 different blood transcriptome modules (BTMs) from existing transcriptomic data in public repositories. The study revealed three distinctive transcriptomic programs, which could potentially be used to predict vaccine efficacy. One

transcriptomic program was a protein recall response that correlated with the antibody response to TIV and a portion of MCV4. Another transcriptomic program was a primary viral response elicited by YF-17D. The final transcriptomic program was an anti-polysaccharide signature induced by the polysaccharide portions of MCV4 and MPSV4 (10).

Hepatitis B Virus (HBV) Vaccine

In 2016, Fourati et al. identified transcriptomic patterns associated with aging and correlated these transcriptomic modules with biological pathways after HBV vaccination. An aggregate score depicting age-related transcriptomic changes (BioAge signature), a surrogate for B-cell activation, was shown to predict the response to the HBV vaccine with a 60% accuracy. Higher levels of baseline memory B cells and CD4+ T cells were associated with a sufficient immune response to vaccination. Additionally, 15 gene expression patterns related to inflammation and interferon signaling pathways are significantly different between vaccine responders and non-responders (11). Such immunologic patterns may be used in addition to age and patient demographics to account for baseline heterogeneity when conducting vaccine clinical trials; leading to more personalized vaccine research. A systems biology approach has also been undertaken to evaluate new adjuvants for the HBV vaccine (12).

SYSTEMS VACCINOLOGY IN VULNERABLE POPULATIONS

Systems biology approaches have emerged to assess vaccination in vulnerable populations such as in people living with HIV (13) while vaccination in other vulnerable populations such as neonates has yet be studied using a systems biology approach; these populations may benefit as well. Another vulnerable population in regard to infection and suboptimal response to vaccination is the elderly which constitute 16% of the US population. More than 90% of seasonal influenza-related deaths occur among people over 60 years of age (14). Stressing the importance of better understanding immunosenescence to design more effective vaccines for a subpopulation most affected by influenza mortality (15). Nakaya et al. applied a systems biology approach comparing the immune responses to influenza vaccine in young adults and elderly across many seasons (16). The fold changes in hemagglutination inhibition titers (HAI) were statistically higher in the younger versus the older group revealing a correlation of decreased antibody responses to influenza vaccine with age. When compared to the younger group, the older group exhibited a diminished B cell and an increased frequency and activation of NK cell responses after vaccination as well as an enhanced monocyte response pre and post vaccination. There was also a difference in expressed genes between the two groups mostly noted one day after vaccination with a greater number of both up- and downregulated genes observed in the younger group. While both groups had similar temporal expression profiles by clusters, the magnitude of the expression of interferon-related genes was also higher in the younger group. Studies have shown methylation and the transcriptome may play a role in and predict humoral immunity. One analysis looked at how methylation affects the expression of genes known to play a role in humoral immunity (17). Gene signatures associated with influenza-specific memory B-cell responses were identified by transcriptome-wide profiling of peripheral blood mononuclear cells (PBMCs) (18). The suboptimal vaccine immune responses in the elderly could be improved by the use of FDA approved seasonal influenza vaccine products such as adjuvant (MF59 oil in water adjuvant) (19) or high-dose vaccines (20) (with 60 mcg of hemagglutinin per strain, the equivalent of four times the current amount of HA in seasonal influenza vaccines). Immunosenescence has been a key focus of systems vaccinology and can likely provide insight into the immune defects to vaccination SOTRs possess.

IMMUNOSUPPRESSION AND INFECTION IN SOTRs

Historically, acute rejection was common after transplant, but over the years, T cell-mediated allo-immune responses have been targeted for most immunosuppression drug development in transplantation (21). In SOTRs, the survival of the patient and graft rely on lifelong modulation of the immune system. Immunosuppressive agents are given perioperatively to prevent allograft rejection. This induction therapy serves to deplete T cells, thereby reducing acute rejection rates and enhancing allograft survival. Maintenance immunosuppression consists of multiple medications, which target various aspects of the immune response. Most transplant centers use a triple-drug regiment including the second-generation calcineurin inhibitor (CNI) tacrolimus, the antiproliferative agent mycophenolic acid, and a corticosteroid; rapamycin-based therapies are sometimes used instead of calcineurin-based therapies to preserve long-term renal function (22). Calcineurin inhibitors such as cyclosporine and tacrolimus work by reducing interleukin-2 (IL-2) production and IL-2 receptor expression, which leads to decreased T-cell activation (23). Inhibitors of mammalian target of rapamycin (mTOR) such as sirolimus and everolimus work later in the cell cycle to prevent IL-2-mediated T-cell proliferation and can act synergistically with cyclosporine and tacrolimus (22). Mycophenolic acids such as mycophenolate mofetil (MMF) act by interfering with purine synthesis to selectively inhibit T and B-lymphocyte proliferation (22). Finally, corticosteroids act through multiple mechanisms, including inhibition of interleukins in macrophages and monocytes, inhibition of the expression of cytokines, and inducing programmed cell death of T cells (22). The effects of corticosteroids on the human immunome have also been described. One study showed that systemic glucocorticoids down-regulate inflammatory cytokine levels in humans and that there was an inhibitory effect on transcription modules associated with inflammation at early time points (24). Their study suggested that anti-inflammatory effects of glucocorticoids are a result of modulation of mRNA levels (24).

The immunome of recipients often determines the degree of response to vaccination. Models based on a small subset of

immune cells may be sufficient to predict immune reactivity, whether to vaccines or auto-immune disease flares (25, 26). As aforementioned, immunosuppressive agents strongly alter the immune landscape, and would predictably alter the response to vaccination. Multiple studies have shown that vaccines are less immunogenic in SOTRs (27), and some studies have demonstrated a direct effect of particular immunosuppressive agents used in this population. In fact, it has been shown that MMF has a dose-dependent response where higher doses, particularly greater than or equal to 2 grams daily were associated with lower seroconversion rates to influenza vaccination (28). Additionally, m-TOR inhibitors were shown to decrease antibody response to the pandemic H1N1-2009 vaccination (29). Another study showed that less seroprotection for influenza after vaccination was achieved in renal transplant patients who had received tacrolimus-based regimens compared with healthy controls (30). Corticosteroids and other immunosuppressive agents used in this population were associated with significantly impaired response to the 23-valent pneumococcal polysaccharide vaccination (23vPPV) (31). Liver transplant patients have been shown to infrequently benefit from hepatitis B vaccination as one study showed only 20% of patients developed measurable anti-HBs in response to vaccination whereas seroconversion rates in healthy adults are greater than 90% (32).

SYSTEMS VACCINOLOGY IN SOTRs

Most studies related to vaccinology in SOTR have looked mostly at serologic markers to assess vaccine immunogenicity. Seroprotection and seroconversion in SOTRs in response to influenza vaccination has varied between 15–93% (33). SOTRs may have high titers of cross-reactive antibodies due to frequent yearly influenza vaccination, which may explain in part the low seroconversion rate among this population (34). Similarly, vaccine-induced serologic immunity to the measles vaccine in SOTR pediatric population was shown to wane over time, along with impaired measles-specific B-cell distribution and immune senescence (35). Few studies have tried to assess the association between the antibody responses and the cellular, and cytokine responses. A study in lung transplant recipients showed an impaired cell-mediated immune response to influenza vaccination by assessing granzyme B and interleukin production (36). Different studies have alluded to an association between humoral and cellular responses (36–38). Some are summarized in **Table 1**. There is a paucity of data surrounding vaccine-induced immunity in SOTRs relevant to the innate immunity and systems biology in general, so it is vital that more studies investigate this area.

Immunosuppressive agents dramatically reduce the risk of rejection in transplanted patients while at the same time increasing the patient's risk for opportunistic infections. Thus, general strategies such as vaccination, universal prophylaxis, and preemptive therapies are used to mitigate the risk of infection. Current guidelines recommend the need for immunization be evaluated, and if possible completed, before transplantation as vaccinations may not be as immunogenic after transplantation (40, 41). Immunosuppressive regimens vary between organ transplants, and some organs like the heart require more aggressive and long-term immunosuppression. Cases of clinical operational tolerance have been described in kidney and liver transplants, but rarely in pancreatic, intestinal, heart, or lung transplants (42). This suggests a varied immune landscape

TABLE 1 | Summation of studies utilizing a systems biology approach in SOTRs.

First Author	Year	Title	Vaccine	Transplant	Data Assessed	Findings
Soesman (39)	2000	Efficacy of influenza vaccination in adult liver transplant recipients.	Influenza	Liver	Humoral and Cellular Immunity	Postvaccination virus-specific T cell proliferation lower than controls (not statistically significant).
Mazzone (36)	2004	Cell-mediated immune response to influenza vaccination in lung transplant recipients	Influenza	Lung	Humoral and Cellular Immunity	Virus-specific responses (Granzyme B & cytokine production) impaired, while antibody response maintained.
Ballet (38)	2006	Humoral and cellular responses to influenza vaccination in human recipients naturally tolerant to a kidney allograft	Influenza	Kidney	Humoral and Cellular Immunity	Comparable humoral and cellular responses to vaccination in SOTRs after cessation of immunosuppressive therapy.
Candon (37)	2009	Humoral and cellular immune responses after influenza vaccination in kidney transplant recipients	Influenza	Kidney	Humoral and Cellular Immunity	Increase in interferon producing T cells post-vaccination in SOTRs and healthy controls, no association with humoral response.
Cagigi (13)	2013	Premature ageing of the immune system relates to increased anti-lymphocyte antibodies (ALA) after an immunization in HIV-1-infected and kidney-transplanted patients	Influenza	Kidney	B-cell biomarkers	Diminished levels of interleukin-21 and interleukin-21 receptor expression in SOTRs postvaccination, along with higher levels of mature activation of B cells and double negative B cells compared to healthy controls.
Rinaldi (34)	2014	B-sides serologic markers of immunogenicity in kidney transplanted patients: report from 2012-2013 flu vaccination experience	Influenza	Kidney	B-cell biomarkers	Influenza specific memory B-cell postvaccination in SOTR similar to healthy controls independent of seroconversion.
Rocca (35)	2016	Waning of vaccine-induced immunity to measles in kidney transplanted children	Measles	Kidney	B-cell biomarkers	Waning of antibody and B-cell responses to measles in pediatric patients Seroprotection depends on immune status at vaccination.

among SOTRs, which requires further characterization through systems biology studies. A better immunologic understanding behind a tailored preventative approach through immunization is needed for SOTRs.

FUTURE DIRECTIONS FOR SYSTEMS VACCINOLOGY

While studies have utilized systems vaccinology to help better understand and predict how well a vaccine will work in the elderly and improve that response, it is vital that we use systems vaccinology to improve vaccines for immunosuppressed populations such as SOTRs.

Vaccine Design in Solid Organ Transplant

Various vaccination strategies have been discussed in the literature to combat the decreased immunogenicity of vaccines in SOTRs particularly to influenza vaccines (43, 44).

Adjuvants

Adjuvants enhance the immune response to vaccine antigen by nonspecifically stimulating cells of the innate immune system; however, they represent a diverse range of materials from small synthetic molecules to heterogeneous extracts of natural products. Aluminum salts (Alum) have historically been the most common adjuvant included in vaccines. Over the past few decades, vaccines have been formulated with novel adjuvants; these include vaccines against HBV, HPV, influenza, and VZV (45). Some have been studied in the elderly (46) and transplant populations (47) to determine efficacy and safety. Adjuvants work by delivering a localized activation signal to the innate immune system, thereby promoting antigen-specific adaptive immunity. Comparative studies of different adjuvants are sparse, and the mechanism of action is poorly understood (48). Future studies elucidating such knowledge can improve vaccine design and implementation. A systems biology approach can be utilized to select the ideal antigen/adjuvant combination through an evidence-based approach allowing for the more expedited development of effective adjuvanted vaccines in SOTRs. Additionally, a systems approach may represent a better technique for risk surveillance and mitigation through better prediction of immune reactivity and potential transplant rejection (49).

However, adjuvants could represent a safety concern in transplant patients. One study, which compared an adjuvanted influenza vaccine containing an oil-in-water emulsion adjuvant (MF59) to a nonadjuvanted formulation showed comparable immunogenicity and seroprotection; a subgroup analysis of the 18–64-year-old group showed greater seroconversion rates in the adjuvanted vaccine group. There was no increase in Human Leukocyte Antigen (HLA) alloantibodies in those receiving the adjuvanted vaccine, suggesting it was safe in these patients (50).

Timing of Vaccination

If vaccinations are not given before transplant, current guidelines recommend transplant patients receive vaccinations approximately 3–6 months after transplantation when baseline immunosuppression levels are obtained; however, there is little data regarding the ideal timing of vaccination post-transplant (41). One study of influenza vaccination showed that those less than 6 months after transplant and on daily MMF and prednisone were at risk for poor vaccine response largely due to the intensity of immunosuppression in the first 6 months (28). A study showed in liver transplant patients that only 14% responded to influenza vaccine 4 months post-transplant, 67% seroconverted at 4–12 months, and 86% after 12 months (51). This supports the current recommendation for influenza vaccination administration 3–6 months post-transplant when patients are on less intense immunosuppressive regimens (41). In contrast to these studies, a multicenter prospective cohort study in adult SOTRs looked at influenza vaccination over four influenza seasons from 2009–2013 (52). After adjusting for confounders, they found that seroprotection was similar in those vaccinated within 6 months of transplantation and those vaccinated more than 6 months after transplantation (52). Our group is currently investigating the optimal timing of the AS01-adjuvanted varicella zoster virus subunit (HZ/su) vaccine in kidney transplant recipients. (NCT 03993717) Systems biology may also be aimed to detect time points of optimal immune activation, potentially leading to personalized vaccine administration schedules per real-time immune status of patients (26).

Vaccine Dosing

Another vaccine strategy that could increase immunogenicity in SOTRs is increasing vaccine dosing. A recent RCT conducted by the TRANSGRIPE 1–2 Study Group used a booster dose of inactivated influenza vaccine 5 weeks from the original dose in SOTRs after one month of transplant. It showed that this was associated with higher short-term seroconversion rates in per-protocol analysis, but not in the intention to treat group; seroprotection as 10 weeks was also higher in the booster group with the number needed to treat being less than 10 (53). Another study looked at two doses of the influenza A/H1N1 (2009) pandemic vaccine in kidney transplant patients and showed this provided significantly improved seroprotection (54). A systematic literature review and meta-analysis, which pooled data from multiple influenza vaccination studies showed no enhanced immunogenicity of a booster dose of influenza vaccine in renal transplant patients (55). More recently, a double-blind, randomized trial showed that high-dose influenza vaccine (including 3 vaccine strains) had significantly improved immunogenicity and similar safety in SOTRs (56).

Delivery Method

Vaccines can be delivered intramuscularly, intradermally, subcutaneously, orally, and intranasally; the latter two routes are not used in SOTRs as they are live-attenuated vaccines. Most commonly, vaccines have been administered intramuscularly and subcutaneously; however, intradermal vaccines are thought to improve immunogenicity by increasing exposure of the antigen to antigen presenting cells such as dendritic cells. A 2011 cohort study of 85 lung transplant recipients receiving the seasonal 2008–9 inactivated influenza vaccination showed a poor

response in both the 6 μg intradermal group and the 15 μg intramuscular group (57). Later, a study looked at higher doses, 18 μg intradermal and 15 μg intramuscular and showed improved, but similar immunogenicity in lung transplant patients (28). Another novel delivery route is microneedle patch technology that can be self-administered, thermostable and leaves no sharp waste (58). This technology has been studied as a mechanism to administer the influenza vaccine (59). Since microneedle patch targets the superficial layers of the skin rich in dendritic cells it may offer antigen sparing and better antigen delivery ultimately leading to an enhanced immune response particularly in vulnerable and immunocompromised populations (60).

DISCUSSION

SOTRs represent a vulnerable population when it comes to infection, and vaccination remains one of the most effective means to prevent infection in this population. While current guidelines recommend vaccination prior to transplant, there is significant variability in implementation of this recommendation in SOTRs. Furthermore, vaccination in SOTRs, is known to produce suboptimal immune responses compared with immunocompetent individuals. Most transplant centers initiate vaccination 3–6 months post-transplant, at the time immunosuppression levels are obtained, for those who have not completed all vaccinations prior to transplant. Influenza vaccinations can be given as early as 1 month after transplant. It is recommended that serologic response be obtained a minimum of 4 weeks after vaccination to document seroconversion based on protective titers in established literature. However, serology is not necessarily an accurate measure of immunity, particularly post-transplant (41). Furthermore, decreased vaccine-specific immune responses and waning titers after transplant are well-documented (61). Consequently, vaccination should not follow a "one-size fits all" model, particularly in immunosuppressed and SOTRs. It is important that we focus on the rational design and implementation of efficacious vaccinations as well as evaluation of their immunogenicity in this vulnerable population. There are many research questions that we must ask when considering optimal vaccination strategies in SOTRs. What is the optimal timing of vaccination in SOTRs in relation to immunosuppression? Are adjuvants necessary to boost the immune response in SOTRs, and is the use of adjuvants safe in this population? Do SOTRs need a higher dose, or repeated vaccination in contrast to immunocompetent individuals? And what is the ideal delivery method for vaccinations in this population? Innovative systems biology approaches can be utilized to model critical determinants to predict vaccine success, better characterization of SOTR immune profile, better assessment of patient heterogeneity in research, vaccine response, and prediction of side effects. These systems biology approaches can help us to answer each of the aforementioned questions and determine the optimal timing, potential need for adjuvants, dosing strategy, and delivery method in this unique population. We highly recommend adapting systems biology approaches to optimize vaccination strategies in SOTRs.

AUTHOR CONTRIBUTIONS

All authors contributed to the article and approved the submitted version.

FUNDING

This work was supposed by the NIH R38 Stimulating Access to Research in Residency (StARR) grant (5R38AI140299-02).

ACKNOWLEDGMENTS

The authors would like to acknowledge The Hope Clinic of Emory University.

REFERENCES

1. Aderem A. Systems Biology: Its Practice and Challenges. *Cell* (2005) 121:511–13. doi: 10.1016/j.cell.2005.04.020
2. Pulendran B, Li S, Nakaya HI. Systems Vaccinology. *Immunity* (2010) 33:516–29. doi: 10.1016/j.immuni.2010.10.006
3. Ideker T, Galitski T, Hood L. A new approach to decoding life: Systems Biology. *Annu Rev Genomics Hum Genet* (2001) 2:343–72. doi: 10.1146/annurev.genom.2.1.343
4. Davis MM, Tato CM, Furman D. Systems Immunology: Just Getting Started. *Nat Immunol* (2017) 18:725–32. doi: 10.1038/ni.3768
5. Pulendran B. Systems Vaccinology: Probing Humanity's Diverse Immune Systems with Vaccines. *Proc Natl Acad Sci U S A* (2014) 111:12300–306. doi: 10.1073/pnas.1400476111
6. Gaucher D, Therrien R, Kettaf N, Angermann BR, Boucher G, Filali-Mouhim A, et al. Yellow Fever Vaccine Induces Integrated Multilineage and Polyfunctional Immune Responses. *J Exp Med* (2008) 205:3119–31. doi: 10.1084/jem.20082292
7. Querec TD, Akondy RS, Lee EK, Cao W, Nakaya HI, Teuwen D, et al. Systems Biology Approach Predicts Immunogenicity of the Yellow Fever Vaccine in Humans. *Nat Immunol* (2009) 10:116–25. doi: 10.1038/ni.1688
8. Nakaya HI, Wrammert J, Lee EK, Racioppi L, Marie-Kunze S, Haining WN, et al. Systems Biology of Seasonal Influenza Vaccination in Humans. *Nat Immunol* (2011) 12:786–95. doi: 10.1038/ni.2067
9. Team, HIPC-CHI Signatures Project and Hipc-I. Consortium. Multicohort Analysis Reveals Baseline Transcriptional Predictors of Influenza Vaccination Responses. *Sci Immunol* (2017) 2:1–13. doi: 10.1126/sciimmunol.aal4656
10. Li S, Rouphael N, Duraisingham S, Romero-Steiner S, Presnell S, Davis C, et al. Molecular Signatures of Antibody Responses Derived from a Systems Biology Study of Five Human Vaccines. *Nat Immunol* (2014) 15:195–204. doi: 10.1038/ni.2789
11. Fourati S, Cristescu R, Loboda A, Talla A, Filali A, Railkar R, et al. Pre-Vaccination Inflammation and B-Cell Signalling Predict Age-Related Hyporesponse to Hepatitis B Vaccination. *Nat Commun* (2016) 7:10369. doi: 10.1038/ncomms10369
12. Wang J, Liu R, Liu B, Yang Y, Xie J, Zhu N. Systems Pharmacology-Based Strategy to Screen New Adjuvant for Hepatitis B Vaccine from Traditional

Chinese Medicine Ophiocordyceps Sinensis. *Sci Rep* (2017) 7:44788. doi: 10.1038/srep44788
13. Cagigi A, Rinaldi S, Santilli V, Mora N, Manno EC, Cotugno N, et al. Premature Ageing of the Immune System Relates to Increased Anti-Lymphocyte Antibodies (ALA) after an Immunization in HIV-1-Infected and Kidney-Transplanted Patients. *Clin Exp Immunol* (2013) 174:274–80. doi: 10.1111/cei.12173
14. Sprenger MJ, Mulder PG, Beyer WE, Van Strik R, Masurel N. Impact of Influenza on Mortality in Relation to Age and Underlying Disease, 1967–1989. *Int J Epidemiol* (1993) 22:334–40. doi: 10.1093/ije/22.2.334
15. Duraisingham SS, Rouphael N, Cavanagh MM, Nakaya HI, Goronzy JJ, Pulendran B. Systems Biology of Vaccination in the Elderly. *Curr Topics Microbiol Immunol* (2013) 363:117–42. doi: 10.1007/82_2012_250
16. Nakaya HI, Hagan T, Duraisingham SS, Lee EK, Kwissa M, Rouphael N, et al. Systems Analysis of Immunity to Influenza Vaccination across Multiple Years and in Diverse Populations Reveals Shared Molecular Signatures. *Immunity* (2015) 43:1186–98. doi: 10.1016/j.immuni.2015.11.012
17. Zimmermann MT, Oberg AL, Grill DE, Ovsyannikova IG, Haralambieva IH, Kennedy RB, et al. System-Wide Associations between DNA-Methylation, Gene Expression, and Humoral Immune Response to Influenza Vaccination. *PloS One* (2016) 11:1–21. doi: 10.1371/journal.pone.0152034
18. Haralambieva IH, Ovsyannikova IG, Kennedy RB, Zimmermann MT, Grill DE, Oberg AL, et al. Transcriptional Signatures of Influenza A/H1N1-Specific IgG Memory-like B Cell Response in Older Individuals. *Vaccine* (2016) 34:3993–4002. doi: 10.1016/j.vaccine.2016.06.034
19. De Donato S, Granoff D, Minutello M, Lecchi G, Faccini M, Agnello M, et al. Safety and Immunogenicity of MF59-Adjuvanted Influenza Vaccine in the Elderly. *Vaccine* (1999) 17:3094–101. doi: 10.1016/S0264-410X(99)00138-3
20. DiazGranados CA, Dunning AJ, Kimmel M, Kirby D, Treanor J, Collins A, et al. Efficacy of High-Dose versus Standard-Dose Influenza Vaccine in Older Adults. *N Engl J Med* (2014) 371:635–45. doi: 10.1056/NEJMoa1315727. Massachusetts Medical Society.
21. Lim MA, Kohli J, Bloom RD. Immunosuppression for Kidney Transplantation: Where Are We Now and Where Are We Going? *Transplant Rev* (2017) 31:10–7. doi: 10.1016/j.trre.2016.10.006
22. Holt CD. Overview of Immunosuppressive Therapy in Solid Organ Transplantation. *Anesthesiol Clinics* (2017) 35:365–80. doi: 10.1016/j.anclin.2017.04.001
23. Holzner ML, Wadhera V, Basu A, Sander F, Shapiro R. 17 - Calcineurin Inhibitors. In: SJ Knechtle, LP Marson, PJ Morris, editors. *Kidney Transplantation - Principles and Practice, Eighth Edition*. Elsevier (2019). p. 242–60. Content Repository Only. doi: 10.1016/B978-0-323-53186-3.00017-6
24. Olnes MJ, Kotliarov Y, Biancotto A, Cheung F, Chen J, Shi R, et al. Effects of Systemically Administered Hydrocortisone on the Human Immunome. *Sci Rep* (2016) 6:23002. doi: 10.1038/srep23002
25. Tsang JS, Schwartzberg PL, Kotliarov Y, Biancotto A, Xie Z, Germain RN, et al. Global Analyses of Human Immune Variation Reveal Baseline Predictors of Postvaccination Responses. *Cell* (2014) 157:499–513. doi: 10.1016/j.cell.2014.03.031
26. Kotliarov Y, Sparks R, Martins AJ, Mulè MP, Lu Y, Goswami M, et al. Broad Immune Activation Underlies Shared Set Point Signatures for Vaccine Responsiveness in Healthy Individuals and Disease Activity in Patients with Lupus. *Nat Med* (2020) 26:618–29. doi: 10.1038/s41591-020-0769-8
27. O'Shea D, Widmer LA, Stelling J, Egli A. Changing Face of Vaccination in Immunocompromised Hosts. *Curr Infect Dis Rep* (2014) 16:420. doi: 10.1007/s11908-014-0420-2
28. Baluch A, Humar A, Eurich D, Egli A, Liacini A, Hoschler K, et al. Randomized Controlled Trial of High-Dose Intradermal Versus Standard-Dose Intramuscular Influenza Vaccine in Organ Transplant Recipients. *Am J Transplant* (2013) 13:1026–33. doi: 10.1111/ajt.12149
29. Cordero E, Perez-Ordoñez A, Aydillo TA, Torre-Cisneros J, Gavalda J, Lara R, et al. Therapy With M-TOR Inhibitors Decreases the Response to the Pandemic Influenza A H1N1 Vaccine in Solid Organ Transplant Recipients. *Am J Transplant* (2011) 11:2205–13. doi: 10.1111/j.1600-6143.2011.03692.x
30. Birdwell KA, Ikizler MR, Sannella EC, Wang L, Byrne DW, Ikizler TA, et al. Decreased Antibody Response to Influenza Vaccination in Kidney Transplant Recipients: A Prospective Cohort Study. *Am J Kidney Dis* (2009) 54:112–21. doi: 10.1053/j.ajkd.2008.09.023
31. Van Kessel DA, Hoffman TW, van Velzen-Blad H, van de Graaf EA, Grutters JC, Rijkers GT. Immune Status Assessment in Adult Lung Transplant Candidates. *Transplant Immunol* (2017) 40:31–4. doi: 10.1016/j.trim.2016.11.001
32. Carey W, Pimentel R, Westveer MK, Vogt D, Broughan T. Failure of Hepatitis B Immunization in Liver Transplant Recipients: Results of a Prospective Trial. *Am J Gastroenterol* (1990) 85:1590–92.
33. Kumar D, Blumberg EA, Danziger-Isakov L, Kotton CN, Halasa NB, Ison MG, et al. Influenza Vaccination in the Organ Transplant Recipient: Review and Summary Recommendations†. *Am J Transplant* (2011) 11:2020–30. doi: 10.1111/j.1600-6143.2011.03753.x
34. Rinaldi S, Cagigi A, Santilli V, Zotta F, di Martino A, Castrucci MR, et al. B-Sides Serologic Markers of Immunogenicity in Kidney Transplanted Patients: Report from 2012-2013 Flu Vaccination Experience. *Transplantation* (2014) 98:259–66. doi: 10.1097/TP.0000000000000209
35. Rocca S, Santilli V, Cotugno N, Concato C, Manno EC, Nocentini G, et al. Waning of Vaccine-Induced Immunity to Measles in Kidney Transplanted Children. *Medicine* (2016) 95:1–7. doi: 10.1097/MD.0000000000004738
36. Mazzone PJ, Mossad SB, Mawhorter SD, Mehta AC, Mauer JR. Cell-Mediated Immune Response to Influenza Vaccination in Lung Transplant Recipients. *J Heart Lung Transplant* (2004) 23:1175–81. doi: 10.1016/j.healun.2003.08.033
37. Candon S, Thervet E, Lebon P, Suberbielle C, Zuber J, Lima C, et al. Humoral and Cellular Immune Responses after Influenza Vaccination in Kidney Transplant Recipients. *Am J Transplant* (2009) 9:2346–54. doi: 10.1111/j.1600-6143.2009.02787.x
38. Ballet C, Roussey-Kesler G, Aubin JT, Brouard S, Giral M, Miqueu P, et al. Humoral and Cellular Responses to Influenza Vaccination in Human Recipients Naturally Tolerant to a Kidney Allograft. *Am J Transplant* (2006) 6:2796–801. doi: 10.1111/j.1600-6143.2006.01533.x
39. Soesman NMR, Rimmelzwaan GF, Nieuwkoop NJ, Beyer WEP, Tilanus HW, Kemmeren MH, et al. Efficacy of Influenza Vaccination in Adult Liver Transplant Recipients. *J Med Virol* (2000) 61, 1:85–93. doi: 10.1002/(SICI)1096-9071(200005)61:1<85::AID-JMV14>3.0.CO;2-H
40. Fishman JA. Infection in Solid-Organ Transplant Recipients. *New Engl J Med* (2007) 357:2601–14. doi: 10.1056/NEJMra064928
41. Danzinger-Isakov L, Kumar D. Guidelines for Vaccination of Solid Organ Transplant Candidates and Recipients. *Am J Transplant* (2009) 9:S258–62. doi: 10.1111/j.1600-6143.2009.02917.x
42. Orlando G, Hematti P, Stratta RJ, Burke GW, Di Cocco P, Pisani F, et al. Clinical Operational Tolerance After Renal Transplantation. *Ann Surg* (2010) 252:915–28. doi: 10.1097/SLA.0b013e3181f3efb0
43. Chong PP, Handler L, Weber DJ. A Systematic Review of Safety and Immunogenicity of Influenza Vaccination Strategies in Solid Organ Transplant Recipients. *Clin Infect Dis* (2018) 66:1802–11. doi: 10.1093/cid/cix1081
44. Bosaeed M, Kumar D. Seasonal Influenza Vaccine in Immunocompromised Persons. *Hum Vaccines Immunotherapeut* (2018) 14:1311–22. doi: 10.1080/21645515.2018.1445446
45. O'Hagan DT, Friedland LR, Hanon E, Didierlaurent AM. Towards an Evidence Based Approach for the Development of Adjuvanted Vaccines. *Curr Opin Immunol Vaccines* (2017) 2017:93–102. doi: 10.1016/j.coi.2017.07.010
46. Weinberger B. Adjuvant Strategies to Improve Vaccination of the Elderly Population. *Curr Opin Pharmacol • Cancer • Immunomodulation* (2018) 41:34–41. doi: 10.1016/j.coph.2018.03.014
47. Vink P, Ramon Torrell JM, Fructuoso AS, Kim SJ, Kim SI, Zaltzman J, et al. Immunogenicity and Safety of the Adjuvanted Recombinant Zoster Vaccine in Chronically Immunosuppressed Adults Following Renal Transplant: A Phase 3, Randomized Clinical Trial. *Clin Infect Dis: Off Publ Infect Dis Soc America* (2020) 70:181–90. doi: 10.1093/cid/ciz177
48. Crooke SN, Ovsyannikova IG, Poland GA, Kennedy RB. Immunosenescence: A Systems-Level Overview of Immune Cell Biology and Strategies for Improving Vaccine Responses. *Exp Gerontol* (2019) 124:110632. doi: 10.1016/j.exger.2019.110632
49. Günther OP, Shin H, Ng RT, McMaster WR, McManus BM, Keown PA, et al. Novel Multivariate Methods for Integration of Genomics and Proteomics Data: Applications in a Kidney Transplant Rejection Study. *Omics: A J Integr Biol* (2014) 18:682–95. doi: 10.1089/omi.2014.0062

50. Kumar D, Campbell P, Hoschler K, Hidalgo L, Al-Dabbagh M, Wilson L, et al. Randomized Controlled Trial of Adjuvanted Versus Nonadjuvanted Influenza Vaccine in Kidney Transplant Recipients. *Transplantation* (2016) 100:662–69. doi: 10.1097/TP.0000000000000861
51. Lawal A, Basler C, Branch A, Gutierrez J, Schwartz M, Schiano TD. Influenza Vaccination in Orthotopic Liver Transplant Recipients: Absence of Post Administration ALT Elevation. *Am J Transplant* (2004) 4:1805–9. doi: 10.1111/j.1600-6143.2004.00564.x
52. Pérez-Romero P, Bulnes-Ramos A, Torre-Cisneros J, Gavaldá J, Aydillo TS, Moreno A, et al. Influenza Vaccination during the First 6 Months after Solid Organ Transplantation Is Efficacious and Safe. *Clin Microbiol Infect* (2015) 21:1040.e11–1040.e18. doi: 10.1016/j.cmi.2015.07.014
53. Cordero E, Roca-Oporto C, Bulnes-Ramos A, Aydillo T, Gavaldà J, Moreno A, et al. Two Doses of Inactivated Influenza Vaccine Improve Immune Response in Solid Organ Transplant Recipients: Results of TRANSGRIPE 1–2, a Randomized Controlled Clinical Trial. *Clin Infect Dis* (2017) 64:829–38. doi: 10.1093/cid/ciw855
54. Le Corre N, Thibault F, Noble CP, Meiffrédy V, Daoud S, Cahen R, et al. Effect of Two Injections of Non-Adjuvanted Influenza A H1N1pdm2009 Vaccine in Renal Transplant Recipients: INSERM C09-32 TRANSFLUVAC Trial. *Vaccine* (2012) 30:7522–28. doi: 10.1016/j.vaccine.2012.10.047
55. Liao Z, Xu X, Liang Y, Xiong Y, Chen R, Ni J. Effect of a Booster Dose of Influenza Vaccine in Patients with Hemodialysis, Peritoneal Dialysis and Renal Transplant Recipients: A Systematic Literature Review and Meta-Analysis. *Hum Vaccines Immunotherapeut* (2016) 12:2909–15. doi: 10.1080/21645515.2016.1201623
56. Natori Y, Shiotsuka M, Slomovic J, Hoschler K, Ferreira V, Ashton P, et al. A Double-Blind, Randomized Trial of High-Dose vs Standard-Dose Influenza Vaccine in Adult Solid-Organ Transplant Recipients. *Clin Infect Dis* (2018) 66:1698–704. doi: 10.1093/cid/cix1082
57. Manuel O, Humar A, Berutto C, Ely L, Giulieri S, Lien D, et al. Low-Dose Intradermal versus Intramuscular Trivalent Inactivated Seasonal Influenza Vaccine in Lung Transplant Recipients. *J Heart Lung Transplant* (2011) 30:679–84. doi: 10.1016/j.healun.2011.01.705
58. Criscuolo E, Caputo V, Diotti RA, Sautto GA, Kirchenbaum GA, Clementi N. Alternative Methods of Vaccine Delivery: An Overview of Edible and Intradermal Vaccines. *J Immunol Res* (2019) 20191–13. doi: 10.1155/2019/8303648
59. Rouphael NG, Paine M, Mosley R, Henry S, McAllister DV, Kalluri H, et al. The Safety, Immunogenicity, and Acceptability of Inactivated Influenza Vaccine Delivered by Microneedle Patch (TIV-MNP 2015): A Randomised, Partly Blinded, Placebo-Controlled, Phase 1 Trial. *Lancet (London England)* (2017) 390:649–58. doi: 10.1016/S0140-6736(17)30575-5
60. Rouphael NG, Mulligan MJ. Microneedle Patch for Immunization of Immunocompromised Hosts. *Oncotarget* (2017) 8:93311–12. doi: 10.18632/oncotarget.22072
61. Moal V, Motte A, Vacher-Coponat H, Tamalet C, Berland Y, Colson P. Considerable Decrease in Antibodies against Hepatitis B Surface Antigen Following Kidney Transplantation. *J Clin Virol* (2015) 68:32–6. doi: 10.1016/j.jcv.2015.04.011

Conflict of Interest: NR received research funding unrelated to this paper from Sanofi-Pasteur, Pfizer, Quidel, Eli Lilly, and Merck.

The remaining authors declare that the research was conducted in the absence of any commercial or financial relationships that could be construed as a potential conflict of interest.

frontiers in Immunology

ORIGINAL RESEARCH
published: 30 November 2020
doi: 10.3389/fimmu.2020.578801

Multi-Omic Data Integration Allows Baseline Immune Signatures to Predict Hepatitis B Vaccine Response in a Small Cohort

Casey P. Shannon[1,2†], Travis M. Blimkie[3†], Rym Ben-Othman[4,5†], Nicole Gladish[6], Nelly Amenyogbe[5,7], Sibyl Drissler[8], Rachel D. Edgar[6,9], Queenie Chan[10], Mel Krajden[11], Leonard J. Foster[10], Michael S. Kobor[6], William W. Mohn[3], Ryan R. Brinkman[8], Kim-Anh Le Cao[12], Richard H. Scheuermann[13,14,15], Scott J. Tebbutt[1,2,16], Robert E.W. Hancock[3], Wayne C. Koff[17], Tobias R. Kollmann[4,5‡], Manish Sadarangani[4,18*‡] and Amy Huei-Yi Lee[19*‡]*

[1] Prevention of Organ Failure (PROOF) Centre of Excellence and Centre for Heart Lung Innovation, St. Paul's Hospital, Vancouver, BC, Canada, [2] UBC Centre for Heart Lung Innovation, St. Paul's Hospital, Vancouver, BC, Canada, [3] Department of Microbiology and Immunology, Life Sciences Institute, University of British Columbia, Vancouver, BC, Canada, [4] Department of Pediatrics, University of British Columbia, Vancouver, BC, Canada, [5] Telethon Kids Institute, Perth Children's Hospital, University of Western Australia, Nedlands, WA, Australia, [6] Centre for Molecular Medicine and Therapeutics, BC Children's Hospital Research Institute, Department of Medical Genetics, The University of British Columbia, Vancouver, BC, Canada, [7] Department of Experimental Medicine, University of British Columbia, Vancouver, BC, Canada, [8] Terry Fox Laboratory, British Columbia Cancer Agency, Vancouver, BC, Canada, [9] European Molecular Biology Laboratory, European Bioinformatics Institute, Wellcome Genome Campus, Cambridge, United Kingdom, [10] Department of Biochemistry & Molecular Biology, Michael Smith Laboratories, University of British Columbia, Vancouver, BC, Canada, [11] British Columbia Centre for Disease Control, Vancouver, BC, Canada, [12] Melbourne Integrative Genomics, School of Mathematics and Statistics, The University of Melbourne, Parkville, VIC, Australia, [13] Department of Informatics, J. Craig Venter Institute, La Jolla, CA, United States, [14] Department of Pathology, University of California, San Diego, CA, United States, [15] Division of Vaccine Discovery, La Jolla Institute for Immunology, La Jolla, CA, United States, [16] Department of Medicine, Division of Respiratory Medicine, University of British Columbia, Vancouver, BC, Canada, [17] Human Vaccines Project, New York, NY, United States, [18] Vaccine Evaluation Center, BC Children's Hospital Research Institute, Vancouver, BC, Canada, [19] Department of Molecular Biology and Biochemistry, Simon Fraser University, Burnaby, BC, Canada

Background: Vaccination remains one of the most effective means of reducing the burden of infectious diseases globally. Improving our understanding of the molecular basis for effective vaccine response is of paramount importance if we are to ensure the success of future vaccine development efforts.

Methods: We applied cutting edge multi-omics approaches to extensively characterize temporal molecular responses following vaccination with hepatitis B virus (HBV) vaccine. Data were integrated across cellular, epigenomic, transcriptomic, proteomic, and fecal microbiome profiles, and correlated to final HBV antibody titres.

Results: Using both an unsupervised molecular-interaction network integration method (NetworkAnalyst) and a data-driven integration approach (DIABLO), we uncovered baseline molecular patterns and pathways associated with more effective vaccine responses to HBV. Biological associations were unravelled, with signalling pathways such as JAK-STAT and interleukin signalling, Toll-like receptor cascades, interferon

OPEN ACCESS

Edited by:
Cornelis Joseph Melief,
Leiden University, Netherlands

Reviewed by:
Mohamed H. Shamji,
Medical Research Council and Asthma UK Centre in Allergic Mechanisms of Asthma, United Kingdom
Vladimir Ryabov,
University of Heidelberg, Germany

***Correspondence:**
Amy Huei-Yi Lee
amy_lee_10@sfu.ca
Manish Sadarangani
msadarangani@bcchr.ubc.ca
Tobias R. Kollmann
Tobias.Kollmann@telethonkids.org.au

[†]These authors have contributed equally to this work

[‡]These authors have contributed equally to this work

Specialty section:
This article was submitted to Vaccines and Molecular Therapeutics, a section of the journal Frontiers in Immunology

Received: 01 July 2020
Accepted: 15 October 2020
Published: 30 November 2020

Citation:
Shannon CP, Blimkie TM, Ben-Othman R, Gladish N, Amenyogbe N, Drissler S, Edgar RD, Chan Q, Krajden M, Foster LJ, Kobor MS, Mohn WW, Brinkman RR, Le Cao K-A, Scheuermann RH, Tebbutt SJ, Hancock REW, Koff WC, Kollmann TR, Sadarangani M and Lee AH-Y (2020) Multi-Omic Data Integration Allows Baseline Immune Signatures to Predict Hepatitis B Vaccine Response in a Small Cohort. Front. Immunol. 11:578801. doi: 10.3389/fimmu.2020.578801

signalling, and Th17 cell differentiation emerging as important pre-vaccination modulators of response.

Conclusion: This study provides further evidence that baseline cellular and molecular characteristics of an individual's immune system influence vaccine responses, and highlights the utility of integrating information across many parallel molecular datasets.

Keywords: multi-omic analysis, hepatitis B vaccination, baseline immunity, network analysis, vaccine response

INTRODUCTION

Hepatitis B is a viral infection that primarily affects the liver of infected individuals, and can cause both acute and chronic disease. The WHO estimates that 257 million people had a chronic hepatitis B infection in 2015 (1), with nearly one million deaths occurring as a result of hepatitis B infections causing cirrhosis and liver cancer. Fortunately, there are highly efficacious vaccines available for hepatitis B with rates of protection above 90% if given in a two- or three-dose schedule (2). The antibody response to hepatitis B virus (HBV) vaccine is one of the best correlates of protection from infection with well characterized quantitative levels associated with degree of protection, allowing clinicians and researchers to easily determine if an individual is sufficiently protected after receipt of the vaccination series.

Unfortunately, the response to vaccination is highly variable in older adults, with some individuals quickly producing high levels of HBV antibodies, while others never develop protective levels (3). While this can be overcome by additional booster doses, the reasons for this reduced efficacy in older populations remains unclear. Age-related immuno-senescence is one proposed mechanism, but a better understanding of the reasons that underlie this variable response in older adults is still needed. This could be accomplished with a large study involving many individuals, but recruiting large numbers of participants for vaccine studies can be difficult and costly. Researchers are thus tasked with attempting to draw significant and meaningful conclusions from relatively small cohorts, typically assessed using only a small variety of methods. To overcome this issue, we used multiple omics technologies together with computational integration methods to generate a more comprehensive picture of vaccine response.

Here, in a cohort of 15 healthy adults ranging from 44 to 73 years of age, we profiled a broad variety of molecular modalities from peripheral whole blood, including immune cell composition, DNA methylation, gene expression, protein abundance, as well as fecal 16S microbiome, to provide the most comprehensive picture of the immune response to an aluminium-adjuvanted HBV vaccine. Antibody measurements to HBV surface antigens were used as the quantitatively defined endpoint in our model to address two main questions: (1) can we identify baseline immune signatures that predict vaccine responses and differentiate between responders and non-responders, and (2) what temporal molecular changes occur following HBV vaccination? Baseline differences correlating with final HBV vaccine response could be identified in this small (n = 15) cohort of adults by using a multi-omics integration approach. This general concept of specific baseline immune signatures predicting vaccine responses has been demonstrated in large cohort studies in the context of HBV, influenza, and malaria vaccines (4–7). However, the benefit of integrating multi-omics baseline data in the context of small sample size has not previously been documented. This approach has substantial implications not only in the field of bioinformatics-driven analyses, but also in systems vaccinology and vaccine development.

MATERIALS AND METHODS

Participant Recruitment and Study Design

A prospective, observational study (ClinicalTrials.gov; NCT03083158) of immune responses to the HBV vaccine (ENGERIX®-B) was undertaken, with recruitment occurring at the Vaccine Evaluation Center (VEC), BC Children's Hospital Research Institute in Vancouver, Canada. Participants were recruited by e-mail, mail and telephone. All participants enrolled in the study provided written informed consent under a research protocol (H17-00175) approved by the University of British Columbia Women's and Children's research ethics board. All initial sample processing was undertaken at the VEC laboratory. Participants were healthy adults aged 44–73 years who were seronegative to HBV and with no prior history to HBV infection or vaccination, with demographics shown in **Figure 1**. In brief, screening of participants was performed by blood sampling to determine their antibody titers to HBV surface antigens. Participants with anti-hepatitis B surface antigen (HBs) antibody levels under 3.1IU/L were considered seronegative and a total of 15 eligible individuals enrolled to participate in the study. For detailed inclusion/exclusion criteria, see the HBV vaccine Methods manuscript: *Systems biology methods applied to blood and tissue for a comprehensive analysis of immune response to Hepatitis B vaccine in adults* (8). Enrolled individuals attended the first study visit involving the collection of clinical history, a physical examination as well as pre-vaccination biospecimen collection (blood and fecal microbiome samples). One ml (20 micrograms) of HBV vaccine was administered *via* intramuscular deltoid injection at three different times throughout the study (0, 28, and 180 days). At each visit, a number of molecular and clinical tests were performed on the collected biospecimens (**Figure 1**). HBV serology of study participants at baseline were performed at the BC Centre for Disease Control. In total, participants were monitored during 12 visits spanning the course of seven months

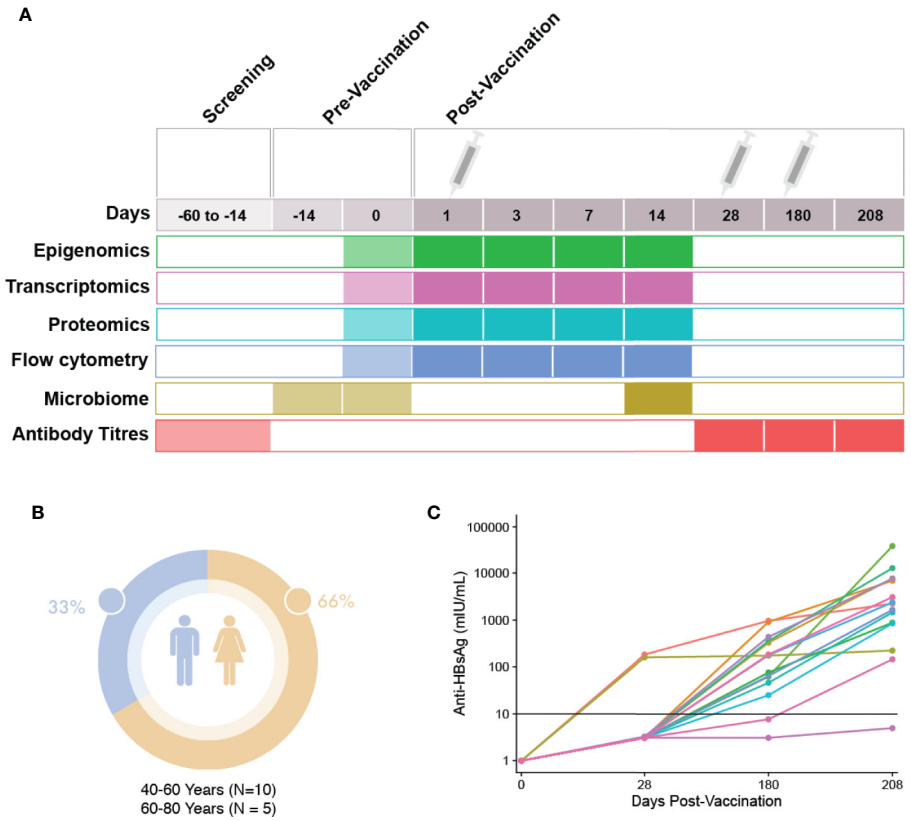

FIGURE 1 | Study visit schedule and cohort demographics. **(A)** Immunization and sampling schedule: Screening of patients eligible for this study occurred 14–60 days prior to the first vaccine dose. Eligible participants returned 14 days prior to vaccination to complete enrolment and have blood and microbiome samples taken. At day 0, the first vaccine dose was administered after blood and microbiome sampling. Blood sampling then occurred at days 1, 3, 7, and 14 post-vaccination. At day 28, blood sampling and the second HBV dose was administered. At day 180, blood sampling and the last dose of HBV was given, followed by a final blood sample taken at day 208. **(B)** Demographics: Participant sex and age. **(C)** Patient anti-HBs antibody titres at 28, 180, and 208 days post first HBV vaccination dose.

(8). HBV titres were measured once during the screening phase, and at three additional time points, corresponding to 28, 180, and 208 days after the first dose of HBV vaccine.

Cellular Profiling, Omics, and Statistical Analysis of the Time Course

Various omics studies were performed as described in the **Supplementary Materials and Methods**, with workflow figure shown in **Supplementary Figure 1**. Briefly, peripheral whole blood cells were profiled by flow cytometry, genome-wide DNA methylation (Illumina Infinium MethylationEPIC BeadChip), transcript abundance (whole blood, bulk RNA-Seq), and proteome-wide protein abundance (mass spectrometry) at various time points (**Figure 1**). Additionally, the bacterial composition (microbiome) of the gut was assessed by 16S rRNA microbiome profiling pre- (Day -14 and 0) and post-vaccination (Day 14). The gating strategy used for immune cell phenotyping is included in **Supplementary Figure S3**.

To identify global changes pre- versus post- vaccination across different omics data, we used multi-level principal component analysis (multi-level PCA) from *mixOmics* to highlight the effect of vaccination (treatment effect) within subjects separately from the biological variation that existed between subjects (9, 10). Based on the temporal trends observed, Day 1 and 14 post-vaccination were further investigated using univariate statistical tests within each omics method to identify differentially methylated CpG sites, expressed genes, and proteins following vaccination (refer to **Supplementary Materials and Methods** for further details on each of these methods).

Identifying Features Associated With HBV Vaccine Response From Single Omics Data

To identify baseline differences between participants who responded to vaccine and those who did not, we used the HBV-specific antibody titre levels from Day 180 to divide the participants into either responders or non-responders, based on the well-established correlate of protection of 10 mIU/ml (6). This demarcation was used in analyzing the transcriptomic and proteomic data. For analysis of the epigenetic data, the same titre values from Day 180 were instead treated as a continuous

variable. For more details on how each of these datasets were analyzed, refer to the **Supplementary Methods** section.

Lists of genes or proteins identified through these methods were submitted to NetworkAnalyst (11, 12) for unsupervised construction of Protein-Protein Interaction (PPI; direct, metabolic or regulatory interactions) networks, to facilitate biological enrichment of the results. In these PPI networks, nodes represent individual proteins, while the edges which connect nodes correspond to a known, curated interaction between a given pair of proteins. Node tables representing all members of a network were downloaded from NetworkAnalyst to test for enriched Reactome pathways using the R package *Sigora* (13), with pathways being considered significantly enriched with a Bonferroni-corrected p-value of <0.001.

Identifying Features Associated With HBV Vaccine Response From Multi-Omic Data

To identify features that could be used to predict vaccine response (anti-HB titres) from baseline omics profiles, we used two complementary data integration strategies: NetworkAnalyst and DIABLO.

NetworkAnalyst

NetworkAnalyst is an online tool which leverages known protein-protein interactions to construct biological networks in an unsupervised manner to provide biological insights (11, 12). Genes or proteins identified when comparing responders and non-responders (using Day 180 titres as detailed previously) using combinations of three different omics data (epigenetics, proteomics, and transcriptomics) were uploaded to NetworkAnalyst and combined to build minimally-connected first order PPI networks, with the commonly-occurring promiscuous node UBC (Ubiquitin C; 10,837 known interactions at www.innatedb.com) removed. To highlight novel nodes in the combined networks, networks were constructed individually for the different omics methods and their node tables downloaded to enable comparison to the node table from the combined network. This allowed identification of nodes that were present in the combined network, but absent when examining each omics network separately. Node tables downloaded from NetworkAnalyst were tested for enriched Reactome or KEGG pathways using the R package *Sigora* as previously described (13, 14).

DIABLO

DIABLO, part of the *mixOmics* framework, is a supervised, data-driven, hypothesis-free multi-omics integration approach that has been successfully applied, by us and others, to derive novel, robust biomarkers, and increase our understanding of the molecular regulatory mechanisms that underlie health and disease (15–17). DIABLO extends sparse Generalized Canonical Correlation Analysis (sGCCA) for multi-omics and supervised integration (18, 19). DIABLO performs multivariate dimensionality reduction and selects correlated variables across different datasets by maximizing the covariance between linear combinations of variables (latent component scores), across datasets (blocks; flow cytometry, epigenomic, transcriptomic, and proteomic profiling, fecal 16S rRNA microbiome) and an outcome variable (response; log-transformed anti-HBs IgG level measured at the final follow-up). Feature selection is performed internally using lasso penalties. The data are then projected into a smaller dimensional subspace spanned by the components for prediction. The ability of the integrative model to predict final anti-HBs IgG titres was then evaluated using leave-one-out cross-validation.

Mapping of Identifiers to Facilitate Biological Interpretation

To facilitate biological interpretation, features were mapped, where possible, to HUGO Gene Nomenclature Committee (HGNC) gene symbols. Methylated CpG dimers were mapped using the annotation provided by Illumina (*IlluminaHumanMethylationEPICanno.ilm10b2.hg19* R package). Ensemble gene IDs and UniProt protein IDs were mapped using the Biomart service from Ensembl (20). Gene set enrichment was assessed against the Broad Institute's MSigDB (C2 collection: manually curated gene sets from KEGG, REACTOME, etc.) using a hypergeometric test, or *Sigora*, as detailed previously (13).

RESULTS

Response of Older Adults to a Three-Dose Schedule of HBV Vaccine

To enable analyses aimed at identifying differences between HBV vaccine responders and non-responders, we first examined the titre levels for each participant over the course of this study. As described previously, participants' anti-HB titres were measured three times following the first dose of HBV vaccine (**Figure 1C**). At the first antibody titre measurement on Day 28, after only a single dose of HBV vaccine, 2 out of 15 participants (aged 63 and 72, both female) showed titres that would classify them as responders, with titre levels above the correlate of protection, 10 mIU/ml. Based on a multi-level PCA, we saw little difference between these two individuals and the remainder of our cohort (**Supplementary Figure S5**). By Day 180, after having received two doses, 13 of 15 participants showed titre levels equal to or greater than 10mIU/mL, measures which have been shown to correlate well with protection. At the final titre measurement 30 days after the third vaccination (208 Days after the first dose), all but a single participant showed titre levels above the correlate of protection. We also examined if there was any relationship between DNAm-based age acceleration and titre levels at Day 180, and found no correlation (**Supplementary Figure 4**).

Immune Cell Phenotyping

To identify potential immune cell types important for HBV vaccine responses, Spearman correlation analysis was performed using the baseline counts of various immune cell types (defined by 15 anchor makers; **Supplementary Table 1**) and the HBV antibody titres measured at Day 180. No statistically significant baseline cell type differences were identified from correlations to

Day 180 titres (**Supplementary Figure 2**). However, we observed a trend of positive correlation between $CD3^+$ T cells on Day 7 and 14 to HB antibody titres measured at Day 180. In contrast, we observed a trend of negative correlation between $CD56^{dim}$ $CD16^{+/-}$ NK cell populations on Day 7 and 14 to HB antibody titres measured at Day 180. While there was no definitive immune phenotype that could potentially identify vaccine responders to non-responders, our data suggested that T cell subsets might potentially be important in the immune response to hepatitis B during infection or vaccination (21).

Molecular Changes Following Vaccination

Our goal was to first define the molecular changes that occurred following HBV vaccination. To do this while removing intra-individual differences, we performed multi-level PCA of the flow cytometry, epigenomic, transcriptomics, and proteomic data (**Figure 2**). For both the epigenomic and transcriptomic profiles, we observed rapid changes one day after HBV vaccination, followed by a return to baseline on Day 14 (**Figures 2B, C**). In contrast, cell population and proteomic profiles were most distinct from baseline two weeks after HBV vaccination (**Figures 2A, D**).

From the epigenomic data, we identified a total of 18 unique DNA methylation sites using a univariate analysis, located in twelve genes that were significantly differently methylated following vaccination, when compared to baseline (**Figure 3A**, **Supplementary Table 2**). A number of these genes are known to participate in immune functions, including: BAIAP2L1 that plays a role in actin organization; a cytotoxic and regulatory T Cell-associated molecule (CRTAM); a negative regulator of TGF-β signalling LDL receptor (LDLRAD4); a transcriptional repressor of activation protein-1 (ZNF12); anti-viral and cytidine deaminase (APOBEC3A_B); and a guanine exchange factor and endosome dynamics regulator (ANKRD27). Similarly, we observed minimal transcriptomic changes following HBV vaccination, with only 14 significantly differentially expressed (DE) genes (adjusted p-value <0.05 and absolute fold change >1.5; **Supplementary Table 3**) when comparing Day 14 to pre-vaccination Day 0 (**Figure 3B**). Among these were the genes CAMP (22), encoding host defence peptide LL-37 that has a known association with immune and inflammatory responses, and the neutrophil-associated elastase gene ELANE (23), which can alter the roles of NK cells, monocytes, and granulocytes. These results point to a detectable change in the immune response of inoculated individuals as early as two weeks after having received the vaccine. No statistically significant changes were observed in proteomics or the fecal microbiome following vaccination (**Figures 3C, D**).

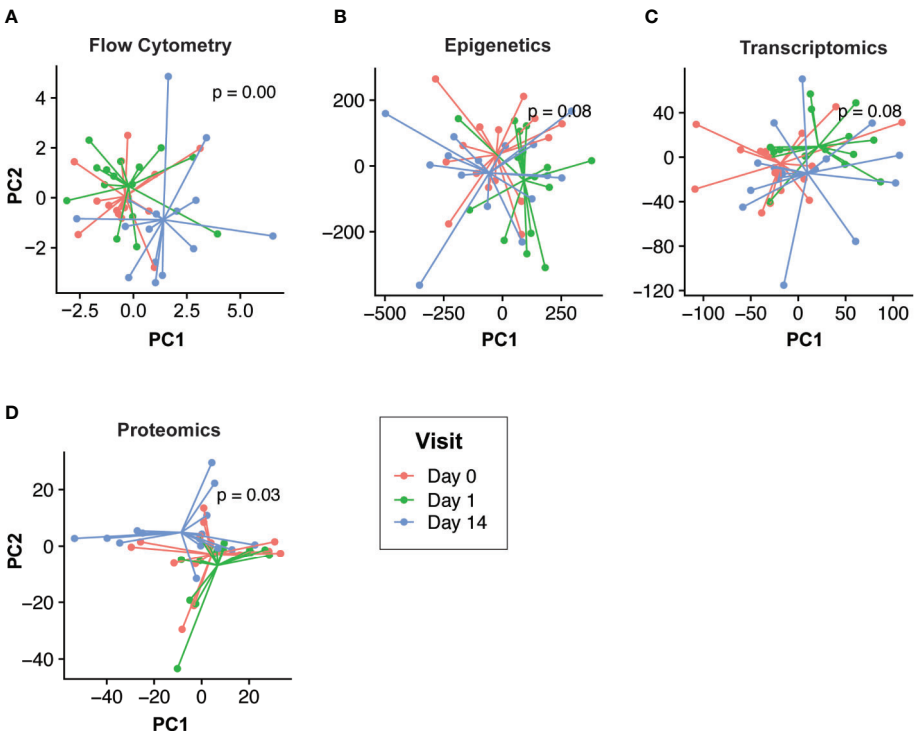

FIGURE 2 | Temporal response profiles following HBV vaccination differs across omics compartments. Low dimensional projection of the flow cytometry **(A)**, epigenomic **(B)**, transcriptomic **(C)**, and proteomic **(D)** data using multilevel principal component analysis to visualize global changes across time. In each panel, different post-vaccination time points for each individual are shown in red (Day 0), green (Day 1), and blue (Day 14). We observed differing global temporal patterns of change following vaccination across the various omics compartments. Epigenomic and transcriptomic profiles changed rapidly post-vaccination (Day 1; green vs. blue/red) before returning to baseline by Day 14. Conversely, flow cytometry and proteomic profiles were most distinct by Day 14 (blue vs. red/green).

Influence of Immune Baseline on Vaccine Response

We then turned our attention to identifying baseline differences between participants who responded to the HBV vaccine and those who did not based on the well-established correlate of protection of 10 mIU/ml. Comparing the responders and non-responders (defined at Day 180) using only the pre-vaccine transcriptomic data, 40 differentially expressed (DE) genes were identified, and used to construct a minimally-connected first-order PPI network (a first order network in which the interconnecting grey nodes that connect to only a single DE gene are removed), as shown in **Figure 4A**. Some of the genes found to be differentially expressed (adjusted p-value <0.05; **Supplementary Table 4**) included up-regulation of CD8A and CD8B that are involved in cytotoxic T-cell mediated immune responses, THEMIS, implicated in T-cell lineage selection and maturation, and transcription factor RORA that regulates cytokine expression in T-regulatory cells (24, 25). Downregulated genes included CEBPB that acts in the suppression of T-cells through transcription factor MYC and SLC11A1, a divalent metal ion transporter important for iron metabolism and host resistance to pathogens (26).

For the proteomic analysis, we were able to identify 267 unique peptides that changed in expression when comparing responders and non-responders at the pre-vaccine baseline (adjusted p-value <0.05; **Supplementary Table 5**). Some of the proteins identified by this analysis include: monocyte marker CD14, calcium binding inhibitor of HCV replication S100A6 (27), and TRIM25, a mediator of signal transduction in response to viral infections (28, 29). Pathway enrichment with Sigora (Bonferroni-corrected p-value <0.001; **Supplementary Table 6**) yielded multiple pathways, including "Neutrophil degranulation" and "Gene and protein expression by JAK-STAT signalling after Interleukin-12 stimulation". The greatest number of changes were observed in the epigenomic analysis, with identification of 898 DNA methylation CpG sites located within 632 genes (p-value ≤0.005 and change in beta >5%, with beta defined as proportion of methylated DNA at a particular locus; **Supplementary Table 7**). These genes were enriched for ERBB4 signalling pathways, a tyrosine protein kinase involved in downstream signalling of the B Cell Receptor, Notch-HLH transcription pathways, and implicated in various inflammatory diseases (p-value ≤ 0.005) (full list in **Supplementary Table 8**) (30).

Multi-Omics Data Integration by a Functional Approach, NetworkAnalyst, Identified Novel Pathways Contributing to Vaccine Responses

Since we were only able to identify limited baseline molecular differences between responders and non-responders from the individual omics data, we next applied a proven (14) multi-omics integration method to identify consistent signatures associated with robust vaccine responses. To determine the molecular and immunological differences that might influence vaccine responses, an integrative analysis was performed using either two or three omics datasets (transcriptomics, proteomics and/or epigenomics) comparing responders vs. non-responders using NetworkAnalyst (**Figure 4**). Both integrations revealed a dense minimally-connected network containing many novel nodes (**Figures 4B, C**, highlighted in orange), including: EOMES (eomesodermin), which is involved in the differentiation of $CD8^+$ T cells, active against viral infections (31); VCP involved in T cell activation (32); and EGR1 that stimulates T cell activation and promotes IL2 production (33). Interestingly the T-cell modulatory genes found using transcriptomics were well integrated into this network and several new T-cell modulators were identified, including ILF2 that mediates expression of IL2 by T-cells, PP1A that modulates T-cell cytokine expression, and FN1 which is Th1-specific in humans (34).

To gain mechanistic and biological insight into the immune pathways, we then tested the nodes from **Figures 4B or C** for enriched pathways with *Sigora*, using both Reactome and KEGG databases. Some of the significant pathways include innate immunity pathways such as "Neutrophil degranulation", "Gene and protein expression by JAK-STAT signaling after Interleukin-12 stimulation", and "Toll-like Receptor 4 (TLR4) Cascade". In addition, we identified some signatures of adaptive immune responses such as "IL17 signaling" and "Th17 cell differentiation", providing further insights into immune differences between responders and non-responders. In particular, JAK-STAT is a major anti-viral pathway that when activated can lead to inhibition of HBV infections (35), while TLR4 activation suppresses HBV infections (36). The full list of enriched pathways is included in **Supplementary Tables 9–12**.

Multi-Omics Data Integration Using a Data-Driven Approach Improved Our Understanding of Vaccine Response in a Small Cohort

In addition, we used the supervised, data-driven, multivariate integration method DIABLO to identify baseline (pre-vaccination) predictors of vaccine responses based on multiple high-throughput datasets (flow cytometry, epigenomic, transcriptomic, and proteomic profiling, as well as fecal 16S rRNA microbiome profiling). To determine whether integrating the data in this manner resulted in models with better predictive performance, we fit DIABLO models of varying complexity (total number of variables selected), and compared them to sparse partial least squares regression [sPLS (18)] models fit on each of the individual high-throughput datasets with similar number of variables selected. We assessed predictive performance using leave-one-out cross-validation and found that the integrative DIABLO model generally outperformed single-omic sPLS models (**Supplementary Figure 6**).

Based on this rigorous statistical assessment, we chose to characterize the variables selected by the DIABLO (17) model that achieved the best overall performance (lowest error rate; **Figure 5A**). Where possible (CpGs, transcripts, proteins) individual features were mapped to gene symbols, while features identified by either the integrative model or by models derived from the individual omics datasets were compared.

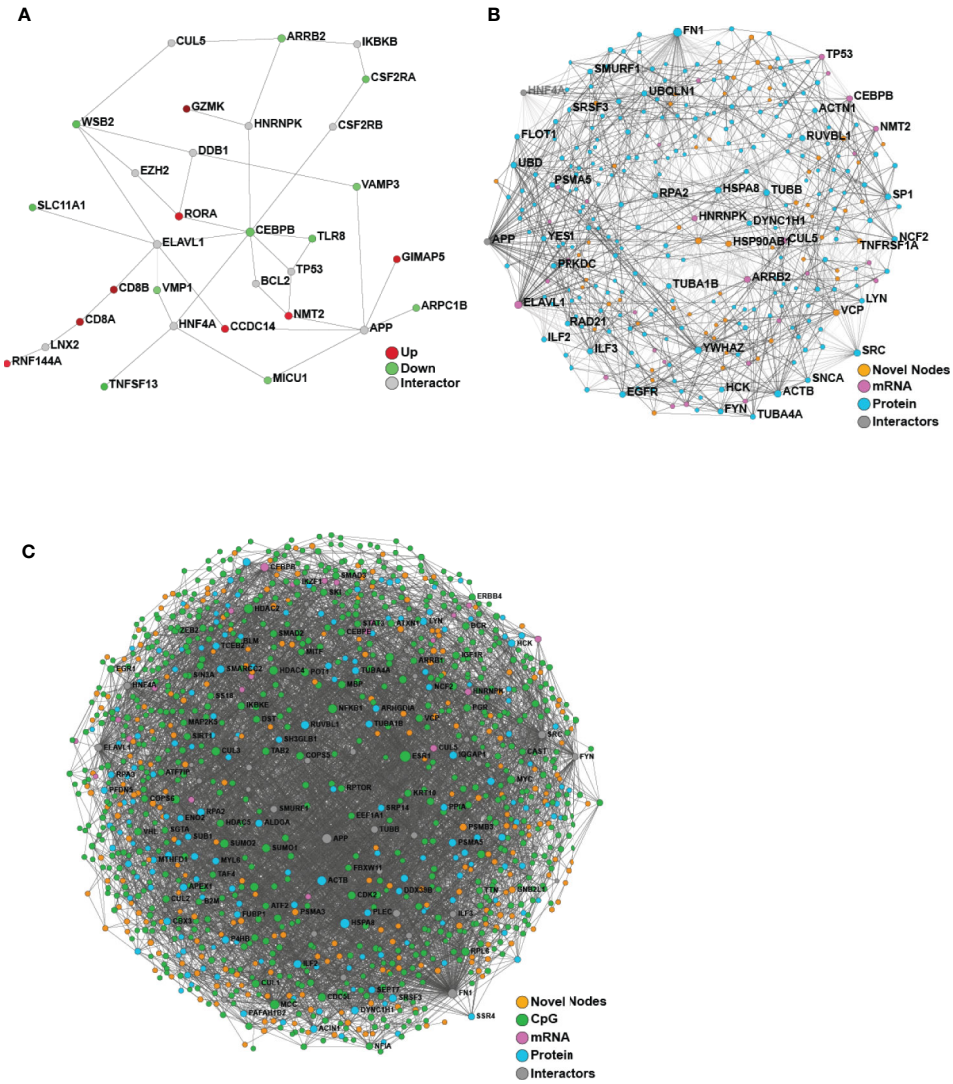

FIGURE 4 | Network analysis of transcriptomics and proteomics data reveal baseline differences between vaccine responders and non-responders. **(A)** Minimum-connected network from the 40 DE genes identified when comparing responders to non-responders (defined using Day 180 titre measures). **(B)** Minimally-connected first-order integrated protein-protein interaction network of the same 40 DE genes combined with the 267 differentially expressed proteins when comparing responders to non-responders (Day 180 post-vaccination). **(C)** Minimally-connected first-order integrated protein-protein interaction network of differentially expressed transcripts and proteins from B with the addition of differentially methylated genes (898 CpG sites) when comparing responders to non-responders (Day 180 post-vaccination). Novel nodes, not present in individual transcriptomic or proteomics networks are highlighted in orange.

Interestingly there was very little overlap between gene symbols identified by the individual omics models and the integrative model (**Supplementary Figure 7**). To rule out the possibility that the approaches were simply identifying different, but functionally-redundant, genes (involved in the same biological functions), the feature sets were assessed for pathway over-representation, and it was found that the various models identified largely distinct biological pathways (**Supplementary Figure 7**). Moreover, the features identified by the integrative model were enriched for a larger number of curated gene sets (Broad Institute MSigDB C2 collection), when compared to those identified individually based on data for the individual omics methods, suggesting that the integrative model features were consistent with well annotated biological pathways. We have made similar observations in a number of larger multi-omics studies (14, 17).

Additionally, to assess the biological function of DIABLO selected features (from transcriptomics, proteomics, and epigenomics), we used NetworkAnalyst to construct PPI networks to determine whether these genes and proteins formed an interconnected biological network (**Figure 5B**). Importantly the resultant first-order minimally-connected network was highly integrated and composed of nodes from each of the omics methods, indicating that transcriptomic,

proteomic, and epigenomic data were reporting on the same underlying biology. Furthermore, we identified additional nodes from this network that might provide insights into the effectiveness of the vaccine response, including: VDR (vitamin D receptor, involved in T cell function and influences HBV responses) (37); IL18 (pro-inflammatory cytokine for T-helper and NK cells) (38, 39); IKBKE (modulates T cell responses and essential for antiviral responses) (40); and ILF3 (participates in the innate antiviral response) (41); TMEM173 (innate immune signalling) (42); and BCL2L1 (minor role in inflammation attenuation) (43). As previously observed, pathway enrichment using both the statistical integration method DIABLO and biologically-driven PPI integration method NetworkAnalyst separately identified similar functional enrichments, highlighting potential pathways at immune baseline that predict HBV vaccine response (**Figure 5C**; **Supplementary Figures 8, 9**; **Supplementary Tables 13, 14**).

Plotting integration by DIABLO- or NetworkAnalyst-selected features showed that IRF9 (promotes inflammation and type III interferon signaling) was more highly expressed in non-responders **(Figure 5D**). In contrast, NEDD4 (E3 ubiquitin ligase that inhibits inflammatory pathways p38α and TNFα) (44) demonstrated lower expression in non-responders (**Figure 5E**). We observed similar correlation patterns in the baseline proteomics data with T cell activation, and proinflammatory dendritic cell, myeloid cell response, positively and negatively correlated, respectively, with vaccine response. This was further supported by a previous transcriptomic study demonstrating that an enrichment of pro-inflammatory pathways at immune baseline leads to a poor HBV vaccine response (45).

Finally, DIABLO identified a number of taxa from the baseline microbiome data, including *Butyricicoccus* and *Phascolarctobacterium*, which were positively associated with anti-HB antibody titre response (**Supplementary Figure 10A**). Interestingly, these two taxa have both been previously shown to regulate host immune responses. *Butyricicoccus* is a butyrate producer that has been used to modulate immune responses (46–48), while *Phascolarctobacterium* showed evidence of reduced abundance in individuals with an anti-inflammatory signatures (based on low lipopolysaccharide-binding protein and C-reactive protein) (49).

DISCUSSION

A better understanding of the complex regulatory interplay involved in the immune response to vaccination is a necessary step in the development of precision vaccinology. Leveraging systems biology approaches and collections of high-dimensional molecular immune readouts obtained from clinical cohorts may yield important insights. While these datasets are complex to synthesize and analyze, the complementary information they encode may strengthen biological findings and improve the accuracy of predictive models derived from them. Here we performed extensive molecular profiling of individuals receiving HBV vaccine to investigate vaccine response in adults. To our knowledge, this study constitutes the most comprehensive set of molecular immune readouts on a common set of individuals before and after HBV vaccination. Fifteen healthy HBV-seronegative adults received three doses of HBV vaccine to assess the correlate(s) of protection. We profiled the blood of participants before and after vaccination and defined both temporal changes in the various omics following vaccination, as well as baseline characteristics associated with a robust vaccine response (**Figure 1**).

Using multi-omics integration strategies described herein, we were able to identify significant biological features and pathways from a small sample size of 15 participants. Where possible, we leveraged resampling strategies (leave-one-out cross-validation) to ensure the robustness of our findings, though we acknowledge the limits of doing so in so few samples. While larger studies will be able to provide more robust results, ours was designed to further demonstrate the feasibility of a multi-omics approach to studying vaccine response, even when applied to a relatively small cohort. As omics-based vaccine studies with large numbers of participants are prohibitively expensive to conduct, our integrative multi-omics strategy on a smaller cohort will help ensure these larger studies are conducted in a manner which extracts as much biological meaning as possible. Select findings could then be targeted for further validation in larger cohorts, using cost-effective platforms with more well-defined paths to clinical implementation.

When analyzing patterns of change over time following vaccination, we were able to detect certain differences between pre- and post-vaccination samples (**Figures 2**, **3**). In particular, despite the very substantial impact of variation in underlying genetics, diet, environment and microbiome, transcriptomic analyses of participants 14 days post-vaccination compared to each individual's baseline pre-vaccination still revealed certain changes in the expression of genes such as ELANE and CAMP, both known to have important roles in the immune responses of many immune cells (50, 51). It is also interesting to note that the greatest differences identified by transcriptomics and epigenomics came from different time points, reinforcing the idea that using multiple omics methods can provide a more complete picture of complex biological phenomena through complementation.

Given that baseline immune profiles are known to predict vaccine responses to many agents (7, 45, 50), we were interested in identifying baseline molecular patterns associated with anti-HBs antibody titre response. When we analyzed each omics dataset separately with respect to vaccine responses, as measured by antibody titre (at Day 120, Day 208), we found only modest differences in the immune baseline between responders and non-responders. However, when this small number of methylation sites, differentially expressed transcripts, and proteins were projected onto PPI networks using NetworkAnalyst integration methods, we uncovered potential biological themes based on the principle of "guilt by association" (52). Specifically, PPI linkages between two nodes imply that there is shared biology (given that PPI are based on curated interactions, involving direct binding, consecutive positions in metabolic pathways, or regulatory interactions), such that PPI networks can be mined for

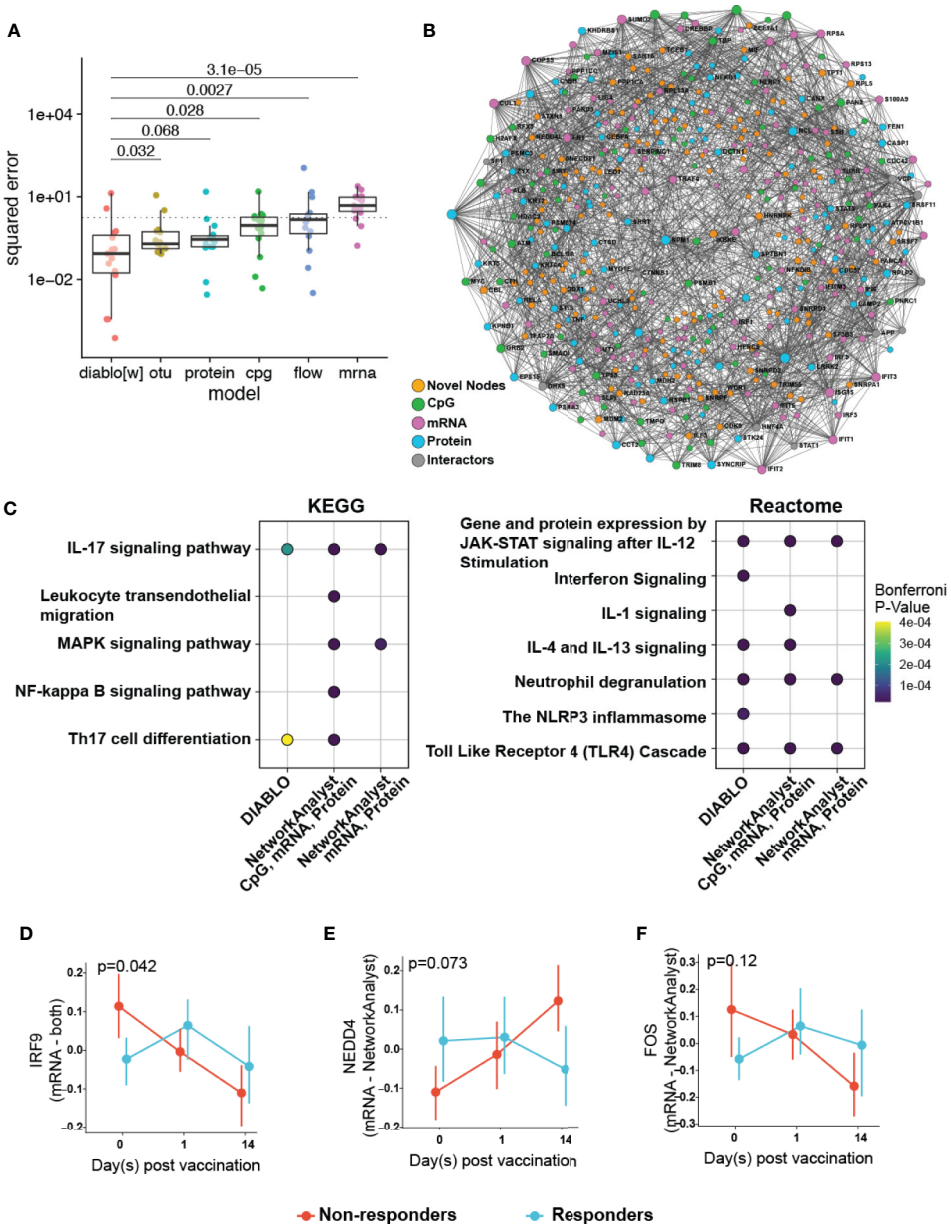

FIGURE 5 | Multi-omics integration to reduce overfitting by identifying of more biologically relevant features. **(A)** Comparison of the performance of a multi-omics model (DIABLO) to that of single-omics models of equivalent complexities, fit separately to individual omics datasets (otu, operating taxonomic units of the fecal microbiome; cpg, blood-based DNA methylation; protein, plasma proteomics; flow, cell counts by flow cytometry; mrna, whole blood transcriptomics). Mean squared error (MSE) differed significantly across all models (Kruskal-Wallis test; p = 0.0023), with the multi-omics model achieving significantly lower error (and better performance) when compared to all other models, with the exception of the proteomics-derived model (p = 0.068). **(B)** Integrated minimally-connected first-order network of features identified by DIABLO from transcriptomic, proteomics, and epigenetic data. Novel nodes identified from integration are highlighted in orange. **(C)** Selected enriched pathways and **(D–F)** selected enriched genes (mRNA) or proteins (proteomics) identified from integration (NetworkAnalyst, DIABLO, or both methods) are shown.

mechanistic information, based not on single gene products but consortia of gene products reflecting pathways and ontologies. Thus, when we used NetworkAnalyst to perform multi-omics integration based on function-related PPI networks, novel nodes and enriched pathways important in HBV vaccine response were identified (**Figure 4**, **Supplementary Figures 8, 9**). The integrated networks shown in **Figure 4** demonstrate the benefit of this approach, since a multitude of novel nodes that provide the "glue" to optimize the network, were identified.

In addition, we applied a multivariate statistical method to carry out multi-omics data integration (DIABLO) and identify baseline features that could predict vaccine response. A

particular concern with these methods is overfitting, particularly in studies with a relatively small *n* i.e. few (tens, up to a hundred) biological samples, and a substantially larger *p* i.e. number of molecules or variables (several tens of thousands). This is sometimes referred to as the "**small *n* big *p***" (or p>>>n) problem and can result in poor reproducibility and/or models that fail to generalize well to new data. DIABLO implements a number of strategies to tackle these challenges. First, it reduces the influence of noisy variables by means of dimensionality reduction techniques that summarise and/or identify useful and robust information from the data, leveraging penalisation (lasso) to carry out variable selection (18, 19). Second, it cross-references information across biological spaces by utilizing different types of data and looking for reinforcing biological dynamics, which works as long as these data report on the same basic underlying biological mechanisms.

We used DIABLO to derive a multi-omics model capable of predicting vaccine response from baseline molecular profiles. Critically, this DIABLO model outperformed models of comparable complexity derived from the individual omics analyses, highlighting the utility of multi-omics integration (**Figure 5**). Further, we tested whether the improved performance could be due to a reduced tendency to overfit data as a result of the additional imposed constraints, i.e. enforcing covariance across the omics datasets. We compared the features identified by our integrative model with those identified with single omics approaches, and found these to be almost entirely distinct. Moreover, features selected by DIABLO can be used to construct coherent and highly interconnected protein-protein interaction networks (48). These DIABLO selected features were enriched for a greater number of annotated gene sets, and critically delivered data overlapping with our functional integration approach using NetworkAnalyst (**Figure 5**, and **Supplementary Figures 8, 9**). Taken together, the superior performance in cross-validation and selection of largely distinct sets of features demonstrate that DIABLO was less likely to identify spurious associations and overfit the data on which it was trained. Furthermore, these results suggest that, by taking advantage of the differing effect of background noise and technical confounders across the various omics, and focusing on the consensus information related to the outcome, multi-omics integration can reduce overfitting and result in more robust and generalizable models (14, 17), even in studies where p>>>n.

Functionally, pathway enrichment of our integrative analyses comparing responders and non-responders using NetworkAnalyst and DIABLO yielded some of the same pathways that provide insights into immune baseline features that may contribute to HBV vaccine response (**Figure 5**, and **Supplementary Figures 8, 9**). This overlap in significant biological phenomena reinforces the validity of these two approaches used separately and conjointly since they converged on the same (or similar) biology, including several key innate immune pathways such as JAK-STAT signalling/IL-12 stimulation, TLR activation and neutrophil degranulation. The JAK-STAT signalling pathway is an anti-viral pathway, and modulation of this pathway would play an important role in an effective response to infection, and most likely, vaccination (53). The apparent role of TLR4 signalling is also in agreement with studies showing the important role of this signalling pathway during chronic HBV infection (54) and T cell activation (55). Furthermore, TLR4 signalling cascade as well as IL12 and TLR/IL-1 signaling, are important in the response to vaccines with aluminum-based adjuvants (which is used in ENGERIX®-B), suggesting that individuals who respond to vaccination may have greater intrinsic responses to adjuvant compared to non-responders (54, 56). Additionally, pathway enrichment of both integration methods revealed adaptive immune signatures such as IL-17 signalling and Th17 cell differentiation. Lastly, interferon signaling, identified by both integration methods, may play a role in linking innate and adaptive immunity through signal transduction *via* inflammasomes (such as the NLRP3) (57, 58).

In this study, two participants did not reach the minimum titre threshold to be considered protected against HBV infection, even after receiving all three vaccine doses. These individuals were 63 and 72 years of age, placing them in the upper end of the range within our cohort of 15 adults. This implies that immunosenescence (3) may be a contributing factor towards their lack of response to HBV vaccination. To investigate this possibility further, we examined the potential relationship between titre (measured at Day 180) and age acceleration as defined through DNA methylation markers (59–61), and saw no correlation between the two (**Supplementary Figure 4**). It also warrants mention that other participants of equivalent or older age did respond well by the clinical endpoint, indicating that there is likely more than age-related immune changes at play.

One important limitation of our integration paradigm is that, in order to increase statistical power, the information extracted from the data in this manner must be statistically independent, implying a null correlation between sets of identified information. The proposed framework is only attainable if complementary information exists *between* data sets (i.e. flow cytometry, epigenomic, transcriptomic, and proteomic profiling, and fecal 16S rRNA microbiome), and can be extracted with a statistical model that will appropriately aggregate independent information to increase statistical power. Such a requirement may seem to go against the key biological assumption that molecular data are inherently interrelated, i.e. it is believed that they act in unison within biological pathways. However, it remains unclear whether interrelatedness between molecules of different types directly implies statistical correlation (62, 63). The distinct patterns of temporal response across molecular data identified in the current study suggests the underlying biological complexity will be difficult to adequately capture statistically, as e.g. DNA methylation and transcript abundance leading to delayed changes in protein and cell abundances follow different time lines.

In summary, single omics analysis revealed some important signatures and showed trends when contrasting vaccine responder groups. In line with previous studies, our work demonstrated that integrative data analysis across several biological domains can provide a comprehensive view of the

molecular pathways and biological networks important in vaccine responses (14, 64, 65). Importantly, our findings revealed that data integration of pre-immunization multi-omics signatures in a small sample size can predict response to HBV vaccination.

DATA AVAILABILITY STATEMENT

RNA-Seq data was deposited to NCBI's Gene Expression Omnibus (GEO), and is available under GSE155198. The mass spectrometry proteomics data have been deposited to the ProteomeXchange Consortium via the PRIDE partner repository with the dataset identifier PXD020474. Microbiome data is available at the NCBI Short Read Archive (SRA) under accession number PRJNA658597. Flow cytometry data is available at flowRepository with the ID FR-FCM-Z2R9. Epigenetic data has been submitted to GEO and is available under GSE161020.

ETHICS STATEMENT

The studies involving human participants were reviewed and approved by the University of British Columbia Clinical Research Ethics Board. The patients/participants provided their written informed consent to participate in this study.

AUTHOR CONTRIBUTIONS

CS advised on all omics analyses and carried out DIABLO integrative analysis. TB performed RNA-Seq and proteomics bioinformatics analyses. RB-O, TK, and MS recruited patients, collected samples, and coordinated data acquisition. NG and RE performed epigenomic analyses. NA performed microbiome sample processing and analyses. SD performed immune cell phenotyping bioinformatics analysis. QC performed initial screening and processing of proteomics samples. MK performed HBV serology for all participants. LF supervised proteomics sample collection, processing, and analysis. MS supervised epigenomics sample collection, processing, and analysis. WWM supervised microbiome sample collection, processing, and analysis. RB supervised immune cell phenotyping bioinformatics analysis. KL conceived and supervised the DIABLO integrative analysis. RHC supervised data deposition and contributed to conception of the manuscript. ST supervised the DIABLO integrative analysis. RH coordinated RNA-Seq sample collection and processing and supervised the RNA-Seq analysis. WK conceived the study and secured funding. TK and MS conceived the study and secured funding. CS, ST, RH, TK, MS and AL contributed to the conception of the manuscript. AL guided and advised on all omics and integrative analyses. CS, TB, RB-O, NG, NA, SD, LF, WWM, KLC, RH, TK, MS, and AL all contributed to manuscript writing. All authors contributed to the article and approved the submitted version.

FUNDING

We acknowledge funding from the Human Vaccines Project. REWH was the recipient of a UBC Killam Professorship and a Canada Research Chair in Health and Genomics. REWH acknowledges funding from the Canadian Institutes of Health Research (CIHR) [funding reference number FDN-154287]. Mass spectrometry infrastructure used here was funded by the Canada Foundation for Innovation and the BC Knowledge Development Fund. Its operation is supported by Genome Canada and Genome BC (214PRO). NA and WWM were supported by a Project Grant (148781) from the Canadian Institutes for Health Research. MS is supported *via* salary awards from the BC Children's Hospital Foundation, the Canadian Child Health Clinician Scientist Program and the Michael Smith Foundation for Health Research. MS has been an investigator on projects funded by GlaxoSmithKline, Merck, Pfizer, Sanofi-Pasteur, Seqirus, Symvivo and VBI Vaccines. All funds have been paid to his institute, and he has not received any personal payments. KL was supported in part by the National Health and Medical Research Council (NHMRC) Career Development fellowship (GNT1159458). TB, CS, and ST were supported by the National Institute of Health/National Institute of Allergy & Infectious Diseases Human Immunology Project Consortium Grant 5U19AI118608. AL is supported by Simon Fraser University New Faculty Start-up Grant.

SUPPLEMENTARY MATERIAL

The Supplementary Material for this article can be found online at: https://www.frontiersin.org/articles/10.3389/fimmu.2020.578801/full#supplementary-material

REFERENCES

1. Hutin Y, Nasrullah M, Easterbrook P, Nguimfack BD, Burrone E, Averhoff F, et al. Access to Treatment for Hepatitis B Virus Infection - Worldwide, 2016. *MMWR Morb Mortal Wkly Rep* (2018) 67:773–7. doi: 10.15585/mmwr.mm6728a2
2. Meireles LC, Marinho RT, Van Damme P. Three decades of hepatitis B control with vaccination. *World J Hepatol* (2015) 7:2127–32. doi: 10.4254/wjh.v7.i18.2127
3. McElhaney JE, Effros RB. Immunosenescence: what does it mean to health outcomes in older adults? *Curr Opin Immunol* (2009) 21:418–24. doi: 10.1016/j.coi.2009.05.023
4. Banatvala J, Van Damme P, Oehen S. Lifelong protection against hepatitis B: the role of vaccine immunogenicity in immune memory. *Vaccine* (2000) 19:877–85. doi: 10.1016/S0264-410X(00)00224-3
5. Havenar-Daughton C, Lee JH, Crotty S. Tfh cells and HIV bnAbs, an immunodominance model of the HIV neutralizing antibody generation problem. *Immunol Rev* (2017) 275:49–61. doi: 10.1111/imr.12512

6. Schillie SF, Murphy TV. Seroprotection after recombinant hepatitis B vaccination among newborn infants: a review. *Vaccine* (2013) 31:2506–16. doi: 10.1016/j.vaccine.2012.12.012
7. Tsang JS, Dobano C, VanDamme P, Moncunill G, Marchant A, Othman RB, et al. Improving Vaccine-Induced Immunity: Can Baseline Predict Outcome? *Trends Immunol* (2020) 41(6):457–65. doi: 10.1016/j.it.2020.04.001
8. Ben-Othman R, Cai B, Liu AC, Varankovich N, He D, Blimkie TM, et al. Systems Biology Methods Applied to Blood and Tissue for a Comprehensive Analysis of Immune Response to Hepatitis B Vaccine in Adults. *Front Immunol* (2020). doi: 10.3389/fimmu.2020.580373
9. Westerhuis JA, van Velzen EJ, Hoefsloot HC, Smilde AK. Multivariate paired data analysis: multilevel PLSDA versus OPLSDA. *Metabolomics* (2010) 6:119–28. doi: 10.1007/s11306-009-0185-z
10. Liquet B, Le Cao KA, Hocini H, Thiebaut R. A novel approach for biomarker selection and the integration of repeated measures experiments from two assays. *BMC Bioinf* (2012) 13:325. doi: 10.1186/1471-2105-13-325
11. Xia J, Gill EE, Hancock RE. NetworkAnalyst for statistical, visual and network-based meta-analysis of gene expression data. *Nat Protoc* (2015) 10:823–44. doi: 10.1038/nprot.2015.052
12. Zhou G, Soufan O, Ewald J, Hancock REW, Basu N, Xia J. NetworkAnalyst 3.0: a visual analytics platform for comprehensive gene expression profiling and meta-analysis. *Nucleic Acids Res* (2019) 47:W234–41. doi: 10.1093/nar/gkz240
13. Foroushani AB, Brinkman FS, Lynn DJ. Pathway-GPS and SIGORA: identifying relevant pathways based on the over-representation of their gene-pair signatures. *PeerJ* (2013) 1:e229. doi: 10.7717/peerj.229
15. Langenberg MCC, Hoogerwerf MA, Koopman JPR, Janse JJ, Kos-van Oosterhoud J, Feijt C, et al. A controlled human Schistosoma mansoni infection model to advance novel drugs, vaccines and diagnostics. *Nat Med* (2020) 26:326–32. doi: 10.1038/s41591-020-0759-x
14. Lee AH, Shannon CP, Amenyogbe N, Bennike TB, Diray-Arce J, Idoko OT, et al. Dynamic molecular changes during the first week of human life follow a robust developmental trajectory. *Nat Commun* (2019) 10:1092. doi: 10.1038/s41467-019-08794-x
16. Rohart F, Gautier B, Singh A, Le Cao KA. mixOmics: An R package for 'omics feature selection and multiple data integration. *PLoS Comput Biol* (2017) 13: e1005752. doi: 10.1371/journal.pcbi.1005752
17. Singh A, Shannon CP, Gautier B, Rohart F, Vacher M, Tebbutt SJ, et al. DIABLO: an integrative approach for identifying key molecular drivers from multi-omics assays. *Bioinformatics* (2019) 35:3055–62. doi: 10.1093/bioinformatics/bty1054
18. Le Cao KA, Boitard S, Besse P. Sparse PLS discriminant analysis: biologically relevant feature selection and graphical displays for multiclass problems. *BMC Bioinf* (2011) 12:253. doi: 10.1186/1471-2105-12-253
19. Tenenhaus A, Philippe C, Guillemot V, Le Cao KA, Grill J, Frouin V. Variable selection for generalized canonical correlation analysis. *Biostatistics* (2014) 15:569–83. doi: 10.1093/biostatistics/kxu001
20. Kinsella RJ, Kahari A, Haider S, Zamora J, Proctor G, Spudich G, et al. Ensembl BioMarts: a hub for data retrieval across taxonomic space. *Database (Oxford)* (2011) 2011:bar030. doi: 10.1093/database/bar030
21. Weihrauch MR, von Bergwelt-Baildon M, Kandic M, Weskott M, Klamp W, Rosler J, et al. T cell responses to hepatitis B surface antigen are detectable in non-vaccinated individuals. *World J Gastroenterol* (2008) 14:2529–33. doi: 10.3748/wjg.14.2529
22. Moore AR, Willoughby DA. The role of cAMP regulation in controlling inflammation. *Clin Exp Immunol* (1995) 101:387–9. doi: 10.1111/j.1365-2249.1995.tb03123.x
23. Tralau T, Meyer-Hoffert U, Schroder JM, Wiedow O. Human leukocyte elastase and cathepsin G are specific inhibitors of C5a-dependent neutrophil enzyme release and chemotaxis. *Exp Dermatol* (2004) 13:316–25. doi: 10.1111/j.0906-6705.2004.00145.x
24. Simpson-Abelson MR, Hernandez-Mir G, Childs EE, Cruz JA, Poholek AC, Chattopadhyay A, et al. CCAAT/Enhancer-binding protein beta promotes pathogenesis of EAE. *Cytokine* (2017) 92:24–32. doi: 10.1016/j.cyto.2017.01.005
25. Espinoza JA, Jara EL, Kalergis AM. THEMIS, the new kid on the block for T-cell development. *Cell Mol Immunol* (2017) 14:721–3. doi: 10.1038/cmi.2017.34
26. Blackwell JM, Goswami T, Evans CA, Sibthorpe D, Papo N, White JK, et al. SLC11A1 (formerly NRAMP1) and disease resistance. *Cell Microbiol* (2001) 3:773–84. doi: 10.1046/j.1462-5822.2001.00150.x
27. Tani J, Shimamoto S, Mori K, Kato N, Moriishi K, Matsuura Y, et al. Ca(2+) /S100 proteins regulate HCV virus NS5A-FKBP8/FKBP38 interaction and HCV virus RNA replication. *Liver Int* (2013) 33:1008–18. doi: 10.1111/liv.12151
28. Gack MU, Shin YC, Joo CH, Urano T, Liang C, Sun L, et al. TRIM25 RING-finger E3 ubiquitin ligase is essential for RIG-I-mediated antiviral activity. *Nature* (2007) 446:916–20. doi: 10.1038/nature05732
29. Oshiumi H, Miyashita M, Matsumoto M, Seya T. A distinct role of Riplet-mediated K63-Linked polyubiquitination of the RIG-I repressor domain in human antiviral innate immune responses. *PLoS Pathog* (2013) 9:e1003533. doi: 10.1371/journal.ppat.1003533
30. Schumacher MA, Hedl M, Abraham C, Bernard JK, Lozano PR, Hsieh JJ, et al. ErbB4 signaling stimulates pro-inflammatory macrophage apoptosis and limits colonic inflammation. *Cell Death Dis* (2017) 8:e2622. doi: 10.1038/cddis.2017.42
31. Atreya I, Schimanski CC, Becker C, Wirtz S, Dornhoff H, Schnurer E, et al. The T-box transcription factor eomesodermin controls CD8 T cell activity and lymph node metastasis in human colorectal cancer. *Gut* (2007) 56:1572–8. doi: 10.1136/gut.2006.117812
32. Egerton M, Ashe OR, Chen D, Druker BJ, Burgess WH, Samelson LE. VCP, the mammalian homolog of cdc48, is tyrosine phosphorylated in response to T cell antigen receptor activation. *EMBO J* (1992) 11:3533–40. doi: 10.1002/j.1460-2075.1992.tb05436.x
33. Collins S, Wolfraim LA, Drake CG, Horton MR, Powell JD. Cutting Edge: TCR-induced NAB2 enhances T cell function by coactivating IL-2 transcription. *J Immunol* (2006) 177:8301–5. doi: 10.4049/jimmunol.177.12.8301
34. Sandig H, McDonald J, Gilmour J, Arno M, Lee TH, Cousins DJ. Fibronectin is a TH1-specific molecule in human subjects. *J Allergy Clin Immunol* (2009) 124:528–35, 535 e1-5. doi: 10.1016/j.jaci.2009.04.036
35. Zhu X, Xie C, Li YM, Huang ZL, Zhao QY, Hu ZX, et al. TMEM2 inhibits hepatitis B virus infection in HepG2 and HepG2.2.15 cells by activating the JAK-STAT signaling pathway. *Cell Death Dis* (2016) 7:e2239. doi: 10.1038/cddis.2016.146
36. Das D, Sarkar N, Sengupta I, Pal A, Saha D, Bandopadhyay M, et al. Anti-viral role of toll like receptor 4 in hepatitis B virus infection: An in vitro study. *World J Gastroenterol* (2016) 22:10341–52. doi: 10.3748/wjg.v22.i47.10341
37. Kongsbak M, Levring TB, Geisler C, von Essen MR. The vitamin d receptor and T cell function. *Front Immunol* (2013) 4:148. doi: 10.3389/fimmu.2013.00148
38. Kato Z, Jee J, Shikano H, Mishima M, Ohki I, Ohnishi H, et al. The structure and binding mode of interleukin-18. *Nat Struct Biol* (2003) 10:966–71. doi: 10.1038/nsb993
39. Tsutsumi N, Kimura T, Arita K, Ariyoshi M, Ohnishi H, Yamamoto T, et al. The structural basis for receptor recognition of human interleukin-18. *Nat Commun* (2014) 5:5340. doi: 10.1038/ncomms6340
40. Zhang J, Feng H, Zhao J, Feldman ER, Chen SY, Yuan W, et al. IkappaB Kinase epsilon Is an NFATc1 Kinase that Inhibits T Cell Immune Response. *Cell Rep* (2016) 16:405–18. doi: 10.1016/j.celrep.2016.05.083
41. Harashima A, Guettouche T, Barber GN. Phosphorylation of the NFAR proteins by the dsRNA-dependent protein kinase PKR constitutes a novel mechanism of translational regulation and cellular defense. *Genes Dev* (2010) 24:2640–53. doi: 10.1101/gad.1965010
42. Kranzusch PJ, Wilson SC, Lee AS, Berger JM, Doudna JA, Vance RE. Ancient Origin of cGAS-STING Reveals Mechanism of Universal 2',3' cGAMP Signaling. *Mol Cell* (2015) 59:891–903. doi: 10.1016/j.molcel.2015.07.022
43. Bruey JM, Bruey-Sedano N, Luciano F, Zhai D, Balpai R, Xu C, et al. Bcl-2 and Bcl-XL regulate proinflammatory caspase-1 activation by interaction with NALP1. *Cell* (2007) 129:45–56. doi: 10.1016/j.cell.2007.01.045
44. Liu Q, Zhang S, Chen G, Zhou H. E3 ubiquitin ligase Nedd4 inhibits AP-1 activity and TNF-alpha production through targeting p38alpha for polyubiquitination and subsequent degradation. *Sci Rep* (2017) 7:4521. doi: 10.1038/s41598-017-04072-2
45. Fourati S, Cristescu R, Loboda A, Talla A, Filali A, Railkar R, et al. Pre-vaccination inflammation and B-cell signalling predict age-related hyporesponse to hepatitis B vaccination. *Nat Commun* (2016) 7:10369. doi: 10.1038/ncomms10369
46. Boesmans L, Valles-Colomer M, Wang J, Eeckhaut V, Falony G, Ducatelle R, et al. Butyrate Producers as Potential Next-Generation Probiotics: Safety

Assessment of the Administration of Butyricicoccus pullicaecorum to Healthy Volunteers. *mSystems* (2018) 3(6). doi: 10.1128/mSystems.00094-18
47. Lopetuso LR, Scaldaferri F, Petito V, Gasbarrini A. Commensal Clostridia: leading players in the maintenance of gut homeostasis. *Gut Pathog* (2013) 5:23. doi: 10.1186/1757-4749-5-23
48. Furusawa Y, Obata Y, Fukuda S, Endo TA, Nakato G, Takahashi D, et al. Commensal microbe-derived butyrate induces the differentiation of colonic regulatory T cells. *Nature* (2013) 504:446–50. doi: 10.1038/nature12721
49. Citronberg JS, Curtis KR, White E, Newcomb PA, Newton K, Atkinson C, et al. Association of gut microbial communities with plasma lipopolysaccharide-binding protein (LBP) in premenopausal women. *ISME J* (2018) 12:1631–41. doi: 10.1038/s41396-018-0064-6
50. Tsang JS, Schwartzberg PL, Kotliarov Y, Biancotto A, Xie Z, Germain RN, et al. Global analyses of human immune variation reveal baseline predictors of postvaccination responses. *Cell* (2014) 157:499–513. doi: 10.1016/j.cell.2014.03.031
51. Ahrends T, Spanjaard A, Pilzecker B, Babala N, Bovens A, Xiao Y, et al. CD4 (+) T Cell Help Confers a Cytotoxic T Cell Effector Program Including Coinhibitory Receptor Downregulation and Increased Tissue Invasiveness. *Immunity* (2017) 47:848–61.e5. doi: 10.1016/j.immuni.2017.10.009
52. Piovesan D, Giollo M, Ferrari C, Tosatto SC. Protein function prediction using guilty by association from interaction networks. *Amino Acids* (2015) 47:2583–92. doi: 10.1007/s00726-015-2049-3
53. Fleming SB. Viral Inhibition of the IFN-Induced JAK/STAT Signalling Pathway: Development of Live Attenuated Vaccines by Mutation of Viral-Encoded IFN-Antagonists. *Vaccines (Basel)* (2016) 4(3). doi: 10.3390/vaccines4030023
54. Wei XQ, Guo YW, Liu JJ, Wen ZF, Yang SJ, Yao JL. The significance of Toll-like receptor 4 (TLR4) expression in patients with chronic hepatitis B. *Clin Invest Med* (2008) 31:E123–30. doi: 10.25011/cim.v31i3.3469
55. Gonzalez-Navajas JM, Fine S, Law J, Datta SK, Nguyen KP, Yu M, et al. TLR4 signaling in effector CD4+ T cells regulates TCR activation and experimental colitis in mice. *J Clin Invest* (2010) 120:570–81. doi: 10.1172/JCI40055
56. Jain A, Pasare C. Innate Control of Adaptive Immunity: Beyond the Three-Signal Paradigm. *J Immunol* (2017) 198:3791–800. doi: 10.4049/jimmunol.1602000
57. Kagan JC, Iwasaki A. Phagosome as the organelle linking innate and adaptive immunity. *Traffic* (2012) 13:1053–61. doi: 10.1111/j.1600-0854.2012.01377.x
58. Evavold CL, Kagan JC. How Inflammasomes Inform Adaptive Immunity. *J Mol Biol* (2018) 430:217–37. doi: 10.1016/j.jmb.2017.09.019
59. Fahy GM, Busse RT, Watson JP, Dittmar G, Good Z, Vasanawala SS, et al. Reversal of epigenetic aging and immunosenescent trends in humans. *Aging Cell* (2019) 18(6):e13028.
60. Bannister S, Messina NL, Novakovic B, Curtis N. The emerging role of epigenetics in the immune response to vaccination and infection: a systematic review. *Epigenetics* (2020) 15(6-7):555–93.
61. Gensous N, Franceschi C, Blomberg BB, Pirazzini C, Ravaioli F, Gentilini D. Responders and non-responders to influenza vaccination: A DNA methylation approach on blood cells. *Exp Gerontol* (2018) 105:94–100.
62. Schwanhausser B, Busse D, Li N, Dittmar G, Schuchhardt J, Wolf J, et al. Global quantification of mammalian gene expression control. *Nature* (2011) 473:337–42. doi: 10.1038/nature10098
63. van Eijk KR, de Jong S, Boks MP, Langeveld T, Colas F, Veldink JH, et al. Genetic analysis of DNA methylation and gene expression levels in whole blood of healthy human subjects. *BMC Genomics* (2012) 13:636. doi: 10.1186/1471-2164-13-636
64. Ghaemi MS, DiGiulio DB, Contrepois K, Callahan B, Ngo TTM, Lee-McMullen B, et al. Multiomics modeling of the immunome, transcriptome, microbiome, proteome and metabolome adaptations during human pregnancy. *Bioinformatics* (2019) 35:95–103. doi: 10.1093/bioinformatics/bty537
65. Zhou W, Sailani MR, Contrepois K, Zhou Y, Ahadi S, Leopold SR, et al. Longitudinal multi-omics of host-microbe dynamics in prediabetes. *Nature* (2019) 569:663–71. doi: 10.1038/s41586-019-1236-x

Conflict of Interest: The authors declare that the research was conducted in the absence of any commercial or financial relationships that could be construed as a potential conflict of interest.

frontiers in Immunology

ORIGINAL RESEARCH
published: 08 December 2020
doi: 10.3389/fimmu.2020.604413

CD8$^+$ T Cells Directed Against a Peptide Epitope Derived From Peptidoglycan-Associated Lipoprotein of *Legionella pneumophila* Confer Disease Protection

Sun Jin Kim[1], *Jeong-Im Sin*[2] *and Min Ja Kim*[1,3,4]*

[1] Department of Medicine, College of Medicine, Korea University, Seoul, South Korea, [2] Department of Microbiology, School of Medicine, Kangwon National University, Chuncheon, Gangwon-do, South Korea, [3] Division of Infectious Diseases, Department of Internal Medicine, Korea University Anam Hospital, Korea University College of Medicine, Seoul, South Korea, [4] Institute of Emerging Infectious Diseases, Korea University College of Medicine, Seoul, South Korea

OPEN ACCESS

Edited by:
Francesco Borriello,
Harvard Medical School, United States

Reviewed by:
Markus Philipp Radsak
Johannes Gutenberg University
Mainz, Germany
Sylvie Fournel,
Université de Strasbourg, France

***Correspondence:**
Min Ja Kim
macropha@korea.ac.kr

Specialty section:
This article was submitted to Vaccines and Molecular Therapeutics, a section of the journal Frontiers in Immunology

Received: 09 September 2020
Accepted: 06 November 2020
Published: 08 December 2020

Citation:
Kim SJ, Sin JI and Kim MJ (2020) CD8$^+$ T Cells Directed Against a Peptide Epitope Derived From Peptidoglycan-Associated Lipoprotein of Legionella pneumophila Confer Disease Protection. Front. Immunol. 11:604413. doi: 10.3389/fimmu.2020.604413

Legionella pneumophila, an intracellular bacterium, may cause life-threatening pneumonia in immunocompromised individuals. Mononuclear cells and antibodies have been reported to be associated with the host defense response against *L. pneumophila*. This study is to determine whether *Legionella* peptidoglycan-associated lipoprotein (PAL)-specific CD8$^+$ T cells are directly associated with protection against *L. pneumophila*, with a focus on potential epitopes. Synthetic peptides derived from PAL of *L. pneumophila* were obtained and tested through in *vitro* and *in vivo* cytotoxic T lymphocyte (CTL) assays for immunogenicity. PAL DNA vaccines or a peptide epitope with or without CpG-oligodeoxynucleotides (ODN) was evaluated for protection against *L. pneumophila* infection in animal models. When mice were immunized with DNA vaccines expressing the PAL of *L. pneumophila*, they were significantly protected against a lethal challenge with *L. pneumophila* through induction of antigen-specific CD8$^+$ CTLs. Of the 13 PAL peptides tested, $PAL_{92\text{-}100}$ (EYLKTHPGA) was the most immunogenic and induced the strongest CTL responses. When mice were immunized with the $PAL_{92\text{-}100}$ peptide plus CpG-ODN, they were protected against the lethal challenge, while control mice died within 3–6 days after the challenge. Consistent with lung tissue histological data, bacterial counts in the lungs of immunized mice were significantly lower than those in control mice. Also, the amino acid sequence of $PAL_{92\text{-}100}$ peptides is conserved among various *Legionella* species. To our knowledge, this study is the first to demonstrate that $PAL_{92\text{-}100}$-specific CD8$^+$ T cells play a central role in the host defense response against *L. pneumophila*.

Keywords: *Legionella pneumophila*, peptidoglycan-associated lipoprotein, peptide epitope, cytotoxic T-lymphocyte, adaptive immunity

INTRODUCTION

Legionella pneumophila is the causative pathogen of a severe form of pneumonia, Legionnaires' disease, with high mortality and morbidity. The *L. pneumophila* bacterium is a Gram-negative facultative intracellular pathogen, which is commonly found in the natural environment and in immunocompromised individuals (1–4). Whether sporadic, epidemic, nosocomial, or community-acquired, Legionnaires' disease can be deadly, especially among patients with reduced immune competence. *L. pneumophila* enters the human respiratory tract as a result of inhalation of aerosols from a contaminated water source, and thereafter infects human alveolar macrophage and lung epithelial cells (5–8).

Cell-mediated immunity, but not humoral immunity, appears to play an important role in the host defense response against *L. pneumophila* (9–11). In human studies, activated mononuclear cells inhibited the intracellular multiplication of *L. pneumophila* (9, 11). Moreover, alveolar macrophages were suggested to be an effector cell acting to inhibit bacterial multiplication (11). In animal models, antibodies were also associated with protection during early stages of airway infection (12). Similarly, immunization with *L. pneumophila* membranes resulted in induction of strong cellular immune responses and protective immunity against a lethal challenge with *L. pneumophila* (13). In addition, the major secretory and outer membrane proteins of *L. pneumophila* were reported to be effective at inducing protective immunity against *L. pneumophila* (14, 15).

The 19-kDa peptidoglycan-associated lipoprotein (PAL) is an outer membrane lipoprotein that is conserved among various *Legionella* species; in 1991, PAL was sequenced and characterized as the most prominent *Legionella* surface antigen (16). As PAL has been found in the urine of infected patients, it has also been used as a diagnostic antigen for legionellosis (17, 18). PAL activates murine macrophages through Toll-like receptor (TLR) 2-mediated signaling, which stimulates the released of pro-inflammatory cytokines, such as IL-6 and TNF-α (19). Immunization with a full-length 528-bp *pal* gene vaccine induced IFN-γ and IL-2 production from spleen cells, as well as potent cytotoxic T lymphocyte (CTL) responses (20). Recombinant PAL (rPAL) also induced protective immunity against *L. pneumophila* infection (21). Together, the results of these studies suggest that PAL may be a potential vaccine target for prevention of *L. pneumophila* infection. In our animal study, PAL DNA and rPAL vaccines induced antigen-specific antibody and CTL responses (20). However, it is still unclear whether PAL-specific antibody or the $CD8^+$ CTL response is mainly responsible for protecting animals from *Legionella* infection.

In this study, we demonstrated that PAL-specific $CD8^+$ CTLs were responsible for protection from infection with *L. pneumophila*. Among 13 peptide candidates derived from the *L. pneumophila* PAL, one peptide ($PAL_{92\text{-}100}$) was recognized by PAL-specific $CD8^+$ T cells. Immunization with the $PAL_{92\text{-}100}$ peptide resulted in the induction of antigen-specific $CD8^+$ CTL responses, improved survival, and reduced lung bacterial burden after *L. pneumophila* infection. Thus, this study clearly demonstrates that $PAL_{92\text{-}100}$-specific $CD8^+$ CTLs mediate anti-*Legionella* protective immunity, and that peptides containing a well-conserved PAL epitope may be effective vaccines against various *Legionella* species.

MATERIALS AND METHODS

Prediction of Class I MHC Binding Epitopes

Peptides derived from the PAL of *L. pneumophila* serogroup 1 were designed using three Class I MHC binding molecule prediction programs, RANKPEP (http://bio.dfci.harvard.edu/RANKPEP), BIMAS (http://bimas.cit.nih.gov), and SYFPEITHI (http://syfpeithi.de). The programs were used to predict the binding activity of each peptide to Class I MHC haplotypes from BALB/c mice. The following selection criteria were used. First, 9-mer sequences with a high Class I MHC binding score were pre-selected from the full-length *Legionella* PAL sequence. Next, the peptides with the best Class I MHC binding scores were selected from within the entire sequence and were ranked according to the Class I MHC binding score for each online algorithm. Finally, the results from all algorithms were combined (consensus prediction).

Synthetic Peptides

The PAL peptides were synthesized by Sigma-Aldrich (St. Louis, MO, USA) and PEPTRON (Daejeon, Korea). The purity of peptide was synthesized to over 90%. The synthetic peptide amino acid sequences were as follows: $PAL_{1\text{-}9}$ (MKAGSFYKL: P1), $PAL_{4\text{-}24}$ (GSFYKLGLLVASAVLVAACS: P2), $PAL_{37\text{-}47}$ (DGDATAQGL: P3), $PAL_{55\text{-}63}$ (EPGESYTTQ: P4), $PAL_{65\text{-}73}$ (PHNQLYLFA: P5), $P_{76\text{-}84}$ (DSTLASKYL: P6), $PAL_{86\text{-}94}$ (SVNAQAEYL: P7), $PAL_{92\text{-}100}$ (EYLKTHPGA: P8), $PAL_{97\text{-}105}$ (HPGARVMIA: P9), $PAL_{112\text{-}119}$ (GSREYNVA: P10), $PAL_{124\text{-}132}$ (RADTVAEIL: P11), $PAL_{135\text{-}147}$ (AGVSRQQIRVVSY: P12), $PAL_{163\text{-}171}$ (AQNRRVEFI: P13), as shown in **Table 1**.

Bacteria

L. pneumophila strain Philadelphia-1 (ATCC 33152), an isolate from the lung tissue of a Legionnaires' disease patient from

TABLE 1 | Predicted MHC class I-restricted peptides derived from peptidoglycan-associated lipoprotein of *Legionella pneumophila*.

Peptide No.	Position	Peptide Sequence	Haplotype
P1	$PAL_{1\text{-}9}$	MKAGSFYKL	H-2L^d
P2	$PAL_{4\text{-}24}$	GSFYKLGLLVASAVLVAACSK	H-2L^d
P3	$PAL_{37\text{-}45}$	DGDATAQGL	H-2D^d
P4	$PAL_{55\text{-}63}$	EPGESYTTQ	H-2D^d
P5	$PAL_{65\text{-}73}$	PHNQLYLFA	H-2L^d
P6	$PAL_{76\text{-}84}$	DSTLASKYL	H-2L^d
P7	$PAL_{86\text{-}94}$	SVNAQAEYL	H-2L^d
P8	$PAL_{92\text{-}100}$	EYLKTHPGA	H-2K^d
P9	$PAL_{97\text{-}105}$	HPGARVMIA	H-2L^d
P10	$PAL_{112\text{-}119}$	GSREYNVA	H-2L^d
P11	$PAL_{124\text{-}132}$	RADTVAEIL	H-2K^d
P12	$PAL_{135\text{-}147}$	AGVSRQQIRVVSY	H-2K^d
P13	$PAL_{163\text{-}171}$	AQNRRVEFI	H-2D^d

Philadelphia, Pennsylvania (32), was tested in this study. Bacteria were cultured from frozen stock on buffered charcoal yeast extract (BCYE-α) agar plates supplemented with L-cysteine, ferric pyrophosphate, and α-ketoglutaric acid, incubated at 37°C with 5% CO_2 for 72 h. The bacteria were maintained at –80°C before use in infection.

Experimental Animals

Female BALB/c (H-2^d) mice, 6 to 8 weeks of age, were purchased from Oriental Bio Inc. (Chungbuk, Korea).

Immunization of Mice

Mice were immunized with PAL plasmid DNAs (pcDNA3-PAL) (20) or synthetic PAL peptides. For DNA immunization, 100 μg of pcDNA3-PAL was injected into the tibialis anterior muscle of both legs and the mice received booster injections at the same dose at 1-week intervals. For synthetic peptide immunization, mice were immunized subcutaneously (s.c.) with 20 μg of PAL peptides plus 20 μg of CpG-oligodeoxynucleotide (ODN) in 100 μl of phosphate-buffered saline (PBS). They mice received booster injections at the same dose at 1-week intervals. The CpG-ODN (5'-TCCATGACGTTCCTGACGTT-3') containing a phosphorothioate backbone was purchased from GenoTech, Daejeon, Korea.

In Vivo Depletion of $CD8^+$ T Cells

Anti-CD8 IgGs (100 μg) were injected intraperitoneally (i.p.) into mice on the indicated days. A hybridoma cell line (clone 2.43) was purchased from the American Type Culture Collection (Manassas, VA, USA), and anti-CD8 IgGs were purified as previously described (22). Control IgGs were purchased from Sigma-Aldrich (St. Louis, MO, USA). Anti-CD8 IgG administration resulted in more than 98% depletion of $CD8^+$ T cell at 3–5 days following antibody treatment.

Measurement of Cytokine Production

Cytokine (IFN-γ and TNF-α) concentrations were measured by ELISA. The splenocytes were incubated at 37°C with/without antigens. Cytokine concentrations in the cell culture supernatants were measured using IFN-γ (BD Biosciences, San Jose, CA, USA) and TNF-α (BioLegend, San Diego, CA, USA) ELISA kits according to the manufacturer's instructions. The analyses were completed in triplicate, and cytokine concentrations were calculated by regression analyses of a standard curve.

In Vitro CTL Assay

Splenocytes were collected 1 week after the final immunization and mixed with 2×10^6 naive splenocytes that had been previously treated with mitomycin C and cultured in the presence of P8 peptides (5 μg/ml) in a 24-well plate for 5 days at 37°C. The cells were washed twice with complete RPMI 1640 and then used as effector cells. Syngeneic naive splenocytes were prepared by adsorption of P8 peptides (5 μg/ml) and rPAL (5 μg/ml) for 3 days at 37°C, washed three times with complete RPMI 1640, and resuspended at a concentration of 5×10^6 cells per ml for use as target cells. The pulsed target (T) cells (1×10^4 cells/well) were added to a 96-well plate, and effector cells (E) were then added a E:T ratios of 50:1, 30:1, or 10:1. After incubation for 4 h, antigen-specific lysis was measured using the CytoTox 96® Non-Radioactive Cytotoxic Assay (Promega, Madison, WI, USA) in accordance with the manufacturer's instructions. The percent specific lysis was calculated as follows: % specific lysis = 100 × (experimental – spontaneous) / (maximal – spontaneous).

In Vivo CTL Assay

Splenocytes from naïve mice were incubated with 5 μg/ml of P8 peptides at 37°C for 90 min. They were prepared by being divided into two tubes containing 2×10^7 cells/ml in RPMI-1640 with 2.5% FBS, and the fluorescent carboxylfluorescein diacetate succinimidyl ester (CFSE) dye (BD Bioscience) added at 2.5 μM ($CFSE^{low}$) or 20 μM ($CFSE^{high}$), then the cells were resuspended and incubated at 37°C for 40 min. The stained cells were washed two times with PBS. Each mouse received an intravenous injection of a mixture of 1×10^7 $CFSE^{low}$ and 1×10^7 $CFSE^{high}$ cells in a total volume of 200 μl of RPMI 1640 without serum. After 18 h, mice were sacrificed in a CO_2 chamber, and the spleens were removed and processed for flow cytometry. The percent lysis was calculated as $[100 \times (1 - [\gamma_{unprimed}/\gamma_{primed}])]$. The γ (ratio) was calculated as $\%CFSE^{low}/\%CFSE^{high}$.

Intravenous and Intranasal Challenges With *L. pneumophila*

Mice were challenged intravenously (i.v.) with 100 μl of a bacterial suspension containing 2×10^7 CFU of *L. pneumophila*. Mice were also challenged intranasally (i.n.) with 40 μl of bacterial suspension containing 1×10^9 CFU of *L. pneumophila*. In this case, mice were administered cyclophosphamide (75 mg/kg or 150 mg/kg) every day for 3 days prior to intranasal challenge. The approximate number of bacteria was estimated by measuring the absorbance at 600 nm (1 OD value at 600 nm was assumed as 1×10^9 CFU/ml). Survival of infected mice was assessed daily for 10–14 days following the bacterial challenge. Percent survival was calculated as [the number of dead mice/the number of all tested mice × 100].

Bacterial Burden Assay

Mice were challenged i.n. with *L. pneumophila*. Forty-eight hours after the challenge, the mice were sacrificed and the lungs removed and homogenized in sterile PBS using a tissue homogenizer (Pyrex Corning, Greencastle, PA, USA). Ten-fold serial dilutions of the lung homogenates were plated on BCYE-α agar containing cefamandole, polymyxin B, and vancomycin. The bacteria were cultured for 72 to 96 h at 37°C in 5% CO_2 for determination of the number of viable *L. pneumophila*.

Histological Analyses

After an intranasal challenge with *L. pneumophila*, mice were sacrificed and the lungs were harvested for histopathologic measurements. Mouse lungs were fixed using 4% paraformaldehyde for 48 h, dehydrated, and embedded in paraffin. The sections (3 μm) were stained with hematoxylin and eosin (H&E) to visualize inflammatory cells infiltrating the lungs.

Statistical Analyses

All statistical analyses were performed by one-way analysis of variance (ANOVA) with *post-hoc* Dunnett's test and chi-square test (Fisher's exact test) using the SPSS13.0 program. Unless noted, ANOVA was used. The values of the experimental groups were compared with the values of the control group. Any p values <0.05 were considered to be significant.

RESULTS

Major Roles of CD8$^+$ T Cells in Protection From *L. pneumophila* Infection and Identification of the Class I MHC Epitopes

We previously reported that both PAL DNA and rPAL vaccines induce antigen-specific antibody and CTL responses (20). It was also reported that rPAL confers protective immunity against a lethal dose of *L. pneumophila* challenge (21). In this study, we used the PAL DNA vaccine model to determine whether CD8$^+$ T cells were responsible for protection from a lethal challenge with *L. pneumophila*. For this test, animals were immunized with PAL DNA vaccines and challenged i.v. with *L. pneumophila*, in the presence of CD8$^+$ T cell depletion (**Figure 1A**). After the lethal challenge, 50% of control mice immunized with PAL DNA vaccines survived, however, survival rates of mice depleted of CD8$^+$ T cells were 0%, similar to naïve control mice (**Figure 1B**). This result suggests that CD8$^+$ T cells are indeed responsible for protection against *L. pneumophila*. Next, we determined which peptides of PAL proteins might be recognized by PAL-specific CD8$^+$ T cells. For these experiments, we predicted CD8$^+$ T cell-specific epitopes from 176 amino acid residues of the full-length *pal* gene of *L. pneumophila* using three Class I MHC binding molecule prediction programs (RANKPEP, BIMAS, and SYFPEITHI software). The peptides were selected based upon their binding affinity for the Class I MHC haplotypes (H-2L^d, H-2D^d, H-2K^d) of BALB/c mice and their amino acid length (a 9-mer). To this end, we obtained 13 peptides with a high Class I MHC binding scores, among which 11 peptides were 9-mers while two others, PAL$_{4\text{-}24}$ (P2) and PAL$_{135\text{-}147}$ (P12), had more than nine amino acids (**Table 1**). To determine which peptides might be recognized by PAL-specific CD8$^+$ T cells, we used each of the 13 peptides to stimulate spleen cells (containing PAL-specific CD8$^+$ T cells) from mice immunized with PAL plasmid DNAs. The IFN-γ concentrations in the cell culture supernatants were assessed. As seen in **Figure 2A**, P8 peptides induced the greatest IFN-γ production among the peptides tested. The other 12 peptides showed some or little induction of IFN-γ production. To confirm this result, we again stimulated the immune cells with an increasing dose of P8 peptides in parallel with P10 peptides as a control. As shown in **Figure 2B**, P8 peptides increased IFN-γ production in a concentration-dependent fashion, as opposed to P10 peptides which induced little IFN-γ production. Therefore, these results reveal that PAL-specific CD8$^+$ T cells can recognize the P8 (PAL$_{92\text{-}100}$) peptide in conjunction with Class I MHC molecules expressed on the cells from BALB/c mice.

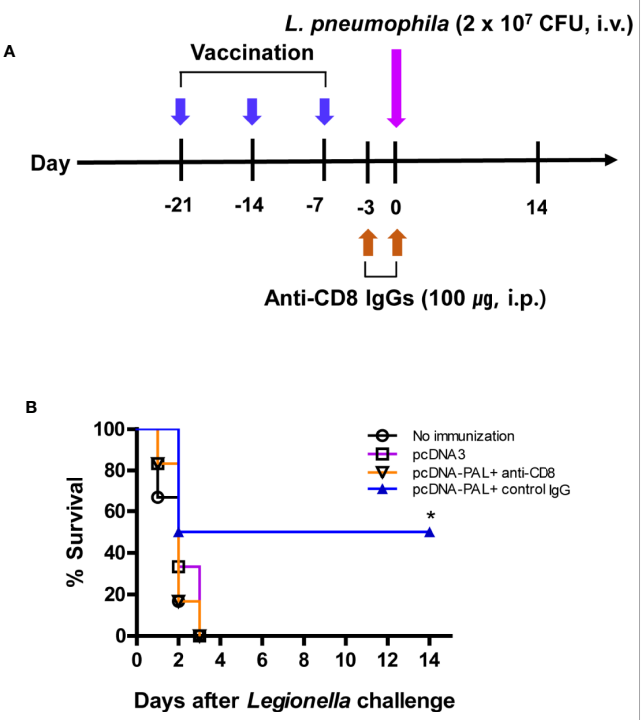

FIGURE 1 | PAL DNA vaccination, CD8+ T cell depletion, and survival of mice after lethal challenge with *L. pneumophila*. **(A)** Schematic diagram showing PAL DNA vaccination, CD8+ T cell depletion, and bacterial challenge. Each group of mice (n = 6/group) was immunized intramuscularly with 100 μg of pcDNA3-PAL at 0, 1, and 2 weeks. At 3 weeks, the mice were challenged intravenously (i.v.) with *L. pneumophila* at 2 × 10^7 CFU per mouse. For depletion of CD8+ T cell subsets, the animals were injected with 100 μg of anti-CD8 antibody and control IgGs on days –3 and 0 of bacterial challenge. **(B)** Percent survival. Surviving animals from bacterial challenge were counted at the indicated time points.

In Vitro and *In Vivo* CTL Responses to P8 Peptides

To investigate whether P8 (PAL$_{92\text{-}100}$) peptides might increase PAL-specific CTL populations, we immunized mice with PAL DNA vaccines and obtained the spleen cells, which were stimulated *in vitro* with P8 peptides. These cells were used as effector cells against target cells primed with either P8 peptides or rPAL in an *in vitro* CTL assay. As shown in **Figure 2C**, a significantly greater degree of CTL activity was directed toward target cells that had been primed with P8 and rPAL, as compared to unprimed control target cells. In particular, CTL activity toward target cells that had been primed with P8 was 11% greater than for target cells primed with rPAL at an effector to target cell ratio of 50:1 (51% for P8 *vs.* 40% for rPAL). This result suggests that as an antigen, P8 (PAL$_{92\text{-}100}$) peptide can stimulate PAL-specific CD8$^+$ CTL cell populations, thereby enhancing their target cell killing activity *in vitro*. Next, we evaluated whether P8 peptides could induce antigen-specific CTL responses *in vivo*. As seen in **Figure 2D,** the groups of mice immunized with P8 plus CpG-ODN had dramatically greater CTL lytic activity than those immunized with either the P8

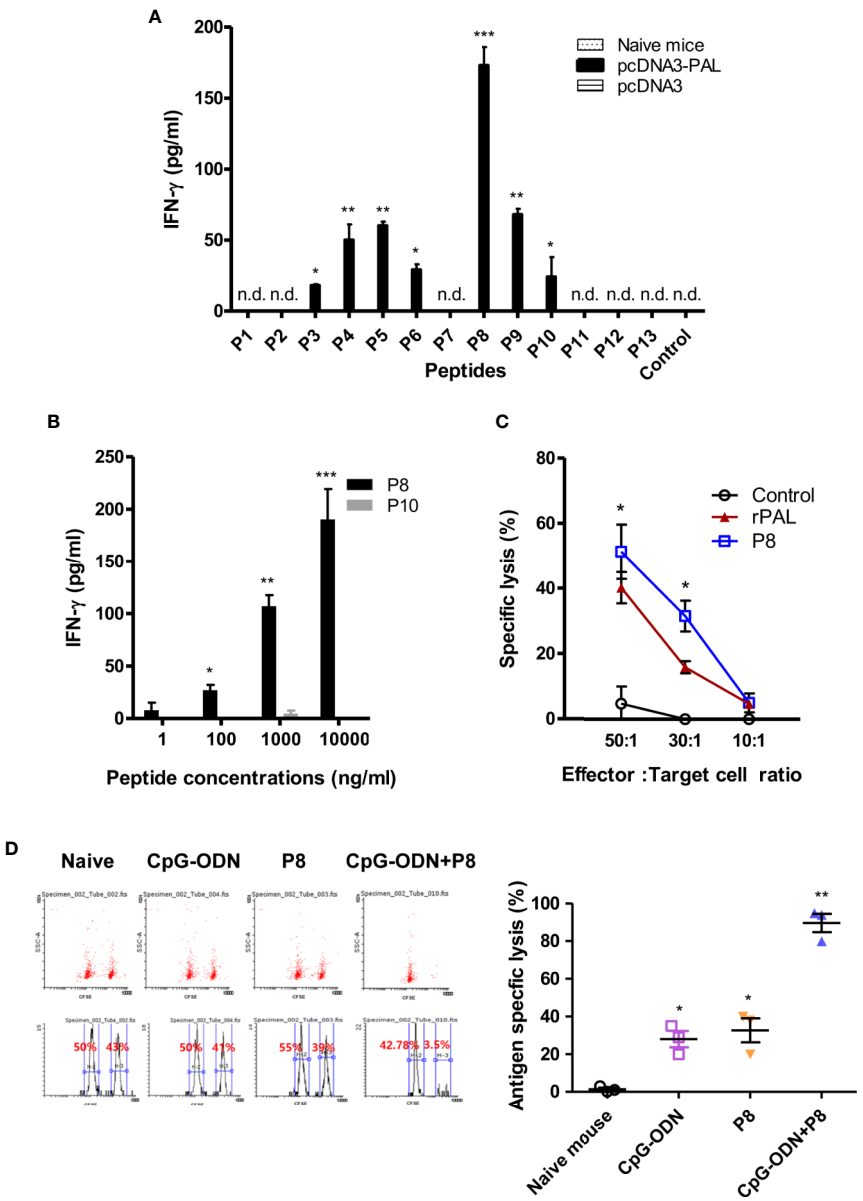

FIGURE 2 | IFN-γ and CTL responses to PAL peptides. **(A)** To determine which peptides were able to induce IFN-γ production from PAL-specific spleen cells, mice were immunized with pcDNA3-PAL at 0, 1, and 2 weeks. At 3 weeks, the mice were sacrificed and the spleens were harvested. Six × 10^6 splenocytes were stimulated for 2 days at 37°C with each of 13 peptides (P1–P13) at a final concentration of 5 μg/ml. The cell culture supernatants were collected and IFN-γ concentrations measured. n.d. (not detectable). *$p < 0.05$ compared to control, **$p < 0.05$ compared to P6, ***$p < 0.05$ compared to P9. **(B)** We repeated the above experiments, except that the splenocytes were stimulated with P8 or P10 (as a control) at final concentrations of 1, 200, 1,000, or 10,000 ng/ml. *$p < 0.05$ compared to 1 ng/ml, **$p < 0.05$ compared to 100 ng/ml, ***$p < 0.05$ compared to 1,000 ng/ml. **(C)** Mice were immunized and the spleens were obtained as above. *In vitro* lytic activity was measured using the splenocytes as effector cells and syngeneic targets (primed with P8 or rPAL) in the LDH release cytotoxicity assay, as described in the *Methods and Materials*. *$p < 0.05$ compared to control. **(D)** A CFSE-based cytotoxicity assay was performed to measure *in vivo* lytic activity, as described in the *Methods and Materials*. Cells with low and high density CFSE staining were gated and the CFSE intensity, as assessed by flow cytometry, was plotted. One representative result (% lysis) is shown. The values and bars represent mean IFN-γ concentrations and percent lysis and the SDs, respectively. *$p <$ 0.05 compared to naïve mouse, **$p < 0.05$ compared to CpG-ODN or P8.

peptide or CpG-ODN alone. For example, P8-plus-CpG-ODN-immunized animals displayed 98% lytic activity. However, control mice and the groups immunized with either P8 or CpG-ODN alone had similar lytic activity (**Figure 2D**). In this study, a TLR9 agonist CpG-ODN was used as a peptide vaccine adjuvant. It has been reported that CpG-ODN elicits antigen-specific CTL responses when co-injected with proteins or peptides (as an immunogen) (23, 24). Collectively, these data indicate that the P8 (PAL_{92-100}) peptide can induce and stimulate antigen-specific $CD8^+$ CTL responses *in vitro* and *in vivo*.

Survival of Mice Immunized With P8 Plus CpG-ODN After Lethal Intravenous or Intranasal Challenge With *L. pneumophila*

To investigate whether P8 (PAL_{92-100}) peptides improve survival after *Legionella* infection, we immunized mice with P8 plus CpG-ODN, followed by a lethal intravenous challenge with 2×10^7 CFU of *L. pneumophila*. As seen in **Figure 3A**, the mouse groups immunized with P8 plus CpG-ODN had 100% survival after the lethal challenge, while the mouse groups immunized with either P8 or CpG-ODN alone, as well as naïve control groups, died within 3 days after the challenge. *L. pneumophila* infects humans through the respiratory tract and most frequently causes disease in immunosuppressed patients (5, 6). Therefore, we evaluated the protective efficacy of P8 peptides against bacterial infection when immunosuppressed animals were challenged i.n. with *L. pneumophila*. Cyclophosphamide has been used previously to render animals immunosuppressed and more susceptible to challenge with *L. pneumophila* (25). Cyclophosphamide is an alkylating chemotherapeutic agent, and as a cytotoxic drug has immunosuppressive effects (26, 27). In addition, lymphocyte counts were reported to reach a nadir four days after treatment with 150 mg/kg of cyclophosphamide (28). In consideration of these findings, immunized mice were administered a low (75 mg/kg of body weight) or high (150 mg/kg of body weight) dose of cyclophosphamide prior to intranasal challenge with *L. pneumophila*. When the groups immunized with P8 plus CpG-ODN were administered 75 mg/kg of cyclophosphamide, 85.7% of mice were alive 14 days after the intranasal challenge (1×10^9 CFU per mouse; **Figure 3B**). However, the mouse groups immunized with either P8 or CpG-ODN alone, as well as the naïve control group died within 6 days after the challenge. When the groups immunized with P8 plus CpG-ODN were treated with 150 mg/kg of cyclophosphamide, 75% of mice were alive 14 days after the intranasal challenge (**Figure 3C**). However, the mouse groups immunized with either P8 or CpG-ODN alone, as well as naïve control groups died within 4 days after the challenge. Taken together, these data suggest that P8 (PAL_{92-100}) peptides can induce resistance to *Legionella* infection in mice, with 75–100% survival, even in immunosuppressed animals after otherwise lethal infection with *L. pneumophila*.

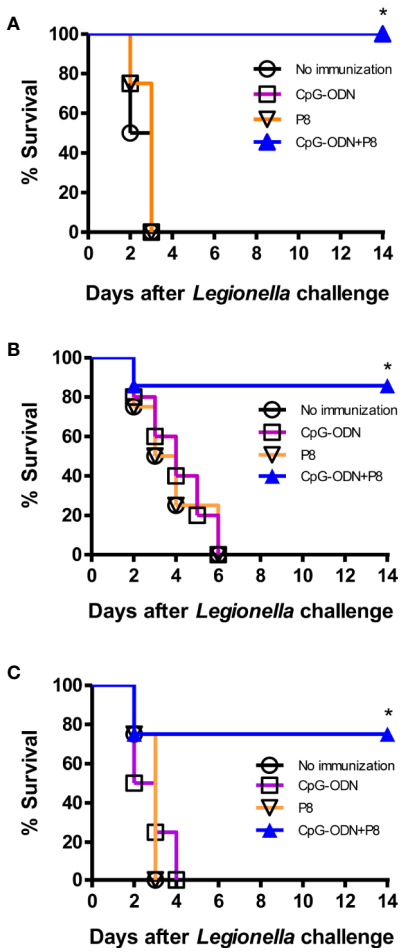

FIGURE 3 | Survival of mice immunized with P8 plus CpG-ODN prior to lethal intravenous or intranasal challenge with *L. pneumophila*. **(A)** Each group of mice (n = 4/group) was immunized s.c. with P8 plus CpG-ODN at 0, 1, and 2 weeks. At 3 weeks, the mice were challenged i.v. with *L. pneumophila* at 2×10^7 CFU per mouse. Surviving mice were counted at the indicated time points. **(B, C)** Each group of mice (n = 7 per group) was immunized as above. At 3 weeks, the mice were treated i.p. with 75 mg/kg **(B)** or 150 mg/kg **(C)** of cyclophosphamide every day for 3 days. The next day, the mice were challenged i.n. with *L. pneumophila* at 1×10^9 CFU per mouse. Surviving mice were counted at the indicated time points. *$p < 0.05$ using Chi-square test compared to non-immunization.

Bacterial Burdens in the Lungs of Mice Immunized With P8 Plus CpG-ODN and Cytokine Production by Spleen Cells After a Lethal Challenge With *L. pneumophila*

We next tested whether P8 (PAL_{92-100}) peptides might be able to reduce the bacterial burden in the lungs after *Legionella* infection. For this test, animals were immunized with P8 plus CpG-ODN, and challenged i.v. with *L. pneumophila*. As seen in **Figure 4A**, bacterial counts in the lung tissues of P8+CpG-ODN-immunized mice were reduced approximately 200-fold compared to control groups (naïve control and mice immunized with either P8 or CpG-ODN). A similar result was obtained when mice were challenged i.n. with *L. pneumophila* in the presence of immune suppression due to cyclophosphamide administration (150 mg/kg; **Figure 4B**). These findings are consistent with survival rates we observed previously. It is likely that the reduction in bacteria counts is mediated by antigen-specific $CD8^+$ CTLs that are elicited by immunization with P8 plus CpG-ODN. We also measured IFN-γ and TNF-α production of the spleen cells from immunized mice administered cyclophosphamide (150 mg/kg). As seen in **Figures 4C, D**, spleen cells from the mice immunized with P8 plus CpG-ODN produced significantly more IFN-γ (C) and TNF-α (D) than cells from mice immunized with either P8 or CpG-ODN, as well as negative control mice producing a basal level of cytokines. It is notable that this cytokine production was measured in the absence of any antigen stimulation *in vitro*, suggesting that the cytokines were likely released from PAL_{92-100}-

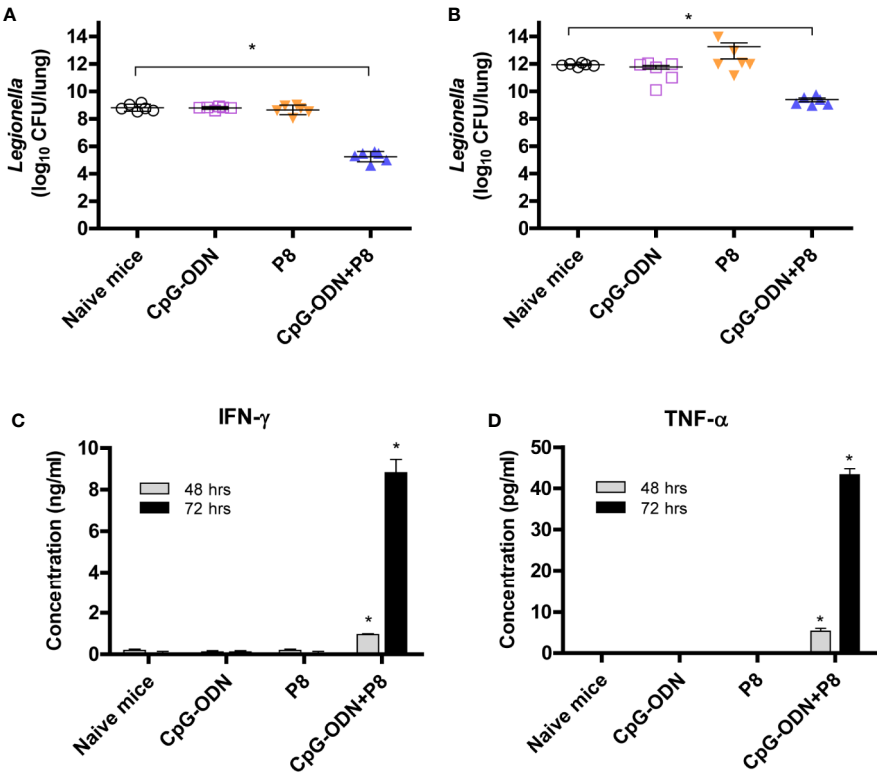

FIGURE 4 | Both bacterial burden and cytokine induction in spleen cells of mice after lethal intravenous or intranasal challenge with *L. pneumophila*. **(A)** Each group of mice (n = 6/group) was immunized s.c. with P8 plus CpG-ODN at 0, 1, and 2 weeks. At 3 weeks, the mice were challenged i.v. with *L. pneumophila* at 2 × 10^7 CFU per mouse. The mice were sacrificed 48 h post-challenge, the lungs were harvested, and the number of viable bacteria in the lung tissues was determined. **(B)** Each group of mice (n = 6/group) was immunized as above. At 3 weeks, the mice were administered 150 mg/kg of cyclophosphamide i.p. every day for 3 days. The next day, the mice were challenged i.n. with 1 × 10^9 CFU of *L. pneumophila*. The mice were sacrificed 48 h post-challenge, the lungs were removed, and viable bacteria from the lung tissue were counted. **(C, D)** Each group of mice (n = 3/group) was immunized and administered cyclophosphamide, as described in panel B. The mice were sacrificed 16 h following the intranasal challenge and the spleens removed. The splenocytes were stimulated *in vitro* for 48–72 h at 37°C and the cell supernatants were collected for measurement of IFN-γ **(C)** and TNF-α **(D)**. *p < 0.05 compared to naïve mice.

specific spleen cells under stimulation with prior intranasal exposure to *L. pneumophila*. Therefore, these results demonstrate that P8 ($PAL_{92\text{-}100}$) peptides can induce cytokine responses even in immunosuppressed animals.

Histological Analyses of Mouse Lung Tissues After *L. pneumophila* Infection

To compare histological changes in the lungs of mice immunized with P8 ($PAL_{92\text{-}100}$) plus CpG-ODN following infection with *L. pneumophila*, the lungs were harvested and stained with H&E. Hemorrhage, destruction of alveolar tissue, hyperplasia of alveolar walls, interstitial edema, and infiltration of numerous inflammatory cells were evident in lung tissues from the control group and groups immunized with either P8 or CpG-ODN alone (**Figure 5**). However, significant reductions in inflammatory infiltration in alveolar and interstitial space were noted in the groups immunized with P8 plus CpG-ODN. These data suggest that animals immunized with P8 plus CpG-ODN alone can protect against lung tissue damage resulting from infection with *L. pneumophila*.

Presence of Conserved P8 Peptide Region in the PAL of *Legionella* Species

To determine if the P8 ($PAL_{92\text{-}100}$) peptide sequences of PAL proteins were similar among 20 *Legionella* species, we used the multiple alignment sequence program, CLUSTALW. As shown in **Figure 6**, the $PAL_{92\text{-}100}$ peptide sequence was located in a conserved region in the PAL sequence of *L. pneumophila* and the genus *Legionella*, including *L. pneumophila* (ATCC 33152), *L. sainthelensi* (ATCC 33152), *L. parisiensis* (ATCC 35299), *L. moravica* (ATCC 43877), *L. shakespearei* (ATCC 49655), *L. gratiana* (ATCC 49413), *L. longbeachae* serogroup 1 (ATCC 33462), *L. dumoffii* (ATCC 33279), *L. wadsworthii* (ATCC 33877), *L. gormanii* (ATCC 33297), *L. anisa* (ATCC 35292), *L. bozemanii* serogroup 1 (ATCC 33217), *L. bozemanii* serogroup 2 (ATCC 35745), *L. longbeachae* serogroup 2 (ATCC 33484), *L. maceachemii* (ATCC 35300), *L. jordanis* (ATCC 33623), *L. heckeliea* serogroup 2 (ATCC 35999), *L. heckeliea* serogroup 1 (ATCC 35250), *L. lansingesis* (ATCC 49751), and *L. nautarum* (ATCC 49506). In this alignment, there was 100% homology in

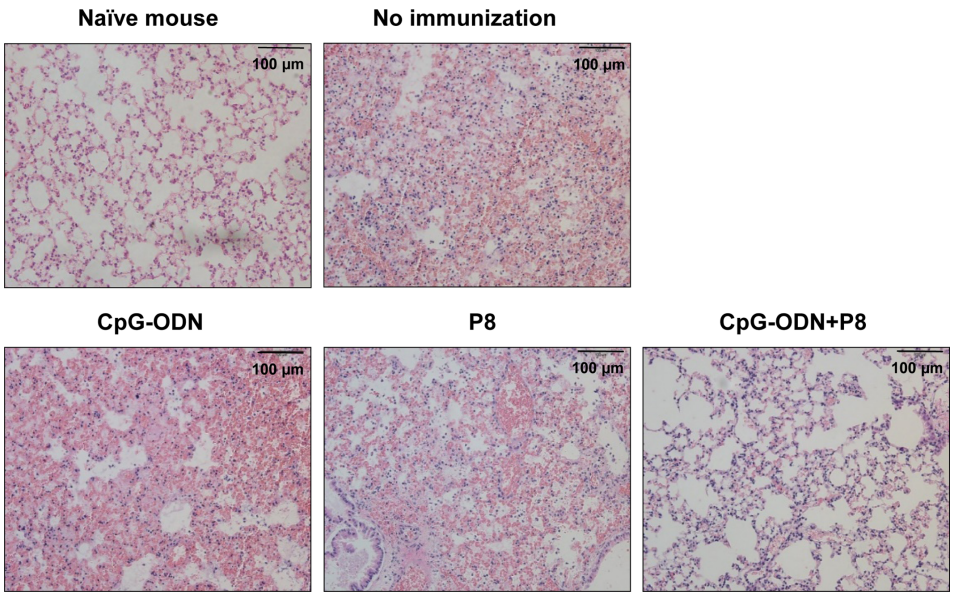

FIGURE 5 | Histopathology of the lungs of mice challenged with a lethal dose of *L. pneumophila*. Each group of mice (n = 3/group) was immunized s.c. with P8 plus CpG-ODN at 0, 1, and 2 weeks. At 3 weeks, the mice were treated i.p. with 150 mg/kg of cyclophosphamide every day for 3 days. Next day, the mice were challenged i.n. with 1×10^9 CFU of *L. pneumophila*. Upon animal death after the challenge, the lungs were removed from the mice and the lung tissues were sectioned, followed by staining with hematoxylin-eosin. Cell nuclei were stained dark blue, and cytoplasm were pink. Representative images of inflammatory lesions are shown (magnification, × 200).

the $PAL_{92\text{-}100}$ sequences between the *L. pneumophila* serogroup 1 and other *Legionella* species analyzed, with the exception of *L. lansingesis* and *L. nautarum*.

DISCUSSION

In this study, we determined that antigen-specific $CD8^+$ T cells were mainly responsible for protection from *Legionella* infection in our PAL vaccine model. Our findings are somewhat consistent with those of previous published studies (9–11). In those studies, however, alveolar mononuclear cells (such as macrophages) were suggested to be effector cells against *L. pneumophila*. As we observed in this study, it is likely that cytokines (IFN-γ and TNF-α) released from PAL-specific $CD8^+$ T cells may be also associated with resistance to *L. pneumophila* through activation of host's mononuclear cells. Furthermore, our findings are fully compatible with those of a previous report indicating $CD8^+$ T cells exert a major effector function in protection from infection with intracellular bacteria, such as *Rickettsia* and *Listeria monocytogenes* (29). In this process, $CD8^+$ cytotoxic T cells kill infected cells by releasing granules (perforin and granzymes), as well as by granule-independent pathways.

In the present study, we also identified *Legionella* PAL-specific $CD8^+$ T cell epitopes using three Class I MHC binding prediction programs, as well as IFN-γ and CTL assays. Out of the 13 predicted peptides, the P8 peptide, $PAL_{92\text{-}100}$ (EYLKTHPGA) stimulated the greatest degree of IFN-γ production from the spleen cells of mice immunized with PAL DNA vaccines. Consistent with this finding, the $PAL_{92\text{-}100}$ peptide stimulated PAL-specific $CD8^+$ T cells as effector cells against target cells in an *in vitro* CTL assay. Moreover, the $PAL_{92\text{-}100}$ peptide induced antigen-specific CTL activity in mice receiving co-immunization with a CpG-ODN adjuvant. Therefore, our findings support the notion that the $PAL_{92\text{-}100}$ peptide is indeed an H-$2K^d$-restricted $CD8^+$ T cell epitope that can induce both INF-γ production from PAL-specific $CD8^+$ T cells and CTL lytic activity *in vitro* and *in vivo*. Given peptide vaccines have been developed against various cancers and infectious diseases (30), we propose that Class I HLA epitopes of PAL proteins might be peptide vaccine candidates for protection from infection with *L. pneumophila* in humans.

We also demonstrated that the $PAL_{92\text{-}100}$ peptide effectively induced protection against a lethal challenge with *L. pneumophila*. Mice immunized with the $PAL_{92\text{-}100}$ peptide plus CpG-ODN had 100% survival after a lethal intravenous challenge with *L. pneumophila*, while all control animal groups died within several days after the challenge. Similarly, mice immunized with the $PAL_{92\text{-}100}$ peptide plus CpG-ODN had 75–85.7% survival 14 days after a lethal intranasal challenge, as opposed to the control groups which had 0% survival after the challenge. The CpG-ODN adjuvant has been previously found to be an effective peptide vaccine adjuvant (24). The survival data were consistent with the bacterial burdens in the lungs of infected mice: bacterial counts were significantly lower in the lung tissues of the groups immunized with $PAL_{92\text{-}100}$ peptide plus CpG-ODN than in the control groups (non-immunized mice and mice immunized with either the $PAL_{92\text{-}100}$ peptide or CpG-ODN). Moreover, the IFN-γ and TNF-α concentrations produced by cultured splenocytes from cyclophosphamide-treated immunosuppressed mice were significantly greater in the groups

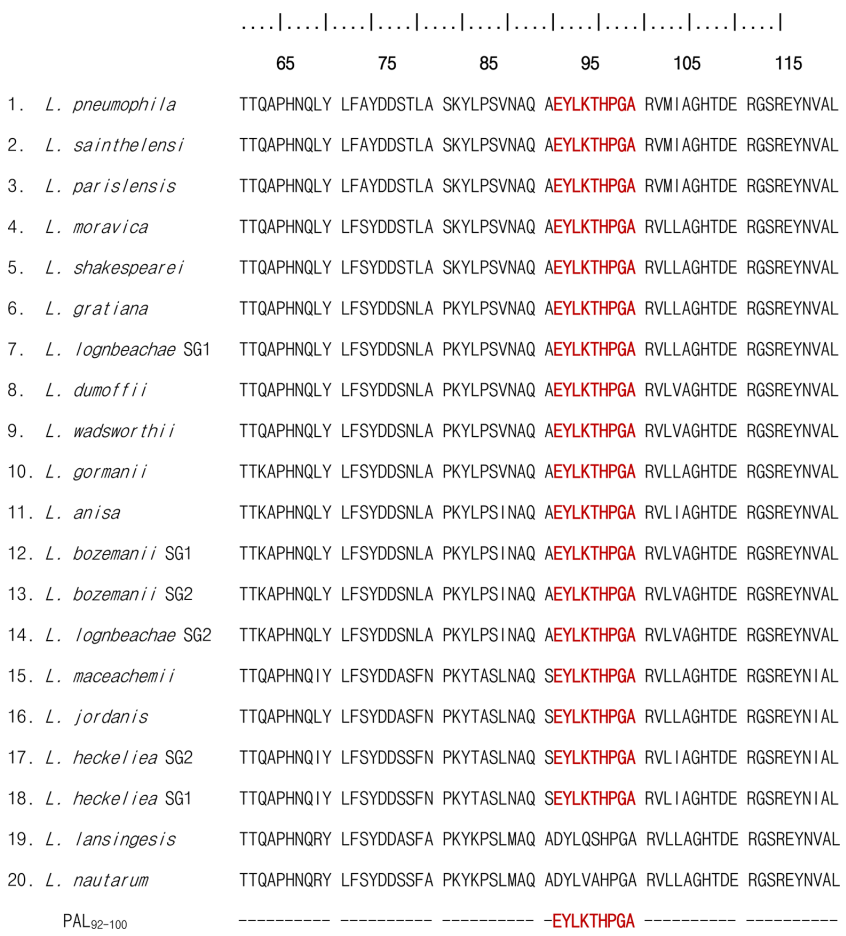

FIGURE 6 | Multi-sequence alignment of the PAL sequence of *L. pneumophila* serogroup and 19 non-pneumophila *Legionella* species. Multi-sequence alignment of amino acid positions from 60 to 120 is shown. P8 (PAL_{92-100}) peptide sequences are shared, as indicated by the red color.

immunized with PAL_{92-100} peptide plus CpG-ODN than in the control groups secreting basal concentrations of cytokines. Given the immunosuppressed mice were treated with 150 mg/kg cyclophosphamide, we first speculated that little, if any, protective immunity might be induced in these mice after immunization with the PAL_{92-100} peptide plus CpG-ODN. In the immunosuppressed animals, however, immunization with the PAL_{92-100} peptide not only increased survival rates after lethal infection with *L. pneumophila*, but also reduced bacterial burden in the lungs of infected mice. This result was consistent with lung pathology data indicating almost normal status after immunization with the PAL_{92-100} peptide plus CpG-ODN. Here it is highly likely that PAL_{92-100}-specific CD8+ T cells are directly associated with protection from lung tissue damage resulting from *Legionella* infection. This is based upon the fact that PAL_{92-100}-specific CD8+ T cells alone were inducible by this immunization scheme. However, this needs to be demonstrated by measuring the infiltration and functional status of CD8+ T cells in the lung tissues. These results suggest that the PAL_{92-100} epitope can induce a strong CTL response, thus leading to the eradication of intracellular *L. pneumophila* and normalization of lung tissues even in immunosuppressed animals. Our results underscore the possible utility of PAL vaccines for protection against *L. pneumophila* in elderly patients with weakened immunity. Taken together, our findings indicate it is highly likely that PAL_{92-100} epitopes induce antigen-specific $CD8^+$ CTLs, thereby exerting protective activity against *L. pneumophila*. In addition, we found the PAL_{92-100} amino acid sequences of PAL proteins were highly conserved among serogroups of *L. pneumophila* and other *Legionella* species. In an international survey, *L. pneumophila* accounted for about 85 to 90% of cases of Legionnaires' disease, but other *Legionella* species were also implicated in human infections (31). Therefore, it is plausible that the PAL_{92-100} peptide, as well as the native PAL protein, may be effective at inducing protective immunity against various *Legionella* species. On the other hand, we observed in our therapeutic study that the PAL_{92-100} peptide had no therapeutic activity against *L. pneumophila* (data not shown). This result might be ascribed to the short-term survival (*i.e.*, 4 days) in the mice after bacterial challenge. Within this short interval, the PAL_{92-100} peptides were unlikely to stimulate antigen-specific CTL responses which were essential for anti-bacterial activity. Moreover, cyclophosphamide treatment required

for this mortality study might have inhibited immune induction by $PAL_{92\text{-}100}$ peptides. It is also possible that prompt administration of $PAL_{92\text{-}100}$-specific $CD8^+$ CTLs (generated *ex vivo*) to *Legionella*-infected animals may engender therapeutic activity against *L. pneumophila*. However, this theory needs to be tested. Taken together, this result suggests that the appropriate timing and magnitude of induction of antigen-specific $CD8^+$ T cells may be a key factor in the development of protection against *L. pneumophila*.

In conclusion, to our knowledge, this is the first study to demonstrate that $PAL_{92\text{-}100}$-specific $CD8^+$ CTLs play an important role as effector cells in the host defense response against *L. pneumophila* in infected mice. Furthermore, *Legionella* PAL containing a well-conserved epitope might be useful as a vaccine against infection with various *Legionella* species.

DATA AVAILABILITY STATEMENT

The original contributions presented in the study are included in the article/supplementary material; further inquiries can be directed to the corresponding author.

ETHICS STATEMENT

The animal study was reviewed and approved by the Institutional Animal Care and Use Committee (IACUC) of the College of medicine, Korea University.

AUTHOR CONTRIBUTIONS

MJK developed the concept and the design of the study project, and directed the project. SJK carried out the experiments. J-IS encouraged SJK to undertake additional protection assays and supervised the findings of this work. SJK drafted the manuscript. All authors contributed to the article and approved the submitted version.

FUNDING

This work was supported by a National Research Foundation of Korea (NRF) grant funded by the Korean government (Ministry of Science and ICT) (No. NRF-2017R1D1A1B03034363).

REFERENCES

1. Foy HM, Broome CV, Hayes PS, Allan I, Cooney MK, Tobe R. Legionnaires' disease in a prepaid medical-care group in Seattle 1963–75. *Lancet* (1979) 1:767–70. doi: 10.1016/s0140-6736(79)91219-4
2. Fields BS, Benson RF, Besser RE. Legionella and Legionnaires' disease: 25 years of investigation. *Clin Microbiol Rev* (2002) 15:506–26. doi: 10.1128/cmr.15.3.506-526.2002
3. Diederen BM. Legionella spp. and Legionnaires' disease. *J Infect* (2008) 56:1–12. doi: 10.1016/j.jinf.2007.09.010
4. Vergis EN, Akbas E, Yu VL. Legionella as a cause of severe pneumonia. *Semin Respir Crit Care Med* (2000) 21:295–304. doi: 10.1055/s-2000-9862
5. Abu Kwaik Y, Gao LY, Stone BJ, Venkataraman C, Harb OS. Invasion of protozoa by Legionella pneumophila and its role in bacterial ecology and pathogenesis. *Appl Environ Microbiol* (1998) 64:3127–33. doi: 10.1128/aem.64.9.3127-3133.1998
6. Fields BS. The molecular ecology of legionellae. *Trends Microbiol* (1996) 4:286–90. doi: 10.1016/0966-842x(96)10041-x
7. Isberg RR, O'Connor TJ, Heidtman M. The Legionella pneumophila replication vacuole: making a cosy niche inside host cells. *Nat Rev Microbiol* (2009) 7:13–24. doi: 10.1038/nrmicro1967
8. Ham H, Sreelatha A, Orth K. Manipulation of host membranes by bacterial effectors. *Nat Rev Microbiol* (2011) 9:635–46. doi: 10.1038/nrmicro2602
9. Horwitz MA. Cell-mediated immunity in Legionnaires' disease. *J Clin Invest* (1983) 71:1686–97. doi: 10.1172/jci110923
10. Horwitz MA, Silverstein SC. Interaction of the legionnaires' disease bacterium (Legionella pneumophila) with human phagocytes. II. Antibody promotes binding of L. pneumophila to monocytes but does not inhibit intracellular multiplication. *J Exp Med* (1981) 153:398–406. doi: 10.1084/jem.153.2.398
11. Nash TW, Libby DM, Horwitz MA. Interaction between the legionnaires' disease bacterium (Legionella pneumophila) and human alveolar macrophages. Influence of antibody, lymphokines, and hydrocortisone. *J Clin Invest* (1984) 74:771–82. doi: 10.1172/jci111493
12. Weber SS, Stoycheva D, Nimmerjahn F, Oxenius A. Two sequential layers of antibody-mediated control of Legionella pneumophila infection. *Eur J Immunol* (2019) 49:1415–20. doi: 10.1002/eji.201948106
13. Blander SJ, Horwitz MA. Vaccination with Legionella pneumophila membranes induces cell-mediated and protective immunity in a guinea pig model of Legionnaires' disease. Protective immunity independent of the major secretory protein of Legionella pneumophila. *J Clin Invest* (1991) 87:1054–9. doi: 10.1172/jci115065
14. Blander SJ, Horwitz MA. Vaccination with the major secretory protein of Legionella induces humoral and cell-mediated immune responses and protective immunity across different serogroups of Legionella pneumophila and different species of Legionella. *J Immunol* (1991) 147:285–91.
15. Xu JN, Yang ZW, Chen JP, Chen DL, Wang T, Liu MJ, et al. Protective immunity against Legionnaires' disease in an A/J mouse model using a DNA vaccine composed of an outer membrane protein (29 kDa) and the pilE fusion protein. *Diagn Microbiol Infect Dis* (2012) 73:9–15. doi: 10.1016/j.diagmicrobio.2012.02.013
16. Engleberg NC, Howe DC, Rogers JE, Arroyo J, Eisenstein BI. Characterization of a Legionella pneumophila gene encoding a lipoprotein antigen. *Mol Microbiol* (1991) 5:2021–9. doi: 10.1111/j.1365-2958.1991.tb00824.x
17. Harrison TG, Doshi N. Evaluation of the Bartels Legionella Urinary Antigen enzyme immunoassay. *Eur J Clin Microbiol Infect Dis* (2001) 20:738–40. doi: 10.1007/s100960100598
18. Kim MJ, Sohn JW, Park DW, Park SC, Chun BC. Characterization of a lipoprotein common to Legionella species as a urinary broad-spectrum antigen for diagnosis of Legionnaires' disease. *J Clin Microbiol* (2003) 41:2974–9. doi: 10.1128/jcm.41.7.2974-2979.2003
19. Shim HK, Kim JY, Kim MJ, Sim HS, Park DW, Sohn JW, et al. Legionella lipoprotein activates toll-like receptor 2 and induces cytokine production and expression of costimulatory molecules in peritoneal macrophages. *Exp Mol Med* (2009) 41:687–94. doi: 10.3858/emm.2009.41.10.075
20. Yoon WS, Park SH, Park YK, Park SC, Sin JI, Kim MJ. Comparison of responses elicited by immunization with a Legionella species common lipoprotein delivered as naked DNA or recombinant protein. *DNA Cell Biol* (2002) 21:99–107. doi: 10.1089/104454902753604970
21. Mobarez AM, Rajabi RA, Salmanian AH, Khoramabadi N, Hosseini Doust SR. Induction of protective immunity by recombinant peptidoglycan associated lipoprotein (rPAL) protein of Legionella pneumophila in a BALB/c mouse model. *Microb Pathog* (2019) 128:100–5. doi: 10.1016/j.micpath.2018.12.014
22. Han BS, Jang HY, Racine T, Qiu X, Sin JI. Purification and characterization of monoclonal IgG antibodies recognizing Ebola virus glycoprotein. *Clin Exp Vaccine Res* (2018) 7:119–28. doi: 10.7774/cevr.2018.7.2.119
23. Bae SH, Park YJ, Park JB, Choi YS, Kim MS, Sin JI. Therapeutic synergy of human papillomavirus E7 subunit vaccines plus cisplatin in an animal tumor model: causal involvement of increased sensitivity of cisplatin-treated tumors

to CTL-mediated killing in therapeutic synergy. *Clin Cancer Res* (2007) 13:341–9. doi: 10.1158/1078-0432.Ccr-06-1838
24. Sin J-I, Park J-B, Lee IH, Park D, Choi YS, Choe J, et al. Intratumoral electroporation of IL-12 cDNA eradicates established melanomas by Trp2 180–188-specific CD8+ CTLs in a perforin/granzyme-mediated and IFN-γ-dependent manner: application of Trp2 180–188 peptides. *Cancer Immunol Immunother* (2012) 61:1671–82. doi: 10.1007/s00262-012-1214-8
25. Widen R, Klein T, Friedman H. Enhanced susceptibility of cyclophosphamide-treated mice to infection with Legionella pneumophila. *J Infect Dis* (1984) 149:1023–4. doi: 10.1093/infdis/149.6.1023
26. Lake RA, Robinson BW. Immunotherapy and chemotherapy–a practical partnership. *Nat Rev Cancer* (2005) 5:397–405. doi: 10.1038/nrc1613
27. Sistigu A, Viaud S, Chaput N, Bracci L, Proietti E, Zitvogel L. Immunomodulatory effects of cyclophosphamide and implementations for vaccine design. *Semin Immunopathol* (2011) 33:369–83. doi: 10.1007/s00281-011-0245-0
28. Huyan XH, Lin YP, Gao T, Chen RY, Fan YM. Immunosuppressive effect of cyclophosphamide on white blood cells and lymphocyte subpopulations from peripheral blood of Balb/c mice. *Int Immunopharmacol* (2011) 11:1293–7. doi: 10.1016/j.intimp.2011.04.011
29. Harty JT, Bevan MJ. Responses of CD8(+) T cells to intracellular bacteria. *Curr Opin Immunol* (1999) 11:89–93. doi: 10.1016/s0952-7915(99)80016-8
30. Naz RK, Dabir P. Peptide vaccines against cancer, infectious diseases, and conception. *Front Biosci* (2007) 12:1833–44. doi: 10.2741/2191
31. Yu VL, Plouffe JF, Pastoris MC, Stout JE, Schousboe M, Widmer A, et al. Distribution of Legionella species and serogroups isolated by culture in patients with sporadic community-acquired legionellosis: an international collaborative survey. *J Infect Dis* (2002) 86(1):127–8. doi: 10.1086/341087

Conflict of Interest: The authors declare that the research was conducted in the absence of any commercial or financial relationships that could be construed as a potential conflict of interest.

frontiers in Immunology

ORIGINAL RESEARCH
published: 05 February 2021
doi: 10.3389/fimmu.2020.613496

Systematic Evaluation of Kinetics and Distribution of Muscle and Lymph Node Activation Measured by ^{18}F-FDG- and ^{11}C-PBR28-PET/CT Imaging, and Whole Blood and Muscle Transcriptomics After Immunization of Healthy Humans With Adjuvanted and Unadjuvanted Vaccines

Zarni Win[1†], January Weiner 3rd[2,3†], Allan Listanco[4], Neva Patel[1], Rohini Sharma[5], Aldona Greenwood[6], Jeroen Maertzdorf[2], Hans-Joachim Mollenkopf[2], Kat Pizzoferro[6], Thomas Cole[4], Caroline L. Bodinham[6], Stefan H. E. Kaufmann[2], Philippe Denoel[7], Giuseppe Del Giudice[7] and David J. M. Lewis[4,6]*

[1] Department of Nuclear Medicine and Radiological Sciences Unit, Imperial College Healthcare NHS Trust (ICHNT), London, United Kingdom, [2] Department for Immunology, Max Planck Institute for Infection Biology, Berlin, Germany, [3] Core Unit for Bioinformatics (CUBI), Berlin Institute of Health, Berlin, Germany, [4] National Institute for Health Research (NIHR) Imperial Clinical Research Facility (NICRF), Imperial College Healthcare NHS Trust, London, United Kingdom, [5] Department of Surgery & Cancer, Imperial College London (ICL), London, United Kingdom, [6] Surrey Clinical Research Centre, University of Surrey, Guildford, United Kingdom, [7] External R&D, GSK, Rixenstart, Belgium and Siena, Italy

Systems vaccinology has been applied to detect signatures of human vaccine induced immunity but its ability, together with high definition *in vivo* clinical imaging is not established to predict vaccine reactogenicity. Within two European Commission funded high impact programs, BIOVACSAFE and ADITEC, we applied high resolution positron emission tomography/computed tomography (PET/CT) scanning using tissue-specific and non-specific radioligands together with transcriptomic analysis of muscle biopsies in a clinical model systematically and prospectively comparing vaccine-induced immune/inflammatory responses. 109 male participants received a single immunization with licensed preparations of either AS04-adjuvanted hepatitis B virus vaccine (AHBVV); MF59C-adjuvanted (ATIV) or unadjuvanted seasonal trivalent influenza vaccine (STIV); or alum-OMV-meningococcal B protein vaccine (4CMenB), followed by a PET/CT scan (n = 54) or an injection site muscle biopsy (n = 45). Characteristic kinetics was observed with a localized intramuscular focus associated with increased tissue glycolysis at the site of immunization detected by ^{18}F-fluorodeoxyglucose (FDG) PET/CT, peaking after 1–3 days and strongest and most prolonged after 4CMenB, which correlated with clinical

OPEN ACCESS

Edited by:
Simon Daniel Van Haren, Boston Children's Hospital and Harvard Medical School, United States

Reviewed by:
Daniel Fredric Hoft, Saint Louis University, Philippines
Daniel O'Connor, University of Oxford, United Kingdom

***Correspondence:**
David J. M. Lewis
vaccinst@outlook.com

[†]These authors have contributed equally to this work

Specialty section:
This article was submitted to Vaccines and Molecular Therapeutics, a section of the journal Frontiers in Immunology

Received: *02 October 2020*
Accepted: *24 December 2020*
Published: *05 February 2021*

Citation:
Win Z, Weiner 3rd J, Listanco A, Patel N, Sharma R, Greenwood A, Maertzdorf J, Mollenkopf H-J, Pizzoferro K, Cole T, Bodinham CL, Kaufmann SHE, Denoel P, Del Giudice G and Lewis DJM (2021) Systematic Evaluation of Kinetics and Distribution of Muscle and Lymph Node Activation Measured by ^{18}F-FDG- and ^{11}C-PBR28-PET/CT Imaging, and Whole Blood and Muscle Transcriptomics After Immunization of Healthy Humans With Adjuvanted and Unadjuvanted Vaccines. Front. Immunol. 11:613496. doi: 10.3389/fimmu.2020.613496

experience. Draining lymph node activation peaked between days 3–5 and was most prominent after ATIV. Well defined uptake of the immune cell-binding radioligand ^{11}C-PBR28 was observed in muscle lesions and draining lymph nodes. Kinetics of muscle gene expression module upregulation reflected those seen previously in preclinical models with a very early (~6hrs) upregulation of monocyte-, TLR- and cytokine/chemokine-associated modules after AHBVV, in contrast to a response on day 3 after ATIV, which was bracketed by whole blood responses on day 1 as antigen presenting, inflammatory and innate immune cells trafficked to the site of immunization, and on day 5 associated with activated CD4+ T cells. These observations confirm the use of PET/CT, including potentially tissue-, cell-, or cytokine/chemokine-specific radioligands, is a safe and ethical quantitative technique to compare candidate vaccine formulations and could be safely combined with biopsy to guide efficient collection of samples for integrated whole blood and tissue systems vaccinology in small-scale but intensive human clinical models of immunization and to accelerate clinical development and optimisation of vaccine candidates, adjuvants, and formulations.

Keywords: PET/CT (positron emission tomography/computed tomography), transcriptomics, systems vaccinology, reactogenicity, muscle, fluorodeoxyglucose (F-FDG) 18, TSPO (18kda translocator protein)

INTRODUCTION

While licensed vaccines are generally safe and effective, their development is both time consuming and expensive requiring many thousands of trial participants to generate a safety database before licensing, and potentially ongoing surveillance thereafter. This can lead to difficult decisions about selection of dose, formulation, schedule and other factors (1) that are rarely fully explored during development but may lead to failure in Phase 3 efficacy trials, or unexpected safety concerns post licensing (2–4). While such failures are unwelcome at any time they are especially acute during epidemics or pandemics, such as recent outbreaks of Ebola, SARS-CoV-1 and SARS- CoV-2 where vaccine development may be expedited. The potential for small-scale but intensive clinical studies that may identify biomarkers of both vaccine efficacy and safety/reactogenicity is therefore attractive (5). While the use of whole blood transcriptomics profiling ("systems vaccinology") is well established for identification of biomarkers of immunogenicity (6, 7), very little has been established to predict vaccine safety or reactogenicity. With increasing use of adjuvants, live viral or other novel delivery systems such as RNA, the regulatory field is increasingly exploring the application of high throughput, precision techniques in early phase clinical trials to augment pre-clinical models for the evaluation and optimisation of candidate vaccine formulations (8). With this in mind the European Commission supported two High Impact research programs: "ADITEC" for the application of advanced immunology techniques for more effective vaccines (9, 10); and *via* the Innovative Medicines Initiative-Joint Undertaking (11), "BIOVACSAFE" to assess the ability of systems vaccinology and other high throughput, precision technologies to develop clinical and pre-clinical biomarkers of vaccine safety and reactogenicity (12).

Increased muscle and lymph node ^{18}F-FDG PET/CT activity following immunization has been described in scattered case reports (13–16), or in retrospective series of patients with oncological or inflammatory conditions (17–20) serendipitously scanned sometime after immunization. Lymph node activity was generally highest within 7–12 days, e.g., after H1N1 influenza vaccines (19) especially those adjuvanted with AS03 (DL-α-tocopherol (vitamin E), squalene and polysorbate 80) or MF59C (17, 18). Similarly in a small study of healthy female trial volunteers receiving either alum- or AS04-adjuvanted Human Papilloma Virus vaccines (21) axillary lymph node activity was universally seen sometime between 8 and 14 days after immunization, with decreased frequency after 30 days, and contralateral activity only after AS04 adjuvanted vaccine. However these studies were generally opportunistic and the participants generally unrepresentative of early stage vaccine trials. We therefore prospectively and systematically characterized early tissue responses to unadjuvanted and adjuvanted vaccines in healthy adult volunteers, with a special focus on the intramuscular site of immunization as a marker of vaccine reactogenicity.

We have already reported the application of systems vaccinology in BIOVACSAFE to identify biomarkers of reactogenicity in preclinical models (22); and using whole blood in small but highly intensive comparative clinical studies of vaccines and adjuvants (23), and in pregnancy (24). We report here linked clinical studies applying precision positron emission tomography/computed tomography (PET/CT) scanning with tissue-specific and non-specific radioligands, and systems vaccinology analysis of gene expression changes in local tissue at the site of immunization, to systematically and prospectively compare inflammatory and immune responses to a range of adjuvanted and unadjuvanted licensed vaccines (**Table 1**). These studies provide a safe and ethical

TABLE 1 | Summary of vaccines, antigens, adjuvants and principal findings on PET/CT and Gene Expression.

Vaccine acronym	Antigen/manufacturer	Adjuvant	Principal findings	
			PET/CT	Gene expression
4CMenB	Meningococcal group B subunit proteins, Outer Membrane Vesicles/GSK	alum	↑↑↑ muscle, peak D5, remains ↑ ↑ lymph nodes, peak D5	
AHBVV	Hepatitis B virus surface antigen/GSK	AS04C: 3Odesacyl4' monophosphoryl lipid A (MPL) adsorbed on aluminium salt		**Blood**: ↑D3: innate immunity, IFNs **Muscle**: ↑↑3h: monocytes, TLR signalling, antigen presentation, cytokines, neutrophils
ATIV	Subunit seasonal trivalent influenza vaccine/ Seqirus Vaccines and Diagnostics	MF59C: squalene, polysorbate 80, sorbitan trioleate, oil-in-water emulsion	↑↑ muscle, peak D3 then ↓ ↑↑lymph nodes, peak D5	**Blood**: ↑↑D1: innate immunity, IFNs, dendritic cells, neutrophils, monocytes ↑↑D5: CD4 T cells **Muscle**: ↑↑↑D3: antigen presentation, monocytes, TLR signalling, cytokines, IFNs, dendritic cells, T cells
STIV	Split virion inactivated seasonal trivalent influenza vaccine/Sanofi Pasteur		↑ muscle, peak D3 then ↓ ↑ lymph nodes, peak D3	

clinical model that can be applied to the evaluation and optimisation of novel vaccine candidates, adjuvants, and formulations in early phase clinical development.

MATERIALS AND METHODS

Participants, Immunizations, Muscle Biopsy and Reactogenicity Scoring

^{18}F-FDG- and ^{11}C-PBR28 -PET/CT Imaging Protocol

Male participants aged 18–55 deemed healthy by medical history and symptoms-directed physical examination were eligible for enrolment at the NICRF, London subject to the following inclusion criteria: able to understand and signed the informed consent form (ICF); body mass index 19–27 kg/m^2; pre-immunized with a hepatitis B vaccine on the basis of immunization history if AHBVV to be the study vaccine, and have not received any meningococcal B vaccine on the basis of immunization history if 4CMenB to be the study vaccine (immunization history and existing immunity not recorded for other vaccines); have not undergone research radiation exposures, and agree to avoid such exposures for 12 months before/after this study; willing to avoid vigorous exercise or contact sports between vaccination and PET scan; no history of hypersensitivity to any of the vaccine components or a history of any allergy; no use of steroids or immunosuppressive/immunomodulating drugs either orally or parenterally within 3 months of the PET scan; not currently participating in a clinical study with a drug or device; do not express TSPO with low-affinity to PBR28 on the basis of TSPO genotype (^{11}C-PBR28 PET imaging only).

All immunizations were a 0.5 ml intramuscular injection on one occasion, randomised to right or left side, using a 25 mm long 23 gauge (G) needle into the antero-lateral thigh with the manufacturer recommended dose. In the ^{18}F-FDG PET/CT protocol participants received one of the following commercially sourced vaccines: 4CMenB (Meningococcal group B subunit/ Outer Membrane Vesicles - alum, GSK); AHBVV (Hepatitis B virus surface antigen adjuvanted by AS04C containing 3*O*desacyl4' monophosphoryl lipid A (MPL) adsorbed on aluminium salt, GSK); ATIV (subunit seasonal trivalent influenza vaccine adjuvanted with MF59C, Seqirus Vaccines and Diagnostics) or STIV (split virion inactivated seasonal trivalent influenza vaccine, Sanofi Pasteur). Those receiving STIV were also injected with saline control in the contralateral leg. In the ^{11}C-PBR28-PET protocol participants received 4CMenB and saline control in the contralateral leg.

^{18}F-FDG PET/CT imaging participants completed a daily diary card recording and scoring severity of solicited symptoms of redness or swelling (score 0 or 1); injection site pain, feeling hot, headache, myalgia, arthralgia, malaise, nausea/vomiting, and an overall score (score 0–4 each). Individual symptom scores were added together to calculate a total reactogenicity score for each subject on each day after immunization.

Muscle Biopsy Transcriptomics Protocol

Male participants aged 18–55 deemed healthy by medical history and symptoms-directed physical examination were eligible for enrolment at the Surrey Clinical Research Centre, Guildford subject to the following inclusion criteria: able to understand and signed the ICF; body mass index 19–27 kg/m^2;

pre-immunized with a hepatitis B virus (HBV) vaccine on the basis of immunization history and seropositive for anti-HBV sAb, negative for HBV sAg and cAb (evidence of HBV immunization but not prior infection; ATIV immunization history and existing immunity not recorded); human immunodeficiency virus 1 and 2 antibodies negative; hepatitis C virus antibodies negative; no history of hypersensitivity to any of the vaccine components, injected local anesthetics or a history of any allergy; no use of steroids or immunosuppressive/immunomodulating drugs either orally or parenterally within 3 months of the immunization; not currently participating in a clinical study with a drug or device; no known immune or coagulation disorder or clinically significant abnormalities of platelets, hemoglobin or coagulation on screening blood tests.

On the day of immunization blood was first drawn into PaxGene tubes for whole blood transcriptomics. Participants then received a 0.5 ml intramuscular immunization, randomised to right or left side, using a 25 mm long 23G needle introduced at right angles to the full length of the needle into the antero-lateral thigh (targeting vastus lateralis muscle) with the manufacturer recommended dose of one of the following commercially sourced vaccines: AHBVV, ATIV or normal saline control. The injection site was marked with indelible marker.

On the allocated day of muscle biopsy blood was first drawn into PaxGene tubes for whole blood transcriptomics. The biopsy was obtained using a well-established technique (25): the site of immunization, and an anatomically matched site on the unimmunized contralateral leg was identified and sterilized using 4% w/v chlorhexidine before being infiltrated intradermally and subcutaneously with 2–5 ml 1% lidocaine (without epinephrine) using a 23G needle. After approximately 5 min a 21G needle was advanced slowly at a 45 degree angle into the subcutaneous tissue, taking care not to penetrate the muscle fascia, and the biopsy site infiltrated with 10–15 ml 1% lidocaine (without epinephrine) in a diamond pattern. This technique ensured that the subcutaneous tissue and muscle fascia is anesthetized without affecting the muscle sample to be biopsied. After a further 5 min a 5–10 mm stab incision was made with a surgical blade inserted far enough to make a small incision in the muscle fascia. A modified Bergström needle with a Luer lock attachment to the inner cannula to allow application of suction during the procedure, and with the exact depth of the needle used for immunization engraved on the shaft, was used to obtain the biopsy. The needle was introduced perpendicularly, through the muscle fascia to the marked depth and a slight vacuum created by pulling back on the plunger of an attached 60 ml syringe. Simultaneously the hole at the top of the Bergström needle was sealed and the inner trocar with the cutting edge pulled up, opening the cutting window in the outer needle. The trocar was then pushed down to excise a piece of muscle and repeated three to four times while maintaining the vacuum. The needle was withdrawn, the inner cannula removed and the muscle sample removed with non-toothed forceps or hypodermic needle tip and immediately placed in 1.5 ml RNA*later* (Invitrogen) reagent in a 2 ml tube. After at least overnight storage at 4°C the tubes were transferred to -80°C freezer for storage prior to RNA extraction and analysis in batches.

PET/CT Scanning and Image Analysis

In order to keep the radiation dose below acceptable exposure levels of 10 milliSieverts (mSv) per annum in this healthy young adult population, each participant had a single PET/CT scan on one occasion only. To calibrate the ^{18}F-FDG PET/CT scan an iterative time series was initially performed at the Clinical Imaging Facility (CIF), Imperial College over 20–60 min after ^{18}F-FDG administration to one participant who had received AHBVV three days previously. Uptake in the muscle ROI increased until it reached a plateau between 50–60 min (data not shown). Therefore, a standard ^{18}F-FDG PET/CT scan protocol was employed thereafter as follows: the participants' height and weight were recorded and plasma glucose checked before a weight corrected dose of ^{18}F-FDG (2.9 MBecquerel/kg [MBq/kg] with a dose constraint of 200 MBq, effective dose 4.0 mSv) was injected intravenously. The participant then remained resting to avoid any muscle use until 55 min post injection when they voided the urinary bladder before being placed in a Siemens Biograph 64 scanner. A CT topogram for position was performed followed by an attenuation correction two bed positions (bp) low dose CT scan from the pelvic brim down to just past vaccine injection site (120 keV, 100mA, rotation 0.5 s, 50 mAs, total CT dose restricted to 2.5 mSv). This was followed by a two bp static PET scan linked to the first CT, then a half body non-attenuation corrected PET scan from eyes to mid-thigh. This protocol was confirmed by scanning a second participant at the CIF 3 days after immunization with AHBVV, and used thereafter for the other study vaccines for which scans were performed at the Department of Nuclear Medicine and Radiological Sciences Unit, Imperial College Healthcare NHS Trust.

For analysis, ^{18}F-FDG -PET/CT uptake was converted into dose- and weight-corrected Standardised Uptake Values (SUV) (26) and attenuation corrected and reconstructed PET images created using the CT scan and Ordered Subset Expectation Maximization (OSEM) algorithms with 4 iterations and 8 subsets, and the Siemens scanner software. DICOM images were imported into Osirix MD (Pixmeo, Geneva. FDA cleared as a Class II Medical Device for diagnostic imaging in medicine, compliant with European Directive 93/42/EEC concerning medical devices, Class IIa product) for calculation of regions of interest (ROI) of increased activity at muscle injection site and lymph nodes using inbuilt minimum-maximum thresholding algorithms. Standard parameters for PET quantification (26) were calculated using the Osirix software tools: SUVpeak (average SUV of a 1 cm^3 sphere centered on the SUVmax voxel); Volume Of Interest (VOI, by combining and interpolating 2D ROI) and SUVmax, SUVmean and Total Lesion Glycolysis (SUVmean x VOI cm^3) within the 3D VOI. A fixed threshold of 0.9 SUV was found to give optimal muscle segmentation at the different time points after immunization. In addition an Osirix software plugin (available at https://github.com/djmlewis/mirrorroi.git) was created which used anatomical

features on the CT scan to accurately mirror each 2D ROI onto the contralateral uninjected leg for calculation of control SUVmax and SUVmean. Scans were analyzed by an experienced consultant radiology and nuclear medicine clinician (ZW) blinded to treatment, who identified increased lymph node activity and anatomical location.

Individual ^{11}C-PBR28 doses were prepared using an on-site cyclotron and used immediately. For the ^{11}C-PBR28 PET/CT protocol, a weight adjusted ^{11}C-PBR28 (target activity 400 MBq, effective dose 2.64 mSv) PET/low dose CT scan (1.26 mSv dose constraint) was performed at Invicro, London on days 1, 3, 5, or 7 after immunization. Preliminary time-series analysis revealed a rapid accumulation of ^{11}C-PBR28 at injection site over 15 min with a plateau thereafter to 80 min (data not shown). Thereafter, ^{11}C-PBR28 analysis was performed on acquisition between 30–50 min after ^{11}C-PBR28 administration using OSEM algorithms with 3 iterations and 21 subsets.

Whole Blood and Muscle Biopsy Transcriptomics Analysis

Microarray Analysis, Normalization and Quality Control

RNA was extracted from whole blood in PaxGene tubes (PreAnalytiX) on the automated QIAcube system (Qiagen) using the PaxGene Blood RNA kit (Qiagen) according to the manufacturer's instructions. Muscle biopsies in RNA*easy* were defrosted before total RNA isolation (including microRNA [miRNA] species) was performed using the miRNeasy mini kit (Qiagen, UK), as described previously (22). Quality control and quantification of isolated RNA was analyzed with an Agilent 2100 Bioanalyzer (Agilent Technologies) and a NanoDrop 1000 UV-Vis spectrophotometer (Thermo Fisher Scientific). Microarray experiments were performed as single-color hybridization, and RNA was labeled with the Low Input Quick-Amp Labeling Kit (Agilent Technologies) as described previously (23). Scanning of microarrays was performed with 3 μm resolution and 20-bit image depth, using a G2565CA high-resolution laser microarray scanner (Agilent Technologies). Microarray image data were processed with the Image Analysis/Feature Extraction software G2567AA v. A.11.5.1.1 (Agilent Technologies), using default settings and the GE1_1105_Oct12 extraction protocol. Blinded primary readouts of the microarrays were read, background corrected, normalized and controlled for quality using the R package limma (23). The normalized data were locked and unblinded for further analysis. All primary readouts and the background corrected and normalized data are available from the Gene Expression Omnibus database (GEO, accession number GSE124719) and under the BioProject identifier PRJNA513261.

Differential Gene Expression, Gene Set Enrichment, and Individual Variability Analysis

Prior to analysis, hybridization control samples were removed from the data set, and gene expression values averaged for each probe over all replicates of that probe on the microarray, using the 'avereps' function from limma (23). Differences in gene expression for each vaccine at each time point tested were assessed using linear models in limma and p-values corrected for false discovery rate using the Benjamini and Hochberg (BH) procedure (23). For whole blood, the expression was fit to time point, vaccine group and subject and the contrast tested for a given vaccine and a given time point was the interaction between the difference in expression between this time point and the pre-immunization time point. For muscle biopsy, the difference in expression was between the biopsy from the injection site and the biopsy from the uninjected leg; or the vaccine group and the saline control injection group for the injected leg biopsy only. Gene set enrichment was tested with the CERNO algorithm implemented in the R package tmod (23, 27). Area under curve (AUC) as described previously (27) was used as effect size estimate. P-values from the CERNO test were corrected using the Benjamini and Hochberg (BH) procedure. For testing, the gene sets [blood transcriptional modules (BTMs)] defined by Li et al (28). and Chaussabel et al (29). were used. p-values were corrected using the BH procedure; gene set enrichments with $p_{adjusted} < 0.05$ were considered significant. Individual variability was analyzed by ordering genes according to a difference in expression between the relevant condition and a comparable control and applying the CERNO algorithm and the above mentioned gene sets to the list of genes ordered by decreasing absolute difference. For blood, the difference in expression between the given time point and the baseline was calculated and used to order the genes. For biopsies, the difference between the uninjected site and the vaccine injection site was used to order the genes.

Ethics Approval and Registry

The PET/CT imaging and muscle transcriptomics protocols were approved by the London–Surrey Borders Research Ethics Committee (references 15/LO/2039 and 14/LO/2226 respectively) and registered on clinicalTrials.gov (NCT02368327 and NCT04515368). The administration of radionucleotides and the PET/CT scanning protocol were approved by the UK Administration of Radioactive Substances Advisory Committee (research certificate number RPC 44/3681/35747).

RESULTS

Participants and Immunizations

A total of 109 male participants were enrolled sequentially into the treatment groups at two study sites. For ^{18}F-FDG PET/CT, 54 participants (median age 28, range 19–55 years) were enrolled and immunized in the NICRF with either 4CMenB (n = 21), ATIV (n = 19), STIV (n = 12, and with simultaneous saline control in contralateral leg) or AHBVV (n = 2). ^{18}F-FDG PET/CT scans were performed in the Clinical Imaging Facility, Imperial College London on day 3 after AHBVV to define the scanning protocol. Thereafter, ^{18}F-FDG PET/CT scans were performed in the Department of Nuclear Medicine, Imperial

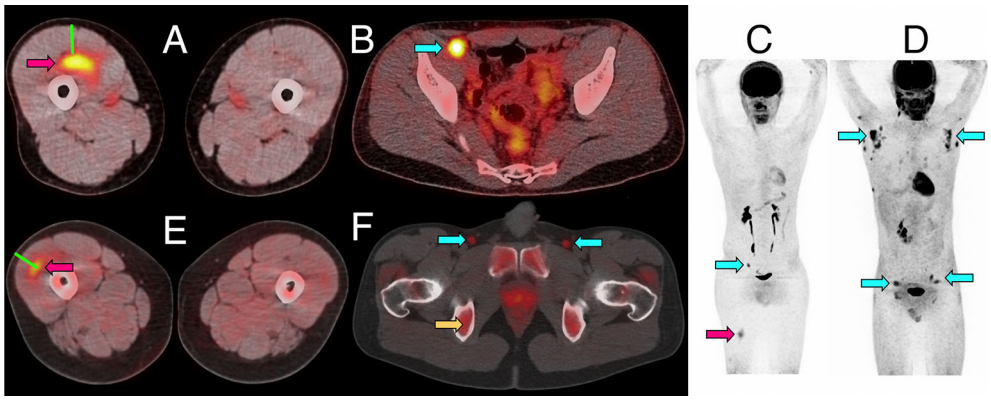

FIGURE 1 | Representative PET/CT images of intramuscular injection site and draining lymph nodes. **(A–C)** Fused ^{18}F-FDG PET/CT images (linear scale) from one participant 5 days after immunization with 4CMenB, demonstrating increased activity at right anterior thigh intramuscular injection site (**A**, red arrow) and right external iliac lymph node (**B**, cyan arrow); whole body PET scan anterior view **(C)** demonstrating level of injection site (red arrow) and activated lymph node (cyan arrow). **(D)** Whole body ^{18}F-FDG PET scan anterior view demonstrating disseminated axillary and pelvic lymph node activity (cyan arrows) 1 day after immunization with ATIV. **(E, F)** Fused ^{11}C-PBR28-PET/CT images (linear scale) from two participants immunized with 4CMenB demonstrating increased ^{11}C-PBR28 binding in right thigh injection site (**E**: red arrow, day +3); and right and left deep inguinal lymph nodes (**F**: cyan arrows, day +7, right thigh injected). Increased bone marrow binding of ^{11}C-PBR28 also visible (**F**: yellow arrow). Green bars **(A, E)** indicate length of immunization needle, actual track unknown. Diffuse uptake of ^{18}F-FDG can be seen in bowel **(B)**, and for both radionucleotides in urinary collecting system and bladder **(B–D, F)**.

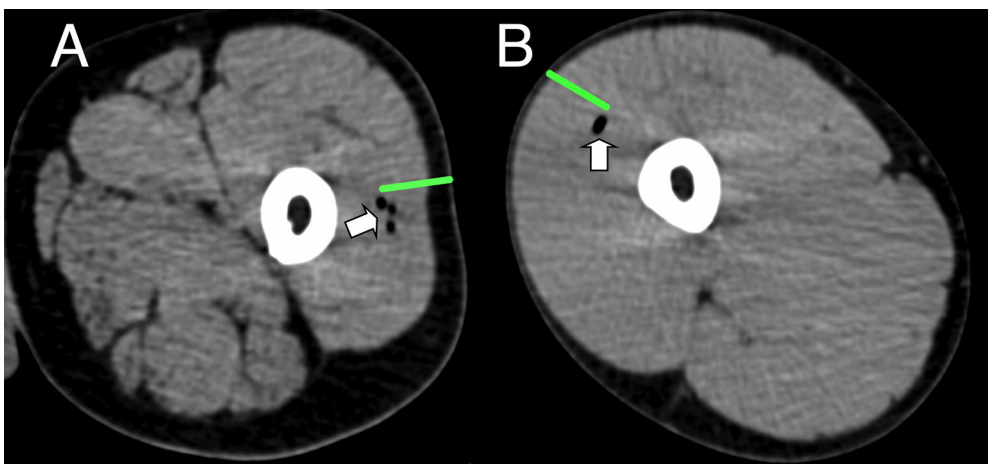

FIGURE 2 | Representative CT imaging of intramuscular immunization site 3 h post injection. Transient inclusions (white arrows) visible at site of immunization with ATIV **(A)** and 4CMenB **(B)**. Green bars indicate length of immunization needle, actual injection track unknown.

College Healthcare NHS Trust at 3 hours, 1, 3, 5, 7, or 10 days after immunization with 4CMenB and ATIV; and at 3 hours, 1, 3, and 7 days after STIV. For ^{11}C-PBR28-PET/CT, 10 participants (median age 25, range 21–51 years) were enrolled and immunized in the NICRF with 4CMenB (and with simultaneous saline control in contralateral leg) and scans performed 1, 3, 5, or 7 days after immunization at Invicro, London. For whole blood and muscle biopsy transcriptomics, a total of 45 male participants (median age of 18, range 23–36 years) were enrolled, immunized with either AHBVV, ATIV or saline control (n = 15 per treatment group, n = 3 per time point per group) and biopsied in the Surrey Clinical Research Centre at 3 hours, 1, 3, or 5 days post-immunization.

^{18}F-FDG and ^{11}C-PBR28 PET Activity in Muscle at Site of Immunization

^{18}F-FDG PET/CT indirectly detects metabolically hyperactive cells by quantifying the concentration of radiolabeled glucose and hence tissue glycolysis (26). We found SUVmax and SUVpeak (30), which has been proposed as more accurate in small VOI and less influenced by a few voxels with high activity (31), to be useful, together with SUVmean which mitigated for

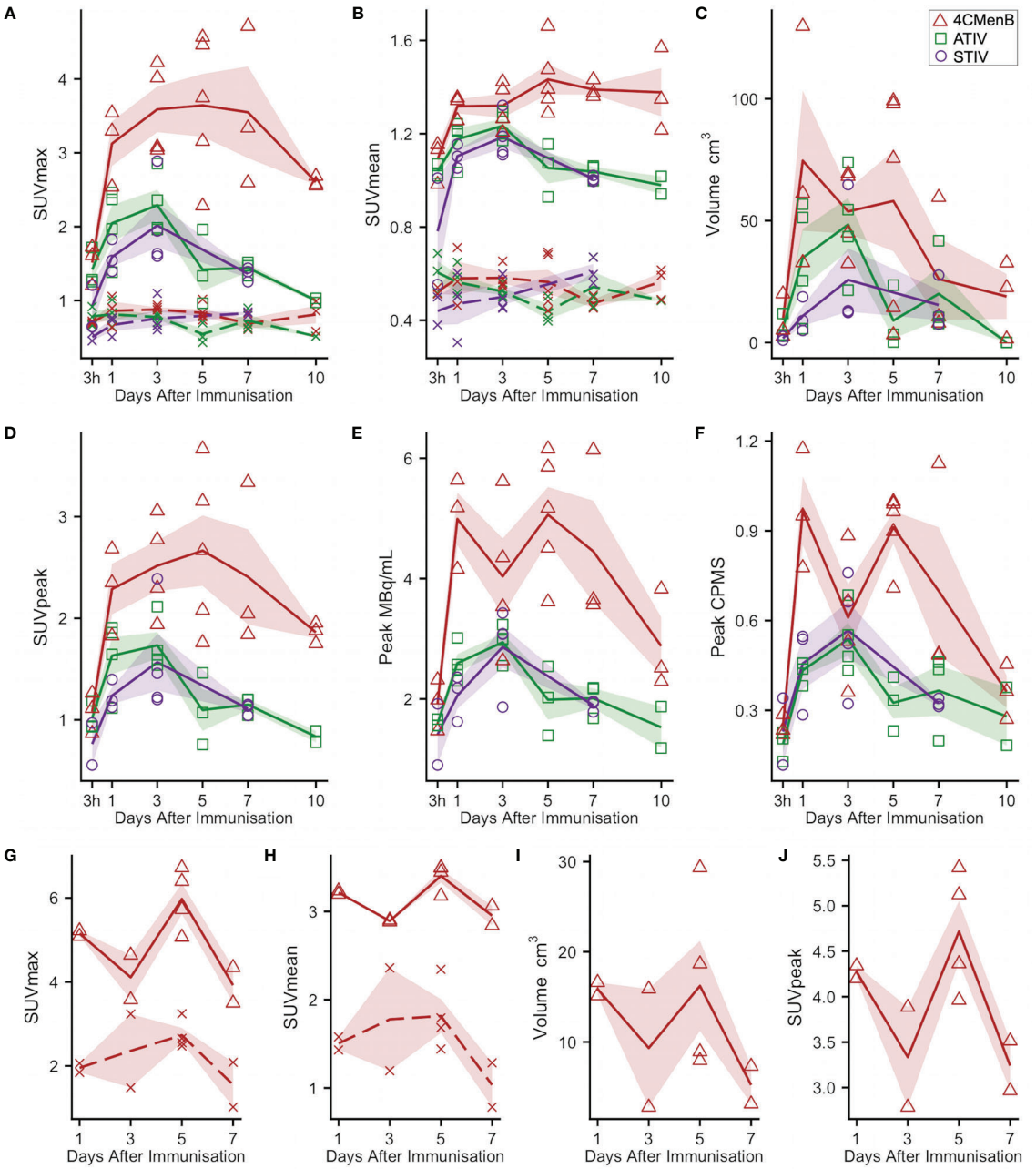

FIGURE 3 | Kinetics of injection site muscle PET/CT activity after immunization **(A–F)** ^{18}F-FDG PET/CT. Panels **(G–J)**: ^{11}C-PBR28 PET/CT. Each point indicates data from one participant immunized with 4CMenB (red triangles), ATIV (green squares) or STIV (purple circles). Lines indicate group mean by vaccine and day of scan, shaded area: SEM. For SUVmax and SUVmean: solid lines: immunized muscle; broken lines/crosses: contralateral muscle.

the lack of a baseline scan by comparing injected and uninjected leg muscle. No increased ^{18}F-FDG or ^{11}C-PBR28 uptake was detectable after saline injection at any time point (**Figure 1E**). An intramuscular inclusion extending up to ~45 mm in the cranial - caudal axis and often branching was visible on CT scan at the site of vaccine injection at 3 hours (**Figure 2**), but not thereafter. A distinct VOI with increased uptake could be detected at the site of vaccine injection in both ^{18}F-FDG- and ^{11}C-PBR28-PET (**Figure 1**). The ^{18}F-FDG PET/CT SUVmean and SUVmax of the immunization site VOI were increased relative to the contralateral uninjected or saline injected muscle at all time points post-immunization. The kinetics of the muscle PET activity are shown in **Figure 3**. A similar level and pattern of response kinetics for all measured parameters was evident after

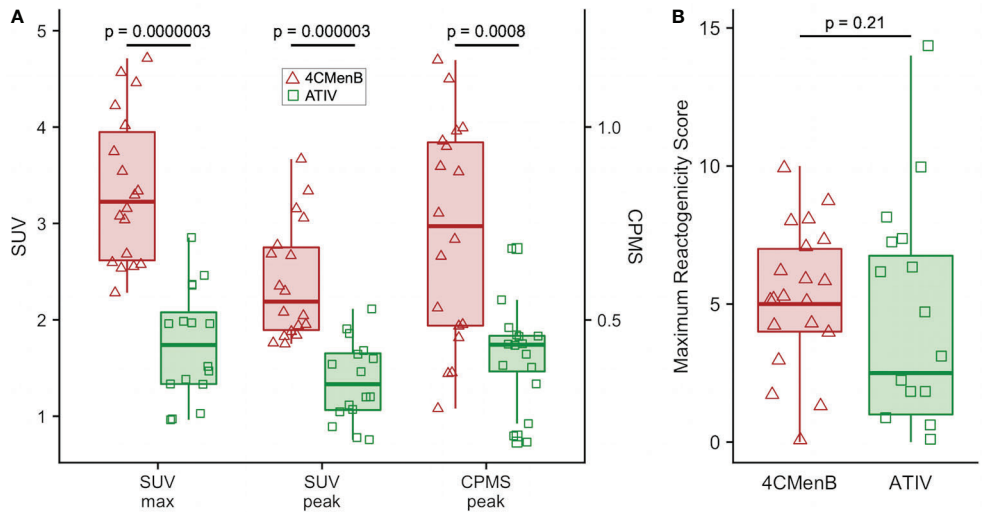

FIGURE 4 | Comparison of 4CMenB and ATIV ^{18}F-FDG PET/CT muscle activity and solicited symptoms severity scores. **(A)** SUVmax, SUVpeak and CPMS peak activity in muscle for all participants at all time points after receiving 4CMenB (pink, triangles) or ATIV (green, squares). **(B)** Maximum reactogenicity score on any day after immunization for all participants after receiving 4CMenB (red, triangles) or ATIV (green, squares). Horizontal bar: vaccine group median, shaded box: 95% confidence interval, whiskers: range. p values: Wilcoxon signed-rank test between vaccine groups.

ATIV and STIV immunization, with a progressive increase in SUVmax and SUVpeak to day 3 before falling to near the 3 h level by days 7–10 (**Figure 3**). In contrast 4CMenB induced a higher and more prolonged increase with a maximal SUVmax and SUVpeak on days 3–5 followed by only a slight decrease up to day 10 but without returning to 3 hour levels, possibly due to a depot effect of the alum formulation. The kinetics and relative levels of activity of each vaccine were also similar when attenuation corrected but not weight standardised MBq/ml values were plotted, and even with uncorrected raw counts per millisecond (CPMS) from the PET, although a relationship with VOI volume could be seen with these parameters compared with SUV (**Figures 3C–F**) as is to be expected (26). We were able to scan two participants, using a different ^{18}F-FDG PET/CT scanner, both on day 3 after immunization with AHBVV who both had a typical VOI of increased glycolysis detectable at the site of immunization with SUVmax, SUVpeak and VOI volumes of 2.3, 3.0 SUV; 1.8, 2.3 SUV; and 13.4, 36.7 cm^3 respectively (data not shown on **Figure 3**).

Although this was a small preliminary study some exploratory statistical comparisons were made between injection site ^{18}F-FDG PET/CT glycolysis in 4CMenB and ATIV immunized participants as comparable numbers and time points were available for these vaccines. The difference in the glycolysis recorded at the injection site was significantly higher after 4CMenB immunization whether SUVmax, SUVpeak or raw CPMS were compared (**Figure 4A**), which correlated with a non-significant trend to increased reactogenicity from diary card recording in participants immunized with 4CMenB (**Figure 4B**). The ^{18}F-FDG PET/CT findings reflect the post licensing clinical experience as while 4CMenB has an acceptable safety profile (32), fever was recorded in 69–79% of infants co-administered with routine vaccines, for which prophylactic use of antipyretic medication has been recommended (33) in various countries; and in adolescents and adults pain at injection site, malaise, myalgia, arthralgia and headache are very common (34). *Neisseria meningitidis* OMVs contain immunostimulatory membrane components such as lipids, proteins and lipopolysaccharide (LPS) and while detergent extraction removes the majority of LPS, residual soluble endotoxin toxicity is ameliorated by complexing OMVs with alum (35). Nevertheless, *ex vivo* whole blood stimulation assays demonstrate that 4CMenB OMVs induced the release of inflammatory cytokines TNF and IL-1β, while alum appeared to have the effect of lowering IFNγ and chemokine CXCL10 (interferon inducible 10) release (36).

For ^{11}C-PBR28-PET only 4CMenB immunization and scanning on days 1, 3, 5, and 7 were studied as the intention was only to determine whether PET/CT was sensitive enough to detect changes in ^{11}C-PBR28 binding in immunized muscle and lymph nodes and experience with ^{18}F-FDG PET/CT suggested this would be a good positive control. A distinct intramuscular VOI of increased binding was observed (**Figure 1E**) and increased SUV mean and SUV max compared with saline injected contralateral leg were detected in all subjects (**Figures 3G, H**). Generally the ^{11}C-PBR28-PET kinetics were similar to those seen with ^{18}F-FDG PET/CT at the same time points (**Figures 3G–J**).

^{18}F-FDG and ^{11}C-PBR28 PET Activity in Draining Lymph Nodes

Increased glycolysis could be identified in at least one lymph node in 38/53 subjects studied with ^{18}F-FDG PET/CT at some time after immunization (**Figures 5A–C**), which was ipsilateral

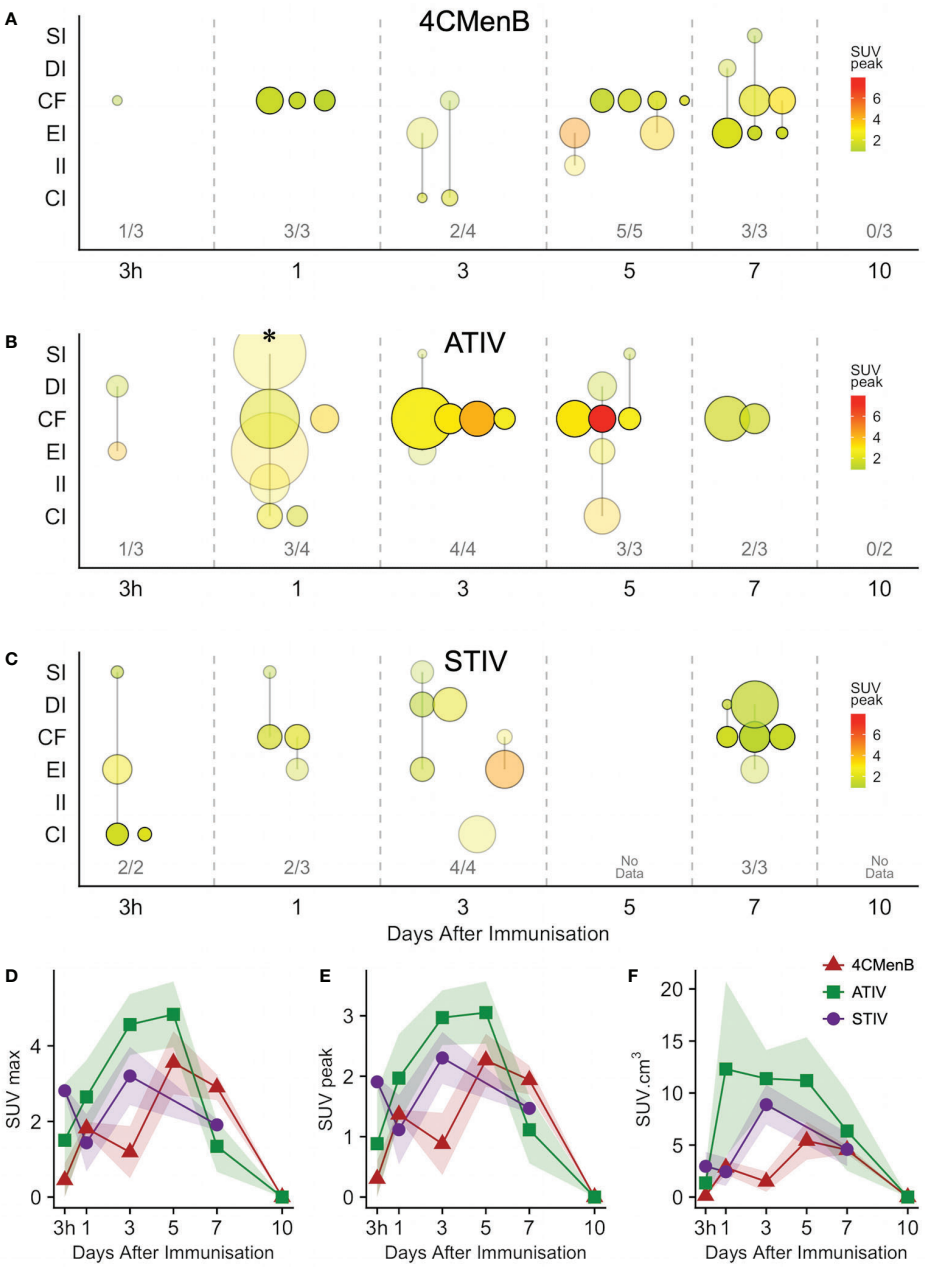

FIGURE 5 | Anatomical distribution and kinetics of lymph node ^{18}F-FDG PET activity after immunization. **(A–C)** bubble chart of lymph node ^{18}F-FDG PET activity after immunization with 4CMenB **(A)**, ATIV **(B)** or STIV **(C)**. X axis: time between scan and immunization (3 h, 1 - 10 days). Y axis: anatomical lymph node group: SI - superficial inguinal; DI - deep inguinal; CF - common femoral; EI - external iliac; II - internal iliac; CI - common iliac. Bubble diameter: lymph node volume; bubble transparency: proportion of participants with detectable lymph node activity in each anatomical group per time point; bubble color: SUVpeak. Figures above X axis: number of participants with detectable lymph node activity at each time point per total participants in group. **(D–F)** Group mean SUVmax **(D)**, SUVpeak **(E)** and total lymph node glycolysis (SUVmean x volume), **(F)** at different time points after immunization with 4CMenB (red triangles), ATIV (green squares) or STIV (purple circles). Shaded area: SEM. * participant with widely disseminated lymph node activity (**Figure 1D**).

to the side of vaccine injection in 31, contralateral in 3, and bilateral in 4 participants. As radiation exposure restrictions precluded a baseline scan it is not possible to exclude chance pre-existing increased lymph node glycolysis, although the strong ipsilateral association with vaccine injection and the kinetics of the lymph node SUV max, SUV peak and total lesion glycolysis (37) together with proportion of participants with detectable lymph nodes which showed an increase to a peak around days 3, 5, and 7 followed by a fall by day 10 (**Figures 5D, E**), strongly suggest the activation observed was induced by

immunization. The anatomical location of lymph nodes (**Figures 5A–C**) also suggests a response to immunization as across all the vaccines the most frequently observed lymph node group was the common femoral (in 28 participants), which is to be expected as it is part of the deep inguinal lymph nodes which drain the thigh muscles; followed by the external iliac nodes which drain the deep inguinal nodes (15 participants), and then common iliac (8 participants), superficial inguinal and deep inguinal (7 participants each), and internal iliac (2 participants). Due to radiation exposure restrictions the attenuation CT scan was limited to the pelvis and thigh, which precluded accurate identification of extra-pelvic nodes, but within the pelvis 18/38 participants with identifiable lymph node activity had more than one lymph node group involved, but only one participant had widely disseminated lymph node activity–on day 1 after ATIV immunization (**Figure 1D** and indicated on **Figure 5B** by *). No participants scanned on day 10 had detectable lymph nodes, although data was not available for STIV. Increased lymph node PBR28 binding was also clearly visible with ^{11}C-PBR28-PET (**Figure 1F**), which also labeled bone marrow as would be expected.

Generally ATIV immunization resulted in the highest lymph node volume and peak SUV (**Figure 5B**), which peaked on days 3 and 5 when all participants had detectable lymph nodes. This correlates with murine models in which intramuscular neutrophils and monocytes recruited by MF59C efficiently take up antigen, aided by the emulsion, and transport it to draining LNs (38) where the differentiation of monocytes to dendritic cells is enhanced by MF59C (39), resulting in enhanced triggering of antigen-specific CD4 T cell responses (39). Additionally, MF59C B cell adjuvanticity appears to be mediated by potent induction of T follicular helper cells which directly control LN germinal centre responses (40) and also correlate with long-term functional immunity (41). In contrast, we observed relatively smaller nodes with lower peak SUV (**Figure 5A**) after 4CMenB which was in marked contrast to the relative intensity of the associated muscle activation, and in keeping with murine models of immunization with OMVs containing native or genetically attenuated LPS which demonstrated that increased intramuscular inflammation was not associated with increased immunogenicity (36).

Whole Blood and Muscle Biopsy Transcriptomics Analysis

Bergström needle muscle biopsies have been used for decades with a good safety record [minor complication rate of 0.15% (25)] and provide adequate samples for histologic, ultrastructural, DNA, RNA and enzyme analysis, from a wide range of muscles (25), although the larger mass of the anterior thigh muscles is most amenable, and is an acceptable site of immunization in UK (42). Adequate RNA for analysis was obtained from all whole blood samples, and all muscle biopsies except for one taken from the contralateral unimmunized leg on day 1 after ATIV immunization.

Analysis of whole blood gene expression in blood transcriptional modules (BTMs) after ATIV immunization (**Figure 6A**) revealed the kinetics we had observed in a previous study with a larger sample size (23) with upregulation on day 1 of modules relating to innate immunity, inflammation, monocytes and IFN-related responses (LI.M67, LI.M150, LI.M75, LI.M127, LI.M165, LI.M111.1, LI.M37.0, LI.M.16, LI.M11.0, LI.S4) and cell cycle/transcription (LI.M4.0) that were also seen in the previous study, plus additional related modules (LI.M111.0, LI.M37.0, LI.S5 and LI.M.118), and in LI.M5.0 (antigen presentation). As in the previous study no upregulated whole blood gene expression was seen on day 3, but upregulation of late-phase response modules governing CD4 T cells, C-MYC and PLK1 signalling (LI.M4.4, LI.M4.2, LI.M4.10, LI.M8, LI.M46, LI.M4.7, LI.M4.5, LI.M4.1, LI.M6, LI.M102, LI.M10.0) observed in the previous study were again seen on day 5, and correlate with the enhanced antigen-specific CD4+ T cell responses we previously observed with MF59C adjuvant using flow cytometry (41).

The kinetics of whole blood gene expression changes suggest a trafficking of immune cells to and from the site of immunization, and indeed analysis of ATIV immunized muscle biopsy gene expression (compared with the uninjected muscle–**Figure 6C**) revealed a strong upregulation of modules on day 3 that were also upregulated in whole blood on day 1 (LI.M4.0, LI.M111.0, LI.M37.0, LI.MS4, LI.M11.0, LI.M16, LI.M5.0, LI.MS5, LI.M75, LI.M111.1, LI.M150, LI.M165, LI.M127, LI.M67) and associated with antigen presentation and interferon responses; together with additional modules not seen in whole blood responses (LI.M95.1, LI.M4.3, LI.M71, LI.M146, LI.M7.0, LI.M95.0, LI.M112.0, LI.M29, LI.MS10) but also strongly associated with antigen presentation. Some of the modules upregulated in muscle on day 3 were also slightly upregulated in muscle on days 1 and 7. The kinetics of these gene expression changes correlated with the level of glycolysis seen in muscle detected by ^{18}F-FDG PET/CT (**Figures 3A–F**), and correspond closely to murine models (38, 43) in which sequential muscle infiltration with neutrophils (peak 16 h), eosinophils/monocytes (peak days 2–3), and macrophages/dendritic cells (peak day 3) occurs, associated with chemokine MCP-1 (CCL-2), IL-8 (CXCL-8), CCL3 and CCL4 production. MF59C, unlike alum, also induces the release of extracellular ATP from muscle that may act as endogenous danger signal (44).

MPL, present in AS04 (45) is a detoxified lipopolysaccharide (LPS) that signals through Toll-like receptor 4 (TLR-4) although in a different way to LPS (45). Alum does not appear to synergise with MPL but prolongs the cytokine responses over the first 24h *via* a depot effect (44). In contrast with ATIV, we observed that gene expression changes in whole blood were largely absent after immunization with AHBVV, apart from a signal on day 3 in one participant in a subset of BTMs also upregulated on day 3 after immunization with ATIV (**Figure 7A**). Also in contrast with ATIV, significant upregulated gene expression could be detected in the muscle biopsy from the site of immunization at 3 h after immunization with AHBVV (**Figure 6B**), in a subset of BTMs also upregulated in muscle on day 3 after ATIV immunization and associated with TLR signalling, monocytes, neutrophils and immune activation. Looking at the individual gene expression

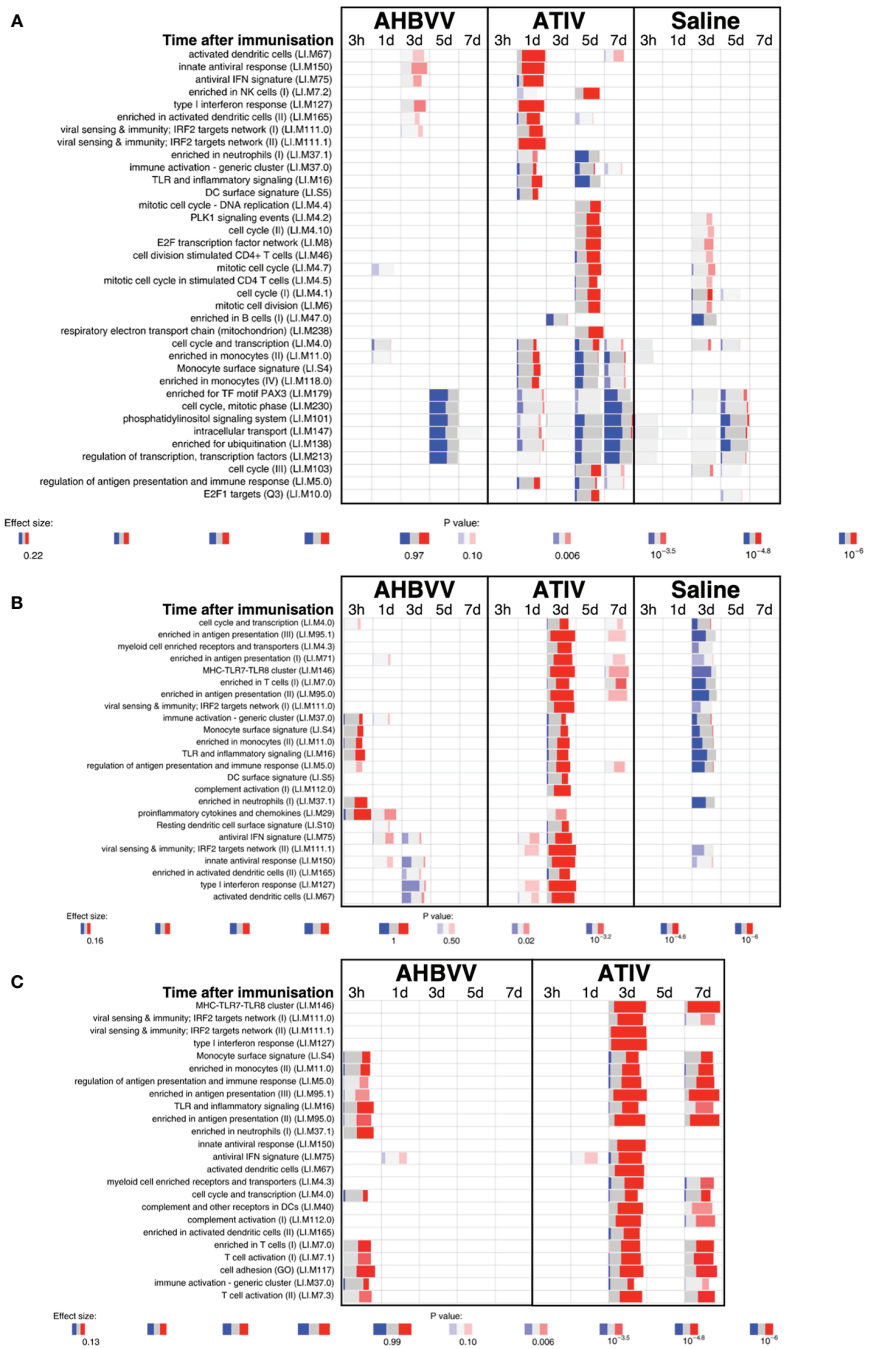

FIGURE 6 | Gene expression in whole blood and muscle at different time points after immunization. Gene set enrichment analysis of signatures at different time points after immunization in the whole blood [pre-immunization time point control **(A)**] and immunized leg muscle biopsy [**(B)** paired unimmunized leg biopsy as control; **(C)** saline group as control]. Bar sizes correspond to effect size (AUC) in the enrichment and intensity of color to the adjusted p value of enrichment (stronger color corresponds to lower adjusted p value). Red and blue boxes indicate fractions of genes that have, respectively, a significantly higher or lower expression in the test group compared to control.

profiles of participants biopsied at 3 h, 1 and 3 days after AHBVV immunization (**Figure 7B**), 6/9 had upregulation of modules also upregulated in muscle on day 3 after ATIV immunization, albeit at lower levels; whereas none of the 6 biopsied on days 5 and 7 had significant upregulation of gene expression. The upregulation of BTMs we observed closely match the kinetics and phenotype of cellular infiltrates seen murine models in which AS04 induced intramuscular production of

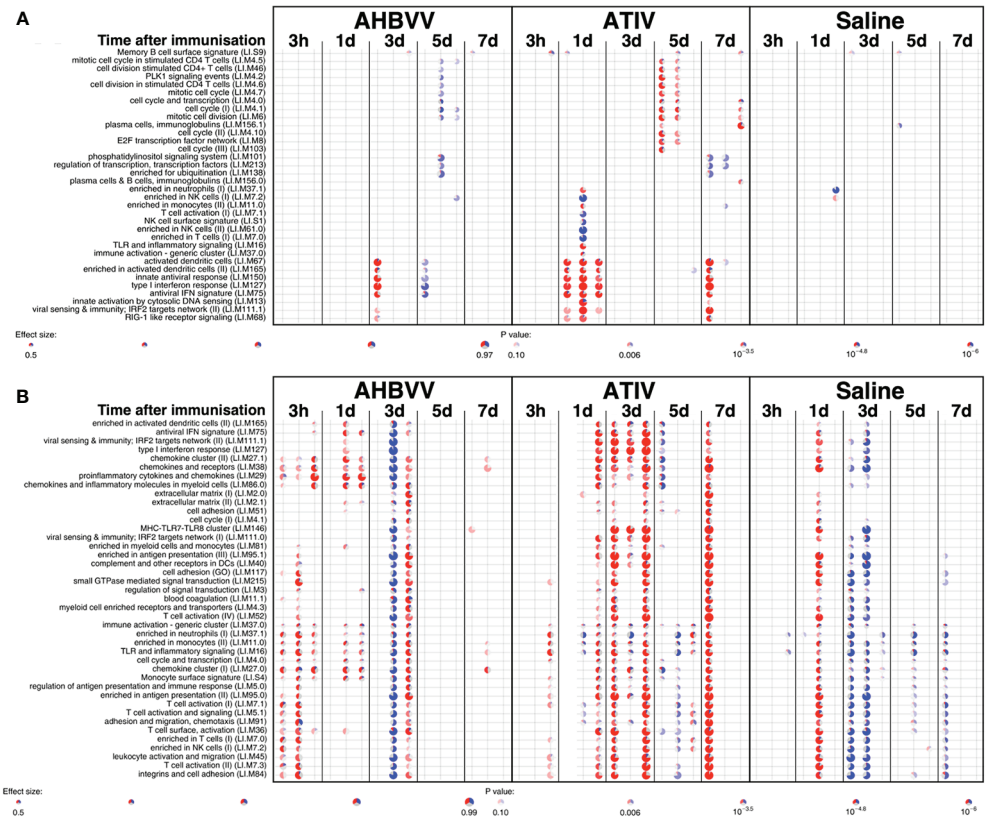

FIGURE 7 | Gene expression in whole blood and muscle from individual participants at different time points after immunization. Gene set enrichment analysis of signatures at different time points after immunization in the whole blood [pre-immunization time point control **(A)**] and immunized leg muscle biopsy [paired unimmunized leg biopsy as control, **(B)**]. Pie diameters correspond to effect size (AUC) in the enrichment and intensity of color to p value of enrichment (stronger color indicates lower p value). Red and blue sectors indicate fractions of genes that have, respectively, a higher or lower [abs(log2FC) > 0.5] expression in test group compared to control.

proinflammatory cytokines and chemokines within 3–6 h that returned to baseline by 22h (46), with an increase in activated antigen-loaded monocytes and dendritic cells within the first day after injection (44).

When gene expression of BTMs in the muscle biopsies from the site of immunization taken from participants immunized with AHBVV or ATIV was contrasted with that in the biopsies from the site of saline injection taken from participants in the control group (**Figure 6C**), the difference in the timing of the gene activation events between ATIV and AHBVV seen in the comparison between immunized and unimmunised leg biopsies was reinforced with upregulated gene expression in muscle on days 3 and to a lesser degree day 7 after immunization with ATIV, but at 3 h after immunization with AHBVV and involving a subset of the same BTMs seen after ATIV (**Figure 6C**).

We used lidocaine local anesthetic without epinephrine which has been shown to affect gene transcription (47) and took great efforts to accurately biopsy the same region of muscle that had been injected, by marking the injection site and engraving the biopsy needle to align the side port through which muscle is extracted with the exact length of the needle for injection. Nevertheless we observed significant inter-subject variation in the muscle gene expression (**Figure 7B**), which probably represents a mixture of technical biopsy issues together with biological variations in vaccine responses, which we also observed in whole blood gene expression in a previously published study (23). Furthermore, ^{18}F-FDG PET/CT revealed that it might have been better to biopsy some millimeters deeper than the needle length where the peak activity was focused (**Figures 1A, E**), and as the injectate often took a bifurcating path (**Figure 2**) it is inevitable that this and operator technique meant we probably missed the muscle region with maximal changes on some occasions.

DISCUSSION

The evaluation of vaccine reactogenicity and tolerability is traditionally undertaken during Phase 1/2 clinical trials in which participants keep a diary card of solicited and unsolicited local injection site and systemic symptoms. However, the methodology is not precise as the symptoms are typically quantified only on a four level categorical scale based on interference with activities of daily living and tend to be skewed

heavily to the first and occasionally second level (mild or moderate). This, together with inter-subject variation in perception of severity requires a large number of respondents to obtain meaningful data. While this technique may be satisfactory for the rule-out of unacceptable reactogenicity based on a benefit-risk calculation for licensing purposes, it is inefficient for the comparison of vaccine candidates and adjuvants, or fine-tuning vaccine formulations during development (1). The BIOVACSAFE project had as a major focus the application of systems vaccinology and high precision techniques to identify biomarkers of vaccine safety and reactogenicity. We therefore undertook an exploratory analysis of the ability of PET/CT scan to predict the known reactogenicity profile of these vaccines. In addition participants recorded symptoms in diary cards and we calculated a simple daily reactogenicity score based on the sum of the scores for each of the solicited symptoms. As may be expected from the published data on reactogenicity obtained during clinical development and post-licensure monitoring, the median of the maximum reactogenicity score recorded in diaries after 4CMenB immunization was higher than for ATIV, but because of the high inter-participant variance this was not clinically significant (**Figure 4B**), reinforcing the need for a large sample size when assessing vaccine reactogenicity this way. In contrast, the higher median SUVmax and SUVpeak detected by ^{18}F-FDG PET/CT was highly significantly different (**Figure 4A** and **Table 1**), and therefore predicted the extended clinical experience with these vaccines using a very small number of participants.

We selected young adults as most representative of Phase 1/2 clinical vaccine trials, which required a 10 mSv total radiation dose limit (category IIb defined by the International Commission for Radiological Protection, effective dose 1 to 10 mSv). For comparison, the average annual natural background radiation dose in the UK is 2.7 mSv (6.9 in Cornwall) and 6.2 in the USA (48). We accommodated this ethical constraint by omitting a baseline PET/CT scan, to reduce the total radiation dose to 6.0 mSv (^{18}F-FDG PET) or 3.9 mSv (^{11}C-PBR28 PET) which corresponds to approximately 2.2/1.4 years natural background radiation in the UK, and 11.6/7.5 months in the USA for the ^{18}F-FDG PET/^{11}C-PBR28 PET protocols respectively. The risk from exposure to ionizing radiation is the induction of cancers and using the risk factor for a UK population of both sexes for ages 18 −64 years has been estimated at 5% per Sievert (49), the lifetime risk of inducing a cancer in a healthy individual is therefore approximately 1 in 3300 from a dose of 6.0 mSv, although no epidemiological data actually exists for an increased risk from doses less than 10 mSv (50). This should be compared with the natural incidence rate for cancer in the UK of ~1 in 4. Furthermore, ^{18}F-FDG radioactivity is usually eliminated from the body in a few hours, and as the half-life of ^{11}C is 20 min most of the radioactivity is eliminated from the body before the subject leaves the imaging unit. While the intramuscular activity could be controlled by the contralateral unimmunized leg, we could not rule out baseline increased nodal activity, although the kinetics and distribution of observed nodal activation strongly suggests a response to the vaccines. We also chose to do a CT scan to allow PET activity correction for tissue attenuation and the anatomical location of increased activity—especially within lymph nodes. However, it is interesting that the intramuscular ^{18}F-FDG PET activity measured only by the CPMS, without correction for tissue attenuation or the body mass of the participant, was still highly significantly different between 4CMenB and ATIV (**Figure 4A**), suggesting that PET alone could be used to quantify the early intramuscular inflammatory immune events, and PET may be calibrated using fixed radiation sources. Therefore, the total radiation dose could be reduced by omitting the CT scan which could permit baseline and serial scans on the same participant. Alternatively, PET/MRI scanning is increasingly available and has been shown to work with tissue-specific radioligands such as ^{11}C-PBR28 (51). These alternatives, together with potentially injecting different formulations and controls into the limbs of the same participant, or recruiting older participants for whom a higher total dose is acceptable, would allow the quantification and kinetics of the inflammatory events that will lead to the immune responses to different vaccines, adjuvants, formulations or doses to be evaluated in far fewer people than are currently required in Phase 1 and 2 trials.

While the application of systems biology techniques to biopsy material is an attractive way to study immune interactions following human immunization, it would be preferable to employ non-invasive techniques where possible. The development of highly specific radioligands suitable for clinical use that can be radiolabeled and target defined tissue or cell markers is now well established in the study of neurological disease, malignancy and pharmacokinetics. However, the use of such radioligands to characterize immune activation events following immunization has not been reported. We therefore took advantage of local expertise with one such ligand, PBR28 and the availability of an onsite cyclotron and scanning facility to conduct a very preliminary study of ^{11}C-PBR28-PET/CT responses to immunization, selecting 4CMenB and days 1–7 scans to optimize the likelihood of detecting a signal. The 18-kDa translocator protein (TSPO; formerly known as the peripheral benzodiazepine receptor, PBR) is a mitochondrial membrane protein involved in steroidogenesis and cholesterol transport expressed throughout the body, and highly upregulated in microglia, macrophages (52) and CD4+ T cells (53) during inflammation. It has therefore been used as a PET imaging target for the investigation of inflammatory diseases involving microglial activation and/or macrophage recruitment (54–58). As the affinity of PBR28 depends on a single polymorphism (rs6971) in the TSPO gene (59), individuals who expressed only low-affinity TSPO were excluded by genetic screening. We postulated that ^{11}C-PBR28 would identify activated macrophages and other immune cells at the vaccine injection site and draining lymph nodes. Indeed, ^{11}C-PBR28-PET/CT revealed a well-defined VOI with increased ^{11}C-PBR28 binding at the site of immunization in all participants scanned between days 1–7 (**Figures 1** and **3**), which correlated well with ^{18}F-FDG PET/CT, and further supports the expected infiltration of immune cells. Increased ^{11}C-PBR28 binding within draining lymph nodes was also evident, with sharply defined anatomy

in comparison with ^{18}F-FDG/CT (**Figure 1**). These findings suggest that PET/CT employing radiolabeled molecules such as monoclonal antibodies certified for clinical use targeting immune cell surface markers or cytokines and chemokines within target tissues may be a practical technique to characterize *in vivo* immune responses to vaccines, and to quantify pro-inflammatory and pro-immunogenicity responses to different adjuvants, formulations and doses in humans.

While whole blood gene expression is an effective way to study trafficking immune cells, there is increased interest in applying systems biology and high precision techniques to sites of immune interaction in humans, especially lymph nodes (60). In this study we complemented our previously published (23) studies comparing whole blood gene expression responses of humans to different live, subunit and adjuvanted/unadjuvanted vaccines, to further characterize the muscle activation observed on PET/CT by obtaining tissue biopsies from the injection site after intramuscular immunization with the adjuvanted vaccines AHBVV and ATIV, or a saline control. The kinetics and gene signatures associated with activated BTMs correlated very well with animal models characterizing the cellular infiltrates and immune responses at the site of immunization and in draining lymph nodes, and "closed the loop" on the patterns previously seen in whole blood by demonstrating the tissue migration and then efflux of activated cells (summarised in **Table 1**). This study demonstrates that tissue biopsy after immunization is both practical and ethical in human models of immunity and inflammation. While the Bergström technique is safe, well tolerated and provides a large tissue sample (25), it may be that multiple, radiologically-guided fine needle aspirates may be more efficient at obtaining a representative muscle biopsy with less trauma. Our PET/CT data also show that different vaccines and adjuvants induce different patterns of lymph node activation, and while the anatomical location of activated lymph nodes may be broadly predicted by knowledge of drainage patterns, there was significant inter-participant variation with often only one activated node in a group. ^{18}F-FDG PET/CT, combined with guided fine needle aspiration therefore offers a technique to increase the chance that only lymph nodes that are actually responding to immunization are aspirated and at the optimal time point, which is especially important in systems biology and high precision techniques where practical sample sizes are often small and aggregated data may be biased by non-responding tissue samples. Indeed in a recent human study of immunization with an unadjuvanted influenza vaccine (60), weekly lymph node aspirates provided useful samples for flow cytometry in only 3/8 participants, which the authors concluded could have been due to the aspiration of a non-responding node and/or mis-timing the response. In our studies with 4CMenB, ATIV and STIV we observed a peak response in lymph nodes around days 3–5, which contrasts with some case series where increased lymph node ^{18}F-FDG PET/CT activity could be detected some weeks after immunization. However, these studies were opportunistic retrospective observations in patients undergoing ^{18}F-FDG PET/CT as part of cancer or other treatment, and in whom the exact vaccine and immunization date was not recorded as part of the study, and highlights the importance of prospectively and systematically determining the kinetics of ^{18}F-FDG PET/CT and tissue site responses for each vaccine candidate or adjuvant to optimize systems vaccinology and high precision imaging techniques.

In conclusion we have demonstrated that PET/CT and gene expression analysis of tissue biopsies are ethically and practically acceptable for intensive, small scale predictive clinical studies of vaccine inflammatory and immune responses, and with the application of target-specific radioligands, radioactive dose-reducing techniques and temporally- and anatomically-guided biopsies may contribute to a better understanding of the balance between inflammatory and immune responses, and the selection and optimisation of candidate vaccines and adjuvants with shorter development times and enhanced safety and reactogenicity profiles.

DATA AVAILABILITY STATEMENT

The datasets presented in this study can be found in online repositories. The name of the repository and accession number can be found here: https://www.ncbi.nlm.nih.gov/geo/, GSE124719.

ETHICS STATEMENT

The studies involving human participants were reviewed and approved by London - Surrey Borders Research Ethics Committee Health Research Authority. The participants provided their written informed consent to participate in this study.

AUTHOR CONTRIBUTIONS

ZW interpretation and analysis of PET/CT, manuscript review. JW analysis of transcriptomics, manuscript review. NP and RS design of PET/CT protocols, conducting scans, manuscript review. JM, H-JM, and KP preparation and processing of tissue samples, study design, manuscript review. AG and AL collection of samples, clinical management, manuscript review. TC and CB clinical project management, manuscript review. PD, GG, and SK manuscript review. DL project design, manuscript initial draft, and review. All authors contributed to the article and approved the submitted version.

FUNDING

This is a summary of independent research carried out at the NICRF and funded in part by the Imperial Biological Research Centre. The views expressed are those of the authors and not necessarily those of the funders, NHS, the NIHR or the Department of Health. Funding was also received from the Innovative Medicines Initiative Joint Undertaking

"BIOVACSAFE" under grant agreement no. 115308, resources of which are composed of financial contribution from the European Union's Seventh Framework Programme (FP7/2007-2013) and EFPIA companies' in kind contribution; and the European Union's Seventh Framework Programme under grant agreement no. 280873 "ADITEC".

ACKNOWLEDGMENTS

We thank E Aboagye and A Busza ICL, and K Nijran ICHNT for advice and assistance with ^{18}F-FDG PET/CT; R Janisch, G Searle, A Saleem, Invicro London for ^{11}C-PBR28-PET/CT; and DR Owen, ICL for advice on TSPO.

REFERENCES

1. Della Cioppa G, Jonsdottir I, Lewis D. Challenges in early clinical development of adjuvanted vaccines. *Vaccine* (2015) 33 Suppl 2:B47–51. doi: 10.1016/j.vaccine.2015.02.031
2. Edwards K, Lambert PH, Black S. Narcolepsy and Pandemic Influenza Vaccination: What We Need to Know to be Ready for the Next Pandemic. *Pediatr Infect Dis J* (2019) 38(8):873–6. doi: 10.1097/INF.0000000000002398
3. Kassim P, Eslick GD. Risk of intussusception following rotavirus vaccination: An evidence based meta-analysis of cohort and case-control studies. *Vaccine* (2017) 35(33):4276–86. doi: 10.1016/j.vaccine.2017.05.064
4. Mutsch M, Zhou W, Rhodes P, Bopp M, Chen RT, Linder T, et al. Use of the inactivated intranasal influenza vaccine and the risk of Bell's palsy in Switzerland. *N Engl J Med* (2004) 350(9):896–903. doi: 10.1056/NEJMoa030595
5. Rappuoli R, Siena E, Finco O. Will Systems Biology Deliver Its Promise and Contribute to the Development of New or Improved Vaccines? Systems Biology Views of Vaccine Innate and Adaptive Immunity. *Cold Spring Harb Perspect Biol* (2018) 10(8):1–9. doi: 10.1101/cshperspect.a029256
6. Olafsdottir TA, Lindqvist M, Nookaew I, Andersen P, Maertzdorf J, Persson J, et al. Comparative Systems Analyses Reveal Molecular Signatures of Clinically tested Vaccine Adjuvants. *Sci Rep* (2016) 6:39097. doi: 10.1038/srep39097
7. Querec TD, Akondy RS, Lee EK, Cao W, Nakaya HI, Teuwen D, et al. Systems biology approach predicts immunogenicity of the yellow fever vaccine in humans. *Nat Immunol* (2009) 10(1):116–25. doi: 10.1038/ni.1688
8. Mastelic B, Lewis DJ, Golding H, Gust I, Sheets R, Lambert PH. Potential use of inflammation and early immunological event biomarkers in assessing vaccine safety. *Biologicals* (2013) 41(2):115–24. doi: 10.1016/j.biologicals.2012.10.005
9. Medaglini D, Andersen P, Rappuoli R. Editorial: Advanced Immunization Technologies for Next Generation Vaccines. *Front Immunol* (2020) 11:878. doi: 10.3389/fimmu.2020.00878
10. Rappuoli R, Medaglini D. ADITEC: joining forces for next-generation vaccines. *Sci Transl Med* (2012) 4(128):128cm4. doi: 10.1126/scitranslmed.3003826
11. Denoel P, Londono-Hayes P, Chlebus M, de Azero MR. Impact of the Innovative Medicines Initiative on vaccine development. *Nat Rev Drug Discovery* (2018) 17(11):769–70. doi: 10.1038/nrd.2018.72
12. Lewis DJ, Lythgoe MP. Application of "Systems Vaccinology" to Evaluate Inflammation and Reactogenicity of Adjuvanted Preventative Vaccines. *J Immunol Res* (2015) 2015:909406. doi: 10.1155/2015/909406
13. Ayati N, Jesudason S, Berlangieri SU, Scott AM. Generalized Lymph Node Activation after Influenza Vaccination on (18)F FDG-PET/CT Imaging, an Important Pitfall in PET Interpretation. *Asia Ocean J Nucl Med Biol* (2017) 5 (2):148–50. doi: 10.22038/aojnmb.2017.8702
14. Galloway TL, Johnston MJ, Starsiak MD, Silverman ED. A Unique Case of Increased 18F-FDG Metabolic Activity in the Soft Tissues of the Bilateral Upper Thighs Due to Immunizations in a Pediatric Patient. *World J Nucl Med* (2017) 16(1):59–61. doi: 10.4103/1450-1147.176886
15. Mingos M, Howard S, Giacalone N, Kozono D, Jacene H. Systemic Immune Response to Vaccination on FDG-PET/CT. *Nucl Med Mol Imaging* (2016) 50 (4):358–61. doi: 10.1007/s13139-015-0385-6
16. Kim JE, Kim EK, Lee DH, Kim SW, Suh C, Lee JS. False-positive hypermetabolic lesions on post-treatment PET-CT after influenza vaccination. *Korean J Intern Med* (2011) 26(2):210–2. doi: 10.3904/kjim.2011.26.2.210
17. Burger IA, Husmann L, Hany TF, Schmid DT, Schaefer NG. Incidence and intensity of F-18 FDG uptake after vaccination with H1N1 vaccine. *Clin Nucl Med* (2011) 36(10):848–53. doi: 10.1097/RLU.0b013e3182177322
18. Panagiotidis E, Exarhos D, Housianakou I, Bournazos A, Datseris I. FDG uptake in axillary lymph nodes after vaccination against pandemic (H1N1). *Eur Radiol* (2010) 20(5):1251–3. doi: 10.1007/s00330-010-1719-5
19. Shirone N, Shinkai T, Yamane T, Uto F, Yoshimura H, Tamai H, et al. Axillary lymph node accumulation on FDG-PET/CT after influenza vaccination. *Ann Nucl Med* (2012) 26(3):248–52. doi: 10.1007/s12149-011-0568-x
20. Thomassen A, Lerberg Nielsen A, Gerke O, Johansen A, Petersen H. Duration of 18F-FDG avidity in lymph nodes after pandemic H1N1v and seasonal influenza vaccination. *Eur J Nucl Med Mol Imaging* (2011) 38(5):894–8. doi: 10.1007/s00259-011-1729-9
21. Coates EE, Costner PJ, Nason MC, Herrin DM, Conant S, Herscovitch P, et al. Lymph Node Activation by PET/CT Following Vaccination With Licensed Vaccines for Human Papillomaviruses. *Clin Nucl Med* (2017) 42(5):329–34. doi: 10.1097/RLU.0000000000001603
22. McKay PF, Cizmeci D, Aldon Y, Maertzdorf J, Weiner J, Kaufmann SH, et al. Identification of potential biomarkers of vaccine inflammation in mice. *Elife* (2019) 8:1–23. doi: 10.7554/eLife.46149
23. Weiner J, Lewis DJM, Maertzdorf J, Mollenkopf HJ, Bodinham C, Pizzoferro K, et al. Characterization of potential biomarkers of reactogenicity of licensed antiviral vaccines: randomized controlled clinical trials conducted by the BIOVACSAFE consortium. *Sci Rep* (2019) 9(1):20362. doi: 10.1038/s41598-019-56994-8
24. Tregoning JS, Weiner J, Cizmeci D, Hake D, Maertzdorf J, Kaufmann SHE, et al. Pregnancy has a minimal impact on the acute transcriptional signature to vaccination. *NPJ Vaccin* (2020) 5:29. doi: 10.1038/s41541-020-0177-6
25. Tarnopolsky MA, Pearce E, Smith K, Lach B. Suction-modified Bergstrom muscle biopsy technique: experience with 13,500 procedures. *Muscle Nerve* (2011) 43(5):717–25. doi: 10.1002/mus.21945
26. Sarikaya I, Sarikaya A. Assessing PET Parameters in Oncologic (18)F-FDG Studies. *J Nucl Med Technol* (2020) 48(3):278–82. doi: 10.2967/jnmt.119.236109
27. Zyla J, Marczyk M, Domaszewska T, Kaufmann SHE, Polanska J, Weiner J. Gene set enrichment for reproducible science: comparison of CERNO and eight other algorithms. *Bioinformatics* (2019) 35(24):5146–54. doi: 10.1093/bioinformatics/btz447
28. Li S, Rouphael N, Duraisingham S, Romero-Steiner S, Presnell S, Davis C, et al. Molecular signatures of antibody responses derived from a systems biology study of five human vaccines. *Nat Immunol* (2014) 15(2):195–204. doi: 10.1038/ni.2789
29. Chaussabel D, Quinn C, Shen J, Patel P, Glaser C, Baldwin N, et al. A modular analysis framework for blood genomics studies: application to systemic lupus erythematosus. *Immunity* (2008) 29(1):150–64. doi: 10.1016/j.immuni.2008.05.012
30. Julyan PJ, Taylor JH, Hastings DL, Williams HA, Zweit J. SUVpeak: a new parameter for quantification of uptake in FDG PET. *Nucl Med Commun* (2004) 25:407. doi: 10.1097/00006231-200404000-00040
31. Akamatsu G, Ikari Y, Nishida H, Nishio T, Ohnishi A, Maebatake A, et al. Influence of Statistical Fluctuation on Reproducibility and Accuracy of SUVmax and SUVpeak: A Phantom Study. *J Nucl Med Technol* (2015) 43 (3):222–6. doi: 10.2967/jnmt.115.161745
32. Bryan P, Seabroke S, Wong J, Donegan K, Webb E, Goldsmith C, et al. Safety of multicomponent meningococcal group B vaccine (4CMenB) in routine infant immunisation in the UK: a prospective surveillance study. *Lancet Child Adolesc Health* (2018) 2(6):395–403. doi: 10.1016/S2352-4642(18)30103-2
33. Public Health England. *Meningococcal B Vaccination Information for healthcare professionals* (2019). Available at: https://assets.publishing.service.gov.uk/government/uploads/system/uploads/attachment_data/file/770824/Men_B_HCP_Information_December_2018 (Accessed September 7, 2020).
34. electronic medicines compendium. *Bexsero Meningococcal Group B vaccine for injection in pre-filled syringe* (2019). Available at: https://www.medicines.org.uk/emc/product/5168/smpc (Accessed September 7, 2020).

35. Fredriksen JH, Rosenqvist E, Wedege E, Bryn K, Bjune G, Froholm LO, et al. Production, characterization and control of MenB-vaccine "Folkehelsa": an outer membrane vesicle vaccine against group B meningococcal disease. *NIPH Ann* (1991) 14(2):67–79; discussion -80.
36. Dowling DJ, Sanders H, Cheng WK, Joshi S, Brightman S, Bergelson I, et al. A Meningococcal Outer Membrane Vesicle Vaccine Incorporating Genetically Attenuated Endotoxin Dissociates Inflammation from Immunogenicity. *Front Immunol* (2016) 7:562. doi: 10.3389/fimmu.2016.00562
37. McDonald JE, Kessler MM, Gardner MW, Buros AF, Ntambi JA, Waheed S, et al. Assessment of Total Lesion Glycolysis by (18)F FDG PET/CT Significantly Improves Prognostic Value of GEP and ISS in Myeloma. *Clin Cancer Res* (2017) 23(8):1981–7. doi: 10.1158/1078-0432.CCR-16-0235
38. Calabro S, Tortoli M, Baudner BC, Pacitto A, Cortese M, O'Hagan DT, et al. Vaccine adjuvants alum and MF59 induce rapid recruitment of neutrophils and monocytes that participate in antigen transport to draining lymph nodes. *Vaccine* (2011) 29(9):1812–23. doi: 10.1016/j.vaccine.2010.12.090
39. Cioncada R, Maddaluno M, Vo HTM, Woodruff M, Tavarini S, Sammicheli C, et al. Vaccine adjuvant MF59 promotes the intranodal differentiation of antigen-loaded and activated monocyte-derived dendritic cells. *PloS One* (2017) 12(10):e0185843. doi: 10.1371/journal.pone.0185843
40. Mastelic Gavillet B, Eberhardt CS, Auderset F, Castellino F, Seubert A, Tregoning JS, et al. MF59 Mediates Its B Cell Adjuvanticity by Promoting T Follicular Helper Cells and Thus Germinal Center Responses in Adult and Early Life. *J Immunol* (2015) 194(10):4836–45. doi: 10.4049/jimmunol.1402071
41. Spensieri F, Siena E, Borgogni E, Zedda L, Cantisani R, Chiappini N, et al. Early Rise of Blood T Follicular Helper Cell Subsets and Baseline Immunity as Predictors of Persisting Late Functional Antibody Responses to Vaccination in Humans. *PloS One* (2016) 11(6):e0157066. doi: 10.1371/journal.pone.0157066
42. Public Health England. *Immunisation against infectious disease*. (2014). Available at: https://www.gov.uk/government/collections/immunisation-against-infectious-disease-the-green-book.
43. O'Hagan DT, Ott GS, De Gregorio E, Seubert A. The mechanism of action of MF59 - an innately attractive adjuvant formulation. *Vaccine* (2012) 30 (29):4341–8. doi: 10.1016/j.vaccine.2011.09.061
44. Del Giudice G, Rappuoli R, Didierlaurent AM. Correlates of adjuvanticity: A review on adjuvants in licensed vaccines. *Semin Immunol* (2018) 39:14–21. doi: 10.1016/j.smim.2018.05.001
45. Shi S, Zhu H, Xia X, Liang Z, Ma X, Sun B. Vaccine adjuvants: Understanding the structure and mechanism of adjuvanticity. *Vaccine* (2019) 37(24):3167–78. doi: 10.1016/j.vaccine.2019.04.055
46. Didierlaurent AM, Morel S, Lockman L, Giannini SL, Bisteau M, Carlsen H, et al. AS04, an aluminum salt- and TLR4 agonist-based adjuvant system, induces a transient localized innate immune response leading to enhanced adaptive immunity. *J Immunol* (2009) 183(10):6186–97. doi: 10.4049/jimmunol.0901474
47. Trappe TA, Standley RA, Liu SZ, Jemiolo B, Trappe SW, Harber MP. Local anesthetic effects on gene transcription in human skeletal muscle biopsies. *Muscle Nerve* (2013) 48(4):591–3. doi: 10.1002/mus.23860
48. Public Health England. *Ionising radiation: dose comparisons* (2011). Available at: https://www.gov.uk/government/publications/ionising-radiation-dose-comparisons/ionising-radiation-dose-comparisons (Accessed 17 November 2020).
49. McKinlay AF AF, Allen SG, Dimbylow PJ, Muirhead CR, Saunders RD, Stather JW. *Documents of the National Radiation Protection Board*. (1993).
50. Lin EC. Radiation risk from medical imaging. *Mayo Clin Proc* (2010) 85 (12):1142–6; quiz 6. doi: 10.4065/mcp.2010.0260
51. Alshikho MJ, Zurcher NR, Loggia ML, Cernasov P, Reynolds B, Pijanowski O, et al. Integrated magnetic resonance imaging and [(11) C]-PBR28 positron emission tomographic imaging in amyotrophic lateral sclerosis. *Ann Neurol* (2018) 83(6):1186–97. doi: 10.1002/ana.25251
52. Kopecky C, Pandzic E, Parmar A, Szajer J, Lee V, Dupuy A, et al. Translocator protein localises to CD11b(+) macrophages in atherosclerosis. *Atherosclerosis* (2019) 284:153–9. doi: 10.1016/j.atherosclerosis.2019.03.011
53. Narayan N, Owen DR, Mandhair H, Smyth E, Carlucci F, Saleem A, et al. Translocator Protein as an Imaging Marker of Macrophage and Stromal Activation in Rheumatoid Arthritis Pannus. *J Nucl Med* (2018) 59(7):1125–32. doi: 10.2967/jnumed.117.202200
54. Banati RB, Newcombe J, Gunn RN, Cagnin A, Turkheimer F, Heppner F, et al. The peripheral benzodiazepine binding site in the brain in multiple sclerosis: quantitative in vivo imaging of microglia as a measure of disease activity. *Brain* (2000) 123(Pt 11):2321–37. doi: 10.1093/brain/123.11.2321
55. Cagnin A, Brooks DJ, Kennedy AM, Gunn RN, Myers R, Turkheimer FE, et al. In-vivo measurement of activated microglia in dementia. *Lancet* (2001) 358 (9280):461–7. doi: 10.1016/S0140-6736(01)05625-2
56. Edison P, Archer HA, Gerhard A, Hinz R, Pavese N, Turkheimer FE, et al. Microglia, amyloid, and cognition in Alzheimer's disease: An [11C](R) PK11195-PET and [11C]PIB-PET study. *Neurobiol Dis* (2008) 32(3):412–9. doi: 10.1016/j.nbd.2008.08.001
57. Gerhard A, Pavese N, Hotton G, Turkheimer F, Es M, Hammers A, et al. In vivo imaging of microglial activation with [11C](R)-PK11195 PET in idiopathic Parkinson's disease. *Neurobiol Dis* (2006) 21(2):404–12. doi: 10.1016/j.nbd.2005.08.002
58. Ramsay SC, Weiller C, Myers R, Cremer JE, Luthra SK, Lammertsma AA, et al. Monitoring by PET of macrophage accumulation in brain after ischaemic stroke. *Lancet* (1992) 339(8800):1054–5. doi: 10.1016/0140-6736(92)90576-o
59. Owen DR, Yeo AJ, Gunn RN, Song K, Wadsworth G, Lewis A, et al. An 18-kDa translocator protein (TSPO) polymorphism explains differences in binding affinity of the PET radioligand PBR28. *J Cereb Blood Flow Metab* (2012) 32(1):1–5. doi: 10.1038/jcbfm.2011.147
60. Turner JS, Zhou JQ, Han J, Schmitz AJ, Rizk AA, Alsoussi WB, et al. Human germinal centres engage memory and naive B cells after influenza vaccination. *Nature* (2020) 586(7827):127–32. doi: 10.1038/s41586-020-2711-0

Conflict of Interest: PD and GG are employees of the GSK group of companies, and report receiving restricted shares of the company.

The remaining authors declare that the research was conducted in the absence of any commercial or financial relationships that could be construed as a potential conflict of interest.

frontiers in Immunology

ORIGINAL RESEARCH
published: 04 March 2021
doi: 10.3389/fimmu.2020.559382

Polymeric Pathogen-Like Particles-Based Combination Adjuvants Elicit Potent Mucosal T Cell Immunity to Influenza A Virus

Brock Kingstad-Bakke[1], Randall Toy[2], Woojong Lee[1], Pallab Pradhan[2], Gabriela Vogel[2], Chandranaik B. Marinaik[1], Autumn Larsen[1], Daisy Gates[1], Tracy Luu[1], Bhawana Pandey[2], Yoshihoro Kawaoka[1], Krishnendu Roy[2] and M. Suresh[1]**

[1] Department of Pathobiological Sciences, University of Wisconsin-Madison, Madison, WI, United States, [2] The Wallace H. Coulter Department of Biomedical Engineering Georgia Institute of Technology and Emory University, Atlanta, GA, United States

OPEN ACCESS

Edited by:
Jay Evans,
University of Montana, United States

Reviewed by:
Tomoko Hayashi,
University of California, San Diego, United States
Kaitlyn Morabito,
Vaccine Research Center (NIAID), United States

***Correspondence:**
Krishnendu Roy
krish.roy@gatech.edu
M. Suresh
sureshm@vetmed.wisc.edu

Specialty section:
This article was submitted to Vaccines and Molecular Therapeutics, a section of the journal Frontiers in Immunology

Received: 06 May 2020
Accepted: 21 December 2020
Published: 04 March 2021

Citation:
Kingstad-Bakke B, Toy R, Lee W, Pradhan P, Vogel G, Marinaik CB, Larsen A, Gates D, Luu T, Pandey B, Kawaoka Y, Roy K and Suresh M (2021) Polymeric Pathogen-Like Particles-Based Combination Adjuvants Elicit Potent Mucosal T Cell Immunity to Influenza A Virus. Front. Immunol. 11:559382. doi: 10.3389/fimmu.2020.559382

Eliciting durable and protective T cell-mediated immunity in the respiratory mucosa remains a significant challenge. Polylactic-co-glycolic acid (PLGA)-based cationic pathogen-like particles (PLPs) loaded with TLR agonists mimic biophysical properties of microbes and hence, simulate pathogen-pattern recognition receptor interactions to safely and effectively stimulate innate immune responses. We generated micro particle PLPs loaded with TLR4 (glucopyranosyl lipid adjuvant, GLA) or TLR9 (CpG) agonists, and formulated them with and without a mucosal delivery enhancing carbomer-based nanoemulsion adjuvant (ADJ). These adjuvants delivered intranasally to mice elicited high numbers of influenza nucleoprotein (NP)-specific CD8+ and CD4+ effector and tissue-resident memory T cells (T_{RM}s) in lungs and airways. PLPs delivering TLR4 versus TLR9 agonists drove phenotypically and functionally distinct populations of effector and memory T cells. While PLPs loaded with CpG or GLA provided immunity, combining the adjuvanticity of PLP-GLA and ADJ markedly enhanced the development of airway and lung T_{RM}s and CD4 and CD8 T cell-dependent immunity to influenza virus. Further, balanced CD8 (Tc1/Tc17) and CD4 (Th1/Th17) recall responses were linked to effective influenza virus control. These studies provide mechanistic insights into vaccine-induced pulmonary T cell immunity and pave the way for the development of a universal influenza and SARS-CoV-2 vaccines.

Keywords: adjuvants, CD8, tissue-resident memory, CD4, influenza A virus, vaccine, polyfunctional

INTRODUCTION

Respiratory infections in adults and children have been among the top three leading causes of death and disability in the world for decades (1, 2). Novel respiratory pathogens are emerging and can quickly spread due to the ease of transmission, as witnessed in the current coronavirus (3–5) and past influenza pandemics (6). Vaccines are essential for the control and elimination of these diseases by eliciting antibody and/or T cell-mediated immune responses (CMI). The necessity for effective T

cell-based vaccines to respiratory pathogens is exemplified by continued seasonal influenza endemics and sporadic pandemics, despite wide vaccine availability and high virus infection rates.

Widely used inactivated influenza vaccines (IIV) function by eliciting subtype-specific antibodies to mutation-prone surface hemagglutinin (HA) and neuraminidase (NA) proteins, and must be reformulated annually to match seasonal strains due to antigenic drift and shift (7). Further, these IIVs are poorly immunogenic for CD8 T cells. Influenza viral infection can generate strong antibody and T cell-mediated immunity (CMI), and while antibodies are still strongly strain matched in terms of protection, heterosubtypic protection to influenza requires CMI to conserved viral epitopes (7, 8).

Robust T cell control of heterosubtypic influenza infection has been closely associated with the development of mucosally residing tissue resident memory (T_{RM}) CD4+ and CD8+ cells (9, 10). However, the numbers of T_{RM} cells after influenza infection have been observed to wane over time with a concomitant decrease in heterosubtypic protection (10–12). Indeed, neither mass vaccination with current IIV or widespread infection have adequately curtailed the continuous infection of influenza virus in human populations. Therefore, development of vaccination strategies to potently elicit long-lived T_{RM} cells and understanding of what factors govern these responses are crucially needed to control respiratory infections such as influenza.

Several groups have developed vaccines to elicit influenza-specific lung T_{RM} cells that confer heterosubtypic protection to influenza virus challenge using live attenuated influenza viruses (13), or viral vectors (14). Recently, we have tested a novel adjuvant, Adjuplex (ADJ, a nano emulsion of carbomer and soy lethicin (15)), that when combined with subunit or IIV proteins potently induced CD8+ lung T_{RM} cell responses after mucosal administration, and conferred substantial protection to influenza virus challenge (16, 17). These studies highlight the importance for identification of novel adjuvants that can elicit mucosal CMI to non-replicating antigens, particularly so we can dissect and study the individual effects these adjuvants have on the magnitude and nature of the resultant mucosal CMI responses.

TLR ligands as adjuvants for influenza vaccines have been widely studied and are typically delivered in monomeric, soluble formulations (18). In order to mimic biophysical interactions between pattern-recognition receptors and their ligands on pathogens, we have developed TLR agonist-loaded polylactic-co-glycolic acid (PLGA)-based pathogen-like particles (PLPs) (19). Varying the size of the PLPs and the density of the loaded TLR agonist CpG, modulated the signaling circuitry within dendritic cells *in vitro* and altered the nature of antibody (T_H1 versus T_H2-driven) responses. Additionally, agonists presented simultaneously on PLPs have been shown to differentially modulate immune responses *in vitro*, compared with soluble counterparts, while potentially improving safety by reducing toxicity from systemic diffusion (20, 21). The ability of TLR-agonist-loaded PLPs to stimulate antigen-specific T cell responses, especially in the respiratory mucosa, has not yet been investigated.

Here, we investigated whether CpG- or glucopyranosyl lipid adjuvant (22) (GLA)-loaded PLP adjuvants mixed with influenza virus nucleoprotein (NP) protein, with or without ADJ could elicit antigen-specific CD4 and CD8 T cells, and analyzed their numbers, frequencies, and phenotypes in mucosal compartments. We found that PLP vaccine formulations elicited strong, yet phenotypically and functionally distinct T_{RM} CD8+ and CD4+ responses in the lungs of vaccinated mice. Further, we observed that PLP-based adjuvants afforded strong and durable protection from influenza challenge that was closely associated with distinct functional recall profiles of CD4 and CD8 T cells unique to the PLP vaccine formulation. These results highlight that PLP-loaded adjuvants can distinctly program effective CMI and can be leveraged to study immunity and develop vaccines to respiratory pathogens such as influenza virus and SARS-CoV-2.

METHODS

Experimental Animals

Six- to 12-week-old C57BL/6J (B6) were purchased from Jackson Laboratory or from restricted-access specific-pathogen-free (SPF) mouse breeding colonies at the University of Wisconsin-Madison Biotron Laboratory. All mice were housed in SPF conditions in the animal facilities at the University of Wisconsin-Madison (Madison, WI).

Ethics Statement

These studies were carried out in strict accordance with recommendations set forth in the National Institutes of Health Guide for the Care and Use of Laboratory Animals. All animals and animal facilities were under the control of the School of Veterinary Medicine with oversight from the University of Wisconsin Research Animal Resource Center. The protocol was approved by the University of Wisconsin Animal Care and Use Committee (Protocol number V005308). The animal committee mandates that institutions and individuals using animals for research, teaching, and/or testing much acknowledge and accept both legal and ethical responsibility for the animals under their care, as specified in the Animal Welfare Act (AWA) and associated Animal Welfare Regulations (AWRs) and Public Health Service (PHS) Policy.

Cells and Viruses

Murine bone marrow-derived dendritic cells (BMDCs) were differentiated from bone marrow cells isolated from C57BL/6 mice. The bone marrow was processed into single cell suspensions and treated with RBC lysis buffer. Cells were then plated into Petri dishes and cultured in BMDC differentiation medium (RPMI, 10% FBS, 1% penicillin-streptomycin, 1x sodium pyruvate, 1x β-mercaptoethanol) supplemented with GM-CSF (PeproTech, Rocky Hill, NJ). Media was refreshed on days 2, 4, and 6. On day 7, BMDCs were harvested and replated for experiments.

Madin-Darby canine kidney (MDCK) cells were obtained from ATCC (ATCC; Manassas, VA, USA) and propagated in growth media containing Modified Eagle's Medium (MEM) with 10% fetal bovine serum (FBS; Hyclone, Logan, UT), 2 mM L-glutamine, 1.5 g/l sodium bicarbonate, non-essential amino acids, 100 U/ml of penicillin, 100 μg/ml of streptomycin (flu media), and incubated at 37°C in 5% CO2. Reverse genetics-derived influenza virus strain A/PR/8/34 H1N1 (PR8) were propagated in MDCK cells, and viral titers were determined by plaque-forming assay (23, 24). Briefly, MDCK cells grown to 90% confluency were infected with serial dilutions of influenza virus samples, and incubated for 1 h while periodically shaking under growth conditions. Cells were then washed with PBS and incubated in flu media containing 1% SeaPlaque agarose (Lonza, Basel, Switzerland). After 48 h incubation, cells were fixed in 10% neutral buffered formalin (NBF), agarose plugs were removed, and distinct plaques were counted at a given dilution to determine the plaque forming units (PFU) of virus per sample.

Viral Challenge

For PR8 challenge studies, mice were inoculated with 500 PFU of PR8 by intranasal (IN) instillation in 50ul PBS applied to the nares under isoflurane anesthesia, and were humanely euthanized at 6 days post infection. Lung tissues for viral titration (left lobe) were frozen at −80°C. To assess the role of CD4 T cells and CD8 T cells in protective immunity, mice were administered 200 μg of anti-CD4 (Bio X Cell, Clone: GK1.5) or CD8 T cells (Bio X Cell; Clone 2.43) intravenously and intranasally at days -5. -3, -1 and 1, 3, and 5 relative to challenge with influenza A virus. Fingolimod (FTY720, Selleck Chemicals) was administered to mice by intravenous injection at a dose of 5mg/kg bodyweight on days. -3, -1 and 1, 3, and 5 relative to challenge with influenza virus.

Vaccines and Vaccinations

PR8 nucleoprotein (NP) was purchased from Sino Biological Inc (Beijing, China). CpG ODN 1826 (CpG) oligonucleotide adjuvant was purchased from InivivoGen (San Diego, CA). The synthetic monophosphoryl lipid A adjuvant, Glucopyranosyl Lipid Adjuvant (GLA) was purchased from Avanti Polar Lipids, Inc. (Alabaster, AL). Adjuplex is a proprietary preparation consisting of an emulsion of polyacrylic acid and soy lecithin, purchased from Advanced BioAdjuvants, LLC. PLPs were synthesized by the double emulsion method. Briefly, PLGA was dissolved in dichloromethane in the presence or absence of GLA adjuvant (10 μg GLA/mg PLGA). DI H_2O was added and the mixture was homogenized to create the first emulsion. One percent PVA was then added and the mixture was homogenized to create the second emulsion. Excess dichloromethane was removed by solvent evaporation and particles were washed with DI H_2O by centrifugation. Following lyophilization, branched PEI was conjugated to the PLP surface by reaction with EDC and sulfo-NHS (Thermo Fisher Scientific, Bedford, MA). PLPs were washed again sequentially with 1 mM NaCl and DI H_2O. CpG adjuvant was loaded onto PLPs (10 μg CpG/mg PLGA) without GLA in sodium phosphate buffer (pH = 6.5) overnight at 4C. Particle size and zeta potential at pH 7.4 was measured using a Malvern Zetasizer and were measured to be within range of what was previously reported for both PLP-CpG and PLP-GLA/MPLA particles (PLP-MPLA/GLA 1.69 μm ± 0.29 μm, -7.59 mV ± 0.15 mV; PLP-CpG 1.72 μm ± 0.37 μm, -20.56 mV ± 4.62 mV) (21). All vaccinations were given *via* IN instillation under isoflurane anesthesia in 50μl saline with 10 μg NP formulated in various adjuvants as follows: 10% ADJ (ADJ) +/-; 1 mg PLGA (PLP-E); 1 mg PLGA loaded with 10μg CpG (PLP-CpG); 1 mg PLGA loaded with 10 μg GLA (PLP-GLA); 10% ADJ. For all studies, mice were boosted with an identical dose 3 weeks after primary vaccination.

BMDC Activation and Proliferation

Murine BMDCs were plated in 96-well plates (300,000 cells/well). BMDCs were incubated with ADJ (1%) and/or PLP adjuvants (50 μg PLGA/mL). After 24 h, supernatants were collected. IFN-β, IL-1β, and IL-18, were measured by ELISA (Bio-Techne, Minneapolis, MN). Cells were then incubated with CellTiter 96 Aqueous One Solution Proliferation Solution for 1 h (Promega, Fitchburg, WI). Absorbance of the solution was then read at 490 nm. Measurements were normalized to untreated cells at the same timepoint of incubation.

Flow Cytometry

For indicated studies, vascular staining of T-cells was performed by IV injection of fluorochrome-labeled CD45.2 3 min prior to animal euthanasia. Single-cell suspensions from spleen and lung were prepared using standard techniques as described (17). Bronchoalveolar lavage (BAL) cells were collected from euthanized mice by cannulating the trachea and flushing 3 times with 1 ml cold 10% FBS-RPMI, followed by cell pelleting. Prior to antibody staining, cells were stained for viability with Fixable Viability 780 (eBioscience, San Diego, CA) according to manufacturer's instructions. Fluorochrome-labeled antibodies against the cell-surface antigens, Ly5.2 (CD45.2), CD4, CD8α, CD44, CD62L, KLRG-1, CD127, CD103, CD69, CD49A, CD127, CXCR3, CX3CR1, and intracellular antigens IFN-γ, TNF-α, IL-2, IL-17, TBET, EOMES, IRF-4, and granzyme B were purchased from BD Biosciences (San Jose, CA), BioLegend (San Diego, CA), eBioscience (San Diego, CA), Invitrogen (Grand Island, NY), or Tonbo Biosciences (**Supplementary Table 2**). Fluorochrome-conjugated I-A^b and H-2/D^b tetramers bearing influenza nucleoprotein peptides, QVYSLIRPNENPAHK (NP311) and ASNENMETM (NP366), respectively, were kindly provided by the NIH Tetramer Core Facility (Emory University, Atlanta, GA). For class-II tetramer NP311, cells were incubated at 37°C for 90 min. For class-I tetramers, cells were incubated with tetramer and antibodies for 60 min on ice in the dark. Stained cells were fixed with 2% paraformaldehyde in PBS for 20 min, then transferred to FACS buffer. All samples were acquired on a LSRFortessa (BD Biosciences) analytical flow cytometer. Data were analyzed with FlowJo software (TreeStar, Ashland, OR).

Intracellular Cytokine Stimulation

For intracellular cytokine staining, one million cells were plated on flat-bottom tissue-culture-treated 96-well plates. Cells were

stimulated for 5 h at 37°C in the presence of human recombinant IL-2 (10 U/well), and brefeldin A (1 µl/ml, GolgiPlug, BD Biosciences), with one of the following peptides: NP366, NP311 (thinkpeptides®, ProImmune Ltd. Oxford, UK) at 0.1 ug/ml, or without peptide. After stimulation, cells were stained for surface markers, and then processed with Cytofix/Cytoperm kit (BD Biosciences, Franklin Lakes, NJ). Figures presenting cytokine expression in this manuscript are from peptide stimulated cells only, as unstimulated cells produced low frequencies and levels of cytokines determined by intracellular staining (**Supplementary Figure 8**)

Statistical Analyses

Total cell numbers are calculated = frequency (percent/100) of marker expression in live cells **x** total cell count per tissue. Statistical analyses were performed using GraphPad software (La Jolla, CA). All comparisons were made using one-way ANOVA test with Tukey corrected multiple comparisons where $p<0.05$ = *, $p<0.005$ = **, $p<0.0005$ = ***, etc. were considered significantly different among groups. Viral titers were log transformed prior to analysis. Error bars in all figures represent the standard error of the mean (SEM). For correlation analysis, a simple linear regression was performed and significance values represent if the slope was significantly non-zero.

RESULTS

Adjuplex Modifies Responses of Murine BMDCs to TLR Agonist-Loaded PLPs

We first assessed the extent to which ADJ modulated the responses of murine DCs to TLR agonists CpG and monophosphoryl lipid A (MPLA) presented as PLPs. Data in **Figure 1A** show that PLP-CpG triggered potent IFN-β responses from murine BMDCs. Interestingly, ADJ or PLP-MPLA alone did not induce an IFN-β response, but ADJ dampened the IFN-β response induced by PLP-CpG (**Figure 1A**). Next, we explored whether MPLA and synthetic MPLA (GLA) triggered production of other pro-inflammatory cytokines such as IL-1β in BMDCs. Data in **Figures 1B, C** show that ADJ, PLP-CpG, PLP-MPLA, or PLP-GLA alone failed to induce IL-1β from murine BMDCs. However, ADJ+PLP-MPLA and ADJ+PLP-GLA but not ADJ+CpG induced strong IL-1β response in DCs (**Figures 1B, C**). Taken together, data in **Figure 1** showed that ADJ in combination with CpG and MPLA/GLA stimulated disparate cytokine responses from BMDCs.

Combination PLP Adjuvants Elicit Contrasting CD8 and CD4 T Cell Effector Responses

Here, we compared the ability of various TLR agonist-loaded PLPs formulated with or without ADJ to elicit pulmonary CD8 T cell responses to the subunit protein, influenza virus nucleoprotein (NP). Mice were vaccinated intranasally (IN) twice at an interval of 3 weeks. On the 8th day after the booster vaccination, we quantified NP-specific effector T cell responses in lungs and airways. Gating strategy for visualizing NP-specific CD8 T cell responses is shown (**Supplementary Figure 1**). All PLP adjuvants elicited robust CD8 T cell responses in the lungs and airways of vaccinated mice (**Figure 2A**). Remarkably a mean of 30%–50% of CD8 T cells in the airways (BAL) were specific to the immunodominant epitope NP366 in PLP-CpG and PLP-GLA groups (**Figure 2A**). Combination of PLP-CpG or PLP-GLA with ADJ did not significantly ($P<0.05$) affect the frequencies of such cells in lungs or airways. While PLP-GLA+/-ADJ seemed to drive the highest numbers of NP366-specific CD8 T cells in lungs, PLP-CpG groups had lower levels of these effector cells. Mice administered NP with empty PLP (PLP-E) had relatively low frequencies and numbers of NP366-specific CD8 T cells, indicating that the PLP particles alone did not substantively contribute to the induction of this immune response, and were excluded from further phenotypic analysis due to unreliably low numbers (**Supplementary Figure 1B**).

We assessed whether adjuvants differed in terms of regulating the differentiation of effector T cells. T cells expressing higher levels of IL-7 receptor (CD127) and lower levels of a terminal

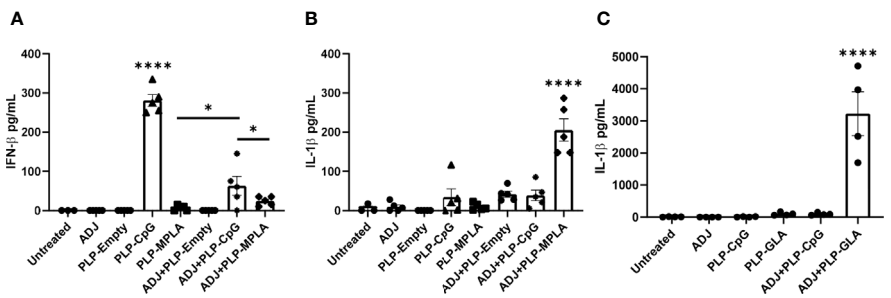

FIGURE 1 | Murine BMDC response to Adjuplex and TLR agonist-loaded PLP adjuvants. Murine BMDCs were treated with Adjuplex (ADJ) and/or PLPs with CpG, MPLA or GLA. **(A)** IFN-β response from BMDCs after 24 h of treatment with ADJ and/or PLP-CpG or PLP-MPLA. **(B, C)** IL-1β response from BMDCs after 24 h of treatment with ADJ and/or PLP-CpG, PLP-MPLA or PLP-GLA. Data are representative of two independent experiments. *, and **** indicate significance at $P<0.1$ and 0.0001 respectively.

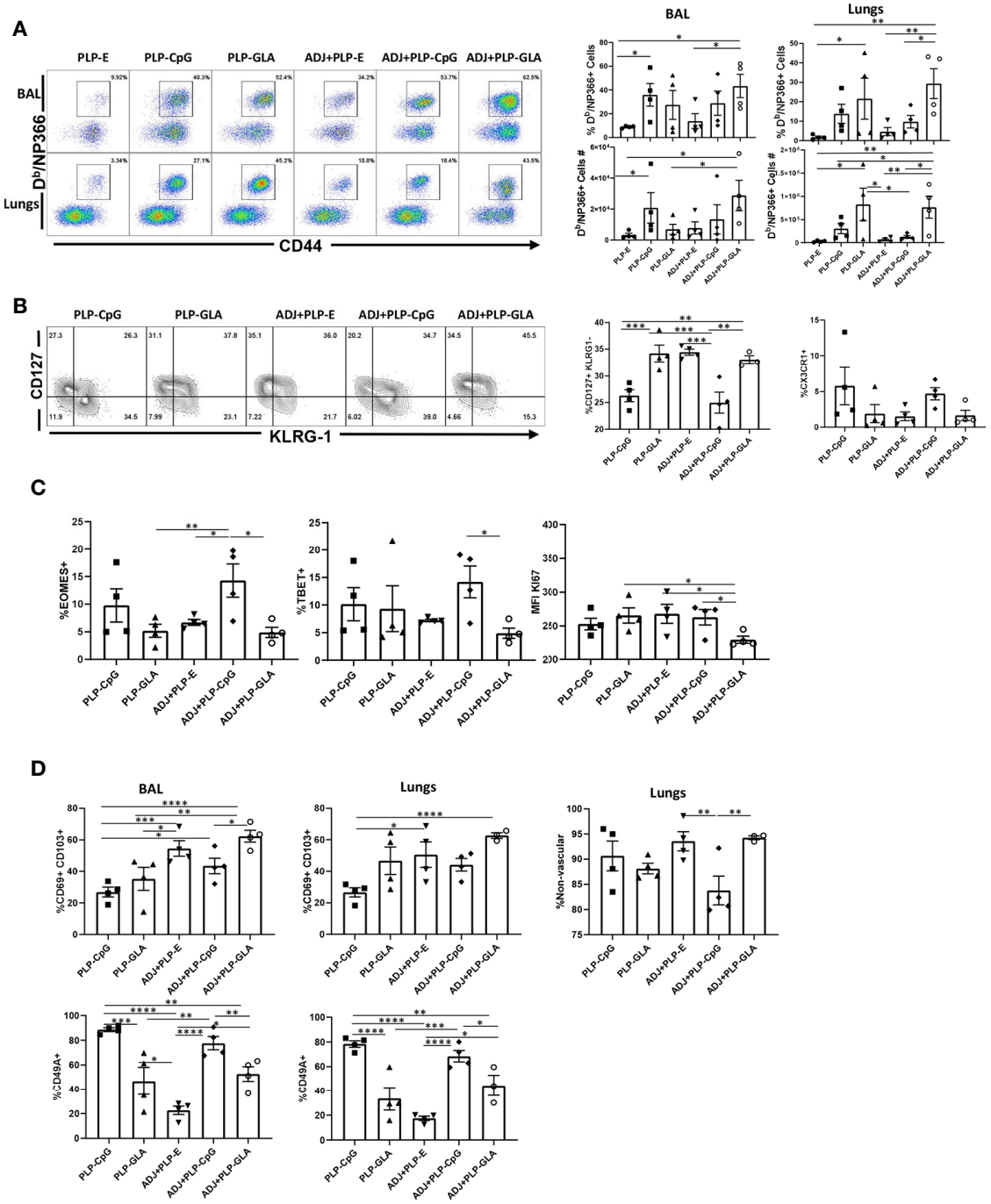

FIGURE 2 | Effector CD8 T cell response to adjuvanted vaccines. C57BL/6J mice were vaccinated intranasally twice (3 weeks apart) with influenza virus nucleoprotein (NP) formulated with the indicated adjuvants. At day 8 post boost, cells in the lungs and bronco-alveolar lavage (BAL) were stained with D^b/NP366 tetramers and the indicated antibodies. **(A)** FACS plots are gated on live CD8 T cells and the numbers are the percentages of tetramer-binding CD8 T cells among CD8 T cells. FACS plots and graphs in panels **(B–D)** show indicated percentages of the subsets among gated tetramer-binding CD8 T cells in respective gates/quadrants or median fluorescence intensities (MFI) for the molecules as indicated. Data are representative of three independent experiments. *, **, ***, and **** indicate significance at $P < 0.1$, 0.01, 0.001, and 0.0001, respectively.

differentiation/senescence marker KLRG-1 are associated with greater memory potential (25). Of the PLP preparations tested, PLP-CpG and ADJ+PLP-CpG induced significantly ($P<0.05$) lower frequencies of $CD127^{HI}$ and $CD127^{HI}$/KLRG-1^{LO} CD8 T cells than all other combination PLP adjuvants (**Figure 2B** and **Supplementary Figure 2**). PLP-CpG also drove a strong trend

for increased frequencies of CX3CR1^{HI} CD8 T cells (**Figure 2B**), a marker associated with increased effector differentiation (26). We quantified transcription factors EOMES and TBET, which are known to regulate differentiation of effector CD8 T cells in spleen (27). Interestingly, while the combination of ADJ+PLP-CpG induced high levels of transcription factors TBET and EOMES, the combination of ADJ+PLP-GLA had a suppressive effect, leading to lower levels of these transcription factors and lower levels of KI67 expression, a marker of cell proliferation (**Figure 2C**). Thus, increased expressions of EOMES and TBET were associated with greater terminal differentiation of CD8 T cells in the ADJ+PLP-CpG group.

To determine whether combination PLP adjuvants differentially regulated mucosal imprinting of lung CD8 T cells, we analyzed CD69 and CD103 expression. ADJ and PLP-GLA both increased CD69^{HI}/CD103^{HI} CD8 T cells in the lungs of vaccinated animals, while PLP-CpG appeared to decrease this mucosal imprinting (**Figure 2D**). The combination of ADJ+PLP-GLA led to significantly (P<0.05) higher levels of mucosal imprinting in airways and lungs compared with PLP-CpG, ADJ+PLP-CpG, or PLP-GLA; ADJ alone strongly induced CD69 and CD103 expression. Another marker that is expressed on lung tissue-resident memory cells (T_{RM}), is CD49a (28). In our studies, CD49A expression on CD8 T cells appeared to be closely associated with PLP-CpG treatment (**Figure 2D**), and unlike CD69 and CD103, CD49a was expressed to significantly lower levels on CD8 T cells from groups administered ADJ+/-PLP-GLA. To determine the localization of effector CD8 T cells in lungs, we performed vascular staining of T cells shortly before euthanasia. Levels of non-vascular cells were highest in the ADJ and ADJ+PLP-GLA groups, which more closely associated with CD69/CD103 levels than CD49A levels (**Figure 2D**). Additionally, we did not observe a difference in CD69/CD103 positivity between total and exclusively non-vascular NP366-specifc CD8 T cells (**Supplementary Figure 3**) because the vast majority of these cells, in all treatment groups, were found in the non-vascular compartment. Thus, ADJ+/-PLP-GLA enhanced expression of CD103 and CD69, and promoted mucosal imprinting of effector CD8 T cells in lungs. By contrast, PLP-CpG appeared to dampen the expression of CD103/CD69, and limit non-vascular localization of effector CD8 T cells.

CpG/GLA-loaded PLPs+/-ADJ elicited high frequencies of antigen-specific CD4 T cells in lungs and airways (**Figure 3A**). GLA- and/or CpG-loaded PLP adjuvants induced higher accumulation of NP311-specific CD4 T cells in lungs compared to groups that received empty PLPs (**Figure 3A**). Similar to CD8 T cell responses, combination of ADJ+PLP-GLA showed a trend for highest levels of antigen-specific responses, however in contrast to NP366-specific CD8 T cell responses, PLP-CpG+/-ADJ also appeared sufficient to induce high frequencies and numbers of NP311-specific CD4 T cells in the respiratory tract (**Figure 3A**).

Pertaining to the differentiation of effector CD4 T cells, only the combination of ADJ+PLP-GLA induced greater percentages of CD127^{HI}/KLRG-1^{LO} CD4 T cells, relative to other treatment groups (**Figure 3B**). The expression of CX3CR1 and transcription factors (TBET/EOMES/IRF4) were not significantly (P<0.05) different between treatment groups (**Supplementary Figure 4A**). However, CD4 T cells isolated from mice that were vaccinated with ADJ+PLP-GLA appeared to be proliferating at significantly (P<0.05) lower levels, as measured by lower Ki67 staining (**Figure 3B**). Interestingly, the frequencies of PD-1^{HI} NP311-specific CD4 T cells and FoxP3^{HI} regulatory CD4 T cells were significantly (P<0.05) higher in both the PLP-GLA and ADJ+PLP-E groups. Similar to the findings for CD8 T cells, ADJ and ADJ+PLP-GLA fostered mucosal imprinting of CD4 T cells, as these groups had significantly (P<0.05) higher frequencies of CD69^{HI}/CD103^{HI} NP311-specific CD4 T cells (**Figure 3C**). However, CD49A expression and proportions of non-vascular T cells were not significantly different between treatment groups (**Supplementary Figure 4B**).

Distinct Functional Programming of CD8 and CD4 T Cells by Combination PLP Adjuvants

At day 8 after booster vaccination, we assessed cytokine production by NP366 peptide-stimulated CD8 T cells in lungs. All PLP-based adjuvants elicited strong CD8 Tc1 responses, measured by IFNγ secretion after *ex vivo* NP366 peptide stimulation (**Figure 4A**), with the exception of the PLP-E which failed to elicit any detectable cytokine expression from stimulated cells. In general, the frequency of IFNγ-secreting CD8 T cells from PLP-CpG/PLP-GLA groups were at least two-folds higher than the ADJ+PLP-E group, which suggested that PLP-TLR4/9 agonists + ADJ favored Tc1 programming. Production of IL-17α in CD8 T cells was significantly increased by PLP-GLA-containing adjuvant formulations, yet was barely detectable in PLP-CpG groups, highlighting the contrasting functional programming of TLR4 and TLR9 agonists, respectively (**Figure 4A**). Though not statistically significant (P<0.05), there was a trend for higher polyfunctionality as measured by frequency of TNFα+/IL-2+/IFNγ+ CD8 T cells in PLP-GLA mice +/- ADJ (**Figure 4B**). Overall, PLP-CpG adjuvants appear to skew towards Tc1 polarization, while PLP-GLA resulted in balanced Tc1/Tc17 responses and greater functional diversity. We also evaluated whether adjuvants differed in terms of inducing effector differentiation, as measured by expression of granzyme B. Expression of the effector molecule granzyme B in CD8 T cells was not associated with administration of PLP-CpG, and conversely NP366-specific CD8 T cells in mice receiving PLP-GLA had significantly (P<0.05) higher levels for granzyme B, compared to all other adjuvant combinations (**Figure 4C**).

In stark contrast to CD8 T cell functionality, PLP-CpG tended to drive balanced Th1/Th17 responses in CD4 T cells, compared with PLP-GLA, which directed skewed T_H17 differentiation (**Figure 4D**). PLP-CpG+/-ADJ groups had significantly (P<0.05) higher frequencies of IFNγ+ CD4 T cells, while all combination PLP adjuvant groups exhibited similar frequencies of IL-17-producing CD4 T cells (**Figure 4D**). Further, the PLP-CpG+/-ADJ groups had higher frequencies of polyfunctional

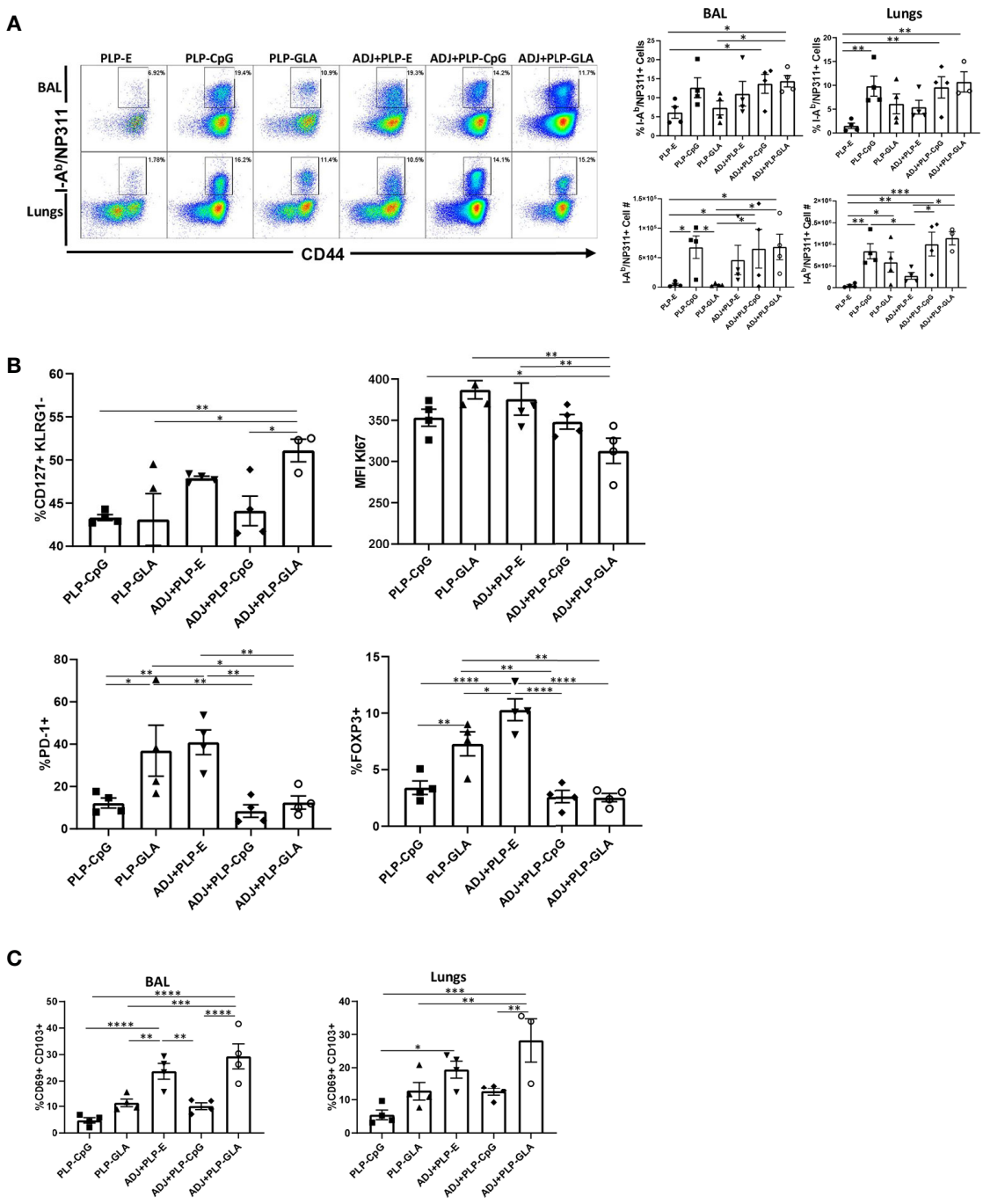

FIGURE 3 | Effector CD4 T cell response to PLP-based vaccines. Cohorts of mice were vaccinated as in **Figure 2**. At day 8 post booster vaccination, cells from lungs and BAL were stained with I-A^b/NP311 tetramers and the indicated antibodies. **(A)** FACS plots show numbers and percentages of tetramer-binding cells among CD4 T cells. Graphs in **(B, C)** show percentages of subsets among gated tetramer-binding CD4 T cells in respective gates/quadrants or median fluorescence intensities (MFI) for the indicated molecules. Data are representative of three independent experiments. *, **, ***, and **** indicate significance at $P < 0.1$, 0.01, 0.001, and 0.0001, respectively.

triple cytokine-producing- (IFNγ, TNF, and IL-2) CD4 cells than the ADJ+PLP-E and PLP-GLA groups (**Figure 4D**). When the functional polarization of CD4 and CD8 T cells is considered together, ADJ+PLP-GLA induced the most balanced and potent Tc1/Tc17 and Th1/Th17 immunity. These results also demonstrated that the type of TLR agonist conjugated to PLPs can have disparate programming effects on CD4 and CD8 T cell functionality during the effector phase of vaccination.

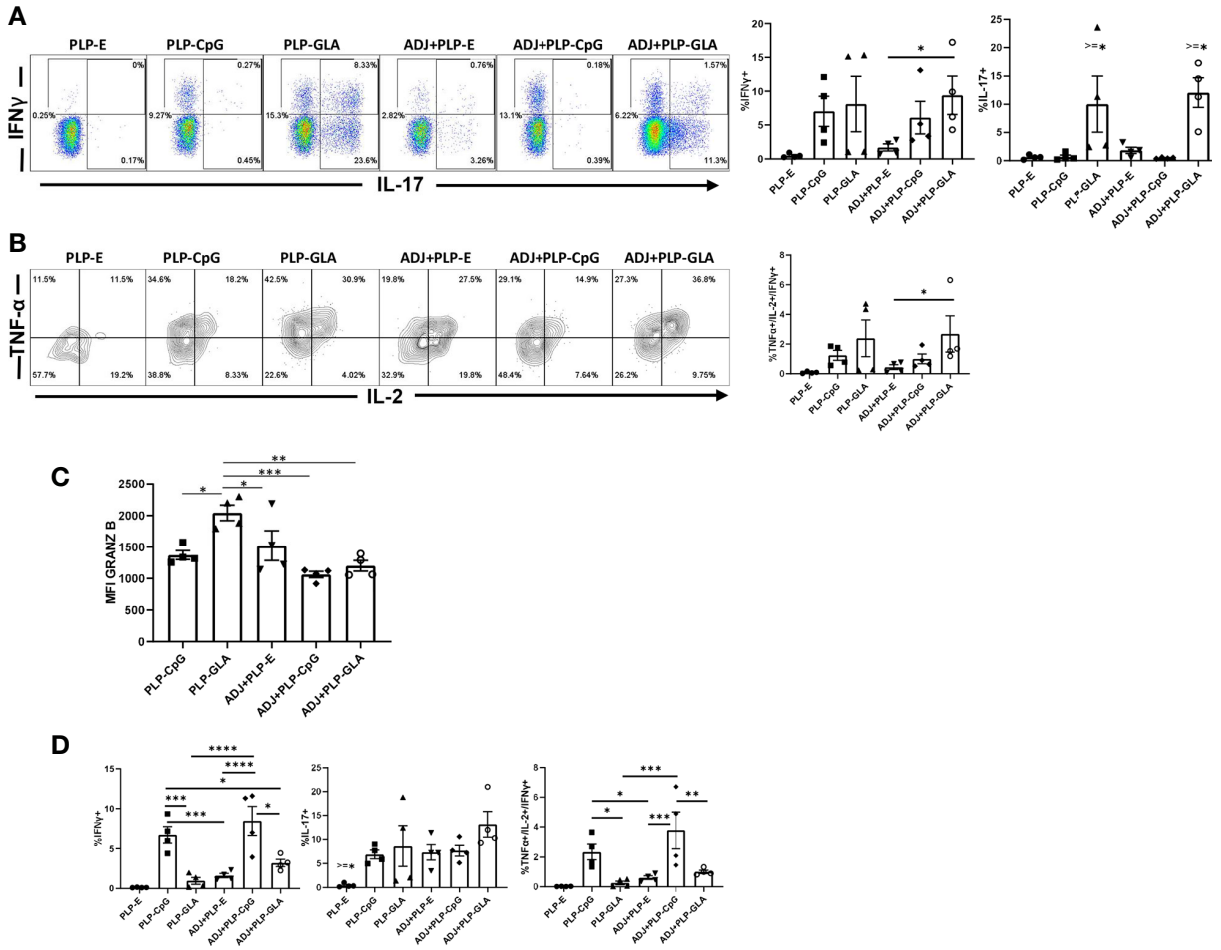

FIGURE 4 | Functional polarization of effector CD8 and CD4 T cells in vaccinated mice. Mice were vaccinated as described in **Figure 2**. On the 8th day after booster vaccination, lung cells were stimulated *ex vivo* with NP366 or NP311 peptides for 5 h. The percentages of NP366 peptide-stimulated CD8 T cells or NP311 peptide-stimulated CD4 T cells that produced IFN-γ, IL-17, TNF-α, and IL-2 were quantified by intracellular cytokine staining. **(A)** FACS plots and graphs show the percentages of cytokine-producing cells among the gated CD8 T cells. **(B)** Data in graphs are percentages among gated IFN-γ-producing CD8 T cells. **(C)** Graphs show the percentages of cytokine-producing cells among CD4 T cells or IFN-γ-producing CD4 T cells ($TNF^{+}IL\text{-}2^{+}$). **(D)** Cells were stained with anti-CD8, D^{b}/NP366 tetramers and anti-granzyme B antibodies directly ex vivo. Graph shows MFI for granzyme B staining in NP366-specific CD8 T cells. Data are representative of three independent experiments. *, **, ***, and **** indicate significance at $P < 0.1$, 0.01, 0.001, and 0.0001, respectively.

PLP Adjuvants Affect the Magnitude and Functionality of CD4 and CD8 T Cell Memory

Cohorts of mice were vaccinated twice (3 weeks apart) with NP protein formulated in various adjuvants, and NP-specific memory T cells were quantified in the lungs and airways, at 100 days after booster vaccination. While all combination PLP adjuvants elicited readily detectable levels of NP366-specific memory CD8 T cells at D100 post boost, the ADJ+PLP-GLA group had significantly (P<0.05) higher frequencies and/or total numbers of memory CD8 T cells in both airways and lungs than other groups (**Figure 5A**). The greater numbers of memory CD8 T cells in lungs of ADJ+PLP-GLA mice are linked to reduced contraction between day 8 and day 100 after vaccination; while the number NP366-specific CD8 T cells dropped by ~100 fold in other groups, there was only a ~20-fold drop in the ADJ+PLP-GLA group (**Supplementary Figure 5**). There were no substantial differences in CD49a, CD62L, CD69, CD103, CD127, CXCR3, CX3CR1, or KLRG1+ frequencies among NP366-specific memory CD8 T cells in various adjuvant groups. Notably however, the numbers of non-vascular parenchymal $CD69^{+ve}CD103^{+ve}$ T_{RM} CD8 T cells in lungs of ADJ+PLP-GLA mice were significantly (P<0.05) higher, as compared to other adjuvant groups (**Figure 5A**).

At 100 days after vaccination, ADJ+PLP-CpG and ADJ+PLP-GLA groups had significantly (P<0.05) higher frequencies and numbers of NP311-specific memory CD4 T cells in airways than other groups and both groups had significantly (P<0.05) higher numbers in airways and/or lungs than the PLP-GLA group (**Figure 5B**). Among NP311-specific CD4 T cells, the PLP-E

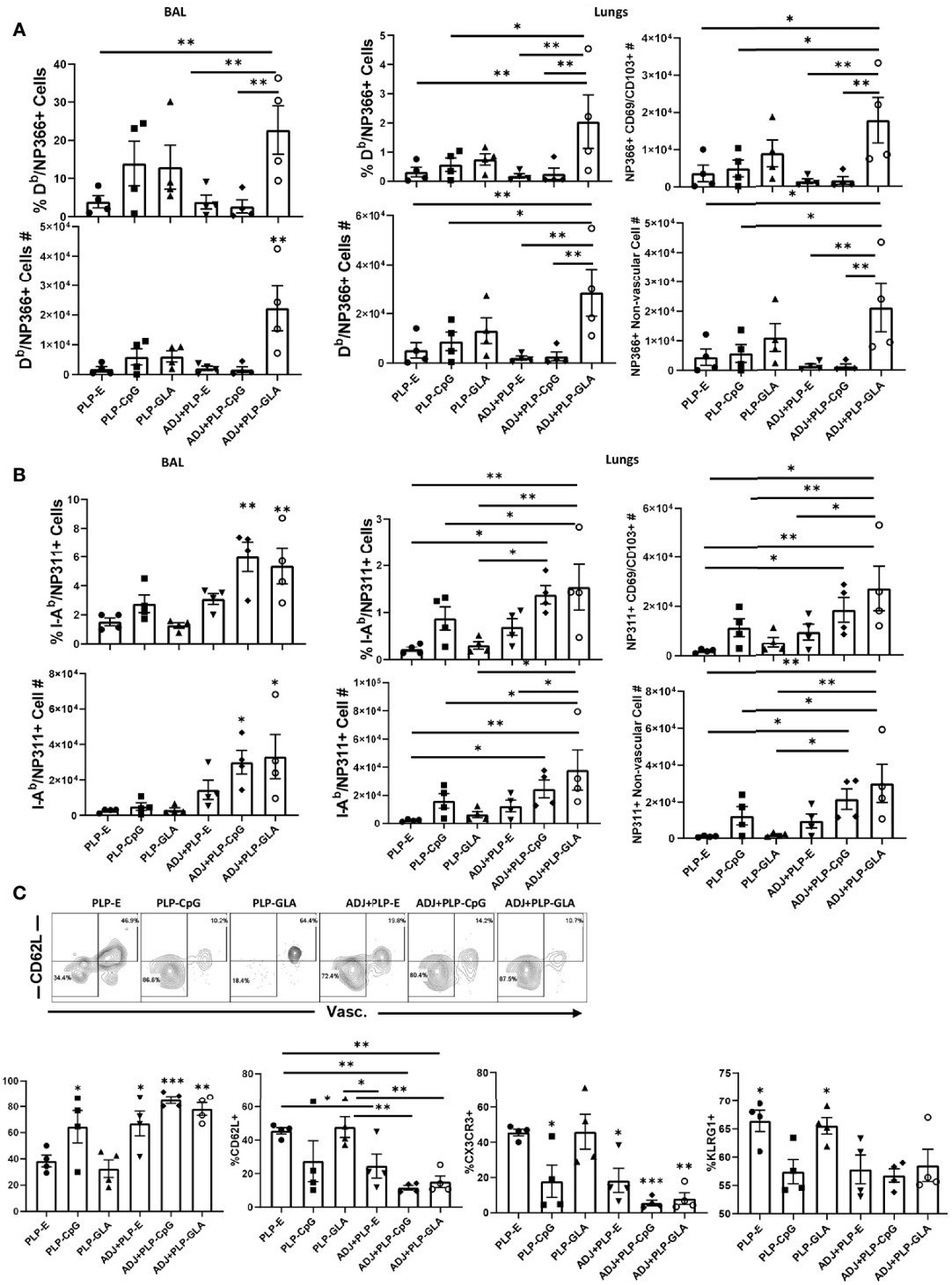

FIGURE 5 | Mucosal CD8 and CD4 T cell memory in vaccinated mice. Cohorts of mice were vaccinated twice, as described in **Figure 2**. At 100 days after booster vaccination, to stain vascular cells, mice were injected intravenously with PE-labeled anti-CD4.2 antibody. Cells from BAL and lungs were stained with D^b/NP366 tetramers or I-A^b/NP311 tetramers along with antibodies for the indicated cell surface molecules. Percentages and total numbers of NP366-specific CD8 T cells or NP311-specific CD4 T cells in BAL or lungs (**A, B**, respectively). Graphs in panels **(A, B)** also show total numbers of $CD103^+CD69^+$ and nonvascular NP366- or NP311-specific T cells in lungs. Plots in **(C)** are gated on NP311-specific T cells and graphs show percentages of the indicated subsets among tetramer-binding CD4 T cells. Data are representative of three independent experiments. *, **, and *** indicate significance at $P<0.1$, 0.01, and 0.001, respectively.

and PLP-GLA groups had a significantly higher proportion of vascular cells and also expressed CD62L, CX3CR1 and KLRG-1 (**Figures 5C**).

The percentages of NP366-specific IFNγ+ memory CD8 T cells in lungs of ADJ+PLP-GLA or ADJ+PLP-CpG groups were higher than in ADJ+PLP-E mice. Percentages of IL-17-producing CD8 T cells in the ADJ+PLP-GLA group were significantly ($P<0.05$) higher than in all other groups (**Figure 6A**). While Tc17 responses in all groups contracted from D8 to D100, this contraction seemed to occur to a lesser degree in the ADJ+PLP-GLA group than the PLP-GLA group; on D8, the numbers and frequencies of NP366-specific CD8 T cells, and frequencies of Tc17 cells were not different between these two groups, but at D100, Tc17 frequencies were significantly higher in ADJ+PLP-GLA than the PLP-GLA group. Interestingly, while both ADJ+PLP-GLA or ADJ+PLP+CpG groups had strong Tc1 responses, the degree of polyfunctionality in the ADJ+PLP-GLA group was significantly higher than all other groups, except PLP-CpG. Further, ADJ appeared to reduce memory CD8 T cell polyfunctionality induced with PLP-CpG but increase polyfunctionality induced with PLP-GLA.

Lungs from all groups contained robust frequencies of IFNγ+ memory CD4 T cells at D100, however, ADJ+PLP-CpG group had significantly ($P<0.05$) higher frequencies of IFNγ-producing NP311-specific memory T cells, than other groups (**Figure 6B**). ADJ+PLP-CpG and ADJ+PLP-GLA were superior to PLP-CpG and PLP-GLA in inducing IL-17-producing and/or polyfunctional memory CD4 T cells (**Figure 6B**). When the functionality of both memory CD4 and CD8 cells are taken together, we observed a similar trend, which is that ADJ+PLP-GLA induced the most robust and balanced Tc1/Th1 and Th17/Tc17 responses.

ADJ+PLP-GLA Induces Durable and Potent Immunity to Influenza Virus

Cohorts of mice were vaccinated twice (at an interval of 3 weeks) intranasally with NP protein formulated in various adjuvants. At day 101 after booster vaccination, vaccinated and unvaccinated animals were challenged with a lethal dose of H1N1 PR8 influenza virus. At D6 post virus challenge, we quantified recall T cell responses and viral titers in the lungs. While vaccination with all PLP formulations resulted in at least ~2 Log_{10} reduction in lung viral titers, the ADJ+PLP-GLA vaccine conferred the highest degree of viral control, reducing viral titers by nearly 7 Log_{10} PFU/gram of lung, as compared to mock (saline) vaccinated mice (**Figure 7A**). Lungs of 4/5 animals in the ADJ+PLP-GLA group contained no detectable infectious virus, indicating nearly complete control of lung viral replication within D6 after challenge.

Interestingly, total numbers and frequencies of recall antigen-specific CD4 and CD8 T cells did not vary significantly between vaccinated groups at this time point (**Figure 7B**). However, there was a nearly significant ($P<0.05$) relationship between frequencies of NP366-specific CD8 T cells and viral lung titers (**Figure 7B**), whereas frequencies or numbers of CD4 T cells did not exhibit such a strong trend. Additionally, there were no noteworthy phenotypic or transcriptional differences between adjuvant groups in CD8 T cells in terms of CD49a, CD62L,

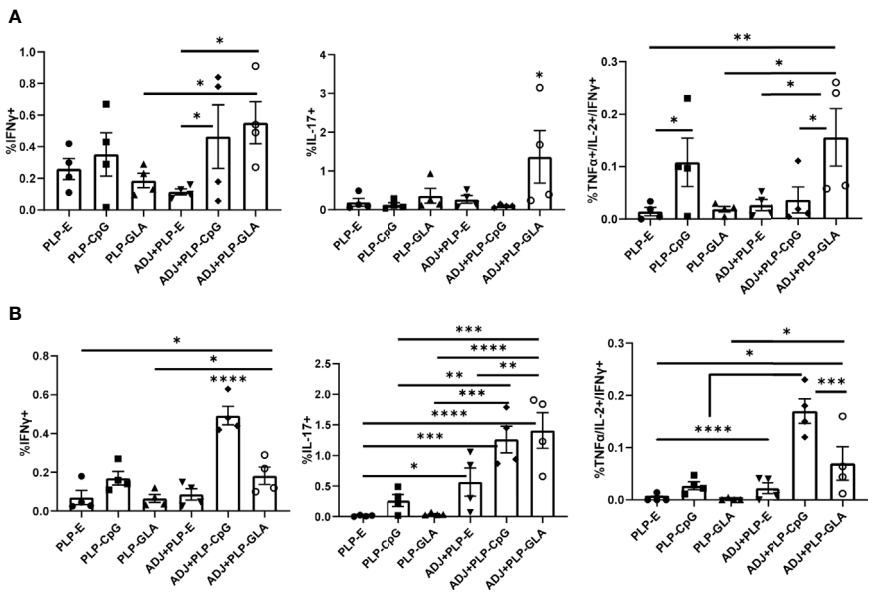

FIGURE 6 | Functional polarization of memory CD8 and CD4 T cells in vaccinated mice. Cohorts of mice were vaccinated twice, as described in **Figure 2**. At 100 days after booster vaccination, lung cells were stimulated with NP366 **(A)** or NP311 **(B)** peptides. Cytokine-producing CD8 or CD4 T cells were quantified by intracellular cytokine staining. Graphs in panel A show percentages of IFN-γ- or IL-17-producing cells among CD8 T cells or TNF-α and IL-2 producing cells among IFN-γ-producing CD8 T cells. Panel B shows percentages of IFN-γ- or IL-17-producing cells among CD4 T cells or TNF-α and IL-2 producing cells among IFN-γ-producing CD4 T cells. Data are representative of three independent experiments. *, **, ***, and **** indicate significance at $P < 0.1$, 0.01, 0.001, and 0.0001, respectively.

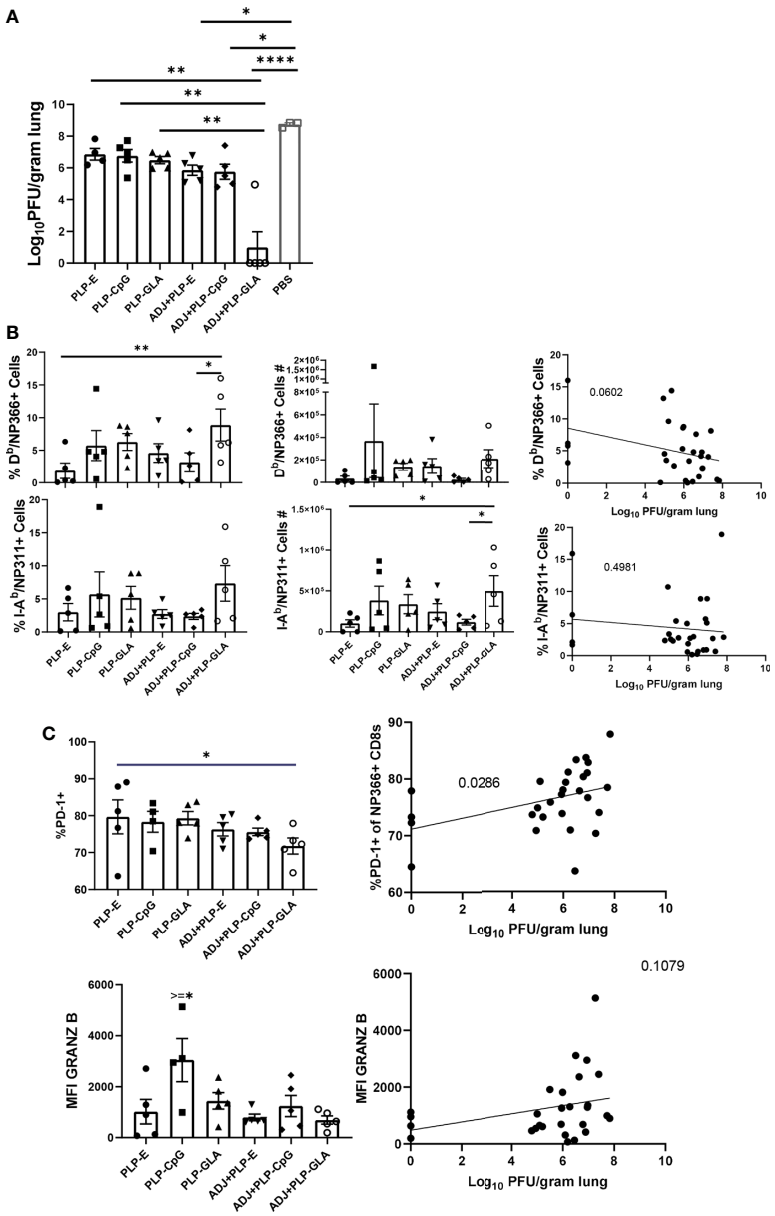

FIGURE 7 | Vaccine-induced protective immunity influenza virus. Cohorts of mice were vaccinated twice, as described in **Figure 2**. At 101 days after booster vaccination, mice were challenged with H1N1/PR8 strain of influenza A virus; unvaccinated mice were challenged as controls. Viral titers were quantified in the lungs on D6 after challenge **(A)**. Percentages or numbers of NP366-specific CD8 T cells and NP311-specific CD4 T cells in lungs **(B)**. Graphs show percentages of cells among the gated NP366-specific CD8 T cells or expression levels of granzyme B in the gated NP366-specific CD8 T cells **(C)**. Data are representative of two independent experiments. *, **, ***, and **** indicate significance at $P < 0.1$, 0.01, 0.001, and 0.0001, respectively. Linear regression curves were plotted for data from individual mice for the indicated cell frequency plotted against its Log_{10} viral titer value.

CD69, CD103, CD127, CXCR3, CX3CR1, KLRG-1, TBET, EOMES, and IRF4 expression. However, we noticed a strong trend for reduced PD-1 expression on recall CD8 T cells in ADJ containing groups, particularly for ADJ+PLP-GLA, and there was a strong correlation between PD-1 expression levels and increased viral lung titers (**Figure 7C**). Further, granzyme B levels were significantly upregulated in recall CD8 T cells in the PLP-CpG group, and there was a negative trend for granzyme B levels and viral titer. Increased PD-1 and granzyme B expression in CD8 T cells might be suggestive of ongoing antigenic stimulation and cytolysis in mice, associated with delayed viral clearance. Finally, we did not observe any strong or clear trends between the aforementioned parameters on recall CD4 T cells and viral control.

Recall T Cell Function Intimately Associates With Influenza Virus Control

Following influenza virus challenge, all PLP groups showed robust IFNγ+ CD8 T-cell recall responses measured by *ex vivo* NP366 peptide stimulation (**Figure 8A**). There was a clear and strong association between the frequency of IFNγ expression in CD8 T cells and the degree of viral control in lungs (**Figure 8A**). ADJ+PLP-GLA seemed to drive increased polyfunctionality among recall CD8 T cells (**Figure 8A**). With the exception of ADJ+PLP-CpG, both ADJ and PLP-GLA groups had significantly increased frequencies of IL-17 expression during virus-induced CD8 T cell recall, with the ADJ+PLP-GLA group having significantly (P<0.05) higher levels than all other groups (**Figure 8A**). Indeed, ADJ+PLP-GLA had the greatest Tc17 recall response and the lowest lung viral titers, and overall there was an extremely close association between IL-17 expression in CD8 T cells and viral control (**Figure 8A**), such that even excluding the ADJ+PLP-GLA animals that had no detectable lung titer from the correlation analysis still resulted in a significant association (**Supplementary Figure 6**).

For CD4 Th1 recall responses, while all groups had robust IFNγ+ CD4 T-cell responses, there were no noteworthy differences between groups and there did not appear to be a strong association with viral control (**Figure 8B**). Interestingly, ADJ+PLP-CpG had significantly higher frequencies of polyfunctional CD4 T cells than all other groups. On the other

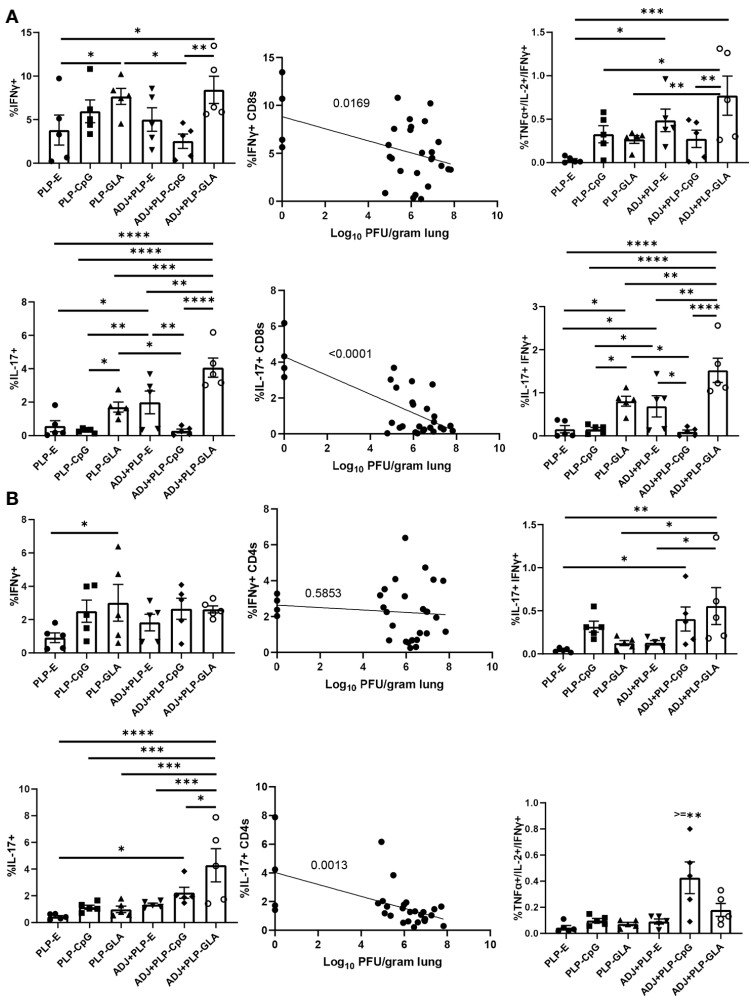

FIGURE 8 | Functional polarization of recall CD8 and CD4 T cells. Cohorts of mice were vaccinated twice, as described in **Figure 2**. 101 days after booster vaccination, mice were challenged with H1N1/PR8 strain of influenza A virus. Lung cells were stimulated *ex vivo* with NP366 or NP311 peptides for 5 h. The percentages of NP366-stimulated CD8, or NP311-stimulated CD4 T cells that produced IFN-γ, IL-17, TNF-α, and IL-2 were quantified by intracellular cytokine staining. Graphs show the percentages of cytokine-producing cells among the gated CD8 T cells or TNF-α and IL-2-producing cells among gated IFN-γ-producing CD8 T cells **(A)**. Graphs show the percentages of cytokine-producing cells among CD4 T cells or TNF-α and IL-2-producing cells among gated IFN-γ-producing CD4 T cells **(B)**. Data are representative of two independent experiments. *, **, ***, and **** indicate significance at P < 0.1, 0.01, 0.001, and 0.0001, respectively. Linear regression curves were plotted for data from individual mice for the indicated cell frequency plotted against its Log_{10} viral titer value.

hand, the ADJ+PLP-GLA group had a significantly ($P<0.05$) higher recall Tc17 response than other groups, and frequencies of IL-17+ cells among CD4 T cells significantly correlated with reduced viral lung titer (**Figure 8B**). Overall, the robust and balanced Tc1/Th1 and Th17/Tc17 functional responses elicited by the ADJ+PLP-GLA vaccine were associated with effective viral control.

ADJ+PLP-GLA Induces Durable Pulmonary T-cell Immunity to Influenza Virus

To test the ability of PLP based adjuvants to elicit durable immunity, cohorts of mice were vaccinated twice (3 weeks apart) with NP protein formulated in various adjuvants. Vaccinated and unvaccinated animals were challenged with a lethal dose of H1N1 PR8 influenza virus at day 362 after booster vaccination. At D6 post virus challenge, we quantified recall T cell responses and viral titers in the lungs. The ADJ+PLP-GLA vaccine conferred effective viral control at this late memory time point, reducing viral titers by nearly 3 Log_{10} PFU/gram of lung, in comparison to mock (saline) vaccinated mice (**Figure 9A**). Note that vaccination with all other PLP formulations resulted in a modest 0.5–1 Log_{10} reduction in lung viral titers. NP366-specific CD8 T-cell frequencies and total numbers were consistently higher in the ADJ+PLP-GLA group (**Figure 9B**), and majority of mice that received other vaccine formulations exhibited poor CD8 T cell recall responses. Interestingly,

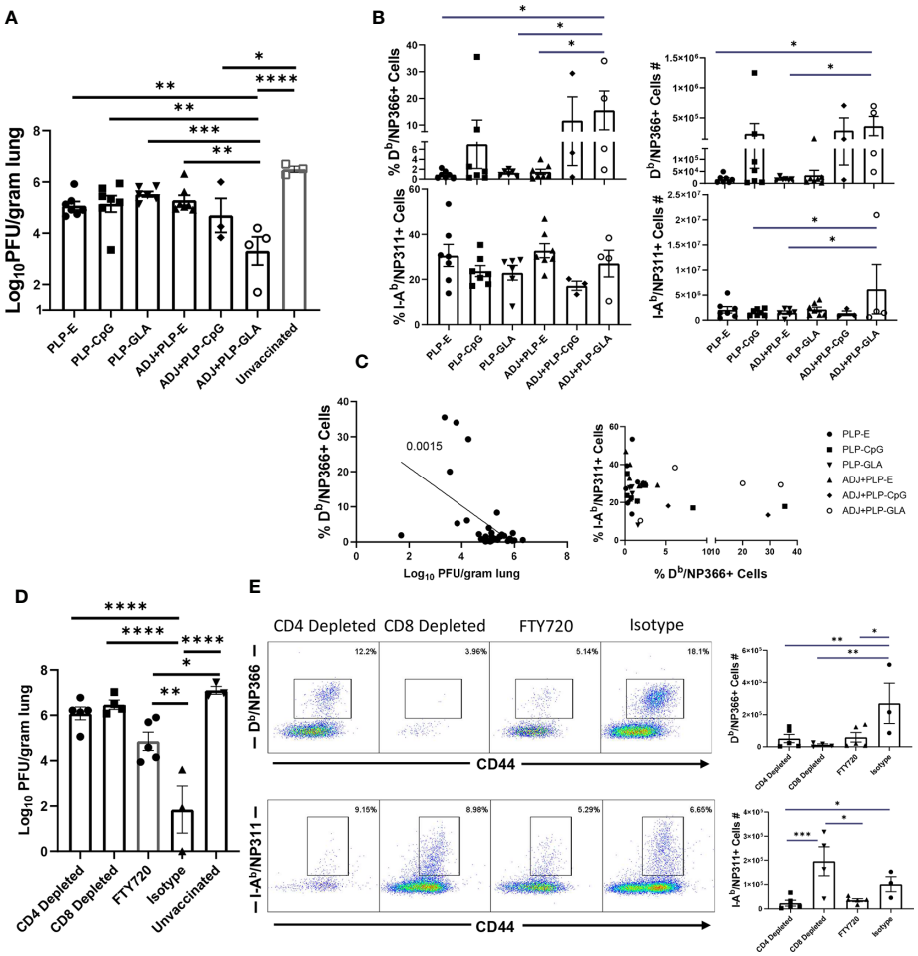

FIGURE 9 | Long term memory and role of CD4 and CD8 T cells in vaccine-induced immunity to influenza virus. Three hundred sixty-two days after booster vaccination, mice were challenged with H1N1/PR8 strain of influenza A virus **(A–C)**. Viral titers were quantified in the lungs on D6 after challenge **(A)**. Numbers and frequencies of NP366-specific CD8 T cells and NP311-specific CD4 T cells in lungs **(B)**. The linear regression curve was plotted for data from individual mice frequencies of NP366-specific CD8 T cells or NP311-specific CD4 T cells plotted against its Log_{10} viral titer value, **(D, E)**: Mice were vaccinated with NP formulated in ADJ+PLP-GLA, and 3 weeks later, either CD4 or CD8 T cells were depleted immediately prior to and during a lethal H1N1 PR8 influenza challenge. An additional cohort of ADJ+PLP-GLA vaccinated mice was treated with FTY720 immediately before and during viral challenge. Viral titers were quantified in the lungs on D6 after challenge **(D)**. Numbers and frequencies of NP366-specific CD8 T cells and NP311-specific CD4 T cells in lungs **(E)**. *, **, ***, and **** indicate significance at $P <$ 0.1, 0.01, 0.001, and 0.0001, respectively.

frequencies and total numbers of NP311-specific recall CD4 T cells were high amongst all vaccine groups (**Figure 9B**). At this late time point, reduction of viral burden in lungs closely associated with the magnitude of NP366-specific CD8 T cell recall response (**Figure 9C**). In general mice vaccinated with ADJ+PLP-GLA had high frequencies of both CD4 and CD8 T cells, as compared with other groups, which suggested that both sets of T cells may be important for viral control at this time point (**Figure 9C**).

Both CD4 and CD8 T Cells Are Required for PLP Vaccine-Induced Protection to Influenza Virus Challenge

As detailed above, ADJ+PLP-GLA elicited potent NP-specific CD4 and CD8 T cell responses during effector and memory time points, which was associated with influenza virus control. To determine the relative roles of T cell subsets in protective immunity, we vaccinated mice with NP protein formulated in ADJ+PLP-GLA. Three weeks after vaccination, we depleted CD4 or CD8 T cells, immediately prior to challenge with a lethal dose of H1N1 PR8 influenza A virus. Depletion of CD4 and CD8 T cells resulted in selective loss of NP311-specific CD4 T cells and NP366-specific CD8 T cells, respectively in lungs (**Figure 9E**). Further, CD4 T-cell depletion significantly reduced CD8 T-cell recall, which suggested that CD4 T cells support recall responses of CD8 T cells. CD8 T cell depletion appeared to increase CD4 T cell recall (**Figure 8E**), which might be suggestive of compensatory CD4 T cell responses, in the absence of CD8 T cells. Vaccinated mice treated with isotype control antibodies displayed >4 Log_{10} reduction in viral load in lungs, as compared to unvaccinated controls (**Figure 9D**). Remarkably, antibody-induced depletion of CD4 or CD8 T cell subsets resulted in significantly ($P<0.05$) increased viral burden in lungs, as compared to isotype control antibody treatment (**Figure 9D**). These findings suggested that both CD4 and CD8 T cells play important roles in controlling influenza viral burdens in lungs of vaccinated mice.

To further investigate the importance of lung T_{RM} in protection against influenza virus challenge, a cohort of ADJ+PLP-GLA-vaccinated mice was treated with FTY720 (Fingolimod), a functional antagonist of sphingosine-1-phosphate receptor (S1PR), that prevents lymphocyte egress from secondary lymphoid organs. As expected, FTY720 treatment markedly reduced the numbers of circulating CD4 and CD8 T cells (**Supplementary Figure 7**). Viral burden in lungs of FTY720-treated animals was significantly lower than in unvaccinated controls (~ 2 Log_{10} reduction). However, lung viral load in FTY720-treated animals was significantly ($P<0.05$) higher than in lungs of mice that were not treated with FTY720 (Isotype control antibodies). Taken together, these data suggested that FTY720 treatment compromised memory CD4 and CD8 T-cell-mediated influenza viral control in vaccinated mice. This in turn implied that both T_{RM} and egress of lymphoid memory T cells might be important for influenza virus control in vaccinated mice. This interpretation comes with a caveat, because FTY720 has been reported to inhibit activation and effector function of T cells (29, 30) and this in turn might have affected recall responses of memory T cells including T_{RM}, leading to ineffective viral control in lungs.

DISCUSSION

Programming potent and durable B and T cell memory is the goal of vaccination programs. Live viral vaccines such as the Yellow fever vaccine (YFV) and the small pox vaccine engender immunity that lasts for decades after vaccination (31). Studies of YFV suggest that engagement of multiple innate immune receptors early in the infection may be key to the programming of long-lived immunological memory (32). This paradigm has triggered a multitude of investigations to explore the possibility of using TLR agonists as adjuvants to program durable immunological memory. One of the downsides of using TLR agonists, such as CpG, in soluble form is their diffusion from vaccination site, leading to systemic toxicity in vaccinees (33). To circumvent this problem and mimic the biophysical attributes of pathogens and their interactions with pattern recognition receptors, we engineered biodegradable PLGA microparticles (i.e. PLPs) that were loaded with optimized densities of TLR agonists CpG and GLA (19). In this manuscript, we document that mucosal delivery of CpG- or GLA-loaded PLPs elicit unexpectedly potent mucosally imprinted antigen-specific CD4 and CD8 T cell responses in the respiratory tract. Interestingly, we find that PLP-CpG and PLP-GLA stimulate disparate transcriptional programs that evoke distinct phenotypic and functional differentiation of antigen-specific T cells. Further, we show that the combination of PLP-GLA, but not PLP-CpG, with the nanoemulsion adjuvant ADJ synergistically augmented the magnitude of lung-resident T cell memory and protective immunity to a lethal influenza virus infection. These studies highlight how the mode of TLR agonist presentation can be leveraged to achieve enhanced immunogenicity without toxicity, and how this feature can be combined with the antigen presenting properties of a nano-emulsion adjuvant to program effective T cell-based protective immunity in the respiratory tract.

In vitro studies show that PLP-CpG, but not PLP-GLA, triggers IFNβ production by BMDCs. Conversely, only PLP-GLA, but not CpG, stimulate IL-1β production when combined with ADJ; differential abilities of PLP-CpG and PLP-GLA in eliciting IFNβ versus IL-1β production need further investigation, but TLR4 agonists are known to promote inflammasome activation and IL-1β release (34, 35). Despite this difference in IFNβ and IL-1β induction, both PLP-CpG and PLP-GLA elicited strong, yet comparable levels of effector CD8 and CD4 T cell responses *in vivo*. This data suggests that: 1) lack of IFNβ induction *in vitro* does not predict failure by an adjuvant to induce T cell responses *in vivo*; 2) PLP-CpG and PLP-GLA likely stimulate different arrays of cytokines in DCs *in vivo*; 3) PLP-CpG and PLP-GLA might engage different pathways to stimulate T cell activation and expansion in the respiratory tract. Consistent with this idea, it is noteworthy that PLP-CpG and PLP-GLA differ when the differentiation of T

cells are compared. In comparison to PLP-GLA, PLP-CpG tended to drive T cells towards terminal differentiation, based on elevated expressions of KLRG-1, CX3CR1, TBET, and EOMES. CpG is known to induce high levels of IL-12 (36), and it is likely that higher induction of IL-12 in DCs by PLP-CpG underlies greater levels of TBET and terminal differentiation of effector T cells in PLP-CpG-vaccinated mice. Pertaining to functional polarization of T cells, PLP-CpG elicited primarily Tc1 CD8 T cells and Th1 CD4 T cells secreting IFNγ, but only a fraction of CD4 T cells also secreted IL-17α. In contrast, PLP-GLA promotes functionally broad CD8 and CD4 T cell responses that secreted IFNγ and/or IL-17α. The differential functional polarization of T cells in PLP-CpG and PLP-GLA-vaccinated mice might be linked to disparate levels of IL-12 and inflammasome activation, respectively (19, 36, 37). In addition to the inflammatory milieu, the strength and/or duration of TCR signaling affects the differentiation of T cells (38). In this context, we have previously reported that ADJ in combination with soluble CpG enhance TCR signaling and promote terminal differentiation of effector CD8 and CD4 T cells (17). By contrast, ADJ in combination with soluble GLA results in dampened TCR signaling, leading to limited terminal differentiation of effectors and development of a larger pool of memory T cells (17). Since TLR4 engagement is known to downregulate antigen-triggered TCR signaling (39), we theorize that disparate TCR signaling induced by CpG and GLA might underlie differential T cell responses to ADJ+CpG versus ADJ +GLA in vaccinated mice.

Total numbers of influenza-specific lung T_{RM} CD8 T cells correlate with protection from rechallenge (10–12). We have previously reported that ADJ, a carbomer-containing nanoemulsion adjuvant induces T_{RM}s in lungs and protects against pathogenic influenza A virus infection (16). In the current study, we explored whether combining ADJ with PLP-CpG or PLP-GLA augmented the adjuvanticity of ADJ and increased the numbers of lung T_{RM} CD8 T cells. PLP-CpG, PLP-GLA, and ADJ alone did not significantly differ in terms of the numbers of lung T_{RM} CD8 T cells. Although ADJ suppresses PLP-CpG-induced IFNβ production *in vitro*, ADJ did not adversely affect CD8 or CD4 T cell responses to PLP-CpG. The numbers of effector CD8 T cells (at the peak of the response) or memory CD8 T cells were not significantly different in PLP-CpG versus ADJ+PLP-CpG groups, though as expected, there was contraction of NP366+ CD8 T cells in lungs from D8 to D100 post boost. Thus, combining ADJ with PLP-CpG did not alter the development of memory CD8 T cells. In striking contrast, combining ADJ with PLP-GLA generally enhanced the number of effector and memory CD8/CD4 T cells, as compared to ADJ or PLP-GLA alone; ADJ+PLP-GLA induced the largest cohort of lung- and airway-resident T_{RM}s, as compared to all other groups. This in turn correlated strongly with the most effective protective immunity against pathogenic influenza virus infection. As discussed above, PLP-CpG with or without ADJ promotes high level of expression of TBET leading to a greater degree of differentiation of KLRG-1^{HI}/CX3CR1^{HI} CD8 T cells. By contrast, the combination of ADJ+PLP-GLA maximizes effector/memory mucosal NP366-specific CD8 T cells and T_{RM} frequencies, and downregulates the levels of KLRG-1, CX3CR1, Granzyme B, TBET, EOMES, and Ki67 (40, 41). Furthermore, engaging the RORγ/Tc17/Th17 differentiation program by ADJ +PLP-GLA might enhance differentiation of long-lived stem cell-like memory T cells (42). Nonetheless, our results are consistent with the axiom that T_{RM} arise from less differentiated effector cells, and terminally differentiated effector cells have diminished capacity to develop into T_{RM}s (43, 44). Collectively, our findings support the rationale and feasibility of combining adjuvants to mitigate terminal differentiation of effectors and enhance the development of T_{RM}.

Memory T cell-dependent protection against influenza virus is dictated by the number of memory CD8 T cells in airways and lung parenchyma (10–12, 45). Consistent with these reports, we find that ADJ+PLP-GLA mice contained significantly greater numbers of T_{RM} and memory T cells in airways, which correlated strongly with the most effective protection against pathogenic influenza infection. Additionally, we find a strong correlative link between recall CD4/CD8 T cell functionality and reduction of influenza virus lung titers, specifically in Tc1/Tc17 and Th1/Th17 responses (factors associated with protection to influenza in the ADJ+PLP-GLA group are listed in **Supplementary Table 1**). The role of IFNγ, and its production in recall lung CD8 T cell responses is established in controlling influenza viral lung replication (46–49). While we also observed a strong correlation between IFNγ expression in lung CD8 T cells and reduction in viral titers, this association did not apply for lung CD4 T cells, indicating that perhaps Tc1 cells are more important than Th1 cells in controlling influenza virus. Interestingly, production of IL-17α from both CD8 and CD4 T cells was closely associated with reduction in lung viral lung titers in this study. IL-17α-producing T cells are well known to be involved in fungal immunity (50, 51), however the role of Tc17/Th17 responses in control of influenza infection is only recently emerging. Lung Tc17 cells appear to be a distinct subset of CD8 T cells, compared with Tc1 cells, and are associated with protection from rechallenge (52, 53). Influenza virus-specific lung Th17 have also been implicated in protection from influenza (54, 55). Overall, more mechanistic studies are required to carefully dissect and correlate the roles of individual functional responses in vaccine-induced lung T cells to influenza viral control.

While antibody-mediated protection against influenza virus is type and subtype specific, memory T cells that recognize conserved epitopes in the internal proteins, such as nucleoprotein, provide heterosubtypic immunity to influenza A virus (56, 57). Hence, there is an impetus to identify strategies to elicit T cell immunity in the lungs towards an universal influenza vaccine (56). Our studies show that both CD4 and CD8 T cells are essential for mediating vaccine immunity to influenza A virus, but the exact mechanisms remain unknown. Our data strongly suggest T-cell-dependent immunity, but our studies do not exclude a role for antibodies in vaccine-induced protection. It is less likely that NP protein induces virus neutralizing antibody responses, but we cannot exclude the possibility that

NP-specific antibodies might promote antigen uptake by FcR-dependent mechanisms, leading to enhanced antigen presentation to CD8 and CD4 T cell responses during vaccination (58–60).

It is clear that recovery from influenza virus infection leads to memory T cell-dependent immunity to reinfection, but this immunity is not durable (10–12). Protection afforded by ADJ +PLP-GLA vaccination was evident at both 100 and 362 days post boost, and T cell dependant. In comparison to published work, we find that T cell responses elicited by ADJ+PLP-GLA differ from those induced by influenza virus infection in two key aspects: 1) A larger proportion of NP366-specific memory CD8 T cells elicited by ADJ+PLP-GLA are mucosally imprinted (CD69+/CD103+) and reside in the lung parenchyma at memory (D100) measurements (**Figure 5A**), while majority of influenza virus-elicited NP366 specific memory CD8 T cells at comparable time points are CD69-/CD103- and/or reside in the vascular compartment (61, 62); 2) Vaccination with PLP adjuvants, particularly ADJ+PLP-GLA, elicits durable antigen specific CD4 memory (**Figure 5B**), unlike influenza infection (63). Mechanisms underpinning differences in vaccine- versus infection-induced T-cell memory needs further investigation.

There are no FDA-approved mucosal vaccines formulated in adjuvants that are known to elicit protective T cell immunity in the respiratory mucosa. In this manuscript, we have explored novel ways of presenting immune components to the immune system to maximize antigen presentation to T cells and evoke innate immune responses that program a strong and enduring mucosal T cell response in the respiratory tract. Specifically, we have identified a novel vaccine formulation consisting of influenza virus NP, TLR-loaded PLPs, and a nanoemulsion adjuvant, that elicits robust mucosally-imprinted T cell memory in the respiratory tract and affords effective protective immunity to a pathogenic influenza virus infection in mice. These findings have significant implications in the development of T cell-based vaccines against respiratory viral pathogens such as influenza virus and SARS-CoV-2.

DATA AVAILABILITY STATEMENT

The raw data supporting the conclusions of this article will be made available by the authors, without undue reservation.

ETHICS STATEMENT

The animal study was reviewed and approved by Animal Care and Use Committee at the UW School of Veterinary Medicine.

AUTHOR CONTRIBUTIONS

MS conceived experiments, analyzed data, and edited the paper. BK-B conceived experiments, performed experiments, analyzed data, and wrote the paper. RT performed experiments, analyzed data, and edited manuscript. WL, PP, GV, CM, DG, TL, BP and AL performed experiments. YK provided critical reagents. All authors contributed to the article and approved the submitted version.

FUNDING

This study was supported by PHS grants from the National Institutes of Health (grant# U01AI124299 and R21 AI149793) and funds from the John E. Butler Professorship to MS. WL was supported by a pre-doctoral fellowship from the American Heart Association. KR was supported by a PHS grant from the National institutes of Health (grant #:U01AI124270).

SUPPLEMENTARY MATERIAL

The Supplementary Material for this article can be found online at: https://www.frontiersin.org/articles/10.3389/fimmu.2020.559382/full#supplementary-material

REFERENCES

1. Wardlaw TM, Johansson EW, Hodge M, World Health OUnited Nations Children's Fund. (World Health Organization, Geneva) (2006).
2. Estimates of the global, regional, and national morbidity, mortality, and aetiologies of lower respiratory infections in 195 countries, 1990-2016: a systematic analysis for the Global Burden of Disease Study 2016. *Lancet Infect Dis* (2018) 18:1191–210. doi: 10.1016/s1473-3099(18)30310-4
3. Rothan HA, Byrareddy SN. The epidemiology and pathogenesis of coronavirus disease (COVID-19) outbreak. *J Autoimmun* (2020) 109:102433. doi: 10.1016/j.jaut.2020.102433
4. Kaneko N, Kuo HH, Boucau J, Farmer JR, Allard-Chamard H, Mahajan VS, et al. Loss of Bcl-6-Expressing T Follicular Helper Cells and Germinal Centers in COVID-19. *Cell* (2020) 183:143–157.e113. doi: 10.1016/j.cell.2020.08.025
5. Sekine T, Perez-Potti A, Rivera-Ballesteros O, Strålin K, Gorin JB, Olsson A, et al. Robust T Cell Immunity in Convalescent Individuals with Asymptomatic or Mild COVID-19. *Cell* (2020) 183:158–68.e114. doi: 10.1016/j.cell.2020.08.017
6. Paules C, Subbarao K. Influenza. *Lancet (London England)* (2017) 390:697–708. doi: 10.1016/s0140-6736(17)30129-0
7. Chen J, Deng YM. Influenza virus antigenic variation, host antibody production and new approach to control epidemics. *Virol J* (2009) 6:30. doi: 10.1186/1743-422x-6-30
8. Assarsson E, Bui HH, Sidney J, Zhang Q, Glenn J, Oseroff C, et al. Immunomic analysis of the repertoire of T-cell specificities for influenza A virus in humans. *J Virol* (2008) 82:12241–51. doi: 10.1128/jvi.01563-08
9. Teijaro JR, Turner D, Pham Q, Wherry EJ, Lefrançois L, Farber DL, et al. Cutting edge: Tissue-retentive lung memory CD4 T cells mediate optimal protection to respiratory virus infection. *J Immunol (Baltimore Md 1950)* (2011) 187:5510–4. doi: 10.4049/jimmunol.1102243
10. Wu T, Hu Y, Lee YT, Bouchard KR, Benechet A, Khanna K, et al. Lung-resident memory CD8 T cells (TRM) are indispensable for optimal cross-protection against pulmonary virus infection. *J Leukocyte Biol* (2014) 95:215–24. doi: 10.1189/jlb.0313180
11. Slütter B, Van Braeckel-Budimir N, Abboud G, Varga SM, Salek-Ardakani S, Harty JT. Dynamics of influenza-induced lung-resident memory T cells underlie waning heterosubtypic immunity. *Sci Immunol* (2017) 2. doi: 10.1126/sciimmunol.aag2031
12. Van Braeckel-Budimir N, Harty JT. Influenza-induced lung Trm: not all memories last forever. *Immunol Cell Biol* (2017) 95:651–5. doi: 10.1038/icb.2017.32

13. Zens KD, Chen JK, Farber DL. Vaccine-generated lung tissue-resident memory T cells provide heterosubtypic protection to influenza infection. *JCI Insight* (2016) 1. doi: 10.1172/jci.insight.85832
14. Lapuente D, Storcksdieck Genannt Bonsmann M, Maaske A, Stab V, Heinecke V, Watzstedt K, et al. IL-1β as mucosal vaccine adjuvant: the specific induction of tissue-resident memory T cells improves the heterosubtypic immunity against influenza A viruses. *Mucosal Immunol* (2018) 11:1265–78. doi: 10.1038/s41385-018-0017-4
15. Wegmann F, Moghaddam AE, Schiffner T, Gartlan KH, Powell TJ, Russell RA, et al. The Carbomer-Lecithin Adjuvant Adjuplex Has Potent Immunoactivating Properties and Elicits Protective Adaptive Immunity against Influenza Virus Challenge in Mice. *Clin Vaccine Immunol* (2015) 22:1004–12. doi: 10.1128/cvi.00736-14
16. Gasper DJ, Neldner B, Plisch EH, Rustom H, Carrow E, Imai H, et al. Effective Respiratory CD8 T-Cell Immunity to Influenza Virus Induced by Intranasal Carbomer-Lecithin-Adjuvanted Non-replicating Vaccines. *PloS Pathog* (2016) 12:e1006064. doi: 10.1371/journal.ppat.1006064
17. Marinaik CB, Kingstad-Bakke B, Lee W, Hatta M, Sonsalla M, Larsen A, et al. Programming Multifaceted Pulmonary T Cell Immunity by Combination Adjuvants. *Cell Rep Med* (2020) 1:100095. doi: 10.1016/j.xcrm.2020.100095
18. Del Giudice G, Rappuoli R, Didierlaurent AM. Correlates of adjuvanticity: A review on adjuvants in licensed vaccines. *Semin Immunol* (2018) 39:14–21. doi: 10.1016/j.smim.2018.05.001
19. Leleux JA, Pradhan P, Roy K. Biophysical Attributes of CpG Presentation Control TLR9 Signaling to Differentially Polarize Systemic Immune Responses. *Cell Rep* (2017) 18:700–10. doi: 10.1016/j.celrep.2016.12.073
20. Dawson E, Leleux JA, Pradhan P, Roy K. Surface-Presentation of CpG and Protein–Antigen on Pathogen-Like Polymer Particles Generate Strong Prophylactic and Therapeutic Antitumor Protection. *ACS Biomater Sci Eng* (2017) 3:169–78. doi: 10.1021/acsbiomaterials.6b00384
21. Madan-Lala R, Pradhan P, Roy K. Combinatorial Delivery of Dual and Triple TLR Agonists via Polymeric Pathogen-like Particles Synergistically Enhances Innate and Adaptive Immune Responses. *Sci Rep* (2017) 7:2530. doi: 10.1038/s41598-017-02804-y
22. Coler RN, Bertholet S, Moutaftsi M, Guderian JA, Windish HP, Baldwin SL, et al. Development and Characterization of Synthetic Glucopyranosyl Lipid Adjuvant System as a Vaccine Adjuvant. *PloS One* (2011) 6:e16333. doi: 10.1371/journal.pone.0016333
23. Ozawa M, Victor ST, Taft AS, Yamada S, Li C, Hatta M, et al. Replication-incompetent influenza A viruses that stably express a foreign gene. *J Gen Virol* (2011) 92:2879–88. doi: 10.1099/vir.0.037648-0
24. Tobita K, Sugiura A, Enomote C, Furuyama M. Plaque assay and primary isolation of influenza A viruses in an established line of canine kidney cells (MDCK) in the presence of trypsin. *Med Microbiol Immunol* (1975) 162:9–14. doi: 10.1007/bf02123572
25. Martin MD, Badovinac VP. Defining Memory CD8 T Cell. *Front Immunol* (2018) 9:2692. doi: 10.3389/fimmu.2018.02692
26. Yan Y, Cao S, Liu X, Harrington SM, Bindeman WE, Adjei AA, et al. CX3CR1 identifies PD-1 therapy-responsive CD8+ T cells that withstand chemotherapy during cancer chemoimmunotherapy. *JCI Insight* (2018) 3. doi: 10.1172/jci.insight.97828
27. Kaech SM, Cui W. Transcriptional control of effector and memory CD8+ T cell differentiation. *Nat Rev Immunol* (2012) 12:749–61. doi: 10.1038/nri3307
28. Topham DJ, Reilly EC. Tissue-Resident Memory CD8+ T Cells: From Phenotype to Function. *Front Immunol* (2018) 9:515. doi: 10.3389/fimmu.2018.00515
29. Baer A, Colon-Moran W, Bhattarai N. Characterization of the effects of immunomodulatory drug fingolimod (FTY720) on human T cell receptor signaling pathways. *Sci Rep* (2018) 8:10910. doi: 10.1038/s41598-018-29355-0
30. Ntranos A, Hall O, Robinson DP, Grishkan IV, Schott JT, Tosi DM, et al. FTY720 impairs CD8 T-cell function independently of the sphingosine-1-phosphate pathway. *J Neuroimmunol* (2014) 270:13–21. doi: 10.1016/j.jneuroim.2014.03.007
31. Miller JD, van der Most RG, Akondy RS, Glidewell JT, Albott S, Masopust D, et al. Human effector and memory CD8+ T cell responses to smallpox and yellow fever vaccines. *Immunity* (2008) 28:710–22. doi: 10.1016/j.immuni.2008.02.020
32. Kasturi SP, Skountzou I, Albrecht RA, Koutsonanos D, Hua T, Nakaya HI, et al. Programming the magnitude and persistence of antibody responses with innate immunity. *Nature* (2011) 470:543–7. doi: 10.1038/nature09737
33. Baxevanis CN, Voutsas IF, Tsitsilonis OE. Toll-like receptor agonists: current status and future perspective on their utility as adjuvants in improving anticancer vaccination strategies. *Immunotherapy* (2013) 5:497–511. doi: 10.2217/imt.13.24
34. Kayagaki N, Wong MT, Stowe IB, Ramani SR, Gonzalez LC, Akashi-Takamura S, et al. Noncanonical inflammasome activation by intracellular LPS independent of TLR4. *Science* (2013) 341:1246–9. doi: 10.1126/science.1240248
35. He Y, Hara H, Nunez G. Mechanism and Regulation of NLRP3 Inflammasome Activation. *Trends Biochem Sci* (2016) 41:1012–21. doi: 10.1016/j.tibs.2016.09.002
36. Yin P, Liu X, Mansfield AS, Harrington SM, Li Y, Yan Y, et al. CpG-induced antitumor immunity requires IL-12 in expansion of effector cells and down-regulation of PD-1. *Oncotarget* (2016) 7:70223–31. doi: 10.18632/oncotarget.11833
37. Deng J, Yu XQ, Wang PH. Inflammasome activation and Th17 responses. *Mol Immunol* (2019) 107:142–64. doi: 10.1016/j.molimm.2018.12.024
38. Jameson SC, Masopust D. Understanding Subset Diversity in T Cell Memory. *Immunity* (2018) 48:214–26. doi: 10.1016/j.immuni.2018.02.010
39. Gonzalez-Navajas JM, Fine S, Law J, Datta SK, Nguyen KP, Yu M, et al. TLR4 signaling in effector CD4+ T cells regulates TCR activation and experimental colitis in mice. *J Clin Invest* (2010) 120:570–81. doi: 10.1172/JCI40055
40. Hombrink P, Helbig C, Backer RA, Piet B, Oja AE, Stark R, et al. Programs for the persistence, vigilance and control of human CD8+ lung-resident memory T cells. *Nat Immunol* (2016) 17:1467–78. doi: 10.1038/ni.3589
41. Behr FM, Chuwonpad A, Stark R, van Gisbergen KPJM. Armed and Ready: Transcriptional Regulation of Tissue-Resident Memory CD8 T Cells. *Front Immunol* (2018) 9:1770. doi: 10.3389/fimmu.2018.01770
42. Muranski P, Borman ZA, Backer SP, Klebanoff CA, Ji Y, Sanchez-Perez L, et al. Th17 cells are long lived and retain a stem cell-like molecular signature. *Immunity* (2011) 35:972–85. doi: 10.1016/j.immuni.2011.09.019
43. Vrisekoop N, den Braber I, de Boer AB, Ruiter AF, Ackermans MT, van der Crabben SN, et al. Sparse production but preferential incorporation of recently produced naive T cells in the human peripheral pool. *Proc Natl Acad Sci USA* (2008) 105:6115–20. doi: 10.1073/pnas.0709713105
44. Szabo PA, Miron M, Farber DL. Location, location, location: Tissue resident memory T cells in mice and humans. *Sci Immunol* (2019) 4:eaas9673. doi: 10.1126/sciimmunol.aas9673
45. Slutter B, Pewe LL, Kaech SM, Harty JT. Lung airway-surveilling CXCR3(hi) memory CD8(+) T cells are critical for protection against influenza A virus. *Immunity* (2013) 39:939–48. doi: 10.1016/j.immuni.2013.09.013
46. Bot A, Bot S, Bona CA. Protective Role of Gamma Interferon during the Recall Response to Influenza Virus. *J Virol* (1998) 72:6637–45. doi: 10.1128/JVI.72.8.6637-6645.1998
47. McMaster SR, Wilson JJ, Wang H, Kohlmeier JE. Airway-Resident Memory CD8 T Cells Provide Antigen-Specific Protection against Respiratory Virus Challenge through Rapid IFN-γ Production. *J Immunol* (2015) 195:203–9. doi: 10.4049/jimmunol.1402975
48. Kang S, Brown HM, Hwang S. Direct Antiviral Mechanisms of Interferon-Gamma. *Immune Netw* (2018) 18:e33. doi: 10.4110/in.2018.18.e33
49. Kohlmeier JE, Cookenham T, Roberts AD, Miller SC, Woodland DL. Type I interferons regulate cytolytic activity of memory CD8(+) T cells in the lung airways during respiratory virus challenge. *Immunity* (2010) 33:96–105. doi: 10.1016/j.immuni.2010.06.016
50. Sparber F, LeibundGut-Landmann S. Interleukin-17 in Antifungal Immunity. *Pathog (Basel Switzerland)* (2019) 8. doi: 10.3390/pathogens8020054
51. Nanjappa SG, McDermott AJ, Fites JS, Galles K, Wüthrich M, Deepe GS Jr., et al. Antifungal Tc17 cells are durable and stable, persisting as long-lasting vaccine memory without plasticity towards IFNγ cells. *PloS Pathog* (2017) 13:e1006356. doi: 10.1371/journal.ppat.1006356
52. Hamada H, Garcia-Hernandez MdIL, Reome JB, Misra SK, Strutt TM, McKinstry KK, et al. Tc17, a Unique Subset of CD8 T Cells That Can Protect against Lethal Influenza Challenge. *J Immunol* (2009) 182:3469–81. doi: 10.4049/jimmunol.0801814
53. Hamada H, Garcia-Hernandez MdLL, Reome JB, Misra SK, Dutton RW. The mechanism of protection against influenza by transfer of Tc17, an IL-17 secreting CD8 T cell subset. *J Immunol* (2009) 18246:45–46.45.

54. McKinstry KK, Strutt TM, Buck A, Curtis JD, Dibble JP, Huston G, et al. IL-10 Deficiency Unleashes an Influenza-Specific Th17 Response and Enhances Survival against High-Dose Challenge. *J Immunol* (2009) 182:7353–63. doi: 10.4049/jimmunol.0900657
55. Christensen D, Mortensen R, Rosenkrands I, Dietrich J, Andersen P. Vaccine-induced Th17 cells are established as resident memory cells in the lung and promote local IgA responses. *Mucosal Immunol* (2017) 10:260–70. doi: 10.1038/mi.2016.28
56. Erbelding EJ, Post DJ, Stemmy EJ, Roberts PC, Augustine AD, Ferguson S, et al. A Universal Influenza Vaccine: The Strategic Plan for the National Institute of Allergy and Infectious Diseases. *J Infect Dis* (2018) 218:347–54. doi: 10.1093/infdis/jiy103
57. Sridhar S. Heterosubtypic T-Cell Immunity to Influenza in Humans: Challenges for Universal T-Cell Influenza Vaccines. *Front Immunol* (2016) 7:195. doi: 10.3389/fimmu.2016.00195
58. Machy P, Serre K, Leserman L. Class I-restricted presentation of exogenous antigen acquired by Fcgamma receptor-mediated endocytosis is regulated in dendritic cells. *Eur J Immunol* (2000) 30:848–57. doi: 10.1002/1521-4141(200003)30:3<848::AID-IMMU848>3.0.CO;2-Q
59. Schuurhuis DH, Ioan-Facsinay A, Nagelkerken B, van Schip JJ, Sedlik C, Melief CJ, et al. Antigen-antibody immune complexes empower dendritic cells to efficiently prime specific CD8+ CTL responses in vivo. *J Immunol* (2002) 168:2240–6. doi: 10.4049/jimmunol.168.5.2240
60. de Jong JM, Schuurhuis DH, Ioan-Facsinay A, van der Voort EI, Huizinga TW, Ossendorp F, et al. Murine Fc receptors for IgG are redundant in facilitating presentation of immune complex derived antigen to CD8+ T cells in vivo. *Mol Immunol* (2006) 43:2045–50. doi: 10.1016/j.molimm.2006.01.002
61. Hayward SL, Scharer CD, Cartwright EK, Takamura S, Li ZT, Boss JM, et al. Environmental cues regulate epigenetic reprogramming of airway-resident memory CD8(+) T cells. *Nat Immunol* (2020) 21:309–20. doi: 10.1038/s41590-019-0584-x
62. Wein AN, McMaster SR, Takamura S, Dunbar PR, Cartwright EK, Hayward SL, et al. CXCR6 regulates localization of tissue-resident memory CD8 T cells to the airways. *J Exp Med* (2019) 216:2748–62. doi: 10.1084/jem.20181308
63. Turner DL, Bickham KL, Thome JJ, Kim CY, D'Ovidio F, Wherry EJ, et al. Lung niches for the generation and maintenance of tissue-resident memory T cells. *Mucosal Immunol* (2014) 7:501–10. doi: 10.1038/mi.2013.67

Conflict of Interest: The authors declare that the research was conducted in the absence of any commercial or financial relationships that could be construed as a potential conflict of interest.

frontiers in Immunology

ORIGINAL RESEARCH
published: 18 March 2021
doi: 10.3389/fimmu.2021.624197

CD169+ Subcapsular Macrophage Role in Antigen Adjuvant Activity

*Christina Lisk[1], Rachel Yuen[2], Jeff Kuniholm[2], Danielle Antos[3], Michael L. Reiser[4] and Lee M. Wetzler[1,2]**

[1] Section of Infectious Diseases, Department of Medicine, Boston Medical Center, Boston, MA, United States, [2] Department of Microbiology, Boston University School of Medicine, Boston, MA, United States, [3] Department of Microbiology and Immunology, University of Pittsburgh School of Medicine, Pittsburgh, PA, United States, [4] DRK-Blutspendedienst, BaWü-Hessen gGmbH, Frankfurt, Germany

Vaccines have played a pivotal role in improving public health, however, many infectious diseases lack an effective vaccine. Controlling the spread of infectious diseases requires continuing studies to develop new and improved vaccines. Our laboratory has been investigating the immune enhancing mechanisms of Toll-like receptor (TLR) ligand-based adjuvants, including the TLR2 ligand Neisseria meningitidis outer membrane protein, PorB. Adjuvant use of PorB increases costimulatory factors on antigen presenting cells (APC), increases antigen specific antibody production, and cytokine producing T cells. We have demonstrated that macrophage expression of MyD88 (required for TLR2 signaling) is an absolute requirement for the improved antibody response induced by PorB. Here-in, we specifically investigated the role of subcapsular CD169+ marginal zone macrophages in antibody production induced by the use of TLR-ligand based adjuvants (PorB and CpG) and non-TLR-ligand adjuvants (aluminum salts). CD169 knockout mice and mice treated with low dose clodronate treated animals (which only remove marginal zone macrophages), were used to investigate the role of these macrophages in adjuvant-dependent antibody production. In both sets of mice, total antigen specific immunoglobulins (IgGs) were diminished regardless of adjuvant used. However, the greatest reduction was seen with the use of TLR ligands as adjuvants. In addition, the effect of the absence of CD169+ macrophages on adjuvant induced antigen and antigen presenting cell trafficking to the lymph nodes was examined using immunofluorescence by determining the relative extent of antigen loading on dendritic cells (DCs) and antigen deposition on follicular dendritic cells (FDC). Interestingly, only vaccine preparations containing PorB had significant decreases in antigen deposition in lymphoid follicles and germinal centers in CD169 knockout mice or mice treated with low dose clodronate as compared to wildtype controls. Mice immunized with CpG containing preparations demonstrated decreased FDC networks in the mice treated with low dose clodronate. Conversely, alum containing preparations only demonstrated significant decreases in IgG in CD169 knockout mice. These studies stress that importance of subcapsular macrophages and their unique role in adjuvant-mediated antibody production,

OPEN ACCESS

Edited by:
Simon Daniel Van Haren, Boston Children's Hospital and Harvard Medical School, United States

Reviewed by:
Constantino López-Macías, Mexican Social Security Institute (IMSS), Mexico
Jovvian Parakkal, New York Blood Center, United States

***Correspondence:**
Lee M. Wetzler
lwetzler@bu.edu

Specialty section:
This article was submitted to Vaccines and Molecular Therapeutics, a section of the journal Frontiers in Immunology

Received: *30 October 2020*
Accepted: *14 January 2021*
Published: *18 March 2021*

Citation:
Lisk C, Yuen R, Kuniholm J, Antos D, Reiser ML and Wetzler LM (2021) CD169+ Subcapsular Macrophage Role in Antigen Adjuvant Activity. Front. Immunol. 12:624197. doi: 10.3389/fimmu.2021.624197

potentially due to an effect of these adjuvants on antigen trafficking to the lymph node and deposition on follicular dendritic cells.

Keywords: adjuvants, TLR-ligand based adjuvants, PorB, Neisseria, TLR2, antibody production, follicular dendritic cells, antigen deposition

INTRODUCTION

Vaccines represent one of the greatest public health advancements of the last 50 years (1–5). However, there is still a great need for new vaccines for many infectious diseases including HIV, malaria, tuberculosis etc (6–10).. It is imperative that vaccine research continue in order to provide protection to these infectious diseases. One way in which vaccine research is progressing is the use of subunit vaccines (9, 11, 12). These vaccines consist of an antigen to protect against and an adjuvant to stimulate the immune response. Adjuvants can be divided up into five main groups – mineral salts, oil emulsion, microbial products, saponins, or synthetic products (13). The microbial product group contains a subclass of adjuvants that stimulate through pattern recognition receptors (PRR), more specifically Toll-like receptors (TLRs) (14–21). TLRs can be either extracellularly or intracellularly within the endosome (22–25). Depending on which TLR is engaged, cellular signal occurs leading to predictable downstream stimulation and effects. This predictableness makes TLR-ligand based adjuvants useful tools to investigate cellular pathways during an immune response (23, 26–28). Our lab has focused on these cellular mechanisms of adjuvants, especially PorB, the major outer membrane protein from *Neisseria meningitidis*, which signals through TLR2/1 heterodimers (29). PorB has been shown to significantly increase adaptive immune responses, such as antigen-specific antibodies (30, 31) and clearance of *Listeria monocytogenes via* $CD8^+$ T cells (32). PorB has also been shown to stimulate antigen presenting cells and enhance adaptive immune responses by increasing their expression of co-stimulatory factors, increase their cytokine expression, and enhance their antigen cross-presentation (30, 33). Most recently, our lab has shown that PorB can also increase deposition of antigen on germinal center follicular dendritic cell (FDC) networks and can even increase the size of such networks (34).

It is well known that innate immune cells have the ability to influence and skew the adaptive immune responses in order to protect against pathogens (19, 35–38). The early induction events within the lymph node and spleen, which lead to germinal center formation and affinity maturation, remain topics of active research. Complete knowledge of such dynamics will lead to a better understanding of infection and prevention by utilizing the immune system. Recently our lab demonstrated that conditional knockouts of the TLR-signaling molecule MyD88 in macrophages specifically prevented the adjuvant effect of PorB as determined by a decrease in the production of OVA-specific IgG (31). Surprisingly, dendritic cells (DC) were not able to rescue the loss of MyD88 signaling within the macrophages. The work presented here which specifically examines the role of subcapsular sinus (SCS) and marginal zone macrophages in improved immune responses after vaccination using various adjuvants, is a follow-up to these studies, as the SCS or marginal zone macrophages have unique functions that DCs cannot perform (39, 40).

Multiple studies have indicated SCS macrophages in antigen and immune complex retention from the lymph, transportation into the lymph node (39–45), and activation of the adaptive immune response including antigen deposition onto follicular dendritic cells (46), antibody production (47) and $CD8^+$ T cell activation (48–50). These studies have determined that SCS macrophages exploit their location within the lymph node, their unique cellular properties, and the expression of singlec 1 (CD169) receptor on the cell surface in order to influence early immune induction events (51–53). The studies described here provide critical information about the potential role of these macrophages in the effect of vaccine adjuvants, including both TLR-ligand based adjuvants (PorB and CpG) and particulate-based adjuvants (Alum) and/or the requirements of CD169 expression for the effects and enhancement of antigen specific antibody production.

METHODS

Animals

Four to eight weeks old C57Bl/6J (referred to as 'wild type', stock #000664) mice were obtained from Jackson laboratories (Bar Harbor, ME). All mice were maintained within the Laboratory Animals Science Center (LASC) at Boston University School of Medicine under Dr. Lee Wetzler's animal protocol 14155. The Boston University Institutional Animal Care and Use Committee (IACUC) approved all research conducted using animal models.

CD169 knockout mice were a gift from Dr. Paul Crocker, University of Dundee. Polymerase chain reaction (PCR) was performed on these animals to ensure the genotype was correct.

Genotyping for CD169 Global Knockout

CD169 knockout animals were ear punched after weaning for genotyping. RedExtract-N-Amp Tissue PCR Kit (Sigma, Cat#E7526) was used according to manufacturer's protocol. PCR reaction was prepared using RedExtract-N-Amp Tissue PCR Kit (Sigma, Cat#R4775) according to manufacturer's protocol.

To determine the effectiveness of the CD169 KO, the following PCR protocol was used. CD169 Primers: Forward - CAC CAC GGT CAC TGT GAC AA, Reverse - GGC CAT ATG TAG GGT CGT CT. Both primers are used at a final concentration of 1μM with the following PCR program:1. 92°C for 2:00, 2. 92°C for 0:30, 3. 57°C for 0:30, 4. 72°C for 1:30, 5.

Repeat step #2 x35, 6. 72°C for 5:00, 7. Store at 4°C. When the transgene is present the expected product is 1,700 bp, as compared to 486 bp in WT mice.

Specificity of Clodronate for Subcapsular Macrophages

Clodronate (Liposoma Research, SKU:C-005) treated animals received intravenous (IV) tail vein injections with different doses of clodronate – either high dose (40 mg/kg) or low dose (6.5 mg/kg). Low dose clodronate has been previously published to deplete the subcapsular subtypes of macrophages within the lymph node (54). Twenty-four hours post IV injection, flow cytometry and immunohistochemistry (IHC) was used to determined depletion of $CD169^+$ macrophages. Briefly, inguinal lymph nodes were isolated and placed in cold PBS for flow cytometry analysis. Iliac lymph nodes were isolated and placed in molds (ThermoFisher) with optimal cutting temperature (OCT) medium (Richard Allan Scientific). These samples were frozen on dry ice for immunohistochemistry (IHC).

Vaccine Regime

Wild type and CD169 knockout mice between the ages of four to eight weeks were immunized subcutaneously with 100 µl vaccine using a 28G insulin syringe (Becton Dickinson Cat# 3294161). Vaccine groups consisted of PBS (vehicle control), ovalbumin (OVA, 10 µg), OVA + PorB (10 µg), OVA+ CpG (10 µg, Invivogen, Cat# ODN1826), and OVA+ aluminum salts (alum, 200 µg Sigma, Cat# A8222). Clodronate treated groups received an IV tail vein injection one day prior to subcutaneous vaccinations. For immunoglobulin (IgG) studies, mice were vaccinated three times, two weeks apart as shown in **Supplemental Figure 3**. Two weeks after the final injection, the animals were sacrificed and the blood collected for antigen (ovalbumin, OVA) specific immunoglobulin ELISAs (n=6–12). The concentrations and volumes for vaccines were from previously determined publications (30). For antigen deposition onto follicular dendritic cells, mice were vaccinated subcutaneously and euthanized 24 h post injection (**Supplemental Figure 4**). Vaccination groups consisted of ovalbumin (OVA) fluorescently labeled with Alexa 594 (OVA-A594, Life technologies) alone, OVA-A594 + PorB, OVA-A594 + CpG, or OVA-A594 + Alum. Draining lymph nodes were isolated for IHC and flow cytometry analysis.

PorB Isolation

Porin B (PorB) was isolated as previously published (55).

Flow Cytometry for $CD169^+$ Macrophages and Follicular Dendritic Cells

Draining lymph nodes were isolated for flow cytometry and placed in cold PBS immediately after isolation. Single cell suspensions were prepared as follows unless indicated otherwise. Tissues were pushed through a 70 µm cell strainer. Samples were then incubated for 3 min in ACK (150 mM NaH_4CL, 50mM $KHCO_3$) buffer to lysis red blood cells. The samples were then washed in PBS and re-filtered through a 70 µm cell strainer. At this point, samples were counted and stained for flow cytometry. Cells were incubated with a live/dead stain (Biolegend, Cat#423105) for 30 min, in the dark at 4°C. Cells were then washed with 5x FACSBuffer (PBS, 0.5%BSA, and 2% EDTA) and spun down at 1,600 rpm at 4°C. Cells were then incubated with CD16/CD32 Fc block (eBioscience, 48-0032-82) for 10 min in the dark at room temperature. Cells were then plated in a 96 V-well bottom plate (Corning, CLS3896-48EA), spun down at 1,600 rpm at 4°C and stained for flow cytometry. All dilutions were 1:200 unless noted. For subcapsular macrophages analysis, antibodies included: CD169-FITC (Bio-Rad, 0308), CD11b–PE (Biolegend, 123128), CD19-BUV395 (BD Horizon, 563557), F4/80–PerCP5.5 (Biolegend, 123128) CD3–eFlour (Invitrogen, 48-0032-82), CD11c–APC (BD Pharmigen, 550261). Gating strategy is shown in **Supplemental Figure 2A**. A fluorescence minus one (FMO) stain was used where all the antibodies in the panel are present with the exception of CD169 as shown in **Supplemental Figure 2B**. For follicular dendritic cells, single cell suspensions were prepared as previously reported (56) and is briefly described. Draining lymph nodes were placed in cold PBS and manually minced on a petri dish with a scalpel. The samples were transferred to a 24-well plate (FisherScientific, Cat #08-772-1H), incubated with DMEM containing 2% FBS (ThermoFisher, Cat#26140079), 33.3 mg/ml collagenase type IV (ThermoFisher, Cat#17104019), and 2,500 U/ml DNase I (ThermoFisher, Cat#18047019). Samples were incubated for 1 h at 37°C. After which, the samples were strained through 70 µm filter, although not pushed through to ensure the integrity of the FDCs remained intact. Cells were spun down at 1200 rmp at 4°C and then stained as described above for flow cytometry. All antibody dilutions were 1:200 unless otherwise noted. CD21/CD35 – BV421, CD45 – APC, CD19 – BUV395 (1:400), ICAM-1 – FITC. Gating strategy is shown in **Supplemental Figure 5A**. A fluorescence minus one (FMO) was stained for all colors within the panel excluding CD21/CD35 shown in **Supplemental Figure 5B**. All samples were analyzed on an LSRII, a machine available within the Boston University flow core, on a low flow setting to ensure the integrity of FDC remained intact.

Immunohistochemistry for Subcapsular Macrophages and Antigen Deposition onto Follicular Dendritic Cells

For specificity of clodronate, lymph nodes were isolated 24 h after IV injections of either vehicle controls, low dose clodronate treatment (6.5 mg/kg), or high dose clodronate treatment (40 mg/kg). Draining lymph nodes were then put into molds containing optimal cutting temperature (OCT) medium (Richard Allan Scientific, Kalamazoo, MI, USA) and frozen on dry ice. Tissues were cut on a microm HM 550 (Microm International GmBH, Germany). 8 µm sections were obtained and placed on Colorfrost Plus slides and stored at -80°C until staining. For staining, sections were air dried for 15 min at room temperature, fixed in acetone at –20°C for 10 min, and air dried for 10 min at room temperature. Sections were re-hydrated in TBS buffer with 0.05% Tween-20 (TBST) then blocked for 30 min at room temperature with TBST with 5% BSA. Sections were rinsed with PBS and then stained with antibodies overnight at 4°C followed by three rinses with PBS. For clodronate specificity studies, the following antibodies and reagents were used: FITC hamster anti-

mouse CD169 (Biolegend, Cat#142405) and F4/80 (Biolegend, Cat#123127). All antibodies were used at 1:200 dilution. For antigen deposition on FDCs, draining lymph nodes were isolated 24 h post subcutaneous injections and stained with conjugated (CD11c, Biolegend, Cat#117309) and primary (FDC-M1, BD Biosciences, Cat#551320) antibodies overnight at 4°C followed by three rinses with PBS. Secondary antibody (anti-rat 488, Biolegend, Cat#405) was added to the slides for 1 h at room temperature followed by three washed in PBS. Antibody concentration for the primary was 1:100. Conjugated and secondary antibodies were used at 1:200 dilution. Stained lymph node sections were mounted in Fluoroshield mounting medium with DAPI (Abcam) and dried overnight at room temperature. A Leica SP5 confocal microscope (Leica AG) was used to examine all sections using the Leica LAS AF the 10x and 63x oil immersion objectives. The images were arranged and analyzed using ImageJ (NIH).

Enzyme-Linked Immunosorbent Assay (ELISA) for Antigen Specific Antibodies

Sera was collected at the time of euthanasia *via* heart sticks from all animals. Ninety-six well immulon 2 HB (ThermonFisher 3455) were coated with 5 μg/ml of OVA in carbonate buffer and incubated overnight at 4°C. Sera was diluted in tris-buffered saline and tween (TBST, 0.05% Tween) starting at 1:50. One hundred microliters of the dilutions were then added to the coated plates. A serial dilution for each sample was done horizontally across the plate. The plates were then incubated overnight in 4°C. The plates were then washed with 200 μl/well with 0.05% TBST three times. Alkaline phosphatase-conjugated anti-mouse total IgG or IgG1or IgG2c subclasses (Sigma Aldrich, St. Louis, MO) was added to each well and incubated at room temperature for 1 h. Total IgG was diluted 1:3,000 and subclasses for IgG was diluted to 1:2,000 in 0.05%TBST. Plates were then washed again and developed with one-step p-nitrophenyl phosphate (Pierce, Rockford, IL). The optical density was measure on BioTek Synergy HT and analyzed with the Gen5 software. For total IgG, colorimetric values were converted to nanograms/milligram from a standard curve created in ImageJ software as previously described (57). End point titers for IgG subclasses were determined by OD x dilution.

Statistics

Statistics were calculated in GraphPad Prism (version 8.0). Differences in OVA-specific IgG and IgG subtypes in were calculated by T tests between wild type control animals and clodronate treated animal or CD169 knockout animals. ANOVA with Sidak's multiple comparisons test was used for all other analysis. *p<0.05, **p<0.01, ***p<0.001, ****p<0.0001

RESULTS

Description of Mouse Models Used for Antibody Production

In the studies describe below we used mice with defects in the subcapsular macrophages, either lacking the CD169 molecule or removal by treatment with low dose clodronate. CD169 global knockout animals were genotyped to ensure their genetic composition was correct. As shown in **Supplemental Figure 1**, the transgene was present at 1,700 base pair (bp) while the wildtype was at 468 bp. To complement our global knockout mouse, we utilized clodronate liposome treatment, which has been shown to deplete macrophages in the lymph nodes and the spleen by causing apoptosis from increased intracellular concentrations of clodronate. At higher doses (40 μg/kg), clodronate liposomes deplete both $CD169^+$ macrophages and conventional ($F4/80^+$) macrophages whereas lower dosages (6.5 μg/kg) result in the preferential depletion of $CD169^+$ macrophages in mice (54). In order to demonstrate the specific depletion of these macrophages, fluorescently labeled antibodies recognizing $CD169^+$ and $F4/80^+$ expressing cells were used in flow cytometry and immunohistochemistry studies to examine the amount of $CD169^+$ macrophages after high dose clodronate treatment, low dose clodronate treatment, and vehicle control animals. These results are shown in **Supplemental Figures 2C–G**. The specificity of low dose clodronate treatment to $CD169^+$ macrophages allowed us to investigate the role of these cells in antibody production. The combination of these mouse models, CD169 knockout and low dose clodronate treatment, allowed for thorough investigations into the role of the subscapular (SCS) macrophages, as well as the expression CD169, in adjuvant mediated vaccine induced antibody production.

$CD169^+$ Macrophages and CD169 Expression are Necessary for TLR-Ligand Adjuvant-Dependent Antibody Production

We hypothesized that use of CD169 KO mice or depletion of $CD169^+$ macrophages by low dose clodronate would adversely affect the ability of PorB, and possibly other adjuvants, to induce OVA specific antibodies. CD169 KO mice or low dose clodronate treated mice were immunized, per our protocol, and OVA-specific IgG was measured from the sera two weeks after the third immunization. These results are displayed in **Figure 1A**. Alum demonstrated the greatest increase in OVA-specific IgG, which was slightly diminished in low dose clodronate treated mice and CD169 knockout mice. Both TLR-ligand based adjuvants, PorB and CpG, also showed significant increases in total OVA-specific IgG in wild type animals, as expected (31), however IgG levels were greatly decreased in the in low dose clodronate treated mice and CD169 knockout mice.

To determine if the loss of $CD169^+$ macrophages or the CD169 molecule influences IgG responses associated with Th1 or Th2 type responses, OVA-specific IgG subtypes in sera from the above-mentioned mice were analyzed by ELISAs. These data would provide insight on whether subcapsular macrophages and/or CD169 influence Th1 or Th2 responses. Th2 responses are characterized by IgG1 production while Th1 response are characterized by IgG2b and IgG2c production (58–60). PorB+ OVA and Alum + OVA immunized mice had significant increases in the OVA-specific IgG1 (**Figure 1B**). However, only low dose clodronate treated mice and CD169 KO mice

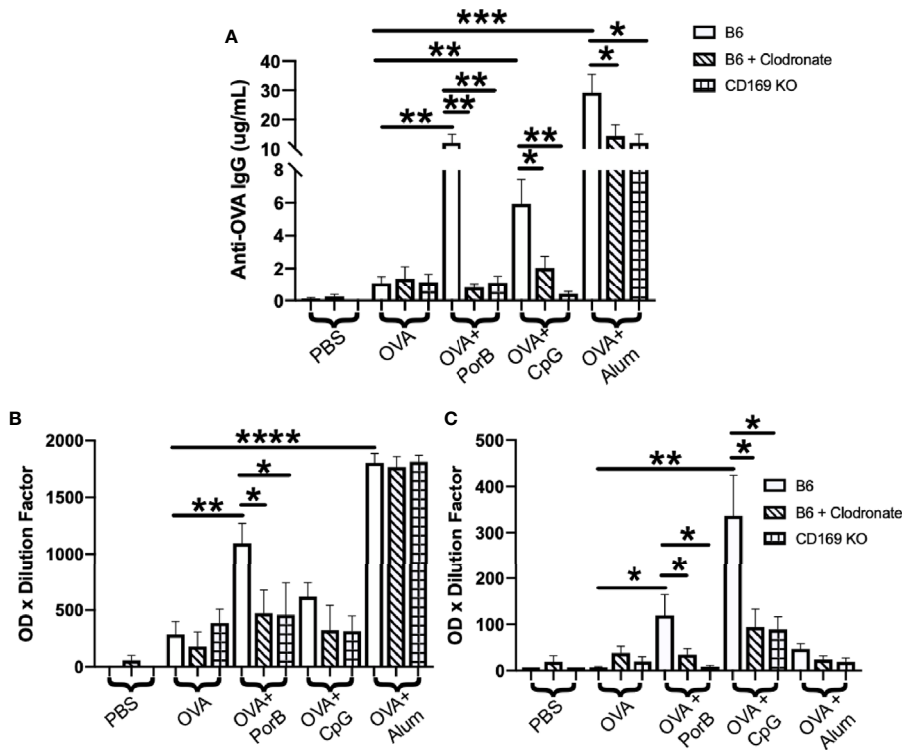

FIGURE 1 | Antigen-specific immunoglobulin (IgG) is significantly decreased in immunized low dose clodronate treated mice and CD169 knockout mice **(A)** Total anti-ovalbumin (OVA)-IgG **(B)** anti-OVA-IgG1 and **(C)** anti-OVA-IgG2c levels were measure by enzyme-linked immunosorbent assay (ELISA) following immunizations with PBS, OVA alone, or OVA + PorB, OVA + CpG, or OVA + Alum. Wildtype (open bars), wildtype treated low dose clodronate (striped bars), or CD169 knockout mice (checkered bars) were immunized three times at 2-week intervals. The results shown are from sera collected 2 weeks after third immunizations. n = 7–14 per group. Statistics were calculated by ordinary one-way ANOVA with Sidak's multiple comparisons test. *p < 0.05, **p < 0.01, ***p < 0.001 ****p < 0.0001.

that were immunized with PorB+OVA had significant decreases in IgG1 as compared to the WT mice (**Figure 1B**). WT mice immunized with either TLR-ligand adjuvant (PorB or CpG) had a significant increase in IgG2c production which was significantly decreased in mice treated with low dose clodronate and CD169 knockout animals.

Adjuvant Induced Increases in Antigen Levels within Lymph Nodes is Influenced by Depletion of CD169$^+$ Macrophages

The diminished antibody responses in total IgG and IgG subtypes led us to hypothesize that low dose clodronate treatment and CD169 knockout were lessening the immune stimulating ability of adjuvants. Antigen deposition on follicular dendritic cells within germinal centers is crucial for effective antibody production by improving B cell receptor affinity maturation (61, 62). To determine if adjuvants affects this process, the total amount of OVA present in the draining lymph nodes was measured 24 h post subcutaneous immunization with OVA with or without adjuvant preparations. As shown in **Figure 2**, PorB was the only adjuvant to significantly increase OVA mean fluorescent intensity (MFI) in the lymph nodes as compared to OVA alone, which was significantly decreased in low dose clodronate

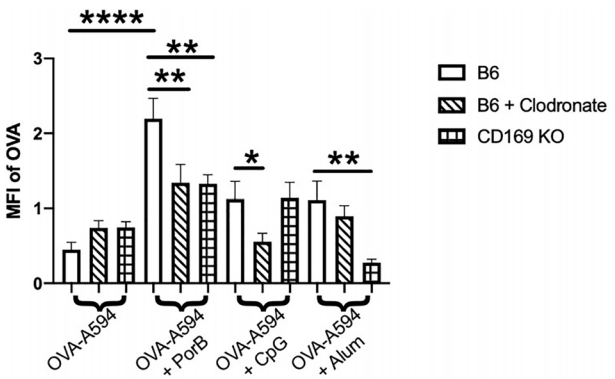

FIGURE 2 | Adjuvant induced antigen presence in draining lymph nodes is affected in immunized low dose clodronate treated mice and CD169 knockout mice. Mean fluorescent intensity (MFI) of antigen (OVA) in draining lymph nodes 24 h post vaccination of either OVA-A594, OVA-A594+PorB, OVA-A594+CpG, or OVA-A594+Alum was measured *via* ImageJ. Wild type control injections are shown in the bars with no pattern. Low dose clodronate treated animals are shown in the striped bars. CD169 knockout mice are shown in checkered bars. MFI of OVA was quantified by the ImageJ measurement tool after the subtraction of the background. n = 8–13. Statistics were calculated by ordinary one-way ANOVA with Sidak's multiple comparisons test. *p < 0.05, **p < 0.01, ****p < 0.0001.

treated mice and CD169 knockout mice. A decrease was also seen with the use of CpG as an adjuvant, but only in mice treated with low dose clodronate. A similar decrease was seen with the use of alum but only in the CD169 KO mice.

Follicular Dendritic Cell Networks Are Affected by Clodronate Treatment

Although a decrease in antigen within the lymph nodes could explain a significant decrease in antibody production, it was also important to determine if depleting CD169 macrophages could also influence the follicular dendritic cell (FDC) network and antigen deposition on FDCs. These experiments follow up our previous published work demonstrating that PorB can greatly enhance both the FDC network and increase antigen deposition on FDCs (34). FDCs and FDC networks are essential for B cell receptor maturation and therefore antibody production. In addition, it has been shown that SCS macrophages are important for entry of particulate matter into the follicle and germinal center to interact with antigen presenting cells (APCs) and FDCs. **Figure 3A** displays representative images of draining lymph nodes for all treatments and immunization groups. FDC staining is shown as a heat map where the highest signal/pixel (px) ratio is shown as white and the lowest signal/px ratio is shown in blue. Similar to our previous work, only the use of TLR-ligand based adjuvants induced increased FDCs in the draining lymph node in immunized WT mice (top row). Interestingly, low dose clodronate treatment and removal of subcapsular macrophages diminished the adjuvant-induced increase of FDCs close to the baseline seen in unimmunized mice. In contrast, the use of CD169 KO mice did not affect the PorB induced increase in FDCs. Next, the MFI of FDC was quantified by the measurement tool within ImageJ (**Figure 3B**) and is consistent with IHC findings (**Figure 3A**). Finally, to further confirm these results, flow cytometric analysis of the draining lymph node were performed to compare the frequency and percentages of FDCs in similar treated and immunized mice. The data was consistent with the IHC and MFI measurements; immunizations including TLR-adjuvants significantly increased

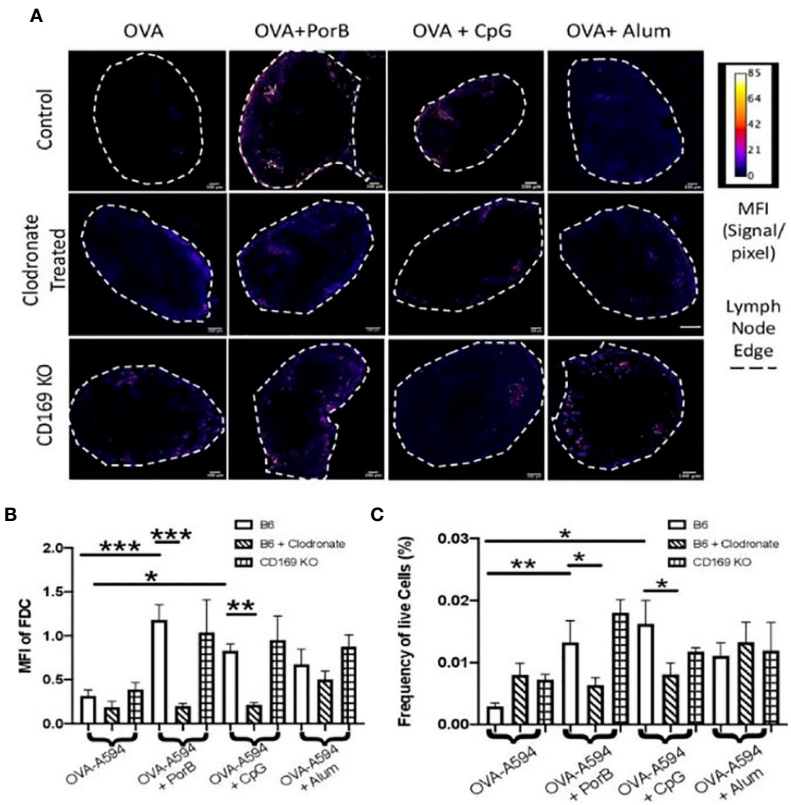

FIGURE 3 | Toll-like receptor (TLR) ligand-adjuvant induced increases in the follicular dendritic cell (FDC) network are affected in low dose clodronate treated mice but not CD169 knockout mice. **(A)** Representative images for FDC networks in draining lymph nodes 24 h post adjuvant+OVA-A594 subcutaneous injections in mice treated with low dose clodronate 24 h prior to these immunizations or CD169 knockout mice. FDC expression is shown as a heat map where white designates the highest signal to pixel ratio and blue designates the lowest signal to pixel ratio. Scale bar is 100 μM. One out of two representative experiments are shown. **(B)** Mean fluorescence intensity (MFI) quantification from ImageJ of FDC in draining lymph nodes 24 h post injection of either OVA-A594, OVA-A594+PorB, OVA-A594+CpG, or OVA-A594+Alum in all three animal models. Wild type control injections are shown in the bars with no pattern. Low dose clodronate treated animals are shown in the stripped bars. CD169 knockout animals are shown in checkered bars. Multiple FDC networks were measured within the lymph nodes. n = 7–15/group. **(C)** Frequency of FDC cells in draining lymph nodes 24 h post subcutaneous injections with OVA-A594 +/- adjuvants. (n = 6). Gating strategy is shown in **Supplemental Figure 5**. Statistics were calculated by ordinary one-way ANOVA with Sidak's multiple comparisons test. *$p < 0.05$, **$p < 0.01$, ***$p < 0.001$.

FDC frequencies in WT mice but was diminished in low dose clodronate treated mice and not in CD169 KO mice (**Figure 3C**).

PorB Induced Increase of Follicular Dendritic Cell Antigen Deposition Is Diminished in Low Dose Clodronate Treated Mice and CD169 Knockout Mice

Above, we demonstrated that PorB effects on FDC frequency was decreased in clodronate treated animals. These studies now determine whether the lack of CD169 macrophages affects PorB's previously demonstrated increase of FDC antigen deposition (34) using Alexa-594 tagged (OVA-594). Consistent with our previous work, PorB induces an increase of colocalization of antigen with FDCs as shown by yellow arrows in **Figure 4A**. Interestingly, this colocalization was diminished when mice treated with low dose clodronate or CD169 KO mice were used (**Figure 4A**). Immunizations using Alum as an adjuvant significantly increased FDC/OVA colocalization in WT mice which was decreased in CD169 KO (**Figure 4C**). Vaccines that contained CpG showed no significant differences in colocalization between FDC and OVA in any of the animal models tested (**Figure 4B**).

OVA Association With DCs and FDCs is Influenced by Depletion of SCS Macrophages

To determine the distribution of antigen, Mander's correlation coefficients were determined *via* JaCoP. This correlation coefficient allows for spilt channels of correlation to be determined (63) as percentages. We measured the percentages of OVA correlated to either dendritic cells (DCs) or FDC. This percent was then multiplied by the MFI of OVA within the lymph node from **Figure 2** to determine the percent of OVA associated with DCs, FDC, or unassociated. We defined "unassociated OVA" as the remaining percentage of OVA that was not associated with either DC or FDC (Unassociated OVA = 1-[MFI of OVA x (Mander's coefficient for OVA/DC + Mander's coefficient for OVA/FDC)]). There are, however, other cell types within the lymph node during this time with which OVA could associate (B cells or macrophages), though unlikely. For the purpose of these studies, these cell types are included in the "unassociated" section because of the importance of antigen loaded DCs and antigen deposited on the FDCs at early timepoints for induction of an adaptive immune response. All adjuvanted immunizations induced increase in OVA associated DCs, and consistent with our previous data (33), PorB induced

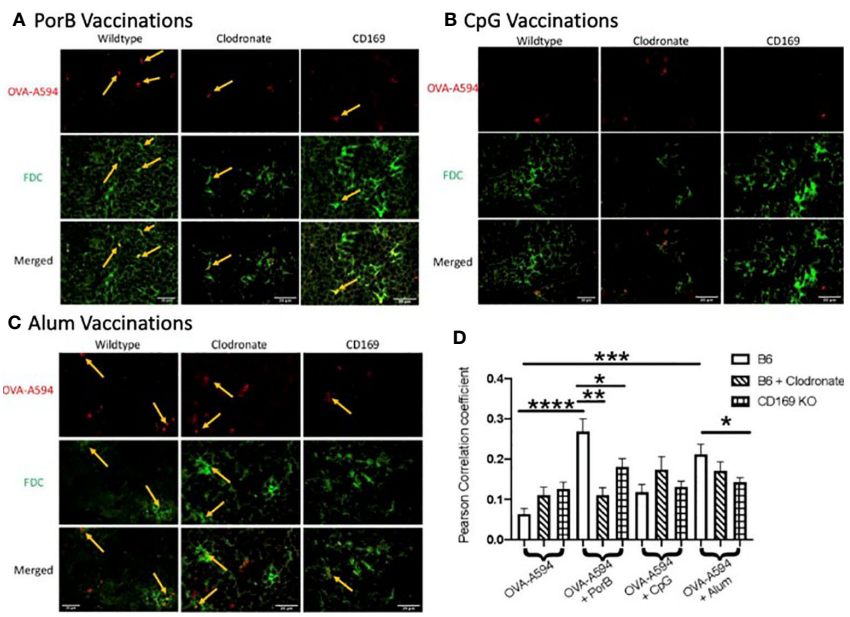

FIGURE 4 | Adjuvant induced increase of antigen deposition on follicular dendritic cells (FDCs) is diminished in low dose clodronate treated mice and CD169 knockout mice. Representative immunohistochemistry images from draining lymph nodes from wildtype, clodronate treated mice, and CD169 knockout mice 24 h post subcutaneous immunizations of ovalbumin (OVA) with PorB **(A)**, CpG **(B)**, or Alum **(C)** and 48 h post clodronate treatment. FDC is shown in green. OVA-A594 is shown in red. Images were taken at 63x objective using a Leica SP5 microscope. Typical areas of co-localization are emphasized with yellow arrows. Scale bar represents 20 μM. One out of six representative experiments is shown. **(D)** Quantification of colocalization between fluorescently labeled OVA-A594 with FDC within draining lymph nodes 24 h post subcutaneous injections. Colocalization was assessed using Pearson Correlation coefficients calculated within JaCoP plugin in ImageJ after background subtraction and unsharp mask filter. n = 8–12/group. Wild type control injections are shown in the bars with no pattern. Low dose clodronate treated animals are shown in the stripped bars. CD169 knockout animals are shown in checkered bars. Statistics were calculated by ordinary one-way ANOVA with Sidak's multiple comparisons test. *$p < 0.05$, **$p < 0.01$, ***$p < 0.001$ ****$p < 0.0001$.

the greatest association (**Figure 5A**). In both low dose clodronate treated mice and CD169 KO mice immunized with OVA + PorB, there were significant decreases in DC/OVA (**Figure 5A**) and FDC/OVA correlation coefficients (**Figure 5B**). Unassociated OVA in both low dose clodronate and CD169 knockout animals had a significant increase over WT mice in animals that received PorB + OVA vaccines (**Figure 5C**). CpG + OVA immunized mice only showed significant differences in DC/OVA correlation in clodronate treated animals (**Figure 5A**). No differences were seen with CpG + OVA immunizations in low dose clodronate treated mice or CD169 KO mice in FDC/OVA (**Figure 5B**). Alum adjuvant usage showed a significant decrease in both DC/OVA (**Figure 5A**) and FDC/OVA in CD169 KO mice (**Figure 5B**) but had no difference in low dose clodronate treated mice. Overall, the increases of OVA association with FDCs or DCs was always greater in mice receiving PorB + OVA immunizations, and the decrease in the low dose clodronate treated mice or CD169KO mice were subsequently greater when PorB was used as an adjuvant as opposed to CpG or Alum.

DISCUSSION

These studies utilized two animal models which interrogate the subcapsular macrophage population in lymph nodes and germinal centers to further characterize cellular mechanisms of adjuvant activity within these structures. Marginal zone and subcapsular macrophages were targeted for analysis for a number of reasons. Our lab has previously demonstrated that a defect in TLR signaling in macrophages, by cell specific genetic depletion of MyD88, greatly diminished the adjuvant effect of PorB (31). This data also demonstrated that no other antigen presenting cell could rescue the depleted antibody production seen in these mice. This focused our attention on macrophage subtypes whose function could not be replaced by dendritic cells or B cells, namely subcapsular and marginal zone macrophages. Importantly, Cyster et al. have shown that subcapsular macrophages are essential for antigen transport and deposition on FDC (64). Our recent publication demonstrates that PorB enhances these processes (34), further implicating the probable involvement of these cells in PorB's adjuvant activity.

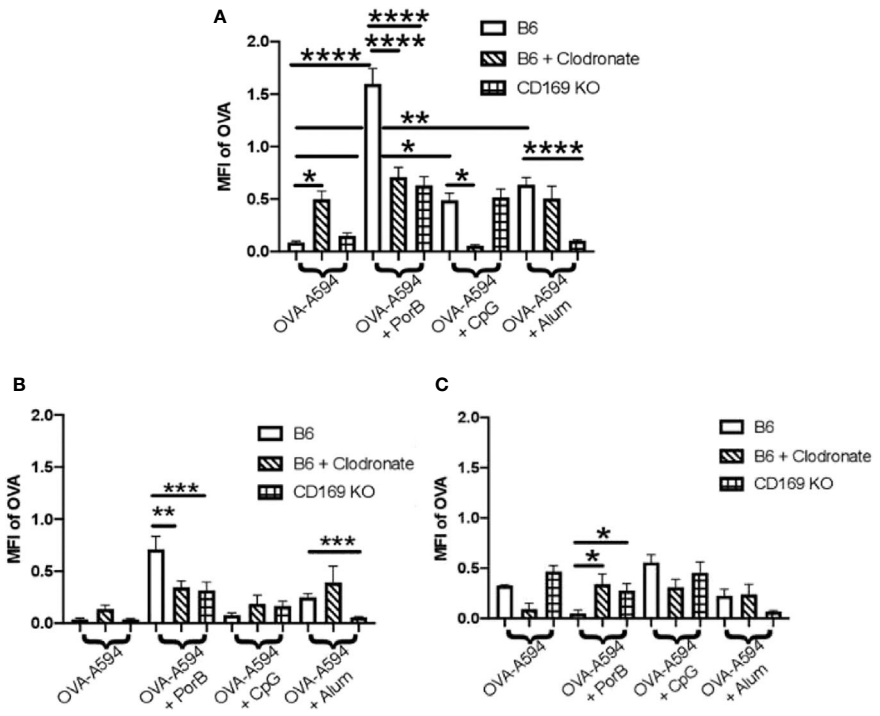

FIGURE 5 | PorB-induced antigen association with dendritic cells (DCs) and follicular dendritic cells (FDCs) is diminished in low dose clodronate treated mice and CD169 knockout mice. These graphs display ovalbumin (OVA)-A594 association with DC and FDC and unassociated OVA within draining lymph node 24 h post subcutaneous immunizations of indicated adjuvants with OVA in WT mice, low dose clodronate mice of CD169 knockout mice. Injection of OVA without adjuvants was used as a control. MFI of OVA=594 associated with DC **(A)**, FDC **(B)**, or unassociated OVA **(C)** was assessed using the JaCoP plugin within ImageJ and determining the Mander's correlation coefficient after subtracting the background and using an unsharp mask filter. The correlation coefficient is the percentage of OVA associated with either FDCs or DCs. This percentage was then multiplied by the total MFI of OVA within the lymph node (**Figure 2**) to determine MFI of OVA associated with DCs or FDCs. Wild type control injections are shown in the bars with no pattern. Low dose clodronate treated animals are shown in the striped bars. CD169 knockout animals are shown in checkered bars. Statistics were calculated by ordinary one-way ANOVA with Sidak's multiple comparisons test. n = 5–7 *p < 0.05, **p < 0.01, ***p < 0.001, ****p < 0.0001.

To investigate the role of these macrophages in adjuvant activity, two mouse models with altered subcapsular macrophages were utilized: 1) mice treated with low dose clodronate which has been shown to cause apoptosis and removal solely of SCS macrophages (65) and 2) CD169 global knockout (KO) mice. It is important to note that while clodronate treatment cause a depletion of a subcapsular macrophages, these cells are still be present in the CD169 KO mice, but do not express CD169 molecule. Immunization with adjuvanted vaccines in both types of mice demonstrated a decreased total antigen-specific antibody response as compared to wild type mice and this decreased was much more dramatic when TLR-ligand based adjuvants, PorB and CpG were used as compared to the use of Alum (**Figure 1A**).

The effects on antigen specific IgG subtypes induced by these adjuvants were investigated to determine if loss of SCS macrophages or CD169 could influence on Th1 or Th2 adaptive immune responses. Alum adjuvanted vaccines almost exclusively induced IgG1 [as expected (66)] which was unaffected in low dose clodronate treated mice and CD169 KO mice (**Figure 1B**), suggesting IgG1 antibody production associated with Alum is not dependent on SCS macrophages or CD169 expression. In contrast, when PorB was used as an adjuvant, OVA-specific IgG1 showed a significant decrease in both clodronate treated and CD169 KO mice as compared to WT mice (**Figure 1B**). The use of CpG as an adjuvant did not induce detectable levels of OVA-specific IgG1. Both TLR-ligand based adjuvants, PorB and CpG, induced OVA-specific IgG2c levels which were significantly decreased in clodronate treated and CD169 KO mice as compared to WT mice (**Figure 1C**). These data emphasize that TLR-ligand based adjuvants likely utilize SCS macrophages to a much greater extent than alum for their adjuvant effect. This is consistent with our MyD88 conditional KO data, as TLR2 and TLR9 both require MyD88 for signaling. To confirm the role of MyD88 in the adjuvant effect of PorB and CpG on these SCS and marginal zone macrophages, future studies will use MyD88 conditional KOs in these $CD169^{+}$ cells utilizing MyD88-floxed mice and CD169-cre-recombinase mice.

As part of these studies, we investigated the potential association of SCS macrophages in relation to B cell receptor affinity maturation and somatic hypermutation which occurs in the germinal center and requires the use of FDCs. The quality of FDCs and the ability of adjuvants to enhance intact antigen deposition on FDCs were investigated. We have recently shown that PorB can increase intact OVA deposition on FDCs (34). As a follow-up, the effect of lacking SCS macrophages or CD169 expression on this process was examined utilizing low dose clodronate treated mice and CD169 KO mice. Results demonstrate that the adjuvants tested here (PorB, CpG, and alum) utilize SCS macrophages by different mechanisms. PorB's effect on trafficking of OVA was greatly affected by loss of either marginal zone macrophages or the global loss of CD169 (**Figure 2**). Additionally, antigen deposition on FDCs (**Figure 4A**) was significantly decreased in both sets of mice as compared to WT groups. In combination, these findings define a mechanism to explain the diminution of OVA specific IgG production in these mice when immunized with PorB + OVA (**Figure 1**). These data also suggest that the adjuvant activity of PorB is likely more dependent on SCS macrophages for enhancing antibody production, when compared to CpG or alum. One explanation is that the native trimeric structure of PorB, which is preserved for these immunizations studies (55, 67), is similar to other particles that have been shown to influence SCS macrophages. Saunderson et al. have shown that exosomes are retained in the SCS macrophages, but in CD169 KO mice, these exosomes now progress into the paracortex of the lymph node (68). We hypothesize that PorB stimulates the marginal zone macrophages (in a MyD88-mediated manner) to a much greater extent than CpG or alum, leading to increased amounts of antigen within the lymph node and increased FDC antigen deposition. Studies examining the direct effect of PorB on SCS macrophages, including the potential role of TLR2 expression and MyD88 are planned to investigate this hypothesis.

Immunizations containing CpG showed significant increases in total OVA-specific IgGs, especially OVA-specific IgG2c (**Figure 1**) which was decreased in low-dose clodronate treated and CD169 KO mice, similar to PorB. However, though also a TLR-ligand based adjuvant, the effect of CpG on antigen levels in the germinal centers, the alterations in the FDC network and antigen deposition on FDCs and results in mice lacking SCS macrophages or CD169 expression was shown to be different as compared to PorB. These differences included a lack of increase in antigen deposition on FDCs (**Figure 3**), a lack of an effect on OVA germinal center association in CD169 KO mice (though decreased in the clodronate treated mice, **Figure 4B**). Similarly, there was a lack of an effect on OVA association with DCs in CD169 KO mice, but significantly decreased in the clodronate treated mice (**Figure 5**). This suggests a different role of these macrophages in the adjuvant activity for CpG which can be discerned in future studies.

To determine if non-TLR ligands have distinctive cellular mechanisms of adjuvanticity as compared to TLR-ligand based adjuvants, we included alum in our studies. Similar to PorB, our results revealed that alum + OVA injections induced total antigen specific IgG was significantly decreased in both low dose clodronate treated and CD169 KO mice when compared to wildtype controls (**Figure 1A**); however, these decreases, were not as robust or significant as the decreases seen when TLR-ligand based adjuvants, PorB and CpG were used. Interestingly, IgG1 subtype levels were similar in the SCS modified mice as compared to WT mice when alum was used as an adjuvant (**Figure 1B**). While investigating innate immune responses to determine if SCS macrophages or CD169 knockout animals influenced alum adjuvanticity, we have found that less antigen is present in the draining lymph nodes of CD169 knockout animals when compared to wildtype (**Figure 2**), including a decrease in antigen deposition onto FDC (**Figures 4C, D** and **5B**) as well as a decrease in OVA associated with DC (**Figure 5A**). Together these data suggests that alum requires expression of CD169 molecule for its adjuvanticity and its ability to allow antigen to enter secondary lymphoid organs, but PorB's adjuvant

activity appears to be more reliant on these cell types as lack of SCS macrophages causes a much greater decrease.

In conclusion, in examining the possible role of subcapsular sinus macrophages and/or the expression of CD169 on these cells we have found that these alterations affects the adjuvant effect of PorB, CpG, and alum but the effects were dependent on the adjuvant used. Interestingly, TLR-ligand based adjuvants had a more dramatic decrease than that of alum immunizations on antibody production. Investigating antigen within the draining lymph node, as well FDC and DC cellular association of antigen, we concluded that these three adjuvants work through different cellular interactions. PorB had the most dramatic defects in both clodronate treated and CD169 knockout mice, leading us to hypothesize that the extracellular TLR1/2 agonist utilizes the SCS macrophages more than the other adjuvants tested here. Since SCS macrophages have been shown to be pivotal for antibody production (69), we believe these data support that PorB has unique characteristics, such as the ability to stimulate both Th1 and Th2 antibody responses and the trimeric structure of the adjuvant, that make PorB a higher quality adjuvant than others.

DATA AVAILABILITY STATEMENT

The raw data supporting the conclusions of this article will be made available by the authors, without undue reservation.

ETHICS STATEMENT

The animal study was reviewed and approved by Boston University IACUC.

AUTHOR CONTRIBUTIONS

The work was performed by CL, with help and advice from RY, JK, and MR and technical help from DA. All the work was planned with LW and CL. CL and LW wrote and edited the manuscript. All authors contributed to the article and approved the submitted version.

FUNDING

These studies were funded by NIH Grant AI0404944 (LW). CL was funded by the Boston University Training Program in Inflammatory Disorders T32AI138933.

ACKNOWLEDGMENTS

We would like to thank Paola Massari and Xiuping Liu for purifying neisserial PorB for the experiments conducted in this manuscript and Maxx Lawson for technical help. We greatly appreciate the usage and technical assistance from the Boston University School of Medicine flow and imaging core. We would also like to thank Kimberly Barker for reviewing and help editing this manuscript.

SUPPLEMENTARY MATERIAL

The Supplementary Material for this article can be found online at: https://www.frontiersin.org/articles/10.3389/fimmu.2021.624197/full#supplementary-material

REFERENCES

1. Hinman AR, Orenstein WA, Schuchat A. Vaccine-preventable diseases, immunizations, and the Epidemic Intelligence Service. *Am J Epidemiol* (2011) 174(11 Suppl):S16–22. doi: 10.1093/aje/kwr306
2. Gould K. Vaccine Safety: Evidence-Based Research Must Prevail. *Dimens Crit Care Nurs* (2017) 36(3):145–7. doi: 10.1097/DCC.0000000000000250
3. Orenstein WA, Ahmed R. Simply put: Vaccination saves lives. *Proc Natl Acad Sci USA* (2017) 114(16):4031–3. doi: 10.1073/pnas.1704507114
4. Andre FE, Booy R, Bock HL, Clemens J, Datta SK, John TJ, et al. Vaccination greatly reduces disease, disability, death and inequity worldwide. *Bull World Health Organ* (2008) 86(2):140–6. doi: 10.2471/blt.07.040089
5. Plotkin SA. Vaccines, vaccination, and vaccinology. *J Infect Dis* (2003) 187 (9):1349–59. doi: 10.1086/374419
6. Gutierrez AH, Spero DM, Gay C, Zimic M, De Groot AS. New vaccines needed for pathogens infecting animals and humans: One Health. *Hum Vaccin Immunother* (2012) 8(7):971–8. doi: 10.4161/hv.20202
7. Taylor K, Nguyen A, Stephenne J. The need for new vaccines. *Vaccine* (2009) 27 Suppl 6:G3–8. doi: 10.1016/j.vaccine.2009.10.014
8. Kaufmann SH, Fensterle J, Hess J. The need for a novel generation of vaccines. *Immunobiology* (1999) 201(2):272–82. doi: 10.1016/S0171-2985(99)80067-9
9. Moyer TJ, Zmolek AC, Irvine DJ. Beyond antigens and adjuvants: formulating future vaccines. *J Clin Invest* (2016) 126(3):799–808. doi: 10.1172/JCI81083
10. Rappuoli R, Pizza M, Del Giudice G, De Gregorio E. Vaccines, new opportunities for a new society. *Proc Natl Acad Sci USA* (2014) 111 (34):12288–93. doi: 10.1073/pnas.1402981111
11. Rueckert C, Guzmán CA. Vaccines: From Empirical Development to Rational Design. *PloS Pathog* (2012) 8(11):e1003001–e1003001. doi: 10.1371/journal.ppat.1003001
12. Di Pasquale A, Preiss S, Tavares Da Silva F, Garçon N. Vaccine Adjuvants: from 1920 to 2015 and Beyond. *Vaccines* (2015) 3(2):320–43. doi: 10.3390/vaccines3020320
13. Reed SG, Orr MT, Fox CB. Key roles of adjuvants in modern vaccines. *Nat Med* (2013) 19(12):1597–608. doi: 10.1038/nm.3409
14. Vasou A, Sultanoglu N, Goodbourn S, Randall RE, Kostrikis LG. Targeting Pattern Recognition Receptors (PRR) for Vaccine Adjuvantation: From Synthetic PRR Agonists to the Potential of Defective Interfering Particles of Viruses. *Viruses* (2017) 9(7):186. doi: 10.3390/v9070186
15. Kawasaki T, Kawai T. Toll-like receptor signaling pathways. *Front Immunol* (2014) 5:461:461. doi: 10.3389/fimmu.2014.00461
16. Steere AC, Sikand VK, Meurice F, Parenti DL, Fikrig E, Schoen RT, et al. Vaccination against Lyme disease with recombinant Borrelia burgdorferi outer-surface lipoprotein A with adjuvant. Lyme Disease Vaccine Study Group. *N Engl J Med* (1998) 339(4):209–15. doi: 10.1056/NEJM199807233390401
17. Beran J, De Clercq N, Dieussaert I, Van Hoecke C. Reactogenicity and immunogenicity of a Lyme disease vaccine in children 2-5 years old. *Clin Infect Dis* (2000) 31(6):1504–7. doi: 10.1086/317479
18. Durier C, Launay O, Meiffredy V, Saidi Y, Salmon D, Levy Y, et al. Clinical safety of HIV lipopeptides used as vaccines in healthy volunteers and HIV-infected adults. *AIDS* (2006) 20(7):1039–49. doi: 10.1097/01.aids.0000222077.68243.22
19. Pulko V, Liu X, Krco CJ, Harris KJ, Frigola X, Kwon ED, et al. TLR3-stimulated dendritic cells up-regulate B7-H1 expression and influence the

magnitude of CD8 T cell responses to tumor vaccination. *J Immunol* (2009) 183(6):3634–41. doi: 10.4049/jimmunol.0900974
20. Tomai MA, Solem LE, Johnson AG, Ribi E. The adjuvant properties of a nontoxic monophosphoryl lipid A in hyporesponsive and aging mice. *J Biol Response Mod* (1987) 6(2):99–107.
21. Johnson AG, Tomai M, Solem L, Beck L, Ribi E. Characterization of a nontoxic monophosphoryl lipid A. *Rev Infect Dis* (1987) 9 Suppl 5:S512–6. doi: 10.1093/clinids/9.supplement_5.s512
22. Gutjahr A, Tiraby G, Perouzel E, Verrier B, Paul S. Triggering Intracellular Receptors for Vaccine Adjuvantation. *Trends Immunol* (2016) 37(10):716. doi: 10.1016/j.it.2016.08.005
23. Reed SG, Hsu FC, Carter D, Orr MT. The science of vaccine adjuvants: advances in TLR4 ligand adjuvants. *Curr Opin Immunol* (2016) 41:85–90. doi: 10.1016/j.coi.2016.06.007
24. van Haren SD, Dowling DJ, Foppen W, Christensen D, Andersen P, Reed SG, et al. Age-Specific Adjuvant Synergy: Dual TLR7/8 and Mincle Activation of Human Newborn Dendritic Cells Enables Th1 Polarization. *J Immunol* (2016) 197(11):4413–24. doi: 10.4049/jimmunol.1600282
25. Akira S. TLR signaling. *Curr Top Microbiol Immunol* (2006) 311:1–16. doi: 10.1007/3-540-32636-7_1
26. Liu Q, Ding JL. The molecular mechanisms of TLR-signaling cooperation in cytokine regulation. *Immunol Cell Biol* (2016) 94(6):538–42. doi: 10.1038/icb.2016.18
27. Gibson SJ, Lindh JM, Riter TR, Gleason RM, Rogers LM, Fuller AE, et al. Plasmacytoid dendritic cells produce cytokines and mature in response to the TLR7 agonists, imiquimod and resiquimod. *Cell Immunol* (2002) 218(1-2):74–86. doi: 10.1016/s0008-8749(02)00517-8
28. Averett DR, Fletcher SP, Li W, Webber SE, Appleman JR. The pharmacology of endosomal TLR agonists in viral disease. *Biochem Soc Trans* (2007) 35(Pt 6):1468–72. doi: 10.1042/BST0351468
29. Massari P, Visintin A, Gunawardana J, Halmen KA, King CA, Golenbock DT, et al. Meningococcal porin PorB binds to TLR2 and requires TLR1 for signaling. *J Immunol* (2006) 176(4):2373–80. doi: 10.4049/jimmunol.176.4.2373
30. Platt A, Macleod H, Massari P, Liu X, Wetzler L. In Vivo and In Vitro Characterization of the Immune Stimulating Activity of the Neisserial Porin PorB. *PloS One* (2013) 8(12):e82171. doi: 10.1371/journal.pone.0082171
31. Mosaheb MM, Reiser ML, Wetzler LM. Toll-Like Receptor Ligand-Based Vaccine Adjuvants Require Intact MyD88 Signaling in Antigen-Presenting Cells for Germinal Center Formation and Antibody Production. *Front Immunol* (2017) 8:225:225. doi: 10.3389/fimmu.2017.00225
32. Mosaheb M, Wetzler LM. Meningococcal PorB induces a robust and diverse antigen specific T cell response as a vaccine adjuvant. *Vaccine* (2018) 36 (50):7689–99. doi: 10.1016/j.vaccine.2018.10.074
33. Reiser ML, Mosaheb MM, Lisk C, Platt A, Wetzler LM. The TLR2 Binding Neisserial Porin PorB Enhances Antigen Presenting Cell Trafficking and Cross-presentation. *Sci Rep* (2017) 7(1):736. doi: 10.1038/s41598-017-00555-4
34. Lisk C, Yuen R, Kuniholm J, Antos D, Reiser ML, Wetzler LM. Toll-Like Receptor Ligand Based Adjuvant, PorB, Increases Antigen Deposition on Germinal Center Follicular Dendritic Cells While Enhancing the Follicular Dendritic Cells Network. *Front Immunol* (2020) 11:1254. doi: 10.3389/fimmu.2020.01254
35. Coffman RL, Sher A, Seder RA. Vaccine Adjuvants: Putting Innate Immunity to Work. *Immunity* (2010) 33(4):492–503. doi: 10.1016/J.IMMUNI.2010.10.002
36. Kawai T, Akira S. The role of pattern-recognition receptors in innate immunity: update on Toll-like receptors. *Nat Immunol* (2010) 11(5):373–84. doi: 10.1038/ni.1863
37. Zhang Y, Roth TL, Gray EE, Chen H, Rodda LB, Liang Y, et al. Migratory and adhesive cues controlling innate-like lymphocyte surveillance of the pathogen-exposed surface of the lymph node. *eLife* (2016) 5(AUGUST):1–29. doi: 10.7554/eLife.18156
38. Fearon DT, Locksley RM. The instructive role of innate immunity in the acquired immune response. *Science* (1996) 272(5258):50–3. doi: 10.1126/science.272.5258.50
39. Louie DAP, Liao S. Lymph Node Subcapsular Sinus Macrophages as the Frontline of Lymphatic Immune Defense. *Front Immunol* (2019) 10:347. doi: 10.3389/fimmu.2019.00347
40. Moran I, Grootveld AK, Nguyen A, Phan TG. Subcapsular Sinus Macrophages: The Seat of Innate and Adaptive Memory in Murine Lymph Nodes. *Trends Immunol* (2019) 40(1):35–48. doi: 10.1016/j.it.2018.11.004
41. Szakal AK, Holmes KL, Tew JG. Transport of immune complexes from the subcapsular sinus to lymph node follicles on the surface of nonphagocytic cells, including cells with dendritic morphology. *J Immunol* (1983) 131 (4):1714–27.
42. Phan TG, Grigorova I, Okada T, Cyster JG. Subcapsular encounter and complement-dependent transport of immune complexes by lymph node B cells. *Nat Immunol* (2007) 8(9):992–1000. doi: 10.1038/ni1494
43. Junt T, Moseman EA, Iannacone M, Massberg S, Lang PA, Boes M, et al. Subcapsular sinus macrophages in lymph nodes clear lymph-borne viruses and present them to antiviral B cells. *Nature* (2007) 450(7166):110–4. doi: 10.1038/nature06287
44. Delputte PL, Van Gorp H, Favoreel HW, Hoebeke I, Delrue I, Dewerchin H, et al. Porcine sialoadhesin (CD169/Siglec-1) is an endocytic receptor that allows targeted delivery of toxins and antigens to macrophages. *PloS One* (2011) 6(2):e16827. doi: 10.1371/journal.pone.0016827
45. Gaya M, Castello A, Montaner B, Rogers N, Reis e Sousa C, Bruckbauer A, et al. Host response. Inflammation-induced disruption of SCS macrophages impairs B cell responses to secondary infection. *Science* (2015) 347(6222):667–72. doi: 10.1126/science.aaa1300
46. Moalli F, Proulx ST, Schwendener R, Detmar M, Schlapbach C, Stein JV. Intravital and whole-organ imaging reveals capture of melanoma-derived antigen by lymph node subcapsular macrophages leading to widespread deposition on follicular dendritic cells. *Front Immunol* (2015) 6:114. doi: 10.3389/fimmu.2015.00114
47. Desbien AL, Dubois Cauwelaert N, Reed SJ, Bailor HR, Liang H, Carter D, et al. IL-18 and Subcapsular Lymph Node Macrophages are Essential for Enhanced B Cell Responses with TLR4 Agonist Adjuvants. *J Immunol* (2016) 197(11):4351–9. doi: 10.4049/jimmunol.1600993
48. Bernhard CA, Ried C, Kochanek S, Brocker T. CD169+ macrophages are sufficient for priming of CTLs with specificities left out by cross-priming dendritic cells. *Proc Natl Acad Sci U S A* (2015) 112(17):5461–6. doi: 10.1073/pnas.1423356112
49. Habbeddine M, Verthuy C, Rastoin O, Chasson L, Bebien M, Bajenoff M, et al. Receptor Activator of NF-kappaB Orchestrates Activation of Antiviral Memory CD8 T Cells in the Spleen Marginal Zone. *Cell Rep* (2017) 21 (9):2515–27. doi: 10.1016/j.celrep.2017.10.111
50. Asano K, Nabeyama A, Miyake Y, Qiu CH, Kurita A, Tomura M, et al. CD169-positive macrophages dominate antitumor immunity by crosspresenting dead cell-associated antigens. *Immunity* (2011) 34(1):85–95. doi: 10.1016/j.immuni.2010.12.011
51. Martinez-Pomares L, Gordon S. CD169+ macrophages at the crossroads of antigen presentation. *Trends Immunol* (2012) 33(2):66–70. doi: 10.1016/j.it.2011.11.001
52. Ludewig B, Cervantes-Barragan L. CD169(+) macrophages take the bullet. *Nat Immunol* (2011) 13(1):13–4. doi: 10.1038/ni.2189
53. Martinez-Pomares L, Gordon S. Antigen presentation the macrophage way. *Cell* (2007) 131(4):641–3. doi: 10.1016/j.cell.2007.10.046
54. McGaha TL, Chen Y, Ravishankar B, Rooijen NV, Karlsson MCI. Marginal zone macrophages suppress innate and adaptive immunity to apoptotic cells in the spleen. *Blood* (2017) 117(20):5403–13. doi: 10.1182/blood-2010-11-320028
55. Massari P, King CA, MacLeod H, Wetzler LM. Improved purification of native meningococcal porin PorB and studies on its structure/function. *Protein Expr Purif* (2005) 44(2):136–46. doi: 10.1016/j.pep.2005.04.021
56. Usui K, Honda S-i, Yoshizawa Y, Nakahashi-Oda C, Tahara-Hanaoka S, Shibuya K, et al. Isolation and characterization of naïve follicular dendritic cells. *Mol Immunol* (2012) 50(3):172–6. doi: 10.1016/j.molimm.2011.11.010
57. Mackinnon FG, Ho Y, Blake MS, Michon F, Chandraker A, Sayegh MH, et al. The role of B/T costimulatory signals in the immunopotentiating activity of neisserial porin. *J Infect Dis* (1999) 180(3):755–61. doi: 10.1086/314966
58. Stevens TL, Bossie A, Sanders VM, Fernandez-Botran R, Coffman RL, Mosmann TR, et al. Regulation of antibody isotype secretion by subsets of antigen-specific helper T cells. *Nature* (1988) 334(6179):255–8. doi: 10.1038/334255a0

59. Snapper CM, Paul WE. Interferon-gamma and B cell stimulatory factor-1 reciprocally regulate Ig isotype production. *Science* (1987) 236(4804):944–7. doi: 10.1126/science.3107127
60. Germann T, Gately MK, Schoenhaut DS, Lohoff M, Mattner F, Fischer S, et al. Interleukin-12/T cell stimulating factor, a cytokine with multiple effects on T helper type 1 (Th1) but not on Th2 cells. *Eur J Immunol* (1993) 23(8):1762–70. doi: 10.1002/eji.1830230805
61. Nossal GJ, Abbot A, Mitchell J. Antigens in immunity. XIV. Electron microscopic radioautographic studies of antigen capture in the lymph node medulla. *J Exp Med* (1968) 127(2):263–76. doi: 10.1084/jem.127.2.263
62. Allen CDC, Cyster JG. Follicular dendritic cell networks of primary follicles and germinal centers: Phenotype and function. *Semin Immunol* (2008) 20 (1):14–25. doi: 10.1016/j.smim.2007.12.001
63. Bolte S, Cordelieres FP. A guided tour into subcellular colocalization analysis in light microscopy. *J Microsc* (2006) 224(Pt 3):213–32. doi: 10.1111/j.1365-2818.2006.01706.x
64. Phan TG, Green JA, Gray EE, Xu Y, Cyster JG. Immune complex relay by subcapsular sinus macrophages and noncognate B cells drives antibody affinity maturation. *Nat Immunol* (2009) 10(7):786–93. doi: 10.1038/ni.1745
65. McGaha TL, Chen Y, Ravishankar B, van Rooijen N, Karlsson MC. Marginal zone macrophages suppress innate and adaptive immunity to apoptotic cells in the spleen. *Blood* (2011) 117(20):5403–12. doi: 10.1182/blood-2010-11-320028
66. Del Giudice G, Rappuoli R, Didierlaurent AM. Correlates of adjuvanticity: A review on adjuvants in licensed vaccines. *Semin Immunol* (2018) 39:14–21. doi: 10.1016/j.smim.2018.05.001
67. Yuen R, Kuniholm J, Lisk C, Wetzler LM. Neisserial PorB immune enhancing activity and use as a vaccine adjuvant. *Hum Vaccines Immunother* (2019) 15 (11):2778–81. doi: 10.1080/21645515.2019.1609852
68. Saunderson SC, Dunn AC, Crocker PR, McLellan AD. CD169 mediates the capture of exosomes in spleen and lymph node. *Blood* (2014) 123(2):208–16. doi: 10.1182/blood-2013-03-489732
69. Veninga H, Borg EG, Vreeman K, Taylor PR, Kalay H, van Kooyk Y, et al. Antigen targeting reveals splenic CD169+ macrophages as promoters of germinal center B-cell responses. *Eur J Immunol* (2015) 45(3):747–57. doi: 10.1002/eji.201444983

Conflict of Interest: The authors declare that the research was conducted in the absence of any commercial or financial relationships that could be construed as a potential conflict of interest.

frontiers in Immunology

ORIGINAL RESEARCH
published: 11 May 2021
doi: 10.3389/fimmu.2021.625030

Immunoprofiling Correlates of Protection Against SHIV Infection in Adjuvanted HIV-1 Pox-Protein Vaccinated Rhesus Macaques

Pinyi Lu[1,2], *Dylan J. Guerin*[3], *Shu Lin*[3], *Sidhartha Chaudhury*[4], *Margaret E. Ackerman*[3], *Diane L. Bolton*[2,5] *and Anders Wallqvist*[1*]

[1] Biotechnology HPC Software Applications Institute, Telemedicine and Advanced Technology Research Center, U.S. Army Medical Research and Development Command, Fort Detrick, MD, United States, [2] Henry M. Jackson Foundation for the Advancement of Military Medicine, Rockville, MD, United States, [3] Thayer School of Engineering, Dartmouth College, Hanover, NH, United States, [4] Center for Enabling Capabilities, Walter Reed Army Institute of Research, Silver Spring, MD, United States, [5] U.S. Military HIV Research Program, Walter Reed Army Institute of Research, Silver Spring, MD, United States

OPEN ACCESS

Edited by:
Jay Evans,
University of Montana, United States

Reviewed by:
Peter Timmerman,
Pepscan, Netherlands
Al Ozonoff,
Harvard Medical School, United States

***Correspondence:**
Anders Wallqvist
awallqvist@bhsai.org

Specialty section:
This article was submitted to Vaccines and Molecular Therapeutics, a section of the journal Frontiers in Immunology

Received: 02 November 2020
Accepted: 27 April 2021
Published: 11 May 2021

Citation:
Lu P, Guerin DJ, Lin S, Chaudhury S, Ackerman ME, Bolton DL and Wallqvist A (2021) Immunoprofiling Correlates of Protection Against SHIV Infection in Adjuvanted HIV-1 Pox-Protein Vaccinated Rhesus Macaques. Front. Immunol. 12:625030. doi: 10.3389/fimmu.2021.625030

Human immunodeficiency virus type 1 (HIV-1) infection remains a major public health threat due to its incurable nature and the lack of a highly efficacious vaccine. The RV144 vaccine trial is the only clinical study to date that demonstrated significant but modest decrease in HIV infection risk. To improve HIV-1 vaccine immunogenicity and efficacy, we recently evaluated pox-protein vaccination using a next generation liposome-based adjuvant, Army Liposomal Formulation adsorbed to aluminum (ALFA), in rhesus monkeys and observed 90% efficacy against limiting dose mucosal SHIV challenge in male animals. Here, we analyzed binding antibody responses, as assessed by Fc array profiling using a broad range of HIV-1 envelope antigens and Fc features, to explore the mechanisms of ALFA-mediated protection by employing machine learning and Cox proportional hazards regression analyses. We found that Fcγ receptor 2a-related binding antibody responses were augmented by ALFA relative to aluminium hydroxide, and these responses were associated with reduced risk of infection in male animals. Our results highlight the application of systems serology to provide mechanistic insights to vaccine-elicited protection and support evidence that antibody effector responses protect against HIV-1 infection.

Keywords: adjuvanted HIV-1 vaccine, systems serology, Fc receptor, immune correlate, rhesus macaque

INTRODUCTION

The HIV-1 AIDS epidemic remains a major public health threat, claiming over half a million lives globally annually (1). An efficacious HIV-1 vaccine is considered the most effective tool to halt the ongoing HIV-1 epidemic (2). To date, the Thai phase 3 HIV vaccine trial RV 144 was the only trial to demonstrate efficacy against HIV acquisition, with 60.5% and 31.2% efficacy one and three years following vaccination, respectively (3, 4). The follow up HVTN 702 trial evaluating a similar pox-protein HIV vaccine regimen did not recapitulate the efficacy observed in RV 144. However, as

numerous parameters differed between these two clinical studies, and several pre-clinical animal studies have supported hypotheses generated by the RV 144 findings, the results of RV 144 remain valid and warrant continued investigation. Therefore, continuous and significant efforts are still required for developing a safe and more effective HIV-1 vaccine.

To improve and sustain HIV vaccine efficacy, multiple novel strategies are being pursued. These include evaluation of other viral vectors, such as adenovirus serotype 26 and cytomegalovirus, and adjuvants. Aluminum salts (alum) are the classical adjuvant and are employed in most licensed vaccines (5). Novel vaccine adjuvants are an active area of product development and have been adopted for vaccines against multiple pathogens. Liposomal adjuvants are particularly promising, as exemplified by the highly successful Shingrix zoster vaccine. We recently evaluated a liposomal adjuvant, ALFA, for HIV-1 Env protein vaccination in combination with pox vector priming for efficacy against SHIV acquisition in rhesus macaques (6). ALFA, or Army Liposome Formulation adsorbed to aluminum hydroxide, consists of liposomes containing saturated phospholipids, cholesterol, and monophosphoryl lipid A, and has exhibited excellent safety and potency in clinical trials (7). Adjuvanting with ALFA reduced the per-exposure SHIV infection risk by 59% compared to controls, while adjuvanting with aluminum hydroxide did not protect against infection. Significant sex differences were observed, with vaccine efficacy limited to male animals (90%). Antibody-dependent neutrophil and monocyte phagocytotic responses, but not binding antibody responses, were increased by ALFA relative to alum, and these responses correlated with protection. Neutralizing antibody responses were robust and comparable between the two active arms, but limited to tier 1. The underlying mechanism(s) for ALFA-mediated protection against infection and augmented phagocytotic responses are unclear.

In the present study, we evaluated a broad range of antibody characteristics relevant to non-neutralizing antibody functions as assessed by an Fc array assay measuring Fv and Fc characteristics of antibodies in the vaccinated macaques. We aimed to determine the immune signature of different adjuvant formulations in a nonhuman primate HIV vaccine model and reveal the underlying mechanism linked to the observed ALFA-enhanced phagocytotic responses. In line with previous findings from hierarchical clustering and principal component analysis (6), our results showed a large overlap in the immune signatures of ALFA- and alum-adjuvanted vaccines, consistent with the overall similar vaccine regimens. The main aspects of variation in the data did not relate to adjuvants, yet differential protection was observed between adjuvants. Thus, we next sought to identify differences in individual immune features that were associated with adjuvants using univariate analysis. We found that ten Fc receptor-related immune responses were significantly enhanced by the vaccine adjuvanted with ALFA compared to alum. We then trained random forest models to determine which adjuvant-associated immune responses can best discriminate two adjuvant formulations on an individual level. Finally, we used a Cox regression analysis to determine whether immune responses most predictive of adjuvant, as identified by random forest models, were associated with reduced risk of infection over time. Among the ten ALFA-specific immune responses, three Fcγ receptor 2a-mediated immune responses strongly correlated with protection, but only in males. Our approach integrating univariate analysis, machine learning, and Cox regression analysis was effective in analyzing high-dimensional immune data and capable of identifying immune features associated with vaccine efficacy and inferring vaccine protection mechanisms.

METHODS

Immunization and SHIV Challenge of Rhesus Macaques

An HIV-1 vaccine NHP study was performed as previously described (6). Briefly, 48 rhesus macaques were assigned to three arms that were balanced across multiple factors, including *TRIM*5 alleles, *TRIMcyp* positivity, sex, weight, and age (**Supplementary Figure 1A**). Animals were primed with MVA encoding HIV-1 *gag-pol* and *env* from multiple subtypes at month 0 and boosted at months 3, 6, and 12 with MVA plus adjuvanted gp145 (CO6980v0c22, subtype C) adjuvanted with either ALFA or aluminum hydroxide (alum). Control animals received MVA lacking HIV-1 inserts and ALFA adjuvant alone. At month 15 macaques were serially challenged intrarectally every other week with SHIV-1157ipd3N4 (AID40) until viremic for up to ten challenges. Immune responses to vaccination were assessed in all three arms at five pre-challenge time points, including months 0, 3, 3.5, 6.5, and 12.5, and at first and sixth challenges (**Supplementary Figure 1B**).

Fc Array

Fc and Fv characteristics of antigen-specific sera polyclonal antibodies raised in response to the vaccines and challenges were evaluated using an Fc array assay (8). Briefly, a panel of thirty-seven recombinant SHIV/HIV-1 proteins were covalently coupled to fluorescent beads. Sera were analyzed at a dilution of 1:1,000 for detection reagents specific for tetramerized rhesus Fcγ receptor (FcγR2A-2, FcγR2A-3, FcγR2A-4, FcγR2B-1, FcγR3A-1, and FcγR3A-3) and human Fcγ receptor (FcγR2aH, FcγR2aR, FcγR2b, FcγR3aF, FcγR3aV, and FcγR3b NA1) detection reagents, whereas the dilutions used for analysis with rhesus IgG (Southern Biotech #6200-09, polyclonal, Lot B0112-YC26B) were 1:1,000 and 1:500. For aHu IgA (Southern Biotech #2050-09, polyclonal, Lot C5213-XA55X) and C1q, the dilution used was 1:250. The optimal serum dilution factors were determined experimentally (9). Beads were first incubated with antibodies, washed, and incubated with Fc detection reagents. Plates were subsequently washed and Median Fluorescence Intensity (MFI) data were collected using an array reader. Prior to analysis, Fc array data were filtered for quality control using a three-step process. First, coefficients of variation (CV) were calculated for all intra-plate sample replicates. The replicates leading to poor reproducibility (CV > 0.15) were identified and excluded.

Second, MFIs below 45 were marked as out of range and excluded. In cases where both replicates had MFIs below 45, these low values were presumed to be correct, and a value of 40 was assigned. Third, the Z-factor was applied to determine whether an Fc array measure has a positive signal, which is a measure of a signal quality using the concept of a separation band between background (pre-immune) and sample (post-immune) signals (10). Fc array data with non-positive signals were excluded.

Data Analysis

Vaccine-elicited immune responses (features) were determined using univariate analysis. Each immune response was compared to its pre-immune reference point and its reference in the Control arm, respectively. Identified vaccine-elicited immune responses were then compared between two vaccination arms, ALFA and alum, to identify differences at the group (adjuvant) level. Following univariate analysis, machine learning (e.g., random forest) was performed to determine how well subjects from the two vaccination arms could be distinguished at the individual level and which combination of immune responses contributed most to the distinction. Finally, Cox regression was used to determine if the immune responses most predictive of adjuvant were also correlated with reduced risk to infection that was observed in the ALFA arm (**Figure 1**).

Univariate analysis. To identify vaccine-elicited immune responses, univariate analysis for each immune measure was performed by comparing post-immune with pre-immune responses. Then, each post-immune response was compared with the corresponding measure from the Control arm. Wilcoxon signed-rank test and Mann-Whitney U test were used to calculate statistical significance, respectively (11). Immune measures in which comparisons to the pre-immune and Control data both showed a significant difference at p-value < 0.05 were selected as vaccine-elicited immune responses. Vaccine-elicited immune responses were further compared between the two adjuvant arms (ALFA vs. alum) using the Mann-Whitney U test to determine group-level difference with respect to adjuvant. To control the false discovery rate (FDR), resampling-based FDR adjustments were employed (12). One thousand permuted datasets were created by randomly shuffling the label (adjuvant) of each subject in the two vaccination arms. For each permuted dataset, the smallest p-value of the Mann-Whitney U tests across all comparisons was selected to create a probability distribution for the 1,000 lowest p-values obtained by random chance. The corrected p-value was calculated by comparing where the uncorrected p-value lies in the permuted distribution of the 1,000 lowest p-values. Adjuvant-associated differences were determined by identifying the vaccine-elicited immune responses that showed a significant difference between ALFA and alum arms at a p-value < 0.05 and a q-value < 0.2.

Multivariate analysis and machine learning. Spearman correlation coefficients between immune measures were calculated to create correlation matrices (13). Correlated immune measures were further clustered using hierarchical clustering (14). The optimal number of clusters was determined using the elbow method. Medoids in each cluster were identified as representative immune measures. The random forest approach was applied to build machine learning models to predict adjuvant arms using immune measures (15). Model training and parameter tunings were carried out using repeated 5-fold cross-validation, subsampling the data set by 5-fold and resampling 100 times. The hyperparameter, mtry (number of variables randomly sampled as candidates at each split), was adjusted to identify the optimal out-of-bag error, an unbiased estimate of the generalization error. To evaluate the predictive accuracy of the RF modeling approach, cross validation were utilized, where data samples were subsampled by bootstrap aggregating for training and prediction performance was evaluated on those observations that were not used in training.

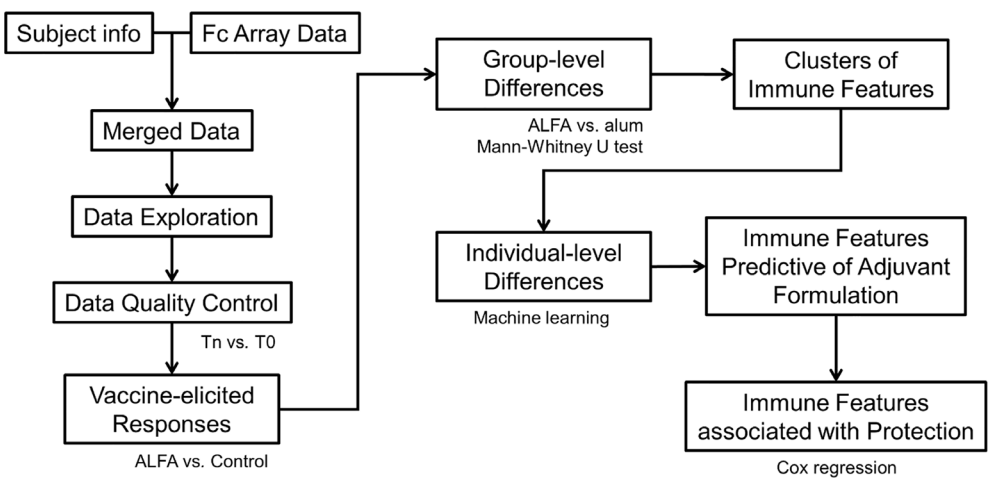

FIGURE 1 | Data analysis pipeline.

Model performance was expressed as both a percentage of correctly predicted outcomes with a Cohen's kappa value (16), and as the area under the curve of the receiver operating characteristic (AUCROC) (17). Cohen's kappa statistic is an unbiased measure for imbalanced class problems. To assess the statistical significance of the RF models and ascertain overfitting that might occur in the machine learning process, AUCROC-based permutation tests were carried out (18). In permutation tests, the labels (i.e., adjuvant type) of the training data were shuffled randomly. Random forest models were then rebuilt using the data with permuted labels 100 times. AUCROC was computed to evaluate prediction performance of permutation models. Based on the AUCROC of the permutation models, null distributions for AUCROC were also estimated.

Survival analysis. Survival analysis was used to investigate the time it takes for a subject to get infected by SHIV (19). The discrete infecting challenge was considered as the time to infection. Subjects that had not been infected by the tenth challenge were treated to be censored. Kaplan–Meier plots were created to visualize survival/time-to-event curves and log-rank test was used to compare the survival/time-to-event curves of two arms. Cox proportional-hazards model was fit to investigate the effect of immune measures on time to infection (20).

All statistical analyses were performed using the R stats package and machine learning were carried out using the R caret package.

RESULTS

Pox-Protein Vaccine Efficacy in Rhesus Macaques

To improve HIV-1 vaccine immunogenicity and efficacy, we recently evaluated pox-protein vaccination using a next generation liposome-based adjuvant, ALFA, in rhesus monkeys (6). It was found that SHIV infection risk trended lower with ALFA-adjuvanted vaccination relative to controls, while no vaccine efficacy was observed in the alum arm (**Supplementary Figures 1A–D**).

Fc Receptor-Related Immune Responses Elicited by ALFA-Adjuvanted Vaccine

To investigate the underlying mechanism(s) linked to the observed efficacy of ALFA-adjuvanted vaccination against SHIV acquisition, Fc array data analyses were performed to characterize the vaccine-elicited, HIV-1 Env-specific antibody effector profiles. Exploration of the whole data set showed that most effector immune responses appeared after the first boost (month 3.5), were sustained or increased with subsequent boosts, and decayed by the time of the first SHIV challenge (month 15). C1q-mediated immune responses declined faster by month 12.5, while IgA responses were limited relative to pre-immunization baseline values (**Figure 2A**). Vaccine-elicited immune responses were determined by comparing each immune response to its pre-immune and control arm values as reference. The broadest range of Fc receptor-related immune responses was identified at month 12.5, two weeks post the last immunization. We identfieid 106 vaccine-elicited immune respones in the active arms at this peak immunogenicity time point and these respones were captured by 14 detection reagents (**Figure 2B**). Comparison of these responses between ALFA and alum arms by PCA was unable to discriminate animals by adjuvant group (**Figure 2C**), indicating that vaccine-elicited immune responses with large variance may not be associated with adjuvants.

Differential Fc Receptor-Related Immune Responses by Adjuvant

Because the main aspects of variation in the data did not relate to adjuvants, yet differential protection was observed between adjuvants, we next sought to identify differences in individual immune features that were associated with adjuvants. Univariate

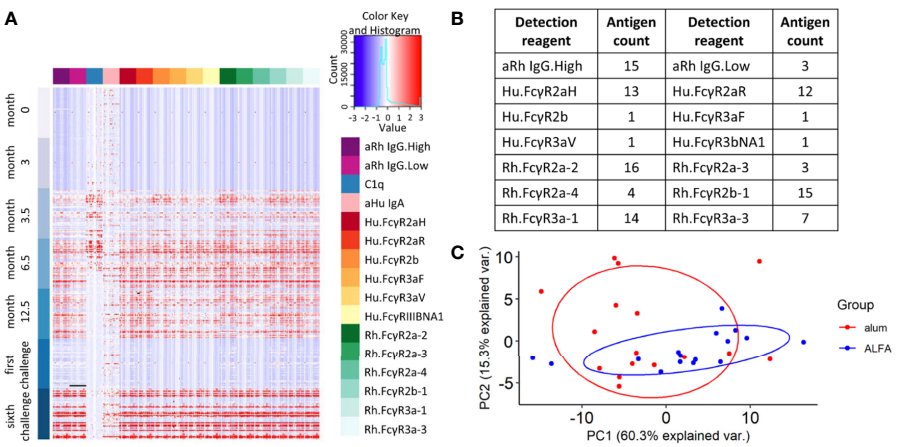

Detection reagent	Antigen count	Detection reagent	Antigen count
aRh IgG.High	15	aRh IgG.Low	3
Hu.FcγR2aH	13	Hu.FcγR2aR	12
Hu.FcγR2b	1	Hu.FcγR3aF	1
Hu.FcγR3aV	1	Hu.FcγR3bNA1	1
Rh.FcγR2a-2	16	Rh.FcγR2a-3	3
Rh.FcγR2a-4	4	Rh.FcγR2b-1	15
Rh.FcγR3a-1	14	Rh.FcγR3a-3	7

FIGURE 2 | Vaccine-elicited and Fc-mediated effector function. **(A)** Heat map for all Fc array measurements performed on all 48 study animals (rows) at each study time point by HIV-1 Env antigen and immune features (columns). **(B)** Fc features of vaccine-elicited immune responses at 12.5 months post-vaccination. **(C)** Principal component analysis on vaccine-elicited immune responses at 12.5 months post-vaccination by active vaccine group.

analyses of the Fc receptor-related immune responses were performed by comparing each vaccine-elicited immune response between the ALFA and alum active arms. While all twelve Fcγ receptors characterized in the Fc array were represented among the vaccine-elicited responses, the two adjuvants arms differed only in ten responses related to just three Fcγ receptors: Hu.FcγR2aR, Rh.FcγR2a-2, and Rh.FcγR2b-1 (**Figures 3A–J**). Fcγ receptors 2a and 2b are close homologs known to be responsible for phagocytosis (21, 22). These ten vaccine-elicited immune responses were also compared between the ALFA and alum active arms using PCA, which distinguished animals by adjuvant when using this subset of vaccine-elicited immune responses (**Figure 3K**). The two principal components, PC1 and PC2, captured over 90% of the variation in the data set. By comparing the PCA plot with the one in **Figure 2C**, we found that the overlap between ALFA and alum clusters is smaller in **Figure 3K**, which indicates that the 10 adjuvant-associated immune responses have stronger classification power for separating adjuvant groups.

Fcγ Receptor 2a-Related Immune Responses Most Predictive of Vaccine Adjuvant

Machine learning was applied to make an individualized assessment of adjuvant-associated effects. A set of random forest models were built (n=100) to predict whether each animal in the active arms received ALFA- or alum-adjuvanted vaccine based on the ten identified vaccine-elicited immune responses that differed between adjuvant groups. We assessed model prediction performance using repeated cross validation and permutation tests. The confusion matrix created from the results of 100 repeated 5-fold cross-validations of the data showed that the random forest model achieved an accuracy of 74%, and a kappa value of 0.50, indicating moderate to strong predictive performance (16) (**Figure 4A**). In order to assess the overfitting, the random forest model was applied using a permutation test whereby the labels (adjuvants) of the data were randomly shuffled. The AUCROC of models built with the randomly shuffled data was 0.52, which was significantly lower than the average AUCROC of actual models, 0.75 (**Figure 4B**). The permutation test also revealed that there was only a 3% probability that the AUCROC of actual models, 0.75, could be obtained at random. The average AUCROC of models built with the randomly shuffled data was close to 0.5, indicating that our model was not overfitted. The importance of the ten vaccine-elicited immune responses that were employed in the random forest model was measured using relative importance scores (**Figure 4C**). We found that three Fcγ receptor 2a-related immune responses were most predictive of vaccine adjuvant: Hu.FcγR2aR_gp120(620345_D11), Rh.FcγR2a-2_gp140C(B.6240), and Rh.FcγR2a-2_gp120(620345_D11).

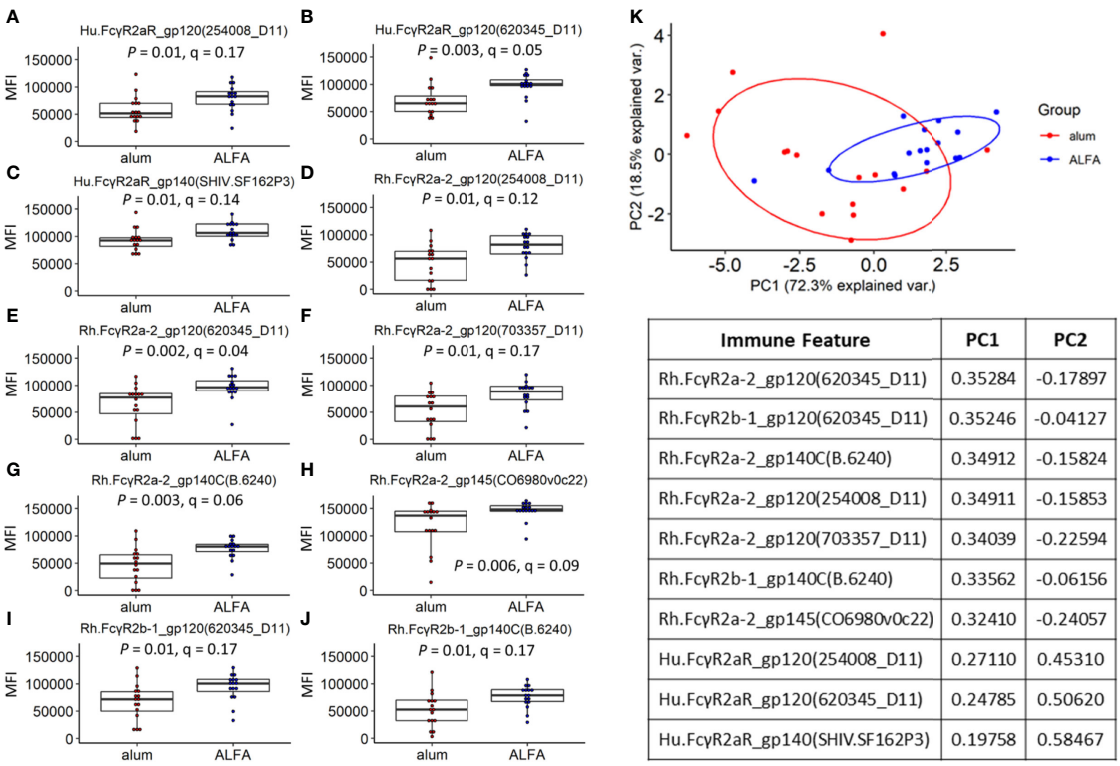

Immune Feature	PC1	PC2
Rh.FcγR2a-2_gp120(620345_D11)	0.35284	-0.17897
Rh.FcγR2b-1_gp120(620345_D11)	0.35246	-0.04127
Rh.FcγR2a-2_gp140C(B.6240)	0.34912	-0.15824
Rh.FcγR2a-2_gp120(254008_D11)	0.34911	-0.15853
Rh.FcγR2a-2_gp120(703357_D11)	0.34039	-0.22594
Rh.FcγR2b-1_gp140C(B.6240)	0.33562	-0.06156
Rh.FcγR2a-2_gp145(CO6980v0c22)	0.32410	-0.24057
Hu.FcγR2aR_gp120(254008_D11)	0.27110	0.45310
Hu.FcγR2aR_gp120(620345_D11)	0.24785	0.50620
Hu.FcγR2aR_gp140(SHIV.SF162P3)	0.19758	0.58467

FIGURE 3 | Vaccine-elicited immune responses that vary by adjuvant. **(A–J)** Vaccine-elicited binding antibody responses differing between the ALFA and alum active arms are shown for each Fc detection reagent and HIV-1 Env antigen combination. MFI, median fluorescence intensity. **(K)** Principal component analysis on adjuvant-associated immune responses.

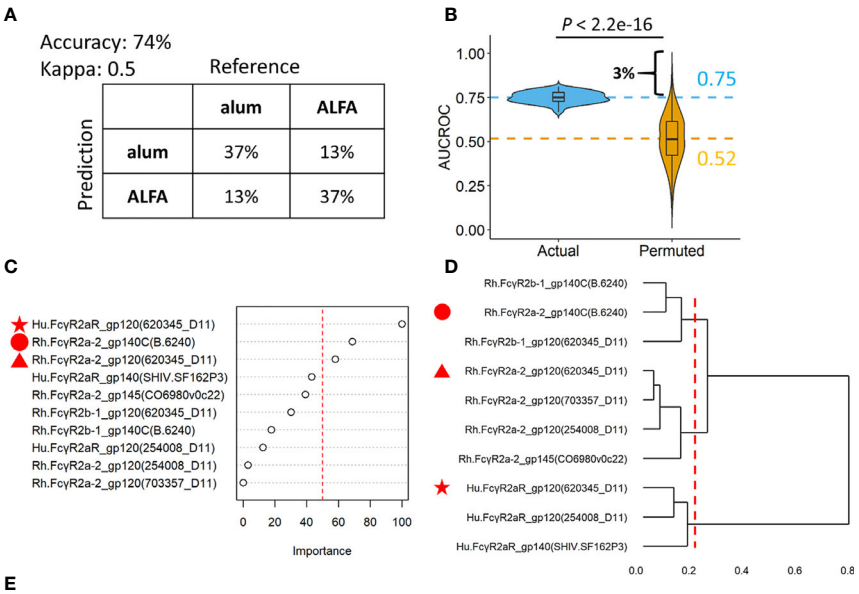

E

Immune Feature	β	*P*	C-index
Hu.FcγR2aR_gp120(620345_D11)	-0.37	0.07	0.7
Rh.FcγR2a-2_gp140C(B.6240)	-0.36	0.08	0.6
Rh.FcγR2a-2_gp120(620345_D11)	-0.35	0.09	0.6

FIGURE 4 | Random forest models revealing individual level differences between ALFA and alum. **(A)** Prediction accuracy, kappa, and confusion matrices. The rows of confusion matrices represent the predicted adjuvant arms, whereas the columns indicate the actual adjuvant arms. **(B)** Comparison of AUCROC values from 100 repetitions of 100 times repeated 5-fold cross-validation using actual (blue) versus permutated (yellow) adjuvant labels. Dashed line represented the mean AUCROC values. **(C)** Immune feature importance in random forest models. **(D)** Hierarchical clustering on immune features used in random forest models. **(E)** Cox regression analysis on three most important immune features identified by random forest models.

These three immune responses belong to three different clusters defined by hierarchical clustering of the ten immune responses employed in the random forest model (**Figure 4D**). The association between these three immune responses and infection risk was investigated using the Cox proportional-hazards model and the pooled data from ALFA and control arms. All three of these responses were negatively associated with infection risk at a significance level of 0.1 (**Figure 4E**). This finding supports an FcγR2a-mediated Env-specific binding antibody-dependent mechanism underlying the protection observed with ALFA-adjuvanted vaccination. Fcγ receptor 2a is known to be responsible for executing phagocytosis, which independently correlated with protection (6).

Sex-Differential Effect of ALFA-Adjuvanted Vaccine

Sex-based differences in vaccine responses are well established both in humans and animal models (23, 24). Two striking sex differences were observed in this macaque study: 1) ALFA-mediated vaccine efficacy was limited to male animals; and 2) the infection rate in females was much lower than that of males, independent of vaccine group (6) (**Supplementary Figures 1E–F**). We explored immune responses associated with challenge outcomes stratified by sex. Using Cox proportional-hazards modeling, the three Fcγ receptor 2a-related immune response features most predictive of vaccine adjuvant at month 12.5 were also negatively associated with infection risk in males at a significance level of 0.01 (**Figure 5A**). However, sex differences in the magnitude of these three immune responses most predictive of adjuvant were not identified, as both males and females immunized with ALFA-adjuvanted vaccine mounted similarly robust responses (**Figures 5B–G**). Therefore inherent sex-based differences in vaccine immunogenicity did not appear to contribute to the discordant challenge outcomes between vaccinated males and females.

DISCUSSION

RV144 and several recent NHP vaccine studies have shown evidence that antibody effector activities are associated with reduced risk to HIV/SHIV infection, highlighting a protective role of non-neutralizing antibodies for HIV vaccine design (22, 25–28). Thus, there is growing interest in studying non-neutralizing Fc functional antibodies and their contributions to novel correlates of protection. The Fc array was applied in this study to capture multi-dimensional profiles of Fc effector

A

Immune Feature	Male			Female		
	β	*P*	C-index	β	*P*	C-index
Hu.FcγR2aR_gp120(620345_D11)	-1.60	0.01	0.9	0.11	0.74	0.5
Rh.FcγR2a-2_gp140C(B.6240)	-1.59	0.01	0.8	0.14	0.71	0.5
Rh.FcγR2a-2_gp120(620345_D11)	-1.63	0.01	0.8	0.37	0.54	0.6

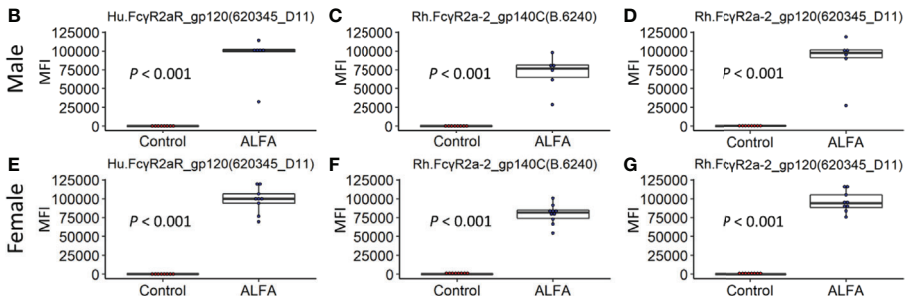

FIGURE 5 | Sex-specific efficacy and vaccine-elicited immune responses. **(A)** Cox regression analysis for Male and Female subjects on three most important immune features identified by random forest models. **(B–D)** Vaccine-elicited immune responses of Male subjects in the ALFA arm. **(E–G)** Vaccine-elicited immune responses of Female subjects in the ALFA arm. MFI, Median Fluorescence Intensity.

functions. We compared antigen-specific binding antibody Fc array immunoprofiles of rhesus macaques enrolled in a pox-protein HIV-1 vaccine efficacy study in which protein was adjuvanted with either conventional alum or ALFA. Characterizing immunoprofiles of adjuvanted vaccines and identifying their immune signatures may aid in understanding protective mechanisms modulated by adjuvants and identifying appropriate vaccine adjuvant(s) for specific pathogens. We found that adjuvanting with ALFA induced stronger Fcγ receptor 2a-related binding antibody responses and these responses were associated with protection against SHIV acquisition.

Fcγ receptor 2a is a cell surface receptor that is expressed on phagocytic cells, such as macrophages, monocytes, neutrophils, and dendritic cells, and involved in phagocytosis. Genetic variations of Fcγ receptor 2a correlate with progression of HIV infection (29), susceptibility to perinatal HIV-1 infection (30), and HIV vaccine effects (31). In addition, Fcγ receptor 2a and 2b-related immune responses have been found to correlate with the phagocytic activity of HIV-specific antibodies (21, 22). Our study not only confirms the findings of the previous study, i.e., that the ALFA-adjuvanted vaccine enhanced induction of phagocytic responses as assessed by functional assays (6), but we can also infer a potential phagocytic mechanism of the ALFA-adjuvanted vaccine, which involves the Fcγ receptor 2a.

Previous studies have shown that females often mount greater antibody responses to immunization or infection than males (32–34), but sex differences in terms of non-neutralizing effector antibody responses have not been investigated in depth. In the present study, we evaluated the sex-differential effect of ALFA-adjuvanted vaccine. The ALFA-adjuvanted vaccine elicited Fcγ receptor 2a-mediated humoral immune responses that were positively correlated with protection, but only in males. Future, well-powered studies including both sexes will be valuable to further identify sex-based differences in vaccine outcomes and immune correlates.

Systems serology is a relatively new data-driven approach that can analyze high-throughput experimental data to comprehensively survey a diverse array of antibody features and functions. This information can be used to identify new correlates of protection from infection and lead to a more comprehensive understanding of vaccine mechanisms that underlie protection (35, 36). Systems serology has been applied to search for immune features that best predict protection induced by HIV vaccines (37–39), malaria vaccines (40–42), and other vaccines (43, 44). In the present study, we developed a systems serology pipeline that integrated both machine learning and Cox proportional hazards regression to analyze high-dimensional Fc array data. We found that antibody-dependent Fcγ receptor 2a-related effector functions were augmented by the ALFA adjuvant, and these responses were associated with enhanced protection in male animals. Our results highlight how systems serology can be used to identify biological mechanisms that underlie vaccine-induced protection. Furthermore, the analyses showcase how to use in-depth statistical analysis of complex data to advance the study and exploration of next generation adjuvants aimed at developing a globally effective HIV vaccine.

DATA AVAILABILITY STATEMENT

The data used in this manuscript can be made available upon request. Requests to access these datasets should be directed to DB, dbolton@hivresearch.org.

AUTHOR CONTRIBUTIONS

PL, SC, DB, and AW designed the project. DG, SL, MA, and DB produced the data. PL performed the data analyses. PL and DB wrote the manuscript. DG, SL, SC, MA, DB, and AW reviewed and edited the manuscript. All authors contributed to the article and approved the submitted version.

FUNDING

This work was supported by the U.S. Army Medical Research and Development Command under Contract No. W81XWH20C0031, by the Military Infectious Disease Research Program and by a cooperative agreement (W81XWH-11-2-0174) between the Henry M. Jackson Foundation for the Advancement of Military Medicine, Inc. (HJF), and the U.S. Department of Defense (DOD).

ACKNOWLEDGMENTS

We would like to thank Drs. Morgane Rolland and Thembi Mdluli for insightful discussion on our project design and manuscript.

SUPPLEMENTARY MATERIAL

The Supplementary Material for this article can be found online at: https://www.frontiersin.org/articles/10.3389/fimmu.2021.625030/full#supplementary-material

REFERENCES

1. UNAIDS. *Global HIV & AIDS Statistics — 2020 Fact Sheet* (2020). Available at: https://www.unaids.org/en/resources/fact-sheet.
2. Gao Y, McKay PF, Mann JFS. Advances in HIV-1 Vaccine Development. *Viruses* (2018) 10(4). doi: 10.3390/v10040167
3. Rerks-Ngarm S, Pitisuttithum P, Nitayaphan S, Kaewkungwal J, Chiu J, Paris R, et al. Vaccination With ALVAC and AIDSVAX to Prevent HIV-1 Infection in Thailand. *New Engl J Med* (2009) 361(23):2209–20. doi: 10.1056/NEJMoa0908492
4. Robb ML, Rerks-Ngarm S, Nitayaphan S, Pitisuttithum P, Kaewkungwal J, Kunasol P, et al. Risk Behaviour and Time as Covariates for Efficacy of the HIV Vaccine Regimen ALVAC-HIV (Vcp1521) and AIDSVAX B/E: A Post-Hoc Analysis of the Thai Phase 3 Efficacy Trial RV 144. *Lancet Infect Dis* (2012) 12(7):531–7. doi: 10.1016/S1473-3099(12)70088-9
5. Shaw AR, Feinberg MB. 90 - Vaccines. In: RR Rich, TA Fleisher, WT Shearer, HW Schroeder, AJ Frew, CM Weyand, editors. *Clinical Immunology*, *4th ed.* London: Content Repository Only (2013). p. 1095–121.
6. Om K, Paquin-Proulx D, Montero M, Peachman K, Shen X, Wieczorek L, et al. Adjuvanted HIV-1 Vaccine Promotes Antibody-Dependent Phagocytic Responses and Protects Against Heterologous SHIV Challenge. *PloS Pathog* (2020) 16(9):e1008764. doi: 10.1371/journal.ppat.1008764
7. Alving CR, Peachman KK, Matyas GR, Rao M, Beck Z. Army Liposome Formulation (ALF) Family of Vaccine Adjuvants. *Expert Rev Vaccines* (2020) 19(3):279–92. doi: 10.1080/14760584.2020.1745636
8. Brown EP, Dowell KG, Boesch AW, Normandin E, Mahan AE, Chu T, et al. Multiplexed Fc Array for Evaluation of Antigen-Specific Antibody Effector Profiles. *J Immunol Methods* (2017) 443:33–44. doi: 10.1016/j.jim.2017.01.010
9. Brown EP, Weiner JA, Lin S, Natarajan H, Normandin E, Barouch DH, et al. Optimization and Qualification of an Fc Array Assay for Assessments of Antibodies Against HIV-1/SIV. *J Immunol Methods* (2018) 455:24–33. doi: 10.1016/j.jim.2018.01.013
10. Zhang JH, Chung TD, Oldenburg KR. A Simple Statistical Parameter for Use in Evaluation and Validation of High Throughput Screening Assays. *J Biomol Screening* (1999) 4(2):67–73. doi: 10.1177/108705719900400206
11. Mann HB, Whitney DR. On a Test of Whether One of Two Random Variables is Stochastically Larger Than the Other. *Ann Math Statistics* (1947) 50–60. doi: 10.1214/aoms/1177730491
12. Yekutieli D, Benjamini Y. Resampling-Based False Discovery Rate Controlling Multiple Test Procedures for Correlated Test Statistics. *J Stat Plann Inference* (1999) 82(1-2):171–96. doi: 10.1016/S0378-3758(99)00041-5
13. Myers JL, Well A. *Research Design and Statistical Analysis*. Lawrence Erlbaum (2003).
14. Nielsen F. Hierarchical Clustering. In: *Introduction to HPC With MPI for Data Science*. Springer (2016). p. 195–211.
15. TK Ho ed. *Random Decision Forests. Proceedings of 3rd International Conference on Document Analysis and Recognition*. IEEE (1995).
16. McHugh ML. Interrater Reliability: The Kappa Statistic. *Biochemia Med* (2012) 22(3):276–82. doi: 10.11613/BM.2012.031
17. Hanley JA, McNeil BJ. The Meaning and Use of the Area Under a Receiver Operating Characteristic (ROC) Curve. *Radiology* (1982) 143(1):29–36. doi: 10.1148/radiology.143.1.7063747
18. Welch WJ. Construction of Permutation Tests. *J Am Stat Assoc* (1990) 85 (411):693–8. doi: 10.1080/01621459.1990.10474929
19. Miller RG Jr. *Survival Analysis*. John Wiley & Sons (2011).
20. Cox D. Regression Models and Life-Tables. *J R Stat Soc Ser B (Methodol)* (1972) 34(2):87–22. doi: 10.1111/j.2517-6161.1972.tb00899.x
21. Ackerman ME, Dugast AS, McAndrew EG, Tsoukas S, Licht AF, Irvine DJ, et al. Enhanced Phagocytic Activity of HIV-Specific Antibodies Correlates With Natural Production of Immunoglobulins With Skewed Affinity for Fcγr2a and Fcγr2b. *J Virol* (2013) 87(10):5468–76. doi: 10.1128/JVI.03403-12
22. Ackerman ME, Das J, Pittala S, Broge T, Linde C, Suscovich TJ, et al. Route of Immunization Defines Multiple Mechanisms of Vaccine-Mediated Protection Against SIV. *Nat Med* (2018) 24(10):1590–8. doi: 10.1038/s41591-018-0161-0
23. Klein SL, Jedlicka A, Pekosz A. The Xs and Y of Immune Responses to Viral Vaccines. *Lancet Infect Diseases* (2010) 10(5):338–49. doi: 10.1016/S1473-3099(10)70049-9
24. Klein SL, Marriott I, Fish EN. Sex-Based Differences in Immune Function and Responses to Vaccination. *Trans R Soc Trop Med Hygiene* (2015) 109(1):9–15. doi: 10.1093/trstmh/tru167
25. Haynes BF, Gilbert PB, McElrath MJ, Zolla-Pazner S, Tomaras GD, Alam SM, et al. Immune-Correlates Analysis of an HIV-1 Vaccine Efficacy Trial. *New Engl J Med* (2012) 366(14):1275–86. doi: 10.1056/NEJMoa1113425
26. Corey L, Gilbert PB, Tomaras GD, Haynes BF, Pantaleo G, Fauci AS. Immune Correlates of Vaccine Protection Against HIV-1 Acquisition. *Sci Trans Med* (2015) 7(310):310rv7. doi: 10.1126/scitranslmed.aac7732
27. Felber BK, Lu Z, Hu X, Valentin A, Rosati M, Remmel CAL, et al. Co-Immunization of DNA and Protein in the Same Anatomical Sites Induces Superior Protective Immune Responses Against SHIV Challenge. *Cell Rep* (2020) 31(6):107624. doi: 10.1016/j.celrep.2020.107624
28. Pittala S, Bagley K, Schwartz JA, Brown EP, Weiner JA, Prado IJ, et al. Antibody Fab-Fc Properties Outperform Titer in Predictive Models of SIV Vaccine-Induced Protection. *Mol Syst Biol* (2019) 15(5):e8747. doi: 10.15252/msb.20188747
29. Forthal DN, Landucci G, Bream J, Jacobson LP, Phan TB, Montoya B. Fcgammariia Genotype Predicts Progression of HIV Infection. *J Immunol (Baltimore Md 1950)* (2007) 179(11):7916–23. doi: 10.4049/jimmunol.179.11.7916
30. Brouwer KC, Lal RB, Mirel LB, Yang C, van Eijk AM, Ayisi J, et al. Polymorphism of Fc Receptor Iia for Igg in Infants is Associated With Susceptibility to Perinatal HIV-1 Infection. *AIDS (London England)* (2004) 18(8):1187–94. doi: 10.1097/00002030-200405210-00012
31. Li SS, Gilbert PB, Carpp LN, Pyo CW, Janes H, Fong Y, et al. Fc Gamma Receptor Polymorphisms Modulated the Vaccine Effect on HIV-1 Risk in the HVTN 505 HIV Vaccine Trial. *J Virol* (2019) 93(21). doi: 10.1128/JVI.02041-18

32. Fischinger S, Boudreau CM, Butler AL, Streeck H, Alter G. Sex Differences in Vaccine-Induced Humoral Immunity. *Semin Immunopathol* (2019) 41 (2):239–49. doi: 10.1007/s00281-018-0726-5
33. Miller-Novak LK, Das J, Musich TA, Demberg T, Weiner JA, Venzon DJ, et al. Analysis of Complement-Mediated Lysis of Simian Immunodeficiency Virus (SIV) and SIV-Infected Cells Reveals Sex Differences in Vaccine-Induced Immune Responses in Rhesus Macaques. *J Virol* (2018) 92(19). doi: 10.1128/JVI.00721-18
34. Aaby P, Benn CS, Flanagan KL, Klein SL, Kollmann TR, Lynn DJ, et al. The Non-Specific and Sex-Differential Effects of Vaccines. *Nat Rev Immunol* (2020) 20(8):464–70. doi: 10.1038/s41577-020-0338-x
35. Arnold KB, Chung AW. Prospects From Systems Serology Research. *Immunology* (2018) 153(3):279–89. doi: 10.1111/imm.12861
36. Chung AW, Alter G. Systems Serology: Profiling Vaccine Induced Humoral Immunity Against HIV. *Retrovirology* (2017) 14(1):57. doi: 10.1186/s12977-017-0380-3
37. Bradley T, Pollara J, Santra S, Vandergrift N, Pittala S, Bailey-Kellogg C, et al. Pentavalent HIV-1 Vaccine Protects Against Simian-Human Immunodeficiency Virus Challenge. *Nat Commun* (2017) 8:15711. doi: 10.1038/ncomms15711
38. Chung AW, Kumar MP, Arnold KB, Yu WH, Schoen MK, Dunphy LJ, et al. Dissecting Polyclonal Vaccine-Induced Humoral Immunity Against HIV Using Systems Serology. *Cell* (2015) 163(4):988–98. doi: 10.1016/j.cell.2015.10.027
39. Pittala S, Morrison KS, Ackerman ME. Systems Serology for Decoding Infection and Vaccine-Induced Antibody Responses to HIV-1. *Curr Opin HIV AIDS* (2019) 14(4):253–64. doi: 10.1097/COH.0000000000000558
40. Suscovich TJ, Fallon JK, Das J, Demas AR, Crain J, Linde CH, et al. Mapping Functional Humoral Correlates of Protection Against Malaria Challenge Following RTS,S/AS01 Vaccination. *Sci Trans Med* (2020) 12(553). doi: 10.1126/scitranslmed.abb4757
41. Chaudhury S, Duncan EH, Atre T, Storme CK, Beck K, Kaba SA, et al. Identification of Immune Signatures of Novel Adjuvant Formulations Using Machine Learning. *Sci Rep* (2018) 8(1):17508. doi: 10.1038/s41598-018-35452-x
42. Pallikkuth S, Chaudhury S, Lu P, Pan L, Jongert E, Wille-Reece U, et al. A Delayed Fractionated Dose RTS,S AS01 Vaccine Regimen Mediates Protection Via Improved T Follicular Helper and B Cell Responses. *eLife* (2020) 9. doi: 10.7554/eLife.51889
43. Srikiatkhachorn A, Yoon IK. Immune Correlates for Dengue Vaccine Development. *Expert Rev Vaccines* (2016) 15(4):455–65. doi: 10.1586/14760584.2016.1116949
44. Sanchez-Lockhart M, Reyes DS, Gonzalez JC, Garcia KY, Villa EC, Pfeffer BP, et al. Qualitative Profiling of the Humoral Immune Response Elicited by Rvsv-ΔG-EBOV-GP Using a Systems Serology Assay, Domain Programmable Arrays. *Cell Rep* (2018) 24(4):1050–9.e5. doi: 10.1016/j.celrep.2018.06.077

Disclaimer: The opinions and assertions contained herein are the private views of the authors and are not to be construed as official or as reflecting the views of the U.S. Army, the U.S. Department of Defense, or The Henry M. Jackson Foundation for the Advancement of Military Medicine, Inc. (HJF). This manuscript has been approved for public release with unlimited distribution.

Conflict of Interest: The authors declare that this study received funding from the Henry M. Jackson Foundation for the Advancement of Military Medicine, Inc. The funder was not involved in the study design, collection, analysis, and interpretation of data, the writing of this article or the decision to submit it for publication.

Advantages of publishing in Frontiers

OPEN ACCESS
Articles are free to read for greatest visibility and readership

FAST PUBLICATION
Around 90 days from submission to decision

HIGH QUALITY PEER-REVIEW
Rigorous, collaborative, and constructive peer-review

TRANSPARENT PEER-REVIEW
Editors and reviewers acknowledged by name on published articles

Frontiers
Avenue du Tribunal-Fédéral 34
1005 Lausanne | Switzerland

Visit us: www.frontiersin.org
Contact us: frontiersin.org/about/contact

REPRODUCIBILITY OF RESEARCH
Support open data and methods to enhance research reproducibility

DIGITAL PUBLISHING
Articles designed for optimal readership across devices

FOLLOW US
@frontiersin

IMPACT METRICS
Advanced article metrics track visibility across digital media

EXTENSIVE PROMOTION
Marketing and promotion of impactful research

LOOP RESEARCH NETWORK
Our network increases your article's readership